THE UNIVERSITY of ADELAIDE

Nonlinear Mechanics of Hyperelastic Structures

by

Hossein Bakhshi Khaniki

In fulfilment of the requirements for the degree of

Doctor of Philosophy

January 2023

School of Mechanical Engineering

The University of Adelaide

Australia

Contents

Declaration

I, Hossein Bakhshi Khaniki, certify that this work contains no material which has been accepted for the award of any other degree or diploma in my name, in any university or other tertiary institution and, to the best of my knowledge and belief, contains no material previously published or written by another person, except where due reference has been made in the text. In addition, I certify that no part of this work will, in the future, be used in a submission in my name, for any other degree or diploma in any university or other tertiary institution without the prior approval of the University of Adelaide and where applicable, any partner institution responsible for the joint-award of this degree.

I acknowledge that copyright of published works contained within this thesis resides with the copyright holder(s) of those works.

I also give permission for the digital version of my thesis to be made available on the web, via the University's digital research repository, the Library Search and also through web search engines, unless permission has been granted by the University to restrict access for a period of time.

This work employed the supercomputing resources provided by the Phoenix HPC service at the University of Adelaide. The HDR scholarship support through The University of Adelaide and Faculty of Engineering, Computer & Mathematical Sciences, the University of Adelaide, is also acknowledged.

Hossein Bakhshi Khaniki

Monday 9th January, 2023

Acknowledgements

I would like to sincerely thank my supervisors, Dr Mergen Ghayesh and Dr Rey Chin for their continuous guidance and kind support throughout this project. Dr Mergen's precious support gave me an excellent research environment to focus on my work. His technical support through this journey upgraded the outcome of this research in all aspects. Dr Rey provided invaluable feedback on my works throughout this thesis. This project would have not been accomplished without the valuable support of my supervisors.

I would also like to acknowledge the precious support of Prof Marco Amabili during this project. His kind guidance has helped me in understanding the fundamentals of hyperelasticity and modelling soft structures. The precious support of my co-authors Prof Li-Qun Chen and Dr Shahid Hussain in the chapters of this thesis is greatly appreciated.

This project includes many experimental tests which would have not been possible without the continuous guidance and support of the staff of the Mechanical Workshop, Chapman Laboratory, Prototyping Laboratory–3D, and Acoustics & Vibration Laboratory of the University of Adelaide helping in design, fabrication and test procedures especially Thomas Stanef, Jon Ayoub, Hayden Westell, Scott Letton, and Pascal Symons.

Most importantly, I sincerely thank my parents Prof Gholamreza Bakhshi Khaniki and Mrs Zahra Behnam. I am greatly indebted to my parents who always wanted the best for me; everything I am is because of you. Thank you for all that you have done for me. The endless love and emotional support I received during this challenging project was indescribable. This thesis is lovingly and respectfully dedicated to them, although nothing can compensate for their love and support.

I have spent a significant time on this project which was not possible without the support of my friends. Thank you all for being there and never leaving me alone. I also appreciate the support I have received from The University of Adelaide and my colleagues.

Abstract

Soft flexible structures have been an important part of many operating systems used by humans in their daily routines. These structures are more likely to undergo large strains and deformation when facing different types of loads, and return to their initial shape when the load is removed. Most structures show a linear stress-strain behaviour only when the strain deformation is significantly small. However, to have a proper analysis of structures facing large strains, it is important to have better and more accurate modelling of their stress-strain behaviour. Rubbers, elastomers, silicones and polymeric-based structures are capable of undergoing large deformations, which mostly show a nonlinear elastic behaviour. Hyperelastic structures are labelled as structures made of non-linear elastic materials that can be modelled following a proper strain energy density function model. The significant capabilities of soft structures, such as infinite degrees of freedom, smooth motion, and safe human-machine interactions, make them ideal for soft robotics, biomechanics, automotive applications, and wearable devices.

In view of the recognition of the capabilities of nonlinear elastic structures, most studies in this field are directed towards their application purposes (e.g., applications of non-linear elastic structures for developing soft robots, wearable devices, packaging, etc.). However, the need to comprehend their mechanical behaviour in order to have a better understanding of the structure's response and, hence, develop optimised designs for hyperelastic structures, has only recently been fully understood. Therefore, this thesis intends to present a comprehensive study of the nonlinear mechanics of different isotropic hyperelastic structures under different conditions, mainly focusing on their nonlinear dynamics behaviour. This thesis is organised using published papers in prestigious peer-reviewed international journals as outcomes of the research.

Paper 1: A detailed review of the static deformation of hyperelastic structures is presented in this paper, focusing on biological tissues and polymeric structures. The main objective of this review paper is to show the application of different hyperelastic strain energy density models for modelling the bending and buckling behaviour of nonlinear elastic structures. For biological structures, a wide range of tissues including brain, artery, cartilage, liver, skeletal muscle, ligament, skin, tongue, heel pad and adipose tissue are discussed and for polymeric structures, beam, column, tube, plate shell and membrane hyperelastic structures are analysed.

Paper 2: The most well-known hyperelastic strain energy density models for analysing soft isotropic structures are reviewed in this paper and the applications of these constitutive laws for modelling the nonlinear dynamics of different hyperelastic structures are discussed using the available literature, up to 2022. Neo-Hookean,

Mooney-Rivlin, Ogden, Eight-chain, Polynomial, Gent and Blatz-Ko hyperelastic strain energy density models are discussed, and the sensitivity of the hyperelastic coefficients for changing the stress-stretch behaviour is analysed. Different studies undertaken on the nonlinear dynamics of hyperelastic beams, plates, shells, membranes and balloons are discussed. Meanwhile, the strength of each hyperelastic strain energy density model for accurately modelling the nonlinear dynamics of such structures is analysed.

Paper 3: Hyperelastic belts provide smooth motion in the performance of belt-operating systems and avoid the propagation of sudden impacts. Since belt-operating systems are one of the main applications of hyperelastic structures, this paper analysed the nonlinear dynamic behaviour of axially-moving, incompressible, isotropic hyperelastic belts. Using the ASTM D638 standard, the nonlinear elastic behaviour of the structure is studied and Yeoh's strain energy density model is used to effectively model the experimental results. A coupled equation of motion is presented for modelling axially-moving hyperelastic belts, and analysing the effect of both hyperelastic coefficients and axial velocity on changing the mode shapes, linear frequencies and the nonlinear dynamic behaviour of the structure.

Paper 4: Porosity and voids are often seen during the fabrication process of soft structures (such as in the injection moulding or 3d-printing processes) or are sometimes added to decrease the overall weight and optimise performance. This paper developed a modified strain energy density model using the Mooney-Rivlin law, which enables consideration of porosity effects. A set of experimental analyses on soft samples with different porosities and infill rates are performed and a modified strain energy model is presented. Using the given model, the nonlinear dynamics of hyperelastic porous beams with uniform and nonuniform porosities is studied and the effects of having different porosity types on the nonlinear vibration behaviour of the structure are discussed.

Paper 5: In many applications, such as packaging, hyperelastic structures are used as a layered (sandwich) structure. This paper investigated the nonlinear dynamics of layered isotropic structures using different shear deformation theories. The importance of proper modelling, layering, and material sorting is analysed comprehensively and the effect of the thickness ratio between layers is investigated.

Paper 6: Some soft structures show significant viscoelastic behaviour together with hyperelasticity. In order to model these soft structures appropriately, this paper investigated the statics and dynamics of hyperelastic and visco-hyperelastic shallow arches. The internal resonance phenomena due to the arch curvature were also investigated in this work, alongside a discussion of the effect of viscoelasticity in damping and changing the rich nonlinear vibration behaviour of the structure.

Paper 7: As hyperelastic structures are used in different sensing applications, this study investigated the mass-sensing behaviour of hyperelastic isotropic plates using both experimental testing and theoretical modelling. The effect of having a concentrated attached mass on changing the nonlinear dynamics of hyperelastic plates was discussed and the internal resonance phenomena due to the geometrical properties of the plate and external attached masses were discussed.

Paper 8: Curved hyperelastic shell structures, including cylindrical, parabolic, and doubly-curved shells are modelled and investigated in this paper as incompressible structures. A comprehensive general model is developed, and the bending,

vibration and internal resonance behaviour of the structure is analysed. The effect of the shell curvatures in causing internal resonance and changing the nonlinear oscillation behaviour of the structure is discussed in detail.

Through the above papers, this thesis investigated the mechanics of hyperelastic structures in a range of well-known applications. With experimental tests supporting the theoretical models, a detailed understanding of the statics and dynamics of such structures has been obtained, which is an important step towards understanding their performance and optimising their use.

Chapter 1

Introduction

1.1 Overview

Given the constant need to improve mechanical structures for different industrial applications, researchers have developed new structures according to the requirements of their research fields. Soft structures have been the focus of much research interest over the past few years due to their superiority in many applications. These structures are more likely to undergo large strains and deformation when facing different types of loads, and providing infinite degrees of freedom, smooth motion, and safe human-machine interactions. Hyperelastic models have been used to model the mechanical behaviour of such structures. For instance, rubber structures are frequently modelled using incompressible isotropic hyperelastic laws [1-3].

The necessity for effectively modelling the non-linear mechanical behaviour of hyperelastic structures can be clearly seen when the applications of such structures are evaluated. Hyperelastic structures are used in various sectors and applications; some of the most well-known applications of hyperelastic structures are energy harvesting systems, biological tissue modelling, prostheses and implants, soft and industrial robots, the packaging industry, belt operating systems, the sport and footwear industry, the automotive industry, surgical and medical supplies, toy and game manufacturing, wearable and smart technologies, the coating and covering industry, vibration and shock absorbers, and the construction industry (Figure 1.1).

Vibration-based hyperelastic energy harvesting is a novel topic in the energy harvesting industry, which can be used for supplying energy for wireless sensor networks [4]. Hyperelastic structures are used in this industry for different purposes, such as tuning the resonant frequency of the harvester with the ambient vibration frequencies of the environment [4]. They have also recently been used as dielectric elastomer energy harvesters, providing lower stiffness and higher dielectric permittivity [5].

Human body organs show a rich hyperelastic and viscoelastic behaviour, for which, depending on the biological tissue, the behaviour can be different [6-8]. The proper modelling of biological tissues has helped scientists with surgery simulations, medical diagnoses and health care [9-11]. Furthermore, knowing the mechanical properties and hyperelastic behaviour of human body organs has improved the design of prostheses and implants [12-15].

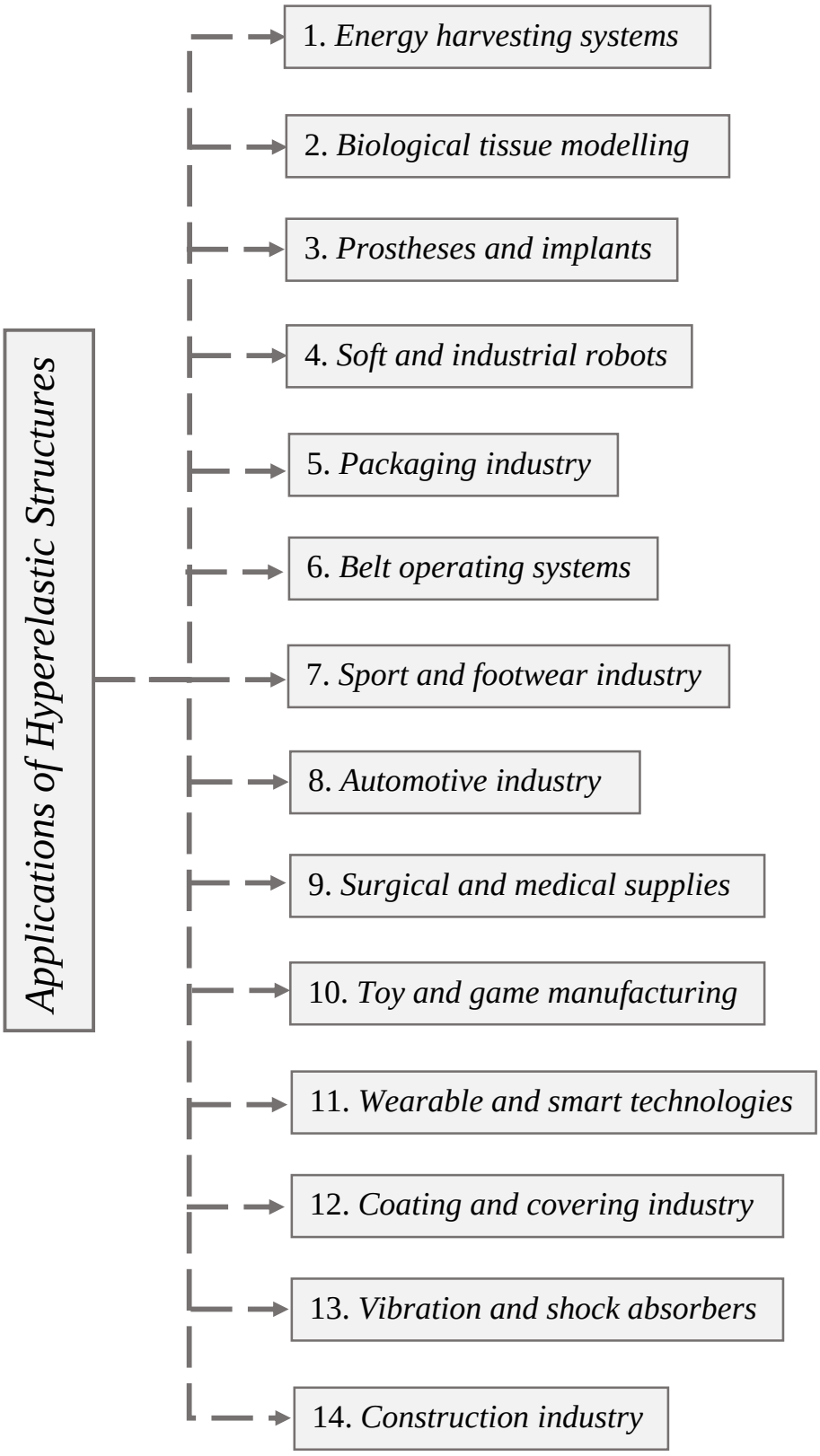

Figure 1.1: Some applications of hyperelastic structures.

Using hyperelastic structures in devices provides infinite degrees of freedom, which is highly beneficial in many applications, such as invasive surgeries in which accessing the target requires a smooth motion in different parts [16-18]. In addition, hyperelastic structures are used in many soft robots for different purposes to provide a significant smooth motion [19-21]. For instance, the infinite degree of freedom provides comfort and strength to patients with muscular dystrophy during physical activities [22, 23].

Since hyperelastic structures are significantly softer than solid structures, they have been used to provide safe physical interactions with humans, used for technologies such as industrial robots, automobiles and toys [24-26]. Another good use of the soft behaviour of hyperelastic structures can be found in sportswear and wearable devices for sensing temperature, glucose, pressure, gas, pulse rate, hydration, and motion [27-29].

Finally, hyperelastic structures provide good resistance against different types of sudden loads and vibrations. This important capability makes these structures great candidates for many diverse applications, such as in food packaging [30-33], coating [34, 35], and vibration/shock absorbers [36-38].

1.2 Aims and objectives

By evaluating the range of applications (above), it can be seen that hyperelastic structures are an important part of human life. To be able to use hyperelastic structures efficiently in different industries, it is important to first have a comprehensive understanding of their mechanical behaviour.

The main aim of this thesis is to develop accurate models of different isotropic incompressible hyperelastic structures in different mechanical conditions. The developed models and analyses create a detailed state of the art study of the nonlinear dynamics and mechanics of hyperelastic structures (including beams, plates and shells). The results in this thesis are applicable to many applications of hyperelastic structures. The listed objectives of this thesis are:

1. To investigate the linear and nonlinear dynamics of axially-travelling incompressible isotropic hyperelastic belts.

2. To understand the influence of porosity on the nonlinear dynamics of hyperelastic structures.

3. To analyse the effect of layering and material sorting on the nonlinear mechanics and dynamics of hyperelastic structures.

4. To combine the effects of viscoelasticity and hyperelasticity on modelling the non- linear dynamics and internal resonance behaviour of soft arches that are slightly curved.

5. To comprehend the mass-sensing behaviour and the internal resonance behaviour of hyperelastic plate structures.

6. To build an understanding of the influence of curvature on the mechanics and dynamics of various hyperelastic curved shell structures.

1.3 Thesis outline

Apart from Chapters 1 and 9, this thesis is organised using already-published/accepted papers in high-quality prestigious journals, along with some that are currently under review. The first chapter presents a brief overview of hyperelastic structures, their applications, and the importance of (and motivation for) studying their mechanical behaviour.

A comprehensive, detailed review of the applications of hyperelasticity in modelling the mechanics and dynamics of hyperelastic structures, focusing on the bending, buck- ling and vibration behaviour of such structures as biological tissues and polymeric structures, is presented in Chapter 2. Chapters 3-8 present critical reviews of the discussed cases, emphasising their significance and novelty for numerous well-known applications.

A continuum-mechanics-based model of axially-travelling hyperelastic belts is presented in Chapter 3, followed by a comprehensive linear and nonlinear analysis of the importance of modelling the large deformations and strains in dynamic conditions accurately.

Chapter 4 presents a modified strain energy model for considering the effect of porosity on the nonlinear stress-strain behaviour of hyperelastic structures, followed by a general model of the nonlinear dynamics of hyperelastic porous beam structures. A detailed analysis of the effect of the presence of voids and porosity on the mechanical behaviour of the structure is also presented in this chapter.

Sandwiched hyperelastic structures made of different hyperelastic materials are analysed in Chapter 5 using different shear modelling approaches, followed by a detailed discussion of the effects of layering and material sorting.

A combination of viscoelasticity and hyperelasticity in modelling visco-hyperelastic structures is employed in Chapter 6 for soft structures, followed by an analysis of the internal resonance behaviour of hyperelastic structures with and without viscoelastic effects.

Mass-sensing analysis in hyperelastic plate structures is presented in Chapter 7 in the framework of nonlinear forced vibrations. The internal resonance phenomena due to geometric aspect ratio and attached mass are also analysed.

The nonlinear statics and dynamics of various curved hyperelastic shell structures including cylindrical, hyperbolic, and parabolic shells are investigated in Chapter 8, followed by internal resonance analysis due to the curvature term in the structure.

Chapter 9 presents a conclusion of the findings of the thesis, followed by potential future work.

1.4 List of publications included as part of the thesis

1. Khaniki, H.B., Ghayesh, M.H., Chin, R. & Amabili, M., (2023). Hyperelastic structures: a review on the mechanics and biomechanics. International Journal of Nonlinear Mechanics, 148, 104275.

   DOI: 10.1016/j.ijnonlinmec.2022.104275

2. Khaniki, H.B., Ghayesh, M.H., Chin, R. & Amabili, M., (2022). A review on the nonlinear dynamics of hyperelastic structures. Nonlinear Dynamics, 110, 963–994.

   DOI: 10.1007/s11071-022-07700-3

3. Khaniki, H. B., Ghayesh, M. H., Chin, R., & Chen, L. Q. (2022). Experimental characteristics and coupled nonlinear forced vibrations of axially travelling hyperelastic beams. Thin-Walled Structures, 170, 108526.

   DOI: 10.1016/j.tws.2021.108526

4. Khaniki, H. B., Ghayesh, M. H., Chin, R., & Amabili, M. (2021). Large amplitude vibrations of imperfect porous-hyperelastic beams via a modified strain energy. Journal of Sound and Vibration, 513, 116416.

   DOI: 10.1016/j.jsv.2021.116416

5. Khaniki, H. B., Ghayesh, M. H., Chin, R., & Hussain, S. (2022). Nonlinear continuum mechanics of thick hyperelastic sandwich beams using various shear deformable beam theories. Continuum Mechanics and Thermodynamics, 34(3), 781-827.

   DOI: 10.1007/s00161-022-01090-y

6. Khaniki, H. B., Ghayesh, M. H., Chin, R., & Hussain, S. (2022). Internal resonance and bending analysis of thick visco-hyper-elastic arches. Continuum Mechanics and Thermodynamics, 1-44.

   DOI: 10.1007/s00161-022-01166-9

7. Khaniki, H. B., Ghayesh, M. H., & Chin, R. (2023). Theory and experiment for dynamics of hyperelastic plates with modal interactions. International Journal of Engineering Science, 182, 103769.

   DOI: 10.1016/j.ijengsci.2022.103769

8. Khaniki, H. B., & Ghayesh, M. H. (2023). Highly nonlinear hyperelastic shells: Statics and dynamics. International Journal of Engineering Science, 183, 103794.

   DOI: 10.1016/j.ijengsci.2022.103794

1.5 Additional publications relevant to the thesis but not forming part of it

1. Khaniki, H. B., Ghayesh, M. H., & Chin, R. (2021, January). Effects of non-uniform cross-section and stiffness on the nonlinear vibration behaviour of soft robotic arms. In ACAM10: 10th Australasian Congress on Applied Mechanics: 10th Australasian Congress on Applied Mechanics (pp. 355-367). Engineers Australia.

2. Khaniki, H. B., Ghayesh, M. H., Chin, R., & Amabili, M. (2022, August). Nonlinear forced oscillation of hyperelastic beams with multiple intermediate mass-spring supports. The First International Conference on Mechanical System Dynamics (1st ICMSD) - Abstract.

References

[1] M. Amabili, Nonlinear mechanics of shells and plates in composite, soft and biological materials, Cambridge University Press, 2018.
[2] A. Muhr, Modeling the stress-strain behavior of rubber, Rubber chemistry and technology, 78 (2005) 391-425.
[3] M. Mansouri, H. Darijani, Constitutive modeling of isotropic hyperelastic materials in an exponential framework using a self-contained approach, International Journal of Solids and Structures, 51 (2014) 4316-4326.
[4] L. Dong, M.D. Grissom, M. Prasad, F.T. Fisher, Application of mechanical stretch to tune the resonance frequency of hyperelastic membrane-based energy harvesters, Sensors and Actuators A: Physical, 252 (2016) 165-173.
[5] G. Boccalero, C. Jean-Mistral, M. Castellano, C. Boragno, Soft, hyper-elastic and highly-stable silicone-organo-clay dielectric elastomer for energy harvesting and actuation applications, Composites Part B: Engineering, 146 (2018) 13-19.
[6] G.A. Holzapfel, R.W. Ogden, S. Sherifova, On fibre dispersion modelling of soft biological tissues: a review, Proceedings of the Royal Society A, 475 (2019) 20180736.
[7] C. Wex, S. Arndt, A. Stoll, C. Bruns, Y. Kupriyanova, Isotropic incompressible hyperelastic models for modelling the mechanical behaviour of biological tissues: a review, Biomedical Engineering/Biomedizinische Technik, 60 (2015) 577-592.
[8] G. Chagnon, M. Rebouah, D. Favier, Hyperelastic energy densities for soft biological tissues: a review, Journal of Elasticity, 120 (2015) 129-160.
[9] S. Marchesseau, T. Heimann, S. Chatelin, R. Willinger, H. Delingette, Fast porous visco-hyperelastic soft tissue model for surgery simulation: application to liver surgery, Progress in biophysics and molecular biology, 103 (2010) 185-196.
[10] R.J. Lapeer, P.D. Gasson, V. Karri, A hyperelastic finite-element model of human skin for interactive real-time surgical simulation, IEEE Transactions on Biomedical Engineering, 58 (2010) 1013-1022.
[11] V. Alastrué, B. Calvo, E. Pena, M. Doblaré, Biomechanical modeling of refractive corneal surgery, (2006).
[12] M. Pawlikowski, K. Skalski, T. Sowiński, Hyper-elastic modelling of intervertebral disc polyurethane implant, Acta of Bioengineering and Biomechanics, 15 (2013)

43–50.
[13] G. Kraaij, A.A. Zadpoor, G.J. Tuijthof, J. Dankelman, R.G. Nelissen, E.R. Valstar, Mechanical properties of human bone–implant interface tissue in aseptically loose hip implants, Journal of the mechanical behavior of biomedical materials, 38 (2014) 59-68.
[14] J. Chen, R. Ahmad, H. Suenaga, W. Li, M. Swain, Q. Li, A comparative study on complete and implant retained denture treatments–a biomechanics perspective, Journal of biomechanics, 48 (2015) 512-519.
[15] E. Biddis, E. Bogoch, S. Meguid, Three-dimensional finite element analysis of prosthetic finger joint implants, International Journal of Mechanics and Materials in Design, 1 (2004) 317-328.
[16] A. Diodato, M. Brancadoro, G. De Rossi, H. Abidi, D. Dall'Alba, R. Muradore, G. Ciuti, P. Fiorini, A. Menciassi, M. Cianchetti, Soft robotic manipulator for improving dexterity in minimally invasive surgery, Surgical innovation, 25 (2018) 69-76.
[17] G. Rateni, M. Cianchetti, G. Ciuti, A. Menciassi, C. Laschi, Design and development of a soft robotic gripper for manipulation in minimally invasive surgery: a proof of concept, Meccanica, 50 (2015) 2855-2863.
[18] M. Runciman, A. Darzi, G.P. Mylonas, Soft robotics in minimally invasive surgery, Soft robotics, 6 (2019) 423-443.
[19] C. Lee, M. Kim, Y.J. Kim, N. Hong, S. Ryu, H.J. Kim, S. Kim, Soft robot review, International Journal of Control, Automation and Systems, 15 (2017) 3-15.
[20] N. Elango, A.A.M. Faudzi, A review article: investigations on soft materials for soft robot manipulations, The International Journal of Advanced Manufacturing Technology, 80 (2015) 1027-1037.
[21] M. Calisti, G. Picardi, C. Laschi, Fundamentals of soft robot locomotion, Journal of The Royal Society Interface, 14 (2017) 20170101.
[22] H.K. Yap, P.M. Khin, T.H. Koh, Y. Sun, X. Liang, J.H. Lim, C.-H. Yeow, A fully fabric-based bidirectional soft robotic glove for assistance and rehabilitation of hand impaired patients, IEEE Robotics and Automation Letters, 2 (2017) 1383-1390.
[23] P. Polygerinos, K.C. Galloway, E. Savage, M. Herman, K. O'Donnell, C.J. Walsh, Soft robotic glove for hand rehabilitation and task specific training, in: 2015 IEEE international conference on robotics and automation (ICRA), IEEE, 2015, pp. 2913-2919.
[24] D. Rus, M.T. Tolley, Design, fabrication and control of soft robots, Nature, 521 (2015) 467-475.
[25] R.E. Khayat, A. Derdouri, Stretch and inflation of hyperelastic membranes as applied to blow moldiing, Polymer Engineering & Science, 35 (1995) 1852-1863.
[26] G. Tamadapu, N.N. Dhavale, A. DasGupta, Geometrical feature of the scaling behavior of the limit-point pressure of inflated hyperelastic membranes, Physical Review E, 88 (2013) 053201.
[27] L. Zhang, K. Chen, S. Wang, S. Chen, S. Niu, Z. Wang, P. Du, Synthesis of percolative hyperelastic conducting composite and demonstrations of application in wearable strain sensors, Materials Letters, 233 (2018) 306-309.
[28] R. Kumar, J. Shin, L. Yin, J.M. You, Y.S. Meng, J. Wang, All-printed, stretchable Zn-Ag2O rechargeable battery via hyperelastic binder for self-powering wearable electronics, Advanced Energy Materials, 7 (2017) 1602096.

[29] M.F. Arif, S. Kumar, T.K. Gupta, K.M. Varadarajan, Strong linear-piezoresistive-response of carbon nanostructures reinforced hyperelastic polymer nanocomposites, Composites Part A: Applied Science and Manufacturing, 113 (2018) 141-149.
[30] A. Athanassiou, Sustainable Food Packaging Technology, John Wiley & Sons, 2020.
[31] A. Lopez-Rubio, E. Almenar, P. Hernandez-Muñoz, J.M. Lagarón, R. Catalá, R. Gavara, Overview of active polymer-based packaging technologies for food applications, Food Reviews International, 20 (2004) 357-387.
[32] I. Majid, G.A. Nayik, S.M. Dar, V. Nanda, Novel food packaging technologies: Innovations and future prospective, Journal of the Saudi Society of Agricultural Sciences, 17 (2018) 454-462.
[33] R. Coles, D. McDowell, M.J. Kirwan, Food packaging technology, CRC press, 2003.
[34] H.Q. Zhu, X.D. Zhang, Calculation of Static Stiffness of Hyperelastic Coating, in: Applied Mechanics and Materials, Trans Tech Publ, 2013, pp. 810-813.
[35] K. Jiang, M. Tao, L.-S. Huang, K.-P. Wang, A Research of Resistance of Hyper-Elastic Coating Structure Based on Impedance Mismatch, in: Mechanics and Materials Science: Proceedings of the 2016 International Conference on Mechanics and Materials Science (MMS2016), World Scientific, 2018, pp. 1108-1116.
[36] D. Giagopoulos, A. Arailopoulos, I. Chatziparasidis, Optimal Modeling of an Elevator Chassis under Crash Scenario Based on Characterization and Validation of the Hyperelastic Material of Its Shock Absorber System, Applied Mechanics, 3 (2022) 227-243.
[37] Y. Qiao, J. Zhang, M. Zhang, L. Liu, P. Zhai, A magneto-hyperelastic model for silicone rubber-based isotropic magnetorheological elastomer under quasi-static compressive loading, Polymers, 12 (2020) 2435.
[38] D. Giagopoulos, A. Arailopoulos, I. Chatziparasidis, Characterization and Validation of Shock Absorbing Hyperelastic Material Using Analytical and Experimental Methods, Proceedings of the 14th International Conference on Vibration Problems, Springer, 2021, pp. 115-125.

Chapter 2

Literature Review

This chapter is based on the following published review articles to represent a comprehensive state-of-the-art review on both statics and dynamics of hyperelastic structures:

• Khaniki, H.B., Ghayesh, M.H., Chin, R. & Amabili, M., (2023). Hyperelastic structures: a review on the mechanics and biomechanics. International Journal of Nonlinear Mechanics, 148, 104275. DOI: 10.1016/j.ijnonlinmec.2022.104275

• Khaniki, H.B., Ghayesh, M.H., Chin, R. & Amabili, M., (2022). A review on the nonlinear dynamics of hyperelastic structures. Nonlinear Dynamics, 110, 963–994. DOI: 10.1007/s11071-022-07700-3.

2.1 Hyperelastic structures: a review on the mechanics and biomechanics

Overview

This section of Chapter 2 introduces the statics of soft structures, focusing on their hyperelastic behaviour in a detailed analysis. Previous studies on soft structures are classified into two main types: soft biological tissues and polymeric structures. The application of hyperelastic strain energy density laws for appropriately modelling body organs is presented, and the strength of each model for the biological tissue type is discussed. Furthermore, the static behaviour of polymeric structures is presented in three subsections, based on the structure type. This literature review is published and available online as: Khaniki, H.B., Ghayesh, M.H., Chin, R. & Amabili, M., (2023). Hyperelastic structures: a review on the mechanics and biomechanics. International Journal of Nonlinear Mechanics, 148, 104275.

Statement of Authorship

Title of Paper	Hyperelastic structures: a review on the mechanics and biomechanics
Publication Status	☑ Published ☐ Accepted for Publication ☐ Submitted for Publication ☐ Unpublished and Unsubmitted w ork w ritten in manuscript style
Publication Details	Khaniki, H. B., Ghayesh, M. H., Chin, R., & Amabili, M. (2023). "Hyperelastic structures: a review on the mechanics and biomechanics". International Journal of Non-Linear Mechanics, 148, 104275.

Principal Author

Name of Principal Author (Candidate)	Hossein Bakhshi Khaniki		
Contribution to the Paper	I carried out the literature search and wrote the manuscript.		
Overall percentage (%)	80%		
Certification:	This paper reports on original research I conducted during the period of my Higher Degree by Research candidature and is not subject to any obligations or contractual agreements with a third party that would constrain its inclusion in this thesis. I am the primary author of this paper.		
Signature		Date	2/11/2022

Co-Author Contributions

By signing the Statement of Authorship, each author certifies that:

i. the candidate's stated contribution to the publication is accurate (as detailed above);

ii. permission is granted for the candidate in include the publication in the thesis; and

iii. the sum of all co-author contributions is equal to 100% less the candidate's stated contribution.

Name of Co-Author	Mergen Ghayesh		
Contribution to the Paper	As the principal supervisor, I helped to construct the manuscript, edit and review the manuscript for submission. I hereby give consent to Hossein Bakhshi Khaniki to present this paper for examination towards the degree of Doctor of Philosophy.		
Signature		Date	3/11/2022

Name of Co-Author	Rey Chin		
Contribution to the Paper	I assisted in the revision and editing of the manuscript. I hereby give consent to Hossein Bakhshi Khaniki to present this paper for examination towards the degree of Doctor of Philosophy.		
Signature		Date	3/11/2022

Name of Co-Author	Marco Amabili			
Contribution to the Paper	I assisted in the construction of the manuscript. I also edited and reviewed the manuscript. I hereby give consent to Hossein Bakhshi Khaniki to present this paper for examination towards the degree of Doctor of Philosophy.			
Signature			Date	7/11/2022

International Journal of Non-Linear Mechanics 148 (2023) 104275

Contents lists available at ScienceDirect

International Journal of Non-Linear Mechanics

journal homepage: www.elsevier.com/locate/nlm

Review

Hyperelastic structures: A review on the mechanics and biomechanics

Hossein B. Khaniki [a,*], Mergen H. Ghayesh [a,*], Rey Chin [a], Marco Amabili [b]

[a] School of Mechanical Engineering, University of Adelaide, South Australia 5005, Australia
[b] Department of Mechanical Engineering, McGill University, 817 Sherbrooke Street West, Montreal H3A 0C3, Canada

ARTICLE INFO

Keywords:
Hyperelastic structures
Mechanics
Biomechanics
Biological tissues
Nonlinear elasticity
Soft robots

ABSTRACT

Soft structures are capable of undergoing reversible large strains and deformations when facing different types of loadings. Due to the limitations of linear elastic models, researchers have developed and employed different nonlinear elastic models capable of accurately modelling large deformations and strains. These models are significantly different in formulation and application. As hyperelastic strain energy density models provide researchers with a good fit for the mechanical behaviour of biological tissues, research studies on using these constitutive models together with different continuum-mechanics-based formulations have reached notable outcomes. With the improvements in biomechanical devices, in-vivo and in-vitro studies have increased significantly in the past few years which emphasises the importance of reviewing the latest works in this field. Besides, since soft structures are used for different mechanical and biomechanical applications such as prosthetics, soft robots, packaging, and wearing devices, the application of a proper hyperelastic strain energy density law in modelling the structure is of high importance. Therefore, in this review, a detailed classified analysis of the mechanics of hyperelastic structures is presented by focusing on the application of different hyperelastic strain energy density models. Previous studies on biological soft parts of the body (brain, artery, cartilage, liver, skeletal muscle, ligament, skin, tongue, heel pad and adipose tissue) are presented in detail and the hyperelastic strain energy models used for each biological tissue is discussed. Besides, the mechanics (deformation, buckling, inflation, etc.) of polymeric structures in different mechanical conditions is presented using previous studies in this field and the strength of hyperelastic strain energy density models in analysing their mechanics is presented.

Contents

* Corresponding authors.
E-mail addresses: hossein.bakhshikhaniki@adelaide.edu (H.B. Khaniki), mergen.ghayesh@adelaide.edu.au (M.H. Ghayesh), rey.chin@adelaide.edu.au (R. Chin), marco.amabili@mcgill.ca (M. Amabili).

https://doi.org/10.1016/j.ijnonlinmec.2022.104275
Received 22 September 2022; Accepted 11 October 2022
Available online 20 October 2022

1. Introduction

Linear elastic assumptions have many limits for modellings of the mechanics of different structures including having a linear elastic constitutive equation valid for small strains. However, in real-world applications, structures might face loadings which lead to large strains where the linear elastic constitutive assumptions become invalid. Besides, in some structures (such as biological tissues), the linear region of the constitutive model is significantly small showing a nonlinear elastic behaviour.

Accordingly, there have been many hyperelastic strain energy density models developed by researchers to accurately take into account the nonlinear elasticity and large strain deformations [1]. Some of the well-known and conventional hyperelastic strain energy density models are named neo-Hookean, Mooney–Rivlin, Ogden, Polynomial, Arruda–Boyce, Yeoh, and Gent. These hyperelastic models have been discussed in detail in a previous review paper on the nonlinear dynamics of soft structures [2]. Hyperelastic strain energy density models for analysing anisotropic materials were also studied and discussed in a review paper presented by Chagnon et al. [3] as well as in books [4,5]. These constitutive models are used by many researchers to understand the mechanics and biomechanics of different structures which have been discussed in this review paper.

Hyperelastic strain energy density models have been employed by researchers for modelling the mechanical behaviour of different biological tissues. Accurately modelling the mechanics of biological tissues have many advantages and helps scientists in different biomedical applications. For instance, hyperelastic models of white and grey matter in the brain have directly helped in brain surgery [6], trauma analysis [7] and injury simulation [8]. A proper hyperelastic model of breast tissues has made a significant help in breast cancer diagnosis and differentiating healthy and unhealthy breast tissues [9–11].

Another important topic of hyperelastic modelling in the biomechanics of biological tissues is predicting plaque rupture in human arteries which has been analysed lately by many researchers [12–14]. Besides, to have a proper understanding of osteoarthritis, researchers have examined the load–displacement behaviour of both healthy and osteoarthritic articular cartilages [15]. Acetabular dysplasia or hip dysplasia have also been modelled by hyperelastic strain energy density models to appropriately understand the biomechanics of healthy and unhealthy acetabulum [16]. The mentioned studies are only a few examples of how important is to develop an accurate hyperelastic model of biological tissues for different applications.

Moreover, since soft structures are more likely to undergo large strains in different mechanical conditions, the linear stress–strain region model is not accurate for modelling the behaviour in larger strains and deformations. To overcome this limit, hyperelastic strain energy models have also been used for modelling the mechanics of soft structures. Soft structures have been used widely in different applications in which most of the applications are achieving more attention in the last few years.

Hyperelasticity definition in mechanics of structure has an important application in prostheses and artificial substitutes for various human tissues. Accurately modelling the mechanics of human tissues and finding an appropriate artificial substitute with the same mechanical behaviour has a significant effect in designing conventional prostheses with the best fit to the behaviour of the real tissue. This importance has been examined by many researchers for different artificial substitutes including lower-limb prosthetics [17], aortic heart valve prosthesis [18], lumbar intervertebral disc prosthesis [19], vascular prosthesis [20–22], and prosthetic finger joint implants [23].

Bio-inspired soft robots are a class of robots which show a nonlinear elastic behaviour in their performance due to large strains in their motions. These structures have been used widely in different industrial sectors. Some of the well-known developed bio-inspired soft robots are octopus-like robots (Octobots) [24–27], inchworm and caterpillar soft robots [28–32], gecko-inspired robots [33–35] and batoid-fish-shaped robots [36–38] which are used for grasping, crawling, lifting and locomotion purposes (Fig. 1).

Since soft robots provide infinite degrees of freedom with a continuous smooth motion due to their hyperelastic behaviour, they have been used in biomedical applications such as wearable robots, drug delivery and surgical tools. For instance, elastomer-based structures have been used in minimally invasive cardiac surgeries [39–42], endoscopy [43,44], optical biopsy [45], catheterization [46] and drug delivery [47] providing a smooth motion with the least damage to the surrounding tissues. Detailed analysis of the application of soft structures in minimally invasive surgeries can be found in Ref. [48].

Besides, wearable robots have been improved by using hyperelastic materials to obtain a conventional motion in their mechanical behaviour for different purposes. Stroke patients with gait impairment can use soft wearable robots for at-home rehabilitation and physical therapy [49,50]. Patients suffering from muscular dystrophy can use wearable soft gloves for exercising and grasping assistance [51] and soft exosuits for motion assistance on arms [52], ankles [53] and other parts of the human body [54]. Detailed analysis on the application of wearable soft robots in human assistance can be found in Ref. [54]. Fig. 2 presents some key applications of biomedical soft robots made of hyperelastic materials [51,55–59].

There have been many comprehensive, valuable review studies on the applications of nonlinear-elastic structures for soft robotics and biomedical applications [57,61–77] which have been listed in Table 1, based on the study type. It can be seen that the topic has attracted significant attention in the last few years. Despite many analyses on the mechanics and biomechanics of hyperelastic structures, a comprehensive review of the application of hyperelastic strain energy density models for studying such structures is missing. Therefore, this study mainly focuses on employing different hyperelastic strain energy density models for appropriately modelling biological tissues and polymeric structures following research studies up to 2022. Previous studies on the mechanics and biomechanics of hyperelastic structures are presented in this review by dividing the studies based on the biological tissues and structures. In Section 2, the application of hyperelastic continuum models to the biomechanics of the body tissues and the capability of the theoretical models in simulating their behaviour are discussed. A comprehensive case study is provided by considering the tissue types; included are brain, artery, cartilage, liver, skeletal muscle, ligament, skin, tongue, heel pad and adipose tissue analyses. The mechanics of hyperelastic structures is discussed in Section 3 for different types of structures. The strength of different hyperelastic constitutive models in properly modelling the static behaviour of hyperelastic structures in different mechanical conditions is investigated using the previous works in this field. Lastly, a detailed analysis and discussion on the current state of the research and outcomes of research works in this field are presented in Section 4.

2. Hyperelasticity of biological tissues

Different biological tissues, such as skin, muscle, and fat, often undergo large deformations and strains while subject to different types

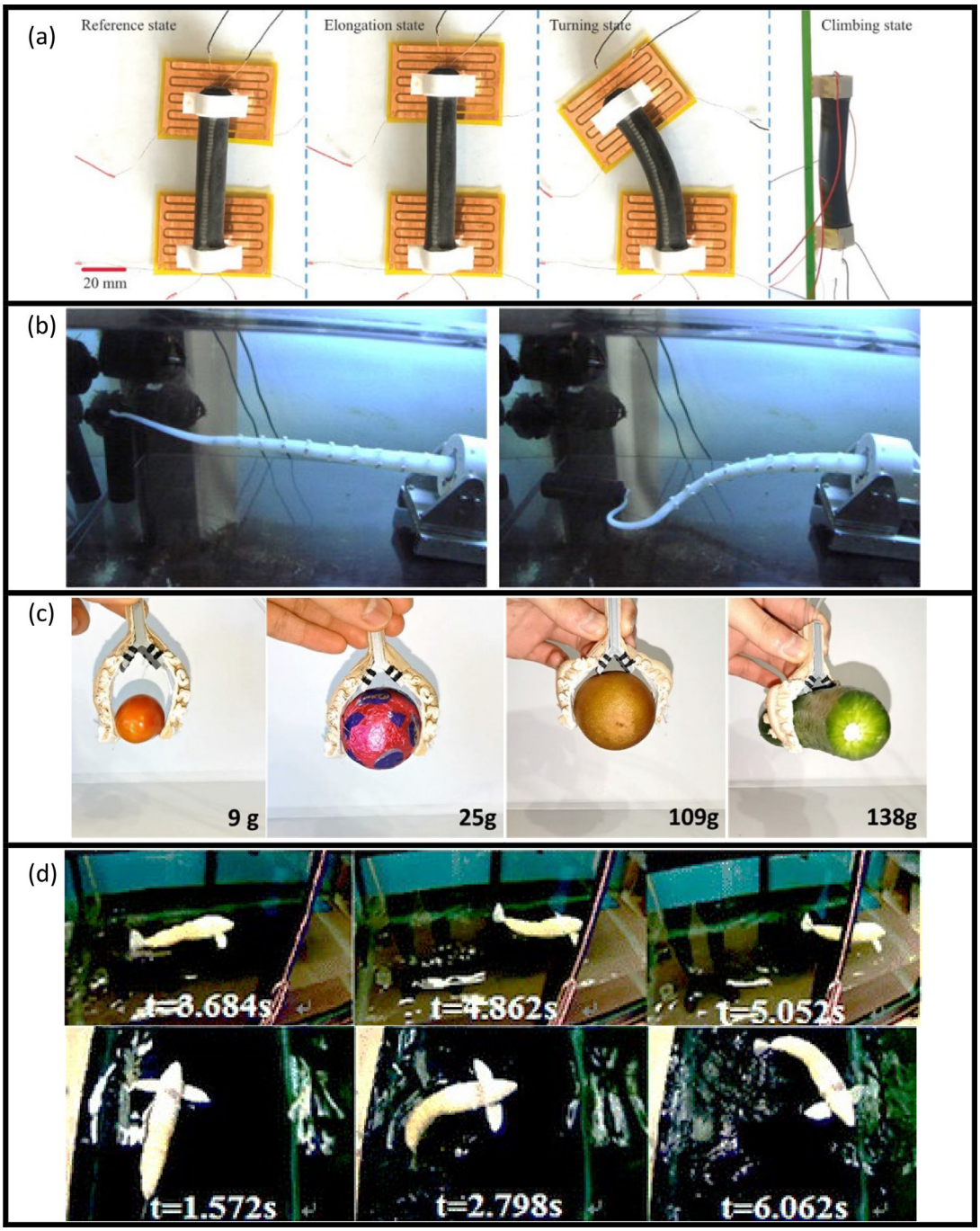

Fig. 1. Some bio-inspired soft robots made of hyperelastic materials: (a) inchworm-inspired robot [28] (Permission obtained from Elsevier), (b) octopus-inspired robot [24] (Permission obtained from Elsevier), (c) gecko-inspired adhesive robot [33] (Permission obtained from Elsevier), and (d) fish-inspired robot [38] (Permission obtained from Springer Nature).

of loadings with a nonlinear stress–strain behaviour, which classifies them as hyperelastic structures. Researchers have employed different hyperelastic constitutive laws to model the mechanical responses of such structures. In this section, the mechanical analysis is divided according to the type of the biological tissue. It is noteworthy that for modelling and analysing biological tissues, viscoelasticity plays an important role as well that must be considered along with hyperelasticity; for more details, interested readers are referred to [4,78–81]. Besides, a detailed study on the nonlinear mechanics of biological materials can be found in Ref. [5].

2.1. Hyperelastic models of the brain tissue

Human brain, as the most important part of the body, has been investigated by researchers over the past years, focusing on its mechanical behaviour under loads. Lately, the importance of having a proper model of the brain for surgery [6], trauma analysis [7] and injury simulation [8] have been emphasised. To have a better understanding of the mechanical behaviour of the brain, Moran et al. [7] experimentally tested different regions of the brain (white matter, grey matter, and corona radiata) under tension, shear and compression forces, and used

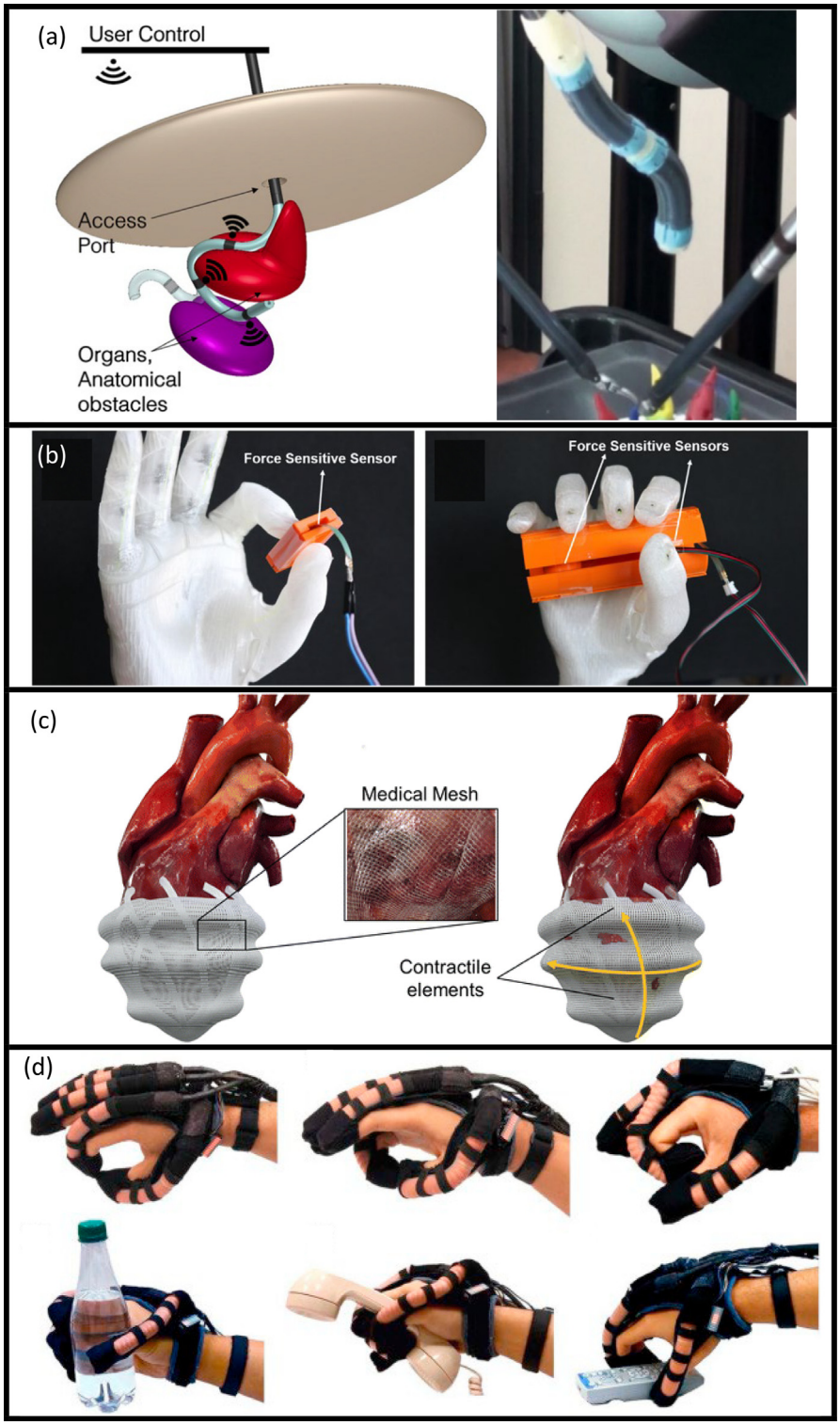

Fig. 2. Some key applications of biomedical soft robots made of hyperelastic materials: (a) minimally invasive surgery application [55,56] (Permission obtained from Springer Nature) (This article is an open access article distributed under the terms and conditions of the Creative Commons Attribution (CC BY) license (https://creativecommons.org/licenses/by/4.0/)), (b) prosthetic application [58] (Permission obtained from PLOS), (c) sleeve supports for heart function [60] (Permission obtained from Springer Nature), and (d) wearable soft robots for rehabilitation [51] (Permission obtained from Elsevier).

the hyperelastic models to compare with the experimental observations. Hyperfoam [82], Ogden [83] and polynomial [84] models were used and the optimised coefficients for each model were presented.

Concentrating on brain elastography, Kaster et al. [6] studied the mechanical characteristics of white and grey matter in brain tissue to differentiate them based on their mechanical properties. Ogden, Polynomial, Yeoh and Arruda–Boyce hyperelasticity strain energy models were examined and the coefficients for each hyperelastic model, for both white and grey matter were presented. It was concluded that the most suitable method for modelling the hyperelastic behaviour of such structures is the Yeoh model. Fig. 3 demonstrates the stress–strain behaviour of different parts of the brain under compression loadings,

Table 1
Review studies on the soft robotic and biomedical applications of hyperelastic structures.

Study	Year	Main application	Reviewed topics
Ng et al. [61]	2021	Motions in soft robots	Locomotion in soft robots including terrestrial locomotion, aquatic locomotion, and aerial locomotion are reviewed.
Xiong et al. [62]	2021	Soft robotics	Wearable robots and human–robot interface and interaction are reviewed.
El-Atab et al. [63]	2020	Soft robotics	Actuating systems for different soft robots are reviewed.
Yap et al. [64]	2020	Manufacturing soft robots	Polymer 3D printing techniques and materials used for soft robotic fabrication are reviewed
Ashuri et al. [65]	2020	Biomedical soft robots	Soft robots with biomedical applications such as artificial muscles, muscle alternatives, prosthetic devices, catheters, stents and surgical instruments are reviewed.
Kumar and Syed [66]	2020	Additive manufacturing in biomedical applications	The fabrication of biomedical components using the selective laser sintering technique is reviewed with hyperelastic behaviour.
Majidi [67]	2019	Materials in soft robotics	Various materials used in soft robotics are reviewed including elastomers, polymer composites, fluids and gels.
Victor et al. [68]	2019	PDMS for biomedical applications	The application of polydimethylsiloxane for aneurysm repair and its biocompatibility is reviewed.
Wang et al. [69]	2018	Sensing technologies in soft robotics	Sensing technologies for soft robots are reviewed including resistive and piezoresistive sensors, capacitive sensors, optical sensors, magnetic sensors, and inductive sensors.
Chu and Patterson [70]	2018	Rehabilitative soft robots	Soft robotic devices for hand rehabilitation are reviewed.
Wallin et al. [71]	2018	3D printed soft robots	Polymers in soft robotics and 3D printing technologies for manufacturing soft robots are reviewed.
Cianchetti et al. [57]	2018	Biomedical application of soft robots	Soft robots in surgery, diagnosis and drug delivery, wearable and assistive devices, prostheses, and artificial organs are reviewed.
Lee et al. [72]	2017	Soft robotics	Different applications of soft robots are reviewed including human–machine interface and interaction, locomotion and exploration, manipulation, medical and surgical applications, rehabilitation and wearable robots.
Polygerinos et al. [73]	2017	Human–Robot Interaction	Fluid-driven intrinsically soft devices are reviewed.
Miao et al. [74]	2017	4D printing of hyperelastic materials	4D printing of polymeric materials for biomedical applications including smart drug or cell delivery, microsurgery devices, and in vivo actuation for biosensing
Rus and Tolley [75]	2015	Soft robotics	Design, manufacturing and actuation systems in soft robots are reviewed.
Kim et al. [76]	2013	Bioinspired soft robots	Different bio-inspired soft robot studies are reviewed including worm-like robots, caterpillar-like robots, and octopus-like robots.
Cho et al. [77]	2009	Manufacturingsoft robots	Processes for manufacturing soft robots including shape deposition manufacturing, nano imprint, laser imaging, micro injection moulding, embed moulding, and multi-nozzle deposition systems are reviewed.

up to 50% strain, via hyperfoam, Ogden and polynomial strain energy density modelling [7].

Since most of the studies on brain matters have presented the hyperelastic coefficients based on a single loading mode, Budday et al. [85] examined different hyperelastic models to find a proper model for characterising the mechanical behaviour of brain tissue under different types of loadings. The strain energy was modelled via five different, well-known hyperelasticity models (neo-Hookean [86], Ogden [87,88], Gent [89], Mooney–Rivlin [90,91] and Demiray [92]). It was claimed that the one-term Ogden hyperelasticity model provides an accurate model for brain tissue facing different loading combinations.

After showing the success of the Ogden hyperelastic constitutive law for modelling brain tissues [85], researchers employed this model for analysing the brain's mechanical behaviour. Hauseux et al. [93] quantified the uncertainty of brain tissue via the Holzapfel and Ogden hyperelastic models [94] to follow the mechanical deformation of the brain. Voyiadjis and Samadi-Dooki [95] examined the influence of having nonslip boundary conditions while modelling the human brain. The Ogden strain energy function was utilised in order to model the hyperelastic behaviour of human brain tissue. By comparing with experimental results, it was shown that mechanical behaviour could be accurately modelled with Ogden hyperelasticity under uniaxial loading. Yousefsani et al. [96] used the one-term Ogden model and embedded an element technique when studying the brain's white matter tissue. The results indicated accurate modelling of the axonal responses, with applications in tumour growth analysis. Labus and Puttlitz [97] studied the mechanical behaviour of the brain's white matter facing biaxial tensile loading. A modified anisotropic model of Ogden strain energy, presented by Velardi et al. [98], was employed to model the hyperelasticity deformation response. It was shown that having both biaxial and uniaxial loading test models could improve the structural model. Fig. 4 shows the preparation of the brain samples and the experimental setup. Budday et al. [99] made the first attempt to identify the relation between the mechanics and microstructure of human brain tissue by presenting a microstructurally developed constitutive model. It was shown that the cell count has a negative effect on stiffness while myelin

content has a positive effect. A detailed review on modelling and testing human brain tissue, its challenges and important characteristics were presented by Budday et al. [100].

2.2. Hyperelastic models of the artery tissue

Another important use of hyperelastic constitutive laws is in modelling the biomechanics of arterial layers. The importance and application of proper models of the arteries for different purposes can be found in the review studies [101–104].

Since arteries consist of three different layers, intima, media and adventitia, Holzapfel et al. [104] presented a new orthotropic constitutive model for specifically analysing arterial wall mechanics. The model requires a total of six material parameters (three for each mechanically relevant layer) for properly modelling the axial extension, torsion and inflation. It was shown that this model is capable to fit the experimental data and takes into account the arterial microstructure. The nonlinear stress–stretch behaviour of the layers of arteries (intima, adventitia, and media) have been obtained by Holzapfel et al. [105], for both circumferential and axial directions.

The fibre dispersion and orientation in arterial layers are key elements in defining the nonlinear behaviour of human arteries. Gasser et al. [106] presented a detailed comprehensive study on the proper modelling of arterial layers in the framework of hyperelastic continuum modelling. By using a modified neo-Hookean strain energy density model with an exponential term to describe the response of collagen fibres, both axial and circular stretches of the thin-walled tube model were obtained and discussed. This study introduced the orientation dispersion of collagen fibres; however, the dispersion was rotationally symmetric. Accordingly, the model was extended into a double dispersion model for representing different in-plane and out-of-plane dispersion of fibre orientation in arteries (nonsymmetric dispersion) by Holzapfel et al. [107] using bivariate von Mises distribution. It was shown that the model was capable of fitting uniaxial testing results of collagen-reinforced arteries with high accuracy. Since arterial layers have a significant collagen fibre dispersion in in-plane directions, the nonsymmetric model shows better accuracy in modelling human arteries. A more detailed discussion on the collagen-fibres dispersion in arteries and other soft biological tissues can be found in a review paper presented by Holzapfel et al. [103].

In studying the nonlinear mechanics of soft fibrous tissues, a possible source of inaccuracy and computational cost is in properly modelling the contribution of compressed fibres in the total strain energy density. To overcome this, Li et al. [108] presented a discrete fibre dispersion model to exclude the fibres under compression loadings from the modelling of soft fibrous solids. In their modelling, they discretised the unit into a finite number of elementary areas. For each element, the fibre density and direction were defined and summed up over all the elements. The fibre strain energy model was presented and used for shear, tension and non-homogeneous uniaxial extension problems showing good accuracy. Breslavsky et al. [109] presented the first model of the compressed collagen fibres exclusion using the double-dispersion model. A novel technique of versatile fibre exclusion to the constitutive model was presented by having different fibre dispersion in both in-plane and out-of-plane. A significant reduction in the computational cost was seen by having in-plane fibre exclusion for modelling the uniaxial tensile test. Besides, it was shown that depending on the fibre orientation and distribution, the thickness of the strips in the uniaxial tensile test might increase.

Sassani et al. [110] experimentally examined the material characteristics of abdominal aortic aneurysms' layers. Fifteen patients were tested and different microstructure-motivated models were used to fit the experimental testings. It was shown that the four-fibre family model presented in Ref. [111] has the most accuracy in modelling the mechanical behaviour of the samples. Besides, it was shown that the collagen arrangement is mainly in the axial direction giving a higher

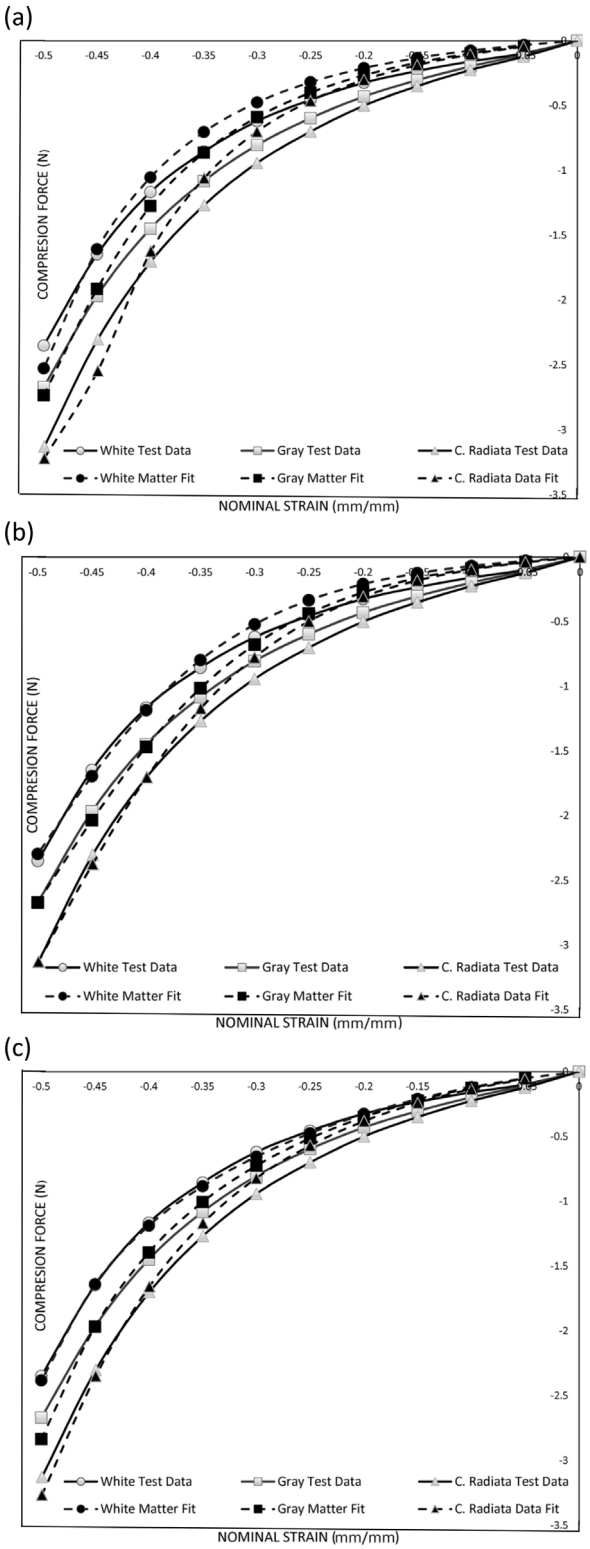

Fig. 3. Nonlinear stress–strain response of brain parts under compression loading and curve fitting using the (a) Ogden energy model, (b) hyperfoam energy model and (c) polynomial energy model [7].
Source: Permission obtained from Elsevier

stiffness to axial strips compared to the circumferential ones. Fig. 5 shows the orientation angles of collagen fibres in the intima, media and adventitia layers and the stretch stress behaviour for the axial and circumferential strips.

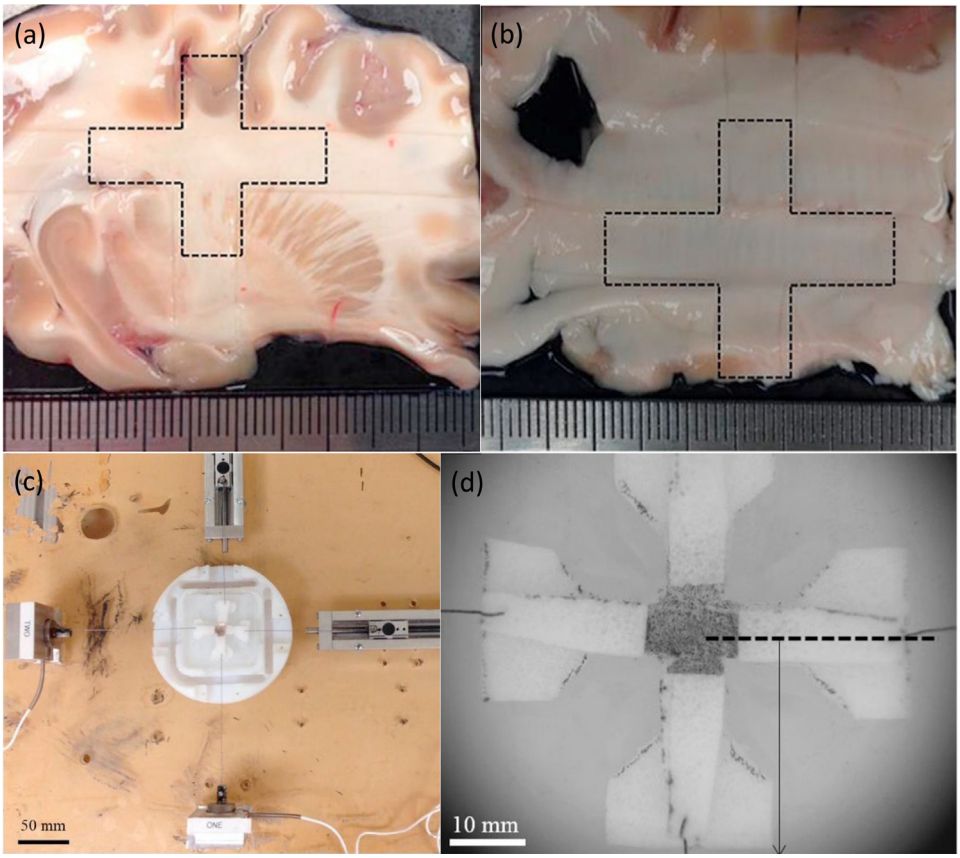

Fig. 4. Testing samples from (a) the corona radiata, (b) the corpus callosum, and (c) the experimental setup for biaxial testing and (d) biaxial samples. [97]. *Source:* Permission obtained from Elsevier.

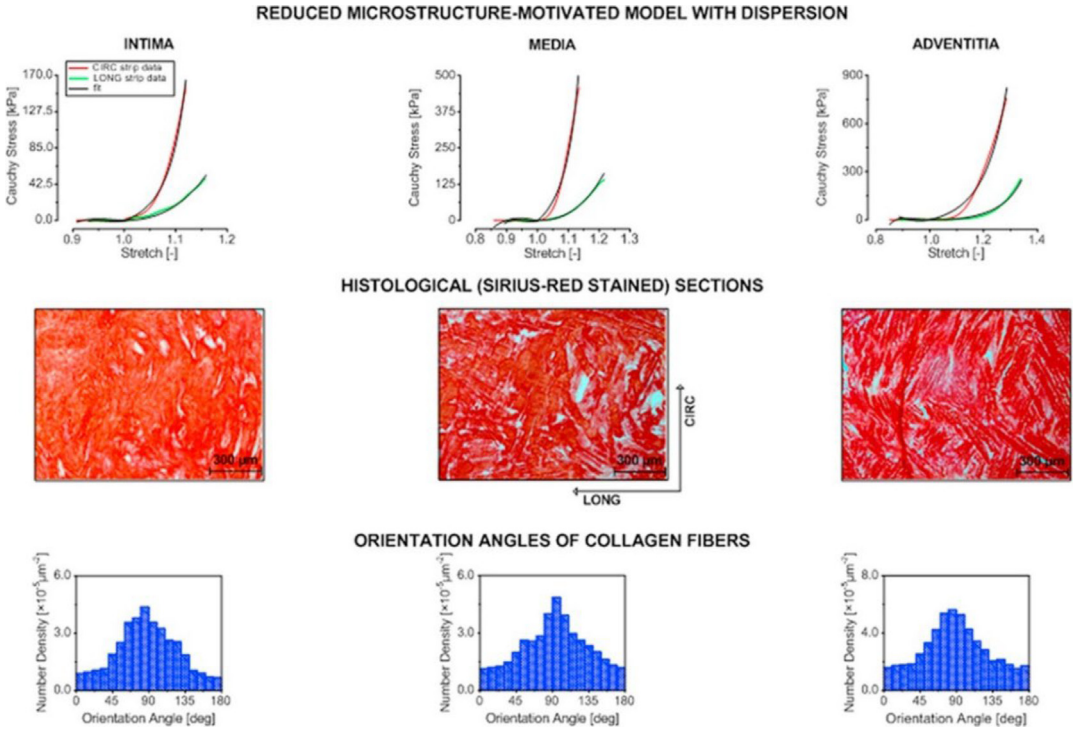

Fig. 5. The orientation angles of collagen fibres in the intima, media and adventitia layers and the stretch stress behaviour for the axial and circumferential strips [110]. *Source:* Permission obtained from Elsevier.

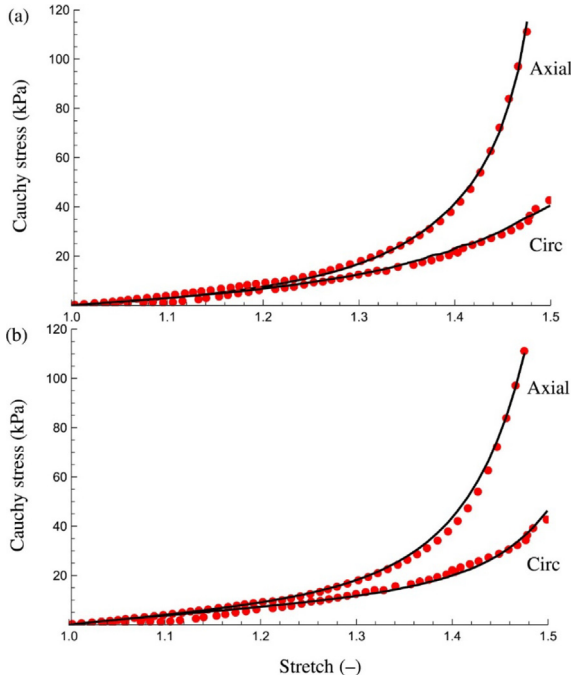

Fig. 6. Capability of the (a) GST and (b) AI models for fitting the experimental results [107] of the human non-atherosclerotic abdominal aorta in both axial and circumferential directions [112].
Source: Permission obtained from Elsevier.

Arterial walls contain randomly dispersed collagen fibres which makes it important to accurately model their large deformation behaviour. Holzapfel and Ogden [112,114] compared two well-known models of fibre-reinforced materials namely generalised structure tensor (GST) [115] and angular integration (AI) [116] methods showing that both models are virtually identical for different cases. Besides, it was emphasised that for the case of using finite element methods, the GST model requires less computational time. Fig. 6 shows the capability of the GST and AI models for fitting the experimental results [107] of the human non-atherosclerotic abdominal aorta in both axial and circumferential directions.

The age factor in changing the nonlinear behaviour of arteries has a key role which cannot be ignored. This importance has been addressed by researchers in studying human arteries. For instance, Amabili et al. [113] examined the visco-hyperelastic behaviour of descending thoracic aortas layers by experimentally testing twelve individual samples of beating heart donors. Axial and circumferential strips were cut from the aorta (Fig. 7) and a uniaxial tensile test and a dynamic test were performed to characterise their properties. This was the first study on the viscoelastic behaviour of aortas by individually analysing each layer. The Gasser–Ogden–Holzapfel material model was used to model the hyperelastic behaviour of each layer. It was concluded that donor age has a direct effect on increasing the stiffness in both circumferential and axial directions. The effect of age on the nonlinear mechanics of arteries was analysed by Jadidi et al. [118] using both theoretical analyses (constitutive modelling) and experiments (biaxial testing). It was shown that the thoracic aorta shows stiffer behaviour with age. Other studies on age dependency can be found in Refs. [119,120].

In another study, a combination of Fung-type (exponential) [121] and neo-Hookean strain energy density models was used by Holzapfel [117] which proposed a new approach for determining arterial wall material characteristics from uniaxial tests. Fig. 8 shows the histological images of circumferential strips of intima, adventitia and media layers indicating that collagen fibres are wavily distributed in the adventitia layer while are almost linearly distributed in intima; it was shown that the presented model is capable of modelling the characteristics of arterial walls (Fig. 9).

An advanced hyperelastic model of aortic tissue based on microstructural characterisation was developed by Amabili et al. [122]. Second-harmonic generation images were used to illustrate the heterogeneity of the structure for each layer (Fig. 10) and the in-plane and

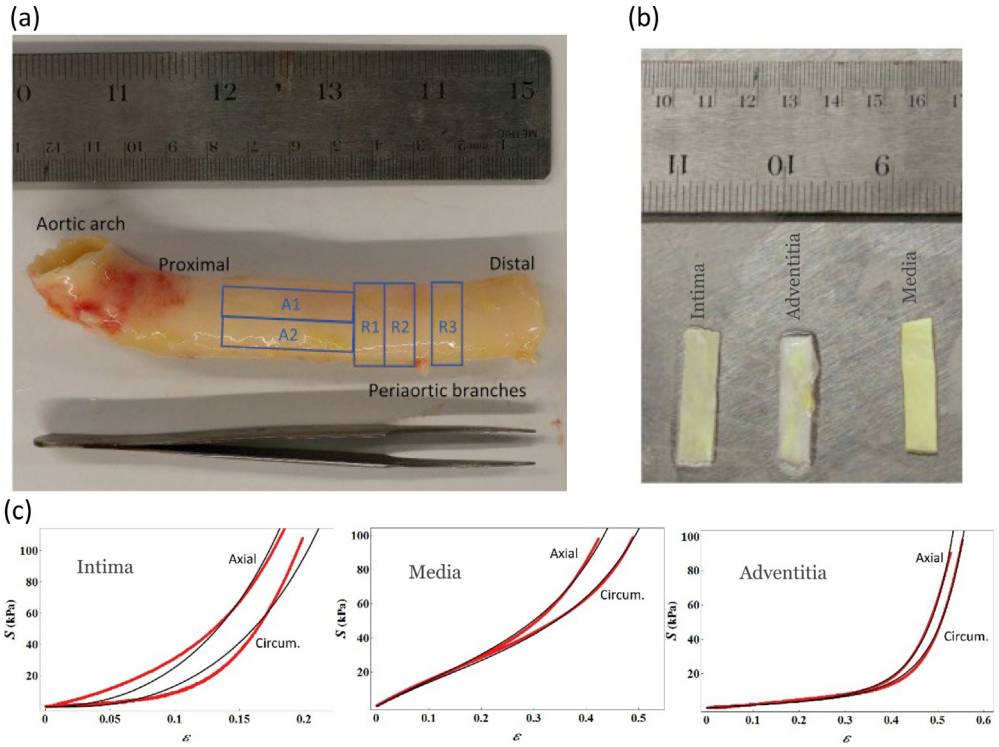

Fig. 7. (a) Donor's aorta, (b) axial strips of the layers, and (c) the stress–strain results for the circumferential and axial strips of each layer [113].
Source: Permission obtained from Elsevier.

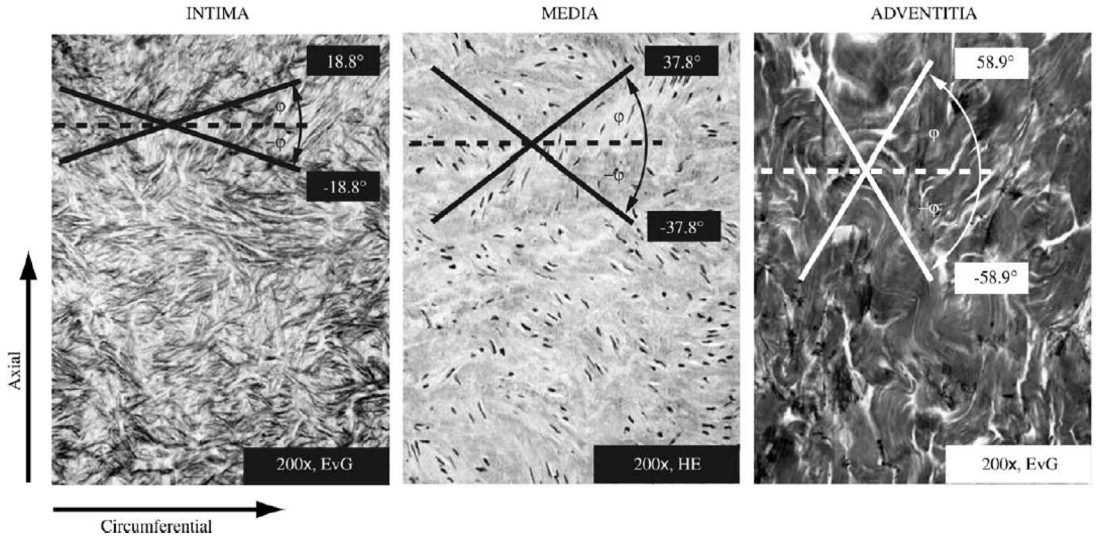

Fig. 8. Histological images of intima, adventitia and media layers [117].
Source: Permission obtained from Elsevier.

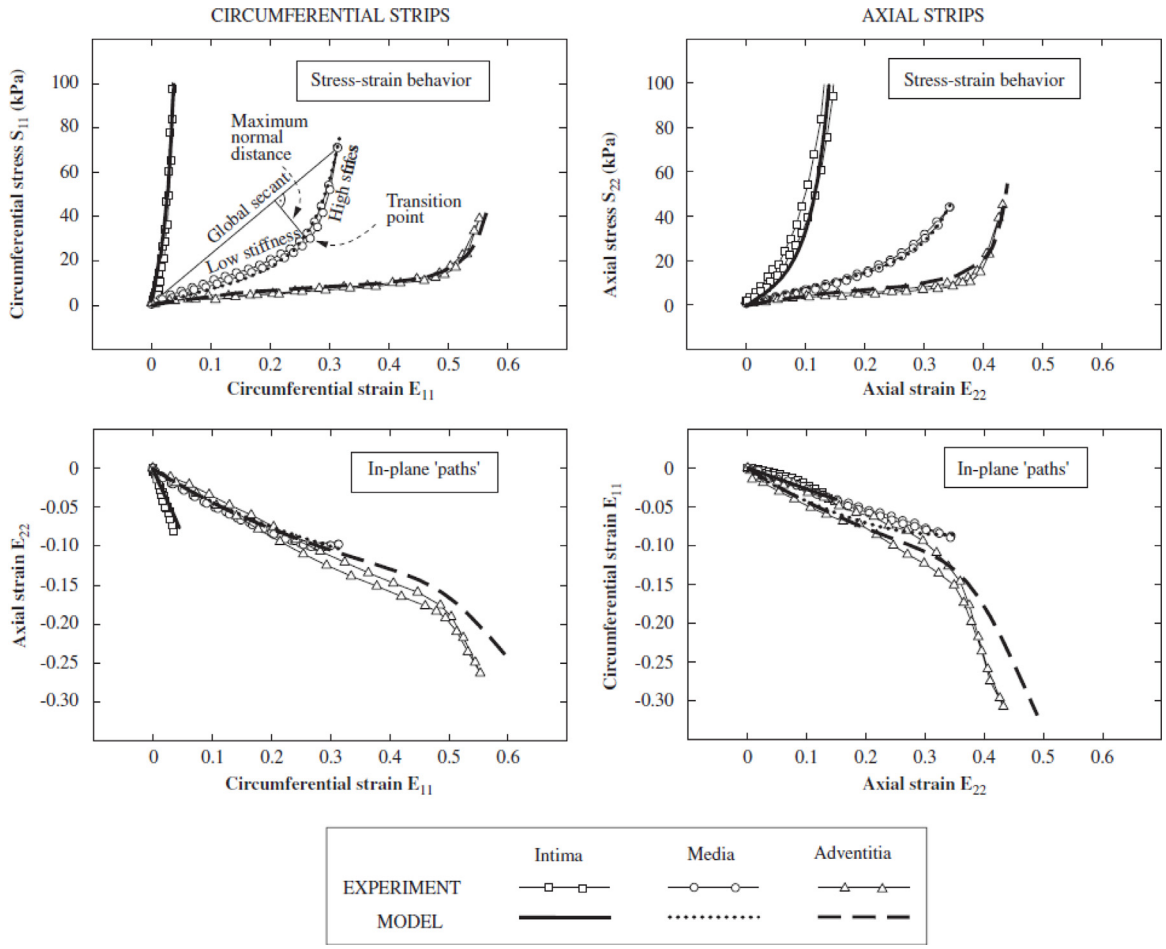

Fig. 9. Comparison of the uniaxial experimental testing on the artery layers with the ones obtained using the model presented in [117].
Source: Permission obtained from Elsevier.

out-of-plane fibre distributions were obtained experimentally and fitted theoretically. Results show that a single family of dispersed collagen fibres is suitable to model the collagen in each aortic layer. Lateral interactions and cross-link of collagen fibres were taken into account by introducing a second family of fibres which is orthogonal to the main one. It was shown that this advanced model is capable of accurately predict the stress–strain result of uniaxial testing of the intima, media and adventitia layers of human aortas (Fig. 11).

To have an appropriate mechanical design of aortic prostheses, Breslavsky and Amabili [123] modelled arteries using a shell

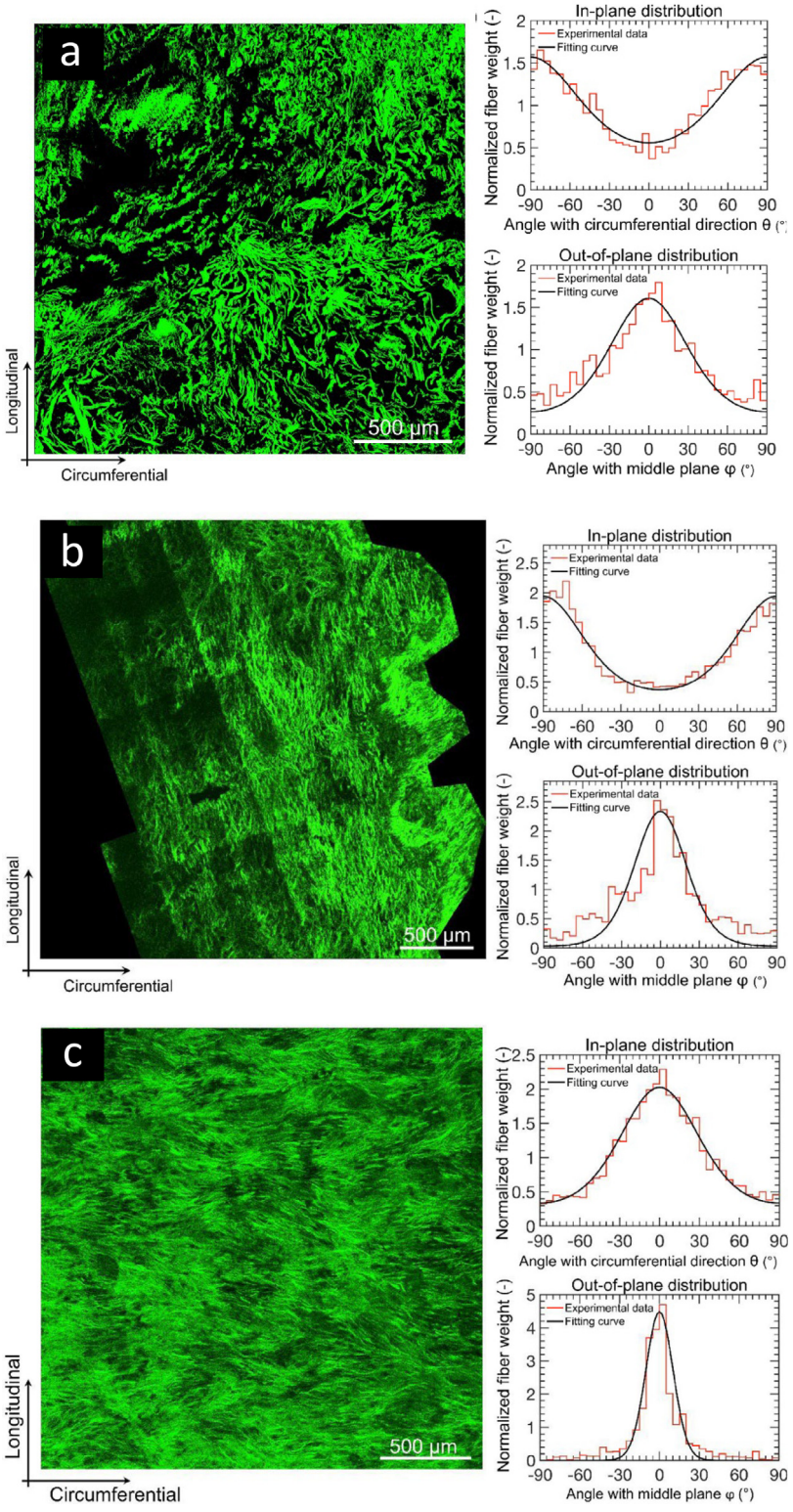

Fig. 10. Second harmonic generation image of an in-plane section of the (a) adventitia (b) intima and (c) media layers with the in-plane and out-of-plane fibre distribution [122]. *Source:* Permission obtained from Elsevier.

deformation model with 8 kinematic parameters. The artery was modelled as a three-layer orthotropic incompressible material in the framework of the Gasser–Ogden–Holzapfel model [124]. Since the current aortic prostheses are stiffer leading to overloading the heart's work [125] and oscillations [126], this study was a step forward in accurately modelling arteries as the commercial finite element programs do not take into account the thickness deformation.

The effect of the contraction of the vascular smooth muscle in arteries increases the wall stiffness. Franchini et al. [127] introduced the first anisotropic hyperelastic model to take into account the vascular smooth muscle activation in both longitudinal and circumferential directions. Their model is capable of fitting with great accuracy experimental results on tensile tests of human aortic strips in passive and active conditions (i.e. with vasoactive agents).

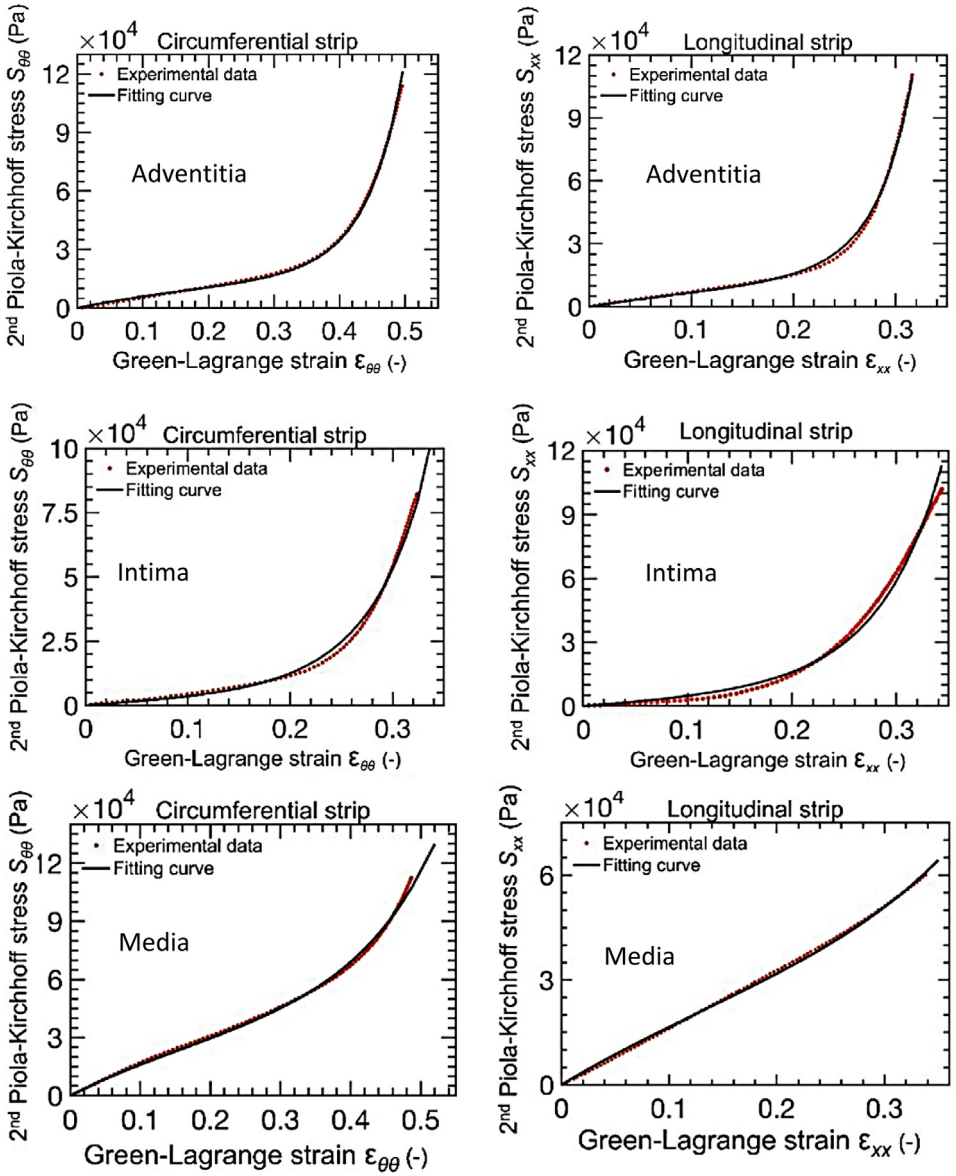

Fig. 11. Stress–strain result of uniaxial testing of the adventitia, intima and media layers with the fitted advanced hyperelastic model given by Amabili et al. [122].
Source: Permission obtained from Elsevier.

2.3. Hyperelastic models of the cartilage and ligament tissues

Cartilages located at the end of long bones of both humans and animals also have a non-linear elastic behaviour when confronting mechanical loadings. Since the weight of the body has a direct effect on these parts, it is important to study the mechanical responses under different conditions. Since articular cartilages repair slowly (due to not having an active blood supply), it is important to have a better understanding of their mechanical properties and differentiate the healthy cartilage from the injured ones (injuries such as osteoarthritis, costochondritis, herniation, achondroplasia and malignant [128–130]).

To this end, Lee et al. [131] studied the mechanical characteristics of articular cartilages in the framework of hyperelasticity. Equine articular cartilages were sampled from horses of different ages, weights, sexes and breeds, and the hyperelasticity of the cartilage was modelled via Ogden's strain energy density model. It was found that variables such as age, weight, sex and breed do not play a significant role in varying the hyperelastic mechanical behaviour of such structures.

Since articular cartilages show different collagen arrangements through the thickness (Fig. 12), Federico et al. [132,133] extended the works on articular cartilage by presenting an analytical approach for modelling the presence of collagen fibres in the framework of nonlinear elasticity. The advantage of this model was that it could analyse the structure with any type of fibre arrangement.

Deneweth et al. [134] focused on simulating the strain behaviour of humans' articular cartilage. Three different eight-chain hyperelastic models were investigated [135–138] to simulate the mechanical behaviour appropriately. It was claimed that the eight-chain transversely isotropic network with freely jointed chains [138] had an excellent fit for the experimental testing data. Results of the nonlinear stress–strain behaviour of articular cartilage under pressure obtained by experimental testing and the theoretical model fitting are presented in Fig. 13.

To have a proper understanding of osteoarthritis, Brown et al. [15] examined the load–displacement behaviour of both healthy and osteoarthritic articular cartilages. Various hyperelastic strain laws were examined to find the best fit indicating that the Yeoh and Mooney–Rivlin models present the best fit for both healthy and osteoarthritic articular cartilages.

Ligaments, which operate as hyperelastic tissue for bone connection, have been investigated using theoretical hyperelastic theories. Huang

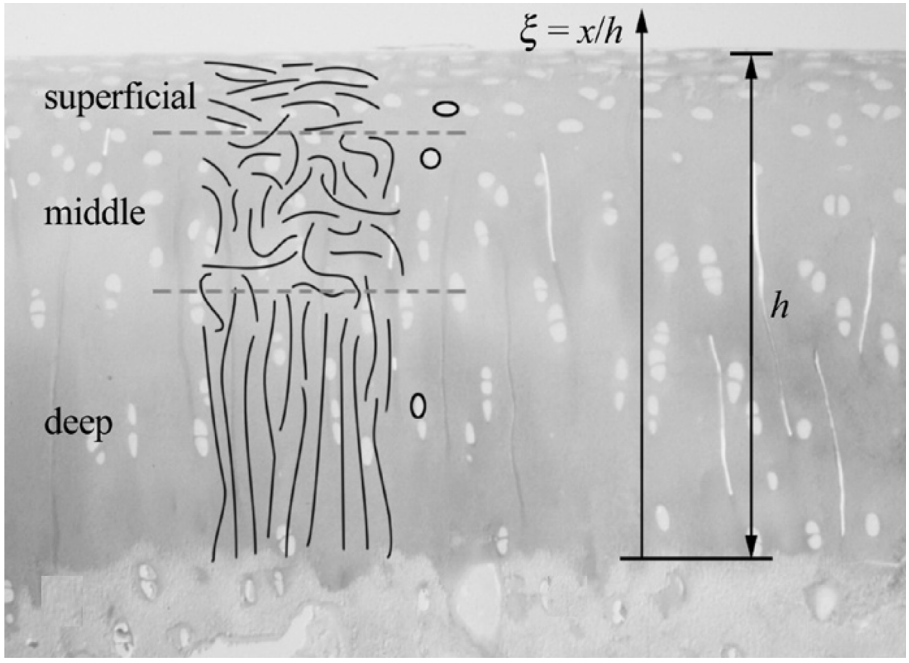

Fig. 12. Collagen arrangement of articular cartilage in-depth direction [132].
Source: Permission obtained from Elsevier.

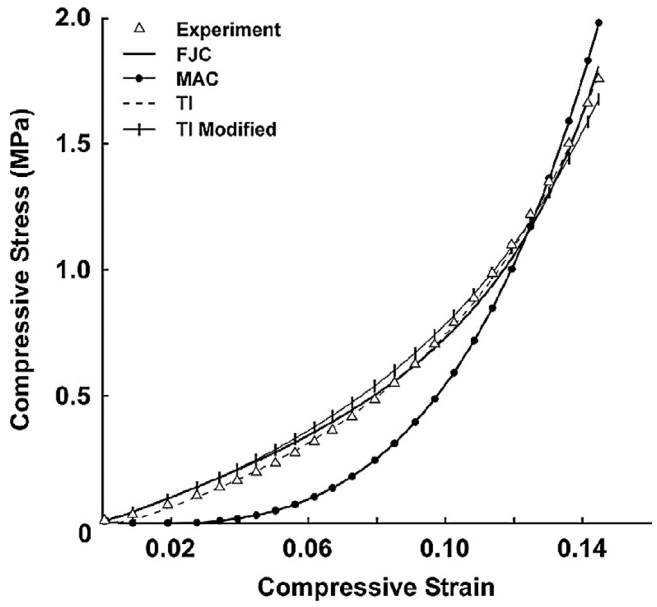

Fig. 13. Nonlinear stress–strain behaviour of articular cartilage under compressive force with fitted hyperelastic models [134].
Source: Permission obtained from Elsevier.

et al. [139] examined the mechanical characterisation of the periodontal ligament, which is the connection between the alveolar bone and the tooth. Hyperelasticity was modelled using an exponential model for strain energy density provided in [140]. It was shown that the simulated model and experimental results are in close agreement and the mechanical model was verified. Fig. 14 shows the experimental setup and the stress–strain behaviour of the periodontal ligament.

Human spine ligaments (Fig. 15(a)) have been analysed by Jiang et al. [141] in the framework of hyperelasticity and viscoelasticity. The neo-Hookean strain energy density model was used to model the substance matrix and a polynomial function for the collagen fibre. It was shown that the model was capable of fitting the stress–strain behaviour of human spine ligaments. Besides, it was shown that for low strain rates, the visco-hyperelastic modellings give similar results as the hyperelastic model (Fig. 15(b)).

2.4. Hyperelastic models of the liver tissue

Liver, as the main body part filtering the blood, has also attracted the attention of researchers for accurate modelling. Since the mechanical behaviour of an unhealthy liver can change significantly due to diseases such as Hepatitis, Cirrhosis, and fatty liver [142,143], modelling their mechanical characteristics using a hyperelastic model can improve our understanding of the liver tissues.

Focusing on liver surgery simulation, Marchesseau et al. [144] modelled the mechanical hyperelastic behaviour of livers. The liver was modelled via the Arruda–Boyce hyperelastic strain energy model and porosity. It was shown that the multiplicative Jacobian energy decomposition method is capable of modelling the strains of the structure with coarse meshing. Madireddy et al. [145] examined the mechanical deformation of bovine liver tissue using experimental observations and hyperelastic laws. Ogden, exponential and Mooney–Rivlin strain energy density models were utilised to track the hyperelasticity of the structure. It was indicated that the two and three-term Ogden models provide good fits, qualitatively. Li et al. [146] studied the mechanical characteristics of sectioned liver samples under loading. Both viscoelasticity and hyperelasticity effects were considered for theoretical modelling using Ogden, neo-Hookean and Mooney–Rivlin strain energy density models, alongside Maxwell, Kelvin–Voigt and combination viscoelasticity models giving an accurate model of the nonlinear stress–strain behaviour of the liver. Estermann et al. [147] examined the hyperelastic and viscoelastic behaviour of bovine and porcine livers by performing uniaxial testing on samples (Fig. 16). By fitting the results with different hyperelastic strain energy density models, it was shown that the most and least accuracy were seen for the Yeoh and neo-Hookean models, respectively (Fig. 17).

2.5. Hyperelastic models of the skeletal muscle tissue

Skeletal muscles, which play an important role in body motions, also indicate hyperelastic behaviour while undergoing mechanical loadings.

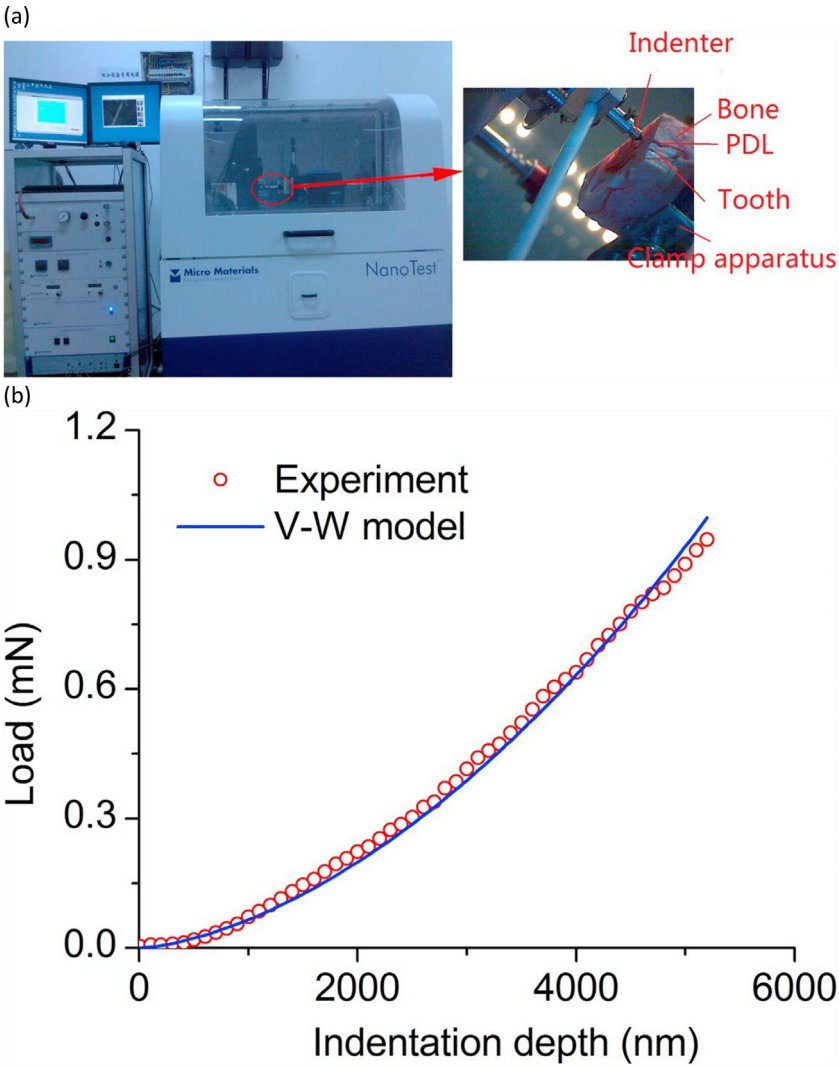

Fig. 14. The (a) experimental setup and (b) load–displacement curve for the periodontal ligament and the hyperelastic fitted model [139].
Source: Permission obtained from Elsevier.

Understanding the mechanical behaviour of skeletal muscles can help researchers in analysing sports injuries.

Focusing on body injury simulations, Lu et al. [148] investigated the behaviour of skeletal muscles by using experimental data from the rabbit tibialis anterior muscle and the neo–Hookean strain energy density model for theoretical analysis. It was claimed that the model was capable of simulating different strain rates and could be useful in simulating human body injuries in car accidents and sports injuries. Jalal and Zidi [149] examined the mechanical behaviour of skeletal muscles at −80 °C under cryopreservation conditions. The first-order Ogden's model, in conjunction with the second-order Maxwell's model, was utilised to model the tissue under uniaxial testing. It was shown that both the tension and the compression behaviour of the tissue varies considerably under cryopreserved conditions. Fig. 18 shows the stress–stretch fit of the tissue samples in cross fibre direction using the first order Ogden's model and experimental data.

An in vitro study on bovine skeletal muscles was performed by Hashemi et al. [150] to determine the passive skeletal muscle's behaviour. Using a genetic algorithm optimisation method, Helmholtz free energy function, and a three-dimensional hyperelastic model [151], the theoretical model of the stress–stretch behaviour of the skeletal muscle was obtained. It was shown that the skeletal muscle shows a toe region, linear elastic region and a nonlinear region before the rupture point. It was also mentioned that the linear region is mostly very small which emphasises the necessity of having a nonlinear elastic model of the skeletal muscle.

2.6. Hyperelastic models of the skin tissue

Skin is the largest organ of the human body facing different mechanical conditions. It is important to understand its behaviour to avoid any damage such as through contact with microneedles, microprojection arrays, micro-indenters and micro-particles as analysed by Meliga et al. [152]. Experimental testings have shown that human skin acts as an incompressible anisotropic material [3,153–155] which requires accurate modelling.

For uniaxial loading, Shergold et al. [156] examined the high and low strain rates of the skin. Pigskin was used for experimental analysis and the one-term Ogden hyperelastic model was used to model the mechanical behaviour theoretically. It was shown that the one-term Ogden strain density function was capable of modelling both the axial tensile and the compression behaviour of skin undergoing uniaxial loading.

Concentrating on humans' skin, Groves et al. [157] studied the mechanical characteristics of human skin via the exponential model of hyperelastic strain energy presented by Weiss et al. [158]. Compared with murine skin, it was shown that human skin can respond differently while facing low loads.

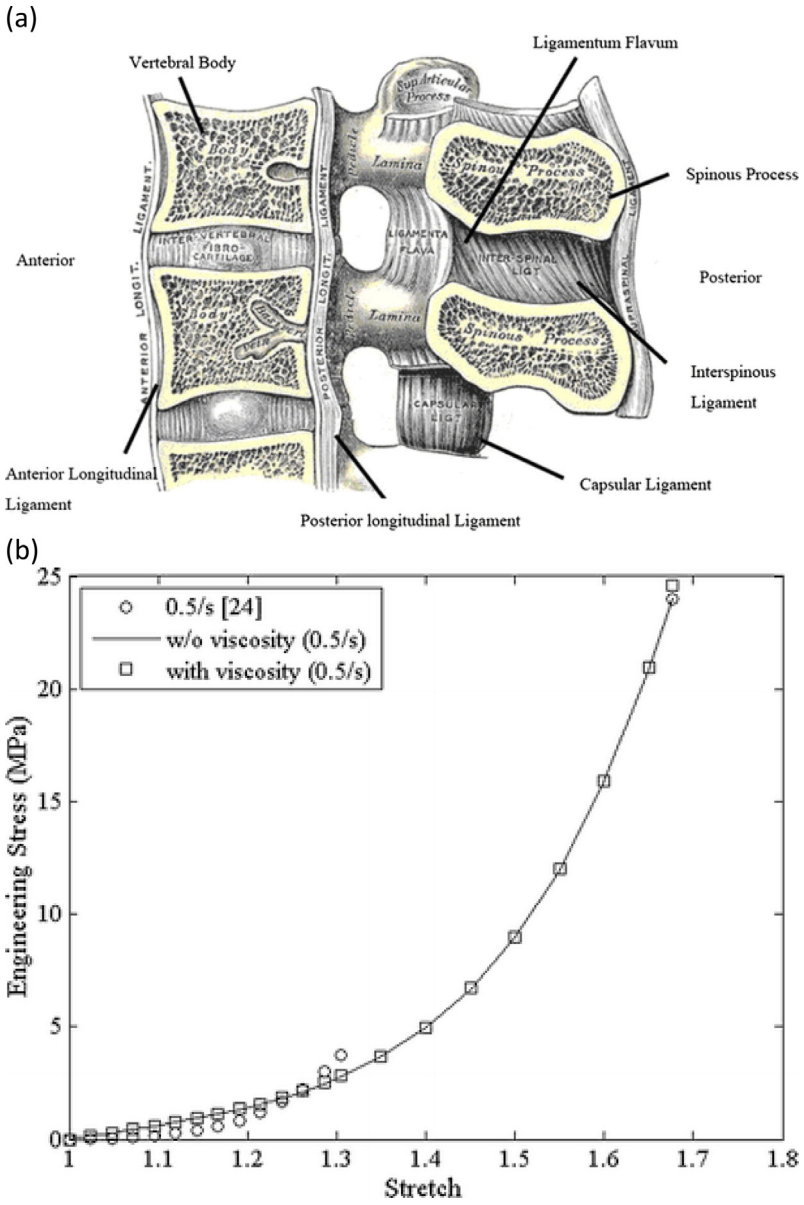

Fig. 15. (a) Sagittal section of spinal ligaments and (b) stress–stretch curve of the uniaxial test on the spine ligaments [141].
Source: Permission obtained from Elsevier.

In vivo experimental measurements and hyperelastic modelling of human skin with a keloid scar (Fig. 19a) have been investigated by Sutula et al. [159] and Chambert et al. [160]. The neo-Hookean strain energy density model was used to model the skin and keloid. It was shown that the given model was capable of accurately modelling the force–displacement of the keloid skin (Fig. 19b).

2.7. Hyperelastic models of the calcaneal and heel pad tissue

Heel pads hold the pressure of the human body's weight, which places it at risk of mechanical trauma. To accurately model the hyperelastic behaviour of heel pad tissues (Fig. 20a), Natali et al. [161] studied the visco-hyperelastic behaviour of human heel pads using both in vitro and in vivo testings. A constitutive model was presented using the Helmholtz free energy function and the hyperelastic model was presented as a combination of exponential and polynomial formulations. It was shown that the model was capable of tracking the stress–stretch behaviour of the heel pad tissue with different strain rates (Fig. 20b). For sub-calcaneal under compression, Isvilanonda et al. [162] utilised first and second-order Ogden hyperelastic strain energy density models to track the stress–strain behaviour. Coefficients for both types of modelling were presented for accuracy.

To understand the risk of mechanical trauma and overloading, Behforootan et al. [163] examined the mechanical behaviour of the heel pad under compression loading. Three different strain energy hyperelastic models (the neo-Hookean, first-order Mooney–Rivlin and first-order Ogden models) were used and it was claimed that the first-order Ogden method is capable of modelling the heel pad accurately, and that changing the stress–strain behaviour could affect the loading distribution through the heel pad which could cause trauma.

2.8. Hyperelastic models of the tongue tissue

The tongue has a valuable role in the digestive system, tasting food and cleaning the mouth which can confront different loads. The mechanics of tongue and properly simulating the muscles has become an important topic for speech production studies [164–167].

Examining hyperelasticity behaviour, Yousefi et al. [168] considered the mechanical properties of the tongue by experimentally

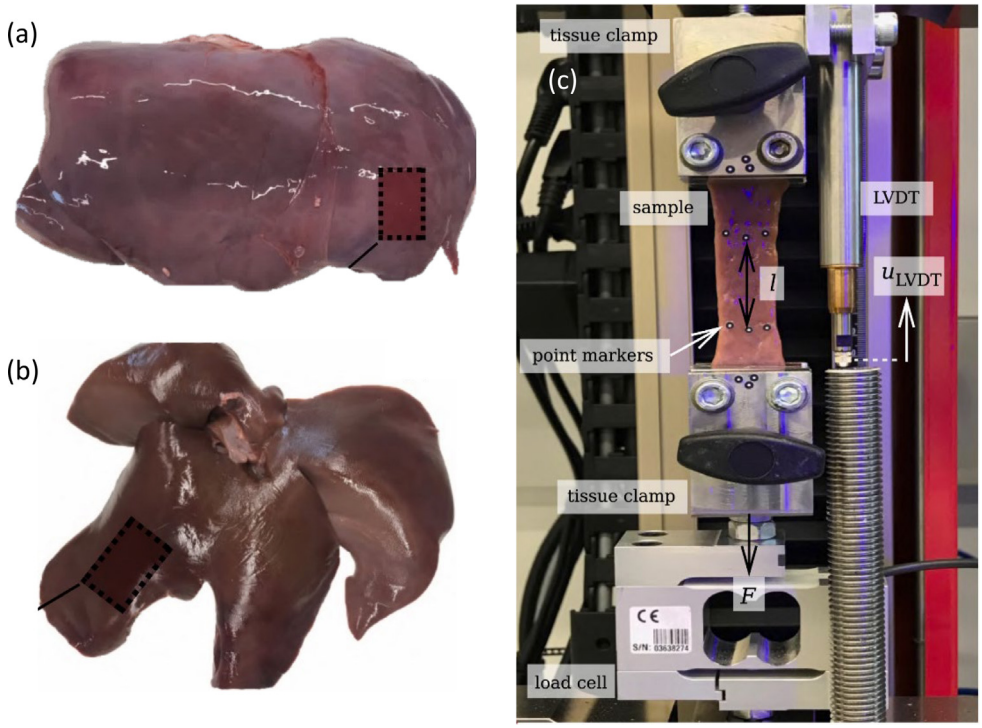

Fig. 16. Liver of (a) bovine and (b) porcine, and (c) the experimental setup for analysing the uniaxial hyperelastic behaviour of the samples [147].
Source: Permission obtained from Elsevier.

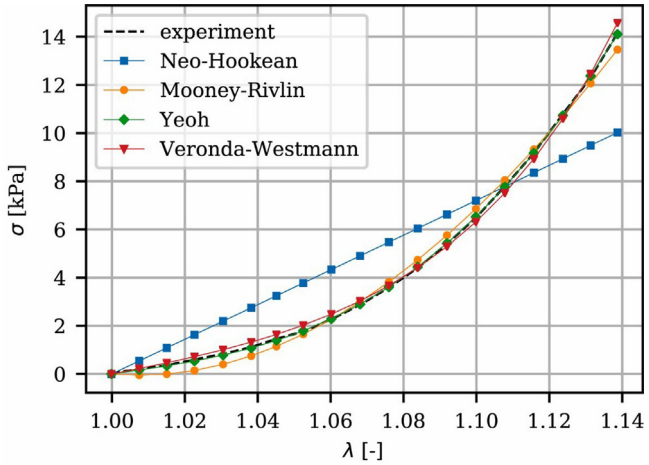

Fig. 17. Stress–strain modelling of liver samples using different hyperelastic samples [147].
Source: Permission obtained from Elsevier.

analysing bovine tongue tissue facing a uniaxial loading test (Fig. 21a), and theoretically modelling via the visco-hyperelastic model presented in [169]. It was indicated that for large deformations, the proposed finite element model (FEM) is capable of modelling the experimental data. Fig. 21(b) shows the stress–stretch behaviour of superior longitudinal muscle of bovine tongue with different fibre directions with a fitted hyperelastic model.

Gérard et al. [170] examined the non-linear elasticity of human tongues. An experimental uniaxial compression testing was performed (Fig. 22(a)) on a tongue of a cadaver 74-year-old woman and the hyperelastic behaviour was modelled theoretically by assuming the tongue incompressible using a Yeoh's strain energy density model. It was shown that the model is capable of modelling the force–displacement behaviour of different parts of the tongue (Fig. 22(b)).

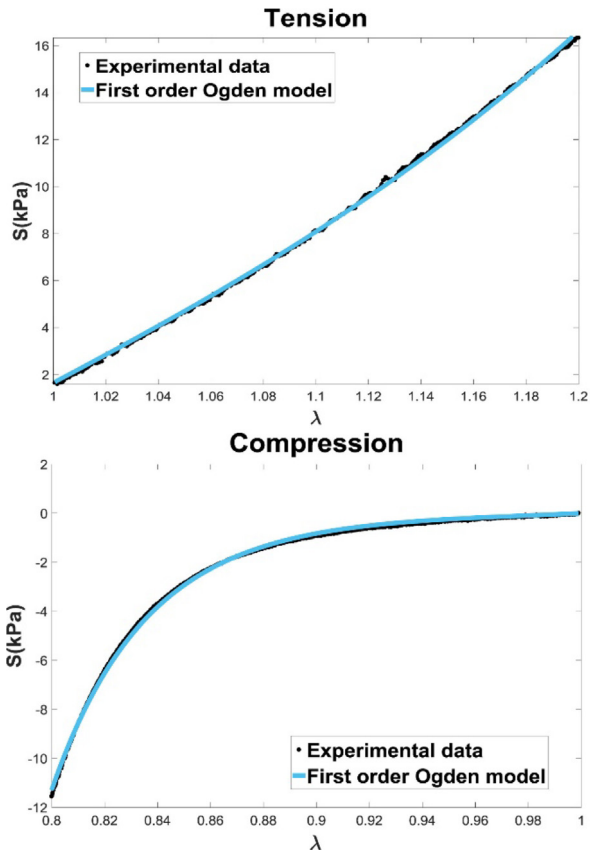

Fig. 18. The stress–stretch fit of the tissue samples in cross fibre direction using the first order Ogden's model and experimental data [149].
Source: Permission obtained from Elsevier.

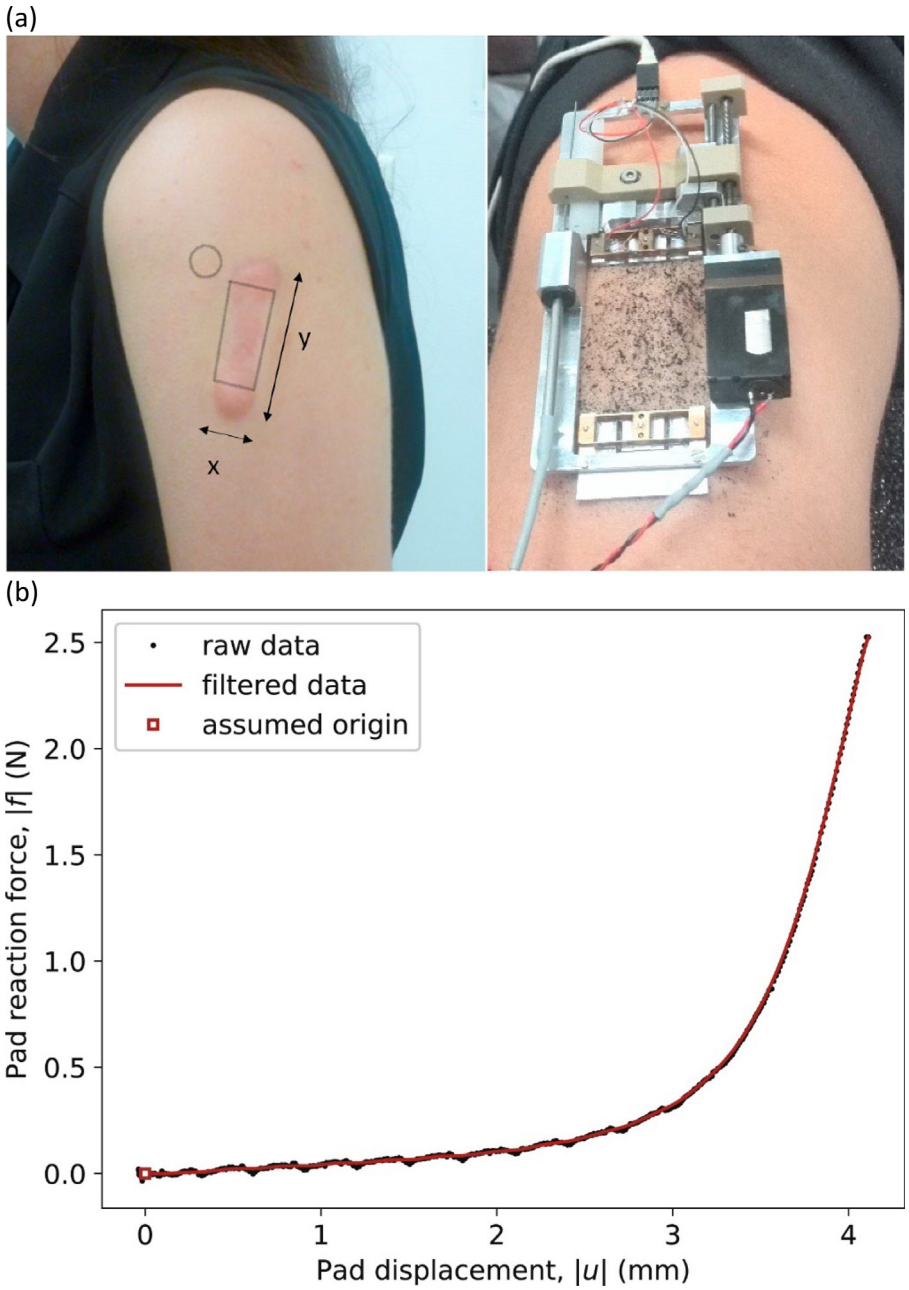

Fig. 19. (a) Keloid and in vitro experimental setup, and (b) load–displacement curve for the keloid and the hyperelastic fitted model [159].
Source: Permission obtained from Elsevier.

Ou et al. [171] examined the mechanical properties of tongues for reaching a better understanding of obstructive sleep apnoea–hypopnoea syndrome (OSAHS). The Mooney–Rivlin hyperelastic law together with the generalised Maxwell model was employed for fitting the stress–strain behaviour of different regions of tongues. They have shown that the stress–strain behaviour of samples from the apex, body and the root of tongue in longitudinal and transverse directions have good fit with the obtained results from the developed hyperelastic model.

2.9. Hyperelastic models of the adipose tissue

Adipose tissues can be found under the skin, in organs and breast tissue. They show non-linear elastic behaviour while being under load. Omidi et al. [172] presented a comprehensive study of decellularised adipose tissue of different parts (breast, abdomen, pericardial, omentum and thymic tissues) (Fig. 23) using various hyperelastic strain energy models. For each decellularised adipose sample, hyperelastic coefficient terms were found using Ogden, Arruda–Boyce, Yeoh and the polynomial model by comparing the results with experimental data.

Sun et al. [173] examined human adipose tissues under different types of shear and compression loadings. It was claimed that the adipose tissues show an isotropic behaviour under high strain rates and large deformations and their mechanical characteristics can be modelled using a quasilinear viscoelasticity model together with the Ogden strain energy density model (Fig. 24).

Breast tissue contains 90 percent adipose tissue [174,175] which properly modelling the mechanical properties of this tissue can significantly help in understanding the stress distribution in breast for industrial purposes (such as sports bra designing [176,177]) and medical treatment (diagnosis and surgery [178,179]). Breast tissue also shows a nonlinear viscoelastic behaviour which has been modelled and examined by researchers in the framework of hyperelasticity.

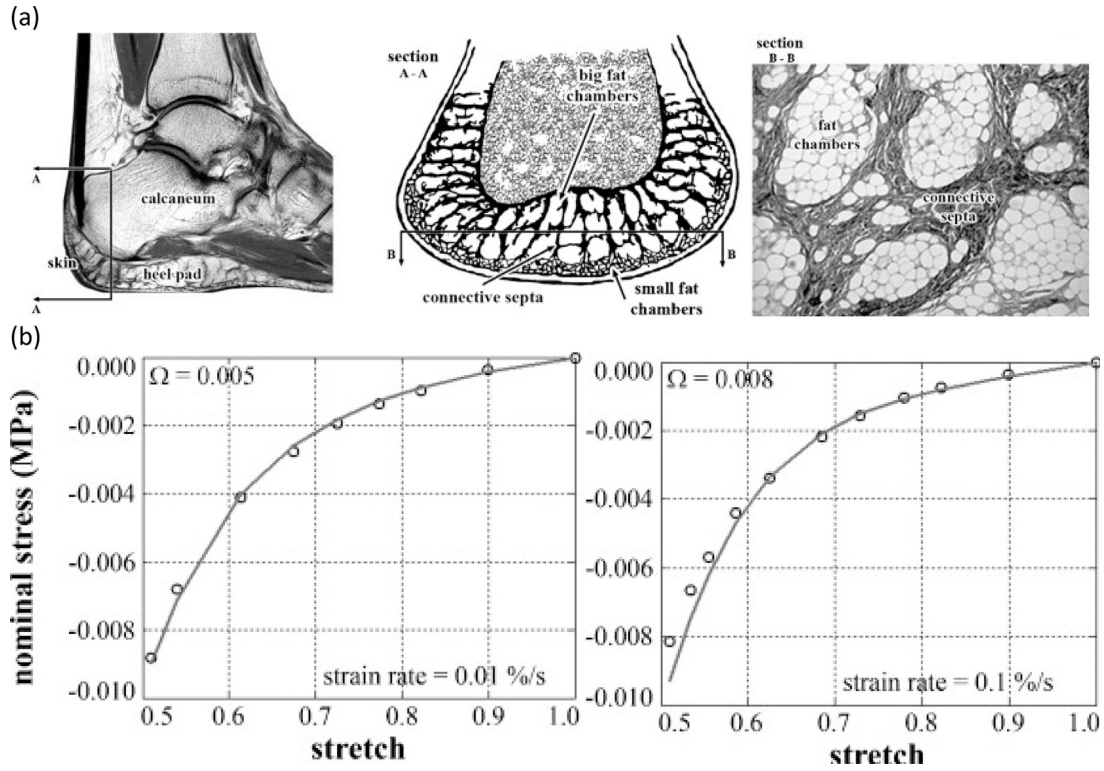

Fig. 20. (a) Histological image of human heel pad for different sections, and (b) the stress–stretch behaviour of human heel pad for different strain rates with a fitted hyperelastic model [161].
Source: Permission obtained from Elsevier.

For differentiating healthy and cancer breast tissues, O'Hagan and Samani [180] tested the hyperelastic behaviour of forty-four breast tissue samples (ex vivo) and used different hyperelastic strain energy models to fit the experimental results. It was shown that the Ogden, Yeoh and polynomial hyperelastic laws show the best fit for modelling breast tissues. Besides, it was emphasised that the cancer breast tissues have considerably different hyperelastic coefficients. In another study by Dempsey et al. [11], the hyperelastic properties of seventy-two healthy breast samples were tested fitted with hyperelastic laws of Polynomial, Ogden, Yeoh, and Veronda–Westmann [140]. It was shown that the nonlinear force–displacement behaviour of the adipose and fibro-glandular is insignificantly different and can be modelled in a mixed model (Fig. 25).

3. Mechanics of hyperelastic structures

Another important matter in hyperelasticity analysis is properly modelling the mechanical behaviour of soft structures. Since hyperelastic structures are used for industrial needs such as packaging [181–184], belt operating systems [185,186], and soft robotics [187–190], accurately modelling their mechanics have been a challenging task for researchers. In this review, the mechanics of soft structures is presented in two subsections for beam-type structures (beams, columns, tubes and arches) and plate-type structures (plates, shells and membranes).

3.1. Hyperelastic beams, columns, tubes and rings

Beam-type hyperelastic structures are used for different applications which makes it important to comprehend their mechanical behaviour. For this part of the review, the mechanics of beam-type hyperelastic structures are divided into two subsections providing the static deformation and buckling analysis. A fundamental study on modelling the elastic deformation of structures can be found in Ref. [83] .

3.1.1. Nonlinear static deformation analysis

For the case of static analysis, Irschik and Gerstmayr [191,192] presented a continuum mechanical model of the hyperelastic Reissner model of shear deformable beams, and analysed bending and axial deformations. The constitutive stress–strain relationship was assumed, as presented in Ref. [193] for isotropic hyperelastic beams. Since the model included the notation of strain and stress, it was claimed that the model was more comprehensive than the Reissner model [194], and therefore applicable for modelling of such structures.

Circular cylindrical hyperelastic blocks have been studied by Sheikhi et al. [195] using the Mooney–Rivlin, neo-Hookean, Arruda–Boyce, and polynomial hyperelastic laws. It was shown that the theoretical modelling of the structure using the left Cauchy–Green tensor definition has a close agreement with those obtained from FE software.

Hyperelastic beam structures strengthened with longitudinal fibres have been investigated by Bacciocchi and Tarantino [196] by considering the anticlastic effect. The structure was modelled as a transverse isotropic beam following the proposed models in Refs. [197,198]. It was claimed that the developed model has good accuracy in modelling many structural systems with application in soft robotics. They [199] also analysed the bending behaviour of laminated hyperelastic beams using the compressible Mooney–Rivlin law.

Jiang and Yu [200] extended the variational asymptotic beam model for hyperelastic beams and different cases were discussed to validate the theory. It was claimed that the model was suitable to be used as an accurate tool for testing experiments. Lanzoni and Tarantino [201,202] presented the anticlastic bending behaviour of beams in the framework of hyperelasticity. The Mooney–Rivlin strain energy density was used to model hyperelastic behaviour. Martins et al. [203] examined the uniaxial tensile behaviour of silicone rubbers and the accuracy of hyperelastic models in simulating the experimental results. It was found from all seven of the hyperelastic strain energy models that the best correlation was observed in the Ogden, Yeoh, and Martins models. Moreover, it was indicated that since biological

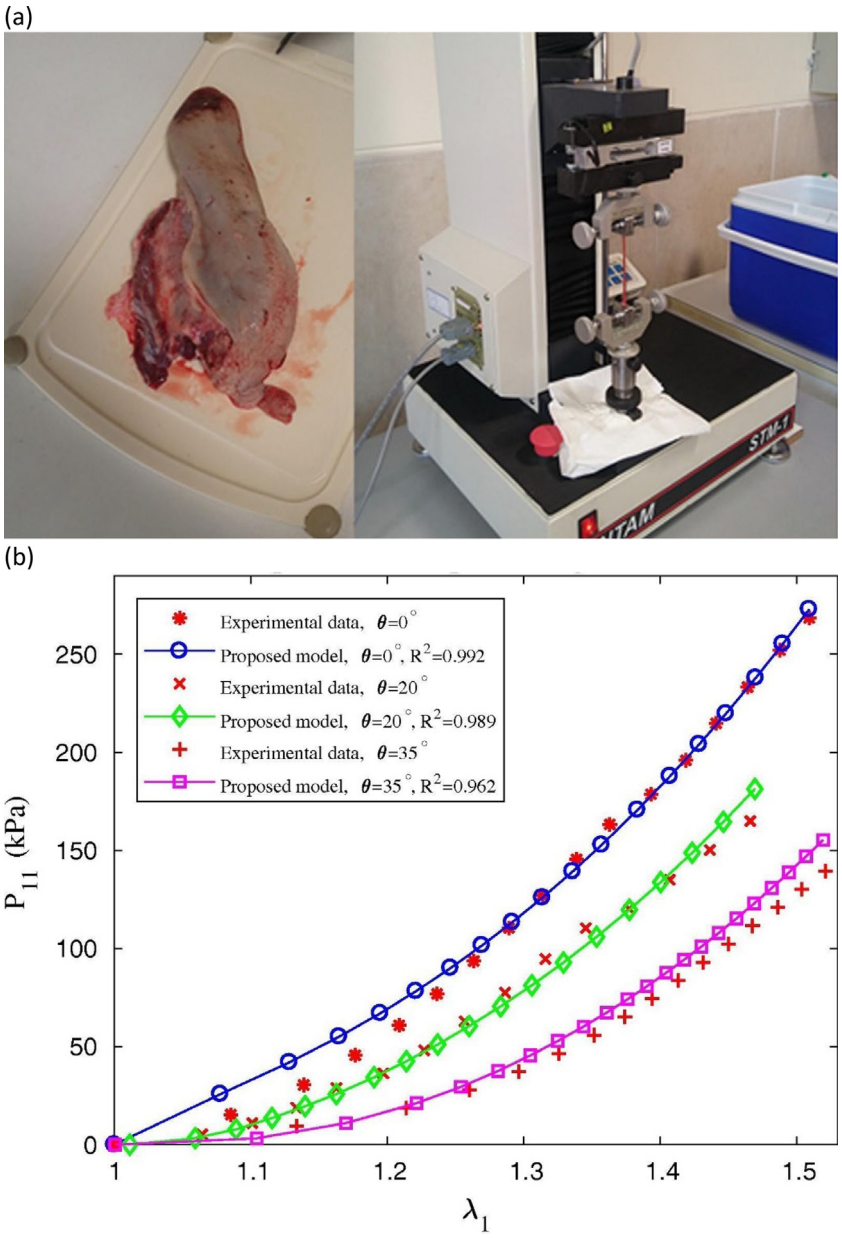

Fig. 21. (a) Bovine tongue with the uniaxial experimental setup, and (b) stress–stretch curve of the superior longitudinal muscle of bovine tongue with different fibre directions with a fitted hyperelastic model [168].
Source: Permission obtained from Elsevier.

tissues are not as homogeneous as elastomers, the hyperelastic models are more capable of modelling the rubbery structures.

For the case of having both hyperelasticity and viscoelasticity in modelling the beam structures, Shojaeifard et al. [204] examined the bending behaviour of soft beam structures. The visco-hyperelastic constitutive model was taken from Ref. [205]. Cantilever hyperelastic beams subjected to an extremely large bending deformation were studied by Falope et al. [206]. The theoretical model developed in Ref. [201] was employed and the effect of the slenderness ratio and the compactness index on the static behaviour of the structure was analysed.

As the displacements and strains are considerably higher in such structures, consideration of the shear effect when modelling hyperelastic structures has been a source of debate for researchers. He et al. [207] considered the thickness stretching effect for shape deformation analysis of hyperelastic beams. Considering the plane-strain Euler–Bernoulli beam model, in conjunction with a neo-Hookean strain energy density model, an analytical solution for pure bending and uniform tension was presented. It was elucidated that for simply-supported beams under large loading, the membrane model is applicable and the stretching deformation is dominant. Zhu et al. [208] discussed the displacement field equations and models. It was emphasised that the small-strain assumption in classic beam theory and the first-order asymptotic expansions presented in Refs. [209,210] are not capable of modelling hyperelastic behaviour in beams since the shear strain effect is neglected. Furthermore, it was discussed that although the coupled series expansions presented in Ref. [211] could be applied for hyperelasticity, the equation and calculations will be too long. Hence, a new leading order model for finite deformations was introduced [208] in which the Poisson's ratio effect was added directly to the displacement equations. The nonlinear time-dependent motion of hyperelastic beams has been controlled by Mylapilli and Udwadia [212] using a constrain motion theory.

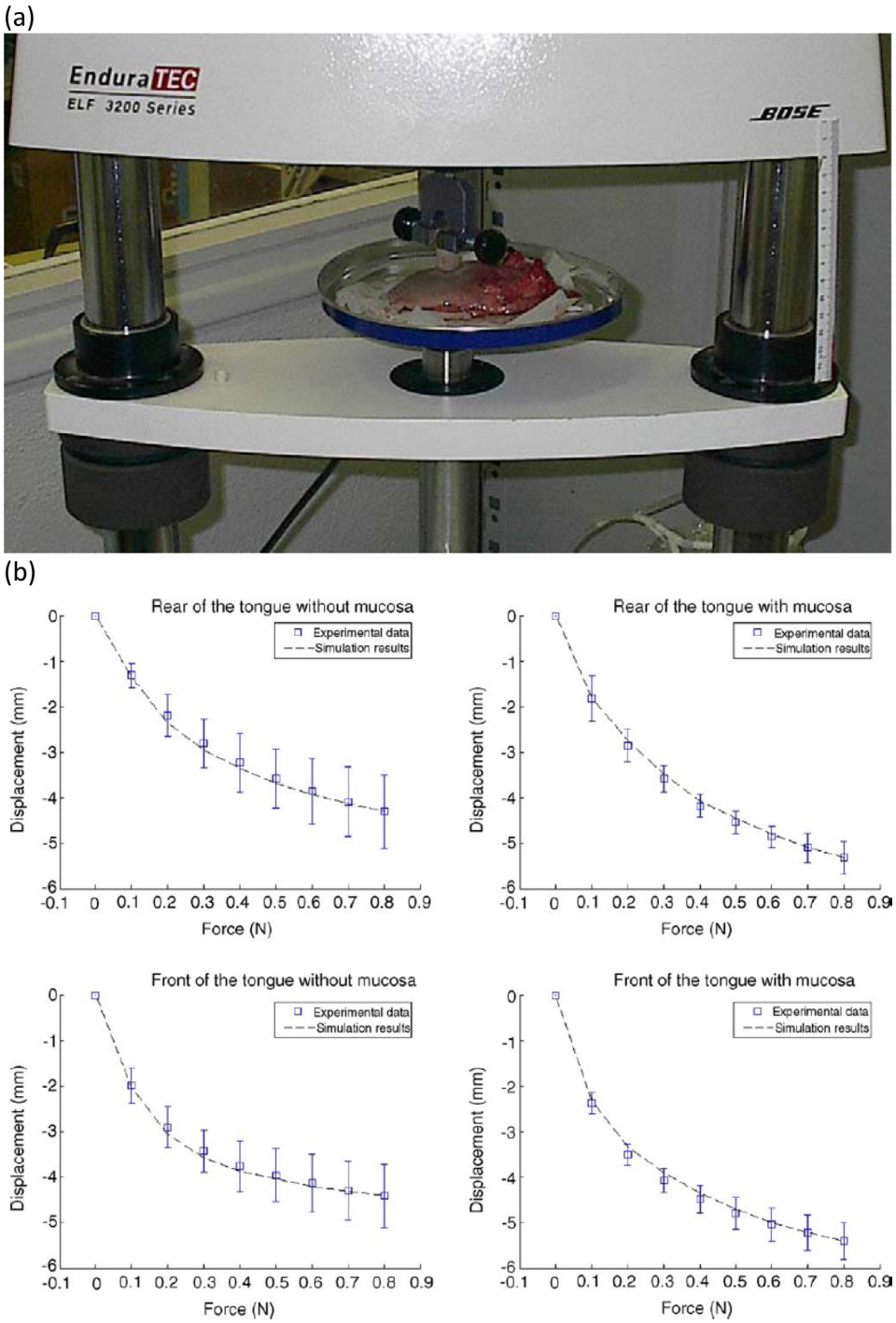

Fig. 22. (a) Uniaxial compression experimental setup on human tongues, and (b) the force–displacement behaviour of different parts of the tongue with a fitted hyperelastic model [170].
Source: Permission obtained from Elsevier.

Hyperelastic and linear-elastic circular rings have been examined by Breslavsky et al. [213] as a benchmark for FE codes. The hyperelasticity was modelled using the incompressible neo-Hookean hyperelastic strain energy density model and the results were compared with those obtained from FE software. It was shown that ANSYS and ABAQUS provide accurate results for the nonlinear elastic material model of the neo-Hookean model (Fig. 26) but the linear elastic model for large strains is not accurate. Wang et al. [214] studied the radial and axial nonlinear motions of cylindrical tubes by using an isotropic compressible neo-Hookean model and travelling wave transformations. Other investigations into hyperelastic beam-type structures for different conditions can be found in Refs. [215–224], discussing the importance of modelling the bending behaviour of hyperelastic beam structures accurately.

3.1.2. Nonlinear buckling analysis

The importance of understanding the buckling behaviour of hyperelastic beam-type soft structures has drawn a lot of attention. Since hyperelastic structures undergo large strains and deformations, buckling is an important phenomenon which must be analysed. For this reason,

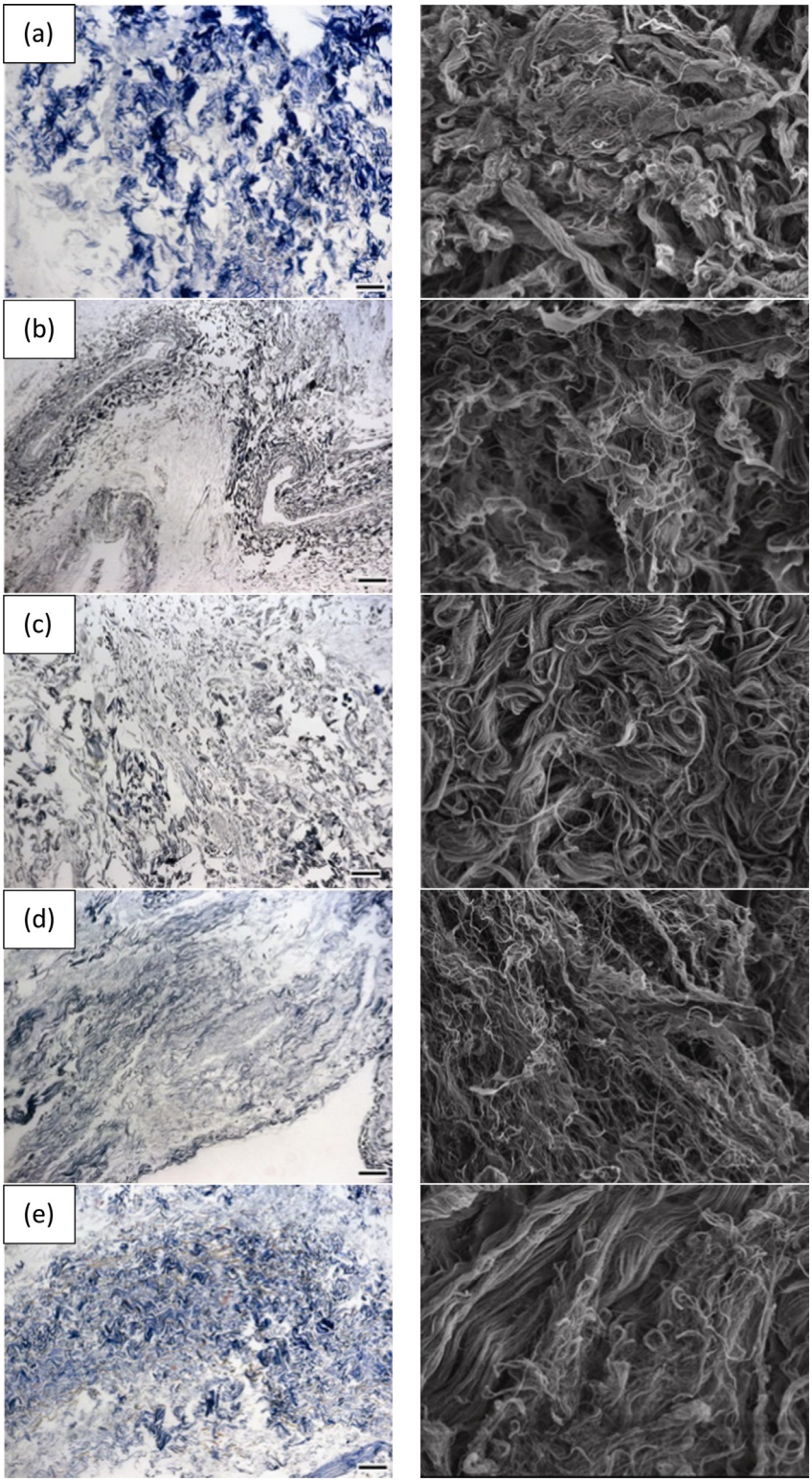

Fig. 23. (a) Histological and SEM images from decellularised (a) breast, (b) thymic remnant, (c) pericardial depot, (d) omentum, and (e) subcutaneous abdominal region adipose tissues [172].
Source: Permission obtained from Elsevier.

Liu [225] studied the axial and transverse buckling of hyperelastic rubber tubes. Continuum mechanics definitions and the hyperelastic strain energy function were utilised to model the buckling behaviour. It was shown that the transaction between axial and transverse buckling occurs when the inner to outer radii ratio is 0.6716.

Slesarenko and Rudykh [226] analysed the appearance of instabilities in fibre-reinforced composites using neo-Hookean strain-energy function and Bloch–Floquet analysis. It was shown that depending on the fibre's volume fraction and based matrix properties, the unit cell can undergo macroscopic or microscopic instabilities. Fig. 27 shows

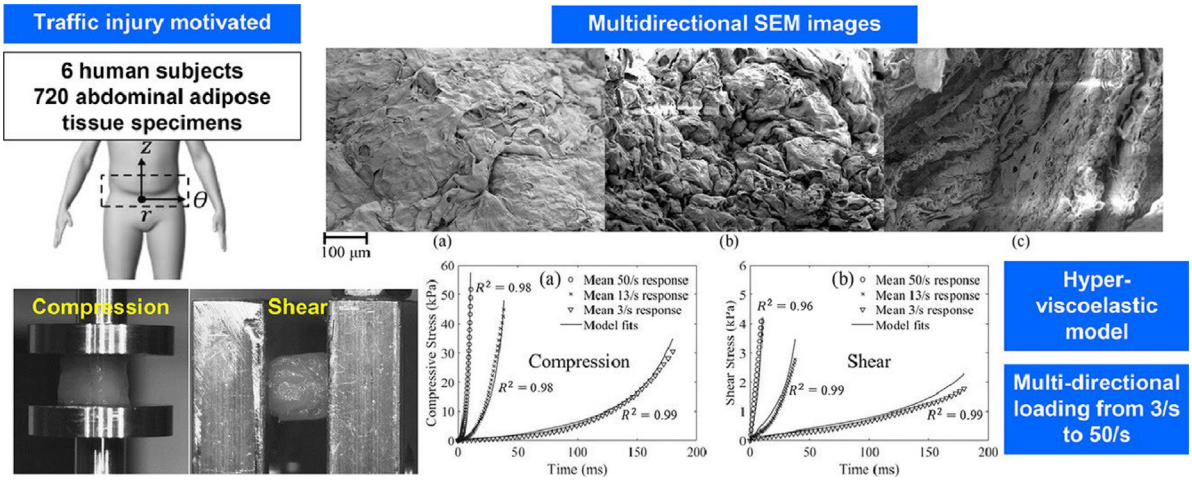

Fig. 24. Compression and shear analysis of adipose tissues with a visco-hyperelastic fit [173].
Source: Permission obtained from Elsevier.

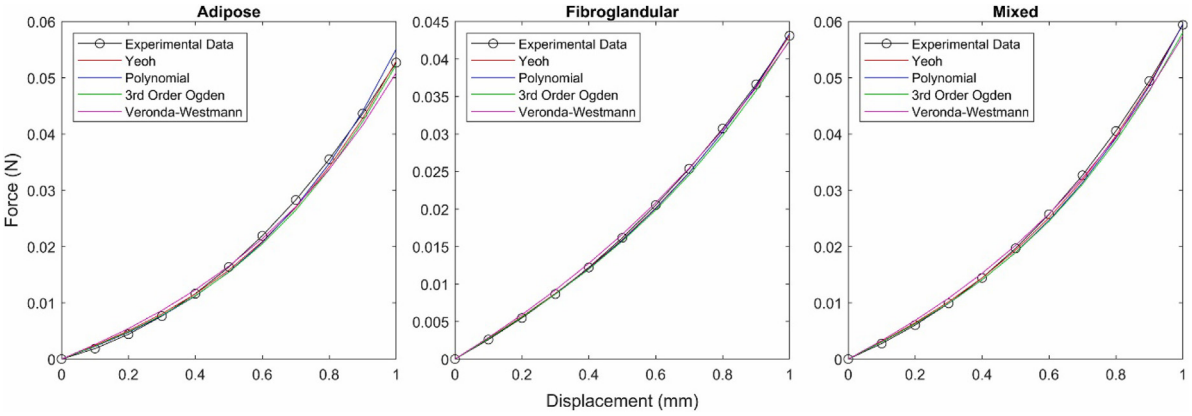

Fig. 25. The nonlinear force–displacement behaviour of the adipose, fibro-glandular and mixed breast tissue with hyperelastic model fits [11].
Source: Permission obtained from Elsevier.

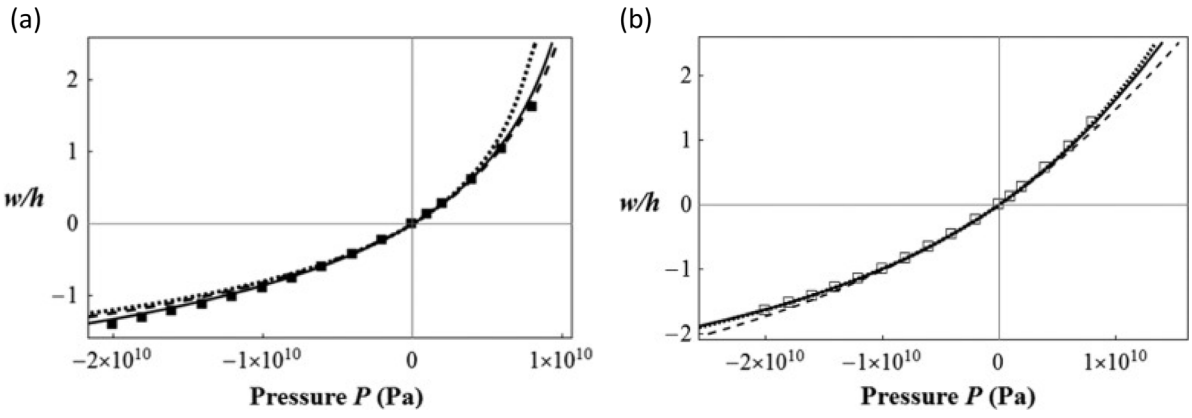

Fig. 26. Comparison of the displacement-pressure behaviour of hyperelastic rings subjected to (a) radial pressure, and (b) displacement-dependent pressure using the nee-Hookean material model and FE software [213].
Source: Permission obtained from Elsevier.

the buckling modes for different fibre volume fractions [226]. Arora et al. [227] improved the instability and buckling behaviour of hyperelastic layered composites by having inhomogeneous interphases.

Flores et al. [228] modelled the post-buckling behaviour of carbon nanotubes (CNTs) via hyperelasticity. The nonlinear elasticity was modelled using the first-term Ogden strain density model by considering the CNT as an incompressible structure. It was found that the main deformation and post-buckling responses of single-walled CNT structures are properly modelled with a hyperelastic Ogden model.

Soft wide columns with hyperelastic behaviour have been investigated by Chen and Jin [229,230] for analysing the snapping-back instability. Experimental testing and neo-Hookean continuum mechanics have been carried out to model the buckling response. It was claimed that due to the hysteresis behaviour of such structures in

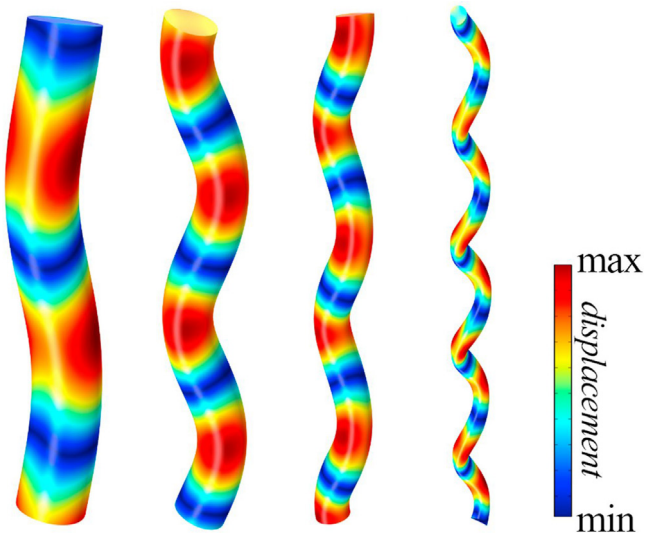

Fig. 27. Buckling modes of fibre reinforced columns with fibre volume fractions from left to right 0.02, 0.01, 0.005, and 0.001 [226].
Source: Permission obtained from Elsevier.

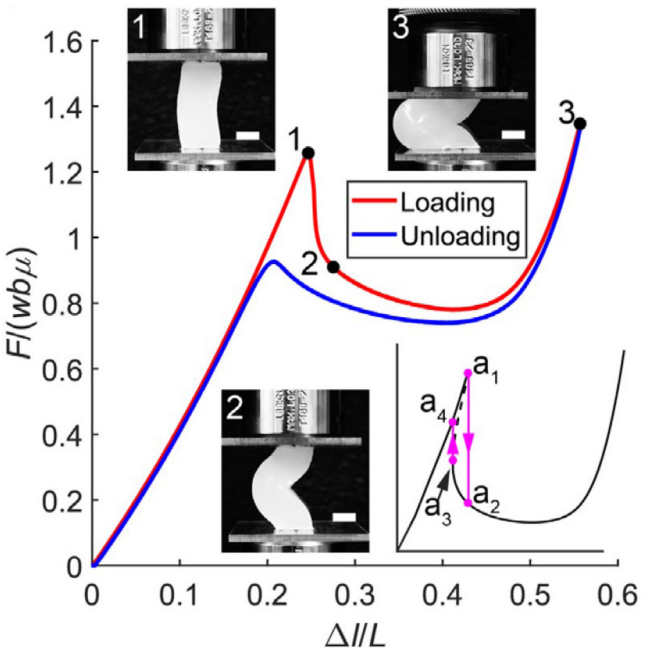

Fig. 28. Force–deformation behaviours of a column under compression loading [229].
Source: Permission obtained from Elsevier.

force–displacement plots, such structures could be useful elements in energy harvesters. The force–deformation behaviour of the structure can be seen in Fig. 28. Attard and Hunt [231] investigated the buckling behaviour of shear deformable hyperelastic columns. A neo-Hookean strain energy density model was employed to model the hyperelasticity behaviour, while the transverse shear effect was modelled via the Timoshenko beam theory. As opposed to previous studies, they [231] claimed that the shear buckling mode does not exist for prismatic isotropic columns. Attard and Kim [232,233] also investigated the lateral buckling of prismatic and sandwich soft beams claiming that most prismatic straight isotropic beams' lateral behaviours are unaffected by shear deformation.

3.2. Hyperelastic plates, shells and membranes

Plate-type hyperelastic structures including soft plates, shells and membranes have been examined by many researchers in both static deformation analysis and buckling/wrinkling analysis. In this section, a detailed discussion of available studies in this field is given in two subsections of nonlinear static deformation analysis and nonlinear buckling analysis.

3.2.1. Nonlinear static deformation analysis

For hyperelastic structures facing rigid body loading, Pamplona et al. [234] analysed the static vertical displacement of a circular membrane under the external load of a rigid body. Experimental testing, numerical modelling and analytical analysis were performed to study the problem. It was found that the incompressible neo-Hookean hyperelastic strain energy model provided a good approximation of the actual model. Selvadurai [235] examined the indentation of a circular rubber membrane acting upon an external rigid spherical in the framework of hyperelasticity. It was shown that the hyperelastic models, named Blatz-Ko and Mooney–Rivlin, have the most correlation with the actual experimental test results.

Pressure loading on hyperelastic structures with several applications in biomechanics [236] has been studied over the past few years. For air pressure loading, Pamplona et al. [237] examined the finite deformations in hyperelastic cylindrical membranes acting upon air pressure inside the structure. Three different constitutive laws were utilised for modelling the hyperelastic behaviour and the coefficients for neo-Hookean, Ogden and Mooney–Rivlin models were obtained via the experimental testing results. Similarly, for fluid pressure loading, the static deformation of hyperelastic circular membranes has been examined by Selvadurai and Shi [236]. By comparing these with the experimental tests, it was shown that Mooney–Rivlin, neo-Hookean, Ogden and Yeoh strain energy density models are capable of modelling the hyperelasticity of the rubber membrane.

Furthermore, Patil and DasGupta [238] studied the effect of initial pressure and pre-stretch on the static deformation of circular hyperelastic membranes. Hyperelasticity had been modelled using the Mooney–Rivlin strain energy density model and solved via the Runge–Kutta method. It was shown that the combination of the base model has a significant effect on the softening and hardening behaviour of the structure. Other studies on hyperelastic membranes and plates can be found in Refs. [239–246], which discuss the importance of modelling the static deformation via a hyperelastic strain energy density model.

The problem of inflation of balloons and membranes for high stretches using different hyperelastic theories is a unique problem of hyperelastic structures which have been examined by researchers in the past few years. Mangan and Destrade [247] studied the inflation of rubber balloons both experimentally and theoretically. The nonlinear elasticity of the spherical balloon was modelled following the Gent-Gent and 3-parameter Mooney hyperelastic models; it was concluded that the Gent-Gent hyperelastic model shows the most accuracy in modelling the inflation of rubber balloons (Fig. 29). Kumar and DasGupta [248] investigated the mechanical response of inflated spherical membranes in contact with an external object. An isotropic hyperelastic Mooney–Rivlin model was employed to model the structure and the contact was assumed to be frictionless and non-slippery; it was shown that for the same contact angle, the frictionless model has a higher pressure compared to the non-slip case. Balloon inflation for high stretches using different hyperelastic theories can be seen in Fig. 30.

3.2.2. Nonlinear buckling analysis

Wrinkling and buckling behaviour of hyperelastic plate and shell structures have been investigated by several researchers. Zhang et al. [249] examined the buckling and post-buckling behaviour of hyperelastic plates. A simply-supported plate model and one edge clamped model were used to study post-buckling behaviour. A perturbation

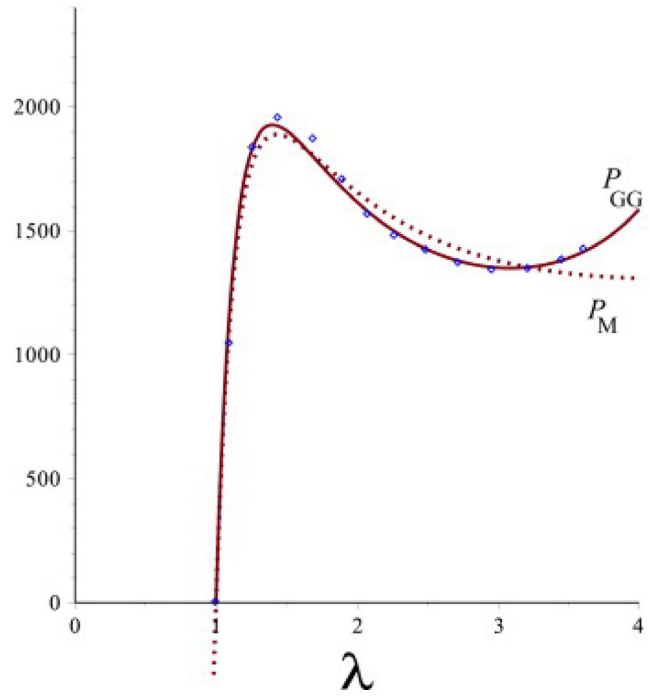

Fig. 29. Pressure–stretch diagram for the inflation of a spherical balloon using Gent-Gent and Mooney hyperelastic models fitted with the experimental data [247].
Source: Permission obtained from Elsevier.

technique of the multiple-scale method was used to solve the model. It was shown that the boundary model has a significant effect on the order of post-buckling response. Diaby et al. [250] analysed the prestressed hyperelastic membranes to understand the buckling and wrinkling behaviour of such structures. The constitutive model was defined using the Saint-Venant Kirchhoff strain energy model. Different cases of inflated torus, pinched hemisphere, shear-loaded membrane, and square airbag were modelled and discussed. It was claimed that the model was capable of predicting the critical values of wrinkling in different cases correctly.

Finite element methods have been employed by Xu et al. [251] to model and study instabilities in hyperelastic thin films using both linear and nonlinear approaches. It was shown that depending on the ratio between the thin film and substrate stiffnesses, the bifurcation curves obtained from the linear elastic model and the neo-Hookean model can differ significantly (Fig. 31).

The limit-point and inflation-jump instabilities have been examined by Anssari-Benam et al. [252] using a new generalised neo-Hookean model for inflation of cylindrical and spherical rubbers. The model was compared to the Gent strain energy model and it was claimed that the results were improved using the new generalised neo-Hookean model and the limit-point and inflation jump instabilities were captured accurately by fitting to the experimental results (Fig. 32). Nayyar et al. [253] examined the wrinkling phenomena in uniaxially stretched rectangular hyperelastic sheets. It was concluded that the wrinkling phenomena can be suppressed by an optimal design in width-to-length and thickness terms or by having stretches larger than the critical strain of the structure.

Buckling in soft structures is not always a failure and in some cases, it can be seen as a protective mechanism. For instance, Hejazi et al. [254] examined inflation and appearance of a bugle in hyperelastic tubes both theoretically (using Ogden's strain energy density model) and experimentally. It was shown that for isotropic hyperelastic tubes, the build-up stress due to inflation can be reduced by buckling in the structure (Fig. 33(a)) and can be seen as a protective fail-safe mechanism (Fig. 33(b)).

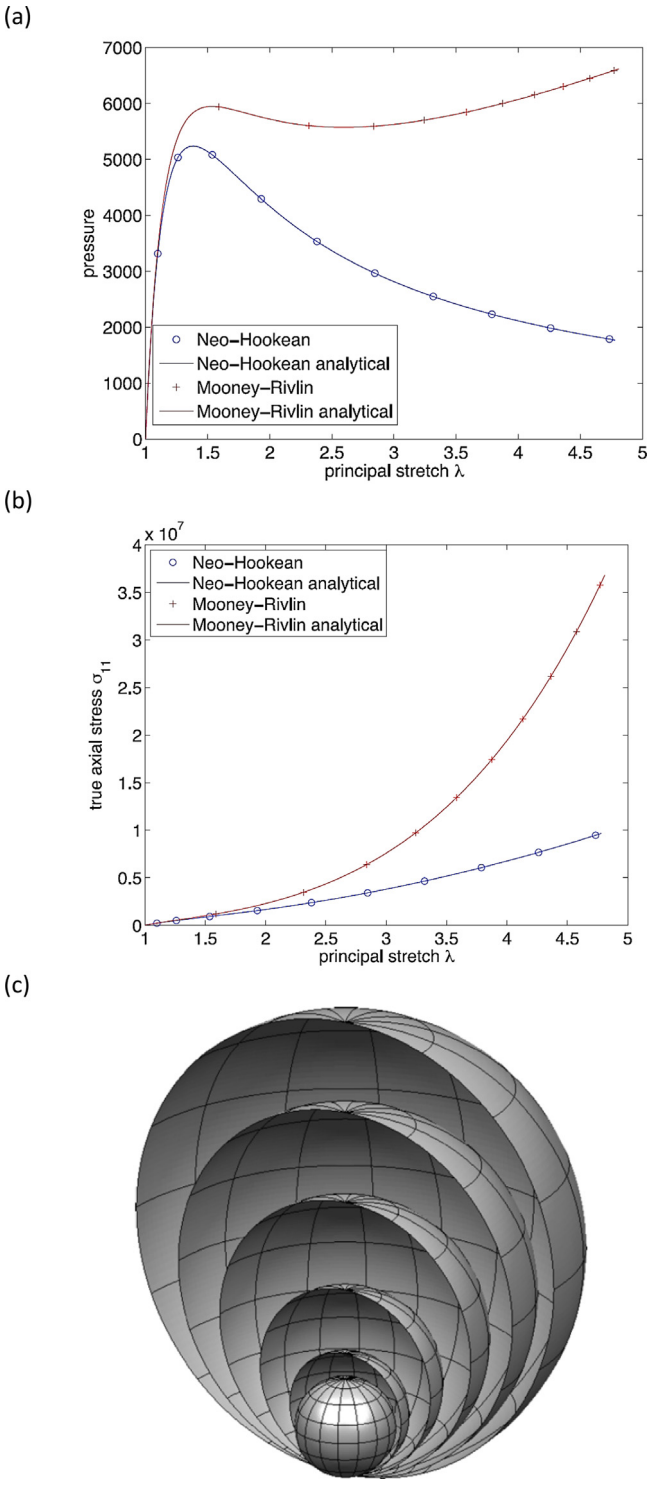

Fig. 30. Differences between the neo-Hookean and Mooney–Rivlin models for (a) pressure and (b) axial stress in balloon inflation for high stretches and (c) schematic view of the balloon [239].
Source: Permission obtained from Elsevier.

Inflated and pressurised hyperelastic spherical structures have also been examined in the past few years. Jiusheng [255] investigated the stability of internally pressurised spherical shells using the neo-Hookean strain energy density model. it was shown that increasing the thickness of the shell leads to higher critical pressure (Fig. 34) and passing this pressure, the shell becomes highly aspherical and unstable. Rodríguez-Martínez et al. [256] investigated the stability of

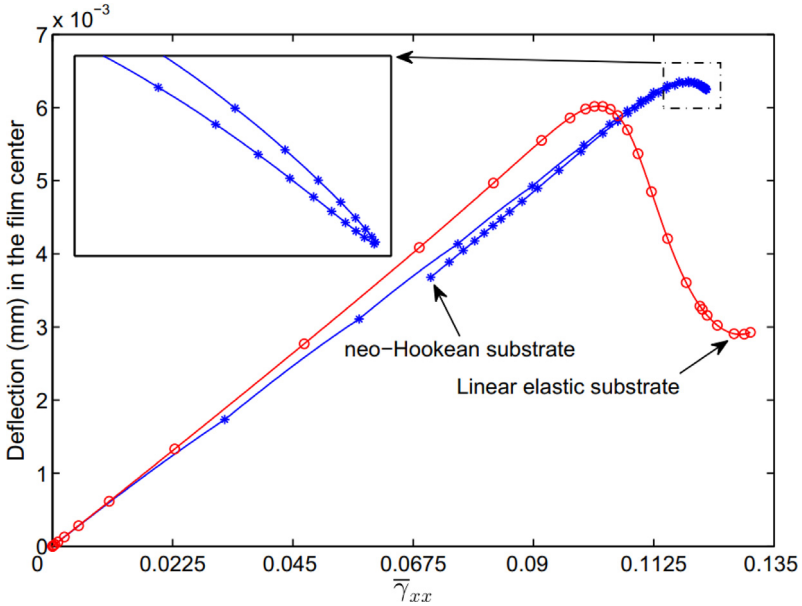

Fig. 31. The linear elastic and hyperelastic modelling of bifurcation curves of equi-biaxially compressed soft films on a rubberlike compliant substrate with a stiffness ratio of 30 [251].
Source: Permission obtained from Elsevier.

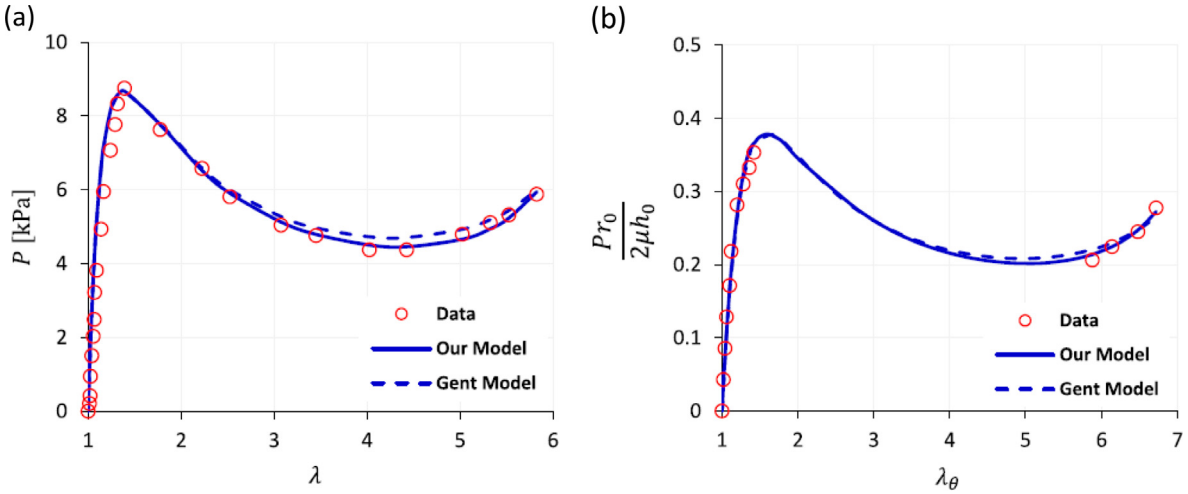

Fig. 32. Comparison of the new generalised neo-Hookean model and Gent model in fitting experimental pressure–stretch curve [252] (This article is an open access article distributed under the terms and conditions of the Creative Commons Attribution (CC BY) license (https://creativecommons.org/licenses/by/4.0/)).

inflated spherical hyperelastic membranes using six different strain energy density models. It was shown that the Yeoh and three-term Ogden model show a stable branch first followed by an unstable branch and another stable branch while the two-term Ogden model shows a consistent stable behaviour with the variation of the circumferential stretch (Fig. 35).

4. Summary and conclusions

This review paper focused on clarifying the importance of having an accurate model of hyperelastic structures in two main subjects of mechanics and biomechanics. A detailed introduction was provided to show the importance of this research topic followed by a comprehensive discussion on literature using over 250 research works until 2022.

One of the essential applications for hyperelastic theoretical modelling is in biomechanical studies. Since almost all the human body organs demonstrate hyperelastic behaviour, the importance of accurately modelling and simulating the organs' behaviours becomes important in different medical analyses, especially for failure prediction, surgery and identifying healthy from unhealthy (tumour, cancer etc.) parts. In this review, the hyperelastic biomechanics of organs were divided into subsections by organ type. The application of different hyperelastic strain energy models and their capability of modelling the soft mechanical behaviour of the body parts was discussed in detail. By reviewing the literature, it was shown that each organ has its significant hyperelastic behaviour, and that the suitable hyperelastic strain energy density model can vary between organs. Most studies on the hyperelastic biomechanics of organs were focused on in vitro tests. The importance of having accuracy in modelling organs was considerably higher when the living organism was studied fresh and the errors in the systems could increase by having in vivo examinations alone [257]. Besides, the accurate developed models in research works in this field emphasise the capability of improving the quality of prosthesis following the hyperelastic characteristics of real human biological tissues.

Since soft structures have been used in many applications including packaging, belt operating systems, and soft robotics, a detailed

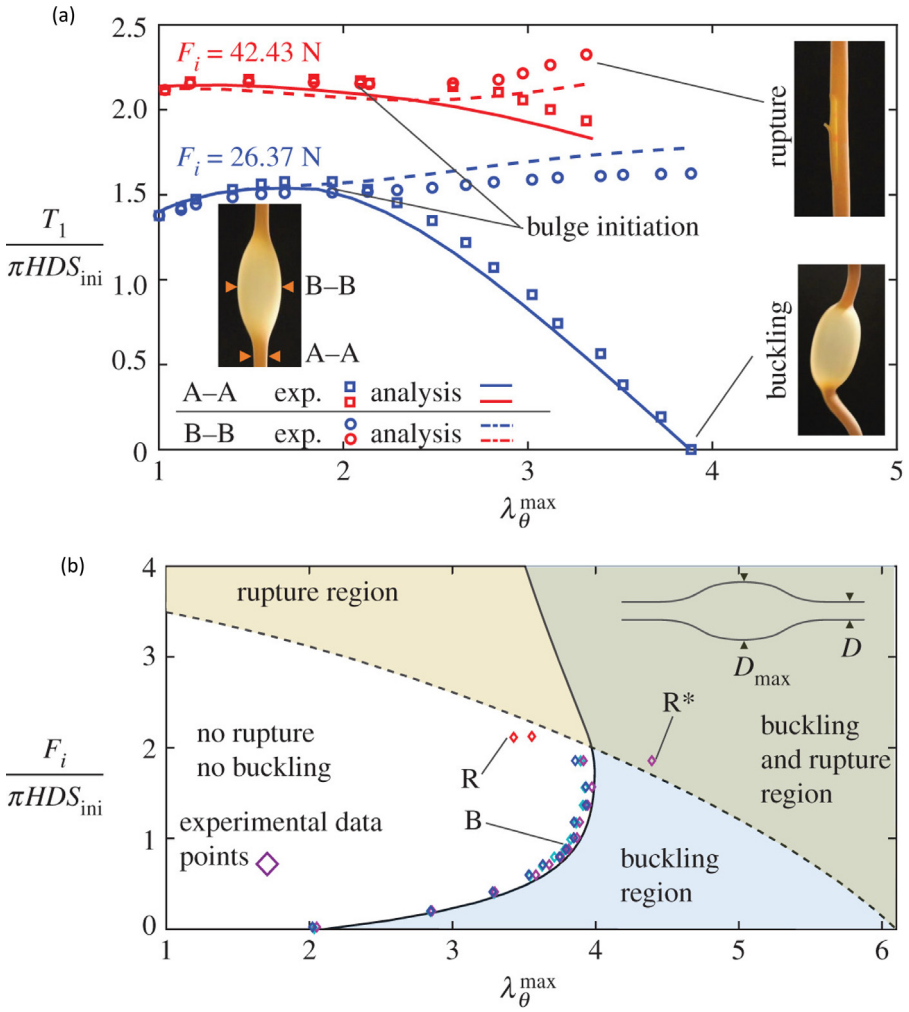

Fig. 33. The (a) tension-radial stretch graph for inflated hyperelastic tube membrane showing bulge initiation, rupture and buckling phenomena and (b) buckling-rupture failing map of the studied inflated balloon showing safety in buckling region [254].
Source: Permission obtained from Royal Society.

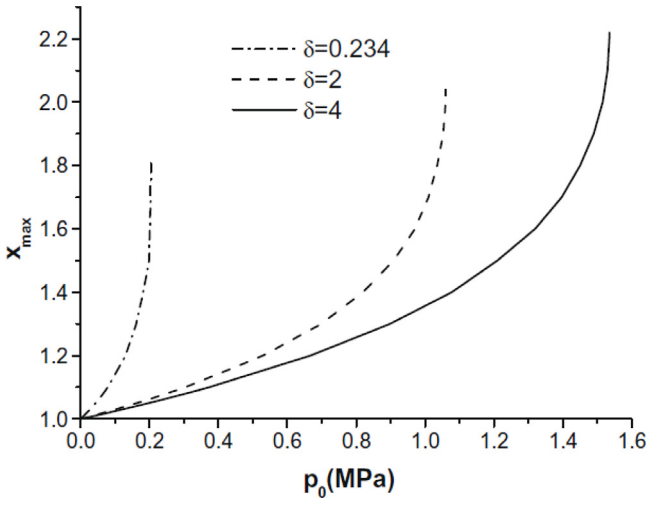

Fig. 34. Critical pressure value of inflated shells with different thicknesses [255].
Source: Permission obtained from Elsevier.

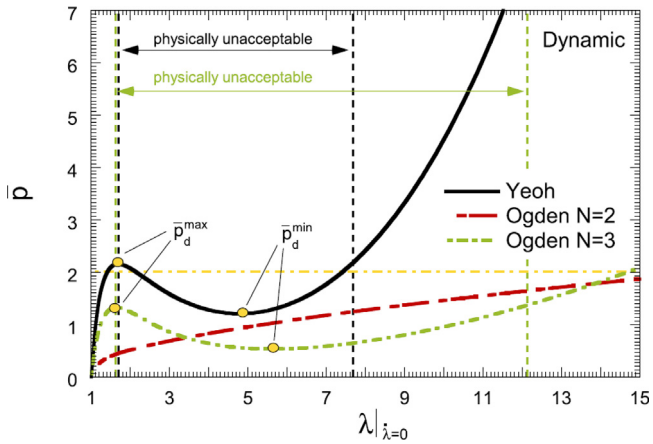

Fig. 35. Pressure–stretch (circumferential stretch) curve of inflated spherical membranes for Yeoh, two-parameter and three-parameter Ogden strain energy density models [256].
Source: Permission obtained from Elsevier.

review on the mechanics of hyperelastic structures was presented in this study. By looking at the previous studies in this field, it can be seen that different types of hyperelastic structures were analysed by researchers for both static and stability analyses. Based on the structure type, hyperelastic strain energy density models were employed in which most of the studies used the neo-Hookean strain energy density

model as it provides a simple definition of nonlinear elasticity. Since modelling hyperelastic structures requires considering both material and geometrical nonlinearities, theoretical models of such structures require considerably more time for solving compared to linear elastic structures. Most of the studies on the mechanics and biomechanics of hyperelastic structures were presented in the last few years and there is still a significant gap in comprehending their mechanical behaviour in different applications which demonstrates the importance, and demands the necessity of more research studies on this topic.

Declaration of competing interest

The authors declare that they have no known competing financial interests or personal relationships that could have appeared to influence the work reported in this paper.

Data availability

No data was used for the research described in the article.

Acknowledgements

The HDR scholarship support through The University of Adelaide and Faculty of Engineering, Computer & Mathematical Sciences, the University of Adelaide, Australia, is acknowledged.

Funding

The authors have not disclosed any funding.

References

[1] J. Bonet, A.J. Gil, R.D. Wood, Nonlinear Solid Mechanics for Finite Element Analysis: Statics, Cambridge University Press, 2016.
[2] H.B. Khaniki, M.H. Ghayesh, R. Chin, M. Amabili, A review on the nonlinear dynamics of hyperelastic structures, Nonlinear Dynam. 110 (2022) 963–994.
[3] G. Chagnon, M. Rebouah, D. Favier, Hyperelastic energy densities for soft biological tissues: a review, J. Elasticity 120 (2015) 129–160.
[4] G. Holzapfel, Nonlinear Solid Mechanics, John Wiley & Sons, Ltd, 2000.
[5] M. Amabili, Nonlinear Mechanics of Shells and Plates in Composite, Soft and Biological Materials, Cambridge University Press, 2018.
[6] T. Kaster, I. Sack, A. Samani, Measurement of the hyperelastic properties of ex vivo brain tissue slices, J. Biomech. 44 (2011) 1158–1163.
[7] R. Moran, J.H. Smith, J.J. García, Fitted hyperelastic parameters for human brain tissue from reported tension, compression, and shear tests, J. Biomech. 47 (2014) 3762–3766.
[8] L. Zhang, K.H. Yang, A.I. King, A proposed injury threshold for mild traumatic brain injury, J. Biomech. Eng. 126 (2004) 226–236.
[9] H. Mehrabian, G. Campbell, A. Samani, A constrained reconstruction technique of hyperelasticity parameters for breast cancer assessment, Phys. Med. Biol. 55 (2010) 7489.
[10] H. Mehrabian, A. Samani, An iterative hyperelastic parameters reconstruction for breast cancer assessment, in: Medical Imaging 2008: Physiology Function, and Structure from Medical Images, SPIE, 2008, pp. 426–434.
[11] S.C. Dempsey, J.J. O'Hagan, A. Samani, Measurement of the hyperelastic properties of 72 normal homogeneous and heterogeneous ex vivo breast tissue samples, J. Mech. Behav. Biomed. Mater. 124 (2021) 104794.
[12] J. Ohayon, P. Teppaz, G. Finet, G. Rioufol, In-vivo prediction of human coronary plaque rupture location using intravascular ultrasound and the finite element method, Coron. Artery Dis. 12 (2001) 655–663.
[13] M. Ahmadi, R. Ansari, Computational simulation of an artery narrowed by plaque using 3D FSI method: influence of the plaque angle, non-Newtonian properties of the blood flow and the hyperelastic artery models, Biomed. Phys. Eng. Express 5 (2019) 045037.
[14] A. Gholipour, M.H. Ghayesh, A. Zander, R. Mahajan, Three-dimensional biomechanics of coronary arteries, Internat. J. Engrg. Sci. 130 (2018) 93–114.
[15] C. Brown, T. Nguyen, H. Moody, R. Crawford, A. Oloyede, Assessment of common hyperelastic constitutive equations for describing normal and osteoarthritic articular cartilage, Proc. Inst. Mech. Eng. H 223 (2009) 643–652.
[16] C.R. Henak, C.L. Abraham, A.E. Anderson, S.A. Maas, B.J. Ellis, C.L. Peters, J.A. Weiss, Patient-specific analysis of cartilage and labrum mechanics in human hips with acetabular dysplasia, Osteoarthr. Cartil. 22 (2014) 210–217.
[17] S. Łagan, A. Liber-Kneć, The determination of mechanical properties of prosthetic liners through experimental and constitutive modelling approaches, Czasopismo Tech. 2018 (2018) 197–209.
[18] H. Mohammadi, D. Boughner, L. Millon, W. Wan, Design and simulation of a poly (vinyl alcohol)—bacterial cellulose nanocomposite mechanical aortic heart valve prosthesis, Proc. Inst. Mech. Eng. H 223 (2009) 697–711.
[19] M. Pawlikowski, K. Skalski, T. Sowiński, Hyper-elastic modelling of intervertebral disc polyurethane implant, Acta Bioeng. Biomech. 15 (2013) 43–50.
[20] M. Zidi, M. Cheref, Mechanical analysis of a prototype of small diameter vascular prosthesis: numerical simulations, Comput. Biol. Med. 33 (2003) 65–75.
[21] J. Schubert, K. Schümann, S. Kischkel, W. Schmidt, N. Grabow, M. Stiehm, S. Pfensig, K.-P. Schmitz, J. Keiler, A. Wree, Numerical simulation of the functionality of a stent structure for venous valve prostheses, Curr. Dir. Biomed. Eng. 5 (2019) 477–479.
[22] M. Zidi, M. Cheref, Finite deformations of a hyperelastic, compressible and fibre reinforced tube, Eur. J. Mech. A Solids 21 (2002) 971–980.
[23] E. Biddis, E. Bogoch, S. Meguid, Three-dimensional finite element analysis of prosthetic finger joint implants, Int. J. Mech. Mater. Des. 1 (2004) 317–328.
[24] M. Cianchetti, A. Arienti, M. Follador, B. Mazzolai, P. Dario, C. Laschi, Design concept and validation of a robotic arm inspired by the octopus, Mater. Sci. Eng. C 31 (2011) 1230–1239.
[25] S. Coyle, C. Majidi, P. LeDuc, K.J. Hsia, Bio-inspired soft robotics: Material selection, actuation, and design, Extrem. Mech. Lett. 22 (2018) 51–59.
[26] S. Campbell, The robotics revolution will be soft: soft robotics proliferate-along with their sources of inspiration, IEEE Pulse 9 (2018) 19–24.
[27] E. Guglielmino, L. Zullo, M. Cianchetti, M. Follador, D. Branson, D.G. Caldwell, The application of embodiment theory to the design and control of an octopus-like robotic arm, in: IEEE International Conference on Robotics and Automation, IEEE, 2012, pp. 5277–5282.
[28] Y. Guo, J. Guo, L. Liu, Y. Liu, J. Leng, Bioinspired multimodal soft robot driven by a single dielectric elastomer actuator and two flexible electroadhesive feet, Extrem. Mech. Lett. 53 (2022) 101720.
[29] P. Karipoth, A. Christou, A. Pullanchiyodan, R. Dahiya, Bioinspired inchworm- and earthworm-like soft robots with intrinsic strain sensing, Adv. Intell. Syst. 4 (2022) 2100092.
[30] E.B. Joyee, Y. Pan, A fully three-dimensional printed inchworm-inspired soft robot with magnetic actuation, Soft Robotics 6 (2019) 333–345.
[31] Y. Zhang, D. Yang, P. Yan, P. Zhou, J. Zou, G. Gu, Inchworm inspired multimodal soft robots with crawling, climbing, and transitioning locomotion, IEEE Trans. Robot. (2021).
[32] T. Duggan, L. Horowitz, A. Ulug, E. Baker, K. Petersen, Inchworm-inspired locomotion in untethered soft robots, in: 2nd IEEE International Conference on Soft Robotics (RoboSoft), IEEE, 2019, pp. 200–205.
[33] T.T. Hoang, J.J.S. Quek, M.T. Thai, P.T. Phan, N.H. Lovell, T.N. Do, Soft robotic fabric gripper with gecko adhesion and variable stiffness, Sensors Actuators A 323 (2021) 112673.
[34] P. Glick, S.A. Suresh, D. Ruffatto, M. Cutkosky, M.T. Tolley, A. Parness, A soft robotic gripper with gecko-inspired adhesive, IEEE Robot. Autom. Lett. 3 (2018) 903–910.
[35] M. Zhou, N. Pesika, H. Zeng, Y. Tian, J. Israelachvili, Recent advances in gecko adhesion and friction mechanisms and development of gecko-inspired dry adhesive surfaces, Friction 1 (2013) 114–129.
[36] S.R. Shin, B. Migliori, B. Miccoli, Y.C. Li, P. Mostafalu, J. Seo, S. Mandla, A. Enrico, S. Antona, R. Sabarish, Electrically driven microengineered bioinspired soft robots, Adv. Mater. 30 (2018) 1704189.
[37] T. Li, G. Li, Y. Liang, T. Cheng, J. Dai, X. Yang, B. Liu, Z. Zeng, Z. Huang, Y. Luo, Fast-moving soft electronic fish, Sci. Adv. 3 (2017) e1602045.
[38] Z. Li, R. Du, Wire-driven robot fish, in: Robot Fish, Springer, 2015, pp. 51–92.
[39] Y. Sun, S. Song, X. Liang, H. Ren, A miniature soft robotic manipulator based on novel fabrication methods, IEEE Robot. Autom. Lett. 1 (2016) 617–623.
[40] L. Lindenroth, C. Duriez, J. Back, K. Rhode, H. Liu, Intrinsic force sensing capabilities in compliant robots comprising hydraulic actuation, in: 2017 IEEE/RSJ International Conference on Intelligent Robots and Systems, IROS, IEEE, 2017, pp. 2923–2928.
[41] Y. Liu, H. Xie, H. Wang, W. Chen, J. Wang, Distance control of soft robot using proximity sensor for beating heart surgery, in: 2016 IEEE/SICE International Symposium on System Integration, SII, IEEE, 2016, pp. 403–408.
[42] H. Wang, R. Zhang, W. Chen, X. Wang, R. Pfeifer, A cable-driven soft robot surgical system for cardiothoracic endoscopic surgery: preclinical tests in animals, Surg. Laparosc. Endosc. Percutan. Tech. 31 (2017) 3152–3158.
[43] R. Stopforth, S. Davrajh, K. Althoefer, Low cost soft endoscope robotic probe, in: 2017 IEEE AFRICON, IEEE, 2017, pp. 1414–1419.
[44] B. Gorissen, M. De Volder, D. Reynaerts, Chip-on-tip endoscope incorporating a soft robotic pneumatic bending microactuator, Biomed. Microdevices 20 (2018) 1–7.
[45] Y. Muramatsu, T. Kobayashi, S. Konishi, Flexible end-effector integrated with scanning actuator and optical waveguide for endoscopic fluorescence imaging diagnosis, in: 2015 28th IEEE International Conference on Micro Electro Mechanical Systems, MEMS, IEEE, 2015, pp. 166–167.

[46] J.-E. Shim, Y.-J. Quan, W. Wang, H. Rodrigue, S.-H. Song, S.-H. Ahn, A smart soft actuator using a single shape memory alloy for twisting actuation, Smart Mater. Struct. 24 (2015) 125033.

[47] W. Hu, G.Z. Lum, M. Mastrangeli, M. Sitti, Small-scale soft-bodied robot with multimodal locomotion, Nature 554 (2018) 81–85.

[48] M. Runciman, A. Darzi, G.P. Mylonas, Soft robotics in minimally invasive surgery, Soft Robotics 6 (2019) 423–443.

[49] S. Kubota, Y. Nakata, K. Eguchi, H. Kawamoto, K. Kamibayashi, M. Sakane, Y. Sankai, N. Ochiai, Feasibility of rehabilitation training with a newly developed wearable robot for patients with limited mobility, Arch. Phys. Med. Rehabil. 94 (2013) 1080–1087.

[50] J. Sung, S. Choi, H. Kim, G. Lee, C. Han, Y. Ji, D. Shin, S. Hwang, D. Yun, H. Jang, Feasibility of rehabilitation training with a newly developed, portable, gait assistive robot for balance function in hemiplegic patients, Ann. Rehabil. Med. 41 (2017) 178–187.

[51] P. Polygerinos, Z. Wang, K.C. Galloway, R.J. Wood, C.J. Walsh, Soft robotic glove for combined assistance and at-home rehabilitation, Robot. Auton. Syst. 73 (2015) 135–143.

[52] M. Xiloyannis, D. Chiaradia, A. Frisoli, L. Masia, Physiological and kinematic effects of a soft exosuit on arm movements, J. Neuroeng. Rehabil. 16 (2019) 1–15.

[53] J. Bae, C. Siviy, M. Rouleau, N. Menard, K. O'Donnell, I. Geliana, M. Athanassiu, D. Ryan, C. Bibeau, L. Sloot, A lightweight and efficient portable soft exosuit for paretic ankle assistance in walking after stroke, in: 2018 IEEE International Conference on Robotics and Automation, ICRA, IEEE, 2018, pp. 2820–2827.

[54] E.Q. Yumbla, Z. Qiao, W. Tao, W. Zhang, Human assistance and augmentation with wearable soft robotics: a literature review and perspectives, Curr. Robotics Rep. (2021) 1–15.

[55] G. Gerboni, T. Ranzani, A. Diodato, G. Ciuti, M. Cianchetti, A. Menciassi, Modular soft mechatronic manipulator for minimally invasive surgery (MIS): overall architecture and development of a fully integrated soft module, Meccanica 50 (2015) 2865–2878.

[56] I. De Falco, M. Cianchetti, A. Menciassi, A soft multi-module manipulator with variable stiffness for minimally invasive surgery, Bioinspiration Biomim. 12 (2017) 056008.

[57] M. Cianchetti, C. Laschi, A. Menciassi, P. Dario, Biomedical applications of soft robotics, Nat. Rev. Mater. 3 (2018) 143–153.

[58] A. Mohammadi, J. Lavranos, H. Zhou, R. Mutlu, G. Alici, Y. Tan, P. Choong, D. Oetomo, A practical 3D-printed soft robotic prosthetic hand with multi-articulating capabilities, PLoS One 15 (2020) e0232766.

[59] E.T. Roche, M.A. Horvath, I. Wamala, A. Alazmani, S.-E. Song, W. Whyte, Z. Machaidze, C.J. Payne, J.C. Weaver, G. Fishbein, Soft robotic sleeve supports heart function, Sci. Transl. Med. 9 (2017) eaaf3925.

[60] M.A. Horvath, C.E. Varela, E.B. Dolan, W. Whyte, D.S. Monahan, C.J. Payne, I.A. Wamala, N.V. Vasilyev, F.A. Pigula, D.J. Mooney, Towards alternative approaches for coupling of a soft robotic sleeve to the heart, Ann. Biomed. Eng. 46 (2018) 1534–1547.

[61] C.S.X. Ng, M.W.M. Tan, C. Xu, Z. Yang, P.S. Lee, G.Z. Lum, Locomotion of miniature soft robots, Adv. Mater. 33 (2021) 2003558.

[62] J. Xiong, J. Chen, P.S. Lee, Functional fibers and fabrics for soft robotics, wearables, and human–robot interface, Adv. Mater. 33 (2021) 2002640.

[63] N. El-Atab, R.B. Mishra, F. Al-Modaf, L. Joharji, A.A. Alsharif, H. Alamoudi, M. Diaz, N. Qaiser, M.M. Hussain, Soft actuators for soft robotic applications: a review, Adv. Intell. Syst. 2 (2020) 2000128.

[64] Y.L. Yap, S.L. Sing, W.Y. Yeong, A review of 3D printing processes and materials for soft robotics, Rapid Prototyp. J. (2020).

[65] T. Ashuri, A. Armani, R. Jalilzadeh Hamidi, T. Reasnor, S. Ahmadi, K. Iqbal, Biomedical soft robots: current status and perspective, Biomed. Eng. Lett. 10 (2020) 369–385.

[66] P. Kumar, Emerging trend in manufacturing of 3D biomedical components using selective laser sintering: A review, in: E3S Web of Conferences, EDP Sciences, 2020, p. 01047.

[67] C. Majidi, Soft-matter engineering for soft robotics, Adv. Mater. Technol. 4 (2019) 1800477.

[68] A. Victor, J. Ribeiro, F.F. Araújo, Study of PDMS characterization and its applications in biomedicine: A review, J. Mech. Eng. Biomech. 4 (2019) 1–9.

[69] H. Wang, M. Totaro, L. Beccai, Toward perceptive soft robots: Progress and challenges, Adv. Sci. 5 (2018) 1800541.

[70] C.-Y. Chu, R.M. Patterson, Soft robotic devices for hand rehabilitation and assistance: a narrative review, J. Neuroeng. Rehabil. 15 (2018) 1–14.

[71] T. Wallin, J. Pikul, R. Shepherd, 3D printing of soft robotic systems, Nat. Rev. Mater. 3 (2018) 84–100.

[72] C. Lee, M. Kim, Y.J. Kim, N. Hong, S. Ryu, H.J. Kim, S. Kim, Soft robot review, Int. J. Control. Autom. Syst. 15 (2017) 3–15.

[73] P. Polygerinos, N. Correll, S.A. Morin, B. Mosadegh, C.D. Onal, K. Petersen, M. Cianchetti, M.T. Tolley, R.F. Shepherd, Soft robotics: Review of fluid-driven intrinsically soft devices; manufacturing, sensing, control, and applications in human–robot interaction, Adv. Energy Mater. 19 (2017) 1700016.

[74] S. Miao, N. Castro, M. Nowicki, L. Xia, H. Cui, X. Zhou, W. Zhu, S. j. Lee, K. Sarkar, G. Vozzi, 4D printing of polymeric materials for tissue and organ regeneration, Mater. Today 20 (2017) 577–591.

[75] D. Rus, M.T. Tolley, Design, fabrication and control of soft robots, Nature 521 (2015) 467–475.

[76] S. Kim, C. Laschi, B. Trimmer, Soft robotics: a bioinspired evolution in robotics, Trends Biotechnol. 31 (2013) 287–294.

[77] K.-J. Cho, J.-S. Koh, S. Kim, W.-S. Chu, Y. Hong, S.-H. Ahn, Review of manufacturing processes for soft biomimetic robots, Int. J. Precis. Eng. Manuf. 10 (2009) 171–181.

[78] M. Amabili, P. Balasubramanian, I. Bozzo, I.D. Breslavsky, G. Ferrari, G. Franchini, F. Giovanniello, C. Pogue, Nonlinear dynamics of human aortas for material characterization, Phys. Rev. X 10 (2020) 011015.

[79] R. Lakes, R.S. Lakes, Viscoelastic Materials, Cambridge University Press, 2009.

[80] R. Christensen, Theory of Viscoelasticity: An Introduction, Elsevier, 2012.

[81] C. Whitford, N.V. Movchan, H. Studer, A. Elsheikh, A viscoelastic anisotropic hyperelastic constitutive model of the human cornea, Biomech. Model. Mechanobiol. 17 (2018) 19–29.

[82] C. Briody, B. Duignan, S. Jerrams, J. Tiernan, The implementation of a visco-hyperelastic numerical material model for simulating the behaviour of polymer foam materials, Comput. Mater. Sci. 64 (2012) 47–51.

[83] R.W. Ogden, Non-Linear Elastic Deformations, Courier Corporation, 1997.

[84] J.L. Calvo-Gallego, J. Martínez-Reina, J. Domínguez, A polynomial hyperelastic model for the mixture of fat and glandular tissue in female breast, Int. J. Numer. Methods Biomed. Eng. 31 (2015) e02723.

[85] S. Budday, G. Sommer, C. Birkl, C. Langkammer, J. Haybaeck, J. Kohnert, M. Bauer, F. Paulsen, P. Steinmann, E. Kuhl, Mechanical characterization of human brain tissue, Acta Biomater. 48 (2017) 319–340.

[86] G.A. Holzapfel, Nonlinear solid mechanics: a continuum approach for engineering science, Meccanica 37 (2002) 489–490.

[87] R. Ogden, Large deformation isotropic elasticity—On the correlation of theory and experiment for incompressible rubberlike solids, Rubber Chem. Technol. 46 (1973) 398–416.

[88] R.W. Ogden, Large deformation isotropic elasticity–on the correlation of theory and experiment for incompressible rubberlike solids, Proc. R. Soc. Lond. Ser. A Math. Phys. Eng. Sci. 326 (1972) 565–584.

[89] A. Gent, A new constitutive relation for rubber, Rubber Chem. Technol. 69 (1996) 59–61.

[90] M. Mooney, A theory of large elastic deformation, J. Appl. Phys. 11 (1940) 582–592.

[91] R. Rivlin, Large elastic deformations of isotropic materials. I. Fundamental concepts, in: Collected Papers of RS Rivlin, Springer, 1997, pp. 23–54.

[92] H. Demiray, A note on the elasticity of soft biological tissues, J. Biomech. 5 (1972) 309–311.

[93] P. Hauseux, J.S. Hale, S. Cotin, S.P. Bordas, Quantifying the uncertainty in a hyperelastic soft tissue model with stochastic parameters, Appl. Math. Model. 62 (2018) 86–102.

[94] G.A. Holzapfel, R.W. Ogden, Constitutive modelling of passive myocardium: a structurally based framework for material characterization, Phil. Trans. R. Soc. A 367 (2009) 3445–3475.

[95] G.Z. Voyiadjis, A. Samadi-Dooki, Hyperelastic modeling of the human brain tissue: Effects of no-slip boundary condition and compressibility on the uniaxial deformation, J. Mech. Behav. Biomed. Mater. 83 (2018) 63–78.

[96] S.A. Yousefsani, A. Shamloo, F. Farahmand, Micromechanics of brain white matter tissue: A fiber-reinforced hyperelastic model using embedded element technique, J. Mech. Behav. Biomed. Mater. 80 (2018) 194–202.

[97] K.M. Labus, C.M. Puttlitz, An anisotropic hyperelastic constitutive model of brain white matter in biaxial tension and structural–mechanical relationships, J. Mech. Behav. Biomed. Mater. 62 (2016) 195–208.

[98] F. Velardi, F. Fraternali, M. Angelillo, Anisotropic constitutive equations and experimental tensile behavior of brain tissue, Biomech. Model. Mechanobiol. 5 (2006) 53–61.

[99] S. Budday, M. Sarem, L. Starck, G. Sommer, J. Pfefferle, N. Phunchago, E. Kuhl, F. Paulsen, P. Steinmann, V. Shastri, Towards microstructure-informed material models for human brain tissue, Acta Biomater. 104 (2020) 53–65.

[100] S. Budday, T.C. Ovaert, G.A. Holzapfel, P. Steinmann, E. Kuhl, Fifty shades of brain: a review on the mechanical testing and modeling of brain tissue, Arch. Comput. Methods Eng. 27 (2020) 1187–1230.

[101] G.A. Holzapfel, R.W. Ogden, Constitutive modelling of arteries, Proc. R. Soc. Lond. Ser. A Math. Phys. Eng. Sci. 466 (2010) 1551–1597.

[102] H.J. Carpenter, A. Gholipour, M.H. Ghayesh, A.C. Zander, P.J. Psaltis, A review on the biomechanics of coronary arteries, Internat. J. Engrg. Sci. 147 (2020) 103201.

[103] G.A. Holzapfel, R.W. Ogden, S. Sherifova, On fibre dispersion modelling of soft biological tissues: a review, Proc. R. Soc. Lond. Ser. A Math. Phys. Eng. Sci. 475 (2019) 20180736.

[104] G.A. Holzapfel, T.C. Gasser, R.W. Ogden, A new constitutive framework for arterial wall mechanics and a comparative study of material models, J. Elasticity Journal of Elasticity 61 (2000) 1–48.

[105] G.A. Holzapfel, G. Sommer, C.T. Gasser, P. Regitnig, Determination of layer-specific mechanical properties of human coronary arteries with nonatherosclerotic intimal thickening and related constitutive modeling, Am. J. Physiol. Circ. Physiol. 289 (2005) H2048–H2058.

[106] T.C. Gasser, R.W. Ogden, G.A. Holzapfel, Hyperelastic modelling of arterial layers with distributed collagen fibre orientations, J. R. Soc. Interface 3 (2005) 15–35.
[107] G.A. Holzapfel, J.A. Niestrawska, R.W. Ogden, A.J. Reinisch, A.J. Schriefl, Modelling non-symmetric collagen fibre dispersion in arterial walls, J. R. Soc. Interface 12 (2015) 20150188.
[108] K. Li, R.W. Ogden, G.A. Holzapfel, A discrete fibre dispersion method for excluding fibres under compression in the modelling of fibrous tissues, J. R. Soc. Interface 15 (2018) 20170766.
[109] I. Breslavsky, G. Franchini, M. Amabili, Effect of fiber exclusion in uniaxial tensile tests of soft biological tissues, J. Mech. Behav. Biomed. Mater. 112 (2020) 104079.
[110] S.G. Sassani, J. Kakisis, S. Tsangaris, D.P. Sokolis, Layer-dependent wall properties of abdominal aortic aneurysms: Experimental study and material characterization, J. Mech. Behav. Biomed. Mater. 49 (2015) 141–161.
[111] S. Baek, R.L. Gleason, K. Rajagopal, J. Humphrey, Theory of small on large: potential utility in computations of fluid–solid interactions in arteries, Comput. Methods Appl. Mech. Engrg. 196 (2007) 3070–3078.
[112] G.A. Holzapfel, R.W. Ogden, Comparison of two model frameworks for fiber dispersion in the elasticity of soft biological tissues, Eur. J. Mech. A Solids 66 (2017) 193–200.
[113] M. Amabili, P. Balasubramanian, I. Bozzo, I.D. Breslavsky, G. Ferrari, Layer-specific hyperelastic and viscoelastic characterization of human descending thoracic aortas, J. Mech. Behav. Biomed. Mater. 99 (2019) 27–46.
[114] G.A. Holzapfel, R.W. Ogden, On fiber dispersion models: exclusion of compressed fibers and spurious model comparisons, J. Elasticity 129 (2017) 49–68.
[115] T.C. Gasser, R.W. Ogden, G.A. Holzapfel, Hyperelastic modelling of arterial layers with distributed collagen fibre orientations, J. R. Soc. Interface 3 (2006) 15–35.
[116] Y. Lanir, Constitutive equations for fibrous connective tissues, J. Biomech. 16 (1983) 1–12.
[117] G.A. Holzapfel, Determination of material models for arterial walls from uniaxial extension tests and histological structure, J. Theoret. Biol. 238 (2006) 290–302.
[118] M. Jadidi, M. Habibnezhad, E. Anttila, K. Maleckis, A. Desyatova, J. MacTaggart, A. Kamenskiy, Mechanical and structural changes in human thoracic aortas with age, Acta Biomater. 103 (2020) 172–188.
[119] S. Roccabianca, C. Figueroa, G. Tellides, J.D. Humphrey, Quantification of regional differences in aortic stiffness in the aging human, J. Mech. Behav. Biomed. Mater. 29 (2014) 618–634.
[120] J.P.V. Geest, M.S. Sacks, D.A. Vorp, Age dependency of the biaxial biomechanical behavior of human abdominal aorta, J. Biomech. Eng. 126 (2004) 815–822.
[121] Y. Fung, K. Fronek, P. Patitucci, Pseudoelasticity of arteries and the choice of its mathematical expression, Am. J. Physiol. Circ. Physiol. 237 (1979) H620–H631.
[122] M. Amabili, M. Asgari, I.D. Breslavsky, G. Franchini, F. Giovanniello, G.A. Holzapfel, Microstructural and mechanical characterization of the layers of human descending thoracic aortas, Acta Biomater. 134 (2021) 401–421.
[123] I. Breslavsky, M. Amabili, Nonlinear model of human descending thoracic aortic segments with residual stresses, Biomech. Model. Mechanobiol. 17 (2018) 1839–1855.
[124] C. O. GasserT, A. HolzapfelG, Hyperelastic modelling of arterial layers with distributed collagen fibre orientations, JR Soc. Interface 3 (2006) 15–35.
[125] C. Spadaccio, F. Nappi, N. Al-Attar, F.W. Sutherland, C. Acar, A. Nenna, M. Trombetta, M. Chello, A. Rainer, Old myths, new concerns: the long-term effects of ascending aorta replacement with dacron grafts. Not all that glitters is gold, J. Cardiovasc. Transl. Res. 9 (2016) 334–342.
[126] E. Tubaldi, G. Ferrari, P. Balasubramanian, I. Breslavskyi, M. Amabili, Viscoelastic characterization of woven dacron for aortic grafts by using direction-dependent quasi-linear viscoelasticity, in: ASME International Mechanical Engineering Congress and Exposition, American Society of Mechanical Engineers, 2018, V003T004A079.
[127] G. Franchini, I.D. Breslavsky, F. Giovanniello, A. Kassab, G.A. Holzapfel, M. Amabili, Role of smooth muscle activation in the static and dynamic mechanical characterization of human aortas, Proc. Natl. Acad. Sci. 119 (2022) e2117232119.
[128] Y. Zhu, M. Yuan, H. Meng, A. Wang, Q. Guo, Y. Wang, J. Peng, Basic science and clinical application of platelet-rich plasma for cartilage defects and osteoarthritis: a review, Osteoarthr. Cartil. 21 (2013) 1627–1637.
[129] J.A. Buckwalter, H.J. Mankin, A.J. Grodzinsky, Articular cartilage and osteoarthritis, Instr. Course Lectures-American Acad. Orthop. Surg. 54 (2005) 465.
[130] L. Laver, N. Marom, L. Dnyanesh, O. Mei-Dan, J. Espregueira-Mendes, A. Gobbi, PRP for degenerative cartilage disease: a systematic review of clinical studies, Cartilage 8 (2017) 341–364.
[131] H. Lee, W.D. Campbell, M.E. Canning, K.M. Theis, H.Y. Ennis, R.L. Jackson, J.C. Wright, R.R. Hanson, Correlation between signalment and the biphasic hyperelastic mechanical properties of equine articular cartilage, Biotribology 7 (2016) 31–37.
[132] S. Federico, W. Herzog, Towards an analytical model of soft biological tissues, J. Biomech. 41 (2008) 3309–3313.
[133] S. Federico, T.C. Gasser, Nonlinear elasticity of biological tissues with statistical fibre orientation, J. R. Soc. Interface 7 (2010) 955–966.
[134] J.M. Deneweth, E.M. Arruda, S.G. McLean, Hyperelastic modeling of location-dependent human distal femoral cartilage mechanics, Int. J. Non-Linear Mech. 68 (2015) 146–156.
[135] E.M. Arruda, M.C. Boyce, A three-dimensional constitutive model for the large stretch behavior of rubber elastic materials, J. Mech. Phys. Solids 41 (1993) 389–412.
[136] J.S. Palmer, M.C. Boyce, Constitutive modeling of the stress–strain behavior of F-actin filament networks, Acta Biomater. 4 (2008) 597–612.
[137] F. MacKintosh, J. Käs, P. Janmey, Elasticity of semiflexible biopolymer networks, Phys. Rev. Lett. 75 (1995) 4425.
[138] J.M. Deneweth, S.G. McLean, E.M. Arruda, Evaluation of hyperelastic models for the non-linear and non-uniform high strain-rate mechanics of tibial cartilage, J. Biomech. 46 (2013) 1604–1610.
[139] H. Huang, W. Tang, Q. Tan, B. Yan, Development and parameter identification of a visco-hyperelastic model for the periodontal ligament, J. Mech. Behav. Biomed. Mater. 68 (2017) 210–215.
[140] D. Veronda, R. Westmann, Mechanical characterization of skin—finite deformations, J. Biomech. 3 (1970) 111–124.
[141] Y. Jiang, Y. Wang, X. Peng, A visco-hyperelastic constitutive model for human spine ligaments, Cell Biochem. Biophys. 71 (2015) 1147–1156.
[142] G. Szabo, T. Csak, Inflammasomes in liver diseases, J. Hepatol. 57 (2012) 642–654.
[143] S. Watanabe, R. Yaginuma, K. Ikejima, A. Miyazaki, Liver diseases and metabolic syndrome, J. Gastroenterol. 43 (2008) 509–518.
[144] S. Marchesseau, T. Heimann, S. Chatelin, R. Willinger, H. Delingette, Fast porous visco-hyperelastic soft tissue model for surgery simulation: application to liver surgery, Prog. Biophys. Mol. Biol. 103 (2010) 185–196.
[145] S. Madireddy, B. Sista, K. Vemaganti, Bayesian calibration of hyperelastic constitutive models of soft tissue, J. Mech. Behav. Biomed. Mater. 59 (2016) 108–127.
[146] L. Li, A. Maccabi, A. Abiri, Y.-Y. Juo, W. Zhang, Y.-J. Chang, G.N. Saddik, L. Jin, W.S. Grundfest, E.P. Dutson, Characterization of perfused and sectioned liver tissue in a full indentation cycle using a visco-hyperelastic model, J. Mech. Behav. Biomed. Mater. 90 (2019) 591–603.
[147] S.-J. Estermann, D.H. Pahr, A. Reisinger, Hyperelastic and viscoelastic characterization of hepatic tissue under uniaxial tension in time and frequency domain, J. Mech. Behav. Biomed. Mater. 112 (2020) 104038.
[148] Y. Lu, H.X. Zhu, S. Richmond, J. Middleton, A visco-hyperelastic model for skeletal muscle tissue under high strain rates, J. Biomech. 43 (2010) 2629–2632.
[149] N. Jalal, M. Zidi, Effect of cryopreservation at- 80 ° C on visco-hyperelastic properties of skeletal muscle tissue, J. Mech. Behav. Biomed. Mater. 77 (2018) 572–577.
[150] S.S. Hashemi, M. Asgari, A. Rasoulian, An experimental study of nonlinear rate-dependent behaviour of skeletal muscle to obtain passive mechanical properties, Proc. Inst. Mech. Eng. H 234 (2020) 590–602.
[151] J. Humphrey, F. Yin, On constitutive relations and finite deformations of passive cardiac tissue: I. A pseudostrain–energy function, J. Biomech. Eng. 109 (1987) 298–394.
[152] S.C. Meliga, J.W. Coffey, M.L. Crichton, C. Flaim, M. Veidt, M.A. Kendall, The hyperelastic and failure behaviors of skin in relation to the dynamic application of microscopic penetrators in a murine model, Acta Biomater. 48 (2017) 341–356.
[153] G. Limbert, Mathematical and computational modelling of skin biophysics: a review, Proc. R. Soc. A 473 (2017) 20170257.
[154] R. Reihsner, E. Menzel, On the orthogonal anisotropy of human skin as a function of anatomical region, Connective Tissue Res. 34 (1996) 145–160.
[155] R. Meijer, L. Douven, C. Oomens, Characterisation of anisotropic and non-linear behaviour of human skin in vivo, Comput. Methods Biomech. Biomed. Eng. 2 (1999) 13–27.
[156] O.A. Shergold, N.A. Fleck, D. Radford, The uniaxial stress versus strain response of pig skin and silicone rubber at low and high strain rates, Int. J. Impact Eng. 32 (2006) 1384–1402.
[157] R.B. Groves, S.A. Coulman, J.C. Birchall, S.L. Evans, An. anisotropic, Hyperelastic model for skin: experimental measurements, finite element modelling and identification of parameters for human and murine skin, J. Mech. Behav. Biomed. Mater. 18 (2013) 167–180.
[158] J.A. Weiss, B.N. Maker, S. Govindjee, Finite element implementation of incompressible, transversely isotropic hyperelasticity, Comput. Methods Appl. Mech. Engrg. 135 (1996) 107–128.
[159] D. Sutula, A. Elouneg, M. Sensale, F. Chouly, J. Chambert, A. Lejeune, D. Baroli, P. Hauseux, S. Bordas, E. Jacquet, An open source pipeline for design of experiments for hyperelastic models of the skin with applications to keloids, J. Mech. Behav. Biomed. Mater. 112 (2020) 103999.

[160] J. Chambert, T. Lihoreau, S. Joly, B. Chatelain, P. Sandoz, P. Humbert, E. Jacquet, G. Rolin, Multimodal investigation of a keloid scar by combining mechanical tests in vivo with diverse imaging techniques, J. Mech. Behav. Biomed. Mater. 99 (2019) 206–215.

[161] A. Natali, C. Fontanella, E. Carniel, Constitutive formulation and analysis of heel pad tissues mechanics, Med. Eng. Phys. 32 (2010) 516–522.

[162] V. Isvilanonda, J.M. Iaquinto, S. Pai, P. Mackenzie-Helnwein, W.R. Ledoux, Hyperelastic compressive mechanical properties of the subcalcaneal soft tissue: An inverse finite element analysis, J. Biomech. 49 (2016) 1186–1191.

[163] S. Behforootan, P.E. Chatzistergos, N. Chockalingam, R. Naemi, A clinically applicable non-invasive method to quantitatively assess the visco-hyperelastic properties of human heel pad, implications for assessing the risk of mechanical trauma, J. Mech. Behav. Biomed. Mater. 68 (2017) 287–295.

[164] S. Buchaillard, M. Brix, P. Perrier, Y. Payan, Simulations of the consequences of tongue surgery on tongue mobility: implications for speech production in post-surgery conditions, Int. J. Med. Robotics Comput. Assist. Surg. 3 (2007) 252–261.

[165] J.-M. Gérard, R. Wilhelms-Tricarico, P. Perrier, Y. Payan, A 3D dynamical biomechanical tongue model to study speech motor control, 2006, arXiv preprint physics/0606148.

[166] C. Jiang, C. Luo, J. Yu, R. Li, Z. Wang, Modeling a realistic 3D physiological tongue for visual speech synthesis, in: 2014 IEEE International Conference on Multimedia and Expo Workshops, ICMEW, IEEE, 2014, pp. 1–6.

[167] N. Koike, S. Ii, T. Yoshinaga, K. Nozaki, S. Wada, Model-based inverse estimation for active contraction stresses of tongue muscles using 3D surface shape in speech production, J. Biomech. 64 (2017) 69–76.

[168] A.-A.K. Yousefi, M.A. Nazari, P. Perrier, M.S. Panahi, Y. Payan, A visco-hyperelastic constitutive model and its application in bovine tongue tissue, J. Biomech. 71 (2018) 190–198.

[169] A. Vogel, L. Rakotomanana, D.P. Pioletti, Viscohyperelastic Strain Energy Function, in: Biomechanics of Living Organs, Elsevier, 2017, pp. 59–78.

[170] J.-M. Gérard, J. Ohayon, V. Luboz, P. Perrier, Y. Payan, Non-linear elastic properties of the lingual and facial tissues assessed by indentation technique: Application to the biomechanics of speech production, Med. Eng. Phys. 27 (2005) 884–892.

[171] T. Ou, D. Wang, C. He, Research on mechanical properties of the tongue muscle with a new composite constitutive model validated by experiments, Int. J. Clin. Exp. Med. 14 (2021) 2483–2495.

[172] E. Omidi, L. Fuetterer, S.R. Mousavi, R.C. Armstrong, L.E. Flynn, A. Samani, Characterization and assessment of hyperelastic and elastic properties of decellularized human adipose tissues, J. Biomech. 47 (2014) 3657–3663.

[173] Z. Sun, B.D. Gepner, S.-H. Lee, J. Rigby, P.S. Cottler, J.J. Hallman, J.R. Kerrigan, Multidirectional mechanical properties and constitutive modeling of human adipose tissue under dynamic loading, Acta Biomater. (2021).

[174] N.K. Pallegar, S.L. Christian, Adipocytes in the tumour microenvironment, Tumor Microenviron. (2020) 1–13.

[175] V. D'Esposito, M.R. Ambrosio, M. Giuliano, S. Cabaro, C. Miele, F. Beguinot, P. Formisano, Mammary adipose tissue control of breast cancer progression: Impact of obesity and diabetes, Front. Oncol. 10 (2020) 1554.

[176] M. Lu, J. Qiu, G. Wang, X. Dai, Mechanical analysis of breast–bra interaction for sports bra design, Mater. Today Commun. 6 (2016) 28–36.

[177] Y. Sun, K. l. Yick, W. Yu, L. Chen, N. Lau, W. Jiao, S. Zhang, 3D bra and human interactive modeling using finite element method for bra design, Comput. Aided Des. 114 (2019) 13–27.

[178] D.J. Gavaghan, J.P. Whiteley, S.J. Chapman, J.M. Brady, P. Pathmanathan, Predicting tumor location by modeling the deformation of the breast, IEEE Trans. Biomed. Eng. 55 (2008) 2471–2480.

[179] A. Samani, D. Plewes, An inverse problem solution for measuring the elastic modulus of intact ex vivo breast tissue tumours, Phys. Med. Biol. 52 (2007) 1247.

[180] J.J. O'Hagan, A. Samani, Measurement of the hyperelastic properties of 44 pathological ex vivo breast tissue samples, Phys. Med. Biol. 54 (2009) 2557.

[181] S. Ügdüler, K.M. Van Geem, R. Denolf, M. Roosen, N. Mys, K. Ragaert, S. De Meester, Towards closed-loop recycling of multilayer and coloured PET plastic waste by alkaline hydrolysis, Green Chem. 22 (2020) 5376–5394.

[182] M. Schulze, F. Schröter, M. Jung, U. Jakop, Evaluation of a panel of spermatological methods for assessing reprotoxic compounds in multilayer semen plastic bags, Sci. Rep. 10 (2020) 1–11.

[183] M.J.G. Ramos, A. Lozano, A.R. Fernández-Alba, High-resolution mass spectrometry with data independent acquisition for the comprehensive non-targeted analysis of migrating chemicals coming from multilayer plastic packaging materials used for fruit purée and juice, Talanta 191 (2019) 180–192.

[184] T.W. Walker, N. Frelka, Z. Shen, A.K. Chew, J. Banick, S. Grey, M.S. Kim, J.A. Dumesic, R.C. Van Lehn, G.W. Huber, Recycling of multilayer plastic packaging materials by solvent-targeted recovery and precipitation, Sci. Adv. 6 (2020) eaba7599.

[185] P.-T. Pham, K.-S. Hong, Dynamic models of axially moving systems: A review, Nonlinear Dynam. 100 (2020) 315–349.

[186] L.-Q. Chen, Y.-Q. Tang, C.W. Lim, Dynamic stability in parametric resonance of axially accelerating viscoelastic Timoshenko beams, J. Sound Vib. 329 (2010) 547–565.

[187] C. De Marco, C.C. Alcântara, S. Kim, F. Briatico, A. Kadioglu, G. de Bernardis, X. Chen, C. Marano, B.J. Nelson, S. Pané, Indirect 3D and 4D printing of soft robotic microstructures, Adv. Mater. Technol. 4 (2019) 1900332.

[188] Y. Yang, Y. Zhang, Z. Kan, J. Zeng, M.Y. Wang, Hybrid jamming for bioinspired soft robotic fingers, Soft Robotics 7 (2020) 292–308.

[189] J.-H. Lee, Y.S. Chung, H. Rodrigue, Long shape memory alloy tendon-based soft robotic actuators and implementation as a soft gripper, Sci. Rep. 9 (2019) 1–12.

[190] X. Ji, X. Liu, V. Cacucciolo, M. Imboden, Y. Civet, A. El Haitami, S. Cantin, Y. Perriard, H. Shea, An autonomous untethered fast soft robotic insect driven by low-voltage dielectric elastomer actuators, Science Robotics 4 (2019) eaaz6451.

[191] H. Irschik, J. Gerstmayr, A hyperelastic Reissner-type model for non-linear shear deformable beams, Proc. Mathmod. 9 (2009) 1–7.

[192] H. Irschik, J. Gerstmayr, A continuum-mechanics interpretation of Reissner's non-linear shear-deformable beam theory, Math. Comput. Model. Dyn. Syst. 17 (2011) 19–29.

[193] J.C. Simo, T.J. Hughes, Computational Inelasticity, Springer Science & Business Media, 2006.

[194] E. Reissner, On one-dimensional finite-strain beam theory: the plane problem, Z. Angew. Math. Phys. 23 (1972) 795–804.

[195] S. Sheikhi, M. Shojaeifard, M. Baghani, Finite bending and straightening of hyperelastic materials: Analytical solution and FEM, Int. J. Appl. Mech. 11 (2019) 1950084.

[196] M. Bacciocchi, A.M. Tarantino, Bending of hyperelastic beams made of transversely isotropic material in finite elasticity, Appl. Math. Model. 100 (2021) 55–76.

[197] J. Merodio, R. Ogden, Mechanical response of fiber-reinforced incompressible non-linearly elastic solids, Int. J. Non-Linear Mech. 40 (2005) 213–227.

[198] A. Zdunek, W. Rachowicz, A mixed higher order FEM for fully coupled compressible transversely isotropic finite hyperelasticity, Comput. Math. Appl. 74 (2017) 1727–1750.

[199] M. Bacciocchi, A.M. Tarantino, Finite anticlastic bending of hyperelastic laminated beams with a rubberlike core, Mech. Adv. Mater. Struct. (2021) 1–24.

[200] F. Jiang, W. Yu, Nonlinear variational asymptotic sectional analysis of hyperelastic beams, AIAA J. 54 (2015) 679–690.

[201] L. Lanzoni, A.M. Tarantino, Finite anticlastic bending of hyperelastic solids and beams, J. Elasticity 131 (2018) 137–170.

[202] L. Lanzoni, A.M. Tarantino, Nonuniform bending theory of hyperelastic beams in finite elasticity, Int. J. Non-Linear Mech. 135 (2021) 103765.

[203] P. Martins, R. Natal Jorge, A. Ferreira, A comparative study of several material models for prediction of hyperelastic properties: Application to silicone-rubber and soft tissues, Strain 42 (2006) 135–147.

[204] M. Shojaeifard, S. Sheikhi, M. Baniassadi, M. Baghani, On finite bending of visco-hyperelastic materials: A novel analytical solution and FEM, Acta Mech. 231 (2020) 3435–3450.

[205] C. Li, J. Lua, A hyper-viscoelastic constitutive model for polyurea, Mater. Lett. 63 (2009) 877–880.

[206] F. Oyedeji Falope, L. Lanzoni, A.M. Tarantino, FE analyses of hyperelastic solids under large bending: The role of the searle parameter and eulerian slenderness, Materials 13 (2020) 1597.

[207] L. He, J. Lou, Y. Dong, S. Kitipornchai, J. Yang, Variational modeling of plane-strain hyperelastic thin beams with thickness-stretching effect, Acta Mech. 229 (2018) 4845–4861.

[208] X. Zhu, Y. Wang, Z. Lou, A study of the critical strain of hyperelastic materials: A new kinematic frame and the leading order term, Mech. Res. Commun. 78 (2016) 20–24.

[209] A.M. Waas, Initial postbuckling behavior of shear deformable symmetrically laminated beams, Int. J. Non-Linear Mech. 27 (1992) 817–832.

[210] A.M. Waas, Initial postbuckling behavior of beams on non-linear elastic foundations, 1990.

[211] H.-H. Dai, Y. Wang, F.-F. Wang, Primary and secondary bifurcations of a compressible hyperelastic layer: Asymptotic model equations and solutions, Int. J. Non-Linear Mech. 52 (2013) 58–72.

[212] H. Mylapilli, F.E. Udwadia, Control of three-dimensional incompressible hyperelastic beams, Nonlinear Dynam. 90 (2017) 115–135.

[213] I.D. Breslavsky, M. Amabili, M. Legrand, F. Alijani, Axisymmetric deformations of circular rings made of linear and Neo-Hookean materials under internal and external pressure: A benchmark for finite element codes, Int. J. Non-Linear Mech. 84 (2016) 39–45.

[214] R. Wang, W. z. Zhang, Z. t. Zhao, H. w. Zhang, X. g. Yuan, Radially and axially symmetric motions of a class of transversely isotropic compressible hyperelastic cylindrical tubes, Nonlinear Dynam. 90 (2017) 2481–2494.

[215] L. He, J. Lou, J. Chen, A. Zhang, J. Yang, An adhesion model for plane-strain shearable hyperelastic beams, Mech. Res. Commun. 90 (2018) 42–46.

[216] T. Kocaturk, S. Akbas, Geometrically non-linear static analysis of a simply supported beam made of hyperelastic material, Struct. Eng. Mech. 35 (2010) 677–697.

[217] G. Orzechowski, J. Frączek, Nearly incompressible nonlinear material models in the large deformation analysis of beams using ANCF, Nonlinear Dynam. 82 (2015) 451–464.

[218] R.D. Rabbitt, J.A. Weiss, G.E. Christensen, M.I. Miller, Mapping of hyperelastic deformable templates using the finite element method, Int. Soc. Opt. Photonics 2573 (1995) 252–265.
[219] F. Jiang, W. Yu, Non-linear Sectional Analysis of Composite Beams with Finite Deformation and Hyperelastic Materials, in: 56th AIAA/ASCE/AHS/ASC Structures, Structural Dynamics, and Materials Conference, 2015, p. 0691.
[220] V.M. Nguyen-Thanh, X. Zhuang, T. Rabczuk, A deep energy method for finite deformation hyperelasticity, Eur. J. Mech. A Solids (2019) 103874.
[221] A. Selvadurai, A. Suvorov, Coupled hydro-mechanical effects in a poro-hyperelastic material, J. Mech. Phys. Solids 91 (2016) 311–333.
[222] M. Zhu, Y. Liu, C. Qu, On the model of the compressible hyperelastic rods and Euler equations on the circle, J. Differential Equations 254 (2013) 648–659.
[223] A. Damanpack, M. Bodaghi, W. Liao, A robust hyper-elastic beam model under bi-axial normal-shear loadings, Int. J. Non-Linear Mech. 95 (2017) 287–295.
[224] L. He, J. Lou, S. Kitipornchai, J. Yang, J. Du, Peeling mechanics of hyperelastic beams: Bending effect, Int. J. Solids Struct. 167 (2019) 184–191.
[225] Y. Liu, Axial and circumferential buckling of a hyperelastic tube under restricted compression, Int. J. Non-Linear Mech. 98 (2018) 145–153.
[226] V. Slesarenko, S. Rudykh, Microscopic and macroscopic instabilities in hyperelastic fiber composites, J. Mech. Phys. Solids 99 (2017) 471–482.
[227] N. Arora, A. Batan, J. Li, V. Slesarenko, S. Rudykh, On the influence of inhomogeneous interphase layers on instabilities in hyperelastic composites, Materials 12 (2019) 763.
[228] S.F. E.I., S. Adhikari, M. Friswell, F. Scarpa, Hyperelastic modelling of post-buckling response in single wall carbon nanotubes under axial compression, Procedia Eng. 10 (2011) 2256–2261.
[229] Y. Chen, L. Jin, Snapping-back buckling of wide hyperelastic columns, Extrem. Mech. Lett. (2019) 100600.
[230] Y. Chen, L. Jin, Reusable energy-absorbing architected materials harnessing snapping-back buckling of wide hyperelastic columns, Adv. Funct. Mater. 31 (2021) 2102113.
[231] M.M. Attard, G.W. Hunt, Column buckling with shear deformations—a hyperelastic formulation, Int. J. Solids Struct. 45 (2008) 4322–4339.
[232] M.M. Attard, M.-Y. Kim, Lateral buckling of beams with shear deformations–A hyperelastic formulation, Int. J. Solids Struct. 47 (2010) 2825–2840.
[233] M.M. Attard, G.W. Hunt, Sandwich column buckling–A hyperelastic formulation, Int. J. Solids Struct. 45 (2008) 5540–5555.
[234] D.C. Pamplona, H.I. Weber, G.R. Sampaio, Analytical, numerical and experimental analysis of continuous indentation of a flat hyperelastic circular membrane by a rigid cylindrical indenter, Int. J. Mech. Sci. 87 (2014) 18–25.
[235] A. Selvadurai, Deflections of a rubber membrane, J. Mech. Phys. Solids 54 (2006) 1093–1119.
[236] A. Selvadurai, M. Shi, Fluid pressure loading of a hyperelastic membrane, Int. J. Non-Linear Mech. 47 (2012) 228–239.
[237] D. Pamplona, P. Goncalves, S. Lopes, Finite deformations of cylindrical membrane under internal pressure, Int. J. Mech. Sci. 48 (2006) 683–696.
[238] A. Patil, A. DasGupta, Finite inflation of an initially stretched hyperelastic circular membrane, Eur. J. Mech. A Solids 41 (2013) 28–36.
[239] J. Kiendl, M.-C. Hsu, M.C. Wu, A. Reali, Isogeometric Kirchhoff–Love shell formulations for general hyperelastic materials, Comput. Methods Appl. Mech. Engrg. 291 (2015) 280–303.
[240] Y. Anani, G.H. Rahimi, Field equations and general solution for axisymmetric thick shell composed of functionally graded incompressible hyperelastic materials, Int. J. Mech. Sci. 144 (2018) 919–928.
[241] Y. Anani, G.H. Rahimi, Stress analysis of rotating cylindrical shell composed of functionally graded incompressible hyperelastic materials, Int. J. Mech. Sci. 108 (2016) 122–128.
[242] R. Hassani, R. Ansari, H. Rouhi, Large deformation analysis of 2D hyperelastic bodies based on the compressible nonlinear elasticity: A numerical variational method, Int. J. Non-Linear Mech. 116 (2019) 39–54.
[243] C. Fu, T. Wang, F. Xu, Y. Huo, M. Potier-Ferry, A modeling and resolution framework for wrinkling in hyperelastic sheets at finite membrane strain, J. Mech. Phys. Solids 124 (2019) 446–470.
[244] J.P. Pascon, Large deformation analysis of functionally graded visco-hyperelastic materials, Comput. Struct. 206 (2018) 90–108.
[245] D. Niu, X. Yuan, C. Cheng, J. Ren, Dynamic characteristics in incompressible hyperelastic cylindrical membranes, Acta Mech. Solida Sin. 23 (2010) 420–427.
[246] Y. Basar, Y. Ding, Finite-element analysis of hyperelastic thin shells with large strains, Comput. Mech. 18 (1996) 200–214.
[247] R. Mangan, M. Destrade, Gent models for the inflation of spherical balloons, Int. J. Non-Linear Mech. 68 (2015) 52–58.
[248] N. Kumar, A. DasGupta, On the contact problem of an inflated spherical hyperelastic membrane, Int. J. Non-Linear Mech. 57 (2013) 130–139.
[249] C. Zhang, J. Wu, K.-C. Hwang, Y. Huang, Postbuckling of hyperelastic plates, J. Appl. Mech. 83 (2016) 051012.
[250] A. Diaby, C. Wielgosz, Buckling and wrinkling of prestressed membranes, Finite Elem. Anal. Des. 42 (2006) 992–1001.
[251] F. Xu, Y. Koutsawa, M. Potier-Ferry, S. Belouettar, Instabilities in thin films on hyperelastic substrates by 3D finite elements, Int. J. Solids Struct. 69 (2015) 71–85.
[252] A. Anssari-Benam, A. Bucchi, G. Saccomandi, Modelling the inflation and elastic instabilities of rubber-like spherical and cylindrical shells using a new generalised neo-Hookean strain energy function, J. Elasticity (2021) 1–31.
[253] V. Nayyar, K. Ravi-Chandar, R. Huang, Stretch-induced stress patterns and wrinkles in hyperelastic thin sheets, Int. J. Solids Struct. 48 (2011) 3471–3483.
[254] M. Hejazi, Y. Hsiang, A. Srikantha Phani, Fate of a bulge in an inflated hyperelastic tube: theory and experiment, Proc. R. Soc. Lond. Ser. A Math. Phys. Eng. Sci. 477 (2021) 20200837.
[255] R. Jiusheng, Dynamics and destruction of internally pressurized incompressible hyper-elastic spherical shells, Internat. J. Engrg. Sci. 47 (2009) 745–753.
[256] J.A. Rodríguez-Martínez, J. Fernández-Sáez, R. Zaera, The role of constitutive relation in the stability of hyper-elastic spherical membranes subjected to dynamic inflation, Internat. J. Engrg. Sci. 93 (2015) 31–45.
[257] F.A. Duck, Physical Properties of Tissues: A Comprehensive Reference Book, Academic Press, 2013.

2.2 A review on the nonlinear dynamics of hyperelastic structures

Overview

This section of Chapter 2 presents a comprehensive literature review of the nonlinear dynamics of hyperelastic structures. Previous studies of hyperelastic structures are classified based on the timeline, showing significant growth and the importance of undertaking this review. A brief explanation of some well-known isotropic hyperelastic strain energy formulations is given, showing the sensitivity of each model in predicting hyperelastic behaviour. A detailed analysis of the nonlinear dynamics of polymeric structures is presented afterwards, showing the current state of research in this field. This literature review is published and available online as: Khaniki, H.B., Ghayesh, M.H., Chin, R. & Amabili, M., (2022). A review on the nonlinear dynamics of hyperelastic structures. Nonlinear Dynamics, 110, 963–994.

Statement of Authorship

Title of Paper	A review on the nonlinear dynamics of hyperelastic structures
Publication Status	☑ Published ☐ Accepted for Publication ☐ Submitted for Publication ☐ Unpublished and Unsubmitted w ork w ritten in manuscript style
Publication Details	Khaniki, H. B., Ghayesh, M. H., Chin, R., & Amabili, M. (2022). A review on the nonlinear dynamics of hyperelastic structures. Nonlinear Dynamics, 110, 963–994.

Principal Author

Name of Principal Author (Candidate)	Hossein Bakhshi Khaniki		
Contribution to the Paper	I carried out the literature search, formal analysis and wrote the manuscript.		
Overall percentage (%)	80%		
Certification:	This paper reports on original research I conducted during the period of my Higher Degree by Research candidature and is not subject to any obligations or contractual agreements with a third party that would constrain its inclusion in this thesis. I am the primary author of this paper.		
Signature		Date	2/11/2022

Co-Author Contributions

By signing the Statement of Authorship, each author certifies that:

i. the candidate's stated contribution to the publication is accurate (as detailed above);

ii. permission is granted for the candidate in include the publication in the thesis; and

iii. the sum of all co-author contributions is equal to 100% less the candidate's stated contribution.

Name of Co-Author	Mergen Ghayesh		
Contribution to the Paper	As the principal supervisor, I helped to construct the manuscript, edit and review the manuscript for submission. I hereby give consent to Hossein Bakhshi Khaniki to present this paper for examination towards the degree of Doctor of Philosophy.		
Signature		Date	3/11/2022

Name of Co-Author	Rey Chin		
Contribution to the Paper	I assisted in the revision and editing of the manuscript. I hereby give consent to Hossein Bakhshi Khaniki to present this paper for examination towards the degree of Doctor of Philosophy.		
Signature		Date	3/11/2022

Name of Co-Author	Marco Amabili
Contribution to the Paper	I assisted in the construction of the manuscript. I also edited and reviewed the manuscript. I hereby give consent to Hossein Bakhshi Khaniki to present this paper for examination towards the degree of Doctor of Philosophy.
Signature	Date 7/11/2022

Nonlinear Dyn (2022) 110:963–994
https://doi.org/10.1007/s11071-022-07700-3

REVIEW

A review on the nonlinear dynamics of hyperelastic structures

Hossein B. Khaniki · Mergen H. Ghayesh · Rey Chin · Marco Amabili

Received: 19 March 2022 / Accepted: 11 July 2022 / Published online: 5 August 2022

Abstract This paper presents a critical review of the nonlinear dynamics of hyperelastic structures. Hyperelastic structures often undergo large strains when subjected to external time-dependent forces. Hyperelasticity requires specific constitutive laws to describe the mechanical properties of different materials, which are characterised by a nonlinear relationship between stress and strain. Due to recent recognition of the high potential of hyperelastic structures in soft robots and other applications, and the capability of hyperelasticity to model soft biological tissues, the number of studies on hyperelastic structures and materials has grown significantly. Thus, a comprehensive explanation of hyperelastic constitutive laws is presented, and different techniques of continuum mechanics, which are suitable to model these materials, are discussed in this literature review. Furthermore, the sensitivity of each hyperelastic strain energy density function to coefficient variation is shown for some well-known hyperelastic models. Alongside this, the application of hyperelasticity to model the nonlinear dynamics of polymeric structures (e.g., beams, plates, shells, membranes and balloons) is discussed in detail with the assistance of previous studies in this field. The advantages and disadvantages of hyperelastic models are discussed in detail. This present review can stimulate the development of more accurate and reliable models.

Keywords Nonlinear dynamics · Hyperelasticity · Hyperelastic beams · Hyperelastic plates · Hyperelastic shells · Nonlinear elasticity

H. B. Khaniki (✉) · M. H. Ghayesh (✉) · R. Chin
School of Mechanical Engineering, University of Adelaide, Adelaide, South Australia 5005, Australia
e-mail: hossein.bakhshikhaniki@adelaide.edu.au

M. H. Ghayesh
e-mail: mergen.ghayesh@adelaide.edu.au

R. Chin
e-mail: rey.chin@adelaide.edu.au

M. Amabili
Department of Mechanical Engineering, McGill University, 817 Sherbrooke Street West, Montreal H3A 0C3, Canada
e-mail: marco.amabili@mcgill.ca

1 Introduction

Hyperelastic structures often undergo large strains when subjected to external forces. The stress–strain relation in such structures is highly complicated, making the linear stress–strain relationship and linear elastic models invalid for simulating their mechanical behaviour. The hyperelastic behaviour can be seen in different soft structures such as rubbers, foams and human body organs. Along with understanding the characteristics of such structures, having accurate modelling of hyperelastic structures could also

provide us with further potential applications in different fields.

1.1 Necessity for this review

By analysing the available database in Scopus on *hyperelasticity*, the significance of the dialogue between scientists and researchers on this topic was obtained. Figure 1a demonstrates the number of published works on *hyperelasticity* from 1990 to 2020. It can be seen that, during this period, the number of published papers on this subject has increased noticeably, reaching more than 1100 research studies published in 2020 alone.

Moreover, analysing the mechanical behaviours (bending, buckling and vibration) of hyperelastic structures (e.g. beams, plates, shells and membranes) shows the same incremental trend indicated in Fig. 1b; from which it can be seen that many studies on hyperelasticity are focused on the mechanics of such structures. The phenomenal growth of studies on this subject clarifies the importance of having a systematic literature review to summarise the achievements to date on this topic.

1.2 Applications of hyperelastic structures

In general, soft structures present hyperelastic behaviours while confronting different conditions. One of the main applications of hyperelastic structures is soft robotics [1–3]; since soft structures can provide higher-order degrees of freedom, movement in robotic

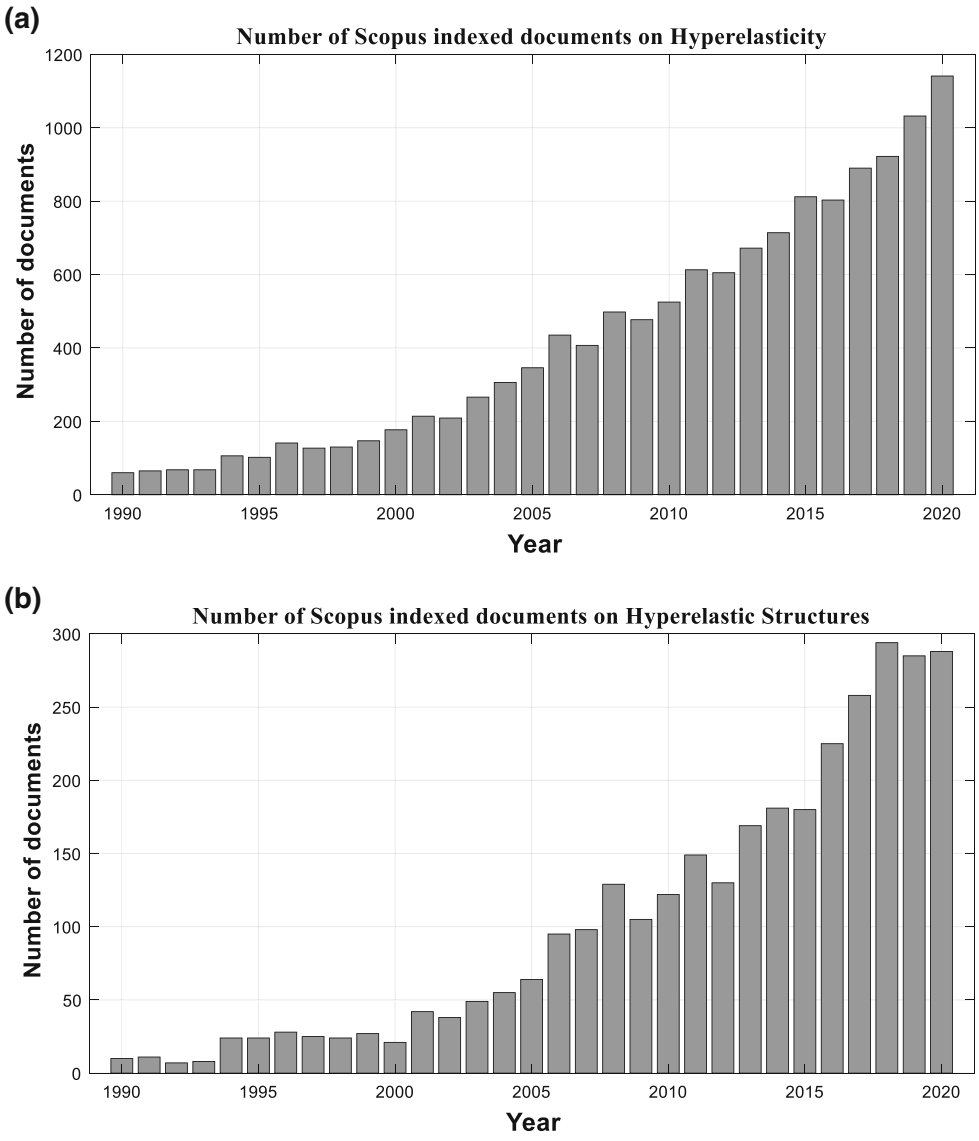

Fig. 1 Tables for the number of documents from 1990 to 2020 on (**a**) hyperelasticity and (**b**) hyperelastic beams, plates and shells

parts could potentially become more smooth than when using rigid and/or firm structures.

Robotic rehabilitation systems for stroke patients can be significantly improved by using soft robotic as they can provide a smooth motion with a safer operation [4]. For instance, soft robotic gloves are capable of helping patients with muscular dystrophy, amyotrophic lateral sclerosis or post-stroke hand function assistance [5–8]. In the work presented by Polygerinos et al. [4], a soft robotic glove is presented to study the hand and fingers' joint motion. In their model, the different mechanical behaviours of bending, twisting and extensions of soft beam-shaped structures were obtained.

Developing soft structures to explore unknown environments is another important application of hyperelastic structures as it can tolerate different types of loadings and impacts. In a study done by Antol et al. [9], it is shown that expensive wheel rovers can be replaced with tumbleweed rovers for Mars exploration. In another study, Trivedi et al. [10] used hyperelastic tubes for soft robotic modelling of Oct-Arm.

Besides, soft robots made of hyperelastic materials have been used for sensing and monitoring environments. For example, a dragonfly-inspired soft robot (DraBot) has been fabricated for measuring the contaminants (such as the presence of oil), pH, and temperature of water surfaces [11–13].

The application of hyperelastic structures in soft robotics has reached a turning point with the capability of 3D printing and the utilisation of soft actuators [14–16]. Hyperelastic structures also have other types of applications, of which some of the main ones are wearable devices [17], stretchable electronics [17], biomedical engineering [17], and energy harvesters [18, 19].

Figure 2 presents a simple robot that is capable of crawling using twisted and coiled actuators [20]. This simple model has been fabricated using hyperelastic beams, and the smooth motion of the robot was obtained by bending. Figure 3 also presents some useful examples of soft structures as actuators in soft robotics, which can be used for grabbing, twisting, motion, lifting and other purposes [15].

Another application of soft structures can be found in belt operating systems. Belt conveyor systems are mainly used for power transmission from the driving

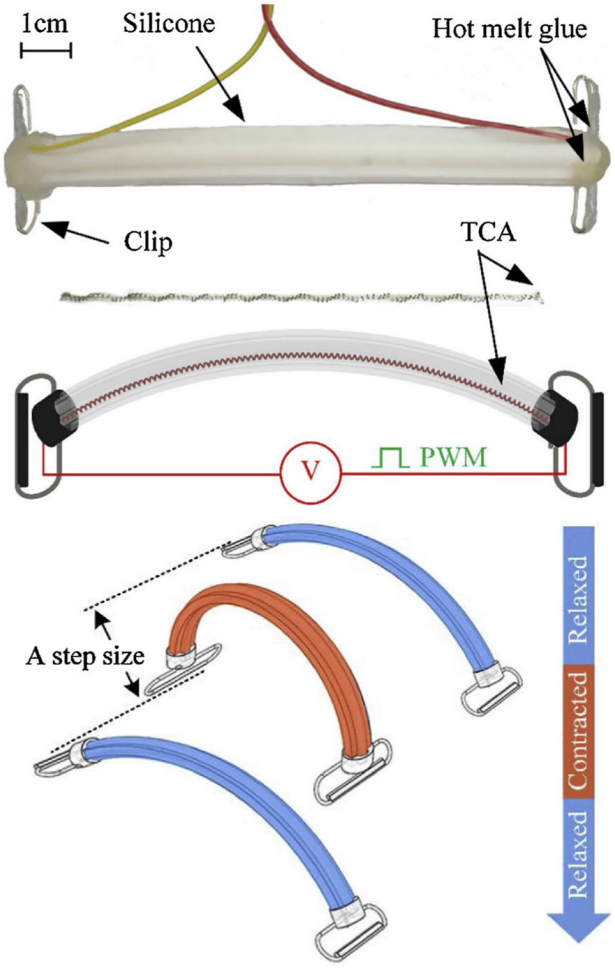

Fig. 2 Schematic view of a crawling robot using soft structures [20]. (Permission obtained from Elsevier)

pulley to the driver one in different engineering fields [21–23].

Layered hyperelastic structures have been used for packaging, especially food industry, as a soft safe layer is required for inside and a stiffer layer for outside. The proper design and material usage are of high importance as the packaging is around 15% of the total variable costs [24, 25]. Waste management and environmentally friendly (biodegradable) packaging [26–28] are also important topics making the discussion of using proper hyperelastic materials for packaging an ongoing novel research topic.

Since human body organs show nonlinear elastic behaviour, researchers have worked on fabricating prosthetics with similar hyperelastic behaviour. Using hyperelastic structures for firstly modelling the human body organs and secondly accurately designing

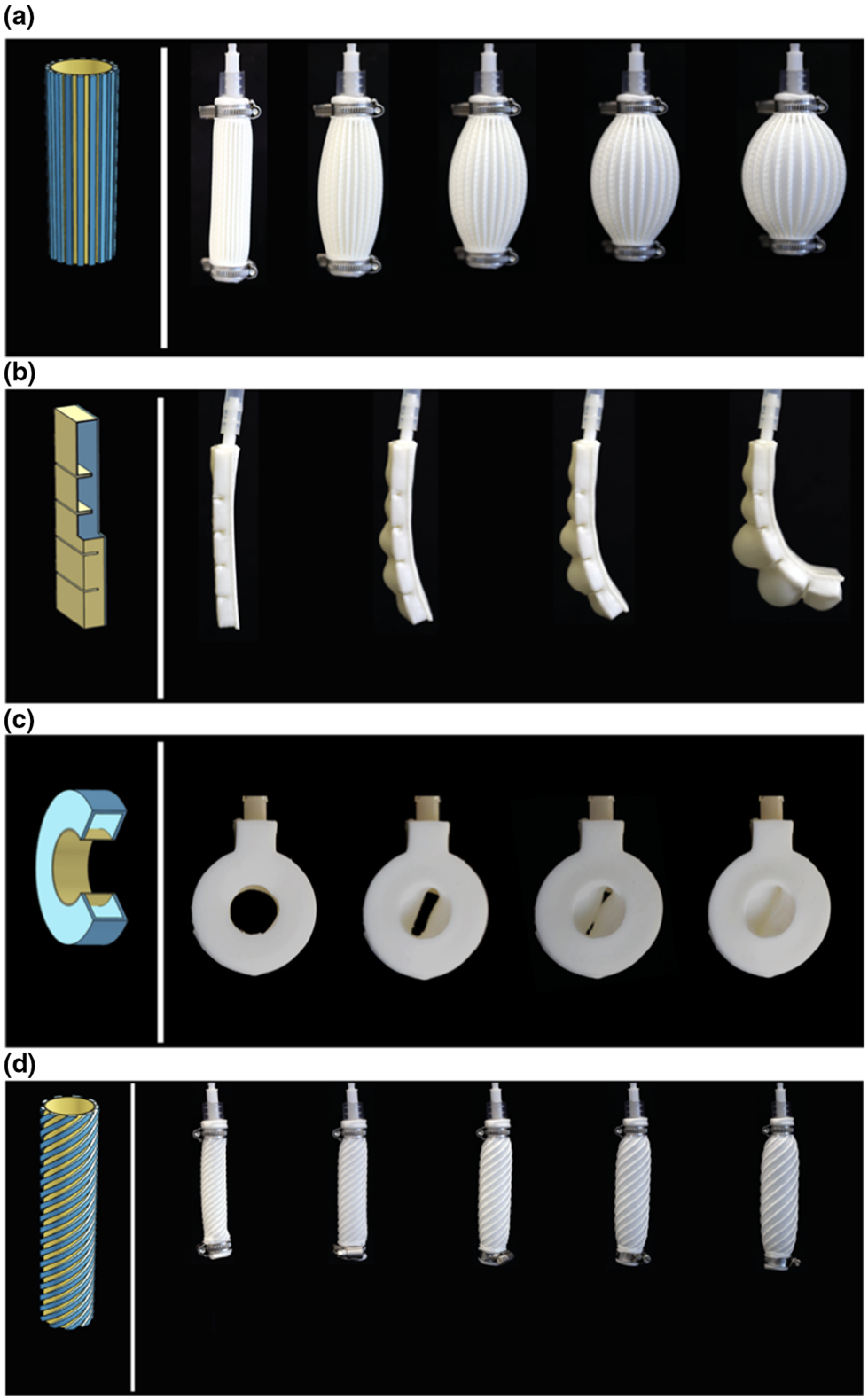

Fig. 3 Actuators made of soft structures with different purposes: **a** contractor; **b** bender; **c** grabber; **d** twister [15]. (This article is an open access article distributed under the terms and conditions of the Creative Commons Attribution (CC BY) license (https://creativecommons.org/licenses/by/4.0/).)

prosthetics have been a novel topic for researchers to invest [29–32].

1.3 Contribution of this paper to the field

The importance of modelling hyperelastic structures accurately has been discussed in the previous subsections. It is shown that there has been a considerable number of researches on hyperelasticity with promising, growing trends over the past few years. The demonstration of the high application potential of these structures in the early years of their development and their future in engineering design [14, 15, 20, 33, 34] emphasises the necessity of having a systematic literature review through the need for categorisation, discussion and explanation of the achievements to date. Accordingly, this review intends to clarify the achievements and goals of this research field by analysing diverse critical hyperelastic studies in the framework of nonlinear dynamics.

1.4 Structure of this review paper

To present a comprehensive investigation on hyperelastic structures, this review is structured in the following order: as shown in the flowchart of Fig. 4, in Sect. 1, a brief introduction to hyperelastic structures is given, indicating the importance of understanding the hyperelastic mechanical behaviour, emphasizing the application's potential and the future of hyperelastic structures, and lastly, demonstrating the contribution of this review to this field. In Sect. 2, some well-known constitutive hyperelastic models for isotropic soft materials are discussed in detail by presenting the fundamental continuum mechanics formulation and definitions related to hyperelastic behaviour. Some of the well-known techniques and models in continuum mechanics are then provided, followed by the sensitivity of the model in tracking hyperelastic behaviour. In Sect. 3, the application of the given and other hyperelastic continuum models on obtaining the nonlinear dynamics of hyperelastic beam structures is discussed. Section 4 concentrates on analysing hyperelastic plate and shell structures in

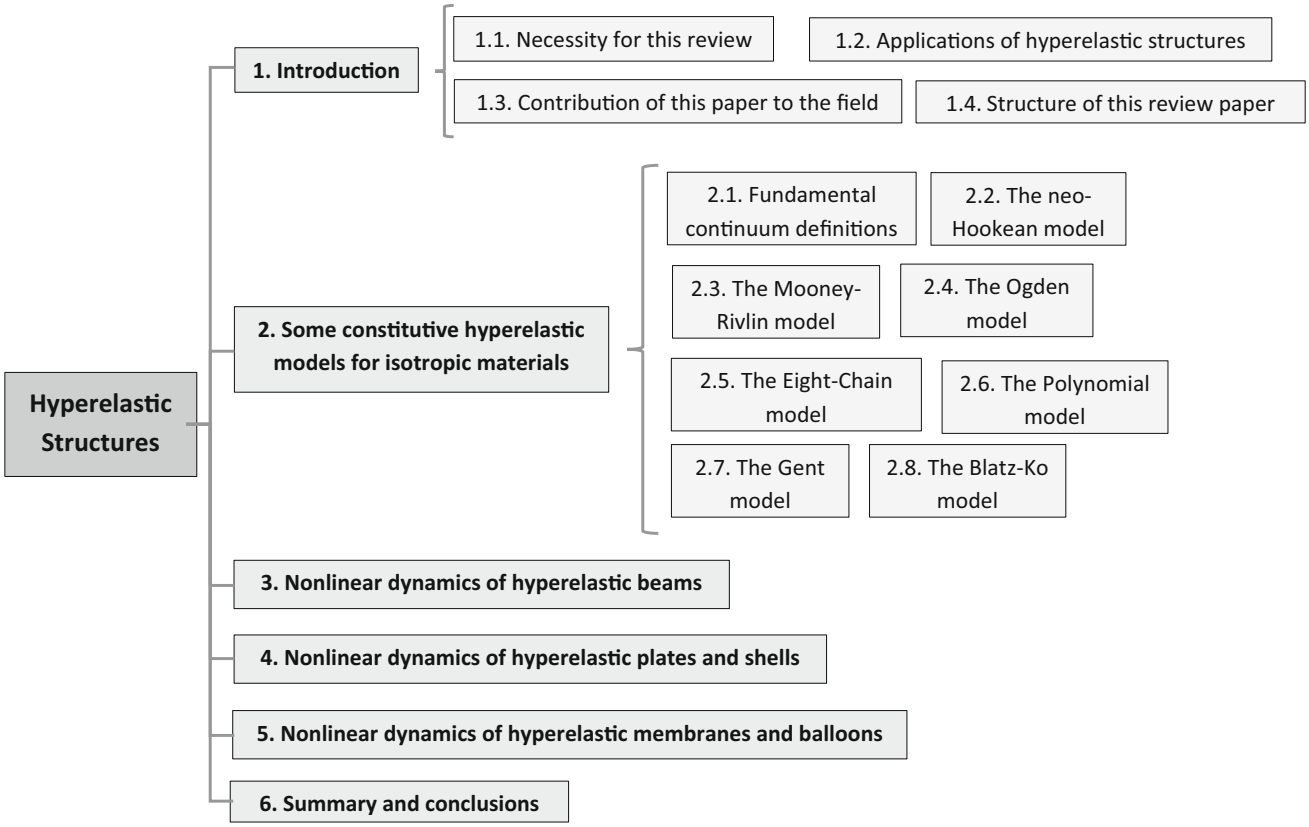

Fig. 4 Flowchart of the structure of this review

the framework of nonlinear dynamics. Different plate and shell theories together with hyperelastic constitutive models are discussed for accurately modelling the nonlinear dynamics of soft plate and shell structures. Section 5 presents a detailed explanation on hyperelastic models and nonlinear dynamics of soft membranes and balloons using different continuum mechanics models. Lastly, in Sect. 6, a comprehensive summary of the analysis performed through this paper is provided, and the achievements and possible potential for improving the modelling of such structures are presented.

2 Some constitutive hyperelastic models for isotropic materials

2.1 Fundamental continuum definitions

In order to define the mechanical characteristics of hyperelastic structures, there are key continuum mechanics definitions that must be presented. In general, the deformation gradient (F) is defined as [35]:

$$\begin{cases} F_{ij} = \delta_{ij} + \dfrac{\partial u_i}{\partial x_j}, \\ J = \det(F), \end{cases} \tag{1}$$

with J is the determinant of the deformation gradient, δ is the Kronecker delta and u_i is the displacement field, which could be rewritten in the principal directions of the structures as [36]:

$$F = \begin{bmatrix} \lambda_1 & 0 & 0 \\ 0 & \lambda_2 & 0 \\ 0 & 0 & \lambda_3 \end{bmatrix} \quad \rightarrow \quad F_{ij} = \delta_{ij}\lambda_i, \tag{2}$$

where λ_i indicates the principal stretch through the principal direction i, defined as

$$\lambda_i = \frac{L_i}{L_i^0}, \tag{3}$$

with L_i and $L_i.^0$ are the deformed and undeformed lengths of the structure through the i direction, respectively. Another important definition in describing hyperelastic structures is the left Cauchy–Green strain tensor (B) which is [36]

$$B = F \cdot F^T \quad \rightarrow \quad B_{ij} = F_{ik}F_{jk} \tag{4}$$

For conventional definitions, the left Cauchy–Green strain tensor's invariants are defined as [37]:

$$\begin{aligned} I_1 &= \frac{Tr(B)}{J^{\frac{2}{3}}} = \frac{B_{ii}}{J^{\frac{2}{3}}}, \\ I_2 &= \frac{1}{2}\left(I_1^2 - \frac{B_{ij}B_{ji}}{J^{\frac{4}{3}}}\right), \\ I_3 &= J^2, \end{aligned} \tag{5}$$

where I_1, I_2 and I_3 are the first, second and third strain invariants for compressible structures, respectively; for incompressible analysis, the first and second invariants will be simplified by having $J = 1$ and the third invariant will be equal to 1 (interested readers are referred to Refs. [38–40] for more information regarding compressible and incompressible materials). The Green–Lagrange strain–displacement can be written regarding the deformation gradient as:

$$E = \frac{1}{2}\left(F^T F - I\right) \rightarrow \; E_{ij} = \frac{1}{2}\left(F_{pi}F_{pj} - \delta_{ij}\right). \tag{6}$$

In the case of having principal stretches, invariants of the left Cauchy–Green strain tensor are:

$$\begin{aligned} I_1 &= \frac{\lambda_1^2 + \lambda_2^2 + \lambda_3^2}{\left(\lambda_1\lambda_2\lambda_3\right)^{\frac{2}{3}}}, \\ I_2 &= \frac{\lambda_1^2\lambda_2^2 + \lambda_1^2\lambda_3^2 + \lambda_2^2\lambda_3^2}{\left(\lambda_1\lambda_2\lambda_3\right)^{\frac{4}{3}}}, \\ I_3 &= \left(\lambda_1\lambda_2\lambda_3\right)^2. \end{aligned} \tag{7}$$

As for the hyperelasticity definition, a structure is hyperelastic if specific strain energy exists which is differentiable from the deformation gradient. In other words, to have a fully elastic behaviour, it is assumed that the strain energy density is directly dependent on the deformation gradient tensor. In another definition, it has been shown that a hyperelastic structure is isotropic if and only if the strain energy term can be rewritten via the three invariants of the left Cauchy–Green strain tensor [41].

According to Richter theorem [41, 42], the constitutive equation of an isotropic solid hyperelastic can be written as:

$$T = \beta_0 I + \beta_1 B + \beta_2 B^2, \tag{8}$$

if and only if the coefficients are defined following a specific relationship defined in the literature. It has been shown that [42], by having an isothermic process,

changes in $-T_0 dS$ (in which T_0 is the absolute temperature and S is the entropy) to become equal to the variation of the Helmholtz free energy. In case of isothermic process, coefficients in Eq. (8) are expressed by Eq. (9) as

$$\begin{aligned}\beta_0 &= \frac{\partial W}{\partial I_1} + I_1 \frac{\partial W}{\partial I_2} + I_2 \frac{\partial W}{\partial I_3},\\ \beta_1 &= -\frac{\partial W}{\partial I_2} - I_1 \frac{\partial W}{\partial I_3},\\ \beta_2 &= \frac{\partial W}{\partial I_3}.\end{aligned} \tag{9}$$

For a simple definition, by having the principal direction stretches, the normal stresses (σ_i) can be defined as [43]:

$$\sigma_i = \frac{\partial W}{\partial \lambda_i}, \quad i = 1,2,3 \tag{10}$$

after which, due to the definition of hyperelastic strain energy (W) being a function of its invariants, Eq. (10) can be rewritten as:

$$\frac{\partial W}{\partial \lambda_i} = \frac{\partial W}{\partial I_3}\frac{\partial I_3}{\partial \lambda_i} + \frac{\partial W}{\partial I_2}\frac{\partial I_2}{\partial \lambda_i} + \frac{\partial W}{\partial I_1}\frac{\partial I_1}{\partial \lambda_i}, \quad i = 1,2,3 \tag{11}$$

which for incompressible structures, the third term (derivation with respect to I_3) will be neglected. Different types of formulation and modelling for hyperelastic strain energy density have been presented in order to predict the nonlinear behaviour accurately. In further subsections, these isotropic models are presented and the formulation procedure for reaching the stress–strain equation is given. These models are used by many researchers to study the nonlinear dynamics of hyperelastic structures which is discussed in further sections.

2.2 The neo-Hookean model

This strain energy density expression is one of the straightforward models of a hyperelastic material in which we only consider the first and third invariant terms as

$$W_{NH} = \sum_{i=0}^{n} C_i \left(\overline{I_1} - 3\right)^i + D_1 (J-1)^2, \tag{12}$$

where W_{NH} is the strain energy density of this model, C_i are the coefficients of the first invariant parameter and D_1 is the compressibility factor, both of which must be obtained experimentally. For $n = 1$ (one-term neo-Hookean model), the axial stress (σ_{uni}) is written as [43]:

$$\begin{aligned}\sigma_{uni} = {} & C_1 \frac{4(1+\nu)}{3} \lambda_1^{-(5+2\nu)/3} \left(\lambda_1^{2+2\nu} - 1\right)\\ & + 2D_1(1-2\nu)\lambda_1^{-2\nu}(J-1),\end{aligned} \tag{13}$$

where ν is the Poisson's ratio. By assuming an incompressible structure, Eq. (13) is simplified as:

$$\sigma_{uni} = 2C_1\left(\lambda - \lambda^{-2}\right), \tag{14}$$

and for equibiaxial (σ_{bi}) stress and pure shear (σ_s) stress, by using the same definition given in Eq. (12), the stress resultants become

$$\sigma_{bi} = 2C_1\left(\lambda - \lambda^{-5}\right), \tag{15}$$

$$\sigma_s = 2C_1\left(\lambda - \lambda^{-3}\right), \tag{16}$$

which coincides with those used in ref [44].

2.3 The Mooney–Rivlin model

One of the popular formulations and models used for predicting the hyperelastic behaviour of structures is the Mooney–Rivlin model [45], which is an extended form of the neo-Hookean model, considering the second invariant term. In the basic form, Mooney defined the strain energy density as a two-parameter model defined as:

$$W_M = C_1\left(\overline{I_1} - 3\right) + C_2\left(\overline{I_2} - 3\right) + D_1(J-1)^2, \tag{17}$$

where W_M is the strain energy density of the two-parameter Mooney model and C_i and D_1 are the coefficients that must be found via the experimental observations (such as the work done by Falope et al. [46] where the coefficients were calibrated using genetic algorithm), which can vary from one soft structure to another. Rivlin [47, 48] extended this equation by writing it in a general form as a polynomial series of the first and second invariant terms:

$$W_{MR} = \sum_{i=0}^{n}\sum_{j=0}^{m} C_{ij}\left(\overline{I_1} - 3\right)^i \left(\overline{I_2} - 3\right)^j + D_1(J-1)^2, \tag{18}$$

where W_{MR} is the strain energy density of the Mooney–Rivlin model, of which some of the well-known models and special cases of this polynomial series are the Biderman model [49], Klosner model [50] and Haines–Wilson model [51]. It has been mentioned already that this model has been widely used for analysing rubbers with less than 200% deformation [52].

For the two-parameter Mooney–Rivlin model under axial load, by having $\lambda_2 = \lambda_3 = \lambda_1^{-v}$, Brown et al. [43] obtained the axial stress as:

$$\sigma_{uni} = \frac{4(1+v)}{3}\lambda_1^{-(5+2v)/3}\left(\lambda_1^{2+2v}-1\right)\left(C_1 + C_2\lambda_1^{-2(1+v)/3}\right) + 2D_1(1-2v)\lambda_1^{-2v}(J-1), \tag{19}$$

from which, by assuming an incompressible structure, Eq. (19) becomes

$$\sigma_{uni} = 2C_1\left(\lambda - \lambda^{-2}\right) + 2C_2\left(1-\lambda^{-3}\right), \tag{20}$$

and for equibiaxial and pure shear stresses, by using the same definition given in Eq. (18), the stress resultants are:

$$\sigma_{bi} = 2C_1\left(\lambda - \lambda^{-5}\right) + 2C_2\left(\lambda^3 - \lambda^{-3}\right), \tag{21}$$

$$\sigma_s = (2C_1 + 2C_2)\left(\lambda - \lambda^{-3}\right), \tag{22}$$

which coincides with those used in ref [44]. To have a better understanding of the Mooney–Rivlin model, the effect of the coefficients C_1 and C_2 on the uniaxial stress is presented in Fig. 5 for axial strain up to 100%. It can be seen that the stress–strain behaviour is completely nonlinear and the curve model is highly sensitive to the two-parameter Mooney–Rivlin coefficients. By having [37] $C_1 = 0.39$ MPa and $C_2 = 0.015$ MPa, in Fig. 5a, the first coefficient term is varied as $[0.5C_1–1.5C_1]$, while in Fig. 5b the second coefficient is varied as $[0.5C_2–5.5C_2]$. Since the formulation of a neo-Hookean model is somewhat similar to the Mooney–Rivlin hyperelastic model (by neglecting the second invariant term), the influence of varying the hyperelastic coefficient C_1 in one-term neo-Hookean models will be very similar to the one presented in Fig. 5a.

2.4 The Ogden model

Ogden [53, 54] proposed a series of models of strain energy density as a direct function of principal stretches

$$W_{Og} = \sum_{i=1}^{n}\frac{2\mu_i}{\alpha_i^2}\left(\lambda_1^{\alpha_i} + \lambda_2^{\alpha_i} + \lambda_3^{\alpha_i} - 3\right) + \sum_{i=1}^{n} D_i(J-1)^{2i} \tag{23}$$

where W_{Og} is the strain energy density of the Ogden model and μ_i, D_i and α_i are the constant properties that must be found using experimental testing. This model is well capable of simulating the typical hardening of rubber materials, which is not included in both neo-

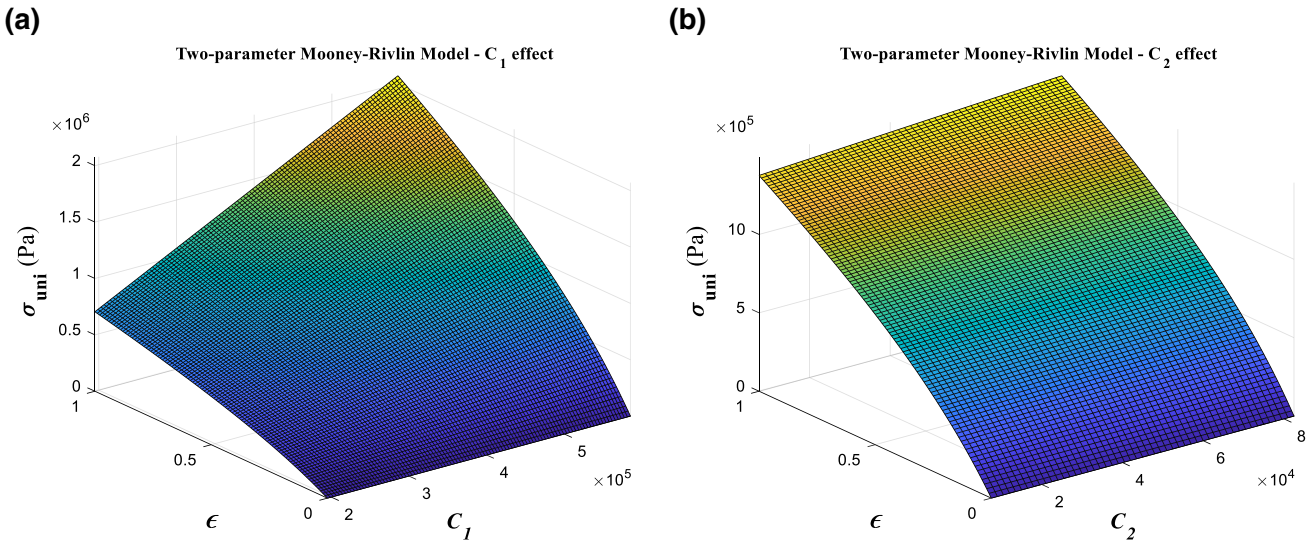

Fig. 5 Uniaxial stress sensitivity to the *two-parameter Mooney–Rivlin* coefficients: **a** C_1; **b** C_2

Hookean and Mooney–Rivlin models. Brown et al. [43] have shown the uniaxial stress for this model to be:

$$\sigma_{uni} = \sum_{i=1}^{n} \frac{2\mu_i}{\alpha_i}\left(\lambda^{\alpha_i - 1} - 2\nu\lambda^{-\alpha_i \nu - 1}\right) + 2\left(1 - 2\nu\lambda^{-2\nu}\right)\sum_{i=1}^{n} iD_i(J-1)^{2i-1} \tag{24}$$

which can be rewritten for incompressible structures as

$$\sigma_{uni} = \sum_{i=1}^{n} \frac{2\mu_i}{\alpha_i^2}\left(\lambda^{\alpha_i - 1} - \lambda^{-\frac{\alpha_i}{2} - 1}\right). \tag{25}$$

Similarly, the equibiaxial and pure shear stresses are:

$$\sigma_{bi} = \sum_{i=1}^{n} \frac{2\mu_i}{\alpha_i^2}\left(\lambda^{\alpha_i - 1} - \lambda^{-2\alpha_i - 1}\right), \tag{26}$$

$$\sigma_s = \sum_{i=1}^{n} \frac{2\mu_i}{\alpha_i^2}\left(\lambda^{\alpha_i - 1} - \lambda^{-\alpha_i - 1}\right). \tag{27}$$

In order to elaborate the impact of each coefficient term on the stress–strain behaviour of Ogden hyperelastic models, uniaxial loading of a three-parameter Ogden model is considered with coefficients and power terms as [37], where $\mu_1 = 0.62$ MPa, $\mu_2 = 0.00118$ MPa, $\mu_3 = 0.00981$ MPa, $\alpha_1 = 1.3$, $\alpha_2 = 5$ and $\alpha_3 = -2$. Figures 6a–f indicate the strong effect of varying three-parameter Ogden model coefficients and power terms by [0.5 μ_1–1.5 μ_1], [0.5α_1–1.5α_1], [0.5μ_2–50.5μ_2], [0.5 α_2–15.5α_2], [0.5μ_3–5.5μ_3] and [0.5α_3–15.5α_3], respectively. It can be seen that each parameter has its own effect on the axial stress magnitude through which, by properly accounting for these terms, the hyperelastic behaviour of rubbery structures can be obtained.

2.5 The eight-chain (Arruda–Boyce) model

Arruda and Boyce [55] proposed the eight-chain model in which the strain energy is described as a function of a polynomial series of the first invariant as

$$W_{AB} = \sum_{i=1}^{n} C_i\left(\overline{I_1^i} - 3^i\right) + \sum_{i=1}^{n} D_i(J-1)^{2i}, \tag{28}$$

where W_{AB} is the strain energy density of the Arruda–Boyce model, for which, under uniaxial loading, the stress-stretch equation will become [43]

$$\sigma_{uni} = \frac{4(1+\nu)}{3}\sum_{i=1}^{n} iC_i\left(\overline{I_1^{i-1}}\right)\lambda^{-(5+2\nu)/3}\left(\lambda^{2+2\nu} - 1\right) + 2(1-2\nu)\sum_{i=1}^{n} iD_i(J-1)^{2i-1}\lambda^{-2\nu}, \tag{29}$$

which for incompressible structures it is simplified as

$$\sigma_{uni} = 2\sum_{i=1}^{n} iC_i\left(\overline{I_1^{i-1}}\right)\left(\lambda - \lambda^{-2}\right), \tag{30}$$

with equibiaxial and pure shear stresses as

$$\sigma_{bi} = 2\sum_{i=1}^{n} iC_i\left(\overline{I_1^{i-1}}\right)\left(\lambda - \lambda^{-5}\right), \tag{31}$$

$$\sigma_s = 2\sum_{i=1}^{n} iC_i\left(\overline{I_1^{i-1}}\right)\left(\lambda - \lambda^{-3}\right). \tag{32}$$

For analysing the coefficient sensitivity of this model, a five-parameter Arruda–Boyce model is considered by having [56] $C_1 = \mu/2$, $C_2 = \mu/20$, $C_3 = 11\mu/1050$, $C_4 = 19\mu/7000$, $C_5 = 519\mu/673750$ where μ is the rubbery shear modulus assumed to be 0.4 MPa. The influence of each coefficient on the uniaxial stress variation can be seen in Fig. 7a–f by varying [0.5μ–1.5μ], [0.5C_1–1.5C_1], [0.5C_2–2C_2], [0.5C_3–2.5C_3], [0.5C_4–5C_4], and [0.5C_5–5C_5], respectively. Here, all the coefficients have a considerable effect on the uniaxial stress term.

2.6 The polynomial model

The strain energy in the polynomial rubber model is defined as [57]

$$W_{Po} = \sum_{i+j=1}^{n} C_{ij}\left(\overline{I_1} - 3\right)^i\left(\overline{I_2} - 3\right)^j + \sum_{i=1}^{n} D_i(J-1)^{2i}, \tag{33}$$

where W_{Po} is the strain energy density of polynomial model, which can also be written as [43]

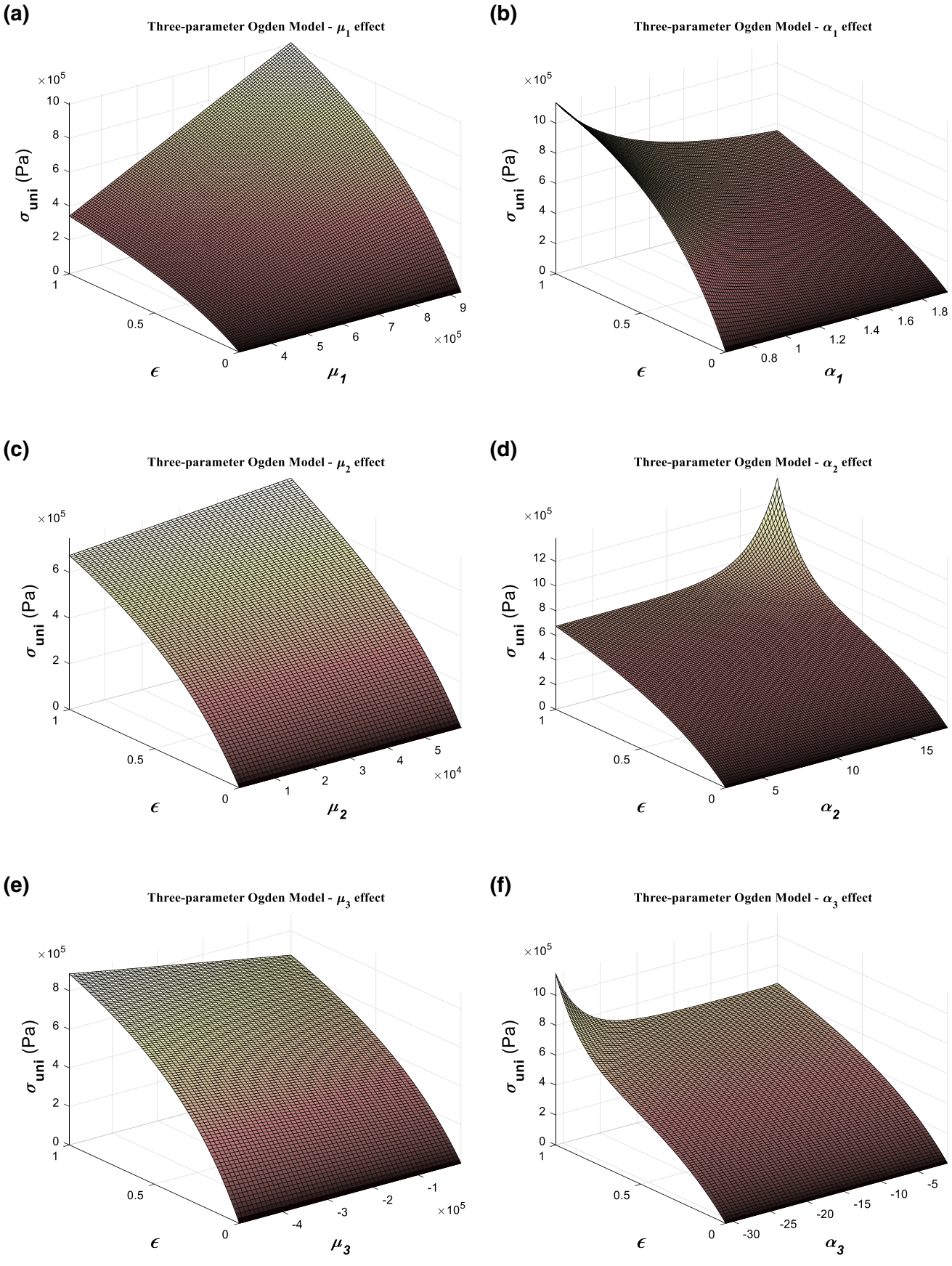
(a)
Three-parameter Ogden Model - μ_1 effect
σ_{uni} (Pa)
ϵ
μ_1
(b)
Three-parameter Ogden Model - α_1 effect
σ_{uni} (Pa)
ϵ
α_1
(c)
Three-parameter Ogden Model - μ_2 effect
σ_{uni} (Pa)
ϵ
μ_2
(d)
Three-parameter Ogden Model - α_2 effect
σ_{uni} (Pa)
ϵ
α_2
(e)
Three-parameter Ogden Model - μ_3 effect
σ_{uni} (Pa)
ϵ
μ_3
(f)
Three-parameter Ogden Model - α_3 effect
σ_{uni} (Pa)
ϵ
α_3

◀**Fig. 6** Uniaxial stress sensitivity to the *three-parameter Ogden* coefficients and power terms: **a** μ_1; **b** α_1; **c** μ_2; **d** α_2; **e** μ_3; **f** α_3

$$W_{Po} = \sum_{i=0}^{n}\sum_{j=1-i}^{n-i} C_{ij}\left(\overline{I}_1 - 3\right)^i\left(\overline{I}_2 - 3\right)^j + \sum_{i=1}^{n} D_i(J-1)^{2i}, \tag{34}$$

leading to an axial stress–stretch relationship as [43]

$$\sigma_{uni} = \frac{4(1+\nu)}{3}\lambda^{-(5+2\nu)/3}\left(\lambda^{2+2\nu}-1\right)\left[\begin{array}{l}\sum_{i=0}^{n}\sum_{j=1-i}^{n-i} iC_{ij}\left(\overline{I}_1-3\right)^{i-1}\left(\overline{I}_2-3\right)^j \\ +\lambda^{-(2+2\nu)/3}\sum_{i=0}^{n}\sum_{j=1-i}^{n-i} jC_{ij}\left(\overline{I}_1-3\right)^i\left(\overline{I}_2-3\right)^{j-1}\end{array}\right] + 2(1-2\nu)\sum_{i=1}^{n} iD_i(J-1)^{2i-1}\lambda^{-2\nu}, \tag{35}$$

which, for incompressible structures using Eq. (33), is rewritten as

$$\sigma_{uni} = 2\sum_{i=0}^{n}\sum_{j=1-i}^{n-i} iC_{ij}\left(\overline{I}_1-3\right)^{i-1}\left(\overline{I}_2-3\right)^j\left(\lambda-\lambda^{-2}\right) + 2\sum_{i=0}^{n}\sum_{j=1-i}^{n-i} jC_{ij}\left(\overline{I}_1-3\right)^i\left(\overline{I}_2-3\right)^{j-1}\left(1-\lambda^{-3}\right), \tag{36}$$

and for equibiaxial and pure shear stresses as

$$\sigma_{bi} = 2\sum_{i=0}^{n}\sum_{j=1-i}^{n-i} iC_{ij}\left(\overline{I}_1-3\right)^{i-1}\left(\overline{I}_2-3\right)^j\left(\lambda-\lambda^5\right) + 2\sum_{i=0}^{n}\sum_{j=1-i}^{n-i} jC_{ij}\left(\overline{I}_1-3\right)^i\left(\overline{I}_2-3\right)^{j-1}\left(\lambda^3-\lambda^{-3}\right), \tag{37}$$

$$\sigma_s = 2\left(\lambda-\lambda^{-3}\right)\left[\begin{array}{l}\sum_{i=0}^{n}\sum_{j=1-i}^{n-i} iC_{ij}\left(\overline{I}_1-3\right)^{i-1}\left(\overline{I}_2-3\right)^j \\ +\sum_{i=0}^{n}\sum_{j=1-i}^{n-i} jC_{ij}\left(\overline{I}_1-3\right)^i\left(\overline{I}_2-3\right)^{j-1}\end{array}\right]. \tag{38}$$

Similar to the previous subsections, by assuming the coefficients to be $C_{10} = 1.44$ MPa, $C_{01} = 0.463$ MPa, $C_{11} = -0.029$ MPa, $C_{20} = -0.151$ MPa, and $C_{02} = -0.0042$ MPa, Fig. 8a–f present the influence of varying the coefficients of the five-parameter polynomial model on the axial stress for strains up to 100%. Coefficients are assumed to vary as $[0.5C_{10}$–$1.5C_{10}]$, $[0.5C_{01}$–$1.5C_{01}]$, $[0.5C_{11}$–$1.5C_{11}]$, $[0.5C_{20}$–$1.5C_{20}]$ and $[0.5C_{20}$–$3C_{02}]$, respectively.

2.7 The Gent model

Gent [57, 58] proposed a simple model of hyperelasticity using the first invariant parameter:

$$W_G = -\frac{\mu}{2}J_m\ln\left(1+\frac{3-I_1}{J_m}\right), \tag{39}$$

where W_G is the strain energy density of the Gent model and J_m is the limiting stretch parameter [59], which for biological tissues is around (0.4–2.3) [60–63] and for plastic structures is in orders of 100 [57, 58]. By increasing the maximum permitted value J_m to infinity, the Gent model will be changed to the neo-Hookean incompressible model. The uniaxial, biaxial and pure shear stresses for this model will be

$$\sigma_{uni} = \mu J_m\left(\lambda-\frac{1}{\lambda^2}\right)\left(1+\frac{3-I_1}{J_m}\right)^{-1}, \tag{40}$$

$$\sigma_{bi} = 2\mu J_m\left(\lambda-\frac{1}{\lambda^5}\right)\left(1+\frac{3-I_1}{J_m}\right)^{-1}, \tag{41}$$

$$\sigma_s = \mu J_m\left(\lambda-\frac{1}{\lambda^3}\right)\left(1+\frac{3-I_1}{J_m}\right)^{-1}, \tag{42}$$

of which Eq. (40) coincides with the uniaxial stress model presented by Ronald [64]. Figure 9a shows the sensitivity of the axial stress parameter to variations of μ for $J_m = 5$ and Fig. 9b shows the sensitivity of the axial stress parameter to variations of J_m for $\mu = 0.4$ MPa. Although the main model presented by Gent is only dependent on the first invariant, modified versions of this model, designed to incorporate the compressibility and other invariant terms, have been extended by several researchers [65–68].

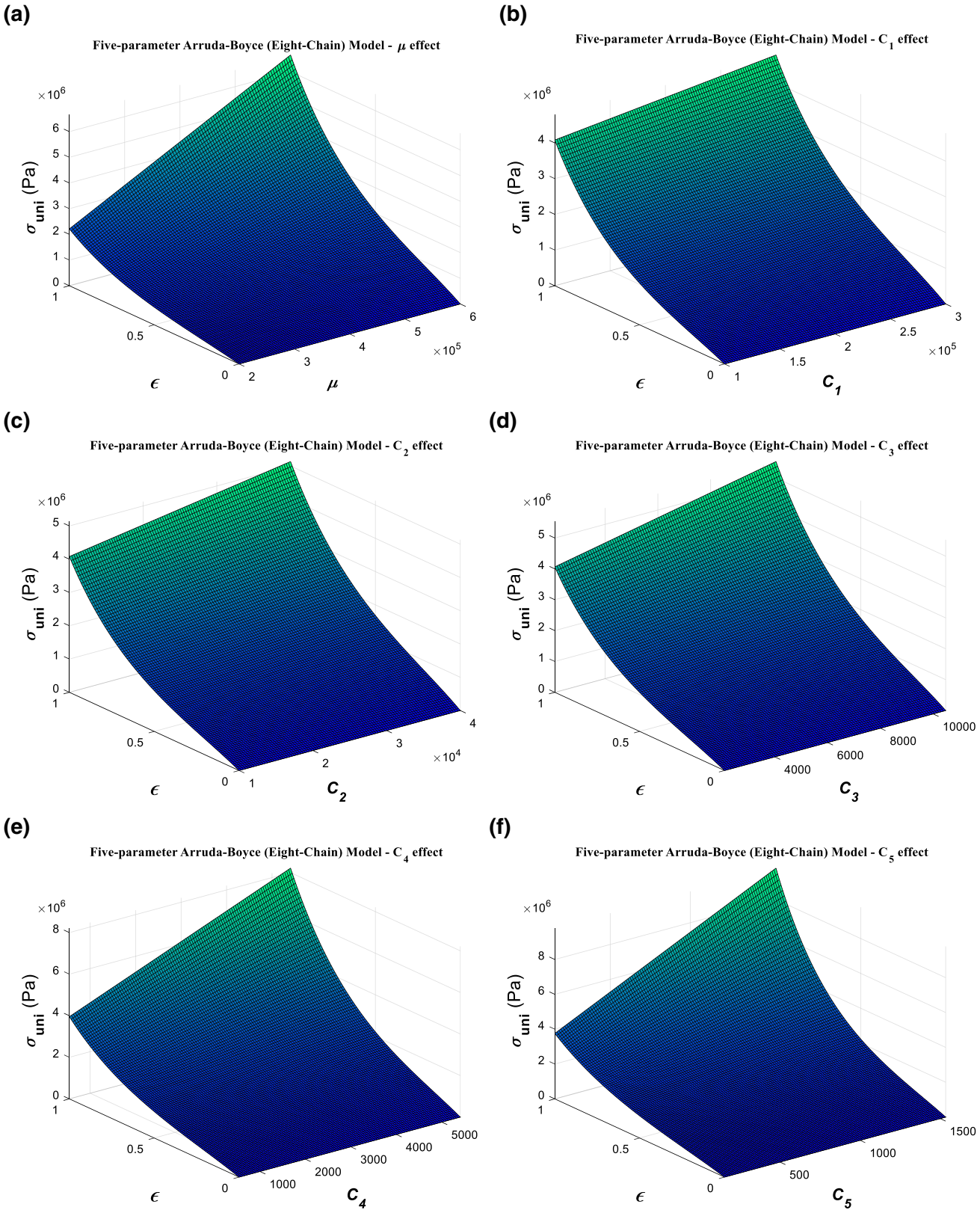

Fig. 7 Uniaxial stress sensitivity to the *five-parameter Arruda–Boyce* (eight-chain) model coefficients: **a** μ; **b** C_1; **c** C_2; **d** C_3; **e** C_4; **f** C_5

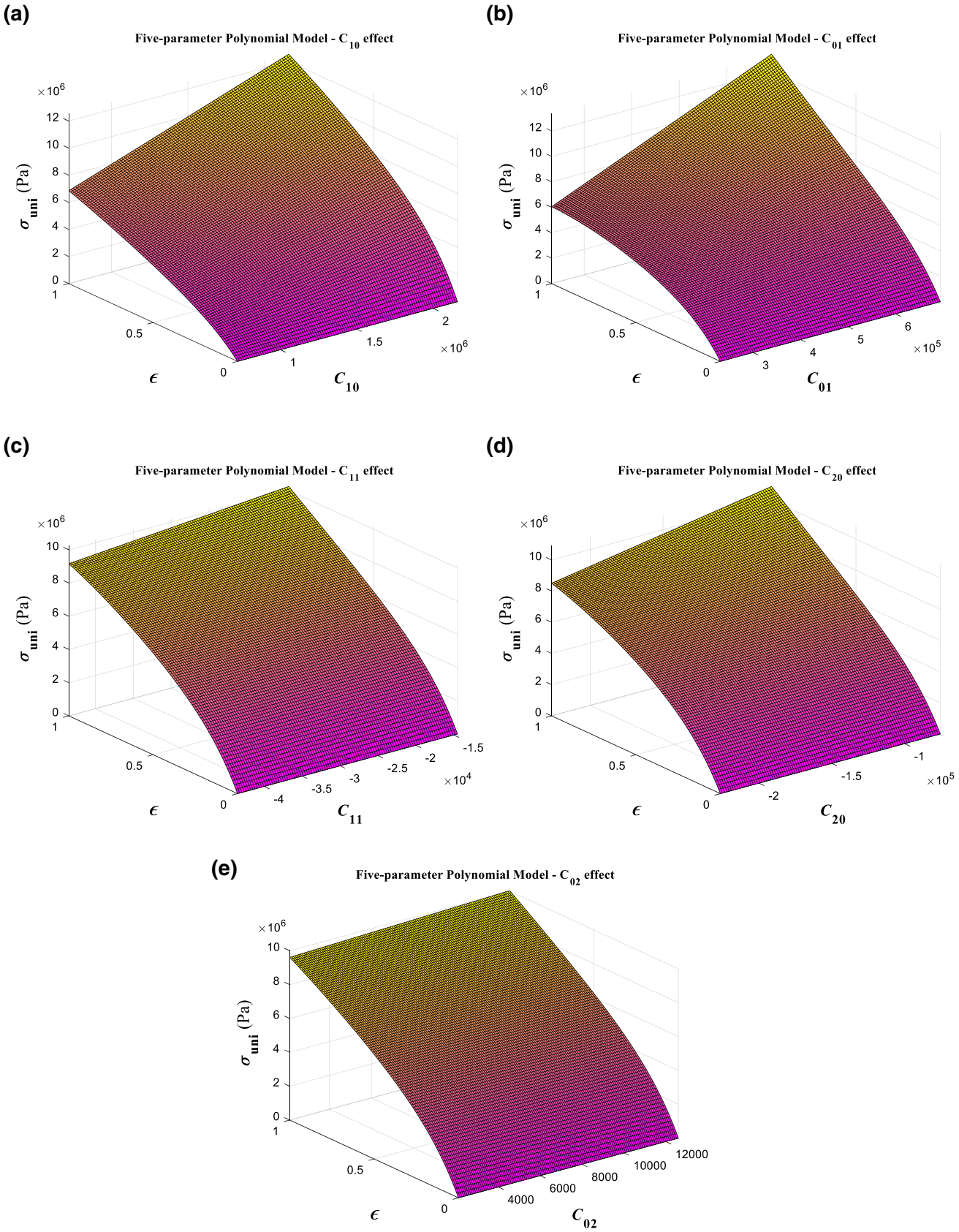

Fig. 8 Uniaxial stress sensitivity to the *five-parameter polynomial* model coefficients: **a** C_{10}; **b** C_{01}; **c** C_{11}; **d** C_{20}; **e** C_{02}

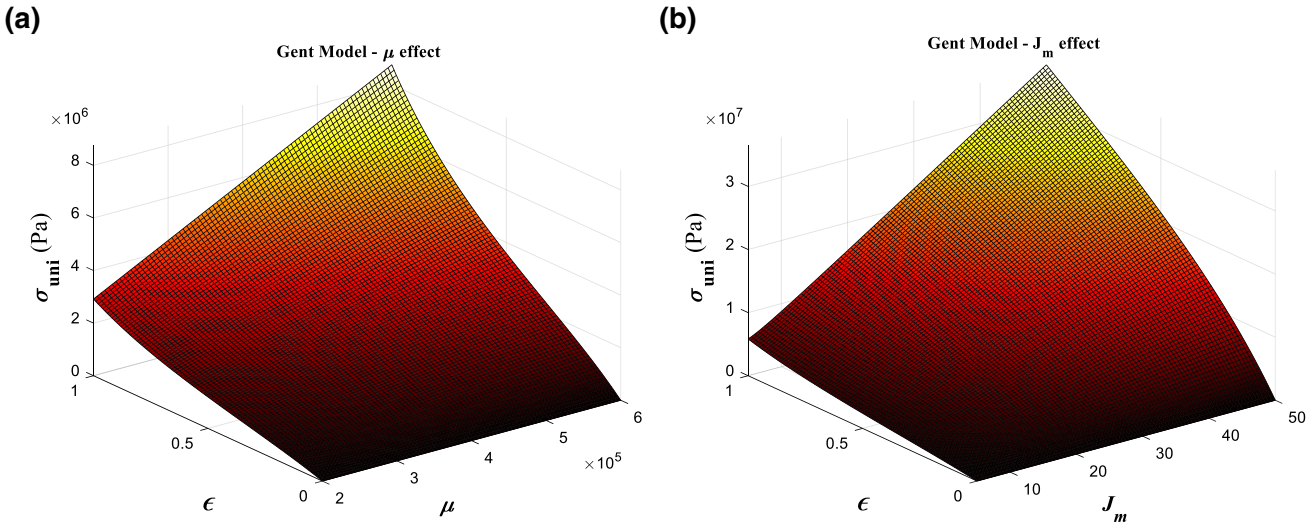

Fig. 9 Uniaxial stress sensitivity to the *Gent* model coefficients: **a** μ; **b** J_m

2.8 The Blatz–Ko model

For the proposed model by Blatz and Ko [69], which is used to characterise foam rubbery structures, the strain energy density is written as [43]:

$$W_{BK} = \frac{\mu}{2}\left(\frac{I_1}{I_2} + 2\sqrt{I_3}\right), \tag{43}$$

where W_{BK} is the Blatz–Ko model of the strain energy density and for the incompressible structures, for axial loading, equibiaxial and pure shear stresses the stress–stretch relationship is, respectively, obtained as:

$$\sigma_{uni} = \frac{\mu}{2\lambda + \lambda^{-2}}\left[\left(\lambda - \lambda^{-2}\right) + \frac{\left(\lambda^2 + 2\lambda^{-1}\right)}{\left(2\lambda + \lambda^{-2}\right)}\left(1 - \lambda^{-3}\right)\right], \tag{44}$$

$$\sigma_{bi} = \frac{\mu}{2\lambda + \lambda^{-2}}\left[\left(\lambda - \lambda^{-5}\right) + \frac{\left(\lambda^2 + 2\lambda^{-1}\right)}{\left(2\lambda + \lambda^{-2}\right)}\left(\lambda^3 - \lambda^{-3}\right)\right], \tag{45}$$

$$\sigma_s = \frac{\mu}{2\lambda + \lambda^{-2}}\left(\lambda - \lambda^{-3}\right)\left[1 + \frac{\left(\lambda^2 + 2\lambda^{-1}\right)}{\left(2\lambda + \lambda^{-2}\right)}\right]. \tag{46}$$

Figure 10 presents the influence of varying the Blatz–Ko coefficient on the nonlinear stress–strain behaviour of uniaxial loaded structures. There are many other models presented by researchers to model the hyperelastic behaviour of such structures [41], such as the Rivlin–Saunders model [41], the Murnaghan model [70], the Ciarlet model [71], the Valanis–Landel model [72], the Hill model [73] and the Attard model [74].

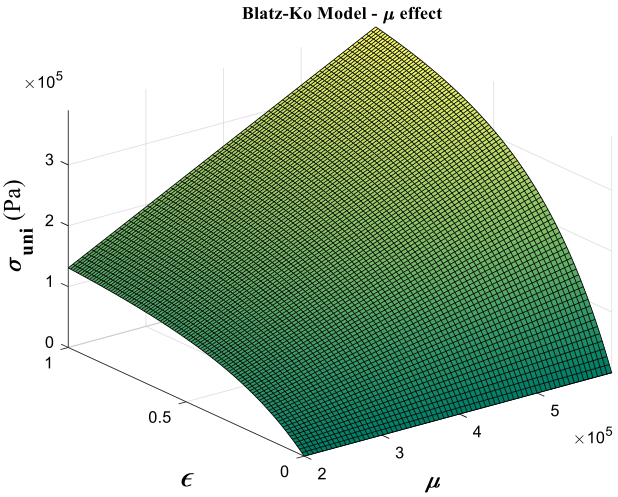

Fig. 10 Uniaxial stress sensitivity to the *Blatz–Ko* model coefficient

The given models are mainly used for isotropic hyperelastic materials; however, some structures (especially biological tissues) show a more complicated behaviour which requires orthotropic and anisotropic modelling in their hyperelastic constitutive models. These models are developed mainly for a specific type of hyperelastic materials. A more detailed explanation on orthotropic and anisotropic modelling can be found in refs [75–80] and [81–90], respectively.

An important topic in hyperelasticity analysis is properly modelling the nonlinear dynamics of different soft structures. Since hyperelastic structures have been used lately in many different industrial needs

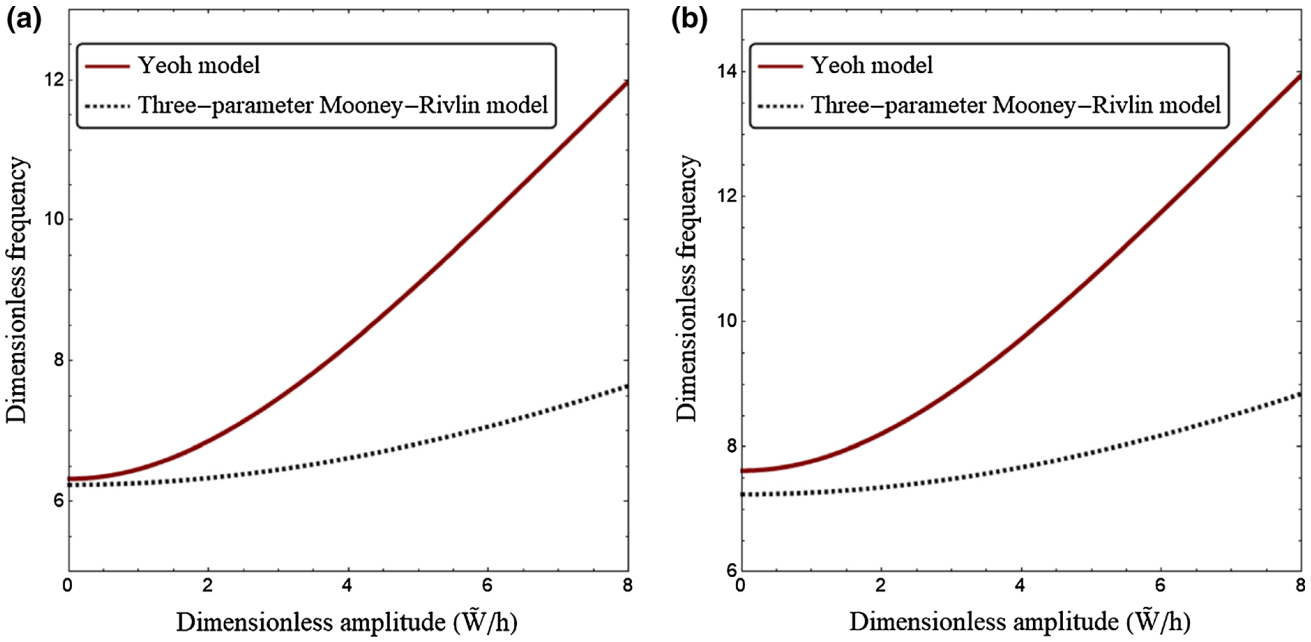

Fig. 11 The nonlinear frequencies of hyperelastic tube models using Yeoh and Mooney–Rivlin strain energy density models for **a** pinned–pinned and **b** clamped–clamped boundary conditions [106]. (Permission obtained from Springer Nature)

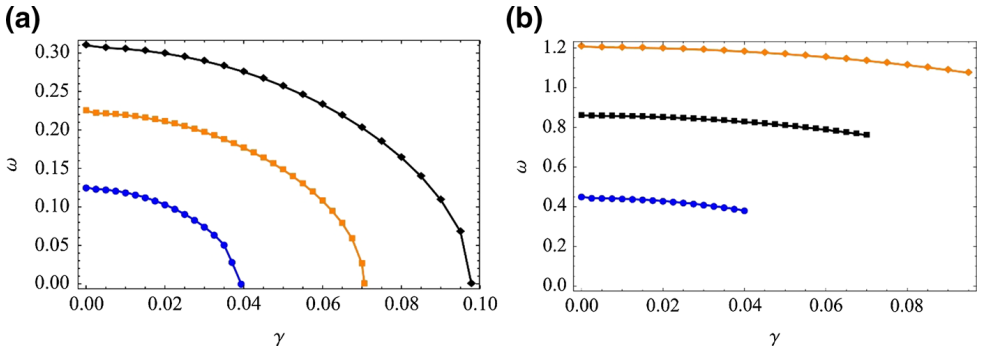

Fig. 12 Variation of the **a** first and **b** second natural frequencies of neo-Hookean axially moving beams with respect to the velocity parameter for different geometrical parameters [109]. (Permission obtained from ELSEVIER)

such as soft robotics [91–94], understanding their nonlinear time-dependant behaviour in different mechanical conditions is of high importance. Studies in this field can be classified based on the structure type and the mechanical analysis. In this review, the nonlinear dynamics of hyperelastic structures is presented in three sections for beams, plates/shells and membranes/balloons.

3 Nonlinear dynamics of hyperelastic beams

One-dimensional structures, including beams, tubes and columns, as the critical part of many mechanical structures, undergo different types of dynamic loads. Since rubber-like beams undergo large strains and deformations, classical linear material models cannot define the nonlinear dynamics accurately; therefore, an accurate hyperelastic model of the structure should be derived and examined. In this section, the nonlinear dynamics of hyperelastic beams is reviewed using literature for different mechanical conditions. Since this review is focused on the nonlinear dynamics, interested readers on the statics of hyperelastic beam structures are referred to [17, 95–100].

For hyperelastic beams laying on a foundation, a mathematical formulation was presented by Forsat [101] to examine the nonlinear free vibration behaviour of silicone rubbers and natural rubbers. A higher-order shear deformation beam theory together with four different nonlinear elasticity models was utilised for modelling the soft beam. The structure was assumed to be sitting on a Pasternak–Winkler medium. Equations of motion were solved and

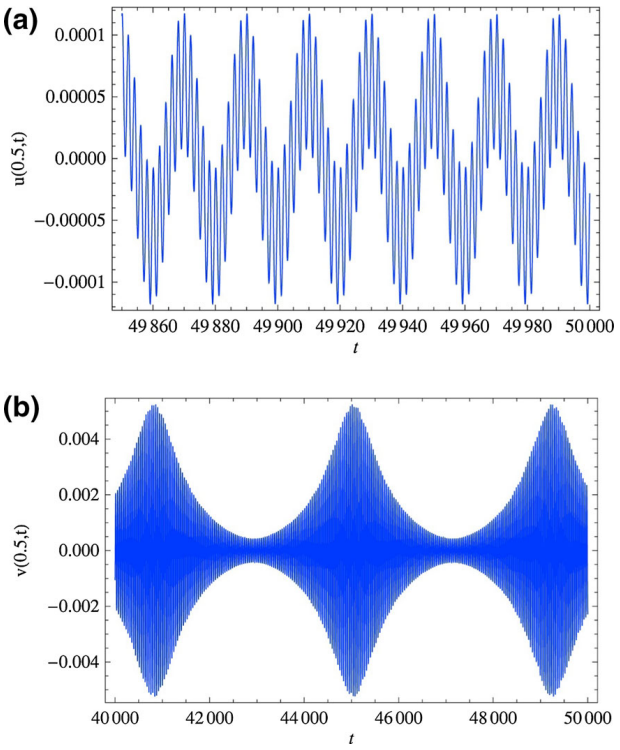

Fig. 13 The time traces for the **a** axial and **b** transverse vibrations of axially accelerated neo-Hookean beams [112]. (Permission obtained from ELSEVIER)

obtained using Galerkin's scheme and Hamilton's principle (which have been used by researchers for studying elastic structures [102–105]), respectively; it was claimed that the shear strain effects were neglected in the Yeoh strain energy. In another study, Mirjavadi et al. [106] used the Euler–Bernoulli beam assumptions showing that for hyperelastic tube models, by increasing the amplitude of vibration, since the effect of nonlinear terms in the structure modelling increases and due to different stress invariant considerations, the difference between the Yeoh and two-parameter Mooney–Rivlin results increased. Figure 11 shows the nonlinear frequencies of hyperelastic tube models using Yeoh and Mooney–Rivlin strain energy density models. In both of these studies, the material was assumed to be incompressible; however, the incompressibility condition, which leads to strains in thickness directions, was neglected.

Since belt operating systems are one of the well-known applications of hyperelastic structures [107, 108], researchers focused on the nonlinear dynamics of axially moving hyperelastic beams to understand their mechanical behaviour in such conditions. Wang et al. [109] used a finite deformation leading-order model (presented in [110, 111]) to investigate the nonlinear oscillations of axially travelling soft beams. Using the Hamilton's principle and neo-Hookean strain energy density model, the equations of motion were obtained. It was claimed that the natural frequencies of the Euler–Bernoulli beam model are lower than the ones obtained for this model. The variation of the natural frequencies with respect to the axial velocity parameter for this model is shown in Fig. 12. In another study by Wang et al. [112], they analysed accelerated longitudinal motion in soft beams using multiple scale perturbation methods and Galerkin's scheme. The time traces for the axial and transverse vibrations of this model are shown in Fig. 13. Khaniki et al. [113] investigated the nonlinear forced oscillation of axially moving hyperelastic belts by employing the Yeoh's strain energy. Different nonlinear elastic models were examined to find the best fit with the experimental testing of hyperelastic properties. The influence of the longitudinal speed on the natural frequencies, mode shapes and nonlinear frequency response was investigated showing a significant effect in changing the mechanical behaviour (Figs. 14 and 15).

For the case of having both thermal and hyperelasticity effects, a wave propagation method was employed by Mirparizi and Fotuhi [114] to understand the nonlinear dynamics of thermo-hyperelastic one-dimensional structures. Hyperelasticity was modelled using a Mooney–Rivlin strain energy density model. It was elucidated that the maximum amplitude of oscillation in the structure is significantly higher than for elastic ones. Figure 16 shows the stress wave propagation with respect to time showing a large difference between the hyperelastic and linear elastic models response.

Since hyperelastic structures are mostly made by moulding and 3D printing, the presence of voids and porosity is highly possible. To understand the effect of having porosities in the nonlinear dynamics of hyperelastic structures, Khaniki et al. [115] studied the characteristics of hyperelastic samples experimentally with different porosities (the infill rate). A general constitutive model for hyperelastic-porous was presented via the Mooney–Rivlin hyperelastic strain energy model, showing that the porosity has a nonlinear effect in varying the hyperelastic constitutive model (Fig. 17). For the derived model, they modelled the nonlinear vibrations of porous

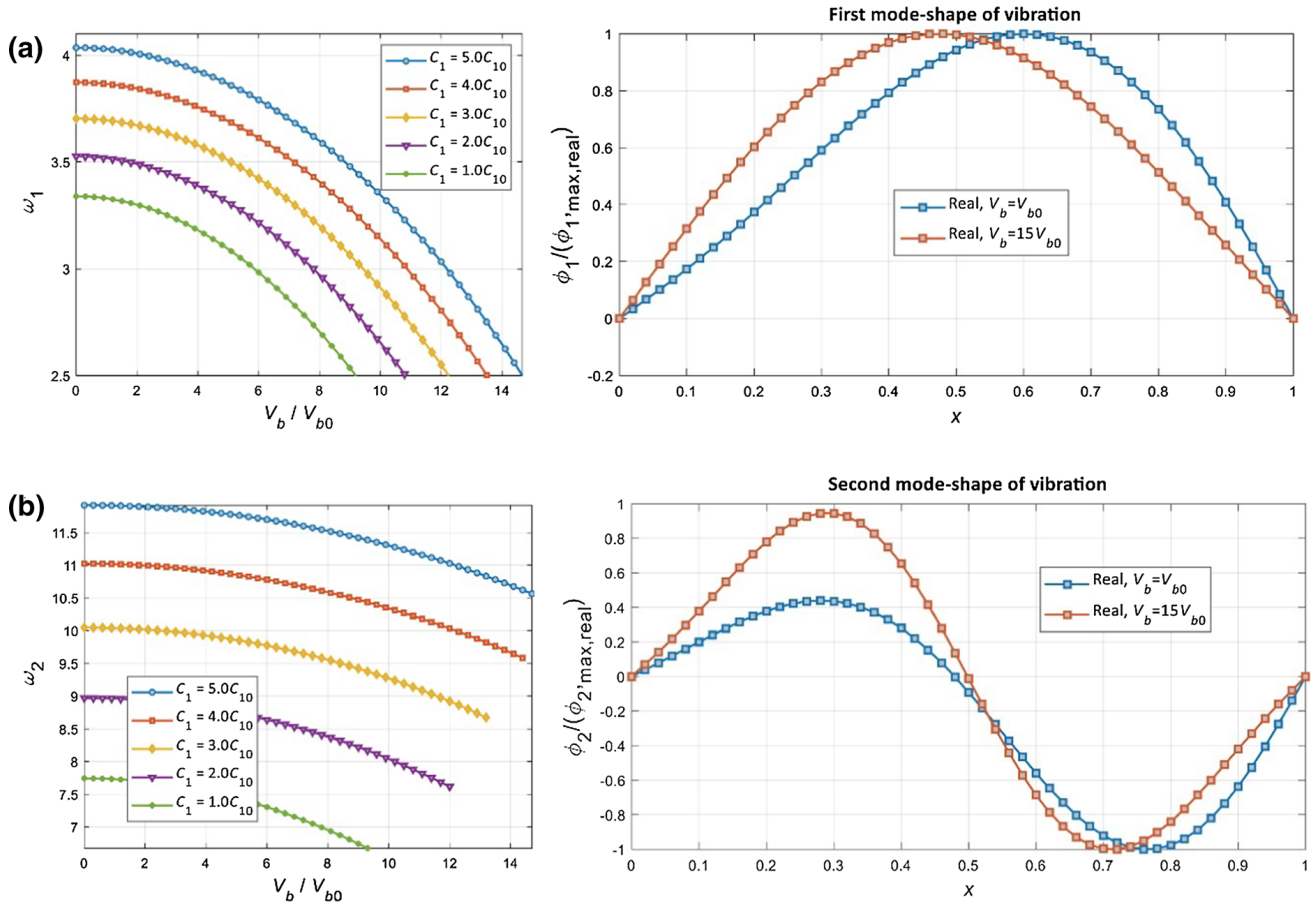

Fig. 14 The natural frequency and mode shapes of axially moving hyperelastic beams versus the speed parameter **a** first and **b** second modes of vibration [113]. (Permission obtained from ELSEVIER)

hyperelastic beams under externally time-dependent forces, showing that increasing the porosity in the structure has a significant effect in changing the stiffness softening behaviour of the structure to a combination of hardening and softening behaviour (Fig. 18).

Layered hyperelastic structures have many applications in packaging industry (especially food packaging) [116–119], which makes it important to comprehend the behaviour of layered hyperelastic structures made of different materials. For this reason, Khaniki et al. [120] examined five different shear deformable beam theories together with the Mooney–Rivlin strain energy model for analysing the nonlinear dynamics of sandwich soft beams. It was shown that considering the shear effect, layering and material positioning can highly affect the nonlinear resonance behaviour of the thick sandwich soft beam. Figure 19 shows the effect of material ordering in changing the nonlinear dynamic behaviour of higher-order shear deformable three-layered beam structures.

Longitudinal vibrations of neo-Hookean beams have been examined by Wang and Zhu [121, 122] in its subcritical buckling regime and under different axial loads. Using a linear bifurcation analysis, the critical buckling loads were obtained showing a high sensitivity of material and geometrical properties. Using the pseudo-arc-length method, the nonlinear frequency response of the system was calculated. Figure 20 shows the axial frequency response of the neo-Hookean beam model for different material and geometrical properties.

In recent years, hyperelasticity has been employed for modelling the static and dynamic responses of

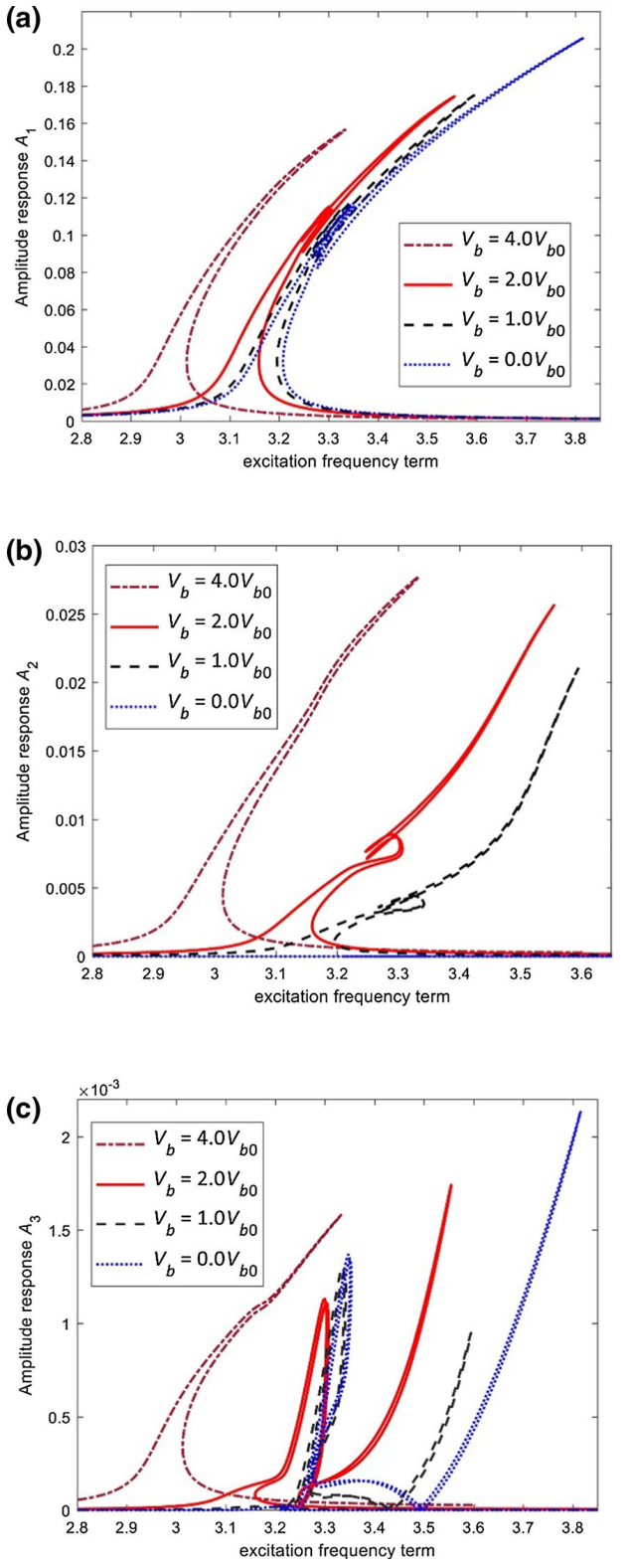

Fig. 15 The transverse amplitude–frequency response of axially moving hyperelastic beams with different velocities **a** first, **b** second, and **c** third coordinates [113]. (Permission obtained from ELSEVIER)

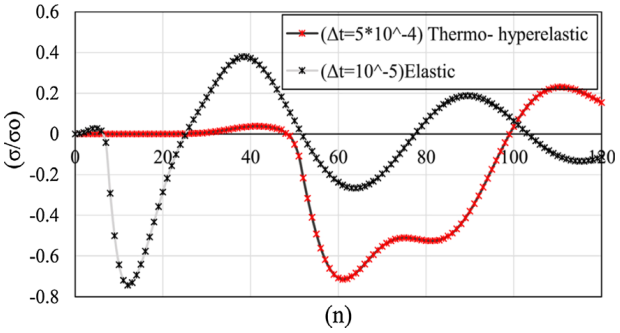

Fig. 16 Stress wave propagation in hyperelastic and elastic structures [114]. (Permission obtained from ELSEVIER)

nano-/micromaterials [123–126], which have crucial importance in new technologies. For instance, micro-scale beam structures made by hyperelastic materials have been studied by Alibakhshi et al. [127] using the Euler–Bernoulli beam theory, modified couple stress theory (which have been used previously for studying small-scale elastic structures [128–132]), and Gent strain energy density model. It was shown that the force–amplitude response of the structure is highly sensitive to the stiffness parameter of Gent model (Fig. 21). Studies on the nonlinear dynamics of hyperelastic beams are summarised in Table 1.

4 Nonlinear dynamics of hyperelastic plates and shells

Both shells and plates are an important element in structural design, and the extensive usage of rubbery structures makes it necessary to comprehend the nonlinear dynamics of the hyperelastic plate and shell structures. For this reason, this section focuses on the investigations undertaken to comprehend the nonlinear dynamics of such structures.

For isotropic hyperelastic plate structures, a combination of the nonlinear von Kármán plate theory and the neo-Hookean strain energy density model was used by Breslavsky et al. [133] for examining the large amplitude vibrations of thin rectangular hyperelastic plates. The equations of motion were presented with quadratic and cubic nonlinear terms by considering both material and geometrical nonlinearities; it was shown that for small strains, the material nonlinearity terms have a weak effect, while this effect increases significantly by having larger strains. Figure 22 shows the amplitude response and backbone curves of the

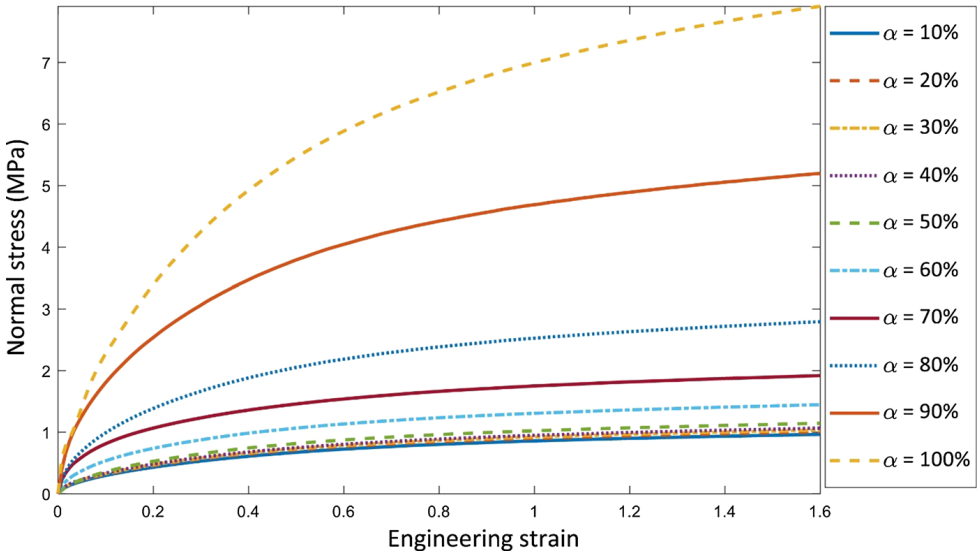

Fig. 17 Experimental results for stress–strain behaviours of porous hyperelastic structures with different infill rates (α) [115]. (Permission obtained from ELSEVIER)

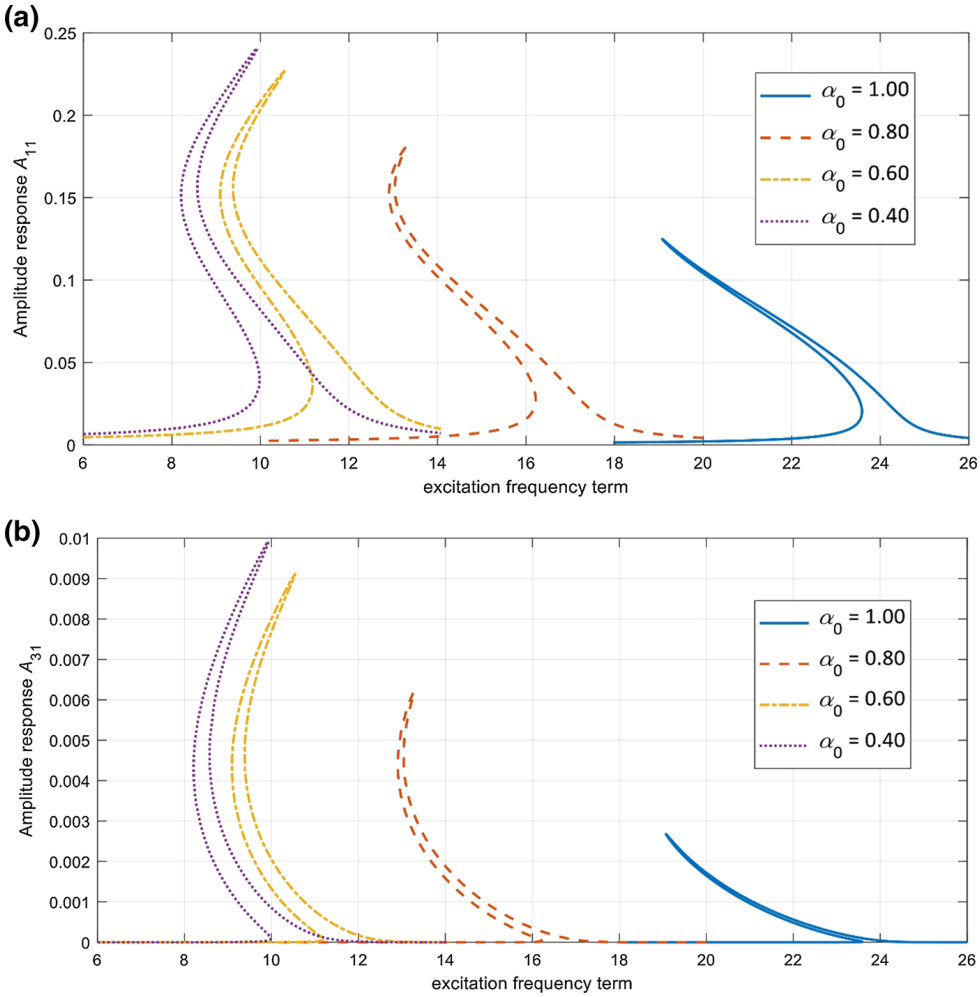

Fig. 18 Influence of the infill rate (porosity) in varying the nonlinear frequency response of porous hyperelastic beams **a** first and **b** third dynamic coordinates. [115]. (Permission obtained from ELSEVIER)

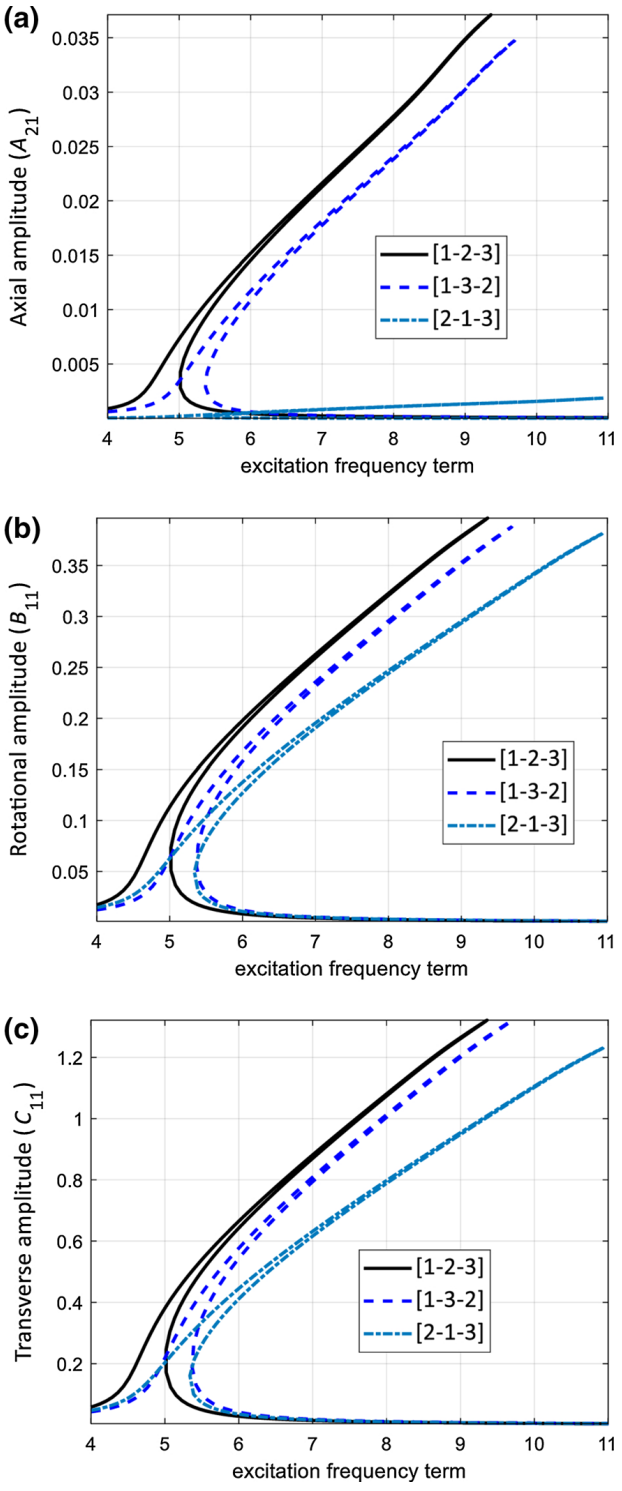

Fig. 19 The effect of hyperelastic material layering on the nonlinear dynamics Mooney–Rivlin shear deformable beams for the **a** axial, **b** rotational and **c** transverse motions [120]. (This article is an open access article distributed under the terms and conditions of the Creative Commons Attribution (CC BY) license (https://creativecommons.org/licenses/by/4.0/).)

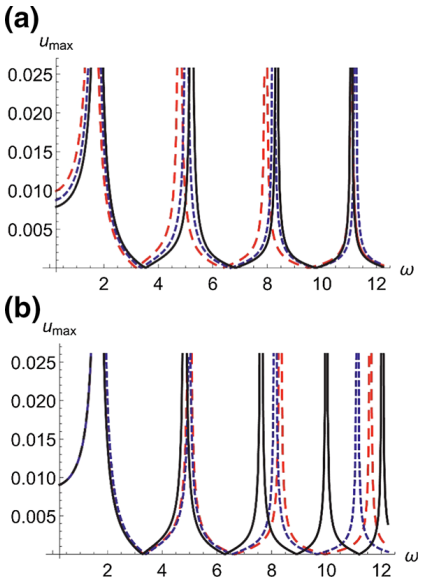

Fig. 20 The axial nonlinear frequency response of the neo-Hookean beam model for different **a** material and **b** geometrical properties [121]. (Permission obtained from ELSEVIER)

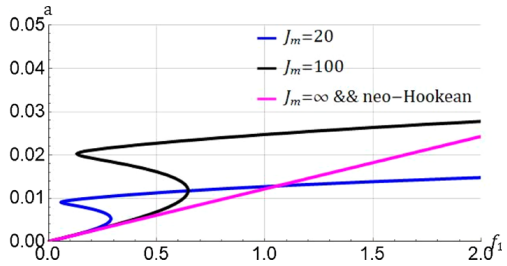

Fig. 21 The force–amplitude response of micro-hyperelastic beam for different Gent coefficients[127]. (Permission obtained from MDPI)

first mode of vibration with two peaks associated with the 2:1 in-plane resonance. Amabili et al. [134] investigated the vibration behaviour of hyperelastic plates. A two-parameter incompressible Mooney–Rivlin model was used to describe the nonlinearity of the structure using Novozhilov nonlinear shell theory to model the deformations. The governing equations were obtained using Hamilton's principle; it was shown that the experimental results are in good agreement with the proposed dynamic model.

The nonlinear dynamics of cylindrical shell structures have been examined lately by many researchers. Zhang et al. [135] modelled the nonlinear vibrations of thin-walled hyperelastic cylindrical shells using Donnell's nonlinear shallow shell theory. Using the

Table 1 Studies on the nonlinear dynamics of hyperelastic beams

Study	Year	Hyperelastic strain energy density model	Formulation methods/Experiments	Solution methods	Analysis
Forsat [101]	2019	Neo-Hookean, Ishihara, Mooney–Rivlin, and Yeoh models	Higher-order shear deformation theory, Hamilton's principle	Galerkin's scheme, Extended Hamiltonian method	Nonlinear free vibrations of hyperelastic beams
Mirjavadi et al. [106]	2019	Neo-Hookean, Ishihara, Mooney–Rivlin, and Yeoh models	Euler–Bernoulli beam theory, Hamilton's principle	Galerkin's scheme, Extended Hamiltonian method	Nonlinear free vibrations of hyperelastic tubes
Wang et al. [109, 112]	2018, 2019	Neo-Hookean model	The leading order model for finite deformation, Hamilton's principle	Multi-scale perturbation techniques Galerkin's method	Nonlinear vibrations of axially moving hyperelastic beams
Khaniki et al. [113]	2020	Arruda–Boyce (Eight-Chain), neo-Hookean, Gent, and Yeoh models	Experimental analysis, Euler–Bernoulli beam theory, Hamilton's principle, von Kármán theory	Galerkin's scheme, Dynamic equilibrium technique	Nonlinear forced vibrations of axially moving hyperelastic beams
Mirparizi and Fotuhi [114]	2020	Mooney-Rivlin strain energy model	Helmholtz's free energy function	Direct iteration method	Wave propagation in thermo-hyperelastic beams
Khaniki et al. [115]	2021	Mooney-Rivlin model	Experimental analysis, Euler–Bernoulli beam theory, Hamilton's principle, von Kármán theory	Galerkin's scheme, Dynamic equilibrium technique	Nonlinear forced vibration of porous-hyperelastic beams
Khaniki et al. [120]	2022	Mooney-Rivlin strain energy model	Euler–Bernoulli, Timoshenko, third-order, trigonometric and exponential beam theories, von Kármán theory, Hamilton's principle	Galerkin's scheme, Dynamic equilibrium technique	Nonlinear forced vibration of sandwich thick hyperelastic beams
Wang and Zhu [121, 122]	2021, 2021	Neo-Hookean model	Euler–Bernoulli beam theory,1 Hamilton's principle	Harmonic balance method, Galerkin's scheme	Nonlinear vibrations of axially loaded hyperelastic beams
Alibakhshi et al. [127]	2021	Gent model	Euler–Bernoulli beam theory, Hamilton's principle, modified couple stress theory, von Kármán theory	Multiple Scales Method	Nonlinear vibrations of small-scale hyperelastic beams

Lagrange equation together with the Mooney–Rivlin strain energy density model, the equations of motion were obtained. It was shown that radius-to-thickness ratio has a significant effect in changing the radial vibration behaviour. Figure 23 shows the Poincare section and bifurcation diagram of the hyperelastic cylindrical shell for different excitation forces. Xu et al. [136, 137] examined the nonlinear dynamics of

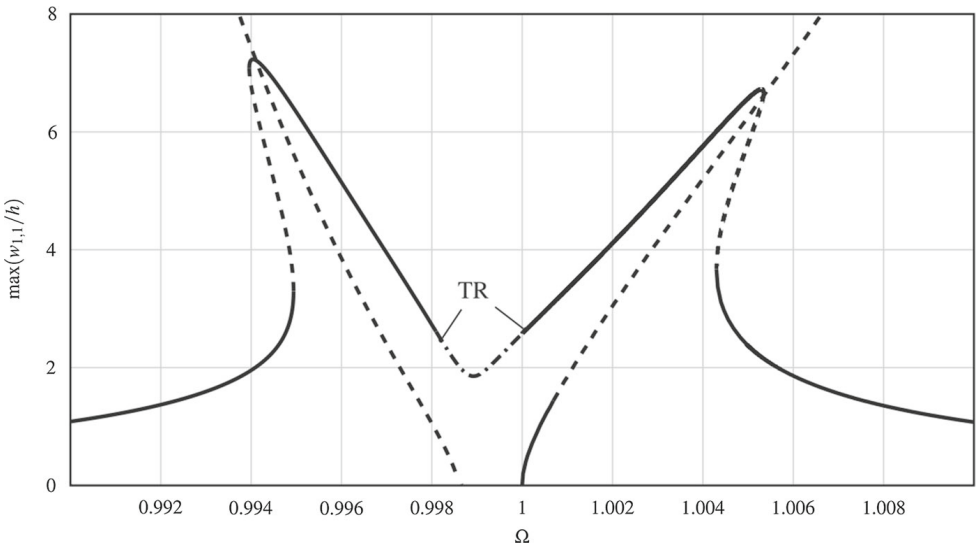

Fig. 22 Amplitude–frequency response and backbone curves of the first mode of vibration of a rectangular hyperelastic plate with two peaks associated with the 2:1 in-plane resonance [133]. (Permission obtained from ELSEVIER)

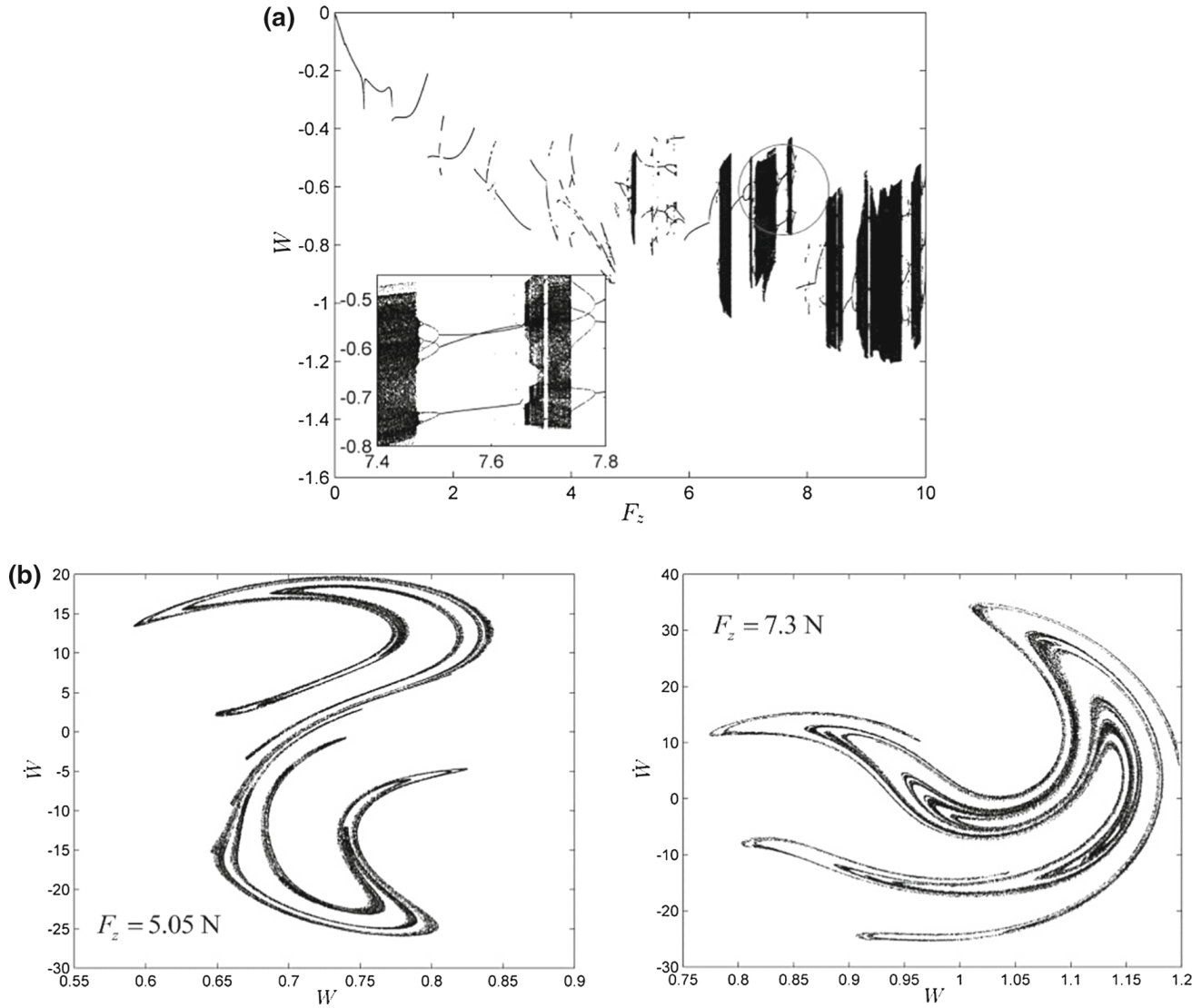

Fig. 23 **a** Bifurcation diagram and **b** Poincaré sections of a thin-walled Mooney–Rivlin cylindrical shell for different excitation forces [135]. (Permission obtained from Springer Nature)

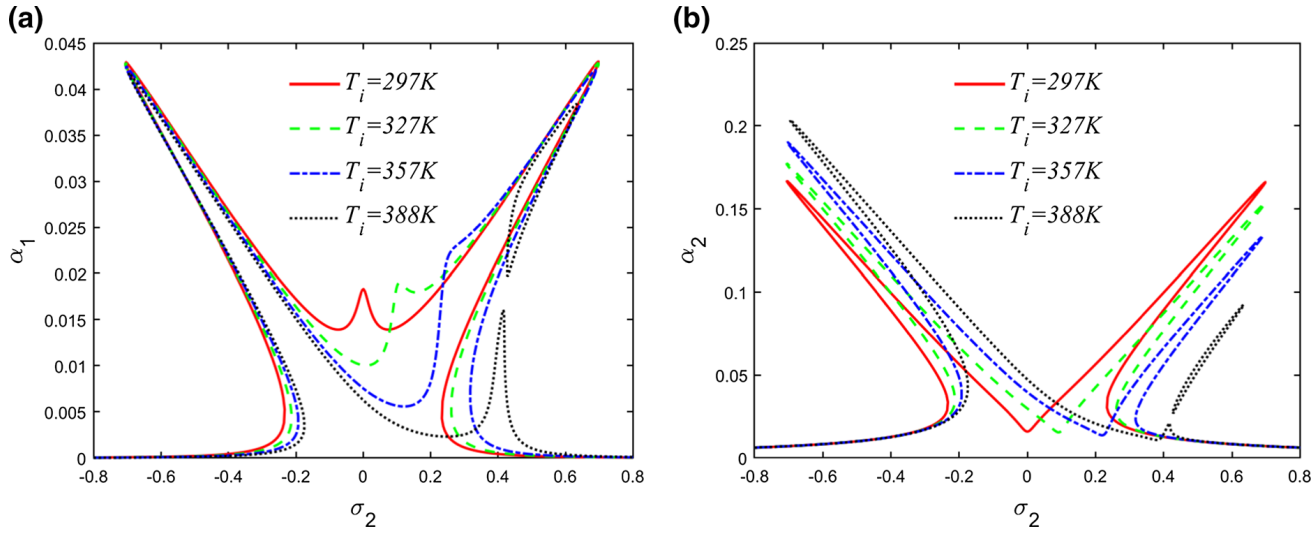

Fig. 24 The nonlinear response of the cylindrical shell with different temperature loads for the (**a**) axisymmetric and (**b**) asymmetric modes [136]. (Permission obtained from WSPC)

thin and thick hyperelastic cylindrical shells subjected to a time-dependant thermal load. It was shown that the single-mode model of such structures gives inaccurate results and the diameter-to-length ratio has a significant influence in the internal resonance phenomena. Figure 24 shows the nonlinear response of the cylindrical shell with different temperature loads for the axisymmetric and asymmetric modes. Breslavsky et al. [44, 138] investigated the free and forced nonlinear responses of circular cylindrical hyperelastic shells and square hyperelastic plates in the framework of large deformations. Hyperelasticity was modelled using the neo-Hookean model in conjunction with the Fung model, while the shell was assumed to be made of arterial bio-tissues. It was shown that the single-mode response is weak; however, the resonant response considering both companion and driven modes, was found with nonlinear complicated dynamics.

In the case of analysing electrostrictive–hyperelastic structures, Tripathi and Bajaj [139, 140] studied the internal resonances due to transverse vibration when designing hyperelastic and electrostrictive–hyperelastic plates. The Mooney–Rivlin and neo-Hookean hyperelastic strain energy models were investigated, while the plate was modelled using Kirchhoff plate theory. These showed that for nearly incompressible structures, the level of nonlinearity in the strain energy model of neo-Hookean is insufficient to lead to 1:2 internal resonances. A visco-hyperelastic model was presented by Zhao et al. [141] for modelling the chaotic motion of spherical shells. Other studies on the dynamic behaviour of hyperelastic plates and shells can be found in refs [142–148], emphasising the importance of considering hyperelasticity in studying the dynamic response of such structures. Studies on the nonlinear dynamics of hyperelastic plates and shells are summarised in Table 2.

5 Nonlinear dynamics of hyperelastic membranes and balloons

Comprehending the nonlinear dynamics of hyperelastic membranes and balloons has been a challenging task for researchers in the past few years. For circular membranes, Goncalves et al. [149, 150] studied the nonlinear vibration behaviour of isotropic homogeneous circular hyperelastic membranes stretched radially. Hyperelasticity was modelled using the neo-Hookean strain energy density model, and the motion equations were derived via Hamilton's principle. Natural frequencies were obtained analytically and compared with finite element modelling. It was revealed that all the hyperelastic models, namely the Arruda–Boyce model, Ogden model, Yeoh model and Mooney–Rivlin model, present similar nonlinear frequency–amplitude responses, qualitatively. The influence of the pre-stretch ratio on the nonlinear

Table 2 Studies on the nonlinear dynamics of hyperelastic plates/shells

Study	Year	Hyperelastic strain energy density model	Formulation methods/ Experiments	Solution methods	Analysis
Breslavsky et al. [133]	2014	Neo-Hookean model	Von Kármán non-linear plate theory, Lagrange equation	Fourier expansion, Pseudo-arc-length continuation and collocation method	Nonlinear forced vibrations of hyperelastic plates
Amabili et al. [134]	2016	Mooney-Rivlin model	Experimental analysis, Novozhilov nonlinear shell theory	Finite-element coding, Analytical procedure, Meshless approach	Nonlinear free vibrations of hyperelastic thin plates
Zhang et al. [135]	2019	Mooney-Rivlin model	Donnell's nonlinear shallow shell theory, Kirchhoff–Love hypothesis, Lagrange equation	Fourth-order Runge–Kutta method	Nonlinear vibrations of cylindrical hyperelastic shells
Xu et al. [136, 137]	2020, 2021	Arruda–Boyce model	Reddy's third-order shear deformation theory, Kirchhoff–love hypothesis, Lagrange equation	Multiple-scale method, Harmonic balance method	Nonlinear thermal vibrations of cylindrical hyperelastic shells
Breslavsky et al. [138]	2016	Neo-Hookean and Fung models	Lagrange equation, nonlinear higher-order shear deformation theory	Fourier expansion, Pseudo-arc-length continuation and collocation method	Nonlinear forced vibrations of cylindrical hyperelastic shells
Breslavsky et al. [44]	2014	Neo-Hookean, Mooney–Rivlin, and Ogden models	Lagrange equation, Novozhilov nonlinear shell theory	Fourier expansion, Pseudo-arc-length continuation and collocation method	Nonlinear forced vibrations of hyperelastic thin plates
Tripathi and Bajaj [139, 140]	2016, 2014	Neo-Hookean and Mooney–Rivlin models	Thin plate Kirchhoff theory, Lagrange equation	Method of averaging FE software	Topology optimisation and internal resonance in hyperelastic plates
Zhao et al. [141]	2020	Gent model	Finite deformation theory	Perturbation theory	Nonlinear dynamics of spherical viscoelastic hyperelastic shells
Iglesias et al. [142, 143]	2018, 2015	Seven invariants orthotropic model	Theory of a generalised Cosserat membrane	Poincaré maps and Lyapunov exponents	Nonlinear vibrations of orthotropic hyperelastic cylinders
Mason, and Maluleke [144]	2007	Mooney–Rivlin model	Ermakov–Pinney equation, First Integral Theorem of Mean Value	Lie point symmetry generator	Nonlinear radial vibrations of hyperelastic shells
Xu et al. [145]	2019	Yeoh model	Experimental analysis, Spatial tridimensional higher-order plate element, Lagrange equation	Newton–Raphson iteration and Newmark numerical techniques	Nonlinear dynamics of thick hyperelastic plates
Iglesias et al. [146]	2017	Mooney–Rivlin and Ogden models	Finite differences modelling	FE software	Nonlinear oscillations of hyperelastic shells
Wang et al. [148]	2021	Mooney–Rivlin model	Hamilton's principle, Classical theory of thermo-elasticity	Analytical and numerical solutions	Nonlinear wave propagation over thermo-hyperelastic cylindrical shells

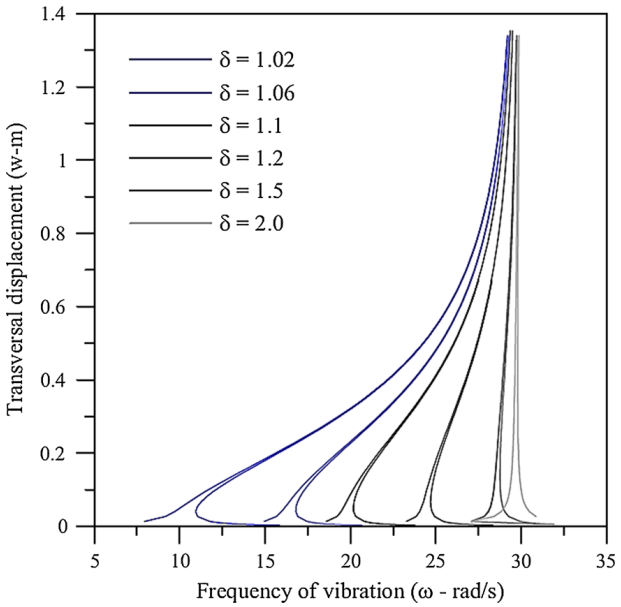

Fig. 25 Amplitude–frequency responses of hyperelastic circular membranes for different pre-stretch ratios [149]. (Permission obtained from ELSEVIER)

amplitude–frequency response of the circular hyperelastic membrane can be seen in Fig. 25.

The nonlinear breathing motion of hyperelastic spherical membranes has been examined by Soares et al. [151] using an incompressible isotropic Mooney–Rivlin strain energy density model. It was shown that the linear viscous damping term has a significant effect in changing the nonlinear resonance behaviour of the spherical membranes (Fig. 26).

Since it was shown by Mangan and Destrade [152] that the hyperelastic Gent–Gent model shows a good accuracy in modelling the nonlinear elasticity of inflated balloons, Alibakhshi and Heidari [59] used this model for studying the chaotic motion of dielectric elastomer balloons; it was shown that the chaotic motion of the dielectric elastomer balloons could be suppressed by the presence of the second invariant term in the Gent–Gent model (Fig. 27). Ilssar and Gat [153] examined the fluid–structure interaction of liquid-filled balloons using the incompressible Mooney–Rivlin strain energy density model. By verifying the model with results obtained from the finite element scheme, it was shown that the simplified presented model was capable of studying the static and

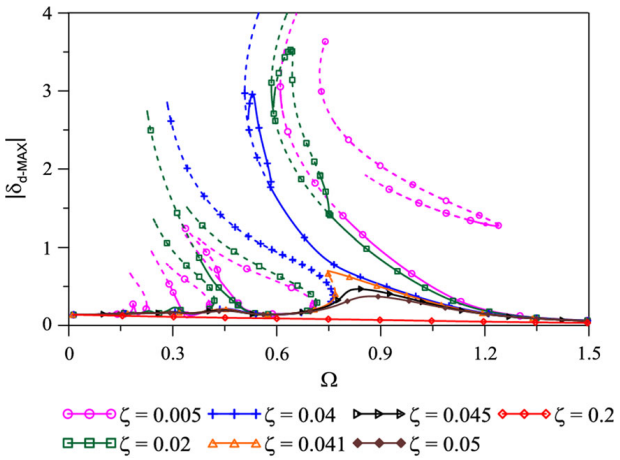

Fig. 26 The nonlinear resonance response of hyperelastic spherical membranes for different linear damping parameters [151]. (Permission obtained from Springer Nature)

dynamic behaviour of such structures. Other studies on the dynamic behaviour of hyperelastic membranes and balloons can be found in refs [19, 154–156]. Studies on the nonlinear dynamics of hyperelastic balloons and membranes are summarised in Table 3.

6 Summary and conclusions

Over the past few decades, accurately modelling the hyperelastic behaviour of polymeric structures has been a challenging task in terms of the complexity in both material and structural nonlinearities. Dozens of constitutive hyperelastic models have been presented by researchers for different materials, which some of the most practical and well-known isotropic models are presented and formulated, and the characteristics of each model are discussed. In terms of the case studies, each of these models has advantages and disadvantages in terms of accurate and inaccurate modelling for material nonlinearity and computational time cost.

Hyperelastic structures, such as rubbers and elastomers, have been analysed in different shapes and mechanical conditions. Most studies into these types of structures have been published over the past few years, since their applications are only now becoming understood. Recently, novel outcomes from rubbery

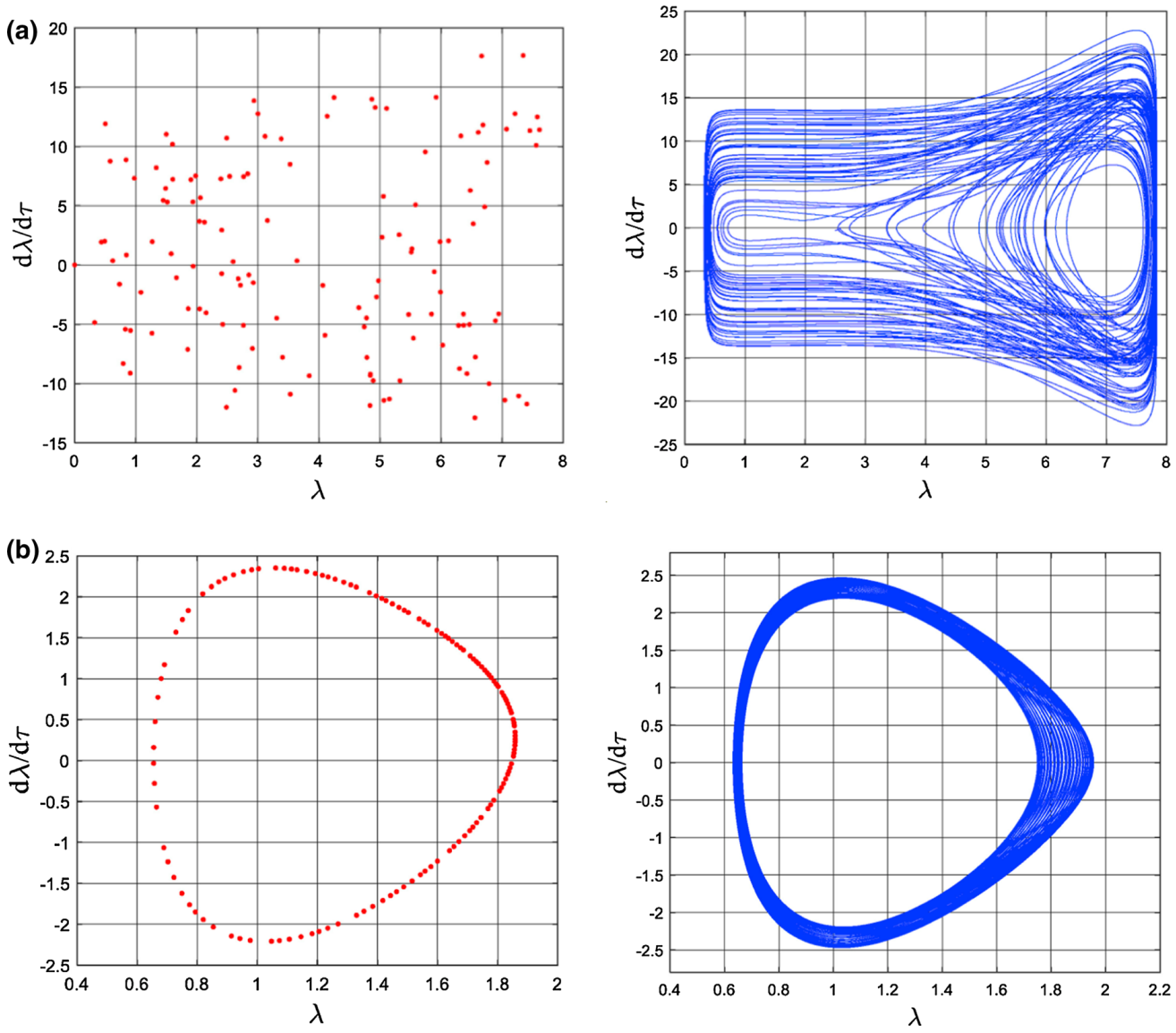

Fig. 27 Variation of the motion from **a** chaotic motion to **b** quasiperiodic vibration by increasing the second invariant parameter of the Gent–Gent model in the dielectric elastomer balloons [59]. (Permission obtained from ELSEVIER)

structures in soft robotics have moved forward such study significantly, notably in terms of achieving smooth deformations and higher the degrees of freedom. The high potential for the application of soft-based structures helped researchers to realise the importance of modelling the dynamic behaviour of hyperelasticity accurately. To demonstrate the achievements and investigations made into hyperelastic structures, a comprehensive review was presented for different structures types (beams, plates, shells, membranes and balloons) in the frameworks of nonlinear dynamics. It was shown that there has been progress in simulating the hyperelastic dynamic response using various continuum mechanic techniques in conjunction with hyperelastic strain energy density models. Since the theoretical modelling of such structures could require highly complex and long theoretical models, many studies in this field are based on simplified models ignoring the higher terms of displacement and strain. Furthermore, since soft

Table 3 Studies on the nonlinear dynamics of hyperelastic membranes/balloons

Study	Year	Hyperelastic strain energy density model	Formulation methods/ Experiments	Solution methods	Analysis
Goncalves et al. [149]	2009	Neo-Hookean, Mooney–Rivlin, Yeoh, Arruda–Boyce, and Ogden models	Lagrange function, Halmilton's principle	Galerkin method, Reduced order models, Floquet theory	Nonlinear dynamics of hyperelastic circular membranes
Soares and Goncalves [150]	2012	Neo-Hookean model	Lagrange function	Shooting method, Galerkin method	Instability and nonlinear oscillation of hyperelastic circular membranes
Soares et al. [151]	2020	Neo-Hookean and Mooney–Rivlin models	Lagrange function	Continuation techniques, Floquet theory	Nonlinear dynamics of hyperelastic spherical shells
Alibakhshi and Heidari [59]	2020	Gent-Gent model	Euler–Lagrange energy method	Time integration-based solver	Chaotic motion of hyperelastic balloons
Ilssar and Gat [153]	2020	Mooney–Rivlin model	Reduced order model	Finite-element simulations, semi-analytical model	Deflation and inflation of fluid filled hyperelastic balloons
Dong et al. [19]	2016	Yeoh model	Generic lumped parameter model, Experimental analysis	Finite element software, analytical solutions	Nonlinear dynamics of hyperelastic membrane energy harvesters
Verron et al. [154]	1999	Mooney–Rivlin model	Conservation of momentum equation	sixth-order Runge–Kutta method	Nonlinear inflation behaviour of spherical hyperelastic membranes
Li et al. [155]	2018	Gent model	Principle of virtual work, Theory of dielectric elastomers	Analytical solution	Nonlinear vibrations of dielectric hyperelastic membranes
Chaudhuri and DasGupta [156]	2014	Mooney–Rivlin model	Perturbation dynamics, Lagrange function	Iterative Ritz method	Wrinkling in inflated circular hyperelastic membranes

structures largely deform when subjected to external loads, the importance of using appropriate nonlinear large-deformation modelling is undeniable.

In summary, by analysing more than 150 research works related to this field from basic analysis to specified simulations, it can be seen that although there have been several studies on each subject of hyperelastic structure behaviour, the field is under-researched and requires further investigations to model and analyse hyperelastic structures.

Acknowledgements The HDR scholarship support through The University of Adelaide and Faculty of Engineering, Computer & Mathematical Sciences, the University of Adelaide, is acknowledged.

Funding Open Access funding enabled and organized by CAUL and its Member Institutions. The authors have not disclosed any funding.

Data availability The authors have not disclosed any funding. The datasets generated during the current study are available from the corresponding author on reasonable request.

Declarations

Conflict of interest The authors declare that there is no conflict of interest with respect to the research, authorship and/or publication of this paper.

References

1. Chen, L., et al.: Design and modeling of a soft robotic surface with hyperelastic material. Mech. Mach. Theory **130**, 109–122 (2018)
2. Case, J.C., White, E.L., Kramer, R.K.: Soft material characterization for robotic applications. Soft Rob. **2**(2), 80–87 (2015)
3. Vignali, E., et al.: Modeling biomechanical interaction between soft tissue and soft robotic instruments: importance of constitutive anisotropic hyperelastic formulations. Int. J. Rob. Res. **40**(1), 224–235 (2021)
4. Polygerinos, P., et al.: Soft robotic glove for combined assistance and at-home rehabilitation. Robot. Auton. Syst. **73**, 135–143 (2015)
5. Yap, H.K., et al.: Design and preliminary feasibility study of a soft robotic glove for hand function assistance in stroke survivors. Front. Neurosci. **11**, 547 (2017)
6. Wang, B., et al. Design and development of a glove for post-stroke hand rehabilitation. In: 2017 IEEE international conference on advanced intelligent mechatronics (AIM). 2017. IEEE
7. Proulx, C.E., et al.: Review of the effects of soft robotic gloves for activity-based rehabilitation in individuals with reduced hand function and manual dexterity following a neurological event. J Rehabil Assist Technol Eng **7**, 2055668320918130 (2020)
8. Polygerinos, P., et al.: EMG controlled soft robotic glove for assistance during activities of daily living. In 2015 IEEE international conference on rehabilitation robotics (ICORR), IEEE
9. Antol, J. and J.F. P Calhoun, *Low CostMars Surface Exploration: the Mars Tumbleweed*. Washington DC: National Aeronauticsand Space Administration. NASA/TM-2003–212411
10. Trivedi, D., Lotfi, A., Rahn, C.D.: Geometrically exact models for soft robotic manipulators. IEEE Trans. Rob. **24**(4), 773–780 (2008)
11. Kumar, V., et al.: Supporting information for microengineered materials with self-healing features for soft robotics. Authorea Preprints, (2021)
12. Liu, J., et al.: Current research, key performances and future development of search and rescue robots. Front. Mech. Eng. China **2**(4), 404–416 (2007)
13. Kumar, V., et al.: Dragonfly inspired smart soft robot. bioRxiv, (2020)
14. Wallin, T., Pikul, J., Shepherd, R.: 3D printing of soft robotic systems. Nat. Rev. Mater. **3**(6), 84 (2018)
15. Schaffner, M., et al.: 3D printing of robotic soft actuators with programmable bioinspired architectures. Nat. Commun. **9**(1), 878 (2018)
16. Yap, H.K., Ng, H.Y., Yeow, C.-H.: High-force soft printable pneumatics for soft robotic applications. Soft Rob. **3**(3), 144–158 (2016)
17. He, L., et al.: Variational modeling of plane-strain hyperelastic thin beams with thickness-stretching effect. Acta Mech. **229**(12), 4845–4861 (2018)
18. Chen, Y., Jin, L.: Snapping-back buckling of wide hyperelastic columns. Extreme Mech. Lett. **34**, 100600 (2019)
19. Dong, L., et al.: Application of mechanical stretch to tune the resonance frequency of hyperelastic membrane-based energy harvesters. Sens. Actuators, A **252**, 165–173 (2016)
20. Tang, X., et al.: A soft crawling robot driven by single twisted and coiled actuator. Sens. Actuators, A **291**, 80–86 (2019)
21. Chen, T., Lee, D., Sung, C.-K.: An experimental study on transmission efficiency of a rubber V-belt CVT. Mech. Mach. Theory **33**(4), 351–363 (1998)
22. Bertini, L., Carmignani, L., Frendo, F.: Analytical model for the power losses in rubber V-belt continuously variable transmission (CVT). Mech. Mach. Theory **78**, 289–306 (2014)
23. Kolosov, A.: The stress-strain state of the belt in the operating changes of the burdening conveyor parameters. In: Theoretical and Practical Solutions of Mineral Resources Mining, pp. 585–590. CRC Press (2015)
24. Esse, R., *Flexible packaging end-use market analysis.* Linthicum, Md.: Flexible Packaging Assn, (2002)
25. Brody, A.L., et al.: Innovative food packaging solutions. J. Food Sci. **73**(8), 107–116 (2008)
26. Siracusa, V., et al.: Biodegradable polymers for food packaging: a review. Trends Food Sci. Technol. **19**(12), 634–643 (2008)
27. Dilkes-Hoffman, L.S., et al.: Environmental impact of biodegradable food packaging when considering food waste. J. Clean. Prod. **180**, 325–334 (2018)
28. Muller, J., González-Martínez, C., Chiralt, A.: Combination of poly (lactic) acid and starch for biodegradable food packaging. Materials **10**(8), 952 (2017)
29. Kim, H.S., Nonlinear multi-scale anisotropic material and structural models for prosthetic and native aortic heart valves. (2009) Georgia Institute of Technology
30. Schendel, M.J. and C.F. Popelar: Numerical methods for design and evaluation of prosthetic heart valves, in Heart Valves. (2013), Springer. pp. 321-341
31. Dickinson, A., Steer, J., Worsley, P.: Finite element analysis of the amputated lower limb: a systematic review and recommendations. Med. Eng. Phys. **43**, 1–18 (2017)

32. Mohammadi, H., Mequanint, K.: Prosthetic aortic heart valves: modeling and design. Med. Eng. Phys. **33**(2), 131–147 (2011)
33. Zolfagharian, A., Kaynak, A., Kouzani, A.: Closed-loop 4D-printed soft robots. Mater. Des. **188**, 108411 (2019)
34. Ijaz, S., et al.: Magnetically actuated miniature walking soft robot based on chained magnetic microparticles-embedded elastomer. Sens. Actuators, A **301**, 111707 (2020)
35. Bonet, J., Wood, R.D.: Nonlinear continuum mechanics for finite element analysis. Cambridge University Press, Cambridge (1997)
36. Holzapfel, G.A.: Nonlinear solid mechanics: a continuum approach for engineering science. Meccanica **37**(4–5), 489–490 (2002)
37. Bower, A.F.: Applied mechanics of solids. CRC Press, London (2009)
38. Steck, D., et al.: Mechanical responses of Ecoflex silicone rubber: compressible and incompressible behaviors. J. Appl. Polym. Sci. **136**(5), 47025 (2019)
39. Moerman, K.M., Fereidoonnezhad, B., McGarry, J.P.: Novel hyperelastic models for large volumetric deformations. Int. J. Solids Struct. **193**, 474–491 (2020)
40. Pelliciari, M., Tarantino, A.M.: Equilibrium paths for von Mises trusses in finite elasticity. J. Elast. **138**(2), 145–168 (2020)
41. Bertram, A.: Elasticity and plasticity of large deformations. (2012) Springer
42. Capurro, M. and F. Barberis: Evaluating the mechanical properties of biomaterials. In: Biomaterials for Bone Regeneration. (2014), Elsevier. pp. 270–323
43. Brown, C., et al.: Assessment of common hyperelastic constitutive equations for describing normal and osteoarthritic articular cartilage. Proc. Inst. Mech. Eng. [H] **223**(6), 643–652 (2009)
44. Breslavsky, I.D., Amabili, M., Legrand, M.: Nonlinear vibrations of thin hyperelastic plates. J. Sound Vib. **333**(19), 4668–4681 (2014)
45. Mooney, M.: A theory of large elastic deformation. J. Appl. Phys. **11**(9), 582–592 (1940)
46. Falope, F.O., et al.: Snap-through and Eulerian buckling of the bi-stable von Mises truss in nonlinear elasticity: a theoretical, numerical and experimental investigation. Int. J. Non-Linear Mech. **134**, 103739 (2021)
47. Rivlin, R.: Large elastic deformations of isotropic materials IV. Further developments of the general theory. Philos. Trans. R. Soc. Lond. Ser. A Math. Phys. Sci. **241**(835), 379–397 (1948)
48. Rivlin, R.: Large elastic deformations of isotropic materials VI. Further results in the theory of torsion, shear and flexure. Philos. Trans. R. Soc. Lond. Ser. A Math. Phys. Sci. **242**(845), 173–195 (1949)
49. Biderman, V., Calculation of rubber parts. Rascheti na prochnost, 1958. **40**.
50. Klosner, J.M. and A. Segal: Mechanical characterization of a natural rubber (1969)
51. James, A., Green, A., Simpson, G.: Strain energy functions of rubber. I. Characterization of gum vulcanizates. J. Appl. Polym. Sci. **19**(7), 2033–2058 (1975)
52. Marckmann, G., Verron, E.: Comparison of hyperelastic models for rubber-like materials. Rubber Chem. Technol. **79**(5), 835–858 (2006)
53. Ogden, R.: Large deformation isotropic elasticity—On the correlation of theory and experiment for incompressible rubberlike solids. Rubber Chem. Technol. **46**(2), 398–416 (1973)
54. Ogden, R.W.: Large deformation isotropic elasticity–on the correlation of theory and experiment for incompressible rubberlike solids. Proc. R. Soc. Londn. A Math. Phys. Sci. **326**(1567), 565–584 (1972)
55. Arruda, E.M., Boyce, M.C.: A three-dimensional constitutive model for the large stretch behavior of rubber elastic materials. J. Mech. Phys. Solids **41**(2), 389–412 (1993)
56. Liu, Y., A.E. Kerdok, and R.D. Howe. A nonlinear finite element model of soft tissue indentation. In: international symposium on medical simulation (2004) Springer
57. Gent, A.: A new constitutive relation for rubber. Rubber Chem. Technol. **69**(1), 59–61 (1996)
58. Gent, A.: Elastic instabilities of inflated rubber shells. Rubber Chem. Technol. **72**(2), 263–268 (1999)
59. Alibakhshi, A., Heidari, H.: Nonlinear dynamics of dielectric elastomer balloons based on the Gent-Gent hyperelastic model. Eur. J. Mech.-A/Solids **82**, 103986 (2020)
60. Horgan, C.O.: The remarkable Gent constitutive model for hyperelastic materials. Int. J. Non-Linear Mech. **68**, 9–16 (2015)
61. Destrade, M., Annaidh, A.N., Coman, C.D.: Bending instabilities of soft biological tissues. Int. J. Solids Struct. **46**(25–26), 4322–4330 (2009)
62. Goriely, A., Destrade, M., Amar, M.B.: Instabilities in elastomers and in soft tissues. Q. J. Mech. Appl. Math. **59**(4), 615–630 (2006)
63. Horgan, C., Saccomandi, G.: A description of arterial wall mechanics using limiting chain extensibility constitutive models. Biomech. Model. Mechanobiol. **1**(4), 251–266 (2003)
64. Roland, C.M., Viscoelastic behavior of rubbery materials. 2011: OUP Oxford
65. Bischoff, J.E., Arruda, E.M., Grosh, K.: A new constitutive model for the compressibility of elastomers at finite deformations. Rubber Chem. Technol. **74**(4), 541–559 (2001)
66. Mac Donald, B.J.: Practical stress analysis with finite elements. Glasnevin Publishing, Dublin (2007)
67. Horgan, C.O., Saccomandi, G.: Constitutive models for compressible nonlinearly elastic materials with limiting chain extensibility. J. Elast. **77**(2), 123–138 (2004)
68. Beda, T.: Modeling hyperelastic behavior of rubber: a novel invariant-based and a review of constitutive models. J. Polym. Sci., Part B: Polym. Phys. **45**(13), 1713–1732 (2007)
69. Blatz, P.J., Ko, W.L.: Application of finite elastic theory to the deformation of rubbery materials. Trans. Soc. Rheol. **6**(1), 223–252 (1962)
70. Murnaghan, F.D.: Finite deformations of an elastic solid. Am. J. Math. **59**(2), 235–260 (1937)
71. Ciarlet, P.G.: Mathematical Elasticity: Volume I: three-dimensional elasticity. (1988): North-Holland
72. Valanis, K., Landel, R.F.: The strain-energy function of a hyperelastic material in terms of the extension ratios. J. Appl. Phys. **38**(7), 2997–3002 (1967)

73. Hill, R.: Aspects of invariance in solid mechanics, advances in applied mechanics, pp. 1–75. Elsevier, London (1979)
74. Attard, M.M.: Finite strain—isotropic hyperelasticity. Int. J. Solids Struct. **40**(17), 4353–4378 (2003)
75. Bischoff, J., Arruda, E., Grosh, K.: A microstructurally based orthotropic hyperelastic constitutive law. J. Appl. Mech. **69**(5), 570–579 (2002)
76. Itskov, M.: A generalized orthotropic hyperelastic material model with application to incompressible shells. Int. J. Numer. Meth. Eng. **50**(8), 1777–1799 (2001)
77. Latorre, M., Montáns, F.J.: Material-symmetries congruency in transversely isotropic and orthotropic hyperelastic materials. Eur. J. Mech.-A/Solids **53**, 99–106 (2015)
78. Motevalli, M., et al.: Geometrically nonlinear simulation of textile membrane structures based on orthotropic hyperelastic energy functions. Compos. Struct. **223**, 110908 (2019)
79. Bonet, J., Burton, A.: A simple orthotropic, transversely isotropic hyperelastic constitutive equation for large strain computations. Comput. Methods Appl. Mech. Eng. **162**(1–4), 151–164 (1998)
80. Itskov, M., Aksel, N.: A class of orthotropic and transversely isotropic hyperelastic constitutive models based on a polyconvex strain energy function. Int. J. Solids Struct. **41**(14), 3833–3848 (2004)
81. Diani, J., et al.: Directional model for isotropic and anisotropic hyperelastic rubber-like materials. Mech. Mater. **36**(4), 313–321 (2004)
82. Sun, S. and W. Chen: An anisotropic hyperelastic constitutive model with bending stiffness interaction for cord-rubber composites: comparison of simulation results with experimental data. Math. Probl. Eng., 2020. **2020**
83. Gültekin, O., Dal, H., Holzapfel, G.A.: On the quasi-incompressible finite element analysis of anisotropic hyperelastic materials. Comput. Mech. **63**(3), 443–453 (2019)
84. Chaimoon, K., Chindaprasirt, P.: An anisotropic hyperelastic model with an application to soft tissues. Eur. J. Mech.-A/Solids **78**, 103845 (2019)
85. Cai, R., et al.: A new hyperelastic model for anisotropic hyperelastic materials with one fiber family. Int. J. Solids Struct. **84**, 1–16 (2016)
86. Nolan, D.R., et al.: A robust anisotropic hyperelastic formulation for the modelling of soft tissue. J. Mech. Behav. Biomed. Mater. **39**, 48–60 (2014)
87. Chen, Z.-W., Joli, P., Feng, Z.-Q.: Anisotropic hyperelastic behavior of soft biological tissues. Comput. Methods Biomech. Biomed. Engin. **18**(13), 1436–1444 (2015)
88. Guerin, H.L., Elliott, D.M.: Quantifying the contributions of structure to annulus fibrosus mechanical function using a nonlinear, anisotropic, hyperelastic model. J. Orthop. Res. **25**(4), 508–516 (2007)
89. Peng, X., et al.: A simple anisotropic hyperelastic constitutive model for textile fabrics with application to forming simulation. Compos. B Eng. **52**, 275–281 (2013)
90. Fernández, M., et al.: Anisotropic hyperelastic constitutive models for finite deformations combining material theory and data-driven approaches with application to cubic lattice metamaterials. Comput. Mech. **67**(2), 653–677 (2021)
91. De Marco, C., et al.: Indirect 3D and 4D printing of soft robotic microstructures. Adv. Mater. Technol. **4**(9), 1900332 (2019)
92. Yang, Y., et al.: Hybrid jamming for bioinspired soft robotic fingers. Soft Rob. **7**(3), 292–308 (2020)
93. Lee, J.-H., Chung, Y.S., Rodrigue, H.: Long shape memory alloy tendon-based soft robotic actuators and implementation as a soft gripper. Sci. Rep. **9**(1), 1–12 (2019)
94. Ji, X., et al.: An autonomous untethered fast soft robotic insect driven by low-voltage dielectric elastomer actuators. Sci. Robot. **4**(37), 6451 (2019)
95. Irschik, H., Gerstmayr, J.: A hyperelastic Reissner-type model for non-linear shear deformable beams. Proc. Mathmod. **9**, 1–7 (2009)
96. Irschik, H., Gerstmayr, J.: A continuum-mechanics interpretation of Reissner's non-linear shear-deformable beam theory. Math. Comput. Model. Dyn. Syst. **17**(1), 19–29 (2011)
97. Jiang, F., Yu, W.: Nonlinear variational asymptotic sectional analysis of hyperelastic beams. AIAA J. **54**(2), 679–690 (2015)
98. Lanzoni, L., Tarantino, A.M.: Finite anticlastic bending of hyperelastic solids and beams. J. Elast. **131**(2), 137–170 (2018)
99. Wang, R., et al.: Radially and axially symmetric motions of a class of transversely isotropic compressible hyperelastic cylindrical tubes. Nonlinear Dyn. **90**(4), 2481–2494 (2017)
100. Ogden, R.W.: Non-linear elastic deformations. Courier Corporation, United States (1997)
101. Forsat, M.: Investigating nonlinear vibrations of higher-order hyper-elastic beams using the Hamiltonian method. Acta Mech. **231**, 125–138 (2019)
102. Lotfan, S., et al.: Nonlinear resonances of axially functionally graded beams rotating with varying speed including Coriolis effects. Nonlinear Dyn. **107**(1), 533–558 (2022)
103. Tian, Y., Daeichin, M., Towfighian, S.: Dynamic behavior of T-beam resonator with repulsive actuation. Nonlinear Dyn. **107**(1), 15–31 (2022)
104. Ghayesh, M.H.: Dynamical analysis of multilayered cantilevers. Commun. Nonlinear Sci. Numer. Simul. **71**, 244–253 (2019)
105. Ghayesh, M.H.: Asymmetric viscoelastic nonlinear vibrations of imperfect AFG beams. Appl. Acoust. **154**, 121–128 (2019)
106. Mirjavadi, S.S., Forsat, M., Badnava, S.: Nonlinear modeling and dynamic analysis of bioengineering hyper-elastic tubes based on different material models. Biomech. Model. Mechanobiol. **19**, 971–983 (2019)
107. Pham, P.-T., Hong, K.-S.: Dynamic models of axially moving systems: a review. Nonlinear Dyn. **100**(1), 315–349 (2020)
108. Chen, L.-Q., Tang, Y.-Q., Lim, C.W.: Dynamic stability in parametric resonance of axially accelerating viscoelastic Timoshenko beams. J. Sound Vib. **329**(5), 547–565 (2010)
109. Wang, Y., Ding, H., Chen, L.-Q.: Vibration of axially moving hyperelastic beam with finite deformation. Appl. Math. Model. **71**, 269–285 (2019)
110. Zhu, X., Wang, Y., Lou, Z.: A study of the critical strain of hyperelastic materials: a new kinematic frame and the

leading order term. Mech. Res. Commun. **78**, 20–24 (2016)
111. Chen, W., Wang, L., Dai, H.: Nonlinear free vibration of hyperelastic beams based on neo-Hookean model. Int. J. Struct. Stab. Dyn. **20**(01), 2050015 (2020)
112. Wang, Y., Ding, H., Chen, L.-Q.: Nonlinear vibration of axially accelerating hyperelastic beams. Int. J. Non-Linear Mech. **99**, 302–310 (2018)
113. Khaniki, H.B., et al.: Experimental characteristics and coupled nonlinear forced vibrations of axially travelling hyperelastic beams. Thin-Wall. Struct. **170**, 108526 (2022)
114. Mirparizi, M., Fotuhi, A.: Nonlinear coupled thermo-hyperelasticity analysis of thermal and mechanical wave propagation in a finite domain. Physica A **537**, 122755 (2020)
115. Khaniki, H.B., et al.: Large amplitude vibrations of imperfect porous-hyperelastic beams via a modified strain energy. J. Sound Vib. **513**, 116416 (2021)
116. Ügdüler, S., et al.: Towards closed-loop recycling of multilayer and coloured PET plastic waste by alkaline hydrolysis. Green Chem. **22**(16), 5376–5394 (2020)
117. Schulze, M., et al.: Evaluation of a panel of spermatological methods for assessing reprotoxic compounds in multilayer semen plastic bags. Sci. Rep. **10**(1), 1–11 (2020)
118. Ramos, M.J.G., Lozano, A., Fernández-Alba, A.R.: High-resolution mass spectrometry with data independent acquisition for the comprehensive non-targeted analysis of migrating chemicals coming from multilayer plastic packaging materials used for fruit purée and juice. Talanta **191**, 180–192 (2019)
119. Walker, T.W., et al.: Recycling of multilayer plastic packaging materials by solvent-targeted recovery and precipitation. Sci. Adv. **6**(47), 7599 (2020)
120. Khaniki, H.B., et al.: Nonlinear continuum mechanics of thick hyperelastic sandwich beams using various shear deformable beam theories. Cont. Mech. Thermodyn. **34**, 781–827 (2022)
121. Wang, Y., Zhu, W.: Nonlinear transverse vibration of a hyperelastic beam under harmonic axial loading in the subcritical buckling regime. Appl. Math. Model. **94**, 597–618 (2021)
122. Wang, Y., Zhu, W.: Nonlinear transverse vibration of a hyperelastic beam under harmonically varying axial loading. J. Comput. Nonlinear Dyn. **16**(3), 031006 (2021)
123. Faghihi, S., et al.: Graphene oxide/poly (acrylic acid)/gelatin nanocomposite hydrogel: experimental and numerical validation of hyperelastic model. Mater. Sci. Eng., C **38**, 299–305 (2014)
124. Pelliciari, M., Tarantino, A.M.: Equilibrium and stability of anisotropic hyperelastic graphene membranes. J. Elast. **144**(2), 169–195 (2021)
125. Pelliciari, M., Tarantino, A.M.: A nonlinear molecular mechanics model for graphene subjected to large in-plane deformations. Int. J. Eng. Sci. **167**, 103527 (2021)
126. Höller, R., Libisch, F., Hellmich, C.: A membrane theory for circular graphene sheets, based on a hyperelastic material model for large deformations. Mech. Adv. Mater. Struct. **29**(5), 651–661 (2022)
127. Alibakhshi, A., et al.: Nonlinear free and forced vibrations of a hyperelastic micro/nanobeam considering strain stiffening effect. Nanomaterials **11**(11), 3066 (2021)
128. Yang, F., et al.: Couple stress based strain gradient theory for elasticity. Int. J. Solids Struct. **39**(10), 2731–2743 (2002)
129. Ma, H., Gao, X.-L., Reddy, J.: A microstructure-dependent Timoshenko beam model based on a modified couple stress theory. J. Mech. Phys. Solids **56**(12), 3379–3391 (2008)
130. Park, S., Gao, X.: Bernoulli-Euler beam model based on a modified couple stress theory. J. Micromech. Microeng. **16**(11), 2355 (2006)
131. Ghayesh, M.H.: Nonlinear dynamics of multilayered microplates. J. Comput. Nonlinear Dyn. **13**(2), 021006 (2018)
132. Ghayesh, M.H.: Mechanics of tapered AFG shear-deformable microbeams. Microsyst. Technol. **24**(4), 1743–1754 (2018)
133. Breslavsky, I.D., Amabili, M., Legrand, M.: Physically and geometrically non-linear vibrations of thin rectangular plates. Int. J. Non-Linear Mech. **58**, 30–40 (2014)
134. Amabili, M., et al.: Experimental and numerical study on vibrations and static deflection of a thin hyperelastic plate. J. Sound Vib. **385**, 81–92 (2016)
135. Zhang, J., et al.: Nonlinear vibration analyses of cylindrical shells composed of hyperelastic materials. Acta Mech. Solida Sin. **32**(4), 463–482 (2019)
136. Xu, J., et al.: Nonlinear vibrations of thermo-hyperelastic moderately thick cylindrical shells with 2: 1 internal resonance. Int. J. Struct. Stab. Dyn. **20**(05), 2050067 (2020)
137. Xu, J., et al.,: Internal resonance of hyperelastic thin-walled cylindrical shells under harmonic axial excitation and time-varying temperature field (2021)
138. Breslavsky, I.D., Amabili, M., Legrand, M.: Static and dynamic behavior of circular cylindrical shell made of hyperelastic arterial material. J. Appl. Mech. **83**(5), 051002 (2016)
139. Tripathi, A., Bajaj, A.K.: Topology optimization and internal resonances in transverse vibrations of hyperelastic plates. Int. J. Solids Struct. **81**, 311–328 (2016)
140. Tripathi, A., Bajaj, A.K.: Design for 1: 2 internal resonances in in-plane vibrations of plates with hyperelastic materials. J. Vib. Acoust. **136**(6), 061005 (2014)
141. Zhao, Z., et al.: Nonlinear dynamics of loaded visco-hyperelastic spherical shells. Nonlinear Dyn. **101**(2), 911–933 (2020)
142. Aranda-Iglesias, D., Rodríguez-Martínez, J., Rubin, M.: Nonlinear axisymmetric vibrations of a hyperelastic orthotropic cylinder. Int. J. Non-Linear Mech. **99**, 131–143 (2018)
143. Aranda-Iglesias, D., Vadillo, G., Rodríguez-Martínez, J.: Constitutive sensitivity of the oscillatory behaviour of hyperelastic cylindrical shells. J. Sound Vib. **358**, 199–216 (2015)
144. Mason, D., Maluleke, G.: Non-linear radial oscillations of a transversely isotropic hyperelastic incompressible tube. J. Math. Anal. Appl. **333**(1), 365–380 (2007)
145. Xu, Q., Liu, J and Qu, L.: A higher-order plate element formulation for dynamic analysis of hyperelastic silicone plate. J Mech pp 1–14
146. Aranda-Iglesias, D., Vadillo, G., Rodríguez-Martínez, J.: Oscillatory behaviour of compressible hyperelastic shells

subjected to dynamic inflation: a numerical study. Acta Mech. **228**(6), 2187–2205 (2017)
147. Amabili, M., Breslavsky, I., Reddy, J.: Nonlinear higher-order shell theory for incompressible biological hyperelastic materials. Comput. Methods Appl. Mech. Eng. **346**, 841–861 (2019)
148. Wang, R., et al.: Nonlinear singular traveling waves in a slightly compressible thermo-hyperelastic cylindrical shell. Nonlinear Dyn. **107**(2), 1495–1509 (2022)
149. Gonçalves, P.B., Soares, R.M., Pamplona, D.: Nonlinear vibrations of a radially stretched circular hyperelastic membrane. J. Sound Vib. **327**(1–2), 231–248 (2009)
150. Soares, R.M., Gonçalves, P.B.: Nonlinear vibrations and instabilities of a stretched hyperelastic annular membrane. Int. J. Solids Struct. **49**(3–4), 514–526 (2012)
151. Soares, R.M., et al.: Nonlinear breathing motions and instabilities of a pressure-loaded spherical hyperelastic membrane. Nonlinear Dyn. **99**(1), 351–372 (2020)
152. Mangan, R., Destrade, M.: Gent models for the inflation of spherical balloons. Int. J. Non-Linear Mech. **68**, 52–58 (2015)
153. Ilssar, D., Gat, A.D.: On the inflation and deflation dynamics of liquid-filled, hyperelastic balloons. J. Fluids Struct. **94**, 102936 (2020)
154. Verron, E., et al.: Dynamic inflation of hyperelastic spherical membranes. J. Rheol. **43**(5), 1083–1097 (1999)
155. Li, Y., et al.: Nonlinear dynamic analysis and active control of visco-hyperelastic dielectric elastomer membrane. Int. J. Solids Struct. **152**, 28–38 (2018)
156. Chaudhuri, A., DasGupta, A.: On the static and dynamic analysis of inflated hyperelastic circular membranes. J. Mech. Phys. Solids **64**, 302–315 (2014)

Chapter 3

Axially travelling hyperelastic beams

Overview

After showing the importance of understanding the mechanics of hyperelastic structures in Chapter 2, this chapter and the next five chapters focus on the mechanics of hyperplastic structures in some of the most common applications and mechanical conditions. One of the well-known applications of polymeric structures is in belt-operating systems (such as power transmission systems, roll-to-roll systems and conveyors). This chapter aims to understand the linear and nonlinear mechanical behaviour of isotropic incompressible hyperelastic belts in axially-travelling conditions. Experimental tests are undertaken to obtain the nonlinear elastic behaviour, and different hyperelastic theories are explored to find the best fit. By finding the proper hyperelastic strain energy density model for the case, the mechanics of axially-travelling hyperelastic belts are presented under a harmonic external load. This research study is published and available online as: Khaniki, H. B., Ghayesh, M. H., Chin, R., & Chen, L. Q. (2022). Experimental characteristics and coupled nonlinear forced vibrations of axially travelling hyperelastic beams. Thin-Walled Structures, 170, 108526. DOI: 10.1016/j.tws.2021.108526

Statement of Authorship

Title of Paper	Experimental characteristics and coupled nonlinear forced vibrations of axially travelling hyperelastic beams
Publication Status	☑ Published ☐ Accepted for Publication ☐ Submitted for Publication ☐ Unpublished and Unsubmitted w ork w ritten in manuscript style
Publication Details	Khaniki, H. B., Ghayesh, M. H., Chin, R., & Chen, L. Q. (2022). Experimental characteristics and coupled nonlinear forced vibrations of axially travelling hyperelastic beams. Thin-Walled Structures, 170, 108526.

Principal Author

Name of Principal Author (Candidate)	Hossein Bakhshi Khaniki		
Contribution to the Paper	I carried out the literature review, conceptualization, formal analysis, investigation, methodology, software, validation, visualization and wrote the manuscript.		
Overall percentage (%)	80%		
Certification:	This paper reports on original research I conducted during the period of my Higher Degree by Research candidature and is not subject to any obligations or contractual agreements with a third party that would constrain its inclusion in this thesis. I am the primary author of this paper.		
Signature		Date	2/11/2022

Co-Author Contributions

By signing the Statement of Authorship, each author certifies that:

i. the candidate's stated contribution to the publication is accurate (as detailed above);

ii. permission is granted for the candidate in include the publication in the thesis; and

iii. the sum of all co-author contributions is equal to 100% less the candidate's stated contribution.

Name of Co-Author	Mergen Ghayesh		
Contribution to the Paper	As the principal supervisor, I helped to construct the manuscript, edit and review the manuscript for submission. I assisted in the conceptualization, investigation, methodology, review and editing. I hereby give consent to Hossein Bakhshi Khaniki to present this paper for examination towards the degree of Doctor of Philosophy.		
Signature		Date	3/11/2022

Name of Co-Author	Rey Chin		
Contribution to the Paper	I assisted in review and editing of the manuscript. I hereby give consent to Hossein Bakhshi Khaniki to present this paper for examination towards the degree of Doctor of Philosophy.		
Signature		Date	3/11/2022

Name of Co-Author	Li-Qun Chen		
Contribution to the Paper	I assisted in the conceptualization, review and editing of the manuscript. I hereby give consent to Hossein Bakhshi Khaniki to present this paper for examination towards the degree of Doctor of Philosophy.		
Signature		Date	2022.11.4.

Thin-Walled Structures 170 (2022) 108526

Contents lists available at ScienceDirect

Thin-Walled Structures

journal homepage: www.elsevier.com/locate/tws

Full length article

Experimental characteristics and coupled nonlinear forced vibrations of axially travelling hyperelastic beams

Hossein B. Khaniki [a,*], Mergen H. Ghayesh [a,*], Rey Chin [a], Li-Qun Chen [b]

[a] School of Mechanical Engineering, University of Adelaide, South Australia 5005, Australia
[b] School of Mechanics and Engineering Science, Shanghai University, Shanghai 200072, China

ARTICLE INFO

Keywords:
Hyperelastic
Nonlinear vibration
Nonlinear dynamics
Hyperelastic beams
Axially moving beams

ABSTRACT

Comprehensively investigated in this paper is the coupled nonlinear dynamics of hyperelastic beams. Experimental testing is performed to accurately model the hyperelasticity using different hyperelastic energy density models. Samples were fabricated using 3D printing technique for flexible thermoplastic polyurethane filaments following the ASTM D638 guidance and tested using a tensile testing machine. For a proper hyperelastic energy density model, coupled nonlinear equations of motion are obtained via the von Kármán geometrical nonlinearity and Hamilton's principle. Free natural vibration response of the gyroscopic system is analysed using a generalised modal decomposition method and the influence of different parameters such as the hyperelastic stiffness term and the axial velocity on the natural frequencies is investigated. Complex mode shapes are obtained and the influence of axial velocity on altering the real and imaginary parts is discussed. Furthermore, a comprehensive analysis on the coupled nonlinear dynamics of the system is presented using a combination of Galerkin's scheme and a dynamic equilibrium technique. The frequency response to different design parameters such as axial speed, axial tension, harmonic external load, hyperelastic parameters and geometrical imperfection is discussed in detail. It is shown that the system shows a wide range of rich nonlinear dynamics including hardening depending on the characteristics of the system.

1. Introduction

Axially moving structures play an important role in many mechanical systems with applications in multiple engineering disciplines [1]. In these systems, an element of the system has an axial motion which the dynamic behaviour of the whole system and the critical designing parameters relies on the accuracy of modelling and understanding the mechanical behaviour of the moving element [2–9].

1.1. Applications

Hyperelastic axially moving beams have a wide range of applications in different mechanical systems such as conveyors, belt operating power transmission systems, treadmills, technical textile manufacturing process, roll-to-roll systems, flexible electronics and nanotechnology and continuously variable transmissions (CVTs) [1,10]. Since the moving element in such structures is soft and undergo large strains, modelling it using linear elastic theories can lead to high errors. Therefore, to have a proper designing of mechanical systems with an axially moving hyperelastic element, it is necessary to use a proper modelling for the hyperelasticity. Fig. 1 shows a schematic of a belt operating mechanical system which the moving element is modelled as an axially moving hyperelastic beam.

Another important application of hyperelastic structures can be found in soft robotics which smooth motion and higher degrees of freedom are required [11–15]. Axially moving hyperelastic arms and robots have been studied previously showing great possible applications in future. To optimise the designing and performance of soft robots, it is crucial to comprehend the physics behind the mechanical behaviour of these robots.

1.2. Brief review on axially moving beam structures

Axially moving *linear elastic* beam structures have been investigated in the past few decades by many researchers [16–19]. For beam structures, Wickert [20] examined the nonlinear vibration behaviour of axially moving simply-supported elastic beams using the Euler–Bernoulli beam theory and a second-order perturbation solution. Chen and Yang [21] investigated the viscoelastic behaviour of axially moving simply-supported beams using a method of multiple scales, showing

* Corresponding authors.
E-mail addresses: hossein.bakhshikhaniki@adelaide.edu (H.B. Khaniki), mergen.ghayesh@adelaide.edu.au (M.H. Ghayesh), rey.chin@adelaide.edu.au (R. Chin), lqchen@shu.edu.cn (L.-Q. Chen).

https://doi.org/10.1016/j.tws.2021.108526
Received 18 August 2021; Accepted 2 October 2021
Available online 22 October 2021

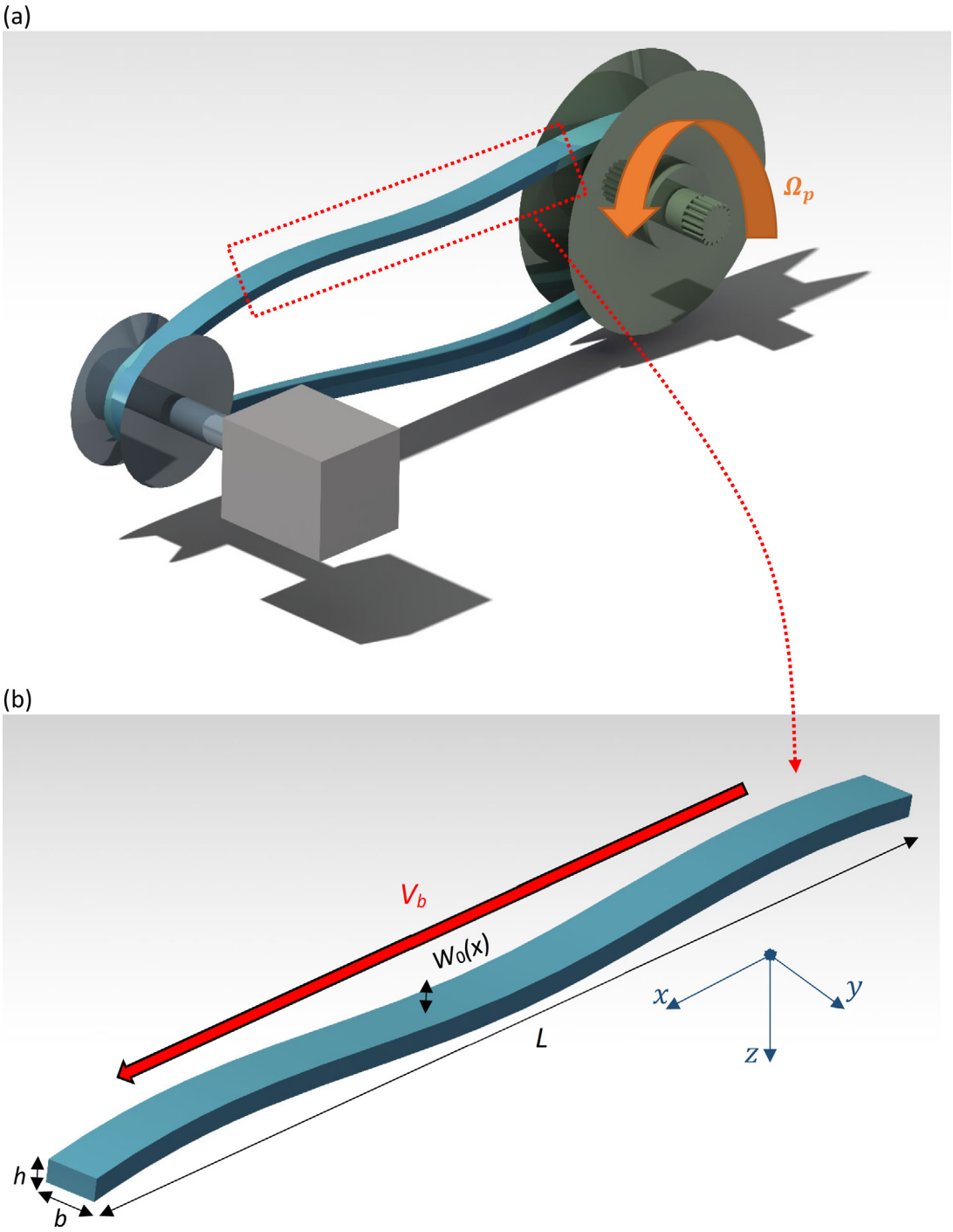

Fig. 1. (a) Schematic of a belt operating power transmission system and (b) the geometrical properties of the axially moving element of the system.

that increasing the viscosity coefficient decreases the damped frequencies. Pellicano and Vestroni [22] studied the bifurcations and nonlinear dynamics of axially moving simply-supported elastic beams. The Galerkin method and a complex adaptive step-size Runge–Kutta scheme were used to discretise the equations of motion; it was shown that in the supercritical speed range, only the first bifurcated position is stable. Öz et al. [23] studied time-dependent velocity of axially travelling Euler–Bernoulli simply-supported elastic beams using a scale method; it was shown that by increasing the speed, the natural frequency terms decrease which leads to divergence instability. Sub/super-critical nonlinear dynamics of axially moving simply-supported elastic beams have been investigated by Ghayesh et al. [24] using a pseudo-arclength continuation method; it was shown that the system shows energy transition from the first to the second mode.

For cantilever *elastic* beams, Chang et al. [25] examined the dynamics of axially moving elastic beams. The Rayleigh beam theory and Runge–Kutta algorithm were used to obtain and solve the problem showing that the unstable regions of the system are close to the linear combination of natural frequencies.

Axially moving *elastic* beams immersed in a fluid have been studied by researchers. Lin and Qiao [26] investigated the mechanical response of axially moving simply-supported elastic beams surrounded in a fluid. A differential quadrature method (DQM) was used to solve the problem showing that as the moving speed of the beam increases, the divergence in the first mode occurs.

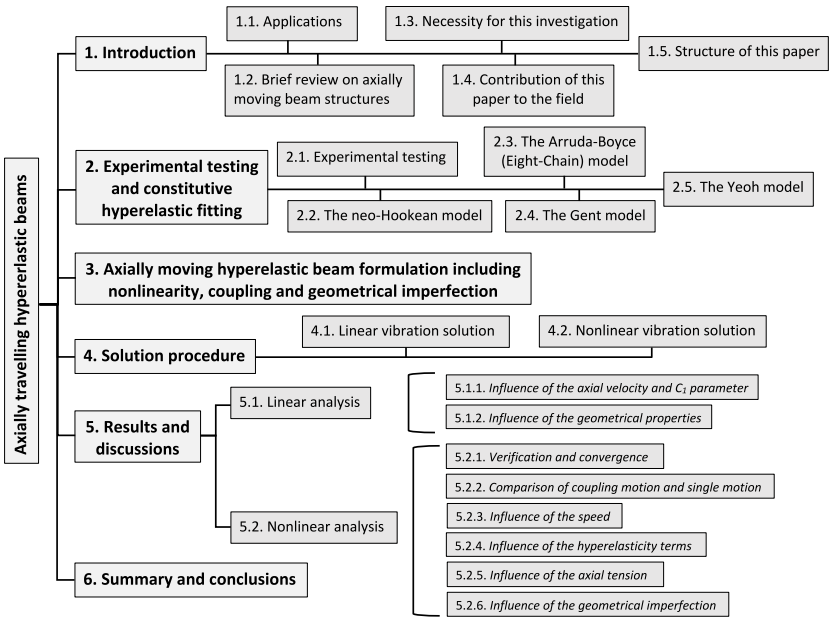

Fig. 2. Flowchart of this paper.

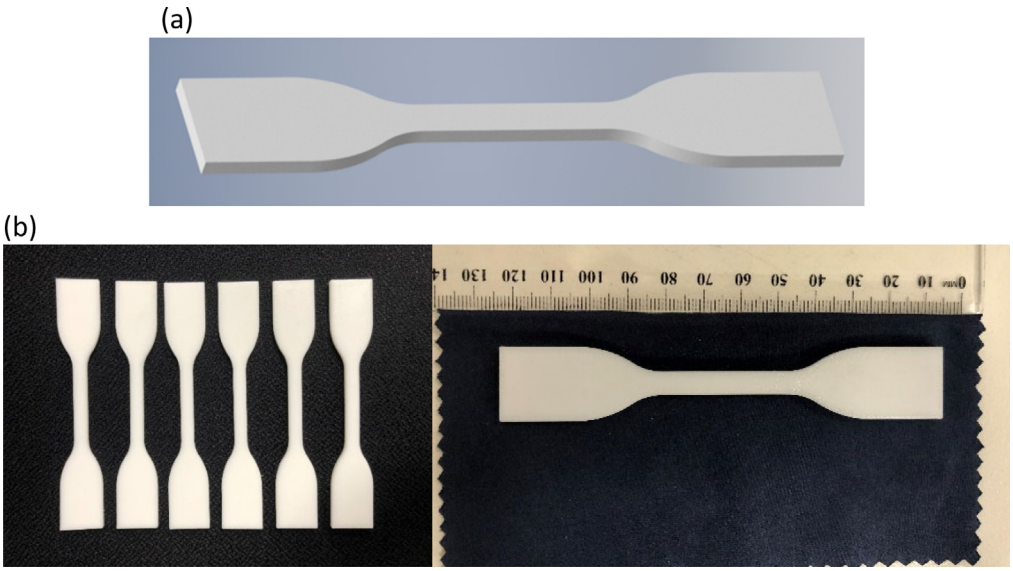

Fig. 3. (a) CAD drawing of dumbbell samples and (b) fabricated dumbbell samples.

The rotation has been combined with the axial motion and studied by Yuh and Young [27]. They investigated the dynamic behaviour of axially moving beams both experimentally and theoretically; it was shown that the approximated dynamic model was capable of tracking the experimental data on time-deflections of the tip.

Internal resonances for *elastic* beams have been examined by many researchers. In one study, Huang et al. [28] examined three-to-one internal resonances of axially moving elastic beams. The incremental harmonic balance (IHB) method together with the Floquet theory and Hsu's method was employed to solve the problem showing that hardening-spring nonlinear characteristics were obtained for the problem.

Influence of having intermediate spring support on the mechanical response of axially moving hyperelastic beams have been investigated by Ghayesh et al. [29]. Hamilton's principle was used to reach the equation of motion and was solved through the pseudo-arclength continuation technique and variable step size Runge–Kutta method; it was shown that the position of the spring support has a rich effect in varying the stiffness hardening behaviour of the system.

For more information about axially moving elastic structures, interested readers are referred to the comprehensive review on axially moving beams by Pham and Hong [1] in 2020 and controlling systems for axially moving beams by Hong and Pham [30] in 2019.

1.3. Necessity for this investigation

In mechanical systems with a moving element, the axially moving component do not necessarily follow *linear elastic constitutive models* and encounters large strains while undergoing loadings which makes the analysis complicated and out of the linear elasticity regime [31]. To have an accurate model of the moving element, *hyperelastic* constitutive models should be used. Previously, axially travelling hyperelastic compressible beams have been modelled using the neo-Hookean strain energy density model and were solved using a variable step-size Runge–Kutta method and a multiple scales method [32,33]. These studies were

the first steps in investigating the nonlinear mechanics of hyperelastic axially moving structures.

In this study, it is shown experimentally that the neo-Hookean model is not the best strain energy density model for simulating the hyperelasticity of some hyperelastic structures such as 3D printed thermoplastic polyurethane; this importance was previously discussed for silicone rubber samples in [34] by mentioning "*neo-Hookean model showed the worst performance, unable to capture the nonlinearity of the mechanical properties*". Therefore, by showing the importance of having a proper modelling of hyperelasticity, different strain energy models are examined in this paper using experimental analysis data and a proper strain energy density model is chosen for further investigations on the dynamic response of the system.

1.4. Contribution of this paper to the field

So far, there have been limited investigations on the nonlinear dynamic response of hyperelastic axially moving beams. This paper has the novelties of:

(i) The experimental testing results for the mechanical characteristics of flexible thermoplastic polyurethane samples are presented for the first time in the framework of hyperelasticity.
(ii) Different hyperelastic strain energy density models are analysed and the best fit for flexible thermoplastic polyurethane samples is presented.
(iii) Coupled nonlinear equations of motion of axially moving hyperelastic beams are presented for the first time in the framework of Yeoh's hyperelastic strain energy density model.
(iv) Geometrical imperfection is added to the coupled dynamic formulation of hyperelastic beams for the first time.
(v) Natural frequencies and complex mode shapes for the given axially moving thermoplastic polyurethane moving beam are presented.
(vi) A dynamic equilibrium technique is provided to solve the coupled highly nonlinear equations of motion.
(vii) Influence of design and operating parameters (hyperelastic strain energy density terms, velocity, axial tension and geometrical imperfection) on the nonlinear dynamics of the system is presented.
(viii) The importance of correctly modelling the structure using hyperelastic strain energy density models and considering the coupled motion is investigated.

1.5. Structure of this paper

In order to present a comprehensive study in this field, this paper is structured as follow (Fig. 2). In Section 1, after clarifying the applications of the current study, a brief literature review on axially moving soft beam models is presented and the necessity for hyperelastic modelling of axially moving beam structures is given and the contribution of this paper to the field is clarified. In Section 2, a set of experimental testing is performed following standards and some of the well-known hyperelastic constitutive models suitable for the current problem are analysed and the coefficients for each hyperelastic strain energy density models for the experimental testing results are obtained. In Section 3, nonlinear dynamics of axially moving hyperelastic beams are formulated by considering both axial and transverse motions using a proper model of strain energy density obtained from Section 2. In Section 4, the solution procedure for solving the coupled equations of motion is presented for both linear and nonlinear analysis of the system and in Section 5, a detailed explanation and discussion on the mechanical response of the system is presented and influence of different parameters on the linear and nonlinear mechanical response of the system is investigated. Finally, in Section 6, a summary of the achievement of this paper is presented with listed conclusions obtained in this study.

2. Experimental testing and constitutive hyperelastic fitting

In this section, some of the well-known hyperelastic constitutive models are examined and their capability for modelling the mechanical behaviour of soft structures is analysed by fitting the model with experimental results. Since 3D printed structures are widely being used for many purposes, in this section, samples are fabricated using this procedure to describe the mechanical characteristics of the sample structures.

2.1. Experimental testing

There are different standards available for analysing the mechanical behaviour of hyperelastic structures. ASTM D638 is one of the well-known standards used by many researchers to obtain the tensile behaviour of soft structures. Accordingly, in this study, dumbbell samples have been fabricated using 3D printing for flexible thermoplastic polyurethane filaments [35] with 100% infill following the ASTM D638 standard (Fig. 3). The samples were tested using an INSTRON testing machine with the speed of 500 mm/min (Fig. 4). Testing is repeated five times and the force–displacement and stress–strain behaviour are obtained as shown in Fig. 5.

It can be seen that the samples show high nonlinear behaviour in their force–deformation response and the linear elasticity constitutive models are invalid for analysing these structures. By having the stress–strain behaviour of the soft structure, different strain energy density models are investigated in the following subsections to determine a proper model with hyperelastic coefficients.

2.2. The neo-Hookean model

The neo-Hookean model is one of the simplest expressions of hyperelastic strain density model in which the influence of the second invariant term on the strain energy density is neglected as [36]

$$W_{NH} = C_1\left(\overline{I}_1 - 3\right) + D_1\left(J-1\right)^2, \tag{1}$$

where W_{NH} is the strain energy density of the neo-Hookean model, C_1 is the coefficient of the first invariant parameter and D_1 is the coefficient for compressibility. By using curve fitting techniques, the closest model of the neo-Hookean energy density model for predicting the stress–strain behaviour is shown in Fig. 6 with $C_1 = 1.549$ MPa which can be seen that has a significant error

2.3. The Arruda–Boyce (Eight-Chain) model

In Arruda and Boyce [37] model, the strain energy density is a function of the first invariant as a polynomial series

$$W_{AB} = \sum_{i=1}^{n} C_i\left(\overline{I}_1^i - 3^i\right) + \sum_{i=1}^{n} D_i\left(J-1\right)^{2i}, \tag{2}$$

where W_{AB} is the strain energy density of the Arruda–Boyce model. For a two-parameter Arruda–Boyce model, the results for curve fitting is shown in Fig. 7 with the coefficients as $C_1 = 2.412$ MPa and $C_2 = -40.605$ kPa.

2.4. The Gent model

For the Gent [38,39] model, the hyperelastic strain energy density is written using the natural logarithm as

$$W_G = -\frac{C_1 C_2}{2}\ln\left(1 + \frac{3 - I_1}{C_1}\right), \tag{3}$$

where W_G is the strain energy density of Gent model and C_1 is a maximum permitted value in the order of 100 for plastic structures [38,39] and with lower magnitudes (0.4 – 2.3) for biological tissues [40–43]. For the current problem, the fitting gives the result of $C_1 = -9.938$, $C_2 = -0.4981$ MPa for the coefficients as shown in Fig. 8.

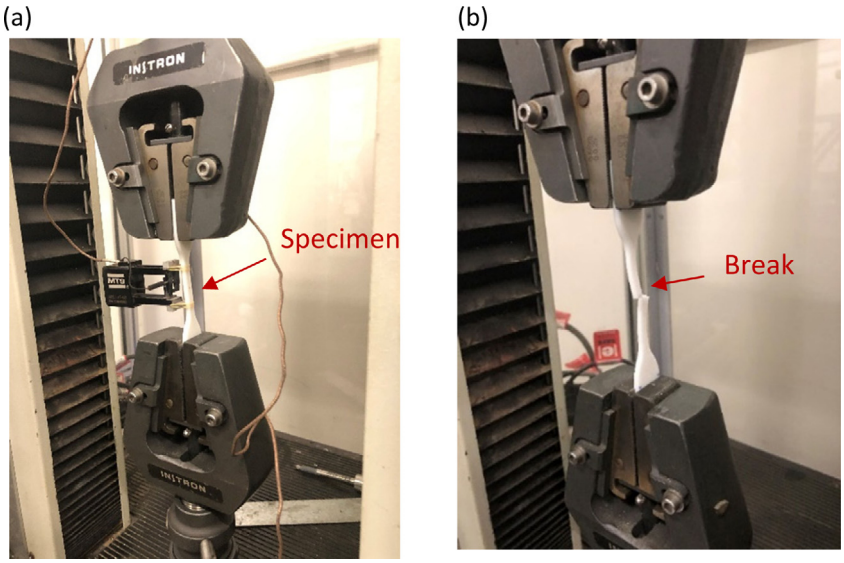

Fig. 4. Tensile testing the 3D printed thermoplastic polyurethane dumbbell samples (a) before, and (b) after application of a tensile load.

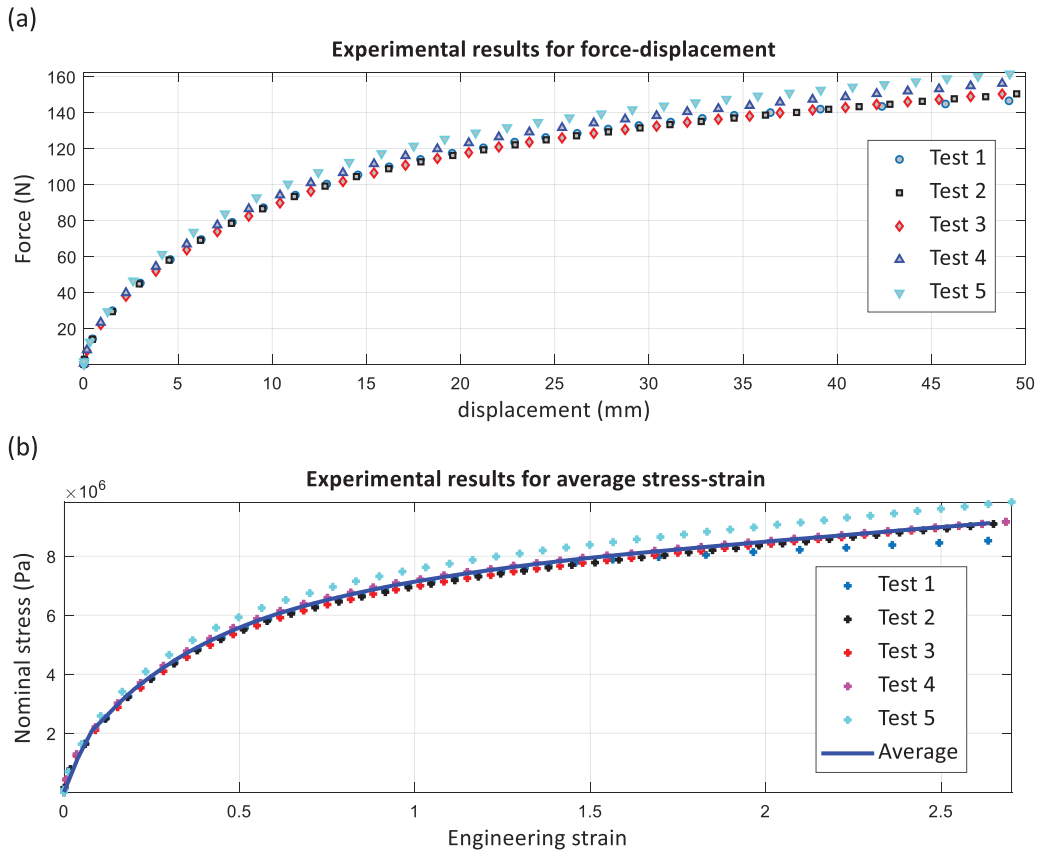

Fig. 5. Experimental testing results of soft dumbbell samples (a) force–displacement and (b) stress–strain.

2.5. The Yeoh model

Yeoh's hyperelastic model presents the strain energy density of the structure as

$$W_Y = C_1 (I_1 - 3) + C_2 (I_1 - 3)^2 + C_3 (I_1 - 3)^3, \tag{4}$$

where W_Y is the strain energy density of Yeoh's model and C_i are the hyperelastic coefficients which for the given experimental test results, the coefficients are obtained as $C_1 = 2.631$ MPa $C_2 = -0.1404$ MPa and $C_3 = 5016$ Pa (Fig. 9). Table 1 shows the strain energy hyperelastic coefficients for best fitting with the experimental testing results.

3. Axially moving hyperelastic beam formulation including nonlinearity, coupling and geometrical imperfection

For thin hyperelastic beams, by assuming the slope of the initial rise of the curved support is small compared to unity, and considering the von Kármán nonlinearity, displacements and strains are written using

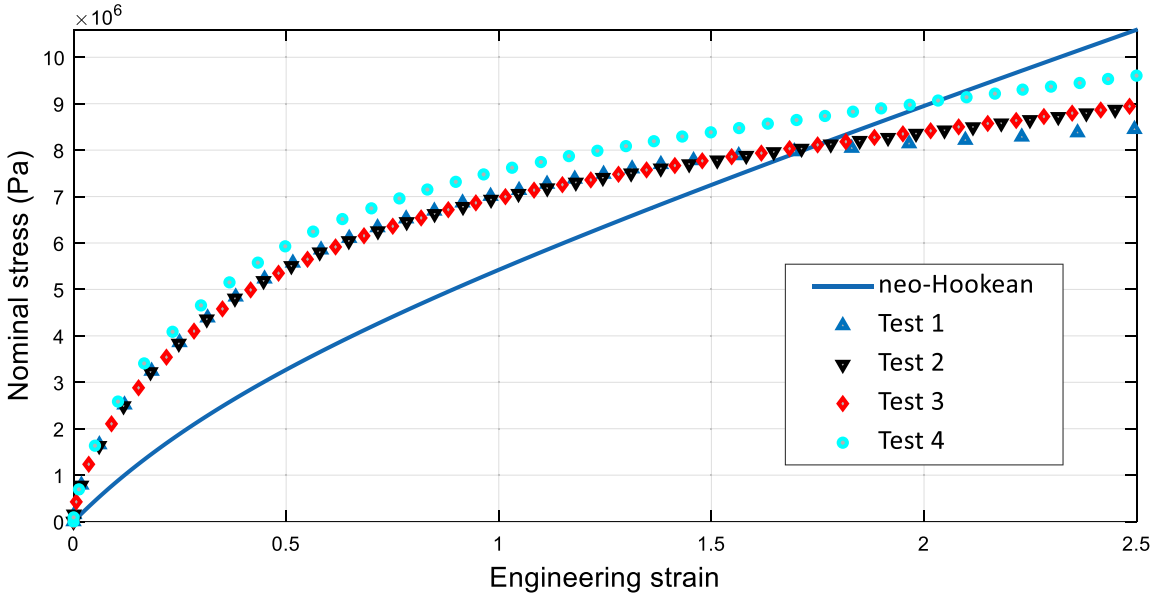

Fig. 6. Stress–strain modelling using *neo-Hookean* hyperelastic strain energy density model.

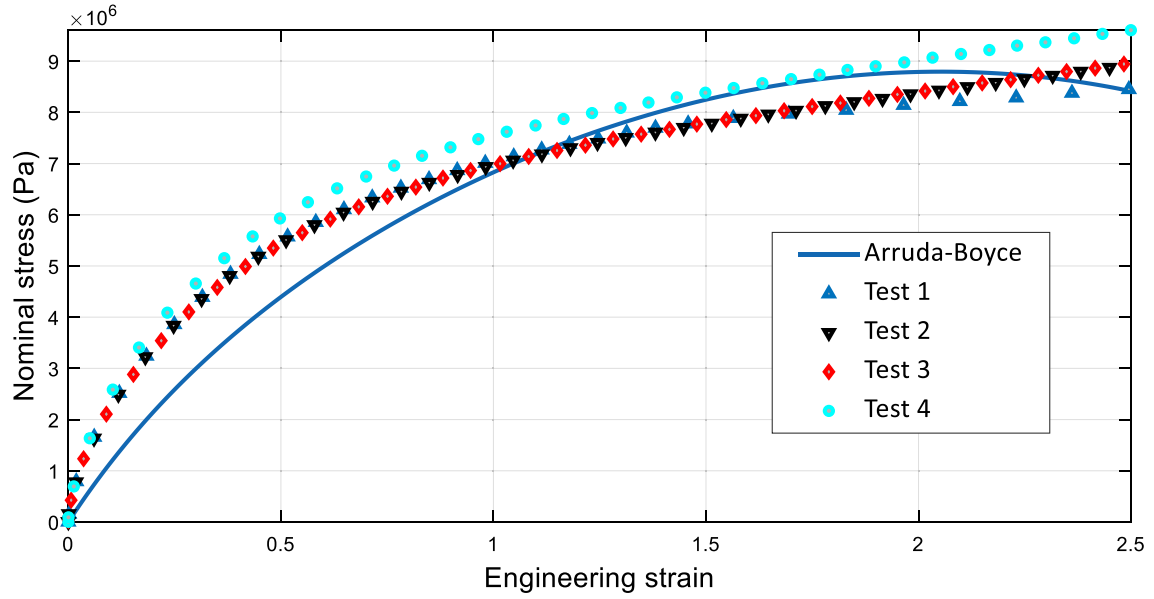

Fig. 7. Stress–strain modelling using *Arruda–Boyce (eight-chain)* hyperelastic strain energy density model.

Table 1
Strain energy density coefficients for different hyperelastic models.

Strain energy density model	C_1	C_2	C_3
Neo-Hookean	1.549e+06	–	–
Arruda–Boyce	2.412e+06	−4.605e+04	–
Gent	−9.938	−4.981e+05	–
Yeoh	2.631e6	−1.404e5	5016

hollow beam model as [44]

$$\begin{cases} u(x,y,z,t) = u(x,t) - z\dfrac{\partial w(x,t)}{\partial x}, \\ v(x,y,z,t) = 0, \\ w(x,y,z,t) = w(x,t) - w_0(x), \end{cases} \tag{5}$$

$$\varepsilon_x = \frac{\partial u}{\partial x} - z\frac{\partial^2 w}{\partial x^2} + \frac{1}{2}\left(\frac{\partial w}{\partial x}\right)^2 - \frac{\partial w}{\partial x}\frac{dw_0}{dx}, \quad \varepsilon_y \neq 0, \quad \varepsilon_z \neq 0, \tag{6}$$

where u, v and w are the displacements in x, y and z directions (shown in Fig. 1b), w_0 is the geometrical imperfection and ε_i is the strain in i direction. The deformation gradient (F) is defined as [45]

$$\begin{cases} F_{ij} = \delta_{ij} + \dfrac{\partial u_i}{\partial x_j}, \\ J = \det(F), \end{cases} \tag{7}$$

where J is the determinant of F and δ is the Kronecker delta. The left Cauchy–Green strain tensor (B) can be written as

$$\boldsymbol{B} = \boldsymbol{F} \bullet \boldsymbol{F}^T \rightarrow B_{ij} = F_{ik}F_{jk}, \tag{8}$$

with the left Cauchy–Green strain tensor invariants (I_1, I_2 and I_3) as

$$\begin{aligned} I_1 &= B_{ii} = tr(B) = \lambda_1^2 + \lambda_2^2 + \lambda_3^2, \\ I_2 &= \frac{1}{2}\left(I_1^2 - B_{ij}B_{ji}\right) = \frac{1}{2}\left(I_1^2 - tr\left(B^2\right)\right) = \lambda_1^2\lambda_2^2 + \lambda_1^2\lambda_3^2 + \lambda_2^2\lambda_3^2, \\ I_3 &= J^2 = \det(B) = \lambda_1^2\lambda_2^2\lambda_3^2, \end{aligned} \tag{9}$$

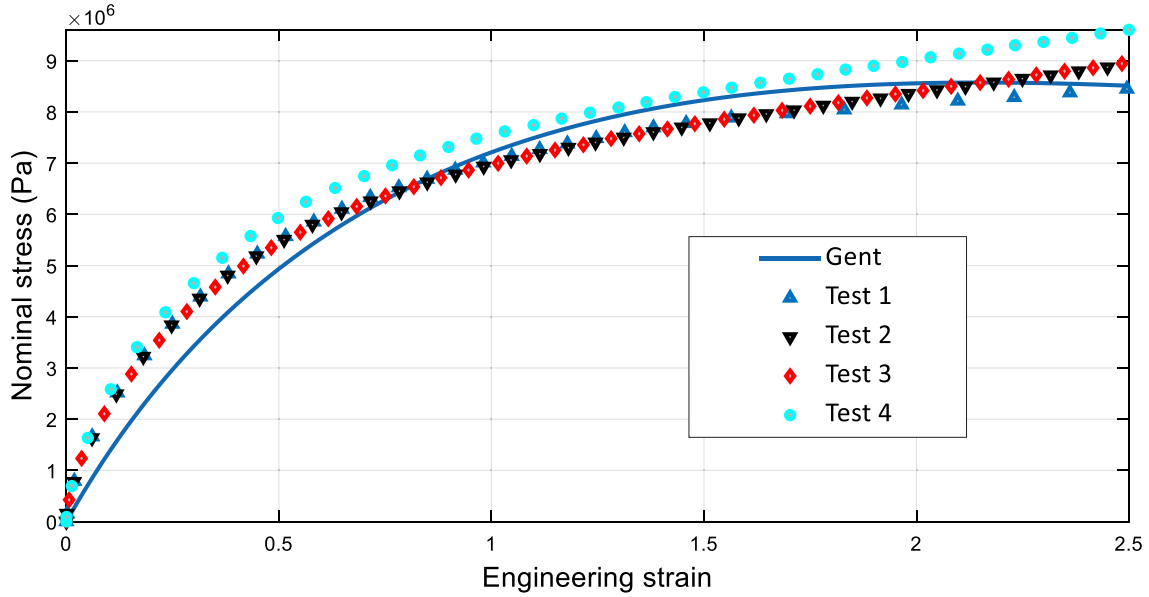

Fig. 8. Stress–strain modelling using *Gent* hyperelastic strain energy density model.

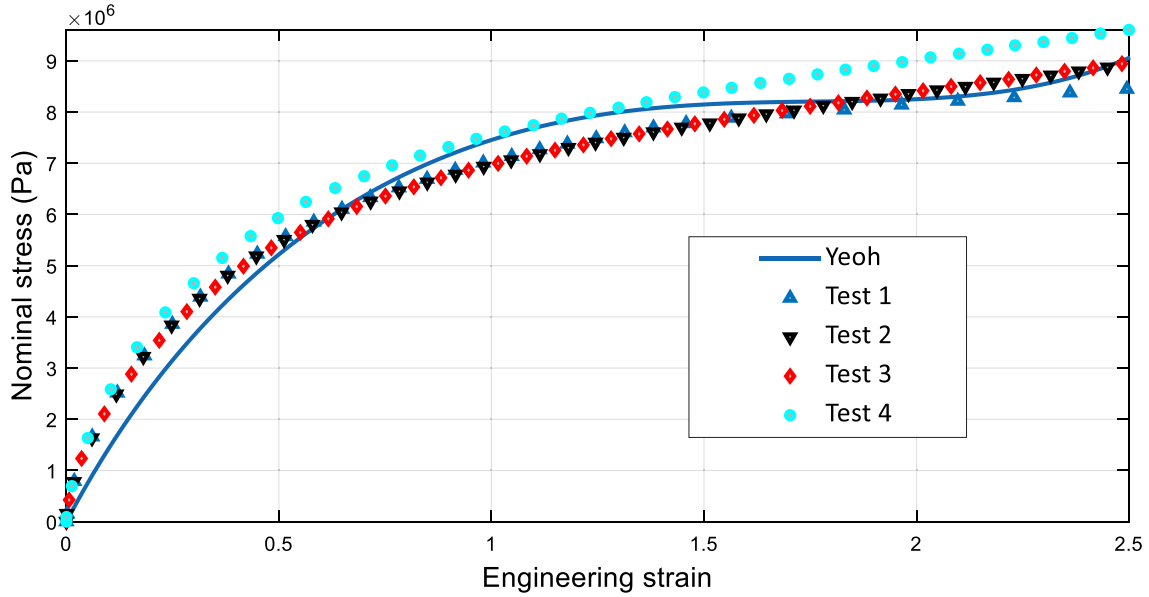

Fig. 9. Stress–strain modelling using *Yeoh* hyperelastic strain energy density model.

where λ_i is the stretch of the structure in i direction. It is known that for incompressible structures, J and accordingly I_3 will be equal to 1. The strain tensor (E) of any structure could be defined as

$$E = \frac{1}{2}(FF - I); \quad E_{ij} = \frac{1}{2}\left(F_{ik}F_{jk} - \delta_{ij}\right), \tag{10}$$

and the relation between the left Cauchy–Green deformation tensor and the strain tensor is written as

$$[C] = 2[E] + [I]. \tag{11}$$

The invariants of the left Cauchy–Green deformation tensor for hollow beams are rewritten as

$$\begin{aligned} I_1 &= (1+\varepsilon_{xx})^2 + \frac{2}{(1+\varepsilon_{xx})}, \\ I_2 &= 2\left(1+\varepsilon_{xx}\right) + \frac{1}{(1+\varepsilon_{xx})^2}, \\ I_3 &= 1 \text{ (if incompressible)}. \end{aligned} \tag{12}$$

It can be seen that the second invariant term shows the same format of the first invariant in hollow beam models which makes the strain energy density models depended on first invariant term sufficient for modelling the structure. Since *Yeoh's hyperelasticity model* has shown a *perfect fit* for modelling the strain energy of the structure, the three-term model is used for further formulation.

Using the defined strain energy density model, the potential energy (U) can be written for axially loaded hyperelastic beams as

$$U = \int_0^L \int_A \left\{ \begin{aligned} &C_1\left[(1+\varepsilon_{xx})^2 + \frac{2}{(1+\varepsilon_{xx})} - 3\right] \\ &+C_2\left[(1+\varepsilon_{xx})^2 + \frac{2}{(1+\varepsilon_{xx})} - 3\right]^2 \\ &+C_3\left[(1+\varepsilon_{xx})^2 + \frac{2}{(1+\varepsilon_{xx})} - 3\right]^3 + P\varepsilon_x \end{aligned} \right\} dA\,dx, \tag{13}$$

where P is the axial tension force and A is the cross-section of the beam. For the case of axially moving hyperelastic beams, the kinetic energy (T) is written as

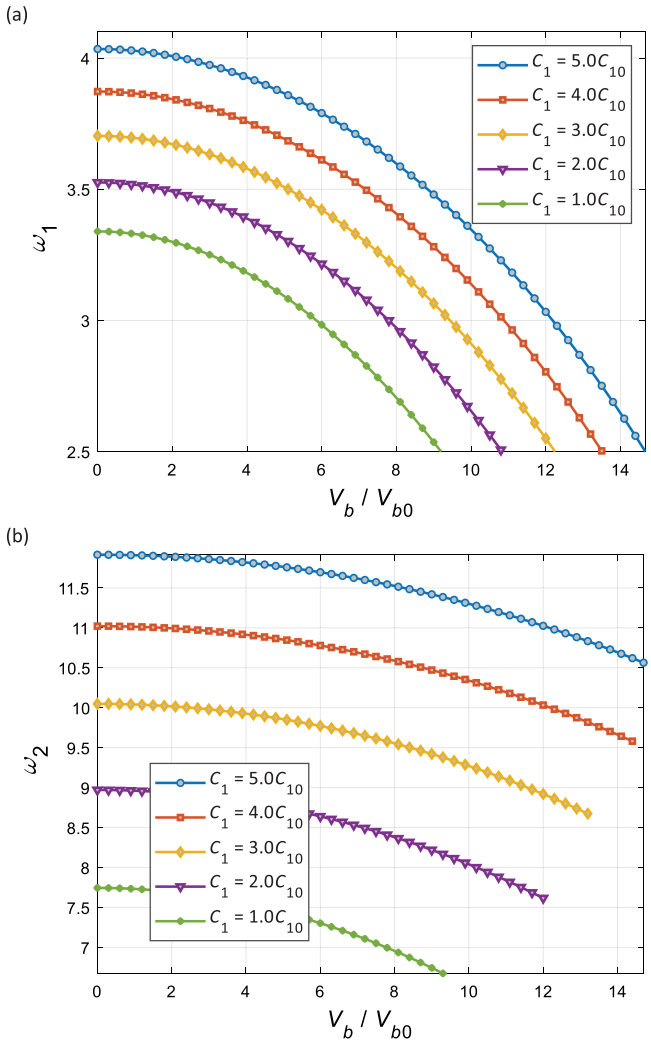

Fig. 10. Linear frequency–velocity response of the thermoplastic polyurethane axially moving hyperelastic beam model for different hyperelastic coefficient C_1(a) first natural frequency and (b) second natural frequency.

$$T = \frac{1}{2}\rho A \int_0^L \left\{ \left[\frac{\partial u}{\partial t} + V_b \left(1 + \frac{\partial u}{\partial x}\right) \right]^2 + \left(\frac{\partial w}{\partial t} + V_b \frac{\partial w}{\partial x} + V_b \frac{dw_0}{dx} \right)^2 \right\} dx, \tag{14}$$

where V_b is the velocity of the axially moving beam. Besides, by having an external harmonic excitation force, the external work (W_F) is written as

$$W_F = \int_0^L F_w \cos(\omega t)\, w dx. \tag{15}$$

By substituting Eqs. (13)–(15) into Hamilton's principle, the coupled equations of motion are formulated as

$$\delta(u): \rho A \left[\frac{\partial^2 u}{\partial t^2} + 2V_b \frac{\partial^2 u}{\partial x \partial t} + V_b^2 \frac{\partial^2 u}{\partial x^2} + \frac{dV_b}{dt}\left(1 + \frac{\partial u}{\partial x}\right) \right]$$
$$-6C_1 \frac{\partial}{\partial x} \begin{bmatrix} A\left(\frac{\partial u}{\partial x}\right) + \frac{1}{2}A\left(\frac{\partial w}{\partial x}\right)^2 - A\left(\frac{\partial w}{\partial x}\right)\left(\frac{dw_0}{dx}\right) \\ -A\left(\frac{\partial u}{\partial x}\right)^2 + 2A\left(\frac{\partial u}{\partial x}\right)\left(\frac{\partial w}{\partial x}\right)\left(\frac{dw_0}{dx}\right) - A\left(\frac{\partial u}{\partial x}\right)\left(\frac{\partial w}{\partial x}\right)^2 \\ -A\left(\frac{\partial w}{\partial x}\right)^2\left(\frac{dw_0}{dx}\right)^2 + A\left(\frac{\partial w}{\partial x}\right)^3\left(\frac{dw_0}{dx}\right) - \frac{1}{4}A\left(\frac{\partial w}{\partial x}\right)^4 \\ -I_{n2}\left(\frac{\partial^2 w}{\partial x^2}\right)^2 \end{bmatrix}$$
$$-36C_2 \frac{\partial}{\partial x} \begin{bmatrix} -\frac{3}{4}A\left(\frac{\partial w}{\partial x}\right)^5\left(\frac{dw_0}{dx}\right) + \frac{3}{4}A\left(\frac{\partial u}{\partial x}\right)\left(\frac{\partial w}{\partial x}\right)^4 \\ +\frac{3}{2}A\left(\frac{\partial w}{\partial x}\right)^4\left(\frac{dw_0}{dx}\right)^2 \\ -A\left(\frac{\partial w}{\partial x}\right)^3\left(\frac{dw_0}{dx}\right)^3 - 3A\left(\frac{\partial u}{\partial x}\right)\left(\frac{\partial w}{\partial x}\right)^3\left(\frac{dw_0}{dx}\right) \\ +\frac{3}{2}A\left(\frac{\partial u}{\partial x}\right)^2\left(\frac{\partial w}{\partial x}\right)^2 \\ +3A\left(\frac{\partial u}{\partial x}\right)\left(\frac{\partial w}{\partial x}\right)^2\left(\frac{dw_0}{dx}\right)^2 - 3A\left(\frac{\partial u}{\partial x}\right)^2\left(\frac{\partial w}{\partial x}\right) \\ \times\left(\frac{dw_0}{dx}\right) + \left(\frac{\partial u}{\partial x}\right)^3 \\ +\frac{3}{2}I_{n2}\left(\frac{\partial w}{\partial x}\right)^2\left(\frac{\partial^2 w}{\partial x^2}\right)^2 - 3I_{n2}\left(\frac{\partial w}{\partial x}\right)\left(\frac{\partial^2 w}{\partial x^2}\right)^2\left(\frac{dw_0}{dx}\right) \\ +3I_{n2}\left(\frac{\partial u}{\partial x}\right)\left(\frac{\partial^2 w}{\partial x^2}\right)^2 + O(6) \end{bmatrix}$$
$$-162C_3 \frac{\partial}{\partial x} \begin{bmatrix} -A\left(\frac{\partial w}{\partial x}\right)^5\left(\frac{dw_0}{dx}\right)^5 + 5A\left(\frac{\partial u}{\partial x}\right)\left(\frac{\partial w}{\partial x}\right)^4\left(\frac{dw_0}{dx}\right)^4 \\ -10A\left(\frac{\partial u}{\partial x}\right)^2\left(\frac{\partial w}{\partial x}\right)^3\left(\frac{dw_0}{dx}\right)^3 \\ +10A\left(\frac{\partial u}{\partial x}\right)^3\left(\frac{\partial w}{\partial x}\right)^2\left(\frac{dw_0}{dx}\right)^2 \\ -5A\left(\frac{\partial u}{\partial x}\right)^4\left(\frac{\partial w}{\partial x}\right)\left(\frac{dw_0}{dx}\right) + A\left(\frac{\partial u}{\partial x}\right)^5 \\ +10I_{n2}\left(\frac{\partial u}{\partial x}\right)^3\left(\frac{\partial^2 w}{\partial x^2}\right)^2 - 10I_{n2}\left(\frac{\partial w}{\partial x}\right)^3 \\ \times\left(\frac{\partial^2 w}{\partial x^2}\right)^2\left(\frac{dw_0}{dx}\right)^3 \\ +30I_{n2}\left(\frac{\partial u}{\partial x}\right)\left(\frac{\partial w}{\partial x}\right)^2\left(\frac{\partial^2 w}{\partial x^2}\right)^2\left(\frac{dw_0}{dx}\right)^2 \\ -30I_{n2}\left(\frac{\partial u}{\partial x}\right)^2\left(\frac{\partial w}{\partial x}\right)\left(\frac{\partial^2 w}{\partial x^2}\right)^2\left(\frac{dw_0}{dx}\right) \\ -5I_{n4}\left(\frac{\partial w}{\partial x}\right)\left(\frac{\partial^2 w}{\partial x^2}\right)^4\left(\frac{dw_0}{dx}\right) + 5I_{n4}\left(\frac{\partial u}{\partial x}\right) \\ \times\left(\frac{\partial^2 w}{\partial x^2}\right)^4 + O(6) \end{bmatrix} = 0, \tag{16}$$

$$\delta(w): \rho A \left[\left(\frac{\partial^2 w}{\partial t^2}\right) + 2V_b\left(\frac{\partial^2 w}{\partial x \partial t}\right) + V_{bt}\left(\frac{\partial w}{\partial x}\right) + V_{bt}\left(\frac{dw_0}{dx}\right) + V_b^2\left(\frac{\partial^2 w}{\partial x^2}\right) + V_b^2\left(\frac{d^2 w_0}{dx^2}\right) \right]$$
$$+6C_1 \frac{\partial^2}{\partial x^2} \begin{bmatrix} I_{n2}\left(\frac{\partial^2 w}{\partial x^2}\right) - 2I_{n2}\left(\frac{\partial u}{\partial x}\right)\left(\frac{\partial^2 w}{\partial x^2}\right) \\ -I_{n2}\left(\frac{\partial w}{\partial x}\right)^2\left(\frac{\partial^2 w}{\partial x^2}\right) + 2I_{n2}\left(\frac{\partial w}{\partial x}\right)\left(\frac{\partial^2 w}{\partial x^2}\right)\left(\frac{dw_0}{dx}\right) \end{bmatrix}$$
$$-6C_1 \frac{\partial}{\partial x} \begin{bmatrix} A\left(\frac{\partial u}{\partial x}\right)\left(\frac{\partial w}{\partial x}\right) + \frac{1}{2}A\left(\frac{\partial w}{\partial x}\right)^3 - A\left(\frac{\partial w}{\partial x}\right)^2\left(\frac{dw_0}{dx}\right) \\ -A\left(\frac{\partial u}{\partial x}\right)^2\left(\frac{\partial w}{\partial x}\right) + 2A\left(\frac{\partial u}{\partial x}\right)\left(\frac{\partial w}{\partial x}\right)^2\left(\frac{dw_0}{dx}\right) \\ -A\left(\frac{\partial u}{\partial x}\right)\left(\frac{\partial w}{\partial x}\right)^3 \\ -A\left(\frac{\partial w}{\partial x}\right)^3\left(\frac{dw_0}{dx}\right)^2 + A\left(\frac{\partial w}{\partial x}\right)^4\left(\frac{dw_0}{dx}\right) \\ -\frac{1}{4}A\left(\frac{\partial w}{\partial x}\right)^5 - I_{n2}\left(\frac{\partial w}{\partial x}\right)\left(\frac{\partial^2 w}{\partial x^2}\right)^2 \end{bmatrix}$$

$$
\begin{aligned}
&+6C_1\frac{\partial}{\partial x}\left[\begin{array}{l}
A\left(\frac{\partial u}{\partial x}\right)\left(\frac{dw_0}{dx}\right)+\frac{1}{2}A\left(\frac{\partial w}{\partial x}\right)^2\left(\frac{dw_0}{dx}\right)-A\left(\frac{\partial w}{\partial x}\right)\left(\frac{dw_0}{dx}\right)^2\\
-A\left(\frac{\partial u}{\partial x}\right)^2\left(\frac{dw_0}{dx}\right)+2A\left(\frac{\partial u}{\partial x}\right)\left(\frac{\partial w}{\partial x}\right)\left(\frac{dw_0}{dx}\right)^2\\
-A\left(\frac{\partial u}{\partial x}\right)\left(\frac{\partial w}{\partial x}\right)^2\left(\frac{dw_0}{dx}\right)-A\left(\frac{\partial w}{\partial x}\right)^2\left(\frac{dw_0}{dx}\right)^3\\
+A\left(\frac{\partial w}{\partial x}\right)^3\left(\frac{dw_0}{dx}\right)\\
^2-\frac{1}{4}A\left(\frac{\partial w}{\partial x}\right)^4\left(\frac{dw_0}{dx}\right)-I_{n2}\left(\frac{\partial^2 w}{\partial x^2}\right)^2\left(\frac{dw_0}{dx}\right)
\end{array}\right]\\
&+36C_2\frac{\partial^2}{\partial x^2}\left[\begin{array}{l}
3I_{n2}\left(\frac{\partial u}{\partial x}\right)^2\left(\frac{\partial^2 w}{\partial x^2}\right)+\frac{3}{4}I_{n2}\left(\frac{\partial^2 w}{\partial x^2}\right)\left(\frac{\partial w}{\partial x}\right)^4\\
-3I_{n2}\left(\frac{\partial^2 w}{\partial x^2}\right)\left(\frac{\partial w}{\partial x}\right)^3\left(\frac{dw_0}{dx}\right)\\
+3I_{n2}\left(\frac{\partial u}{\partial x}\right)\left(\frac{\partial w}{\partial x}\right)^2\left(\frac{\partial^2 w}{\partial x^2}\right)+3I_{n2}\left(\frac{\partial w}{\partial x}\right)^2\\
\times\left(\frac{\partial^2 w}{\partial x^2}\right)\left(\frac{dw_0}{dx}\right)^2\\
-6I_{n2}\left(\frac{\partial u}{\partial x}\right)\left(\frac{\partial w}{\partial x}\right)\left(\frac{\partial^2 w}{\partial x^2}\right)\left(\frac{dw_0}{dx}\right)+I_{n4}\left(\frac{\partial^2 w}{\partial x^2}\right)^3+O(6)
\end{array}\right]\\
&-36C_2\frac{\partial}{\partial x}\left[\begin{array}{l}
\frac{3}{2}A\left(\frac{\partial w}{\partial x}\right)^5\left(\frac{dw_0}{dx}\right)^2-A\left(\frac{\partial w}{\partial x}\right)^4\left(\frac{dw_0}{dx}\right)^3\\
-3A\left(\frac{\partial u}{\partial x}\right)\left(\frac{\partial w}{\partial x}\right)^4\left(\frac{dw_0}{dx}\right)\\
+\frac{3}{2}A\left(\frac{\partial u}{\partial x}\right)^2\left(\frac{\partial w}{\partial x}\right)^3+3A\left(\frac{\partial u}{\partial x}\right)\left(\frac{\partial w}{\partial x}\right)^3\left(\frac{dw_0}{dx}\right)^2\\
-3A\left(\frac{\partial u}{\partial x}\right)^2\left(\frac{\partial w}{\partial x}\right)^2\left(\frac{dw_0}{dx}\right)+A\left(\frac{\partial u}{\partial x}\right)^3\left(\frac{\partial w}{\partial x}\right)\\
+\frac{3}{2}I_{n2}\left(\frac{\partial w}{\partial x}\right)^3\left(\frac{\partial^2 w}{\partial x^2}\right)^2\\
-3I_{n2}\left(\frac{\partial w}{\partial x}\right)^2\left(\frac{\partial^2 w}{\partial x^2}\right)^2\left(\frac{dw_0}{dx}\right)+O(6)
\end{array}\right]\\
&+36C_2\frac{\partial}{\partial x}\left[\begin{array}{l}
-\frac{3}{4}A\left(\frac{\partial w}{\partial x}\right)^5\left(\frac{dw_0}{dx}\right)^2+\frac{3}{4}A\left(\frac{\partial u}{\partial x}\right)\left(\frac{\partial w}{\partial x}\right)^4\left(\frac{dw_0}{dx}\right)\\
+\frac{3}{2}A\left(\frac{\partial w}{\partial x}\right)^4\left(\frac{dw_0}{dx}\right)^3\\
-A\left(\frac{\partial w}{\partial x}\right)^3\left(\frac{dw_0}{dx}\right)^4-3A\left(\frac{\partial u}{\partial x}\right)\left(\frac{\partial w}{\partial x}\right)^3\left(\frac{dw_0}{dx}\right)^2\\
+\frac{3}{2}A\left(\frac{\partial u}{\partial x}\right)^2\left(\frac{\partial w}{\partial x}\right)^2\left(\frac{dw_0}{dx}\right)\\
+3A\left(\frac{\partial u}{\partial x}\right)\left(\frac{\partial w}{\partial x}\right)^2\left(\frac{dw_0}{dx}\right)^3-3A\left(\frac{\partial u}{\partial x}\right)^2\left(\frac{\partial w}{\partial x}\right)\left(\frac{dw_0}{dx}\right)^2\\
+A\left(\frac{\partial u}{\partial x}\right)^3\left(\frac{dw_0}{dx}\right)\\
+\frac{3}{2}I_{n2}\left(\frac{\partial w}{\partial x}\right)^2\left(\frac{\partial^2 w}{\partial x^2}\right)^2\left(\frac{dw_0}{dx}\right)-3I_{n2}\left(\frac{\partial w}{\partial x}\right)\\
\times\left(\frac{\partial^2 w}{\partial x^2}\right)^2\left(\frac{dw_0}{dx}\right)^2\\
+3I_{n2}\left(\frac{\partial u}{\partial x}\right)\left(\frac{\partial^2 w}{\partial x^2}\right)^2\left(\frac{dw_0}{dx}\right)+O(6)
\end{array}\right]
\end{aligned}
\tag{17}
$$

$$
\begin{aligned}
&+162C_3\frac{\partial^2}{\partial x^2}\left[\begin{array}{l}
5I_{n2}\left(\frac{\partial u}{\partial x}\right)^4\left(\frac{\partial^2 w}{\partial x^2}\right)+5I_{n2}\left(\frac{\partial w}{\partial x}\right)^4\left(\frac{\partial^2 w}{\partial x^2}\right)\left(\frac{dw_0}{dx}\right)^4\\
-20I_{n2}\left(\frac{\partial u}{\partial x}\right)^3\left(\frac{\partial w}{\partial x}\right)\left(\frac{\partial^2 w}{\partial x^2}\right)\left(\frac{dw_0}{dx}\right)\\
-20I_{n2}\left(\frac{\partial u}{\partial x}\right)\left(\frac{\partial w}{\partial x}\right)^3\left(\frac{\partial^2 w}{\partial x^2}\right)\left(\frac{dw_0}{dx}\right)^3\\
+30I_{n2}\left(\frac{\partial u}{\partial x}\right)^2\left(\frac{\partial w}{\partial x}\right)^2\left(\frac{\partial^2 w}{\partial x^2}\right)\left(\frac{dw_0}{dx}\right)^2\\
+10I_{n4}\left(\frac{\partial w}{\partial x}\right)^2\left(\frac{\partial^2 w}{\partial x^2}\right)^3\left(\frac{dw_0}{dx}\right)\\
+10I_{n4}\left(\frac{\partial u}{\partial x}\right)^2\left(\frac{\partial^2 w}{\partial x^2}\right)^3-20I_{n4}\left(\frac{\partial u}{\partial x}\right)\left(\frac{\partial w}{\partial x}\right)\left(\frac{\partial^2 w}{\partial x^2}\right)^3\\
\times\left(\frac{dw_0}{dx}\right)+I_{n6}\left(\frac{\partial^2 w}{\partial x^2}\right)^5+O(6)
\end{array}\right]\\
&+162C_3\frac{\partial}{\partial x}\left[\begin{array}{l}
-A\left(\frac{\partial w}{\partial x}\right)^5\left(\frac{dw_0}{dx}\right)^6+5\mathrm{A}\left(\frac{\partial u}{\partial x}\right)\left(\frac{\partial w}{\partial x}\right)^4\left(\frac{dw_0}{dx}\right)^5\\
-10\mathrm{A}\left(\frac{\partial u}{\partial x}\right)^2\left(\frac{\partial w}{\partial x}\right)^3\left(\frac{dw_0}{dx}\right)^4\\
+10\mathrm{A}\left(\frac{\partial u}{\partial x}\right)^3\left(\frac{\partial w}{\partial x}\right)^2\left(\frac{dw_0}{dx}\right)^3-5\mathrm{A}\left(\frac{\partial u}{\partial x}\right)^4\\
\times\left(\frac{\partial w}{\partial x}\right)\left(\frac{dw_0}{dx}\right)^2+\mathrm{A}\left(\frac{\partial u}{\partial x}\right)^5\left(\frac{dw_0}{dx}\right)\\
+10I_{n2}\left(\frac{\partial u}{\partial x}\right)^3\left(\frac{\partial^2 w}{\partial x^2}\right)^2\left(\frac{dw_0}{dx}\right)-10I_{n2}\left(\frac{\partial w}{\partial x}\right)^3\left(\frac{\partial^2 w}{\partial x^2}\right)^2\\
\times\left(\frac{dw_0}{dx}\right)^4\\
+30I_{n2}\left(\frac{\partial u}{\partial x}\right)\left(\frac{\partial w}{\partial x}\right)^2\left(\frac{\partial^2 w}{\partial x^2}\right)^2\left(\frac{dw_0}{dx}\right)^3\\
-30I_{n2}\left(\frac{\partial u}{\partial x}\right)^2\left(\frac{\partial w}{\partial x}\right)\left(\frac{\partial^2 w}{\partial x^2}\right)^2\left(\frac{dw_0}{dx}\right)^2\\
-5I_{n4}\left(\frac{\partial w}{\partial x}\right)\left(\frac{\partial^2 w}{\partial x^2}\right)^4\left(\frac{dw_0}{dx}\right)^2+5I_{n4}\left(\frac{\partial u}{\partial x}\right)\left(\frac{\partial^2 w}{\partial x^2}\right)^4\\
\times\left(\frac{dw_0}{dx}\right)+O(6)
\end{array}\right]\\
&-F_w\cos(\omega t)-P\left(\frac{\partial^2 w}{\partial x^2}\right)=0.
\end{aligned}
\tag{18}
$$

The terms related to coefficient C_1 in Eqs. (14) and (15) are the elastic terms and the terms related to coefficients C_2 and C_3 are the hyperelastic terms of the equation. It can be seen that considering the geometrical imperfection in the system increases the coupling axial-transverse motion terms significantly.

4. Solution procedure

Since the scale of parameters are different, nondimensional terms are defined as

$$
x^*=\frac{x}{L},\quad w^*=\frac{w}{L},\quad {w_0}^*=\frac{w_0}{L},\quad {C_1}^*=\frac{C_1A}{P},\quad {C_2}^*=\frac{C_2}{C_1},\quad {C_3}^*=\frac{C_3}{C_1},
$$

$$
{F_w}^*=\frac{F_wL}{P},
$$

$$
\Omega=\omega\sqrt{\frac{\rho AL^2}{P}},\quad {V_b}^*=V_b\sqrt{\frac{\rho A}{P}},\quad \gamma_2=\sqrt{\frac{I_{n1}}{AL^2}},\quad \gamma_4=\sqrt{\frac{I_{n2}}{AL^4}},
$$

$$
\gamma_6=\sqrt{\frac{I_{n3}}{AL^6}},\quad t^*=t\sqrt{\frac{P}{\rho AL^2}},
$$

and the equations of motions are rewritten in a nondimensional form as

$$\frac{\partial^2 u}{\partial t^2}+2V_b\frac{\partial^2 u}{\partial x\partial t}+V_b^2\frac{\partial^2 u}{\partial x^2}+\frac{dV_b}{dt}\left(1+\frac{\partial u}{\partial x}\right)$$

$$-6C_1\frac{\partial}{\partial x}\begin{bmatrix}\left(\frac{\partial u}{\partial x}\right)+\frac{1}{2}\left(\frac{\partial w}{\partial x}\right)^2-\left(\frac{\partial w}{\partial x}\right)\left(\frac{dw_0}{dx}\right)-\left(\frac{\partial u}{\partial x}\right)^2\\+2\left(\frac{\partial u}{\partial x}\right)\left(\frac{\partial w}{\partial x}\right)\left(\frac{dw_0}{dx}\right)\\-\left(\frac{\partial u}{\partial x}\right)\left(\frac{\partial w}{\partial x}\right)^2-\left(\frac{\partial w}{\partial x}\right)^2\left(\frac{dw_0}{dx}\right)^2+\left(\frac{\partial w}{\partial x}\right)^3\left(\frac{dw_0}{dx}\right)\\-\frac{1}{4}\left(\frac{\partial w}{\partial x}\right)^4-\gamma_2^2\left(\frac{\partial^2 w}{\partial x^2}\right)^2\end{bmatrix}$$

$$-36C_1C_2\frac{\partial}{\partial x}\begin{bmatrix}-\frac{3}{4}\left(\frac{\partial w}{\partial x}\right)^5\left(\frac{dw_0}{dx}\right)+\frac{3}{4}u_x\left(\frac{\partial w}{\partial x}\right)^4+\frac{3}{2}\left(\frac{\partial w}{\partial x}\right)^4\left(\frac{dw_0}{dx}\right)^2\\-\left(\frac{\partial w}{\partial x}\right)^3\left(\frac{dw_0}{dx}\right)^3-3u_x\left(\frac{\partial w}{\partial x}\right)^3\left(\frac{dw_0}{dx}\right)\\+\frac{3}{2}\left(\frac{\partial u}{\partial x}\right)^2\left(\frac{\partial w}{\partial x}\right)^2\\+3u_x\left(\frac{\partial w}{\partial x}\right)^2\left(\frac{dw_0}{dx}\right)^2-3u_x^2\left(\frac{\partial w}{\partial x}\right)\left(\frac{dw_0}{dx}\right)+\left(\frac{\partial u}{\partial x}\right)^3\\+\frac{3}{2}\gamma_2^2\left(\frac{\partial w}{\partial x}\right)^2\left(\frac{\partial^2 w}{\partial x^2}\right)^2-3\gamma_2^2\left(\frac{\partial w}{\partial x}\right)\left(\frac{\partial^2 w}{\partial x^2}\right)^2\left(\frac{dw_0}{dx}\right)\\+3\gamma_2^2u_x\left(\frac{\partial^2 w}{\partial x^2}\right)^2\end{bmatrix}$$

$$-162C_1C_3\frac{\partial}{\partial x}\begin{bmatrix}-\left(\frac{\partial w}{\partial x}\right)^5\left(\frac{dw_0}{dx}\right)^5+5u_x\left(\frac{\partial w}{\partial x}\right)^4\left(\frac{dw_0}{dx}\right)^4\\-5\gamma_4^2\left(\frac{\partial w}{\partial x}\right)\left(\frac{\partial^2 w}{\partial x^2}\right)^4\left(\frac{dw_0}{dx}\right)\\-10u_x^2\left(\frac{\partial w}{\partial x}\right)^3\left(\frac{dw_0}{dx}\right)^3+10u_x^3\left(\frac{\partial w}{\partial x}\right)^2\left(\frac{dw_0}{dx}\right)^2\\-5u_x^4\left(\frac{\partial w}{\partial x}\right)\left(\frac{dw_0}{dx}\right)+\left(\frac{\partial u}{\partial x}\right)^5\\+10\gamma_2^2\left(\frac{\partial u}{\partial x}\right)^3\left(\frac{\partial^2 w}{\partial x^2}\right)^2\\-10\gamma_2^2\left(\frac{\partial w}{\partial x}\right)^3\left(\frac{\partial^2 w}{\partial x^2}\right)^2\left(\frac{dw_0}{dx}\right)^3\\+5\gamma_4^2\left(\frac{\partial u}{\partial x}\right)\left(\frac{\partial^2 w}{\partial x^2}\right)^4\\+30\gamma_2^2\left(\frac{\partial u}{\partial x}\right)\left(\frac{\partial w}{\partial x}\right)^2\left(\frac{\partial^2 w}{\partial x^2}\right)^2\left(\frac{dw_0}{dx}\right)^2\\-30\gamma_2^2\left(\frac{\partial u}{\partial x}\right)^2\left(\frac{\partial w}{\partial x}\right)\left(\frac{\partial^2 w}{\partial x^2}\right)^2\left(\frac{dw_0}{dx}\right)\end{bmatrix}=0 \tag{19}$$

$$\delta(w):\left(\frac{\partial^2 w}{\partial t^2}\right)+2V_b\left(\frac{\partial^2 w}{\partial x\partial t}\right)+V_{bt}\left(\frac{\partial w}{\partial x}\right)+V_{bt}\left(\frac{dw_0}{dx}\right)$$

$$+V_b^2\left(\frac{\partial^2 w}{\partial x^2}\right)+V_b^2\left(\frac{d^2 w_0}{dx^2}\right)$$

$$+6C_1\frac{\partial^2}{\partial x^2}\begin{bmatrix}\gamma_2^2\left(\frac{\partial^2 w}{\partial x^2}\right)-2\gamma_2^2\left(\frac{\partial u}{\partial x}\right)\left(\frac{\partial^2 w}{\partial x^2}\right)-\gamma_2^2\left(\frac{\partial w}{\partial x}\right)^2\left(\frac{\partial^2 w}{\partial x^2}\right)\\+2\gamma_2^2\left(\frac{\partial w}{\partial x}\right)\left(\frac{\partial^2 w}{\partial x^2}\right)\left(\frac{dw_0}{dx}\right)\end{bmatrix}$$

$$-6C_1\frac{\partial}{\partial x}\begin{bmatrix}\left(\frac{\partial u}{\partial x}\right)\left(\frac{\partial w}{\partial x}\right)+\frac{1}{2}\left(\frac{\partial w}{\partial x}\right)^3-\left(\frac{\partial w}{\partial x}\right)^2\left(\frac{dw_0}{dx}\right)\\-\left(\frac{\partial u}{\partial x}\right)^2\left(\frac{\partial w}{\partial x}\right)+2\left(\frac{\partial u}{\partial x}\right)\left(\frac{\partial w}{\partial x}\right)^2\left(\frac{dw_0}{dx}\right)-\left(\frac{\partial u}{\partial x}\right)\left(\frac{\partial w}{\partial x}\right)^3\\-\left(\frac{\partial w}{\partial x}\right)^3\left(\frac{dw_0}{dx}\right)^2+\left(\frac{\partial w}{\partial x}\right)^4\left(\frac{dw_0}{dx}\right)-\frac{1}{4}\left(\frac{\partial w}{\partial x}\right)^5\\-\gamma_2^2\left(\frac{\partial w}{\partial x}\right)\left(\frac{\partial^2 w}{\partial x^2}\right)^2\end{bmatrix}$$

$$+6C_1\frac{\partial}{\partial x}\begin{bmatrix}\left(\frac{\partial u}{\partial x}\right)\left(\frac{dw_0}{dx}\right)+\frac{1}{2}\left(\frac{\partial w}{\partial x}\right)^2\left(\frac{dw_0}{dx}\right)-\left(\frac{\partial w}{\partial x}\right)\left(\frac{dw_0}{dx}\right)^2\\-\left(\frac{\partial u}{\partial x}\right)^2\left(\frac{dw_0}{dx}\right)+2\left(\frac{\partial u}{\partial x}\right)\left(\frac{\partial w}{\partial x}\right)\left(\frac{dw_0}{dx}\right)^2\\-\left(\frac{\partial u}{\partial x}\right)\left(\frac{\partial w}{\partial x}\right)^2\left(\frac{dw_0}{dx}\right)-\left(\frac{\partial w}{\partial x}\right)^2\left(\frac{dw_0}{dx}\right)^3\\+\left(\frac{\partial w}{\partial x}\right)^3\left(\frac{dw_0}{dx}\right)^2-\frac{1}{4}\left(\frac{\partial w}{\partial x}\right)^4\left(\frac{dw_0}{dx}\right)\\-\gamma_2^2\left(\frac{\partial^2 w}{\partial x^2}\right)^2\left(\frac{dw_0}{dx}\right)\end{bmatrix}$$

$$+36C_1C_2\frac{\partial^2}{\partial x^2}\begin{bmatrix}3\gamma_2^2\left(\frac{\partial u}{\partial x}\right)^2\left(\frac{\partial^2 w}{\partial x^2}\right)+\frac{3}{4}\gamma_2^2\left(\frac{\partial^2 w}{\partial x^2}\right)\left(\frac{\partial w}{\partial x}\right)^4\\+\gamma_4^2\left(\frac{\partial^2 w}{\partial x^2}\right)^3\\-3\gamma_2^2\left(\frac{\partial^2 w}{\partial x^2}\right)\left(\frac{\partial w}{\partial x}\right)^3\left(\frac{dw_0}{dx}\right)\\+3\gamma_2^2\left(\frac{\partial u}{\partial x}\right)\left(\frac{\partial w}{\partial x}\right)^2\left(\frac{\partial^2 w}{\partial x^2}\right)\\+3\gamma_2^2\left(\frac{\partial w}{\partial x}\right)^2\left(\frac{\partial^2 w}{\partial x^2}\right)\left(\frac{dw_0}{dx}\right)^2\\-6\gamma_2^2u_x\left(\frac{\partial w}{\partial x}\right)\left(\frac{\partial^2 w}{\partial x^2}\right)\left(\frac{dw_0}{dx}\right)\end{bmatrix}$$

$$-36C_1C_2\frac{\partial}{\partial x}\begin{bmatrix}\frac{3}{2}\left(\frac{\partial w}{\partial x}\right)^5\left(\frac{dw_0}{dx}\right)^2-\left(\frac{\partial w}{\partial x}\right)^4\left(\frac{dw_0}{dx}\right)^3\\-3\left(\frac{\partial u}{\partial x}\right)\left(\frac{\partial w}{\partial x}\right)^4\left(\frac{dw_0}{dx}\right)+\frac{3}{2}\left(\frac{\partial u}{\partial x}\right)^2\left(\frac{\partial w}{\partial x}\right)^3\\+3\left(\frac{\partial u}{\partial x}\right)\left(\frac{\partial w}{\partial x}\right)^3\left(\frac{dw_0}{dx}\right)^2-3\left(\frac{\partial u}{\partial x}\right)^2\left(\frac{\partial w}{\partial x}\right)^2\left(\frac{dw_0}{dx}\right)\\+\left(\frac{\partial u}{\partial x}\right)^3\left(\frac{\partial w}{\partial x}\right)+\frac{3}{2}\gamma_2^2\left(\frac{\partial w}{\partial x}\right)^3\left(\frac{\partial^2 w}{\partial x^2}\right)^2\\-3\gamma_2^2\left(\frac{\partial w}{\partial x}\right)^2\left(\frac{\partial^2 w}{\partial x^2}\right)^2\left(\frac{dw_0}{dx}\right)\end{bmatrix}$$

$$+36C_1C_2\frac{\partial}{\partial x}\begin{bmatrix}-\frac{3}{4}\left(\frac{\partial w}{\partial x}\right)^5\left(\frac{dw_0}{dx}\right)^2+\frac{3}{4}\left(\frac{\partial u}{\partial x}\right)\left(\frac{\partial w}{\partial x}\right)^4\left(\frac{dw_0}{dx}\right)\\+\frac{3}{2}\left(\frac{\partial w}{\partial x}\right)^4\left(\frac{dw_0}{dx}\right)^3\\-\left(\frac{\partial w}{\partial x}\right)^3\left(\frac{dw_0}{dx}\right)^4-3u_x\left(\frac{\partial w}{\partial x}\right)^3\left(\frac{dw_0}{dx}\right)^2\\+\frac{3}{2}\left(\frac{\partial u}{\partial x}\right)^2\left(\frac{\partial w}{\partial x}\right)^2\left(\frac{dw_0}{dx}\right)\\+3u_x\left(\frac{\partial w}{\partial x}\right)^2\left(\frac{dw_0}{dx}\right)^3-3\left(\frac{\partial u}{\partial x}\right)^2\left(\frac{\partial w}{\partial x}\right)\left(\frac{dw_0}{dx}\right)^2\\+\left(\frac{\partial u}{\partial x}\right)^3\left(\frac{dw_0}{dx}\right)+\frac{3}{2}\gamma_2^2\left(\frac{\partial w}{\partial x}\right)^2\left(\frac{\partial^2 w}{\partial x^2}\right)^2\left(\frac{dw_0}{dx}\right)\\-3\gamma_2^2\left(\frac{\partial w}{\partial x}\right)\left(\frac{\partial^2 w}{\partial x^2}\right)^2\left(\frac{dw_0}{dx}\right)^2\\+3\gamma_2^2\left(\frac{\partial u}{\partial x}\right)\left(\frac{\partial^2 w}{\partial x^2}\right)^2\left(\frac{dw_0}{dx}\right)\end{bmatrix} \tag{20}$$

$$
\begin{aligned}
&+162C_1C_3\frac{\partial^2}{\partial x^2}\left[\begin{array}{l}
5\gamma_2^2u_x^4\left(\frac{\partial^2 w}{\partial x^2}\right)+5\gamma_2^2\left(\frac{\partial w}{\partial x}\right)^4\left(\frac{\partial^2 w}{\partial x^2}\right)\left(\frac{dw_0}{dx}\right)^4\\
-20\gamma_2^2\left(\frac{\partial u}{\partial x}\right)^3\left(\frac{\partial w}{\partial x}\right)\left(\frac{\partial^2 w}{\partial x^2}\right)\left(\frac{dw_0}{dx}\right)\\
-20\gamma_2^2\left(\frac{\partial u}{\partial x}\right)\left(\frac{\partial w}{\partial x}\right)^3\left(\frac{\partial^2 w}{\partial x^2}\right)\left(\frac{dw_0}{dx}\right)^3\\
+30\gamma_2^2\left(\frac{\partial u}{\partial x}\right)^2\left(\frac{\partial w}{\partial x}\right)^2\left(\frac{\partial^2 w}{\partial x^2}\right)\left(\frac{dw_0}{dx}\right)^2\\
+10\gamma_4^2\left(\frac{\partial w}{\partial x}\right)^2\left(\frac{\partial^2 w}{\partial x^2}\right)^3\left(\frac{dw_0}{dx}\right)\\
+10\gamma_4^2\left(\frac{\partial u}{\partial x}\right)^2\left(\frac{\partial^2 w}{\partial x^2}\right)^3-20\gamma_4^2\left(\frac{\partial u}{\partial x}\right)\left(\frac{\partial w}{\partial x}\right)\left(\frac{\partial^2 w}{\partial x^2}\right)^3\\
\left(\frac{dw_0}{dx}\right)+\gamma_6^2\left(\frac{\partial^2 w}{\partial x^2}\right)^5
\end{array}\right]\\
&+162C_1C_3\frac{\partial}{\partial x}\left[\begin{array}{l}
-\left(\frac{\partial w}{\partial x}\right)^5\left(\frac{dw_0}{dx}\right)^6+5\left(\frac{\partial u}{\partial x}\right)\left(\frac{\partial w}{\partial x}\right)^4\left(\frac{dw_0}{dx}\right)^5\\
-10\left(\frac{\partial u}{\partial x}\right)^2\left(\frac{\partial w}{\partial x}\right)^3\left(\frac{dw_0}{dx}\right)^4\\
+10\left(\frac{\partial u}{\partial x}\right)^3\left(\frac{\partial w}{\partial x}\right)^2\left(\frac{dw_0}{dx}\right)^3-5\left(\frac{\partial u}{\partial x}\right)^4\left(\frac{\partial w}{\partial x}\right)\left(\frac{dw_0}{dx}\right)^2\\
+\left(\frac{\partial u}{\partial x}\right)^5\left(\frac{dw_0}{dx}\right)+10\gamma_2^2\left(\frac{\partial u}{\partial x}\right)^3\left(\frac{\partial^2 w}{\partial x^2}\right)^2\left(\frac{dw_0}{dx}\right)\\
-10\gamma_2^2\left(\frac{\partial w}{\partial x}\right)^3\left(\frac{\partial^2 w}{\partial x^2}\right)^2\left(\frac{dw_0}{dx}\right)^4\\
+30\gamma_2^2\left(\frac{\partial u}{\partial x}\right)\left(\frac{\partial w}{\partial x}\right)^2\left(\frac{\partial^2 w}{\partial x^2}\right)^2\left(\frac{dw_0}{dx}\right)^3\\
-30\gamma_2^2\left(\frac{\partial u}{\partial x}\right)^2\left(\frac{\partial w}{\partial x}\right)\left(\frac{\partial^2 w}{\partial x^2}\right)^2\left(\frac{dw_0}{dx}\right)^2\\
-5\gamma_4^2\left(\frac{\partial w}{\partial x}\right)\left(\frac{\partial^2 w}{\partial x^2}\right)^4\left(\frac{dw_0}{dx}\right)^2\\
+5\gamma_4^2\left(\frac{\partial u}{\partial x}\right)\left(\frac{\partial^2 w}{\partial x^2}\right)^4\left(\frac{dw_0}{dx}\right)
\end{array}\right]\\
&-F_w\cos(\Omega t)-\left(\frac{\partial^2 w}{\partial x^2}\right)=0.
\end{aligned}
$$

where '*' symbol is neglected for the sake of brevity. It can be seen that by neglecting the terms with coefficients C_2 and C_3, the equations of motion for elastic axially moving beam will be obtained which is similar to those presented in the literature [20,22,23,46,47].

4.1. Linear vibration solution

Non-dimensional equations of motion can be linearised for perfect beam models by only considering transverse vibration model as

$$w_{tt}+2V_bw_{xt}+V_{bt}w_x+\left(V_b^2-1\right)w_{xx}+6C_1\gamma_2^2w_{xxxx}=0, \tag{21}$$

which by assuming harmonic motion [48]

$$w(x,t)=\phi_n(x)e^{i\omega_nt}+\overline{\phi_n}(x)e^{-i\omega_nt}, \tag{22}$$

the linearised equation is rewritten for a constant speed as

$$
\begin{aligned}
&-\omega_n^2\phi_n(x)+2iV_b\omega_n\frac{d\phi_n(x)}{dx}+\left(V_b^2-1\right)\frac{d^2\phi_n(x)}{dx^2}\\
&+6C_1\gamma_2^2\frac{d^4\phi_n(x)}{dx^4}=0.
\end{aligned} \tag{23}
$$

The general form of the solution for Eq. (23) can be written as [46]

$$\phi_n(x)=A_{1n}\left(e^{i\theta_{1n}x}+A_{2n}e^{i\theta_{2n}x}+A_{3n}e^{i\theta_{3n}x}+A_{4n}e^{i\theta_{4n}x}\right), \tag{24}$$

and by substituting Eq. (24) into Eq. (23), one can reach to

$$6C_1\gamma_2^2\theta_{in}^4-\left(V_b^2-1\right)\theta_{in}^2-2V_b\omega_n\theta_{in}-\omega_n^2=0, \tag{25}$$

where θ is obtained as a function of ω_n. For a simply-supported hyperelastic beam model, the mode shapes and the natural frequency terms are obtained using [49]

$$\begin{bmatrix}1&1&1&1\\ \theta_{1n}^2&\theta_{2n}^2&\theta_{3n}^2&\theta_{4n}^2\\ e^{i\theta_{1n}}&e^{i\theta_{2n}}&e^{i\theta_{3n}}&e^{i\theta_{4n}}\\ \theta_{1n}^2e^{i\theta_{1n}}&\theta_{2n}^2e^{i\theta_{2n}}&\theta_{3n}^2e^{i\theta_{3n}}&\theta_{4n}^2e^{i\theta_{4n}}\end{bmatrix}\begin{Bmatrix}A_{1n}\\ A_{1n}A_{3n}\\ A_{1n}A_{2n}\\ A_{1n}A_{4n}\end{Bmatrix}=0, \tag{26}$$

which the determinant of the equation must be zero to have a nontrivial solution.

4.2. Nonlinear vibration solution

By considering coupled motion and employing the Galerkin's scheme, and by assuming the first N modes of transverse and M modes of axial vibration as

$$u(x,t)=\sum_{j=1}^{M}\phi_j(x)r_j(t), \tag{27}$$

$$w(x,t)=\sum_{i=1}^{N}\psi_i(x)q_i(t), \tag{28}$$

the governing coupled equations of motion are discretised as

$$
\begin{aligned}
&M_1\ddot{r}+C_1\dot{r}+K_{11}^Lr+K_{12}^Lq+K_{11}^{NL}r^2+K_{12}^{NL}rq+K_{13}^{NL}q^2+K_{14}^{NL}r^3\\
&+K_{15}^{NL}r^2q+K_{16}^{NL}rq^2+K_{17}^{NL}q^3+K_{18}^{NL}r^2q^2+K_{19}^{NL}rq^3+K_{110}^{NL}q^4\\
&+K_{111}^{NL}r^5+K_{112}^{NL}r^4q+K_{113}^{NL}r^3q^2+K_{114}^{NL}r^2q^3+K_{115}^{NL}rq^4+K_{116}^{NL}q^5=0,
\end{aligned} \tag{29}
$$

$$
\begin{aligned}
&M_2\ddot{q}+C_2\dot{q}+K_{21}^Lr+K_{22}^Lq+K_{20}^L+K_{21}^{NL}r^2+K_{22}^{NL}rq+K_{23}^{NL}q^2+K_{24}^{NL}r^3\\
&+K_{25}^{NL}r^2q+K_{26}^{NL}rq^2+K_{27}^{NL}q^3+K_{28}^{NL}r^3q+K_{29}^{NL}r^2q^2\\
&+K_{210}^{NL}rq^3+K_{211}^{NL}q^4\\
&+K_{212}^{NL}r^5+K_{213}^{NL}r^4q+K_{214}^{NL}r^3q^2+K_{215}^{NL}r^2q^3+K_{216}^{NL}rq^4+K_{217}^{NL}q^5=F.
\end{aligned} \tag{30}
$$

where

$$M_1(l,i)=\int\phi_l\phi_i\,dx, \tag{31}$$

$$C_1(l,i)=2V_b\int\phi_l\left(\frac{d\phi_i}{dx}\right)dx, \tag{32}$$

$$K_{11}^L(l,i)=\left(V_b^2-6C_1\right)\int\phi_l\left(\frac{d^2\phi_i}{dx^2}\right)dx, \tag{33}$$

$$K_{12}^L(l,i)=6C_1\int\phi_l\frac{d}{dx}\left[\left(\frac{d\psi_i}{dx}\right)\left(\frac{d\psi_0}{dx}\right)\right]dx, \tag{34}$$

$$K_{11}^{NL}(l,i,j)=6C_1\int\phi_l\frac{d}{dx}\left[\left(\frac{d\phi_i}{dx}\right)\left(\frac{d\phi_j}{dx}\right)\right]dx, \tag{35}$$

$$
\begin{aligned}
K_{12}^{NL}(l,i,j)=-12C_1\int\phi_l\frac{d}{dx}\Bigg[&\left(\frac{d\phi_i}{dx}\right)\\
&\times\left(\frac{d\psi_j}{dx}\right)\left(\frac{d\psi_0}{dx}\right)\Bigg]dx,
\end{aligned} \tag{36}
$$

$$
\begin{aligned}
K_{13}^{NL}(l,i,j)=&-3C_1\int\phi_l\frac{d}{dx}\left[\left(\frac{d\psi_i}{dx}\right)\left(\frac{d\psi_j}{dx}\right)\right]dx\\
&+6C_1\int\phi_l\frac{d}{dx}\left[\left(\frac{d\psi_i}{dx}\right)\left(\frac{d\psi_j}{dx}\right)\left(\frac{d\psi_0}{dx}\right)^2\right]dx\\
&+6C_1\gamma_2^2\int\phi_l\frac{d}{dx}\left[\left(\frac{d^2\psi_i}{dx^2}\right)\left(\frac{d^2\psi_j}{dx^2}\right)\right]dx,
\end{aligned} \tag{37}
$$

$$K_{14}^{NL}(l,i,j,k) = -36C_1C_2 \times \int \phi_l \frac{d}{dx}\left[\left(\frac{d\phi_i}{dx}\right)\left(\frac{d\phi_j}{dx}\right)\left(\frac{d\phi_k}{dx}\right)\right]dx, \tag{38}$$

$$K_{15}^{NL}(l,i,j,k) = 108C_1C_2 \times \int \phi_l \frac{d}{dx}\left[\left(\frac{d\phi_i}{dx}\right)\left(\frac{d\phi_j}{dx}\right)\left(\frac{d\psi_k}{dx}\right)\left(\frac{d\psi_0}{dx}\right)\right]dx, \tag{39}$$

$$\begin{aligned} K_{16}^{NL}(l,i,j,k) &= 6C_1 \int \phi_l \frac{d}{dx}\left[\left(\frac{d\phi_i}{dx}\right) \times \left(\frac{d\psi_j}{dx}\right)\left(\frac{d\psi_k}{dx}\right)\right] \\ &\quad -108C_1C_2 \int \phi_l \frac{d}{dx}\left[\left(\frac{d\phi_i}{dx}\right) \times \left(\frac{d\psi_j}{dx}\right)\left(\frac{d\psi_k}{dx}\right)\left(\frac{d\psi_0}{dx}\right)^2\right]dx \\ &\quad -108\gamma_2^2C_1C_2 \int \phi_l \frac{d}{dx}\left[\left(\frac{d\phi_i}{dx}\right)\left(\frac{d^2\psi_j}{dx^2}\right)\left(\frac{d^2\psi_k}{dx^2}\right)\right]dx, \end{aligned} \tag{40}$$

$$\begin{aligned} K_{17}^{NL}(l,i,j,k) &= -6C_1 \int \phi_l \frac{d}{dx}\left[\left(\frac{d\psi_i}{dx}\right)\left(\frac{d\psi_j}{dx}\right) \times \left(\frac{d\psi_k}{dx}\right)\left(\frac{d\psi_0}{dx}\right)\right]dx \\ &\quad +36C_1C_2 \int \phi_l \frac{d}{dx}\left[\left(\frac{d\psi_i}{dx}\right)\left(\frac{d\psi_j}{dx}\right)\left(\frac{d\psi_k}{dx}\right)\left(\frac{d\psi_0}{dx}\right)^3\right]dx \\ &\quad +108\gamma_2^2C_1C_2 \int \phi_l \frac{d}{dx}\left[\left(\frac{d\psi_i}{dx}\right)\left(\frac{d^2\psi_j}{dx^2}\right) \times \left(\frac{d^2\psi_k}{dx^2}\right)\left(\frac{d\psi_0}{dx}\right)\right]dx, \end{aligned} \tag{41}$$

$$K_{18}^{NL}(l,i,j,k,m) = -54C_1C_2 \int \phi_l \frac{d}{dx} \times \left[\left(\frac{d\phi_i}{dx}\right)\left(\frac{d\phi_j}{dx}\right)\left(\frac{d\psi_k}{dx}\right)\left(\frac{d\psi_m}{dx}\right)\right]dx, \tag{42}$$

$$K_{19}^{NL}(l,i,j,k,m) = -108C_1C_2 \int \phi_l \frac{d}{dx}\left[\left(\frac{d\phi_i}{dx}\right)\left(\frac{d\psi_j}{dx}\right) \times \left(\frac{d\psi_k}{dx}\right)\left(\frac{d\psi_m}{dx}\right)\left(\frac{d\psi_0}{dx}\right)\right]dx, \tag{43}$$

$$\begin{aligned} K_{110}^{NL}(l,i,j,k,m) &= \frac{3}{2}C_1 \int \phi_l \frac{d}{dx}\left[\left(\frac{d\psi_i}{dx}\right)\left(\frac{d\psi_j}{dx}\right) \times \left(\frac{d\psi_k}{dx}\right)\left(\frac{d\psi_m}{dx}\right)\right]dx \\ &\quad -54C_1C_2 \int \phi_l \frac{d}{dx}\left[\left(\frac{d\psi_i}{dx}\right)\left(\frac{d\psi_j}{dx}\right)\left(\frac{d\psi_k}{dx}\right) \times \left(\frac{d\psi_m}{dx}\right)\left(\frac{d\psi_0}{dx}\right)^2\right]dx \\ &\quad -54\gamma_2^2C_1C_2 \int \phi_l \frac{d}{dx}\left[\left(\frac{d\psi_i}{dx}\right)\left(\frac{d\psi_j}{dx}\right) \times \left(\frac{d^2\psi_k}{dx^2}\right)\left(\frac{d^2\psi_m}{dx^2}\right)\right]dx, \end{aligned} \tag{44}$$

$$K_{111}^{NL}(l,i,j,k,m,n) = -162C_1C_3 \int \phi_l \frac{d}{dx}\left[\left(\frac{d\phi_i}{dx}\right)\left(\frac{d\phi_j}{dx}\right) \times \left(\frac{d\phi_k}{dx}\right)\left(\frac{d\phi_m}{dx}\right)\left(\frac{d\phi_n}{dx}\right)\right]dx, \tag{45}$$

$$K_{112}^{NL}(l,i,j,k,m,n) = 810C_1C_3 \int \phi_l \frac{d}{dx}\left[\left(\frac{d\phi_i}{dx}\right)\left(\frac{d\phi_j}{dx}\right) \times \left(\frac{d\phi_k}{dx}\right)\left(\frac{d\phi_m}{dx}\right)\left(\frac{d\psi_n}{dx}\right)\left(\frac{d\psi_0}{dx}\right)\right]dx, \tag{46}$$

$$\begin{aligned} K_{113}^{NL}(l,i,j,k,m,n) &= -1620C_1C_3 \int \phi_l \frac{d}{dx}\left[\left(\frac{d\phi_i}{dx}\right) \times \left(\frac{d\phi_j}{dx}\right)\left(\frac{d\phi_k}{dx}\right)\left(\frac{d\psi_m}{dx}\right)\left(\frac{d\psi_n}{dx}\right)\left(\frac{d\psi_0}{dx}\right)^2\right]dx \\ &\quad -1620\gamma_2^2C_1C_3 \int \phi_l \frac{d}{dx}\left[\left(\frac{d\phi_i}{dx}\right)\left(\frac{d\phi_j}{dx}\right)\left(\frac{d\phi_k}{dx}\right) \times \left(\frac{d^2\psi_m}{dx^2}\right)\left(\frac{d^2\psi_n}{dx^2}\right)\right]dx, \end{aligned} \tag{47}$$

$$\begin{aligned} K_{114}^{NL} &= 1620C_1C_3 \int \phi_l \frac{d}{dx}\left[\left(\frac{d\phi_i}{dx}\right)\left(\frac{d\phi_j}{dx}\right)\left(\frac{d\psi_k}{dx}\right) \times \left(\frac{d\psi_m}{dx}\right)\left(\frac{d\psi_n}{dx}\right)\left(\frac{d\psi_0}{dx}\right)^3\right]dx \\ &\quad +4860\gamma_2^2C_1C_3 \int \phi_l \frac{d}{dx}\left[\left(\frac{d\phi_i}{dx}\right)\left(\frac{d\phi_j}{dx}\right)\left(\frac{d\psi_k}{dx}\right) \times \left(\frac{d^2\psi_m}{dx^2}\right)\left(\frac{d^2\psi_n}{dx^2}\right)\left(\frac{d\psi_0}{dx}\right)\right]dx, \end{aligned} \tag{48}$$

$$\begin{aligned} K_{115}^{NL}(l,i,j,k,m,n) &= -27C_1C_2 \int \phi_l \frac{d}{dx}\left[\left(\frac{d\phi_i}{dx}\right)\left(\frac{d\psi_j}{dx}\right) \times \left(\frac{d\psi_k}{dx}\right)\left(\frac{d\psi_m}{dx}\right)\left(\frac{d\psi_n}{dx}\right)\right]dx \\ &\quad -810C_1C_3 \int \phi_l \frac{d}{dx}\left[\left(\frac{d\phi_i}{dx}\right)\left(\frac{d\psi_j}{dx}\right)\left(\frac{d\psi_k}{dx}\right) \times \left(\frac{d\psi_m}{dx}\right)\left(\frac{d\psi_n}{dx}\right)\left(\frac{d\psi_0}{dx}\right)^4\right]dx \\ &\quad -4860\gamma_2^2C_1C_3 \int \phi_l \frac{d}{dx}\left[\left(\frac{d\phi_i}{dx}\right)\left(\frac{d\psi_j}{dx}\right)\left(\frac{d\psi_k}{dx}\right) \times \left(\frac{d^2\psi_m}{dx^2}\right)\left(\frac{d^2\psi_n}{dx^2}\right)\left(\frac{d\psi_0}{dx}\right)^2\right]dx \\ &\quad -810\gamma_4^2C_1C_3 \int \phi_l \frac{d}{dx}\left[\left(\frac{d\phi_i}{dx}\right)\left(\frac{d^2\psi_j}{dx^2}\right)\left(\frac{d^2\psi_k}{dx^2}\right) \times \left(\frac{d^2\psi_m}{dx^2}\right)\left(\frac{d^2\psi_n}{dx^2}\right)\right]dx, \end{aligned} \tag{49}$$

$$\begin{aligned} K_{116}^{NL}(l,i,j,k,m,n) &= 27C_1C_2 \int \phi_l \frac{d}{dx}\left[\left(\frac{d\psi_i}{dx}\right)\left(\frac{d\psi_j}{dx}\right) \times \left(\frac{d\psi_k}{dx}\right)\left(\frac{d\psi_m}{dx}\right)\left(\frac{d\psi_n}{dx}\right)\left(\frac{d\psi_0}{dx}\right)\right]dx \\ &\quad +162C_1C_3 \int \phi_l \frac{d}{dx}\left[\left(\frac{d\psi_i}{dx}\right)\left(\frac{d\psi_j}{dx}\right)\left(\frac{d\psi_k}{dx}\right) \times \left(\frac{d\psi_m}{dx}\right)\left(\frac{d\psi_n}{dx}\right)\left(\frac{d\psi_0}{dx}\right)^5\right]dx \\ &\quad +1620\gamma_2^2C_1C_3 \int \phi_l \frac{d}{dx}\left[\left(\frac{d\psi_i}{dx}\right)\left(\frac{d\psi_j}{dx}\right)\left(\frac{d\psi_k}{dx}\right) \times \left(\frac{d^2\psi_m}{dx^2}\right)\left(\frac{d^2\psi_n}{dx^2}\right)\left(\frac{d\psi_0}{dx}\right)^3\right]dx \\ &\quad +810\gamma_4^2C_1C_3 \int \phi_l \frac{d}{dx}\left[\left(\frac{d\psi_i}{dx}\right)\left(\frac{d^2\psi_j}{dx^2}\right)\left(\frac{d^2\psi_k}{dx^2}\right) \times \left(\frac{d^2\psi_m}{dx^2}\right)\left(\frac{d^2\psi_n}{dx^2}\right)\left(\frac{d\psi_0}{dx}\right)\right]dx, \end{aligned} \tag{50}$$

$$M_2(l,i) = \int \psi_l \psi_i dx, \tag{51}$$

$$C_2(l,i) = 2V_b \int \psi_l \left(\frac{d\psi_i}{dx}\right) dx, \tag{52}$$

$$K_{21}^L(l,i) = 6C_1 \int \psi_l \frac{d}{dx}\left[\left(\frac{d\phi_i}{dx}\right)\left(\frac{d\psi_0}{dx}\right)\right] dx, \tag{53}$$

$$\begin{aligned} K_{22}^L(l,i) &= \left(V_b^2 - 1\right) \int \psi_l \left(\frac{d^2\psi_i}{dx^2}\right) dx \\ &+6C_1\gamma_2^2 \int \psi_l \left(\frac{d^4\psi_i}{dx^4}\right) dx \\ &-6C_1 \int \psi_l \frac{d}{dx}\left[\left(\frac{d\psi_i}{dx}\right)\left(\frac{d\psi_0}{dx}\right)^2\right] dx, \end{aligned} \tag{54}$$

$$K_{20}^L = V_b^2 \int \psi_l \left(\frac{d^2\psi_0}{dx^2}\right) dx, \tag{55}$$

$$K_{21}^{NL}(l,i,j) = -6C_1 \int \psi_l \frac{d}{dx}\left[\left(\frac{d\phi_i}{dx}\right)\left(\frac{d\phi_j}{dx}\right)\left(\frac{d\psi_0}{dx}\right)\right] dx, \tag{56}$$

$$\begin{aligned} K_{22}^{NL}(l,i,j) &= -12\gamma_2^2 C_1 \int \psi_l \frac{d^2}{dx^2}\left[\left(\frac{d\phi_i}{dx}\right)\left(\frac{d^2\psi_j}{dx^2}\right)\right] dx \\ &-6C_1 \int \psi_l \frac{d}{dx}\left[\left(\frac{d\phi_i}{dx}\right)\left(\frac{d\psi_j}{dx}\right)\right] dx \\ &+12C_1 \int \psi_l \frac{d}{dx}\left[\left(\frac{d\phi_i}{dx}\right)\left(\frac{d\psi_j}{dx}\right)\left(\frac{d\psi_0}{dx}\right)^2\right] dx, \end{aligned} \tag{57}$$

$$\begin{aligned} K_{23}^{NL}(l,i,j) &= 12\gamma_2^2 C_1 \int \psi_l \frac{d^2}{dx^2} \\ &\times \left[\left(\frac{d\psi_i}{dx}\right)\left(\frac{d^2\psi_j}{dx^2}\right)\left(\frac{d\psi_0}{dx}\right)\right] dx \\ &+9C_1 \int \psi_l \frac{d}{dx}\left[\left(\frac{d\psi_i}{dx}\right)\left(\frac{d\psi_j}{dx}\right)\left(\frac{d\psi_0}{dx}\right)\right] dx \\ &-6C_1 \int \psi_l \frac{d}{dx}\left[\left(\frac{d\psi_i}{dx}\right)\left(\frac{d\psi_j}{dx}\right)\left(\frac{d\psi_0}{dx}\right)^3\right] dx \\ &-6\gamma_2^2 C_1 \int \psi_l \frac{d}{dx}\left[\left(\frac{d^2\psi_i}{dx^2}\right)\left(\frac{d^2\psi_j}{dx^2}\right)\left(\frac{d\psi_0}{dx}\right)\right] dx, \end{aligned} \tag{58}$$

$$K_{24}^{NL}(l,i,j,k) = 36C_1C_2 \int \psi_l \frac{d}{dx}\left[\left(\frac{d\phi_i}{dx}\right)\left(\frac{d\phi_j}{dx}\right)\left(\frac{d\phi_k}{dx}\right)\left(\frac{d\psi_0}{dx}\right)\right] dx, \tag{59}$$

$$\begin{aligned} K_{25}^{NL}(l,i,j,k) &= 6C_1 \int \psi_l \frac{d}{dx}\left[\left(\frac{d\phi_i}{dx}\right)\left(\frac{d\phi_j}{dx}\right)\left(\frac{d\psi_k}{dx}\right)\right] dx \\ &+108\gamma_2^2 C_1C_2 \int \psi_l \frac{d^2}{dx^2}\left[\left(\frac{d\phi_i}{dx}\right)\left(\frac{d\phi_j}{dx}\right)\left(\frac{d^2\psi_k}{dx^2}\right)\right] dx \\ &-108C_1C_2 \int \psi_l \frac{d}{dx}\left[\left(\frac{d\phi_i}{dx}\right)\left(\frac{d\phi_j}{dx}\right)\left(\frac{d\psi_k}{dx}\right)\left(\frac{d\psi_0}{dx}\right)^2\right] dx, \end{aligned} \tag{60}$$

$$\begin{aligned} K_{26}^{NL}(l,i,j,k) &= -18C_1 \int \psi_l \frac{d}{dx}\left[\left(\frac{d\phi_i}{dx}\right)\left(\frac{d\psi_j}{dx}\right)\left(\frac{d\psi_k}{dx}\right)\left(\frac{d\psi_0}{dx}\right)\right] dx \\ &-216\gamma_2^2 C_1C_2 \int \psi_l \frac{d^2}{dx^2}\left[\left(\frac{d\phi_i}{dx}\right)\left(\frac{d\psi_j}{dx}\right)\left(\frac{d^2\psi_k}{dx^2}\right)\left(\frac{d\psi_0}{dx}\right)\right] dx \\ &+108C_1C_2 \int \psi_l \frac{d}{dx}\left[\left(\frac{d\phi_i}{dx}\right)\left(\frac{d\psi_j}{dx}\right)\left(\frac{d\psi_k}{dx}\right)\left(\frac{d\psi_0}{dx}\right)^3\right] dx \\ &+108\gamma_2^2 C_1C_2 \int \psi_l \frac{d}{dx}\left[\left(\frac{d\phi_i}{dx}\right)\left(\frac{d^2\psi_j}{dx^2}\right)\left(\frac{d^2\psi_k}{dx^2}\right)\left(\frac{d\psi_0}{dx}\right)\right] dx, \end{aligned} \tag{61}$$

$$\begin{aligned} K_{27}^{NL}(l,i,j,k) &= -6\gamma_2^2 C_1 \int \psi_l \frac{\partial^2}{\partial x^2}\left[\left(\frac{d\psi_i}{dx}\right)\left(\frac{d\psi_j}{dx}\right)\left(\frac{d^2\psi_k}{dx^2}\right)\right] dx \\ &-3C_1 \int \psi_l \frac{d}{dx}\left[\left(\frac{d\psi_i}{dx}\right)\left(\frac{d\psi_j}{dx}\right)\left(\frac{d\psi_k}{dx}\right)\right] dx \\ &+12C_1 \int \psi_l \frac{d}{dx}\left[\left(\frac{d\psi_i}{dx}\right)\left(\frac{d\psi_j}{dx}\right)\left(\frac{d\psi_k}{dx}\right)\left(\frac{d\psi_0}{dx}\right)^2\right] dx \\ &+6\gamma_2^2 C_1 \int \psi_l \frac{d}{dx}\left[\left(\frac{d\psi_i}{dx}\right)\left(\frac{d^2\psi_j}{dx^2}\right)\left(\frac{d^2\psi_k}{dx^2}\right)\right] dx \\ &+108\gamma_2^2 C_1C_2 \int \psi_l \frac{d^2}{dx^2}\left[\left(\frac{d\psi_i}{dx}\right)\left(\frac{d\psi_j}{dx}\right)\left(\frac{d^2\psi_k}{dx^2}\right)\left(\frac{d\psi_0}{dx}\right)^2\right] dx \\ &+36\gamma_4^2 C_1C_2 \int \psi_l \frac{d^2}{dx^2}\left[\left(\frac{d^2\psi_i}{dx^2}\right)\left(\frac{d^2\psi_j}{dx^2}\right)\left(\frac{d^2\psi_k}{dx^2}\right)\right] dx \\ &-36C_1C_2 \int \psi_l \frac{d}{dx}\left[\left(\frac{d\psi_i}{dx}\right)\left(\frac{d\psi_j}{dx}\right)\left(\frac{d\psi_k}{dx}\right)\left(\frac{d\psi_0}{dx}\right)^4\right] dx \\ &-108\gamma_2^2 C_1C_2 \int \psi_l \frac{d}{dx}\left[\left(\frac{d\psi_i}{dx}\right)\left(\frac{d^2\psi_j}{dx^2}\right)\left(\frac{d^2\psi_k}{dx^2}\right)\left(\frac{d\psi_0}{dx}\right)^2\right] dx, \end{aligned} \tag{62}$$

$$\begin{aligned} K_{28}^{NL}(l,i,j,k,m) &= -36C_1C_2 \\ &\times \int \psi_l \frac{d}{dx}\left[\left(\frac{d\phi_i}{dx}\right)\left(\frac{d\phi_j}{dx}\right)\left(\frac{d\phi_k}{dx}\right)\left(\frac{d\psi_m}{dx}\right)\right] dx, \end{aligned} \tag{63}$$

$$\begin{aligned} K_{29}^{NL}(l,i,j,k,m) &= 162C_1C_2 \int \psi_l \frac{d}{dx}\left[\left(\frac{d\phi_i}{dx}\right)\left(\frac{d\phi_j}{dx}\right)\right. \\ &\left.\times \left(\frac{d\psi_k}{dx}\right)\left(\frac{d\psi_m}{dx}\right)\left(\frac{d\psi_0}{dx}\right)\right] dx, \end{aligned} \tag{64}$$

$$\begin{aligned} K_{210}^{NL}(l,i,j,k,m) &= 6C_1 \int \psi_l \frac{d}{dx}\left[\left(\frac{d\phi_i}{dx}\right)\left(\frac{d\psi_j}{dx}\right)\left(\frac{d\psi_k}{dx}\right)\left(\frac{d\psi_m}{dx}\right)\right] dx \\ &+108\gamma_2^2 C_1C_2 \int \psi_l \frac{d^2}{dx^2}\left[\left(\frac{d\phi_i}{dx}\right)\left(\frac{d\psi_j}{dx}\right)\left(\frac{d\psi_k}{dx}\right)\left(\frac{d^2\psi_m}{dx^2}\right)\right] dx \\ &-162C_1C_2 \int \psi_l \frac{d}{dx}\left[\left(\frac{d\phi_i}{dx}\right)\left(\frac{d\psi_j}{dx}\right)\left(\frac{d\psi_k}{dx}\right)\left(\frac{d\psi_m}{dx}\right)\right. \\ &\left.\times \left(\frac{d\psi_0}{dx}\right)^2\right] dx, \end{aligned} \tag{65}$$

$$\begin{aligned} K_{211}^{NL}(l,i,j,k,m) &= -\frac{15}{2}C_1 \int \psi_l \frac{d}{dx}\left[\left(\frac{d\psi_i}{dx}\right)\left(\frac{d\psi_j}{dx}\right)\right. \\ &\left.\times \left(\frac{d\psi_k}{dx}\right)\left(\frac{d\psi_m}{dx}\right)\left(\frac{d\psi_0}{dx}\right)\right] dx \\ &-108\gamma_2^2 C_1C_2 \int \psi_l \frac{d^2}{dx^2}\left[\left(\frac{d\psi_i}{dx}\right)\left(\frac{d\psi_j}{dx}\right)\left(\frac{d\psi_k}{dx}\right)\right. \\ &\left.\times \left(\frac{d^2\psi_m}{dx^2}\right)\left(\frac{d\psi_0}{dx}\right)\right] dx \\ &+90C_1C_2 \int \psi_l \frac{d}{dx}\left[\left(\frac{d\psi_i}{dx}\right)\left(\frac{d\psi_j}{dx}\right)\left(\frac{d\psi_k}{dx}\right)\right. \\ &\left.\times \left(\frac{d\psi_m}{dx}\right)\left(\frac{d\psi_0}{dx}\right)^3\right] dx \\ &+162\gamma_2^2 C_1C_2 \int \psi_l \frac{d}{dx}\left[\left(\frac{d\psi_i}{dx}\right)\left(\frac{d\psi_j}{dx}\right)\right. \\ &\left.\times \left(\frac{d^2\psi_k}{dx^2}\right)\left(\frac{d^2\psi_m}{dx^2}\right)\left(\frac{d\psi_0}{dx}\right)\right] dx, \end{aligned} \tag{66}$$

$$K_{212}^{NL}(l,i,j,k,m,n) = 162C_1C_3 \int \psi_l \frac{d}{dx}\left[\left(\frac{d\phi_i}{dx}\right)\left(\frac{d\phi_j}{dx}\right)\right.$$

$$\times \left(\frac{d\phi_k}{dx}\right)\left(\frac{d\phi_m}{dx}\right)\left(\frac{d\phi_n}{dx}\right)\left(\frac{d\psi_0}{dx}\right)\Big] dx, \tag{67}$$

$$\begin{aligned}K_{213}^{NL}(l,i,j,k,m,n) = {} & 810\gamma_2^2 C_1 C_3 \int \psi_l \frac{d^2}{dx^2}\left[\left(\frac{d\phi_i}{dx}\right)\left(\frac{d\phi_j}{dx}\right)\left(\frac{d\phi_k}{dx}\right)\right. \\ & \times \left(\frac{d\phi_m}{dx}\right)\left(\frac{d^2\psi_n}{dx^2}\right)\Big] dx \\ & -810 C_1 C_3 \int \psi_l \frac{d}{dx}\left[\left(\frac{d\phi_i}{dx}\right)\left(\frac{d\phi_j}{dx}\right)\left(\frac{d\phi_k}{dx}\right)\right. \\ & \times \left(\frac{d\phi_m}{dx}\right)\left(\frac{d\psi_n}{dx}\right)\left(\frac{d\psi_0}{dx}\right)^2\Big] dx,\end{aligned} \tag{68}$$

$$\begin{aligned}K_{214}^{NL}(l,i,j,k,m,n) = {} & -3240\gamma_2^2 C_1 C_3 \int \psi_l \frac{d^2}{dx^2}\left[\left(\frac{d\phi_i}{dx}\right)\left(\frac{d\phi_j}{dx}\right)\left(\frac{d\phi_k}{dx}\right)\right. \\ & \times \left(\frac{d\psi_m}{dx}\right)\left(\frac{d^2\psi_n}{dx^2}\right)\left(\frac{d\psi_0}{dx}\right)\Big] dx \\ & +1620 C_1 C_3 \int \psi_l \frac{d}{dx}\left[\left(\frac{d\phi_i}{dx}\right)\left(\frac{d\phi_j}{dx}\right)\left(\frac{d\phi_k}{dx}\right)\right. \\ & \times \left(\frac{d\psi_m}{dx}\right)\left(\frac{d\psi_n}{dx}\right)\left(\frac{d\psi_0}{dx}\right)^3\Big] dx \\ & +1620\gamma_2^2 C_1 C_3 \int \psi_l \frac{d}{dx}\left[\left(\frac{d\phi_i}{dx}\right)\left(\frac{d\phi_j}{dx}\right)\left(\frac{d\phi_k}{dx}\right)\right. \\ & \times \left(\frac{d^2\psi_m}{dx^2}\right)\left(\frac{d^2\psi_n}{dx^2}\right)\left(\frac{d\psi_0}{dx}\right)\Big] dx,\end{aligned} \tag{69}$$

$$\begin{aligned}K_{215}^{NL}(l,i,j,k,m,n) = {} & -54 C_1 C_2 \int \psi_l \frac{d}{dx}\left[\left(\frac{d\phi_i}{dx}\right)\left(\frac{d\phi_j}{dx}\right)\right. \\ & \times \left(\frac{d\psi_k}{dx}\right)\left(\frac{d\psi_m}{dx}\right)\left(\frac{d\psi_n}{dx}\right)\Big] dx \\ & +4860\gamma_2^2 C_1 C_3 \int \psi_l \frac{d^2}{dx^2}\left[\left(\frac{d\phi_i}{dx}\right)\left(\frac{d\phi_j}{dx}\right)\left(\frac{d\psi_k}{dx}\right)\right. \\ & \times \left(\frac{d\psi_m}{dx}\right)\left(\frac{d^2\psi_n}{dx^2}\right)\left(\frac{d\psi_0}{dx}\right)^2\Big] dx \\ & +1620\gamma_4^2 C_1 C_3 \int \psi_l \frac{d^2}{dx^2}\left[\left(\frac{d\phi_i}{dx}\right)\left(\frac{d\phi_j}{dx}\right)\left(\frac{d^2\psi_k}{dx^2}\right)\left(\frac{d^2\psi_m}{dx^2}\right)\right. \\ & \times \left(\frac{d^2\psi_n}{dx^2}\right)\Big] dx \\ & -1620 C_1 C_3 \int \psi_l \frac{d}{dx}\left[\left(\frac{d\phi_i}{dx}\right)\left(\frac{d\phi_j}{dx}\right)\left(\frac{d\psi_k}{dx}\right)\right. \\ & \times \left(\frac{d\psi_m}{dx}\right)\left(\frac{d\psi_n}{dx}\right)\left(\frac{d\psi_0}{dx}\right)^4\Big] dx \\ & -4860\gamma_2^2 C_1 C_3 \int \psi_l \frac{d}{dx}\left[\left(\frac{d\phi_i}{dx}\right)\left(\frac{d\phi_j}{dx}\right)\left(\frac{d\psi_k}{dx}\right)\right. \\ & \times \left(\frac{d^2\psi_m}{dx^2}\right)\left(\frac{d^2\psi_n}{dx^2}\right)\left(\frac{d\psi_0}{dx}\right)^2\Big] dx,\end{aligned} \tag{70}$$

$$\begin{aligned}K_{216}^{NL}(l,i,j,k,m,n) = {} & 132 C_1 C_2 \int \psi_l \frac{d}{dx}\left[\left(\frac{d\phi_i}{dx}\right)\left(\frac{d\psi_j}{dx}\right)\left(\frac{d\psi_k}{dx}\right)\right. \\ & \times \left(\frac{d\psi_m}{dx}\right)\left(\frac{d\psi_n}{dx}\right)\left(\frac{d\psi_0}{dx}\right)\Big] dx \\ & -3240\gamma_2^2 C_1 C_3 \int \psi_l \frac{d^2}{dx^2}\left[\left(\frac{d\phi_i}{dx}\right)\left(\frac{d\psi_j}{dx}\right)\left(\frac{d\psi_k}{dx}\right)\right. \\ & \times \left(\frac{d\psi_m}{dx}\right)\left(\frac{d^2\psi_n}{dx^2}\right)\left(\frac{d\psi_0}{dx}\right)^3\Big] dx \\ & -3240\gamma_2^2 C_1 C_3 \int \psi_l \frac{d^2}{dx^2}\left[\left(\frac{d\phi_i}{dx}\right)\left(\frac{d\psi_j}{dx}\right)\left(\frac{d^2\psi_k}{dx^2}\right)\right. \\ & \times \left(\frac{d^2\psi_m}{dx^2}\right)\left(\frac{d^2\psi_n}{dx^2}\right)\left(\frac{d\psi_0}{dx}\right)\Big] dx \\ & +810 C_1 C_3 \int \psi_l \frac{d}{dx}\left[\left(\frac{d\phi_i}{dx}\right)\left(\frac{d\psi_j}{dx}\right)\left(\frac{d\psi_k}{dx}\right)\right. \\ & \times \left(\frac{d\psi_m}{dx}\right)\left(\frac{d\psi_n}{dx}\right)\left(\frac{d\psi_0}{dx}\right)^5\Big] dx \\ & +4860\gamma_2^2 C_1 C_3 \int \psi_l \frac{d}{dx}\left[\left(\frac{d\phi_i}{dx}\right)\left(\frac{d\psi_j}{dx}\right)\left(\frac{d\psi_k}{dx}\right)\right. \\ & \times \left(\frac{d^2\psi_m}{dx^2}\right)\left(\frac{d^2\psi_n}{dx^2}\right)\left(\frac{d\psi_0}{dx}\right)^3\Big] dx \\ & +810\gamma_4^2 C_1 C_3 \int \psi_l \frac{d}{dx}\left[\left(\frac{d\phi_i}{dx}\right)\left(\frac{d^2\psi_j}{dx^2}\right)\left(\frac{d^2\psi_k}{dx^2}\right)\right. \\ & \times \left(\frac{d^2\psi_m}{dx^2}\right)\left(\frac{d^2\psi_n}{dx^2}\right)\left(\frac{d\psi_0}{dx}\right)\Big] dx,\end{aligned} \tag{71}$$

$$\begin{aligned}K_{217}^{NL}(l,i,j,k,m,n) = {} & \frac{3}{2} C_1 \int \psi_l \frac{d}{dx}\left[\left(\frac{d\psi_i}{dx}\right)\left(\frac{d\psi_j}{dx}\right)\left(\frac{d\psi_k}{dx}\right)\right. \\ & \times \left(\frac{d\psi_m}{dx}\right)\left(\frac{d\psi_n}{dx}\right)\Big] dx \\ & +27\gamma_2^2 C_1 C_2 \int \psi_l \frac{d^2}{dx^2}\left[\left(\frac{d\psi_i}{dx}\right)\left(\frac{d\psi_j}{dx}\right)\left(\frac{d\psi_k}{dx}\right)\right. \\ & \times \left(\frac{d\psi_m}{dx}\right)\left(\frac{d^2\psi_n}{dx^2}\right)\Big] dx \\ & -81 C_1 C_2 \int \psi_l \frac{d}{dx}\left[\left(\frac{d\psi_i}{dx}\right)\left(\frac{d\psi_j}{dx}\right)\left(\frac{d\psi_k}{dx}\right)\left(\frac{d\psi_m}{dx}\right)\right. \\ & \times \left(\frac{d\psi_n}{dx}\right)\left(\frac{d\psi_0}{dx}\right)^2\Big] dx \\ & -54\gamma_2^2 C_1 C_2 \int \psi_l \frac{d}{dx}\left[\left(\frac{d\psi_i}{dx}\right)\left(\frac{d\psi_j}{dx}\right)\left(\frac{d\psi_k}{dx}\right)\right. \\ & \times \left(\frac{d^2\psi_m}{dx^2}\right)\left(\frac{d^2\psi_n}{dx^2}\right)\Big] dx \\ & +810\gamma_2^2 C_1 C_3 \int \psi_l \frac{d^2}{dx^2}\left[\left(\frac{d\psi_i}{dx}\right)\left(\frac{d\psi_j}{dx}\right)\left(\frac{d\psi_k}{dx}\right)\right. \\ & \times \left(\frac{d\psi_m}{dx}\right)\left(\frac{d^2\psi_n}{dx^2}\right)\left(\frac{d\psi_0}{dx}\right)^4\Big] dx \\ & +1620\gamma_4^2 C_1 C_3 \int \psi_l \frac{d^2}{dx^2}\left[\left(\frac{d\psi_i}{dx}\right)\left(\frac{d\psi_j}{dx}\right)\left(\frac{d^2\psi_k}{dx^2}\right)\right. \\ & \times \left(\frac{d^2\psi_m}{dx^2}\right)\left(\frac{d^2\psi_n}{dx^2}\right)\left(\frac{d\psi_0}{dx}\right)\Big] dx \\ & +162\gamma_6^2 C_1 C_3 \int \psi_l \frac{d^2}{dx^2}\left[\left(\frac{d^2\psi_i}{dx^2}\right)\left(\frac{d^2\psi_j}{dx^2}\right)\left(\frac{d^2\psi_k}{dx^2}\right)\right. \\ & \times \left(\frac{d^2\psi_m}{dx^2}\right)\left(\frac{d^2\psi_n}{dx^2}\right)\Big] dx \\ & -162 C_1 C_3 \int \psi_l \frac{d}{dx}\left[\left(\frac{d\psi_i}{dx}\right)\left(\frac{d\psi_j}{dx}\right)\left(\frac{d\psi_k}{dx}\right)\right. \\ & \times \left(\frac{d\psi_m}{dx}\right)\left(\frac{d\psi_n}{dx}\right)\left(\frac{d\psi_0}{dx}\right)^6\Big] dx \\ & -1620\gamma_2^2 C_1 C_3 \int \psi_l \frac{d}{dx}\left[\left(\frac{d\psi_i}{dx}\right)\left(\frac{d\psi_j}{dx}\right)\left(\frac{d\psi_k}{dx}\right)\left(\frac{d^2\psi_m}{dx^2}\right)\right. \\ & \times \left(\frac{d^2\psi_n}{dx^2}\right)\left(\frac{d\psi_0}{dx}\right)^4\Big] dx \\ & -810\gamma_4^2 C_1 C_3 \int \psi_l \frac{d}{dx}\left[\left(\frac{d\psi_i}{dx}\right)\left(\frac{d^2\psi_j}{dx^2}\right)\left(\frac{d^2\psi_k}{dx^2}\right)\left(\frac{d^2\psi_m}{dx^2}\right)\right. \\ & \times \left(\frac{d^2\psi_n}{dx^2}\right)\left(\frac{d\psi_0}{dx}\right)^2\Big] dx,\end{aligned} \tag{72}$$

which can be rewritten in a matrix form as Eq. (73) is as given in Box I where

$$\{p_1, p_2, \ldots, p_{M+N}\} = \{r_1, r_2, \ldots, r_N, q_1, q_2, \ldots, q_M\}. \tag{74}$$

$$
\begin{bmatrix} \mu_{11} & & zeros \\ & \mu_{22} & \\ & \ddots & \\ zeros & & \mu_{(M+N)(M+N)} \end{bmatrix} \begin{Bmatrix} \ddot{p}_1 \\ \ddot{p}_2 \\ \vdots \\ \ddot{p}_{(M+N)} \end{Bmatrix} + \begin{bmatrix} \varsigma_{11} & \varsigma_{12} & \cdots & \varsigma_{1(M+N)} \\ \varsigma_{21} & \varsigma_{22} & & \vdots \\ \vdots & & \ddots & \\ \varsigma_{(M+N)1} & \cdots & & \varsigma_{(M+N)(M+N)} \end{bmatrix} \begin{Bmatrix} \dot{p}_1 \\ \dot{p}_2 \\ \vdots \\ \dot{p}_{(M+N)} \end{Bmatrix}
$$

$$
+ \begin{bmatrix} \kappa^L_{11} & \kappa^L_{12} & \cdots & \kappa^L_{1(M+N)} \\ \kappa^L_{21} & \kappa^L_{22} & & \vdots \\ \vdots & & \ddots & \\ \kappa^L_{(M+N)1} & \cdots & & \kappa^L_{(M+N)(M+N)} \end{bmatrix} \begin{Bmatrix} p_1 \\ p_2 \\ \vdots \\ p_{(M+N)} \end{Bmatrix}
$$

$$
+ \begin{bmatrix} \kappa^{NL}_{11}\left(p_1, p_2, \ldots, p_{(M+N)}\right) & \kappa^{NL}_{12}\left(p_1, p_2, \ldots, p_{(M+N)}\right) & \cdots & \kappa^{NL}_{1(M+N)}\left(p_1, p_2, \ldots, p_{(M+N)}\right) \\ \kappa^{NL}_{21}\left(p_1, p_2, \ldots, p_{(M+N)}\right) & \kappa^{NL}_{22}\left(p_1, p_2, \ldots, p_{(M+N)}\right) & & \vdots \\ \vdots & & \ddots & \\ \kappa^{NL}_{(M+N)1}\left(p_1, p_2, \ldots, p_{(M+N)}\right) & \cdots & & \kappa^{NL}_{(M+N)(M+N)}\left(p_1, p_2, \ldots, p_{(M+N)}\right) \end{bmatrix} \begin{Bmatrix} p_1 \\ p_2 \\ \vdots \\ p_{(M+N)} \end{Bmatrix}
$$

$$
= \begin{Bmatrix} f_1 \\ f_2 \\ \vdots \\ f_N \end{Bmatrix} \cos(\Omega t). \tag{73}
$$

Box I.

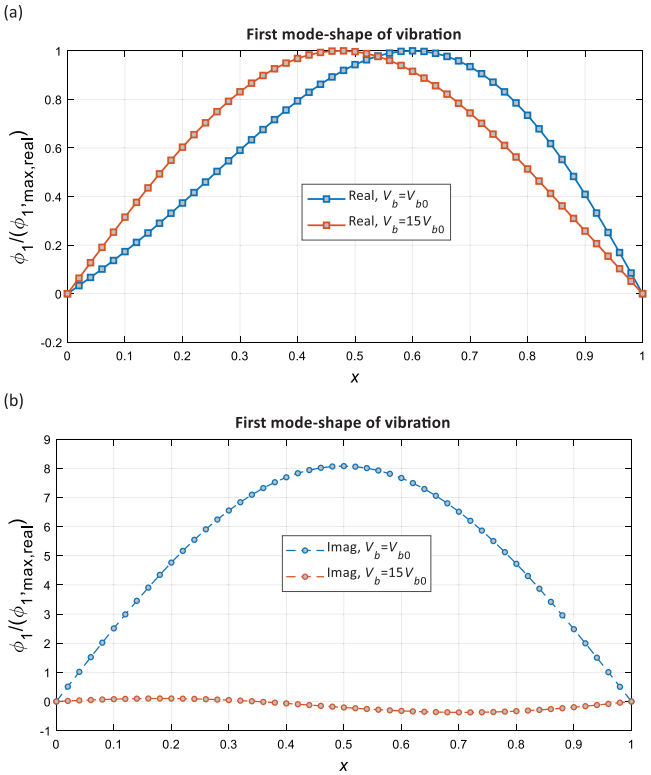

Fig. 11. First mode shapes of the thermoplastic polyurethane axially moving hyperelastic beam model for different velocities (a) real, and (b) imaginary parts.

Using the given assumptions and employing a dynamic equilibrium technique, the dynamic equilibrium coefficients are written in an exponential series as

$$
p_m = \sum_{n=-(M+N)}^{(M+N)} A_{mn} e^{in\omega t}, \tag{75}
$$

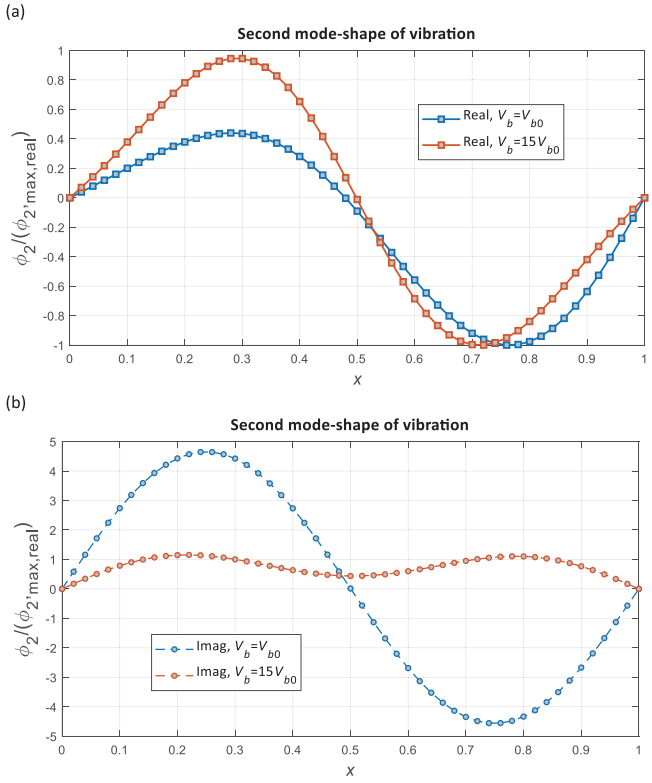

Fig. 12. Second mode shapes of the thermoplastic polyurethane axially moving hyperelastic beam model for different velocities (a) real, and (b) imaginary parts.

and the dynamic complex equilibrium equations is obtained as

$$\left\{-\omega^2\left[M_T\right]+i\omega\left[C_T\right]+\left[K_T^L\right]+\left[K_T^{NL}\left(\sum_{n=-(M+N)}^{(M+N)}A_{mn}e^{in\omega t}\right)\right]\right\}$$

$$\times\left\{\sum_{n=-(M+N)}^{(M+N)}A_{mn}e^{in\omega t}\right\}=\{f\}\cos(\Omega t), \tag{76}$$

which by solving the dynamic equilibrium equations, the nonlinear dynamic response of the system is obtained.

5. Results and discussions

In the previous sections, the coupled nonlinear dynamics of axially travelling hyperelastic beams is formulated and solved. In this section, the dynamic response of the system in a coupled regime is analysed and discussed in two subsections of linear and nonlinear analysis.

In order to analyse the mechanical behaviour of the system, the following properties are assumed as $L = 200$ mm, $h = 10$ mm, $b = 20$ mm; $\rho = 1000\,\text{kg/m}^3$, $P_0 = 50$ N, $V_{b0} = 1$ m/s, together with hyperelastic coefficients for Yeoh's strain energy density model as $C_1 = 2.631\text{e}6$ Pa $C_2 = -1.404\text{e}5$ Pa and $C_3 = 5016$ Pa for the thermoplastic polyurethane experimental testing model and as $C_1 = 0.24162\text{e}6$ Pa, $C_2 = 0.19977\text{e}6$ Pa, $C_3 = -0.00541\text{e}6$ Pa for silicone rubber [34] acted upon an external harmonic load as $F_0 = 0.01$ N.

5.1. Linear analysis

For the given properties, in the following subsections, the influence of different parameters on the linear frequency response of the system is discussed.

5.1.1. Influence of the axial velocity and C_1 parameter

For the first step, by using the defined properties, the velocity and C_1 hyperelasticity strain energy density terms are varied and the variation of the first two frequency parameters are calculated and shown in Fig. 10 for thermoplastic polyurethane model; it can be seen that the linear natural frequency terms decrease by increasing the axial velocity and decreasing term C_1.

Besides, the first two mode shapes for the axially moving hyperelastic beam model with velocity as $V_b = [V_b, 15V_{b0}]$ are shown in Figs. 11 and 12, respectively for the 3D printed thermoplastic polyurethane model; it can be seen that the mode shapes contain real and imaginary parts and varying the velocity changes the mode shapes significantly with more influence on the imaginary part.

5.1.2. Influence of the geometrical properties

To show the influence of the geometrical properties on the linear frequency vibration response of the system, the velocity and γ are varied together as $0.5\gamma_0 \le \gamma \le 2\gamma_0$ and $0.5V_{b0} \le V_b \le 10V_{b0}$. Results are shown in Fig. 13(a) and (b) for first and second natural frequency terms of thermoplastic polyurethane beam, respectively; it can be seen that the fundamental natural frequency term shows more sensitivity to variation of the axial velocity for all the γ terms compare to the second mode of vibration.

5.2. Nonlinear analysis

In this section, the nonlinear dynamic response of axially moving hyperelastic beams is investigated. Since hyperelastic structures show nonlinear mechanical properties and this importance is combined with large strains due to soft behaviour, nonlinear analysis of the system plays an important role in understanding their mechanical behaviour in different conditions. To this end, at the first stage of this section, the current methodology and solution procedure is verified. The importance of considering coupling motion and the influence of different parameters on the nonlinear response are discussed afterwards.

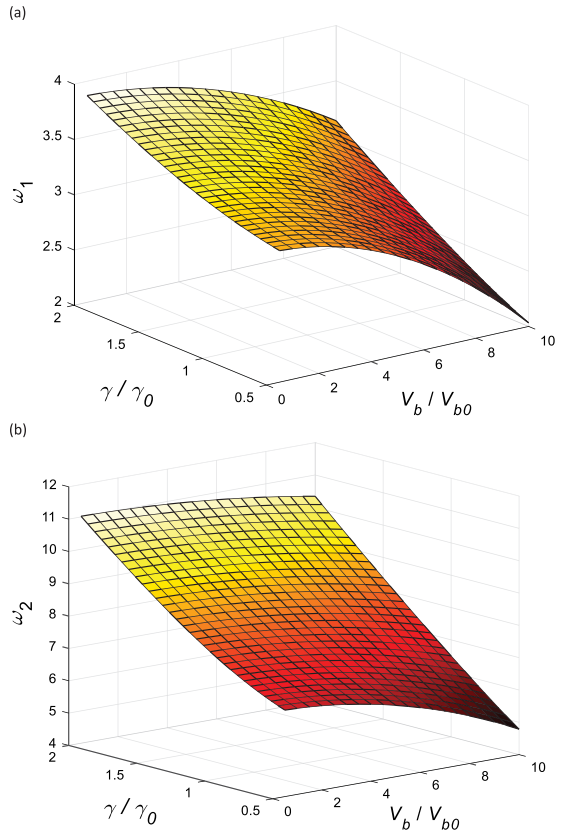

Fig. 13. Geometrical properties effect on the natural frequencies of the thermoplastic polyurethane axially moving hyperelastic beam model for different velocities (a) first natural frequency, and (b) second natural frequency.

5.2.1. Verification and convergence

In order to verify the current methodology, two-different approaches are provided; first, the coefficients are chosen in a way to convert the equations from hyperelasticity to elasticity by neglecting the hyperelasticity terms as ($C_2 = C_3 = 0$). Accordingly, by neglecting the coupled motion ($M = 0$) and only considering the transverse motion, properties are rewritten for internal resonance as $\omega_{20} = 3\omega_{10}$. By considering the first two series coordinate terms and first two Galerkin' parameters ($N = 2$), the amplitude–frequency response of the system is obtained as shown in Appendix A; it can be seen that the results are in a great agreement with Ref. [47] which shows the accuracy of the current methodology.

Besides, the convergence of the current methodology is analysed by increasing the total number of modes. To this end, the axially moving hyperelastic beam is modelled following the given properties at the beginning of this section for silicone-rubber and $F = 0.1\ F_0$, and the total number of modes is varied as shown in Appendix B for the first three dynamic equilibrium coordinates; it can be seen that by increasing the number of modes from six to fourteen, convergence is obtained after considering ten modes which this number of modes will be used in this study.

5.2.2. Comparison of coupling motion and single motion response

Axially moving elastic beam models have mainly been modelled previously using single motion analysis. In this study, the formulation and solution procedure is presented for coupled axial and transverse motions of hyperelastic beam model. The importance of considering couple motion is examined by showing the amplitude–frequency response of single and couple motion analysis in Fig. 14 for perfect and Fig. 15 for imperfect silicone-rubber with imperfection as $A_0 = 0.02$; it can be seen that the stiffness hardening behaviour is overestimated

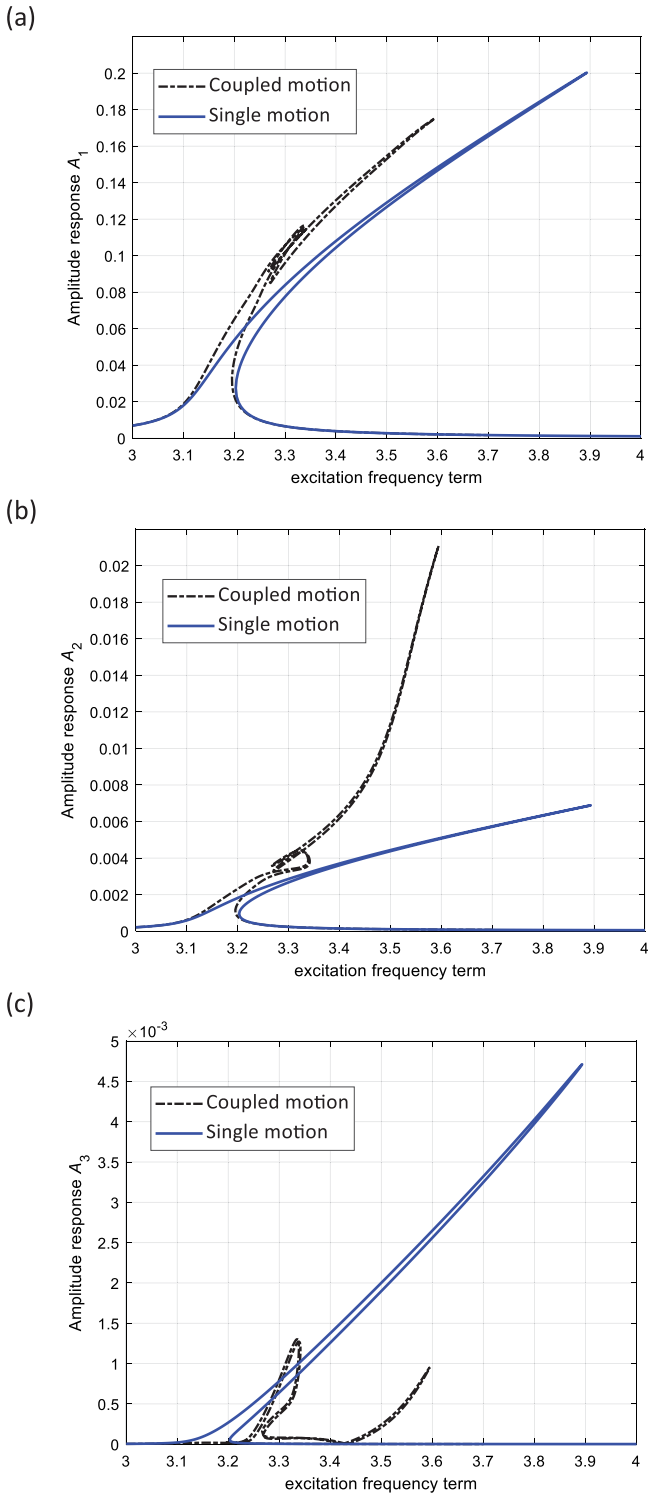

Fig. 14. Comparison between single motion and coupled motion nonlinear frequency response of perfect silicone rubber axially moving hyperelastic beam model (a) first coordinate, (b) second coordinate and (c) third coordinate.

for the all the coordinates of imperfect beam model and the first and third coordinates of perfect beam model when only transverse motion is considered, and the internal resonances are not seen.

5.2.3. Influence of the speed

As shown in the linear analysis, the speed of the axially moving beam plays a dominant role in varying the mechanical behaviour of

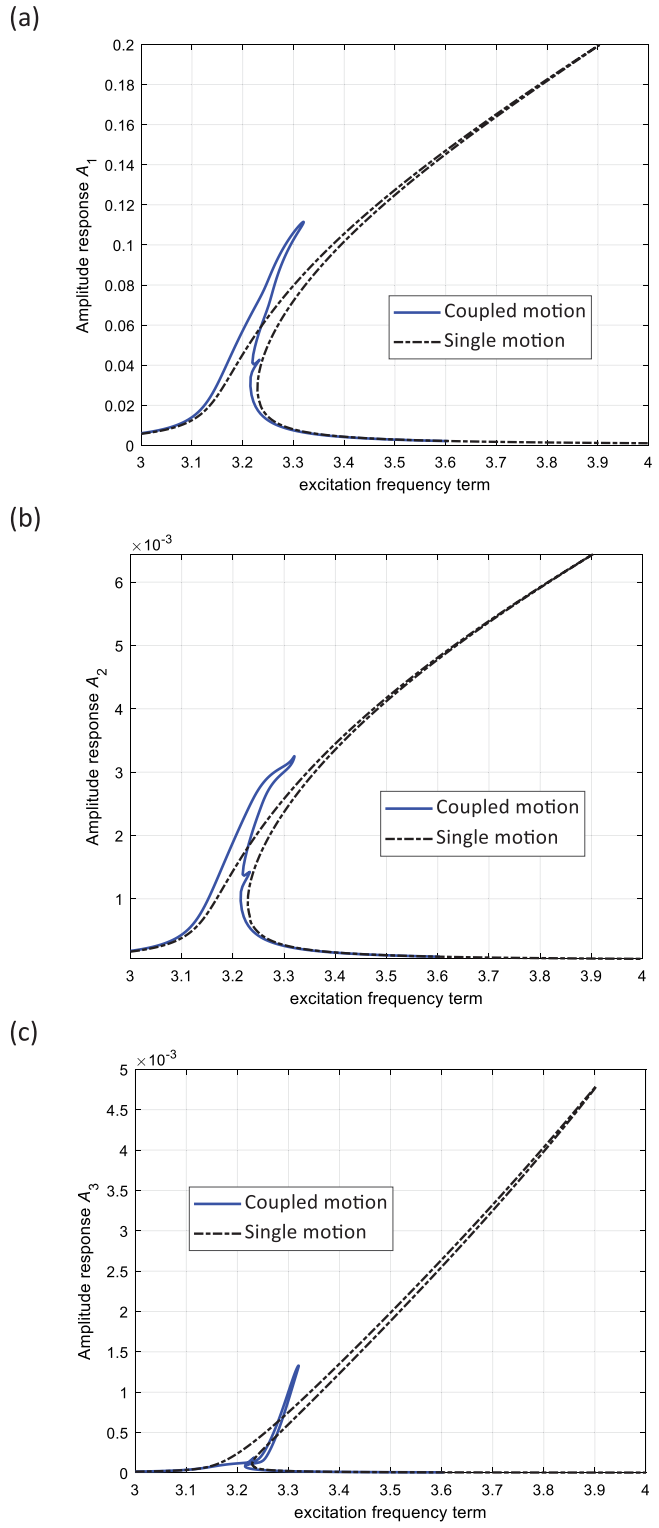

Fig. 15. Comparison between single motion and coupled motion nonlinear frequency response of imperfect silicone rubber axially moving hyperelastic beam model (a) first coordinate, (b) second coordinate and (c) third coordinate.

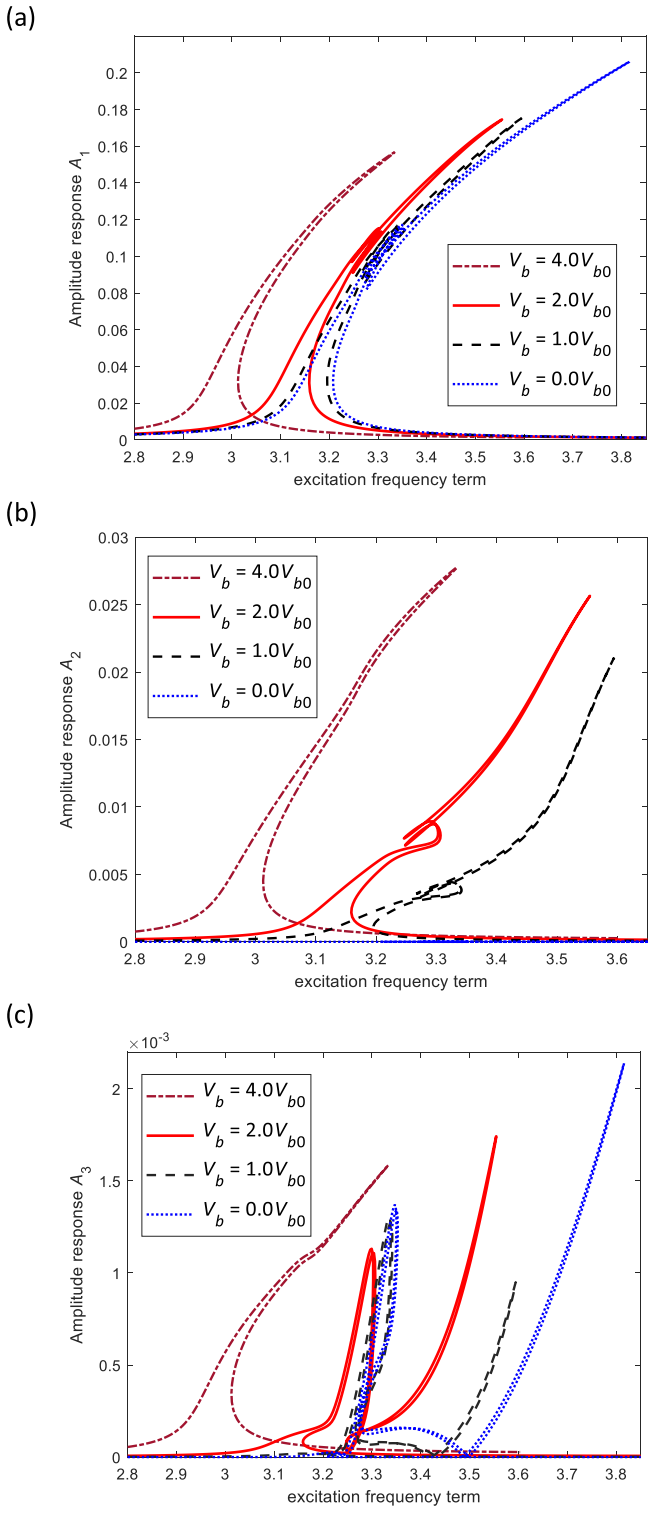

Fig. 16. Influence of the axial velocity parameter on the frequency response of perfect silicone rubber axially moving hyperelastic beam model (a) first coordinate, (b) second coordinate, and (c) third coordinate.

the system. To show the influence of this parameter on the nonlinear frequency–amplitude response, the previous properties are used and the velocity is varied as $V_b = [0, 1.0V_{b0}, 2.0V_{b0}, 4.0V_{b0}]$ by having $F = 0.1 F_0$. Fig. 16 indicates the influence of varying the axial velocity for the first three dynamic equilibrium coordinates; it can be seen that for the first dynamic equilibrium coordinate, by increasing the velocity, the nonlinear response moves to lower excitation frequencies while the maximum amplitude decrease. However, the second equilibrium coordinate shows a different behaviour; it can be seen that increasing the velocity increases the maximum amplitude of the second dynamic equilibrium coordinate which indicates more coupling between the first two modes of vibration by increasing the velocity.

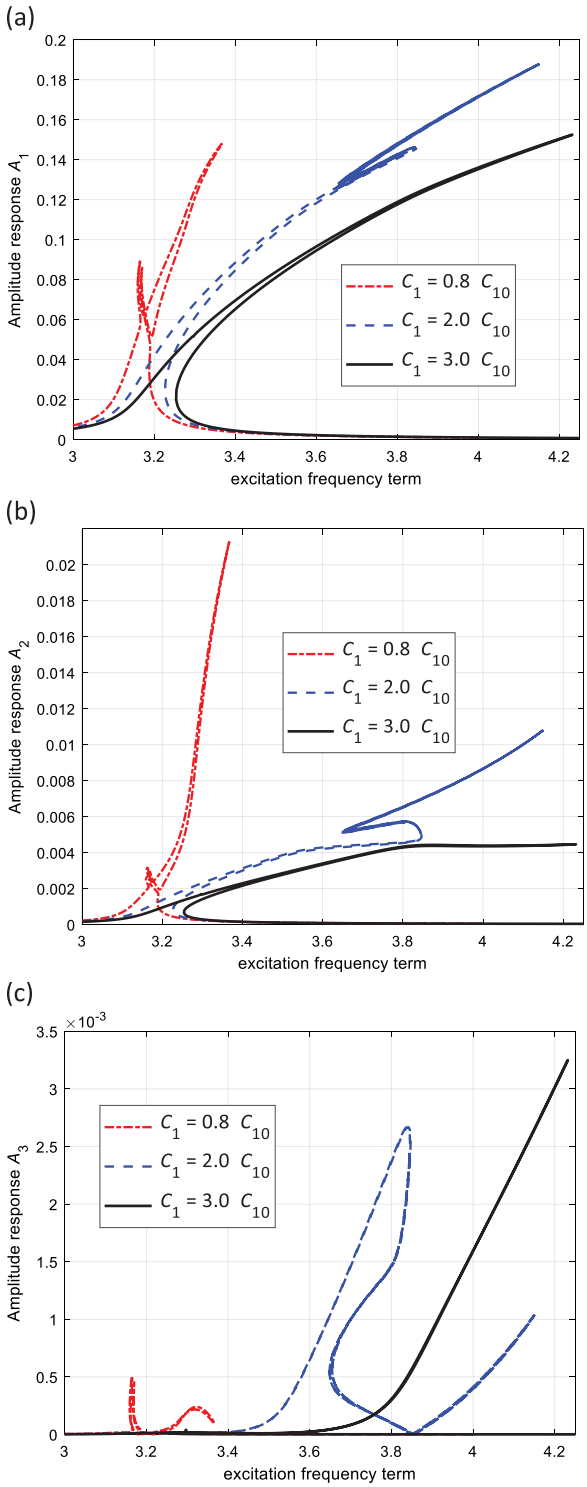

Fig. 17. Influence of the hyperelastic parameter C_1 on the frequency response of silicone rubber axially moving hyperelastic beam model (a) first coordinate, (b) second coordinate, and (c) third coordinate.

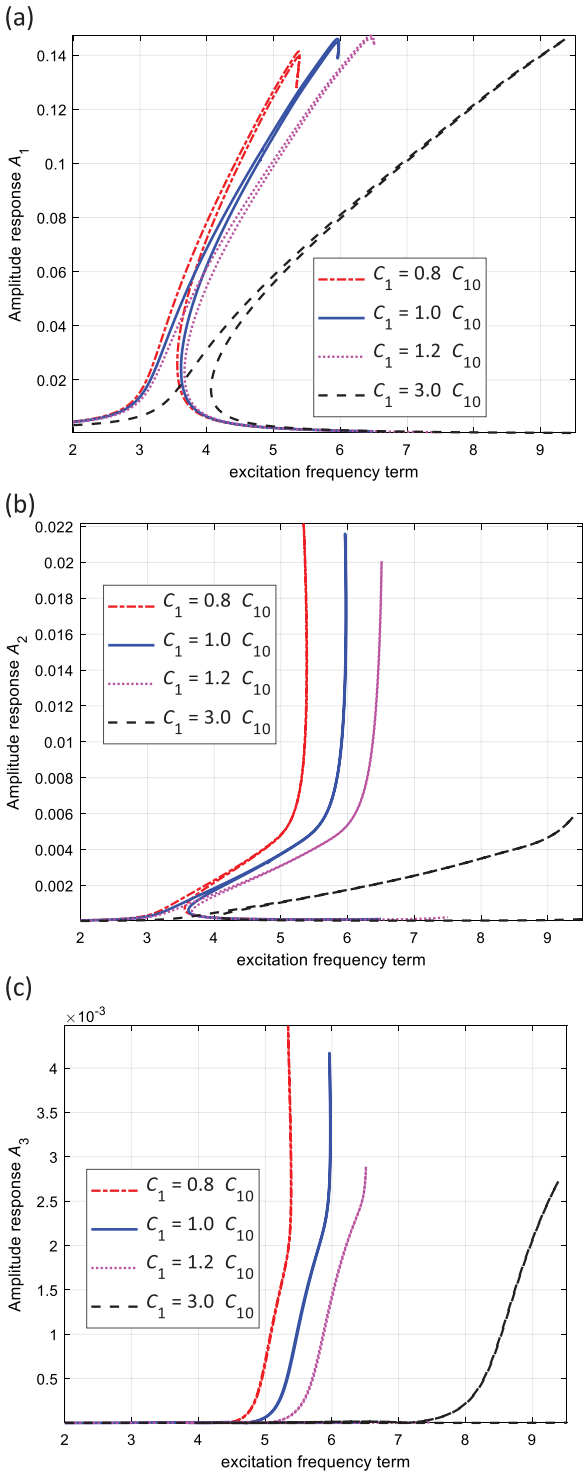

Fig. 18. Influence of the hyperelastic parameter C_1 on the frequency response of thermoplastic axially moving hyperelastic beam model (a) first coordinate, (b) second coordinate, and (c) third coordinate.

5.2.4. Influence of the hyperelasticity terms

Another important term in analysing the mechanical characteristics of the hyperelastic systems is the strain energy density terms. Therefore, in this subsection, the influence of varying hyperelastic term C_1 is discussed. For silicone-Rubber beam model, the hyperelastic strain term C_1 is varied as $C_1 = [0.8C_{10}, 2.0C_{10}, 3.0C_{10}]$ by having $F = 0.1F_0$ and the frequency–amplitude response is analysed as shown in Fig. 17. Similarly, for thermoplastic polyurethane, the first three dynamic equilibrium coordinate response are shown in Fig. 18 for $C_1 = [0.8C_{10}, 1.0C_{10}, 1.2C_{10}, 3.0C_{10}]$; it can be seen that for the thermoplastic polyurethane beam model, the maximum amplitude of the first coordinate does not change significantly while for the silicone-rubber model, this variation is noticeable. Besides, the contribution of the second generalised coordinate is less for higher strain energy density term C_1 for both models.

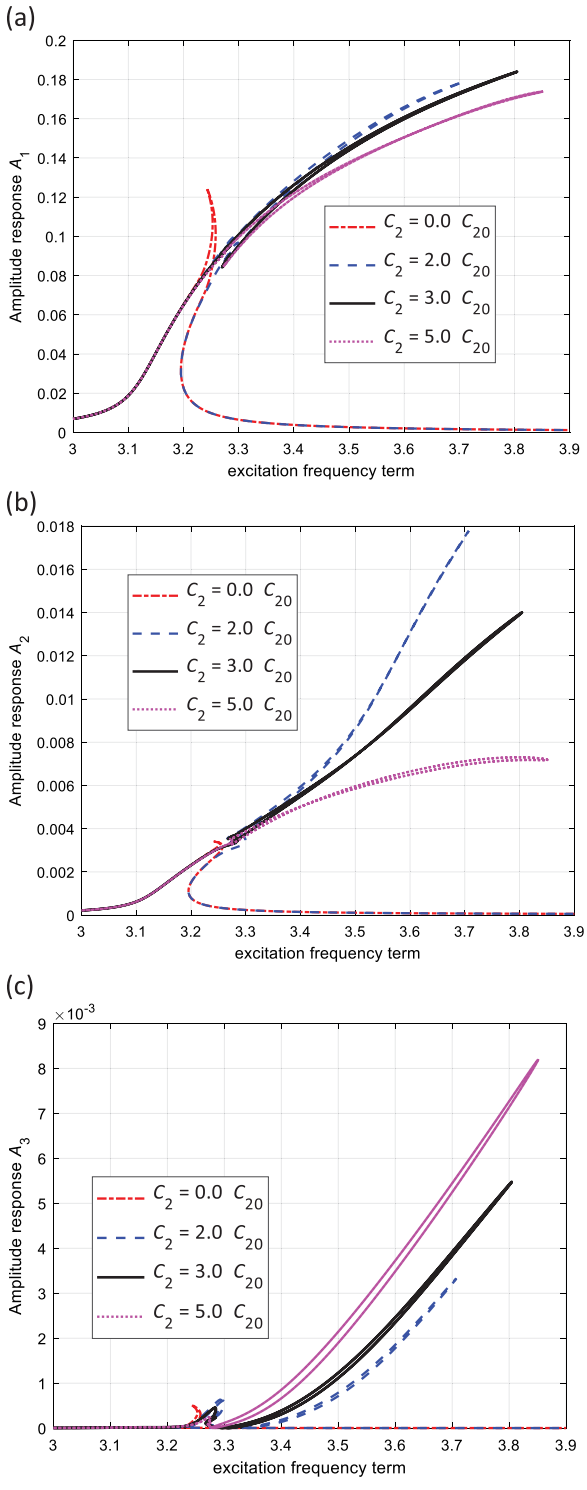

Fig. 19. Influence of the hyperelastic parameter C_2 on the frequency response of silicone rubber axially moving hyperelastic beam model (a) first coordinate, (b) second coordinate, and (c) third coordinate.

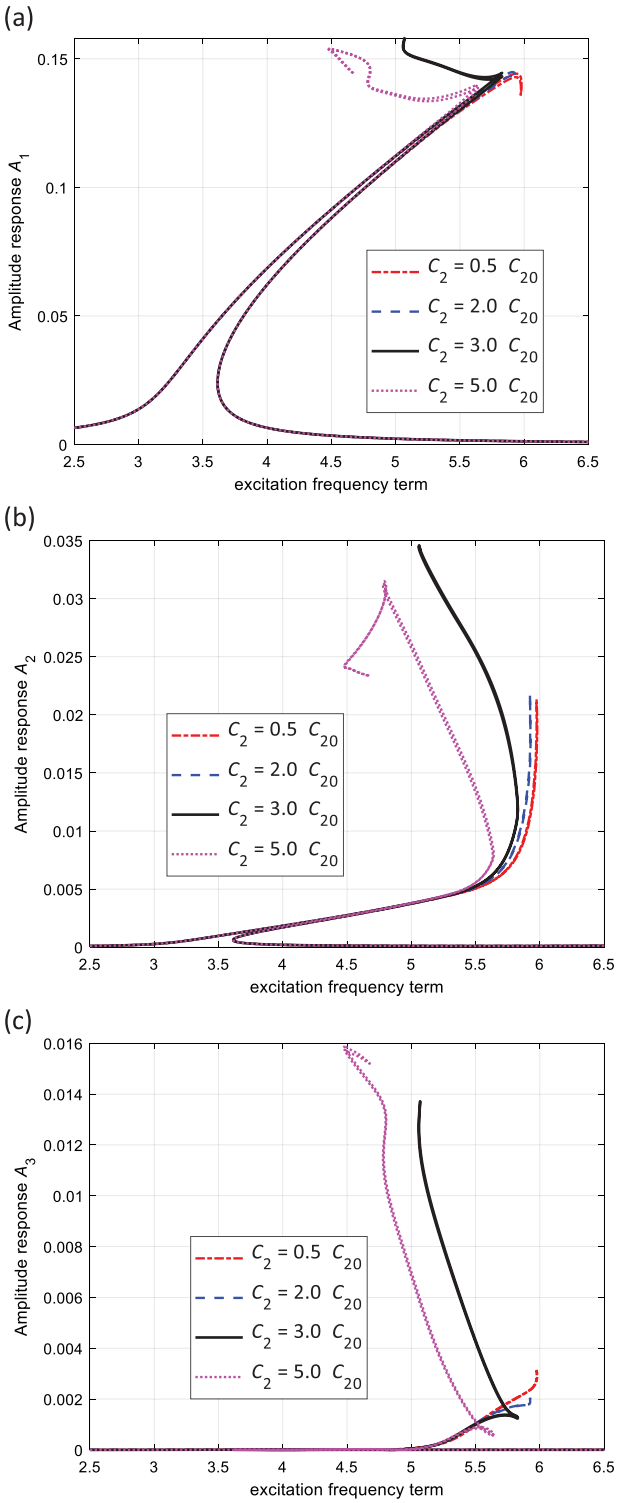

Fig. 20. Influence of the hyperelastic parameter C_2 on the frequency response of thermoplastic axially moving hyperelastic beam model (a) first coordinate, (b) second coordinate, and (c) third coordinate.

Besides, the strain energy nonlinear term C_2 plays an important role in varying the nonlinear response of the system. To this end, C_2 is varied as $C_2 = [0.0C_{20}, 2.0C_{20}, 3.0C_{20}, 5.0C_{20}]$ for silicone-rubber and $C_2 = [0.5C_{20}, 2.0C_{20}, 3.0C_{20}, 5.0C_{20}]$ for thermoplastic polyurethane beam model; from Figs. 19 and 20 can be seen that the natural frequency term does not change by varying this parameter however, it has a rich effect in varying the amplitude-response in higher amplitudes.

5.2.5. *Influence of the axial tension*

Axial tension is required for belt operating systems for properly transmitting power from one pulley to another. Therefore, in this subsection, by varying the axial tension force, the nonlinear frequency response of the axially moving beam is examined for both silicone-rubber and thermoplastic polyurethane beam models. Figs. 21–23 shows the first three dynamic equilibrium coordinates for thermoplastic

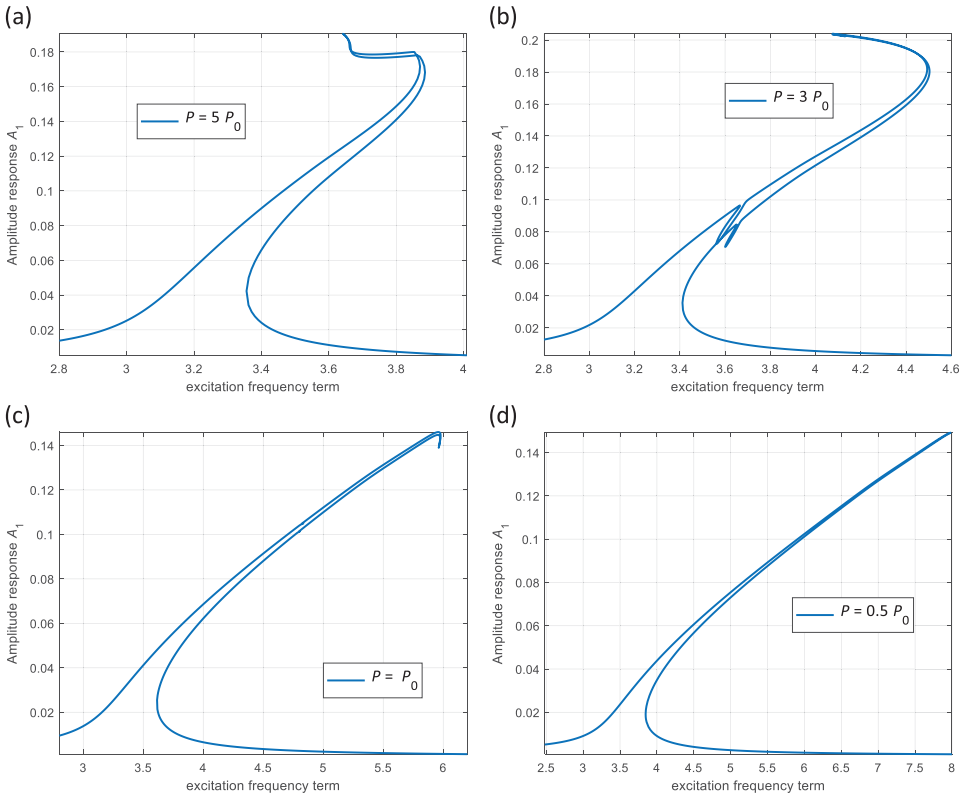

Fig. 21. Influence of the axial tension on the first dynamic coordinate frequency response of thermoplastic polyurethane axially moving hyperelastic beam model (a) $P = 5P_0$, (b) $P = 3P_0$, (c) $P = P_0$, and (d) $P = 0.5P_0$.

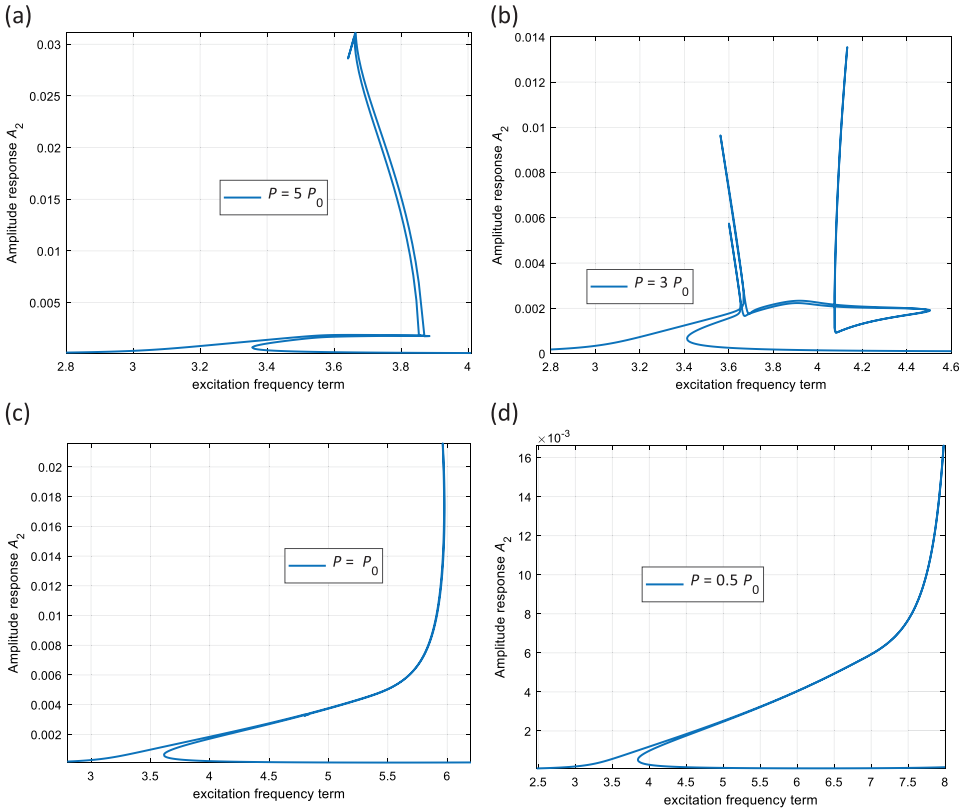

Fig. 22. Influence of the axial tension on the second dynamic coordinate frequency response of thermoplastic polyurethane axially moving hyperelastic beam model (a) $P = 5P_0$, (b) $P = 3P_0$, (c) $P = P_0$, and (d) $P = 0.5P_0$.

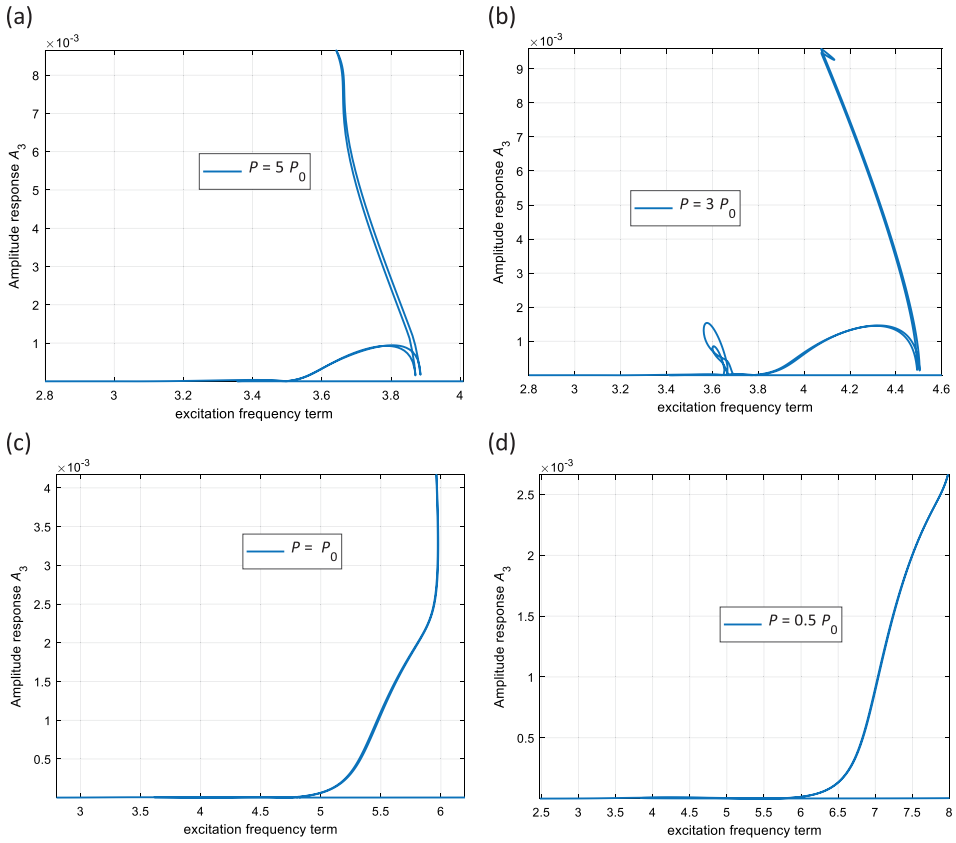

Fig. 23. Influence of the axial tension on the third dynamic coordinate frequency response of thermoplastic polyurethane axially moving hyperelastic beam model (a) $P = 5P_0$, (b) $P = 3P_0$, (c) $P = P_0$, and (d) $P = 0.5P_0$.

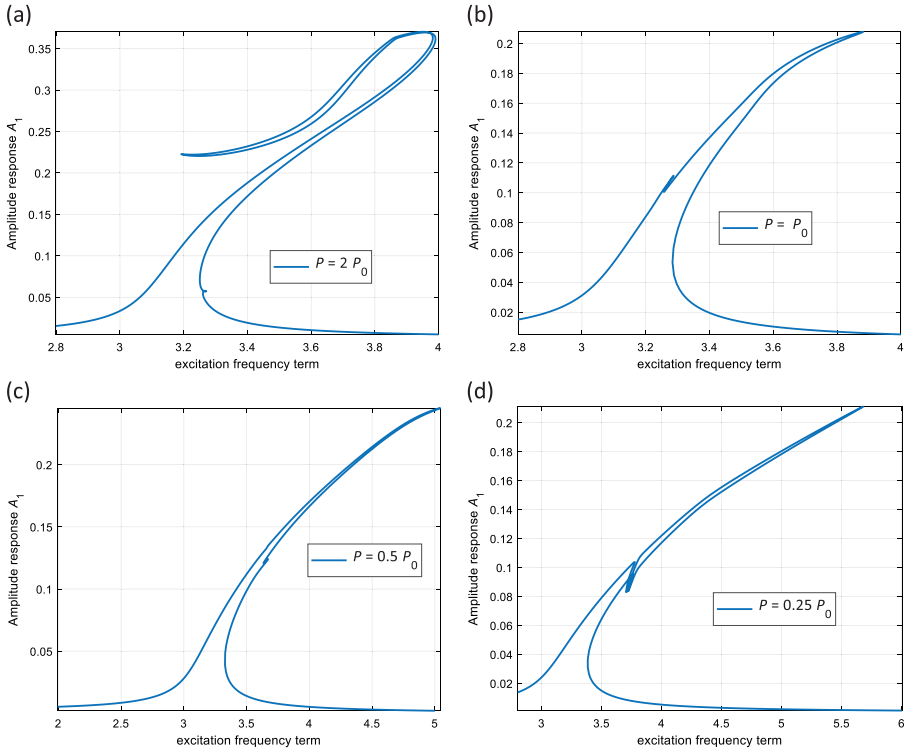

Fig. 24. Influence of the axial tension on the first dynamic coordinate frequency response of silicone rubber axially moving hyperelastic beam model (a) $P = 2P_0$, (b) $P = P_0$, (c) $P = 0.5P_0$, and (d) $P = 0.25P_0$.

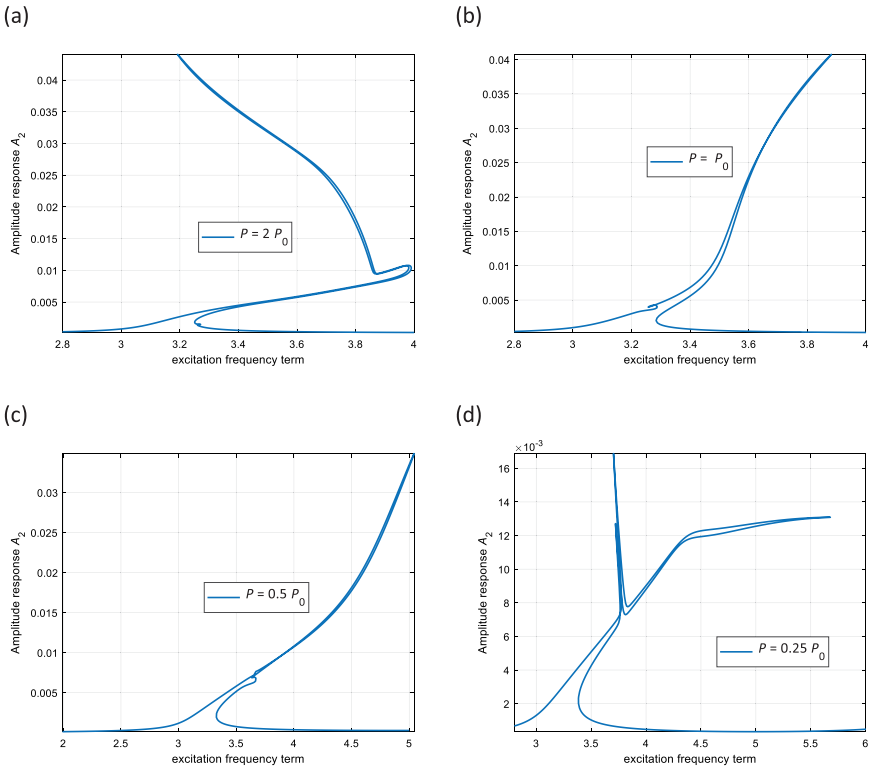

Fig. 25. Influence of the axial tension on the second dynamic coordinate frequency response of silicone rubber axially moving hyperelastic beam model (a) $P = 2P_0$, (b) $P = P_0$, (c) $P = 0.5P_0$, and (d) $P = 0.25P_0$.

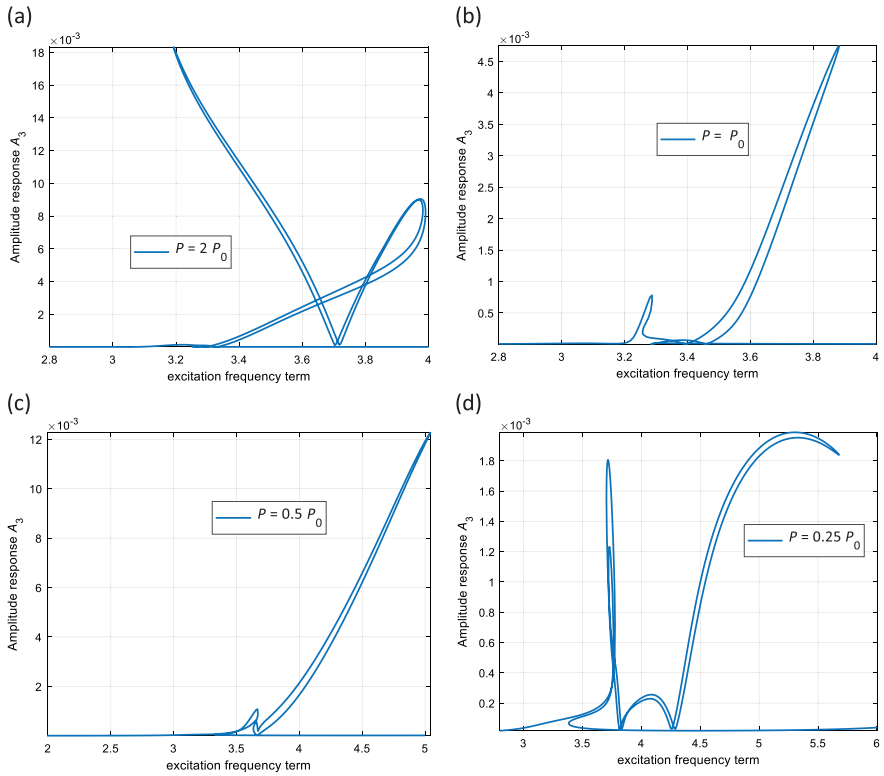

Fig. 26. Influence of the axial tension on the third dynamic coordinate frequency response of silicone rubber axially moving hyperelastic beam model (a) $P = 2P_0$, (b) $P = P_0$, (c) $P = 0.5P_0$, and (d) $P = 0.25P_0$.

polyurethane beam with $P = [0.5P_0,\ P_0,\ 3P_0,\ 5P_0]$, and Figs. 24–26 shows the first three dynamic equilibrium coordinates for silicone-rubber beam with $P = [0.25P_0,\ 0.5P_0,\ P_0,\ 2P_0]$. It can be seen that the system is highly sensitive to the variation of tension force which combination of softening and hardening behaviour is obtained for the first generalised coordinates for higher axial tensions.

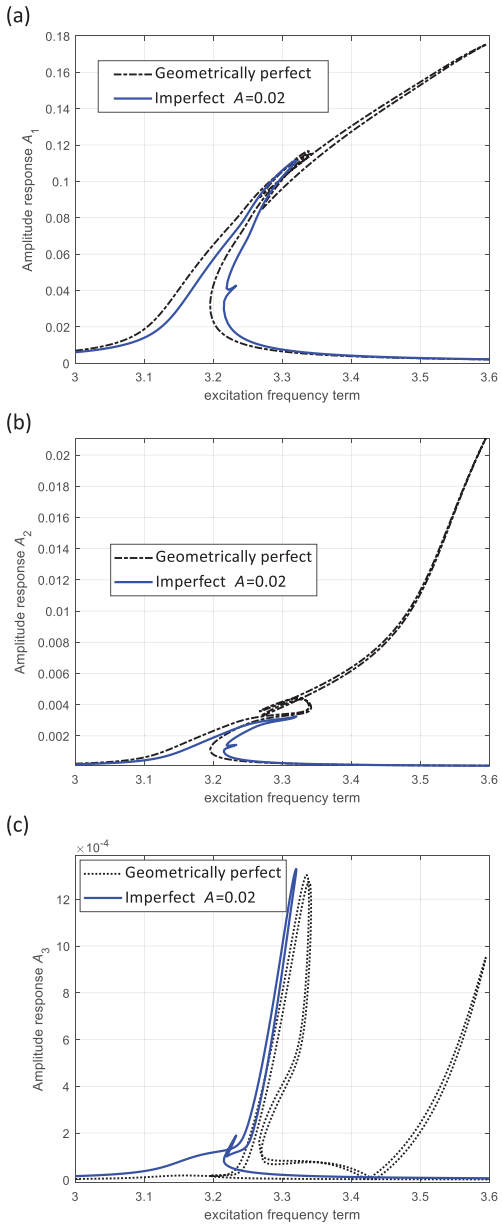

Fig. 27. Influence of the geometrical imperfection on the frequency response of silicone rubber axially moving hyperelastic beam model (a) first coordinate, (b) second coordinate, and (c) fourth coordinate.

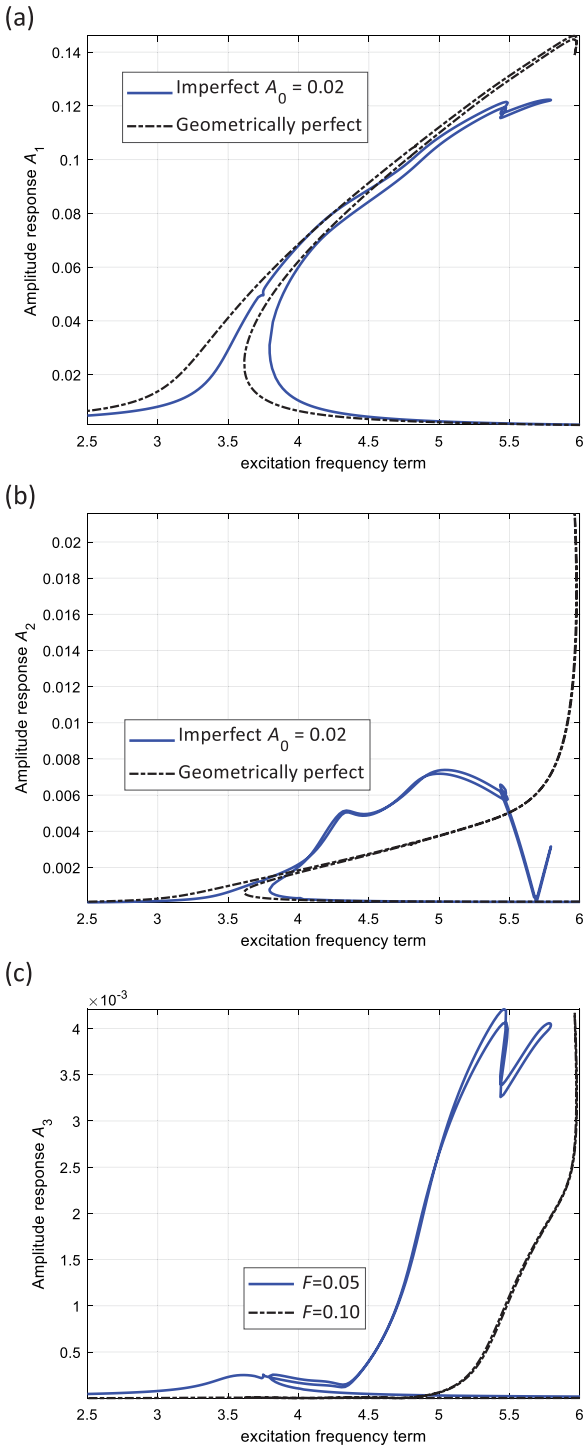

Fig. 28. Influence of the geometrical imperfection on the frequency response of thermoplastic polyurethane axially moving hyperelastic beam model (a) first coordinate, (b) second coordinate, and (c) fourth coordinate.

5.2.6. *Influence of the geometrical imperfection*

Since hyperelastic structures are soft, geometrical imperfection is a part of their physical characteristics which should be included when analysing hyperelastic structures. To show this influence, the geometrical imperfection is presented as a scale of the first mode of vibration with a constant coefficient A_0. By having $A_0 = 0.02$ and $F = 0.1F_0$, the amplitude–frequency response of the system is calculated as shown in Figs. 27 and 28 for silicone-rubber and thermoplastic polyurethane, respectively; it can be seen that the imperfection leads to lower amplitude of vibration in silicone-rubber beam and more complicated rich nonlinear vibration response for thermoplastic polyurethane beam.

6. Summary and conclusions

In this study, a comprehensive analysis on coupled nonlinear dynamics of axially moving hyperelastic beam was presented. At the first part of this paper, experimental testing was performed on rubbery structures and the mechanical stress–strain behaviour of the samples was recorded following the ASTM D638 guidance. Different hyperelastic strain energy density models were investigated and the best fitting between models and experimental data were presented. It was shown that the neo-Hookean model is incapable of properly modelling the behaviour of experimental results and Yoeh's strain energy density model presents a fair fit.

Accordingly, by having the data from the experimental analysis, the axially moving hyperelastic beam was formulated using Yeoh's

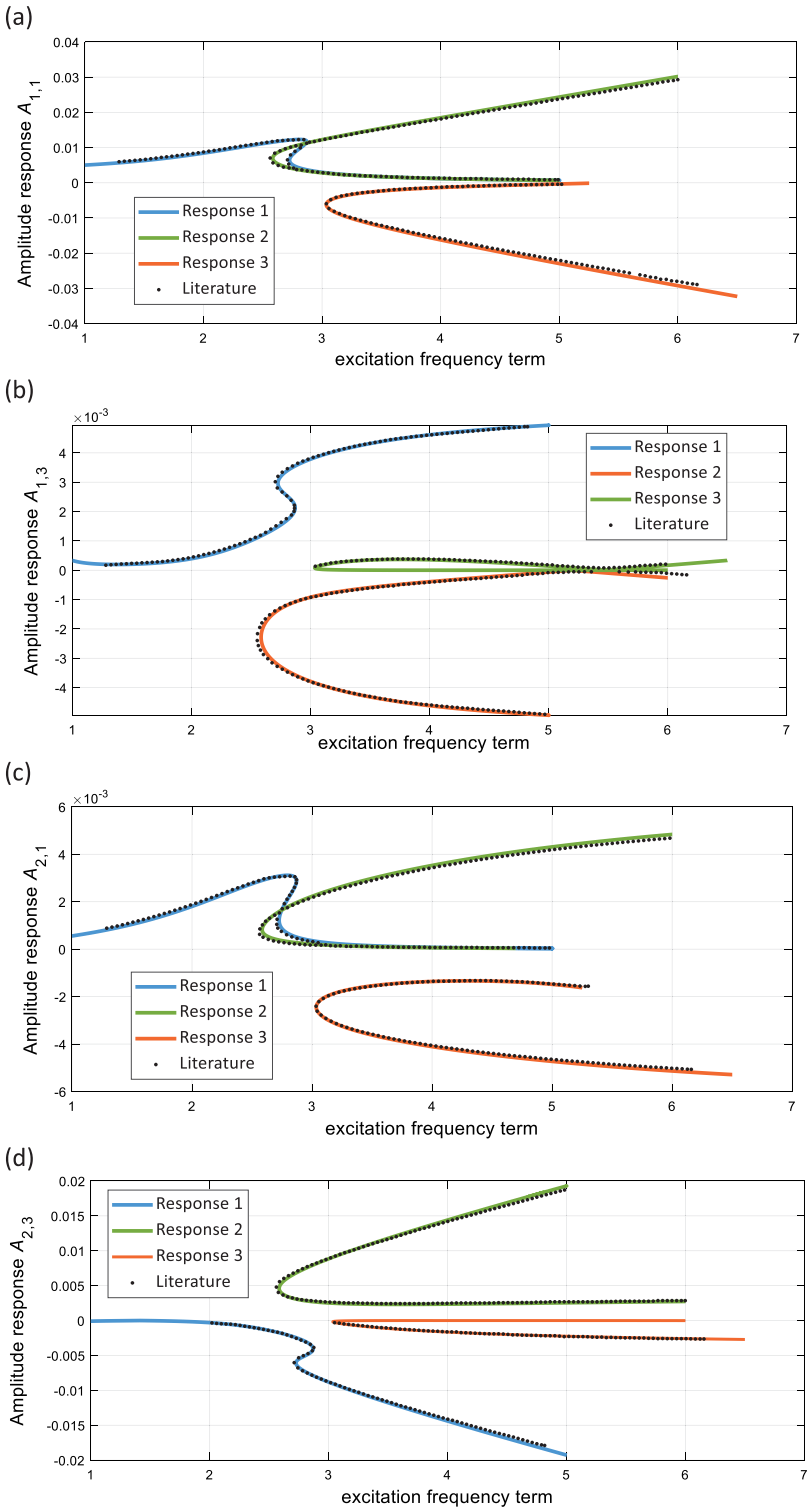

Fig. A.1. Comparison of amplitude–frequency response of an axially moving elastic beam at internal resonance with Ref. [47].

hyperelastic strain energy density model and von Kármán geometrical nonlinearity considering geometrical imperfection as well. Coupled equations of motion for the axial and transverse motions were obtained using Hamilton's principle and solved for linear and nonlinear analysis using a generalised decomposition technique, Galerkin's scheme and a dynamic equilibrium method. A comprehensive analysis on the mechanical response of the system due to the variation of different physical and geometrical properties of the beam was presented. It was shown that

- Considering higher number of Galerkin modes converges the nonlinear results and the low number of modes cannot track the internal resonance phenomena.

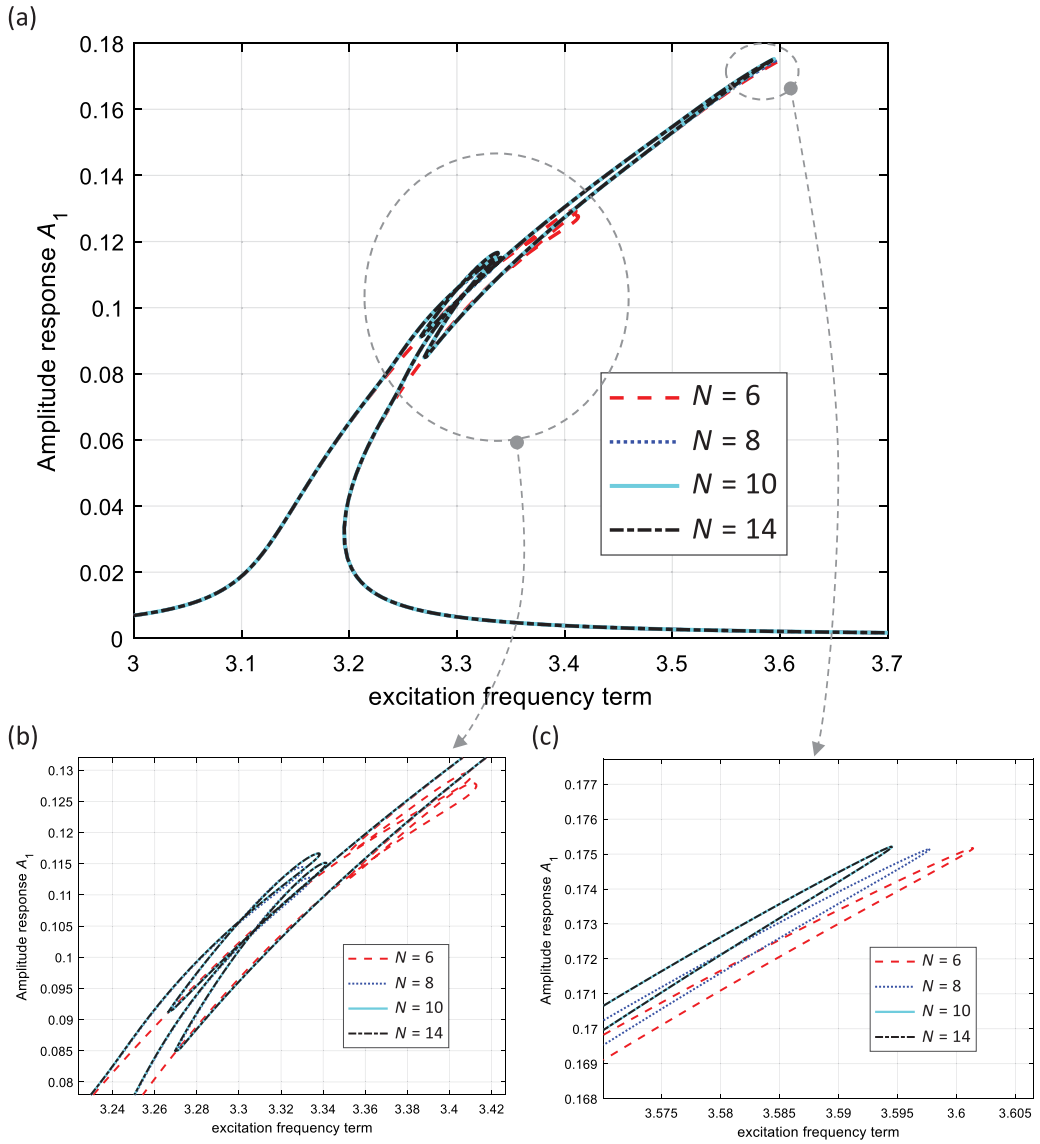

Fig. B.1. Convergence of the amplitude–frequency response of an axially moving silicone rubber beam–*first* coordinate.

- By comparing single motion and coupling motion between axial and transverse motions, it was shown that the single motion model overestimates the hardening behaviour of the beam which shows the importance of considering the coupled motion. Similarly, the imperfect beam model shows a great difference between single and coupled motion responses.
- Increasing the velocity of axially moving hyperelastic beams leads to lower nondimensional natural frequencies and sweeps the nonlinear frequency amplitude response of the system to the left side.
- The maximum amplitude of the first generalised vibration decreases while the second generalised vibration amplitude increases significantly by increasing the speed which shows more coupling between modes.
- The system shows high sensitivity to variation of the hyperelastic parameters which by increasing C_1, the linear natural frequencies increase and the nonlinear amplitude–frequency response sweeps to right side. However, the second hyperelastic term (C_2) shows no effect in varying the position of the stiffness hardening phenomena.
- Increasing the hyperelastic parameter C_1 leads to more hardening response in the system and the turning point moves to higher excitation frequencies for all the dynamic equilibrium coordinates and beam models.
- Increasing the hyperelastic parameter C_2 has a significant effect on the nonlinear vibration response by changing the peak of the stiffness hardening model to lower excitation frequencies or even stiffness softening behaviour.
- Both imaginary and real parts of the first two mode shapes are affected by the variation of the axial speed which the imaginary part shows higher sensitivity to this variation. These mode shapes are not symmetric due to the axial travelling speed.
- Linear natural frequencies show high sensitivity to geometrical designing terms, axial velocity and the hyperelastic parameter C_1.

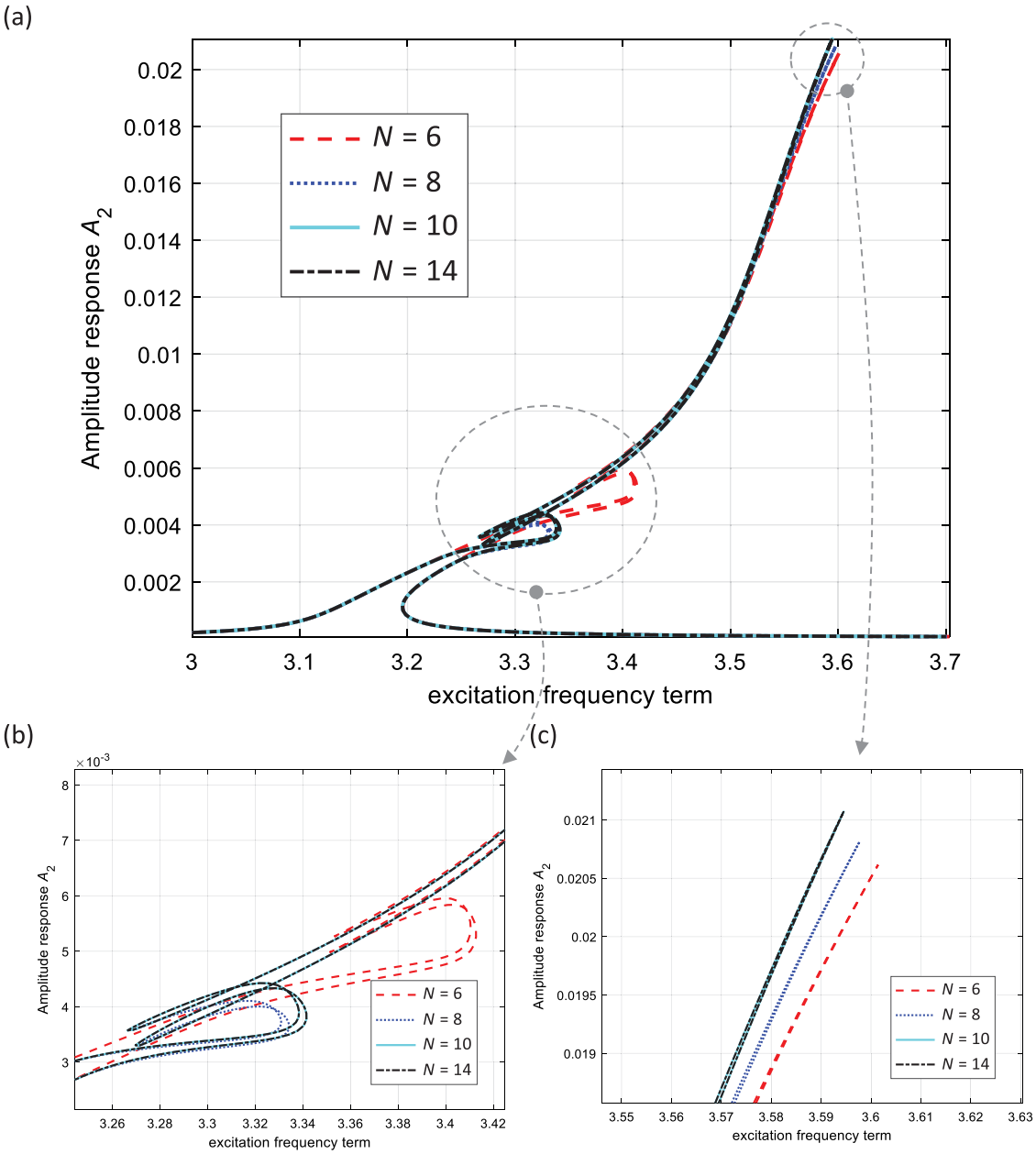

Fig. B.2. Convergence of the amplitude–frequency response of an axially moving silicone rubber beam–*second* coordinate.

- Importance of axial tension on varying the nonlinear frequency response is discussed in the study showing that increasing the axial force enriches the nonlinear frequency–amplitude response.
- Geometrical imperfection has a significant effect in increasing the coupling between modes and considering it in studying the system can increase the accuracy of the modelling.

Declaration of competing interest

The authors declare that they have no known competing financial interests or personal relationships that could have appeared to influence the work reported in this paper.

Acknowledgements

This work employed the supercomputing resources provided by the Phoenix HPC service at the University of Adelaide. The authors would like to thank the HDR scholarship support through The University of Adelaide and Faculty of Engineering, Computer & Mathematical Sciences, The University of Adelaide, Australia is also acknowledged.

Appendix A

See Fig. A.1.

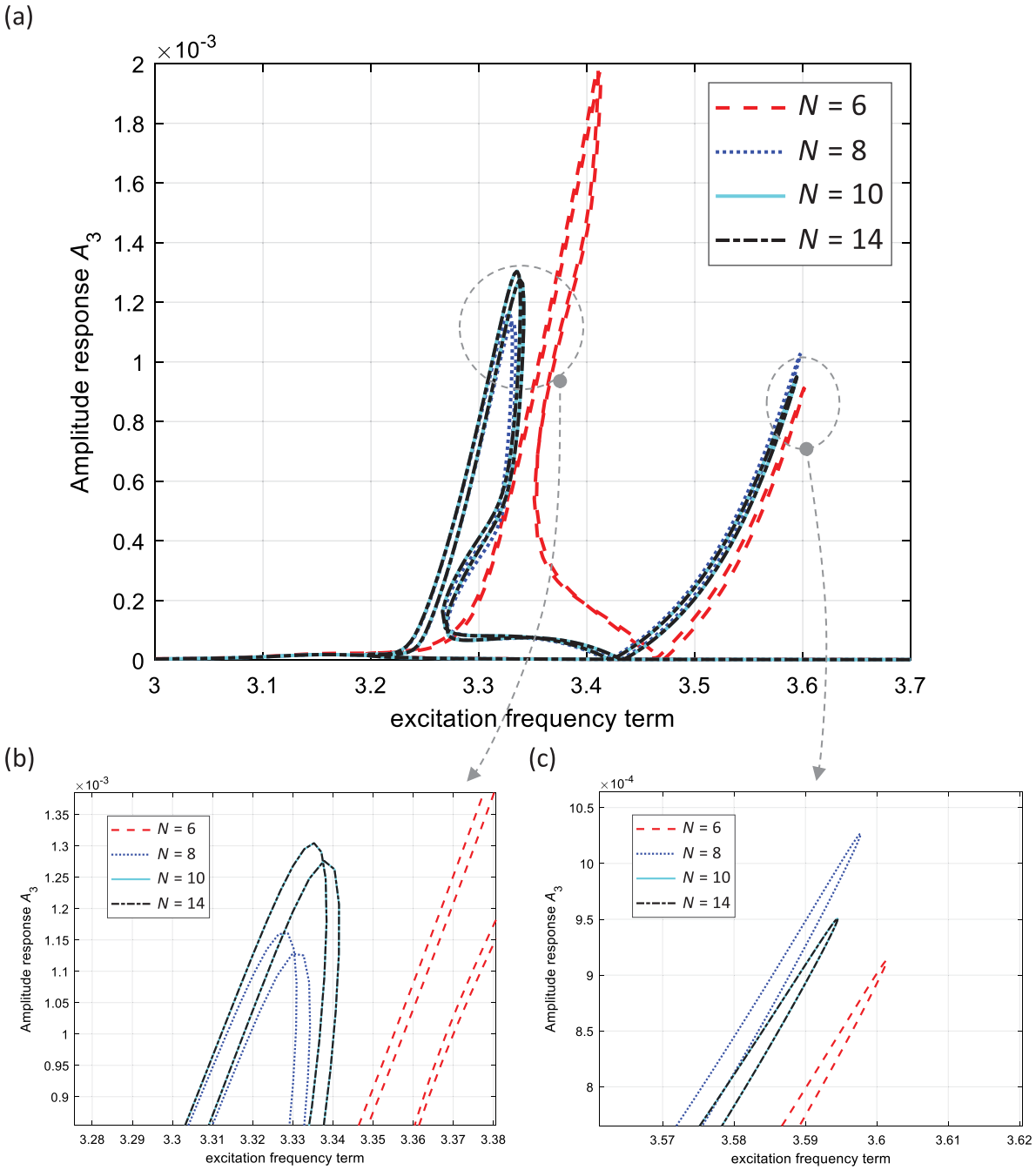

Fig. B.3. Convergence of the amplitude–frequency response of an axially moving silicone rubber beam–*third* coordinate.

Appendix B

See Figs. B.1–B.3.

References

[1] P.-T. Pham, K.-S. Hong, Dynamic models of axially moving systems: A review, Nonlinear Dynam. (2020) 1–35.

[2] D. Karličić, M. Cajić, S. Paunović, S. Adhikari, Periodic response of a nonlinear axially moving beam with a nonlinear energy sink and piezoelectric attachment, Int. J. Mech. Sci. 195 (2021) 106230.

[3] L.-Q. Chen, Y.-Q. Tang, J.W. Zu, Nonlinear transverse vibration of axially accelerating strings with exact internal resonances and longitudinally varying tensions, Nonlinear Dynam. 76 (2014) 1443–1468.

[4] Y. Li, Y. Dong, Y. Qin, H. Lv, Nonlinear forced vibration and stability of an axially moving viscoelastic sandwich beam, Int. J. Mech. Sci. 138 (2018) 131–145.

[5] L.-Q. Chen, Y.-Q. Tang, Combination and principal parametric resonances of axially accelerating viscoelastic beams: recognition of longitudinally varying tensions, J. Sound Vib. 330 (2011) 5598–5614.

[6] L.-Q. Chen, Y.-Q. Tang, C.W. Lim, Dynamic stability in parametric resonance of axially accelerating viscoelastic Timoshenko beams, J. Sound Vib. 329 (2010) 547–565.

[7] A. Mokhtari, H.R. Mirdamadi, M. Ghayour, Wavelet-based spectral finite element dynamic analysis for an axially moving Timoshenko beam, Mech. Syst. Signal Process. 92 (2017) 124–145.

[8] J. Wang, H. Shen, B. Zhang, J. Liu, Y. Zhang, Complex modal analysis of transverse free vibrations for axially moving nanobeams based on the nonlocal strain gradient theory, Physica E 101 (2018) 85–93.

[9] L.-Q. Chen, B. Wang, Stability of axially accelerating viscoelastic beams: asymptotic perturbation analysis and differential quadrature validation, Eur. J. Mech. A Solids 28 (2009) 786–791.
[10] M.H. Ghayesh, M. Amabili, H. Farokhi, Coupled global dynamics of an axially moving viscoelastic beam, Int. J. Non-Linear Mech. 51 (2013) 54–74.
[11] J.-H. Lee, Y.S. Chung, H. Rodrigue, Long shape memory alloy tendon-based soft robotic actuators and implementation as a soft gripper, Sci. Rep. 9 (2019) 1–12.
[12] H. Jia, E. Mailand, J. Zhou, Z. Huang, G. Dietler, J.M. Kolinski, X. Wang, M.S. Sakar, Universal soft robotic microgripper, Small 15 (2019) 1803870.
[13] X. Ji, X. Liu, V. Cacucciolo, M. Imboden, Y. Civet, A. El Haitami, S. Cantin, Y. Perriard, H. Shea, An autonomous untethered fast soft robotic insect driven by low-voltage dielectric elastomer actuators, Science Robotics 4 (2019).
[14] Y. Yang, Y. Zhang, Z. Kan, J. Zeng, M.Y. Wang, Hybrid jamming for bioinspired soft robotic fingers, Soft Robot. 7 (2020) 292–308.
[15] C. De Marco, C.C. Alcântara, S. Kim, F. Briatico, A. Kadioglu, G. de Bernardis, X. Chen, C. Marano, B.J. Nelson, S. Pané, Indirect 3D and 4D printing of soft robotic microstructures, Adv. Mater. Technol. 4 (2019) 1900332.
[16] S. Lu, N. Xue, W. Zhang, X. Song, W. Ma, Dynamic stability of axially moving graphene reinforced laminated composite plate under constant and varied velocities, Thin-Walled Struct. 167 (2021) 108176.
[17] S. Lotfan, M.R. Anamagh, B. Bediz, A general higher-order model for vibration analysis of axially moving doubly-curved panels/shells, Thin-Walled Struct. 164 (2021) 107813.
[18] A. Mohamadi, M. Shahgholi, F.A. Ghasemi, Nonlinear vibration of axially moving simply-supported circular cylindrical shell, Thin-Walled Struct. 156 (2020) 107026.
[19] M.T. Piovan, R. Sampaio, Vibrations of axially moving flexible beams made of functionally graded materials, Thin-Walled Struct. 46 (2008) 112–121.
[20] J. Wickert, Non-linear vibration of a traveling tensioned beam, Int. J. Non-Linear Mech. 27 (1992) 503–517.
[21] L.-Q. Chen, X.-D. Yang, Vibration and stability of an axially moving viscoelastic beam with hybrid supports, Eur. J. Mech. A Solids 25 (2006) 996–1008.
[22] F. Pellicano, F. Vestroni, Nonlinear dynamics and bifurcations of an axially moving beam, J. Vib. Acoust. 122 (2000) 21–30.
[23] H. Öz, M. Pakdemirli, H. Boyacı, Non-linear vibrations and stability of an axially moving beam with time-dependent velocity, Int. J. Non-Linear Mech. 36 (2001) 107–115.
[24] M.H. Ghayesh, H.A. Kafiabad, T. Reid, Sub-and super-critical nonlinear dynamics of a harmonically excited axially moving beam, Int. J. Solids Struct. 49 (2012) 227–243.
[25] J.-R. Chang, W.-J. Lin, C.-J. Huang, S.-T. Choi, Vibration and stability of an axially moving Rayleigh beam, Appl. Math. Model. 34 (2010) 1482–1497.
[26] W. Lin, N. Qiao, Vibration and stability of an axially moving beam immersed in fluid, Int. J. Solids Struct. 45 (2008) 1445–1457.
[27] J. Yuh, T. Young, Dynamic modeling of an axially moving beam in rotation: simulation and experiment, J. Dyn. Syst. Meas. Control (1991).
[28] J. Huang, R. Su, W. Li, S. Chen, Stability and bifurcation of an axially moving beam tuned to three-to-one internal resonances, J. Sound Vib. 330 (2011) 471–485.
[29] M.H. Ghayesh, M. Amabili, M.P. Païdoussis, Nonlinear vibrations and stability of an axially moving beam with an intermediate spring support: two-dimensional analysis, Nonlinear Dynam. 70 (2012) 335–354.
[30] K.-S. Hong, P.-T. Pham, Control of axially moving systems: a review, Int. J. Control Autom. Syst. 17 (2019) 2983–3008.
[31] W. Zhao, J. Zhang, W. Zhang, X. Yuan, Internal resonance characteristics of hyperelastic thin-walled cylindrical shells composed of Mooney–Rivlin materials, Thin-Walled Struct. 163 (2021) 107754.
[32] Y. Wang, H. Ding, L.-Q. Chen, Vibration of axially moving hyperelastic beam with finite deformation, Appl. Math. Model. 71 (2019) 269–285.
[33] Y. Wang, H. Ding, L.-Q. Chen, Nonlinear vibration of axially accelerating hyperelastic beams, Int. J. Non-Linear Mech. 99 (2018) 302–310.
[34] P. Martins, R. Natal Jorge, A. Ferreira, A comparative study of several material models for prediction of hyperelastic properties: Application to silicone-rubber and soft tissues, Strain 42 (2006) 135–147.
[35] https://www.3dprintergear.com.au/filaform-select-white-tpu-500g.
[36] C. Brown, T. Nguyen, H. Moody, R. Crawford, A. Oloyede, Assessment of common hyperelastic constitutive equations for describing normal and osteoarthritic articular cartilage, Proc. Inst. Mech. Eng. H 223 (2009) 643–652.
[37] E.M. Arruda, M.C. Boyce, A three-dimensional constitutive model for the large stretch behavior of rubber elastic materials, J. Mech. Phys. Solids 41 (1993) 389–412.
[38] A. Gent, A new constitutive relation for rubber, Rubber Chem. Technol. 69 (1996) 59–61.
[39] A. Gent, Elastic instabilities of inflated rubber shells, Rubber Chem. Technol. 72 (1999) 263–268.
[40] C.O. Horgan, The remarkable Gent constitutive model for hyperelastic materials, Int. J. Non-Linear Mech. 68 (2015) 9–16.
[41] M. Destrade, A.N. Annaidh, C.D. Coman, Bending instabilities of soft biological tissues, Int. J. Solids Struct. 46 (2009) 4322–4330.
[42] A. Goriely, M. Destrade, M. Ben Amar, Instabilities in elastomers and in soft tissues, Q. J. Mech. Appl. Math. 59 (2006) 615–630.
[43] C. Horgan, G. Saccomandi, A description of arterial wall mechanics using limiting chain extensibility constitutive models, Biomech. Model. Mechanobiol. 1 (2003) 251–266.
[44] P. Heyliger, J. Reddy, A higher order beam finite element for bending and vibration problems, J. Sound Vib. 126 (1988) 309–326.
[45] J. Bonet, R.D. Wood, Nonlinear Continuum Mechanics for Finite Element Analysis, Cambridge University Press, 1997.
[46] H. Öz, M. Pakdemirli, Vibrations of an axially moving beam with time-dependent velocity, J. Sound Vib. 227 (1999) 239–257.
[47] K. Sze, S.a. Chen, J. Huang, The incremental harmonic balance method for nonlinear vibration of axially moving beams, J. Sound Vib. 281 (2005) 611–626.
[48] Y.-Q. Tang, L.-Q. Chen, X.-D. Yang, Natural frequencies, modes and critical speeds of axially moving Timoshenko beams with different boundary conditions, Int. J. Mech. Sci. 50 (2008) 1448–1458.
[49] Y.-Q. Tang, L.-Q. Chen, X.-D. Yang, Parametric resonance of axially moving Timoshenko beams with time-dependent speed, Nonlinear Dynam. 58 (2009) 715.

Chapter 4

Porous-hyperelastic beams

Overview

Since many polymeric structures are fabricated by injection moulding and 3d-printing, this chapter focuses on comprehension of the mechanics of hyperelastic structures with the presence of porosities and voids. A set of samples with different porosities is fabricated and the effect of having different infill rates on the stress-stretch behaviour is investigated. A modified hyperelastic strain energy density model is provided in the framework of the Mooney-Rivlin model. The developed model is then used for modelling incompressible isotropic porous-hyperelastic beam structures. The porosity is assumed to be uniform or functionally-graded through the length of the structure. A detailed analysis is presented, showing the effect of porosity on changing the mechanical behaviour of the hyperelastic structure. This research study is published and available online as: Khaniki, H. B., Ghayesh, M. H., Chin, R., & Amabili, M. (2021). Large amplitude vibrations of imperfect porous-hyperelastic beams via a modified strain energy. Journal of Sound and Vibration, 513, 116416. DOI: 10.1016/j.jsv.2021.116416

Statement of Authorship

Title of Paper	Large amplitude vibrations of imperfect porous-hyperelastic beams via a modified strain energy
Publication Status	☑ Published ☐ Accepted for Publication ☐ Submitted for Publication ☐ Unpublished and Unsubmitted w ork w ritten in manuscript style
Publication Details	Khaniki, H. B., Ghayesh, M. H., Chin, R., & Amabili, M. (2021). Large amplitude vibrations of imperfect porous-hyperelastic beams via a modified strain energy. Journal of Sound and Vibration, 513, 116416.

Principal Author

Name of Principal Author (Candidate)	Hossein Bakhshi Khaniki		
Contribution to the Paper	I carried out the literature review, conceptualization, formal analysis, investigation, methodology, software, validation, visualization and wrote the manuscript.		
Overall percentage (%)	80%		
Certification:	This paper reports on original research I conducted during the period of my Higher Degree by Research candidature and is not subject to any obligations or contractual agreements with a third party that would constrain its inclusion in this thesis. I am the primary author of this paper.		
Signature		Date	2/11/2022

Co-Author Contributions

By signing the Statement of Authorship, each author certifies that:

i. the candidate's stated contribution to the publication is accurate (as detailed above);

ii. permission is granted for the candidate in include the publication in the thesis; and

iii. the sum of all co-author contributions is equal to 100% less the candidate's stated contribution.

Name of Co-Author	Mergen Ghayesh		
Contribution to the Paper	As the principal supervisor, I helped to construct the manuscript, edit and review the manuscript for submission. I assisted in the conceptualization, investigation, methodology, review and editing. I hereby give consent to Hossein Bakhshi Khaniki to present this paper for examination towards the degree of Doctor of Philosophy.		
Signature		Date	3/11/2022

Name of Co-Author	Rey Chin		
Contribution to the Paper	I assisted in review and editing of the manuscript. I hereby give consent to Hossein Bakhshi Khaniki to present this paper for examination towards the degree of Doctor of Philosophy.		
Signature		Date	3/11/2022

Name of Co-Author	Marco Amabili		
Contribution to the Paper	I assisted in the conceptualization, investigation, review and editing of the manuscript. I hereby give consent to Hossein Bakhshi Khaniki to present this paper for examination towards the degree of Doctor of Philosophy.		
Signature		Date	7/11/2022

Journal of Sound and Vibration 513 (2021) 116416

Contents lists available at ScienceDirect

Journal of Sound and Vibration

journal homepage: www.elsevier.com/locate/jsvi

Large amplitude vibrations of imperfect porous-hyperelastic beams via a modified strain energy

Hossein B. Khaniki [a,*], Mergen H. Ghayesh [a,*], Rey Chin [a], Marco Amabili [b]

[a] School of Mechanical Engineering, University of Adelaide, South Australia 5005, Australia
[b] Department of Mechanical Engineering, McGill University, 817 Sherbrooke Street West, Montreal, Canada

ARTICLE INFO

Keywords:
Hyperelastic
Porosity
Porous beam
Nonlinear vibration
Nonlinear dynamics
Hyperelastic beams

ABSTRACT

In this paper, the porous-hyperelastic properties of soft materials are obtained experimentally and a general model for a combination of porosity (of functional type) and hyperelasticity using the Mooney-Rivlin strain energy density is obtained. Porous-hyperelastic samples are fabricated using thermoplastics with different porosities by varying the infill rate of 3D-printing. Following the available standards, the stress-strain behaviour for different samples are obtained and a general model for hyperelastic closed-cell porosity is presented. After obtaining model's characteristics from the experimental testings, a general beam formulation is presented for hyperelastic beams with functional porosity through the length. Both the axial and transverse motions are considered in the model of hyperelastic beams in the framework of the Mooney-Rivlin material model and Hamilton's principle. A geometrical imperfection of the beam is also considered in the formulation. The nonlinear forced vibrations of the imperfect porous-hyperelastic beam are studied by simultaneously solving the axial and transverse nonlinear coupled equations using a dynamic equilibrium technique. It is shown that having a uniform and functional porosity has a significant effect in changing the nonlinear frequency response of the system. Geometrical imperfection leads to a significant coupling between the axial and transverse coordinates when the porosity varies functionally through the length which shows the importance of considering both motions while analysing such structures. The results are useful for better understanding the effects of imperfections in studying the mechanics of soft structures and can be useful in designing soft robotics and artificial organs.

1. Introduction

Voids and porosities are the commonly known production defects of many available structural components [1–4]. These types of imperfection happen during the fabrication process or intentionally added to a component based on the application and requirement of the design [5–7]. For soft structures made of thermoplastics, elastomers or silicone-rubbers, the fabrication procedure (e.g. 3D-printing and injection moulding [8]) can cause porous/perforated soft structures.

Since the mechanical properties of porous structures are affected by the porosity type [9] (e.g. closed-cell or open-cell), volume fraction and distribution through the structure (e.g. uniformly or functionally), researchers have analysed these effects in different mechanical conditions in the framework of *linear elasticity*. Due to the possibility to vary the porosity through a direction [10,11],

* Corresponding authors.
E-mail addresses: hossein.bakhshikhaniki@adelaide.edu (H.B. Khaniki), mergen.ghayesh@adelaide.edu.au (M.H. Ghayesh).

https://doi.org/10.1016/j.jsv.2021.116416
Received 9 June 2021; Received in revised form 8 August 2021; Accepted 23 August 2021
Available online 24 August 2021

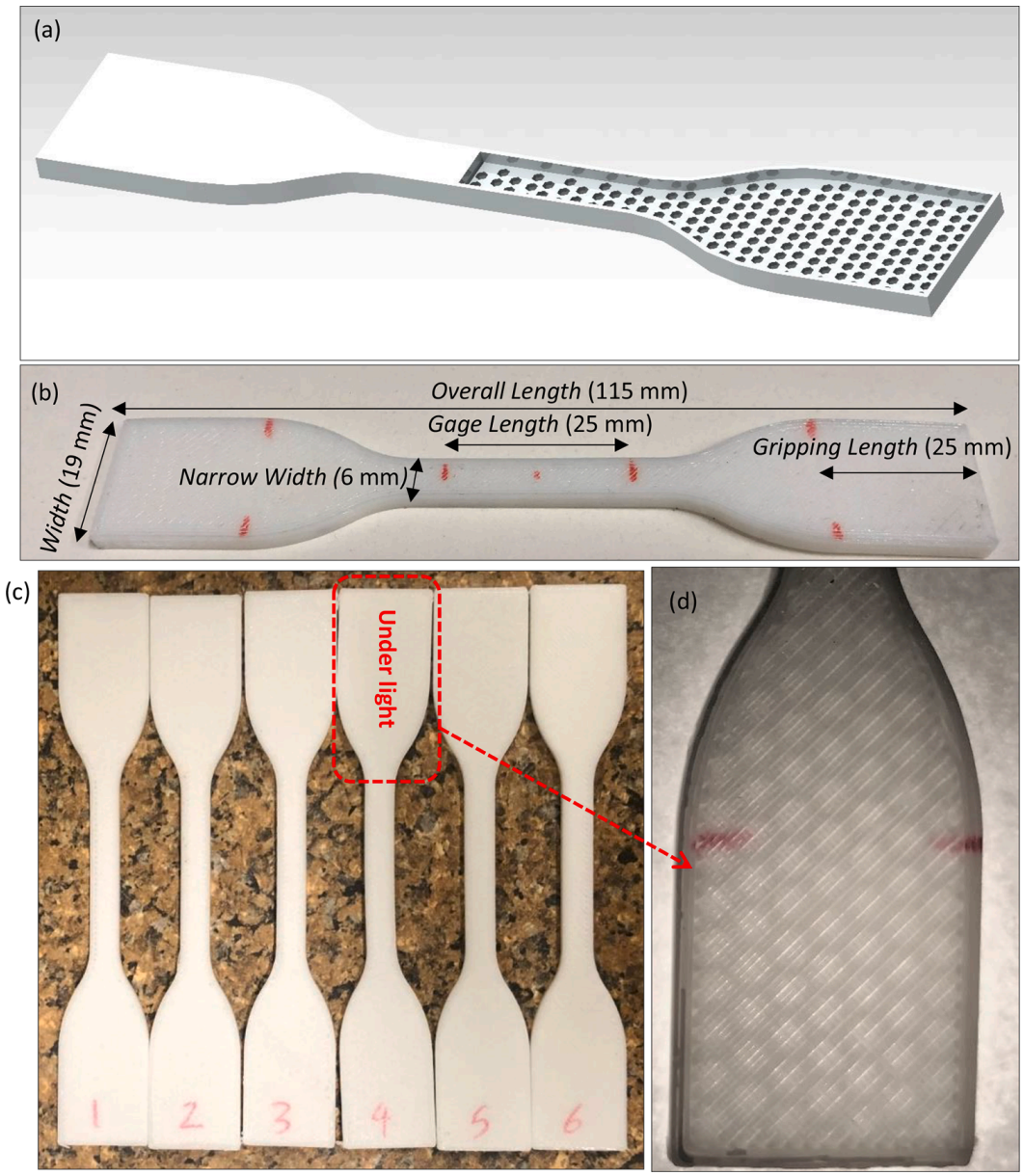

Fig. 1. Sample preparation for porosity-hyperelasticity testing (a) schematic representation of closed-cell porous dumbbells (b) dimensions following standards (c) fabricated porous-hyperelastic samples (d) closed-cell hexagonal porosity in samples.

functionally porous elastic beams have been examined by many researchers. Chen et al. [12] investigated the static deformation and buckling of functionally porous elastic beams for open-cell metal foam beams. Porosity was varied in the thickness direction of the beam following symmetrical and unsymmetrical models; it was shown that by increasing the porosity of the structure, the critical buckling decreases while the maximum deflection increases. Jena et al. [13] examined beams made of functionally graded materials with uniform porosity through the thickness and analysed the linear vibration behaviour; using the Navier's technique and Rayleigh-Ritz method, it was shown that considering the uniform porosity causes lower natural frequencies for power-law functional beam models.

Beams strengthened with fibres also possess different types of porosities between the matrix and fibres. This importance has been investigated by Kitipornchai et al. [14] and Chen et al. [15] for graphene strengthened structures; it was shown that the porosity and its distribution in the beam structure can significantly change the mechanical behaviour and stiffness of the structures emphasizing on the importance of considering this effect for such structures. Akbaş [16] studied the influence of having even and uneven CNT distribution models on the forced vibration response of simply-supported beams. The linear elastic structure was assumed with material variation through the thickness; it was shown that by choosing a proper material distribution in the structure, the unpleasant effects of having porosity can be decreased.

On the other hand, since *soft* structures made of plastics, rubbers and elastomers go through large nonlinear strains in their elastic region, the conventional linear elastic continuum mechanic models fail to predict their behaviour accurately and a proper hyperelastic

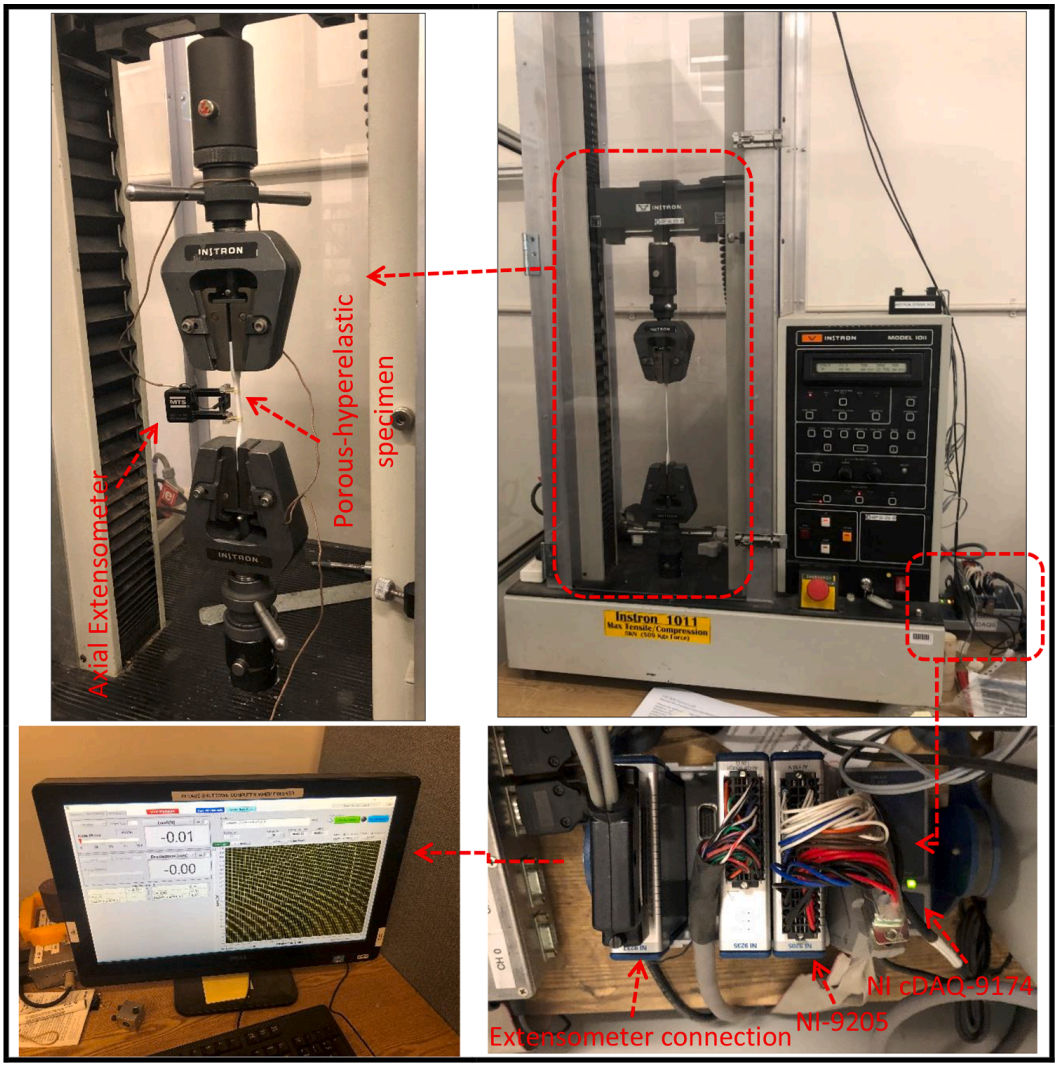

Fig. 2. Tensile test on the fabricated porous-hyperelastic samples using Instron testing machine.

formulation and definition is required. Soft structures without porosity and geometry imperfection have been examined in the past few years due to the increasing demand for their application in soft robotics [17,18], surgical tools [19,20], artificial organs and implants [21–23]. The nonlinear mechanics of hyperelastic plate [24–26] and shell [27,28] structures have been examined using Ogden and neo-Hookean strain energy density models; it was shown that the hyperelastic-model predictions match with the experimental results.

However, the importance of having voids and porosities in soft structures have not been examined yet. Since most of the soft structures are fabricated by moulding and printing, it is important to comprehend the influence of this imperfection on their mechanical behaviour. Besides, since soft structures undergo large strains while facing different types of loading, the geometrical imperfection also plays a key role in accurately defining the initial condition of the beam.

To reach this understanding, this paper deeply investigates the nonlinear mechanics of imperfect porous-hyperelastic soft beams by the means of continuum mechanics and experimental testing which is structured as follows. In Section 2, the porosity and hyperelastic properties of thermal polyurethane (TPU) samples made by 3D-printing are investigated using experimental testing and a proper porous-hyperelastic model is presented based on the Mooney-Rivlin strain energy density model with porosity dependent coefficients. In Section 3, the coupled nonlinear dynamics of porous-hyperelastic beams is presented by considering a geometrical imperfection and the possibility of porosity variation through the length of the beam. The coupled highly nonlinear equations of motion are solved in Section 4 by employing a dynamic equilibrium technique and Galerkin's scheme. In Section 5, the nonlinear forced vibration response of the structure is presented in detailed subsections and the influence of the uniform/functional porosity, hyperelastic material parameters, geometrical imperfection and the external load on the nonlinear dynamic behaviour is discussed. Section 6 presents the conclusion and highlights the outcomes of this study.

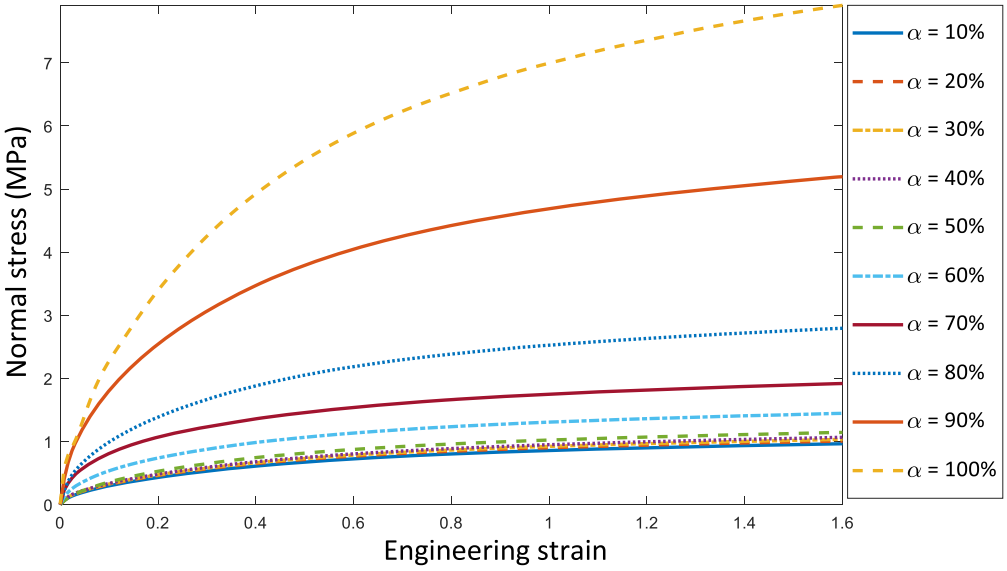

Fig. 3. Average stress-strain behaviour of porous-hyperelastic samples for different infill rates based on the experimental results.

Table 1
Porous-hyperelastic and mas density coefficients for experimental samples with different infills with $C_1^{perfect} = 2.463e5$ Pa, $C_2^{perfect} = 3.512e6$ Pa and $\rho^{perfect} = 1152.5$ kg/m^3.

Model	Infill	$\rho^{porous}/\rho^{perfect}$	$C_1^{porous}/C_1^{perfect}$	$C_2^{porous}/C_2^{perfect}$	*R*-Square
1	10%	0.5981	0.0180	0.1381	0.9908
2	20%	0.6269	0.0316	0.1434	0.9894
3	30%	0.6558	0.0439	0.1452	0.9892
4	40%	0.6808	0.0589	0.1474	0.989
5	50%	0.7173	0.0814	0.1558	0.9998
6	60%	0.7327	0.0989	0.1995	0.9992
7	70%	0.7654	0.1198	0.2721	0.9973
8	80%	0.8173	0.1484	0.3833	0.9964
9	90%	0.8980	0.5416	0.6936	0.9711
10	100%	1.0000	1.0000	1.0000	0.9999

2. Experimental characterisation of the porous-hyperelastic material

Hyperelastic structures show nonlinear behaviour in their stress-strain diagram making the linear classic models inaccurate for defining their stiffness properties. In order to obtain the hyperelasticity properties of a soft structure, one should obtain the stress-strain behaviour following the related standards for hyperelastic structures. This study follows the ASTM-D638 standard by fabricating dumbbell samples using a 3D-printer for thermal polyurethane. Different types of hexagonal infill rates are considered in manufacturing the samples indicating closed-cell porosity in the structure (Fig. 1). Each sample is considered to be isotropic, due to a uniform distribution of the porosity through the sample.

For each porosity model (with infill rate varying from 10 to 100%), five thermal polyurethane dumbbell samples are manufactured and tested following ASTM-D638 recommendations and using an Instron 1011 testing machine (Fig. 2). The connection between the Instron machine and the computer is done using a Compact-DAQ USB chassis (NI cDAQ-9174) which is suitable for portable sensor measurement systems (Fig. 2); the data acquisition for force/deformation is done using a 16-Bit 32-Channel DAQ system (NI-9205) which is the left slot on the chassis in Fig. 2 and an MTS axial extensometer is connected to the chassis at the right slot (Fig. 2). For each infill rate, the experiment is repeated five times with the speed of 50 mm/min and 200 samples per second. After performing the tests, the stress-strain behaviour is recorded and the results are presented in Fig. 3 for different infill rates (porosities); it can be seen that increasing the infill rate from 10 to 100% (decreasing the porosity rate from 90 to 0%) increases the stiffness, nonlinearly and the most sensitivity is seen when the infill rate is high.

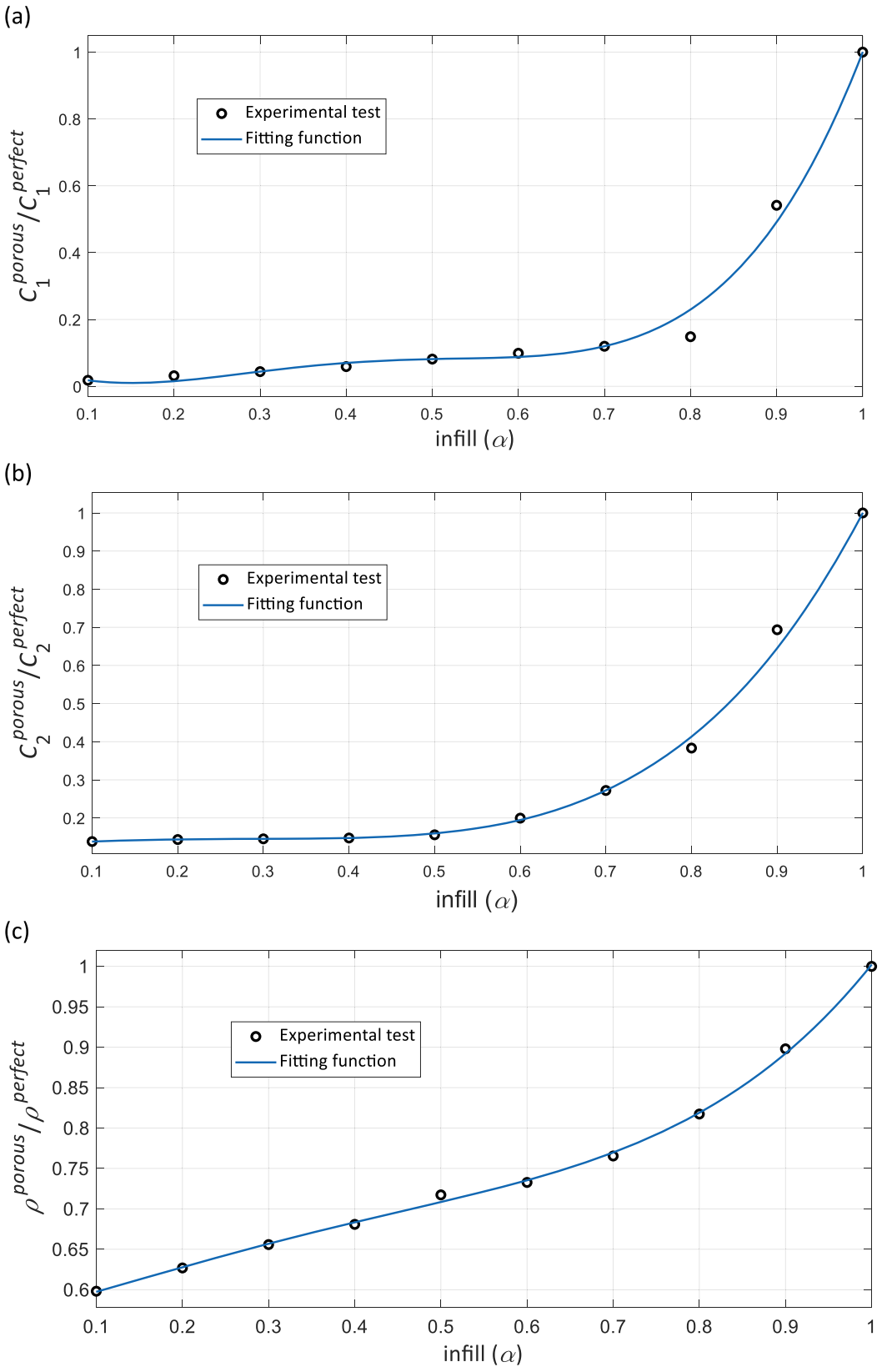

Fig. 4. Fitting the experimental results with the theoretical modelling (a) C_1 ratio, (b) C_2 ratio and (c) mass density ratio.

Table 2
Porous-hyperelastic and mas density coefficients for curve fitting with experimental results.

i	Coefficient	a_{i1}	a_{i2}	a_{i3}	a_{i4}	a_{i5}	R-Square
1	$C_1^{porous}/\ C_1^{perfect}$	8.93625	-14.51887	8.03085	-1.55217	0.10649	0.9892
2	$C_2^{porous}/\ C_2^{perfect}$	1.85051	-1.05951	-0.03058	0.11153	0.12813	0.9973
3	$\rho^{porous}/\rho^{perfect}$	0.89110	-1.06203	0.34160	0.26299	0.56859	0.9989

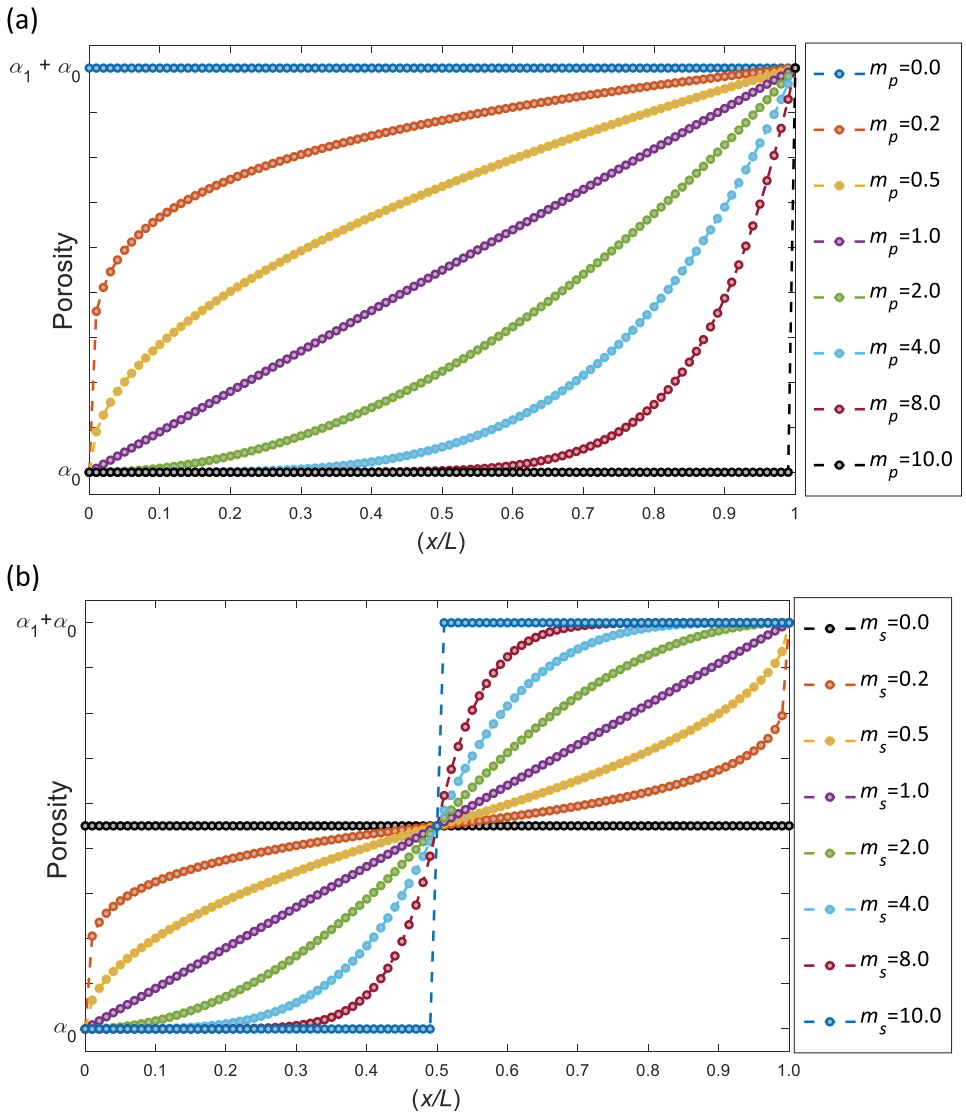

Fig. 5. Porosity variation through the length of the beam for different (a) power-law and (b) sigmoid parameters using the variation formulation given in Eq. (10).

By having the nonlinear stress-strain behaviour of such structures, the Mooney-Rivlin strain energy density model, which have shown good accuracy in modelling isotropic soft materials structure [29], is employed to model the stress-strain behaviour.

The strain energy density of the Mooney-Rivlin hyperelastic model is a function of the strain tensor invariants as [29]

$$W_{MR} = C_1(I_1 - 3) + C_2(I_2 - 3) + \frac{\kappa}{2}(J-1)^2, \tag{1}$$

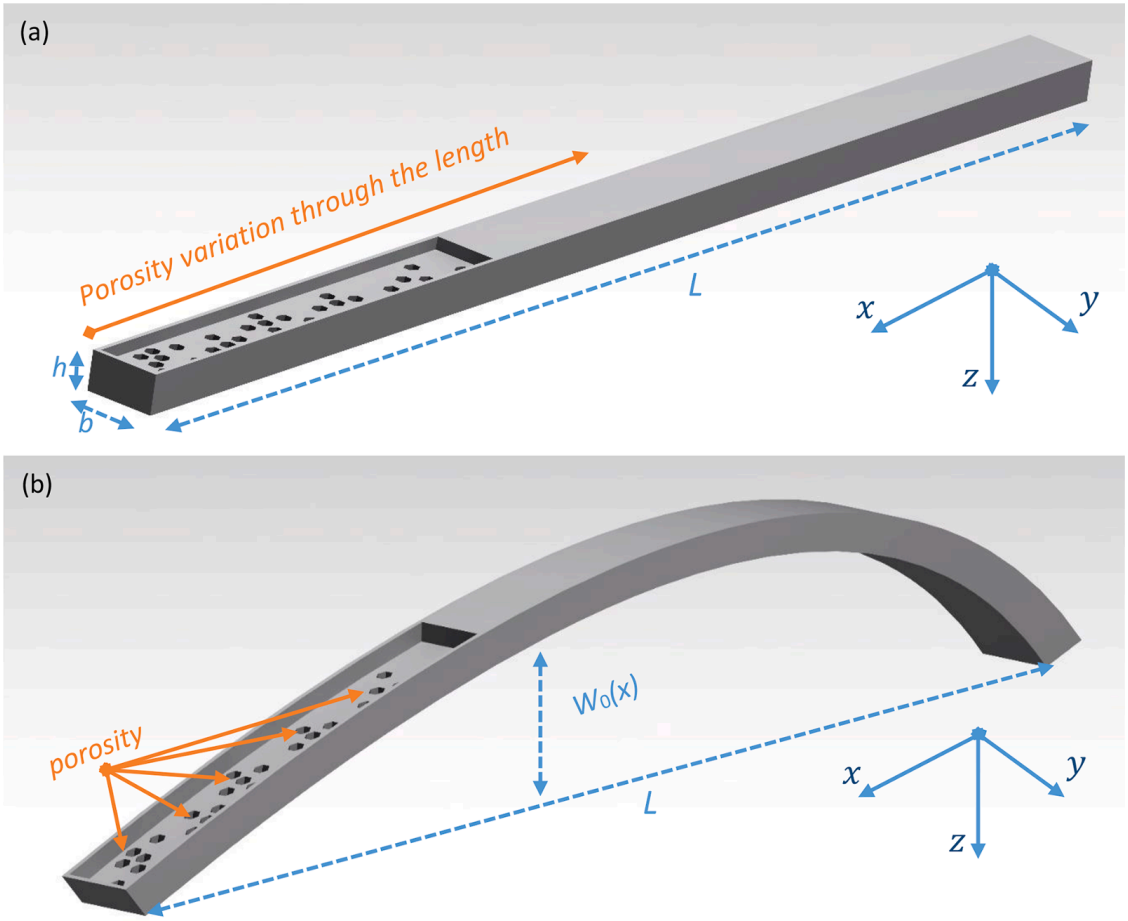

Fig. 6. Schematic representation of closed-cell porous-hyperelastic beam (with a cut section to show the porosity) (a) geometrical perfect and (b) geometrical imperfect.

where C_1, C_2 and κ are the hyperelastic coefficients that should be identified experimentally and I_1, I_2 and J are strain invariants. For an incompressible material, $J = 1$ [28]. The stress invariants are written as

$$I_1 = \lambda_1^2 + \lambda_2^2 + \lambda_3^2, \tag{2}$$

$$I_2 = \lambda_1^2\lambda_2^2 + \lambda_1^2\lambda_3^2 + \lambda_2^2\lambda_3^2, \tag{3}$$

where λ_i (with $i = 1$, 2, and 3) is the stretch of the structure in the ith principal direction. By performing a curve fitting with the experimental testing, the Mooney-Rivlin hyperelastic coefficients for each infill is obtained, as shown in Table 1. Fitting is performed using the R-square correlation technique which is defined as [30]

$$R^2 = 1 - \frac{T_{ss}}{R_{ss}}, \tag{4}$$

where T_{ss} and R_{ss} are the total and residual sum of squares, respectively, defined as

$$T_{ss} = \sum_i w_i (y_i - f_i)^2, \tag{5}$$

$$R_{ss} = \sum_i w_i (y_i - \bar{y})^2, \quad \bar{y} = \frac{1}{n}\sum_{i=1}^{n} y_i, \tag{6}$$

where y_i and f_i denote the values marked and fitted, respectively; w_i is the applied weight for each data (usually assumed as 1) and $\bar{y}$ is the mean marked data; it can be seen that the fitting result shows a great correlation (Table 1). Fitting results are shown in Appendix A for the sake of brevity.

To have a general formulation for porous-hyperelastic structures, the hyperelastic coefficients (C_1 and C_2) and mass density (ρ) are defined as a function of porosity with respect to the material properties when there is no porosity (perfect), each parameter is presented as a polynomial function of infill rate as

$$\frac{C_1^{porous}(x)}{C_1^{perfect}} = a_{11}\alpha^4(x) + a_{12}\alpha^3(x) + a_{13}\alpha^2(x) + a_{14}\alpha(x) + a_{15}, \tag{7}$$

$$\frac{C_2^{porous}(x)}{C_2^{perfect}} = a_{21}\alpha^4(x) + a_{22}\alpha^3(x) + a_{23}\alpha^2(x) + a_{24}\alpha(x) + a_{25}, \tag{8}$$

$$\frac{\rho^{porous}(x)}{\rho^{perfect}} = a_{31}\alpha^4(x) + a_{32}\alpha^3(x) + a_{33}\alpha^2(x) + a_{34}\alpha(x) + a_{35}, \tag{9}$$

where a_{ij} indicates the fitting coefficients and ${C_1}^{perfect}$, ${C_2}^{perfect}$ and $\rho^{perfect}$ are the Mooney-Rivlin hyperelastic and mass density terms of the soft samples without any porosity. By performing a curve fitting (Fig. 4), the coefficients for each parameter are obtained as shown in Table 2; it can be seen that the R-square is very close to 1 showing the accuracy of the proposed model for porous-hyperelastic coefficients and mass density terms as a function of porosity.

In this paper, it is assumed that structure's porosity can vary through the length direction (1 - $\alpha(x)$); therefore, the infill rate is assumed as a function of the longitudinal direction term x following a power-law or sigmoid functions as

$$\alpha(x) = \begin{cases} powerlaw: \ \alpha_1\left(\dfrac{x}{L}\right)^{m_p} + \alpha_0, & 0 \le x \le L, \\ sigmoid: \begin{cases} \alpha_0 + \dfrac{1}{2}\alpha_1\left(\dfrac{2x}{L}\right)^{m_s}, & 0 \le x \le \dfrac{L}{2}, \\ \alpha_0 + \alpha_1 - \dfrac{\alpha_1}{2}\left(2 - \dfrac{2x}{L}\right)^{m_s}, & \dfrac{L}{2} \le x \le L, \end{cases} \end{cases} \tag{10}$$

where α_0 and α_1 are the infill rate coefficients (the infill rate at the left and right ends are α_0 and (α_0+α_1), respectively), m_p and m_s are the varying terms for power-law and sigmoid functions, respectively, and L is the length of the beam which is assumed that the porosity varies through it. The variation of infill rate for both models are shown in Fig. 5; it can be seen that by having $m_p = 0$, a uniform infill rate ($\alpha_0 + \alpha_1$) through the length is obtained and by having $m_p = 1$, linear variation model for porosity is presented. Similarly, for the sigmoidal model, by having $m_s = 0$ and $m_s = 1$, a uniform infill rate ($\alpha_0 + 0.5\alpha_1$) and linear variation through the length are obtained.

3. Porous-hyperelastic beam formulation via the Mooney-Rivlin model

For a hollow porous-hyperelastic beam with the thickness of h, length L and width b (Fig. 6a), by considering a geometrical imperfection (Fig. 6b) of von Kármán geometric nonlinearity in the strain-displacement relationships and assuming that the slope of the initial rise is smaller than unity, the kinetic energy (KE) is written following the displacement field of Euler-Bernoulli beam theory as [31]

$$KE = \frac{1}{2}\int_V \rho(x)\left[\left(\frac{\partial u(x,t)}{\partial t} - z\frac{\partial^2 w(x,t)}{\partial x \partial t}\right)^2 + \left(\frac{\partial w(x,t)}{\partial t}\right)^2\right] \mathrm{dV}, \tag{11}$$

where u and w are the displacements in x and z directions (x is along the length) and t is time; dV is the elementary volume element of the beam. The invariants (I_1, I_2 and J) for the described beam model, by considering strains in all three directions and assuming the same strain in the y and z directions (i.e. orthogonally to the transverse deflection w), are rewritten as

$$I_1 = \frac{2 + \left(1 + \frac{\partial u}{\partial x} - z\frac{\partial^2 w}{\partial x^2} + \frac{1}{2}\left(\frac{\partial w}{\partial x}\right)^2 - \frac{\partial w}{\partial x}\frac{dw_0}{dx}\right)^3}{\frac{1}{2}\left(\frac{\partial w}{\partial x}\right)^2 - z\frac{\partial^2 w}{\partial x^2} + \frac{\partial u}{\partial x} - \frac{\partial w}{\partial x}\frac{dw_0}{dx} + 1}, \tag{12}$$

$$I_2 = \frac{1+2\left(1+\frac{\partial u}{\partial x}-z\frac{\partial^2 w}{\partial x^2}+\frac{1}{2}\left(\frac{\partial w}{\partial x}\right)^2-\frac{\partial w}{\partial x}\frac{dw_0}{dx}\right)^3}{1+2\frac{\partial u}{\partial x}-2z\frac{\partial^2 w}{\partial x^2}+\left(\frac{\partial w}{\partial x}\right)^2-2\frac{\partial w}{\partial x}\frac{dw_0}{dx}+\left(\frac{\partial u}{\partial x}-z\frac{\partial^2 w}{\partial x^2}+\frac{1}{2}\left(\frac{\partial w}{\partial x}\right)^2-\frac{\partial w}{\partial x}\frac{dw_0}{dx}\right)^2}, \tag{13}$$

$$J = 1 \rightarrow \varepsilon_y = \varepsilon_z = \sqrt{\frac{\left(\frac{\partial u}{\partial x}-z\frac{\partial^2 w}{\partial x^2}+\frac{1}{2}\left(\frac{\partial w}{\partial x}\right)^2-\frac{\partial w}{\partial x}\frac{dw_0}{dx}+2\left[1-\sqrt{1+\frac{\partial u}{\partial x}-z\frac{\partial^2 w}{\partial x^2}+\frac{1}{2}\left(\frac{\partial w}{\partial x}\right)^2-\frac{\partial w}{\partial x}\frac{dw_0}{dx}}\right]\right)}{1+\frac{\partial u}{\partial x}-z\frac{\partial^2 w}{\partial x^2}+\frac{1}{2}\left(\frac{\partial w}{\partial x}\right)^2-\frac{\partial w}{\partial x}\frac{dw_0}{dx}}} \tag{14}$$

where w_0 is the geometrical imperfection (Fig. 6b). By using the Mooney-Rivlin hyperelastic strain energy density model [29,32], the potential energy of the beam can be written as

$$\begin{aligned} PE &= \int_0^L \int_A [C_1(I_1-3)+C_2(I_2-3)]dAdx \\ &= \int_0^L \int_A \left[C_1 \frac{2+\left(1+\frac{\partial u}{\partial x}-z\frac{\partial^2 w}{\partial x^2}+\frac{1}{2}\left(\frac{\partial w}{\partial x}\right)^2-\frac{\partial w}{\partial x}\frac{dw_0}{dx}\right)^3}{\frac{1}{2}\left(\frac{\partial w}{\partial x}\right)^2-z\frac{\partial^2 w}{\partial x^2}+\frac{\partial u}{\partial x}-\frac{\partial w}{\partial x}\frac{dw_0}{dx}+1} - 3(C_1+C_2) \right. \\ &\left. + C_2 \frac{1+2\left(1+\frac{\partial u}{\partial x}-z\frac{\partial^2 w}{\partial x^2}+\frac{1}{2}\left(\frac{\partial w}{\partial x}\right)^2-\frac{\partial w}{\partial x}\frac{dw_0}{dx}\right)^3}{1+2\frac{\partial u}{\partial x}-2z\frac{\partial^2 w}{\partial x^2}+\left(\frac{\partial w}{\partial x}\right)^2-2\frac{\partial w}{\partial x}\frac{dw_0}{dx}+\left(\frac{\partial u}{\partial x}-z\frac{\partial^2 w}{\partial x^2}+\frac{1}{2}\left(\frac{\partial w}{\partial x}\right)^2-\frac{\partial w}{\partial x}\frac{dw_0}{dx}\right)^2} \right] dAdx, \end{aligned} \tag{15}$$

By using Hamilton's principle, the coupled equations of motion are obtained (given in Appendix B for the sake of brevity). Since the scale of parameters in the equations of motion are significantly different, nondimensional terms are defined as

$$\begin{aligned} &x* = \frac{x}{L},\ w* = \frac{w}{h},\ w_0* = \frac{w_0}{h},\ u* = \frac{u}{h},\ F* = \frac{FL^4}{(C_{10}+C_{20})hI_2},\ \rho* = \frac{\rho}{\rho_0},\ \eta = \frac{h}{L},\ \gamma_2 = \sqrt{\frac{AL^2}{I_2}},\ \gamma_4 = \sqrt{\frac{I_4}{I_2L^2}}, \\ &C_1* = \frac{C_1}{C_{1,\alpha=1}+C_{2,\alpha=1}},\ C_2* = \frac{C_2}{C_{1,\alpha=1}+C_{2,\alpha=1}},\ t* = t\sqrt{\frac{(C_{1,\alpha=1}+C_{2,\alpha=1})I_2}{\rho_0AL^4}},\ \Omega = \omega\sqrt{\frac{\rho_0AL^4}{(C_{1,\alpha=1}+C_{2,\alpha=1})I_2}}, \end{aligned} \tag{16}$$

which by using the nondimensional terms, one can rewrite the equations of motion in a nondimensional form which is given in Appendix B. It can be seen that the nondimensional equations of motion are highly nonlinear due to hyperelastic nonlinearities, porosity variation, geometrical imperfections, large deflection and the coupling between the axial and transverse motions. In order to obtain the nonlinear dynamic behaviour of soft porous beams, one has to solve the coupled system of nonlinear equations simultaneously which is discussed in the next section.

4. Solution procedure

By considering coupled motion and by assuming the first 2N modes of vibration (N modes of axial motion and N modes of transverse motion) in Galerkin's scheme as

$$u(x,t) = \chi_1(x)\tau_1(t)+\chi_2(x)\tau_2(t)+\chi_3(x)\tau_3(t)+\cdots+\chi_N(x)\tau_N(t), \tag{17}$$

$$w(x,t) = \xi_1(x)\vartheta_1(t)+\xi_2(x)\vartheta_2(t)+\xi_3(x)\vartheta_3(t)+\cdots+\xi_N(x)\vartheta_N(t), \tag{18}$$

and the governing coupled equations of motion are discretised and rewritten with coefficients for each term as

$$
\begin{aligned}
&\sum_{l=1}^{N}\sum_{i=1}^{N} M2_{li}\frac{d^2}{dt^2}\vartheta_i(t)+\sum_{l=1}^{N}\sum_{i=1}^{N} KL21_{li}\tau_i(t)+\sum_{l=1}^{N}\sum_{i=1}^{N} KL22_{li}\vartheta_i(t)-\sum_{l=1}^{N} F_l\cos(\Omega t)\\
&+\sum_{l=1}^{N}\sum_{i=1}^{N}\sum_{j=1}^{N} KN21_{lij}\tau_i(t)\tau_j(t)+\sum_{l=1}^{N}\sum_{i=1}^{N}\sum_{j=1}^{N} KN22_{lij}\tau_i(t)\vartheta_j(t)\\
&+\sum_{l=1}^{N}\sum_{i=1}^{N}\sum_{j=1}^{N} KN23_{lij}\vartheta_i(t)\vartheta_j(t)+\sum_{l=1}^{N}\sum_{i=1}^{N}\sum_{j=1}^{N}\sum_{k=1}^{N} KN24_{lijk}\tau_i(t)\tau_j(t)\tau_k(t)\\
&+\sum_{l=1}^{N}\sum_{i=1}^{N}\sum_{j=1}^{N}\sum_{k=1}^{N} KN25_{lijk}\tau_i(t)\tau_j(t)\vartheta_k(t)+\sum_{l=1}^{N}\sum_{i=1}^{N}\sum_{j=1}^{N}\sum_{k=1}^{N} KN26_{lijk}\tau_i(t)\vartheta_j(t)\vartheta_k(t)\\
&+\sum_{l=1}^{N}\sum_{i=1}^{N}\sum_{j=1}^{N}\sum_{k=1}^{N} KN27_{lijk}\vartheta_i(t)\vartheta_j(t)\vartheta_k(t)+\sum_{l=1}^{N}\sum_{i=1}^{N}\sum_{j=1}^{N}\sum_{k=1}^{N}\sum_{m=1}^{N} KN28_{lijkm}\tau_i(t)\tau_j(t)\tau_k(t)\vartheta_m(t)\\
&+\sum_{l=1}^{N}\sum_{i=1}^{N}\sum_{j=1}^{N}\sum_{k=1}^{N}\sum_{m=1}^{N} KN29_{lijkm}\tau_i(t)\tau_j(t)\vartheta_k(t)\vartheta_m(t)\\
&+\sum_{l=1}^{N}\sum_{i=1}^{N}\sum_{j=1}^{N}\sum_{k=1}^{N}\sum_{m=1}^{N} KN210_{lijkm}\tau_i(t)\vartheta_j(t)\vartheta_k(t)\vartheta_m(t)\\
&+\sum_{l=1}^{N}\sum_{i=1}^{N}\sum_{j=1}^{N}\sum_{k=1}^{N}\sum_{m=1}^{N} KN211_{lijkm}\vartheta_i(t)\vartheta_j(t)\vartheta_k(t)\vartheta_m(t)\\
&+\sum_{l=1}^{N}\sum_{i=1}^{N}\sum_{j=1}^{N}\sum_{k=1}^{N}\sum_{m=1}^{N}\sum_{n=1}^{N} KN212_{lijkmn}\tau_i(t)\tau_j(t)\vartheta_k(t)\vartheta_m(t)\vartheta_n(t)\\
&+\sum_{l=1}^{N}\sum_{i=1}^{N}\sum_{j=1}^{N}\sum_{k=1}^{N}\sum_{m=1}^{N}\sum_{n=1}^{N} KN213_{lijkmn}\tau_i(t)\vartheta_j(t)\vartheta_k(t)\vartheta_m(t)\vartheta_n(t)\\
&+\sum_{l=1}^{N}\sum_{i=1}^{N}\sum_{j=1}^{N}\sum_{k=1}^{N}\sum_{m=1}^{N}\sum_{n=1}^{N} KN214_{lijkmn}\vartheta_i(t)\vartheta_j(t)\vartheta_k(t)\vartheta_m(t)\vartheta_n(t)\\
&+\sum_{l=1}^{N}\sum_{i=1}^{N}\sum_{j=1}^{N}\sum_{k=1}^{N}\sum_{m=1}^{N}\sum_{n=1}^{N}\sum_{o=1}^{N} KN215_{lijkmno}\tau_i(t)\vartheta_j(t)\vartheta_k(t)\vartheta_m(t)\vartheta_n(t)\vartheta_o(t)\\
&+\sum_{l=1}^{N}\sum_{i=1}^{N}\sum_{j=1}^{N}\sum_{k=1}^{N}\sum_{m=1}^{N}\sum_{n=1}^{N}\sum_{o=1}^{N} KN216_{lijkmno}\vartheta_i(t)\vartheta_j(t)\vartheta_k(t)\vartheta_m(t)\vartheta_n(t)\vartheta_o(t)\\
&+\sum_{l=1}^{N}\sum_{i=1}^{N}\sum_{j=1}^{N}\sum_{k=1}^{N}\sum_{m=1}^{N}\sum_{n=1}^{N}\sum_{o=1}^{N}\sum_{p=1}^{N} KN217_{lijkmnop}\vartheta_i(t)\vartheta_j(t)\vartheta_k(t)\vartheta_m(t)\vartheta_n(t)\vartheta_o(t)\vartheta_p(t)=0,
\end{aligned}
\tag{19}
$$

$$\sum_{l=1}^{N}\sum_{i=1}^{N} M1_{li}\frac{d^2}{dt^2}\tau_i(t)+\sum_{l=1}^{N}\sum_{i=1}^{N} KL11_{li}\tau_i(t)+\sum_{l=1}^{N}\sum_{i=1}^{N} KL12_{li}\vartheta_i(t)+\sum_{l=1}^{N}\sum_{i=1}^{N}\sum_{j=1}^{N} KN11_{lij}\tau_i(t)\tau_j(t)$$
$$+\sum_{l=1}^{N}\sum_{i=1}^{N}\sum_{j=1}^{N} KN12_{lij}\tau_i(t)\vartheta_j(t)+\sum_{l=1}^{N}\sum_{i=1}^{N}\sum_{j=1}^{N} KN13_{lij}\vartheta_i(t)\vartheta_j(t)$$
$$+\sum_{l=1}^{N}\sum_{i=1}^{N}\sum_{j=1}^{N}\sum_{k=1}^{N} KN14_{lijk}\tau_i(t)\tau_j(t)\tau_k(t)+\sum_{l=1}^{N}\sum_{i=1}^{N}\sum_{j=1}^{N}\sum_{k=1}^{N} KN15_{lijk}\tau_i(t)\tau_j(t)\vartheta_k(t)$$
$$+\sum_{l=1}^{N}\sum_{i=1}^{N}\sum_{j=1}^{N}\sum_{k=1}^{N} KN16_{lijk}\tau_i(t)\vartheta_j(t)\vartheta_k(t)+\sum_{l=1}^{N}\sum_{i=1}^{N}\sum_{j=1}^{N}\sum_{k=1}^{N} KN17_{lijk}\vartheta_i(t)\vartheta_j(t)\vartheta_k(t)$$
$$+\sum_{l=1}^{N}\sum_{i=1}^{N}\sum_{j=1}^{N}\sum_{k=1}^{N}\sum_{m=1}^{N} KN18_{lijkm}\tau_i(t)\tau_j(t)\vartheta_k(t)\vartheta_m(t) \tag{20}$$
$$+\sum_{l=1}^{N}\sum_{i=1}^{N}\sum_{j=1}^{N}\sum_{k=1}^{N}\sum_{m=1}^{N} KN19_{lijkm}\tau_i(t)\vartheta_j(t)\vartheta_k(t)\vartheta_m(t)$$
$$+\sum_{l=1}^{N}\sum_{i=1}^{N}\sum_{j=1}^{N}\sum_{k=1}^{N}\sum_{m=1}^{N} KN110_{lijkm}\vartheta_i(t)\vartheta_j(t)\vartheta_k(t)\vartheta_m(t)$$
$$+\sum_{l=1}^{N}\sum_{i=1}^{N}\sum_{j=1}^{N}\sum_{k=1}^{N}\sum_{m=1}^{N}\sum_{n=1}^{N} KN111_{lijkmn}\vartheta_i(t)\vartheta_j(t)\vartheta_k(t)\vartheta_m(t)\vartheta_n(t)+$$
$$+\sum_{l=1}^{N}\sum_{i=1}^{N}\sum_{j=1}^{N}\sum_{k=1}^{N}\sum_{m=1}^{N}\sum_{n=1}^{N}\sum_{o=1}^{N} KN112_{lijkmno}\vartheta_i(t)\vartheta_j(t)\vartheta_k(t)\vartheta_m(t)\vartheta_n(t)\vartheta_o(t)=0,$$

which for the sake of brevity, the coefficients are defined in Appendix C. In this study, the boundary conditions are assumed to be fixed-fixed which leads to the spatial functions as [33]

$$\chi_p(x)=\sin(p\pi x) \tag{21}$$

$$\xi_p(x)=\frac{\cos(\mu_p)-\cosh(\mu_p)}{\sin(\mu_p)-\sinh(\mu_p)}\left[\sinh(\mu_p x)-\sin(\mu_p x)\right]+\cosh(\mu_p x)-\cos(\mu_p x) \tag{22}$$

where μ_p is the pth root of the transcendental equation. The equilibrium coefficients can be rewritten by employing a dynamic equilibrium technique as

$$\tau_m=A_{m(-n)}e^{-ni\omega t}+\cdots+A_{m(-2)}e^{-2i\omega t}+A_{m(-1)}e^{-i\omega t}+A_{m0}+A_{m1}e^{i\omega t}+A_{m2}e^{2i\omega t}+\cdots+A_{mn}e^{ni\omega t}, \tag{23}$$

$$\vartheta_m=B_{m(-n)}e^{-ni\omega t}+\cdots+B_{m(-2)}e^{-2i\omega t}+B_{m(-1)}e^{-i\omega t}+B_{m0}+B_{m1}e^{i\omega t}+B_{m2}e^{2i\omega t}+\cdots+B_{mn}e^{ni\omega t}, \tag{24}$$

and the dynamic complex equilibrium equation is obtained as

$$\left\{-\omega^2[M_T]+\left[K_T^L\right]\right\}\begin{Bmatrix}\sum_{n=-N}^{N} B_{mn}e^{in\omega t}\\ \sum_{n=-N}^{N} A_{mn}e^{in\omega t}\end{Bmatrix}+K_T^{NL}\left(A_{mn},B_{mn},e^{in\omega t}\right)\begin{Bmatrix}\sum_{n=-N}^{N} B_{mn}e^{in\omega t}\\ \sum_{n=-N}^{N} A_{mn}e^{in\omega t}\end{Bmatrix}=\{f\}\cos(\Omega t), \tag{25}$$

which by solving the dynamic equilibrium equations in Eq. (25), the nonlinear dynamic response of the system is obtained. To solve Eq. (25), the frequency term Ω is firstly guessed and inserted into this system of equations for obtaining the dynamic complex equilibrium coefficients (A_{mn} and B_{mn}). The frequency term is evolved afterwards with a small iteration in the previous frequency term as

$$\Omega_{new}=\Omega_{previous}+\Delta\Omega, \tag{26}$$

which for the new frequency term, the dynamic complex equilibrium coefficients are computed again and the process is repeated (interested readers are referred to Refs. [34–36]). For linear analysis and obtaining the natural frequencies of the soft structure, the nonlinear parts of the equations of motion are neglected and a modal decomposition technique [37] is used.

5. Results and discussions

The coupled equations of motion of porous-hyperelastic beams with uniform/functional porosity through the length have been

Table 3
Nondimensional fundamental frequency parameter of a porous elastic beam with different geometrical imperfection.

$A_0/[\eta(I_2/A)^{0.5}]$	0.0	0.1	0.2	0.3	0.4	0.5
Ref. [38]	9.8696	9.8942	9.9678	10.0892	10.2568	10.4683
Present	9.8696044	9.8942474	9.9678108	10.0892246	10.2568795	10.4682895

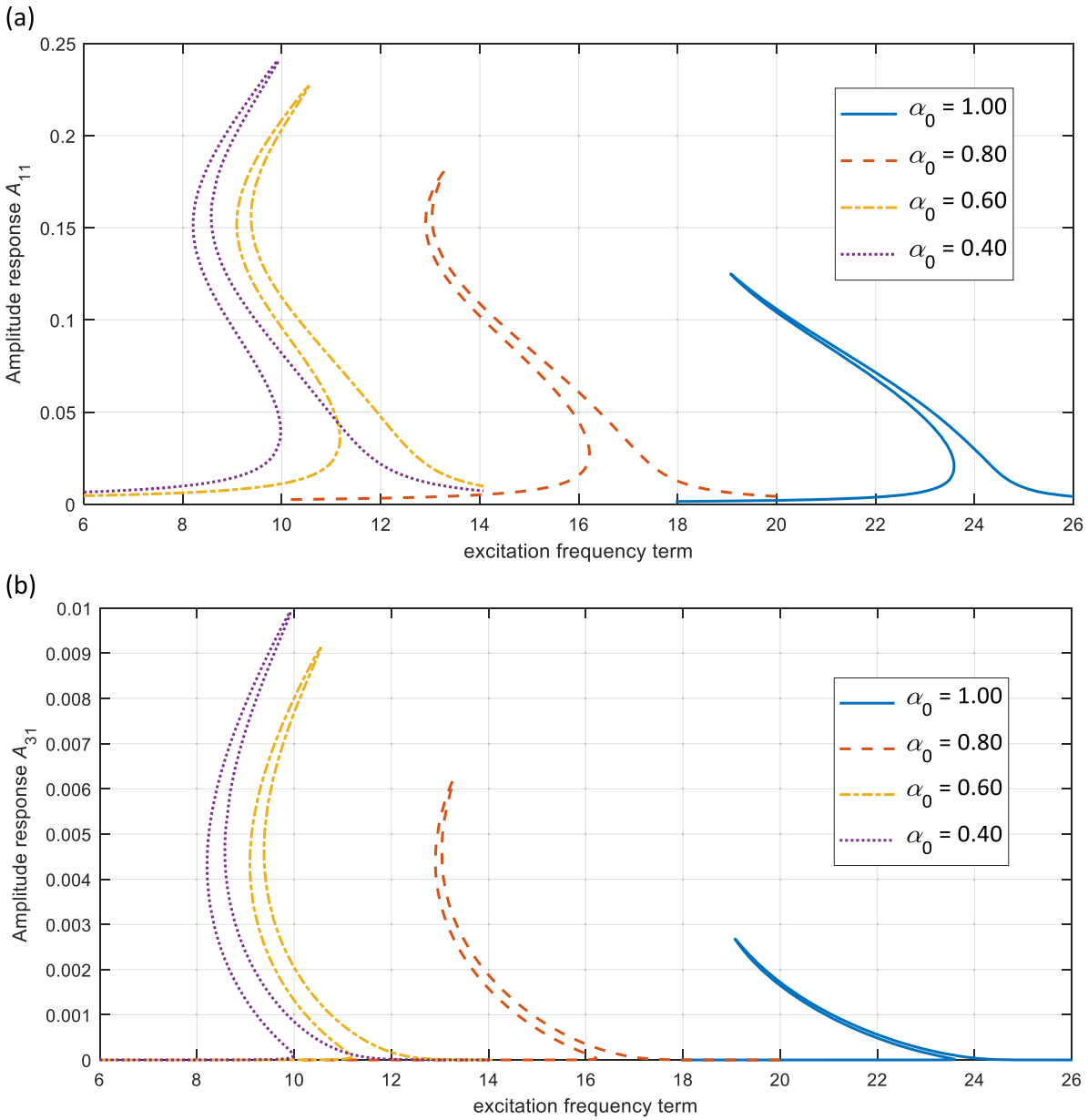

Fig. 7. Transverse amplitude-frequency response of uniformly porous-hyperelastic beams with different infill rates for the (a) first and (b) third dynamic coordinates.

formulated based on the experimental results and solved in the previous sections. In this section, the nonlinear dynamic response of such structures is investigated and different case studies are presented.

5.1. Model validation

For the sake of verifying the current methodology, a geometrically imperfect *elastic* beam model with even porosity is modelled using the given formulation. To reach this model, the equations of motion are simplified by neglecting the higher order strain terms and defining the Young's modulus of the system equal to the hyperelastic parameter as

$$\rho A u_{tt} - EA\left(\frac{\partial^2 u}{\partial x^2} + \frac{\partial w}{\partial x}\frac{\partial^2 w}{\partial x^2} - \frac{\partial^2 w}{\partial x^2}\frac{\mathrm{d}w_0}{\mathrm{d}x} - \frac{\partial w}{\partial x}\frac{\mathrm{d}^2 w_0}{\mathrm{d}x^2}\right) = 0, \tag{27}$$

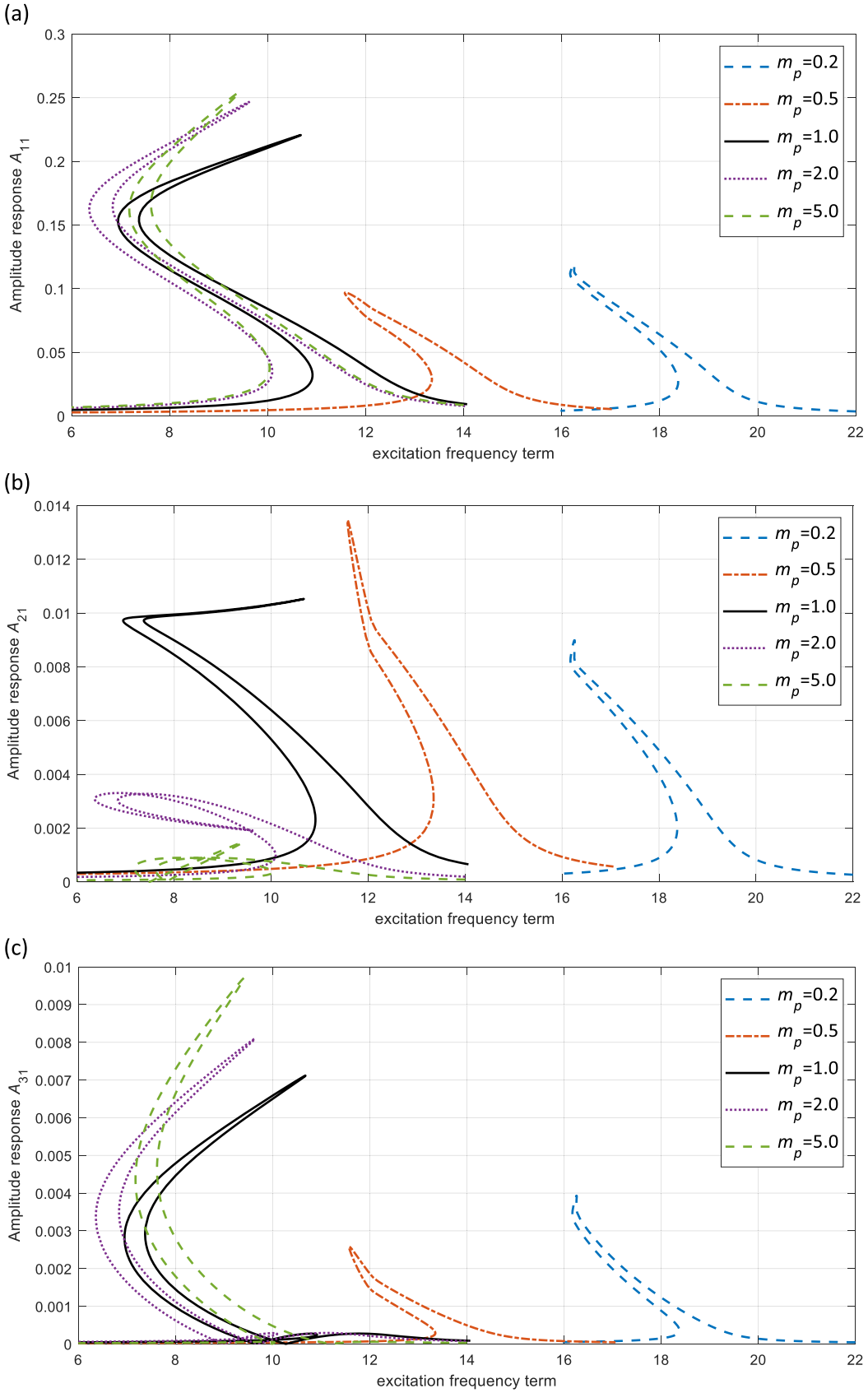

Fig. 8. Transverse amplitude-frequency response of power-law porous-hyperelastic beams for the (a) first, (b) second and (c) third dynamic coordinates.

$$\rho A w_{tt} - I_2\rho\frac{\partial^4 w}{\partial x^2\partial t^2} + I_2 E\left(\frac{\partial^4 w}{\partial x^4}\right) + AE\left(\frac{\partial u}{\partial x}\frac{\mathrm{d}^2 w_0}{\mathrm{d}x^2} - \frac{\partial w}{\partial x}\frac{\mathrm{d}w_0}{\mathrm{d}x}\frac{\mathrm{d}^2 w_0}{\mathrm{d}x^2}\right) + AE\left(\frac{\partial^2 u}{\partial x^2}\frac{\mathrm{d}w_0}{\mathrm{d}x} + \frac{\partial w}{\partial x}\frac{\partial^2 w}{\partial x^2}\frac{\mathrm{d}w_0}{\mathrm{d}x} - \frac{\partial^2 w}{\partial x^2}\left(\frac{\mathrm{d}w_0}{\mathrm{d}x}\right)^2 - \frac{\partial w}{\partial x}\frac{dw_0}{dx}\frac{\mathrm{d}^2 w_0}{\mathrm{d}x^2}\right) = 0, \tag{28}$$

which is equal to those obtained by literature [38] and validates the formulation procedure given in this paper. By varying the geometrical imperfection term as $A_0 = [0\ 0.1\ 0.2\ 0.3\ 0.4\ 0.5]\eta(I_2/A)^{0.5}$ and having even porosity in the structure as [38]

$$\begin{Bmatrix}\rho\\ E\end{Bmatrix} = (1-\mu_0)\begin{Bmatrix}\rho_0\\ E_0\end{Bmatrix}, \tag{29}$$

the nondimensional fundamental frequency terms are obtained using the modal decomposition technique [37] after non-dimensionalisation (for $\mu_0 = 0.1$) and shown in Table 3 which are in good agreement with the literature.

5.2. Porosity effect

Porosity is one of the main defects seen in hyperelastic structures. To understand the influence of porosity in varying the mechanical behaviour of soft structures, a geometrically perfect beam is considered with the dimensions as $L = 0.2$ m, $b = 0.02$ m and $h = 0.01$ m and the porosity is assumed to be either uniformly constant or varied via a function through the length. A modal damping term of $\xi = 0.08$ is also considered.

- Uniform porosity

For the case of having porous soft structure with uniform porosity, the infill rate is assumed to be constant through the length ($\alpha(x) = \alpha_0$), which regarding Eqs. (7)–(9), the porous-hyperelastic coefficients and mass density will be independent of x. An external nondimensional excitation load of $F = 1.5$ is applied to the structure and the porosity is assumed by having the infill rate as $\alpha = [0.4, 0.6, 0.8, 1.0]$. The frequency responses of the defined porous-hyperelastic beams are shown in Fig. 7(a) and (b) for the transverse dynamic coordinates, respectively; it can be seen that the first transverse generalised coordinate of the fully infilled beam model (α =1.0) shows stiffness softening behaviour while by decreasing the infill rate (to α =0.8, 0.6 and 0.4), a combination of stiffness softening and hardening is obtained. Besides, form Fig. 7(a) and (b), it is seen that decreasing the infill rate (increasing the porosity) shifts the resonance towards lower frequencies; this is due to losing stiffness in the structure by increasing the porosity. The dynamic coordinates lose amplitude by increasing the infill rate for all the dynamic coordinates while the contribution of the second coordinate is negligible (significantly small).

- Functional porosity

In many structures, the porosity is not distributed evenly through the structure and can vary because of the fabrication procedure or the engineering need for functional porosity. To have a general model of porosity, this study presented the porosity in the form of power-law and sigmoid functions as shown in Section 2. The influence of having functional porosity along the length of the current beam model is studied in this section for both power-law and sigmoid models.

- Power-law porosity

In the case of varying the porosity using a power-law function, the porosity distribution and infill rate vary through the length as shown in Fig. 5a. The nonlinear vibration behaviour of a porous-hyperelastic beam with the given geometry in the previous section is analysed by increasing the power-law parameter as $m_p = [0.2, 0.5, 1.0, 2.0, 5.0]$ in Fig. 8(a–c) for the first three dynamic coordinates of transverse motion; it can be seen that decreasing the power-law parameter from 1.0 to 0.2 has a higher effect in changing the nonlinear vibration behaviour than increasing it from 1.0 to 5.0; the reason for this significant difference is due to the definition given for power-law porosity in Eq. (10) which can be seen that decreasing the power-law parameter from 1.0 to 0.2 has lower porosity in the whole structure and as shown in Fig. (3), the structure shows more sensitivity to porosity changes when the overall porosity is low. Besides, lowering the power-law parameter shifts the resonance phenomenon to higher frequencies and lowers the maximum amplitude of the first transverse coordinate—the axial coordinates are significantly smaller than the transverse ones which for the sake of brevity, are not shown here.

- Sigmoid porosity

For the case of varying the porosity through the length of the porous-hyperelastic beam using a sigmoid function (Fig. 5b), the nonlinear frequency responses for transverse dynamic coordinates are shown in Fig. 9(a–c) for $m_s = [0.2, 0.5, 1.0, 2.0, 5.0]$; as shown, increasing the sigmoid parameter causes lower amplitude peak and shifts the resonance to higher frequencies, slightly—this effect is considerably lower than the power-law porosity variation model (given in Fig. 8(a–c)). The reason for this difference can be seen by comparing sigmoid and power-law porosity variation in Fig. (5); the sigmoid porosity model gives the overall same amount of porosity

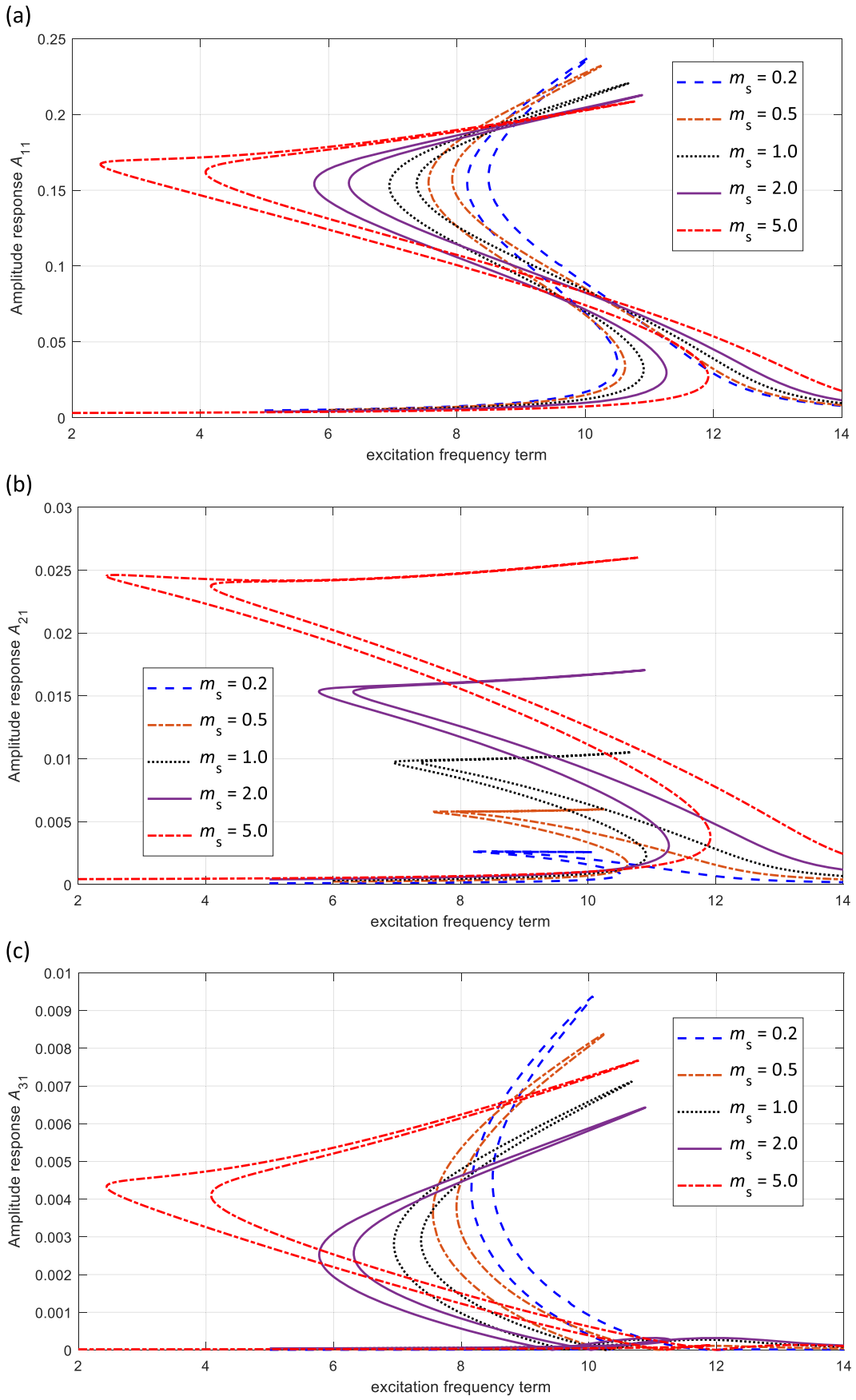

Fig. 9. Transverse amplitude-frequency response of sigmoid porous-hyperelastic beams for the (a) first, (b) second and (c) third dynamic coordinates.

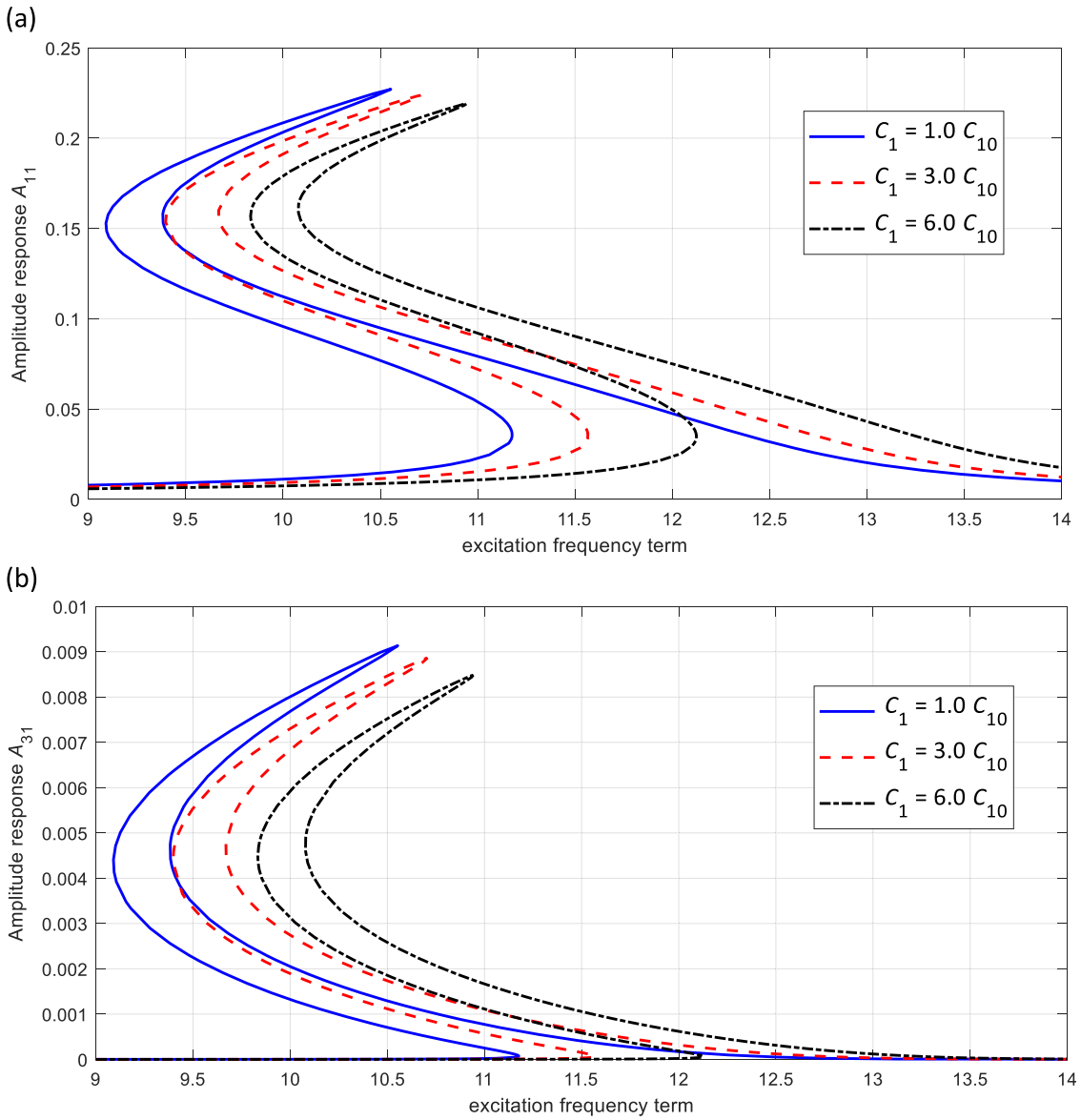

Fig. 10. Influence of the first Mooney-Rivlin hyperelastic coefficient (C_1) on the transverse amplitude-frequency response of uniformly porous-hyperelastic beams for the (a) first and (b) third dynamic coordinates.

in the whole structure by varying the porosity term while this is not the case for power-law porosity model as the overall porosity changes significantly by changing the power-law parameter. Similarly, for the axial coordinates, the variation of the amplitude response to the sigmoid variation is lower than the power-law model as well which is not shown here for the sake of brevity.

5.3. Effect of the hyperelastic material parameters

The strain energy density of the beam is defined based on the Mooney-Rivlin hyperelastic model with stiffness coefficients C_1 and C_2. To show the effects of correctly defining the values of these coefficients, this section will analyse the influence of the Mooney-Rivlin coefficients on varying the nonlinear response of both uniformly and functionally porous-hyperelastic beam models.

– Uniform porosity

For having a uniformly distributed porosity in the beam (with the infill rate as $\alpha = 0.6$), the influence of varying the porous-hyperelastic parameters is discussed here. The first parameter of the Mooney-Rivlin strain energy density model has a direct effect on the first strain invariant (I_1) of the beam. By defining the initial nondimensional term as

$$C_{10} = \frac{C_{1,\,\alpha=0.6}}{\left(C_{1,\,\alpha=1.0} + C_{2,\,\alpha=1.0}\right)}, \tag{30}$$

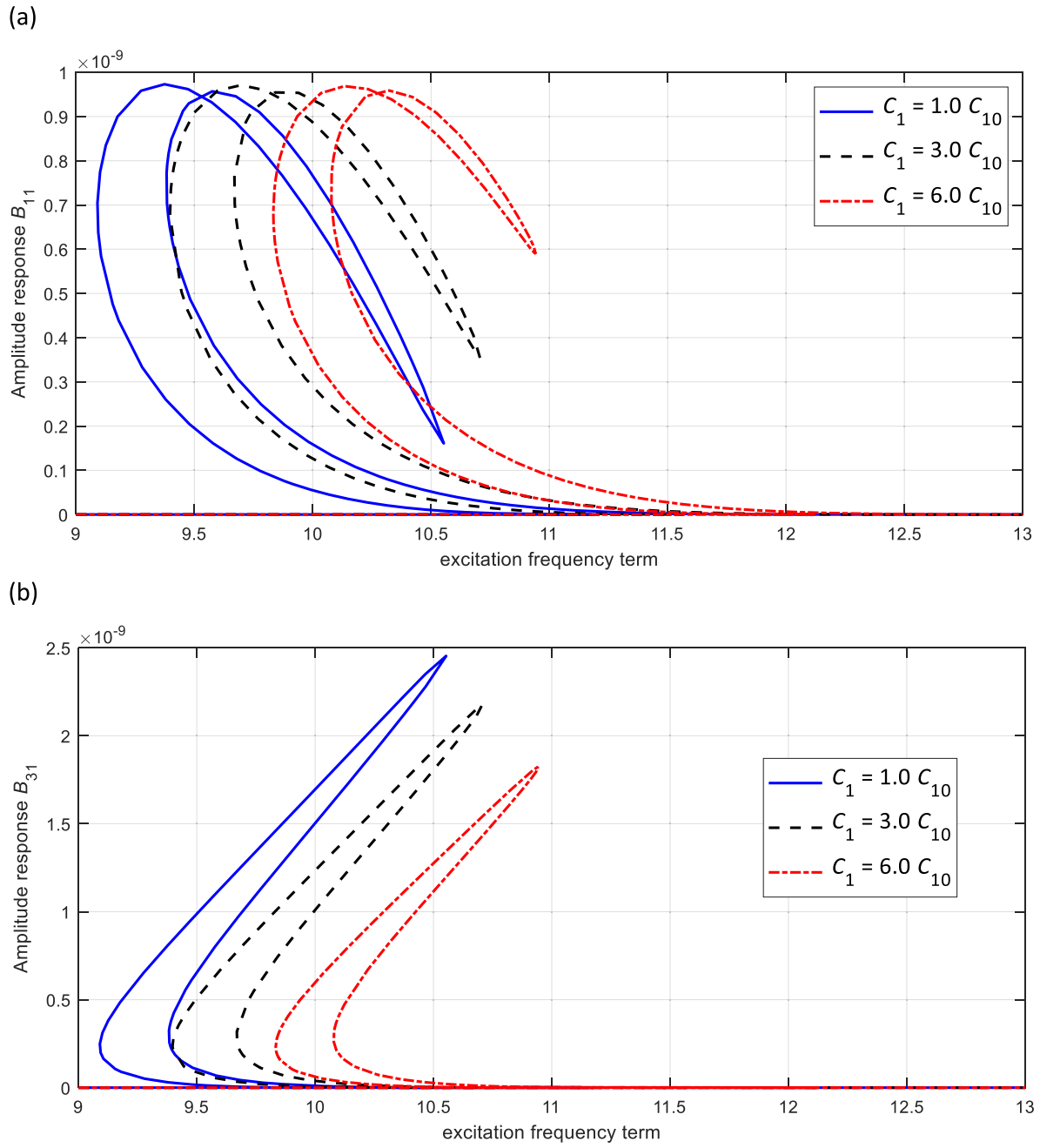

Fig. 11. Influence of the first Mooney-Rivlin hyperelastic coefficient (C_1) on the axial amplitude-frequency response of uniformly porous-hyperelastic beams for the (a) first and (b) third dynamic coordinates.

where $C_{1,\alpha=0.6}$ indicates the first parameter of the Mooney-Rivlin strain energy density model for infill rate 0.6, the variation of this term is presented by $C_1 = [1.0, 3.0 \text{ and } 6.0]C_{10}$. By solving the equations of motion for this definition, the nonlinear frequency response is shown in Figs. (10) and (11) for the transverse and axial coordinates, respectively. Similarly, by defining the second porous-hyperelastic parameter C_2 (which directly affects the second strain invariant I_2) as

$$C_{20} = \frac{C_{2,\,\alpha=0.6}}{\left(C_{1,\,\alpha=1.0} + C_{2,\,\alpha=1.0}\right)}, \tag{31}$$

and $C_2 = [0.9, 1.2, 2.0, 3.0, 4.0, \text{ and } 5.0]C_{20}$, the nonlinear frequency response is shown in Figs. (12) and (13) for the transverse and axial coordinates, respectively. For both the axial and transverse coordinates, it is seen that increasing the Mooney-Rivlin hyperelastic parameters shifts the amplitude peak to higher frequencies and decreases the maximum amplitude of the generalised axial and transverse coordinates; the physical reason behind this change in the amplitude response is that by increasing the hyperelastic coefficient terms, the material is stiffer and therefore the natural frequencies will be higher. This effect is stronger for the second porous-hyperelastic parameter as the magnitude of this term is considerably higher for the material defined for this study case.

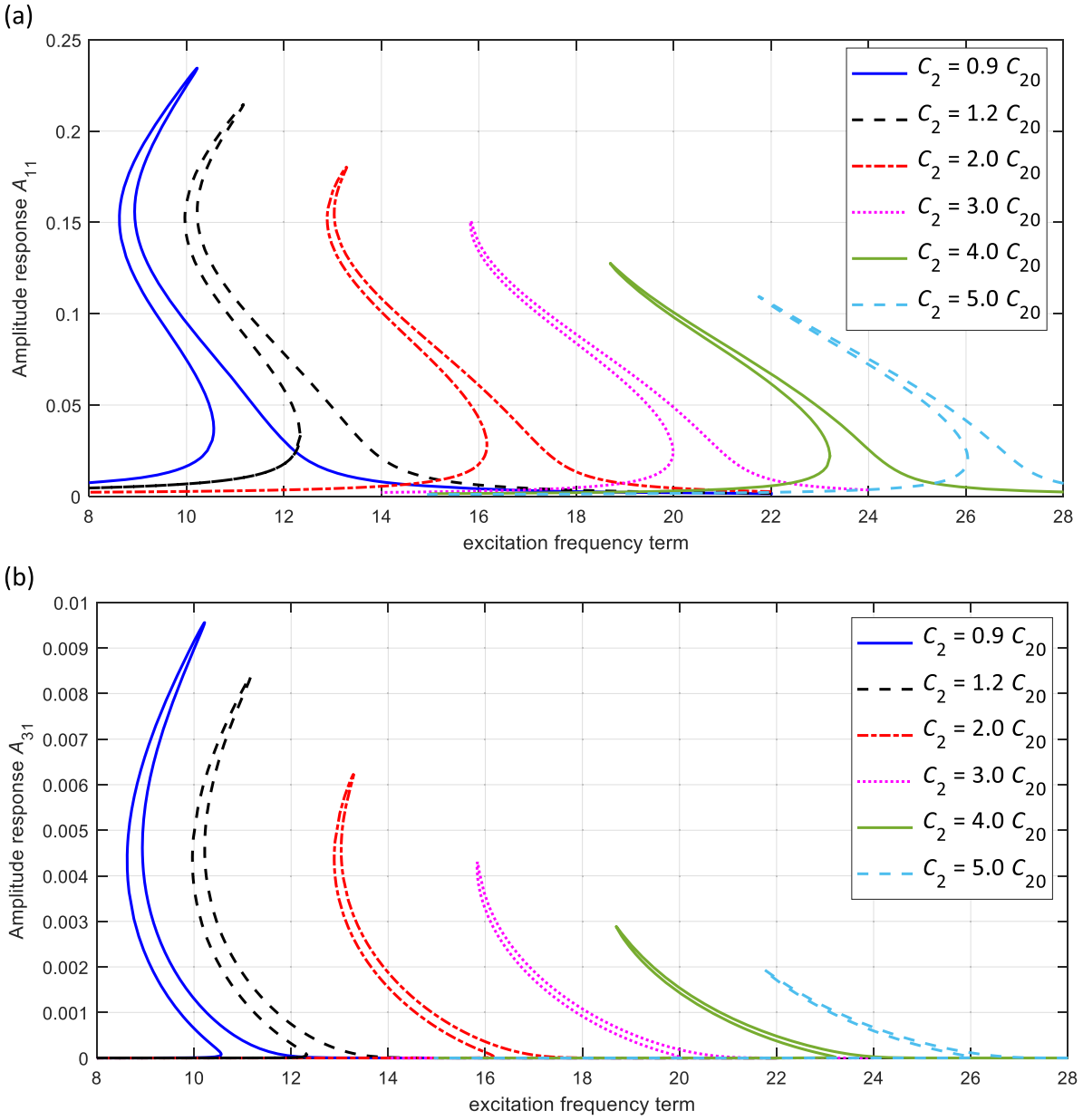

Fig. 12. Influence of the second Mooney-Rivlin hyperelastic coefficient (C_2) on the transverse amplitude-frequency response of uniformly porous-hyperelastic beams for the (a) first and (b) third dynamic coordinates.

- Functional porosity

For having a linear variation of infill rate from $\alpha = 0.1$ at the left end to $\alpha = 1.0$ at the right end, the influence of changing the porous-hyperelastic parameters on the nonlinear oscillation response is analysed. To this end, the first term of porous-hyperelasticity is defined as

$$C_{10}(x) = \frac{a_{11}\alpha^4(x) + a_{12}\alpha^2(x) + a_{13}\alpha^3(x) + a_{14}\alpha(x) + a_{15}}{\left(C_{1,\,\alpha=1.0} + C_{2,\,\alpha=1.0}\right)}, \tag{32}$$

with $C_1(x) = [1.0, 3.0 \text{ and } 6.0]C_{10}(x)$. Figs. (14) and (15) show the first three dynamic coordinates of the transverse and axial motions, respectively, for variation of the first porous-hyperelastic parameter ($C_1(x)$). Similarly, for the second porous-hyperelastic parameter, the initial term is defined as

$$C_{20}(x) = \frac{a_{21}\alpha^4(x) + a_{22}\alpha^2(x) + a_{23}\alpha^3(x) + a_{24}\alpha(x) + a_{25}}{\left(C_{1,\,\alpha=1.0} + C_{2,\,\alpha=1.0}\right)}, \tag{33}$$

with $C_2(x) = [0.9, 1.2, 2.0, 3.0, 4.0, \text{and } 5.0]C_{20}(x)$. For functional porous-hyperelastic beams, the influence of the second Mooney-

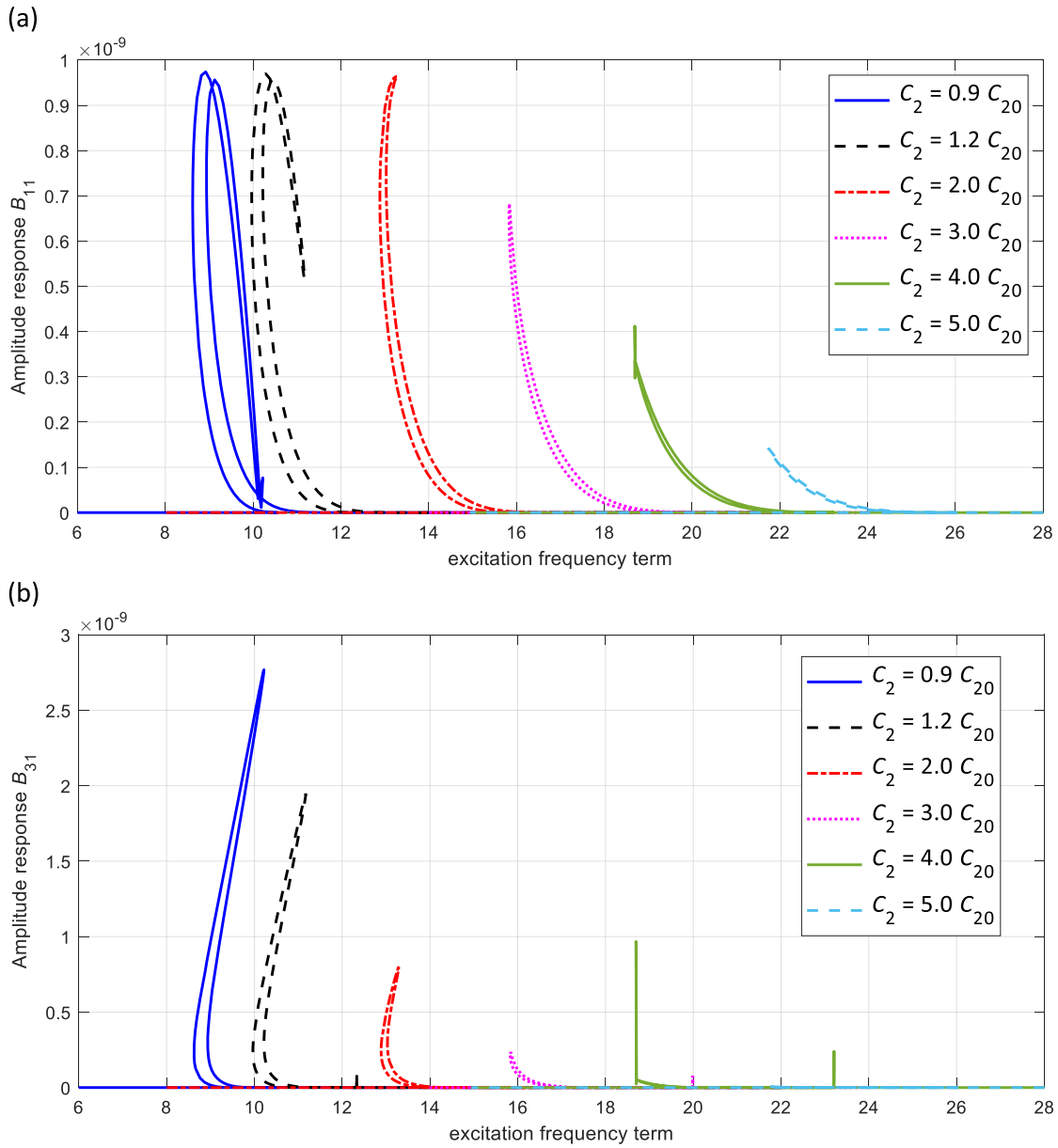

Fig. 13. Influence of the second Mooney-Rivlin hyperelastic coefficient (C_2) on the axial amplitude-frequency response of uniformly porous-hyperelastic beams for the (a) first and (b) third dynamic coordinates.

Rivlin coefficient is shown in Figs. (16) and (17) for the transverse and axial motions, respectively; it can be seen that increasing the porous-hyperelastic parameters moves the resonance peak to higher frequencies as discussed in the previous section and for the given case, the influence of the second porous-hyperelastic parameter is significantly higher. The second dynamic coordinate shows contribution in the dynamic response of the functional porous-hyperelastic beam model (which was zero for the uniform porous model) and increasing the C_2/C_{20} ratio from 0.9 to 5.0 changes the behaviour of the first two transverse coordinates to nonlinear softening behaviour. The reason for different frequency responses in uniform and functionally graded porous models can be seen in the equations of motion given in Appendix B; for the uniform porosity model, the hyperelastic terms will not be a function of x which means many terms will be neglected and some coupling terms will not be there. For axial dynamic coordinates shown in Fig. (17), it can be seen that for lower values of C_2, there is a local loss in the amplitude of the first two dynamic coordinates while the third dynamic coordinate increases significantly which physically shows the energy transmission from the first two axial coordinates to the third coordinate.

5.4. Effect of geometric imperfection

- Comparison

Due to the properties of soft structures, these structures can have a geometrical imperfection which can also be caused by the

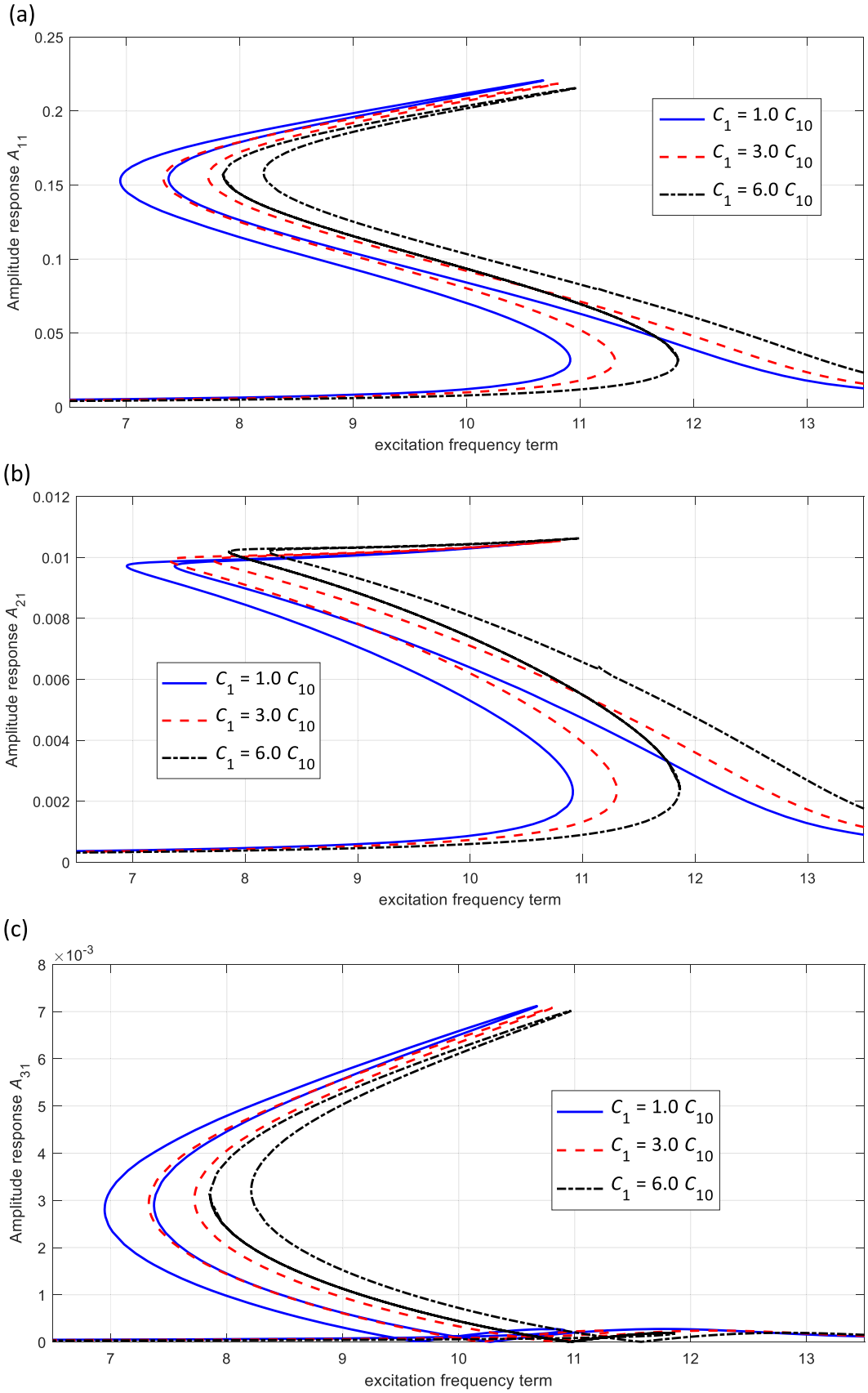

Fig. 14. Influence of the first Mooney-Rivlin hyperelastic coefficient (C_1) on the transverse amplitude-frequency response of functionally porous-hyperelastic beams for the (a) first, (b) second and (c) third dynamic coordinates.

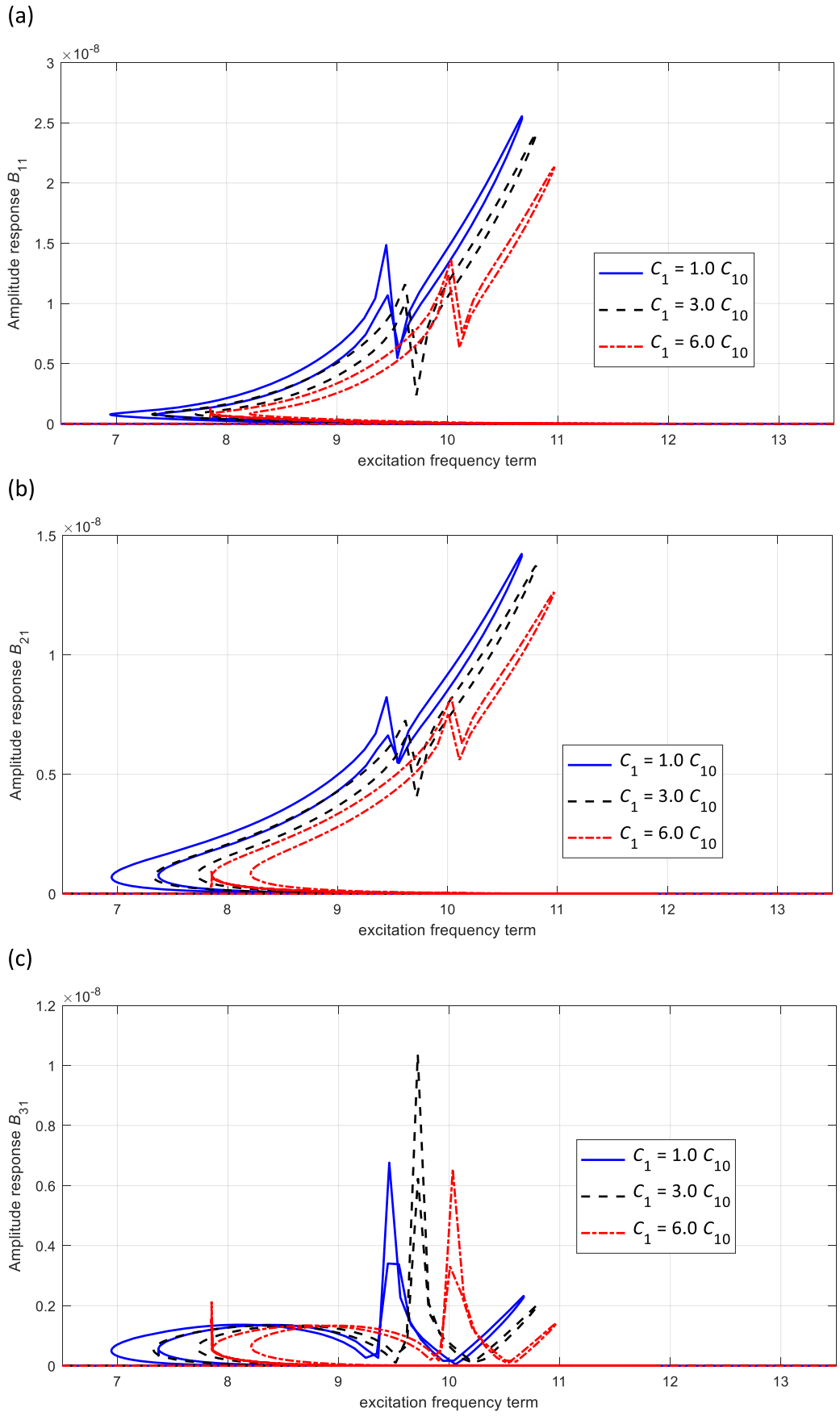

Fig. 15. Influence of the first Mooney-Rivlin hyperelastic coefficient (C_1) on the axial amplitude-frequency response of functionally porous-hyperelastic beams for the (a) first, (b) second and (c) third dynamic coordinates.

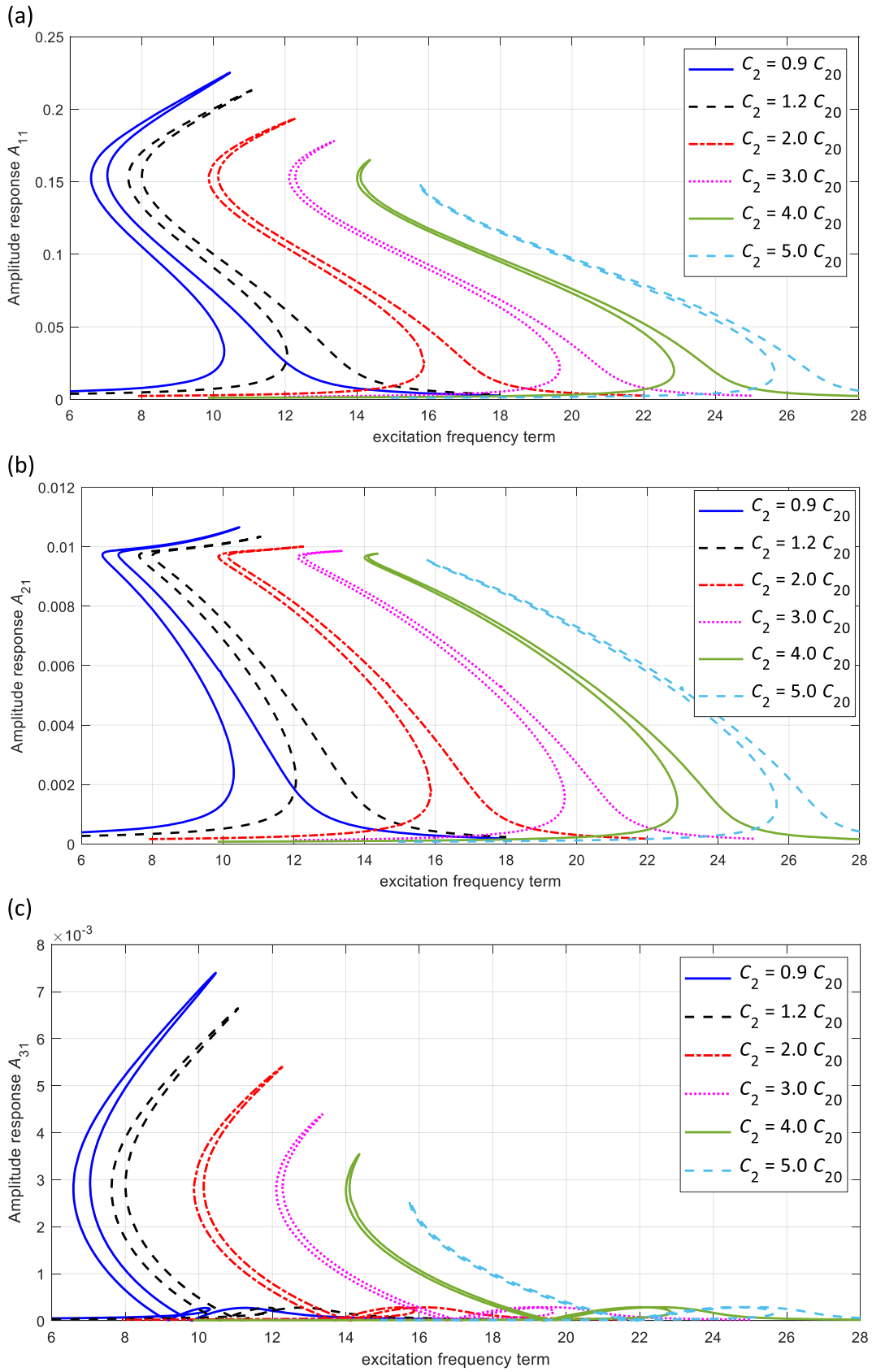

Fig. 16. Influence of the second Mooney-Rivlin hyperelastic coefficient (C_2) on the transverse amplitude-frequency response of functionally porous-hyperelastic beams for the (a) first, (b) second and (c) third dynamic coordinates.

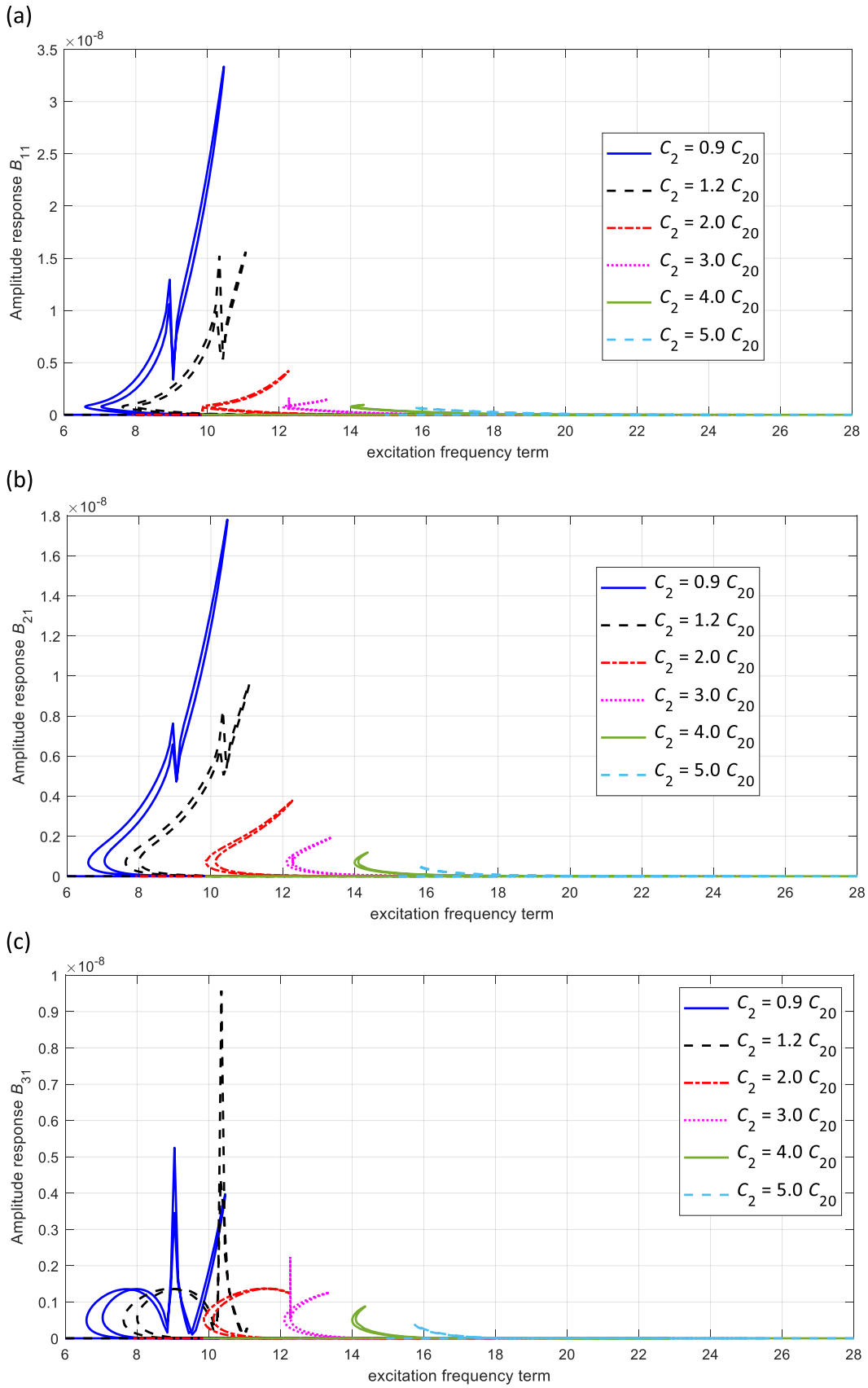

Fig. 17. Influence of the second Mooney-Rivlin hyperelastic coefficient (C_2) on the axial amplitude-frequency response of functionally porous-hyperelastic beams for the (a) first, (b) second and (c) third dynamic coordinates.

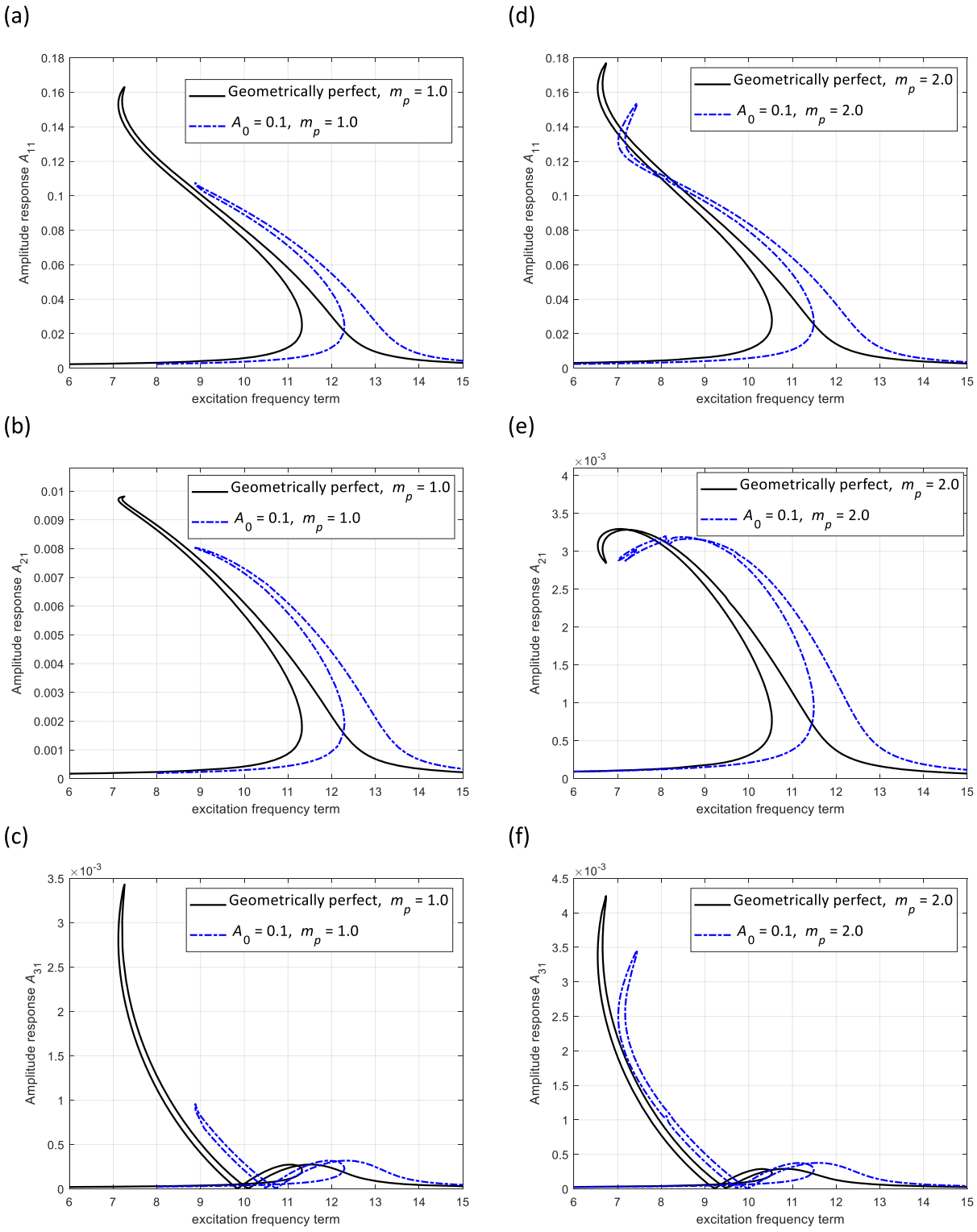

Fig. 18. Comparison of the transverse amplitude-frequency response of geometrically perfect and imperfect powerlaw porous-hyperelastic beams for the (a) first, (b) second and (c) third dynamic coordinates with $m_p = 1.0$ and the (d) first, (e) second and (f) third dynamic coordinates with $m_p = 2.0$.

fabrication procedure or the working environment. In Appendix B (Eqs. (B.1) and (B.2)), it is shown that the geometrical imperfection has a significant effect in adding nonlinear and linear terms to the equations of motion of these structures. To clarify the effects of these terms, Figs. (18) and (19) show the first three dynamic coordinates of the transverse and axial motions for $m_p = 1$ and 2 and the nondimensional external force as $F = 0.75$; it can be seen that for both the models, the geometric nonlinearity has a significant effect in increasing the amplitude of the axial motion and the coupling between the transverse and axial motions—this demonstrates the importance of considering couple motion in analysing geometrical imperfect porous-hyperelastic beams. Besides, the geometrical

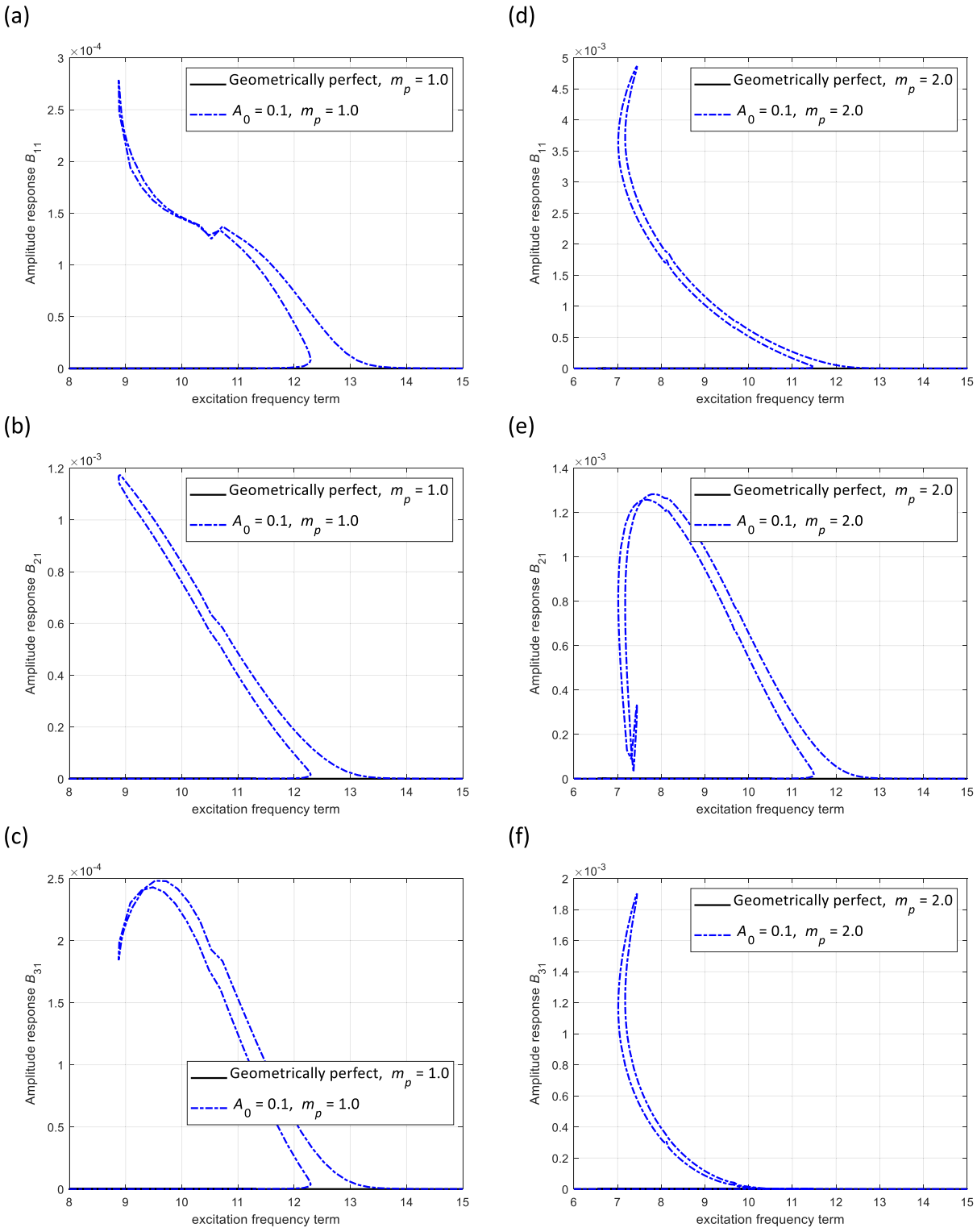

Fig. 19. Comparison of the axial amplitude-frequency response of geometrically perfect and imperfect powerlaw porous-hyperelastic beams for the (a) first, (b) second and (c) third dynamic coordinates with $m_p = 1.0$ and the (d) first, (e) second and (f) third dynamic coordinates with $m_p = 2.0$.

imperfection moves the frequency response to higher frequencies.

- Power-law porosity

For a geometrically imperfect ($A_0 = 0.1$) porous-hyperelastic beam with power-law porosity variation through the length, the first three dynamic coordinates of the transverse and axial motions are shown in Figs. (20) and (21) for $m_p = [0.2, 0.5, 1.0, \text{and } 2.0]$; this shows that increasing the power-law parameter causes higher amplitude for both axial and transverse first coordinates and shifts the

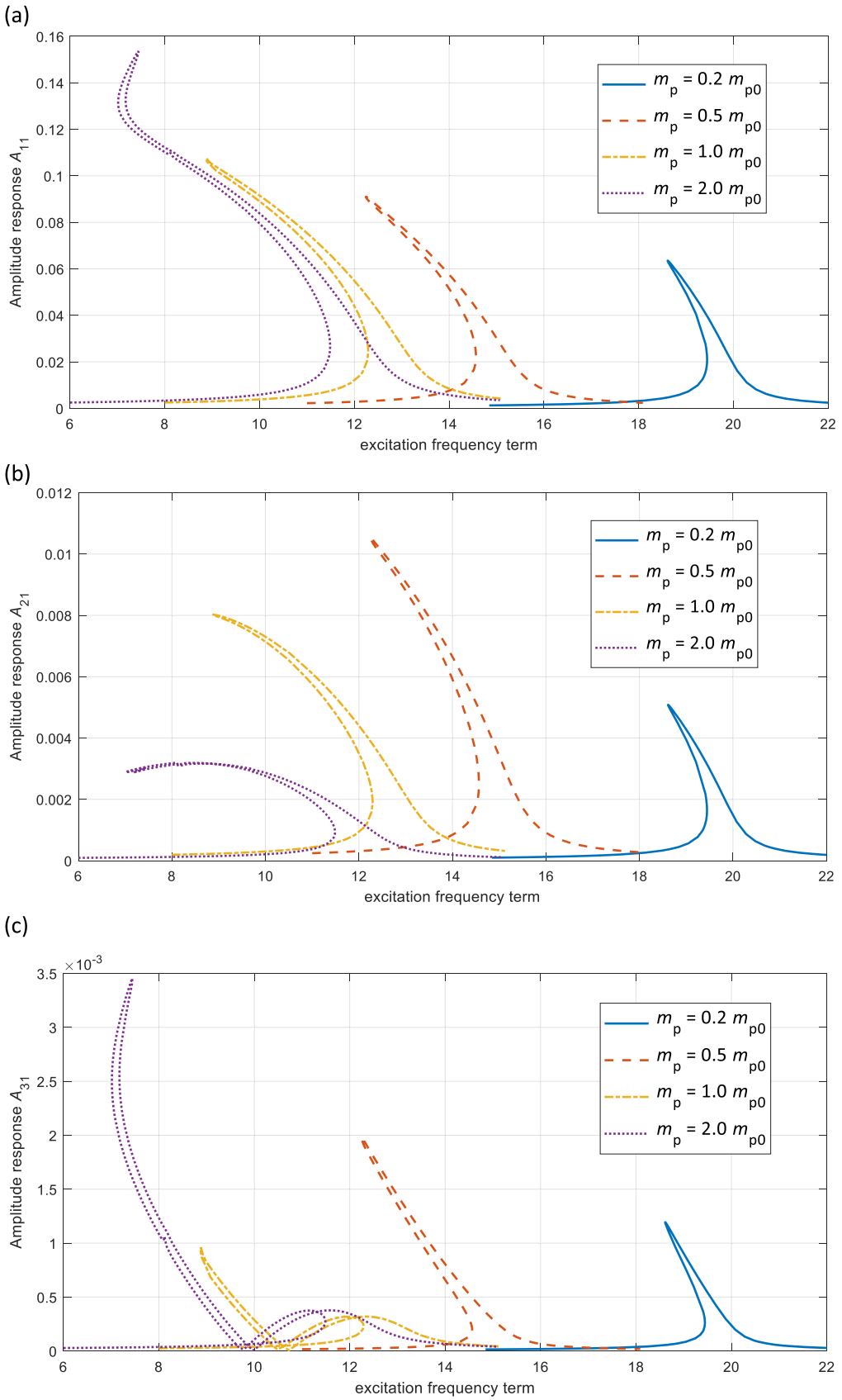

Fig. 20. Transverse amplitude-frequency response of geometrically imperfect power-law porous-hyperelastic beams for the (a) first, (b) second and (c) third dynamic coordinates.

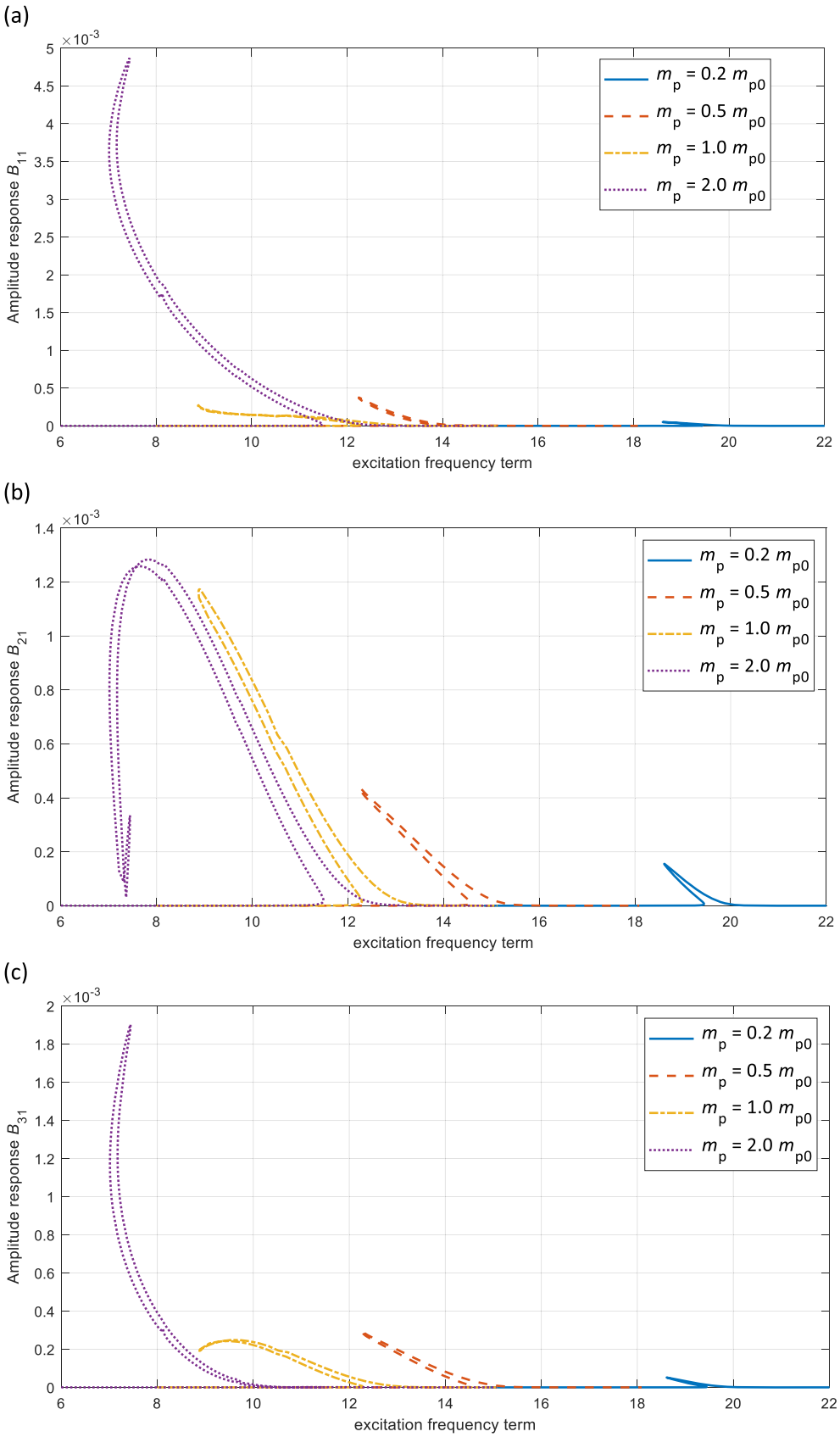

Fig. 21. Axial amplitude-frequency response of geometrically imperfect power-law porous-hyperelastic beams for the (a) first, (b) second and (c) third dynamic coordinates.

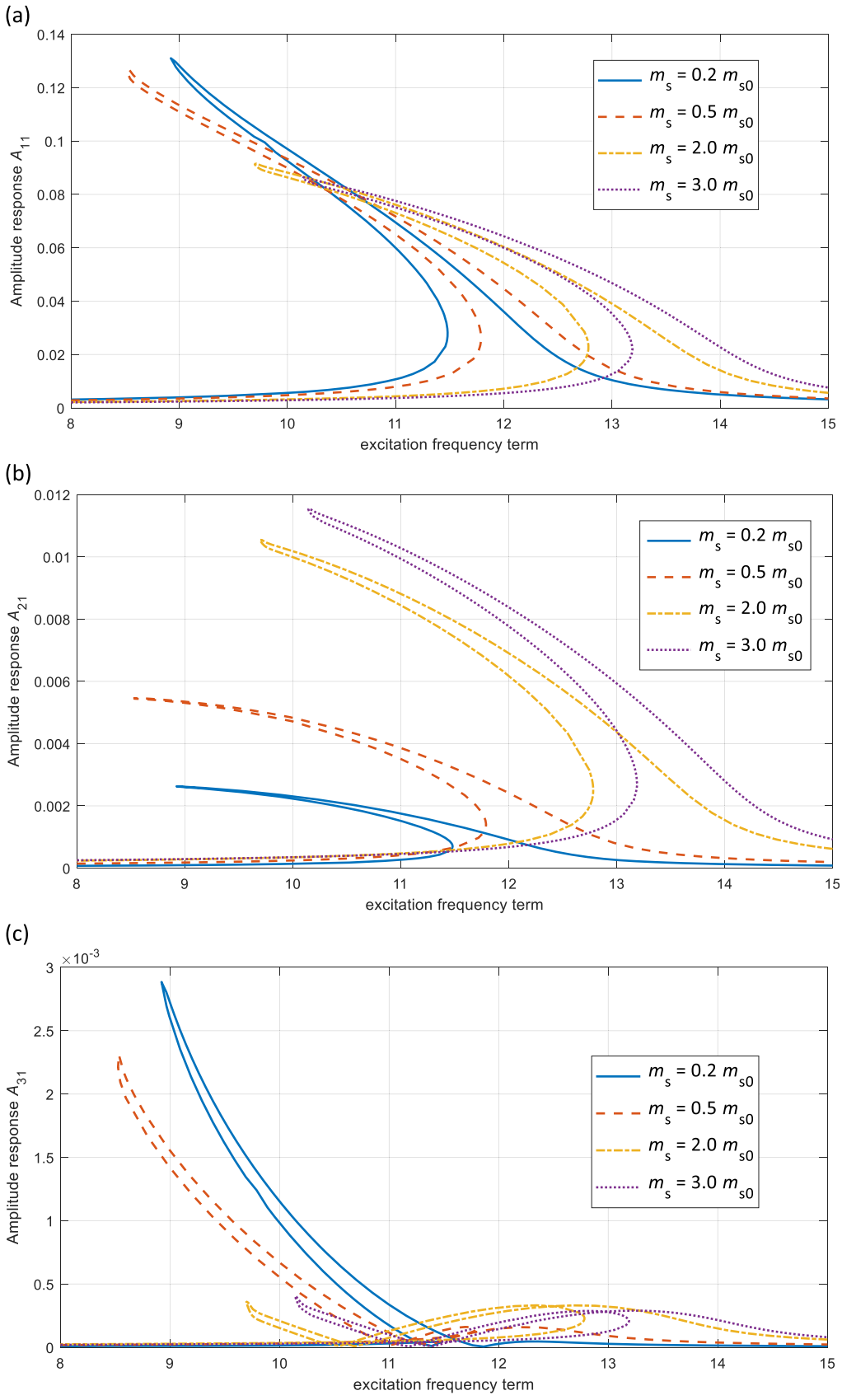

Fig. 22. Transverse amplitude-frequency response of geometrically imperfect sigmoid porous-hyperelastic beams for the (a) first, (b) second and (c) third dynamic coordinates.

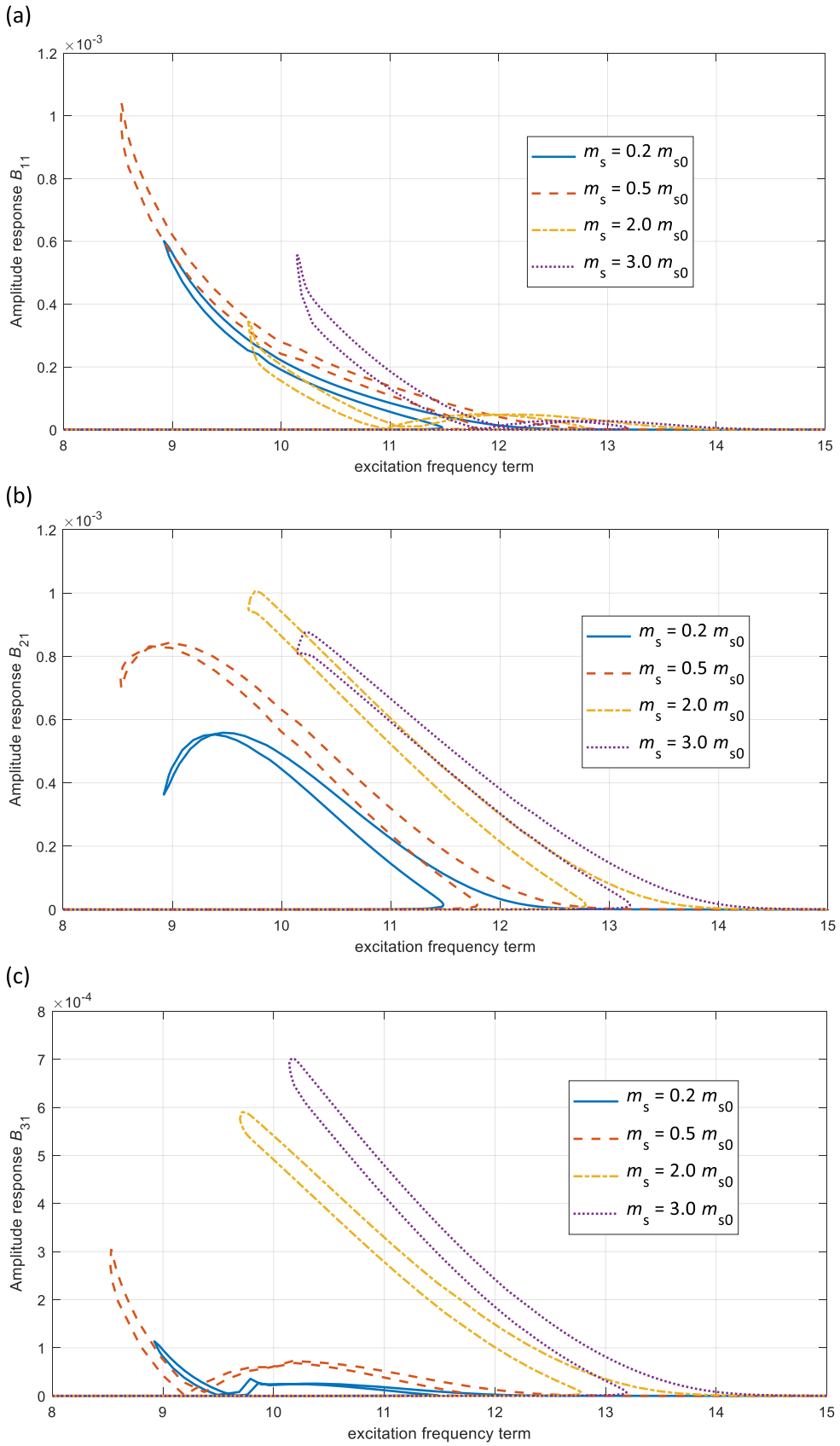

Fig. 23. Axial amplitude-frequency response of geometrically imperfect sigmoid porous-hyperelastic beams for the (a) first, (b) second and (c) third dynamic coordinates.

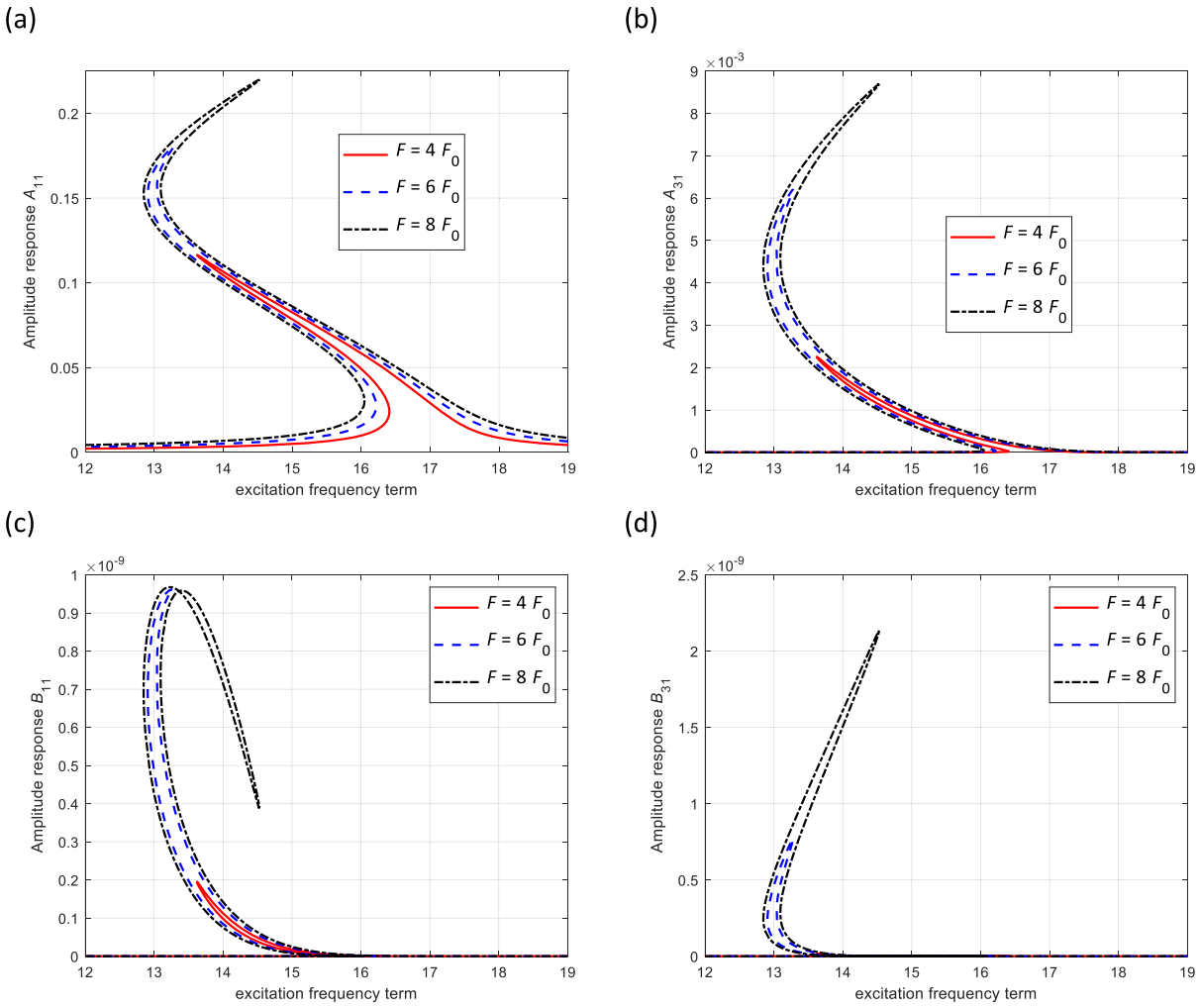

Fig. 24. Influence of the external excitation force on the amplitude-frequency response of uniformly porous-hyperelastic beams for the (a) first and (b) third transverse dynamic coordinates and the (c) first and (d) third axial dynamic coordinates.

resonance to lower frequencies. The reason for this behaviour can be seen in Fig. (5) which by increasing the power-law term, the infill rate increases leading to stiffer behaviour in the structure.

- Sigmoid porosity

Moreover, for sigmoid porosity variation through the length of the geometrical imperfect beam, the frequency response of the porous-hyperelastic beam is shown in Figs. (22) and (23) for the transverse and axial coordinates, respectively by varying the sigmoid porosity as $m_s = [0.2, 0.5, 2.0, \text{and } 3.0]$. The nonlinear frequency shows less sensitivity to the sigmoid function compare to the power-law porosity model for the given porous-hyperelastic beam as it can be seen from Fig. (5). Besides, increasing the sigmoid parameter from 0.2 to 3.0 increases the coupling between the first two transverse dynamic coordinates and decreases the effect of the third transverse coordinate. Comparing the sigmoid and power-law models, it can be seen that for the given case study, the contribution of the second axial generalised coordinate in the sigmoid model is higher than the power-law model and, in some cases, it overtakes the first coordinate in magnitude.

5.5. External force effect

The external excitation force on the structure plays an important role in varying the nonlinear mechanics of the porous-hyperelastic beams. To demonstrate this effect, the nondimensional external load is defined as $F_0 = 0.25$ and the effects on the nonlinear vibration response of porous-hyperelastic beams with uniform ($\alpha_0 = 0.8$) and functional ($m_p = 1$) porosity is analysed. Figs. (24) and (25) show the amplitude-frequency response of uniform and functionally porous-hyperelastic beams for coupled dynamic coordinates, respectively; it can be seen that for the functionally porous model, the axial coordinates are relatively more affected by increasing the force compared to the transverse coordinates. For both uniform and functionally porous models, the porous-hyperelastic beam shows a stiffness softening behaviour in their first three transverse coordinates while increasing this force leads to a combination of softening/hardening behaviour. For axial dynamic coordinates shown in Fig. (25), it can be seen that there is a local loss in the amplitude of the

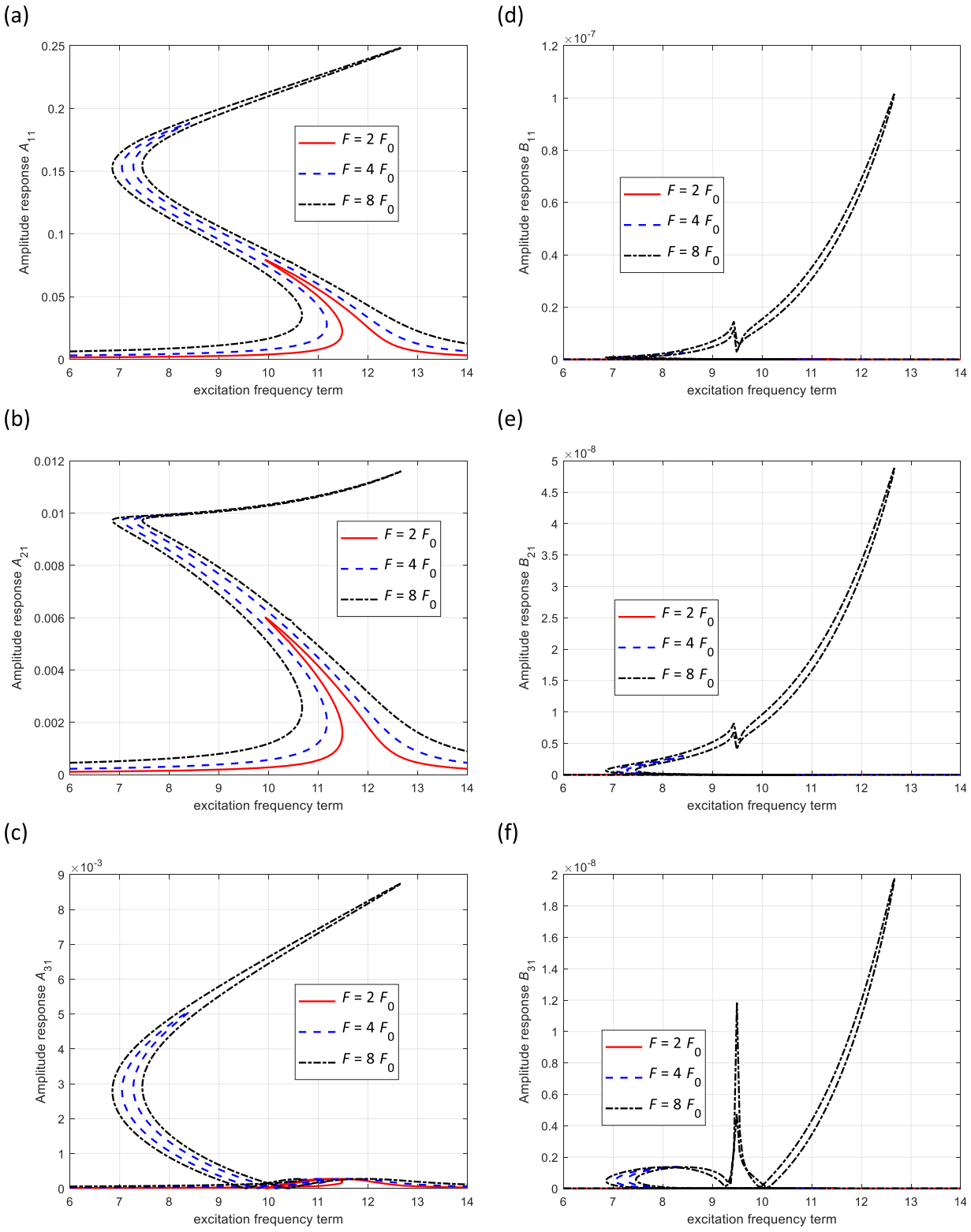

Fig. 25. Influence of the external excitation force on the amplitude-frequency response of functionally porous-hyperelastic beams for the (a) first, (b) second and (c) third transverse dynamic coordinates and the (d) first, (e) second and (f) third axial dynamic coordinates.

first two dynamic coordinates while the third dynamic coordinate increases significantly which physically shows the energy transmission from the first two axial coordinates to the third coordinate.

6. Summary and conclusion

The nonlinear dynamics of imperfect porous-hyperelastic beams have been investigated in this paper by a combination of

experimental characterisation and theoretical analysis. Different dumbbell samples were fabricated using thermal polyurethane filament and a 3D-printing machine following the dimensions given in ASTM D638 standard with different hexagonal infill rates. For each infill rate, samples are tested and the stress-strain curves are obtained following the standard; it is shown that by increasing the porosity (decreasing the infill rate), the stiffness of the samples decreases nonlinearly but the form of the porous-hyperelastic behaviour remains.

Using the experimental results for porous-hyperelasticity and porosity imperfection, a general strain energy density model is provided based on the Mooney-Rivlin model with porosity dependent coefficients. By using this nonlinear porous-hyperelastic model, soft imperfect beams are formulated by assuming the possibility of porosity variation through the longitudinal direction following a power-law or sigmoid function. Besides, the geometrical imperfection and large nonlinear deformations are considered to accurately model the deformations of soft components. Coupled transverse-longitudinal equations of motion are derived by employing Hamilton's principle showing higher-order nonlinear terms derived from the nonuniform porosity, hyperelasticity and geometrical imperfection. The equations of motion are solved using a dynamic equilibrium technique and a Galerkin's scheme. From the case studies reported in this paper, it is concluded that:

- The porosity type (uniform or functional through the length) have a significant effect in varying the nonlinear dynamic response which by increasing the porosity (decreasing the infill rate parameter), the stiffness softening behaviour turns into a combination of softening and hardening behaviour for the first transverse coordinate.
- The axial coordinate terms show a significant increase in magnitude by considering a small amount of geometrical imperfection. This shows the importance of considering both axial and transverse motions when analysing the geometrical imperfect porous-hyperelastic beam.
- For the studied uniformly porous model, decreasing the infill rate (increasing the porosity) moves the resonance peak to lower frequencies and increases the maximum amplitude. These effects are more severe for higher infill rates.
- By comparing the functional porosity models of power-law and sigmoid, it is shown that the frequency response of the structure is more sensitive to the power-law model.
- Increasing the power-law parameter for functional porosity through the length moves the amplitude peak to lower frequencies for the studied model and increases the amplitude of the first transverse dynamic coordinate. However, decreasing the sigmoid term in the functionally porous model decreases the amplitude of the first transverse dynamic coordinate and increases the amplitude of the second coordinate showing a higher coupling between the first and second coordinates.
- Porous-hyperelastic coefficients of the model, which are defined as a function of porosity in a Mooney-Rivlin based model have shown a great influence in changing the mechanical behaviour of the structure. For all the studied cases (uniform and functionally porous models), it is shown that increasing either porous-hyperelastic coefficients moves the resonance peak to higher frequencies and decreases the amplitude peak of the first transverse dynamic coordinate.
- By comparing the results obtained for geometrically perfect and imperfect porous-hyperelastic beams, it is seen that the geometrically imperfect beam model has a lower maximum amplitude for the first transverse coordinate and significantly higher for the axial coordinates. Besides, for the given model, the maximum amplitude moves to higher frequencies by considering the geometrical imperfection in the modelling.
- The applied external force has an important role in changing the stiffness softening behaviour of the model to a combination of softening and hardening which happens by increasing the magnitude of the force.
- Comparing the porous-hyperelastic beam's nonlinear response to available studies on linear elastic structures; it can be seen that conventional elastic structures either show a pure hardening or softening behaviour while for porous-hyperelastic structures, due to their material nonlinearity, a combination of softening and hardening behaviour with a rich resonant response is obtained.

CRediT authorship contribution statement

Hossein B. Khaniki: Conceptualization, Methodology, Investigation, Software, Visualization, Formal analysis, Validation, Writing – original draft, Writing – review & editing. **Mergen H. Ghayesh:** Conceptualization, Investigation, Methodology, Supervision, Writing – review & editing. **Rey Chin:** Supervision, Writing – review & editing. **Marco Amabili:** Conceptualization, Investigation, Writing – review & editing.

Declaration of Competing Interest

The authors declare that they have no known competing financial interests or personal relationships that could have appeared to influence the work reported in this paper.

Acknowledgments

This work was supported with supercomputing resources provided by the Phoenix HPC service at the University of Adelaide. The scholarship support through The University of Adelaide and Faculty of Engineering, Computer & Mathematical Sciences, The University of Adelaide is also acknowledged.

Appendix A

Fig. A1

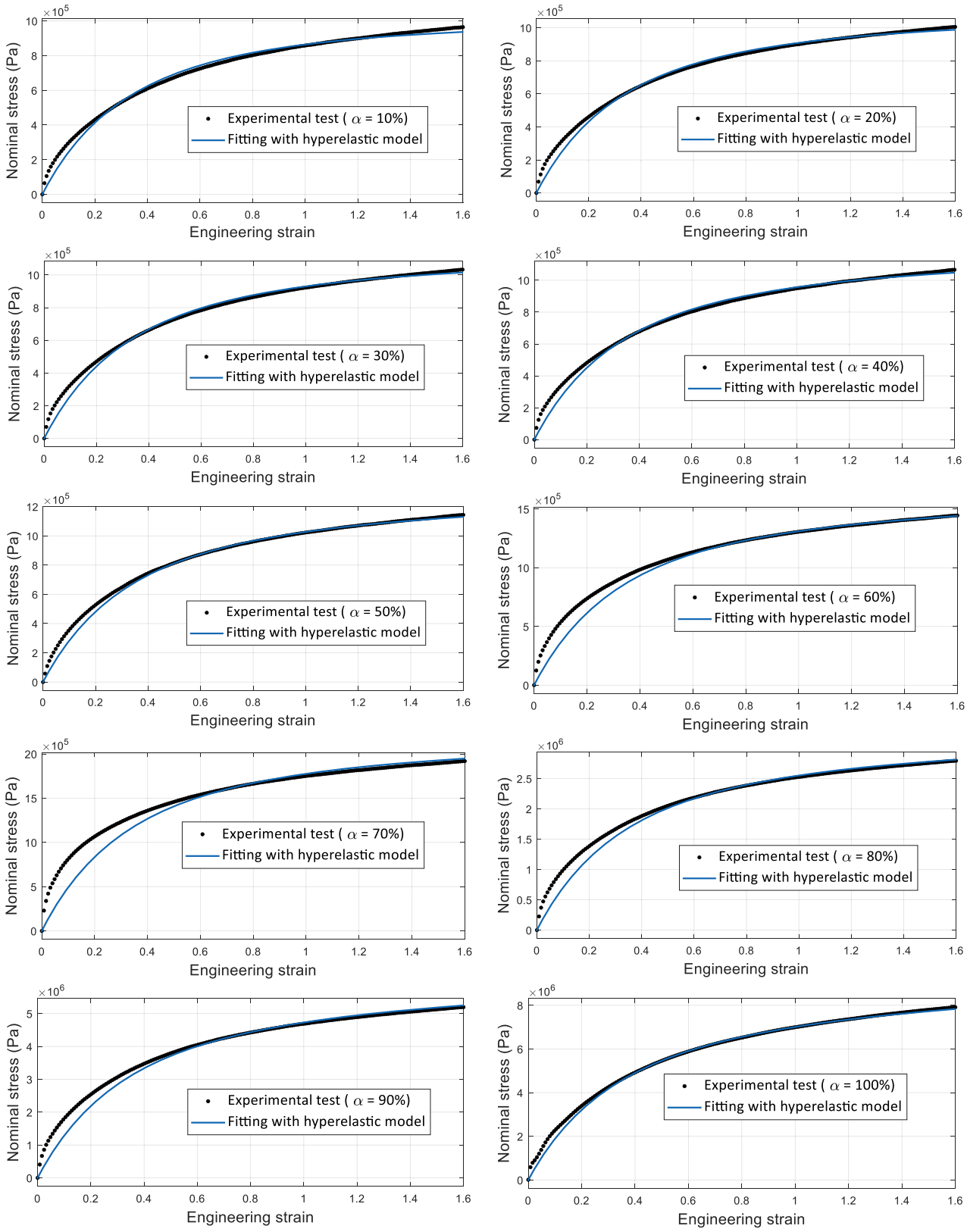

Fig. A1. Curve fitting results for porous-hyperelastic samples with different infill rates via the Mooney-Rivlin model.

Appendix B

The equations of motion are obtained as

$$
\begin{aligned}
&\rho(x)Au_{tt} - A[6C_1(x) + 6C_2(x)]\left(\frac{\partial^2 u}{\partial x^2} + \frac{\partial w}{\partial x}\frac{\partial^2 w}{\partial x^2} - \frac{\partial^2 w}{\partial x^2}\frac{dw_0}{dx} - \frac{\partial w}{\partial x}\frac{d^2 w_0}{dx^2}\right)\\
&+2A[6C_1(x) + 12C_2(x)]\left(\frac{\partial u}{\partial x} + \frac{1}{2}\left(\frac{\partial w}{\partial x}\right)^2 - \frac{\partial w}{\partial x}\frac{dw_0}{dx}\right)\left(\begin{array}{l}\frac{\partial^2 u}{\partial x^2} + \frac{\partial w}{\partial x}\frac{\partial^2 w}{\partial x^2}\\ \\ -\frac{\partial^2 w}{\partial x^2}\frac{dw_0}{dx} - \frac{\partial w}{\partial x}\frac{d^2 w_0}{dx^2}\end{array}\right)\\
&+2I_2[6C_1(x) + 12C_2(x)]\left(\frac{\partial^2 w}{\partial x^2}\frac{\partial^3 w}{\partial x^3}\right)\\
&-3A[8C_1(x) + 20C_2(x)]\left(\begin{array}{l}\frac{\partial^2 u}{\partial x^2} + \frac{\partial w}{\partial x}\frac{\partial^2 w}{\partial x^2}\\ \\ -\frac{\partial^2 w}{\partial x^2}\frac{dw_0}{dx} - \frac{\partial w}{\partial x}\frac{d^2 w_0}{dx^2}\end{array}\right)\left(\frac{\partial u}{\partial x} + \frac{1}{2}\left(\frac{\partial w}{\partial x}\right)^2 - \frac{\partial w}{\partial x}\frac{dw_0}{dx}\right)^2\\
&-3I_2[8C_1(x) + 20C_2(x)]\left(\frac{\partial^2 u}{\partial x^2} + \frac{\partial w}{\partial x}\frac{\partial^2 w}{\partial x^2} - \frac{\partial^2 w}{\partial x^2}\frac{dw_0}{dx} - \frac{\partial w}{\partial x}\frac{d^2 w_0}{dx^2}\right)\left(\frac{\partial^2 w}{\partial x^2}\right)^2\\
&-6I_2[8C_1(x) + 20C_2(x)]\left(\frac{\partial u}{\partial x} + \frac{1}{2}\left(\frac{\partial w}{\partial x}\right)^2 - \frac{\partial w}{\partial x}\frac{dw_0}{dx}\right)\left(\frac{\partial^2 w}{\partial x^2}\frac{\partial^3 w}{\partial x^3}\right)\\
&-A\left[6\frac{\partial C_1(x)}{\partial x} + 6\frac{\partial C_2(x)}{\partial x}\right]\left(\frac{\partial u}{\partial x} + \frac{1}{2}\left(\frac{\partial w}{\partial x}\right)^2 - \frac{\partial w}{\partial x}\frac{dw_0}{dx}\right)\\
&+A\left[6\frac{\partial C_1(x)}{\partial x} + 12\frac{\partial C_2(x)}{\partial x}\right]\left(\frac{\partial u}{\partial x} + \frac{1}{2}\left(\frac{\partial w}{\partial x}\right)^2 - \frac{\partial w}{\partial x}\frac{dw_0}{dx}\right)^2\\
&+I_2\left[6\frac{\partial C_1(x)}{\partial x} + 12\frac{\partial C_2(x)}{\partial x}\right]\left(\frac{\partial^2 w}{\partial x^2}\right)^2\\
&-A\left[8\frac{\partial C_1(x)}{\partial x} + 20\frac{\partial C_2(x)}{\partial x}\right]\left(\frac{\partial u}{\partial x} + \frac{1}{2}\left(\frac{\partial w}{\partial x}\right)^2 - \frac{\partial w}{\partial x}\frac{dw_0}{dx}\right)^3\\
&-3I_2\left[8\frac{\partial C_1(x)}{\partial x} + 20\frac{\partial C_2(x)}{\partial x}\right]\left(\frac{\partial u}{\partial x} + \frac{1}{2}\left(\frac{\partial w}{\partial x}\right)^2 - \frac{\partial w}{\partial x}\frac{dw_0}{dx}\right)\left(\frac{\partial^2 w}{\partial x^2}\right)^2 = 0,
\end{aligned}
\tag{B.1}
$$

Eqs. (B.1) and (B.2) are nondimensionalised using the new parameters given in Eq. (16) and rewritten as

$$
\begin{aligned}
&\ldots - A[8C_1(x)+20C_2(x)]\left(\frac{\partial u}{\partial x}+\frac{1}{2}\left(\frac{\partial w}{\partial x}\right)^2-\frac{\partial w}{\partial x}\frac{dw_0}{dx}\right)^3\left(\frac{\partial^2 w}{\partial x^2}-\frac{d^2w_0}{dx^2}\right)\\
&+3I_2[8C_1(x)+20C_2(x)]\frac{\partial^2}{\partial x^2}\left(\left(\frac{\partial u}{\partial x}+\frac{1}{2}\left(\frac{\partial w}{\partial x}\right)^2-\frac{\partial w}{\partial x}\frac{dw_0}{dx}\right)^2\left(\frac{\partial^2 w}{\partial x^2}\right)\right)\\
&+3I_4[8C_1(x)+20C_2(x)]\left(2\left(\frac{\partial^2 w}{\partial x^2}\right)\left(\frac{\partial^3 w}{\partial x^3}\right)^2+\left(\frac{\partial^2 w}{\partial x^2}\right)^2\left(\frac{\partial^4 w}{\partial x^4}\right)\right)\\
&+2I_2\left[6\frac{\partial C_1(x)}{\partial x}+6\frac{\partial C_2(x)}{\partial x}\right]\left(\frac{\partial^3 w}{\partial x^3}\right)\\
&-A\left[6\frac{\partial C_1(x)}{\partial x}+6\frac{\partial C_2(x)}{\partial x}\right]\left(\frac{\partial u}{\partial x}+\frac{1}{2}\left(\frac{\partial w}{\partial x}\right)^2-\frac{\partial w}{\partial x}\frac{dw_0}{dx}\right)\left(\frac{\partial w}{\partial x}-\frac{dw_0}{dx}\right)\\
&+A\left[6\frac{\partial C_1(x)}{\partial x}+12\frac{\partial C_2(x)}{\partial x}\right]\left(\frac{\partial u}{\partial x}+\frac{1}{2}\left(\frac{\partial w}{\partial x}\right)^2-\frac{\partial w}{\partial x}\frac{dw_0}{dx}\right)^2\left(\frac{\partial w}{\partial x}-\frac{dw_0}{dx}\right)\\
&+I_2\left[6\frac{\partial C_1(x)}{\partial x}+12\frac{\partial C_2(x)}{\partial x}\right]\left(\frac{\partial^2 w}{\partial x^2}\right)^2\left(\frac{\partial w}{\partial x}-\frac{dw_0}{dx}\right)\\
&\left[6\frac{\partial C_1(x)}{\partial x}+12\frac{\partial C_2(x)}{\partial x}\right]\frac{\partial}{\partial x}\left(\left(\frac{\partial u}{\partial x}+\frac{1}{2}\left(\frac{\partial w}{\partial x}\right)^2-\frac{\partial w}{\partial x}\frac{dw_0}{dx}\right)\left(\frac{\partial^2 w}{\partial x^2}\right)\right)\\
&-3I_2\left[8\frac{\partial C_1(x)}{\partial x}+20\frac{\partial C_2(x)}{\partial x}\right]\left(\frac{\partial u}{\partial x}+\frac{1}{2}\left(\frac{\partial w}{\partial x}\right)^2-\frac{\partial w}{\partial x}\frac{dw_0}{dx}\right)\left(\frac{\partial^2 w}{\partial x^2}\right)^2\left(\frac{\partial w}{\partial x}-\frac{dw_0}{dx}\right)\\
&-A\left[8\frac{\partial C_1(x)}{\partial x}+20\frac{\partial C_2(x)}{\partial x}\right]\left(\frac{\partial u}{\partial x}+\frac{1}{2}\left(\frac{\partial w}{\partial x}\right)^2-\frac{\partial w}{\partial x}\frac{dw_0}{dx}\right)^3\left(\frac{\partial w}{\partial x}-\frac{dw_0}{dx}\right)\\
&+6I_2\left[8\frac{\partial C_1(x)}{\partial x}+20\frac{\partial C_2(x)}{\partial x}\right]\frac{\partial}{\partial x}\left(\left(\frac{\partial u}{\partial x}+\frac{1}{2}\left(\frac{\partial w}{\partial x}\right)^2-\frac{\partial w}{\partial x}\frac{dw_0}{dx}\right)^2\left(\frac{\partial^2 w}{\partial x^2}\right)\right)\\
&+6I_4\left[8\frac{\partial C_1(x)}{\partial x}+20\frac{\partial C_2(x)}{\partial x}\right]\left(\frac{\partial^2 w}{\partial x^2}\right)^2\left(\frac{\partial^3 w}{\partial x^3}\right)\\
&+I_2\left[6\frac{\partial^2 C_1(x)}{\partial x^2}+6\frac{\partial^2 C_2(x)}{\partial x^2}\right]\left(\frac{\partial^2 w}{\partial x^2}\right)\\
&-2I_2\left[6\frac{\partial^2 C_1(x)}{\partial x^2}+12\frac{\partial^2 C_2(x)}{\partial x^2}\right]\left(\frac{\partial u}{\partial x}+\frac{1}{2}\left(\frac{\partial w}{\partial x}\right)^2-\frac{\partial w}{\partial x}\frac{dw_0}{dx}\right)\left(\frac{\partial^2 w}{\partial x^2}\right)\\
&+3I_2\left[8\frac{\partial^2 C_1(x)}{\partial x^2}+20\frac{\partial^2 C_2(x)}{\partial x^2}\right]\left(\left(\frac{\partial u}{\partial x}+\frac{1}{2}\left(\frac{\partial w}{\partial x}\right)^2-\frac{\partial w}{\partial x}\frac{dw_0}{dx}\right)^2\left(\frac{\partial^2 w}{\partial x^2}\right)\right)\\
&+I_4\left[8\frac{\partial^2 C_1(x)}{\partial x^2}+20\frac{\partial^2 C_2(x)}{\partial x^2}\right]\left(\frac{\partial^2 w}{\partial x^2}\right)^3=F\cos(\omega t).
\end{aligned}
\tag{B.2}
$$

$$
\begin{aligned}
&\rho(x)u_{tt} - {\gamma_2}^2[6C_1(x) + 6C_2(x)]\left(\frac{\partial^2 u}{\partial x^2} + \eta\frac{\partial w}{\partial x}\frac{\partial^2 w}{\partial x^2} - \eta\frac{\partial^2 w}{\partial x^2}\frac{dw_0}{dx} - \eta\frac{\partial w}{\partial x}\frac{d^2 w_0}{dx^2}\right)\\
&+2{\gamma_2}^2[6C_1(x) + 12C_2(x)]\left(\eta\frac{\partial u}{\partial x} + \frac{1}{2}\eta^2\left(\frac{\partial w}{\partial x}\right)^2 - \eta^2\frac{\partial w}{\partial x}\frac{dw_0}{dx}\right)\left(\begin{array}{l}\frac{\partial^2 u}{\partial x^2} + \eta\frac{\partial w}{\partial x}\frac{\partial^2 w}{\partial x^2}\\ \\ -\eta\frac{\partial^2 w}{\partial x^2}\frac{dw_0}{dx} - \eta\frac{\partial w}{\partial x}\frac{d^2 w_0}{dx^2}\end{array}\right)\\
&+2\eta[6C_1(x) + 12C_2(x)]\left(\frac{\partial^2 w}{\partial x^2}\frac{\partial^3 w}{\partial x^3}\right)\\
&-3{\gamma_2}^2[8C_1(x) + 20C_2(x)]\left(\begin{array}{l}\frac{\partial^2 u}{\partial x^2} + \eta\frac{\partial w}{\partial x}\frac{\partial^2 w}{\partial x^2}\\ \\ -\eta\frac{\partial^2 w}{\partial x^2}\frac{dw_0}{dx} - \eta\frac{\partial w}{\partial x}\frac{d^2 w_0}{dx^2}\end{array}\right)\left(\eta\frac{\partial u}{\partial x} + \frac{1}{2}\eta^2\left(\frac{\partial w}{\partial x}\right)^2 - \eta^2\frac{\partial w}{\partial x}\frac{dw_0}{dx}\right)^2\\
&-3[8C_1(x) + 20C_2(x)]\left(\frac{\partial^2 u}{\partial x^2} + \eta\frac{\partial w}{\partial x}\frac{\partial^2 w}{\partial x^2} - \eta\frac{\partial^2 w}{\partial x^2}\frac{dw_0}{dx} - \eta\frac{\partial w}{\partial x}\frac{d^2 w_0}{dx^2}\right)\left(\frac{\partial^2 w}{\partial x^2}\right)^2 \qquad \text{(B.3)}\\
&-6[8C_1(x) + 20C_2(x)]\left(\frac{\partial u}{\partial x} + \frac{1}{2}\eta\left(\frac{\partial w}{\partial x}\right)^2 - \eta\frac{\partial w}{\partial x}\frac{dw_0}{dx}\right)\left(\frac{\partial^2 w}{\partial x^2}\frac{\partial^3 w}{\partial x^3}\right)\\
&-{\gamma_2}^2\left[6\frac{\partial C_1(x)}{\partial x} + 6\frac{\partial C_2(x)}{\partial x}\right]\left(\frac{\partial u}{\partial x} + \frac{1}{2}\eta\left(\frac{\partial w}{\partial x}\right)^2 - \eta\frac{\partial w}{\partial x}\frac{dw_0}{dx}\right)\\
&+{\gamma_2}^2\left[6\frac{\partial C_1(x)}{\partial x} + 12\frac{\partial C_2(x)}{\partial x}\right]\left(\frac{\partial u}{\partial x} + \frac{1}{2}\eta\left(\frac{\partial w}{\partial x}\right)^2 - \eta\frac{\partial w}{\partial x}\frac{dw_0}{dx}\right)^2\\
&+\eta\left[6\frac{\partial C_1(x)}{\partial x} + 12\frac{\partial C_2(x)}{\partial x}\right]\left(\frac{\partial^2 w}{\partial x^2}\right)^2\\
&-{\gamma_2}^2\frac{1}{\eta}\left[8\frac{\partial C_1(x)}{\partial x} + 20\frac{\partial C_2(x)}{\partial x}\right]\left(\eta\frac{\partial u}{\partial x} + \frac{1}{2}\eta^2\left(\frac{\partial w}{\partial x}\right)^2 - \eta^2\frac{\partial w}{\partial x}\frac{dw_0}{dx}\right)^3\\
&-3\left[8\frac{\partial C_1(x)}{\partial x} + 20\frac{\partial C_2(x)}{\partial x}\right]\left(\frac{\partial u}{\partial x} + \frac{1}{2}\eta\left(\frac{\partial w}{\partial x}\right)^2 - \eta\frac{\partial w}{\partial x}\frac{dw_0}{dx}\right)\left(\frac{\partial^2 w}{\partial x^2}\right)^2 = 0,
\end{aligned}
$$

$$
\begin{aligned}
&\ldots\\
&-{\gamma_2}^2[8C_1(x)+20C_2(x)]\left(\eta\frac{\partial u}{\partial x}+\frac{1}{2}\eta^2\left(\frac{\partial w}{\partial x}\right)^2-\eta^2\frac{\partial w}{\partial x}\frac{dw_0}{dx}\right)^3\left(\frac{\partial^2 w}{\partial x^2}-\frac{d^2w_0}{dx^2}\right)\\
&+3[8C_1(x)+20C_2(x)]\frac{\partial^2}{\partial x^2}\left(\left(\eta\frac{\partial u}{\partial x}+\frac{1}{2}\eta^2\left(\frac{\partial w}{\partial x}\right)^2-\eta^2\frac{\partial w}{\partial x}\frac{dw_0}{dx}\right)^2\left(\frac{\partial^2 w}{\partial x^2}\right)\right)\\
&+3{\gamma_4}^2\eta^2[8C_1(x)+20C_2(x)]\left(2\left(\frac{\partial^2 w}{\partial x^2}\right)\left(\frac{\partial^3 w}{\partial x^3}\right)^2+\left(\frac{\partial^2 w}{\partial x^2}\right)^2\left(\frac{\partial^4 w}{\partial x^4}\right)\right)\\
&+2\left[6\frac{\partial C_1(x)}{\partial x}+6\frac{\partial C_2(x)}{\partial x}\right]\left(\frac{\partial^3 w}{\partial x^3}\right)\\
&-{\gamma_2}^2\left[6\frac{\partial C_1(x)}{\partial x}+6\frac{\partial C_2(x)}{\partial x}\right]\left(\eta\frac{\partial u}{\partial x}+\frac{1}{2}\eta^2\left(\frac{\partial w}{\partial x}\right)^2-\eta^2\frac{\partial w}{\partial x}\frac{dw_0}{dx}\right)\left(\frac{\partial w}{\partial x}-\frac{dw_0}{dx}\right)\\
&+\left[6\frac{\partial C_1(x)}{\partial x}+12\frac{\partial C_2(x)}{\partial x}\right]\left(\begin{array}{l}{\gamma_2}^2\left(\eta\frac{\partial u}{\partial x}+\frac{1}{2}\eta^2\left(\frac{\partial w}{\partial x}\right)^2-\eta^2\frac{\partial w}{\partial x}\frac{dw_0}{dx}\right)^2\\ \\ +\eta^2\left(\frac{\partial^2 w}{\partial x^2}\right)^2\end{array}\right)\left(\frac{\partial w}{\partial x}-\frac{dw_0}{dx}\right)\\
&-4\left[6\frac{\partial C_1(x)}{\partial x}+12\frac{\partial C_2(x)}{\partial x}\right]\frac{\partial}{\partial x}\left(\left(\eta\frac{\partial u}{\partial x}+\frac{1}{2}\eta^2\left(\frac{\partial w}{\partial x}\right)^2-\eta^2\frac{\partial w}{\partial x}\frac{dw_0}{dx}\right)\left(\frac{\partial^2 w}{\partial x^2}\right)\right)\\
&-3\eta^2\left[8\frac{\partial C_1(x)}{\partial x}+20\frac{\partial C_2(x)}{\partial x}\right]\left(\eta\frac{\partial u}{\partial x}+\frac{1}{2}\eta^2\left(\frac{\partial w}{\partial x}\right)^2-\eta^2\frac{\partial w}{\partial x}\frac{dw_0}{dx}\right)\left(\frac{\partial^2 w}{\partial x^2}\right)^2\left(\frac{\partial w}{\partial x}-\frac{dw_0}{dx}\right)\\
&-{\gamma_2}^2\left[8\frac{\partial C_1(x)}{\partial x}+20\frac{\partial C_2(x)}{\partial x}\right]\left(\eta\frac{\partial u}{\partial x}+\frac{1}{2}\eta^2\left(\frac{\partial w}{\partial x}\right)^2-\eta^2\frac{\partial w}{\partial x}\frac{dw_0}{dx}\right)^3\left(\frac{\partial w}{\partial x}-\frac{dw_0}{dx}\right)\\
&+6\left[8\frac{\partial C_1(x)}{\partial x}+20\frac{\partial C_2(x)}{\partial x}\right]\frac{\partial}{\partial x}\left(\left(\eta\frac{\partial u}{\partial x}+\frac{1}{2}\eta^2\left(\frac{\partial w}{\partial x}\right)^2-\eta^2\frac{\partial w}{\partial x}\frac{dw_0}{dx}\right)^2\left(\frac{\partial^2 w}{\partial x^2}\right)\right)\\
&+6{\gamma_4}^2\eta^2\left[8\frac{\partial C_1(x)}{\partial x}+20\frac{\partial C_2(x)}{\partial x}\right]\left(\frac{\partial^2 w}{\partial x^2}\right)^2\left(\frac{\partial^3 w}{\partial x^3}\right)\\
&+\left[6\frac{\partial^2 C_1(x)}{\partial x^2}+6\frac{\partial^2 C_2(x)}{\partial x^2}\right]\left(\frac{\partial^2 w}{\partial x^2}\right)\\
&-2\left[6\frac{\partial^2 C_1(x)}{\partial x^2}+12\frac{\partial^2 C_2(x)}{\partial x^2}\right]\left(\left(\eta\frac{\partial u}{\partial x}+\frac{1}{2}\eta^2\left(\frac{\partial w}{\partial x}\right)^2-\eta^2\frac{\partial w}{\partial x}\frac{dw_0}{dx}\right)\left(\frac{\partial^2 w}{\partial x^2}\right)\right)\\
&+3\left[8\frac{\partial^2 C_1(x)}{\partial x^2}+20\frac{\partial^2 C_2(x)}{\partial x^2}\right]\left(\left(\eta\frac{\partial u}{\partial x}+\frac{1}{2}\eta^2\left(\frac{\partial w}{\partial x}\right)^2-\eta^2\frac{\partial w}{\partial x}\frac{dw_0}{dx}\right)^2\left(\frac{\partial^2 w}{\partial x^2}\right)\right)\\
&+{\gamma_4}^2\eta^2\left[8\frac{\partial^2 C_1(x)}{\partial x^2}+20\frac{\partial^2 C_2(x)}{\partial x^2}\right]\left(\frac{\partial^2 w}{\partial x^2}\right)^3=F\cos(\Omega t).
\end{aligned}
\tag{B.4}
$$

Appendix C

Coefficients of Eqs. (19) and (20) in Section 4 are defined as

$$M1_{li}=\int_0^1\chi_l(x)\rho(x)\chi_i(x)dx, \tag{C.1}$$

$$KL11_{li}=-{\gamma_2}^2\int_0^1\chi_l(x)\frac{d}{dx}\{[6C_1(x)+6C_2(x)]\chi'_i(x)\}dx, \tag{C.2}$$

$$KL12_{li} = \eta{\gamma_2}^2 \int_0^1 \chi_l(x) \frac{d}{dx}\{[6C_1(x)+6C_2(x)]{\xi'}_0(x){\xi'}_i(x)\}dx, \tag{C.3}$$

$$KN11_{lij} = \eta{\gamma_2}^2 \int_0^1 \chi_l(x) \frac{d}{dx}\{[6C_1(x)+12C_2(x)]{\chi'}_i(x){\chi'}_j(x)\}dx, \tag{C.4}$$

$$KN12_{lij} = -2\eta^2{\gamma_2}^2 \int_0^1 \chi_l(x) \frac{d}{dx}\{[6C_1(x)+12C_2(x)]{\chi'}_i(x){\xi'}_j(x){\xi'}_0(x)\}dx, \tag{C.5}$$

$$\begin{aligned} KN13_{lij} &= -\frac{1}{2}\eta{\gamma_2}^2 \int_0^1 \chi_l(x) \frac{d}{dx}\{[6C_1(x)+6C_2(x)]{\xi'}_i(x){\xi'}_j(x)\}dx \\ &+\eta^3{\gamma_2}^2 \int_0^1 \chi_l(x) \frac{d}{dx}\{[6C_1(x)+12C_2(x)]{\xi'}_0{}^2(x){\xi'}_i(x){\xi'}_j(x)\}dx \\ &+\eta{\gamma_2}^2 \int_0^1 \chi_l(x) \frac{d}{dx}\{[6C_1(x)+12C_2(x)]\xi_i''(x)\xi_j''(x)\}dx, \end{aligned} \tag{C.6}$$

$$KN14_{lijk} = -\eta^2{\gamma_2}^2 \int_0^1 \chi_l(x) \frac{d}{dx}\{[8C_1(x)+20C_2(x)]{\chi'}_i(x){\chi'}_j(x){\chi'}_k(x)\}dx, \tag{C.7}$$

$$KN15_{lijk} = +3\eta^3{\gamma_2}^2 \int_0^1 \chi_l(x) \frac{d}{dx}\left\{[8C_1(x)+20C_2(x)]\begin{pmatrix}{\chi'}_i(x){\chi'}_j(x)\\ {\xi'}_k(x){\xi'}_0(x)\end{pmatrix}\right\}dx, \tag{C.8}$$

$$\begin{aligned} KN16_{lijk} &= \eta^2{\gamma_2}^2 \int_0^1 \chi_l(x) \frac{d}{dx}\{[6C_1(x)+12C_2(x)]{\chi'}_i(x){\xi'}_j(x){\xi'}_k(x)\}dx \\ &-3\eta^4{\gamma_2}^2 \int_0^1 \chi_l(x) \frac{d}{dx}\{[8C_1(x)+20C_2(x)]{\xi'}_0{}^2(x){\chi'}_i(x){\xi'}_j(x){\xi'}_k(x)\}dx \\ &-3\eta^2 \int_0^1 \chi_l(x) \frac{d}{dx}\{[8C_1(x)+20C_2(x)]{\chi'}_i(x)\xi_j''(x)\xi_k''(x)\}dx, \end{aligned} \tag{C.9}$$

$$\begin{aligned} KN17_{lijk} &= -\eta^3{\gamma_2}^2 \int_0^1 \chi_l(x) \frac{d}{dx}\{[6C_1(x)+12C_2(x)]{\xi'}_0(x){\xi'}_i(x){\xi'}_j(x){\xi'}_k(x)\}dx \\ &+\eta^5{\gamma_2}^2 \int_0^1 \chi_l(x) \frac{d}{dx}\{[8C_1(x)+20C_2(x)]{\xi'}_0{}^3(x){\xi'}_i(x){\xi'}_j(x){\xi'}_k(x)\}dx \\ &+3\eta^3 \int_0^1 \chi_l(x) \frac{d}{dx}\{[8C_1(x)+20C_2(x)]{\xi'}_0(x){\xi'}_i(x)\xi_j''(x)\xi_k''(x)\}dx, \end{aligned} \tag{C.10}$$

$$KN18_{lijkm} = -\frac{3}{2}\eta^3{\gamma_2}^2 \int_0^1 \chi_l(x) \frac{d}{dx}\left\{[8C_1(x)+20C_2(x)]\begin{pmatrix}{\chi'}_i(x){\chi'}_j(x)\\ {\xi'}_k(x){\xi'}_m(x)\end{pmatrix}\right\}dx, \tag{C.11}$$

$$KN19_{lijkm} = +3\eta^4{\gamma_2}^2 \int_0^1 \chi_l(x) \frac{d}{dx}\left\{[8C_1(x)+20C_2(x)]\begin{pmatrix}{\xi'}_0(x){\chi'}_i(x){\xi'}_j(x)\\ {\xi'}_k(x){\xi'}_m(x)\end{pmatrix}\right\}dx, \tag{C.12}$$

$$KN110_{lijkm} = \eta^3 \frac{{\gamma_2}^2}{4} \int_0^1 \chi_l(x) \frac{d}{dx} \left\{ [6C_1(x) + 12C_2(x)] {\xi'}_i(x) {\xi'}_j(x) {\xi'}_k(x) {\xi'}_m(x) \right\} dx$$

$$-\frac{3}{2}\eta^5 {\gamma_2}^2 \int_0^1 \chi_l(x) \frac{d}{dx} \left\{ [8C_1(x) + 20C_2(x)] {\xi'}_0{}^2(x) {\xi'}_i(x) {\xi'}_j(x) {\xi'}_k(x) {\xi'}_m(x) \right\} dx \tag{C.13}$$

$$-\frac{3}{2}\eta^3 \int_0^1 \chi_l(x) \frac{d}{dx} \left\{ [8C_1(x) + 20C_2(x)] {\xi'}_i(x) {\xi'}_j(x) \xi_k''(x) \xi_m''(x) \right\} dx,$$

$$KN111_{lijkmn} = +\frac{3}{4}\eta^5 {\gamma_2}^2 \int_0^1 \chi_l(x) \frac{d}{dx} \left\{ [8C_1(x) + 20C_2(x)] \begin{pmatrix} {\xi'}_0(x) {\xi'}_i(x) {\xi'}_j(x) \\ {\xi'}_k(x) {\xi'}_m(x) {\xi'}_n(x) \end{pmatrix} \right\} dx, \tag{C.14}$$

$$KN112_{lijkmno} = -\eta^5 \frac{{\gamma_2}^2}{8} \int_0^1 \chi_l(x) \frac{d}{dx} \left\{ [8C_1(x) + 20C_2(x)] \begin{pmatrix} {\xi'}_i(x) {\psi'}_j(x) {\xi'}_k(x) \\ {\xi'}_m(x) {\xi'}_n(x) {\xi'}_o(x) \end{pmatrix} \right\} dx, \tag{C.15}$$

$$M2_{li} = \int_0^1 \xi_l(x) \rho(x) \xi_i(x) dx - \frac{1}{{\gamma_2}^2} \int_0^1 \xi_l \frac{d}{dx} [\rho(x) {\xi'}_i(x)] dx, \tag{C.16}$$

$$KL21_{li} = \eta {\gamma_2}^2 \int_0^1 \xi_l(x) \frac{d}{dx} \{ [6C_1(x) + 6C_2(x)] {\xi'}_0(x) {\chi'}_i(x) \} dx, \tag{C.17}$$

$$KL22_{li} = -\eta^2 {\gamma_2}^2 \int_0^1 \xi_l(x) \frac{d}{dx} \left\{ [6C_1(x) + 6C_2(x)] {\xi'}_0{}^2(x) {\xi'}_i(x) \right\} dx$$
$$+ \int_0^1 \xi_l(x) \frac{d^2}{dx^2} \{ [6C_1(x) + 6C_2(x)] \xi_i''(x) \} dx, \tag{C.18}$$

$$KN21_{lij} = -\eta^2 {\gamma_2}^2 \int_0^1 \xi_l(x) \frac{d}{dx} \left\{ [6C_1(x) + 12C_2(x)] {\xi'}_0(x) {\chi'}_i(x) {\chi'}_j(x) \right\} dx, \tag{C.19}$$

$$KN22_{lij} = -\eta {\gamma_2}^2 \int_0^1 \xi_l(x) \frac{d}{dx} \left\{ [6C_1(x) + 6C_2(x)] {\chi'}_i(x) {\xi'}_j(x) \right\} dx$$
$$+2\eta^3 {\gamma_2}^2 \int_0^1 \xi_l(x) \frac{d}{dx} \left\{ [6C_1(x) + 12C_2(x)] \, {\xi'}_0{}^2(x) {\chi'}_i(x) {\xi'}_j(x) \right\} dx \tag{C.20}$$
$$-2\eta \int_0^1 \xi_l(x) \frac{d^2}{dx^2} \left\{ [6C_1(x) + 12C_2(x)] {\chi'}_i(x) \xi_j''(x) \right\} dx,$$

$$KN23_{lij} = +\frac{3}{2}\eta^2{\gamma_2}^2\int_0^1 \xi_l(x)\frac{d}{dx}\left\{[6C_1(x)+6C_2(x)]\xi'_0(x)\xi'_i(x)\xi'_j(x)\right\}dx$$
$$-\eta^4{\gamma_2}^2\int_0^1 \xi_l(x)\frac{d}{dx}\left\{[6C_1(x)+12C_2(x)]\,\xi'^3_0(x)\,\xi'_i(x)\xi'_j(x)\right\}dx$$
$$-\eta^2\int_0^1 \xi_l(x)\frac{d}{dx}\left\{[6C_1(x)+12C_2(x)]\xi'_0(x)\xi_i''(x)\xi_j''(x)\right\}dx \qquad \text{(C.21)}$$
$$+2\eta^2\int_0^1 \xi_l(x)\frac{d^2}{dx^2}\left\{[6C_1(x)+12C_2(x)]\,\xi'_0(x)\xi'_i(x)\xi_j''(x)\right\}dx,$$

$$KN24_{lijk} = +\eta^3{\gamma_2}^2\int_0^1 \xi_l(x)\frac{d}{dx}\left\{[8C_1(x)+20C_2(x)]\xi'_0(x)\chi'_i(x)\chi'_j(x)\chi'_k(x)\right\}dx, \qquad \text{(C.22)}$$

$$KN25_{lijk} = +\eta^2{\gamma_2}^2\int_0^1 \xi_l(x)\frac{d}{dx}\left\{[6C_1(x)+12C_2(x)]\chi'_i(x)\chi'_j(x)\xi'_k(x)\right\}dx$$
$$-3\eta^4{\gamma_2}^2\int_0^1 \xi_l(x)\frac{d}{dx}\left\{[8C_1(x)+20C_2(x)]\psi'^2_0(x)\chi'_i(x)\chi'_j(x)\xi'_k(x)\right\}dx \qquad \text{(C.23)}$$
$$+3\eta^2\int_0^1 \xi_l(x)\frac{d^2}{dx^2}\left\{[8C_1(x)+20C_2(x)]\chi'_i(x)\chi'_j(x)\xi_k''(x)\right\}dx,$$

$$KN26_{lijk} = -3\eta^3{\gamma_2}^2\int_0^1 \xi_l(x)\frac{d}{dx}\left\{[6C_1(x)+12C_2(x)]\begin{pmatrix}\xi'_0(x)\chi'_i(x)\\ \xi'_j(x)\xi'_k(x)\end{pmatrix}\right\}dx$$
$$+3\eta^3\int_0^1 \xi_l(x)\frac{d}{dx}\left\{[8C_1(x)+20C_2(x)]\xi'_0(x)\chi'_i(x)\xi_j''(x)\xi_k''(x)\right\}dx$$
$$+3\eta^5{\gamma_2}^2\int_0^1 \xi_l(x)\frac{d}{dx}\left\{[8C_1(x)+20C_2(x)]\xi'^3_0(x)\chi'_i(x)\xi'_j(x)\xi'_k(x)\right\}dx \qquad \text{(C.24)}$$
$$-6\eta^3\int_0^1 \xi_l(x)\frac{d^2}{dx^2}\left\{[8C_1(x)+20C_2(x)]\xi'_0(x)\chi'_i(x)\xi'_j(x)\xi_k''(x)\right\}dx,$$

$$
\begin{aligned}
KN27_{lijk} &= -\frac{1}{2}\eta^2{\gamma_2}^2\int_0^1 \xi_l(x)\frac{d}{dx}\left\{[6C_1(x)+6C_2(x)]\xi'_i(x)\xi'_j(x)\xi'_k(x)\right\}dx \\
&+2\eta^4{\gamma_2}^2\int_0^1 \xi_l(x)\frac{d}{dx}\left\{[6C_1(x)+12C_2(x)]{\xi'_0}^2(x)\xi'_i(x)\xi'_j(x)\xi'_k(x)\right\}dx \\
&+\eta^2\int_0^1 \xi_l(x)\frac{d}{dx}\left\{[6C_1(x)+12C_2(x)]\xi'_i(x)\xi_j''(x)\xi_k''(x)\right\}dx \\
&-\eta^2\int_0^1 \xi_l(x)\frac{d^2}{dx^2}\left\{[6C_1(x)+12C_2(x)]\xi'_i(x)\xi'_j(x)\xi_k''(x)\right\}dx \\
&-3\eta^4\int_0^1 \xi_l(x)\frac{d}{dx}\left\{[8C_1(x)+20C_2(x)]{\xi'_0}^2(x)\xi'_i(x)\xi_j''(x)\xi_k''(x)\right\}dx \\
&-\eta^6{\gamma_2}^2\int_0^1 \xi_l(x)\frac{d}{dx}\left\{[8C_1(x)+20C_2(x)]{\xi'_0}^4(x)\xi'_i(x)\xi'_j(x)\xi'_k(x)\right\}dx \\
&+3\eta^4\int_0^1 \xi_l(x)\frac{d^2}{dx^2}\left\{[8C_1(x)+20C_2(x)]{\xi'_0}^2(x)\xi'_i(x)\xi'_j(x)\xi_k''(x)\right\}dx \\
&+\eta^2{\gamma_4}^2\int_0^1 \xi_l(x)\frac{d^2}{dx^2}\left\{[8C_1(x)+20C_2(x)]\xi_i''(x)\xi_j''(x)\xi_k''(x)\right\}dx,
\end{aligned}
\tag{C.25}
$$

$$
KN28_{lijkm} = -\eta^3{\gamma_2}^2\int_0^1 \xi_l(x)\frac{d}{dx}\left\{[8C_1(x)+20C_2(x)]\begin{pmatrix}\chi'_i(x)\chi'_j(x)\\ \chi'_k(x)\xi'_m(x)\end{pmatrix}\right\}dx,
\tag{C.26}
$$

$$
KN29_{lijkm} = \frac{9}{2}\eta^4{\gamma_2}^2\int_0^1 \xi_l(x)\frac{d}{dx}\left\{[8C_1(x)+20C_2(x)]\begin{pmatrix}\xi'_0(x)\chi'_i(x)\chi'_j(x)\\ \xi'_k(x)\xi'_m(x)\end{pmatrix}\right\}dx,
\tag{C.27}
$$

$$
\begin{aligned}
KN210_{lijkm} &= \eta^3{\gamma_2}^2\int_0^1 \xi_l(x)\frac{d}{dx}\left\{[6C_1(x)+12C_2(x)]\begin{pmatrix}\chi'_i(x)\xi'_j(x)\\ \xi'_k(x)\xi'_m(x)\end{pmatrix}\right\}dx \\
&-3\eta^3\int_0^1 \xi_l(x)\frac{d}{dx}\left\{[8C_1(x)+20C_2(x)]\chi'_i(x)\xi'_j(x)\xi_k''(x)\xi_m''(x)\right\}dx \\
&-6\eta^5{\gamma_2}^2\int_0^1 \xi_l(x)\frac{d}{dx}\left\{[8C_1(x)+20C_2(x)]{\xi'_0}^2(x)\chi'_i(x)\xi'_j(x)\xi'_k(x)\xi'_m(x)\right\}dx \\
&+3\eta^3\int_0^1 \xi_l(x)\frac{d^2}{dx^2}\left\{[8C_1(x)+20C_2(x)]\chi'_i(x)\xi'_j(x)\xi'_k(x)\xi_m''(x)\right\}dx,
\end{aligned}
\tag{C.28}
$$

$$KN211_{lijkm} = -\frac{5}{4}\eta^4{\gamma_2}^2\int_0^1 \xi_l(x)\frac{d}{dx}\left\{[6C_1(x)+12C_2(x)]\begin{pmatrix}\xi'_0(x)\xi'_i(x)\xi'_j(x)\\ \xi'_k(x)\xi'_m(x)\end{pmatrix}\right\}dx$$
$$+\frac{9}{2}\eta^4\int_0^1 \xi_l(x)\frac{d}{dx}\left\{[8C_1(x)+20C_2(x)]\xi'_0(x)\xi'_i(x)\xi'_j(x)\xi_k''(x)\xi_m''(x)\right\}dx$$
$$+\frac{5}{2}\eta^6{\gamma_2}^2\int_0^1 \xi_l(x)\frac{d}{dx}\left\{[8C_1(x)+20C_2(x)]\,{\xi'_0}^3(x)\xi'_i(x)\xi'_j(x)\xi'_k(x)\xi'_m(x)\right\}dx$$
$$-3\eta^4\int_0^1 \xi_l(x)\frac{d^2}{dx^2}\left\{[8C_1(x)+20C_2(x)]\,\xi'_0(x)\xi'_i(x)\xi'_j(x)\xi'_k(x)\xi_m''(x)\right\}dx, \tag{C.29}$$

$$KN212_{lijkmn} = -\frac{3}{2}\eta^4{\gamma_2}^2\int_0^1 \xi_l(x)\frac{d}{dx}\left\{\begin{bmatrix}8C_1(x)\\ +20C_2(x)\end{bmatrix}\begin{pmatrix}\chi'_i(x)\chi'_j(x)\xi'_k(x)\\ \xi'_m(x)\xi'_n(x)\end{pmatrix}\right\}dx, \tag{C.30}$$

$$KN213_{lijkmn} = +\frac{15}{4}\eta^5{\gamma_2}^2\int_0^1 \xi_l(x)\frac{d}{dx}\left\{\begin{bmatrix}8C_1(x)\\ +20C_2(x)\end{bmatrix}\begin{pmatrix}\xi'_0(x)\chi'_i(x)\xi'_j(x)\\ \xi'_k(x)\xi'_m(x)\xi'_n(x)\end{pmatrix}\right\}dx, \tag{C.31}$$

$$KN214_{lijkmn} = +\frac{\eta^4}{4}{\gamma_2}^2\int_0^1 \xi_l(x)\frac{d}{dx}\left\{[6C_1(x)+12C_2(x)]\begin{pmatrix}\xi'_i(x)\xi'_j(x)\xi'_k(x)\\ \xi'_m(x)\xi'_n(x)\end{pmatrix}\right\}dx$$
$$-\frac{3}{2}\eta^4\int_0^1 \xi_l(x)\frac{d}{dx}\left\{[8C_1(x)+20C_2(x)]\xi'_i(x)\xi'_j(x)\xi'_k(x)\xi_m''(x)\xi_n''(x)\right\}dx$$
$$-\frac{9}{4}\eta^6{\gamma_2}^2\int_0^1 \xi_l(x)\frac{d}{dx}\left\{[8C_1(x)+20C_2(x)]{\xi'_0}^2(x)\xi'_i(x)\xi'_j(x)\xi'_k(x)\xi'_m(x)\xi'_n(x)\right\}dx$$
$$+\frac{3}{4}\eta^4\int_0^1 \xi_l(x)\frac{d^2}{dx^2}\left\{[8C_1(x)+20C_2(x)]\xi'_i(x)\xi'_j(x)\xi'_k(x)\xi'_m(x)\xi_n''(x)\right\}dx, \tag{C.32}$$

$$KN215_{lijkmno} = -\frac{3}{4}\eta^5{\gamma_2}^2\int_0^1 \xi_l(x)\frac{d}{dx}\left\{\begin{bmatrix}8C_1(x)\\ +20C_2(x)\end{bmatrix}\begin{pmatrix}\chi'_i(x)\xi'_j(x)\xi'_k(x)\\ \xi'_m(x)\xi'_n(x)\xi'_o(x)\end{pmatrix}\right\}dx, \tag{C.33}$$

$$KN216_{lijkmno} = +\frac{7}{8}\eta^6{\gamma_2}^2\int_0^1 \xi_l(x)\frac{d}{dx}\left\{\begin{bmatrix}8C_1(x)\\ +20C_2(x)\end{bmatrix}\begin{pmatrix}\xi'_0(x)\xi'_i(x)\xi'_j(x)\\ \xi'_k(x)\xi'_m(x)\xi'_n(x)\xi'_o(x)\end{pmatrix}\right\}dx, \tag{C.34}$$

$$KN217_{lijkmnop} = -\frac{\eta^6}{8}{\gamma_2}^2\int_0^1 \xi_l(x)\frac{d}{dx}\left\{\begin{bmatrix}8C_1(x)\\ +20C_2(x)\end{bmatrix}\begin{pmatrix}\xi'_i(x)\xi'_j(x)\xi'_k(x)\\ \xi'_m(x)\xi'_n(x)\xi'_o(x)\xi'_p(x)\end{pmatrix}\right\}dx, \tag{C.35}$$

References

[1] R. Biswal, X. Zhang, A.K. Syed, M. Awd, J. Ding, F. Walther, S. Williams, Criticality of porosity defects on the fatigue performance of wire+ arc additive manufactured titanium alloy, Int. J. Fatigue 122 (2019) 208–217.

[2] Y. Nikishkov, G. Seon, A. Makeev, Structural analysis of composites with porosity defects based on X-ray computed tomography, J. Compos. Mater. 48 (2014) 2131–2144.

[3] A. Jakus, N. Geisendorfer, P. Lewis, R. Shah, 3D-printing porosity: a new approach to creating elevated porosity materials and structures, Acta Biomater. 72 (2018) 94–109.

[4] S. Zhang, J. Wu, W. Qi, J. Wang, Effect of porosity defects on the long-term corrosion behaviour of Fe-based amorphous alloy coated mild steel, Corros. Sci. 110 (2016) 57–70.

[5] P. Colombo, C. Vakifahmetoglu, S. Costacurta, Fabrication of ceramic components with hierarchical porosity, J. Mater. Sci. 45 (2010) 5425–5455.

[6] F. Tang, H. Fudouzi, Y. Sakka, Fabrication of macroporous alumina with tailored porosity, J. Am. Ceram. Soc. 86 (2003) 2050–2054.

[7] W. Van Grunsven, E. Hernandez-Nava, G.C. Reilly, R. Goodall, Fabrication and mechanical characterisation of titanium lattices with graded porosity, Metals 4 (2014) 401–409.
[8] L. Zhang, G. Zhao, G. Wang, Formation mechanism of porous structure in plastic parts injected by microcellular injection molding technology with variable mold temperature, Appl. Therm. Eng. 114 (2017) 484–497.
[9] L.J. Gibson, M.F. Ashby, Cellular Solids, Structure and Properties, Cambridge University Press, Cambridge, 1997.
[10] M. Afshar, A.P. Anaraki, H. Montazerian, J. Kadkhodapour, Additive manufacturing and mechanical characterization of graded porosity scaffolds designed based on triply periodic minimal surface architectures, J. Mech. Behav. Biomed. Mater. 62 (2016) 481–494.
[11] Y. Torres, P. Trueba, J. Pavón, E. Chicardi, P. Kamm, F. García-Moreno, J. Rodríguez-Ortiz, Design, processing and characterization of titanium with radial graded porosity for bone implants, Mater. Des. 110 (2016) 179–187.
[12] D. Chen, J. Yang, S. Kitipornchai, Elastic buckling and static bending of shear deformable functionally graded porous beam, Compos. Struct. 133 (2015) 54–61.
[13] S.K. Jena, S. Chakraverty, M. Malikan, Application of shifted Chebyshev polynomial-based Rayleigh–Ritz method and Navier's technique for vibration analysis of a functionally graded porous beam embedded in Kerr foundation, Eng. Comput. (2020) 1–21.
[14] S. Kitipornchai, D. Chen, J. Yang, Free vibration and elastic buckling of functionally graded porous beams reinforced by graphene platelets, Mater. Des. 116 (2017) 656–665.
[15] D. Chen, J. Yang, S. Kitipornchai, Nonlinear vibration and postbuckling of functionally graded graphene reinforced porous nanocomposite beams, Compos. Sci. Technol. 142 (2017) 235–245.
[16] Ş.D. Akbaş, Forced vibration analysis of functionally graded porous deep beams, Compos. Struct. 186 (2018) 293–302.
[17] M. Cianchetti, C. Laschi, A. Menciassi, P. Dario, Biomedical applications of soft robotics, Nat. Rev. Mater. 3 (2018) 143–153.
[18] Y. Zhang, M. Lu, A review of recent advancements in soft and flexible robots for medical applications, Int. J. Med. Robot. Comput. Assist. Surg. 16 (2020) e2096.
[19] M.W. Gifari, H. Naghibi, S. Stramigioli, M. Abayazid, A review on recent advances in soft surgical robots for endoscopic applications, Int. J. Med. Robot. Comput. Assist. Surg. 15 (2019) e2010.
[20] A. Ghosh, C. Yoon, F. Ongaro, S. Scheggi, F.M. Selaru, S. Misra, D.H. Gracias, Stimuli-responsive soft untethered grippers for drug delivery and robotic surgery, Front. Mech. Eng. 3 (2017) 7.
[21] A. Menciassi, V. Iacovacci, Implantable Biorobotic Organs, AIP Publishing LLC, 2020.
[22] W. Wu, S. Zhang, Z. Wu, S. Qin, F. Li, T. Song, X. Cao, Z.L. Wang, L. Zhang, On the understanding of dielectric elastomer and its application for all-soft artificial heart, Sci. Bull. 66 (10) (2021) 981–990.
[23] P.S. Malchesky, Artificial organs 2018: a year in review, Artif. Organs 43 (2019) 288–317.
[24] I.D. Breslavsky, M. Amabili, M. Legrand, Physically and geometrically non-linear vibrations of thin rectangular plates, Int. J. Non Linear Mech. 58 (2014) 30–40.
[25] I.D. Breslavsky, M. Amabili, M. Legrand, Nonlinear vibrations of thin hyperelastic plates, J. Sound Vib. 333 (2014) 4668–4681.
[26] M. Amabili, P. Balasubramanian, I.D. Breslavsky, G. Ferrari, R. Garziera, K. Riabova, Experimental and numerical study on vibrations and static deflection of a thin hyperelastic plate, J. Sound Vib. 385 (2016) 81–92.
[27] I.D. Breslavsky, M. Amabili, M. Legrand, Static and dynamic behavior of circular cylindrical shell made of hyperelastic arterial material, J. Appl. Mech. 83 (5) (2016) 051002.
[28] M. Amabili, I. Breslavsky, J. Reddy, Nonlinear higher-order shell theory for incompressible biological hyperelastic materials, Comput. Methods Appl. Mech. Eng. 346 (2019) 841–861.
[29] M. Mooney, A theory of large elastic deformation, J. Appl. Phys. 11 (1940) 582–592.
[30] J. Miles, R squared adjusted R squared. Encyclopedia of statistics in behavioral science, Wiley Online Library, 2005.
[31] P. Heyliger, J. Reddy, A higher order beam finite element for bending and vibration problems, J. Sound Vib. 126 (1988) 309–326.
[32] M. Amabili, Nonlinear Mechanics of Shells and Plates in Composite, Soft and Biological Materials, Cambridge University Press, 2018.
[33] M.H. Ghayesh, Dynamics of functionally graded viscoelastic microbeams, Int. J. Eng. Sci. 124 (2018) 115–131.
[34] H.B. An, Z.Z. Bai, A globally convergent Newton-GMRES method for large sparse systems of nonlinear equations, Appl. Numer. Math. 57 (2007) 235–252.
[35] L.T. Watson, Globally convergent homotopy algorithms for nonlinear systems of equations, Nonlinear Dyn. 1 (1990) 143–191.
[36] E.G. Birgin, N. Krejić, J.M. Martínez, Globally convergent inexact quasi-Newton methods for solving nonlinear systems, Numer. Algorithm. 32 (2003) 249–260.
[37] S.S. Rao, Vibration of Continuous Systems, John Wiley & Sons, 2019.
[38] L. Li, H. Tang, Y. Hu, Size-dependent nonlinear vibration of beam-type porous materials with an initial geometrical curvature, Compos. Struct. 184 (2018) 1177–1188.

Chapter 5

Hyperelastic sandwich beams

Overview

Layered polymeric structures are widely used in different industries including packaging and layered pipes. This chapter aims to provide a better understanding of how layering, material sorting and design can affect the mechanical behaviour of layered hyperelastic structures. Different shear deformation theories are employed and the coupled axial, rotational and transverse equations of motion of isotropic polymeric structures are presented in the framework of Hamilton's principle. A detailed case study on the nonlinear oscillation behaviour of sandwich hyperelastic beams is presented showing the effect of using different materials on each layer and changing the total number of layers. This research study is published and available online as: Khaniki, H. B., Ghayesh, M. H., Chin, R., & Hussain, S. (2022). Nonlinear continuum mechanics of thick hyperelastic sandwich beams using various shear deformable beam theories. Continuum Mechanics and Thermodynamics, 34, 781-827. DOI: 10.1007/s00161-022-01090-y

Statement of Authorship

Title of Paper	Nonlinear continuum mechanics of thick hyperelastic sandwich beams using various shear deformable beam theories
Publication Status	☑ Published ☐ Accepted for Publication ☐ Submitted for Publication ☐ Unpublished and Unsubmitted w ork w ritten in manuscript style
Publication Details	Khaniki, H. B., Ghayesh, M. H., Chin, R., & Hussain, S. (2022). Nonlinear continuum mechanics of thick hyperelastic sandwich beams using various shear deformable beam theories. Continuum Mechanics and Thermodynamics, 34, 781-827.

Principal Author

Name of Principal Author (Candidate)	Hossein Bakhshi Khaniki		
Contribution to the Paper	I carried out the literature review, conceptualization, formal analysis, investigation, methodology, software, validation, visualization and wrote the manuscript.		
Overall percentage (%)	80%		
Certification:	This paper reports on original research I conducted during the period of my Higher Degree by Research candidature and is not subject to any obligations or contractual agreements with a third party that would constrain its inclusion in this thesis. I am the primary author of this paper.		
Signature		Date	2/11/2022

Co-Author Contributions

By signing the Statement of Authorship, each author certifies that:

i. the candidate's stated contribution to the publication is accurate (as detailed above);

ii. permission is granted for the candidate in include the publication in the thesis; and

iii. the sum of all co-author contributions is equal to 100% less the candidate's stated contribution.

Name of Co-Author	Mergen Ghayesh		
Contribution to the Paper	As the principal supervisor, I helped to construct the manuscript, edit and review the manuscript for submission. I assisted in the conceptualization, investigation, methodology, review and editing. I hereby give consent to Hossein Bakhshi Khaniki to present this paper for examination towards the degree of Doctor of Philosophy.		
Signature		Date	3/11/2022

Name of Co-Author	Rey Chin		
Contribution to the Paper	I assisted in review and editing of the manuscript. I hereby give consent to Hossein Bakhshi Khaniki to present this paper for examination towards the degree of Doctor of Philosophy.		
Signature		Date	3/11/2022

Name of Co-Author	Shahid Hussain		
Contribution to the Paper	I assisted in the conceptualization, review and editing of the manuscript. I hereby give consent to Hossein Bakhshi Khaniki to present this paper for examination towards the degree of Doctor of Philosophy.		
Signature		Date	8/11/2022

Continuum Mech. Thermodyn. (2022) 34:781–827
https://doi.org/10.1007/s00161-022-01090-y

ORIGINAL ARTICLE

Hossein B. Khaniki · Mergen H. Ghayesh · Rey Chin · Shahid Hussain

Nonlinear continuum mechanics of thick hyperelastic sandwich beams using various shear deformable beam theories

Received: 22 September 2021 / Accepted: 1 February 2022 / Published online: 9 March 2022

Abstract In this study, the time-dependent mechanics of multilayered thick hyperelastic beams are investigated for the first time using five different types of shear deformation models for modelling the beam (i.e. the Euler–Bernoulli, Timoshenko, third-order, trigonometric and exponential shear deformable models), together with the von Kármán geometrical nonlinearity and Mooney–Rivlin hyperelastic strain energy density. The laminated hyperelastic beam is assumed to be resting on a nonlinear foundation and undergoing a time-dependent external force. The coupled highly nonlinear hyperelastic equations of motion are obtained by considering the longitudinal, transverse and rotation motions and are solved using a dynamic equilibrium technique. Both the linear and nonlinear time-dependent mechanics of the structure are analysed for clamped–clamped and pinned–pinned boundaries, and the impact of considering the shear effect using different shear deformation theories is discussed in detail. The influence of layering, each layer's thickness, hyperelastic material positioning and many other parameters on the nonlinear frequency response is analysed, and it is shown that the resonance position, maximum amplitude, coupled motion and natural frequencies vary significantly for various hyperelastic and layer properties. The results of this study should be useful when studying layered soft structures, such as multilayer plastic packaging and laminated tubes, as well as modelling layered soft tissues.

Keywords Layered beams · Soft beams · Hyperelastic beams · Nonlinear vibration · Nonlinear dynamics · Laminated beams · Multilayered beams · Sandwich beams

1 Introduction

Layering structures is an effective method for optimising their mechanical, physical and electrical properties for a specific purpose. For instance, in the automotive industry, reducing the weight of the structure and increasing the stiffness lead to significant environmental benefits (lowering the fuel consumption and increasing automobile's performance [1,2]) which is made feasible by fabricating multilayered parts.

Communicated by Andreas Öchsner.

H. B. Khaniki ( ) · M. H. Ghayesh ( ) · R. Chin
School of Mechanical Engineering, University of Adelaide, Adelaide, SA 5005, Australia
E-mail: hossein.bakhshikhaniki@adelaide.edu

M. H. Ghayesh
E-mail: mergen.ghayesh@adelaide.edu.au

S. Hussain
Faculty of Science and Technology, University of Canberra, Canberra, Australia

In many engineering applications, structures are fabricated with three layers (e.g. in laminated packaging); the outer layers are called the skins (upper skin and lower skin) and the middle layer is the core. If the purpose of the design is to increase the strength against bending loads, the core is usually made of a softer material with a higher thickness and the outer skins are thinner and stiffer. If the structure is used in an uncertain environment, the outer skins are made of softer materials to propagate the force throughout the structure and avoid cracks in a brittle core. In some other engineering structures, researchers gradually change the material properties to fabricate functionally graded structures which have been studied in Refs. [3–6].

Over the past few years, researchers have analysed different layered *elastic (versus hyperelastic in this paper)* structures to understand their mechanical behaviour under diverse conditions. A brief review of previous studies in this field is given in this section; however, interested readers seeking a more detailed literature review are referred to Refs. [7–10].

For bending analysis of layered *elastic* beams [11,12], researchers have used different beam theories and analysed layered beam structures. By neglecting the shear effects, Chai and Yap [13] examined the bending behaviour of layered composite structures using classic beam theory (CBT). By comparing the results with those of a finite element modelling (FEM), it was shown that the coupling terms between the layers play a significant role in predicting the mechanical behaviour accurately. Chen et al [14] added the shear influence to the model using the first-order shear deformable beam theory; it was shown that the bending deformation of the Timoshenko beam model is higher than the CBT and the difference is higher for any lower thickness-to-length ratio. Özütok and Madenci [15] used a higher-order shear deformation theory together with FEM for timed-independent analysis of layered composite beams and verified the results by comparing them with those available in the literature.

For *linear* vibration analysis of layered *elastic* beams [16–18], Emam and Nayfeh [19] investigated the free vibration of layered composites using the Euler–Bernoulli beam theory. The axial motion was considered in the formulation and was substituted in the transverse equation of motion. Natural frequencies were obtained for different axial loads and boundary conditions; it was reported that for the studied six-layer beam model, the layer positioning has a significant effect in varying the fundamental frequency for different axial loads. A first-order shear deformable beam theory was used by Banerjee and Sobey [20] to examine the free oscillation of laminated structures under axial loading. A closed-form analytical solution was presented showing accuracy in predicting the natural frequencies and mode shapes of layered beams. Damanpack and Khalili [21] used higher-order beam theory to model the longitudinal–transverse coupled motion of layered structures. Hamilton's principle was used to reach the equations of motion showing that the natural frequencies obtained from this model agree with the experimental results presented in Ref. [22].

For *nonlinear* vibration analysis of *elastic* beams, Zhang et al. [23] studied the nonlinear forced oscillation of laminated beams in a humid thermal condition. Only the transverse motion was considered in the formulation, and a nonlinear energy sink was added to the model. The equations of motion were solved using a fourth-order Rung–Kutta (RK4) method and a two-term harmonic balance (HB) scheme. It was shown that the nonlinear studied model has a hardening behaviour and adding a nonlinear energy sink can reduce the maximum amplitude of the transverse vibration significantly. Shen et al. [24] examined the nonlinear free oscillation behaviour of layered graphene-strengthened beams; Halpin–Tsai model was employed to predict the physical properties of the combination of the matrix and fibres. A higher-order shear deformable theory, together with the von-Kármán geometrical nonlinearity, was used to model the beam. By employing a two-step perturbation technique, it was shown that the layering and positioning of fibres has a significant effect in varying the nonlinear frequency ratio and the natural frequencies. Three-layered and bi-layered shear deformable *elastic* beams have been studied by Ghayesh et al. [25]; it was shown that the resonance region change based on the layer sorting and both hardening and softening behaviour can be observed while considering geometrical imperfections. Other types of layered structures have also been examined by researchers, and interested authors are referred to Refs. [26,27] for more information about layered-plate and layered-shell structures focused investigations.

The previously mentioned studies focus on *elastic* structures that undergo small strains while facing different types of loadings; even the nonlinear ones are based on *geometric* nonlinearities and small strains. Soft structures cannot be modelled as a linear elastic material and require more accurate hyperelastic assumptions and formulations; in other words, a *material* nonlinearity should be taken into account, as done in this paper.

Multilayered *hyper*elastic structures have been used widely in many products. For instance, multilayer plastic packaging is used for packaging different products, such as food packaging which has been a trending topic over the last few years in waste management, recycling and optimised packaging [28–31]. Furthermore, human body organs act as hyperelastic components and many parts are made of different layers, such as the artery, which is made of three hyperelastic layers (intima, media and adventitia) [32].

Previously, axially moving hyperelastic structures and porous-hyperelastic structures have been investigated by Khaniki et al. [33,34]; however, until now, there have been no studies on the time-dependent mechanics of layered hyperelastic structures. In this study, a comprehensive analysis of the mechanics of multilayered thick hyperelastic structures is presented for the first time as having different boundary conditions via different shear theories. Large strain modelling, together with large-amplitude displacements, is modelled using the Mooney–Rivlin strain energy model (for material nonlinearity) and the von Kármán geometrical nonlinearity. Different types of shear deformable beam theories (Euler–Bernoulli, Timoshenko, third-order, trigonometric and exponential shear deformable models) are used to model the layered structures and the influence of layering, material positioning and the thickness of the core and skins is discussed in detail.

2 Layered hyperelastic shear deformable beam formulation

For a thick-layered shear deformable beam (Fig. 1), considering the plane motion, the axial and transverse deformations are written as [35]

$$u(x,z,t) = \chi(z)\, w_x(x,t) - \chi(z)\,\phi(x,t) + u(x,t) - z w_x(x,t), \tag{1}$$

$$w(x,z,t) = w(x,t), \tag{2}$$

where u and w are the axial and transverse displacements in the x and z directions (Fig. 1), respectively, subscript x indicates derivations with respect to x, ϕ is the rotation and $\chi(z)$ is the higher-order shear function, which the definition depends on the shear deformable theory used. In this study, five different definitions for $\chi(z)$ are used, which are defined as [36–39]

$$\text{Case 1 (Euler}-\text{Bernoulli beam theory)}: \quad \chi(z) = 0, \tag{3}$$

$$\text{Case 2 (Timoshenko beam theory)}: \quad \chi(z) = z, \tag{4}$$

$$\text{Case 3 (Third}-\text{order beam theory)}: \quad \chi(z) = z\left(1 - \frac{4}{3}\frac{z^2}{h^2}\right), \tag{5}$$

$$\text{Case 4 (Exponential beam theory)}: \quad \chi(z) = z e^{-2(z/h)^2}, \tag{6}$$

$$\text{Case 5 (Trigonometric beam theory)}: \quad \chi(z) = \frac{h}{\pi}\sin\left(\frac{\pi z}{h}\right), \tag{7}$$

where Case 1 indicates that the shear deformation effect is neglected, following the Euler–Bernoulli beam assumption (classic beam theory) when the rotary inertia is also neglected; the advantage of using this model is that the model is simplified by neglecting the rotational degree of freedom by only considering axial and transverse motions. Case 2 defines a linearly varying shear deformation through the thickness of the beam, which represents the Timoshenko beam theory. In this model, the transverse normal plates do not necessarily remain perpendicular (to the mid-surface) after deformation leading to an extra degree of freedom for the rotary inertia. Case 3 shows the shear deformation using a higher-order model following the third-order shear deformable beam theory [36,37]. In this model, the transverse shear stress in the Cases 4 and 5 defines the shear deformation of the beam using an exponential [38] and trigonometric [39] functions, which follow the beam theories of exponential shear deformable and trigonometric, respectively. For all the five cases, the strains are written as

$$\varepsilon_{xx}(x,y,t) = u_x(x,t) - z w_{xx}(x,t) + \chi(z)\, w_{xx}(x,t) - \chi(z)\,\phi_x(x,t) + \frac{1}{2} {w_x}^2(x,t), \tag{8}$$

$$\gamma_{xz}(x,y,t) = 2\varepsilon_{xz}(x,y,t) = \chi_z(z)\, w_x(x,t) - \chi_z(z)\,\phi(x,t), \tag{9}$$

$$\varepsilon_{zz} \neq 0, \tag{10}$$

where ε_{xx} is the axial strain, γ_{xz} is the shear strain and ε_{zz} is the transverse strain that is not equal to zero and should satisfy the incompressibility condition of hyperelastic structures. The deformation gradient (F) is given in Refs. [33,40] which can be used for defining the left Cauchy–Green strain tensor (C) for planar motion as

$$C = F^T F = \begin{bmatrix} (1+\varepsilon_{xx})^2 + {\varepsilon_{xz}}^2 & 0 & \varepsilon_{xz}(2+\varepsilon_{xx}+\varepsilon_{zz}) \\ 0 & 1 & 0 \\ \varepsilon_{xz}(2+\varepsilon_{xx}+\varepsilon_{zz}) & 0 & (1+\varepsilon_{zz})^2 + {\varepsilon_{xz}}^2 \end{bmatrix}, \tag{11}$$

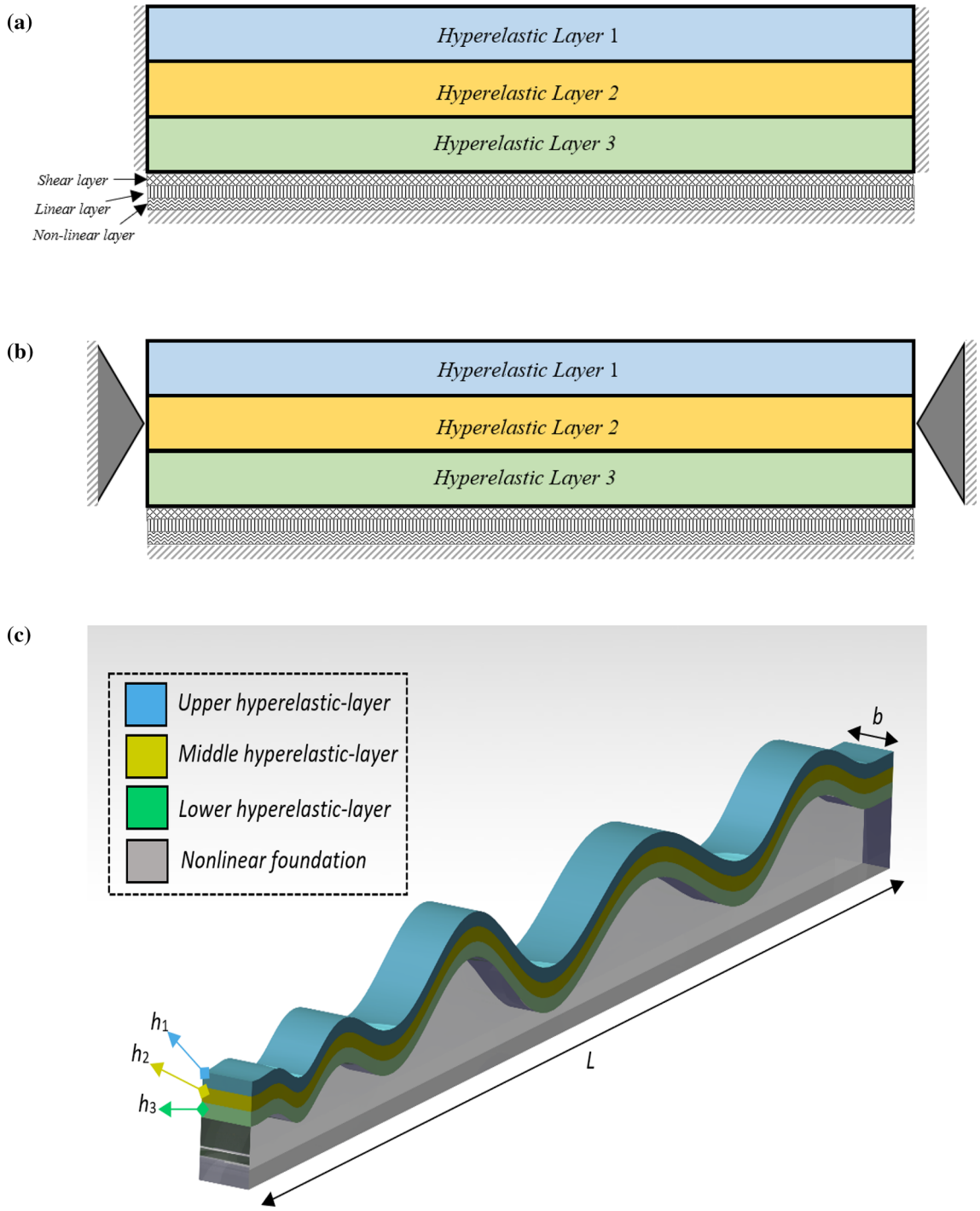

Fig. 1 Schematics of three-layered hyperelastic beam with (**a**) fixed and (**b**) simply supported boundary conditions and (**c**) layer characteristics

where the higher-order strain terms are due to the soft behaviour of hyperelastic materials, which undergo large strains and cannot be ignored. The strain term ε_{zz} can be obtained as a function of ε_{zz} and ε_{zz} by considering $\det(C) = 0$ (the incompressibility condition). For linear elastic models, by neglecting the higher-order strain terms, the Cauchy–Green strain tensor will be [27]

$$C = F^T F = \begin{bmatrix} 1+2\varepsilon_x & 0 & 2\varepsilon_{xz} \\ 0 & 1 & 0 \\ 2\varepsilon_{xz} & 0 & 1+2\varepsilon_z \end{bmatrix}, \tag{12}$$

which is equal to the elastic material strain tensor model. By using the Mooney–Rivlin hyperelastic strain energy density model [41,42], the variation of the total potential energy of the system is written as

$$\begin{aligned} \delta U = \int_0^L \int_A & \left[U_1(x,z)\,\delta u_x(x,t) + U_2(x,z)\,\delta w_x(x,t) \right. \\ & \left. + U_3(x,z)\,\delta w_{xx}(x,t) + U_4(x,z)\,\delta\phi(x,t) + U_5(x,z)\,\delta\phi_x(x,t) \right] \mathrm{d}A\mathrm{d}x, \end{aligned} \tag{13}$$

where

$$\begin{aligned} U_1(x,z) = {} & 8C_T u_x(x,t) + 8C_T[\chi(z) - z]\,w_{xx}(x,t) + 4C_T {w_x}^2(x,t) - 8C_T\chi(z)\,\phi_x(x,t) \\ & - 12C_T {u_x}^2(x,t) - 24C_T[\chi(z) - z]\,u_x(x,t)\,w_{xx}(x,t) + 24C_T\chi(z)\,u_x(x,t)\,\phi_x(x,t) \\ & - 12C_T u_x(x,t)\,{w_x}^2(x,t) - 12C_T[\chi(z) - z]^2 {w_{xx}}^2(x,t) + 12C_T\chi(z)\,{w_x}^2(x,t)\,\phi_x(x,t) \\ & + 24C_T\chi(z)[\chi(z) - z]\,w_{xx}(x,t)\,\phi_x(x,t) - 12C_T[\chi(z) - z]\,{w_x}^2(x,t)\,w_{xx}(x,t) \\ & - 3C_T {w_x}^4(x,t) - 12C_T\chi(z)^2 {\phi_x}^2(x,t) - C_T {\chi_z}^2(z)\,{w_x}^2(x,t) \\ & + 2C_T {\chi_z}^2(z)\,w_x(x,t)\,\phi(x,t) - C_T {\chi_z}^2(z)\,\phi^2(x,t), \end{aligned} \tag{14}$$

$$\begin{aligned} U_2(x,z) = {} & 8C_T u_x(x,t)\,w_x(x,t) + 8C_T[\chi(z) - z]\,w_x(x,t)\,w_{xx}(x,t) + 4C_T {w_x}^3(x,t) \\ & - 8C_T\chi(z)\,w_x(x,t)\,\phi_x(x,t) - 12C_T {u_x}^2(x,t)\,w_x(x,t) \\ & - 24C_T[\chi(z) - z]\,u_x(x,t)\,w_x(x,t)\,w_{xx}(x,t) + 24C_T\chi(z)\,u_x(x,t)\,w_x(x,t)\,\phi_x(x,t) \\ & - 12C_T u_x(x,t)\,{w_x}^3(x,t) - 12C_T[\chi(z) - z]^2 w_x(x,t)\,{w_{xx}}^2(x,t) \\ & + 24C_T\chi(z)[\chi(z) - z]\,w_x(x,t)\,w_{xx}(x,t)\,\phi_x(x,t) + 12C_T\chi(z)\,{w_x}^3(x,t)\,\phi_x(x,t) \\ & - 12C_T[\chi(z) - z]\,{w_x}^3(x,t)\,w_{xx}(x,t) - 3C_T {w_x}^5(x,t) - 12C_T\chi(z)^2 w_x(x,t)\,{\phi_x}^2(x,t) \\ & - C_T {\chi_z}^2(z)\,{w_x}^3(x,t) + 2C_T {\chi_z}^2(z)\,{w_x}^2(x,t)\,\phi(x,t) - C_T {\chi_z}^2(z)\,w_x(x,t)\,\phi^2(x,t) \\ & + 2C_T {\chi_z}^2(z)\,w_x(x,t) - 2C_T {\chi_z}^2(z)\,\phi(x,t) - 2C_T {\chi_z}^2(z)\,u_x(x,t)\,w_x(x,t) \\ & + 2C_T {\chi_z}^2(z)\,u_x(x,t)\,\phi(x,t) - 2C_T {\chi_z}^2(z)[\chi(z) - z]\,w_x(x,t)\,w_{xx}(x,t) \\ & - C_T {\chi_z}^2(z)\,{w_x}^3(x,t) + 2C_T {\chi_z}^2(z)\,\chi(z)\,w_x(x,t)\,\phi_x(x,t) \\ & + 2C_T {\chi_z}^2(z)[\chi(z) - z]\,w_{xx}(x,t)\,\phi(x,t) + C_T {\chi_z}^2(z)\,{w_x}^2(x,t)\,\phi(x,t) \\ & - 2C_T {\chi_z}^2(z)\,\chi(z)\,\phi(x,t)\,\phi_x(x,t), \end{aligned} \tag{15}$$

$$\begin{aligned} U_3(x,z) = {} & 8C_T[\chi(z) - z]\,u_x(x,t) + 8C_T[\chi(z) - z]^2 w_{xx}(x,t) + 4C_T[\chi(z) - z]\,{w_x}^2(x,t) \\ & - 8C_T\chi(z)[\chi(z) - z]\,\phi_x(x,t) - 12C_T[\chi(z) - z]\,{u_x}^2(x,t) \\ & - 24C_T[\chi(z) - z]^2 u_x(x,t)\,w_{xx}(x,t) + 24C_T\chi(z)[\chi(z) - z]\,u_x(x,t)\,\phi_x(x,t) \\ & - 12C_T[\chi(z) - z]\,u_x(x,t)\,{w_x}^2(x,t) - 12C_T[\chi(z) - z]^3 {w_{xx}}^2(x,t) \\ & + 24C_T\chi(z)[\chi(z) - z]^2 w_{xx}(x,t)\,\phi_x(x,t) + 12C_T\chi(z)[\chi(z) - z]\,{w_x}^2(x,t)\,\phi_x(x,t) \\ & - 12C_T[\chi(z) - z]^2 {w_x}^2(x,t)\,w_{xx}(x,t) - 3C_T[\chi(z) - z]\,{w_x}^4(x,t) \\ & - 12C_T\chi(z)^2[\chi(z) - z]\,{\phi_x}^2(x,t) - C_T {\chi_z}^2(z)[\chi(z) - z]\,{w_x}^2(x,t) \\ & + 2C_T {\chi_z}^2(z)[\chi(z) - z]\,w_x(x,t)\,\phi(x,t) - C_T {\chi_z}^2(z)[\chi(z) - z]\,\phi^2(x,t), \end{aligned} \tag{16}$$

$$\begin{aligned} U_4(x,z) = {} & -2C_T {\chi_z}^2(z)\,w_x(x,t) + 2C_T {\chi_z}^2(z)\,\phi(x,t) \\ & + 2C_T {\chi_z}^2(z)\,u_x(x,t)\,w_x(x,t) - 2C_T {\chi_z}^2(z)\,u_x(x,t)\,\phi(x,t) \\ & + 2C_T {\chi_z}^2(z)[\chi(z) - z]\,w_x(x,t)\,w_{xx}(x,t) + C_T {\chi_z}^2(z)\,{w_x}^3(x,t) \\ & - 2C_T\chi(z)\,{\chi_z}^2(z)\,w_x(x,t)\,\phi_x(x,t) - C_T {\chi_z}^2(z)\,{w_x}^2(x,t)\,\phi(x,t) \\ & - 2C_T {\chi_z}^2(z)[\chi(z) - z]\,w_{xx}(x,t)\,\phi(x,t) \\ & + 2C_T\chi(z)\,{\chi_z}^2(z)\,\phi(x,t)\,\phi_x(x,t), \end{aligned} \tag{17}$$

$$
\begin{aligned}
U_5(x,z) = & -8C_T\chi(z)\,u_x(x,t) - 8C_T\chi(z)\,[\chi(z)-z]\,w_{xx}(x,t) \\
& - 4C_T\chi(z)\,{w_x}^2(x,t) + 8C_T{\chi}^2(z)\,\phi_x(x,t) + 12C_T\chi(z)\,{u_x}^2(x,t) \\
& + 24C_T\chi(z)\,[\chi(z)-z]\,u_x(x,t)\,w_{xx}(x,t) - 24C_T{\chi}^2(z)\,u_x(x,t)\,\phi_x(x,t) \\
& + 12C_T\chi(z)\,u_x(x,t)\,{w_x}^2(x,t) + 12C_T\chi(z)\,[\chi(z)-z]^2{w_{xx}}^2(x,t) \\
& - 24C_T{\chi}^2(z)\,[\chi(z)-z]\,w_{xx}(x,t)\,\phi_x(x,t) - 12C_T{\chi}^2(z)\,{w_x}^2(x,t)\,\phi_x(x,t) \\
& + 12C_T\chi(z)\,[\chi(z)-z]\,{w_x}^2(x,t)\,w_{xx}(x,t) + 3C_T\chi(z)\,{w_x}^4(x,t) \\
& + 12C_T{\chi}^3(z)\,{\phi_x}^2(x,t) + C_T\chi(z)\,{\chi_z}^2(z)\,{w_x}^2(x,t) \\
& - 2C_T\chi(z)\,{\chi_z}^2(z)\,w_x(x,t)\,\phi(x,t) + C_T\chi(z)\,{\chi_z}^2(z)\,\phi^2(x,t)\,,
\end{aligned} \tag{18}
$$

for which, by assuming the hyperelastic beam has three layers (Fig. 1) with layers attached perfectly (with no delamination), the stiffness parameters (A_{ii}, B_{ii}, D_{ii} and E_{ii}) are defined as

$$A_{11} = \int_A C_T \mathrm{d}A = \int_{A_1} C_{T1}\mathrm{d}A_1 + \int_{A_2} C_{T2}\mathrm{d}A_2 + \int_{A_3} C_{T3}\mathrm{d}A_3, \tag{19}$$

$$B_{11} = \int_A C_T\chi(z)\,\mathrm{d}A = \int_{A_1} C_{T1}\chi(z)\,\mathrm{d}A_1 + \int_{A_2} C_{T2}\chi(z)\,\mathrm{d}A_2 + \int_{A_3} C_{T3}\chi(z)\,\mathrm{d}A_3, \tag{20}$$

$$
\begin{aligned}
B_{22} = & \int_A C_T\,[\chi(z)-z]\,\mathrm{d}A = \int_{A_1} C_{T1}\,[\chi(z)-z]\,\mathrm{d}A_1 + \int_{A_2} C_{T2}\,[\chi(z)-z]\,\mathrm{d}A_2 + \int_{A_3} C_{T3} \\
& [\chi(z)-z]\,\mathrm{d}A_3,
\end{aligned} \tag{21}
$$

$$D_{11} = \int_A C_T{\chi}^2(z)\mathrm{d}A = \int_{A_1} C_{T1}{\chi}^2(z)\mathrm{d}A_1 + \int_{A_2} C_{T2}{\chi}^2(z)\mathrm{d}A_2 + \int_{A_3} C_{T3}{\chi}^2(z)\mathrm{d}A_3, \tag{22}$$

$$
\begin{aligned}
D_{22} = & \int_A C_T[\chi(z)-z]^2\mathrm{d}A = \int_{A_1} C_{T1}[\chi(z)-z]^2\mathrm{d}A_1 + \int_{A_2} C_{T2}[\chi(z)-z]^2\mathrm{d}A_2 \\
& + \int_{A_3} C_{T3}[\chi(z)-z]^2\mathrm{d}A_3,
\end{aligned} \tag{23}
$$

$$
\begin{aligned}
D_{33} = & \int_A C_T\chi(z)\,[\chi(z)-z]\mathrm{d}A = \int_{A_1} C_{T1}\chi(z)\,[\chi(z)-z]\mathrm{d}A_1 \\
& + \int_{A_2} C_{T2}\chi(z)\,[\chi(z)-z]\mathrm{d}A_2 + \int_{A_3} C_{T3}\chi(z)\,[\chi(z)-z]\mathrm{d}A_3,
\end{aligned} \tag{24}
$$

$$D_{44} = \int_A C_T{\chi_z}^2(z)\mathrm{d}A = \int_{A_1} C_{T1}{\chi_z}^2(z)\mathrm{d}A_1 + \int_{A_2} C_{T2}{\chi_z}^2(z)\mathrm{d}A_2 + \int_{A_3} C_{T3}{\chi_z}^2(z)\mathrm{d}A_3, \tag{25}$$

$$E_{11} = \int_A C_T{\chi}^3(z)\,\mathrm{d}A = \int_{A_1} C_{T1}{\chi}^3(z)\,\mathrm{d}A_1 + \int_{A_2} C_{T2}{\chi}^3(z)\,\mathrm{d}A_2 + \int_{A_3} C_{T3}{\chi}^3(z)\,\mathrm{d}A_3, \tag{26}$$

$$
\begin{aligned}
E_{22} = & \int_A C_T{\chi}^2(z)\,[\chi(z)-z]\,\mathrm{d}A = \int_{A_1} C_{T1}{\chi}^2(z)\,[\chi(z)-z]\,\mathrm{d}A_1 \\
& + \int_{A_2} C_{T2}{\chi}^2(z)\,[\chi(z)-z]\,\mathrm{d}A_2 + \int_{A_3} C_{T3}{\chi}^2(z)\,[\chi(z)-z]\,\mathrm{d}A_3,
\end{aligned} \tag{27}
$$

$$E_{33} = \int_A C_T\chi(z)\,[\chi(z)-z]^2\mathrm{d}A = \int_{A_1} C_{T1}\chi(z)\,[\chi(z)-z]^2\mathrm{d}A_1$$

$$+\int_{A_2} C_{T2}\chi(z)\,[\chi(z)-z]^2 \mathrm{d}A_2+\int_{A_3} C_{T3}\chi(z)\,[\chi(z)-z]^2 \mathrm{d}A_3, \tag{28}$$

$$E_{44}=\int_{A} C_T[\chi(z)-z]^3 \mathrm{d}A=\int_{A_1} C_{T1}[\chi(z)-z]^3 \mathrm{d}A_1$$
$$+\int_{A_2} C_{T2}[\chi(z)-z]^3 \mathrm{d}A_2+\int_{A_3} C_{T3}[\chi(z)-z]^3 \mathrm{d}A_3, \tag{29}$$

$$E_{55}=\int_{A} C_T {\chi_z}^3(z)\,\mathrm{d}A=\int_{A_1} C_{T1}{\chi_z}^3(z)\,\mathrm{d}A_1+\int_{A_2} C_{T2}{\chi_z}^3(z)\,\mathrm{d}A_2+\int_{A_3} C_{T3}{\chi_z}^3(z)\,\mathrm{d}A_3, \tag{30}$$

$$E_{66}=\int_{A} C_T {\chi_z}^2(z)\,[\chi(z)-z]\,\mathrm{d}A=\int_{A_1} C_{T1}{\chi_z}^2(z)\,[\chi(z)-z]\,\mathrm{d}A_1$$
$$+\int_{A_2} C_{T2}{\chi_z}^2(z)\,[\chi(z)-z]\,\mathrm{d}A_2+\int_{A_3} C_{T3}{\chi_z}^2(z)\,[\chi(z)-z]\,\mathrm{d}A_3, \tag{31}$$

$$E_{77}=\int_{A} C_T\chi(z)\,{\chi_z}^2(z)\,\mathrm{d}A=\int_{A_1} C_{T1}\chi(z){\chi_z}^2(z)\,\mathrm{d}A_1+\int_{A_2} C_{T2}\chi(z){\chi_z}^2(z)\,\mathrm{d}A_2$$
$$+\int_{A_3} C_{T3}\chi(z)\,{\chi_z}^2(z)\,\mathrm{d}A_3, \tag{32}$$

which, for the case considering the Timoshenko beam model ($\chi(z)=z$), uses a shear correction factor of $\kappa=5/6$ [43]. Accordingly, by using Eqs. (19–32), the potential energy of a three-layered hyperelastic beam

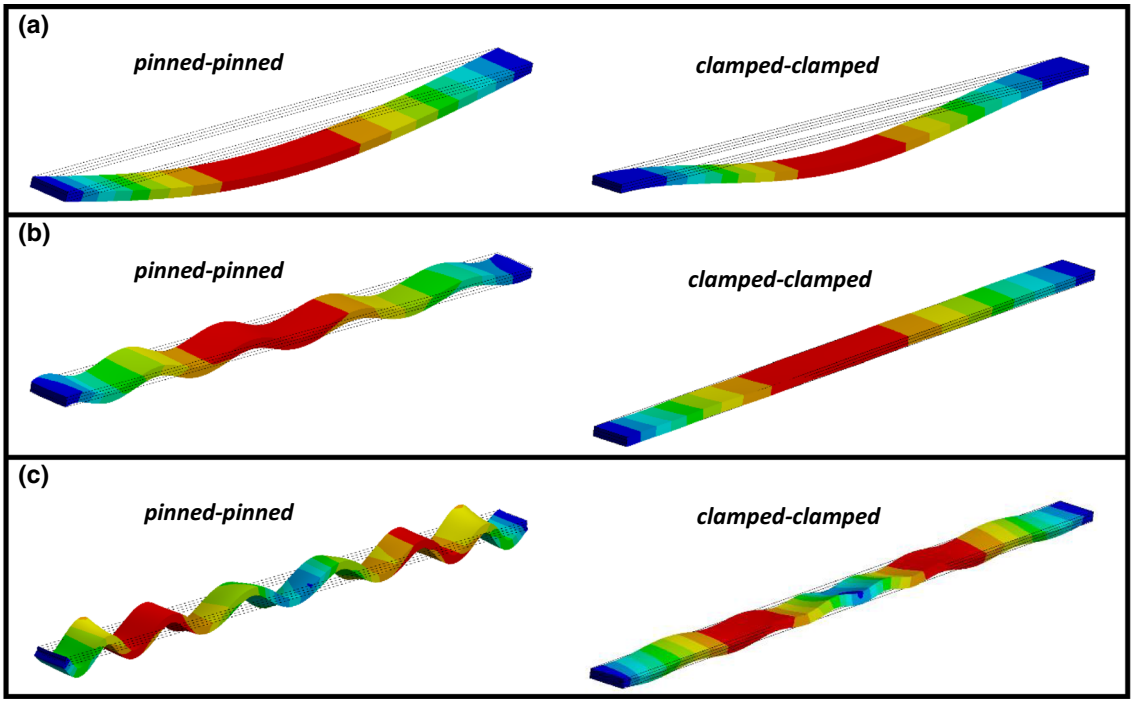

Fig. 2 Mode shapes of the first (**a**) transverse, (**b**) longitudinal and (**c**) rotation vibration modes with clamped–clamped and pinned–pinned boundary conditions

can be rewritten, which is not presented here for the sake of brevity. It should be mentioned that for having more layers in the laminated hyperelastic beam model, Eqs. (19–32) should be rewritten on the right side, based on the number of layers. The kinetic energy of the structure is written as

$$\begin{aligned}\delta KE = &\int_0^L \int_A \rho(z)\left[u_t(x,t) + (\chi(z) - z)\, w_{xt}(x,t) - \chi(z)\,\phi_t(x,t)\right]\delta u_t(x,t)\,\mathrm{d}A\mathrm{d}x \\ &+ \int_0^L \int_A \rho(z)\,(\chi(z) - z)\left[u_t(x,t) + (\chi(z) - z)\, w_{xt}(x,t) - \chi(z)\,\phi_t(x,t)\right]\delta w_{xt}(x,t)\,\mathrm{d}A\mathrm{d}x \\ &- \int_0^L \int_A \rho(z)\chi(z)\left[u_t(x,t) + (\chi(z) - z)\, w_{xt}(x,t) - \chi(z)\,\phi_t(x,t)\right]\delta\phi_t(x,t)\,\mathrm{d}A\mathrm{d}x \\ &+ \int_0^L \int_A \rho(z) w_t(x,t)\,\delta w_t(x,t)\,\mathrm{d}A\mathrm{d}x, \end{aligned} \tag{33}$$

which, by defining the moment of inertia in terms of area (I_i) for a three-layered hyperelastic thick beam, is written as

$$I_0 = \int_A \rho(z)\mathrm{d}A = \int_{A_1} \rho_1 \mathrm{d}A_1 + \int_{A_2} \rho_2 \mathrm{d}A_2 + \int_{A_3} \rho_3 \mathrm{d}A_3, \tag{34}$$

$$I_1 = \int_A \rho(z)\chi(z)\,\mathrm{d}A = \int_{A_1} \rho_1 \chi(z)\,\mathrm{d}A_1 + \int_{A_2} \rho_2 \chi(z)\,\mathrm{d}A_2 + \int_{A_3} \rho_3 \chi(z)\,\mathrm{d}A_3, \tag{35}$$

$$I_2 = \int_A \rho(z)\left[\chi(z) - z\right]\mathrm{d}A = \int_{A_1} \rho_1\left[\chi(z) - z\right]\mathrm{d}A_1 + \int_{A_2} \rho_2\left[\chi(z) - z\right]\mathrm{d}A_2 + \int_{A_3} \rho_3\left[\chi(z) - z\right]\mathrm{d}A_3, \tag{36}$$

$$I_3 = \int_A \rho(z)\,\chi^2(z)\mathrm{d}A = \int_{A_1} \rho_1 \chi^2(z)\mathrm{d}A_1 + \int_{A_2} \rho_2 \chi^2(z)\mathrm{d}A_2 + \int_{A_3} \rho_3 \chi^2(z)\mathrm{d}A_3, \tag{37}$$

$$\begin{aligned} I_4 = &\int_A \rho(z)[\chi(z) - z]^2\mathrm{d}A = \int_{A_1} \rho_1[\chi(z) - z]^2\mathrm{d}A_1 \\ &+ \int_{A_2} \rho_2[\chi(z) - z]^2\mathrm{d}A_2 + \int_{A_3} \rho_3[\chi(z) - z]^2\mathrm{d}A_3, \end{aligned} \tag{38}$$

$$\begin{aligned} I_5 = &\int_A \rho\chi(z)\left[\chi(z) - z\right]\mathrm{d}A = \int_{A_1} \rho_1\chi(z)\left[\chi(z) - z\right]\mathrm{d}A_1 \\ &+ \int_{A_2} \rho_2\chi(z)\left[\chi(z) - z\right]\mathrm{d}A_2 + \int_{A_3} \rho_3\chi(z)\left[\chi(z) - z\right]\mathrm{d}A_3, \end{aligned} \tag{39}$$

and by substituting Eqs. (34–39) into Eq. (33), one can reach the kinetic energy of layered thick hyperelastic beams, as

$$\begin{aligned}\delta KE = \int_0^L &-\left[I_0 u_{tt}(x,t) + I_2 w_{xtt}(x,t) - I_1\phi_{tt}(x,t)\right]\delta u(x,t) \\ &+\left[I_2 u_{xtt}(x,t) + I_4 w_{xxtt}(x,t) - I_5\phi_{xtt}(x,t)\right]\delta w(x,t) \\ &-I_0 w_{tt}(x,t)\,\delta w(x,t) + \left[I_1 u_{tt}(x,t) + I_5 w_{xtt}(x,t) - I_3\phi_{tt}(x,t)\right]\delta\phi(x,t)\,\mathrm{d}x. \end{aligned} \tag{40}$$

Moreover, the beam is assumed to be lying on a nonlinear elastic foundation (Fig. 1) and externally actuated by a periodic load, which gives the external work on the beam as

$$\begin{aligned}\delta U_F &= \int_0^L \left(F_{linear}\left(x,t\right)+F_{nonlinear}\left(x,t\right)+F_{shear}\left(x,t\right)\right)\delta w\mathrm{d}x+\int_0^L F\cos\left(\omega t\right)\delta w\mathrm{d}x\\ &= \int_0^L \left[-K_L w\left(x,t\right)-K_{NL}w^3\left(x,t\right)+K_S w_{xx}\left(x,t\right)+F\cos\left(\omega t\right)\right]\delta w, \end{aligned} \tag{41}$$

where K_L, K_{NL} and K_S are the linear, nonlinear and shear coefficients of the foundation, respectively, and F is the external force acting periodically with a frequency of ω. Using Hamilton's principle, the coupled longitudinal, transverse and rotation equations of motion are obtained as

$$\begin{aligned}
&I_0 u_{tt}\left(x,t\right)+I_2 w_{xtt}\left(x,t\right)-I_1\phi_{tt}\left(x,t\right)-8A_{11}u_{xx}\left(x,t\right)-8B_{22}w_{xxx}\left(x,t\right)+8B_{11}\phi_{xx}\left(x,t\right)\\
&+12A_{11}\frac{\partial}{\partial x}\left[{u_x}^2\left(x,t\right)\right]+24B_{22}\frac{\partial}{\partial x}\left[u_x\left(x,t\right)w_{xx}\left(x,t\right)\right]-24B_{11}\frac{\partial}{\partial x}\left[u_x\left(x,t\right)\phi_x\left(x,t\right)\right]\\
&-\left(4A_{11}-D_{44}\right)\frac{\partial}{\partial x}\left[{w_x}^2\left(x,t\right)\right]+12D_{22}\frac{\partial}{\partial x}\left[{w_{xx}}^2\left(x,t\right)\right]-2D_{44}\frac{\partial}{\partial x}\left[w_x\left(x,t\right)\phi\left(x,t\right)\right]\\
&-24D_{33}\frac{\partial}{\partial x}\left[w_{xx}\left(x,t\right)\phi_x\left(x,t\right)\right]+D_{44}\frac{\partial}{\partial x}\left[\phi^2\left(x,t\right)\right]+12D_{11}\frac{\partial}{\partial x}\left[{\phi_x}^2\left(x,t\right)\right]\\
&+12A_{11}\frac{\partial}{\partial x}\left[u_x\left(x,t\right){w_x}^2\left(x,t\right)\right]+12B_{22}\frac{\partial}{\partial x}\left[{w_x}^2\left(x,t\right)w_{xx}\left(x,t\right)\right]\\
&-12B_{11}\frac{\partial}{\partial x}\left[{w_x}^2\left(x,t\right)\phi_x\left(x,t\right)\right]+3A_{11}\frac{\partial}{\partial x}\left[{w_x}^4\left(x,t\right)\right]=0,
\end{aligned} \tag{42}$$

$$\begin{aligned}
&-I_2 u_{xtt}\left(x,t\right)+I_0 w_{tt}\left(x,t\right)-I_4 w_{xxtt}\left(x,t\right)+I_5\phi_{xtt}\left(x,t\right)-8B_{22}u_{xxx}\left(x,t\right)-2D_{44}w_{xx}\left(x,t\right)\\
&-8D_{22}w_{xxxx}\left(x,t\right)+K_L w\left(x,t\right)-K_S w_{xx}\left(x,t\right)+2D_{44}\phi_x\left(x,t\right)+8D_{33}\phi_{xxx}\left(x,t\right)\\
&+12B_{22}\frac{\partial^2}{\partial x^2}\left[{u_x}^2\left(x,t\right)\right]+24D_{22}\frac{\partial^2}{\partial x^2}\left[u_x\left(x,t\right)w_{xx}\left(x,t\right)\right]\\
&-\left(8A_{11}-2D_{44}\right)\frac{\partial}{\partial x}\left[u_x\left(x,t\right)w_x\left(x,t\right)\right]-24D_{33}\frac{\partial^2}{\partial x^2}\left[u_x\left(x,t\right)\phi_x\left(x,t\right)\right]\\
&-2D_{44}\frac{\partial}{\partial x}\left[u_x\left(x,t\right)\phi\left(x,t\right)\right]-\left(4B_{22}-E_{66}\right)\frac{\partial^2}{\partial x^2}\left[{w_x}^2\left(x,t\right)\right]\\
&-\left(8B_{22}-2E_{66}\right)\frac{\partial}{\partial x}\left[w_x\left(x,t\right)w_{xx}\left(x,t\right)\right]+12E_{44}\frac{\partial^2}{\partial x^2}\left[{w_{xx}}^2\left(x,t\right)\right]\\
&-2E_{66}\frac{\partial^2}{\partial x^2}\left[w_x\left(x,t\right)\phi\left(x,t\right)\right]+\left(8B_{11}-2E_{77}\right)\frac{\partial}{\partial x}\left[w_x\left(x,t\right)\phi_x\left(x,t\right)\right]\\
&-2E_{66}\frac{\partial}{\partial x}\left[w_{xx}\left(x,t\right)\phi\left(x,t\right)\right]-24E_{33}\frac{\partial^2}{\partial x^2}\left[w_{xx}\left(x,t\right)\phi_x\left(x,t\right)\right]\\
&+E_{66}\frac{\partial^2}{\partial x^2}\left[\phi^2\left(x,t\right)\right]+2E_{77}\frac{\partial}{\partial x}\left[\phi\left(x,t\right)\phi_x\left(x,t\right)\right]+12E_{22}\frac{\partial^2}{\partial x^2}\left[{\phi_x}^2\left(x,t\right)\right]\\
&+12A_{11}\frac{\partial}{\partial x}\left[{u_x}^2\left(x,t\right)w_x\left(x,t\right)\right]+12B_{22}\frac{\partial^2}{\partial x^2}\left[u_x\left(x,t\right){w_x}^2\left(x,t\right)\right]\\
&+24B_{22}\frac{\partial}{\partial x}\left[u_x\left(x,t\right)w_x\left(x,t\right)w_{xx}\left(x,t\right)\right]-24B_{11}\frac{\partial}{\partial x}\left[u_x\left(x,t\right)w_x\left(x,t\right)\phi_x\left(x,t\right)\right]\\
&-\left(4A_{11}-2D_{44}\right)\frac{\partial}{\partial x}\left[{w_x}^3\left(x,t\right)\right]+K_{NL}w^3\left(x,t\right)+12D_{22}\frac{\partial}{\partial x}\left[w_x\left(x,t\right){w_{xx}}^2\left(x,t\right)\right]\\
&+12D_{22}\frac{\partial^2}{\partial x^2}\left[{w_x}^2\left(x,t\right)w_{xx}\left(x,t\right)\right]-12D_{33}\frac{\partial^2}{\partial x^2}\left[{w_x}^2\left(x,t\right)\phi_x\left(x,t\right)\right]\\
&-3D_{44}\frac{\partial}{\partial x}\left[{w_x}^2\left(x,t\right)\phi\left(x,t\right)\right]-24D_{33}\frac{\partial}{\partial x}\left[w_x\left(x,t\right)w_{xx}\left(x,t\right)\phi_x\left(x,t\right)\right]
\end{aligned}$$

$$
\begin{aligned}
&+ D_{44}\frac{\partial}{\partial x}\left[w_x\left(x,t\right)\phi^2\left(x,t\right)\right] + 12D_{11}\frac{\partial}{\partial x}\left[w_x\left(x,t\right)\phi_x{}^2\left(x,t\right)\right]\\
&+ 12A_{11}\frac{\partial}{\partial x}\left[u_x\left(x,t\right)w_x{}^3\left(x,t\right)\right] + 3B_{22}\frac{\partial^2}{\partial x^2}\left[w_x{}^4\left(x,t\right)\right] + 12B_{22}\frac{\partial}{\partial x}\left[w_x{}^3\left(x,t\right)w_{xx}\left(x,t\right)\right]\\
&- 12B_{11}\frac{\partial}{\partial x}\left[w_x{}^3\left(x,t\right)\phi_x\left(x,t\right)\right] + 3A_{11}\frac{\partial}{\partial x}\left[w_x{}^5\left(x,t\right)\right] = F\cos\left(\omega t\right), \qquad (43)
\end{aligned}
$$

$$
\begin{aligned}
&-I_1u_{tt}\left(x,t\right) - I_5w_{xtt}\left(x,t\right) + I_3\phi_{tt}\left(x,t\right) + 8B_{11}u_{xx}\left(x,t\right) - 2D_{44}w_x\left(x,t\right) + 8D_{33}w_{xxx}\left(x,t\right)\\
&- 8D_{11}\phi_{xx}\left(x,t\right) + 2D_{44}\phi\left(x,t\right) - 12B_{11}\frac{\partial}{\partial x}\left[u_x{}^2\left(x,t\right)\right] - 24D_{33}\frac{\partial}{\partial x}\left[u_x\left(x,t\right)w_{xx}\left(x,t\right)\right]\\
&+ 2D_{44}u_x\left(x,t\right)w_x\left(x,t\right) + 24D_{11}\frac{\partial}{\partial x}\left[u_x\left(x,t\right)\phi_x\left(x,t\right)\right] - 2D_{44}u_x\left(x,t\right)\phi\left(x,t\right)\\
&+ \left(4B_{11} - E_{77}\right)\frac{\partial}{\partial x}\left[w_x{}^2\left(x,t\right)\right] - 12E_{33}\frac{\partial}{\partial x}\left[w_{xx}{}^2\left(x,t\right)\right] + 2E_{66}w_x\left(x,t\right)w_{xx}\left(x,t\right)\\
&+ 2E_{77}\frac{\partial}{\partial x}\left[w_x\left(x,t\right)\phi\left(x,t\right)\right] + 24E_{22}\frac{\partial}{\partial x}\left[w_{xx}\left(x,t\right)\phi_x\left(x,t\right)\right] - 2E_{77}w_x\left(x,t\right)\phi_x\left(x,t\right)\\
&- 2E_{66}w_{xx}\left(x,t\right)\phi\left(x,t\right) - 12E_{11}\frac{\partial}{\partial x}\left[\phi_x{}^2\left(x,t\right)\right] - E_{77}\frac{\partial}{\partial x}\left[\phi^2\left(x,t\right)\right] + 2E_{77}\phi\left(x,t\right)\phi_x\left(x,t\right)\\
&- 12B_{11}\frac{\partial}{\partial x}\left[u_x\left(x,t\right)w_x{}^2\left(x,t\right)\right] - 12D_{33}\frac{\partial}{\partial x}\left[w_x{}^2\left(x,t\right)w_{xx}\left(x,t\right)\right] + D_{44}w_x{}^3\left(x,t\right)\\
&+ 12D_{11}\frac{\partial}{\partial x}\left[w_x{}^2\left(x,t\right)\phi_x\left(x,t\right)\right] - D_{44}w_x{}^2\left(x,t\right)\phi\left(x,t\right) - 3B_{11}\frac{\partial}{\partial x}\left[w_x{}^4\left(x,t\right)\right] = 0. \qquad (44)
\end{aligned}
$$

It can therefore be seen that the equations of motion are highly nonlinear and coupled, which emphasises the importance of having the axial motion while analysing the mechanical behaviour of the structure. The linear coupling sources between the axial and transverse motions are the stiffness terms B_{11} and B_{22} and inertia terms I_1 and I_2, for which, for a single-layer hyperelastic beam, due to the homogeneity in the thickness direction, these terms will be equal to zero and the linear coupling terms vanish. In the next section, the equations of motion are nondimensionalised, discretised and solved.

3 Solution procedure

For the first step of solving the equations of motion, the new nondimensional parameters are defined as

$$
\begin{aligned}
&\gamma^* = \frac{x}{L}, \beta^* = \frac{w}{h}, \alpha^* = \frac{u}{h}, \phi^* = \phi, A_{11}{}^* = \frac{A_{11}}{A_{110}}, B_{11}{}^* = \frac{B_{11}}{A_{110}h}, B_{22}{}^* = \frac{B_{22}}{A_{110}h}, D_{44}{}^* = \frac{D_{11}}{A_{110}},\\
&D_{11}{}^* = \frac{D_{11}}{A_{110}h^2}, D_{22}{}^* = \frac{D_{11}}{A_{110}h^2}, D_{33}{}^* = \frac{D_{11}}{A_{110}h^2}, E_{11}{}^* = \frac{E_{11}}{A_{110}h^3}, E_{22}{}^* = \frac{E_{22}}{A_{110}h^3},\\
&E_{33}{}^* = \frac{E_{33}}{A_{110}h^3}, E_{44}{}^* = \frac{E_{44}}{A_{110}h^3}, E_{55}{}^* = \frac{E_{55}}{A_{110}}, E_{66}{}^* = \frac{E_{66}}{A_{110}h}, E_{77}{}^* = \frac{E_{77}}{A_{110}h},\\
&I_0{}^* = \frac{I_0}{I_{00}}, I_1{}^* = \frac{I_1}{I_{00}h}, I_2{}^* = \frac{I_2}{I_{00}h}, I_3{}^* = \frac{I_3}{I_{00}h^2}, I_4{}^* = \frac{I_4}{I_{00}h^2}, I_5{}^* = \frac{I_5}{I_{00}h^2},\\
&\eta = \frac{h}{L}, \Omega = \omega\sqrt{\frac{I_{00}L^3}{A_{110}h}}, t^* = t\sqrt{\frac{A_{110}h}{I_{00}L^3}},\\
&F^* = F\frac{L^2}{A_{11}h}, K_L{}^* = K_L\frac{L^2}{A_{11}}, K_{NL}{}^* = K_{NL}\frac{h^2L^2}{A_{11}}, K_S{}^* = K_S\frac{1}{A_{11}}, \qquad (45)
\end{aligned}
$$

and by using these terms, the equations of motion are nondimensionalised as

$$
I_0\eta\alpha_{tt}\left(\gamma,t\right) + I_2\eta^2\beta_{\gamma tt}\left(\gamma,t\right) - I_1\eta\phi_{tt}\left(\gamma,t\right) - 8A_{11}\alpha_{\gamma\gamma}\left(\gamma,t\right) - 8B_{22}\eta\beta_{\gamma\gamma\gamma}\left(\gamma,t\right) + 8B_{11}\phi_{\gamma\gamma}\left(\gamma,t\right)
$$

$$
\begin{aligned}
&+12A_{11}\eta\frac{\partial}{\partial\gamma}\left[{\alpha_\gamma}^2(\gamma,t)\right]+24B_{22}\eta^2\frac{\partial}{\partial\gamma}\left[\alpha_\gamma(\gamma,t)\,\beta_{\gamma\gamma}(\gamma,t)\right]-24B_{11}\eta\frac{\partial}{\partial\gamma}\left[\alpha_\gamma(\gamma,t)\,\phi_\gamma(\gamma,t)\right]\\
&-\eta\left(4A_{11}-D_{44}\right)\frac{\partial}{\partial\gamma}\left[{\beta_\gamma}^2(\gamma,t)\right]+12D_{22}\eta^3\frac{\partial}{\partial\gamma}\left[{\beta_{\gamma\gamma}}^2(\gamma,t)\right]-2D_{44}\frac{\partial}{\partial\gamma}\left[\beta_\gamma(\gamma,t)\,\phi(\gamma,t)\right]\\
&-24D_{33}\eta^2\frac{\partial}{\partial\gamma}\left[\beta_{\gamma\gamma}(\gamma,t)\,\phi_\gamma(\gamma,t)\right]+D_{44}\frac{1}{\eta}\frac{\partial}{\partial\gamma}\left[\phi^2(\gamma,t)\right]+12D_{11}\eta\frac{\partial}{\partial\gamma}\left[{\phi_\gamma}^2(\gamma,t)\right]\\
&+12A_{11}\eta^2\frac{\partial}{\partial\gamma}\left[\alpha_\gamma(\gamma,t)\,{\beta_\gamma}^2(\gamma,t)\right]+12B_{22}\eta^3\frac{\partial}{\partial\gamma}\left[{\beta_\gamma}^2(\gamma,t)\,\beta_{\gamma\gamma}(\gamma,t)\right]\\
&-12B_{11}\eta^2\frac{\partial}{\partial\gamma}\left[{\beta_\gamma}^2(\gamma,t)\,\phi_\gamma(\gamma,t)\right]+3A_{11}\eta^3\frac{\partial}{\partial\gamma}\left[{\beta_\gamma}^4(\gamma,t)\right]=0,
\end{aligned}
\tag{46}
$$

$$
\begin{aligned}
&-I_2\eta^2\alpha_{\gamma tt}(\gamma,t)+I_0\eta\beta_{tt}(\gamma,t)-I_4\eta^3\beta_{\gamma\gamma tt}(\gamma,t)+I_5\eta^2\phi_{\gamma tt}(\gamma,t)-8B_{22}\eta\alpha_{\gamma\gamma\gamma}(\gamma,t)\\
&\quad-2D_{44}\beta_{\gamma\gamma}(\gamma,t)-8D_{22}\eta^2\beta_{\gamma\gamma\gamma\gamma}(\gamma,t)+K_L\beta(\gamma,t)-K_S\beta_{\gamma\gamma}(\gamma,t)+2D_{44}\frac{1}{\eta}\phi_\gamma(\gamma,t)\\
&\quad+8D_{33}\eta\phi_{\gamma\gamma\gamma}(\gamma,t)+12B_{22}\eta^2\frac{\partial^2}{\partial\gamma^2}\left[{\alpha_\gamma}^2(\gamma,t)\right]+24D_{22}\eta^3\frac{\partial^2}{\partial\gamma^2}\left[\alpha_\gamma(\gamma,t)\,\beta_{\gamma\gamma}(\gamma,t)\right]\\
&\quad-\eta\left(8A_{11}-2D_{44}\right)\frac{\partial}{\partial\gamma}\left[\alpha_\gamma(\gamma,t)\,\beta_\gamma(\gamma,t)\right]-24D_{33}\eta^2\frac{\partial^2}{\partial\gamma^2}\left[\alpha_\gamma(\gamma,t)\,\phi_\gamma(\gamma,t)\right]\\
&\quad-2D_{44}\frac{\partial}{\partial\gamma}\left[\alpha_\gamma(\gamma,t)\,\phi(\gamma,t)\right]-\eta^2\left(4B_{22}-E_{66}\right)\frac{\partial^2}{\partial\gamma^2}\left[{\beta_\gamma}^2(\gamma,t)\right]\\
&\quad-\eta^2\left(8B_{22}-2E_{66}\right)\frac{\partial}{\partial\gamma}\left[\beta_\gamma(\gamma,t)\,\beta_{\gamma\gamma}(\gamma,t)\right]+12E_{44}\eta^4\frac{\partial^2}{\partial\gamma^2}\left[{\beta_{\gamma\gamma}}^2(\gamma,t)\right]\\
&\quad-2E_{66}\eta\frac{\partial^2}{\partial\gamma^2}\left[\beta_\gamma(\gamma,t)\,\phi(\gamma,t)\right]+\eta\left(8B_{11}-2E_{77}\right)\frac{\partial}{\partial\gamma}\left[\beta_\gamma(\gamma,t)\,\phi_\gamma(\gamma,t)\right]\\
&\quad-2E_{66}\eta\frac{\partial}{\partial\gamma}\left[\beta_{\gamma\gamma}(\gamma,t)\,\phi(\gamma,t)\right]-24E_{33}\eta^3\frac{\partial^2}{\partial\gamma^2}\left[\beta_{\gamma\gamma}(\gamma,t)\,\phi_\gamma(\gamma,t)\right]\\
&\quad+E_{66}\frac{\partial^2}{\partial\gamma^2}\left[\phi^2(\gamma,t)\right]+2E_{77}\frac{\partial}{\partial\gamma}\left[\phi(\gamma,t)\,\phi_\gamma(\gamma,t)\right]+12E_{22}\eta^2\frac{\partial^2}{\partial\gamma^2}\left[{\phi_\gamma}^2(\gamma,t)\right]\\
&\quad+12A_{11}\eta^2\frac{\partial}{\partial\gamma}\left[{\alpha_\gamma}^2(\gamma,t)\,\beta_\gamma(\gamma,t)\right]+12B_{22}\eta^3\frac{\partial^2}{\partial\gamma^2}\left[\alpha_\gamma(\gamma,t)\,{\beta_\gamma}^2(\gamma,t)\right]\\
&\quad+24B_{22}\eta^3\frac{\partial}{\partial\gamma}\left[\alpha_\gamma(\gamma,t)\,\beta_\gamma(\gamma,t)\,\beta_{\gamma\gamma}(\gamma,t)\right]-24B_{11}\eta^2\frac{\partial}{\partial\gamma}\left[\alpha_\gamma(\gamma,t)\,\beta_\gamma(\gamma,t)\,\phi_\gamma(\gamma,t)\right]\\
&\quad-\eta^2\left(4A_{11}-2D_{44}\right)\frac{\partial}{\partial\gamma}\left[{\beta_\gamma}^3(\gamma,t)\right]+K_{NL}\beta^3(\gamma,t)+12D_{22}\eta^4\frac{\partial}{\partial\gamma}\left[\beta_\gamma(\gamma,t)\,{\beta_{\gamma\gamma}}^2(\gamma,t)\right]\\
&\quad+12D_{22}\eta^4\frac{\partial^2}{\partial\gamma^2}\left[{\beta_\gamma}^2(\gamma,t)\,\beta_{\gamma\gamma}(\gamma,t)\right]-12D_{33}\eta^3\frac{\partial^2}{\partial\gamma^2}\left[{\beta_\gamma}^2(\gamma,t)\,\phi_\gamma(\gamma,t)\right]\\
&\quad-3D_{44}\eta\frac{\partial}{\partial\gamma}\left[{\beta_\gamma}^2(\gamma,t)\,\phi(\gamma,t)\right]-24D_{33}\eta^3\frac{\partial}{\partial\gamma}\left[\beta_\gamma(\gamma,t)\,\beta_{\gamma\gamma}(\gamma,t)\,\phi_\gamma(\gamma,t)\right]\\
&\quad+D_{44}\frac{\partial}{\partial\gamma}\left[\beta_\gamma(\gamma,t)\,\phi^2(\gamma,t)\right]+12D_{11}\eta^2\frac{\partial}{\partial\gamma}\left[\beta_\gamma(\gamma,t)\,{\phi_\gamma}^2(\gamma,t)\right]\\
&\quad+12A_{11}\eta^3\frac{\partial}{\partial\gamma}\left[\alpha_\gamma(\gamma,t)\,{\beta_\gamma}^3(\gamma,t)\right]+3B_{22}\eta^4\frac{\partial^2}{\partial\gamma^2}\left[{\beta_\gamma}^4(\gamma,t)\right]\\
&\quad+12B_{22}\eta^4\frac{\partial}{\partial\gamma}\left[{\beta_\gamma}^3(\gamma,t)\,\beta_{\gamma\gamma}(\gamma,t)\right]-12B_{11}\eta^3\frac{\partial}{\partial\gamma}\left[{\beta_\gamma}^3(\gamma,t)\,\beta_\gamma(\gamma,t)\right]\\
&\quad+3A_{11}\eta^4\frac{\partial}{\partial\gamma}\left[{\beta_\gamma}^5(\gamma,t)\right]=F\cos(\Omega t),
\end{aligned}
\tag{47}
$$

$$
\begin{aligned}
&-I_1\eta\alpha_{tt}(\gamma,t)-I_5\eta^2\beta_{\gamma tt}(\gamma,t)+I_3\eta\phi_{tt}(\gamma,t)+8B_{11}\alpha_{\gamma\gamma}(\gamma,t)-2D_{44}\frac{1}{\eta}\beta_\gamma(\gamma,t)+8D_{33}\eta\beta_{\gamma\gamma\gamma}(\gamma,t)\\
&-8D_{11}\phi_{\gamma\gamma}(\gamma,t)+2D_{44}\frac{1}{\eta^2}\phi(\gamma,t)-12B_{11}\eta\frac{\partial}{\partial\gamma}\left[{\alpha_\gamma}^2(\gamma,t)\right]-24D_{33}\eta^2\frac{\partial}{\partial\gamma}\left[\alpha_\gamma(\gamma,t)\beta_{\gamma\gamma}(\gamma,t)\right]\\
&+2D_{44}\alpha_\gamma(\gamma,t)\beta_\gamma(\gamma,t)+24D_{11}\eta\frac{\partial}{\partial\gamma}\left[\alpha_\gamma(\gamma,t)\phi_\gamma(\gamma,t)\right]-2D_{44}\frac{1}{\eta}\alpha_\gamma\phi(x,t)\\
&+(4B_{11}-E_{77})\eta\frac{\partial}{\partial\gamma}\left[{\beta_\gamma}^2(\gamma,t)\right]-12E_{33}\eta^3\frac{\partial}{\partial\gamma}\left[{\beta_{\gamma\gamma}}^2(\gamma,t)\right]+2E_{66}\eta\beta_\gamma(\gamma,t)\beta_{\gamma\gamma}(\gamma,t)\\
&+2E_{77}\frac{\partial}{\partial\gamma}\left[\beta_\gamma(\gamma,t)\phi(\gamma,t)\right]+24E_{22}\eta^2\frac{\partial}{\partial\gamma}\left[\beta_{\gamma\gamma}(\gamma,t)\phi_\gamma(\gamma,t)\right]-2E_{77}\beta_\gamma(\gamma,t)\phi_\gamma(\gamma,t)\\
&-2E_{66}\beta_{\gamma\gamma}(\gamma,t)\phi(\gamma,t)-12E_{11}\eta\frac{\partial}{\partial\gamma}\left[{\phi_\gamma}^2(\gamma,t)\right]-E_{77}\frac{1}{\eta}\frac{\partial}{\partial\gamma}\left[\phi^2(\gamma,t)\right]+2E_{77}\frac{1}{\eta}\phi(\gamma,t)\phi_\gamma(\gamma,t)\\
&-12B_{11}\eta^2\frac{\partial}{\partial\gamma}\left[\alpha_\gamma(\gamma,t){\beta_\gamma}^2(\gamma,t)\right]-12D_{33}\eta^3\frac{\partial}{\partial\gamma}\left[{\beta_\gamma}^2(\gamma,t)\beta_{\gamma\gamma}(\gamma,t)\right]+D_{44}\eta{\beta_\gamma}^3(\gamma,t)\\
&+12D_{11}\eta^2\frac{\partial}{\partial\gamma}\left[{\beta_\gamma}^2(\gamma,t)\phi_\gamma(\gamma,t)\right]-D_{44}{\beta_\gamma}^2(\gamma,t)\phi(\gamma,t)-3B_{11}\eta^3\frac{\partial}{\partial x}\left[{\beta_\gamma}^4(\gamma,t)\right]=0. \qquad (48)
\end{aligned}
$$

For the sake of brevity and ease notation, the superscript * is neglected in the formulation. Using the Galerkin scheme, each motion component can be written in a series expansion of orthogonal spatial functions as

$$
\begin{Bmatrix}\alpha\\ \phi\\ \beta\end{Bmatrix}=\sum_{n=1}^{N}\begin{Bmatrix}U_n(\gamma)r_n(t)\\ \Phi_n(\gamma)p_n(t)\\ W_n(\gamma)q_n(t)\end{Bmatrix}, \qquad (49)
$$

where U_n, Φ_n, W_n are the set of trial functions that should satisfy the boundary conditions of longitudinal, rotation and transverse motions at the middle of the thickness. (Studies on layered structures based on various thickness assumptions can be found in Refs. [44–50].) For pinned–pinned and fixed–fixed boundary conditions, these trial functions are written as

$$
U_p(\gamma)=\sin\left(\mu_p\gamma\right), \qquad (50)
$$

$$
\begin{cases} Fixed-Fixed \rightarrow W_p(\gamma)=-\cos\left(\mu_p\gamma\right)+\cosh\left(\mu_p\gamma\right)-\psi\left(\mu_p\right)\left[-\sin\left(\mu_p\gamma\right)+\sinh\left(\mu_p\gamma\right)\right],\\ Pinned-Pinned \rightarrow W_p(\gamma)=\sin\left(\mu_p\gamma\right), \end{cases} \qquad (51)
$$

$$
\Phi_p(\gamma)=\left(\frac{1}{\mu_p}\right)\left(\frac{\partial W_p(\gamma)}{\partial x}\right), \qquad (52)
$$

where

$$
\psi\left(\mu_p\right)=\frac{-\cos\left(\mu_p\right)+\cosh\left(\mu_p\right)}{-\sin\left(\mu_p\right)+\sinh\left(\mu_p\right)}, \qquad (53)
$$

and the equations of motion are rewritten as

$$
\begin{aligned}
&\begin{bmatrix}\boldsymbol{M}_{11}&\boldsymbol{M}_{12}&\boldsymbol{M}_{13}\\ \boldsymbol{M}_{21}&\boldsymbol{M}_{22}&\boldsymbol{M}_{23}\\ \boldsymbol{M}_{31}&\boldsymbol{M}_{32}&\boldsymbol{M}_{33}\end{bmatrix}\begin{Bmatrix}\ddot{r}_n\\ \ddot{p}_n\\ \ddot{q}_n\end{Bmatrix}+\begin{bmatrix}\xi&0&0\\ 0&\xi&0\\ 0&0&\xi\end{bmatrix}\begin{Bmatrix}\dot{r}_n\\ \dot{p}_n\\ \dot{q}_n\end{Bmatrix}\\
&+\begin{bmatrix}\boldsymbol{KL}_{11}&\boldsymbol{KL}_{12}&\boldsymbol{KL}_{13}\\ \boldsymbol{KL}_{21}&\boldsymbol{KL}_{22}&\boldsymbol{KL}_{23}\\ \boldsymbol{KL}_{31}&\boldsymbol{KL}_{32}&\boldsymbol{KL}_{33}\end{bmatrix}\begin{Bmatrix}r_n\\ p_n\\ q_n\end{Bmatrix}=\begin{Bmatrix}0\\ 0\\ F_n^{external}\end{Bmatrix}+\begin{Bmatrix}\boldsymbol{KNI}_n^{system}\\ \boldsymbol{KN2}_n^{system}\\ \boldsymbol{KN3}_n^{system}\end{Bmatrix}, \qquad (54)
\end{aligned}
$$

where $\boldsymbol{M}_{ij}$ are the mass tensors of the discretised equations and the components are defined as

$$
M_{11}(l,i):\eta I_0\int_0^1 U_l(\gamma)U_i(\gamma)\,\mathrm{d}\gamma, \qquad (55)
$$

$$M_{12}(l,i) : \eta^2 I_2 \int_0^1 U_l(\gamma) W_i'(\gamma)\,\mathrm{d}\gamma, \tag{56}$$

$$M_{13}(l,i) : -\eta I_1 \int_0^1 U_l(\gamma) \Phi_i(\gamma)\,\mathrm{d}\gamma, \tag{57}$$

$$M_{21} : -\eta^2 I_2 \int_0^1 W_l(\gamma) U_i'(\gamma)\,\mathrm{d}\gamma, \tag{58}$$

$$M_{22}(l,i) : \eta I_0 \int_0^1 W_l(\gamma) W_i(\gamma)\,\mathrm{d}\gamma - \eta^3 I_4 \int_0^1 W_l(\gamma) W_i''(\gamma)\,\mathrm{d}\gamma, \tag{59}$$

$$M_{23}(l,i) : \eta^2 I_5 \int_0^1 W_l(\gamma) \Phi_i'(\gamma)\,\mathrm{d}\gamma, \tag{60}$$

$$M_{31} : -\eta I_1 \int_0^1 \Phi_l(\gamma) U_i(\gamma)\,\mathrm{d}\gamma, \tag{61}$$

$$M_{32}(l,i) : -\eta^2 I_5 \int_0^1 \Phi_l(\gamma) W_i'(\gamma)\,\mathrm{d}\gamma, \tag{62}$$

$$M_{33}(l,i) : \eta I_3 \int_0^1 \Phi_l(\gamma) \Phi_i(\gamma)\,\mathrm{d}\gamma, \tag{63}$$

and $\boldsymbol{KL}_{ij}$ are the linear stiffness tensors, defined as

$$KL_{11}(l,i) : -8A_{11} \int_0^1 U_l(\gamma) U_i''(\gamma)\,\mathrm{d}\gamma, \tag{64}$$

$$KL_{12}(l,i) : -8\eta B_{22} \int_0^1 U_l(\gamma) W_i'''(\gamma)\,\mathrm{d}\gamma, \tag{65}$$

$$KL_{13}(l,i) : 8B_{11} \int_0^1 U_l(\gamma) \Phi_i''(\gamma)\,\mathrm{d}\gamma, \tag{66}$$

$$KL_{21}(l,i) : -8\eta B_{22} \int_0^1 W_l(\gamma) U_i'''(\gamma)\,\mathrm{d}\gamma, \tag{67}$$

$$\begin{aligned} KL_{22}(l,i) : &- \int_0^1 W_l(\gamma) \frac{\mathrm{d}}{\mathrm{d}\gamma}\left[2D_{44} W'_i(\gamma)\right]\mathrm{d}\gamma - 8\eta^2 D_{22} \int_0^1 W_l(\gamma) W_i{}^{(4)}(\gamma)\,\mathrm{d}\gamma \\ &+ K_L \int_0^1 W_l(\gamma) W_i(\gamma)\,\mathrm{d}\gamma - K_S \int_0^1 W_l(\gamma) W''_i(\gamma)\,\mathrm{d}\gamma, \end{aligned} \tag{68}$$

$$KL_{23}(l,i): 2\frac{1}{\eta}D_{44}\int_0^1 W_l(\gamma)\Phi_i'(\gamma)\,\mathrm{d}\gamma + 8\eta D_{33}\int_0^1 W_l(\gamma)\Phi_i'''(\gamma)\,\mathrm{d}\gamma, \tag{69}$$

$$KL_{31}(l,i): 8B_{11}\int_0^1 \Phi_l(\gamma)U_i''(\gamma)\,\mathrm{d}\gamma, \tag{70}$$

$$KL_{32}(l,i): -2\frac{1}{\eta}D_{44}\int_0^1 \Phi_l(\gamma)W_i'(\gamma)\,\mathrm{d}\gamma + 8\eta D_{33}\int_0^1 \Phi_l(\gamma)W_i'''(\gamma)\,\mathrm{d}\gamma, \tag{71}$$

$$KL_{33}(l,i): -8D_{11}\int_0^1 \Phi_l(\gamma)\Phi_i''(\gamma)\,\mathrm{d}\gamma + 2\frac{1}{\eta^2}D_{44}\int_0^1 \Phi_l(\gamma)\Phi_i(\gamma)\,\mathrm{d}\gamma. \tag{72}$$

$KN1$, $KN2$ and $KN3$ are the nonlinear stiffness terms in the coupled equation where

$$\begin{aligned}
\boldsymbol{KN}1_n^{system} &= \boldsymbol{KN}_{11}r^2(t) + \boldsymbol{KN}_{12}r(t)\,p(t) + \boldsymbol{KN}_{13}r(t)\,q(t)\\
&+ \boldsymbol{KN}_{14}p^2(t) + \boldsymbol{KN}_{15}p(t)\,q(t) + \boldsymbol{KN}_{16}q^2(t)\\
&+ \boldsymbol{KN}_{17}r(t)\,p^2(t) + \boldsymbol{KN}_{18}p^3(t) + \boldsymbol{KN}_{19}p^2(t)\,q(t)\\
&+ \boldsymbol{KN}_{110}p^4(t),
\end{aligned} \tag{73}$$

$$\begin{aligned}
\boldsymbol{KN}2_n^{system} &= \boldsymbol{KN}_{21}r^2(t) + \boldsymbol{KN}_{22}r(t)\,p(t) + \boldsymbol{KN}_{23}r(t)\,q(t)\\
&+ \boldsymbol{KN}_{24}p^2(t) + \boldsymbol{KN}_{25}p(t)\,q(t) + \boldsymbol{KN}_{26}q^2(t)\\
&+ \boldsymbol{KN}_{27}r^2(t)\,p(t) + \boldsymbol{KN}_{28}r(t)\,p^2(t)\\
&+ \boldsymbol{KN}_{29}r(t)\,p(t)\,q(t) + \boldsymbol{KN}_{210}p^3(t)\\
&+ \boldsymbol{KN}_{211}p^2(t)\,q(t) + \boldsymbol{KN}_{212}p(t)\,q^2(t)\\
&+ \boldsymbol{KN}_{213}r(t)\,p^3(t) + \boldsymbol{KN}_{214}p^4(t) + \boldsymbol{KN}_{215}p^3(t)\,q(t) + \boldsymbol{KN}_{216}p^5(t),
\end{aligned} \tag{74}$$

$$\begin{aligned}
\boldsymbol{KN}3_n^{system} &= \boldsymbol{KN}_{31}r^2(t) + \boldsymbol{KN}_{32}r(t)\,p(t) + \boldsymbol{KN}_{33}r(t)\,q(t) + \boldsymbol{KN}_{34}p^2(t)\\
&+ \boldsymbol{KN}_{35}p(t)\,q(t) + \boldsymbol{KN}_{36}q^2(t) + \boldsymbol{KN}_{37}r(t)\,p^2(t) + \boldsymbol{KN}_{38}p^3(t)\\
&+ \boldsymbol{KN}_{39}p^2(t)\,q(t) + \boldsymbol{KN}_{310}p^4(t),
\end{aligned} \tag{75}$$

and the coefficients of the nonlinear stiffnesses (KN_{ij}) are defined in "Appendix A" for the sake of brevity. By employing a dynamic equilibrium technique, the time-dependent terms of the degrees of freedom are written in a series expansion of exponential functions as

$$r_m = \sum_{n=-N}^{N} A_{mn}e^{in\Omega t}, \tag{76}$$

$$p_m = \sum_{n=-N}^{N} B_{mn}e^{in\Omega t}, \tag{77}$$

$$q_m = \sum_{n=-N}^{N} C_{mn}e^{in\Omega t}, \tag{78}$$

and the general dynamic complex equilibrium equations are written as

$$\begin{aligned}
&\left\{-n^2\Omega^2\boldsymbol{M}_{3n\times 3n} + in\Omega\boldsymbol{C}_{3n\times 3n} + \boldsymbol{K}_{3n\times 3n}\right\}\begin{Bmatrix} r_n \\ p_n \\ q_n \end{Bmatrix}_{3n\times 1}\\
&= \begin{Bmatrix} 0 \\ 0 \\ \boldsymbol{F}_n^{external}(\Omega) \end{Bmatrix}_{3n\times 1} + \begin{Bmatrix} \boldsymbol{KN}1_n^{system}(A_{mn}, B_{mn}, C_{mn}, \Omega) \\ \boldsymbol{KN}2_n^{system}(A_{mn}, B_{mn}, C_{mn}, \Omega) \\ \boldsymbol{KN}3_n^{system}(A_{mn}, B_{mn}, C_{mn}, \Omega) \end{Bmatrix}_{3n\times 1}.
\end{aligned} \tag{79}$$

By solving the discretised coupled $3N$ equations of motion presented in Eq. (79) using a continuation technique [51–53], the nonlinear forced time-dependent mechanical response of the layered hyperelastic structure is obtained.

4 Results and discussion for linear and nonlinear analyses

The coupled motion of shear deformable layered hyperelastic structures is formulated, discretised and solved in the previous sections. In this section, the linear and nonlinear mechanics of the system are analysed and discussed in two main subsections.

4.1 Linear analysis for different shear models

In this subsection, the natural frequencies of the layered hyperelastic structures are analysed and the influence of layering, shear deformation theory and the foundation is discussed in detail.

4.1.1 Model verification

In the first step, in order to verify the current model for analysing layered beam models, the natural frequencies of a three-layered elastic beam structure are obtained for clamped–clamped and pinned–pinned boundaries. Layering is achieved by having steel as the top layer, aluminium in the middle and silicon carbide at the bottom (the elastic material properties of the layers can be found in Ref. [54]), with geometry properties at a length of $L = 2.4$ m, total thickness of $h = 0.03$ m (0.01 m for each layer) and width of $b = 0.12$ m. The first four transverse natural frequencies and the first axial and rotational natural frequencies are obtained using the third-order shear deformable beam theory and compared with those obtained by ANSYS Workbench [55] in Table 1, and the mode shapes are shown in Fig. 2; it can be seen that the current modelling shows great accuracy in computing the natural frequency terms.

4.1.2 Layer sorting, slenderness ratio and shear model effect

Properly layering the structure can have a significant effect in changing the natural frequencies of a hyperelastic beam. To make this possible, three different soft materials are assumed with known Mooney–Rivlin hyperelastic coefficients, as shown in Table 2. For the first step, by assuming a single-layer homogeneous hyperelastic beam with the length of 0.2 mm and nondimensional foundation of $K_L = 1$ and $K_S = 1$, the slenderness ratio ($r = L/h$) is varied and the fundamental natural frequency is obtained for different shear deformation theories in Table 3. It can be seen that for the single-layer model, the fundamental natural frequency of all the five shear models is in good agreement, especially for the vulcanised rubber beam.

By increasing the number of layers to two and three, the fundamental natural frequencies are given in Tables 4 and 5, respectively. It can be seen that by having more than a single layer, the homogeneity in the thickness direction is lost, the coupling terms are considerable and, therefore, the difference between different shear models is slightly more than for the homogeneous single-layer model. Furthermore, it can be seen that for all the layered models and boundary conditions, by increasing the slenderness ratio (L/h), the shear effect loses its importance and the results for different shear models become unique.

Table 1 Linear natural frequencies of a three-layered elastic beam with pinned–pinned and fixed–fixed boundary conditions in hertz

Model	BCs	Transverse				*Axial*	*Rotation*
		Mode 1	Mode 2	Mode 3	Mode 4	Mode 1	Mode 1
Present	*CC*	41.0802	113.129	221.209	365.317	1479.540	2957.979
ANSYS	*CC*	41.322	113.53	221.66	364.64	1482.3	2956.6
Present	*SS*	18.2554	72.9090	163.911	290.543	1479.623	2957.468
ANSYS	*SS*	18.994	72.492	163.67	288.55	1470.2	2955.4

Table 2 Hyperelastic physical properties of soft materials from the literature [56,57]

Material	Mooney Rivlin parameters		
	C_1 (Pa)	C_2 (Pa)	ρ (kg/m^3)
Silicone	253216	4.709e5	1430
Thermoplastic	2.463e5	3.512e6	1152.5
Vulcanised rubber	0.28e6	0.15e6	950

Table 3 Fundamental natural frequencies of *single-layer* hyperelastic beams with different slenderness ratios and shear deformation theories

$r = L/h$	BC	CBT	Timoshenko	Third-Order	Exponential	Trigonometric
Silicone						
100	*CC*	28.1066315	28.1058381	28.0613949	28.0495963	28.0555882
	SS	26.8844497	26.8844452	26.8790424	26.8776181	26.8783409
50	*CC*	20.0984905	20.0909931	19.9747145	19.9433354	19.9592964
	SS	19.0364669	19.0364162	19.0211706	19.0171500	19.0191906
20	*CC*	13.5165344	13.4300982	13.0894529	12.9940148	13.0427443
	SS	12.1552464	12.1540216	12.0947328	12.0790562	12.0870142
10	*CC*	11.0263991	10.6412455	9.97717584	9.78842630	9.88489544
	SS	8.87847552	8.86563176	8.70696574	8.66466219	8.68615087
3D-printed thermoplastic						
100	*CC*	31.8001428	31.7963715	31.5600876	31.4958815	31.5285720
	SS	30.0096747	30.0096449	29.9784623	29.9702373	29.9744119
50	*CC*	23.5675273	23.5423896	23.0001642	22.8473804	22.9255139
	SS	21.3821135	21.3817796	21.2942338	21.2710974	21.2828424
20	*CC*	18.2377203	18.0294260	16.6267951	16.2247058	16.4307878
	SS	14.2187342	14.2109901	13.8816207	13.7934946	13.8382855
10	*CC*	18.5914253	17.4967291	14.9614247	14.21118716	14.5966669
	SS	11.6305988	11.5580599	10.7552375	10.5334826	10.6465584
Vulcanised rubber						
100	*CC*	34.4280536	34.4274664	34.3947866	34.3861353	34.3905276
	SS	32.9775740	32.9775711	32.9736341	32.9725962	32.9731229
50	*CC*	24.5106362	24.5047782	24.4174210	24.3940465	24.4059248
	SS	23.3366630	23.3366304	23.3255149	23.3225840	23.3240715
20	*CC*	16.1341804	16.0555223	15.7864449	15.7121078	15.7499904
	SS	14.8386764	14.8378850	14.7944946	14.7830357	14.7888520
10	*CC*	12.5987291	12.2434931	11.7111708	11.5615479	11.6378881
	SS	10.6887937	10.6803688	10.5628155	10.5316104	10.5474551

4.1.3 Foundation effect

To show the influence of a foundation support on the natural frequencies of layered hyperelastic beams, the structure is assumed to be three-layered with equal thicknesses, ($L/h = 20$) and the foundation terms are varied as $K_L = [0.0, 1.0, 1.0, 3.0, 4.0, 5.0]$ and $K_S = [0.1, 0.2, 0.4, 0.6, 0.8, 1.0]$. The fundamental natural frequencies are shown for both pinned–pinned and clamped–clamped boundary conditions in Tables 6, 7 and 8 for layering as [thermoplastic–silicone–vulcanised rubber], [thermoplastic– vulcanised rubber–silicone] and [silicone–thermoplastic–vulcanised rubber], respectively, using the third-order shear deformable beam model. It can be seen that the layered hyperelastic beam models are more sensitive to variations of the shear term (K_s) compared with the linear term (K_L), and adding the foundation increases the fundamental frequency parameter significantly.

4.2 Nonlinear analysis

The nonlinear dynamics of layered hyperelastic thick beam structures is investigated in this section for various layer, shear and material position models.

Table 4 Fundamental natural frequencies of *two-layered* hyperelastic beams with different slenderness ratios and shear deformation theories

$r = L/h$	BC	CBT	Timoshenko	Third-Order	Exponential	Trigonometric
Sorting: *Silicone–3D-printed thermoplastic*						
100	*CC*	29.7340907	29.7322132	29.6207112	29.5910476	29.6061242
	SS	28.3089814	28.3089689	28.2956561	28.2922077	28.2939558
50	*CC*	21.5192529	21.5058667	21.2413942	21.1685749	21.2057350
	SS	20.0807042	20.0805804	20.0432020	20.0335084	20.0384230
20	*CC*	15.1241626	15.0300170	14.3361165	14.1404376	14.2406520
	SS	12.9733813	12.9710949	12.8278107	12.7904730	12.8094120
10	*CC*	13.3507029	12.9333003	11.5762041	11.1874505	11.3867605
	SS	9.82337237	9.80184612	9.42775842	9.32851239	9.37894002
Sorting: *3D-printed thermoplastic–vulcanised rubber*						
100	*CC*	32.9025718	32.9007381	32.7954063	32.7675713	32.7817124
	SS	31.3673283	31.3673136	31.3551669	31.3520513	31.3536296
50	*CC*	23.7164675	23.7035445	23.4548446	23.3868036	23.4215140
	SS	22.2348245	22.2346909	22.2007027	22.1919742	22.1963967
20	*CC*	16.3475598	16.2654456	15.6174109	15.4361428	15.528951
	SS	14.2969492	14.2950743	14.1652090	14.1317878	14.1487259
10	*CC*	13.9084386	13.5779696	12.2872118	11.9217392	12.1090495
	SS	10.6682708	10.6525061	10.3088192	10.2191370	10.2646474
Sorting: *Vulcanised rubber–silicone*						
100	*CC*	30.7828884	30.7822099	30.7442483	30.7341990	30.7393013
	SS	29.4676038	29.4676004	29.4630306	29.4618281	29.4624383
50	*CC*	21.9580668	21.9515018	21.8512018	21.8242796	21.8379663
	SS	20.8582540	20.8582149	20.8453158	20.8419207	20.8436436
20	*CC*	14.5905007	14.5104299	14.2102543	14.1267312	14.1693410
	SS	13.2865750	13.2856309	13.2353502	13.2220888	13.2288196
10	*CC*	11.6111038	11.2593795	10.6693876	10.5025821	10.5877820
	SS	9.62848313	9.61850920	9.48290029	9.44689586	9.46517866

Table 5 Fundamental natural frequencies of *three-layered* hyperelastic beams with different slenderness ratios and shear deformation theories

$r = L/h$	BC	CBT	Timoshenko	Third-Order	Exponential	Trigonometric
Sorting: *Silicone–3D-printed thermoplastic– vulcanised rubber*						
100	*CC*	30.9681123	30.9677558	30.9280699	30.917347	30.9228017
	SS	29.6263359	29.6263339	29.6215268	29.620237	29.6208931
50	*CC*	22.1334388	22.1300004	22.0257725	21.997078	22.0116995
	SS	20.9763997	20.9763776	20.9628076	20.959166	20.9610175
20	*CC*	14.8485713	14.8065505	14.5019297	14.413492	14.4587790
	SS	13.3871531	13.3866154	13.3336929	13.319438	13.3266873
10	*CC*	12.052601	11.8570456	11.2633773	11.084178	11.1761513
	SS	9.76211837	9.75638969	9.61347065	9.574479	9.59432579
Sorting: *3D-printed thermoplastic–silicone– vulcanised rubber*						
100	*CC*	31.0792240	31.0771291	30.9822274	30.957249	30.9699350
	SS	29.6369342	29.6369169	29.6262028	29.623464	29.6248515
50	*CC*	22.3854567	22.3707232	22.1464147	22.085406	22.1165090
	SS	21.0057928	21.0056361	20.9756990	20.968037	20.9719186
20	*CC*	15.3767687	15.2849197	14.6992985	14.536812	14.6199287
	SS	13.4959180	13.4938098	13.3798142	13.350614	13.3654096
10	*CC*	12.9909881	12.6319641	11.4549604	11.128466	11.2954731
	SS	10.0454782	10.0282134	9.72613705	9.648189	29.68770610
Sorting: *3D-printed thermoplastic–vulcanised rubber–silicone*						
100	*CC*	31.1189765	31.1164982	31.0054465	30.976079	30.9909968
	SS	29.6422094	29.6421922	29.6292289	29.625888	29.6275813
50	*CC*	22.4882142	22.4706799	22.205782	22.133457	22.1703283
	SS	21.0208307	21.0206653	20.9843036	20.974924	20.9796777
20	*CC*	15.6954145	15.5768274	14.8707311	14.673673	14.7744629
	SS	13.5560659	13.5532475	13.4139315	13.377907	13.3961688
10	*CC*	13.6707649	13.1694255	11.7529818	11.358212	11.5600729
	SS	10.2074657	10.1817722	9.81514643	9.719439	29.76798865

Table 6 Fundamental natural frequencies of three-layered hyperelastic beams [*thermoplastic–silicone–vulcanised rubber*] with different slenderness ratios and shear deformation theories

	$K_S = 0.1$	$K_S = 0.2$	$K_S = 0.4$	$K_S = 0.6$	$K_S = 0.8$	$K_S = 1.0$
Pinned–pinned						
$K_L = 0.0$	4.44576163	5.97334523	8.21583078	9.96541025	11.4504844	12.7637935
$K_L = 1.0$	5.98912959	7.19623324	9.14356823	10.7431088	12.1333669	13.3798142
$K_L = 2.0$	7.20933731	8.23958051	9.98547942	11.4681894	12.7798116	13.9686945
$K_L = 3.0$	8.25102479	9.16491111	10.7617263	12.1500759	13.3950951	14.5337338
$K_L = 4.0$	9.17519864	10.0050236	11.4856302	12.7956757	13.9833313	15.0776128
$K_L = 5.0$	10.0144457	10.7798607	12.1665379	13.4102305	14.5478016	15.6025444
Fixed–fixed						
$K_L = 0.0$	6.06990371	7.46126469	9.61553921	11.3408049	12.8222314	14.1412529
$K_L = 1.0$	7.27559657	8.47125334	10.4188043	12.0294404	13.4351646	14.6992985
$K_L = 2.0$	8.30811966	9.37303420	11.1644234	12.6807332	14.0213286	15.2369188
$K_L = 3.0$	9.22579923	10.1953607	11.8632707	13.3001703	14.5839514	15.7562049
$K_L = 4.0$	10.0601124	10.9561383	12.5231789	13.8920136	15.1256604	16.2589136
$K_L = 5.0$	10.8303428	11.6674130	13.1500116	14.4596519	15.6486275	16.7465377

Table 7 Fundamental natural frequencies of three-layered hyperelastic beams [*thermoplastic–vulcanised rubber–silicone*] with different slenderness ratios and shear deformation theories

	$K_S = 0.1$	$K_S = 0.2$	$K_S = 0.4$	$K_S = 0.6$	$K_S = 0.8$	$K_S = 1.0$
Pinned–pinned						
$K_L = 0.0$	4.56023487	6.05767609	8.27569748	10.0136505	11.4915612	12.7998710
$K_L = 1.0$	6.07392035	7.26582713	9.19695668	10.7874954	12.1718053	13.4139315
$K_L = 2.0$	7.27937245	8.29994197	10.0339844	11.5094268	12.8159938	14.0010860
$K_L = 3.0$	8.31179923	9.21877531	10.8063715	12.1886727	13.4293164	14.5645889
$K_L = 4.0$	9.22944950	10.0539837	11.5271191	12.8320134	14.0158257	15.1070870
$K_L = 5.0$	10.0637695	10.8249409	12.2053789	13.4446043	14.5787582	15.6307676
Fixed–fixed						
$K_L = 0.0$	6.46909276	7.78987081	9.87438670	11.5620699	13.0187251	14.3196948
$K_L = 1.0$	7.61113810	8.76148587	10.6577014	12.2378694	13.6224732	14.8707311
$K_L = 2.0$	8.60288588	9.63561855	11.3872584	12.8782530	14.2005746	15.4020647
$K_L = 3.0$	9.49156616	10.4367915	12.0728072	13.4882660	14.7560438	15.9156689
$K_L = 4.0$	10.3038813	11.1807000	12.7214645	14.0718587	15.2913474	16.4132083
$K_L = 5.0$	11.0566755	11.8781081	13.3386134	14.6321926	15.8085341	16.8961020

Table 8 Fundamental natural frequencies of three-layered hyperelastic beams [*silicone–thermoplastic–vulcanised rubber*] with different slenderness ratios and shear deformation theories

	$K_S = 0.1$	$K_S = 0.2$	$K_S = 0.4$	$K_S = 0.6$	$K_S = 0.8$	$K_S = 1.0$
Pinned–pinned						
$K_L = 0.0$	4.31840975	5.87720585	8.14415800	9.90520367	11.3973154	12.7155232
$K_L = 1.0$	5.89504178	7.11648799	9.07910558	10.6871841	12.0831138	13.3336929
$K_L = 2.0$	7.13122503	8.16989914	9.92637922	11.4157236	12.7320257	13.9244461
$K_L = 3.0$	8.18273922	9.10220306	10.7068131	12.1004787	13.3494312	14.4911363
$K_L = 4.0$	9.11372973	9.94750958	11.4341021	12.7485067	13.9395175	15.0364843
$K_L = 5.0$	9.95805785	10.7264062	12.1178187	13.3651509	14.5056189	15.5627340
Fixed–fixed						
$K_L = 0.0$	5.76095561	7.19395301	9.38000579	11.1192680	12.6096991	13.9357624
$K_L = 1.0$	7.02042195	8.23721111	10.2021634	11.8210913	13.2327187	14.5019297
$K_L = 2.0$	8.08603946	9.16244126	10.9628357	12.4835201	13.8276959	15.0468088
$K_L = 3.0$	9.02672360	10.0024501	11.6740478	13.1125264	14.3981075	15.5726343
$K_L = 4.0$	9.87823054	10.7771835	12.3443516	13.7127101	14.9467664	16.0812756
$K_L = 5.0$	10.6619479	11.4998415	12.9800861	14.2877041	15.4759861	16.5743147

4.2.1 Comparison of different shear models

Five different shear deformable beam theories were used in previous sections for modelling and formulation of the layered hyperelastic beam structure. In this section, the amplitude response of the sandwich structure for different shear models is examined. Three layers are assumed, and the thickness of the layers is assumed as $h = [h/4, h/2, h/4]$ with $L/h = 10$, $K_L = K_{NL} = 1$, $K_s = 0.1$, with the material sorting as [silicone–vulcanised rubber–thermoplastic]. In the first step, the influence of considering the shear effect as negligible (CBT), linear (Timoshenko) or higher order (third order) is examined, and the axial, transverse and rotation amplitudes are obtained, as shown in Figs. 3, 4 and 5 for *clamped–clamped* and Figs. 6, 7 and 8 for *pinned–pinned* boundary conditions. It can be seen that for both boundary conditions, the Timoshenko beam model gives the highest maximum amplitude for the dominant axial, transverse and rotation deformation. Furthermore, increasing the shear effect from the linear model to higher-order moves the resonance peak to lower frequencies.

The influence of using different types of higher-order shear deformable theories on the amplitude response is investigated for the similar three-layered hyperelastic beams with the given properties. Figures 9, 10, 11, 12, 13 and 14 show the axial, transverse and rotation amplitudes of *clamped–clamped* and *pinned–pinned* thick beam models, respectively. The results for the different higher-order shear models are fairly in good agreement, especially for the pinned–pinned boundary condition. Comparing the amplitude response of the dominant terms of axial, transverse and rotation motions, it can be seen that the highest amplitude is for the third-order beam model and the lowest belongs to the exponential beam model.

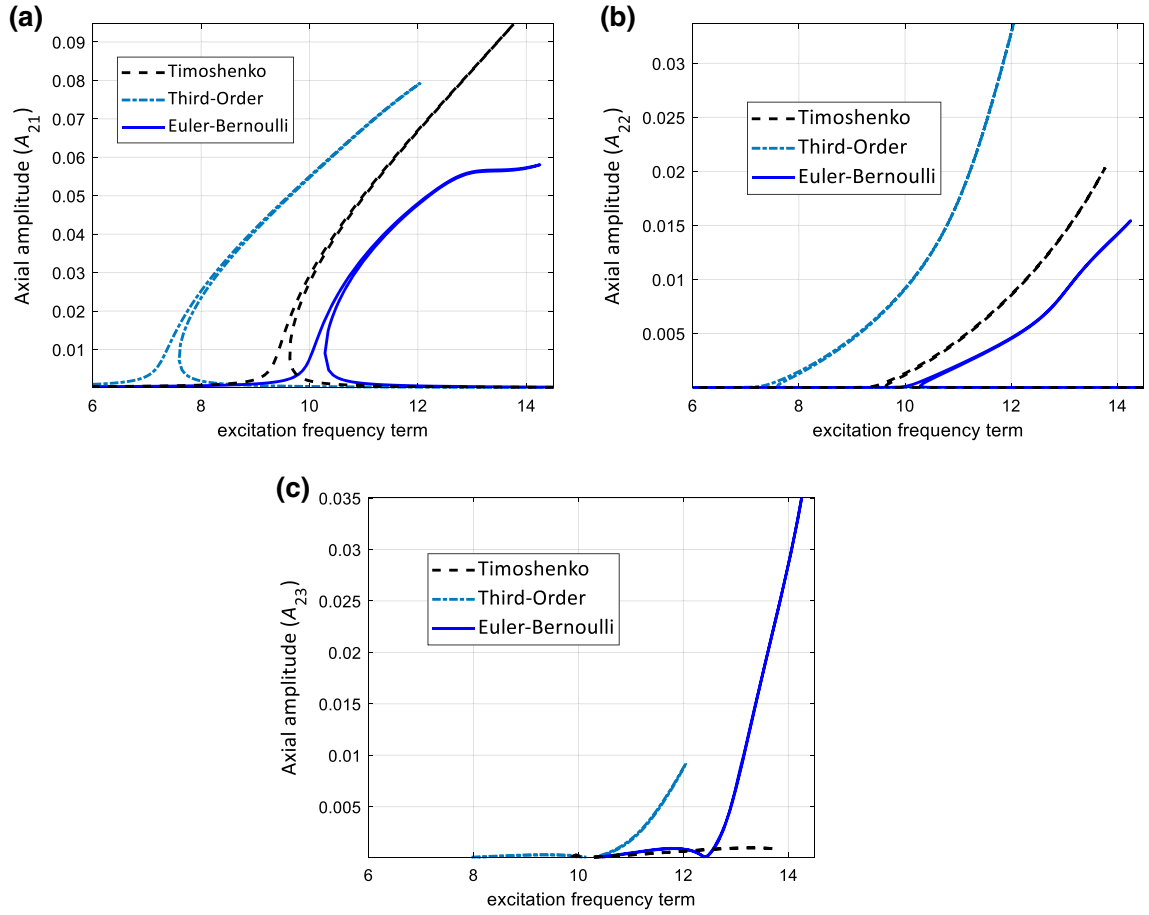

Fig. 3 Influence of considering shear effect on the *axial* amplitude response of the sandwich hyperelastic *clamped–clamped* beam **a** A_{21}, **b** A_{22} and **c** A_{23}

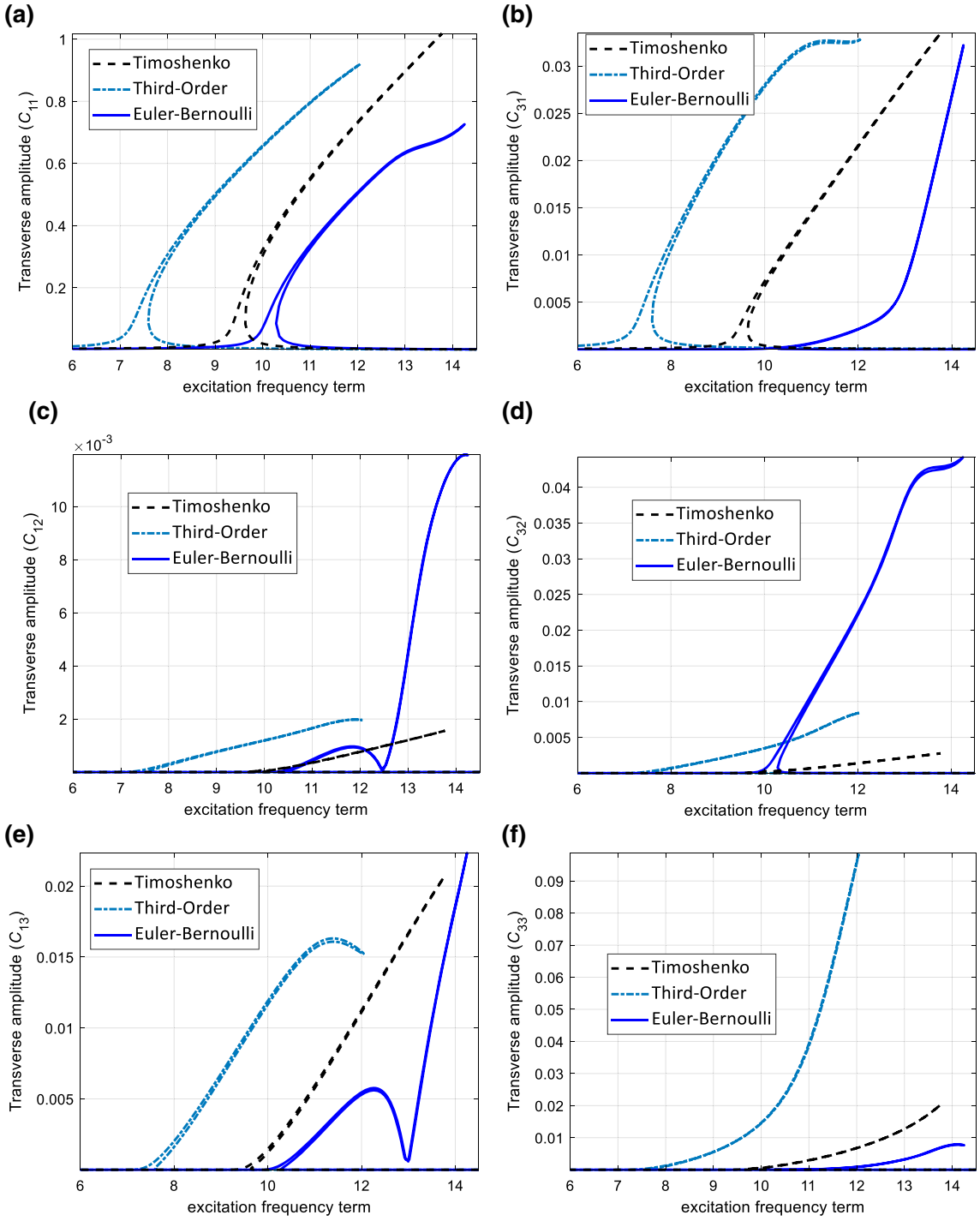

Fig. 4 Influence of considering shear effect on the *transverse* amplitude response of the sandwich hyperelastic *clamped–clamped* beam **a** C_{11}, **b** C_{31}, **c** C_{12}, **d** C_{32}, **e** C_{13}, and **f** C_{33}

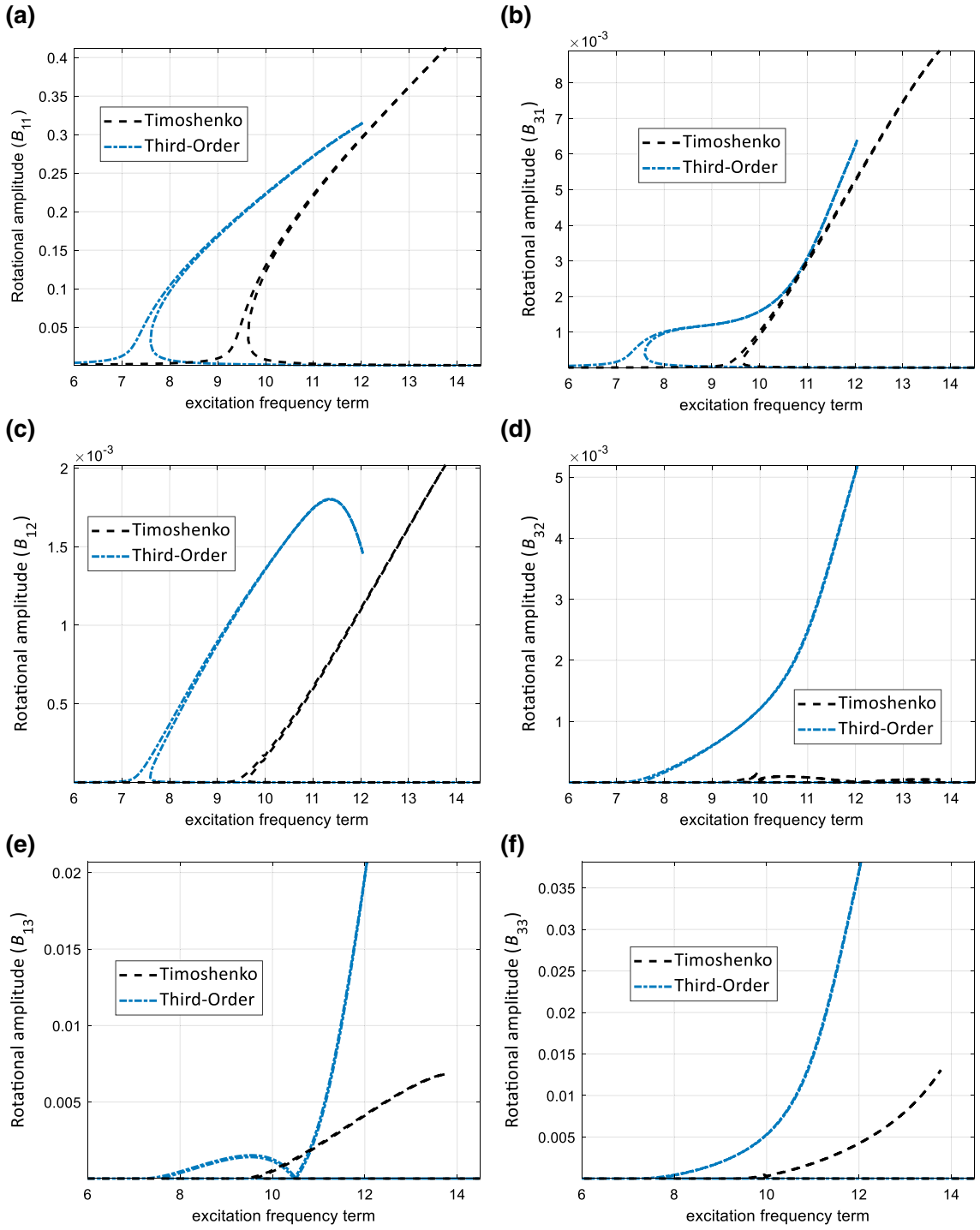

Fig. 5 Influence of considering shear effect on the *rotation* amplitude response of the sandwich hyperelastic *clamped–clamped* beam **a** B_{11}, **b** B_{31}, **c** B_{12}, **d** B_{32}, **e** B_{13}, and **f** B_{33}

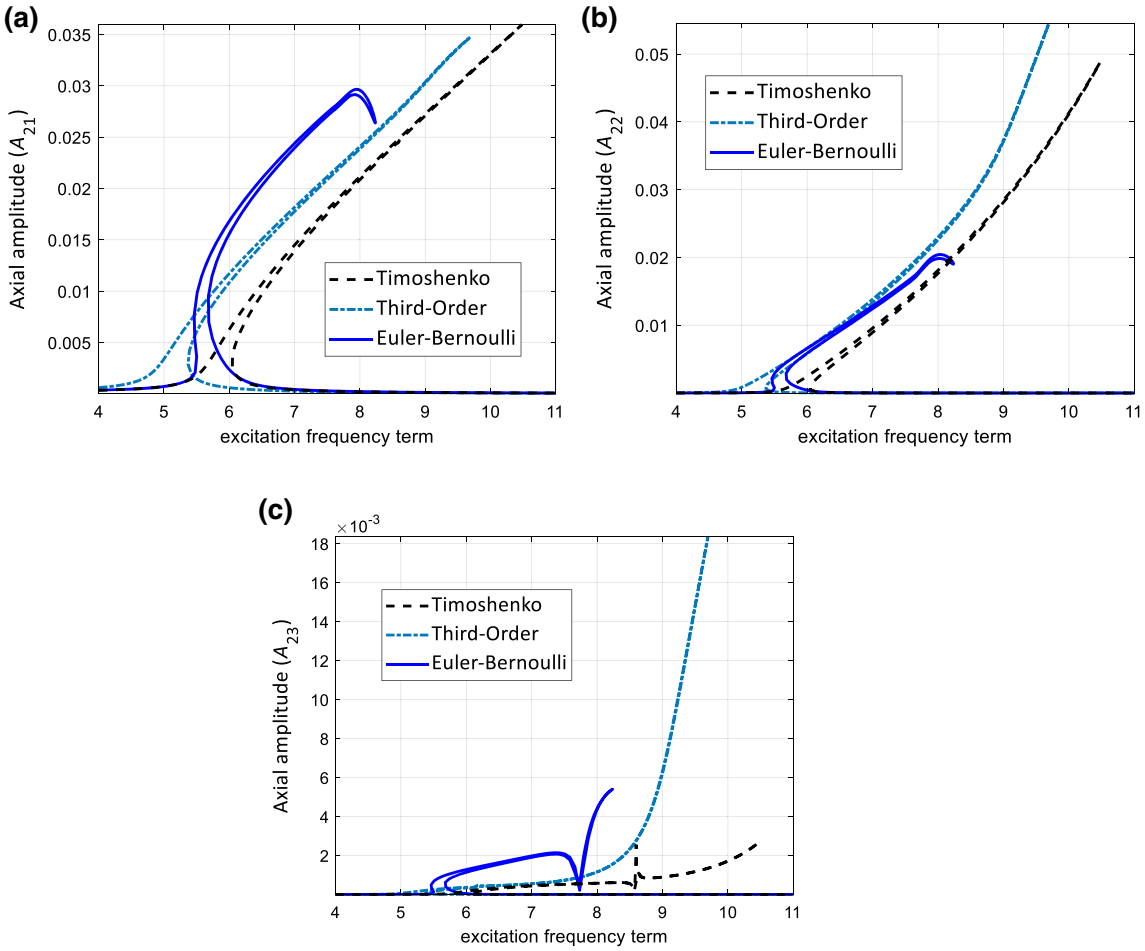

Fig. 6 Influence of considering shear effect on the *axial* amplitude response of the sandwich hyperelastic *pinned–pinned* beam **a** A_{21}, **b** A_{22} and **c** A_{23}

4.2.2 Influence of layering

Layering a hyperelastic structure for different purposes can change the dynamic behaviour of the structure significantly. In Sect. 4.1.1., this influence on the linear vibration response is analysed, and in this section, the nonlinear vibration response of the structure based on the number of layers is examined. To this end, for a homogeneous single-layer structure, the dominant amplitude responses are shown in Fig. 15, for thermoplastic, vulcanised rubber and silicone hyperelastic thick beams using the third-order shear deformable beam theory model. It can be seen that thermoplastic and silicone show a stiffness hardening effect, while the vulcanised rubber beam model shows a drop in the amplitude response of the axial motion while increasing the frequency and continues to go up afterwards.

By increasing the layers to two by having $h_1 = h_2 = h/2$, the dominant longitudinal, transverse and rotation amplitude responses of the structure are shown for different hyperelastic materials in Fig. 16 for a combination of different hyperelastic materials which the combination is given as Mat = ([*mat*1- *mat*2], [*mat*1- *mat*3], [*mat*2- *mat*3]) with *mat*1 = *thermoplastic*, *mat*2 = *silicone*, *mat*3 = *vulcanised rubber*. It can be seen that the highest transverse amplitude belongs to the material combination of [*mat*2- *mat*3], while the other two models have almost the same behaviour.

Finally, by having three layers ($h_1 = h_2 = h_3 = h/3$) and varying the layers as Mat = ([*mat*1-*mat*2-*mat*3], [*mat*2-*mat*1-*mat*3], [*mat*1-*mat*3-*mat*2]), the dominant amplitude responses of the longitudinal, transverse and rotation motions are shown in Fig. 17. It can be seen that the material distribution [*mat*2- *mat*1- *mat*3] has the lowest maximum axial amplitude and the highest transverse and rotation amplitudes; this shows that for

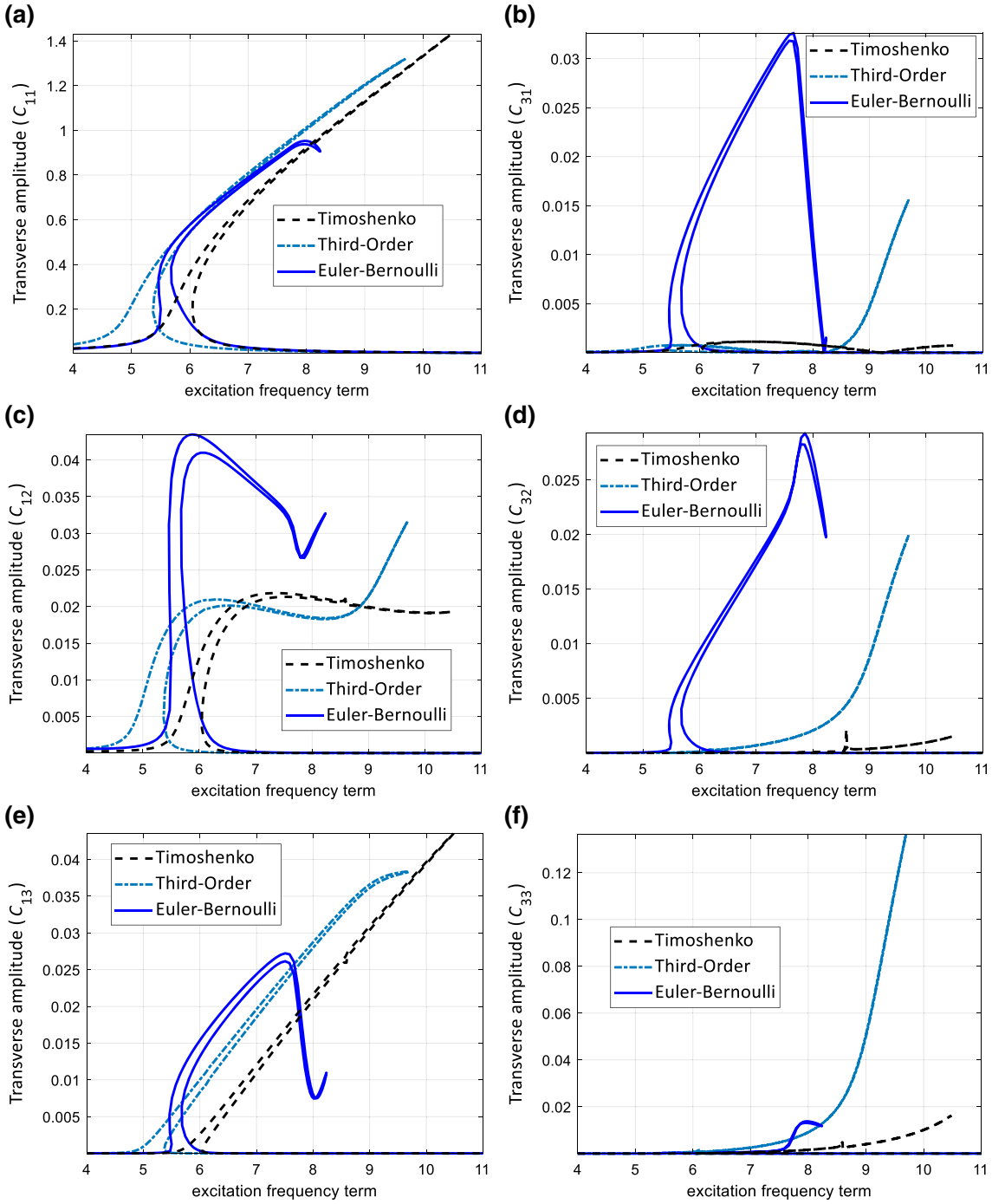

Fig. 7 Influence of considering shear effect on the *transverse* amplitude response of the sandwich hyperelastic *pinned–pinned* beam **a** C_{11}, **b** C_{31}, **c** C_{12}, **d** C_{32}, **e** C_{13} and **f** C_{33}

the other two material models, the coupling between the axial and transverse motion is noticeably higher and should be considered.

4.2.3 Influence of layer thickness

Changing the thickness of the layers can change the nonlinear vibration response of the structure significantly. To show this influence, the material distribution is Mat = [*mat*1-*mat*2-*mat*3] and the thickness of layers are

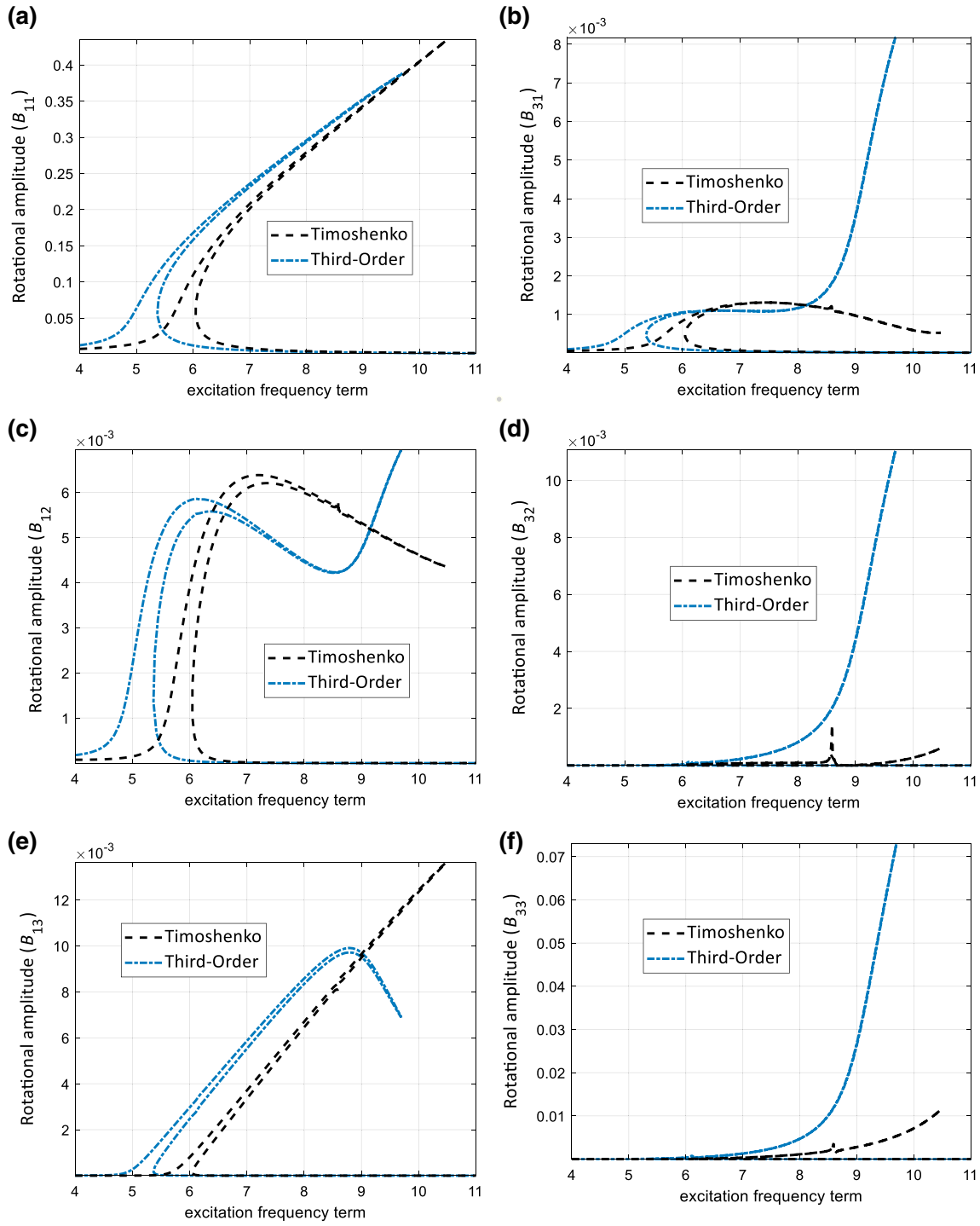

Fig. 8 Influence of considering shear effect on the *rotation* amplitude response of the sandwich hyperelastic *pinned–pinned* beam **a** B_{11}, **b** B_{31}, **c** B_{12}, **d** B_{32}, **e** B_{13} and **f** B_{33}

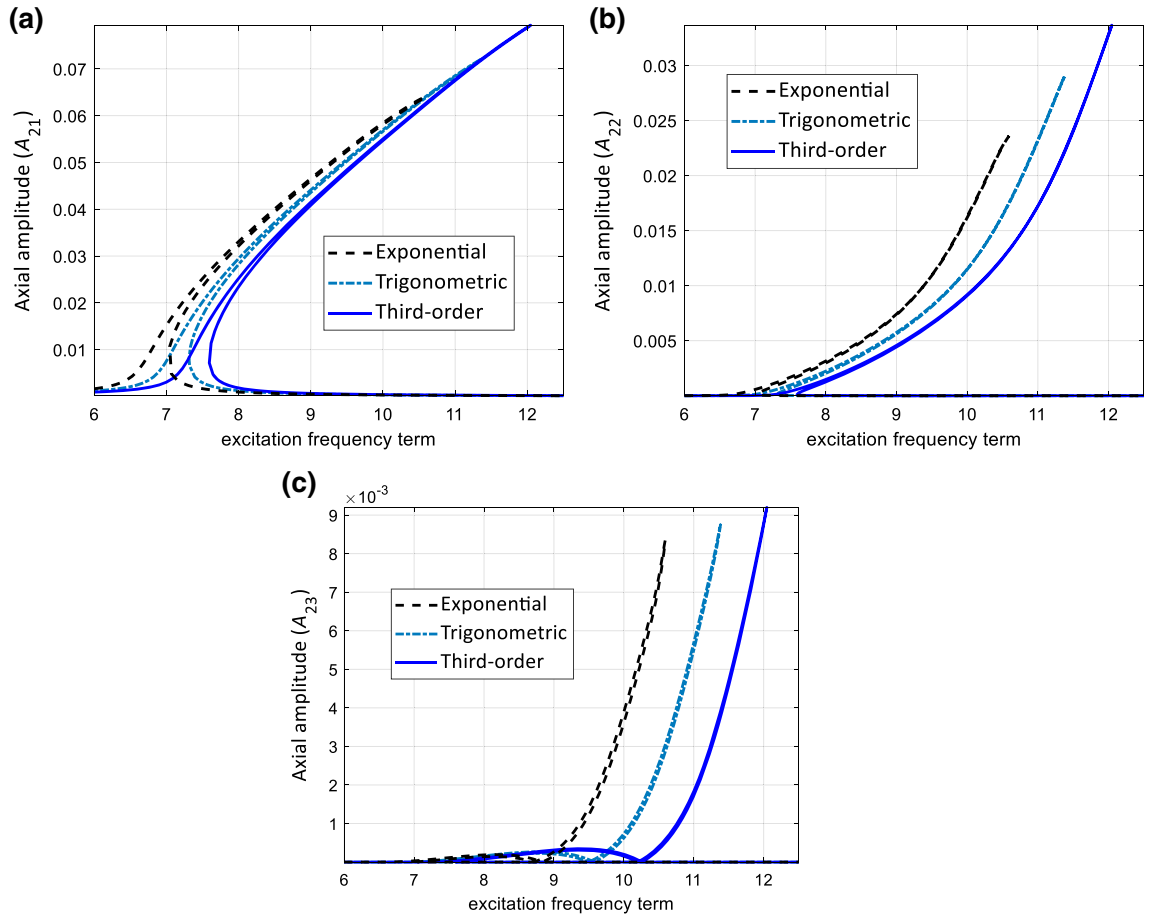

Fig. 9 Influence of different higher-order shear effect models on the *axial* amplitude response of the sandwich hyperelastic *clamped–clamped* beam **a** A_{21}, **b** A_{22}, and **c** A_{23}

$h = ([h/4, h/4, h/2], [h/2\,h/4, h/4], [h/4, h/2, h/4])$. The frequency–amplitude response of the structure is plotted in Figs. 18, 19 and 20 for axial, transverse and rotation deformations, respectively. It can be seen that changing the thickness of the layers has a significant effect in varying the nonlinear behaviour of the system. Besides, the maximum amplitude of all the deformation coordinates moves to higher frequencies for $h = [h/2, h/4, h/4]$ and the other two models show similar behaviour in dominant amplitude coordinates.

4.2.4 Influence of material positioning

To show the importance of the position of the hyperelastic material in a layered structure, a three-layered beam is assumed with the thickness of $h = [h/4, h/2, h/4]$ which shows that the middle layer (the core) is thicker than the outer layers. In this section, by varying the materials in the layers, the nonlinear forced vibration response of the system is studied. To do this, the position of the material is varied and the dominant amplitude–frequency responses in axial, transverse and rotation motions of the structure are shown in Figs. 21 and 22 for pinned–pinned and clamped–clamped conditions, respectively. It can be seen that for both boundary conditions, the maximum amplitudes sweep to lower frequencies when the material positioning is [*mat*1-*mat*2-*mat*3]; the clamped–clamped and pinned-pinned beam models show that the dominant rotation coordinate reaches its highest when the material positioning is [*mat*1-*mat*2-*mat3*].

4.2.5 Influence of layer positioning

Another important goal of this study is to show the influence of layering and positioning the layers in manufacturing sandwich hyperelastic structures. To demonstrate this effect, the position of the layers is varied with

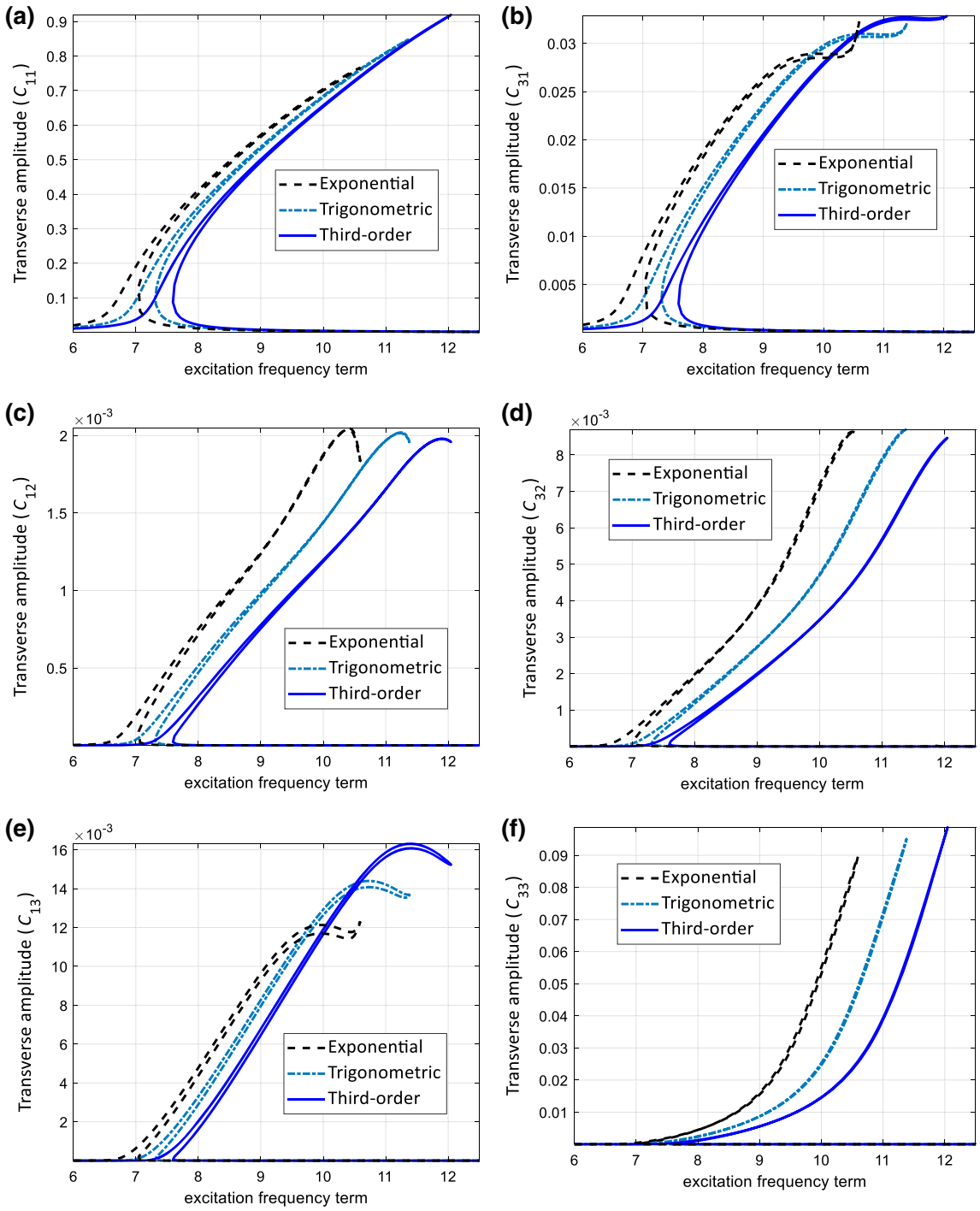

Fig. 10 Influence of different higher-order shear effect models on the *transverse* amplitude response of the sandwich hyperelastic *clamped–clamped* beam **a** C_{11}, **b** C_{31}, **c** C_{12}, **d** C_{32}, **e** C_{13}, and **f** C_{33}

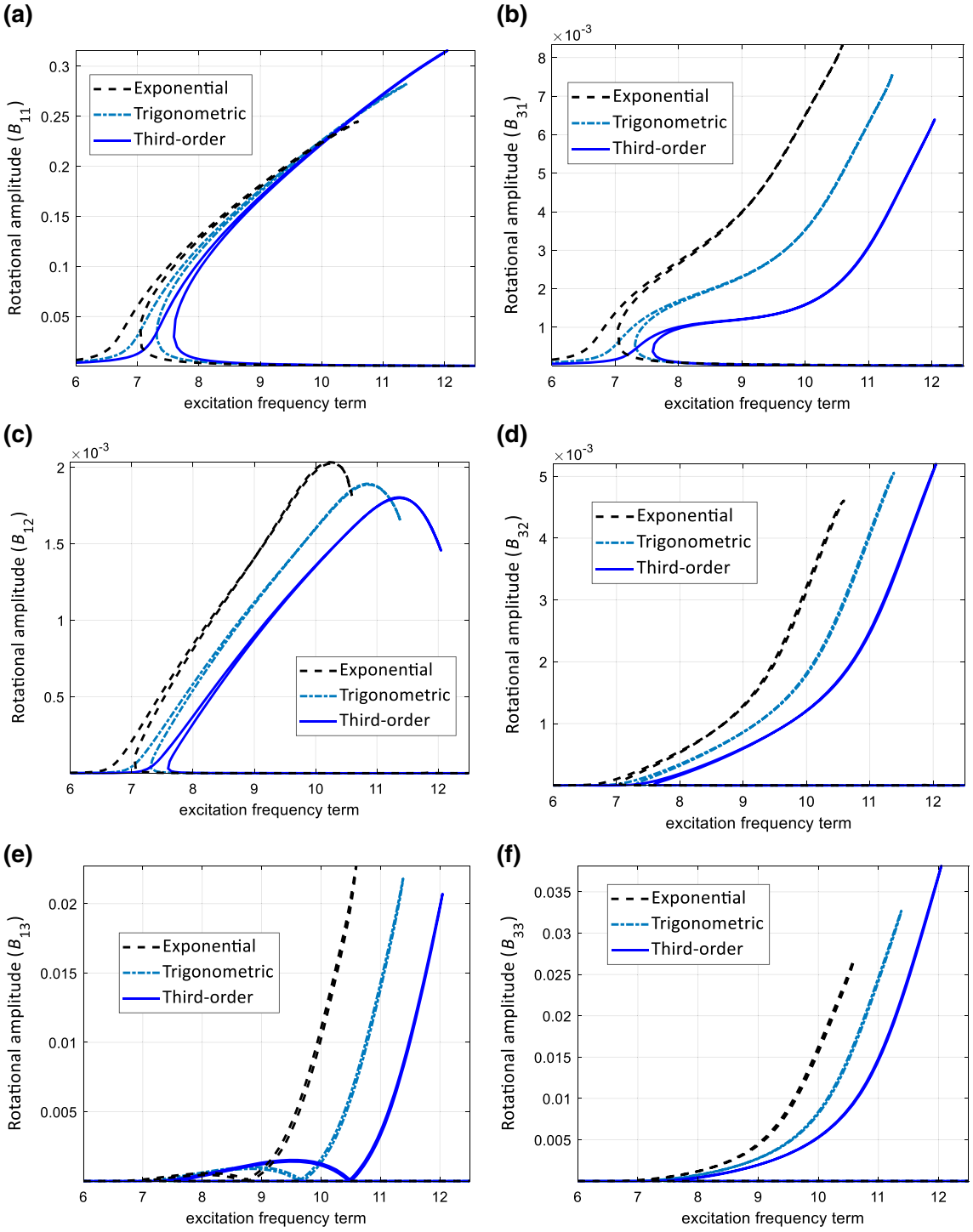

Fig. 11 Influence of different higher-order shear effect models on the *rotation* amplitude response of the sandwich hyperelastic *clamped–clamped* beam **a** B_{11}, **b** B_{31}, **c** B_{12}, **d** B_{32}, **e** B_{13} and **f** B_{33}

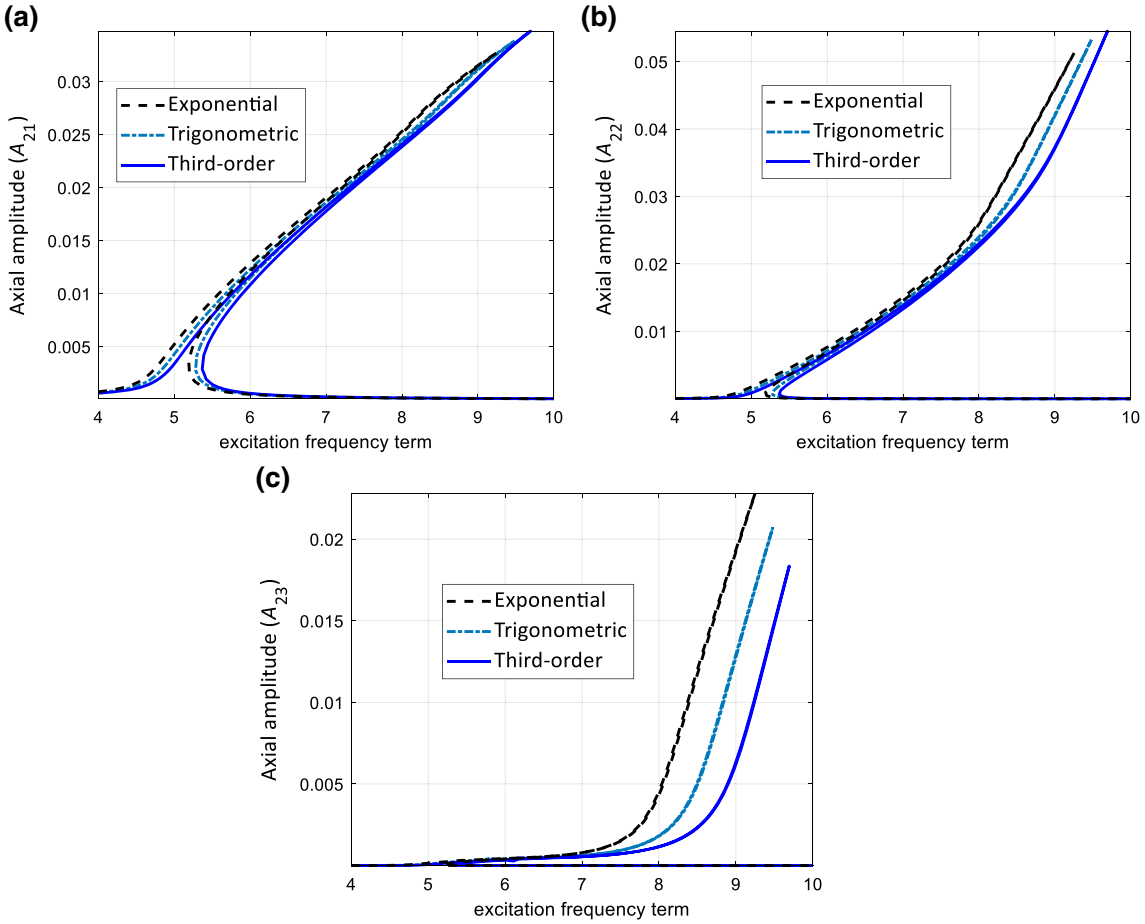

Fig. 12 Influence of different higher-order shear effect models on the *axial* amplitude response of the sandwich hyperelastic *pinned–pinned* beam **a** A_{21}, **b** A_{22} and **c** A_{23}

the thickness of $h = [h/4, h/2, h/4]$ and the amplitude–frequency responses of the structures are shown in Figs. 23, 24 and 25 for clamped–clamped third-order shear deformable hyperelastic thick beams. It can be seen that the layer positioning has a notable effect in changing the coupling motion of the structure, based on the requirements of the design.

5 Summary and conclusions

In this study, a detailed layerwise analysis of the time-dependent mechanics of hyperelastic beams structures is given using five different shear deformation theories. The hyperelasticity was modelled following the Mooney–Rivlin hyperelastic strain energy density model, and the beam was assumed to lie on a foundation including linear, nonlinear and shear layers. Equations of motion were derived using Hamilton's principle together with different shear deformable beam theories. Solving the equations of motion using a dynamic equilibrium technique, it was shown that:

- The classic beam theory predicts the fundamental frequency term of hyperelastic-layered beam models higher than the studied shear deformable beam models.
- By increasing the length-to-thickness ratio, the influence of the type of boundary conditions decreases.
- Similar to elastic beams, the hyperelastic-layered beam model shows higher sensitivity to shear effects when the length-to-thickness ratio is lower.
- The higher-order shear deformable beam models (namely third-order, exponential and trigonometric) give very close results for natural frequency terms, while the nonlinear behaviours are slightly different.

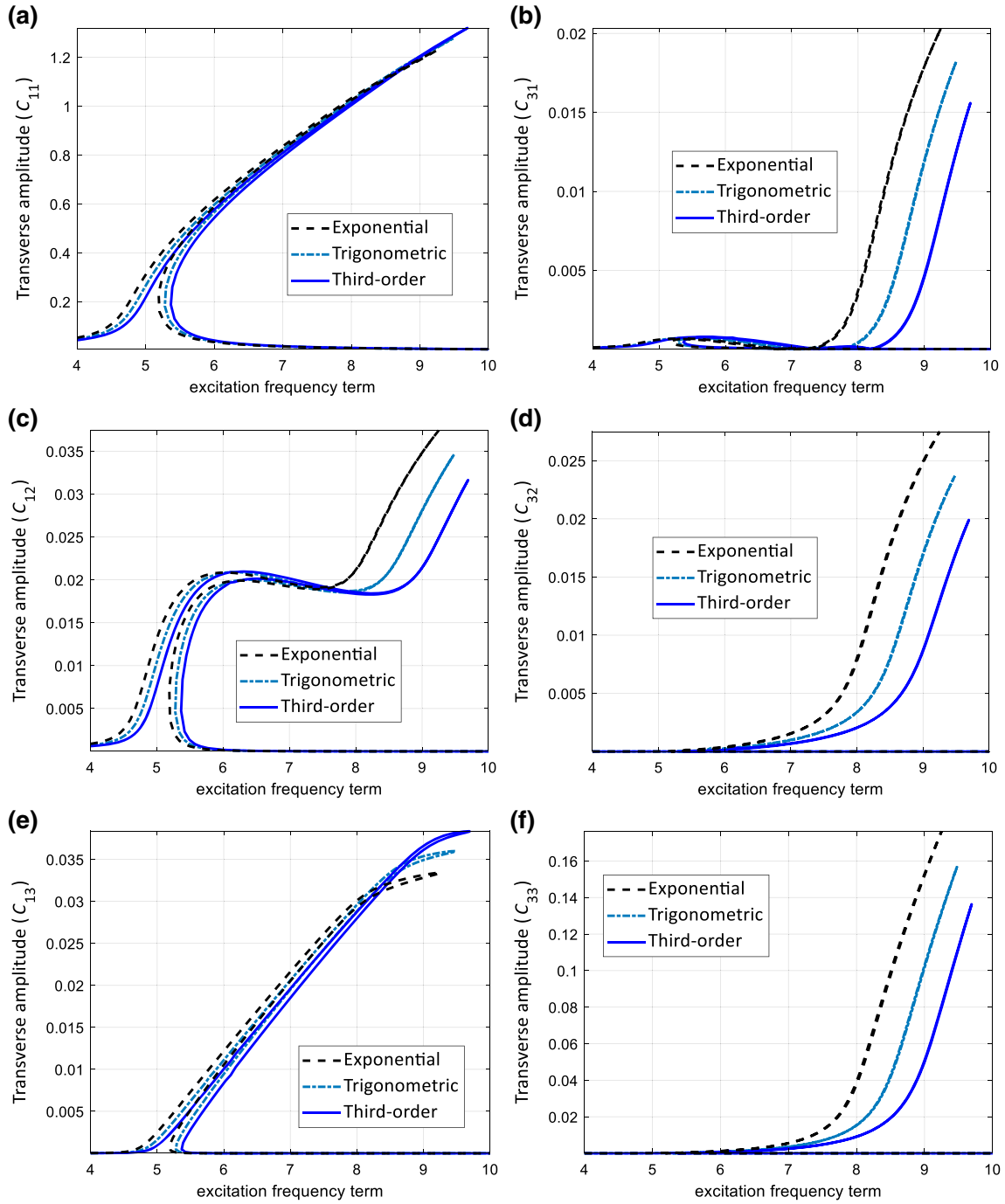

Fig. 13 Influence of different higher-order shear effect models on the *transverse* amplitude response of the sandwich hyperelastic *pinned–pinned* beam **a** C_{11}, **b**)C_{31}, **c** C_{12}, **d** C_{32}, **e** C_{13} and **f** C_{33}

- For linear natural frequencies, it was shown that having a foundation can increase the fundamental natural frequency of hyperelastic-layered beams significantly and this effect is higher for the shear layer compared with the linear layer.
- For nonlinear forced time-dependent analysis of layered hyperelastic beams, the Timoshenko beam model gives the highest maximum amplitude for the dominant longitudinal, transverse and rotation deformations, compared with the other shear deformable models. Similarly, for higher-order shear models, the highest amplitudes are for the third-order beam model and the lowest one belongs to the exponential beam model.

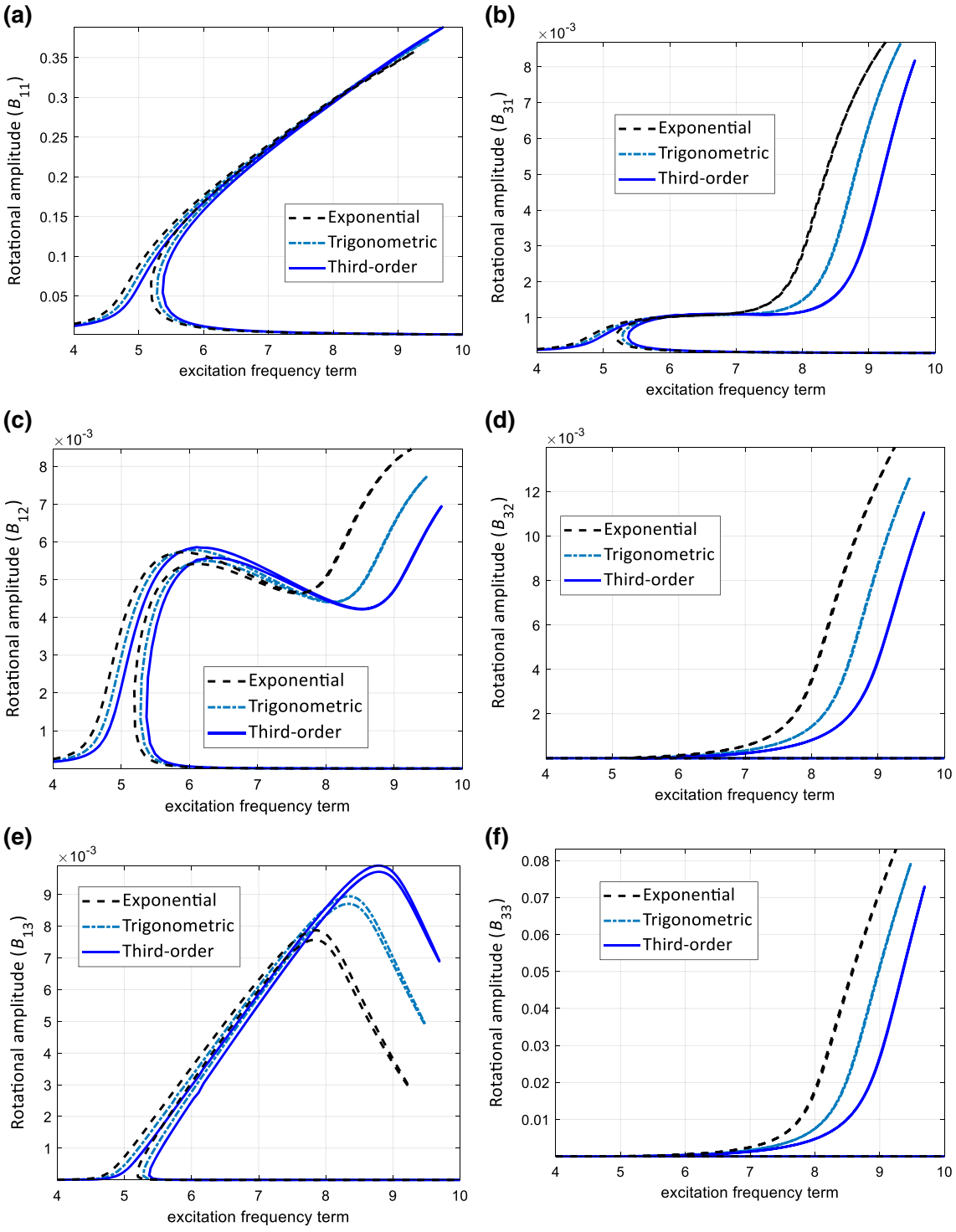

Fig. 14 Influence of different higher-order shear effect models on the *rotation* amplitude response of the sandwich hyperelastic *pinned–pinned* beam **a** B_{11}, **b** B_{31}, **c** B_{12}, **d** B_{32}, **e** B_{13} and **f** B_{33}

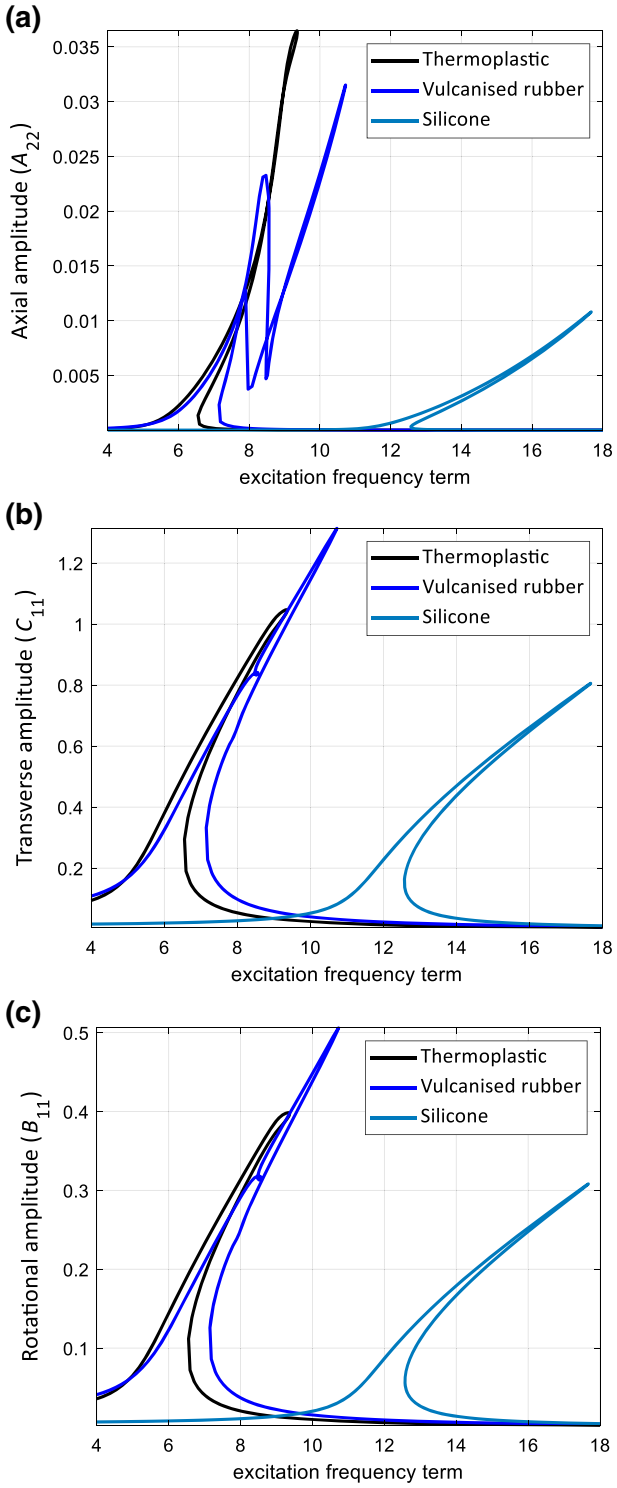

Fig. 15 The amplitude response of the *single-layer* hyperelastic *clamped–clamped* beam **a** A_{22}, **b** C_{11}, **c** B_{11}

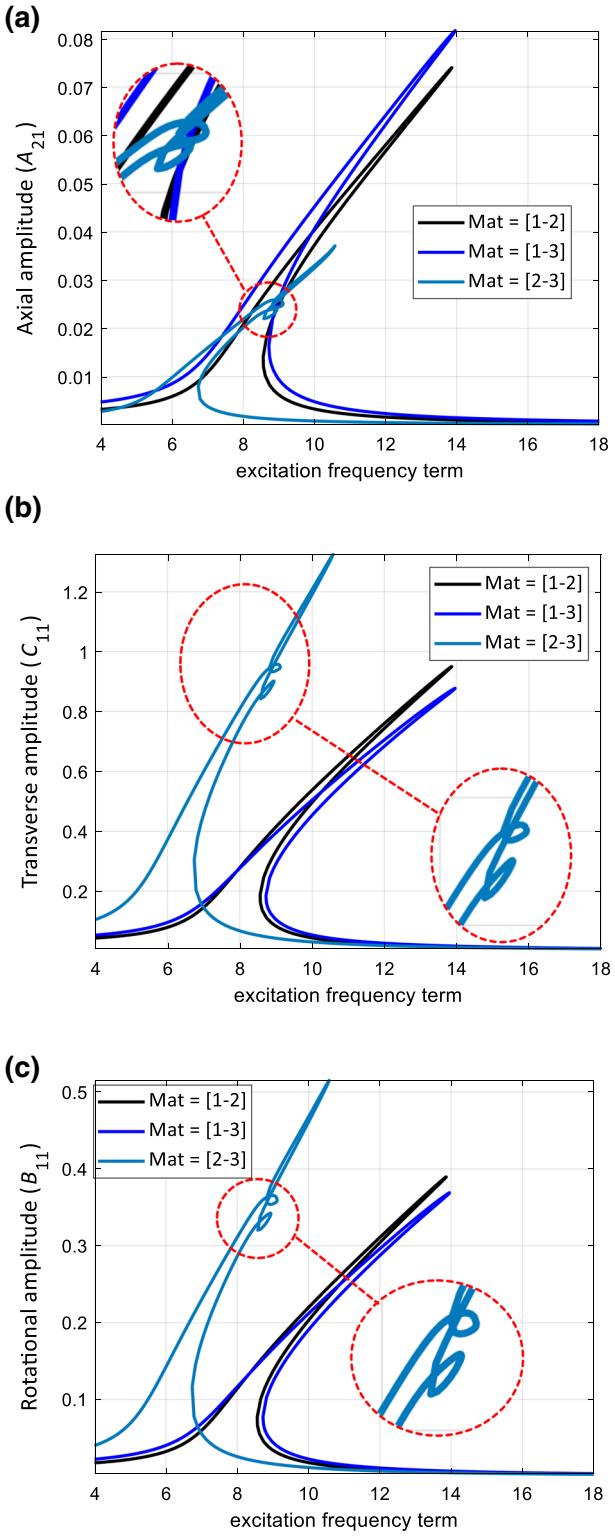

Fig. 16 The amplitude response of the *two-layered* hyperelastic *clamped–clamped* beam **a** A_{21}, **b** C_{11}, **c** B_{11}

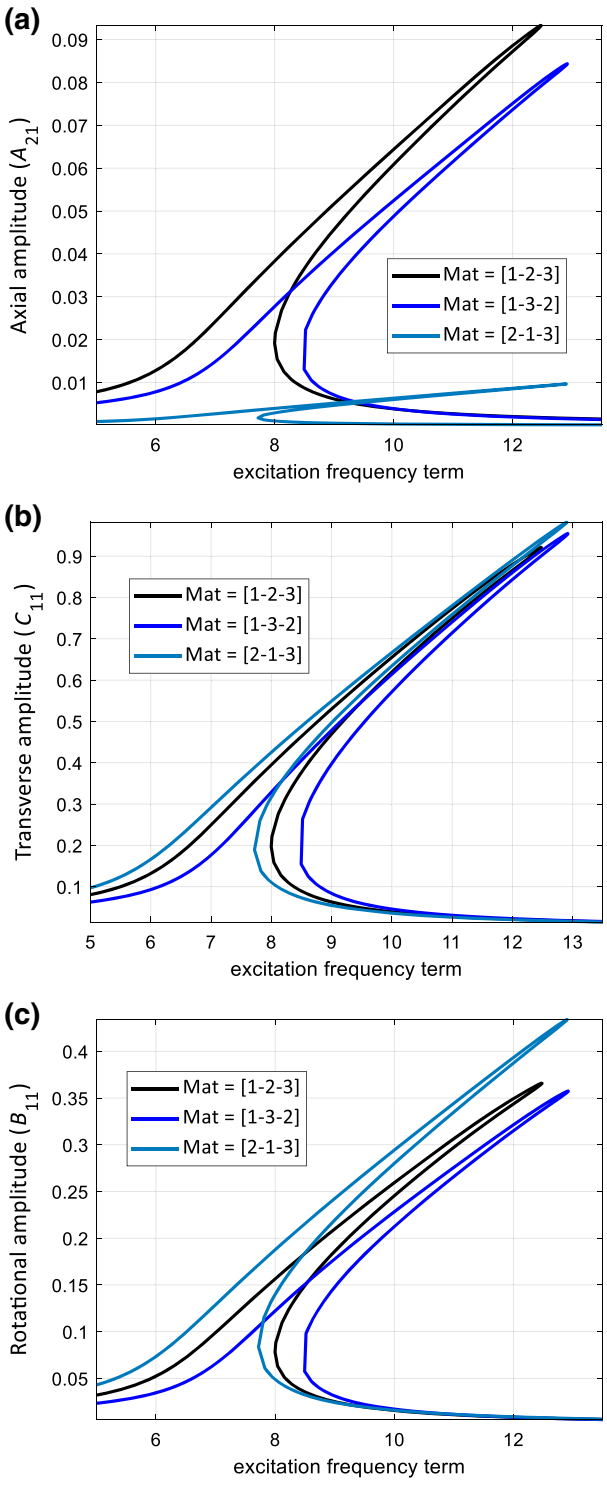

Fig. 17 The amplitude response of the *three-layered* hyperelastic *clamped–clamped* beam **a** A_{21}, **b** C_{11}, **c** B_{11}

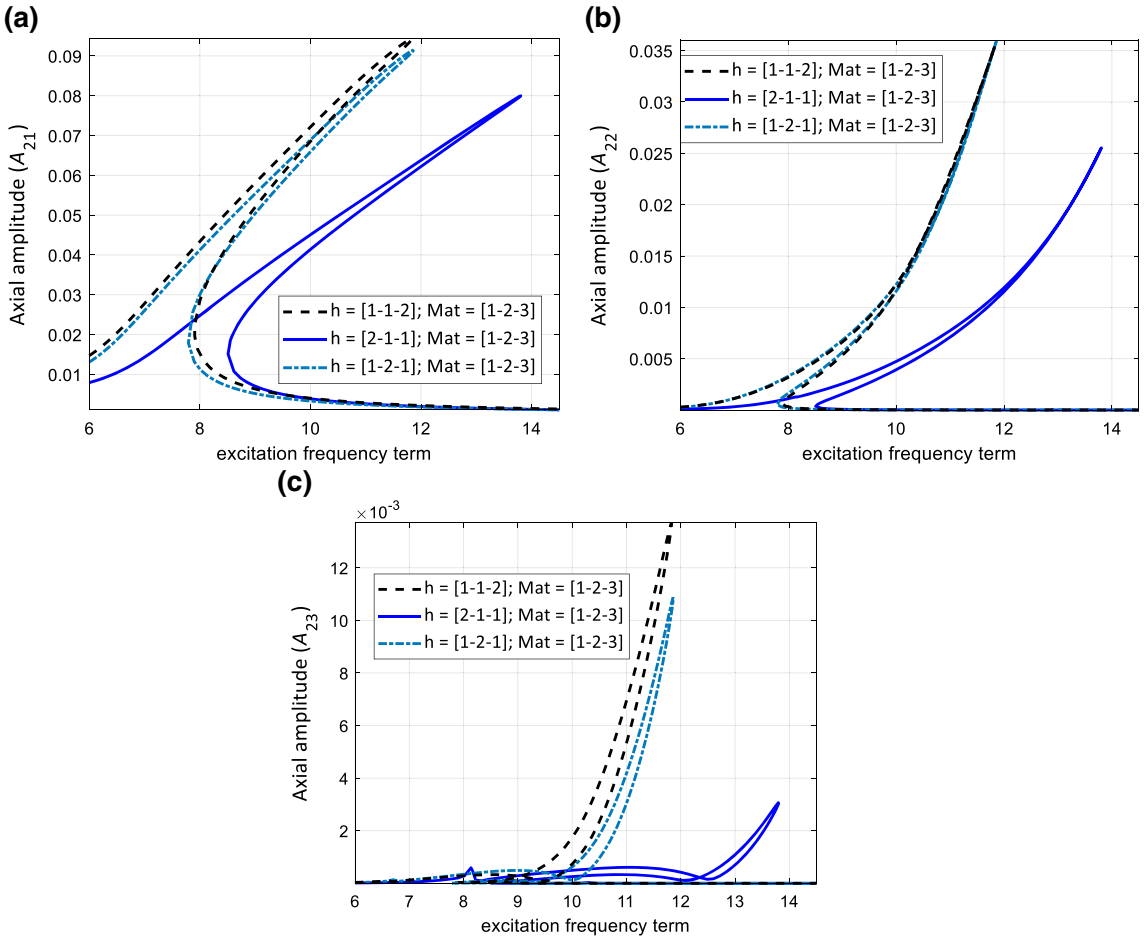

Fig. 18 Influence of the thickness of each layer on the *axial* amplitude response of the sandwich hyperelastic *clamped–clamped* beam **a** A_{21}, **b** A_{22} and **c** A_{23}

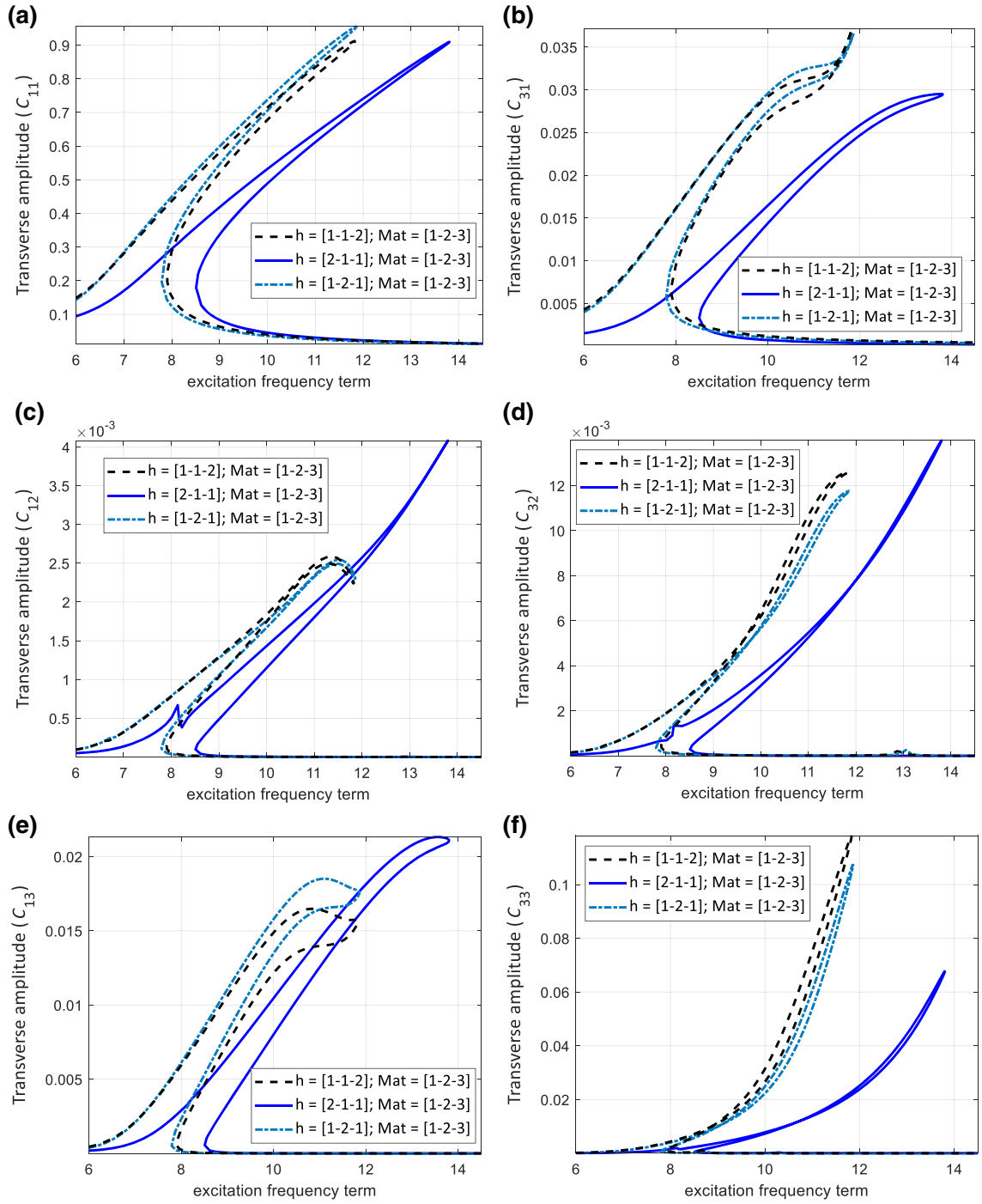

Fig. 19 Influence of the thickness of each layer on the *transverse* amplitude response of the sandwich hyperelastic *clamped–clamped* beam **a** C_{11}, **b** C_{31}, **c** C_{12}, **d** C_{32}, **e** C_{13} and **f** C_{33}

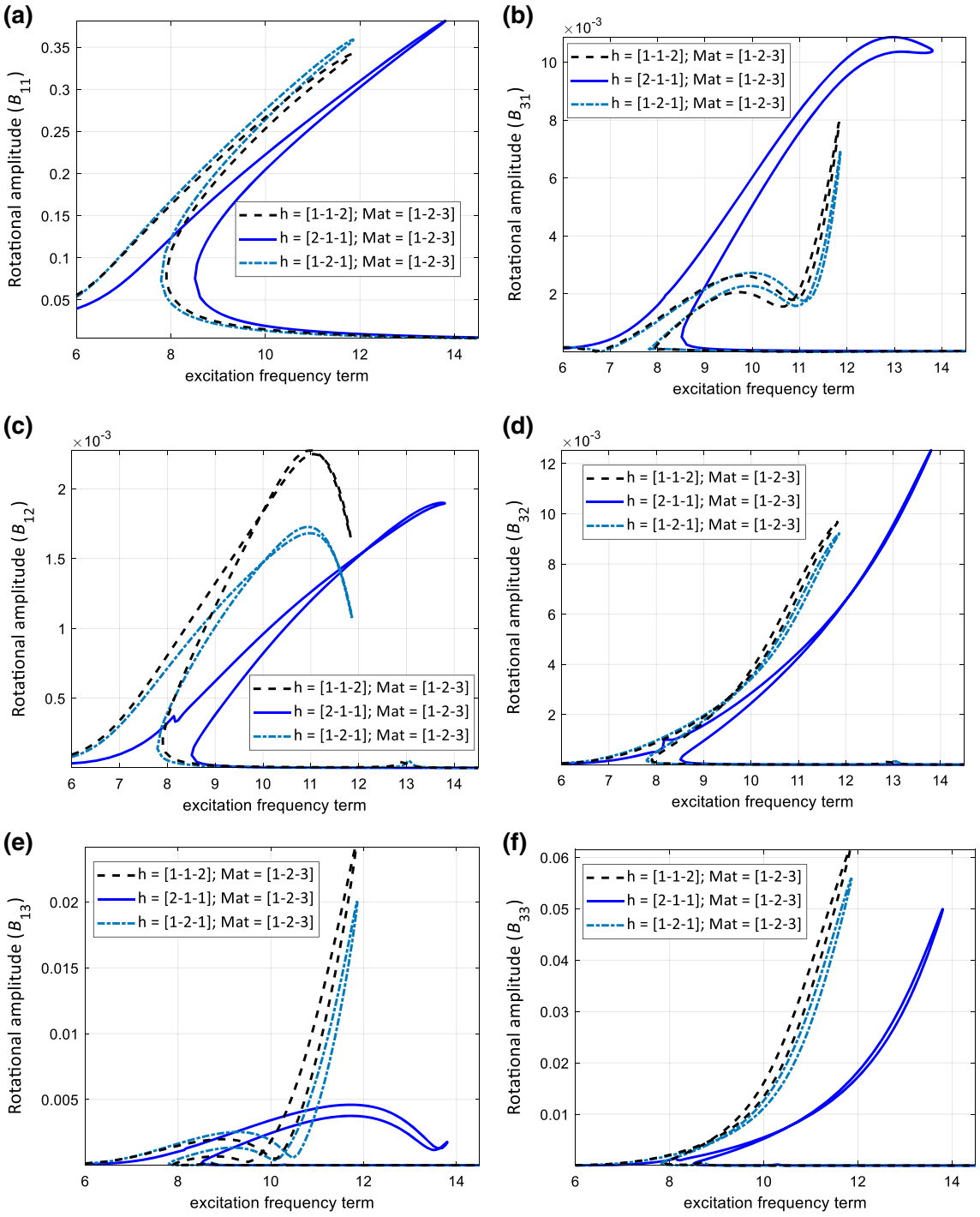

Fig. 20 Influence of the thickness of each layer on the *rotation* amplitude response of the sandwich hyperelastic *clamped–clamped* beam **a** B_{11}, **b** B_{31}, **c** B_{12}, **d** B_{32}, **e** B_{13}, and **f** B_{33}

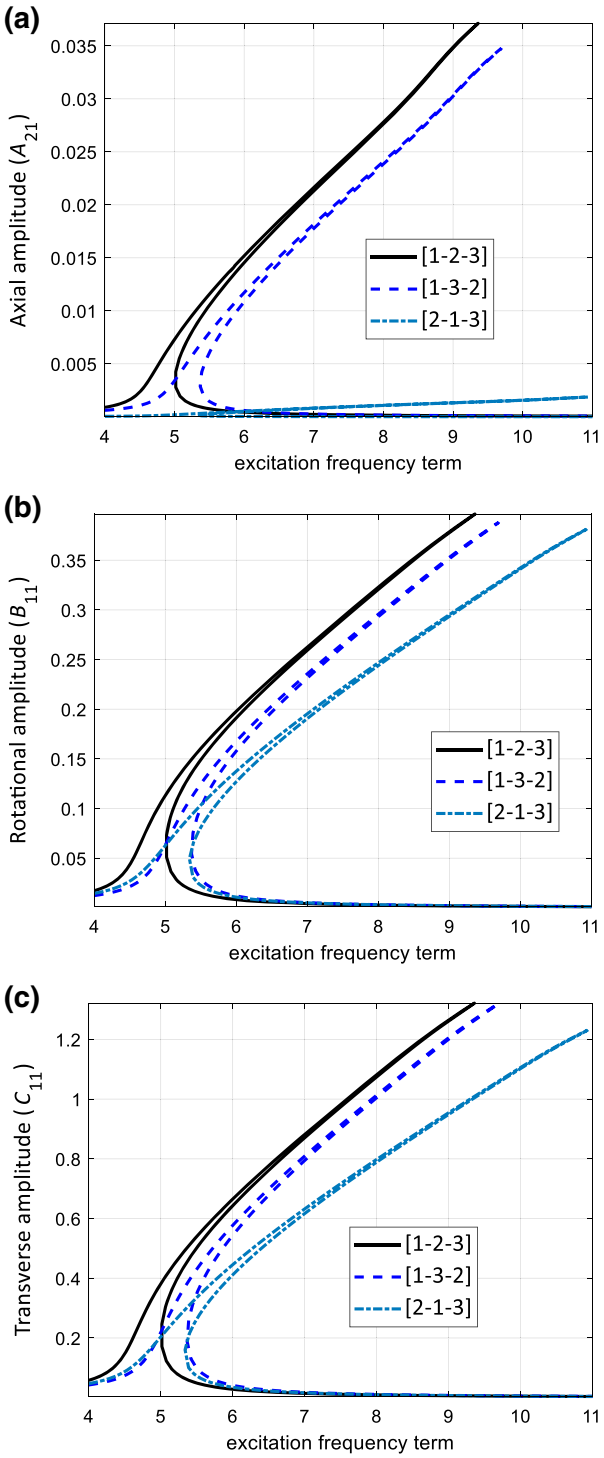

Fig. 21 Influence of the material positioning on the amplitude response of the sandwich hyperelastic *pinned–pinned* beam **a** A_{21}, **b** B_{11}, **c** C_{11}

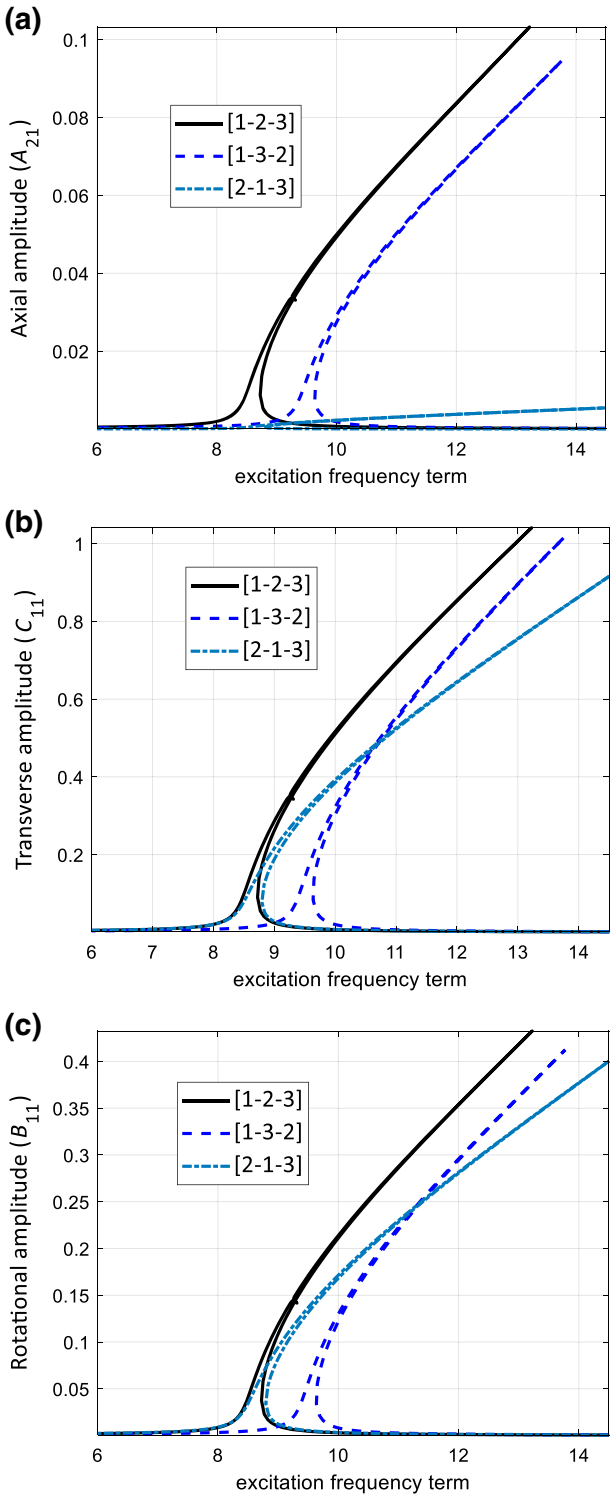

Fig. 22 Influence of the material positioning on the amplitude response of the sandwich hyperelastic *clamped–clamped* beam **a** A_{21}, **b** C_{11}, **c** B_{11}

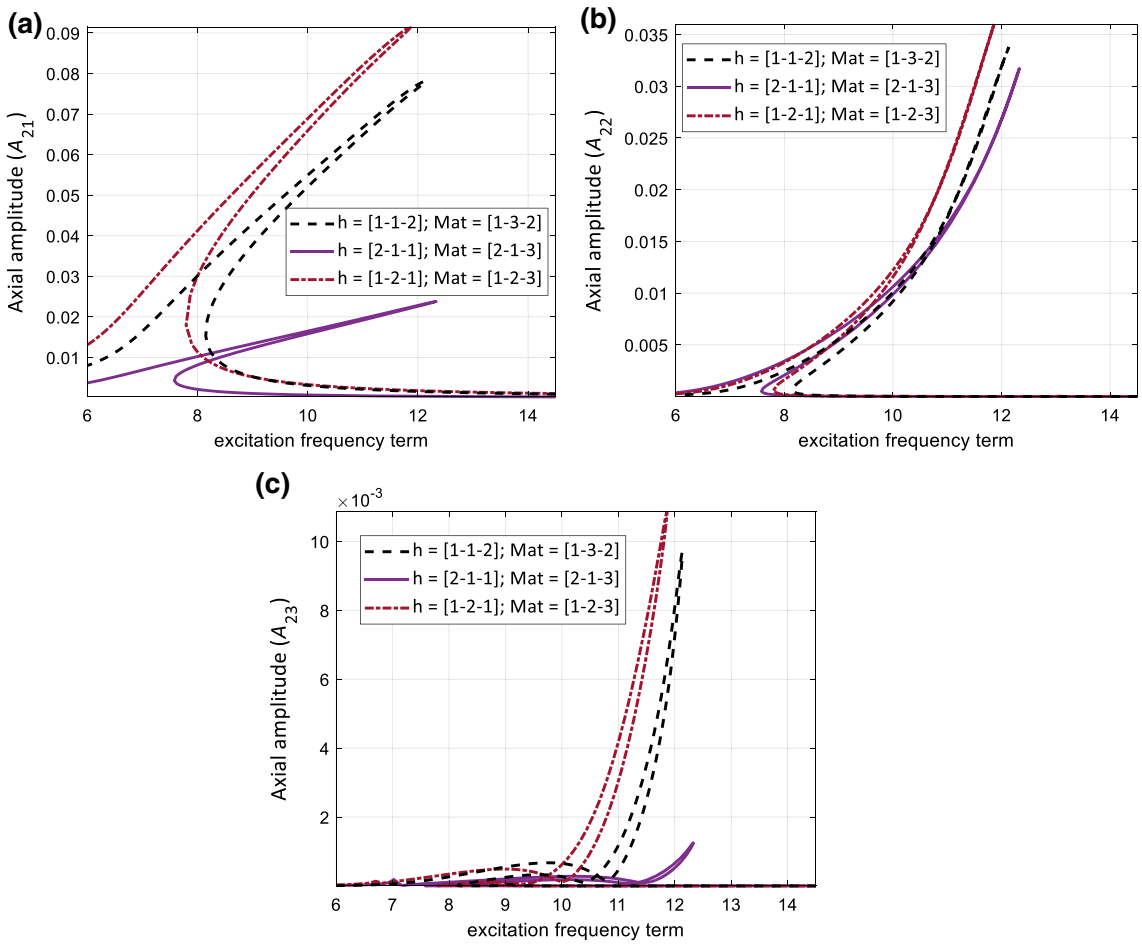

Fig. 23 Influence of the layer positioning on the *axial* amplitude response of the sandwich hyperelastic *clamped–clamped* beam **a** A_{21}, **b** A_{22} and **c** A_{23}

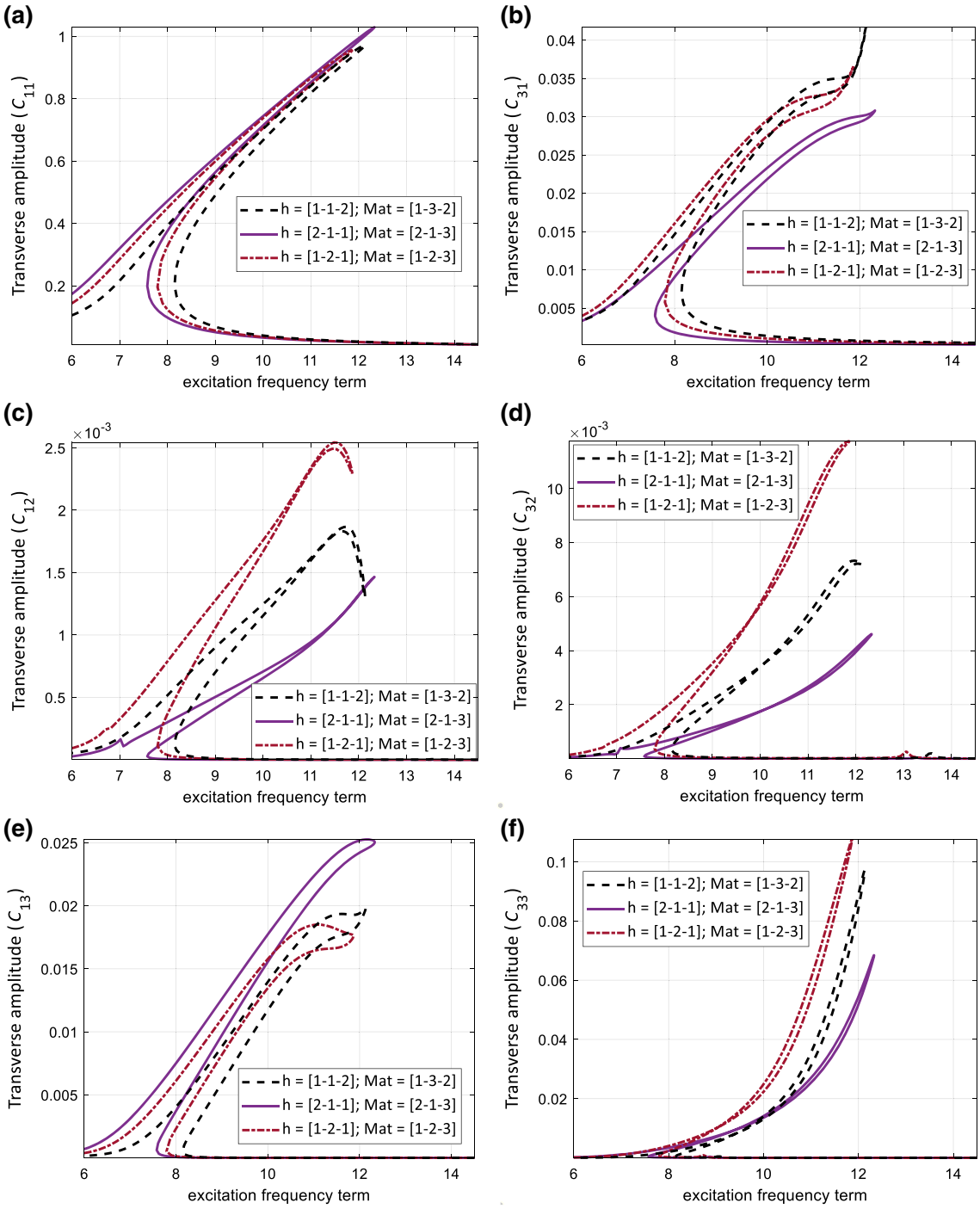

Fig. 24 Influence of the layer positioning on the *transverse* amplitude response of the sandwich hyperelastic *clamped–clamped* beam **a** C_{11}, **b** C_{31}, **c** C_{12}, **d** C_{32}, **e** C_{13} and **f** C_{33}

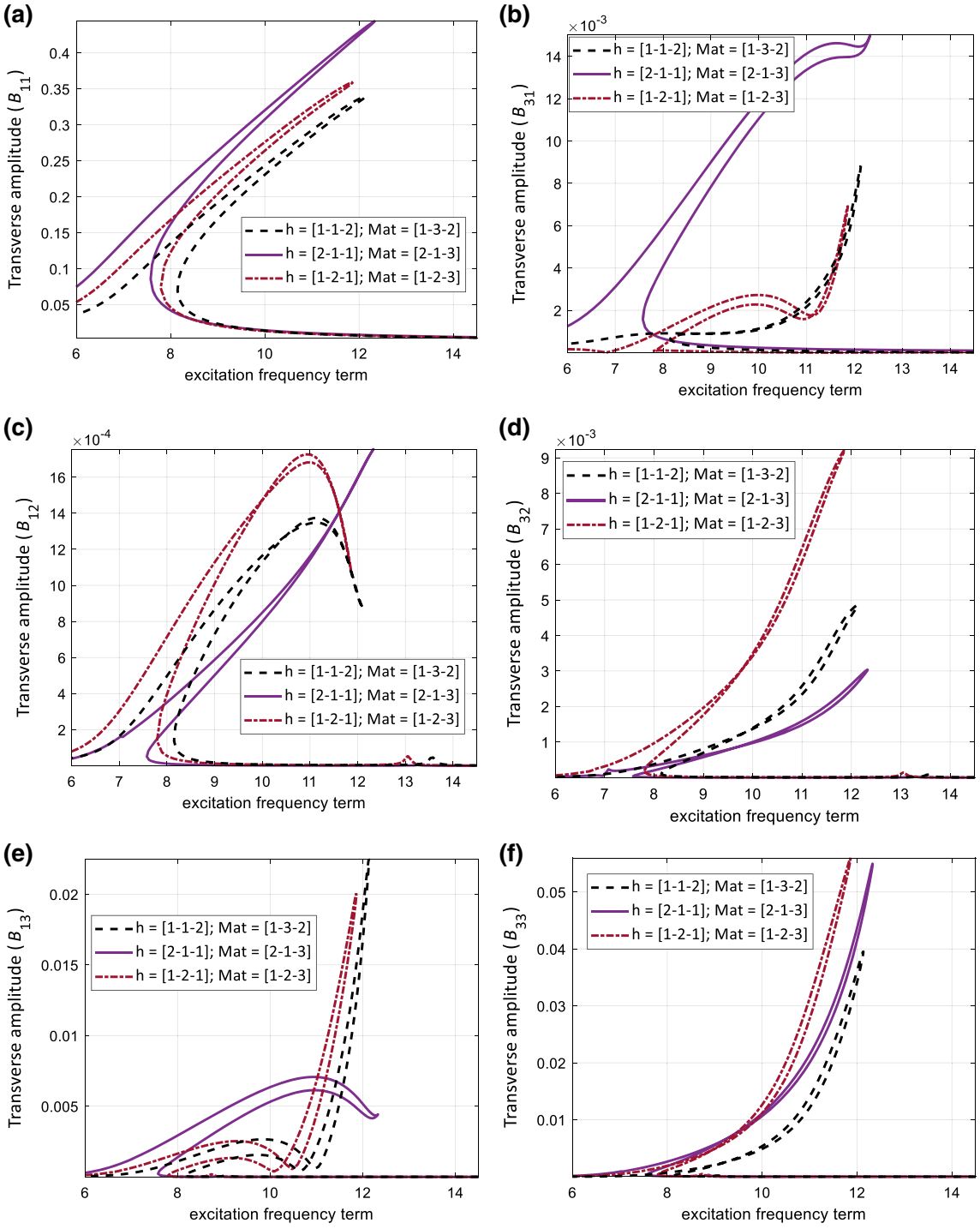

Fig. 25 Influence of the layer positioning on the *rotation* amplitude response of the sandwich hyperelastic *clamped–clamped* beam **a** B_{11}, **b** B_{31}, **c** B_{12}, **d** B_{32}, **e** B_{13} and **f** B_{33}

- For the two-layered hyperelastic beam model examined in this study, it is shown that the highest transverse amplitude belongs to the material combination of silicone and vulcanised rubber. Similarly, for the three-layered model, the material distribution silicone–thermoplastic–vulcanised rubber has the lowest maximum axial amplitude and the highest transverse and rotation amplitudes.
- The influence of each layer's thickness is examined showing that changing the thickness of the layers can change the nonlinear vibration response of the structure significantly.
- Hyperelastic material sorting has been shown to be a promising designing parameter in changing the dynamic behaviour of the structure for both linear and nonlinear analysis. For the studied model, both boundary conditions, the maximum amplitudes sweep to lower frequencies when the material positioning is [*mat*1- *mat*2- *mat*3].

Overall, since layered hyperelastic structures are replacing single-layer hyperelastic structures in many designs and applications such as food packaging, bottles, tubes and pipes, it is important to comprehend and predict the changes in their mechanical behaviour before employing them, especially their coupling motion behaviour. The results of this study are a step forward in realising the changes in the mechanical response of laminated hyperelastic beams when different materials and layers are used.

Acknowledgements This work employed the supercomputing resources provided by the Phoenix HPC service at the University of Adelaide. The HDR scholarship support through The University of Adelaide and Faculty of Engineering, Computer & Mathematical Sciences, the University of Adelaide, is also acknowledged.

Funding Open Access funding enabled and organized by CAUL and its Member Institutions No funding was received for this project.

Declarations

Conflict of interest The authors declare that they have no conflict of interest.

Appendix A

The nonlinear coefficients are defined as

$$KN_{11}(l,i,j) : 12\eta A_{11}\int_0^1 U_l(\gamma)\frac{\mathrm{d}}{\mathrm{d}\gamma}\left[U_i'(\gamma)\,U_j'(\gamma)\right]\mathrm{d}\gamma, \tag{A1}$$

$$KN_{12}(l,i,j) : 24\eta^2 B_{22}\int_0^1 U_l(\gamma)\frac{\mathrm{d}}{\mathrm{d}\gamma}\left[U_i'(\gamma)\,W_j''(\gamma)\right]\mathrm{d}\gamma, \tag{A2}$$

$$KN_{13}(l,i,j) : -24\eta B_{11}\int_0^1 U_l(\gamma)\frac{\mathrm{d}}{\mathrm{d}\gamma}\left[U_i'(\gamma)\,\Phi_j'(\gamma)\right]\mathrm{d}\gamma, \tag{A3}$$

$$\begin{aligned} KN_{14}(l,i,j) : &-\eta(4A_{11}-D_{44})\int_0^1 U_l(\gamma)\frac{\mathrm{d}}{\mathrm{d}\gamma}\left[W'_i(\gamma)\,W'_j(\gamma)\right]\mathrm{d}\gamma \\ &+12\eta^3 D_{22}\int_0^1 U_l(\gamma)\frac{\mathrm{d}}{\mathrm{d}\gamma}\left[W''_i(\gamma)\,W''_j(\gamma)\right]\mathrm{d}\gamma, \end{aligned} \tag{A4}$$

$$KN_{15}(l,i,j): -2D_{44}\int_0^1 U_l(\gamma)\frac{\mathrm{d}}{\mathrm{d}\gamma}\left[W'_i(\gamma)\,\Phi_j(\gamma)\right]\mathrm{d}\gamma - 24\eta^2 D_{33}\int_0^1 U_l(\gamma)\frac{\mathrm{d}}{\mathrm{d}\gamma}\left[W''_i(\gamma)\,\Phi'_j(\gamma)\right]\mathrm{d}\gamma \tag{A5}$$

$$KN_{16}(l,i,j): \frac{1}{\eta}D_{44}\int_0^1 U_l(\gamma)\frac{\mathrm{d}}{\mathrm{d}\gamma}\left[\Phi_i(\gamma)\,\Phi_j(\gamma)\right]\mathrm{d}\gamma + 12\eta D_{11}\int_0^1 U_l(\gamma)\frac{\mathrm{d}}{\mathrm{d}\gamma}\left[\Phi'_i(\gamma)\,\Phi'_j(\gamma)\right]\mathrm{d}\gamma, \tag{A6}$$

$$KN_{17}(l,i,j,k): 12\eta^2 A_{11}\int_0^1 U_l(\gamma)\frac{\mathrm{d}}{\mathrm{d}\gamma}\left[U'_i(\gamma)\,W'_j(\gamma)\,W'_k(\gamma)\right]\mathrm{d}\gamma, \tag{A7}$$

$$KN_{18}(l,i,j,k): 12\eta^3 B_{22}\int_0^1 U_l(\gamma)\frac{\mathrm{d}}{\mathrm{d}\gamma}\left[W'_i(\gamma)\,W'_j(\gamma)\,W''_k(\gamma)\right]\mathrm{d}\gamma, \tag{A8}$$

$$KN_{19}(l,i,j,k): -12\eta^2 B_{11}\int_0^1 U_l(\gamma)\frac{\mathrm{d}}{\mathrm{d}\gamma}\left[W'_i(\gamma)\,W'_j(\gamma)\,\Phi'_k(\gamma)\right]\mathrm{d}\gamma, \tag{A9}$$

$$KN_{110}(l,i,j,k,m): 3\eta^3 A_{11}\int_0^1 U_l(\gamma)\frac{\mathrm{d}}{\mathrm{d}\gamma}\left[W'_i(\gamma)\,W'_j(\gamma)\,W'_k(\gamma)\,W'_m(\gamma)\right]\mathrm{d}\gamma, \tag{A10}$$

$$KN_{21}(l,i,j): 12\eta^2 B_{22}\int_0^1 W_l(\gamma)\frac{\mathrm{d}^2}{\mathrm{d}\gamma^2}\left[U'_i(\gamma)\,U'_j(x)\right]\mathrm{d}\gamma, \tag{A11}$$

$$KN_{22}(l,i,j): 24\eta^3 D_{22}\int_0^1 W_l(\gamma)\frac{\mathrm{d}^2}{\mathrm{d}\gamma^2}\left[U'_i(\gamma)\,W''_j(\gamma)\right]\mathrm{d}\gamma$$
$$-(8A_{11}-2D_{44})\,\eta\int_0^1 W_l(\gamma)\frac{\mathrm{d}}{\mathrm{d}\gamma}\left[U'_i(\gamma)\,W'_j(\gamma)\right]\mathrm{d}\gamma, \tag{A12}$$

$$KN_{23}(l,i,j): -24\eta^2 D_{33}\int_0^1 W_l(\gamma)\frac{\mathrm{d}^2}{\mathrm{d}\gamma^2}\left[U'_i(\gamma)\,\Phi'_j(\gamma)\right]\mathrm{d}\gamma - 2D_{44}\int_0^1 W_l(\gamma)\frac{\mathrm{d}}{\mathrm{d}\gamma}\left[U'_i(\gamma)\,\Phi_j(\gamma)\right]\mathrm{d}\gamma, \tag{A13}$$

$$KN_{24}(l,i,j): -(4B_{22}-E_{66})\,\eta^2\int_0^1 W_l(\gamma)\frac{\mathrm{d}^2}{\mathrm{d}x^2}\left[W'_i(\gamma)\,W'_j(\gamma)\right]\mathrm{d}\gamma$$
$$-(8B_{22}-2E_{66})\,\eta^2\int_0^1 W_l(\gamma)\frac{\mathrm{d}}{\mathrm{d}\gamma}\left[W'_i(\gamma)\,W''_j(\gamma)\right]\mathrm{d}x$$
$$+12\eta^4 E_{44}\int_0^1 W_l(\gamma)\frac{\mathrm{d}^2}{\mathrm{d}\gamma^2}\left[W''_i(\gamma)\,W''_j(\gamma)\right]\mathrm{d}\gamma, \tag{A14}$$

$$KN_{25}(l,i,j): -2\eta E_{66}\int_0^1 W_l(\gamma)\frac{\mathrm{d}^2}{\mathrm{d}\gamma^2}\left[W'_i(\gamma)\,\Phi_j(\gamma)\right]\mathrm{d}\gamma - 24\eta^3 E_{33}\int_0^1 W_l(\gamma)\frac{\mathrm{d}^2}{\mathrm{d}\gamma^2}\left[W''_i(\gamma)\,\Phi'_j(\gamma)\right]\mathrm{d}\gamma$$

$$+(8B_{11}-2E_{77})\,\eta\int_0^1 W_l(\gamma)\frac{\mathrm{d}}{\mathrm{d}\gamma}\left[W'_i(\gamma)\,\Phi'_j(\gamma)\right]\mathrm{d}\gamma-2\eta E_{66}\int_0^1 W_l(\gamma)\frac{\mathrm{d}}{\mathrm{d}\gamma}\left[W''_i(\gamma)\,\Phi_j(\gamma)\right]\mathrm{d}\gamma, \quad \text{(A15)}$$

$$KN_{26}(l,i,j): E_{66}\int_0^1 W_l(\gamma)\frac{\mathrm{d}^2}{\mathrm{d}\gamma^2}\left[\Phi_i(\gamma)\,\Phi_j(\gamma)\right]\mathrm{d}\gamma+2E_{77}\int_0^1 W_l(\gamma)\frac{\mathrm{d}}{\mathrm{d}\gamma}\left[\Phi_i(\gamma)\,\Phi'_j(\gamma)\right]\mathrm{d}\gamma$$

$$+12\eta^2 E_{22}\int_0^1 W_l(\gamma)\frac{\mathrm{d}^2}{\mathrm{d}\gamma^2}\left[\Phi_i'(\gamma)\,\Phi'_j(\gamma)\right]\mathrm{d}\gamma, \quad \text{(A16)}$$

$$KN_{27}(l,i,j,k): 12\eta^2 A_{11}\int_0^1 W_l(\gamma)\frac{\mathrm{d}}{\mathrm{d}\gamma}\left[U_i'(\gamma)\,U'_j(\gamma)\,W'_k(\gamma)\right]\mathrm{d}\gamma, \quad \text{(A17)}$$

$$KN_{28}(l,i,j,k): 12\eta^3 B_{22}\int_0^1 W_l(\gamma)\frac{\mathrm{d}^2}{\mathrm{d}\gamma^2}\left[U'_i(\gamma)\,W'_j(\gamma)\,W'_k(\gamma)\right]\mathrm{d}\gamma$$

$$+24\eta^3 B_{22}\int_0^1 W_l(\gamma)\frac{\mathrm{d}}{\mathrm{d}\gamma}\left[U'_i(\gamma)\,W'_j(\gamma)\,W''_k(\gamma)\right]\mathrm{d}\gamma, \quad \text{(A18)}$$

$$KN_{29}(l,i,j,k): -24\eta^2 B_{11}\int_0^1 W_l(\gamma)\frac{\mathrm{d}}{\mathrm{d}\gamma}\left[U'_i(\gamma)\,W'_j(\gamma)\,\Phi'_k(\gamma)\right]\mathrm{d}\gamma, \quad \text{(A19)}$$

$$KN_{210}(l,i,j,k): -(4A_{11}-2D_{44})\,\eta^2\int_0^1 W_l(\gamma)\frac{\mathrm{d}}{\mathrm{d}\gamma}\left[W'_i(\gamma)\,W_j{}'(\gamma)\,W_k{}'(\gamma)\right]\mathrm{d}\gamma$$

$$-K_{NL}\int_0^1 W_l(\gamma)W_i(\gamma)\,W_j(\gamma)\,W_k(\gamma)\,\mathrm{d}\gamma$$

$$+12\eta^4 D_{22}\int_0^1 W_l(\gamma)\frac{\mathrm{d}}{\mathrm{d}\gamma}\left[W_i{}'(\gamma)\,W_j{}''(\gamma)\,W_k{}''(\gamma)\right]\mathrm{d}\gamma$$

$$+12\eta^4 D_{22}\int_0^1 W_l(\gamma)\frac{\mathrm{d}^2}{\mathrm{d}\gamma^2}\left[W_i{}'(\gamma)\,W_j{}'(\gamma)\,W_k{}''(\gamma)\right]\mathrm{d}\gamma, \quad \text{(A20)}$$

$$KN_{211}(l,i,j,k): -12\eta^3 D_{33}\int_0^1 W_l(\gamma)\frac{\mathrm{d}^2}{\mathrm{d}\gamma^2}\left[W'_i(\gamma)\,W_j{}'(\gamma)\,\Phi'_k(\gamma)\right]\mathrm{d}\gamma$$

$$-3\eta D_{44}\int_0^1 W_l(\gamma)\frac{\mathrm{d}}{\mathrm{d}\gamma}\left[W'_i(\gamma)\,W_j{}'(\gamma)\,\Phi_k(\gamma)\right]\mathrm{d}\gamma$$

$$-24\eta^3 D_{33}\int_0^1 W_l(\gamma)\frac{\mathrm{d}}{\mathrm{d}\gamma}\left[W'_i(\gamma)\,W_j{}''(\gamma)\,\Phi'_k(\gamma)\right]\mathrm{d}\gamma, \quad \text{(A21)}$$

$$KN_{212}(l,i,j,k): D_{44}\int_0^1 W_l(\gamma)\frac{\mathrm{d}}{\mathrm{d}\gamma}\left[W_i{}'(\gamma)\,\Phi_j(\gamma)\,\Phi_k(\gamma)\right]\mathrm{d}\gamma$$

$$+12\eta^2 D_{11}\int_0^1 W_l(\gamma)\frac{\mathrm{d}}{\mathrm{d}\gamma}\left[W_i{}'(\gamma)\,\Phi'_j(\gamma)\,\Phi'_k(\gamma)\right]\mathrm{d}\gamma, \tag{A22}$$

$$KN_{213}(l,i,j,k,m):12\eta^3 A_{11}\int_0^1 W_l(\gamma)\frac{\mathrm{d}}{\mathrm{d}\gamma}\left[U'_i(\gamma)\,W'_j(\gamma)\,W'_k(\gamma)\,W'_m(\gamma)\right]\mathrm{d}\gamma, \tag{A23}$$

$$KN_{214}(l,i,j,k,m):3\eta^4 B_{22}\int_0^1 W_l(\gamma)\frac{\mathrm{d}^2}{\mathrm{d}\gamma^2}\left[W'_i(\gamma)\,W'_j(\gamma)\,W_k{}'(\gamma)\,W_m{}'(\gamma)\right]\mathrm{d}\gamma$$

$$+12\eta^4 B_{22}\int_0^1 W_l(\gamma)\frac{\mathrm{d}}{\mathrm{d}\gamma}\left[W'_i(\gamma)\,W'_j(\gamma)\,W_k{}'(\gamma)\,W_m{}''(\gamma)\right]\mathrm{d}\gamma, \tag{A24}$$

$$KN_{215}(l,i,j,k,m):-12\eta^3 B_{11}\int_0^1 W_l(\gamma)\frac{\mathrm{d}}{\mathrm{d}\gamma}\left[W'_i(\gamma)\,W'_j(\gamma)\,W'_k(\gamma)\,\Phi'_m(\gamma)\right]\mathrm{d}\gamma, \tag{A25}$$

$$KN_{216}(l,i,j,k,m,n):3\eta^4 A_{11}\int_0^1 W_l(\gamma)\frac{\mathrm{d}}{\mathrm{d}\gamma}\left[W'_i(\gamma)\,W'_j(\gamma)\,W'_k(\gamma)\,W'_m(\gamma)\,W'_n(\gamma)\right]\mathrm{d}\gamma, \tag{A26}$$

References

1. Koronis, G., Silva, A., Fontul, M.: Green composites: a review of adequate materials for automotive applications. Compos. B Eng. **44**, 120–127 (2013)
2. Chrysler, F.: Car makers increase their use of composites. Reinf. Plast. **48**, 26–32 (2004)
3. Birsan, M., Sadowski, T., Marsavina, L., Linul, E., Pietras, D.: Mechanical behavior of sandwich composite beams made of foams and functionally graded materials. Int. J. Solids Struct. **50**, 519–530 (2013)
4. Sadowski, T., Birsan, M., Pietras, D.: Multilayered and FGM structural elements under mechanical and thermal loads. Part I: Comparison of finite elements and analytical models. Arch. Civ. Mech. Eng. **15**, 1180–1192 (2015)
5. Birsan, M., Altenbach, H., Sadowski, T., Eremeyev, V., Pietras, D.: Deformation analysis of functionally graded beams by the direct approach. Compos. B Eng. **43**, 1315–1328 (2012)
6. Ivanov, I., Sadowski, T., Pietras, D.: Crack propagation in functionally graded strip under thermal shock. Eur. Phys. J. Spec. Top. **222**, 1587–1595 (2013)
7. Nikbakt, S., Kamarian, S., Shakeri, M.: A review on optimization of composite structures Part I: Laminated composites. Compos. Struct. **195**, 158–185 (2018)
8. Sayyad, A.S., Ghugal, Y.M.: Bending, buckling and free vibration of laminated composite and sandwich beams: a critical review of literature. Compos. Struct. **171**, 486–504 (2017)
9. Li , D.: Layerwise theories of laminated composite structures and their applications: a review. Arch. Comput. Methods Eng. 1–24 (2020)
10. Garg, A., Chalak, H.: A review on analysis of laminated composite and sandwich structures under hygrothermal conditions. Thin-Walled Struct. **142**, 205–226 (2019)
11. Danesh, H., Javanbakht, M., Aghdam, M.M.: A comparative study of 1D nonlocal integral Timoshenko beam and 2D nonlocal integral elasticity theories for bending of nanoscale beams. Continuum Mech. Thermodyn. 1–23 (2021)
12. Bîrsan, M., Pietras, D., Sadowski, T.: Determination of effective stiffness properties of multilayered composite beams. Continuum Mech. Thermodyn. 1–23 (2021)
13. Chai, G.B., Yap, C.W.: Coupling effects in bending, buckling and free vibration of generally laminated composite beams. Compos. Sci. Technol. **68**, 1664–1670 (2008)
14. Chen, W., Li, L., Xu, M.: A modified couple stress model for bending analysis of composite laminated beams with first order shear deformation. Compos. Struct. **93**, 2723–2732 (2011)
15. Özütok, A., Madenci, E.: Static analysis of laminated composite beams based on higher-order shear deformation theory by using mixed-type finite element method. Int. J. Mech. Sci. **130**, 234–243 (2017)
16. Mikhasev, G.: Free high-frequency vibrations of nonlocally elastic beam with varying cross-section area. Continuum Mech. Thermodyn. 1–14 (2021)
17. Szymczak, C., Kujawa, M.: Sensitivity analysis of free torsional vibration frequencies of thin-walled laminated beams under axial load. Continuum Mech. Thermodyn. **32**, 1347–1356 (2020)
18. Warminska, A., Manoach, E., Warminski, J., Samborski, S.: Regular and chaotic oscillations of a Timoshenko beam subjected to mechanical and thermal loadings. Continuum Mech. Thermodyn. **27**, 719–737 (2015)
19. Emam, S.A., Nayfeh, A.H.: Postbuckling and free vibrations of composite beams. Compos. Struct. **88**, 636–642 (2009)

20. Banerjee, J., Sobey, A.: Dynamic stiffness formulation and free vibration analysis of a three-layered sandwich beam. Int. J. Solids Struct. **42**, 2181–2197 (2005)
21. Damanpack, A., Khalili, S.: High-order free vibration analysis of sandwich beams with a flexible core using dynamic stiffness method. Compos. Struct. **94**, 1503–1514 (2012)
22. Sokolinsky, V.S., Von Bremen, H.F., Lavoie, J.A., Nutt, S.R.: Analytical and experimental study of free vibration response of soft-core sandwich beams. J. Sandwich Struct. Mater. **6**, 239–261 (2004)
23. Zhang, Y.-W., Hou, S., Zhang, Z., Zang, J., Ni, Z.-Y., Teng, Y.-Y., Chen, L.-Q.: Nonlinear vibration absorption of laminated composite beams in complex environment. Nonlinear Dyn. 1–18 (2020)
24. Shen, H.-S., Lin, F., Xiang, Y.: Nonlinear vibration of functionally graded graphene-reinforced composite laminated beams resting on elastic foundations in thermal environments. Nonlinear Dyn. **90**, 899–914 (2017)
25. Farokhi, H., Ghayesh, M.H., Gholipour, A., Hussain, S.: Motion characteristics of bilayered extensible Timoshenko microbeams. Int. J. Eng. Sci. **112**, 1–17 (2017)
26. Amabili, M.: Nonlinear vibrations of laminated circular cylindrical shells: comparison of different shell theories. Compos. Struct. **94**, 207–220 (2011)
27. Amabili, M.: Nonlinear Vibrations and Stability of Shells and Plates. Cambridge University Press, Cambridge (2008)
28. Schulze, M., Schröter, F., Jung, M., Jakop, U.: Evaluation of a panel of spermatological methods for assessing reprotoxic compounds in multilayer semen plastic bags. Sci. Rep. **10**, 1–11 (2020)
29. Walker, T.W., Frelka, N., Shen, Z., Chew, A.K., Banick, J., Grey, S., Kim, M.S., Dumesic, J.A., Van Lehn, R.C., Huber, G.W.: Recycling of multilayer plastic packaging materials by solvent-targeted recovery and precipitation. Sci. Adv. **6**, eaba7599 (2020)
30. Ügdüler, S., Van Geem, K.M., Denolf, R., Roosen, M., Mys, N., Ragaert, K., De Meester, S.: Towards closed-loop recycling of multilayer and coloured PET plastic waste by alkaline hydrolysis. Green Chem. **22**, 5376–5394 (2020)
31. Ramos, M.J.G., Lozano, A., Fernández-Alba, A.R.: High-resolution mass spectrometry with data independent acquisition for the comprehensive non-targeted analysis of migrating chemicals coming from multilayer plastic packaging materials used for fruit purée and juice. Talanta **191**, 180–192 (2019)
32. Amabili, M., Balasubramanian, P., Bozzo, I., Breslavsky, I.D., Ferrari, G.: Layer-specific hyperelastic and viscoelastic characterization of human descending thoracic aortas. J. Mech. Behav. Biomed. Mater. **99**, 27–46 (2019)
33. Khaniki, H.B., Ghayesh, M.H., Chin, R., Chen, L.-Q.: Experimental characteristics and coupled nonlinear forced vibrations of axially travelling hyperelastic beams. Thin-Walled Struct. **170**, 108526 (2022)
34. Khaniki, H.B., Ghayesh, M.H., Chin, R., Amabili, M.: Large amplitude vibrations of imperfect porous-hyperelastic beams via a modified strain energy. J. Sound Vib. **513**, 116416 (2021)
35. Thai, H.-T., Vo, T.P.: Bending and free vibration of functionally graded beams using various higher-order shear deformation beam theories. Int. J. Mech. Sci. **62**, 57–66 (2012)
36. Levinson, M.: An accurate, simple theory of the statics and dynamics of elastic plates. Mech. Res. Commun. **7**, 343–350 (1980)
37. Reddy, J.N.: A simple high-order theory of laminated composite plate. J. Appl. Mech. **51**, 745–752 (1984)
38. Karama, M., Afaq, K., Mistou, S.: Mechanical behaviour of laminated composite beam by the new multi-layered laminated composite structures model with transverse shear stress continuity. Int. J. Solids Struct. **40**, 1525–1546 (2003)
39. Touratier, M.: An efficient standard plate theory. Int. J. Eng. Sci. **29**, 901–916 (1991)
40. Bonet, J., Wood, R.D.: Nonlinear continuum mechanics for finite element analysis. Cambridge University Press, Cambridge (1997)
41. Ogden, R.W.: Large deformation isotropic elasticity–on the correlation of theory and experiment for incompressible rubberlike solids, Proceedings of the Royal Society of London A. Math. Phys. Sci. **326**, 565–584 (1972)
42. Mooney, M.: A theory of large elastic deformation. J. Appl. Phys. **11**, 582–592 (1940)
43. Cho, K., Striz, A., Bert, C.: Bending analysis of thick bimodular laminates by higher-order individual-layer theory. Compos. Struct. **15**, 1–24 (1990)
44. Liu, N., Johnson, E.L., Rajanna, M.R., Lua, J., Phan, N., Hsu, M.-C.: Blended isogeometric Kirchhoff-Love and continuum shells. Comput. Methods Appl. Mech. Eng. **385**, 114005 (2021)
45. Liu, N., Jeffers, A.E.: Isogeometric analysis of laminated composite and functionally graded sandwich plates based on a layerwise displacement theory. Compos. Struct. **176**, 143–153 (2017)
46. Liu, N., Jeffers, A.E.: A geometrically exact isogeometric Kirchhoff plate: Feature-preserving automatic meshing and C 1 rational triangular Bézier spline discretizations. Int. J. Numer. Methods Eng. **115**, 395–409 (2018)
47. Liu, N., Jeffers, A.E.: Adaptive isogeometric analysis in structural frames using a layer-based discretization to model spread of plasticity. Comput. Struct. **196**, 1–11 (2018)
48. Liu, N., Plucinsky, P., Jeffers, A.E.: Combining load-controlled and displacement-controlled algorithms to model thermal-mechanical snap-through instabilities in structures. J. Eng. Mech. **143**, 04017051 (2017)
49. Liu, N., Ren, X., Lua, J.: An isogeometric continuum shell element for modeling the nonlinear response of functionally graded material structures. Compos. Struct. **237**, 111893 (2020)
50. Liu, N., Beata, P.A., Jeffers, A.E.: A mixed isogeometric analysis and control volume approach for heat transfer analysis of nonuniformly heated plates. Numer. Heat Transf. Part B Fundam. **75**, 347–362 (2019)
51. An, H.-B., Bai, Z.-Z.: A globally convergent Newton-GMRES method for large sparse systems of nonlinear equations. Appl. Numer. Math. **57**, 235–252 (2007)
52. Watson, L.T.: Globally convergent homotopy algorithms for nonlinear systems of equations. Nonlinear Dyn. **1**, 143–191 (1990)
53. Birgin, E.G., Krejić, N., Martínez, J.M.: Globally convergent inexact quasi-Newton methods for solving nonlinear systems. Numer. Algorithms **32**, 249–260 (2003)
54. Ghayesh, M.H., Farokhi, H., Gholipour, A.: Vibration analysis of geometrically imperfect three-layered shear-deformable microbeams. Int. J. Mech. Sci. **122**, 370–383 (2017)

55. ANSYS® Multiphysics™, Workbench 19.2, Workbench User's Guide, ANSYS Workbench Systems, Analysis Systems, Modal
56. Amabili, M., Balasubramanian, P., Breslavsky, I.D., Ferrari, G., Garziera, R., Riabova, K.: Experimental and numerical study on vibrations and static deflection of a thin hyperelastic plate. J. Sound Vib. **385**, 81–92 (2016)
57. Fukahori, Y., Seki, W.: Molecular behaviour of elastomeric materials under large deformation: 1. Re-evaluation of the Mooney–Rivlin plot. Polymer **33**, 502–508 (1992)

Chapter 6

Visco-hyper-elastic arches

Overview

Since most biological tissues and some polymeric structures show a combination of hyperelastic and viscoelastic behaviour, this chapter presents the nonlinear mechanics of visco-hyperelastic structures. The visco-hyperelasticity is presented using a combination of the Kelvin-Voigt viscoelastic scheme and Mooney-Rivlin hyperelastic theory, both of which have shown good accuracy in modelling visco-hyperelasticity in previous studies. The structure is assumed to have curvatures, and the shear effects are taken into account. The bending and vibration behaviour are analysed and the effect of having viscoelasticity on the nonlinear forced vibrations in a three-to-one internal resonance stage is discussed. This research study is published online as: Khaniki, H. B., Ghayesh, M. H., Chin, R., & Hussain, S. (2022). Internal resonance and bending analysis of thick visco-hyper-elastic arches. Continuum Mechanics and Thermodynamics, 1-44. DOI: 10.1007/s00161-022-01166-9

Statement of Authorship

Title of Paper	Internal resonance and bending analysis of thick visco-hyper-elastic arches
Publication Status	☐ Published ☑ Accepted for Publication ☐ Submitted for Publication ☐ Unpublished and Unsubmitted w ork w ritten in manuscript style
Publication Details	Khaniki, H. B., Ghayesh, M. H., Chin, R., & Hussain, S. (2022). Internal resonance and bending analysis of thick visco-hyper-elastic arches. Continuum Mechanics and Thermodynamics, Accepted for publication at 19/Oct/2022.

Principal Author

Name of Principal Author (Candidate)	Hossein Bakhshi Khaniki		
Contribution to the Paper	I carried out the literature review, conceptualization, formal analysis, investigation, methodology, software, validation, visualization and wrote the manuscript.		
Overall percentage (%)	80%		
Certification:	This paper reports on original research I conducted during the period of my Higher Degree by Research candidature and is not subject to any obligations or contractual agreements with a third party that would constrain its inclusion in this thesis. I am the primary author of this paper.		
Signature		Date	2/11/2022

Co-Author Contributions

By signing the Statement of Authorship, each author certifies that:

i. the candidate's stated contribution to the publication is accurate (as detailed above);

ii. permission is granted for the candidate in include the publication in the thesis; and

iii. the sum of all co-author contributions is equal to 100% less the candidate's stated contribution.

Name of Co-Author	Mergen Ghayesh		
Contribution to the Paper	As the principal supervisor, I helped to construct the manuscript, edit and review the manuscript for submission. I assisted in the conceptualization, investigation, methodology, review and editing. I hereby give consent to Hossein Bakhshi Khaniki to present this paper for examination towards the degree of Doctor of Philosophy.		
Signature		Date	3/11/2022

Name of Co-Author	Rey Chin		
Contribution to the Paper	I assisted in review and editing of the manuscript. I hereby give consent to Hossein Bakhshi Khaniki to present this paper for examination towards the degree of Doctor of Philosophy.		
Signature		Date	3/11/2022

Name of Co-Author	Shahid Hussain		
Contribution to the Paper	I assisted in the conceptualization, review and editing of the manuscript. I hereby give consent to Hossein Bakhshi Khaniki to present this paper for examination towards the degree of Doctor of Philosophy.		
Signature		Date	8/11/2022

Continuum Mech. Thermodyn.
https://doi.org/10.1007/s00161-022-01166-9

ORIGINAL ARTICLE

Hossein B. Khaniki · Mergen H. Ghayesh · Rey Chin · Shahid Hussain

Internal resonance and bending analysis of thick visco-hyper-elastic arches

Received: 9 June 2022 / Accepted: 19 October 2022

Abstract In this study, a comprehensive analysis of visco-hyper-elastic thick soft arches under an external time-independent as well as time-dependent loads is presented from bending and internal resonance phenomenon perspectives. Axial, transverse and rotation motions are considered for modelling the thick and soft arch in the framework of the Mooney–Rivlin and Kelvin–Voigt visco-hyper-elastic schemes and third-order shear deformable models. The arch is assumed to be incompressible and is modelled using von Kármán geometric nonlinearity in the strain–displacement relationship. Using a virtual work method, the bending equations are derived. For the vibration analysis, three, coupled, highly nonlinear equations of motions are obtained using force-moment balance method. The Newton–Raphson method together with the dynamic equilibrium technique is used for the bending and vibration analyses. A detailed study on the influence of having visco-hyper-elasticity and arch curvature in the frequency response of the system is given in detail, and the bending deformation due to the applied static load is presented. The influence of having thick, soft arches with different slenderness ratios is shown, and the forced vibration response is discussed. Moreover, internal resonance in the system is studied showing that the curvature term in the structure can lead to three-to-one internal resonances, showing a rich nonlinear frequency response. The results of this study are a step forward in studying the visco-hyper-elastic behaviour of biological structures and soft tissues.

Keywords Internal resonance · Visco-elastic · Visco-hyper-elastic · Arch · Mooney–Rivlin · Kelvin–Voigt · Bending · Nonlinear vibration

1 Introduction

Arches are one of the main curved structures used in different engineering applications including civil and mechanical engineering. In civil engineering, arches have been employed for different construction purposes such as bridges and subway stations [1,2] as it can carry greater loads compared to straight structures. As an application in the field of mechanical engineering, arch structures have been used in designing different types of energy harvesters to optimise the efficiency of the system [3–6]. For instance, in a study presented by Yang

Communicated by Andreas Öchsner.

H. B. Khaniki ( ) · M. H. Ghayesh ( ) · R. Chin
School of Mechanical Engineering, University of Adelaide, Adelaide, South Australia 5005, Australia
E-mail: hossein.bakhshikhaniki@adelaide.edu

M. H. Ghayesh
E-mail: mergen.ghayesh@adelaide.edu.au

S. Hussain
Faculty of Science and Technology, University of Canberra, Canberra, Australia

et al. [7], it was shown that by using arch structures, the total harvested power was 200% times more power compared to straight structures. As another example, shallow arches have also been used and examined for microelectromechanical systems (MEMS) [8].

During the last few years, researchers have studied the mechanical behaviour of both flat structures (including beams and plates) [9–15] and curved structures (including shells and arches) [16–23] to be able to use them efficiently for specific purposes. Focusing on arch structures, their behaviour in different engineering conditions has been examined lately. To name a few, Yang et al. [24] reinforced elastic arch structures using graphene nanoplatelets and studied the linear vibration behaviour of graphene-reinforced arches. Different fibre distribution was modelled using Halpin–Tsai micromechanics model and Hamilton's principle showing that out-of-plane and in-plane linear frequencies of the elastic arch are highly affected by the fibre distribution and percentage. For dynamic instability analysis, Zhao et al. [25] studied the influence of having porosity in modelling graphene-reinforced elastic arches; it was shown that the best dynamic instability resistance can be seen in the symmetric porosity distribution model. The nonlinear mechanics of elastic shallow arches with nonuniform cross section made of functionally graded materials (FGMs) have been investigated by Ghayesh and Farokhi [26]. Coupled axial-transverse equations of motion were obtained using Euler-Bernoulli theory and Hamilton's principle; it was shown that as the arch curvature increases, the maximum amplitude of transverse vibration decreases. For MEMS structures, Farokhi et al. [27] studied the pull-in phenomena in micro-scale arch structures. Using a high-dimensional reduced-order Galerkin model and generalised Hamilton's principle, it was shown that by increasing the curvature of the arch, the DC voltage for pull-in phenomena increases.

The previous studies were mainly focused on linear-elastic structures under small strains. However, soft materials undergo large strains, which makes the classic linear modelling of the behaviour inaccurate for many hyper-elastic structures. There has been a significant attention on hyper-elastic structures in the past few years focusing on the statics [28–31] and dynamics [32–35]. In some recent studies, the anti-clastic bending of hyper-elastic beams in finite elasticity has been investigated by Lanzoni and Tarantino [36–38]. Khaniki et al. [39,40] have examined the nonlinear vibration and mechanics of axially moving hyper-elastic structures and layered hyper-elastic beams. In another study, Khaniki et al. [41] investigated the effect of having porosity in hyper-elastic structures providing a porous-hyper-elastic strain energy model and modelling the vibration behaviour of porous soft beams. A detailed review on the nonlinear dynamic behaviour of different hyper-elastic structures can be found in Ref. [42].

However, since some soft structures show a combination of viscoelasticity and hyper-elasticity, researchers have developed different models for such structures [43–47]. In a recent study presented by Li et al. [48], a wide range of visco-hyper-elastic constitutive models were developed. The viscoelasticity was modelled via Maxwell and Kelvin–Voigt models, and the hyper-elasticity was modelled via neo-Hookean, Mooney–Rivlin, and Ogden models. It was shown that the proposed models are capable of modelling both hyper-elasticity and viscoelasticity of the biological structure. Since visco-hyper-elastic structures are widely applicable for modelling human body organs, soft robots and prosthesis, the visco-hyper-elastic constitutive models are useful for studying and manufacturing accurate mechanical and biomechanical structures in different environments.

Besides, since most of the hyper-elastic structures are significantly softer than linear-elastic structures, it is very likely to have them bent (like arches and shells) in real-life applications. Accordingly, in this study, *visco-hyper-elastic* thick soft shallow arches are examined in the framework of nonlinear bending and vibrations (with and without internal resonances). Since the soft arch is assumed to be thick, a third-order shear deformable theory is used and the visco-hyper-elasticity is modelled following Ref. [48] by using Mooney–Rivlin and Kelvin–Voigt models. The bending behaviour of the soft arch is formulated using the virtual work method and solved using the Newton–Raphson method. For the vibration analysis, the equations of motion are obtained using the force-moment balance method and solved using a dynamic equilibrium technique. The effect of having curvature in the structure is analysed, and the internal resonance phenomena caused by having this nonlinearity in the system are discussed. A detailed discussion of the influence of curvature term, the slenderness ratio and three-to-one internal resonance is given.

2 Bending of hyper-elastic thick arch formulation

For a thick, soft, shallow arch, using a higher-order shear deformation theory, by considering plane motion, von Kármán's geometric nonlinearity, and curvature in the thickness direction, the nonlinear *static* strain terms

are obtained as

$$\varepsilon_{11}(x_1,x_3)=\frac{\mathrm{d}u_1(x_1)}{\mathrm{d}x_1}+\frac{1}{2}\left(\frac{\mathrm{d}u_3(x_1)}{\mathrm{d}x_1}\right)^2+\frac{\mathrm{d}u_3(x_1)}{\mathrm{d}x_1}\frac{\mathrm{d}u_{30}(x_1)}{\mathrm{d}x_1}+x_3\frac{\mathrm{d}\phi(x_1)}{\mathrm{d}x_1}+\Im_1\left[\frac{d^2u_3(x_1)}{\mathrm{d}x_1^2}+\frac{\mathrm{d}\phi(x_1)}{\mathrm{d}x_1}\right], \tag{1}$$

$$\varepsilon_{13}(x_1)=\Im_2\left(\frac{\mathrm{d}u_3(x_1)}{\mathrm{d}x_1}+\phi(x_1)\right), \tag{2}$$

$$\varepsilon_{33}\neq 0 \quad \text{(should satisfy the incompressibility condition)} \tag{3}$$

with

$$\Im_1=-\frac{4}{3}\frac{x_3^3}{h^2},\qquad \Im_2=\frac{1}{2}\left(1-4\frac{x_3^2}{h^2}\right), \tag{4}$$

where u_1 and u_3 are the displacements of the arch in the x_1 and x_3 directions (shown in Fig. 1a), u_{30} is the curvature of the shallow arch, ε_{11} and ε_{33} are the axial strains in the x_1 and x_3 directions and ε_{13} is the shear strain. By considering plane motion and incompressible material, the right Cauchy-Green strain tensor is written as [49]

$$C=\begin{bmatrix}(1+\varepsilon_{11})^2+\varepsilon_{13}^2 & 0 & \varepsilon_{11}\varepsilon_{13}+2\varepsilon_{13}+\varepsilon_{33}\varepsilon_{13}\\ 0 & 1 & 0\\ \varepsilon_{11}\varepsilon_{13}+2\varepsilon_{13}+\varepsilon_{33}\varepsilon_{13} & 0 & (1+\varepsilon_{33})^2+\varepsilon_{13}^2\end{bmatrix}, \tag{5}$$

which contains nonlinear higher-order strain terms since *hyper-elastic* structures undergo large strains and cannot be modelled by considering the linear part alone, as is undertaken for *elastic* structures.

The principle of virtual work is not only for linear elastic structures and can be applied for hyper-elastic structures [50]. To this end, by using the Mooney–Rivlin hyper-elastic strain energy density [51,52] and the principle of virtual work, the variation of the energy term, due to the static applied forces, can be written in three variation terms for axial ($PE1$), transverse ($PE2$) and rotation ($PE3$) variations as

$$\int_0^L\left[F_{s1}\delta u_1+F_{s3}\delta u_3+F_{s2}\delta\phi\right]\mathrm{d}x_1=\int_0^L\left[(PE1)\,\delta u_1+(PE2)\,\delta u_3+(PE3)\,\delta\phi\right]\mathrm{d}x_1, \tag{6}$$

where $PE1$, $PE2$, $PE3$ are given in Appendix A for the sake of brevity, with the moment of area coefficients defined as

$$I_{00}=\int_A 1dA,\quad I_{11}=\int_A u_3\mathrm{d}A,\quad I_{22}=\int_A\Im_1\mathrm{d}A,\quad I_{33}=\int_A(u_3+\Im_1)\,\mathrm{d}A,$$

$$I_{44}=\int_A\Im_1^2\mathrm{d}A,\quad I_{55}=\int_A\Im_2^2\mathrm{d}A,$$

$$I_{66}=\int_A\Im_1(u_3+\Im_1)\,\mathrm{d}A,\quad I_{77}=\int_A\left(1-\Im_2^2\right)\mathrm{d}A,$$

$$I_{88}=\int_A\left(1-2\Im_2^2\right)\mathrm{d}A,\quad I_{99}=\int_A(\Im_1+u_3)^2\,\mathrm{d}A,$$

$$I_{1010}=\int_A\Im_1^3\mathrm{d}A,\quad I_{1111}=\int_A\Im_1\Im_2^2\mathrm{d}A,\quad I_{1212}=\int_A\Im_1\left(1-\Im_2^2\right)\mathrm{d}A,\quad I_{1313}=\int_A\Im_2^2(\Im_1+u_3)\,\mathrm{d}A,$$

$$I_{1414}=\int_A\Im_1^2(\Im_1+u_3)\,\mathrm{d}A,\quad I_{1515}=\int_A\Im_1(\Im_1+u_3)^2\,\mathrm{d}A,\quad I_{1616}=\int_A(\Im_1+u_3)^3\,\mathrm{d}A,$$

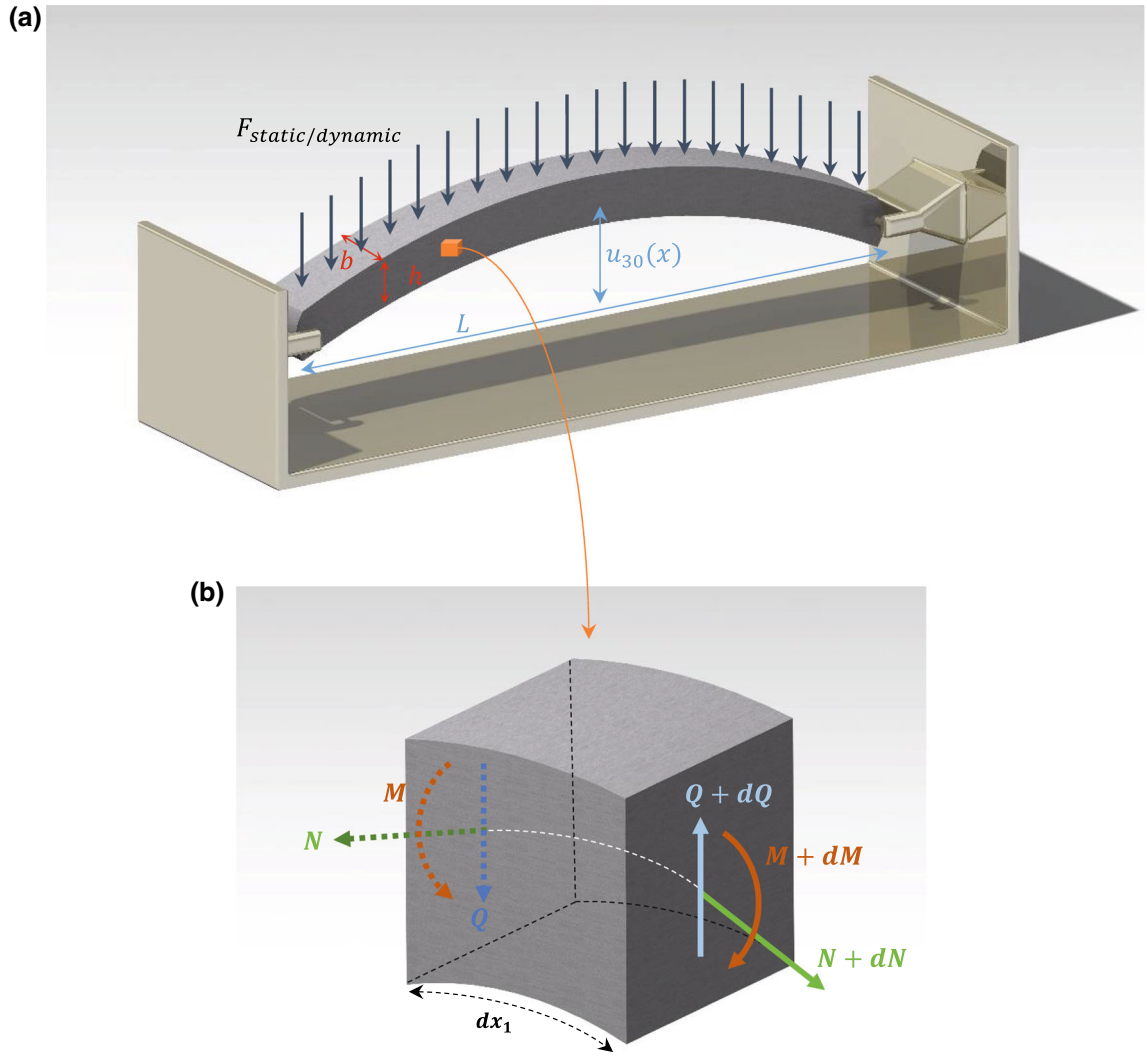

Fig. 1 Schematic figure of a visco-hyper-elastic thick shallow arch with simply supported boundary conditions

$$I_{1717} = \int_A u_3 \left(u_3 + \Im_1\right) \Im_2^2 \mathrm{d}A, \quad I_{1818} = \int_A \Im_2^3 \mathrm{d}A, \quad I_{1919} = \int_A \left(u_3 + \Im_1\right) \left(\Im_2^2 - 1\right) \mathrm{d}A. \tag{7}$$

Using Eqs. (1–7), three equilibrium equations for the bending analysis are obtained by having homogeneity in the arch as

$$\begin{aligned}
&-8C_T I_{00} u_{1x_1x_1} - 8C_T I_{00} \frac{\mathrm{d}}{\mathrm{d}x_1}\left(u_{3x_1} u_{30x_1}\right) + 12C_T I_{00} \frac{\mathrm{d}}{\mathrm{d}x_1}\left(u_{1x_1}^2\right) + 24C_T I_{00} \frac{\mathrm{d}}{\mathrm{d}x_1}\left(u_{1x_1} u_{3x_1} u_{30x_1}\right) \\
&-4C_T I_{77} \frac{\mathrm{d}}{\mathrm{d}x_1}\left(u_{3x_1}^2\right) + 12C_T I_{00} \frac{\mathrm{d}}{\mathrm{d}x_1}\left(u_{3x_1}^2 u_{30x_1}^2\right) + 12C_T I_{44} \frac{\mathrm{d}}{\mathrm{d}x_1}\left(u_{3x_1x_1}^2\right) \\
&+24C_T I_{66} \frac{\mathrm{d}}{\mathrm{d}x_1}\left(u_{3x_1x_1} \phi_{x_1}\right) + 8C_T I_{55} \frac{\mathrm{d}}{\mathrm{d}x_1}\left(u_{3x_1} \phi\right) + 12C_T I_{99} \frac{\mathrm{d}}{\mathrm{d}x_1}\left(\phi_{x_1}^2\right) + 4C_T\, I_{55} \frac{\mathrm{d}}{\mathrm{d}x_1}\left(\phi^2\right) \\
&+12C_T I_{00} \frac{\mathrm{d}}{\mathrm{d}x_1}\left(u_{1x_1} u_{3x_1}^2\right) + 12C_T I_{00} \frac{\mathrm{d}}{\mathrm{d}x_1}\left(u_{30x_1} u_{3x_1}^3\right) + 3C_T I_{00} \frac{\mathrm{d}}{\mathrm{d}x_1}\left(u_{3x_1}^4\right) = F_{S1}, \qquad (8) \\
&-8C_T I_{66} u_{3x_1x_1x_1} + 8C_T I_{55} u_{3x_1} - 8C_T I_{99} \phi_{x_1x_1} + 8C_T I_{55} \phi + 24C_T I_{66} \frac{\mathrm{d}}{\mathrm{d}x_1}\left(u_{1x_1} u_{3x_1x_1}\right) - 8C_T I_{55} u_{1x_1} u_{3x_1}
\end{aligned}$$

$$
\begin{aligned}
&+24C_T I_{99}\frac{\mathrm{d}}{\mathrm{d}x_1}\left(u_{1x_1}\phi_{x_1}\right)-8C_T I_{55}u_{1x_1}\phi+24C_T I_{66}\frac{\mathrm{d}}{\mathrm{d}x_1}\left(u_{3x_1}u_{3x_1x_1}u_{30x_1}\right)-8C_T I_{55}u_{3x_1}^2u_{30x_1}\\
&+24C_T I_{99}\frac{\mathrm{d}}{\mathrm{d}x_1}\left(u_{3x_1}\phi_{x_1}u_{30x_1}\right)-8C_T I_{55}u_{3x_1}\phi u_{30x_1}+12C_T I_{66}\frac{\mathrm{d}}{\mathrm{d}x_1}\left(u_{3x_1}^2u_{3x_1x_1}\right)-4C_T I_{55}u_{3x_1}^3\\
&+12C_T I_{99}\frac{\mathrm{d}}{\mathrm{d}x_1}\left(u_{3x_1}^2\phi_{x_1}\right)-4C_T I_{55}u_{3x_1}^2\phi=F_{S2}. \qquad (9)\\
&-8C_T I_{00}\frac{\mathrm{d}}{\mathrm{d}x_1}\left(u_{1x_1}u_{30x_1}\right)-8C_T I_{00}\frac{\mathrm{d}}{\mathrm{d}x_1}\left(u_{3x_1}u_{30x_1}^2\right)\\
&+8C_T I_{44}u_{3x_1x_1x_1x_1}-8C_T\ I_{55}u_{3x_1x_1}+8C_T I_{66}\phi_{x_1x_1x_1}-8C_T I_{55}\phi_{x_1}\\
&+12C_T I_{00}\frac{\mathrm{d}}{\mathrm{d}x_1}\left(u_{1x_1}^2u_{30x_1}\right)-8C_T I_{77}\frac{\mathrm{d}}{\mathrm{d}x_1}\left(u_{1x_1}u_{3x_1}\right)\\
&+24C_T I_{00}\frac{\mathrm{d}}{\mathrm{d}x_1}\left(u_{1x_1}u_{3x_1}u_{30x_1}^2\right)-24C_T I_{44}\frac{d^2}{\mathrm{d}x_1^2}\left(u_{1x_1}u_{3x_1x_1}\right)\\
&-24C_T I_{66}\frac{d^2}{\mathrm{d}x_1^2}\left(u_{1x_1}\phi_{x_1}\right)+8C_T I_{55}\frac{\mathrm{d}}{\mathrm{d}x_1}\left(u_{1x_1}\phi\right)\\
&-12C_T I_{77}\frac{\mathrm{d}}{\mathrm{d}x_1}\left(u_{3x_1}^2u_{30x_1}\right)+12C_T I_{00}\frac{\mathrm{d}}{\mathrm{d}x_1}\left(u_{3x_1}^2u_{30x_1}^3\right)\\
&+12C_T I_{44}\frac{\mathrm{d}}{\mathrm{d}x_1}\left(u_{3x_1x_1}^2u_{30x_1}\right)-24C_T I_{44}\frac{\mathrm{d}^2}{\mathrm{d}x_1^2}\left(u_{3x_1}u_{3x_1x_1}u_{30x_1}\right)+24C_T I_{66}\frac{\mathrm{d}}{\mathrm{d}x_1}\left(u_{3x_1x_1}\phi_{x_1}u_{30x_1}\right)\\
&+16C_T I_{55}\frac{\mathrm{d}}{\mathrm{d}x_1}\left(u_{3x_1}\phi u_{30x_1}\right)-24C_T I_{66}\frac{\mathrm{d}^2}{\mathrm{d}x_1^2}\left(u_{3x_1}\phi_{x_1}u_{30x_1}\right)\\
&+12C_T I_{99}\frac{\mathrm{d}}{\mathrm{d}x_1}\left(\phi_{x_1}^2u_{30x_1}\right)+4C_T I_{55}\frac{\mathrm{d}}{\mathrm{d}x_1}\left(\phi^2u_{30x_1}\right)\\
&+12C_T I_{00}\frac{\mathrm{d}}{\mathrm{d}x_1}\left(u_{1x_1}^2u_{3x_1}\right)+36C_T I_{00}\frac{\mathrm{d}}{\mathrm{d}x_1}\left(u_{1x_1}u_{3x_1}^2u_{30x_1}\right)\\
&-4C_T I_{88}\frac{\mathrm{d}}{\mathrm{d}x_1}\left(u_{3x_1}^3\right)+24C_T I_{00}\frac{\mathrm{d}}{\mathrm{d}x_1}\left(u_{3x_1}^3u_{30x_1}^2\right)\\
&+12C_T I_{44}\frac{\mathrm{d}}{\mathrm{d}x_1}\left(u_{3x_1}u_{3x_1x_1}^2\right)-12C_T I_{44}\frac{\mathrm{d}^2}{\mathrm{d}x_1^2}\left(u_{3x_1}^2u_{3x_1x_1}\right)\\
&+24C_T I_{66}\frac{\mathrm{d}}{\mathrm{d}x_1}\left(u_{3x_1}u_{3x_1x_1}\phi_{x_1}\right)+12C_T I_{55}\frac{\mathrm{d}}{\mathrm{d}x_1}\left(u_{3x_1}^2\phi\right)\\
&-12C_T I_{66}\frac{\mathrm{d}^2}{\mathrm{d}x_1^2}\left(u_{3x_1}^2\phi_{x_1}\right)+12C_T I_{99}\frac{\mathrm{d}}{\mathrm{d}x_1}\left(u_{3x_1}\phi_{x_1}^2\right)+4C_T I_{55}\frac{\mathrm{d}}{\mathrm{d}x_1}\left(u_{3x_1}\phi^2\right)+12C_T I_{00}\frac{\mathrm{d}}{\mathrm{d}x_1}\left(u_{1x_1}u_{3x_1}^3\right)\\
&+15C_T I_{00}\frac{\mathrm{d}}{\mathrm{d}x_1}\left(u_{30x_1}u_{3x_1}^4\right)+3C_T I_{00}\frac{\mathrm{d}}{\mathrm{d}x_1}\left(u_{3x_1}^5\right)=F_{S3}, \qquad (10)
\end{aligned}
$$

It can be seen that the equilibrium equations are highly nonlinear in hyper-elasticity terms, with a high coupling between the axial, rotation and transverse motions. The equilibrium equations can be validated by comparing them to those presented in Ref. [40] by neglecting the curvature terms from these equations and unsymmetrical and time-dependant terms in the equations of motion of Ref. [40]. By employing the solution procedure given in Sect. 4, the bending behaviour of soft thick shallow arches will be obtained.

3 Dynamics of visco-hyper-elastic thick arch formulation via force-moment balance method

For the time-dependent analysis and modelling of soft thick shallow arches, using the same assumptions given in Sect. 2, the nonlinear strain terms are written as

$$\varepsilon_{11}\left(x_1,x_3,t\right)=\frac{\partial u_1\left(x_1,t\right)}{\partial x_1}+\frac{1}{2}\left(\frac{\partial u_3\left(x_1,t\right)}{\partial x_1}\right)^2+\frac{\partial u_3\left(x_1,t\right)}{\partial x_1}\frac{\mathrm{d}u_{30}\left(x_1\right)}{\mathrm{d}x_1}$$

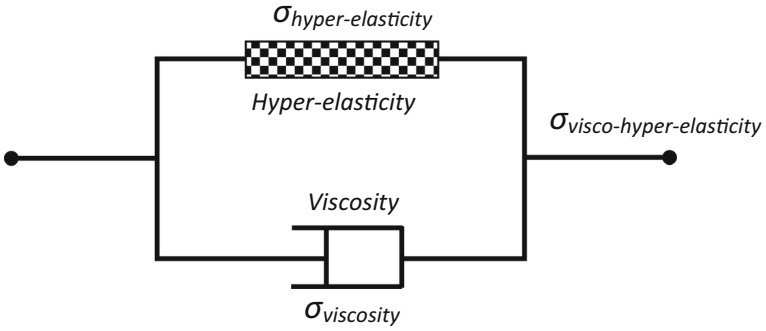

Fig. 2 Constitutive model of Kelvin–Voigt visco-hyper-elasticity

$$+x_3\frac{\partial\phi\left(x_1,t\right)}{\partial x_1}+\Im_1\left[\frac{\partial^2 u_3\left(x_1,t\right)}{\partial x_1^2}+\frac{\partial\phi\left(x_1,t\right)}{\partial x_1}\right], \tag{11}$$

$$\varepsilon_{13}\left(x_1,t\right)=\Im_2\left(\frac{\partial u_3\left(x_1,t\right)}{\partial x_1}+\phi\left(x_1,t\right)\right), \tag{12}$$

$$\varepsilon_{33}\neq 0 \quad \text{(should satisfy the incompressibility condition)}. \tag{13}$$

For visco-hyper-elastic structures, Li et al. [48] have shown that the visco-hyper Kelvin–Voigt model has a good accuracy in modelling visco-hyper-elastic structures while using Mooney–Rivlin, neo-Hookean and Ogden strain energy density models. The visco-hyper-elastic model (Fig. 2) is presented as [48]

$$\sigma_{\text{visco-hyper}}=\sigma_{\text{hyperelastic}}+\xi_k\dot{\varepsilon}, \tag{14}$$

(Talk about the feasible applicability of the approach) For an element of the thick visco-hyper-elastic arch, shown in Fig. 2b, Newton's law is applied for the rotational motion, as well as translational ones by having [53]

$$\frac{\partial N\left(x_1,x_3,t\right)}{\partial x_1}=-\rho I_{00}u_{1tt}-\rho I_{22}u_{3xtt}-\rho I_{33}\phi_{tt}, \tag{15}$$

$$\frac{\partial Q\left(x_1,x_3,t\right)}{\partial x_1}+F_{\text{external}}\left(x_1,x_3,t\right)=\rho I_{22}u_{1xtt}+\rho I_{44}u_{3xxtt}+\rho I_{66}\phi_{xtt}-\rho I_{00}u_{3tt}, \tag{16}$$

$$\frac{\partial M\left(x_1,x_3,t\right)}{\partial x_1}-Q\left(x_1,x_3,t\right)=-\rho I_{33}u_{1tt}-\rho I_{66}u_{3xtt}-\rho I_{99}\phi_{tt}, \tag{17}$$

where the stress resultants are defined as [54]

$$N=\int_A \sigma_{\text{visco-hyper},x_1x_1}\mathrm{d}A, \tag{18}$$

$$M=\int_A x_3\sigma_{\text{visco-hyper},x_1x_1}\mathrm{d}A, \tag{19}$$

$$Q=\int_A \sigma_{\text{visco-hyper},x_1x_3}\mathrm{d}A, \tag{20}$$

and the applied external periodic load with the magnitude of F is given as

$$F_{\text{external}}=F\cos\left(\omega t\right). \tag{21}$$

For isotropic visco-hyper-elastic shallow arches, by using force-moment balance method, one can reach the coupled equations of motions which are shown in Appendix B for the sake of brevity. By neglecting the viscoelasticity and the arch-related terms, the equations of motion can be validated through Ref. [40]. It can be seen that all three equations of motion are highly nonlinear in visco-elasticity and hyper-elasticity terms, with a high coupling between the axial, rotation and transverse motions. By using the solution procedure given in Sect. 5, the vibration behaviour of soft thick shallow arches will be obtained.

4 Solution procedure for hyper-elastic bending analysis

By assuming only transverse external load on the system ($F_{s1} = F_{S2} = 0$ and $F_{S3} = F$) and defining nondimensional terms as

$$
\begin{aligned}
&{x_1}^* = \frac{x_1}{L}, \quad {u_1}^* = \frac{u_1}{h}, \quad {u_3}^* = \frac{u_3}{h}, \quad {u_{30}}^* = \frac{u_{30}}{h}, \quad {I_{00}}^* = \frac{I_{00}h^2}{I_{44}},\\
&{I_{55}}^* = \frac{I_{55}h^2}{I_{44}}, \quad {I_{66}}^* = \frac{I_{66}}{I_{44}}, \quad {I_{77}}^* = \frac{I_{77}h^2}{I_{44}},\\
&{I_{88}}^* = \frac{I_{88}h^2}{I_{44}}, \quad {I_{99}}^* = \frac{I_{99}}{I_{44}}, \quad \eta = \frac{h}{L}, \quad F^* = \frac{FL^4}{C_T I_{44} h},
\end{aligned} \tag{22}
$$

the nondimensional equilibrium equations are written as

$$
\begin{aligned}
&-8I_{00}\frac{1}{\eta^2}u_{1x_1x_1} - 8I_{00}\frac{1}{\eta}\frac{\mathrm{d}}{\mathrm{d}x_1}\left(u_{3x_1}u_{30x_1}\right)\\
&+12I_{00}\frac{1}{\eta}\frac{\mathrm{d}}{\mathrm{d}x_1}\left(u_{1x_1}^2\right) + 24I_{00}\frac{\mathrm{d}}{\mathrm{d}x_1}\left(u_{1x_1}u_{3x_1}u_{30x_1}\right) - 4I_{77}\frac{1}{\eta}\frac{\mathrm{d}}{\mathrm{d}x_1}\left(u_{3x_1}^2\right) + 12I_{00}\eta\frac{\mathrm{d}}{\mathrm{d}x_1}\left(u_{3x_1}^2u_{30x_1}^2\right)\\
&+12\eta\frac{\mathrm{d}}{\mathrm{d}x_1}\left(u_{3x_1x_1}^2\right) + 24I_{66}\frac{\mathrm{d}}{\mathrm{d}x_1}\left(u_{3x_1x_1}\phi_{x_1}\right) + 8I_{55}\frac{1}{\eta^2}\frac{\mathrm{d}}{\mathrm{d}x_1}\left(u_{3x_1}\phi\right) + 12I_{99}\frac{1}{\eta}\frac{\mathrm{d}}{\mathrm{d}x_1}\left(\phi_{x_1}^2\right) + 4I_{55}\frac{1}{\eta^3}\frac{\mathrm{d}}{\mathrm{d}x_1}\left(\phi^2\right)\\
&+12I_{00}\frac{\mathrm{d}}{\mathrm{d}x_1}\left(u_{1x_1}u_{3x_1}^2\right) + 12I_{00}\eta\frac{\mathrm{d}}{\mathrm{d}x_1}\left(u_{30x_1}u_{3x_1}^3\right) + 3I_{00}\eta\frac{\mathrm{d}}{\mathrm{d}x_1}\left(u_{3x_1}^4\right) = 0,
\end{aligned} \tag{23}
$$

$$
\begin{aligned}
&-8I_{00}\frac{1}{\eta}\frac{\mathrm{d}}{\mathrm{d}x_1}\left(u_{1x_1}u_{30x_1}\right) - 8I_{00}\frac{\mathrm{d}}{\mathrm{d}x_1}\left(u_{3x_1}u_{30x_1}^2\right) + 8u_{3x_1x_1x_1x_1} - 8I_{55}\frac{1}{\eta^2}u_{3x_1x_1} + 8I_{66}\frac{1}{\eta}\phi_{x_1x_1x_1} - 8I_{55}\frac{1}{\eta^3}\phi_{x_1}\\
&+12I_{00}\frac{\mathrm{d}}{\mathrm{d}x_1}\left(u_{1x_1}^2u_{30x_1}\right) - 8I_{77}\frac{1}{\eta}\frac{\mathrm{d}}{\mathrm{d}x_1}\left(u_{1x_1}u_{3x_1}\right) + 24I_{00}\eta\frac{\mathrm{d}}{\mathrm{d}x_1}\left(u_{1x_1}u_{3x_1}u_{30x_1}^2\right) - 24\eta\frac{\mathrm{d}^2}{\mathrm{d}x_1^2}\left(u_{1x_1}u_{3x_1x_1}\right)\\
&-24I_{66}\frac{\mathrm{d}^2}{\mathrm{d}x_1^2}\left(u_{1x_1}\phi_{x_1}\right) + 8I_{55}\frac{1}{\eta^2}\frac{\mathrm{d}}{\mathrm{d}x_1}\left(u_{1x_1}\phi\right) - 12I_{77}\frac{\mathrm{d}}{\mathrm{d}x_1}\left(u_{3x_1}^2u_{30x_1}\right) + 12I_{00}\eta^2\frac{\mathrm{d}}{\mathrm{d}x_1}\left(u_{3x_1}^2u_{30x_1}^3\right)\\
&+12\eta^2\frac{\mathrm{d}}{\mathrm{d}x_1}\left(u_{3x_1x_1}^2u_{30x_1}\right) - 24\eta^2\frac{\mathrm{d}^2}{\mathrm{d}x_1^2}\left(u_{3x_1}u_{3x_1x_1}u_{30x_1}\right) + 24I_{66}\eta\frac{\mathrm{d}}{\mathrm{d}x_1}\left(u_{3x_1x_1}\phi_{x_1}u_{30x_1}\right)\\
&+16I_{55}\frac{1}{\eta}\frac{\mathrm{d}}{\mathrm{d}x_1}\left(u_{3x_1}\phi u_{30x_1}\right) - 24I_{66}\eta\frac{\mathrm{d}^2}{\mathrm{d}x_1^2}\left(u_{3x_1}\phi_{x_1}u_{30x_1}\right) + 12I_{99}\frac{\mathrm{d}}{\mathrm{d}x_1}\left(\phi_{x_1}^2u_{30x_1}\right)\\
&+4I_{55}\frac{1}{\eta^2}\frac{\mathrm{d}}{\mathrm{d}x_1}\left(\phi^2u_{30x_1}\right) + 12I_{00}\frac{\mathrm{d}}{\mathrm{d}x_1}\left(u_{1x_1}^2u_{3x_1}\right) + 36I_{00}\eta\frac{\mathrm{d}}{\mathrm{d}x_1}\left(u_{1x_1}u_{3x_1}^2u_{30x_1}\right) - 4I_{88}\frac{\mathrm{d}}{\mathrm{d}x_1}\left(u_{3x_1}^3\right)\\
&+24I_{00}\frac{\mathrm{d}}{\mathrm{d}x_1}\left(u_{3x_1}^3u_{30x_1}^2\right) + 12\eta^2\frac{\mathrm{d}}{\mathrm{d}x_1}\left(u_{3x_1}u_{3x_1x_1}^2\right) - 12\eta^2\frac{\mathrm{d}^2}{\mathrm{d}x_1^2}\left(u_{3x_1}^2u_{3x_1x_1}\right)\\
&+24I_{66}\eta\frac{\mathrm{d}}{\mathrm{d}x_1}\left(u_{3x_1}u_{3x_1x_1}\phi_{x_1}\right) + 12I_{55}\frac{1}{\eta}\frac{\mathrm{d}}{\mathrm{d}x_1}\left(u_{3x_1}^2\phi\right) - 12I_{66}\eta\frac{\mathrm{d}^2}{\mathrm{d}x_1^2}\left(u_{3x_1}^2\phi_{x_1}\right)\\
&+12I_{99}\frac{\mathrm{d}}{\mathrm{d}x_1}\left(u_{3x_1}\phi_{x_1}^2\right) + 4I_{55}\frac{1}{\eta^2}\frac{\mathrm{d}}{\mathrm{d}x_1}\left(u_{3x_1}\phi^2\right) + 12I_{00}\eta\frac{\mathrm{d}}{\mathrm{d}x_1}\left(u_{1x_1}u_{3x_1}^3\right) + 15I_{00}\eta^2\frac{\mathrm{d}}{\mathrm{d}x_1}\left(u_{30x_1}u_{3x_1}^4\right)\\
&+3I_{00}\eta^2\frac{\mathrm{d}}{\mathrm{d}x_1}\left(u_{3x_1}^5\right) = F,
\end{aligned} \tag{24}
$$

$$
\begin{aligned}
&-8I_{66}\eta u_{3x_1x_1x_1} + 8I_{55}\frac{1}{\eta}u_{3x_1} - 8I_{99}\phi_{x_1x_1} + 8I_{55}\frac{1}{\eta^2}\phi + 24I_{66}\eta^2\frac{\mathrm{d}}{\mathrm{d}x_1}\left(u_{1x_1}u_{3x_1x_1}\right) - 8I_{55}u_{1x_1}u_{3x_1}\\
&+24I_{99}\eta\frac{\mathrm{d}}{\mathrm{d}x_1}\left(u_{1x_1}\phi_{x_1}\right) - 8I_{55}\frac{1}{\eta}u_{1x_1}\phi + 24I_{66}\eta^3\frac{\mathrm{d}}{\mathrm{d}x_1}\left(u_{3x_1}u_{3x_1x_1}u_{30x_1}\right) - 8I_{55}\eta u_{3x_1}^2u_{30x_1}\\
&+24I_{99}\eta^2\frac{\mathrm{d}}{\mathrm{d}x_1}\left(u_{3x_1}\phi_{x_1}u_{30x_1}\right) - 8I_{55}u_{3x_1}\phi u_{30x_1} + 12I_{66}\eta^3\frac{\mathrm{d}}{\mathrm{d}x_1}\left(u_{3x_1}^2u_{3x_1x_1}\right) - 4I_{55}\eta u_{3x_1}^3\\
&+12I_{99}\eta^2\frac{\mathrm{d}}{\mathrm{d}x_1}\left(u_{3x_1}^2\phi_{x_1}\right) - 4I_{55}u_{3x_1}^2\phi = 0.
\end{aligned} \tag{25}
$$

where * is neglected from the parameters for the sake of brevity. By employing a series expansion, the degrees of freedom are written as

$$u_1(x_1) = \sum_{j=1}^{M} \Re_j U_j(x_1), \tag{26}$$

$$u_3(x_1) = \sum_{i=1}^{N} \aleph_i W_i(x_1), \tag{27}$$

$$\phi(x_1) = \sum_{i=1}^{N} \kappa_i \psi_i(x_1), \tag{28}$$

$$u_{30}(x_1) = W_0(x_1), \tag{29}$$

and the equations of motion are discretised as

$$K_{11}^{L}\Re + K_{12}^{L}\aleph + K_{11}^{NL}\Re^2 + K_{12}^{NL}\Re\aleph + K_{13}^{NL}\aleph^2 + K_{14}^{NL}\aleph\kappa + K_{15}^{NL}\kappa^2 + K_{16}^{NL}\Re\aleph^2 + K_{17}^{NL}\aleph^3 + K_{18}^{NL}\aleph^4 = 0, \tag{30}$$

$$K_{21}^{L}\Re + K_{22}^{L}\aleph + K_{22}^{L}\kappa + K_{21}^{NL}\Re^2 + K_{22}^{NL}\Re\aleph + K_{23}^{NL}\Re\kappa + K_{24}^{NL}\aleph^2 + K_{25}^{NL}\aleph\kappa + K_{26}^{NL}\kappa^2 + K_{27}^{NL}\Re^2\aleph + K_{28}^{NL}\Re\aleph^2 + K_{29}^{NL}\aleph^3 + K_{210}^{NL}\aleph^2\kappa + K_{211}^{NL}\aleph\kappa^2 + K_{212}^{NL}r\aleph^3 + K_{213}^{NL}\aleph^4 + K_{214}^{NL}\aleph^5 = F, \tag{31}$$

$$K_{32}^{L}\aleph + K_{33}^{L}\kappa + K_{31}^{NL}\Re\aleph + K_{32}^{NL}\Re\kappa + K_{33}^{NL}\aleph^2 + K_{34}^{NL}\aleph\kappa + K_{35}^{NL}\aleph^3 + K_{36}^{NL}\aleph^2\kappa = 0. \tag{32}$$

The linear stiffness coefficients (K_{ij}^{L}) of the bending equilibrium equations are defined as

$$K_{11}^{L} = -8\frac{1}{\eta^2} I_{00} \int_0^1 U_p(x_1) U_i''(x_1)\,\mathrm{d}x_1, \tag{33}$$

$$K_{12}^{L} = -8\frac{1}{\eta} I_{00} \int_0^1 U_p(x_1) \frac{\mathrm{d}}{\mathrm{d}x_1}\left(W_i'(x_1)\, W_0'(x_1)\right)\mathrm{d}x_1, \tag{34}$$

$$K_{21}^{L} = -8 I_{00}\frac{1}{\eta} \int_0^1 W_l(x_1) \frac{\mathrm{d}}{\mathrm{d}x_1}\left(U_i'(x_1)\, W_0'(x_1)\right)\mathrm{d}x_1, \tag{35}$$

$$K_{22}^{L} = -8 I_{00} \int_0^1 W_l(x_1) \frac{\mathrm{d}}{\mathrm{d}x_1}\left(W_i'(x_1)\, W_0'^2(x_1)\right)\mathrm{d}x_1 + 8\int_0^1 W_l(x_1) W_i^{(4)}(x_1)\,\mathrm{d}x_1 - 8 I_{55}\frac{1}{\eta^2}\int_0^1 W_l(x_1) W_i''(x_1)\,\mathrm{d}x_1, \tag{36}$$

$$K_{23}^{L} = +8 I_{66}\frac{1}{\eta}\int_0^1 W_l(x_1)\psi_i'''(x_1)\,\mathrm{d}x_1 - 8 I_{55}\frac{1}{\eta^3}\int_0^1 W_l(x_1)\psi_i'(x_1)\,\mathrm{d}x_1, \tag{37}$$

$$K_{32}^{L} = -8 I_{66}\eta \int_0^1 \psi_l(x_1) W_i''' \ (x_1)\,\mathrm{d}x_1 + 8 I_{55}\frac{1}{\eta}\int_0^1 \psi_l(x_1) W_i'(x_1)\,\mathrm{d}x_1, \tag{38}$$

$$K_{33}^{L} = +8 I_{55}\frac{1}{\eta^2}\int_0^1 \psi_l(x_1)\psi_i(x_1)\,\mathrm{d}x_1 - 8 I_{99}\int_0^1 \psi_l(x_1)\psi_i''(x_1)\,\mathrm{d}x_1, \tag{39}$$

and the nonlinear stiffness coefficients (K_{ij}^{NL}) are defined as

$$K_{11}^{NL} = +12\frac{1}{\eta}I_{00}\int_0^1 U_p\left(x_1\right)\frac{\mathrm{d}}{\mathrm{d}x_1}\left(U_i'\left(x_1\right)U_j'\left(x_1\right)\right)\mathrm{d}x_1, \tag{40}$$

$$K_{12}^{NL} = +24I_{00}\int_0^1 U_p\left(x_1\right)\frac{\mathrm{d}}{\mathrm{d}x_1}\left(U_i'\left(x_1\right)W_j'\left(x_1\right)W_0'\left(x_1\right)\right)\mathrm{d}x_1, \tag{41}$$

$$\begin{aligned} K_{13}^{NL} = &-4\frac{1}{\eta}I_{77}\int_0^1 U_p\left(x_1\right)\frac{\mathrm{d}}{\mathrm{d}x_1}\left(W_i'\left(x_1\right)W_j'\left(x_1\right)\right)\mathrm{d}x_1 \\ &+12\eta I_{00}\int_0^1 U_p\left(x_1\right)\frac{\mathrm{d}}{\mathrm{d}x_1}\left(W_i'\left(x_1\right)W_j'\left(x_1\right)W_0'^2\left(x_1\right)\right)\mathrm{d}x_1 \\ &+12\eta\int_0^1 U_p\left(x_1\right)\frac{\mathrm{d}}{\mathrm{d}x_1}\left(W_i''\left(x_1\right)W_j''\left(x_1\right)\right)\mathrm{d}x_1, \end{aligned} \tag{42}$$

$$K_{14}^{NL} = +24I_{66}\int_0^1 U_p\left(x_1\right)\frac{\mathrm{d}}{\mathrm{d}x_1}\left(W_i''\left(x_1\right)\psi_j'\left(x_1\right)\right)\mathrm{d}x_1 + 8\frac{1}{\eta^2}I_{55}\int_0^1 U_p\left(x_1\right)\frac{\mathrm{d}}{\mathrm{d}x_1}\left(W_i'\left(x\right)\psi_j\left(x_1\right)\right)\mathrm{d}x_1, \tag{43}$$

$$K_{15}^{NL} = +12\frac{1}{\eta}I_{99}\int_0^1 U_p\left(x_1\right)\frac{\mathrm{d}}{\mathrm{d}x_1}\left(\psi_i'\left(x_1\right)\psi_j'\left(x_1\right)\right)\mathrm{d}x_1 + 4\frac{1}{\eta^3}I_{55}\int_0^1 U_p\left(x_1\right)\frac{\mathrm{d}}{\mathrm{d}x_1}\left(\psi_i\left(x_1\right)\psi_j\left(x_1\right)\right)\mathrm{d}x_1, \tag{44}$$

$$K_{16}^{NL} = +12I_{00}\int_0^1 U_p\left(x_1\right)\frac{\mathrm{d}}{\mathrm{d}x_1}\left(U_i'\left(x_1\right)W_j'\left(x_1\right)W_k'\left(x_1\right)\right)\mathrm{d}x_1, \tag{45}$$

$$K_{17}^{NL} = +12\eta I_{00}\int_0^1 U_p\left(x_1\right)\frac{\mathrm{d}}{\mathrm{d}x_1}\left(W_i'\left(x_1\right)W_j'\left(x_1\right)W_k'\left(x_1\right)W_0'\left(x_1\right)\right)\mathrm{d}x_1, \tag{46}$$

$$K_{18}^{NL} = +3\eta I_{00}\int_0^1 U_p\left(x_1\right)\frac{\mathrm{d}}{\mathrm{d}x_1}\left(W_i'\left(x_1\right)W_j'\left(x_1\right)W_k'\left(x_1\right)W_m'\left(x_1\right)\right)\mathrm{d}x_1, \tag{47}$$

$$K_{21}^{NL} = +12I_{00}\int_0^1 W_l\left(x_1\right)\frac{\mathrm{d}}{\mathrm{d}x_1}\left(U_i'\left(x_1\right)U_j'\left(x_1\right)W_0'\left(x_1\right)\right)\mathrm{d}x_1, \tag{48}$$

$$\begin{aligned} K_{22}^{NL} = &-8I_{77}\frac{1}{\eta}\int_0^1 W_l\left(x_1\right)\frac{\mathrm{d}}{\mathrm{d}x_1}\left(U_i'\left(x_1\right)W_j'\left(x_1\right)\right)\mathrm{d}x_1 - 24\eta\int_0^1 W_l\left(x_1\right)\frac{\mathrm{d}^2}{\mathrm{d}x_1^2}\left(U_i'\left(x_1\right)W_j''\left(x_1\right)\right)\mathrm{d}x_1 \\ &+24I_{00}\eta\int_0^1 W_l\left(x_1\right)\frac{\mathrm{d}}{\mathrm{d}x_1}\left(U_i'\left(x_1\right)W_j'\left(x_1\right)W_0'^2\left(x_1\right)\right)\mathrm{d}x_1, \end{aligned} \tag{49}$$

$$K_{23}^{NL} = -24I_{66}\int_0^1 W_l\left(x_1\right)\frac{\mathrm{d}^2}{\mathrm{d}x_1^2}\left(U_i'\left(x_1\right)\psi_j'\left(x_1\right)\right)\mathrm{d}x_1 + 8I_{55}\frac{1}{\eta^2}\int_0^1 W_l\left(x_1\right)\frac{\mathrm{d}}{\mathrm{d}x_1}\left(U_i'\left(x_1\right)\psi_j\left(x_1\right)\right)\mathrm{d}x_1, \tag{50}$$

$$K_{24}^{NL} = -12I_{77}\int_0^1 W_l(x_1)\frac{\mathrm{d}}{\mathrm{d}x_1}\left(W_i'(x_1)\,W_j'(x_1)\,W_0'(x_1)\right)\mathrm{d}x_1$$
$$+12I_{00}\eta^2\int_0^1 W_l(x_1)\frac{\mathrm{d}}{\mathrm{d}x_1}\left(W_i'(x_1)\,W_j'(x_1)\,W_0'^3(x_1)\right)\mathrm{d}x_1$$
$$+12\eta^2\int_0^1 W_l(x_1)\frac{\mathrm{d}}{\mathrm{d}x_1}\left(W_i''(x_1)\,W_j''(x_1)\,W_0'(x_1)\right)\mathrm{d}x_1$$
$$-24\eta^2\int_0^1 W_l(x_1)\frac{\mathrm{d}^2}{\mathrm{d}x_1^2}\left(W_i'(x_1)\,W_j''(x_1)\,W_0'(x_1)\right)\mathrm{d}x_1, \tag{51}$$

$$K_{25}^{NL} = +24I_{66}\eta\int_0^1 W_l(x_1)\frac{\mathrm{d}}{\mathrm{d}x_1}\left(W_i''(x_1)\,\psi_j'(x_1)\,W_0'(x_1)\right)\mathrm{d}x_1$$
$$+16I_{55}\frac{1}{\eta}\int_0^1 W_l(x_1)\frac{\mathrm{d}}{\mathrm{d}x_1}\left(W_i'(x_1)\,\psi_j(x_1)\,W_0'(x_1)\right)\mathrm{d}x_1$$
$$-24I_{66}\eta\int_0^1 W_l(x_1)\frac{\mathrm{d}^2}{\mathrm{d}x_1^2}\left(W_i'(x_1)\,\psi_j'(x_1)\,W_0'(x_1)\right)\mathrm{d}x_1, \tag{52}$$

$$K_{26}^{NL} = +12I_{99}\int_0^1 W_l(x_1)\frac{\mathrm{d}}{\mathrm{d}x_1}\left(\psi_i'(x_1)\,\psi_j'(x_1)\,W_0'(x_1)\right)\mathrm{d}x_1$$
$$+4I_{55}\frac{1}{\eta^2}\int_0^1 W_l(x_1)\frac{\mathrm{d}}{\mathrm{d}x_1}\left(\psi_i(x_1)\,\psi_j(x_1)\,W_0'(x_1)\right)\mathrm{d}x_1, \tag{53}$$

$$K_{27}^{NL} = +12I_{00}\int_0^1 W_l(x_1)\frac{\mathrm{d}}{\mathrm{d}x_1}\left(U_i'(x_1)\,U_j'(x_1)\,W_k'(x_1)\right)\mathrm{d}x_1, \tag{54}$$

$$K_{28}^{NL} = +36I_{00}\eta\int_0^1 W_l(x_1)\frac{\mathrm{d}}{\mathrm{d}x_1}\left(U_i'(x_1)\,W_j'(x_1)\,W_k'(x_1)\,W_0'(x_1)\right)\mathrm{d}x_1, \tag{55}$$

$$K_{29}^{NL} = -4I_{88}\int_0^1 W_l(x_1)\frac{\mathrm{d}}{\mathrm{d}x_1}\left(W_i'(x_1)\,W_j'(x_1)\,W_k'(x_1)\right)\mathrm{d}x_1$$
$$+24I_{00}\int_0^1 W_l(x_1)\frac{\mathrm{d}}{\mathrm{d}x_1}\left(W_i'(x_1)\,W_j'(x_1)\,W_k'(x_1)\,W_0'^2(x_1)\right)\mathrm{d}x_1$$
$$+12\eta^2\int_0^1 W_l(x_1)\frac{\mathrm{d}}{\mathrm{d}x_1}\left(W_i'(x_1)\,W_j''(x_1)\,W_k''(x_1)\right)\mathrm{d}x_1$$
$$-12\eta^2\int_0^1 W_l(x_1)\frac{\mathrm{d}^2}{\mathrm{d}x_1^2}\left(W_i'(x_1)\,W_j'(x_1)\,W_k''(x_1)\right)\mathrm{d}x_1, \tag{56}$$

$$K_{210}^{NL} = +24I_{66}\eta \int_0^1 W_l(x_1) \frac{\mathrm{d}}{\mathrm{d}x_1} \left(W_i'(x_1)\, W_j''(x_1)\, \psi_k'(x_1) \right) \mathrm{d}x_1$$

$$+12I_{55} \frac{1}{\eta} \int_0^1 W_l(x_1) \frac{\mathrm{d}}{\mathrm{d}x_1} \left(W_i'(x_1)\, W_j'(x_1)\, \psi_j(x_1) \right) \mathrm{d}x_1$$

$$-12I_{66}\eta \int_0^1 W_l(x_1) \frac{\mathrm{d}^2}{\mathrm{d}x_1^2} \left(W_i'(x_1)\, W_j'(x_1)\, \psi_k'(x_1) \right) \mathrm{d}x_1, \tag{57}$$

$$K_{211}^{NL} = +12I_{99} \int_0^1 W_l(x_1) \frac{\mathrm{d}}{\mathrm{d}x_1} \left(W_i'(x_1)\, \psi_j'(x_1)\, \psi_k'(x_1) \right) \mathrm{d}x_1$$

$$+4I_{55} \frac{1}{\eta^2} \int_0^1 W_l(x_1) \frac{\mathrm{d}}{\mathrm{d}x_1} \left(W_i'(x_1)\, \psi_j(x_1)\, \psi_k(x_1) \right) \mathrm{d}x_1, \tag{58}$$

$$K_{212}^{NL} = +12I_{00}\eta \int_0^1 W_l(x_1) \frac{\mathrm{d}}{\mathrm{d}x_1} \left(U_i'(x_1)\, W_j'(x_1)\, W_k'(x_1)\, W_m'(x_1) \right) \mathrm{d}x_1, \tag{59}$$

$$K_{213}^{NL} = +15I_{00}\eta^2 \int_0^1 W_l(x_1) \frac{\mathrm{d}}{\mathrm{d}x_1} \left(W_i'(x_1)\, W_j'(x_1)\, W_k'(x_1)\, W_m'(x_1)\, W_0'(x_1) \right) \mathrm{d}x_1, \tag{60}$$

$$K_{214}^{NL} = +3I_{00}\eta^2 \int_0^1 W_l(x_1) \frac{\mathrm{d}}{\mathrm{d}x_1} \left(W_i'(x_1)\, W_j'(x_1)\, W_k'(x_1)\, W_m'(x_1)\, W_n'(x_1) \right) \mathrm{d}x_1, \tag{61}$$

$$K_{31}^{NL} = -8I_{55} \int_0^1 \psi_l(x_1) U_i'(x_1)\, W_j'(x_1)\, \mathrm{d}x_1 + 24I_{66}\eta^2 \int_0^1 \psi_l(x_1) \frac{\mathrm{d}}{\mathrm{d}x_1} \left(U_j'(x_1)\, W_j''(x_1) \right) \mathrm{d}x_1, \tag{62}$$

$$K_{32}^{NL} = +24I_{99}\eta \int_0^1 \psi_l(x_1) \frac{\mathrm{d}}{\mathrm{d}x_1} \left(U_i'(x_1)\, \psi_j'(x_1) \right) \mathrm{d}x_1 - 8I_{55} \frac{1}{\eta} \int_0^1 \psi_l(x_1) U_i'(x_1)\, \psi_j(x_1)\, \mathrm{d}x_1, \tag{63}$$

$$K_{33}^{NL} = +24I_{66}\eta^3 \int_0^1 \psi_l(x_1) \frac{\mathrm{d}}{\mathrm{d}x_1} \left(W_i'(x_1)\, W_j''(x_1)\, W_0'(x_1) \right) \mathrm{d}x_1$$

$$-8I_{55}\eta \int_0^1 \psi_l(x_1) W_i'(x_1)\, W_j'(x_1)\, W_0'(x_1)\, \mathrm{d}x_1, \tag{64}$$

$$K_{34}^{NL} = +24I_{99}\eta^2 \int_0^1 \psi_l(x_1) \frac{\mathrm{d}}{\mathrm{d}x_1} \left(W_i'(x_1)\, \psi_i'(x_1)\, W_0'(x_1) \right) \mathrm{d}x_1$$

$$-8I_{55} \int_0^1 \psi_l(x_1) W_i'(x_1)\, \psi_i(x_1)\, W_0'(x_1)\, \mathrm{d}x_1, \tag{65}$$

$$K_{35}^{NL} = +12I_{66}\eta^3 \int_0^1 \psi_l(x_1)\frac{\mathrm{d}}{\mathrm{d}x_1}\left(W_i'(x_1)\,W_j'(x_1)\,W_k''(x_1)\right)\mathrm{d}x_1$$
$$-4I_{55}\eta \int_0^1 \psi_l(x_1)W_i'(x_1)\,W_j'(x_1)\,W_k'(x_1)\,\mathrm{d}x_1, \tag{66}$$

$$K_{36}^{NL} = +12I_{99}\eta^2 \int_0^1 \psi_l(x_1)\frac{\mathrm{d}}{\mathrm{d}x_1}\left(W_i'(x_1)\,W_j'(x_1)\,\psi_k'(x_1)\right)\mathrm{d}x_1$$
$$-4I_{55} \int_0^1 \psi_l(x_1)W_i'(x_1)\,W_j'(x_1)\,\psi_k(x_1)\,\mathrm{d}x_1. \tag{67}$$

which by solving the nonlinear polynomial equations of motion using the Newton–Raphson method, the static bending due to the external static force can be obtained.

5 Solution procedure for visco-hyper-elastic vibrations

Using the given nondimensional terms in Sect. 4 and additional nondimensional terms as

$$\Omega = \omega\sqrt{\frac{\rho I_{00}L^4}{C_T I_{44}}}, \quad t* = t\sqrt{\frac{C_T I_{44}}{\rho A L^4}}, \quad \xi_k = \frac{\xi_k}{C_T} * \sqrt{\frac{C_T I_{44}}{\rho A L^4}}, \tag{68}$$

the nondimensional equations of motion are written as

$$\begin{aligned}
&u_{1tt} - \xi_k I_{00}\frac{1}{\eta^2}u_{1x_1x_1t} - \xi_k I_{00}\frac{1}{\eta}\frac{\partial}{\partial x_1}\left(u_{30x_1}u_{3x_1t}\right) + 2\xi_k I_{00}\frac{1}{\eta}\frac{\partial}{\partial x_1}\left(u_{1x_1}u_{1x_1t}\right) + 2\xi_k I_{00}\frac{\partial}{\partial x_1}\left(u_{3x_1}u_{30x_1}u_{1x_1t}\right)\\
&+2\xi_k I_{00}\frac{\partial}{\partial x_1}\left(u_{1x_1}u_{30x_1}u_{3x_1t}\right) - \xi_k I_{77}\frac{1}{\eta}\frac{\partial}{\partial x_1}\left(u_{3x_1}u_{3x_1t}\right)\\
&+2\xi_k I_{00}\eta\frac{\partial}{\partial x_1}\left(u_{3x_1}u_{30x_1}^2u_{3x_1t}\right) + 2\xi_k\eta\frac{\partial}{\partial x_1}\left(u_{3x_1x_1}u_{3x_1x_1t}\right)\\
&+2\xi_k I_{66}\frac{\partial}{\partial x_1}\left(\phi_{x_1}u_{3x_1x_1t}\right) + \xi_k I_{55}\frac{1}{\eta^2}\frac{\partial}{\partial x_1}\left(\phi u_{3x_1t}\right) + 2\xi_k I_{66}\frac{\partial}{\partial x_1}\left(u_{3x_1x_1}\phi_{x_1t}\right) + \xi_k I_{55}\frac{1}{\eta^2}\frac{\partial}{\partial x_1}\left(u_{3x_1}\phi_t\right)\\
&+2\xi_k I_{99}\frac{1}{\eta}\frac{\partial}{\partial x_1}\left(\phi_{x_1}\phi_{x_1t}\right) + \xi_k I_{55}\frac{1}{\eta^3}\frac{\partial}{\partial x_1}\left(\phi\phi_t\right) + \xi_k I_{00}\frac{\partial}{\partial x_1}\left(u_{3x_1}^2u_{1x_1t}\right) + 2\xi_k I_{00}\frac{\partial}{\partial x_1}\left(u_{1x_1}u_{3x_1}u_{3x_1t}\right)\\
&+3\xi_k I_{00}\eta\frac{\partial}{\partial x_1}\left(u_{3x_1}^2u_{30x_1}u_{3x_1t}\right) + \xi_k I_{00}\eta\frac{\partial}{\partial x_1}\left(u_{3x_1}^3u_{3x_1t}\right) - 8I_{00}\frac{1}{\eta^2}u_{1x_1x_1} - 8I_{00}\frac{1}{\eta}\frac{\partial}{\partial x_1}\left(u_{3x_1}u_{30x_1}\right)\\
&+12I_{00}\frac{1}{\eta}\frac{\partial}{\partial x_1}\left(u_{1x_1}^2\right) + 24I_{00}\frac{\partial}{\partial x_1}\left(u_{1x_1}u_{3x_1}u_{30x_1}\right) - 4I_{77}\frac{1}{\eta}\frac{\partial}{\partial x_1}\left(u_{3x_1}^2\right) + 12I_{00}\eta\frac{\partial}{\partial x_1}\left(u_{3x_1}^2u_{30x_1}^2\right)\\
&+12\eta\frac{\partial}{\partial x_1}\left(u_{3x_1x_1}^2\right) + 24I_{66}\frac{\partial}{\partial x_1}\left(u_{3x_1x_1}\phi_{x_1}\right) + 8I_{55}\frac{1}{\eta^2}\frac{\partial}{\partial x_1}\left(u_{3x_1}\phi\right)\\
&+12I_{99}\frac{1}{\eta}\frac{\partial}{\partial x_1}\left(\phi_{x_1}^2\right) + 4I_{55}\frac{1}{\eta^3}\frac{\partial}{\partial x_1}\left(\phi^2\right)\\
&+12I_{00}\frac{\partial}{\partial x_1}\left(u_{1x_1}u_{3x_1}^2\right) + 12I_{00}\eta\frac{\partial}{\partial x_1}\left(u_{30x_1}u_{3x_1}^3\right) + 3I_{00}\eta\frac{\partial}{\partial x_1}\left(u_{3x_1}^4\right) = 0,
\end{aligned} \tag{69}$$

$$\begin{aligned}
&\frac{I_{66}}{I_{00}}\eta^3u_{3x_1tt} + \frac{I_{99}}{I_{00}}\eta^2\phi_{tt} - \xi_k\eta I_{66}u_{3x_1x_1x_1t} + \frac{1}{2}\xi_k I_{55}\frac{1}{\eta}u_{3x_1t} - \xi_k I_{99}\phi_{x_1x_1t}\\
&+\frac{1}{2}\xi_k I_{55}\frac{1}{\eta^2}\phi_t + 2\xi_k I_{66}\eta^2\frac{\partial}{\partial x_1}\left(u_{3x_1x_1}u_{1x_1t}\right)
\end{aligned}$$

$$
\begin{aligned}
&-\xi_k I_{55} u_{3x_1} u_{1x_1t} + 2\xi_k I_{99}\eta \frac{\partial}{\partial x_1}\left(\phi_{x_1} u_{1x_1t}\right) - \xi_k I_{55}\frac{1}{\eta}\phi u_{1x_1t} + 2\xi_k I_{66}\eta^2 \frac{\partial}{\partial x_1}\left(u_{1x_1} u_{3x_1x_1t}\right)\\
&+2\xi_k I_{66}\eta^3 \frac{\partial}{\partial x_1}\left(u_{3x_1x_1} u_{30x_1} u_{3x_1t}\right) - \xi_k I_{55}\eta u_{3x_1} u_{30x_1} u_{3x_1t}\\
&+\xi_k 2I_{99}\eta^2 \frac{\partial}{\partial x_1}\left(\phi_{x_1} u_{30x_1} u_{3x_1t}\right) - \xi_k I_{55}\phi u_{30x_1} u_{3x_1t}\\
&+2\xi_k I_{99}\eta \frac{\partial}{\partial x_1}\left(u_{1x_1}\phi_{x_1t}\right) + 2\xi_k I_{99}\eta^2 \frac{\partial}{\partial x_1}\left(u_{3x_1} u_{30x_1}\phi_{x_1t}\right) + 2\xi_k I_{66}\eta^3 \frac{\partial}{\partial x_1}\left(u_{3x_1} u_{3x_1x_1} u_{3x_1t}\right)\\
&+\xi_k I_{66}\eta^3 \frac{\partial}{\partial x_1}\left(u_{3x_1}^2 u_{3x_1x_1t}\right) + 2\xi_k I_{66}\eta^3 \frac{\partial}{\partial x_1}\left(u_{3x_1} u_{30x_1} u_{3x_1x_1t}\right)\\
&-\xi_k I_{55}\eta u_{3x_1}^2 u_{3x_1t} + 2\xi_k I_{99}\eta^2 \frac{\partial}{\partial x_1}\left(u_{3x_1}\phi_{x_1} u_{3x_1t}\right)\\
&-\xi_k I_{55} u_{3x_1}\phi u_{3x_1t} + \xi_k I_{99}\eta^2 \frac{\partial}{\partial x_1}\left(u_{3x_1}^2\phi_{x_1t}\right) - 8I_{66}\eta u_{3x_1x_1x_1} + 8I_{55}\frac{1}{\eta}u_{3x_1} - 8I_{99}\phi_{x_1x_1} + 8I_{55}\frac{1}{\eta^2}\phi\\
&+24I_{66}\eta^2 \frac{\partial}{\partial x_1}\left(u_{1x_1} u_{3x_1x_1}\right) - 8I_{55} u_{1x_1} u_{3x_1} + 24I_{99}\eta \frac{\partial}{\partial x_1}\left(u_{1x_1}\phi_{x_1}\right)\\
&-8I_{55}\frac{1}{\eta}u_{1x_1}\phi + 24I_{66}\eta^3 \frac{\partial}{\partial x_1}\left(u_{3x_1} u_{3x_1x_1} u_{30x_1}\right)\\
&-8I_{55}\eta u_{3x_1}^2 u_{30x_1} + 24I_{99}\eta^2 \frac{\partial}{\partial x_1}\left(u_{3x_1}\phi_{x_1} u_{30x_1}\right) - 8I_{55} u_{3x_1}\phi u_{30x_1}\\
&+12I_{66}\eta^3 \frac{\partial}{\partial x_1}\left(u_{3x_1}^2 u_{3x_1x_1}\right) - 4I_{55}\eta u_{3x_1}^3\\
&+12I_{99}\eta^2 \frac{\partial}{\partial x_1}\left(u_{3x_1}^2\phi_{x_1}\right) - 4I_{55} u_{3x_1}^2\phi = 0.
\end{aligned}
\tag{70}
$$

$$
\begin{aligned}
&-\frac{1}{I_{00}}\eta^2 u_{3x_1x_1tt} - \frac{I_{66}}{I_{00}}\eta\phi_{x_1tt} + u_{3tt} - \xi_k I_{00}\frac{1}{\eta}\frac{\partial}{\partial x_1}\left(u_{30x_1} u_{1x_1t}\right)\\
&+\xi_k\, u_{3x_1x_1x_1x_1t} - \xi_k I_{00}\frac{\partial}{\partial x_1}\left(u_{30x_1}^2 u_{3x_1t}\right) - \frac{1}{2}\xi_k I_{55}\frac{1}{\eta^2}u_{3x_1x_1t}\\
&+\xi_k\, I_{66}\frac{1}{\eta}\phi_{x_1x_1x_1t} - \frac{1}{2}\xi_k I_{55}\frac{1}{\eta^3}\phi_{x_1t} + 2\xi_k I_{00}\frac{\partial}{\partial x_1}\left(u_{1x_1} u_{30x_1} u_{1x_1t}\right)\\
&+2\xi_k I_{00}\eta \frac{\partial}{\partial x_1}\left(u_{3x_1} u_{30x_1}^2 u_{1x_1t}\right) - \xi_k I_{00}\frac{1}{\eta}\frac{\partial}{\partial x_1}\left(u_{3x_1} u_{1x_1t}\right)\\
&-2\,\xi_k\eta \frac{\partial^2}{\partial x_1^2}\left(u_{3x_1x_1} u_{1x_1t}\right) + \xi_k I_{55}\frac{1}{\eta}\frac{\partial}{\partial x_1}\left(u_{3x_1} u_{1x_1t}\right) - 2\xi_k I_{66}\frac{\partial^2}{\partial x_1^2}\left(\phi_{x_1} u_{1x_1t}\right) + \xi_k I_{55}\frac{1}{\eta^2}\frac{\partial}{\partial x_1}\left(\phi u_{1x_1t}\right)\\
&+2\xi_k I_{00}\eta \frac{\partial}{\partial x_1}\left(u_{1x_1} u_{30x_1}^2 u_{3x_1t}\right) - 2\,\xi_k\eta \frac{\partial^2}{\partial x_1^2}\left(u_{1x_1} u_{3x_1x_1t}\right)\\
&-\xi_k\, I_{77}\frac{\partial}{\partial x_1}\left(u_{3x_1} u_{30x_1} u_{3x_1t}\right) + 2\xi_k I_{00}\eta^2 \frac{\partial}{\partial x_1}\left(u_{3x_1} u_{30x_1}^3 u_{3x_1t}\right)\\
&+2\xi_k\eta^2 \frac{\partial}{\partial x_1}\left(u_{3x_1x_1} u_{30x_1} u_{3x_1x_1t}\right) - \xi_k I_{00}\frac{\partial}{\partial x_1}\left(u_{30x_1} u_{3x_1} u_{3x_1t}\right)\\
&+\xi_k I_{55}\frac{\partial}{\partial x_1}\left(u_{3x_1} u_{30x_1} u_{3x_1t}\right) - 2\xi_k\eta^2 \frac{\partial^2}{\partial x_1^2}\left(u_{3x_1x_1} u_{30x_1} u_{3x_1t}\right)\\
&+2\xi_k I_{66}\eta \frac{\partial}{\partial x_1}\left(\phi_{x_1} u_{30x_1} u_{3x_1x_1t}\right) + 2\xi_k I_{55}\frac{1}{\eta}\frac{\partial}{\partial x_1}\left(\phi u_{30x_1} u_{3x_1t}\right)\\
&-2\xi_k I_{66}\eta \frac{\partial^2}{\partial x_1^2}\left(\phi_{x_1} u_{30x_1} u_{3x_1t}\right) - 2\xi_k I_{66}\frac{\partial^2}{\partial x_1^2}\left(u_{1x_1}\phi_{x_1t}\right)
\end{aligned}
$$

$$
\begin{aligned}
&+2\xi_k I_{66}\eta\frac{\partial}{\partial x_1}\left(u_{3x_1x_1}u_{30x_1}\phi_{x_1t}\right)+\xi_k I_{55}\frac{1}{\eta}\frac{\partial}{\partial x_1}\left(u_{3x_1}u_{30x_1}\phi_t\right)\\
&-2\xi_k I_{66}\eta\frac{\partial^2}{\partial x_1^2}\left(u_{3x_1}u_{30x_1}\phi_{x_1t}\right)+2\xi_k I_{99}\frac{\partial}{\partial x_1}\left(\phi_{x_1}u_{30x_1}\phi_{x_1t}\right)\\
&+\xi_k I_{55}\frac{1}{\eta^2}\frac{\partial}{\partial x_1}\left(\phi u_{30x_1}\phi_t\right)+2\xi_k I_{00}\frac{\partial}{\partial x_1}\left(u_{1x_1}u_{3x_1}u_{1x_1t}\right)\\
&+3\xi_k I_{00}\eta\frac{\partial}{\partial x_1}\left(u_{3x_1}^2u_{30x_1}u_{1x_1t}\right)+4\xi_k I_{00}\eta\frac{\partial}{\partial x_1}\left(u_{1x_1}u_{3x_1}u_{30x_1}u_{3x_1t}\right)\\
&+5\xi_k I_{00}\eta^2\frac{\partial}{\partial x_1}\left(u_{3x_1}^2u_{30x_1}^2u_{3x_1t}\right)-\xi_k I_{77}\frac{\partial}{\partial x_1}\left(u_{3x_1}^2u_{3x_1t}\right)\\
&+2\xi_k\,\eta^2\frac{\partial}{\partial x_1}\left(u_{3x_1}u_{3x_1x_1}u_{3x_1x_1t}\right)-2\xi_k\eta^2\frac{\partial^2}{\partial x_1^2}\left(u_{3x_1}u_{3x_1x_1}u_{3x_1t}\right)\\
&-\xi_k\eta^2\frac{\partial^2}{\partial x_1^2}\left(u_{3x_1}^2u_{3x_1x_1t}\right)-2\xi_k\eta^2\frac{\partial^2}{\partial x_1^2}\left(u_{3x_1}u_{30x_1}u_{3x_1x_1t}\right)\\
&+\xi_k I_{55}\frac{\partial}{\partial x_1}\left(u_{3x_1}^2u_{3x_1t}\right)+2\xi_k I_{66}\eta\frac{\partial}{\partial x_1}\left(u_{3x_1}\phi_{x_1}u_{3x_1x_1t}\right)\\
&+2\xi_k I_{55}\frac{1}{\eta}\frac{\partial}{\partial x_1}\left(u_{3x_1}\phi u_{3x_1t}\right)-2\xi_k I_{66}\eta\frac{\partial^2}{\partial x_1^2}\left(u_{3x_1}\phi_{x_1}u_{3x_1t}\right)\\
&+2\,\xi_k I_{66}\eta\frac{\partial}{\partial x_1}\left(u_{3x_1}u_{3x_1x_1}\phi_{x_1t}\right)+\xi_k I_{55}\frac{1}{\eta}\frac{\partial}{\partial x_1}\left(u_{3x_1}^2\phi_t\right)\\
&-\xi_k I_{66}\eta\frac{\partial^2}{\partial x_1^2}\left(u_{3x_1}^2\phi_{x_1t}\right)+2\xi_k I_{99}\frac{\partial}{\partial x_1}\left(u_{3x_1}\phi_{x_1}\phi_{x_1t}\right)+\xi_k I_{55}\frac{1}{\eta^2}\frac{\partial}{\partial x_1}\left(u_{3x_1}\phi\phi_t\right)+\xi_k I_{00}\eta\frac{\partial}{\partial x_1}\left(u_{3x_1}^3u_{1x_1t}\right)\\
&+2\xi_k I_{00}\eta\frac{\partial}{\partial x_1}\left(u_{1x_1}u_{3x_1}^2u_{3x_1t}\right)+4\xi_k I_{00}\eta^2\frac{\partial}{\partial x_1}\left(u_{3x_1}^3u_{30x_1}u_{3x_1t}\right)\\
&+\xi_k I_{00}\eta^2\frac{\partial}{\partial x_1}\left(u_{3x_1}^4u_{3x_1t}\right)-8I_{00}\frac{1}{\eta}\frac{\partial}{\partial x_1}\left(u_{1x_1}u_{30x_1}\right)\\
&-8I_{00}\frac{\partial}{\partial x_1}\left(u_{3x_1}u_{30x_1}^2\right)+8u_{3x_1x_1x_1x_1}-8I_{55}\,\frac{1}{\eta^2}u_{3x_1x_1}+8I_{66}\frac{1}{\eta}\phi_{x_1x_1x_1}\\
&-8I_{55}\frac{1}{\eta^3}\phi_{x_1}+12I_{00}\frac{\partial}{\partial x_1}\left(u_{1x_1}^2u_{30x_1}\right)\\
&-8I_{77}\frac{1}{\eta}\frac{\partial}{\partial x_1}\left(u_{1x_1}u_{3x_1}\right)+24I_{00}\eta\frac{\partial}{\partial x_1}\left(u_{1x_1}u_{3x_1}u_{30x_1}^2\right)\,-24\eta\frac{\partial^2}{\partial x_1^2}\left(u_{1x_1}u_{3x_1x_1}\right)-24I_{66}\frac{\partial^2}{\partial x_1^2}\left(u_{1x_1}\phi_{x_1}\right)\\
&+8I_{55}\frac{1}{\eta^2}\frac{\partial}{\partial x_1}\left(u_{1x_1}\phi\right)-12I_{77}\frac{\partial}{\partial x_1}\left(u_{3x_1}^2u_{30x_1}\right)+12I_{00}\eta^2\frac{\partial}{\partial x_1}\left(u_{3x_1}^2u_{30x_1}^3\right)+12\eta^2\frac{\partial}{\partial x_1}\left(u_{3x_1x_1}^2u_{30x_1}\right)\\
&-24\eta^2\frac{\partial^2}{\partial x_1^2}\left(u_{3x_1}u_{3x_1x_1}u_{30x_1}\right)+24I_{66}\eta\frac{\partial}{\partial x_1}\left(u_{3x_1x_1}\phi_{x_1}u_{30x_1}\right)+16I_{55}\,\frac{1}{\eta}\frac{\partial}{\partial x_1}\left(u_{3x_1}\phi u_{30x_1}\right)\\
&-24I_{66}\eta\frac{\partial^2}{\partial x_1^2}\left(u_{3x_1}\phi_{x_1}u_{30x_1}\right)+12I_{99}\frac{\partial}{\partial x_1}\left(\phi_{x_1}^2u_{30x_1}\right)+4I_{55}\,\frac{1}{\eta^2}\frac{\partial}{\partial x_1}\left(\phi^2u_{30x_1}\right)+12I_{00}\frac{\partial}{\partial x_1}\left(u_{1x_1}^2u_{3x_1}\right)\\
&\ldots\\
&\ldots\\
&+36I_{00}\eta\frac{\partial}{\partial x_1}\left(u_{1x_1}u_{3x_1}^2u_{30x_1}\right)-4I_{88}\frac{\partial}{\partial x_1}\left(u_{3x_1}^3\right)+24I_{00}\frac{\partial}{\partial x_1}\left(u_{3x_1}^3u_{30x_1}^2\right)+12\eta^2\frac{\partial}{\partial x_1}\left(u_{3x_1}u_{3x_1x_1}^2\right)\\
&-12\eta^2\frac{\partial^2}{\partial x_1^2}\left(u_{3x_1}^2u_{3x_1x_1}\right)+24I_{66}\eta\frac{\partial}{\partial x_1}\left(u_{3x_1}u_{3x_1x_1}\phi_{x_1}\right)+12I_{55}\,\frac{1}{\eta}\frac{\partial}{\partial x_1}\left(u_{3x_1}^2\phi\right)-12I_{66}\eta\frac{\partial^2}{\partial x_1^2}\left(u_{3x_1}^2\phi_{x_1}\right)
\end{aligned}
$$

$$+12I_{99}\frac{\partial}{\partial x_1}\left(u_{3x_1}\phi_{x_1}^2\right)+4I_{55}\frac{1}{\eta^2}\frac{\partial}{\partial x_1}\left(u_{3x_1}\phi^2\right)+12I_{00}\eta\frac{\partial}{\partial x_1}\left(u_{1x_1}u_{3x_1}^3\right)+15I_{00}\eta^2\frac{\partial}{\partial x_1}\left(u_{30x_1}u_{3x_1}^4\right)$$
$$+3I_{00}\eta^2\frac{\partial}{\partial x_1}\left(u_{3x_1}^5\right)=F\cos\left(\Omega t\right), \tag{71}$$

For time-dependant analysis, by employing the Galerkin's procedure, the degrees of freedom are written as

$$u_1\left(x_1,t\right)=\sum_{j=1}^{M}U_j\left(x_1\right)\Re_j\left(t\right), \tag{72}$$

$$u_3\left(x_1,t\right)=\sum_{i=1}^{N}W_i\left(x_1\right)\aleph_i\left(t\right), \tag{73}$$

$$\phi\left(x_1,t\right)=\sum_{i=1}^{N}\psi_i\left(x_1\right)\kappa_i\left(t\right), \tag{74}$$

and the equations of motion are discretised as

$$M_{11}\ddot{\Re}+C_{11}^{L}\dot{\Re}+C_{12}^{L}\dot{\aleph}+C_{11}^{NL}\Re\dot{\Re}+C_{12}^{NL}\aleph\dot{\Re}+C_{13}^{NL}\Re\dot{\aleph}+C_{14}^{NL}\aleph\dot{\aleph}+C_{15}^{NL}\kappa\dot{\aleph}+C_{16}^{NL}\aleph\dot{\kappa}+C_{17}^{NL}\kappa\dot{\kappa}$$
$$+C_{18}^{NL}\aleph^2\dot{\Re}+C_{19}^{NL}\Re\aleph\dot{\aleph}+C_{110}^{NL}\aleph^2\dot{\aleph}+C_{111}^{NL}\aleph^3\dot{\aleph}+K_{11}^{L}\Re+K_{12}^{L}\aleph+K_{11}^{NL}\Re^2+K_{12}^{NL}\Re\aleph+K_{13}^{NL}\aleph^2$$
$$+K_{14}^{NL}\aleph\kappa+K_{15}^{NL}\kappa^2+K_{16}^{NL}\Re\aleph^2+K_{17}^{NL}\aleph^3+K_{18}^{NL}\aleph^4=0, \tag{75}$$

$$M_{22}\ddot{\aleph}+M_{23}\ddot{\kappa}+C_{21}^{L}\dot{\Re}+C_{22}^{L}\dot{\aleph}+C_{23}^{L}\dot{\kappa}+C_{21}^{NL}\Re\dot{\Re}+C_{22}^{NL}\aleph\dot{\Re}+C_{23}^{NL}\kappa\dot{\Re}+C_{24}^{NL}\Re\dot{\aleph}+C_{25}^{NL}\aleph\dot{\aleph}$$
$$+C_{26}^{NL}\kappa\dot{\aleph}+C_{27}^{NL}\Re\dot{\kappa}+C_{28}^{NL}\aleph\dot{\kappa}+C_{29}^{NL}\kappa\dot{\kappa}+C_{210}^{NL}\Re\aleph\dot{\Re}+C_{211}^{NL}\aleph^2\dot{\Re}+C_{212}^{NL}\Re\aleph\dot{\aleph}+C_{213}^{NL}\aleph^2\dot{\aleph}$$
$$+C_{214}^{NL}\aleph\kappa\dot{\aleph}+C_{215}^{NL}\aleph^2\dot{\kappa}+C_{216}^{NL}\aleph\kappa\dot{\kappa}+C_{217}^{NL}\aleph^3\dot{\Re}+C_{218}^{NL}\Re\aleph^2\dot{\aleph}+C_{219}^{NL}\aleph^3\dot{\aleph}+C_{220}^{NL}\aleph^4\dot{\aleph}+K_{21}^{L}\Re$$
$$+K_{22}^{L}\aleph+K_{22}^{L}\kappa+K_{21}^{NL}\Re^2+K_{22}^{NL}\Re\aleph+K_{23}^{NL}\Re\kappa+K_{24}^{NL}\aleph^2$$
$$+K_{25}^{NL}\aleph\kappa+K_{26}^{NL}\kappa^2+K_{27}^{NL}\Re^2\aleph+K_{28}^{NL}\Re\aleph^2$$
$$+K_{29}^{NL}\aleph^3+K_{210}^{NL}\aleph^2\kappa+K_{211}^{NL}\aleph\kappa^2+K_{212}^{NL}r\aleph^3+K_{213}^{NL}\aleph^4+K_{214}^{NL}\aleph^5=F\cos\left(\Omega t\right), \tag{76}$$

$$M_{32}\ddot{\aleph}+M_{33}\ddot{\kappa}+C_{31}^{L}\dot{\aleph}+C_{32}^{L}\dot{\kappa}+C_{31}^{NL}\aleph\dot{\Re}+C_{32}^{NL}\kappa\dot{\Re}+C_{33}^{NL}\Re\dot{\aleph}+C_{34}^{NL}\aleph\dot{\aleph}+C_{35}^{NL}\kappa\dot{\aleph}+C_{36}^{NL}\Re\dot{\kappa}$$
$$+C_{37}^{NL}\aleph\dot{\kappa}+C_{38}^{NL}\aleph^2\dot{\aleph}+C_{39}^{NL}\aleph\kappa\dot{\aleph}+C_{310}^{NL}\aleph^2\dot{\kappa}+K_{32}^{L}\aleph+K_{33}^{L}\kappa+K_{31}^{NL}\Re\aleph+K_{32}^{NL}\Re\kappa+K_{33}^{NL}\aleph^2$$
$$+K_{34}^{NL}\aleph\kappa+K_{35}^{NL}\aleph^3+K_{36}^{NL}\aleph^2\kappa=0, \tag{77}$$

with the mass coefficients (M_{ij}) as

$$M_{11}=\int_0^1 U_p\left(x_1\right)U_i\left(x_1\right)\mathrm{d}x_1, \tag{78}$$

$$M_{22}=+\int_0^1 W_l\left(x_1\right)W_i\left(x_1\right)\mathrm{d}x_1-\frac{1}{I_{00}}\eta^2\int_0^1 W_l\left(x_1\right)W_i''\left(x_1\right)\mathrm{d}x_1, \tag{79}$$

$$M_{23}=-\frac{I_{66}}{I_{00}}\eta\int_0^1 W_l\left(x_1\right)\psi_i'\left(x_1\right)\mathrm{d}x_1, \tag{80}$$

$$M_{32}=+\frac{I_{66}}{I_{00}}\eta^3\int_0^1 \psi_l\left(x_1\right)W_i'\left(x_1\right)\mathrm{d}x_1, \tag{81}$$

$$M_{33}=+\frac{I_{99}}{I_{00}}\eta^2\int_0^1 \psi_l\left(x_1\right)\psi_i\left(x_1\right)\mathrm{d}x_1, \tag{82}$$

and the linear visco-elastic coefficients (C_{ij}^{L}) as

$$C_{11}^{L} : -\xi_k I_{00} \frac{1}{\eta^2} \int_0^1 U_l(x_1) U_i''(x_1)\, \mathrm{d}x_1, \tag{83}$$

$$C_{12}^{L} : -\xi_k I_{00} \frac{1}{\eta} \int_0^1 U_l(x_1) \frac{\mathrm{d}}{\mathrm{d}x_1} \left(W_i'(x_1)\, W_0'(x_1) \right) \mathrm{d}x_1, \tag{84}$$

$$C_{21}^{L} : -\xi I_{00} \frac{1}{\eta} \int_0^1 W_l(x_1) \frac{\mathrm{d}}{\mathrm{d}x_1} \left(U_i'(x_1)\, W_0'(x_1) \right) \mathrm{d}x, \tag{85}$$

$$\begin{aligned} C_{22}^{L} : &+\xi \int_0^1 W_l(x_1) W_i^{(4)}(x_1)\, \mathrm{d}x_1 - \xi I_{00} \int_0^1 W_l(x_1) \frac{\mathrm{d}}{\mathrm{d}x_1} \left(W_i'(x_1)\, W_0'^2(x_1) \right) \mathrm{d}x_1 \\ &-\frac{1}{2} \xi I_{55} \frac{1}{\eta^2} \int_0^1 W_l(x_1) W_i''(x_1)\, \mathrm{d}x_1, \end{aligned} \tag{86}$$

$$C_{23}^{L} : +\xi\, I_{66} \frac{1}{\eta} \int_0^1 W_l(x_1) \psi_i'''(x_1)\, \mathrm{d}x_1 - \frac{1}{2} \xi I_{55} \frac{1}{\eta^3} \int_0^1 W_l(x_1) \psi_i'(x_1)\, \mathrm{d}x_1, \tag{87}$$

$$C_{31}^{L} : -\xi_k \eta I_{66} \int_0^1 \psi_l(x_1) W_i'''(x_1)\, \mathrm{d}x_1 + \frac{1}{2} \xi_k I_{55} \frac{1}{\eta} \int_0^1 \psi_l(x_1) W_i'(x_1)\, \mathrm{d}x_1, \tag{88}$$

$$C_{32}^{L} : -\xi_k I_{99} \int_0^1 \psi_l(x_1) \psi_i''(x_1)\, \mathrm{d}x_1 + \frac{1}{2} \xi_k I_{55} \frac{1}{\eta^2} \int_0^1 \psi_l(x_1) \psi_i(x_1)\, \mathrm{d}x_1. \tag{89}$$

The nonlinear damping coefficients (C_{ij}^{NL}) are shown in Appendix C for the sake of brevity, and the stiffness terms are defined in the previous sections. By solving the dynamic equilibrium equations [39,41], the nonlinear vibration response of the system is obtained.

6 Results and discussions for bending and vibration

In this section, the nonlinear bending and vibration responses of thick visco-hyper-elastic shallow arches are modelled for different cases of curvature, slenderness ratio and internal resonances. The hyper-elastic properties are taken from Ref [55] for vulcanised rubbers with the Mooney–Rivlin coefficients as $C_1 = 0.28\text{e}6$ Pa and $C_2 = 0.15\text{e}6$ Pa and mass density $\rho = 950$ kg/m^3.

6.1 Bending analysis

Study 1: Force-bending analysis

As the first part of the analysis, the nonlinear static deformation of thick hyper-elastic shallow arches is analysed following the solution procedure given in Sect. 4 and compared to those obtained using finite element software. The shallow arch is assumed to have the following geometrical properties: $L = 0.3$ m, $h = 0.03$ m, $b = 0.03$ m, with a simply supported boundary condition and assumed to undergo a static pressure (which is varied from -1 to 1 kPa). The maximum transverse deformation is obtained and shown in Table 1 for different curvatures and external loads. By comparing the current results with those obtained from ANSYS [56], it is shown that the results are in very good agreement. Besides, it can be seen that by increasing the curvature term, the maximum deformation of the shallow arch decreases significantly especially for higher external loadings.

Table 1 Comparison of the maximum transverse deformation of the shallow arch for different loads

$R_0 = u_{30}/h$	Maximum transverse deformation (mm)						
	P_0	−1 kPa	−500 Pa	−200 Pa	200 Pa	500 Pa	1 kPa
0.5	Present	6.1184	3.5272	1.6645	2.0481	5.9868	12.2926
	ANSYS	6.4259	3.6742	1.6301	1.9701	6.1897	12.7670
1.0	Present	2.9103	1.5246	0.6643	0.6984	1.7256	3.6963
	ANSYS	3.0089	1.5804	0.6533	0.6861	1.7877	3.8807
1.5	Present	1.7133	0.8725	0.3582	0.3607	0.9051	1.8352
	ANSYS	1.7517	0.8930	0.3616	0.3678	0.9320	1.9089

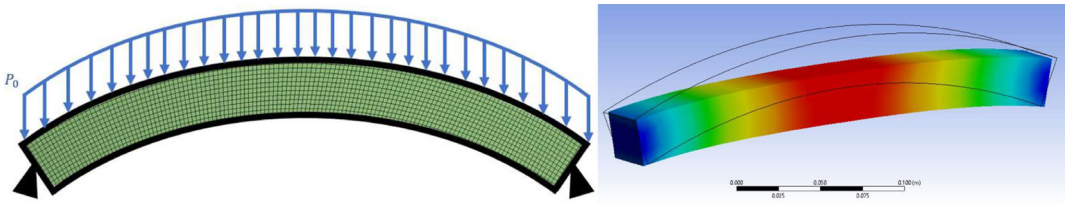

Moreover, to understand the static behaviour of the shallow arch under different types of loadings, the curvature is assumed as following the first mode as $W_0(x_1) = R_0 W_1(x_1)$ where R_0 is the nondimensional curvature term assumed as 0.6. The nondimensional external applied static force (F_{bending}) is modelled using a combination of sin functions as

$$F_{\text{bending}}(x) : f_1 \sin(\pi x) + f_2 \sin(2\pi x), \qquad f_1 = 50\,(n-1)\,, \qquad f_2 = 25\,(n-1)\,, \tag{90}$$

where n is varied from 1 to 70. For the given function, the static force through the length of the arch is shown in Fig. 3a for different values of n. By solving the nonlinear bending equilibrium equations, the nondimensional deformations of the hyper-elastic thick arch are shown in Fig. 3b–d. It can be seen that there is a high coupling between the degrees of freedom; also, the force type and magnitude can change the deformations in the structure, significantly.

Study 2: Influence of the curvature on the bending behaviour

For the same shallow arch with the given properties in the previous subsection, the influence of the curvature in resisting deformation in the structure is analysed. To do this, an external static force following Eq. (93) is given to the structure with f_1 and f_2 as 1000 and -500, respectively. Figure 4a–c shows the axial, transverse and rotation deformation of the shallow arch by varying the curvature term as $R_0 = 0.1$, 0.3, 0.5, 0.7, 0.9, 1.0, and 1.5. It can be seen that increasing the shallow arch curvature leads to higher resistance against the transverse loading. Besides, as shown in Fig. 4a, the coupling between the axial and transverse deformations increases significantly by increasing the curvature term.

Study 3: Influence of considering the higher-order nonlinear terms

Since incompressible hyper-elastic structures show nonlinearity in their constitutive equation as well as large deformations, the importance of considering the higher-order nonlinear terms is discussed in this subsection. Accordingly, for the same shallow arch in previous sections with the curvature of $R_0 = 1.5$, bending behaviour is obtained using both linear and nonlinear models when subjected to an external static force following Eq. (93) with f_1 and f_2 as 10000 and -2500. Figure 5a–c shows the axial, transverse and rotation deformation of the shallow arch by only considering the linear part of the equilibrium equations as well as considering the full equations. It can be seen that the linear simplification of the structure leads to underestimated bending deformations for the axial deformation and inaccurate transverse and rotation motions which indicates the importance of accurately modelling the nonlinear behaviour of the structure.

6.2 Internal resonance and vibration analysis

Study 1: Vibration in the hyper-elasticity framework with internal resonances

Since the curvature of the thick, soft shallow arch can change the linear frequencies of the structure, this section concentrates on detecting the internal resonance behaviour of the arch due to the curvature. For the same shallow arch model given in Sect. 6.1, the ratio of the second natural frequency to the fundamental

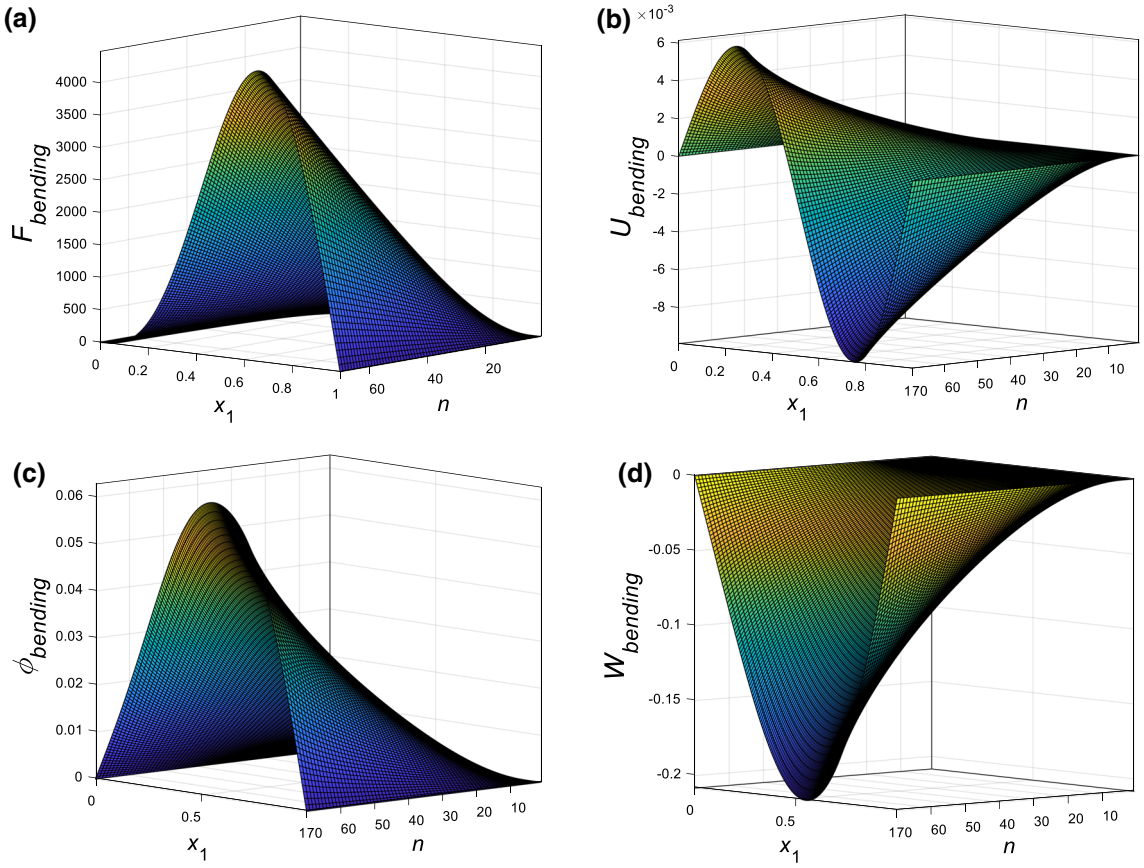

Fig. 3 Nondimensional static force and nondimensional bending deformation response of the hyper-elastic arch **a** applied force, **b** axial deformation, **c** transverse deformation and **d** rotational deformation

natural frequency (ω_2/ω_1) is shown in Fig. 6 by having different curvature terms. It can be seen that around $R_0 = 0.3$, the ratio is equal to 3 and the three-to-one internal resonance in the system occurs. Accordingly, by having $R_0 = 0.3$ (which leads to $\omega_2/\omega_1 \cong 3$), the frequency-amplitude responses of the system are shown in Figs. 7, 8 and 9 for the dominant vibration coordinates in the axial, transverse and rotational directions. It can be seen that a high coupling between modes it obtained, and the system shows a rich nonlinear behaviour, with a combination of hardening, softening and modal interactions.

Study 2: Vibration in the visco-hyper-elasticity framework with internal resonances

Many soft structures show visco-elastic behaviour together with hyper-elasticity (especially biological tissues). To see the influence of this combination on the nonlinear frequency response of the structure with an internal resonance, this section analyses the visco-hyper-elasticity behaviour of thick, soft, shallow arches. Since visco-elasticity is a function of many environmental parameters, such as temperature [57], this property of hyper-elastic structures should be measured for specific working environments. In this study, visco-elasticity is modelled using the Kelvin–Voigt visco-hyper-elastic model which has been shown that has a good accuracy in modelling visco-hyper-elastic materials [48]. The influence of the visco-elasticity on the three-to-one internal resonance of the structure is shown in Figs. 10, 11 and 12 for the axial, transverse and rotational directions by varying the viscoelastic parameter as $\xi_k = [2e{-}3, 2e{-}4, 2e{-}5]$. It can be seen that the visco-hyper-elasticity has a significant effect in changing the nonlinear frequency response, and increasing this term from 2e−5 to 2e−4 decreases the maximum amplitude. By increasing the viscous term to 2e−3, the complicated nonlinear internal resonance behaviour will be fully damped.

Study 3: Curvature sensitivity

One of the main concentrations of this paper is on considering the curvature modelling in soft thick shallow arches. To show the importance and influence of this term on the nonlinear vibration behaviour of the structure, the shallow arch is assumed to have the following geometrical properties given in Sect. 6.1 with a simply supported boundary condition and curvature term varied as $R_0 = [0.0, 0.1, 0.3, 0.5, 0.6, 0.8, 1.0]$.

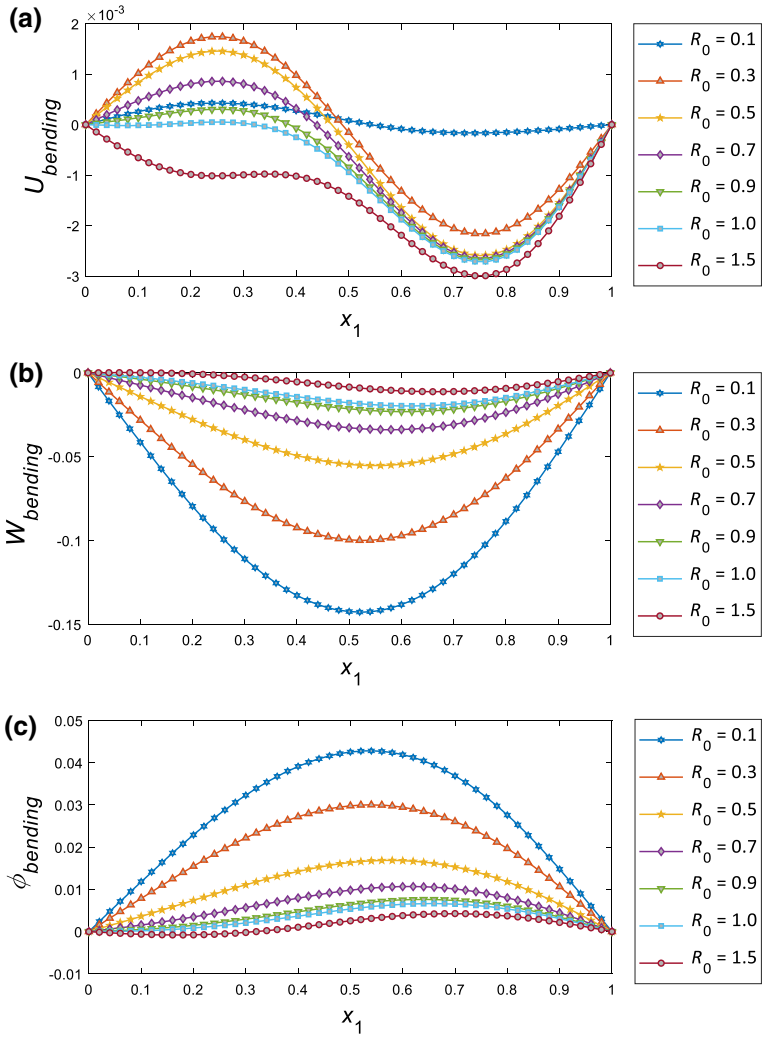

Fig. 4 The nondimensional bending deformation response of the hyper-elastic shallow arch with different curvatures **a** axial deformation, **b** transverse deformation and **c** rotational deformation

The results for the amplitude-frequency response of the soft arch subjected to an external nondimensional load of $F = 0.5$ are shown in Figs. 13, 14 and 15 for the dominant vibration coordinates in the axial, transverse and rotation directions, respectively. It can be seen that increasing the curvature term from 0 to 1.0 moves the amplitude responses to higher frequencies. For higher curvature terms, transverse dynamic equilibriums show a softening effect, while for lower curvature term a combination of hardening and softening behaviour is obtained. Furthermore, by increasing the curvature term, the maximum amplitude of the first transverse dynamic equilibrium coordinate decreases significantly.

Study 4: Slenderness ratio sensitivity

Since a third-order shear deformable model has been used, different length-to-thickness models can be analysed. In this subsection, by assuming the same properties given in Sect. 6.1, the length of the arch is varied to $L = S_L h$ where S_L is the slenderness ratio, which is varied as $S_L = [10, 20, 30, 40, 50]$. The results for varying the length-to-thickness ratio are shown in Figs. 16, 17 and 18 for the axial, transverse and rotation dynamic equilibrium directions. It can be seen that increasing the slenderness ratio increases the stiffness hardening behaviour in the transverse coordinates. The first axial and rotation coordinates' amplitude decreases by increasing the slenderness ratio rate, which means the coupling between the axial and the transverse motion decreases and the rotation motion loses its importance.

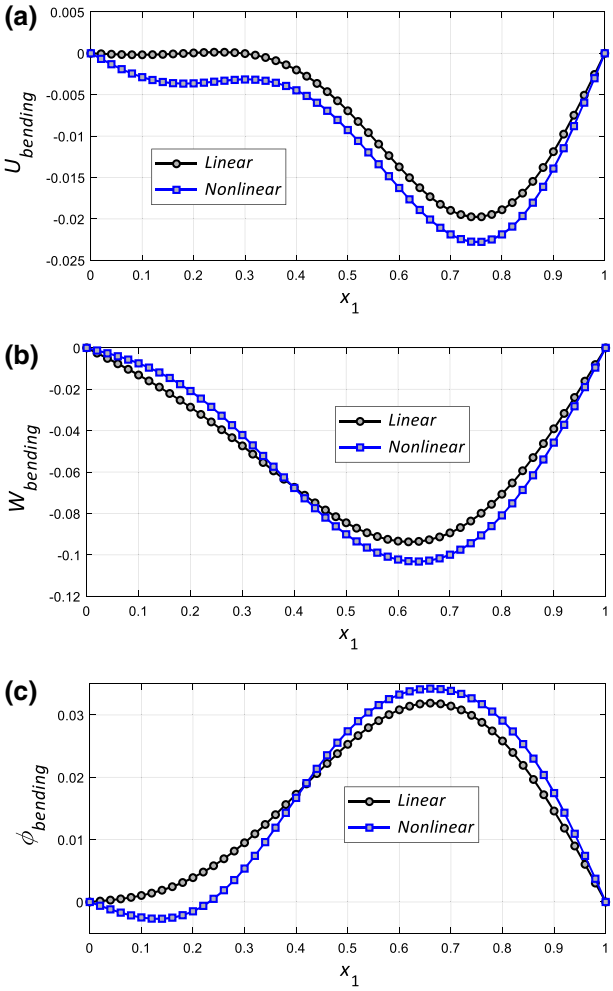

Fig. 5 Comparison of the linear and nonlinear models for bending analysis of the hyper-elastic shallow arch with $R_0 = 1.5$ **a** axial deformation, **b** transverse deformation, and **c** rotational deformation

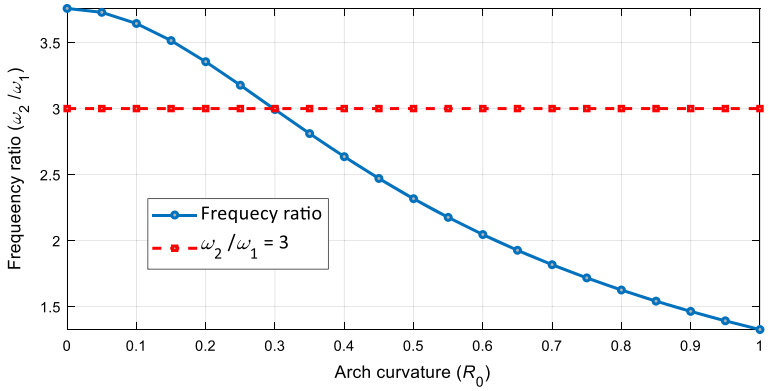

Fig. 6 The frequency ratio of a soft, thick shallow arch with respect to the curvature term

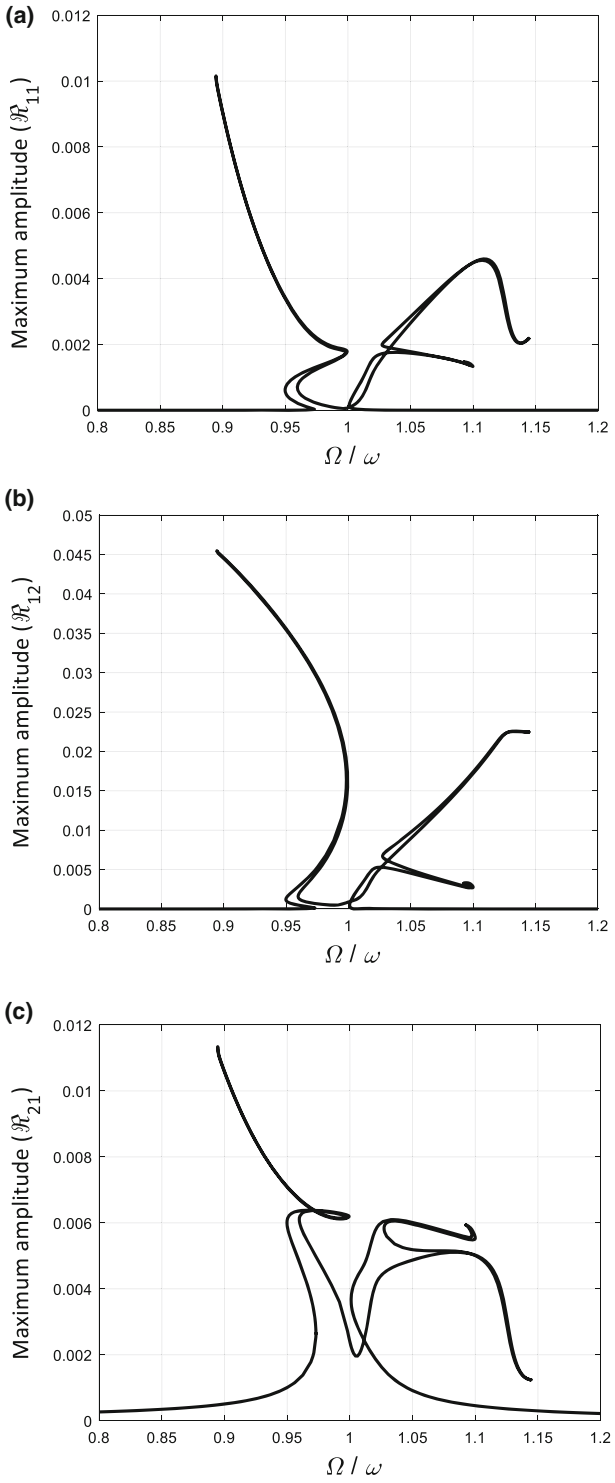

Fig. 7 First three axial nonlinear frequency responses of *hyper-elastic* thick, soft arches at the internal resonance **a** $\mathfrak{R}_{11}$, **b** $\mathfrak{R}_{21}$ and **c** $\mathfrak{R}_{12}$

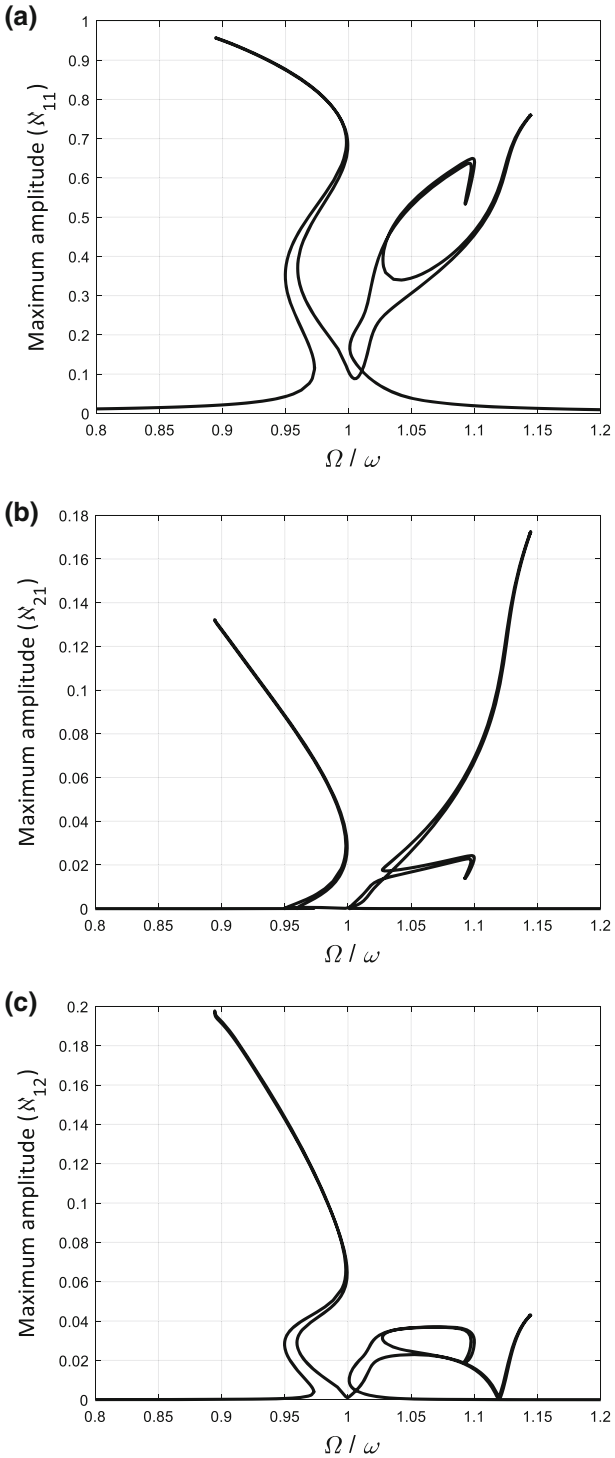

Fig. 8 First three *transverse* nonlinear frequency responses of *hyper-elastic* thick, soft arches at the *internal resonance* **a** $\aleph_{11}$, **b** $\aleph_{12}$ and **c** $\aleph_{21}$

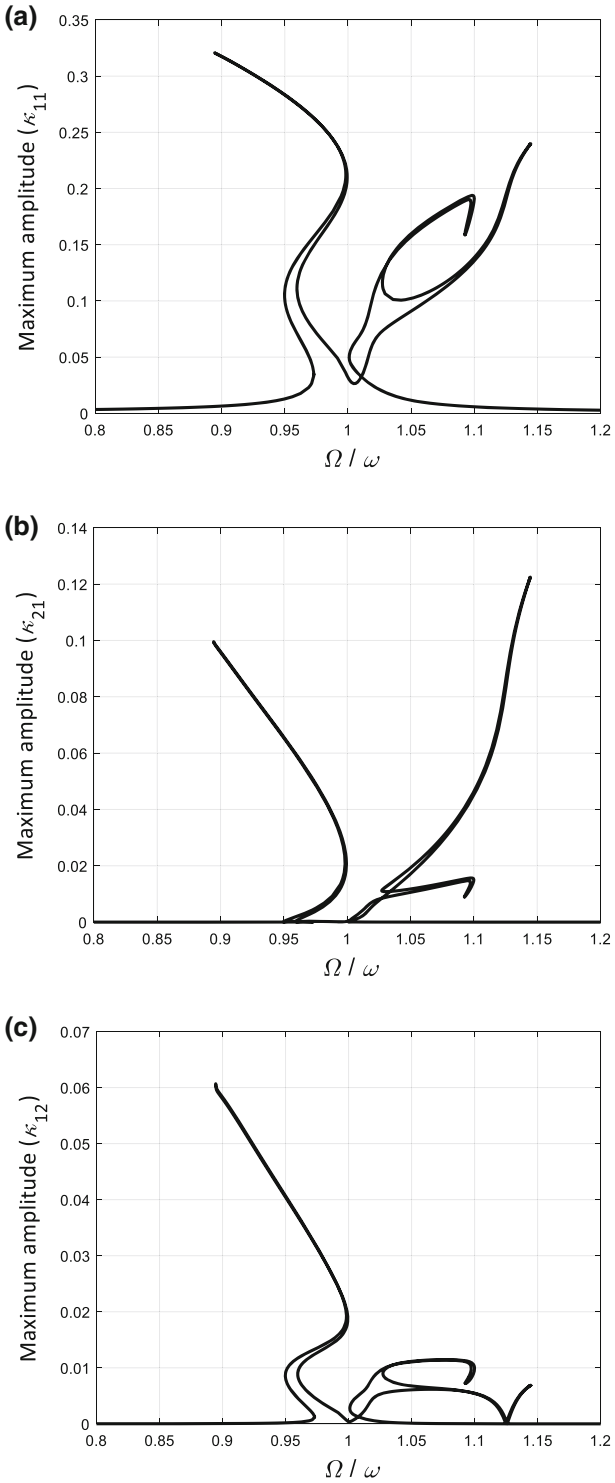

Fig. 9 First three *rotation* nonlinear frequency responses of *hyper-elastic* thick, soft arches at the *internal resonance* **a** k_{11}, **b** κ_{21} and **c** κ_{12}

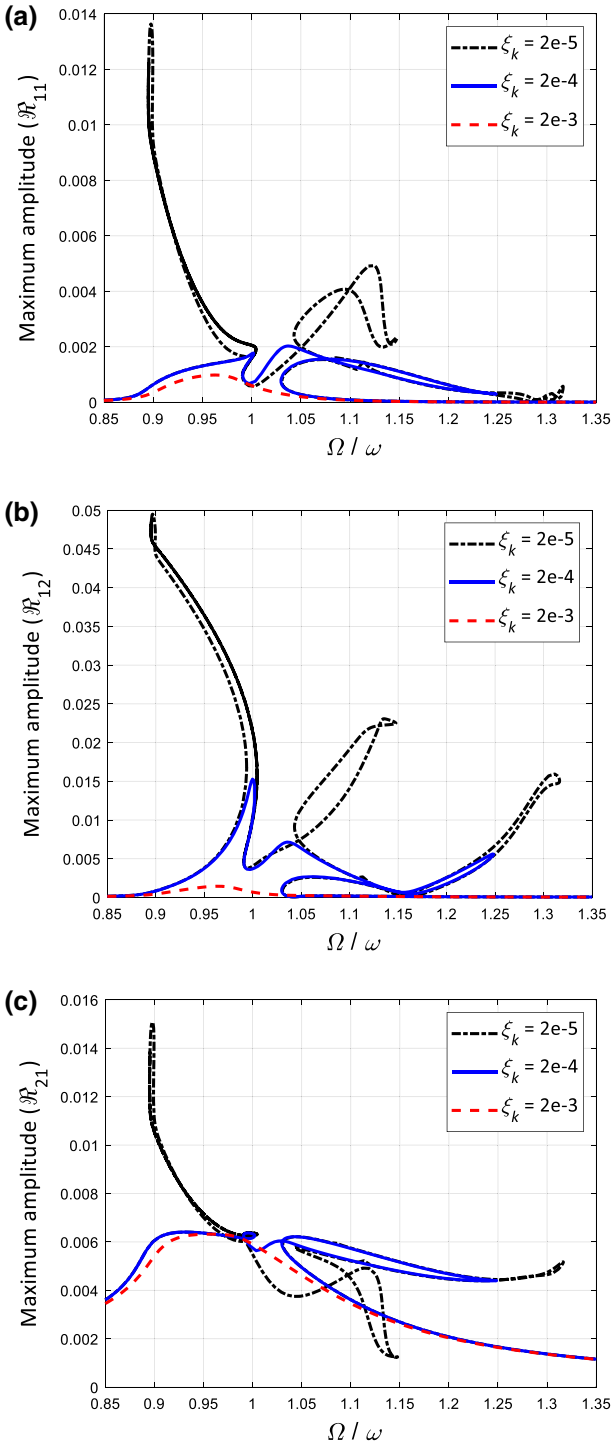

Fig. 10 First three *axial* nonlinear frequency responses of *visco-hyper-elastic* thick, soft arches at the *internal resonance* **a** $\Re_{11}$, **b** $\Re_{21}$ and **c** $\Re_{12}$

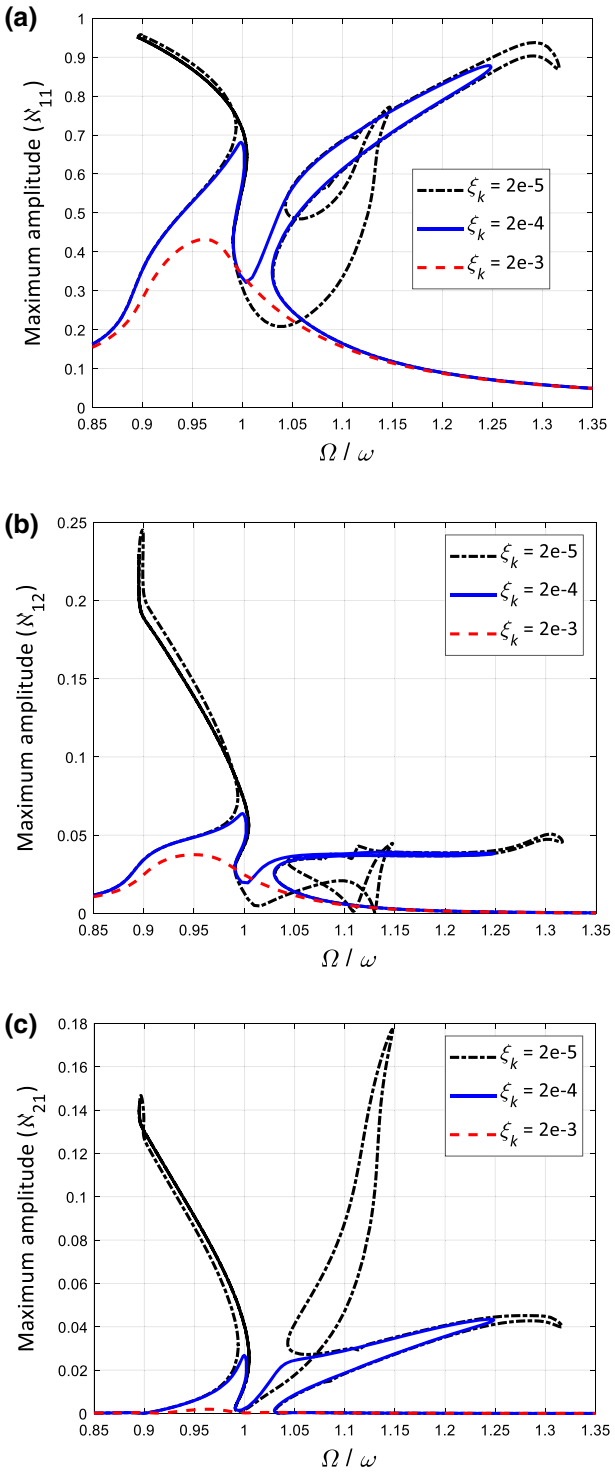

Fig. 11 First three *transverse* nonlinear frequency responses of *visco-hyper-elastic* thick, soft arches at the *internal resonance* **a** $\aleph_{11}$, **b** $\aleph_{12}$ and **c** $\aleph_{21}$

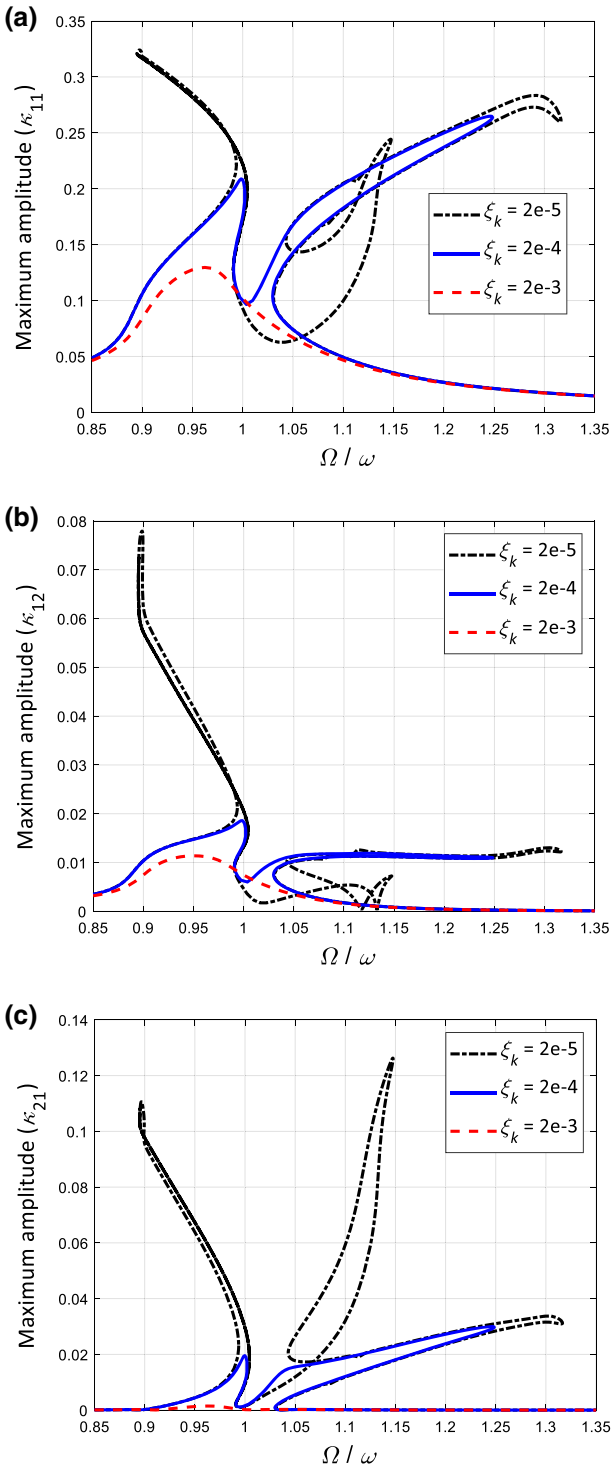

Fig. 12 First three *rotation* nonlinear frequency responses of *visco-hyper-elastic* thick, soft arches at the *internal resonance* **a** k_{11}, **b** κ_{21} and **c** κ_{12}

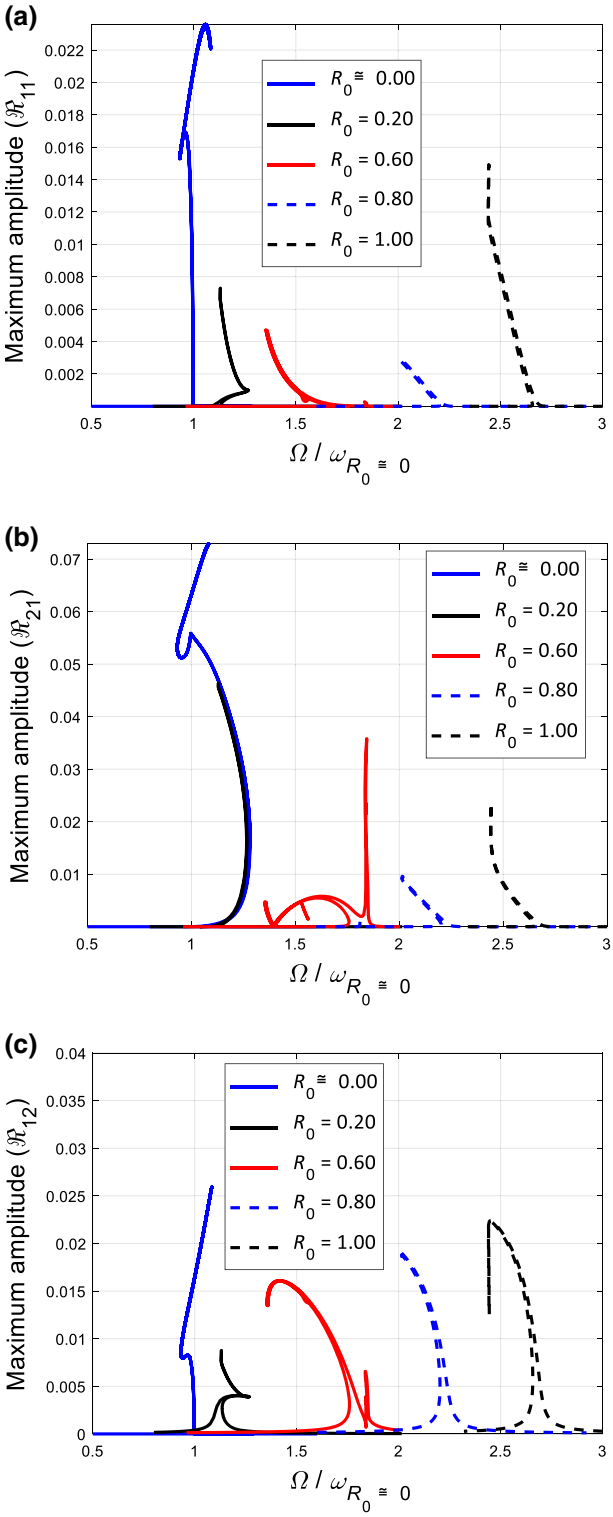

Fig. 13 Influence of the *curvature term* on the first three *axial* nonlinear frequency responses of thick, soft arches **a** $\Re_{11}$, **b** $\Re_{21}$ and **c** $\Re_{12}$

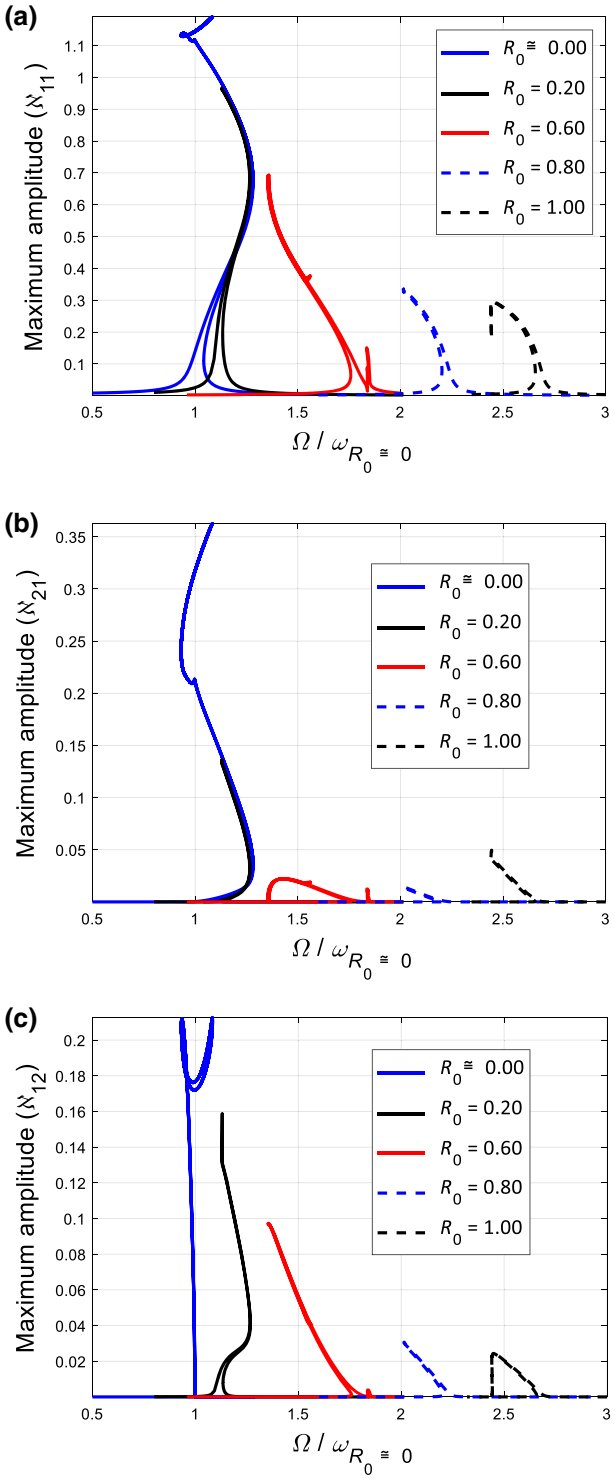

Fig. 14 Influence of *the curvature term* on the first three *transverse* nonlinear frequency responses of thick, soft arches **a** $\aleph_{11}$, **b** $\aleph_{12}$ and (c) $\aleph_{21}$

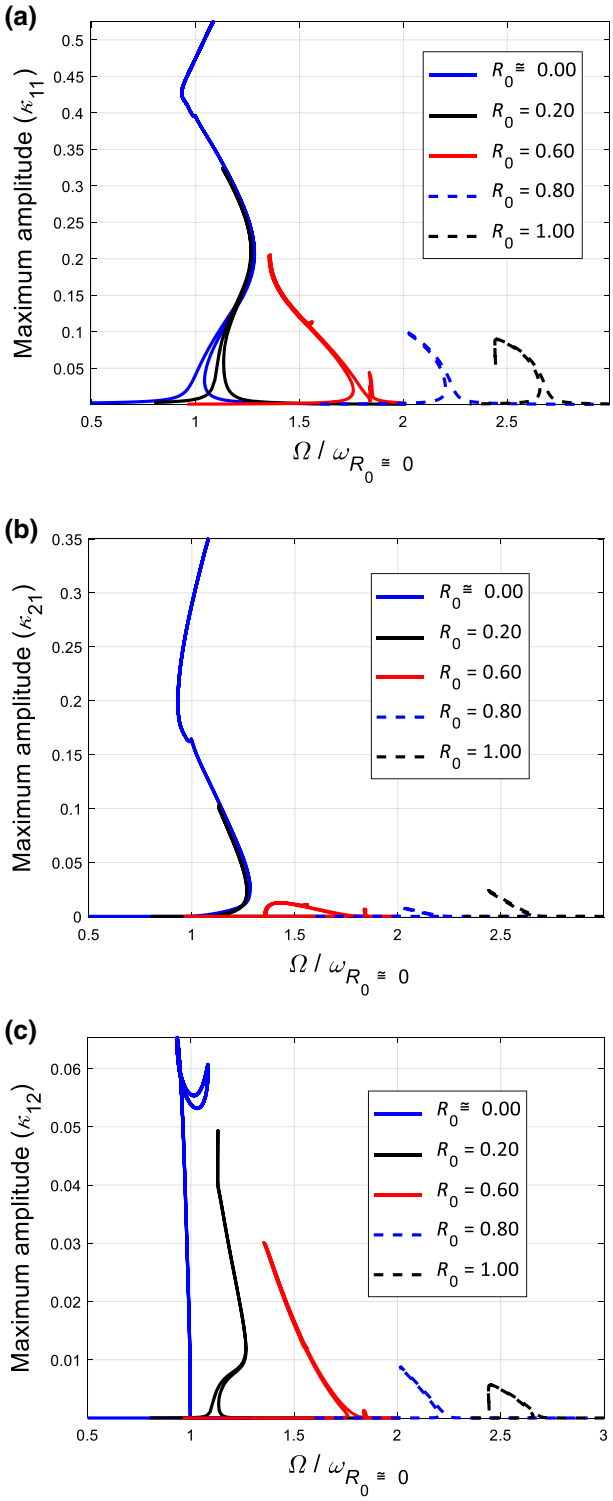

Fig. 15 Influence of the *curvature term* on the first three *rotation* nonlinear frequency responses of thick, soft arches **a** k_{11}, **b** κ_{21} and **c** κ_{12}

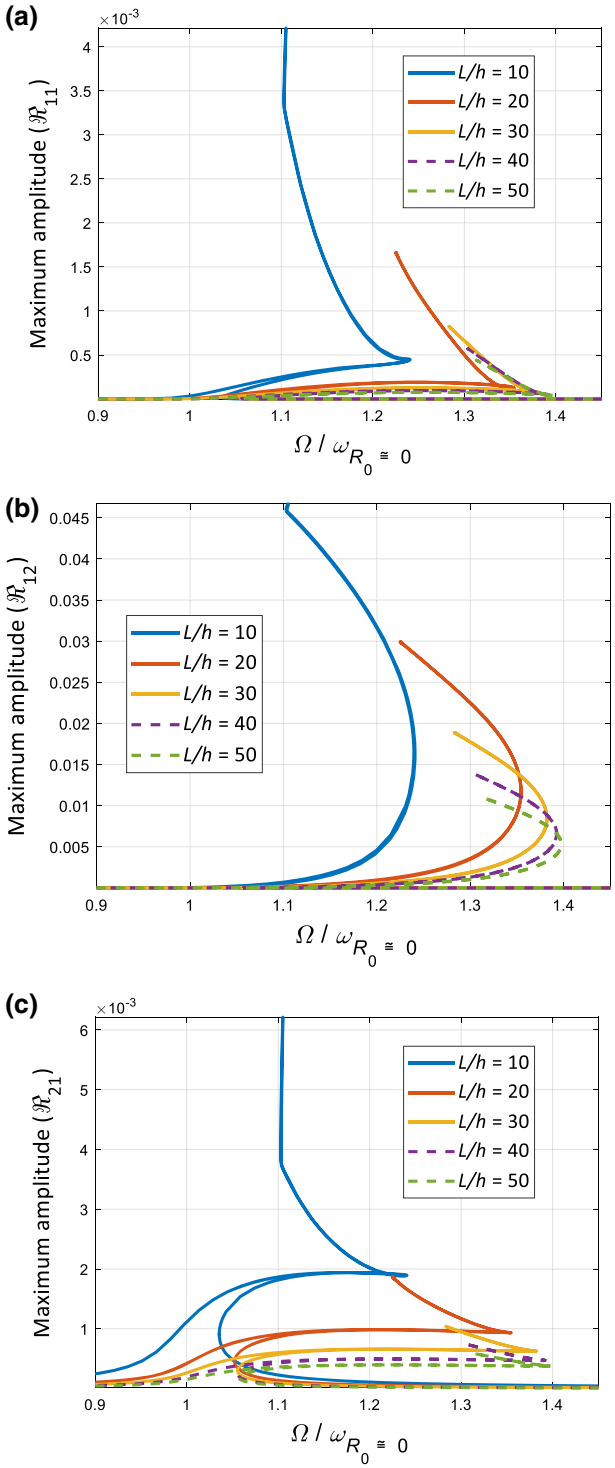

Fig. 16 Influence of the *slenderness ratio* on the first three *axial* nonlinear frequency responses of thick, soft arches **a** $\Re_{11}$, **b** $\Re_{21}$ and **c** $\Re_{12}$

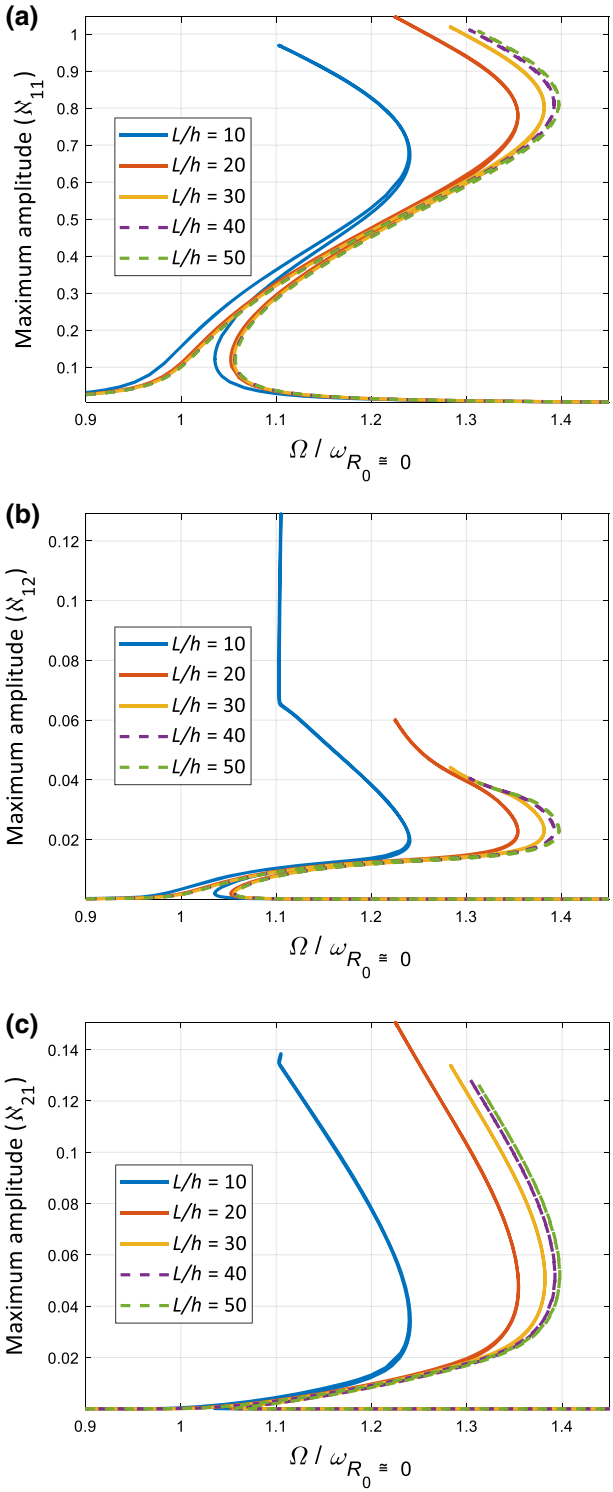

Fig. 17 Influence of the *slenderness ratio* on the first three *transverse* nonlinear frequency responses of thick, soft arches **a** $\aleph_{11}$, **b** $\aleph_{12}$ and **c** $\aleph_{21}$

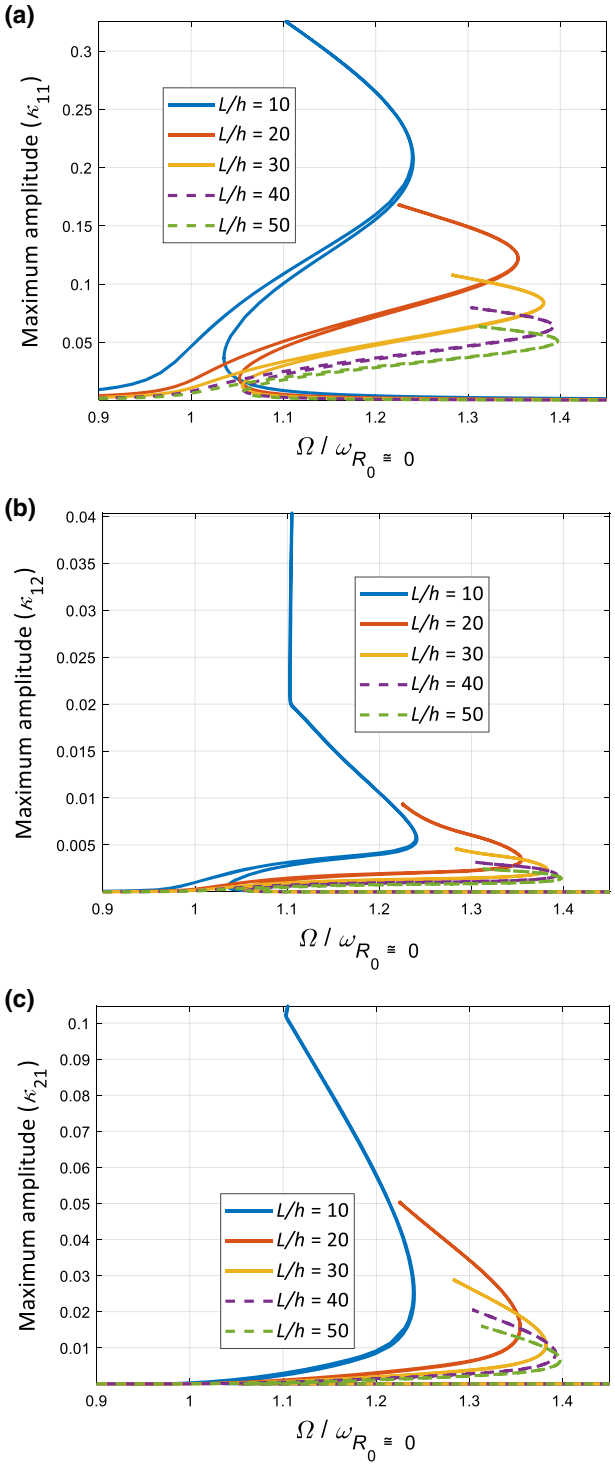

Fig. 18 Influence of the *slenderness ratio* on the first three *transverse* nonlinear frequency responses of thick, soft arches **a** κ_{11}, **b** κ_{12} and **c** κ_{21}

7 Summary and conclusions

The nonlinear bending and vibration behaviours of simply supported, thick, soft, visco-hyper-elastic shallow arches are examined in this study. The visco-hyper-elasticity was modelled using an incompressible Mooney–Rivlin's hyper-elastic strain energy density model, together with Kelvin–Voigt visco-hyper-elasticity. A higher-order shear deformable model was used to model the axial, transverse and rotation motions. The curvature term was added to the model using von Kármán geometric nonlinearity, and the incompressibility condition was satisfied in the strain–displacement definition. The coupled nonlinear equations of motion were obtained and solved using force-moment balance method and the virtual work method for the vibration and bending analyses, respectively, showing that:

(i) Increasing the shallow arch curvature leads to higher resistance against the transverse loading in all axial, transverse and rotation motions of the structure and changed the bending behaviour significantly.
(ii) The linear simplification of the structure leads to underestimated bending deformations for all the axial, transverse and rotation motions which indicates the importance of accurately modelling the nonlinear behaviour of the structure.
(iii) The coupling between the axial and transverse bending increases significantly by increasing the curvature term
(iv) The curvature term can cause internal resonance in the system, leading to high coupling between modes, for which the system shows a rich nonlinear behaviour with a combination of hardening, softening and modal interactions.
(v) The visco-hyper-elasticity has a significant effect in changing the nonlinear frequency response with a three-to-one internal resonance. By increasing the visco-hyper-elastic term to higher numbers, the complicated nonlinear internal resonance behaviour will be fully damped.
(vi) For higher curvature terms, transverse dynamic equilibriums show a softening behaviour, while for lower curvature terms, a combination of hardening and softening behaviour is obtained.
(vii) By increasing the curvature term, the maximum amplitude of the first transverse dynamic equilibrium coordinate decreases significantly.
(viii) Increasing the slenderness ratio increases the stiffness hardening behaviour in the transverse coordinates.
(ix) The dominant axial and rotation coordinates' amplitude decreases by increasing the slenderness ratio rate, which means the coupling between the axial and the transverse motion decreases and the rotation motion loses its importance.

Acknowledgements This work employed the supercomputing resources provided by the Phoenix HPC service at the University of Adelaide. The HDR scholarship support through The University of Adelaide and Faculty of Engineering, Computer & Mathematical Sciences, The University of Adelaide is also acknowledged.

Funding Open Access funding enabled and organized by CAUL and its Member Institutions Open Access funding enabled and organized by CAUL and its Member Institutions. No funding was received for this project.

Declarations

Conflict of interest The authors declare that they have no known competing financial interests or personal relationships that could have appeared to influence the work reported in this paper.

Appendix A

Variations of potential energy terms

$$PE1 = -8C_T I_{00} u_{1x_1x_1} - 8C_T I_{00} \frac{\mathrm{d}}{\mathrm{d}x_1}\left(u_{3x_1} u_{30x_1}\right) - 8C_T I_{22} u_{3x_1x_1x_1} - 8C_T I_{33} \phi_{x_1x_1} + 12C_T I_{00} \frac{\mathrm{d}}{\mathrm{d}x_1}\left(u_{1x_1}^2\right)$$

$$
\begin{aligned}
&+24C_T I_{00}\frac{\mathrm{d}}{\mathrm{d}x_1}\left(u_{1x_1}u_{3x_1}u_{30x_1}\right)+24C_T I_{22}\frac{\mathrm{d}}{\mathrm{d}x_1}\left(u_{1x}u_{3x_1x_1}\right)\\
&+24C_T I_{33}\frac{\mathrm{d}}{\mathrm{d}x_1}\left(u_{1x_1}\phi_{x_1}\right)-4C_T I_{77}\frac{\mathrm{d}}{\mathrm{d}x_1}\left(u_{3x_1}^2\right)\\
&+12C_T I_{00}\frac{\mathrm{d}}{\mathrm{d}x_1}\left(u_{3x_1}^2u_{30x_1}^2\right)+24C_T I_{22}\frac{\mathrm{d}}{\mathrm{d}x_1}\left(u_{3x_1}u_{3x_1x_1}u_{03x_1}\right)+12C_T I_{44}\frac{\mathrm{d}}{\mathrm{d}x_1}\left(u_{3x_1x_1}^2\right)\\
&+24C_T I_{33}\frac{\mathrm{d}}{\mathrm{d}x_1}\left(u_{3x_1}\phi_{x_1}u_{30x_1}\right)+24C_T I_{66}\frac{\mathrm{d}}{\mathrm{d}x_1}\left(u_{3x_1x_1}\phi_{x_1}\right)\\
&+8C_T I_{55}\frac{\mathrm{d}}{\mathrm{d}x_1}\left(u_{3x_1}\phi\right)+12C_T I_{99}\frac{\mathrm{d}}{\mathrm{d}x_1}\left(\phi_{x_1}^2\right)\\
&+4C_T\, I_{55}\frac{\mathrm{d}}{\mathrm{d}x_1}\left(\phi^2\right)+12C_T I_{00}\frac{\mathrm{d}}{\mathrm{d}x_1}\left(u_{1x_1}u_{3x_1}^2\right)+12C_T I_{00}\frac{\mathrm{d}}{\mathrm{d}x_1}\left(u_{30}u_{3x_1}^3\right)+12C_T I_{22}\frac{\mathrm{d}}{\mathrm{d}x_1}\left(u_{3x_1}^2u_{3x_1x_1}\right)\\
&+12C_T I_{33}\frac{\mathrm{d}}{\mathrm{d}x_1}\left(u_{3x_1}^2\phi_{x_1}\right)+3C_T I_{00}\frac{\partial}{\partial x_1}\left(u_{3x_1}^4\right), \qquad \text{(A.1)}\\
PE3 = &-8C_T I_{33}u_{1x_1x_1}-8C_T I_{33}\frac{\mathrm{d}}{\mathrm{d}x_1}\left(u_{3x_1}u_{30x_1}\right)-8C_T I_{66}u_{3x_1x_1x_1}\\
&+8C_T I_{55}u_{3x_1}-8C_T I_{99}\phi_{x_1x_1}+8C_T I_{55}\phi\\
&+12C_T I_{33}\frac{\mathrm{d}}{\mathrm{d}x_1}\left(u_{1x_1}^2\right)+24C_T I_{33}\frac{\mathrm{d}}{\mathrm{d}x_1}\left(u_{1x_1}u_{3x_1}u_{30x_1}\right)+24C_T I_{66}\frac{\mathrm{d}}{\mathrm{d}x_1}\left(u_{1x_1}u_{3x_1x_1}\right)-8C_T I_{55}u_{1x_1}u_{3x_1}\\
&+24C_T I_{99}\frac{\mathrm{d}}{\mathrm{d}x_1}\left(u_{1x_1}\phi_{x_1}\right)-8C_T I_{55}u_{1x_1}\phi-4C_T I_{33}\frac{\mathrm{d}}{\mathrm{d}x_1}\left(u_{3x_1}^2\right)+12C_T I_{33}\frac{\mathrm{d}}{\mathrm{d}x_1}\left(u_{3x_1}^2u_{30x_1}^2\right)\\
&+24C_T I_{66}\frac{\mathrm{d}}{\mathrm{d}x_1}\left(u_{3x_1}u_{3x_1x_1}u_{30x_1}\right)+4C_T I_{1313}\frac{\mathrm{d}}{\mathrm{d}x_1}\left(u_{3x_1}^2\right)+12C_T\, I_{1414}\frac{\mathrm{d}}{\mathrm{d}x_1}\left(u_{3x_1x_1}^2\right)-8C_T I_{55}u_{3x_1}^2u_{30x_1}\\
&-8C_T I_{1111}u_{3x_1}u_{3x_1x_1}+24C_T I_{99}\frac{\mathrm{d}}{\mathrm{d}x_1}\left(u_{3x_1}\phi_{x_1}u_{30x_1}\right)\\
&+24C_T I_{1515}\frac{\mathrm{d}}{\mathrm{d}x_1}\left(u_{3x_1x_1}\phi_{x_1}\right)+8C_T I_{1313}\frac{\mathrm{d}}{\mathrm{d}x_1}\left(u_{3x_1}\phi\right)\\
&-8C_T I_{1313}u_{3x_1}\phi_{x_1}-8C_T I_{55}u_{3x_1}\phi u_{30x_1}-8C_T I_{1111}u_{3x_1x_1}\phi\\
&+12C_T I_{1616}\frac{\mathrm{d}}{\mathrm{d}x_1}\left(\phi_{x_1}^2\right)+4C_T I_{1313}\frac{\mathrm{d}}{\mathrm{d}x_1}\left(\phi^2\right)\\
&-8C_T I_{1313}\phi\phi_{x_1}+12C_T I_{33}\frac{\mathrm{d}}{\mathrm{d}x_1}\left(u_{1x_1}u_{3x_1}^2\right)\\
&+12C_T I_{33}\frac{\mathrm{d}}{\mathrm{d}x_1}\left(u_{30x_1}u_{3x_1}^3\right)+12C_T I_{66}\frac{\mathrm{d}}{\mathrm{d}x_1}\left(u_{3x_1}^2u_{3x_1x_1}\right)\\
&-4C_T I_{55}u_{3x_1}^3+12C_T I_{99}\frac{\mathrm{d}}{\mathrm{d}x_1}\left(u_{3x_1}^2\phi_{x_1}\right)-4C_T I_{55}u_{3x_1}^2\phi+3C_T I_{33}\frac{\mathrm{d}}{\mathrm{d}x_1}\left(u_{3x_1}^4\right), \qquad \text{(A.2)}\\
PE2 = &+8C_T I_{22}u_{1x_1x_1x_1}-8C_T I_{00}\frac{\mathrm{d}}{\mathrm{d}x_1}\left(u_{1x_1}u_{30x_1}\right)-8C_T I_{00}\frac{\mathrm{d}}{\mathrm{d}x_1}\left(u_{3x_1}u_{30x_1}^2\right)-8C_T I_{22}\frac{\mathrm{d}}{\mathrm{d}x_1}\left(u_{30x_1}u_{3x_1x_1}\right)\\
&+8C_T I_{22}\frac{\mathrm{d}^2}{\mathrm{d}x_1^2}\left(u_{3x_1}u_{30x_1}\right)+8C_T I_{44}u_{3x_1x_1x_1x_1}-8C_T\, I_{55}u_{3x_1x_1}\\
&+8C_T I_{66}\phi_{x_1x_1x_1}-8C_T I_{33}\frac{\mathrm{d}}{\mathrm{d}x_1}\left(\phi_{x_1}u_{30x_1}\right)\\
&-8C_T I_{55}\phi_{x_1}-12C_T I_{22}\frac{\mathrm{d}^2}{\mathrm{d}x_1^2}\left(u_{1x_1}^2\right)+12C_T I_{00}\frac{\mathrm{d}}{\mathrm{d}x_1}\left(u_{1x_1}^2u_{30x_1}\right)-8C_T I_{77}\frac{\mathrm{d}}{\mathrm{d}x_1}\left(u_{1x_1}u_{3x_1}\right)\\
&+24C_T I_{00}\frac{\mathrm{d}}{\mathrm{d}x_1}\left(u_{1x_1}u_{3x_1}u_{30x_1}^2\right)-24C_T I_{22}\frac{\mathrm{d}^2}{\mathrm{d}x_1^2}\left(u_{1x_1}u_{3x_1}u_{30x_1}\right)+24C_T I_{22}\frac{\mathrm{d}}{\mathrm{d}x_1}\left(u_{1x_1}u_{3x_1x_1}u_{30x_1}\right)\\
&-24C_T I_{44}\frac{\mathrm{d}^2}{\mathrm{d}x_1^2}\left(u_{1x_1}u_{3x_1x_1}\right)+24C_T I_{33}\frac{\mathrm{d}}{\mathrm{d}x_1}\left(u_{1x_1}\phi_{x_1}u_{30x_1}\right)-24C_T I_{66}\frac{\mathrm{d}^2}{\mathrm{d}x_1^2}\left(u_{1x_1}\phi_{x_1}\right)
\end{aligned}
$$

$$
\begin{aligned}
&+4C_T I_{22}\frac{\mathrm{d}^2}{\mathrm{d}x_1^2}\left(u_{3x_1}^2\right)-4C_T I_{1111}\frac{\mathrm{d}^2}{\mathrm{d}x_1^2}\left(u_{3x_1}^2\right)-12C_T I_{1010}\frac{\mathrm{d}^2}{\mathrm{d}x_1^2}\left(u_{3x_1x_1}^2\right)-12C_T I_{77}\frac{\mathrm{d}}{\mathrm{d}x_1}\left(u_{3x_1}^2u_{30x_1}\right)\\
&-8C_T I_{1212}\frac{\mathrm{d}}{\mathrm{d}x_1}\left(u_{3x_1}u_{3x_1x_1}\right)+12C_T I_{00}\frac{\mathrm{d}}{\mathrm{d}x_1}\left(u_{3x_1}^2u_{30x_1}^3\right)+12C_T I_{44}\frac{\mathrm{d}}{\mathrm{d}x_1}\left(u_{3x_1x_1}^2u_{30x_1}\right)\\
&+24C_T I_{22}\frac{\mathrm{d}}{\mathrm{d}x_1}\left(u_{3x_1}u_{3x_1x_1}u_{30x_1}^2\right)-12C_T I_{22}\frac{\mathrm{d}^2}{\mathrm{d}x_1^2}\left(u_{3x_1}^2u_{30x_1}^2\right)-24C_T I_{44}\frac{\mathrm{d}^2}{\mathrm{d}x_1^2}\left(u_{3x_1}u_{3x_1x_1}u_{30x_1}\right)\\
&-8C_T I_{33}\frac{\mathrm{d}}{\mathrm{d}x_1}\left(u_{30x_1}\phi_{x_1}\right)+8C_T I_{1313}\frac{\mathrm{d}}{\mathrm{d}x_1}\left(u_{3x_1}\phi_{x_1}\right)+24C_T I_{33}\frac{\mathrm{d}}{\mathrm{d}x_1}\left(u_{3x_1}\phi_{x_1}u_{30x_1}^2\right)\\
&+24C_T I_{66}\frac{\mathrm{d}}{\mathrm{d}x_1}\left(u_{3x_1x_1}\phi_{x_1}u_{30x_1}\right)+16C_T I_{55}\frac{\mathrm{d}}{\mathrm{d}x_1}\left(u_{3x_1}\phi u_{30x_1}\right)-8C_T I_{1111}\frac{\mathrm{d}^2}{\mathrm{d}x_1^2}\left(u_{3x_1}\phi\right)\\
&-24C_T I_{66}\frac{\mathrm{d}^2}{\mathrm{d}x_1^2}\left(u_{3x_1}\phi_{x_1}u_{30x_1}\right)-24C_T I_{1414}\frac{\mathrm{d}^2}{\mathrm{d}x_1^2}\left(u_{3x_1x_1}\phi_{x_1}\right)+8C_T I_{1111}\frac{\mathrm{d}}{\mathrm{d}x_1}\left(u_{3x_1x_1}\phi\right)\\
&-4C_T I_{1111}\frac{\mathrm{d}^2}{\mathrm{d}x_1^2}\left(\phi^2\right)-12C_T I_{1515}\frac{\mathrm{d}^2}{\mathrm{d}x_1^2}\left(\phi_{x_1}^2\right)+12C_T I_{99}\frac{\mathrm{d}}{\mathrm{d}x_1}\left(\phi_{x_1}^2u_{30x_1}\right)+8C_T I_{55}\frac{\mathrm{d}}{\mathrm{d}x_1}\left(u_{1x_1}\phi\right)\\
&+4C_T I_{55}\frac{\mathrm{d}}{\mathrm{d}x_1}\left(\phi^2u_{30x_1}\right)+8C_T I_{1313}\frac{\mathrm{d}}{\mathrm{d}x_1}\left(\phi\phi_{x_1}\right)+12C_T I_{00}\frac{\mathrm{d}}{\mathrm{d}x_1}\left(u_{1x_1}^2u_{3x_1}\right)\\
&+36C_T I_{00}\frac{\mathrm{d}}{\mathrm{d}x_1}\left(u_{1x_1}u_{3x_1}^2u_{30x_1}\right)+24C_T I_{22}\frac{\mathrm{d}}{\mathrm{d}x_1}\left(u_{1x_1}u_{3x_1}u_{3x_1x_1}\right)-12C_T I_{22}\frac{\mathrm{d}^2}{\mathrm{d}x_1^2}\left(u_{1x_1}u_{3x_1}^2\right)\\
&+24C_T I_{33}\frac{\mathrm{d}}{\mathrm{d}x_1}\left(u_{1x_1}u_{3x_1}\phi_{x_1}\right)-4C_T I_{88}\frac{\mathrm{d}}{\mathrm{d}x_1}\left(u_{3x_1}^3\right)+24C_T I_{00}\frac{\mathrm{d}}{\mathrm{d}x_1}\left(u_{3x_1}^3u_{30x_1}^2\right)\\
&-12C_T I_{22}\frac{\mathrm{d}^2}{\mathrm{d}x_1^2}\left(u_{30x_1}u_{3x_1}^3\right)+12C_T I_{44}\frac{\mathrm{d}}{\mathrm{d}x_1}\left(u_{3x_1}u_{3x_1x_1}^2\right)+36C_T I_{22}\frac{\mathrm{d}}{\mathrm{d}x_1}\left(u_{3x_1}^2u_{3x_1x_1}u_{30x_1}\right)\\
&-12C_T I_{44}\frac{\mathrm{d}^2}{\mathrm{d}x_1^2}\left(u_{3x_1}^2u_{3x_1x_1}\right)+36C_T I_{33}\frac{\mathrm{d}}{\mathrm{d}x_1}\left(u_{3x_1}^2\phi_{x_1}u_{30x_1}\right)+24C_T I_{66}\frac{\mathrm{d}}{\mathrm{d}x_1}\left(u_{3x_1}u_{3x_1x_1}\phi_{x_1}\right)\\
&+12C_T I_{55}\frac{\mathrm{d}}{\mathrm{d}x_1}\left(u_{3x_1}^2\phi\right)-12C_T I_{66}\frac{\mathrm{d}^2}{\mathrm{d}x_1^2}\left(u_{3x_1}^2\phi_x\right)+12C_T I_{99}\frac{\mathrm{d}}{\mathrm{d}x_1}\left(u_{3x_1}\phi_{x_1}^2\right)\\
&+4C_T I_{55}\frac{\mathrm{d}}{\mathrm{d}x_1}\left(u_{3x_1}\phi^2\right)+12C_T I_{00}\frac{\mathrm{d}}{\mathrm{d}x_1}\left(u_{1x_1}u_{3x_1}^3\right)-3C_T I_{22}\frac{\mathrm{d}^2}{\mathrm{d}x_1^2}\left(u_{3x_1}^4\right)\\
&+15C_T I_{00}\frac{\mathrm{d}}{\mathrm{d}x_1}\left(u_{30x_1}u_{3x_1}^4\right)+12C_T I_{22}\frac{\mathrm{d}}{\mathrm{d}x_1}\left(u_{3x_1}^3u_{3x_1x_1}\right)\\
&+12C_T I_{33}\frac{\mathrm{d}}{\mathrm{d}x_1}\left(u_{3x_1}^3\phi_{x_1}\right)+3C_T I_{00}\frac{\mathrm{d}}{\mathrm{d}x_1}\left(u_{3x_1}^5\right),
\end{aligned}
\tag{A.3}
$$

Appendix B

For homogeneous visco-hyper-elastic shallow arches, due to the homogeneity of the visco-hyper-elastic arch, some of the inertia terms are equal to zero, simplifying the equations of motion to

$$
\begin{aligned}
&\rho I_{00}u_{1tt}-\xi_k I_{00}u_{1x_1x_1t}-\xi_k I_{00}\frac{\partial}{\partial x_1}\left(u_{30x_1}u_{3x_1t}\right)+2\xi_k I_{00}\frac{\partial}{\partial x_1}\left(u_{1x_1}u_{1x_1t}\right)+2\xi_k I_{00}\frac{\partial}{\partial x_1}\left(u_{3x_1}u_{30x_1}u_{x_1t}\right)\\
&+2\xi_k I_{00}\frac{\partial}{\partial x_1}\left(u_{1x_1}u_{30x_1}u_{3x_1t}\right)-\xi_k I_{77}\frac{\partial}{\partial x_1}\left(u_{3x_1}u_{3x_1t}\right)+2\xi_k I_{00}\frac{\partial}{\partial x_1}\left(u_{3x_1}u_{30x_1}^2u_{3x_1t}\right)-8C_T I_{00}u_{1x_1x_1}\\
&+2\xi_k I_{44}\frac{\partial}{\partial x_1}\left(u_{3x_1x_1}u_{3x_1x_1t}\right)+2\xi_k I_{66}\frac{\partial}{\partial x_1}\left(\phi_{x_1}u_{3x_1x_1t}\right)+\xi_k I_{55}\frac{\partial}{\partial x_1}\left(\phi u_{3x_1t}\right)+2\xi_k I_{66}\frac{\partial}{\partial x_1}\left(u_{3x_1x_1}\phi_{x_1t}\right)\\
&+\xi_k I_{55}\frac{\partial}{\partial x_1}\left(u_{3x_1}\phi_t\right)+2\xi_k I_{99}\frac{\partial}{\partial x_1}\left(\phi_{x_1}\phi_{x_1t}\right)+\xi_k I_{55}\frac{\partial}{\partial x_1}\left(\phi\phi_t\right)+\xi_k I_{00}\frac{\partial}{\partial x_1}\left(u_{3x_1}^2u_{xt}\right)+\xi_k I_{00}\frac{\partial}{\partial x_1}\left(u_{3x_1}^3u_{3x_1t}\right)
\end{aligned}
$$

$$
\begin{aligned}
&+2\xi_k I_{00}\frac{\partial}{\partial x_1}\left(u_{1x_1}u_{3x_1}u_{3x_1t}\right)+3\xi_k I_{00}\frac{\partial}{\partial x_1}\left(u_{3x_1}^2u_{30x_1}u_{3x_1t}\right)-8C_T I_{00}\frac{\partial}{\partial x_1}\left(u_{3x_1}u_{30x_1}\right)+12C_T I_{00}\frac{\partial}{\partial x_1}\left(u_{1x_1}^2\right)\\
&+24C_T I_{00}\frac{\partial}{\partial x_1}\left(u_{1x_1}u_{3x_1}u_{30x_1}\right)-4C_T I_{77}\frac{\partial}{\partial x_1}\left(u_{3x_1}^2\right)+12C_T I_{00}\frac{\partial}{\partial x_1}\left(u_{3x_1}^2u_{30x_1}^2\right)+12C_T I_{44}\frac{\partial}{\partial x_1}\left(u_{3x_1x_1}^2\right)\\
&+24C_T I_{66}\frac{\partial}{\partial x_1}\left(u_{3x_1x_1}\phi_{x_1}\right)+8C_T I_{55}\frac{\partial}{\partial x_1}\left(u_{3x_1}\phi\right)+12C_T I_{99}\frac{\partial}{\partial x_1}\left(\phi_{x_1}^2\right)+4C_T\, I_{55}\frac{\partial}{\partial x_1}\left(\phi^2\right)\\
&+12C_T I_{00}\frac{\partial}{\partial x_1}\left(u_{1x_1}u_{3x_1}^2\right)+12C_T I_{00}\frac{\partial}{\partial x_1}\left(u_{30x_1}u_{3x_1}^3\right)+3C_T I_{00}\frac{\partial}{\partial x_1}\left(u_{3x_1}^4\right)=0, \qquad \text{(B.1)}
\end{aligned}
$$

$$
\begin{aligned}
&-\rho I_{44}u_{3x_1x_1tt}-\rho I_{66}\phi_{x_1tt}+\rho I_{00}u_{3tt}-\xi_k I_{00}\frac{\partial}{\partial x_1}\left(u_{30x_1}u_{1x_1t}\right)+\xi_k I_{44}u_{3x_1x_1x_1x_1t}-\xi_k I_{00}\frac{\partial}{\partial x_1}\left(u_{30x_1}^2u_{3x_1t}\right)\\
&-\frac{1}{2}\xi_k I_{55}u_{3x_1x_1t}+\xi_k I_{66}\phi_{x_1x_1x_1t}-\frac{1}{2}\xi_k I_{55}\phi_{x_1t}+2\xi_k I_{00}\frac{\partial}{\partial x_1}\left(u_{1x_1}u_{30x_1}u_{1x_1t}\right)+2\xi_k I_{00}\frac{\partial}{\partial x_1}\left(u_{3x_1}u_{30x_1}^2u_{1x_1t}\right)\\
&-\xi_k I_{00}\frac{\partial}{\partial x_1}\left(u_{3x_1}u_{1x_1t}\right)-2\xi_k I_{44}\frac{\partial^2}{\partial x_1^2}\left(u_{3x_1x_1}u_{1x_1t}\right)+\xi_k I_{55}\frac{\partial}{\partial x_1}\left(u_{3x_1}u_{1x_1t}\right)-2\xi_k I_{66}\frac{\partial^2}{\partial x_1^2}\left(\phi_{x_1}u_{1x_1t}\right)\\
&+\xi_k I_{55}\frac{\partial}{\partial x_1}\left(\phi u_{1x_1t}\right)+2\xi_k I_{00}\frac{\partial}{\partial x_1}\left(u_{1x_1}u_{30x_1}^2u_{3x_1t}\right)-2\xi_k I_{44}\frac{\partial^2}{\partial x_1^2}\left(u_{1x_1}u_{3x_1x_1t}\right)-\xi_k I_{77}\frac{\partial}{\partial x_1}\left(u_{3x_1}u_{30x_1}u_{3x_1t}\right)\\
&+2\xi_k I_{00}\frac{\partial}{\partial x_1}\left(u_{3x_1}u_{30x_1}^3u_{3x_1t}\right)+2\xi_k I_{44}\frac{\partial}{\partial x_1}\left(u_{3x_1x_1}u_{30x_1}u_{3x_1x_1t}\right)-\xi_k I_{00}\frac{\partial}{\partial x_1}\left(u_{30x_1}u_{3x_1}u_{3x_1t}\right)\\
&+\xi_k I_{55}\frac{\partial}{\partial x_1}\left(u_{3x_1}u_{30x_1}u_{3x_1t}\right)-2\xi_k I_{44}\frac{\partial^2}{\partial x_1^2}\left(u_{3x_1x_1}u_{30x_1}u_{3x_1t}\right)+2\xi_k I_{66}\frac{\partial}{\partial x_1}\left(\phi_{x_1}u_{30x_1}u_{3x_1x_1t}\right)\\
&+2\xi_k I_{55}\frac{\partial}{\partial x_1}\left(\phi u_{30x_1}u_{3x_1t}\right)-2\xi_k I_{66}\frac{\partial^2}{\partial x_1^2}\left(\phi_{x_1}u_{30x_1}u_{3x_1t}\right)\\
&-2\xi_k I_{66}\frac{\partial^2}{\partial x_1^2}\left(u_{1x_1}\phi_{x_1t}\right)+2\xi_k I_{66}\frac{\partial}{\partial x_1}\left(u_{3x_1x_1}u_{30x_1}\phi_{x_1t}\right)\\
&+\xi_k I_{55}\frac{\partial}{\partial x_1}\left(u_{3x_1}u_{30x_1}\phi_t\right)-2\xi_k I_{66}\frac{\partial^2}{\partial x_1^2}\left(u_{3x_1}u_{30x_1}\phi_{x_1t}\right)\\
&+2\xi_k I_{99}\frac{\partial}{\partial x_1}\left(\phi_{x_1}u_{30x_1}\phi_{x_1t}\right)+\xi_k I_{55}\frac{\partial}{\partial x_1}\left(\phi u_{30x_1}\phi_t\right)\\
&+2\xi_k I_{00}\frac{\partial}{\partial x_1}\left(u_x u_{3x_1}u_{1x_1t}\right)+3\xi_k I_{00}\frac{\partial}{\partial x_1}\left(u_{3x_1}^2u_{30x_1}u_{1x_1t}\right)+4\xi_k I_{00}\frac{\partial}{\partial x_1}\left(u_{1x_1}u_{3x_1}u_{30x_1}u_{3x_1t}\right)\\
&+5\xi_k I_{00}\frac{\partial}{\partial x_1}\left(u_{3x_1}^2u_{30x_1}^2u_{3x_1t}\right)-\xi_k I_{77}\frac{\partial}{\partial x_1}\left(u_{3x_1}^2u_{3x_1t}\right)+2\xi_k I_{44}\frac{\partial}{\partial x_1}\left(u_{3x_1}u_{3x_1x_1}u_{3x_1x_1t}\right)\\
&\ldots\\
&\ldots\\
&-2\xi_k I_{44}\frac{\partial^2}{\partial x_1^2}\left(u_{3x_1}u_{3x_1x_1}u_{3x_1t}\right)-\xi_k I_{44}\frac{\partial^2}{\partial x_1^2}\left(u_{3x_1}^2u_{3x_1x_1t}\right)\\
&-2\xi_k I_{44}\frac{\partial^2}{\partial x_1^2}\left(u_{3x_1}u_{30x_1}u_{3x_1x_1t}\right)+\xi_k I_{55}\frac{\partial}{\partial x_1}\left(u_{3x_1}^2u_{3x_1t}\right)\\
&+2\xi_k I_{66}\frac{\partial}{\partial x_1}\left(u_{3x_1}\phi_{x_1}u_{3x_1x_1t}\right)+2\xi_k I_{55}\frac{\partial}{\partial x_1}\left(u_{3x_1}\phi u_{3x_1t}\right)\\
&-2\xi_k I_{66}\frac{\partial^2}{\partial x_1^2}\left(u_{3x_1}\phi_{x_1}u_{3x_1t}\right)+2\xi_k I_{66}\frac{\partial}{\partial x_1}\left(u_{3x_1}u_{3x_1x_1}\phi_{x_1t}\right)\\
&+\xi_k I_{55}\frac{\partial}{\partial x_1}\left(u_{3x_1}^2\phi_t\right)-\xi_k I_{66}\frac{\partial^2}{\partial x_1^2}\left(u_{3x_1}^2\phi_{x_1t}\right)+2\xi_k I_{99}\frac{\partial}{\partial x_1}\left(u_{3x_1}\phi_{x_1}\phi_{x_1t}\right)+\xi_k I_{55}\frac{\partial}{\partial x_1}\left(u_{3x_1}\phi\phi_t\right)\\
&+\xi_k I_{00}\frac{\partial}{\partial x_1}\left(u_{3x_1}^3u_{1x_1t}\right)+2\xi_k I_{00}\frac{\partial}{\partial x_1}\left(u_{1x_1}u_{3x_1}^2u_{3x_1t}\right)+4\xi_k I_{00}\frac{\partial}{\partial x_1}\left(u_{3x_1}^3u_{30x_1}u_{3x_1t}\right)+\xi_k I_{00}\frac{\partial}{\partial x_1}\left(u_{3x_1}^4u_{3x_1t}\right)\\
&-8C_T I_{00}\frac{\partial}{\partial x_1}\left(u_{1x_1}u_{30x_1}\right)-8C_T I_{00}\frac{\partial}{\partial x_1}\left(u_{3x_1}u_{30x_1}^2\right)+8C_T I_{44}u_{3x_1x_1x_1x_1}\\
&-8C_T\, I_{55}u_{3x_1x_1}+8C_T I_{66}\phi_{x_1x_1x_1}-8C_T I_{55}\phi_{x_1}
\end{aligned}
$$

$$
\begin{aligned}
&+12C_T I_{00}\frac{\partial}{\partial x_1}\left(u_{1x_1}^2 u_{30x_1}\right) - 8C_T I_{77}\frac{\partial}{\partial x_1}\left(u_{1x_1}u_{3x_1}\right)\\
&+24C_T I_{00}\frac{\partial}{\partial x_1}\left(u_{1x_1}u_{3x_1}u_{30x_1}^2\right) - 24C_T I_{44}\frac{\partial^2}{\partial x_1^2}\left(u_{1x_1}u_{3x_1x_1}\right)\\
&-24C_T I_{66}\frac{\partial^2}{\partial x_1^2}\left(u_{1x_1}\phi_{x_1}\right) + 8C_T I_{55}\frac{\partial}{\partial x_1}\left(u_{1x_1}\phi\right) - 12C_T I_{77}\frac{\partial}{\partial x_1}\left(u_{3x_1}^2 u_{30x_1}\right) + 12C_T I_{00}\frac{\partial}{\partial x_1}\left(u_{3x_1}^2 u_{30x_1}^3\right)\\
&+12C_T I_{44}\frac{\partial}{\partial x_1}\left(u_{3x_1x_1}^2 u_{30x_1}\right) - 24C_T I_{44}\frac{\partial^2}{\partial x_1^2}\left(u_{3x_1}u_{3x_1x_1}u_{30x_1}\right) + 24C_T I_{66}\frac{\partial}{\partial x_1}\left(u_{3x_1x_1}\phi_{x_1}u_{30x_1}\right)\\
&+16C_T I_{55}\frac{\partial}{\partial x_1}\left(u_{3x_1}\phi u_{30x_1}\right) - 24C_T I_{66}\frac{\partial^2}{\partial x_1^2}\left(u_{3x_1}\phi_{x_1}u_{30x_1}\right)\\
&+12C_T I_{99}\frac{\partial}{\partial x_1}\left(\phi_{x_1}^2 u_{30x_1}\right) + 4C_T I_{55}\frac{\partial}{\partial x_1}\left(\phi^2 u_{30x_1}\right)\\
&+12C_T I_{00}\frac{\partial}{\partial x_1}\left(u_{1x_1}^2 u_{3x_1}\right) + 36C_T I_{00}\frac{\partial}{\partial x_1}\left(u_{1x_1}u_{3x_1}^2 u_{30x_1}\right)\\
&-4C_T I_{88}\frac{\partial}{\partial x_1}\left(u_{3x_1}^3\right) + 24C_T I_{00}\frac{\partial}{\partial x_1}\left(u_{3x_1}^3 u_{30x_1}^2\right)\\
&+12C_T I_{44}\frac{\partial}{\partial x_1}\left(u_{3x_1}u_{3x_1x_1}^2\right) - 12C_T I_{44}\frac{\partial^2}{\partial x_1^2}\left(u_{3x_1}^2 u_{3x_1x_1}\right)\\
&+24C_T I_{66}\frac{\partial}{\partial x_1}\left(u_{3x_1}u_{3x_1x_1}\phi_{x_1}\right) + 12C_T I_{55}\frac{\partial}{\partial x_1}\left(u_{3x_1}^2\phi\right)\\
&-12C_T I_{66}\frac{\partial^2}{\partial x_1^2}\left(u_{3x_1}^2\phi_{x_1}\right) + 12C_T I_{99}\frac{\partial}{\partial x_1}\left(u_{3x_1}\phi_{x_1}^2\right)\\
&+4C_T I_{55}\frac{\partial}{\partial x_1}\left(u_{3x_1}\phi^2\right) + 12C_T I_{00}\frac{\partial}{\partial x_1}\left(u_{1x_1}u_{3x_1}^3\right)\\
&+15C_T I_{00}\frac{\partial}{\partial x_1}\left(u_{30x_1}u_{3x_1}^4\right) + 3C_T I_{00}\frac{\partial}{\partial x_1}\left(u_{3x_1}^5\right) = F\cos(\omega t),
\end{aligned}
\tag{B.2}
$$

$$
\begin{aligned}
&\rho I_{66}u_{3x_1tt} + \rho I_{99}\phi_{tt} - \xi_k I_{66}u_{3x_1x_1x_1t} + \frac{1}{2}\xi_k I_{55}u_{3x_1t} - \xi_k I_{99}\phi_{x_1x_1t}\\
&+\frac{1}{2}\xi_k I_{55}\phi_t + 2\xi_k I_{66}\frac{\partial}{\partial x}\left(u_{3x_1x_1}u_{1x_1t}\right)\\
&-\xi_k I_{55}u_{3x_1}u_{1x_1t} + 2\xi_k I_{99}\frac{\partial}{\partial x}\left(\phi_{x_1}u_{1x_1t}\right) - \xi_k I_{55}\phi u_{1x_1t}\\
&+2\xi_k I_{66}\frac{\partial}{\partial x}\left(u_{1x_1}u_{3x_1x_1t}\right) + 2\xi_k I_{66}\frac{\partial}{\partial x}\left(u_{3x_1x_1}u_{30x_1}u_{3x_1t}\right)\\
&-\xi_k I_{55}u_{3x_1}u_{30x_1}u_{3x_1t} + 2\xi_k I_{99}\frac{\partial}{\partial x}\left(\phi_x u_{30x_1}u_{3x_1t}\right) - \xi_k I_{55}\phi u_{30x_1}u_{3x_1t} + 2\xi_k I_{99}\frac{\partial}{\partial x}\left(u_{1x_1}\phi_{x_1t}\right)\\
&+2\xi_k I_{99}\frac{\partial}{\partial x}\left(u_{3x_1}u_{30x_1}\phi_{x_1t}\right) + 2\xi_k I_{66}\frac{\partial}{\partial x}\left(u_{3x_1}u_{3x_1x_1}u_{3x_1t}\right)\\
&+\xi_k I_{66}\frac{\partial}{\partial x}\left(u_{3x_1}^2 u_{3x_1x_1t}\right) + 2\xi_k\, I_{66}\frac{\partial}{\partial x}\left(u_{3x_1}u_{30x_1}u_{3x_1x_1t}\right)\\
&-\xi_k I_{55}u_{3x_1}^2 u_{3x_1t} + 2\xi_k I_{99}\frac{\partial}{\partial x}\left(u_{3x_1}\phi_{x_1}u_{3x_1t}\right) - \xi_k I_{55}u_{3x_1}\phi u_{3x_1t}\\
&+\xi_k I_{99}\frac{\partial}{\partial x}\left(u_{3x_1}^2\phi_{x_1t}\right) - 8C_T I_{66}u_{3x_1x_1x_1} + 8C_T I_{55}u_{3x_1}\\
&-8C_T I_{99}\phi_{x_1x_1} + 8C_T I_{55}\phi\ + 24C_T I_{66}\frac{\partial}{\partial x_1}\left(u_{1x_1}u_{3x_1x_1}\right)\\
&-8C_T I_{55}u_{1x_1}u_{3x_1} + 24C_T I_{99}\frac{\partial}{\partial x_1}\left(u_{1x_1}\phi_{x_1}\right) - 8C_T I_{55}u_{1x_1}\phi\\
&+24C_T I_{66}\frac{\partial}{\partial x_1}\left(u_{3x_1}u_{3x_1x_1}u_{30x_1}\right) - 8C_T I_{55}u_{3x_1}^2 u_{30x_1}\\
&+24C_T I_{99}\frac{\partial}{\partial x_1}\left(u_{3x_1}\phi_{x_1}u_{30x_1}\right) - 8C_T I_{55}u_{3x_1}\phi u_{30x_1}
\end{aligned}
$$

$$+12C_T I_{66}\frac{\partial}{\partial x_1}\left(u_{3x_1}^2 u_{3x_1x_1}\right)-4C_T I_{55}u_{3x_1}^3+12C_T I_{99}\frac{\partial}{\partial x_1}\left(u_{3x_1}^2\phi_{x_1}\right)-4C_T I_{55}u_{3x_1}^2\phi=0. \tag{B.3}$$

Appendix C

$$C_{11}^{NL}:+2\xi_k I_{00}\frac{1}{\eta}\int_0^1 U_l(x_1)\frac{\mathrm{d}}{\mathrm{d}x_1}\left(U_i'(x_1)\,U_j'(x_1)\right)\mathrm{d}x, \tag{C.1}$$

$$C_{12}^{NL}:+2\xi_k I_{00}\int_0^1 U_l(x_1)\frac{\mathrm{d}}{\mathrm{d}x_1}\left(U_i'(x_1)\,W_j'(x_1)\,W_0'(x_1)\right)\mathrm{d}x, \tag{C.2}$$

$$C_{13}^{NL}:+2\xi_k I_{00}\int_0^1 U_l(x_1)\frac{\mathrm{d}}{\mathrm{d}x_1}\left(U_i'(x_1)\,W_j'(x_1)\,W_0'(x_1)\right)\mathrm{d}x_1, \tag{C.3}$$

$$\begin{aligned}C_{14}^{NL}:&-\xi_k I_{77}\frac{1}{\eta}\int_0^1 U_l(x_1)\frac{\mathrm{d}}{\mathrm{d}x_1}\left(W_i'(x_1)\,W_j'(x_1)\right)\mathrm{d}x_1\\&+2\xi_k\eta\int_0^1 U_l(x_1)\frac{\mathrm{d}}{\mathrm{d}x_1}\left(W_i''(x_1)\,W_j''(x_1)\right)\mathrm{d}x_1\\&+2\xi_k I_{00}\eta\int_0^1 U_l(x_1)\frac{\mathrm{d}}{\mathrm{d}x_1}\left(W_i'(x_1)\,W_j'(x_1)\,W_0'^2(x_1)\right)\mathrm{d}x_1,\end{aligned} \tag{C.4}$$

$$\begin{aligned}C_{15}^{NL}:&+2\xi_k I_{66}\int_0^1 U_l(x_1)\frac{\mathrm{d}}{\mathrm{d}x_1}\left(W_i''(x_1)\,\psi_j'(x_1)\right)\mathrm{d}x_1\\&+\xi_k I_{55}\frac{1}{\eta^2}\int_0^1 U_l(x_1)\frac{\mathrm{d}}{\mathrm{d}x_1}\left(W_i'(x_1)\,\psi_j(x_1)\right)\mathrm{d}x_1,\end{aligned} \tag{C.5}$$

$$\begin{aligned}C_{16}^{NL}:&+2\xi_k I_{66}\int_0^1 U_l(x_1)\frac{\mathrm{d}}{\mathrm{d}x_1}\left(W_i''(x_1)\,\psi_j'(x_1)\right)\mathrm{d}x_1\\&+\xi_k I_{55}\frac{1}{\eta^2}\int_0^1 U_l(x_1)\frac{\mathrm{d}}{\mathrm{d}x_1}\left(W_i'(x_1)\,\psi_j(x_1)\right)\mathrm{d}x_1,\end{aligned} \tag{C.6}$$

$$\begin{aligned}C_{17}^{NL}:&+2\xi_k I_{99}\frac{1}{\eta}\int_0^1 U_l(x_1)\frac{\mathrm{d}}{\mathrm{d}x_1}\left(\psi_i'(x_1)\,\psi_j'(x_1)\right)\mathrm{d}x_1\\&+\xi_k I_{55}\frac{1}{\eta^3}\int_0^1 U_l(x_1)\frac{\mathrm{d}}{\mathrm{d}x_1}\left(\psi_i(x_1)\,\psi_j(x_1)\right)\mathrm{d}x_1,\end{aligned} \tag{C.7}$$

$$C_{18}^{NL}:+\xi_k I_{00}\int_0^1 U_l(x_1)\frac{\mathrm{d}}{\mathrm{d}x_1}\left(U_i'(x_1)\,W_j'(x_1)\,W_k'(x_1)\right)\mathrm{d}x_1, \tag{C.8}$$

$$C_{19}^{NL} : +2\xi_k I_{00} \int_0^1 U_l\,(x_1) \frac{\mathrm{d}}{\mathrm{d}x_1} \left(U_i'\,(x_1)\, W_j'\,(x_1)\, W_k'\,(x_1) \right) \mathrm{d}x_1, \tag{C.9}$$

$$C_{110}^{NL} : +3\xi_k I_{00}\eta \int_0^1 U_l\,(x_1) \frac{\mathrm{d}}{\mathrm{d}x_1} \left(W_i'\,(x_1)\, W_j'\,(x_1)\, W_k'\,(x_1)\, W_0^{'}\,(x_1) \right) \mathrm{d}x_1, \tag{C.10}$$

$$C_{111}^{NL} : +\xi_k I_{00}\eta \int_0^1 U_l\,(x_1) \frac{\mathrm{d}}{\mathrm{d}x_1} \left(W_i'\,(x_1)\, W_j'\,(x_1)\, W_k'\,(x_1)\, W_m'\,(x_1) \right) \mathrm{d}x_1, \tag{C.11}$$

$$C_{21}^{NL} : +2\xi_k I_{00} \int_0^1 W_l\,(x_1) \frac{\mathrm{d}}{\mathrm{d}x_1} \left(U_i'\,(x_1)\, U_j'\,(x_1)\, W_0'\,(x_1) \right) \mathrm{d}x_1, \tag{C.12}$$

$$\begin{aligned} C_{22}^{NL} : &+2\xi_k I_{00}\eta \int_0^1 W_l\,(x_1) \frac{\mathrm{d}}{\mathrm{d}x_1} \left(U_i'\,(x_1)\, W_j'\,(x_1)\, W_0'^2\,(x_1) \right) \mathrm{d}x_1 \\ &-\xi_k I_{77} \frac{1}{\eta} \int_0^1 W_l\,(x_1) \frac{\mathrm{d}}{\mathrm{d}x_1} \left(U_i'\,(x_1)\, W_j'\,(x_1) \right) \mathrm{d}x_1 \\ &-2\,\xi_k I_{00}\eta \int_0^1 W_l\,(x_1) \frac{\mathrm{d}^2}{\mathrm{d}x_1^2} \left(U_i'\,(x_1)\, W_j''\,(x_1) \right) \mathrm{d}x_1, \end{aligned} \tag{C.13}$$

$$\begin{aligned} C_{23}^{NL} : &-2\xi_k I_{66} \int_0^1 W_l\,(x_1) \frac{\mathrm{d}^2}{\mathrm{d}x_1^2} \left(U_i'\,(x_1)\, \psi_j'\,(x_1) \right) \mathrm{d}x_1 \\ &+\xi_k I_{55} \frac{1}{\eta^2} \int_0^1 W_l\,(x_1) \frac{\mathrm{d}}{\mathrm{d}x_1} \left(U_i'\,(x_1)\, \psi_j\,(x_1) \right) \mathrm{d}x_1, \end{aligned} \tag{C.14}$$

$$\begin{aligned} C_{24}^{NL} : &+2\xi_k I_{00}\eta \int_0^1 W_l\,(x_1) \frac{\mathrm{d}}{\mathrm{d}x_1} \left(U_i'\,(x_1)\, W_j'\,(x_1)\, W_0'^2\,(x_1) \right) \mathrm{d}x_1 \\ &-2\,\xi_k \eta \int_0^1 W_l\,(x_1) \frac{\mathrm{d}^2}{\mathrm{d}x_1^2} \left(U_i'\,(x_1)\, W_j''\,(x_1) \right) \mathrm{d}x_1, \end{aligned} \tag{C.15}$$

$$\begin{aligned} C_{25}^{NL} : &+2\xi_k I_{00}\eta^2 \int_0^1 W_l\,(x_1) \frac{\mathrm{d}}{\mathrm{d}x_1} \left(W_i'\,(x_1)\, W_j'\,(x_1)\, W_0'^3\,(x_1) \right) \mathrm{d}x_1 \\ &+2\xi_k \eta^2 \int_0^1 W_l\,(x_1) \frac{\mathrm{d}}{\mathrm{d}x_1} \left(W_i''\,(x_1)\, W_j''\,(x_1)\, W_0'\,(x_1) \right) \mathrm{d}x_1 \\ &-2\xi_k I_{77} \int_0^1 W_l\,(x_1) \frac{\mathrm{d}}{\mathrm{d}x_1} \left(W_i'\,(x_1)\, W_j'\,(x_1)\, W_0'\,(x_1) \right) \mathrm{d}x_1 \\ &-2\xi_k \eta^2 \int_0^1 W_l\,(x_1) \frac{\mathrm{d}^2}{\mathrm{d}x_1^2} \left(W_i'\,(x_1)\, W_j''\,(x_1)\, W_0'\,(x_1) \right) \mathrm{d}x_1, \end{aligned} \tag{C.16}$$

$$C_{26}^{NL}: +2\xi_k I_{66}\eta \int_0^1 W_l(x_1)\frac{\mathrm{d}}{\mathrm{d}x_1}\left(W_i''(x_1)\,\psi_j'(x_1)\,W_0'(x_1)\right)\mathrm{d}x_1$$
$$+2\xi_k I_{55}\frac{1}{\eta}\int_0^1 W_l(x_1)\frac{\mathrm{d}}{\mathrm{d}x_1}\left(W_i'(x_1)\,\psi_j(x_1)\,W_0'(x_1)\right)\mathrm{d}x_1$$
$$-2\xi_k I_{66}\eta \int_0^1 W_l(x_1)\frac{\mathrm{d}^2}{\mathrm{d}x_1^2}\left(W_i'(x_1)\,\psi_j'(x_1)\,W_0'(x_1)\right)\mathrm{d}x_1, \tag{C.17}$$

$$C_{27}^{NL}: -2\xi_k I_{66}\int_0^1 W_l(x)\frac{\mathrm{d}^2}{\mathrm{d}x_1^2}\left(U_i'(x_1)\,\psi_j'(x_1)\right)\mathrm{d}x_1, \tag{C.18}$$

$$C_{28}^{NL}: +2\xi_k I_{66}\eta \int_0^1 W_l(x_1)\frac{\mathrm{d}}{\mathrm{d}x_1}\left(W_i''(x_1)\,\psi_j'(x_1)\,W_0'(x_1)\right)\mathrm{d}x_1$$
$$+\xi_k I_{55}\frac{1}{\eta}\int_0^1 W_l(x_1)\frac{\mathrm{d}}{\mathrm{d}x_1}\left(W_i'(x_1)\,\psi_j(x_1)\,W_0'(x_1)\right)\mathrm{d}x_1$$
$$-2\xi_k I_{66}\eta \int_0^1 W_l(x_1)\frac{\mathrm{d}^2}{\mathrm{d}x_1^2}\left(W_i'(x_1)\,\psi_j'(x_1)\,W_0'(x_1)\right)\mathrm{d}x_1, \tag{C.19}$$

$$C_{29}^{NL}: +2\xi_k I_{99}\int_0^1 W_l(x_1)\frac{\mathrm{d}}{\mathrm{d}x_1}\left(\psi_i'(x_1)\,\psi_j'(x_1)\,W_0'(x_1)\right)\mathrm{d}x_1$$
$$+\xi_k I_{55}\frac{1}{\eta^2}\int_0^1 W_l(x_1)\frac{\mathrm{d}}{\mathrm{d}x_1}\left(\psi_i(x_1)\,\psi_j(x_1)\,W_0'(x_1)\right)\mathrm{d}x_1, \tag{C.20}$$

$$C_{210}^{NL}: +2\xi_k I_{00}\int_0^1 W_l(x_1)\frac{\mathrm{d}}{\mathrm{d}x_1}\left(U_i'(x_1)\,U_j'(x_1)\,W_k'(x_1)\right)\mathrm{d}x_1, \tag{C.21}$$

$$C_{211}^{NL}: +3\xi_k I_{00}\eta \int_0^1 W_l(x_1)\frac{\mathrm{d}}{\mathrm{d}x_1}\left(U_i'(x_1)\,W_j'(x_1)\,W_k'(x_1)\,W_0'(x_1)\right)\mathrm{d}x_1, \tag{C.22}$$

$$C_{212}^{NL}: +4\xi_k I_{00}\eta \int_0^1 W_l(x_1)\frac{\mathrm{d}}{\mathrm{d}x_1}\left(U_i'(x_1)\,W_j'(x_1)\,W_k'(x_1)\,W_0'(x_1)\right)\mathrm{d}x_1, \tag{C.23}$$

$$C_{213}^{NL}: +5\xi_k I_{00}\eta^2 \int_0^1 W_l(x_1)\frac{\mathrm{d}}{\mathrm{d}x_1}\left(W_i'(x_1)\,W_j'(x_1)\,W_k'(x_1)\,W_0'^2(x_1)\right)\mathrm{d}x_1$$
$$-\xi_k I_{88}\int_0^1 W_l(x_1)\frac{\mathrm{d}}{\mathrm{d}x_1}\left(W_i'(x_1)\,W_j'(x_1)\,W_k'(x_1)\right)\mathrm{d}x_1$$
$$+2\xi_k\,\eta^2 \int_0^1 W_l(x_1)\frac{\mathrm{d}}{\mathrm{d}x_1}\left(W_i'(x_1)\,W_j''(x_1)\,W_k''(x_1)\right)\mathrm{d}x_1$$

$$-3\xi_k\,\eta^2\int_0^1 W_l\,(x_1)\frac{\mathrm{d}^2}{\mathrm{d}x_1^2}\left(W_i'\,(x_1)\,W_j'\,(x_1)\,W_k''\,(x_1)\right)\mathrm{d}x_1, \tag{C.24}$$

$$\begin{aligned}C_{214}^{NL}:&+2\xi_k\,I_{66}\eta\int_0^1 W_l\,(x_1)\frac{\mathrm{d}}{\mathrm{d}x_1}\left(W_i'\,(x_1)\,W_j''\,(x_1)\,\psi_k'\,(x_1)\right)\mathrm{d}x_1\\&+2\xi_k I_{55}\frac{1}{\eta}\int_0^1 W_l\,(x_1)\frac{\mathrm{d}}{\mathrm{d}x_1}\left(W_i'\,(x_1)\,W_j'\,(x_1)\,\psi_k\,(x_1)\right)\mathrm{d}x_1\\&-2\xi_k I_{66}\eta\int_0^1 W_l\,(x_1)\frac{\mathrm{d}^2}{\mathrm{d}x_1^2}\left(W_i'\,(x_1)\,W_j'\,(x_1)\,\psi_k'\,(x_1)\right)\mathrm{d}x_1,\end{aligned} \tag{C.25}$$

$$\begin{aligned}C_{215}^{NL}:&+2\,\xi_k I_{66}\eta\int_0^1 W_l\,(x_1)\frac{\mathrm{d}}{\mathrm{d}x_1}\left(W_i'\,(x_1)\,W_j''\,(x_1)\,\psi_k'\,(x_1)\right)\mathrm{d}x_1\\&+\xi_k I_{55}\frac{1}{\eta}\int_0^1 W_l\,(x_1)\frac{\mathrm{d}}{\mathrm{d}x_1}\left(W_i'\,(x_1)\,W_j'\,(x_1)\,\psi_k\,(x_1)\right)\mathrm{d}x_1\\&-\xi_k I_{66}\eta\int_0^1 W_l\,(x_1)\frac{\mathrm{d}^2}{\mathrm{d}x_1^2}\left(W_i'\,(x_1)\,W_j'\,(x_1)\,\psi_k'\,(x_1)\right)\mathrm{d}x_1,\end{aligned} \tag{C.26}$$

$$\begin{aligned}C_{216}^{NL}:&+2\xi_k I_{99}\int_0^1 W_l\,(x_1)\frac{\mathrm{d}}{\mathrm{d}x_1}\left(W_i'\,(x_1)\,\psi_j'\,(x_1)\,\psi_k'\,(x_1)\right)\mathrm{d}x_1\\&+\xi_k I_{55}\frac{1}{\eta^2}\int_0^1 W_l\,(x_1)\frac{\mathrm{d}}{\mathrm{d}x_1}\left(W_i'\,(x_1)\,\psi_j\,(x_1)\,\psi_k\,(x_1)\right)\mathrm{d}x_1,\end{aligned} \tag{C.27}$$

$$C_{217}^{NL}:+\xi_k I_{00}\eta\int_0^1 W_l\,(x_1)\frac{\mathrm{d}}{\mathrm{d}x_1}\left(U_i'\,(x_1)\,W_j'\,(x_1)\,W_k'\,(x_1)\,W_m'\,(x_1)\right)\mathrm{d}x_1, \tag{C.28}$$

$$C_{218}^{NL}:+2\xi_k I_{00}\eta\int_0^1 W_l\,(x_1)\frac{\mathrm{d}}{\mathrm{d}x_1}\left(U_i'\,(x_1)\,W_j'\,(x_1)\,W_k'\,(x_1)\,W_m'\,(x_1)\right)\mathrm{d}x_1, \tag{C.29}$$

$$C_{219}^{NL}:+4\xi_k I_{00}\eta^2\int_0^1 W_l\,(x_1)\frac{\mathrm{d}}{\mathrm{d}x_1}\left(W_i'\,(x_1)\,W_j'\,(x_1)\,W_k'\,(x_1)\,W_m'\,(x_1)\,W_0'\,(x_1)\right)\mathrm{d}x_1, \tag{C.30}$$

$$C_{220}^{NL}:+\xi_k I_{00}\eta^2\int_0^1 W_l\,(x_1)\frac{\mathrm{d}}{\mathrm{d}x_1}\left(W_i'\,(x_1)\,W_j'\,(x_1)\,W_k'\,(x_1)\,W_m'\,(x_1)\,W_n'\,(x_1)\right)\mathrm{d}x_1, \tag{C.31}$$

$$C_{31}^{NL}:+2\xi_k I_{66}\eta^2\int_0^1 \psi_l\,(x_1)\frac{\mathrm{d}}{\mathrm{d}x_1}\left(U_j'\,(x_1)\,W_j''\,(x_1)\right)\mathrm{d}x_1-\xi_k I_{55}\int_0^1 \psi_l\,(x_1)U_i'\,(x_1)\,W_j'\,(x_1)\,\mathrm{d}x_1, \tag{C.32}$$

$$C_{32}^{NL}:+2\xi_k I_{99}\eta\int_0^1 \psi_l\,(x_1)\frac{\mathrm{d}}{\mathrm{d}x_1}\left(U_i'\,(x_1)\,\psi_j'\,(x_1)\right)\mathrm{d}x_1-\xi_k I_{55}\frac{1}{\eta}\int_0^1 \psi_l\,(x_1)U_i'\,(x_1)\,\psi_j\,(x_1)\,\mathrm{d}x_1, \tag{C.33}$$

$$C_{33}^{NL}:+2\xi_k I_{66}\eta^2\int_0^1\psi_l\left(x_1\right)\frac{\mathrm{d}}{\mathrm{d}x_1}\left(U_j'\left(x_1\right)W_j''\left(x_1\right)\right)\mathrm{d}x_1, \tag{C.34}$$

$$C_{34}^{NL}:+4\xi_k I_{66}\eta^3\int_0^1\psi_l\left(x_1\right)\frac{\mathrm{d}}{\mathrm{d}x_1}\left(W_i'\left(x_1\right)W_j''\left(x_1\right)W_0'\left(x_1\right)\right)\mathrm{d}x_1$$

$$-\xi_k I_{55}\eta\int_0^1\psi_l\left(x_1\right)W_i'\left(x_1\right)W_j'\left(x_1\right)W_0'\left(x_1\right)\mathrm{d}x_1, \tag{C.35}$$

$$C_{35}^{NL}:+2\xi_k I_{99}\eta^2\int_0^1\psi_l\left(x_1\right)\frac{\mathrm{d}}{\mathrm{d}x_1}\left(W_i'\left(x_1\right)\psi_i'\left(x_1\right)W_0'\left(x_1\right)\right)\mathrm{d}x_1$$

$$-\xi_k I_{55}\int_0^1\psi_l\left(x_1\right)W_i'\left(x_1\right)\psi_i\left(x_1\right)W_0'\left(x_1\right)\mathrm{d}x_1, \tag{C.36}$$

$$C_{36}^{NL}:+2\xi_k I_{99}\eta\int_0^1\psi_l\left(x_1\right)\frac{\mathrm{d}}{\mathrm{d}x_1}\left(U_i'\left(x_1\right)\psi_j'\left(x_1\right)\right)\mathrm{d}x_1, \tag{C.37}$$

$$C_{37}^{NL}:+2\xi_k I_{99}\eta^2\int_0^1\psi_l\left(x_1\right)\frac{\mathrm{d}}{\mathrm{d}x_1}\left(W_i'\left(x_1\right)\psi_i'\left(x_1\right)W_0'\left(x_1\right)\right)\mathrm{d}x_1, \tag{C.38}$$

$$C_{38}^{NL}:+3\xi_k I_{66}\eta^3\int_0^1\psi_l\left(x_1\right)\frac{\mathrm{d}}{\mathrm{d}x_1}\left(W_i'\left(x_1\right)W_j'\left(x_1\right)W_k''\left(x_1\right)\right)\mathrm{d}x_1$$

$$-\xi_k I_{55}\eta\int_0^1\psi_l\left(x_1\right)W_i'\left(x_1\right)W_j'\left(x_1\right)W_k'\left(x_1\right)\mathrm{d}x_1, \tag{C.39}$$

$$C_{39}^{NL}:+2\xi_k I_{99}\eta^2\int_0^1\psi_l\left(x_1\right)\frac{\mathrm{d}}{\mathrm{d}x_1}\left(W_i'\left(x_1\right)W_j'\left(x_1\right)\psi_k'\left(x_1\right)\right)\mathrm{d}x_1$$

$$-\xi_k I_{55}w_x\phi w_{xt}\int_0^1\psi_l\left(x_1\right)W_i'\left(x_1\right)W_j'\left(x_1\right)\psi_k\left(x_1\right)\mathrm{d}x_1, \tag{C.40}$$

$$C_{310}^{NL}:+\xi_k I_{99}\eta^2\int_0^1\psi_l\left(x_1\right)\frac{\mathrm{d}}{\mathrm{d}x_1}\left(W_i'\left(x_1\right)W_j'\left(x_1\right)\psi_k'\left(x_1\right)\right)\mathrm{d}x_1, \tag{C.41}$$

References

1. Yu, L., Zhang, D., Fang, Q., Cao, L., Xu, T., Li, Q.: Surface settlement of subway station construction using pile-beam-arch approach. Tunn. Undergr. Space Technol. **90**, 340–356 (2019)
2. Li, B., Wang, Z.: Numerical study on the response of ground movements to construction activities of a metro station using the pile-beam-arch method. Tunn. Undergr. Space Technol. **88**, 209–220 (2019)
3. Chen, X., Zhang, X., Wang, L., Chen, L.: An arch-linear composed beam piezoelectric energy harvester with magnetic coupling: design, modeling and dynamic analysis. J. Sound Vib. **513**, 116394 (2021)
4. Zhang, X., Chen, L., Chen, X., Zhu, F., Guo, Y.: Time-domain dynamic characteristics analysis and experimental research of tri-stable piezoelectric energy harvester. Micromachines **12**, 1045 (2021)
5. Tzou, H., Zhang, X.: A flexoelectric double-curvature nonlinear shell energy harvester. J. Vib. Acoust. **138**, 031006 (2016)

6. Zhang, X., Zuo, M., Yang, W., Wan, X.: A tri-stable piezoelectric vibration energy harvester for composite shape beam: nonlinear modeling and analysis. Sensors **20**, 1370 (2020)
7. Yang, Z., Wang, Y.Q., Zuo, L., Zu, J.: Introducing arc-shaped piezoelectric elements into energy harvesters. Energy Convers. Manag. **148**, 260–266 (2017)
8. Hafiz, M.A.A., Kosuru, L., Ramini, A., Chappanda, K.N., Younis, M.I.: In-plane MEMS shallow arch beam for mechanical memory. Micromachines **7**, 191 (2016)
9. Liu, N., Plucinsky, P., Jeffers, A.E.: Combining load-controlled and displacement-controlled algorithms to model thermal-mechanical snap-through instabilities in structures. J. Eng. Mech. **143**, 04017051 (2017)
10. Zhao, B., Long, C., Peng, X., Chen, J., Liu, T., Zhang, Z., Lai, A.: Size effect and geometrically nonlinear effect on thermal post-buckling of micro-beams: a new theoretical analysis. Contin. Mech. Thermodyn. **34**, 519–532 (2022)
11. Liu, N., Jeffers, A.E.: Adaptive isogeometric analysis in structural frames using a layer-based discretization to model spread of plasticity. Comput. Struct. **196**, 1–11 (2018)
12. Liu, N., Jeffers, A.E.: Isogeometric analysis of laminated composite and functionally graded sandwich plates based on a layerwise displacement theory. Compos. Struct. **176**, 143–153 (2017)
13. Liu, N., Jeffers, A.E.: A geometrically exact isogeometric Kirchhoff plate: feature-preserving automatic meshing and C 1 rational triangular Bézier spline discretizations. Int. J. Numer. Methods Eng. **115**, 395–409 (2018)
14. Surana, K., Mysore, D., Reddy, J.: Thermodynamic consistency of beam theories in the context of classical and non-classical continuum mechanics and a thermodynamically consistent new formulation. Contin. Mech. Thermodyn. **31**, 1283–1312 (2019)
15. Malikan, M., Wiczenbach, T., Eremeyev, V.A.: Thermal buckling of functionally graded piezomagnetic micro-and nanobeams presenting the flexomagnetic effect. Contin. Mech. Thermodyn. **34**, 1051–1066 (2022)
16. Liu, N., Ren, X., Lua, J.: An isogeometric continuum shell element for modeling the nonlinear response of functionally graded material structures. Compos. Struct. **237**, 111893 (2020)
17. Liu, N., Johnson, E.L., Rajanna, M.R., Lua, J., Phan, N., Hsu, M.-C.: Blended isogeometric Kirchhoff–Love and continuum shells. Comput. Methods Appl. Mech. Eng. **385**, 114005 (2021)
18. Cazzani, A., Malagù, M., Turco, E.: Isogeometric analysis: a powerful numerical tool for the elastic analysis of historical masonry arches. Contin. Mech. Thermodyn. **28**, 139–156 (2016)
19. de Leo, A.M., Contento, A., Di Egidio, A.: Semi-analytical approach for the study of linear static behaviour and buckling of shells with single constant curvature. Contin. Mech. Thermodyn. **27**, 767–785 (2015)
20. Liu, N., Lua, J., Rajanna, M.R., Johnson, E., Hsu, M.-C., Phan, N.D.: Buffet-induced structural response prediction of aircraft horizontal stabilizers based on immersogeometric analysis and an isogeometric blended shell approach. In: AIAA SCITECH 2022 Forum, p. 0852 (2022)
21. Liu, N., Hsu, M.-C., Lua, J., Phan, N.: A large deformation isogeometric continuum shell formulation incorporating finite strain elastoplasticity. Comput. Mech. **70**, 965–976 (2022)
22. Chróścielewski, J., Schmidt, R., Eremeyev, V.A.: Nonlinear finite element modeling of vibration control of plane rod-type structural members with integrated piezoelectric patches. Contin. Mech. Thermodyn. **31**, 147–188 (2019)
23. Liu, N., Rajanna, M.R., Johnson, E.L., Lua, J., Phan, N., Hsu, M.-C.: Isogeometric blended shells for dynamic analysis: simulating aircraft takeoff and the resulting fatigue damage on the horizontal stabilizer. Comput. Mech. **70**, 1013–1024 (2022)
24. Yang, Z., Zhao, S., Yang, J., Lv, J., Liu, A., Fu, J.: In-plane and out-of-plane free vibrations of functionally graded composite arches with graphene reinforcements. Mech. Adv. Mater. Struct. **28**, 2046–2056 (2021)
25. Zhao, S., Yang, Z., Kitipornchai, S., Yang, J.: Dynamic instability of functionally graded porous arches reinforced by graphene platelets. Thin-Walled Struct. **147**, 106491 (2020)
26. Ghayesh, M.H., Farokhi, H.: Mechanics of tapered axially functionally graded shallow arches. Compos. Struct. **188**, 233–241 (2018)
27. Farokhi, H., Ghayesh, M.H., Hussain, S.: Pull-in characteristics of electrically actuated MEMS arches. Mech. Mach. Theory **98**, 133–150 (2016)
28. Bacciocchi, M., Tarantino, A.M.: Bending of hyperelastic beams made of transversely isotropic material in finite elasticity. Appl. Math. Modell. **100**, 55–76 (2021)
29. Du, P., Dai, H.-H., Wang, J., Wang, Q.: Analytical study on growth-induced bending deformations of multi-layered hyperelastic plates. Int. J. Non-Linear Mech. **119**, 103370 (2020)
30. Bacciocchi, M., Tarantino, A.M.: Finite bending of hyperelastic beams with transverse isotropy generated by longitudinal porosity. Eur. J. Mech. A Solids **85**, 104131 (2021)
31. Herrmann, H.: A constitutive model for linear hyperelastic materials with orthotropic inclusions by use of quaternions. Contin. Mech. Thermodyn. **33**, 1375–1384 (2021)
32. Breslavsky, I.D., Amabili, M., Legrand, M.: Nonlinear vibrations of thin hyperelastic plates. J. Sound Vib. **333**, 4668–4681 (2014)
33. Amabili, M., Breslavsky, I., Reddy, J.: Nonlinear higher-order shell theory for incompressible biological hyperelastic materials. Comput. Methods Appl. Mech. Eng. **346**, 841–861 (2019)
34. Amabili, M., Balasubramanian, P., Breslavsky, I.D., Ferrari, G., Garziera, R., Riabova, K.: Experimental and numerical study on vibrations and static deflection of a thin hyperelastic plate. J. Sound Vib. **385**, 81–92 (2016)
35. Breslavsky, I.D., Amabili, M., Legrand, M.: Static and dynamic behavior of circular cylindrical shell made of hyperelastic arterial material. J. Appl. Mech. **83**, 051002 (2016)
36. Lanzoni, L., Tarantino, A.M.: Finite anticlastic bending of hyperelastic solids and beams. J. Elast. **131**, 137–170 (2018)
37. Lanzoni, L., Tarantino, A.M.: Nonuniform bending theory of hyperelastic beams in finite elasticity. Int. J. Non-Linear Mech. **135**, 103765 (2021)
38. Lanzoni, L., Tarantino, A.M.: The bending of beams in finite elasticity. J. Elast. **139**, 91–121 (2020)
39. Khaniki, H.B., Ghayesh, M.H., Chin, R., Chen, L.-Q.: Experimental characteristics and coupled nonlinear forced vibrations of axially travelling hyperelastic beams. Thin-Walled Struct. **170**, 108526 (2022)

40. Khaniki, H.B., Ghayesh, M.H., Chin, R., Hussain, S.: Nonlinear continuum mechanics of thick hyperelastic sandwich beams using various shear deformable beam theories. Contin. Mech. Thermodyn. **34**, 781–827 (2022)
41. Khaniki, H.B., Ghayesh, M.H., Chin, R., Amabili, M.: Large amplitude vibrations of imperfect porous-hyperelastic beams via a modified strain energy. J. Sound Vib. **513**, 116416 (2021)
42. Khaniki, H.B., Ghayesh, M.H., Chin, R., Amabili, M.: A review on the nonlinear dynamics of hyperelastic structures. Nonlinear Dyn. **110**, 963–994 (2022)
43. Altmeyer, G., Panicaud, B., Rouhaud, E., Wang, M., Roos, A., Kerner, R.: Viscoelasticity behavior for finite deformations, using a consistent hypoelastic model based on Rivlin materials. Contin. Mech. Thermodyn. **28**, 1741–1758 (2016)
44. Menga, N., Bottiglione, F., Carbone, G.: Nonlinear viscoelastic isolation for seismic vibration mitigation. Mech. Syst. Signal Process. **157**, 107626 (2021)
45. Penas, R., Balmes, E., Gaudin, A.: A unified non-linear system model view of hyperelasticity, viscoelasticity and hysteresis exhibited by rubber. Mech. Syst. Signal Process. **170**, 108793 (2022)
46. Huang, Y., Oterkus, S., Hou, H., Oterkus, E., Wei, Z., Zhang, S.: Peridynamic model for visco-hyperelastic material deformation in different strain rates. Contin. Mech. Thermodyn. **34**, 977–1011 (2019)
47. Buchen, S., Kröger, N.H., Reppel, T., Weinberg, K.: Time-dependent modeling and experimental characterization of foamed EPDM rubber. Contin. Mech. Thermodyn. **33**, 1747–1764 (2021)
48. Li, L., Maccabi, A., Abiri, A., Juo, Y.-Y., Zhang, W., Chang, Y.-J., Saddik, G.N., Jin, L., Grundfest, W.S., Dutson, E.P.: Characterization of perfused and sectioned liver tissue in a full indentation cycle using a visco-hyperelastic model. J. Mech. Behav. Biomed. Mater. **90**, 591–603 (2019)
49. Amabili, M.: Nonlinear Vibrations and Stability of Shells and Plates. Cambridge University Press (2008)
50. Bower, A.F.: Applied Mechanics of Solids. CRC Press (2009)
51. Rivlin, R.: Large elastic deformations of isotropic materials VI. Further results in the theory of torsion, shear and flexure. Philos. Trans. R. Soc. Lond. Ser. A Math. Phys. Sci. **242**, 173–195 (1949)
52. Mooney, M.: A theory of large elastic deformation. J. Appl. Phys. **11**, 582–592 (1940)
53. Xiang, H., Yang, J.: Free and forced vibration of a laminated FGM Timoshenko beam of variable thickness under heat conduction. Compos. Part B Eng. **39**, 292–303 (2008)
54. Reddy, J.N.: Mechanics of Laminated Composite Plates and Shells: Theory and Analysis. CRC Press (2003)
55. Fukahori, Y., Seki, W.: Molecular behaviour of elastomeric materials under large deformation: 1. Re-evaluation of the Mooney–Rivlin plot. Polymer **33**, 502–508 (1992)
56. ANSYS®Multiphysics^{TM}, Workbench 19.2, Workbench User's Guide, ANSYS Workbench Systems, Analysis Systems, Static Structural
57. Meyers, M.A., Chawla, K.K.: Mechanical Behavior of Materials. Cambridge University Press (2008)

Chapter 7

Hyperelastic plates with modal interactions

Overview

This chapter concentrates on the nonlinear mechanics of hyperelastic plates. Both theoretical and experimental analyses are presented here to understand the nonlinear dynamic response of the structure under different conditions. For the experimental part, different equipment was used and an external excitation setup was prepared. The sensitivity of the structure to the existence of attached mass was studied. The hyperelastic characterisation of the isotropic soft plate was also obtained, using experimental tests following ASTM standards. Theoretical modelling of the nonlinear mechanics of hyperelastic plates is also provided to support the experimental results. Detailed analysis of the nonlinear response of the hyperelastic structure is presented both experimentally and theoretically. This study is published and available online as: Khaniki, H. B., Ghayesh, M. H., & Chin, R. (2023). Theory and experiment for dynamics of hyperelastic plates with modal interactions. International Journal of Engineering Science, 182, 103769. DOI: 10.1016/j.ijengsci.2022.103769

Statement of Authorship

Title of Paper	Theory and experiment for dynamics of hyperelastic plates with modal interactions
Publication Status	☑ Published ☐ Accepted for Publication ☐ Submitted for Publication ☐ Unpublished and Unsubmitted w ork w ritten in manuscript style
Publication Details	Khaniki, H. B., Ghayesh, M. H., & Chin, R. (2023). Theory and experiment for dynamics of hyperelastic plates with modal interactions. International Journal of Engineering Science, 182, 103769.

Principal Author

Name of Principal Author (Candidate)	Hossein Bakhshi Khaniki		
Contribution to the Paper	I carried out the literature review, conceptualization, formal analysis, investigation, methodology, software, validation, visualization and wrote the manuscript.		
Overall percentage (%)	80%		
Certification:	This paper reports on original research I conducted during the period of my Higher Degree by Research candidature and is not subject to any obligations or contractual agreements with a third party that would constrain its inclusion in this thesis. I am the primary author of this paper.		
Signature		Date	2/11/2022

Co-Author Contributions

By signing the Statement of Authorship, each author certifies that:

i. the candidate's stated contribution to the publication is accurate (as detailed above);

ii. permission is granted for the candidate in include the publication in the thesis; and

iii. the sum of all co-author contributions is equal to 100% less the candidate's stated contribution.

Name of Co-Author	Mergen Ghayesh		
Contribution to the Paper	As the principal supervisor, I helped to construct the manuscript, edit and review the manuscript for submission. I assisted in the conceptualization, investigation, methodology, review and editing. I hereby give consent to Hossein Bakhshi Khaniki to present this paper for examination towards the degree of Doctor of Philosophy.		
Signature		Date	3/11/2022

Name of Co-Author	Rey Chin		
Contribution to the Paper	I assisted in review and editing of the manuscript. I hereby give consent to Hossein Bakhshi Khaniki to present this paper for examination towards the degree of Doctor of Philosophy.		
Signature		Date	3/11/2022

International Journal of Engineering Science 182 (2023) 103769

Contents lists available at ScienceDirect

International Journal of Engineering Science

journal homepage: www.elsevier.com/locate/ijengsci

Theory and experiment for dynamics of hyperelastic plates with modal interactions

Hossein B. Khaniki, Mergen H. Ghayesh *, Rey Chin

School of Mechanical Engineering, University of Adelaide, South Australia 5005, Australia

ARTICLE INFO

Keywords:
Hyperelasticity
Plate
Nonlinear elasticity
Mooney-Rivlin
Mass sensing
Vibrations
Dynamics

ABSTRACT

This paper presents a joint experimental and theoretical approach to the dynamics and mass sensitivity of hyperelastic plates including cases with modal interactions. For the theoretical approach, the plate structure is assumed to undergo large strains and deformations using the Mooney-Rivlin hyperelastic strain energy density model and the von-Kármán geometric nonlinearity, respectively. The plate is modelled using the continuum mechanics definitions and the Kirchhoff–Love plate theory. The coupled in-plane and out-of-plane equations of motion are obtained using Hamilton's equation and solved afterwards using a combination of Galerkin's procedure together with a dynamic equilibrium technique. For the experimental analysis, the properties of the material are first obtained by performing a set of stress-strain tests on the samples following the ASTM D-412 standard, and then from the same rubber material, a plate structure is fabricated, and an externally actuated vibration test is performed. The nonlinear frequency response of the structure both with and without a concentrated mass is investigated and the capability of the structure for mass sensing is discussed. By obtaining the amplitude-frequency response of the structure due to the applied external periodic load, using both theoretical and experimental approaches, it is shown that the given model has good accuracy in simulating the nonlinear dynamics of the hyperelastic plate structure under different conditions. Furthermore, a set of analyses on the nonlinear forced vibration behaviour of hyperelastic plates at different internal resonances, using concentrated mass and the length-to-width ratio is presented. The results of this study are useful in designing systems involving hyperelastic plates, such as soft robots and soft functional devices.

1. Introduction

Thin-walled structures have been used widely by researchers in different fields of engineering such as mechanical, civil, automotive and electrical (Barber & Klarbring, 2003). Over the past few years, linear *elastic* structures, including porous (Ashok & Manam, 2021; Hayat & Khan, 2005; Makinde, 2005), functionally graded (Argatov & Sabina, 2022; Yahia et al., 2015), layered (Kushch & Mogilevskaya, 2022; Malikan & Eremeyev, 2022), cracked (Darban et al., 2022; Soni et al., 2018; Yang et al., 2010) and reinforced (Douhou & Ramtani, 2021; Sur & Kanoria, 2018) structures, have been studied by many researchers in different environments such as thermal (Jeyaraj et al., 2008; Wang et al., 2020; Xu et al., 2021) and magnetic (Hu & Wang, 2016; Jalaei et al., 2022; Malikan et al., 2020) fields, just to name a few. One of the most common thin-walled structures used in these fields is *plate* structures. Elastic plate structures

* Corresponding author.
E-mail address: mergen.ghayesh@adelaide.edu.au (M.H. Ghayesh).

https://doi.org/10.1016/j.ijengsci.2022.103769
Received 5 September 2022; Received in revised form 3 October 2022; Accepted 7 October 2022
Available online 25 October 2022

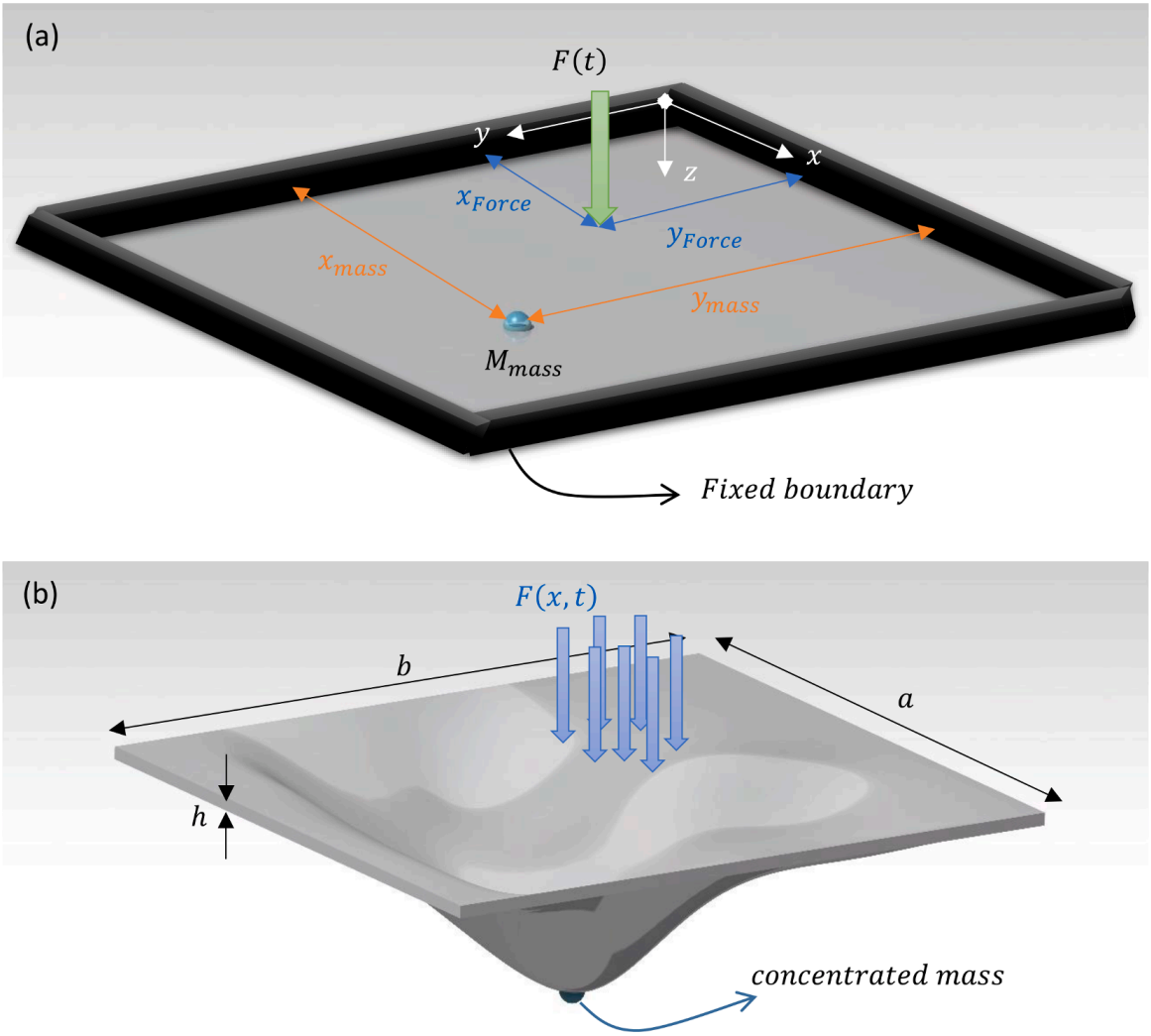

Fig. 1. Schematic of a mass-sensing hyperelastic plate with (a) geometrical properties of the concentrated mass and point load and (b) geometrical properties of the hyperelastic plate under a distributed force.

have been fabricated and investigated for many engineering applications and studied for bending (Berry et al., 2014; Kaplunov et al., 2022), buckling (Bloom & Coffin, 2000; Kubiak, 2013) and vibration (Khadem & Rezaee, 2000; Zheng et al., 2022; Zhou & Cheung, 2000) conditions.

The *elastic* definition is mainly used for structures showing a linear stress-strain behaviour in a small strain loading condition. However, *hyperelastic* structures undergo larger strains with a nonlinear elastic behaviour that makes classic linear constitutive models inaccurate for modelling and predicting their behaviour. Therefore, researchers have developed more accurate models for studying the mechanical behaviour of soft structures, including plate structures.

Over the past few years, the importance of modelling soft structures accurately, motivated some researchers to analyse *hyperelastic* structures. For beam structures, for example, Khaniki et al. investigated hyperelastic beam structures in different mechanical conditions including axially moving hyperelastic beams via Yeoh's strain energy density model (Khaniki et al., 2022), porous hyperelastic beams through the use of the Mooney-Rivlin strain energy density model (Khaniki et al., 2021), and layered sandwich hyperelastic beams by employing different shear deformation theories (Khaniki et al., 2022). The peeling behaviour of hyperelastic beams has been examined by He et al. (2019) using the Euler beam theory. The bending behaviour of multi-layered hyperelastic beams has been studied by Bacciocchi & Tarantino (2021) using the Mooney-Rivlin material model and the Saint Venant-Kirchhoff stored energy function. Other studies on the mechanics of hyperelastic beams can be found in Refs. Kocaturk & Akbas (2010), Forsat (2020), Jiang & Yu (2016), Chen et al. (2020).

For hyperelastic plate structures, Ahmetolan & Teymur (2007) studied the nonlinear shear horizontal (SH) waves in hyperelastic plate structures. The plate was modelled as an incompressible isotropic structure using the generalised neo-Hookean strain energy density model. It was shown that under infinitesimal perturbations, the waves are unstable when the plate material shows softening behaviour in shear. Amabili et al. (2016) and Breslavsky et al. (2014) investigated the static deformation and vibrations of hyperelastic shells using Novozhilov's nonlinear shell theory, the Lagrangian approach and experimental testing. It was shown that the model is capable of predicting the natural frequencies and the static deformation of the structure. The surface instability and wrinkling in hyperelastic compressible plates were investigated by Yang et al. (2020) and Xia et al. (2021) using the neo-Hookean and Gent laws.

Ansari et al. (2021) examined the nonlinear static behaviour of neo-Hookean hyperelastic plates using the minimum total potential energy principle. Zhao et al. (2021) and Xu et al. (2020) examined the 2:1 internal resonance behaviour of soft cylindrical shell structures using multi-scale analysis and considering thermal effects. Islam et al. (2021) studied the deformations in hyperelastic plates strengthened with unidirectional and bidirectional fibres using the Mooney–Rivlin model. Wang et al. (2018) examined the stress-free static behaviour of hyperelastic plates using the neo-Hookean strain energy density model and verified the modelling using experimental testing. The growth-induced deformation and instability of circular hyperelastic plates have been examined by Li et al. (2022) and Mehta et al. (2021), respectively. A detailed review on the dynamic behaviour of hyperelastic structures, including plates, can be found in Ref. Khaniki et al. (2022) for interested readers.

In this study, a Hamiltonian framework for the theoretical dynamics of hyperelastic structures along with experimental verifications are developed and the mass sensitivity of hyperelastic plates and the modal interactions of the structure during different stages are presented via developing a nonlinear continuum mechanics formulation and validating it through several sets of experiments. In Section 1, a brief introduction to hyperelasticity and a literature review on hyperelastic structures are given. Section 2 presents a detailed problem formulation and solution procedure for modelling the nonlinear mechanics of hyperelastic plates with mass imperfection using the Kirchhoff–Love plate theory together with the Mooney-Rivlin hyperelastic strain energy density model. Section 3 explains the experimental preparation and testing performed for obtaining the hyperelastic properties of soft structures and the experimental nonlinear forced vibration behaviour of hyperelastic plates. In Section 4, results of the theoretical modelling and experimental testing on hyperelastic plates are presented and compared showing good agreement with the model. The sensitivity of the structure to the presence of concentrated mass and periodic external load is presented for different cases. Modal interactions and internal resonance phenomena in hyperelastic plates using a concentrated mass and length-to-width ratio variation is presented. The conclusion of the study is highlighted in Section 5.

2. Mooney-Rivlin, thin soft plate formulation and solution procedure

2.1. Hyperelastic plate modelling

For a thin hyperelastic plate with the geometrical properties shown in Fig. 1, the deformation gradient (F) and the left Cauchy-Green deformation tensor (C) are defined as (Bonet & Wood, 1997; Mezzasalma et al., 2022)

$$F = \begin{bmatrix} 1+\varepsilon_x & \varepsilon_{xy} & 0 \\ \varepsilon_{xy} & 1+\varepsilon_y & 0 \\ 0 & 0 & 1+\varepsilon_z \end{bmatrix}, \tag{1}$$

$$C = F^T F = \begin{bmatrix} (1+\varepsilon_x)^2 + {\varepsilon_{xy}}^2 & \varepsilon_{xy}(2+\varepsilon_y+\varepsilon_x) & 0 \\ \varepsilon_{xy}(2+\varepsilon_y+\varepsilon_x) & (1+\varepsilon_y)^2 + {\varepsilon_{xy}}^2 & 0 \\ 0 & 0 & (1+\varepsilon_z)^2 \end{bmatrix}, \tag{2}$$

where ε_x, ε_x, and ε_z are the axial strains in the x, y and z directions and ε_{xy} is the in-plane shear strains defined for the Kirchhoff–Love plate theory as (Reddy, 2003)

$$\begin{Bmatrix} \varepsilon_x \\ \varepsilon_y \end{Bmatrix} = \begin{Bmatrix} \dfrac{\partial u(x,y)}{\partial x} - z\dfrac{\partial^2 w(x,y)}{\partial x^2} + \dfrac{1}{2}\left(\dfrac{\partial w(x,y)}{\partial x}\right)^2 \\ \dfrac{\partial v(x,y)}{\partial y} - z\dfrac{\partial^2 w(x,y)}{\partial y^2} + \dfrac{1}{2}\left(\dfrac{\partial w(x,y)}{\partial y}\right)^2 \end{Bmatrix}, \quad \varepsilon_z \neq 0, \tag{3}$$

$$\varepsilon_{xy} = \frac{\partial u(x,y)}{\partial y} + \frac{\partial v(x,y)}{\partial x} - 2z\frac{\partial^2 w(x,y)}{\partial x \partial y} + \frac{\partial w(x,y)}{\partial x}\frac{\partial w(x,y)}{\partial y}, \tag{4}$$

with u, v and w as the displacements in the x, y and z directions, respectively. Using Eqs. (2)–(4), the first two strain invariants (I_1 and I_2) of the left Cauchy-Green strain tensor are written as

$$I_1 = tr(C) = 3 + 2\varepsilon_x + 2\varepsilon_y + 2\varepsilon_z + {\varepsilon_x}^2 + {\varepsilon_y}^2 + {\varepsilon_z}^2 + 2{\varepsilon_{xy}}^2, \tag{5}$$

$$\begin{aligned} I_2 = \frac{1}{2}\left(tr(C)^2 - tr(C^2)\right) = 3 + 4\varepsilon_x + 4\varepsilon_y + 4\varepsilon_z + 2{\varepsilon_x}^2 + 2{\varepsilon_y}^2 + 2{\varepsilon_z}^2 \\ +4\varepsilon_x\varepsilon_y + 4\varepsilon_x\varepsilon_z + 4\varepsilon_y\varepsilon_z + 2{\varepsilon_x}^2\varepsilon_y + 2{\varepsilon_x}^2\varepsilon_z + 2\varepsilon_x{\varepsilon_y}^2 + 2{\varepsilon_y}^2\varepsilon_z + 2\varepsilon_x{\varepsilon_z}^2 \\ +2\varepsilon_y{\varepsilon_z}^2 + 4{\varepsilon_{xy}}^2\varepsilon_z - 2{\varepsilon_{xy}}^2\varepsilon_y - 2{\varepsilon_{xy}}^2\varepsilon_x, \end{aligned} \tag{6}$$

and from the incompressibility condition on the third invariant ($I_3 = 1$) (Xiao et al., 2022), a constrain relationship is obtained as

$$\varepsilon_z = -\varepsilon_x - \varepsilon_y + 2{\varepsilon_x}^2 + 2{\varepsilon_y}^2 + 2\varepsilon_x\varepsilon_y + 2{\varepsilon_{xy}}^2 + 16{\varepsilon_x}^2\varepsilon_y + 16\varepsilon_x{\varepsilon_y}^2 - 16\varepsilon_x{\varepsilon_{xy}}^2 - 16\varepsilon_y{\varepsilon_{xy}}^2. \tag{7}$$

The strain energy of the incompressible hyperelastic plate can be modelled using the stain invariants in the framework of the hyperelastic Mooney-Rivlin strain energy density model as (Chen & Zhao, 2022; Mooney, 1940)

$$HE = C_1[I_1(x,y,z)-3] + C_2[I_2(x,y,z)-3], \tag{8}$$

where C_1 and C_2 are the material constants of the Mooney-Rivlin strain energy density model. The variation of the potential energy is therefore written as

$$\delta PE = \int \left\{ \left[\begin{array}{l} \left\{ \begin{array}{l} C_1(x,y)\big(+12\varepsilon_x + 6\varepsilon_y - 12{\varepsilon_x}^2 + 48\varepsilon_x\varepsilon_y + 24{\varepsilon_y}^2 - 36{\varepsilon_{xy}}^2\big) \\ +C_2(x,y)\big(+16\varepsilon_x + 8\varepsilon_y + 140\varepsilon_x\varepsilon_y + 70{\varepsilon_y}^2 - 70{\varepsilon_{xy}}^2\big) \end{array} \right\}\delta\varepsilon_x \\ +\left\{ \begin{array}{l} C_1(x,y)\big(+12\varepsilon_y + 6\varepsilon_x - 12{\varepsilon_y}^2 + 24{\varepsilon_x}^2 + 48\varepsilon_x\varepsilon_y - 36{\varepsilon_{xy}}^2\big) \\ +C_2(x,y)\big(+16\varepsilon_y + 8\varepsilon_x + 70{\varepsilon_x}^2 + 140\varepsilon_x\varepsilon_y - 70{\varepsilon_{xy}}^2\big) \end{array} \right\}\delta\varepsilon_y \\ +\left\{ \begin{array}{l} C_1(x,y)\big(+12\varepsilon_{xy} - 72\varepsilon_x\varepsilon_{xy} - 72\varepsilon_y\varepsilon_{xy}\big) \\ +C_2(x,y)\big(+16\varepsilon_{xy} - 140\varepsilon_x\varepsilon_{xy} - 140\varepsilon_y\varepsilon_{xy}\big) \end{array} \right\}\delta\varepsilon_{xy} \end{array} \right] \right\} dAdx. \tag{9}$$

Furthermore, the kinetic energy of the hyperelastic plate and the point mass (M_{mass}) is written as

$$\begin{aligned} T &= \frac{1}{2}\int_V \rho\Big[(u_t - zw_{xt})^2 + \big(v_t - zw_{yt}\big)^2 + (w_t)^2\Big]dV \\ &+\frac{1}{2}\int_0^b\int_0^a M_{mass}\big[(u_t)^2 + (v_t)^2 + (w_t)^2\big]\delta(x-x_{mass})\delta(y-y_{mass})dxdy, \end{aligned} \tag{10}$$

where ρ is the mass density. The plate is assumed to be excited using a point (Fig. 1a) or distributed (Fig. 1b) load (F) with the external work (W_F) as

$$\left\{ \begin{array}{l} \text{Distributed Load}: \quad W_F = \displaystyle\int_A F(x,y,t)wdA, \\ \\ \text{Point Load}: \quad W_F = \displaystyle\int_A F(t)\delta\big(x-x_{force}\big)\delta\big(y-y_{force}\big)wdA. \end{array} \right. \tag{11}$$

Using Hamilton's equations and going through the mathematical calculations, one can reach the nonlinear coupled equations of motion as

$$\begin{aligned} &\rho u_{tt} + M_{mass}\delta(x-x_{mass})\delta(y-y_{mass})u_{tt} - (12C_1+16C_2)u_{xx} - (3C_1+4C_2)u_{yy} - (9C_1+12C_2)v_{xy} \\ &+12C_1\frac{\partial}{\partial x}\big({u_x}^2\big) + \frac{1}{4}(36C_1+70C_2)\frac{\partial}{\partial x}\big({u_y}^2\big) + (18C_1+35C_2)\frac{\partial}{\partial y}\big(u_xu_y\big) \\ &-(48C_1+140C_2)\frac{\partial}{\partial x}\big(u_xv_y\big) + (18C_1+35C_2)\frac{\partial}{\partial x}\big(u_yv_x\big) + (18C_1+35C_2)\frac{\partial}{\partial y}\big(u_xv_x\big) \\ &+(18C_1+35C_2)\frac{\partial}{\partial y}\big(u_yv_y\big) - (24C_1+70C_2)\frac{\partial}{\partial x}\big({v_y}^2\big) + \frac{1}{2}(18C_1+35C_2)\frac{\partial}{\partial x}\big({v_x}^2\big) \\ &+(18C_1+35C_2)\frac{\partial}{\partial y}\big(v_xv_y\big) - (6C_1+8C_2)\frac{\partial}{\partial x}\big(w_x^2\big) - (3C_1+4C_2)\frac{\partial}{\partial x}\Big(w_y^2\Big) + C_1h^2\frac{\partial}{\partial x}\big({w_{xx}}^2\big) \\ &-\frac{1}{12}(24C_1+70C_2)h^2\frac{\partial}{\partial x}\big({w_{yy}}^2\big) - \frac{1}{12}(48C_1+140C_2)h^2\frac{\partial}{\partial x}\big(w_{xx}w_{yy}\big) \\ &+\frac{1}{12}(36C_1+70C_2)h^2\frac{\partial}{\partial x}\big({w_{xy}}^2\big) - (3C_1+4C_2)\frac{\partial}{\partial y}\big(w_xw_y\big) + \frac{1}{6}(18C_1+35C_2)h^2\frac{\partial}{\partial y}\big(w_{xx}w_{xy}\big) \\ &+\frac{1}{6}(18C_1+35C_2)h^2\frac{\partial}{\partial y}\big(w_{xy}w_{yy}\big) + 12C_1\frac{\partial}{\partial x}\big(u_xw_x^2\big) - (24C_1+70C_2)\frac{\partial}{\partial x}\Big(u_xw_y^2\Big) \\ &+(18C_1+35C_2)\frac{\partial}{\partial x}\big(u_yw_xw_y\big) + (18C_1+35C_2)\frac{\partial}{\partial y}\big(u_xw_xw_y\big) + \frac{1}{2}(18C_1+35C_2)\frac{\partial}{\partial y}\big(u_yw_x^2\big) \\ &+\frac{1}{2}(18C_1+35C_2)\frac{\partial}{\partial y}\Big(u_yw_y^2\Big) - (24C_1+70C_2)\frac{\partial}{\partial x}\Big(v_yw_y^2\Big) - (24C_1+70C_2)\frac{\partial}{\partial x}\big(v_yw_x^2\big) \\ &+(18C_1+35C_2)\frac{\partial}{\partial x}\big(v_xw_xw_y\big) + \frac{1}{2}(18C_1+35C_2)\frac{\partial}{\partial y}\big(v_xw_x^2\big) + \frac{1}{2}(18C_1+35C_2)\frac{\partial}{\partial y}\Big(v_xw_y^2\Big) \\ &+(18C_1+35C_2)\frac{\partial}{\partial y}\big(v_yw_xw_y\big) + 3C_1\frac{\partial}{\partial x}\big(w_x^4\big) - \frac{1}{2}(12C_1+35C_2)\frac{\partial}{\partial x}\Big(w_y^4\Big) \\ &-\frac{1}{2}(6C_1+35C_2)\frac{\partial}{\partial x}\Big(w_x^2w_y^2\Big) + \frac{1}{2}(18C_1+35C_2)\frac{\partial}{\partial y}\big(w_x^3w_y\big) + \frac{1}{2}(18C_1+35C_2)\frac{\partial}{\partial y}\Big(w_xw_y^3\Big) = 0, \end{aligned} \tag{12}$$

$$
\begin{aligned}
&\rho v_{tt} + M_{mass}\delta(x-x_{mass})\delta(y-y_{mass})v_{tt} - (9C_1+12C_2)u_{xy} - (12C_1+16C_2)v_{yy} - (3C_1+4C_2)v_{xx} \\
&\quad -(24C_1+70C_2)\frac{\partial}{\partial y}\left(u_x{}^2\right) + \frac{1}{2}(18C_1+35C_2)\frac{\partial}{\partial y}\left(u_y{}^2\right) + (18C_1+35C_2)\frac{\partial}{\partial x}\left(u_x u_y\right) \\
&\quad -(48C_1+140C_2)\frac{\partial}{\partial y}\left(u_x v_y\right) + (18C_1+35C_2)\frac{\partial}{\partial y}\left(u_y v_x\right) + (18C_1+35C_2)\frac{\partial}{\partial x}\left(u_x v_x\right) \\
&\quad +(18C_1+35C_2)\frac{\partial}{\partial x}\left(u_y v_y\right) + 12C_1\frac{\partial}{\partial y}\left(v_y{}^2\right) + \frac{1}{2}(18C_1+35C_2)\frac{\partial}{\partial y}\left(v_x{}^2\right) \\
&\quad +(18C_1+35C_2)\frac{\partial}{\partial x}\left(v_x v_y\right) - (6C_1+8C_2)\frac{\partial}{\partial y}\left(w_y^2\right) - (3C_1+4C_2)\frac{\partial}{\partial y}\left(w_x^2\right) + C_1h^2\frac{\partial}{\partial y}\left(w_{yy}{}^2\right) \\
&\quad -\frac{1}{12}(24C_1+70C_2)h^2\frac{\partial}{\partial y}\left(w_{xx}{}^2\right) - \frac{1}{12}(48C_1+140C_2)h^2\frac{\partial}{\partial y}\left(w_{xx}w_{yy}\right) \\
&\quad +\frac{1}{12}(36C_1+70C_2)h^2\frac{\partial}{\partial y}\left(w_{xy}{}^2\right) - (3C_1+4C_2)\frac{\partial}{\partial x}\left(w_x w_y\right) + \frac{1}{6}(18C_1+35C_2)h^2\frac{\partial}{\partial x}\left(w_{xx}w_{xy}\right) \\
&\quad +\frac{1}{6}(18C_1+35C_2)h^2\frac{\partial}{\partial x}\left(w_{xy}w_{yy}\right) - (24C_1+70C_2)\frac{\partial}{\partial y}\left(u_x w_x^2\right) - (24C_1+70C_2)\frac{\partial}{\partial y}\left(u_x w_y^2\right) \\
&\quad +(18C_1+35C_2)\frac{\partial}{\partial y}\left(u_y w_x w_y\right) + (18C_1+35C_2)\frac{\partial}{\partial x}\left(u_x w_x w_y\right) + \frac{1}{2}(18C_1+35C_2)\frac{\partial}{\partial x}\left(u_y w_x^2\right) \\
&\quad +\frac{1}{2}(18C_1+35C_2)\frac{\partial}{\partial x}\left(u_y w_y^2\right) + (12C_1)\frac{\partial}{\partial y}\left(v_y w_y^2\right) - (24C_1+70C_2)\frac{\partial}{\partial y}\left(v_y w_x^2\right) \\
&\quad +(18C_1+35C_2)\frac{\partial}{\partial y}\left(v_x w_x w_y\right) + \frac{1}{2}(18C_1+35C_2)\frac{\partial}{\partial x}\left(v_x w_x^2\right) + \frac{1}{2}(18C_1+35C_2)\frac{\partial}{\partial x}\left(v_x w_y^2\right) \\
&\quad +(18C_1+35C_2)\frac{\partial}{\partial x}\left(v_y w_x w_y\right) + 3C_1\frac{\partial}{\partial y}\left(w_y^4\right) - \frac{1}{4}(24C_1+70C_2)\frac{\partial}{\partial y}\left(w_x^4\right) \\
&-\frac{1}{4}(12C_1+70C_2)\frac{\partial}{\partial y}\left(w_x^2 w_y^2\right) + \frac{1}{2}(18C_1+35C_2)\frac{\partial}{\partial x}\left(w_x^3 w_y\right) + \frac{1}{2}(18C_1+35C_2)\frac{\partial}{\partial x}\left(w_x w_y^3\right) = 0,
\end{aligned}
\tag{13}
$$

$$
\begin{aligned}
\rho w_{tt} \;&-\; \frac{1}{12}\rho h^2 w_{xxtt} - \frac{1}{12}\rho h^2 w_{yytt} + M_{mass}\delta(x-x_{mass})\delta(y-y_{mass})w_{tt} \\
&+\; \frac{1}{12}(12C_1+16C_2)h^2 w_{xxxx} + \frac{1}{12}(24C_1+32C_2)h^2 w_{xxyy} + \frac{1}{12}(12C_1+16C_2)h^2 w_{yyyy} \\
&-\; 2C_1h^2\frac{\partial^2}{\partial x^2}\left(u_x w_{xx}\right) + \frac{1}{6}(24C_1+70C_2)h^2\frac{\partial^2}{\partial x^2}\left(u_x w_{yy}\right) - \frac{1}{12}(36C_1+70C_2)h^2\frac{\partial^2}{\partial x^2}\left(u_y w_{xy}\right) \\
&-\; (12C_1+16C_2)\frac{\partial}{\partial x}\left(u_x w_x\right) + \frac{1}{6}(24C_1+70C_2)h^2\frac{\partial^2}{\partial y^2}\left(u_x w_{xx}\right) + \frac{1}{6}(24C_1+70C_2)h^2\frac{\partial^2}{\partial y^2}\left(u_x w_{yy}\right) \\
&-\; \frac{1}{12}(36C_1+70C_2)h^2\frac{\partial^2}{\partial y^2}\left(u_y w_{xy}\right) - (6C_1+8C_2)\frac{\partial}{\partial y}\left(u_x w_x\right) - \frac{1}{3}(18C_1+35C_2)h^2\frac{\partial^2}{\partial x\partial y}\left(u_x w_{xy}\right) \\
&-\; \frac{1}{6}(18C_1+35C_2)h^2\frac{\partial^2}{\partial x\partial y}\left(u_y w_{xx}\right) - \frac{1}{6}(18C_1+35C_2)h^2\frac{\partial^2}{\partial x\partial y}\left(u_y w_{yy}\right) - (3C_1+4C_2)\frac{\partial}{\partial x}\left(u_y w_y\right) \\
&-\; (3C_1+4C_2)\frac{\partial}{\partial y}\left(u_y w_x\right) + \frac{1}{3}(18C_1+35C_2)h^2\frac{\partial^2}{\partial x^2}\left(v_y w_{yy}\right) + \frac{1}{6}(24C_1+70C_2)h^2\frac{\partial^2}{\partial x^2}\left(v_y w_{xx}\right) \\
&+\ldots
\end{aligned}
$$

$$
\begin{aligned}
&+ \quad \ldots \\
&+ \quad \frac{1}{12}(48C_1+140C_2)h^2\frac{\partial^2}{\partial x^2}\left(v_y w_{xx}\right) - \frac{1}{12}(36C_1+70C_2)h^2\frac{\partial^2}{\partial x^2}\left(v_x w_{xy}\right) + \frac{1}{6}(24C_1+70C_2)h^2\frac{\partial^2}{\partial x^2}\left(v_y w_{yy}\right) \\
&+ \quad \frac{1}{12}(48C_1+140C_2)h^2\frac{\partial^2}{\partial y^2}\left(v_y w_{xx}\right) - \frac{1}{12}(36C_1+70C_2)h^2\frac{\partial^2}{\partial y^2}\left(v_x w_{xy}\right) - (6C_1+8C_2)\frac{\partial}{\partial x}\left(v_y w_x\right) \\
&- \quad (3C_1+4C_2)\frac{\partial}{\partial y}\left(v_x w_x\right) - (3C_1+4C_2)\frac{\partial}{\partial x}\left(v_x w_y\right) - \frac{1}{3}(18C_1+35C_2)h^2\frac{\partial^2}{\partial x\partial y}\left(v_y w_{xy}\right) \\
&- \quad \frac{1}{6}(18C_1+35C_2)h^2\frac{\partial^2}{\partial x\partial y}\left(v_x w_{yy}\right) - \frac{1}{6}(18C_1+35C_2)h^2\frac{\partial^2}{\partial x\partial y}\left(v_x w_{xx}\right) - (6C_1+8C_2)\frac{\partial}{\partial x}\left(w_x^3\right) \\
&- \quad \frac{1}{2}(12C_1+16C_2)\frac{\partial}{\partial y}\left(w_y^3\right) - (3C_1+4C_2)\frac{\partial}{\partial x}\left(w_x w_y^2\right) - \frac{1}{2}(6C_1+8C_2)\frac{\partial}{\partial y}\left(w_x^2 w_y\right) + C_1h^2\frac{\partial}{\partial x}\left(w_x {w_{xx}}^2\right) \\
&+ \quad C_1h^2\frac{\partial}{\partial y}\left(w_y {w_{yy}}^2\right) - \frac{1}{12}(24C_1+70C_2)h^2\frac{\partial}{\partial x}\left(w_x {w_{yy}}^2\right) - \frac{1}{12}(24C_1+70C_2)h^2\frac{\partial}{\partial y}\left({w_{xx}}^2 w_y\right) \\
&- \quad \frac{1}{12}(48C_1+140C_2)h^2\frac{\partial}{\partial x}\left(w_x w_{xx} w_{yy}\right) - \frac{1}{12}(48C_1+140C_2)h^2\frac{\partial}{\partial y}\left(w_{xx} w_y w_{yy}\right) \\
&+ \quad \frac{1}{12}(36C_1+70C_2)h^2\frac{\partial}{\partial x}\left(w_x {w_{xy}}^2\right) + \frac{1}{12}(36C_1+70C_2)h^2\frac{\partial}{\partial y}\left(w_y {w_{xy}}^2\right) - C_1h^2\frac{\partial^2}{\partial x^2}\left(w_x^2 w_{xx}\right) \\
&- \quad C_1h^2\frac{\partial^2}{\partial y^2}\left(w_y^2 w_{yy}\right) + \frac{1}{12}(24C_1+70C_2)h^2\frac{\partial^2}{\partial x^2}\left(w_y^2 w_{yy}\right) + \frac{1}{12}(24C_1+70C_2)h^2\frac{\partial^2}{\partial y^2}\left(w_x^2 w_{xx}\right) \\
&+ \quad \frac{1}{24}(48C_1+140C_2)h^2\frac{\partial^2}{\partial x^2}\left(w_{xx} w_y^2\right) + \frac{1}{24}(48C_1+140C_2)h^2\frac{\partial^2}{\partial y^2}\left(w_{xx} w_y^2\right) \\
&+ \quad \frac{1}{24}(48C_1+140C_2)h^2\frac{\partial^2}{\partial x^2}\left(w_x^2 w_{yy}\right) + \frac{1}{24}(48C_1+140C_2)h^2\frac{\partial^2}{\partial y^2}\left(w_x^2 w_{yy}\right) \\
&- \quad \frac{1}{12}(36C_1+70C_2)h^2\frac{\partial^2}{\partial x^2}\left(w_x w_y w_{xy}\right) - \frac{1}{12}(36C_1+70C_2)h^2\frac{\partial^2}{\partial y^2}\left(w_x w_y w_{xy}\right) \\
&- \quad \frac{1}{6}(18C_1+35C_2)h^2\frac{\partial^2}{\partial x\partial y}\left(w_x^2 w_{xy}\right) - \frac{1}{6}(18C_1+35C_2)h^2\frac{\partial^2}{\partial x\partial y}\left(w_y^2 w_{xy}\right) \\
&- \quad \frac{1}{6}(18C_1+35C_2)h^2\frac{\partial^2}{\partial x\partial y}\left(w_x w_y w_{yy}\right) - \frac{1}{6}(18C_1+35C_2)h^2\frac{\partial^2}{\partial x\partial y}\left(w_x w_y w_{xx}\right) \\
&- \quad (3C_1+4C_2)\frac{\partial}{\partial x}\left(w_x {w_y}^2\right) - (3C_1+4C_2)\frac{\partial}{\partial y}\left({w_x}^2 w_y\right) + \frac{1}{6}(18C_1+35C_2)h^2\frac{\partial}{\partial x}\left(w_{xx} w_y w_{xy}\right) \\
&+ \quad \frac{1}{6}(18C_1+35C_2)h^2\frac{\partial}{\partial y}\left(w_x w_{xx} w_{xy}\right) + \frac{1}{6}(18C_1+35C_2)h^2\frac{\partial}{\partial x}\left(w_y w_{xy} w_{yy}\right) \\
&+ \quad \frac{1}{6}(18C_1+35C_2)h^2\frac{\partial}{\partial y}\left(w_x w_{xy} w_{yy}\right) + 12C_1\frac{\partial}{\partial x}\left({u_x}^2 w_x\right) - (24C_1+70C_2)\frac{\partial}{\partial y}\left({u_x}^2 w_y\right) \\
&+ \quad \ldots
\end{aligned}
$$

$$
\begin{aligned}
&+\dots\\
&+\frac{1}{4}(36C_1+70C_2)\frac{\partial}{\partial y}\left({u_y}^2 w_y\right)+(18C_1+35C_2)\frac{\partial}{\partial x}\left(u_x u_y w_y\right)+(18C_1+35C_2)\frac{\partial}{\partial y}\left(u_x u_y w_x\right)\\
&+\frac{1}{4}(36C_1+70C_2)\frac{\partial}{\partial x}\left({u_y}^2 w_x\right)-(24C_1+70C_2)\frac{\partial}{\partial x}\left({v_y}^2 w_x\right)+\frac{1}{4}(36C_1+70C_2)\frac{\partial}{\partial x}\left({v_x}^2 w_x\right)\\
&+(18C_1+35C_2)\frac{\partial}{\partial x}\left(v_x v_y w_y\right)+(18C_1+35C_2)\frac{\partial}{\partial y}\left(v_x v_y w_x\right)+\frac{1}{4}(36C_1+70C_2)\frac{\partial}{\partial y}\left({v_x}^2 w_y\right)\\
&-(48C_1+140C_2)\frac{\partial}{\partial x}\left(u_x v_y w_x\right)-(48C_1+140C_2)\frac{\partial}{\partial y}\left(u_x v_y w_y\right)+\frac{1}{2}(36C_1+70C_2)\frac{\partial}{\partial x}\left(u_y v_x w_x\right)\\
&+\frac{1}{2}(36C_1+70C_2)\frac{\partial}{\partial y}\left(u_y v_x w_y\right)+(18C_1+35C_2)\frac{\partial}{\partial x}\left(u_x v_x w_y\right)+(18C_1+35C_2)\frac{\partial}{\partial y}\left(u_y v_y w_x\right)\\
&+(18C_1+35C_2)\frac{\partial}{\partial x}\left(u_y v_y w_y\right)+(18C_1+35C_2)\frac{\partial}{\partial y}\left(u_x v_x w_x\right)+12C_1\frac{\partial}{\partial x}\left(u_x {w_x}^3\right)+12C_1\frac{\partial}{\partial y}\left({v_y}^2 w_y\right)\\
&-\frac{1}{2}(48C_1+140C_2)\frac{\partial}{\partial x}\left(u_x w_x {w_y}^2\right)+\frac{1}{2}(36C_1+70C_2)\frac{\partial}{\partial x}\left(u_y {w_x}^2 w_y\right)-(24C_1+70C_2)\frac{\partial}{\partial y}\left(u_x {w_x}^2 w_y\right)\\
&-\frac{1}{2}(48C_1+140C_2)\frac{\partial}{\partial y}\left(u_x {w_y}^3\right)+\frac{1}{2}(36C_1+70C_2)\frac{\partial}{\partial y}\left(u_y w_x {w_y}^2\right)+(18C_1+35C_2)\frac{\partial}{\partial x}\left(u_x w_x {w_y}^2\right)\\
&+\frac{1}{2}(18C_1+35C_2)\frac{\partial}{\partial x}\left(u_y {w_x}^2 w_y\right)+\frac{1}{2}(18C_1+35C_2)\frac{\partial}{\partial x}\left(u_y {w_y}^3\right)+(18C_1+35C_2)\frac{\partial}{\partial y}\left(u_x {w_x}^2 w_y\right)\\
&+\frac{1}{2}(18C_1+35C_2)\frac{\partial}{\partial y}\left(u_y {w_x}^3\right)+\frac{1}{2}(18C_1+35C_2)\frac{\partial}{\partial y}\left(u_y w_x {w_y}^2\right)+12C_1\frac{\partial}{\partial y}\left(v_y {w_y}^3\right)\\
&-\frac{1}{2}(48C_1+140C_2)\frac{\partial}{\partial y}\left(v_y {w_x}^2 w_y\right)+\frac{1}{2}(36C_1+70C_2)\frac{\partial}{\partial y}\left(v_x w_x {w_y}^2\right)-(24C_1+70C_2)\frac{\partial}{\partial x}\left(v_y w_x {w_y}^2\right)\\
&-\frac{1}{2}(48C_1+140C_2)\frac{\partial}{\partial x}\left(v_y {w_x}^3\right)+\frac{1}{2}(36C_1+70C_2)\frac{\partial}{\partial x}\left(v_x {w_x}^2 w_y\right)+(18C_1+35C_2)\frac{\partial}{\partial y}\left(v_y {w_x}^2 w_y\right)\\
&+\frac{1}{2}(18C_1+35C_2)\frac{\partial}{\partial y}\left(v_x w_x {w_y}^2\right)+\frac{1}{2}(18C_1+35C_2)\frac{\partial}{\partial y}\left(v_x {w_x}^3\right)+(18C_1+35C_2)\frac{\partial}{\partial x}\left(v_y w_x {w_y}^2\right)\\
&+\frac{1}{2}(18C_1+35C_2)\frac{\partial}{\partial x}\left(v_x {w_y}^3\right)+\frac{1}{2}(18C_1+35C_2)\frac{\partial}{\partial x}\left(v_x {w_x}^2 w_y\right)+3C_1\frac{\partial}{\partial x}\left({w_x}^5\right)+3C_1\frac{\partial}{\partial y}\left({w_y}^5\right)\\
&-\frac{1}{4}(24C_1+70C_2)\frac{\partial}{\partial x}\left(w_x {w_y}^4\right)-\frac{1}{4}(24C_1+70C_2)\frac{\partial}{\partial y}\left({w_x}^4 w_y\right)-\frac{1}{4}(12C_1+70C_2)\frac{\partial}{\partial x}\left({w_x}^3 {w_y}^2\right)\\
&-\frac{1}{4}(12C_1+70C_2)\frac{\partial}{\partial y}\left({w_x}^2 {w_y}^3\right)+\frac{1}{2}(18C_1+35C_2)\frac{\partial}{\partial x}\left({w_x}^3 {w_y}^2\right)+\frac{1}{2}(18C_1+35C_2)\frac{\partial}{\partial y}\left({w_x}^2 {w_y}^3\right)\\
&+\frac{1}{2}(18C_1+35C_2)\frac{\partial}{\partial x}\left(w_x {w_y}^4\right)+\frac{1}{2}(18C_1+35C_2)\frac{\partial}{\partial y}\left({w_x}^4 w_y\right)=F(x,y,t).
\end{aligned}
\tag{14}
$$

By neglecting Poisson's effect and deformation in y direction, the equations of motion for hyperelastic beams are obtained which matches perfectly with those obtained in Ref. Khaniki et al. (2021) (when the porosity effect is also neglected).

2.2. Solution procedure

To solve the coupled nonlinear equations of motion of the hyperelastic plate structure, nondimensional parameters are defined as

$$
\begin{aligned}
&x^*=\frac{x}{a},\quad {x_{mass}}^*=\frac{x_{mass}}{a},\quad {x_{Force}}^*=\frac{x_{Force}}{a},\quad {y_{mass}}^*=\frac{y_{mass}}{b},\quad y*=\frac{y}{b},\quad {y_{Force}}^*=\frac{y_{Force}}{b},\\
&z^*=\frac{z}{h},\quad u^*=\frac{u}{h},\quad v^*=\frac{v}{h},\quad w^*=\frac{w}{h},\quad A_1=\frac{C_1}{C_2},\quad A_2=\frac{3C_1+4C_2}{C_2},\quad {M_{mass}}^*=\frac{M_{mass}}{\rho abh},\\
&A_3=\frac{18C_1+35C_2}{C_2},\quad A_4=\frac{24C_1+70C_2}{C_2},\quad A_5=\frac{12C_1+70C_2}{C_2},\quad \eta_a=\frac{h}{a},\quad \eta_b=\frac{h}{b},\\
&F^*=\frac{Fa^2b^2}{C_2h^4},\quad \lambda=\sqrt{\frac{\rho_0 a^2b^2}{C_2h^2}},\quad t^*=t\sqrt{\frac{C_2h^2}{\rho_0 a^2b^2}}=t\frac{h}{ab}\sqrt{\frac{C_2}{\rho_0}},
\end{aligned}
\tag{15}
$$

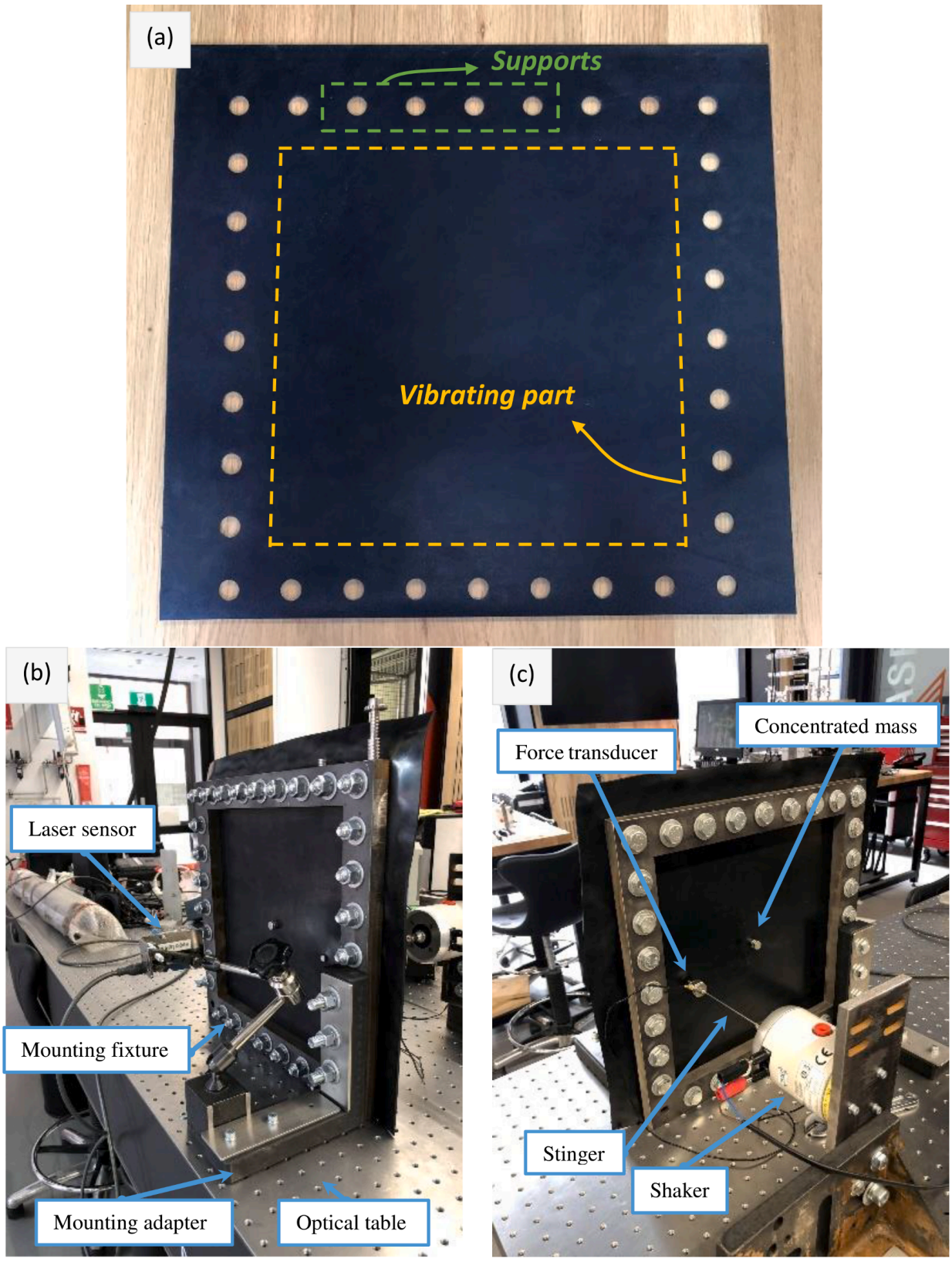

Fig. 2. (a) An EPDM rubber plate, (b) fixture to hold the plate tight with 32 M12 bolts, and (c) mounted fixture to the shaking table using accurate right-angle mounting adapters and M6 steel bolts.

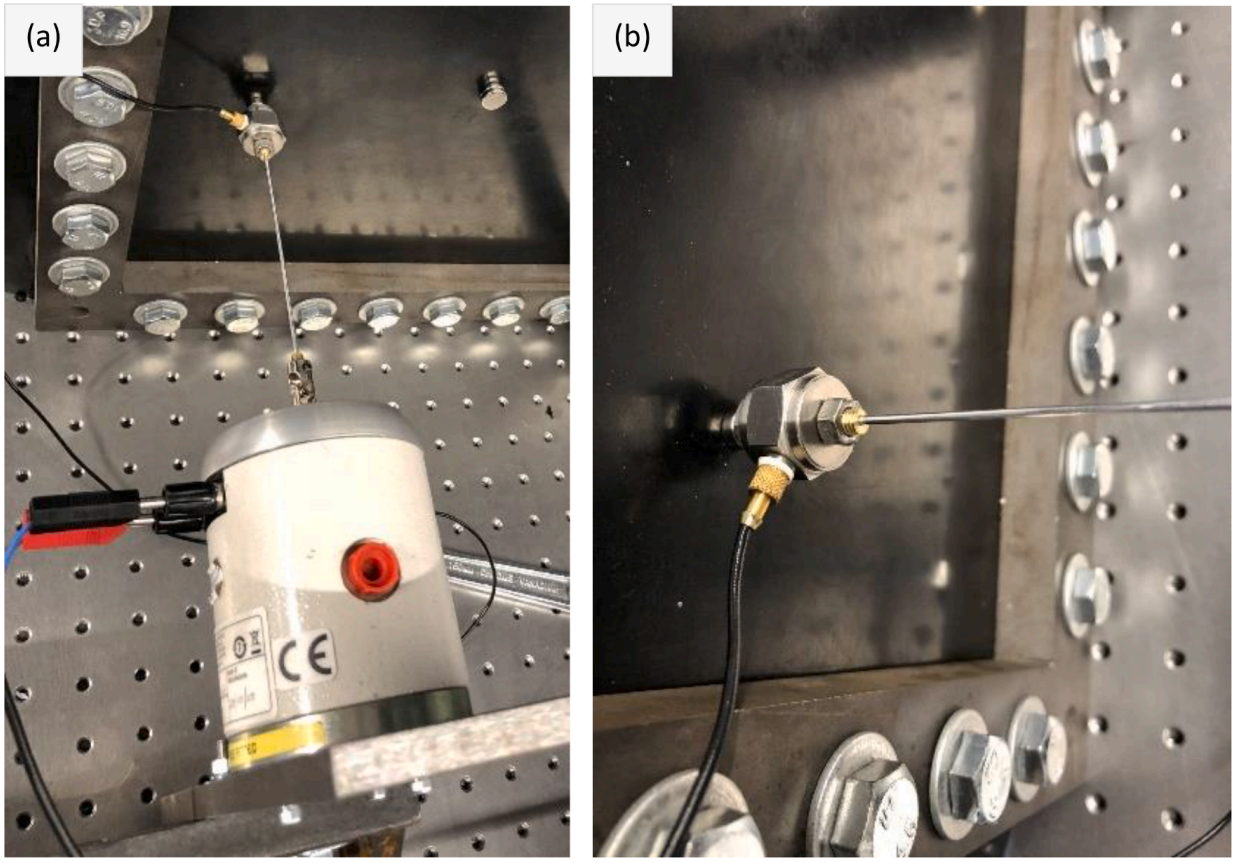

Fig. 3. (a) An LDS permanent magnet V200 Series shaker mounted to the table using a right-angle mounting fixture and connected to the plate using a steel stinger, and (b) a B&K 8200 force transducer added to the end of the steel stinger to measure the applied force.

and the equations of motion are nondimensionalised as

$$
\begin{aligned}
u_{tt} \;+\;& M_{mass}\delta(x-x_{mass})\delta(y-y_{mass})u_{tt} - 4\frac{1}{{\eta_b}^2}A_2u_{xx} - \frac{1}{{\eta_a}^2}A_2u_{yy} - 3\frac{1}{\eta_a\eta_b}A_2v_{xy} + 12\frac{{\eta_a}}{{\eta_b}^2}A_1\frac{\partial}{\partial x}\left({u_x}^2\right)\\
&+ \frac{1}{2}\frac{1}{\eta_a}A_3\frac{\partial}{\partial x}\left({u_y}^2\right) + \frac{1}{\eta_a}A_3\frac{\partial}{\partial y}\left(u_xu_y\right) - 2\frac{1}{\eta_b}A_4\frac{\partial}{\partial x}\left(u_xv_y\right) + \frac{1}{\eta_b}A_3\frac{\partial}{\partial x}\left(u_yv_x\right) + \frac{1}{\eta_b}A_3\frac{\partial}{\partial y}\left(u_xv_x\right)\\
&+ \frac{\eta_b}{{\eta_a}^2}A_3\frac{\partial}{\partial y}\left(u_yv_y\right) - \frac{1}{\eta_a}A_4\frac{\partial}{\partial x}\left({v_y}^2\right) + \frac{1}{2}\frac{\eta_a}{{\eta_b}^2}A_3\frac{\partial}{\partial x}\left({v_x}^2\right) + \frac{1}{\eta_a}A_3\frac{\partial}{\partial y}\left(v_xv_y\right) - 2\frac{\eta_a}{{\eta_b}^2}A_2\frac{\partial}{\partial x}\left(w_x^2\right)\\
&- \frac{1}{\eta_a}A_2\frac{\partial}{\partial x}\left(w_y^2\right) + \frac{{\eta_a}^3}{{\eta_b}^2}A_1\frac{\partial}{\partial x}\left({w_{xx}}^2\right) - \frac{1}{12}\frac{{\eta_b}^2}{\eta_a}A_4\frac{\partial}{\partial x}\left({w_{yy}}^2\right) - \frac{1}{6}\eta_aA_4\frac{\partial}{\partial x}\left(w_{xx}w_{yy}\right)\\
&+ \frac{1}{6}\eta_aA_3\frac{\partial}{\partial x}\left({w_{xy}}^2\right) - \frac{1}{\eta_a}A_2\frac{\partial}{\partial y}\left(w_xw_y\right) + \frac{1}{6}\eta_aA_3\frac{\partial}{\partial y}\left(w_{xx}w_{xy}\right) + \frac{1}{6}\frac{{\eta_b}^2}{\eta_a}A_3\frac{\partial}{\partial y}\left(w_{xy}w_{yy}\right)\\
&+ 12\frac{{\eta_a}^2}{{\eta_b}^2}A_1\frac{\partial}{\partial x}\left(u_xw_x^2\right) - A_4\frac{\partial}{\partial x}\left(u_xw_y^2\right) + A_3\frac{\partial}{\partial x}\left(u_yw_xw_y\right) + A_3\frac{\partial}{\partial y}\left(u_xw_xw_y\right) + \frac{1}{2}A_3\frac{\partial}{\partial y}\left(u_yw_x^2\right)\\
&+ \frac{1}{2}\frac{{\eta_b}^2}{{\eta_a}^2}A_3\frac{\partial}{\partial y}\left(u_yw_y^2\right) - \frac{\eta_b}{\eta_a}A_4\frac{\partial}{\partial x}\left(v_yw_y^2\right) - \frac{\eta_a}{\eta_b}A_4\frac{\partial}{\partial x}\left(v_yw_x^2\right) + \frac{\eta_a}{\eta_b}A_3\frac{\partial}{\partial x}\left(v_xw_xw_y\right)\\
&+ \frac{1}{2}\frac{\eta_a}{\eta_b}A_3\frac{\partial}{\partial y}\left(v_xw_x^2\right) + \frac{1}{2}\frac{\eta_b}{\eta_a}A_3\frac{\partial}{\partial y}\left(v_xw_y^2\right) + \frac{\eta_b}{\eta_a}A_3\frac{\partial}{\partial y}\left(v_yw_xw_y\right) + 3\frac{{\eta_a}^3}{{\eta_b}^2}A_1\frac{\partial}{\partial x}\left(w_x^4\right)\\
&- \frac{1}{4}\frac{{\eta_b}^2}{\eta_a}A_4\frac{\partial}{\partial x}\left(w_y^4\right) - \frac{1}{4}\eta_aA_5\frac{\partial}{\partial x}\left(w_x^2w_y^2\right) + \frac{1}{2}\eta_aA_3\frac{\partial}{\partial y}\left(w_x^3w_y\right) + \frac{1}{2}\frac{{\eta_b}^2}{\eta_a}A_3\frac{\partial}{\partial y}\left(w_xw_y^3\right) = 0,
\end{aligned}
\tag{16}
$$

$$
\begin{aligned}
&w_{tt} - \frac{1}{12}{\eta_a}^2 (w_{xxtt}) + M_{mass}\delta(x - x_{mass})\delta(y - y_{mass})w_{tt} - \frac{1}{12}{\eta_b}^2 \left(w_{yytt}\right) + \frac{1}{3}A_2\frac{1}{\xi^2}w_{xxxx} \\
&+\frac{2}{3}A_2 w_{xxyy} + \frac{1}{3}A_2\frac{{\eta_b}^2}{{\eta_a}^2}\left(w_{yyyy}\right) - 4A_2\frac{\eta_a}{{\eta_b}^2}\frac{\partial}{\partial x}\left(u_x w_x\right) - 2A_1\frac{{\eta_a}^3}{{\eta_b}^2}\frac{\partial^2}{\partial x^2}\left(u_x w_{xx}\right) + \frac{1}{6}A_4\eta_a\frac{\partial^2}{\partial x^2}\left(u_x w_{yy}\right) \\
&-\frac{1}{6}A_3\eta_a\frac{\partial^2}{\partial x^2}\left(u_y w_{xy}\right) + \frac{1}{6}A_4\eta_a\frac{\partial^2}{\partial y^2}\left(u_x w_{xx}\right) + \frac{1}{6}A_4\frac{{\eta_b}^2}{\eta_a}\frac{\partial^2}{\partial y^2}\left(u_x w_{yy}\right) - \frac{1}{6}A_3\frac{{\eta_b}^2}{\eta_a}\frac{\partial^2}{\partial y^2}\left(u_y w_{xy}\right) \\
&-2A_2\frac{1}{\eta_a}\frac{\partial}{\partial y}\left(u_x w_y\right) - A_2\frac{1}{\eta_a}\frac{\partial}{\partial y}\left(u_y w_x\right) - A_2\frac{1}{\eta_a}\frac{\partial}{\partial x}\left(u_y w_y\right) - \frac{1}{3}A_3\eta_a\frac{\partial^2}{\partial x\partial y}\left(u_x w_{xy}\right) \\
&-\frac{1}{6}A_3\eta_a\frac{\partial^2}{\partial x\partial y}\left(u_y w_{xx}\right) - \frac{1}{6}A_3\frac{{\eta_b}^2}{\eta_a}\frac{\partial^2}{\partial x\partial y}\left(u_y w_{yy}\right) - \frac{1}{6}A_3\frac{{\eta_a}^2}{\eta_b}\frac{\partial^2}{\partial x\partial y}\left(v_x w_{xx}\right) - 4A_2\frac{\eta_b}{{\eta_a}^2}\frac{\partial}{\partial y}\left(v_y w_y\right) \\
&-2A_1\frac{{\eta_b}^3}{{\eta_a}^2}\frac{\partial^2}{\partial y^2}\left(v_y w_{yy}\right) + \frac{1}{6}A_4\frac{{\eta_a}^2}{\eta_b}\frac{\partial^2}{\partial x^2}\left(v_y w_{xx}\right) - \frac{1}{6}A_3\frac{{\eta_a}^2}{\eta_b}\frac{\partial^2}{\partial x^2}\left(v_x w_{xy}\right) + \frac{1}{6}A_4\eta_b\frac{\partial^2}{\partial x^2}\left(v_y w_{yy}\right) \\
&+\frac{1}{6}A_4\eta_b\frac{\partial^2}{\partial y^2}\left(v_y w_{xx}\right) - \frac{1}{6}A_3\eta_b\frac{\partial^2}{\partial y^2}\left(v_x w_{xy}\right) - 2A_2\frac{1}{\eta_b}\frac{\partial}{\partial x}\left(v_y w_x\right) - A_2\frac{1}{\eta_b}\frac{\partial}{\partial y}\left(v_x w_x\right) \\
&-A_2\frac{1}{\eta_b}\frac{\partial}{\partial x}\left(v_x w_y\right) - \frac{1}{3}A_3\eta_b\frac{\partial^2}{\partial x\partial y}\left(v_y w_{xy}\right) - \frac{1}{6}A_3\eta_b\frac{\partial^2}{\partial x\partial y}\left(v_x w_{yy}\right) - 2A_2\frac{{\eta_a}^2}{{\eta_b}^2}\frac{\partial}{\partial x}\left(w_x^3\right) \\
&-2A_2\frac{{\eta_b}^2}{{\eta_a}^2}\frac{\partial}{\partial y}\left(w_y^3\right) - A_2\frac{\partial}{\partial x}\left(w_x w_y^2\right) - A_2\frac{\partial}{\partial y}\left(w_x^2 w_y\right) + A_1\frac{{\eta_a}^4}{{\eta_b}^2}\frac{\partial}{\partial x}\left(w_x {w_{xx}}^2\right) + A_1\frac{{\eta_b}^4}{{\eta_a}^2}\frac{\partial}{\partial y}\left(w_y {w_{yy}}^2\right) \\
&-\frac{1}{12}A_4{\eta_b}^2\frac{\partial}{\partial x}\left(w_x {w_{yy}}^2\right) - \frac{1}{12}A_4{\eta_a}^2\frac{\partial}{\partial y}\left({w_{xx}}^2 w_y\right) - \frac{1}{6}A_4{\eta_a}^2\frac{\partial}{\partial x}\left(w_x w_{xx} w_{yy}\right) \\
&-\frac{1}{6}A_4{\eta_b}^2\frac{\partial}{\partial y}\left(w_{xx} w_y w_{yy}\right) + \frac{1}{6}A_3{\eta_a}^2\frac{\partial}{\partial x}\left(w_x {w_{xy}}^2\right) + \frac{1}{6}A_3{\eta_b}^2\frac{\partial}{\partial y}\left(w_y {w_{xy}}^2\right) - A_1\frac{{\eta_a}^4}{{\eta_b}^2}\frac{\partial^2}{\partial x^2}\left(w_x^2 w_{xx}\right) \\
&-A_1\frac{{\eta_b}^4}{{\eta_a}^2}\frac{\partial^2}{\partial y^2}\left(w_y^2 w_{yy}\right) + \frac{1}{12}A_4{\eta_b}^2\frac{\partial^2}{\partial x^2}\left(w_y^2 w_{yy}\right) + \frac{1}{12}A_4{\eta_a}^2\frac{\partial^2}{\partial y^2}\left(w_x^2 w_{xx}\right) + \frac{1}{12}A_4{\eta_a}^2\frac{\partial^2}{\partial x^2}\left(w_{xx} w_y^2\right) \\
&+\frac{1}{12}A_4{\eta_b}^2\frac{\partial^2}{\partial y^2}\left(w_{xx} w_y^2\right) + \frac{1}{12}A_4{\eta_a}^2\frac{\partial^2}{\partial x^2}\left(w_x^2 w_{yy}\right) + \frac{1}{12}A_4{\eta_b}^2\frac{\partial^2}{\partial y^2}\left(w_x^2 w_{yy}\right) \\
&-\frac{1}{6}A_3{\eta_a}^2\frac{\partial^2}{\partial x^2}\left(w_x w_y w_{xy}\right) - \frac{1}{6}A_3{\eta_b}^2\frac{\partial^2}{\partial y^2}\left(w_x w_y w_{xy}\right) - \frac{1}{6}A_3{\eta_a}^2\frac{\partial^2}{\partial x\partial y}\left(w_x^2 w_{xy}\right) \\
&-\frac{1}{6}A_3{\eta_b}^2\frac{\partial^2}{\partial x\partial y}\left(w_y^2 w_{xy}\right) - \frac{1}{6}A_3{\eta_b}^2\frac{\partial^2}{\partial x\partial y}\left(w_x w_y w_{yy}\right) - \frac{1}{6}A_3{\eta_a}^2\frac{\partial^2}{\partial x\partial y}\left(w_x w_y w_{xx}\right) - A_2\frac{\partial}{\partial x}\left(w_x {w_y}^2\right) \\
&-A_2\frac{\partial}{\partial y}\left({w_x}^2 w_y\right) + \frac{1}{6}A_3{\eta_a}^2\frac{\partial}{\partial x}\left(w_{xx} w_y w_{xy}\right) + \frac{1}{6}A_3{\eta_a}^2\frac{\partial}{\partial y}\left(w_x w_{xx} w_{xy}\right) + \frac{1}{6}A_3{\eta_b}^2\frac{\partial}{\partial x}\left(w_y w_{xy} w_{yy}\right) \\
&+\frac{1}{6}A_3{\eta_b}^2\frac{\partial}{\partial y}\left(w_x w_{xy} w_{yy}\right) + 12A_1\frac{{\eta_a}^2}{{\eta_b}^2}\frac{\partial}{\partial x}\left({u_x}^2 w_x\right) - A_4\frac{\partial}{\partial y}\left({u_x}^2 w_y\right) + \frac{1}{2}A_3\frac{{\eta_b}^2}{{\eta_a}^2}\frac{\partial}{\partial y}\left({u_y}^2 w_y\right) \\
&+A_3\frac{\partial}{\partial x}\left(u_x u_y w_y\right) + A_3\frac{\partial}{\partial y}\left(u_x u_y w_x\right) + \frac{1}{2}A_3\frac{\partial}{\partial x}\left({u_y}^2 w_x\right) + 12A_1\frac{{\eta_b}^2}{{\eta_a}^2}\frac{\partial}{\partial y}\left({v_y}^2 w_y\right) - A_4\frac{\partial}{\partial x}\left({v_y}^2 w_x\right) \\
&+\frac{1}{2}A_3\frac{{\eta_a}^2}{{\eta_b}^2}\frac{\partial}{\partial x}\left({v_x}^2 w_x\right) + A_3\frac{\partial}{\partial x}\left(v_x v_y w_y\right) + A_3\frac{\partial}{\partial y}\left(v_x v_y w_x\right) + \frac{1}{2}A_3\frac{\partial}{\partial y}\left({v_x}^2 w_y\right) - 2A_4\frac{\eta_a}{\eta_b}\frac{\partial}{\partial x}\left(u_x v_y w_x\right) \\
&-2A_4\frac{\eta_b}{\eta_a}\frac{\partial}{\partial y}\left(u_x v_y w_y\right) + A_3\frac{\eta_a}{\eta_b}\frac{\partial}{\partial x}\left(u_y v_x w_x\right) + A_3\frac{\eta_b}{\eta_a}\frac{\partial}{\partial y}\left(u_y v_x w_y\right) + A_3\frac{\eta_a}{\eta_b}\frac{\partial}{\partial x}\left(u_x v_x w_y\right) \\
&+\ldots
\end{aligned}
$$

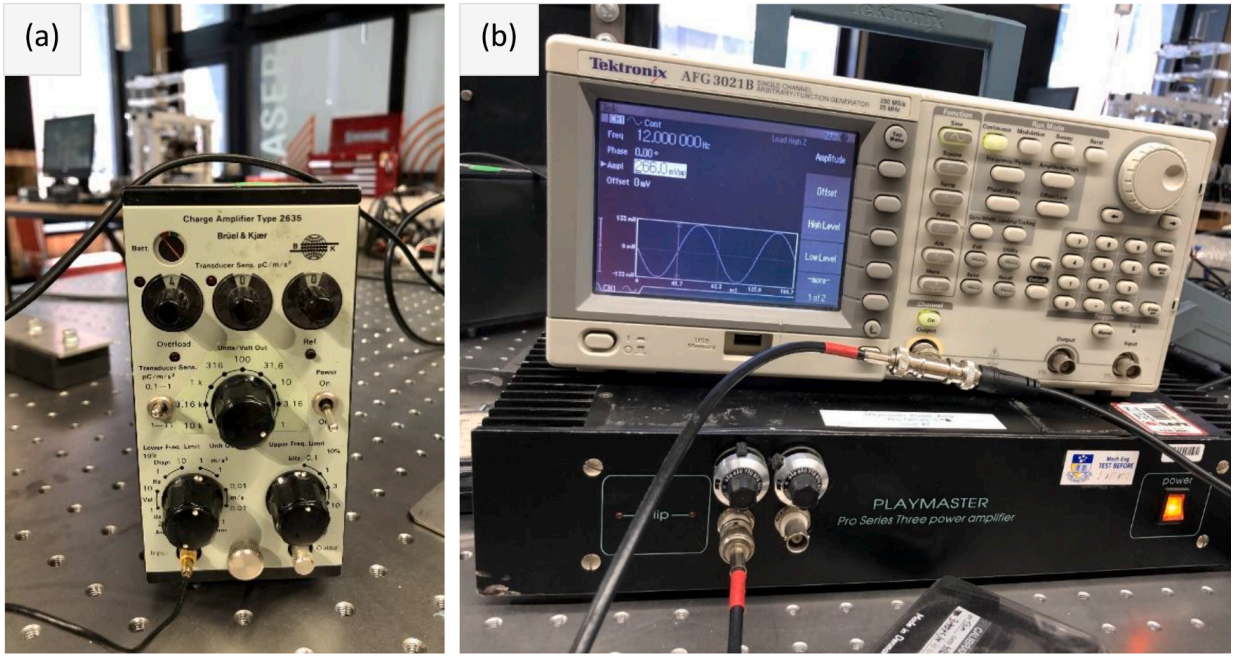

Fig. 4. (a) A B&K 2635 charge amplifier connected to the force transducer, and (b) a Tektronix AFG3021 function generator and a Playmaster pro series 3 power amplifier for generating a sinusoidal excitation with a certain frequency and amplitude.

$$
\begin{aligned}
&+\ldots\\
&+A_3\frac{\eta_b}{\eta_a}\frac{\partial}{\partial y}\left(u_y v_y w_x\right)+A_3\frac{\eta_b}{\eta_a}\frac{\partial}{\partial x}\left(u_y v_y w_y\right)+A_3\frac{\eta_a}{\eta_b}\frac{\partial}{\partial y}\left(u_x v_x w_x\right)+12A_1\frac{{\eta_a}^3}{{\eta_b}^2}\frac{\partial}{\partial x}\left(u_x w_x^3\right)\\
&-A_4\eta_a\frac{\partial}{\partial x}\left(u_x w_x w_y^2\right)+A_3\eta_a\frac{\partial}{\partial x}\left(u_y {w_x}^2 w_y\right)-A_4\eta_a\frac{\partial}{\partial y}\left(u_x w_x^2 w_y\right)-A_4\frac{{\eta_b}^2}{\eta_a}\frac{\partial}{\partial y}\left(u_x w_y^3\right)\\
&+A_3\frac{{\eta_b}^2}{\eta_a}\frac{\partial}{\partial y}\left(u_y w_x {w_y}^2\right)+A_3\eta_a\frac{\partial}{\partial x}\left(u_x w_x {w_y}^2\right)+\frac{1}{2}A_3\eta_a\frac{\partial}{\partial x}\left(u_y w_x^2 w_y\right)+\frac{1}{2}A_3\frac{{\eta_b}^2}{\eta_a}\frac{\partial}{\partial x}\left(u_y w_y^3\right)\\
&+A_3\eta_a\frac{\partial}{\partial y}\left(u_x {w_x}^2 w_y\right)+\frac{1}{2}A_3\eta_a\frac{\partial}{\partial y}\left(u_y w_x^3\right)+\frac{1}{2}A_3\frac{{\eta_b}^2}{\eta_a}\frac{\partial}{\partial y}\left(u_y w_x w_y^2\right)+12A_1\frac{{\eta_b}^3}{{\eta_a}^2}\frac{\partial}{\partial y}\left(v_y w_y^3\right)\\
&-A_4\eta_b\frac{\partial}{\partial y}\left(v_y w_x^2 w_y\right)+A_3\eta_b\frac{\partial}{\partial y}\left(v_x w_x {w_y}^2\right)-A_4\eta_b\frac{\partial}{\partial x}\left(v_y w_x w_y^2\right)-A_4\frac{{\eta_a}^2}{\eta_b}\frac{\partial}{\partial x}\left(v_y w_x^3\right)\\
&+A_3\frac{{\eta_a}^2}{\eta_b}\frac{\partial}{\partial x}\left(v_x {w_x}^2 w_y\right)+A_3\eta_b\frac{\partial}{\partial y}\left(v_y {w_x}^2 w_y\right)+\frac{1}{2}A_3\eta_b\frac{\partial}{\partial y}\left(v_x w_x w_y^2\right)+\frac{1}{2}A_3\frac{{\eta_a}^2}{\eta_b}\frac{\partial}{\partial y}\left(v_x w_x^3\right)\\
&+A_3\eta_b\frac{\partial}{\partial x}\left(v_y w_x {w_y}^2\right)+\frac{1}{2}A_3\eta_b\frac{\partial}{\partial x}\left(v_x w_y^3\right)+\frac{1}{2}A_3\frac{{\eta_a}^2}{\eta_b}\frac{\partial}{\partial x}\left(v_x w_x^2 w_y\right)+3A_1\frac{{\eta_a}^4}{{\eta_b}^2}\frac{\partial}{\partial x}\left(w_x^5\right)\\
&+3A_1\frac{{\eta_b}^4}{{\eta_a}^2}\frac{\partial}{\partial y}\left(w_y^5\right)-\frac{1}{4}A_4{\eta_b}^2\frac{\partial}{\partial x}\left(w_x w_y^4\right)-\frac{1}{4}A_4{\eta_a}^2\frac{\partial}{\partial y}\left(w_x^4 w_y\right)-\frac{1}{4}A_5{\eta_a}^2\frac{\partial}{\partial x}\left(w_x^3 w_y^2\right)\\
&-\frac{1}{4}A_5{\eta_b}^2\frac{\partial}{\partial y}\left(w_x^2 w_y^3\right)+\frac{1}{2}A_3{\eta_a}^2\frac{\partial}{\partial x}\left(w_x^3 {w_y}^2\right)+\frac{1}{2}A_3{\eta_b}^2\frac{\partial}{\partial y}\left({w_x}^2 w_y^3\right)+\frac{1}{2}A_3{\eta_b}^2\frac{\partial}{\partial x}\left(w_x w_y^4\right)\\
&+\frac{1}{2}A_3{\eta_a}^2\frac{\partial}{\partial y}\left(w_x^4 w_y\right)=F\cos(\Omega t),
\end{aligned}
\tag{17}
$$

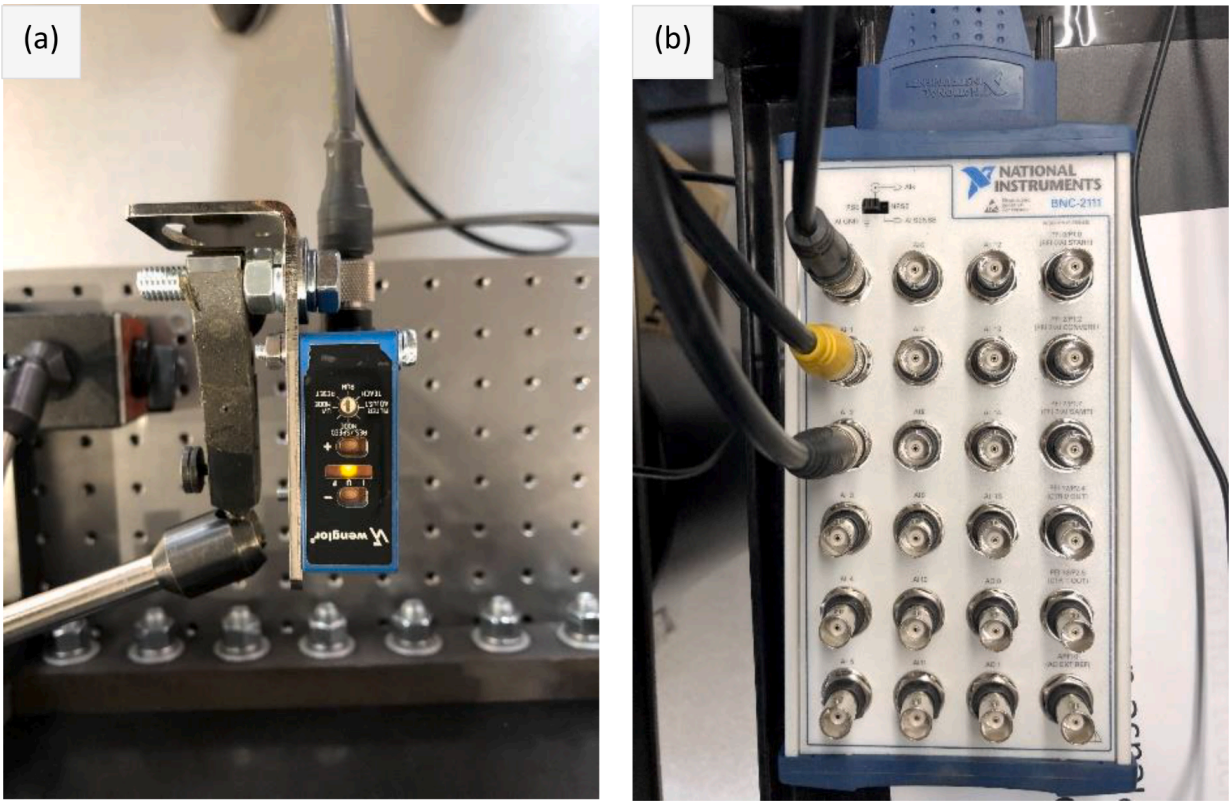

Fig. 5. (a) Wenglor laser distance sensor to record the displacement in the rubber plate, and (b) an NI BNC-2111 shielded connector block to collect the signals.

$$
\begin{aligned}
&v_{tt} + M_{mass}\delta(x-x_{mass})\delta(y-y_{mass})v_{tt} - \frac{3}{\eta_a\eta_b}A_2u_{xy} - \frac{4}{{\eta_a}^2}A_2v_{yy} - \frac{1}{{\eta_b}^2}A_2v_{xx} - \frac{1}{\eta_b}A_4\frac{\partial}{\partial y}\left({u_x}^2\right)\\
&\quad+\frac{1}{2}\frac{\eta_b}{{\eta_a}^2}A_3\frac{\partial}{\partial y}\left({u_y}^2\right) + \frac{1}{\eta_b}A_3\frac{\partial}{\partial x}\left(u_xu_y\right) - \frac{2}{\eta_a}A_4\frac{\partial}{\partial y}\left(u_xv_y\right) + \frac{1}{\eta_a}A_3\frac{\partial}{\partial y}\left(u_yv_x\right)\\
&\quad+\frac{\eta_a}{{\eta_b}^2}A_3\frac{\partial}{\partial x}\left(u_xv_x\right) + \frac{1}{\eta_a}A_3\frac{\partial}{\partial x}\left(u_yv_y\right) + 12\frac{\eta_b}{{\eta_a}^2}A_1\frac{\partial}{\partial y}\left({v_y}^2\right) + \frac{1}{2}\frac{1}{\eta_b}A_3\frac{\partial}{\partial y}\left({v_x}^2\right)\\
&\quad+\frac{1}{\eta_b}A_3\frac{\partial}{\partial x}\left(v_xv_y\right) - 2\frac{\eta_b}{{\eta_a}^2}A_2\frac{\partial}{\partial y}\left(w_y^2\right) - \frac{1}{\eta_b}A_2\frac{\partial}{\partial y}\left(w_x^2\right) + \frac{{\eta_b}^3}{{\eta_a}^2}A_1\frac{\partial}{\partial y}\left({w_{yy}}^2\right)\\
&\quad-\frac{1}{12}\frac{{\eta_a}^2}{\eta_b}A_4\frac{\partial}{\partial y}\left({w_{xx}}^2\right) - \frac{1}{6}\eta_bA_4\frac{\partial}{\partial y}\left(w_{xx}w_{yy}\right) + \frac{1}{6}\eta_bA_3\frac{\partial}{\partial y}\left({w_{xy}}^2\right) - \frac{1}{\eta_b}A_2\frac{\partial}{\partial x}\left(w_xw_y\right)\\
&\quad+\frac{1}{6}\frac{{\eta_a}^2}{\eta_b}A_3\frac{\partial}{\partial x}\left(w_{xx}w_{xy}\right) + \frac{1}{6}\eta_bA_3\frac{\partial}{\partial x}\left(w_{xy}w_{yy}\right) - \frac{\eta_a}{\eta_b}A_4\frac{\partial}{\partial y}\left(u_xw_x^2\right) - \frac{\eta_b}{\eta_a}A_4\frac{\partial}{\partial y}\left(u_xw_y^2\right)\\
&\quad+\frac{\eta_b}{\eta_a}A_3\frac{\partial}{\partial y}\left(u_yw_xw_y\right) + \frac{\eta_a}{\eta_b}A_3\frac{\partial}{\partial x}\left(u_xw_xw_y\right) + \frac{1}{2}\frac{\eta_a}{\eta_b}A_3\frac{\partial}{\partial x}\left(u_yw_x^2\right) + \frac{1}{2}\frac{\eta_b}{\eta_a}A_3\frac{\partial}{\partial x}\left(u_yw_y^2\right)\\
&\quad+12\frac{{\eta_b}^2}{{\eta_a}^2}A_1\frac{\partial}{\partial y}\left(v_yw_y^2\right) - A_4\frac{\partial}{\partial y}\left(v_yw_x^2\right) + A_3\frac{\partial}{\partial y}\left(v_xw_xw_y\right) + \frac{1}{2}\frac{{\eta_a}^2}{{\eta_b}^2}A_3\frac{\partial}{\partial x}\left(v_xw_x^2\right)\\
&\quad+\frac{1}{2}A_3\frac{\partial}{\partial x}\left(v_xw_y^2\right) + A_3\frac{\partial}{\partial x}\left(v_yw_xw_y\right) + 3\frac{{\eta_b}^3}{{\eta_a}^2}A_1\frac{\partial}{\partial y}\left(w_y^4\right) - \frac{1}{4}\frac{{\eta_a}^2}{\eta_b}A_4\frac{\partial}{\partial y}\left(w_x^4\right)\\
&\quad-\frac{1}{4}\eta_bA_4\frac{\partial}{\partial y}\left(w_x^2w_y^2\right) + \frac{1}{2}\frac{{\eta_a}^2}{\eta_b}A_3\frac{\partial}{\partial x}\left(w_x^3w_y\right) + \frac{1}{2}\eta_bA_3\frac{\partial}{\partial x}\left(w_xw_y^3\right) = 0.
\end{aligned}
\tag{18}
$$

Using the Galerkin scheme, the degrees of freedom are written in series functions

$$u(x,y,t) = \sum_{i=1}^{M}\sum_{j=1}^{M}U_{ij}(t)\phi_i(x)\psi_j(y) = \sum_{i=1}^{M}\sum_{j=1}^{M}U_{ij}(t)r_{ij}(x,y), \tag{19}$$

$$v(x,y,t) = \sum_{i=1}^{M}\sum_{j=1}^{M}V_{ij}(t)\phi_i(x)\psi_j(y) = \sum_{i=1}^{M}\sum_{j=1}^{M}V_{ij}(t)p_{ij}(x,y), \tag{20}$$

$$w(x,y,t) = \sum_{i=1}^{M}\sum_{j=1}^{M}W_{ij}(t)X_i(x)Y_j(y) = \sum_{i=1}^{M}\sum_{j=1}^{M}W_{ij}(t)q_{ij}(x,y), \tag{21}$$

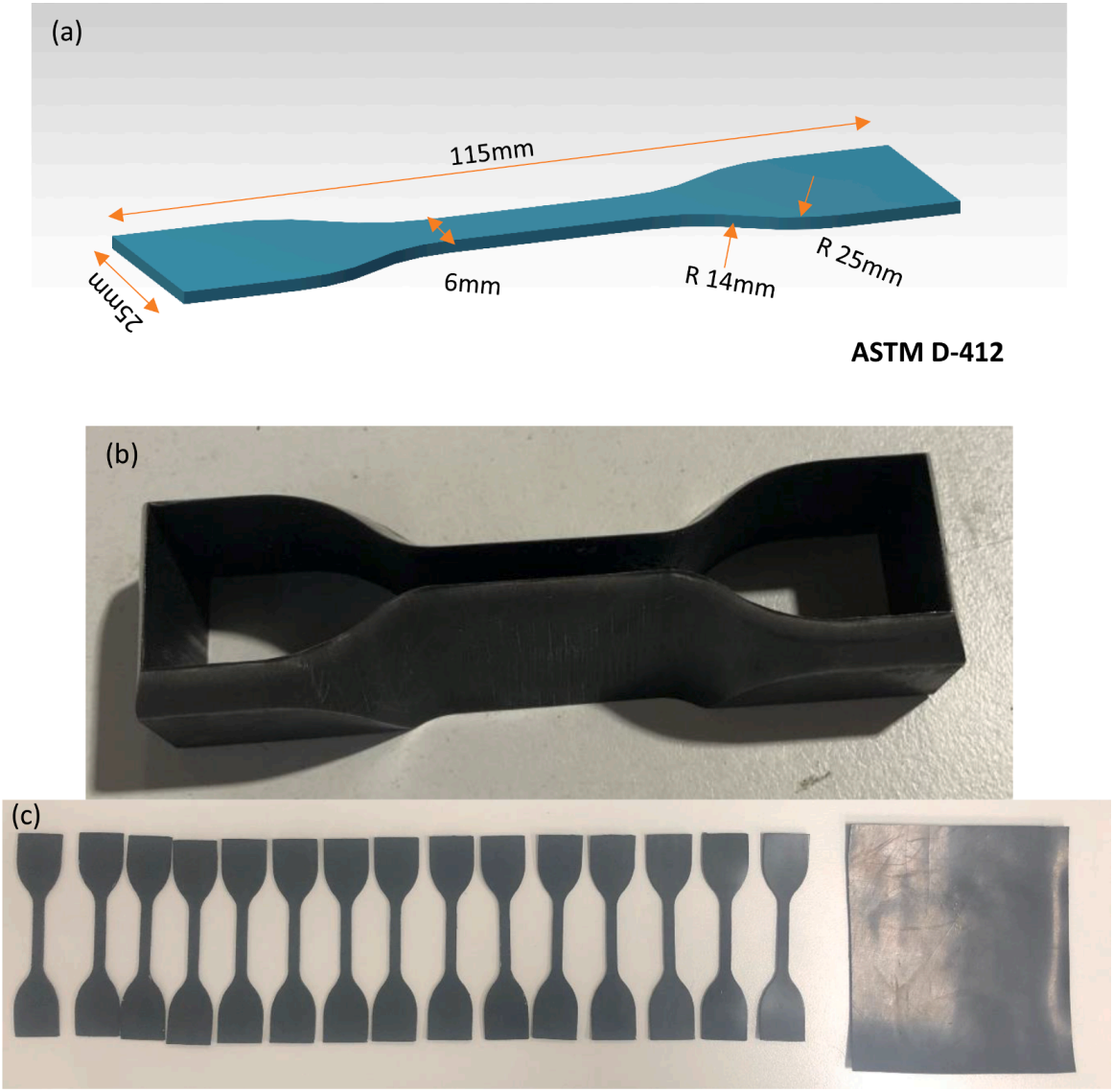

Fig. 6. (a) Dimensions, (b) mould and (c) specimen dumbbell samples for material testing of EPDM rubber following the ASTM D-412 standard.

where for a fully clamped hyperelastic plate model (Ghayesh & Farokhi, 2018)

$$\phi_i(x) = \sin(i\pi x), \tag{22}$$

$$\psi_i(y) = \sin(i\pi y), \tag{23}$$

$$X_i(x) = \cosh(\alpha_i x) - \cos(\alpha_i x) - \frac{\cosh(\alpha_i) - \cos(\alpha_i)}{\sinh(\alpha_i) - \sin(\alpha_i)}[\sinh(\alpha_i x) - \sin(\alpha_i x)], \tag{24}$$

$$Y_i(y) = \cosh(\alpha_i y) - \cos(\alpha_i y) - \frac{\cosh(\alpha_i) - \cos(\alpha_i)}{\sinh(\alpha_i) - \sin(\alpha_i)}[\sinh(\alpha_i y) - \sin(\alpha_i y)]. \tag{25}$$

Eqs. (19)–(21) can be used to discretise the coupled equations of motion and convert them to a system of nonlinear ordinary differential equations as

$$M_{11}\ddot{U} + KL_{11}U + KL_{12}V + KN_{11}U^2 + KN_{12}UV + KN_{13}V^2 + KN_{14}W^2 + KN_{15}UW^2 + KN_{16}VW^2 + KN_{17}W^4 = 0, \tag{26}$$

$$M_{22}\ddot{V} + KL_{21}U + KL_{22}V + KN_{21}U^2 + KN_{22}UV + KN_{23}V^2 + KN_{24}W^2 + KN_{25}UW^2 + KN_{26}VW^2 + KN_{27}W^4 = 0, \tag{27}$$

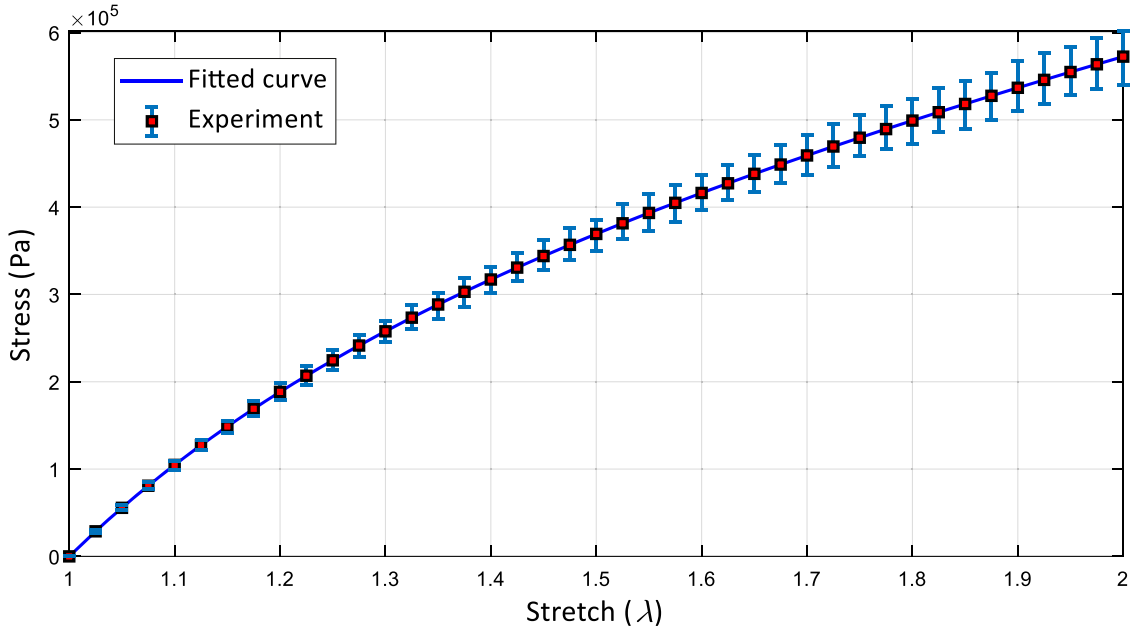

Fig. 7. The stress strain behaviour fitted curve of EPDM rubber following the ASTM D-412 standard with error bars.

$$M_{33}\ddot{W} + KL_{33}W + KN_{31}UW + KN_{32}VW + KN_{33}U^2W + KN_{34}UVW + KN_{35}V^2W \\ +KN_{36}W^3 + KN_{37}UW^3 + KN_{38}VW^3 + KN_{39}W^5 = fcos(\Omega t), \tag{28}$$

with the linear coefficient terms as

$$M_{11} = \int_0^1\int_0^1 r_{ij}(x,y)r_{kl}(x,y)dxdy + M_{mass}\int_0^1\int_0^1 r_{ij}(x,y)r_{kl}(x,y)\delta(x-x_{mass})\delta(y-y_{mass})dxdy, \tag{29}$$

$$KL_{11} = -\frac{4}{{\eta_b}^2}A_2\int_0^1\int_0^1 r_{ij}(x,y)r^{xx}_{kl}(x,y)dxdy - \frac{1}{{\eta_a}^2}A_2\int_0^1\int_0^1 r_{ij}(x,y)r^{yy}_{kl}(x,y)dxdy, \tag{30}$$

$$KL_{12} = -\frac{3}{\eta_a\eta_b}A_2\int_0^1\int_0^1 r_{ij}(x,y)p^{xy}_{kl}(x,y)dxdy, \tag{31}$$

$$M_{22} = \int_0^1\int_0^1 p_{ij}(x,y)p_{kl}(x,y)dxdy + M_{mass}\int_0^1\int_0^1 p_{ij}(x,y)p_{kl}(x,y)\delta(x-x_{mass})\delta(y-y_{mass})dxdy, \tag{32}$$

$$KL_{21} = -\frac{3}{\eta_a\eta_b}A_2\int_0^1\int_0^1 p_{ij}(x,y)r^{xy}_{kl}(x,y)dxdy, \tag{33}$$

$$KL_{22} = -\frac{4}{{\eta_a}^2}A_2\int_0^1\int_0^1 p_{ij}(x,y)p^{yy}_{kl}(x,y)dxdy - \frac{1}{{\eta_b}^2}A_2\int_0^1\int_0^1 p_{ij}(x,y)p^{xx}_{kl}(x,y)dxdy, \tag{34}$$

$$M_{33} = \int_0^1\int_0^1 q_{ij}(x,y)q_{kl}(x,y)dxdy - \frac{1}{12}{\eta_a}^2\int_0^1\int_0^1 q_{ij}(x,y)q^{xx}_{kl}(x,y)dxdy \\ -\frac{1}{12}{\eta_b}^2\int_0^1\int_0^1 q_{ij}(x,y)q^{yy}_{kl}(x,y)dxdy + M_{mass}\int_0^1\int_0^1 q_{ij}(x,y)q_{kl}(x,y)\delta(x-x_{mass})\delta(y-y_{mass})dxdy, \tag{35}$$

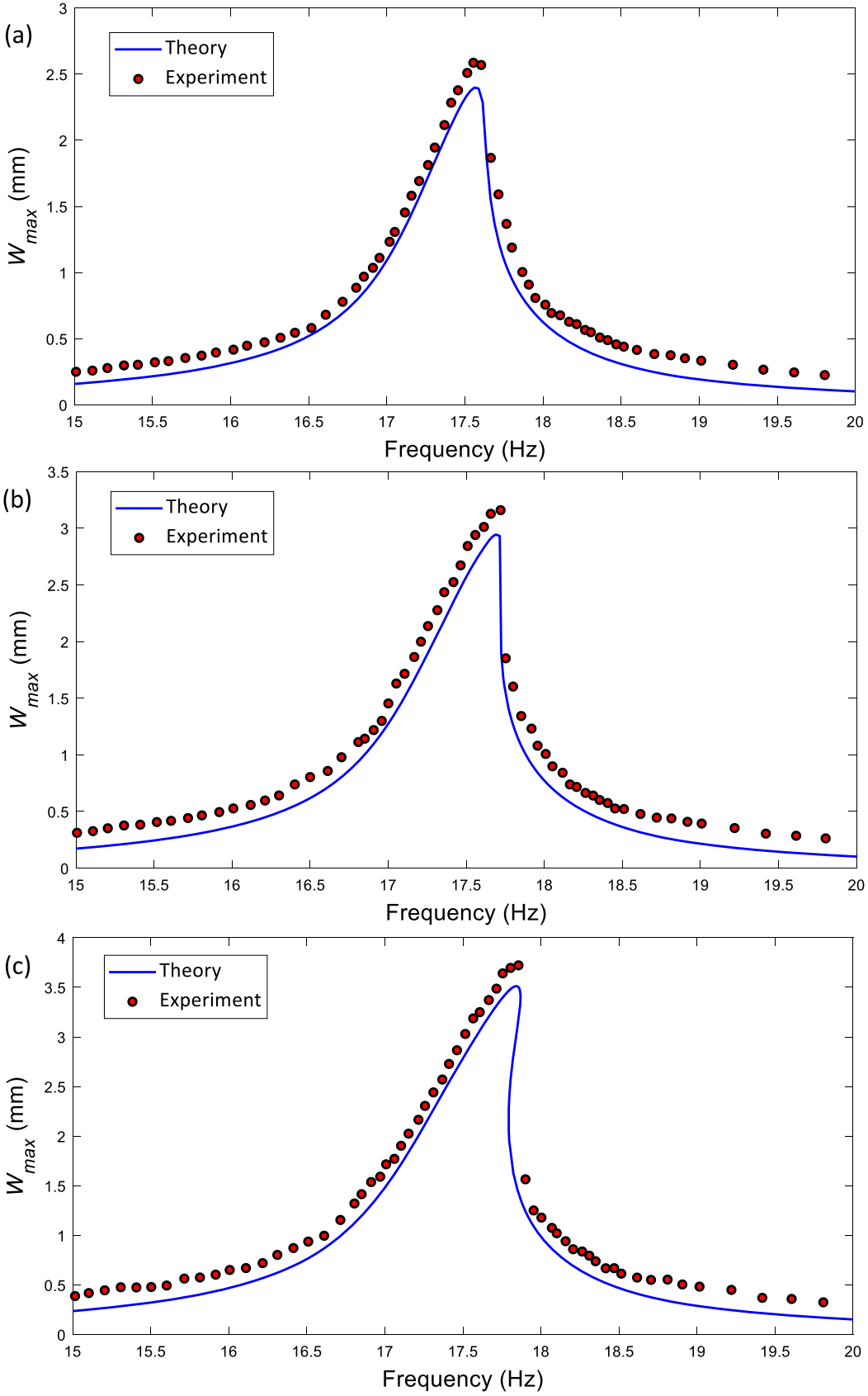

Fig. 8. The maximum transverse amplitude-frequency response of rubber plate excited with a (a) 2N, (b) 2.5N, and (c) 3N point sinusoidal loads.

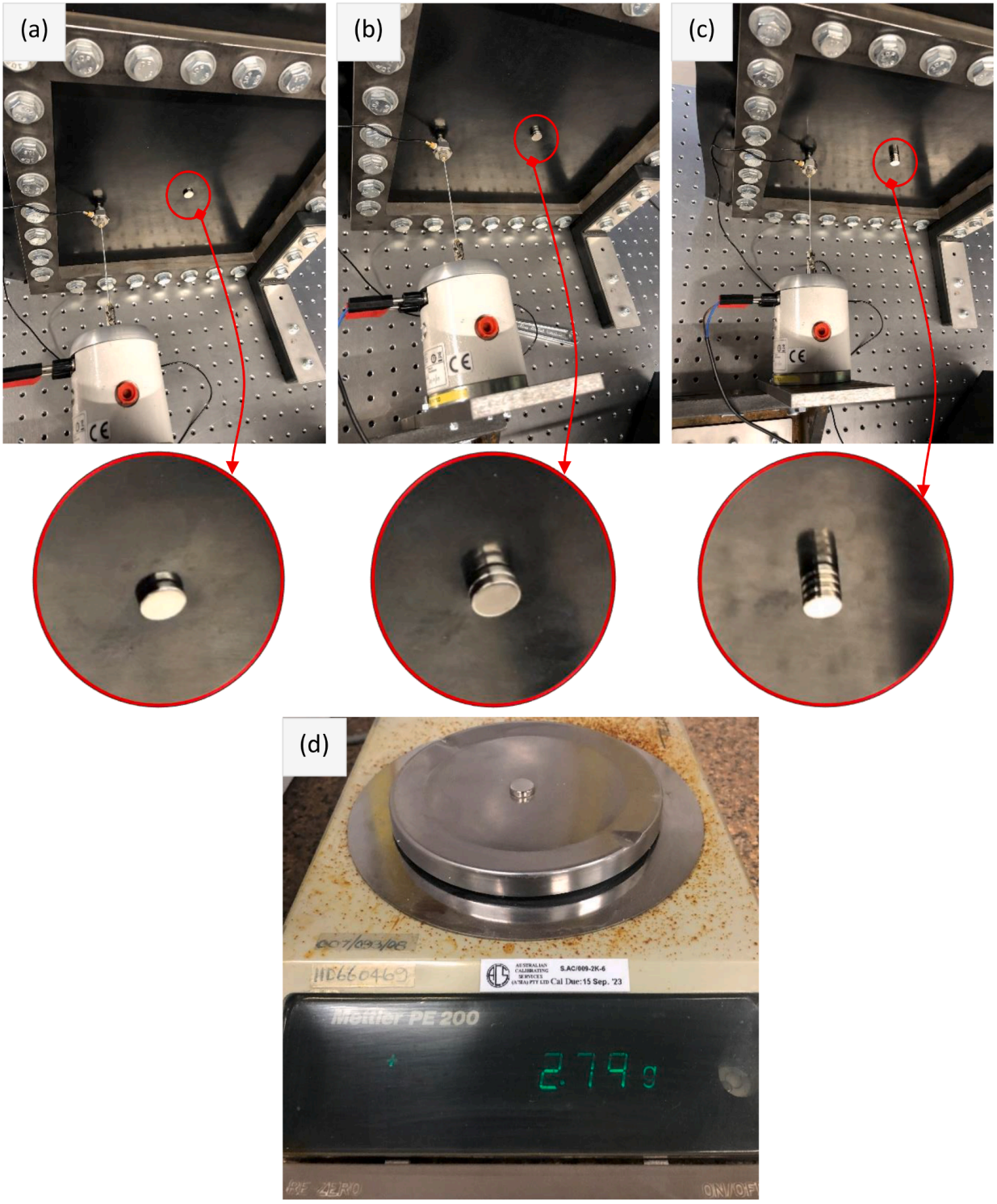

Fig. 9. Mass-sensing experiment setup of the hyperelastic plate with (a) two, (b) four, and (c) six magnets and (d) the weight measurement of each magnet using a METTLER PE 200 digital laboratory scale.

$$KL_{33} = +\frac{1}{3}\frac{\eta_a{}^2}{\eta_b{}^2}A_2\int_0^1\int_0^1 q_{ij}(x,y)q_{kl}^{xxxx}(x,y)dxdy + \frac{2}{3}A_2\int_0^1\int_0^1 q_{ij}(x,y)q_{kl}^{xxyy}(x,y)dxdy$$
$$+N_{xx}\int_0^1\int_0^1 q_{ij}(x,y)q_{kl}^{xx}(x,y)dxdy + N_{yy}\int_0^1\int_0^1 q_{ij}(x,y)q_{kl}^{yy}(x,y)dxdy + \frac{1}{3}\frac{\eta_b{}^2}{\eta_a{}^2}A_2\int_0^1\int_0^1 q_{ij}(x,y)q_{kl}^{yyyy}(x,y)dxdy, \tag{36}$$

and the higher-order nonlinear coefficients as shown in Appendix A. By simultaneously solving the discretised coupled equations of

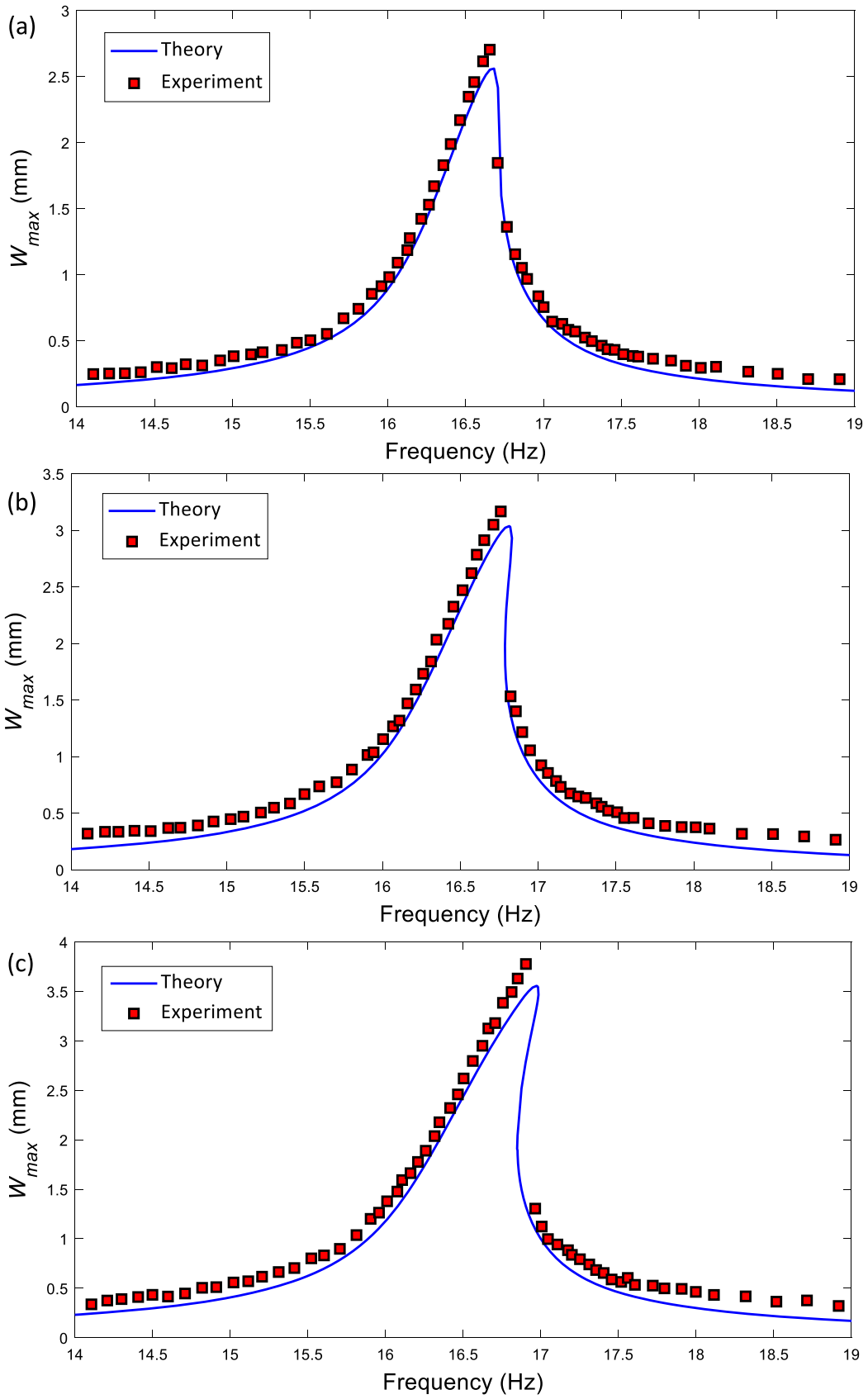

Fig. 10. The mass-sensing response of the rubber plate with two magnets and a (a) 2N, (b) 2.5N, and (c) 3N point sinusoidal loads.

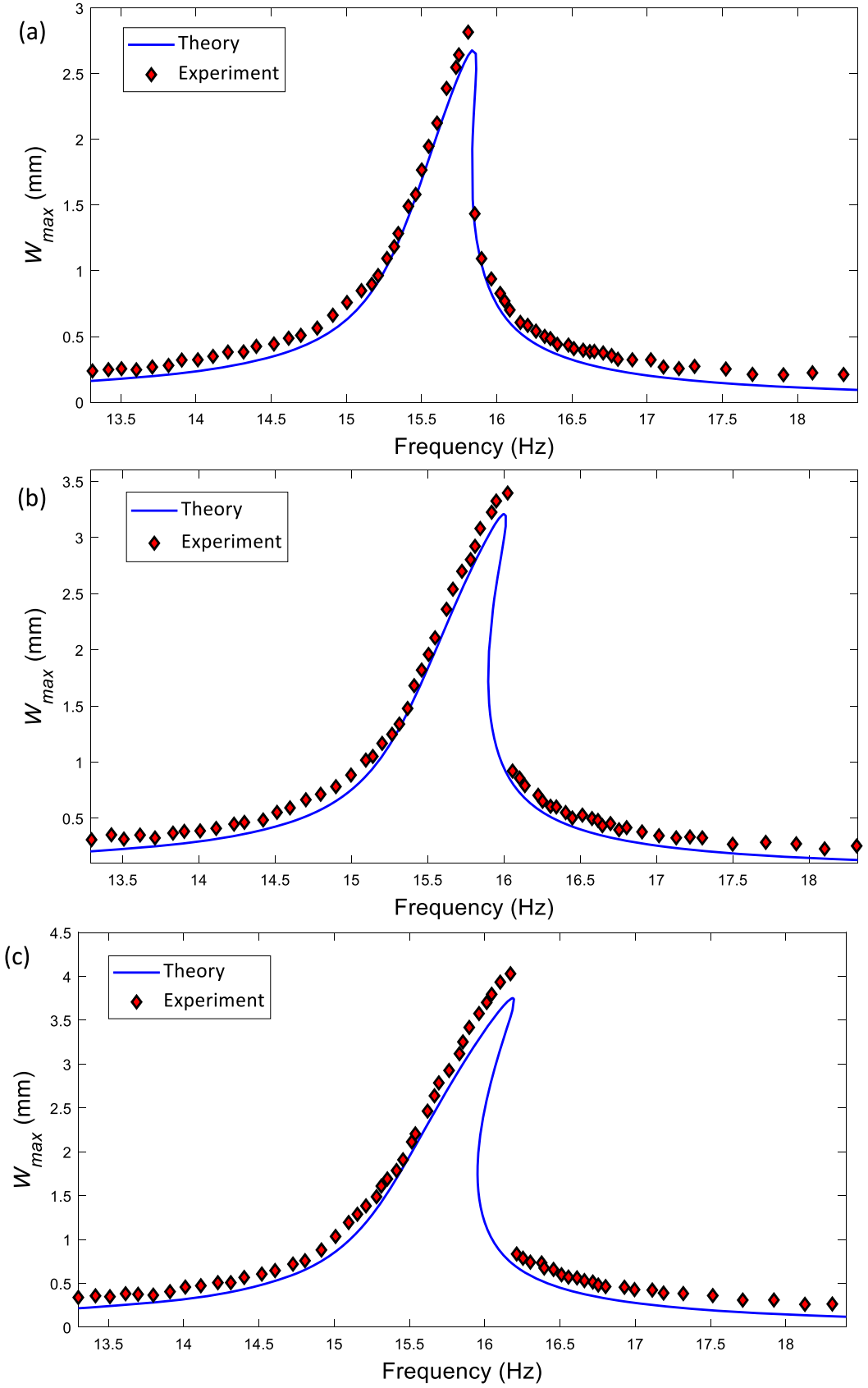

Fig. 11. The mass-sensing response of the rubber plate with four magnets and a (a) 2N, (b) 2.5N, and (c) 3N point sinusoidal loads.

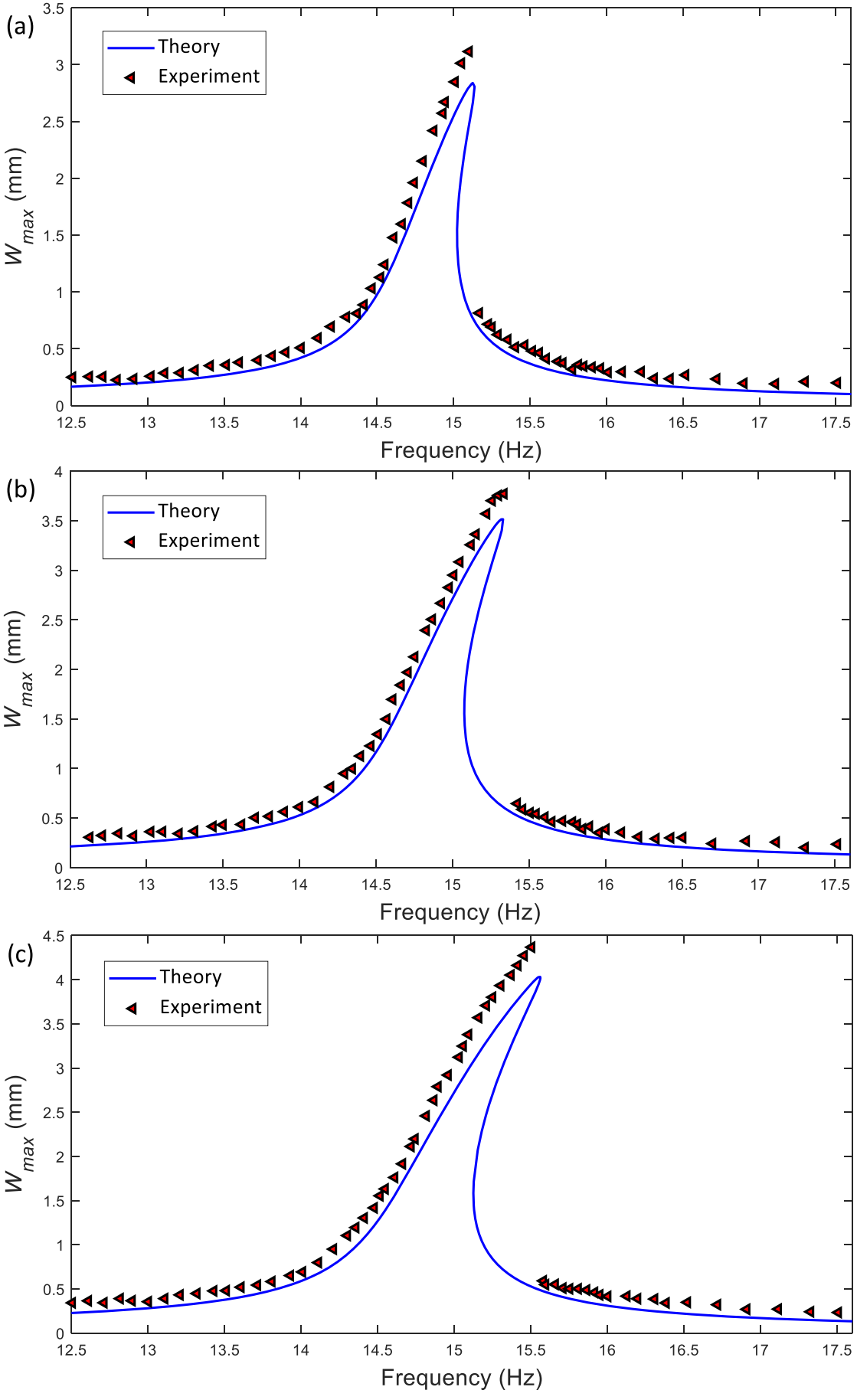

(caption on next page)

Fig. 12. The mass-sensing response of the rubber plate with six magnets and a (a) 2N, (b) 2.5N, and (c) 3N point sinusoidal loads.

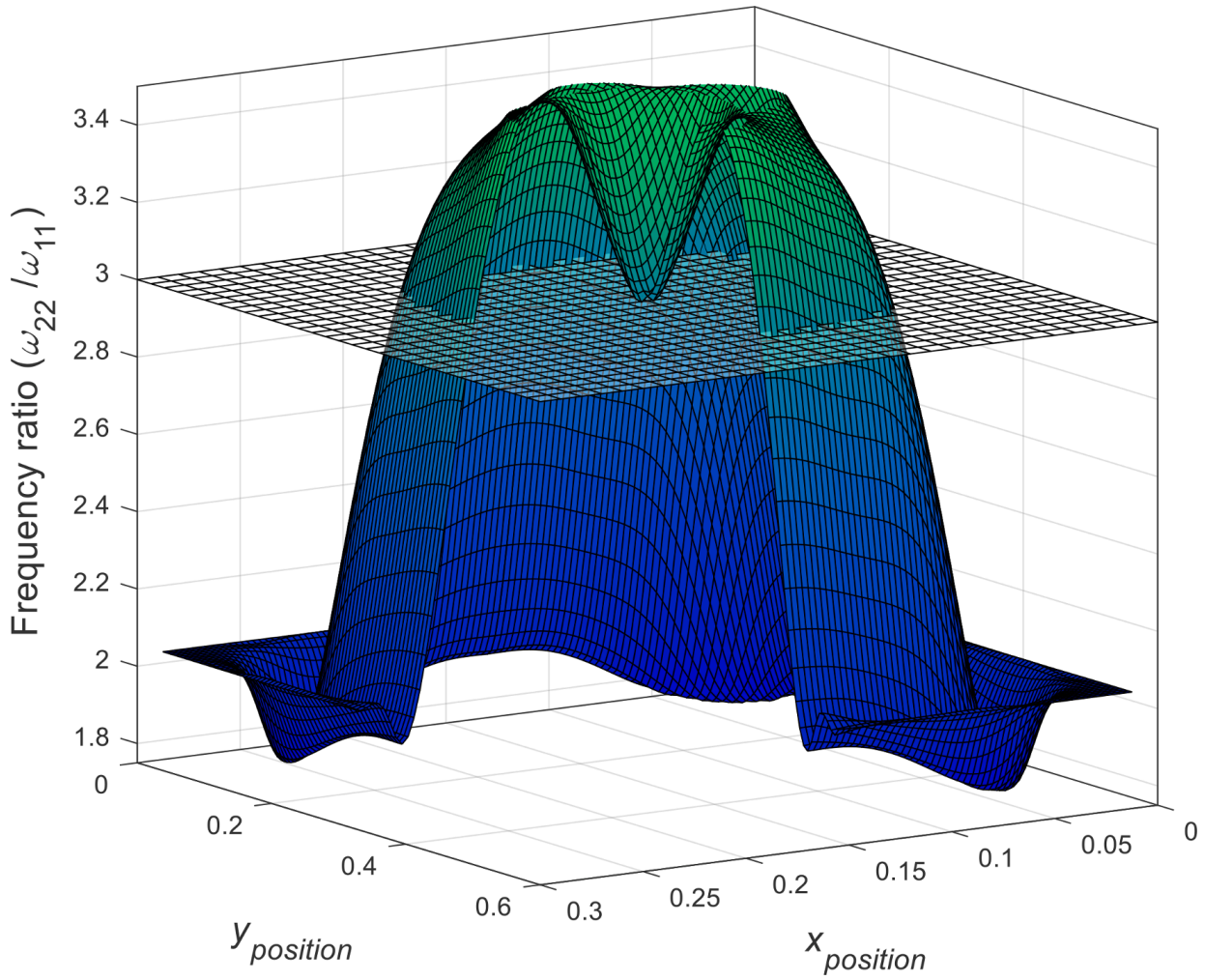

Fig. 13. Natural frequency ratio between ω_{22} and ω_{11} for different positions of the concentrated mass.

motion Eqs. (26)–(28)) using the dynamic equilibrium technique discussed in Refs. Allgower & Georg (2003, 2012); Lu et al. (2016), Mittelmann & Roose (1990), Ortega & Rheinboldt (2000), Polyanin & Zaitsev (2003) and recently in Refs. Khaniki et al. (2022, 2021), the nonlinear mass sensing behaviour of hyperelastic plates can be obtained. Due to complexity and coupling in Eqs. (26)–(28) and having strong modal interactions, the following modes are used: U_{11}, U_{12}, U_{21}, U_{22}, U_{13}, U_{31}, U_{23}, U_{32}, U_{33}, V_{11}, V_{12}, V_{21}, V_{22}, V_{13}, V_{31}, V_{23}, V_{32}, V_{33}, W_{11}, W_{12}, W_{21}, W_{22}, W_{13}, W_{31}, W_{23}, W_{32}, and W_{33}.

3. Experimental setup and testing procedure of mass-sensing hyperelastic plates

The experimental analyses performed in this study are explained and discussed here. In the first subsection, the forced vibration-test experimental setup for obtaining the frequency response of the hyperelastic plate is explained. In the second subsection, the material properties are examined to obtain the Mooney-Rivlin hyperelastic properties of the hyperelastic samples via ASTM D-412 standard; these properties are required for obtaining the nonlinear mechanics of the hyperelastic plate, theoretically.

3.1. Vibration test setup

In order to perform an experimental vibration test on hyperelastic plate structures, an EPDM rubber plate (with the material properties discussed in the next section) was cut as shown in Fig. 2a using waterjet cutting. For the given hyperelastic plate, a fixture was designed to hold the plate tight with 32 M12 bolts (Fig. 2b) with the effective lengths of 300 mm x 300 mm and thickness of 2 mm. The plate was assembled in the fixture and then mounted to the honeycomb optical breadboard of the optical table supported on vibration isolation supports using accurate right-angle mounting adapters and M6 steel bolts (Fig. 2c).

To operate a forced vibration test on the given hyperelastic plate, since the structure is significantly softer than a metal structure (discussed in the next section), a shaker with a low range of operating frequency was used. To do this, an LDS (Ling Dynamic Systems)

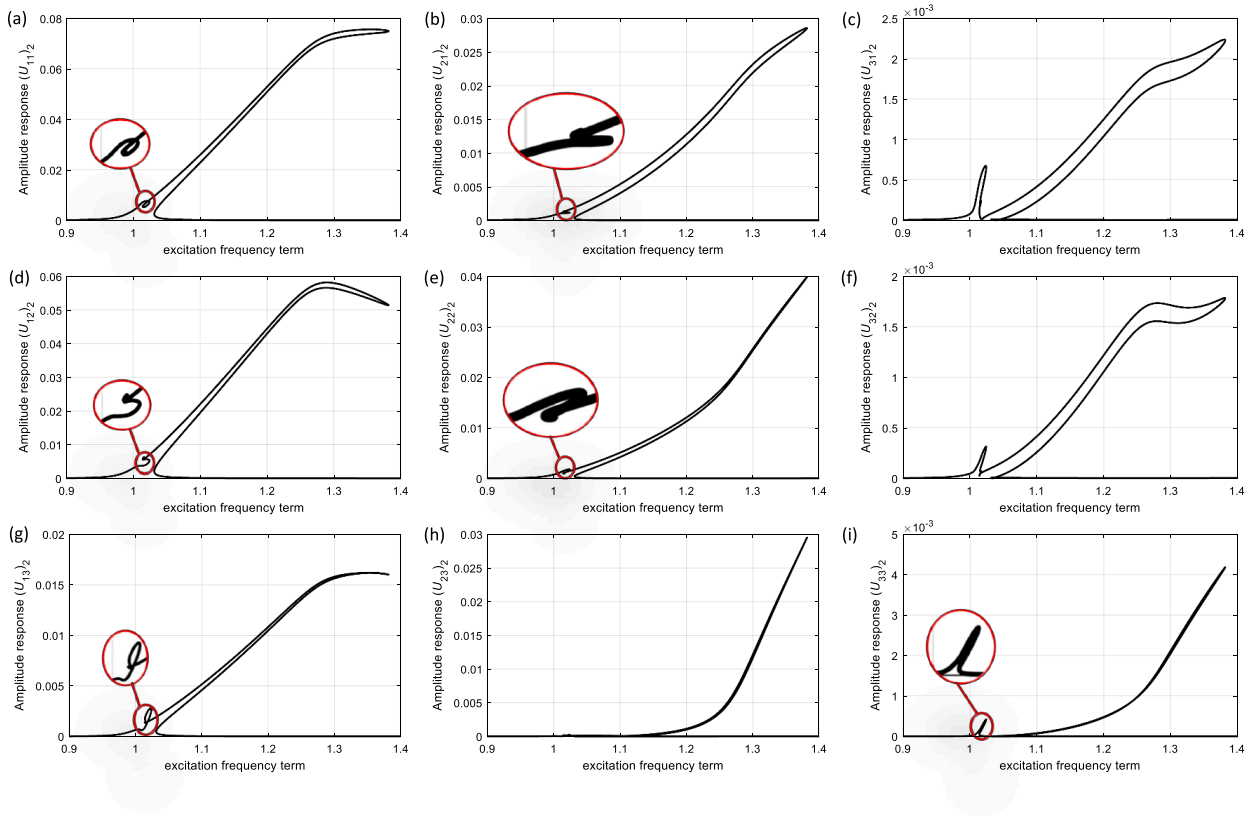

Fig. 14. The maximum in-plane x-direction amplitude-frequency response of the second dynamic coordinates of the hyperelastic plate close to three-to-one ω_{22}/ω_{11} internal resonance (a) U_{11}, (b) U_{21}, (c) U_{31}, (d) U_{12}, (e) U_{22}, (e) U_{32}, (g) U_{13}, (h) U_{23}, and (i) U_{33}.

permanent magnet V200 Series shaker with a sine peak force of 17.8 N was used, which was mounted to the table using right-angle mounting fixtures and connected to the plate using a steel stinger (Fig. 3a). A B&K (Bruel & Kjaer) 8200 force transducer was added to the end of the steel stinger (Fig. 3b) to measure the applied force and convert it to an electrical output signal, which was then sent to a B&K 2635 charge amplifier (Fig. 4a). The shaker was vibrated with a sinusoidal excitation signal with a certain frequency and amplitude using a Tektronix AFG3021 function generator and a Playmaster pro series 3 power amplifier (Fig. 4b). The displacement of the plate was recorded using a Wenglor laser distance sensor (Fig. 5a). The output signals from the signal generator, force transducer and laser distance sensors were all entered into an NI (National Instruments) BNC-2111 shielded connector block (Fig. 5b) to be recorded in a LabView (Bitter et al., 2017) developed model in the computer.

To operate the experimental test, for a constant maximum amplitude of periodic sinusoidal force, the excitation frequency was varied by small steps (0.05–0.10 Hz). The plate was first vibrated for 600 seconds at a frequency of 10 Hz for the sake of stabilisation in the dynamic behaviour and then the frequency sweep was performed. For mass imperfections, a set of rare earth disc magnets are used and placed in the mid-point of the hyperelastic plate. The structure was analysed for different maximum amplitude sinusoidal forces and mass imperfections.

3.2. Hyperelastic material properties via ASTM D-412

In order to analyse the vibration behaviour of hyperelastic plate structures, the material properties of the soft plate should be known. An ethylene propylene diene monomer (EPDM) rubber was used for this study and the mechanical properties of the rubber was obtained in this section. Following the American Society for Testing and Materials (ASTM) D-412 standard (ASTM, D412, 2006), the rubber needs to be cut with the dimensions shown in Fig. 6a; this standard (ASTM D-412) is different to those we used in our previous papers (Khaniki et al., 2022, 2021). To do this, a mould is used with the dimensions given in ASTM D-412 (Fig. 6b) and dumbbell-shaped specimens are prepared for testing (Fig. 6c). Following the testing procedure given in Refs. Khaniki et al. (2022, 2021), the stress-stretch behaviour of the material was obtained.

For this study, the Mooney-Rivlin hyperelastic strain energy density model is used, which is written in a general form as (Mooney, 1940)

$$W_M = C_1(\overline{I}_1 - 3) + C_2(\overline{I}_2 - 3) + D_1(J-1)^2, \tag{37}$$

where C_i and D_1 are the hyperelastic coefficients to be found for each material via the experimental tests. The given model is accurate for modelling structures within a 200% stretch rate (Marckmann & Verron, 2006), which is the range considered for this testing as

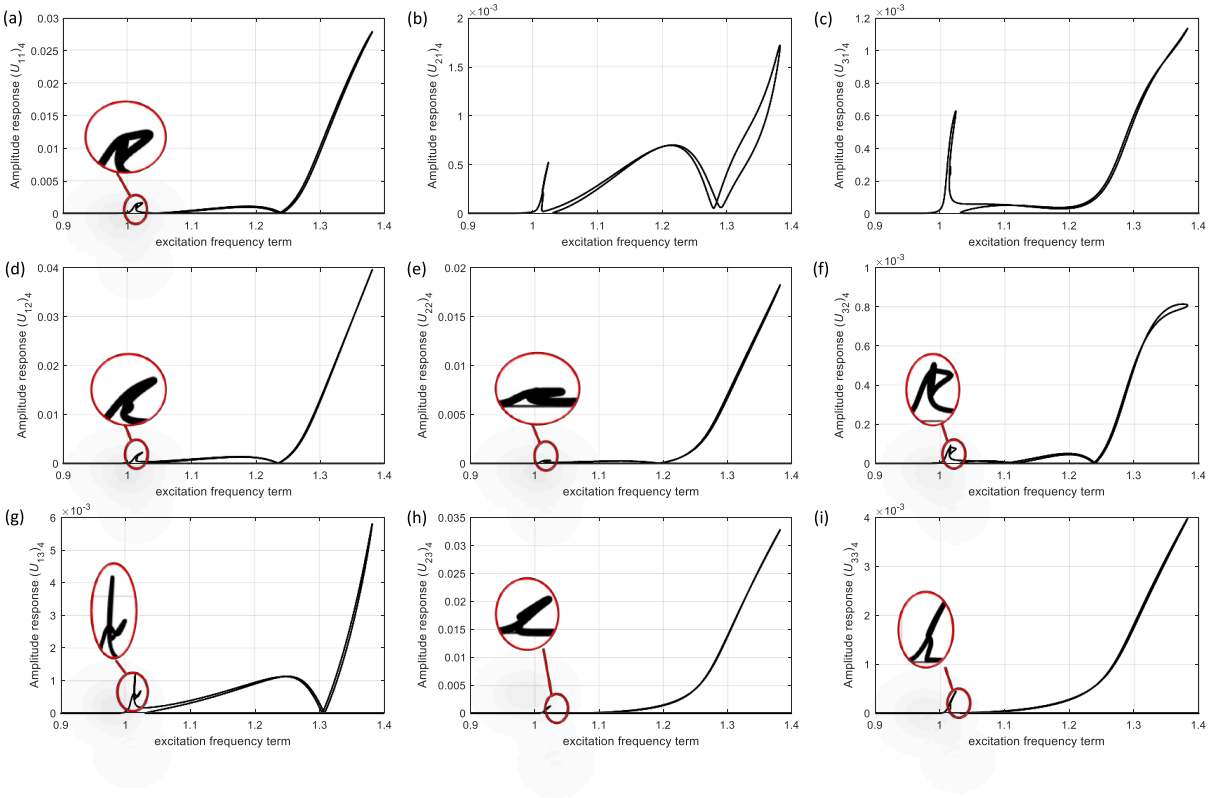

Fig. 15. The maximum in-plane x-direction amplitude-frequency response of the fourth dynamic coordinates of the hyperelastic plate close to three-to-one ω_{22}/ω_{11} internal resonance (a) U_{11}, (b) U_{21}, (c) U_{31}, (d) U_{12}, (e) U_{22}, (e) U_{32}, (g) U_{13}, (h) U_{23}, and (i) U_{33}.

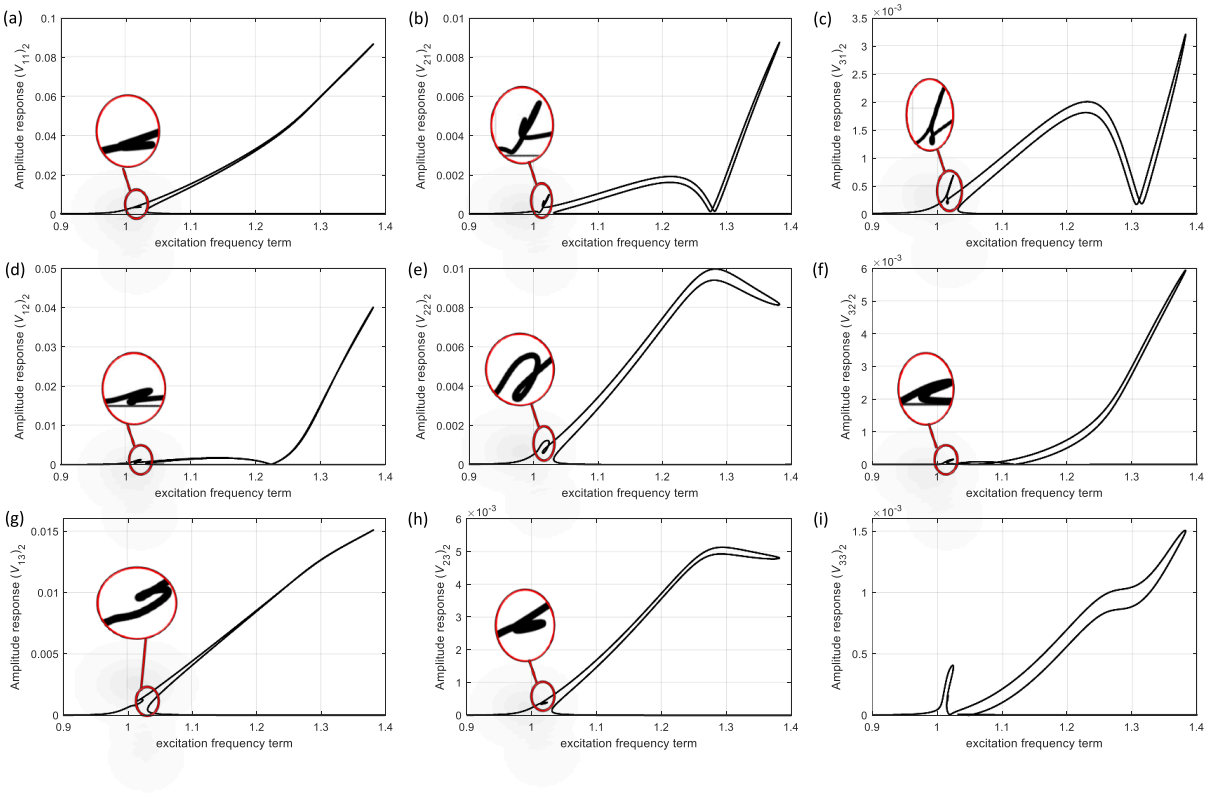

Fig. 16. The maximum in-plane y-direction amplitude-frequency response of the second dynamic coordinates of the hyperelastic plate close to three-to-one ω_{22}/ω_{11} internal resonance (a) V_{11}, (b) V_{21}, (c) V_{31}, (d) V_{12}, (e) V_{22}, (e) V_{32}, (g) V_{13}, (h) V_{23}, and (i) V_{33}.

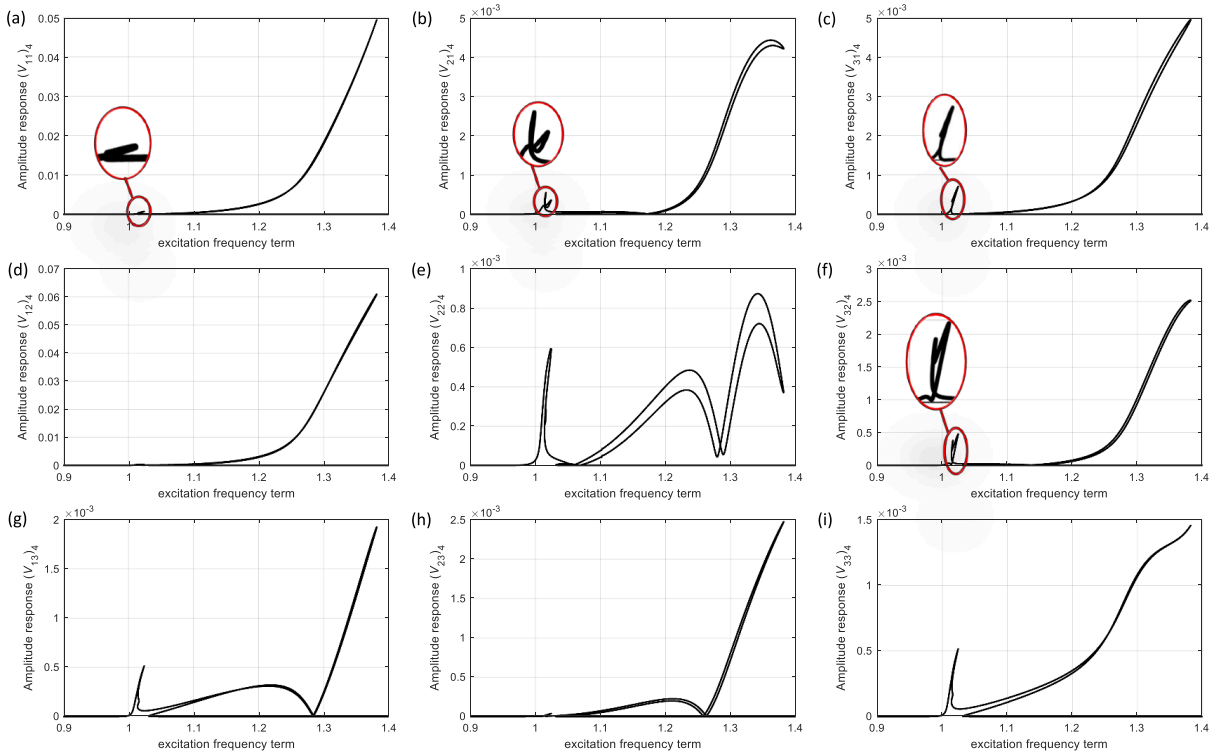

Fig. 17. The maximum in-plane y-direction amplitude-frequency response of the fourth dynamic coordinates of the hyperelastic plate close to three-to-one ω_{22}/ω_{11} internal resonance (a) V_{11}, (b) V_{21}, (c) V_{31}, (d) V_{12}, (e) V_{22}, (e) V_{32}, (g) V_{13}, (h) V_{23}, and (i) V_{33}.

well. Using the given model, the uniaxial stress-strain relationship can be obtained as (Brown et al., 2009)

$$\sigma_{uni} = \frac{4(1+\nu)}{3}\lambda_1^{-(5+2\nu)/3}\left(\lambda_1^{2+2\nu}-1\right)\left(C_1 + C_2\lambda_1^{-2(1+\nu)/3}\right) + 2D_1(1-2\nu)\lambda_1^{-2\nu}(J-1), \tag{38}$$

and for incompressible materials it is simplified as

$$\sigma_{uni} = 2C_1\left(\lambda-\lambda^{-2}\right) + 2C_2\left(1-\lambda^{-3}\right). \tag{39}$$

Using a curve-fitting, the best fit of the Mooney-Rivlin hyperelastic model to the experimental uniaxial testings can be seen in Fig. 7, obtained by having $C_1 = 129350$ Pa and $C_2 = 68400$ Pa. From the stress-stretch behaviour of the material, it can be seen that the hyperelastic plate shows a nonlinear elastic behaviour and is significantly softer than for example, a metal structure. Therefore, for this test, the experimental setup and fixture can be assumed to be a rigid structure (with no deformation).

4. Results and discussion

In this section, the results obtained using the experiments and the theories are presented. The mass-sensing behaviour of the hyperelastic plate is also analysed and structure's behaviour at different internal resonances is presented.

4.1. Experimental validation and mass sensitivity of the structure

As the first step of this section, the theory developed is verified by comparing the theoretical results with those of experiments.

4.1.1. Experimental validation for the case without mass

In the first comparison study, the hyperelastic plate is assumed to be without any attached concentrated mass (i.e. a plain plate). Following the experimental procedure given in Section 3, the nonlinear frequency response of the structure is obtained for a point load at (45 mm, 130 mm) with different magnitudes (2, 2.5 and 3N). Using the given formulation and methodology in Section 2, the Mooney-Rivlin hyperelastic properties used are $C_1 = 129350$ Pa and $C_2 = 68400$ Pa (obtained in Section 3.2) where in-plane nondimensional load is 18860 (for natural frequency fitting). A comparison between the experiment and the theory of the nonlinear vibration behaviour of the hyperelastic plate is given in Figs. 8(a)–(c) for an applied periodic load with a maximum magnitude of 2, 2.5 and 3 N. It can be seen that the nonlinear frequency response of the hyperelastic plate is hardening. Throughout the paper, a linear viscous term in room temperature of 4203 N.s/m (24 lbf.s/inch) (Schaefer, 2010)) was used in the theoretical

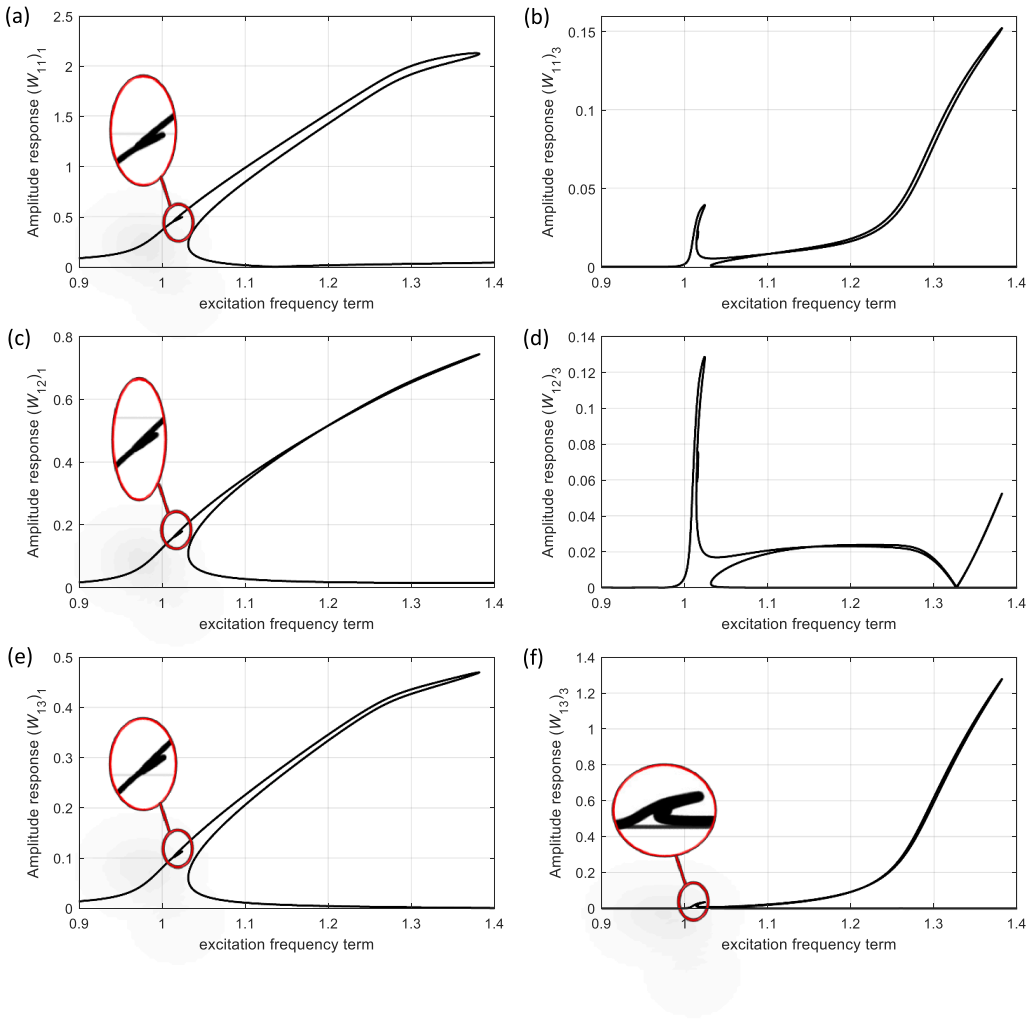

Fig. 18. The maximum transverse amplitude-frequency response of the first and third dynamic coordinates of the hyperelastic plate close to three-to-one ω_{22}/ω_{11} internal resonance (a) $(W_{11})_1$, (b) $(W_{11})_3$, (c) $(W_{12})_1$, (d) $(W_{12})_3$, (e) $(W_{13})_1$, and (f) $(W_{13})_3$.

simulations. Since the plate is hyperelastic, the in-plane motions contribute to the transverse one via modal interactions.

4.1.2. Mass sensitivity of the structure

The mass sensitivity of the hyperelastic plate is analysed in this section using both the theory and experiment. Round rare earth magnets were used, as concentrated mass, and was added to the mid-point of the plate. The mass is small compared to the hyperelastic plate dimensions. The experimental test was operated for different actuation loads with two, four and six magnets (Fig. 9a–c), each having a mass of 2.79 gr (Fig. 9d) equal to a nondimensional mass of 0.0127.

Figs. 10(a)–(c) present the mass-sensing nonlinear behaviour of the hyperelastic plate with two magnets (one on each side of the plate). The theoretical result was also performed by having the concentrated mass $M_{mass} = 5.58$ gr at the midpoint. The results show very good agreement with the experimental ones for different loads. Similarly, Figs. 11 and 12 show the mass-sensing nonlinear behaviour of the setup to four and six magnets (half on each side of the hyperelastic plate) versus the theoretical modelling results, respectively; the maximum amplitude of vibration moves to lower frequencies by increasing the mass, and the nonlinear hardening behaviour increases by increasing the concentrated mass.

4.2. Nonlinear behaviour at different internal resonances and modal interactions

After verifying the current methodology for modelling and analysing the nonlinear dynamics of hyperelastic plates with and without attached masses, the nonlinear behaviour of the hyperelastic plate with different internal resonances (which even makes the modal interactions stronger) is discussed in this section.

4.2.1. Due to concentrated mass

In this section, internal resonance phenomena in the hyperelastic plate due to the presence of a concentrated mass at different

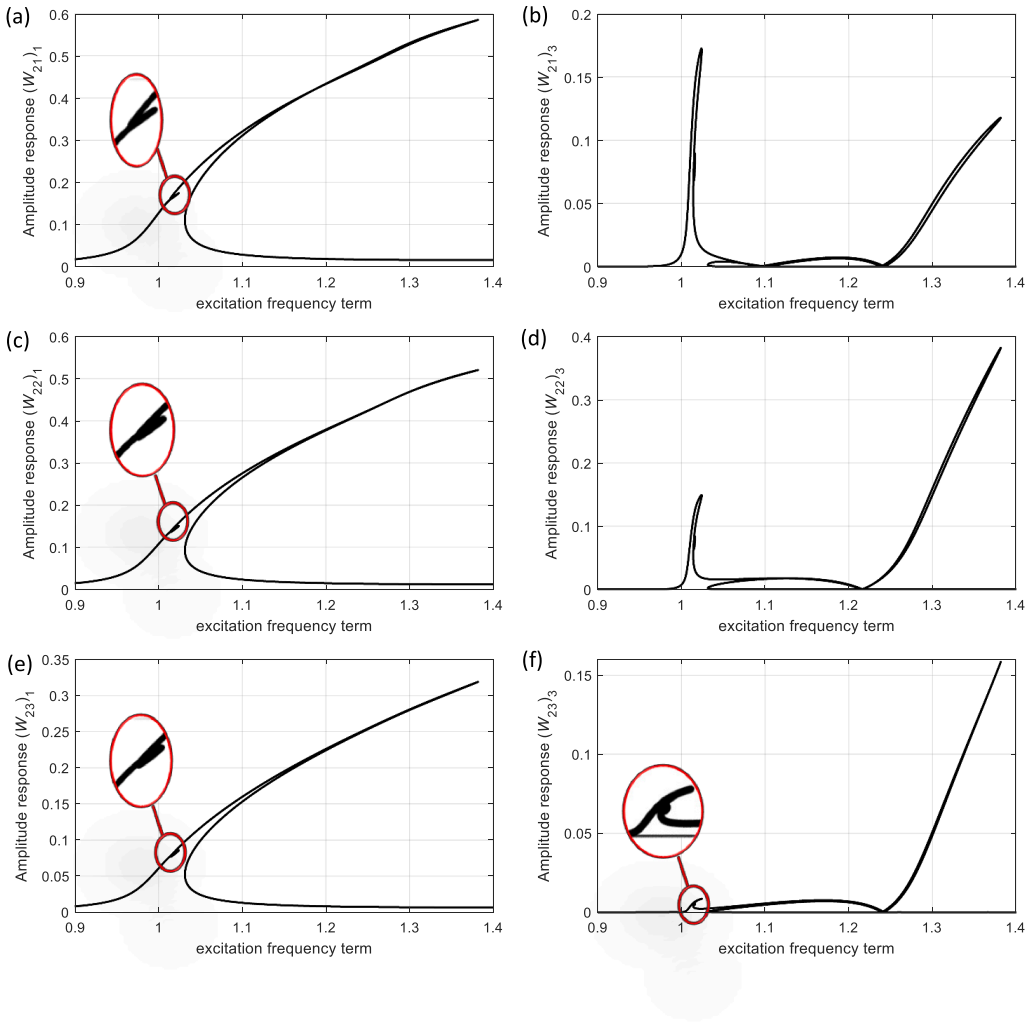

Fig. 19. The maximum transverse amplitude-frequency response of the first and third dynamic coordinates of the hyperelastic plate close to three-to-one ω_{22}/ω_{11} internal resonance (a) $(W_{21})_1$, (b) $(W_{21})_3$, (c) $(W_{22})_1$, (d) $(W_{22})_3$, (e) $(W_{23})_1$, and (f) $(W_{23})_3$.

positions are discussed, showing different types of internal resonances.

4.2.1.1. Case 1: three-to-one ω_{22}/ω_{11} type of internal resonance. For the first case, by having the same previous properties and the geometrical properties as $a = 0.3$ m, $b = 0.6$ m, $h = 2$ mm, a nondimensional mass $M_{mass} = 0.4$ is attached to the hyperelastic plate and its position is varied in the axial and lateral directions. Fig. 13 shows the ratio between ω_{22} and ω_{11} as a function of the position of the concentrated mass. It can be seen that for some positions, the frequency ratio between ω_{32} and ω_{11} is close to three.

To study the behaviour of the system at this resonance, the nondimensional position of the concentrated mass is assumed as $x_m = 0.250$ and $y_m = 0.275$ and a distributed sinusoidal nondimensional load of 1.5 is transversely applied to the plate. Figs. 14–20 present the first two dominant coordinates of the axial, lateral and transverse coordinates, at a three-to-one ω_{22}/ω_{11} internal resonance, respectively, by considering the nondimensional damping term to be 1.5. The results show a significant modal interaction, since the plate is not symmetrical due to the mass positions and a rich nonlinear behaviour in all the axial, lateral and transverse coordinates.

4.2.1.2. Case 2: three-to-one ω_{31}/ω_{11} type of internal resonance. For the second case, a nondimensional mass $M_{mass} = 0.3$ is used and its location on the hyperelastic plate is varied to see the effect on different natural frequencies' ratios. From Fig. 21, it is seen that for different mass positions, the frequency ratio between ω_{31} and ω_{11} is close to three.

In order to obtain the nonlinear dynamic response of the hyperelastic plate at the three-to-one ω_{31}/ω_{11} internal resonance and observe the modal interactions, the position of the concentrated mass is assumed to be $x_m = 0.225$ and $y_m = 0.250$, which gives a frequency ratio of $\omega_{31}/\omega_{11} \approx 3$. Figs. 22–28 present the first two dominant coordinates of the axial, lateral and transverse coordinates, at three-to-one ω_{31}/ω_{11} internal resonance, respectively, by considering the nondimensional viscous term as 2. The results show a significant modal interaction since the plate is not symmetrical due to the mass positions; the rotary inertia is assumed to be negligible. Due to having a three-to-one ω_{31}/ω_{11} internal resonance, the system shows a rich nonlinear behaviour completely different from the previous cases for the in-plane coordinates and a dominant hardening behaviour for the transverse motion.

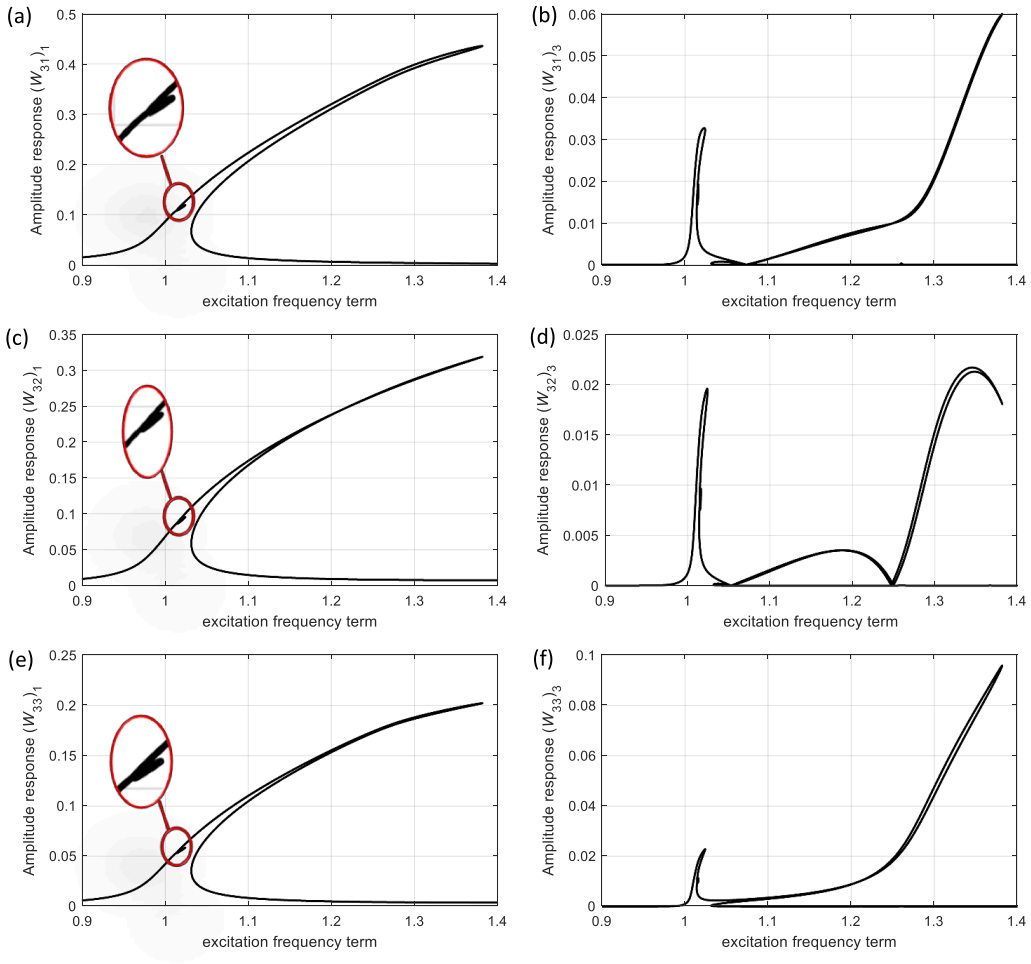

Fig. 20. The maximum transverse amplitude-frequency response of the first and third dynamic coordinates of the hyperelastic plate close to three-to-one ω_{22}/ω_{11} internal resonance (a) $(W_{31})_1$, (b) $(W_{31})_3$, (c) $(W_{32})_1$, (d) $(W_{32})_3$, (e) $(W_{33})_1$, and (f) $(W_{33})_3$.

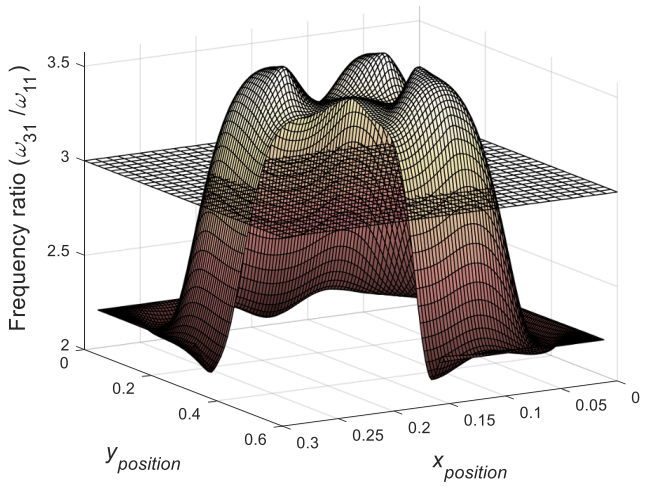

Fig. 21. Natural frequency ratio between ω_{31} and ω_{11} for different positions of the concentrated mass.

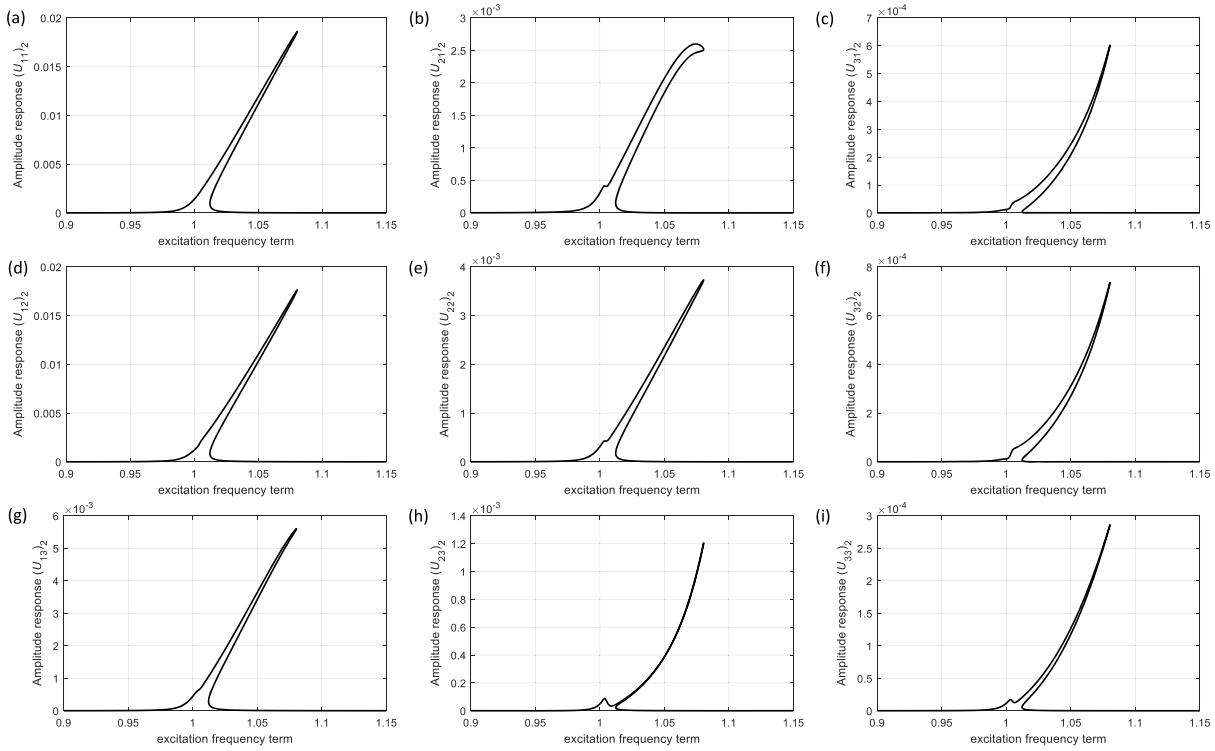

Fig. 22. The maximum in-plane x-direction amplitude-frequency response of the second dynamic coordinates of the hyperelastic plate close to three-to-one ω_{31}/ω_{11} internal resonance (a) U_{11}, (b) U_{21}, (c) U_{31}, (d) U_{12}, (e) U_{22}, (e) U_{32}, (g) U_{13}, (h) U_{23}, and (i) U_{33}.

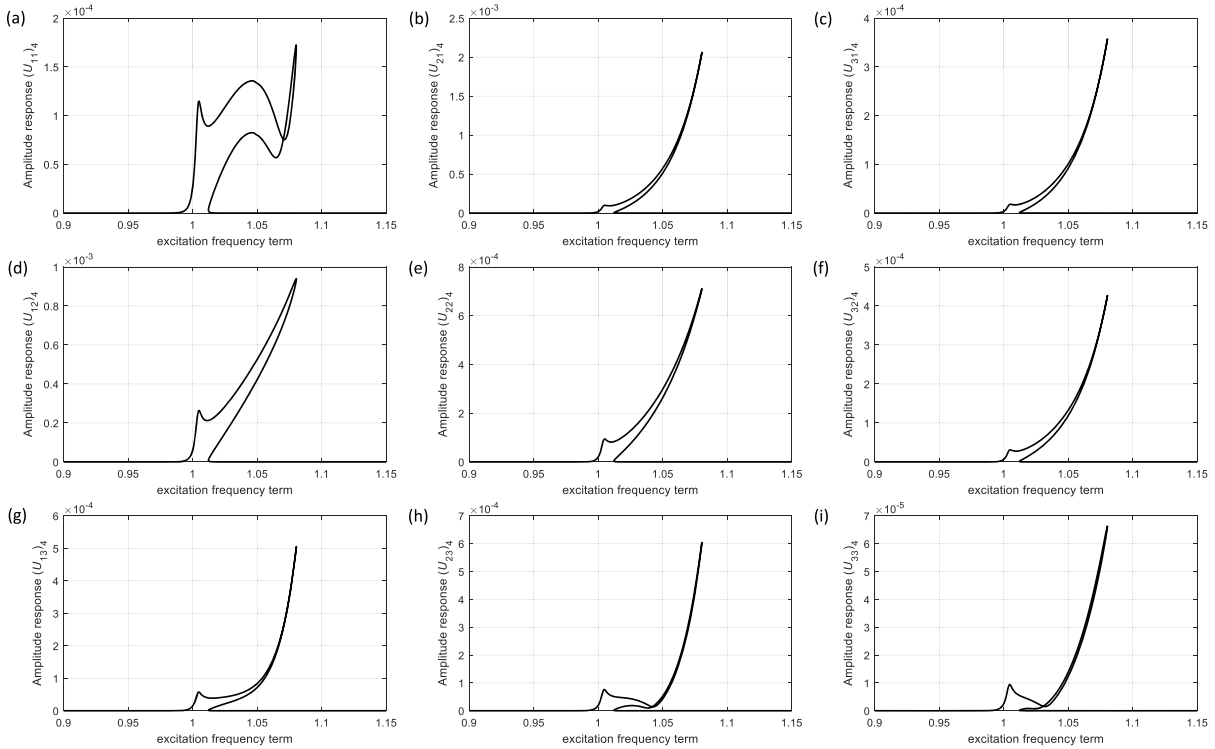

Fig. 23. The maximum in-plane x-direction amplitude-frequency response of the fourth dynamic coordinates of the hyperelastic plate close to three-to-one ω_{31}/ω_{11} internal resonance (a) U_{11}, (b) U_{21}, (c) U_{31}, (d) U_{12}, (e) U_{22}, (e) U_{32}, (g) U_{13}, (h) U_{23}, and (i) U_{33}.

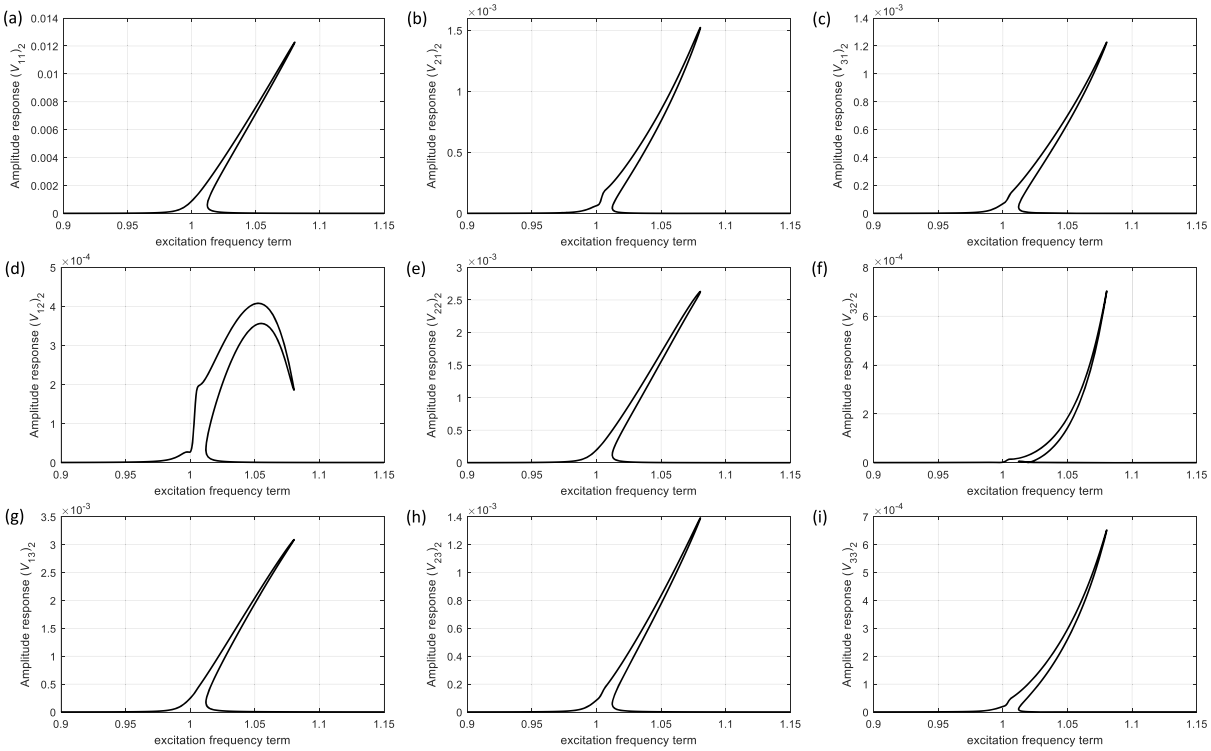

Fig. 24. The maximum in-plane y-direction amplitude-frequency response of the second dynamic coordinates of the hyperelastic plate close to three-to-one ω_{31}/ω_{11} internal resonance (a) V_{11}, (b) V_{21}, (c) V_{31}, (d) V_{12}, (e) V_{22}, (e) V_{32}, (g) V_{13}, (h) V_{23}, and (i) V_{33}.

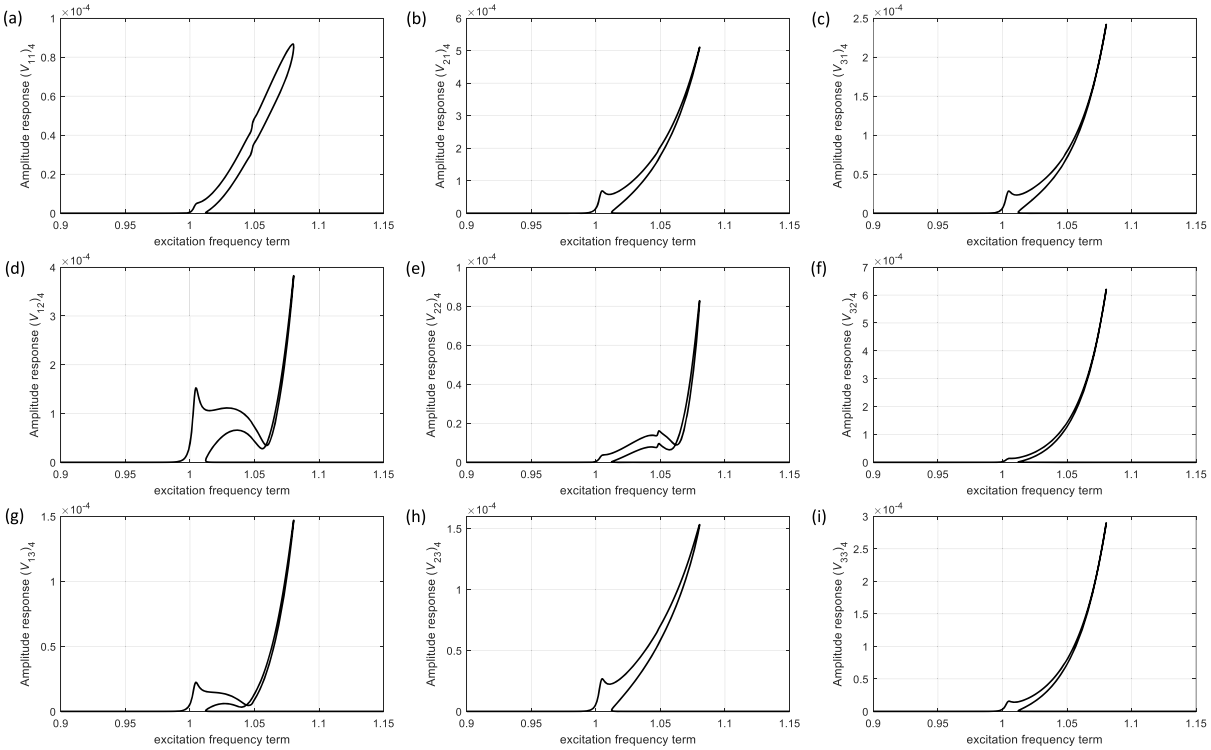

Fig. 25. The maximum in-plane y-direction amplitude-frequency response of the fourth dynamic coordinates of the hyperelastic plate close to three-to-one ω_{31}/ω_{11} internal resonance (a) V_{11}, (b) V_{21}, (c) V_{31}, (d) V_{12}, (e) V_{22}, (e) V_{32}, (g) V_{13}, (h) V_{23}, and (i) V_{33}.

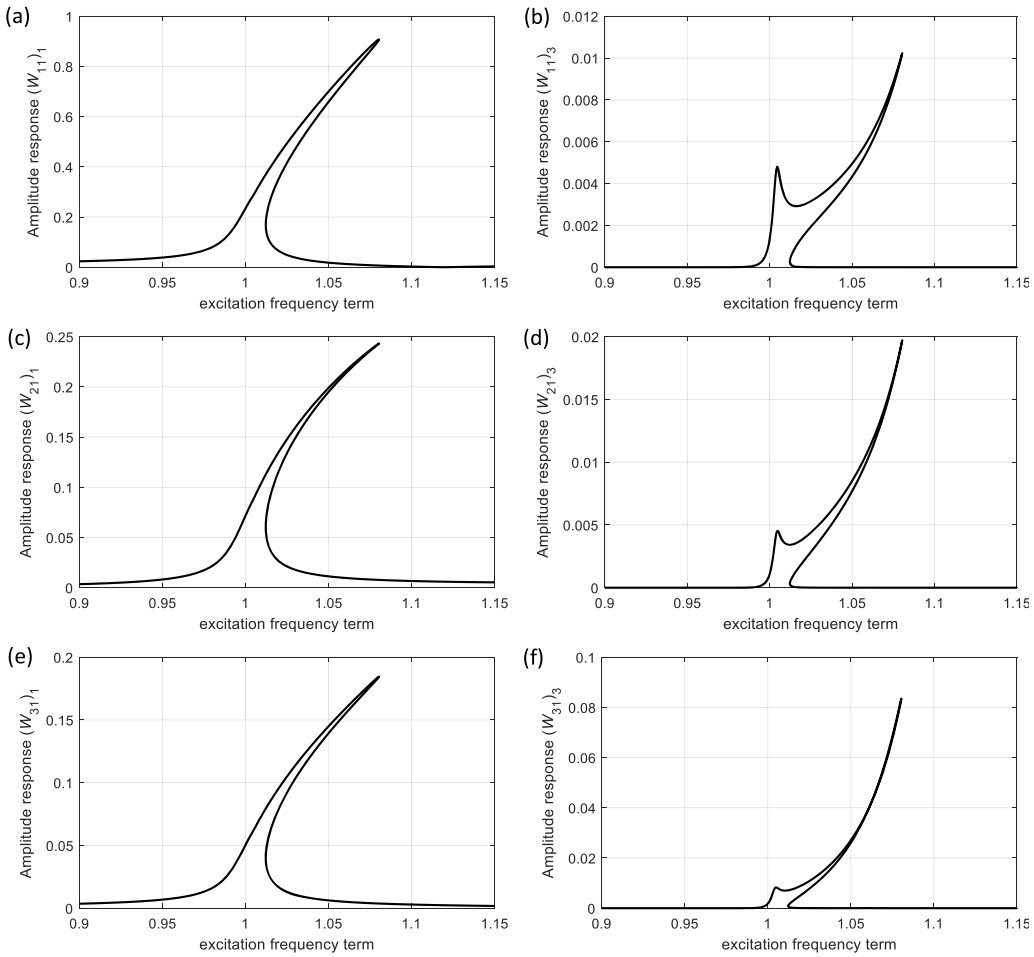

Fig. 26. The maximum transverse amplitude-frequency response of the first and third dynamic coordinates of the hyperelastic plate close to three-to-one ω_{31}/ω_{11} internal resonance (a) $(W_{11})_1$, (b) $(W_{11})_3$, (c) $(W_{21})_1$, (d) $(W_{21})_3$, (e) $(W_{31})_1$, and (f) $(W_{31})_3$.

4.2.2. Due to geometry

For this section, the geometrical properties of the structure are varied for a system prone to an internal resonance. To find the proper geometries, the length (a) and width (b) are varied as

$$a = 0.1 + 0.08a_0, \tag{40}$$

$$b = 0.3 + 0.16b_0, \tag{41}$$

while neglecting the concentrated mass and holding the thickness as $h = 2$ mm. By varying a_0 and b_0 from 0 to 9, it can be seen that for certain lengths and widths, the hyperelastic plate is prone to three-to-one internal resonance between ω_{32} and ω_{11} (Fig. 29). For instance, for $a_0 = 2$ and $b_0 = 8$ (equivalent to $a = 0.26$ m and $b = 1.58$ m), the frequency ratio $\omega_{32}/\omega_{11} \approx 3$; even though the system approaches a beam structure, the solution generality is retained. For the given dimensions and previously defined properties, the nonlinear frequency response of the structure and distributed sinusoidal nondimensional load of 3.9 are shown in Figs. 30–33 for some coordinates of the axial, lateral and transverse coordinates, respectively. From the results, it can be seen that the structure shows a rich nonlinear behaviour and a coupling and interactions between the axial, lateral and transverse modes in the vibration response, mainly following a general hardening behaviour.

5. Summary and conclusions

This study presented a detailed investigation on the mass sensitivity and multiple internal resonances and modal interactions of hyperelastic plates through experiments and theory. For the theoretical part, the coupled equations of motion were obtained using the Mooney-Rivlin strain energy density model, the von-Kármán geometric nonlinearity, the Kirchhoff–Love plate theory and Hamilton's

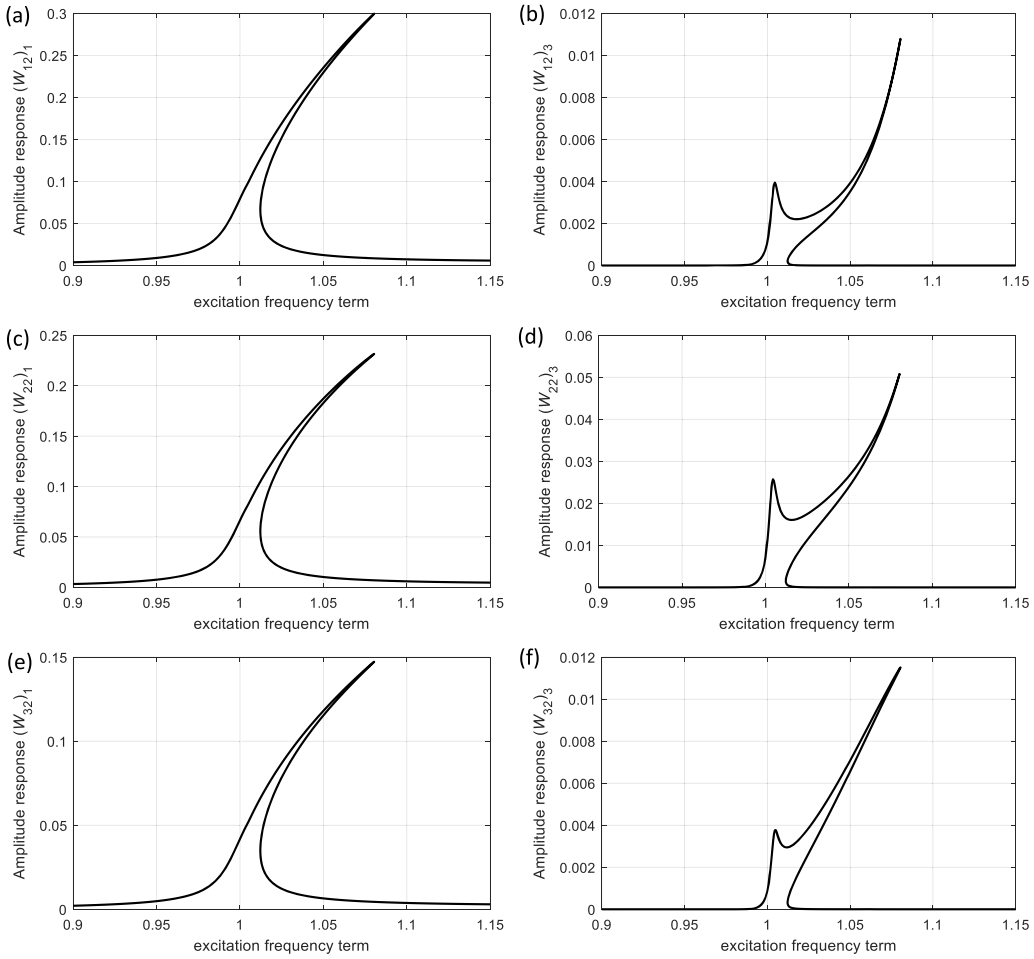

Fig. 27. The maximum transverse amplitude-frequency response of the first and third dynamic coordinates of the hyperelastic plate close to three-to-one ω_{31}/ω_{11} internal resonance (a) $(W_{12})_1$, (b) $(W_{12})_3$, (c) $(W_{22})_1$, (d) $(W_{22})_3$, (e) $(W_{32})_1$, and (f) $(W_{32})_3$.

equations. The coupled in-plane and out-of-plane equations of motion were solved using a combination of Galerkin's scheme and a dynamic equilibrium technique. A detailed explanation for modelling these structures by considering higher-order strain terms was presented. For the experimental analysis, a hyperelastic plate structure was fabricated and an externally actuated vibration test was performed using a set of devices. The nonlinear frequency response of the structure with and without a concentrated mass was investigated under various actuating time-dependent loads, and the capability of the structure for mass sensing was discussed. To obtain the hyperelastic properties, the rubber was cut to dumbbell samples using a mould fabricated following the ASTM D-412 standard and, by performing the tensile tests, the Mooney-Rivlin material coefficients were obtained by finding the best fit to the experimental results. Theory and experiment, in terms of frequency response curves, were shown to be in very good agreement for both mass and plain structures. Both the theoretical and the experimental results show a nonlinear stiffness hardening behaviour in the structure involving modal interactions, and as the mass weight and external applied dynamic force increased, the hardening behaviour increased accordingly.

Furthermore, after verifying the current methodology and modelling in predicting the dynamic behaviour and mass sensitivity of hyperelastic plates, different internal resonance and modal interactions caused (namely three-to-one ω_{22}/ω_{11}, ω_{31}/ω_{11}, and ω_{32}/ω_{11}) were investigated. It was shown that the structure shows a rich nonlinear behaviour that is significantly different for each internal resonance, with a coupling between the axial, lateral and transverse modes in the vibration response, mainly following a hardening behaviour with complexities in the frequency response plots. Since soft structures are widely used for different soft robots and soft functional devices, the results of this study are a step forward in investigating the mechanics of soft structures.

Declaration of Competing Interest

The authors declare that they have no known competing financial interests or personal relationships that could have appeared to influence the work reported in this paper.

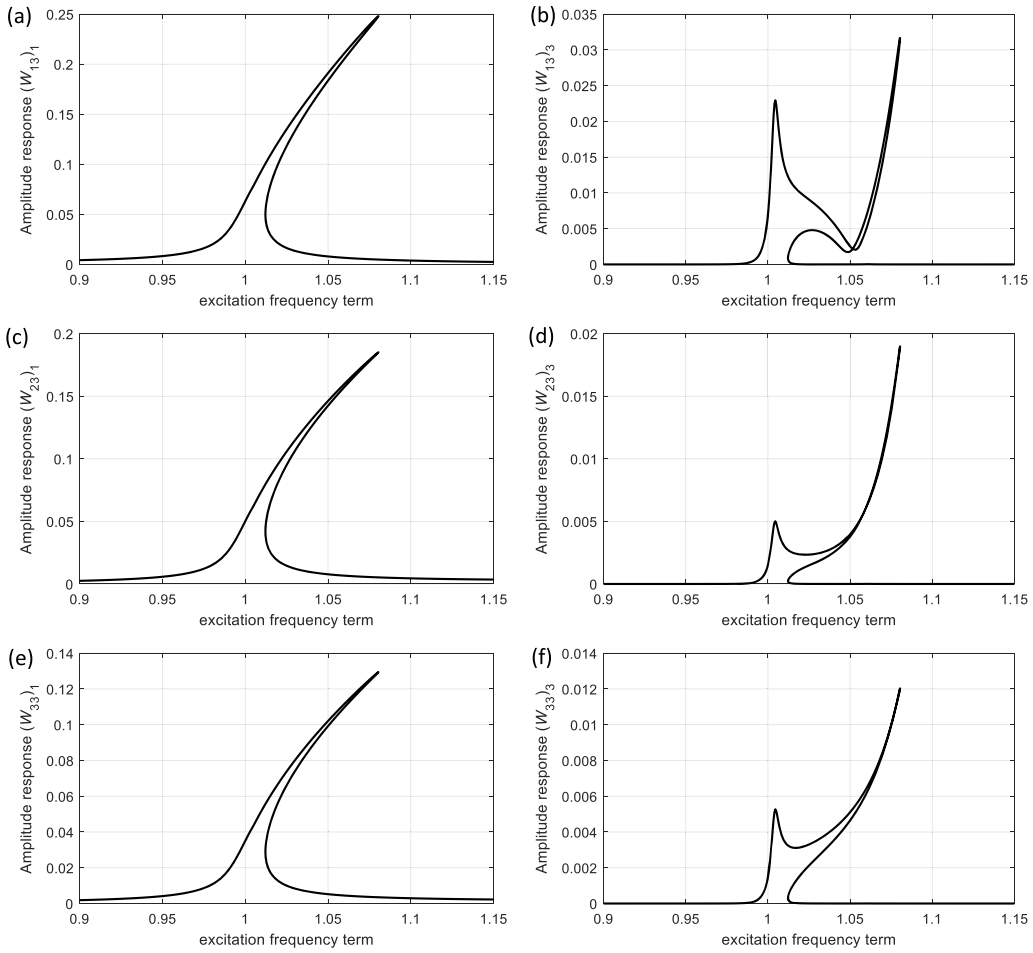

Fig. 28. The maximum transverse amplitude-frequency response of the first and third dynamic coordinates of the hyperelastic plate close to three-to-one ω_{31}/ω_{11} internal resonance (a) $(W_{13})_1$, (b) $(W_{13})_3$, (c) $(W_{23})_1$, (d) $(W_{23})_3$, (e) $(W_{33})_1$, and (f) $(W_{33})_3$.

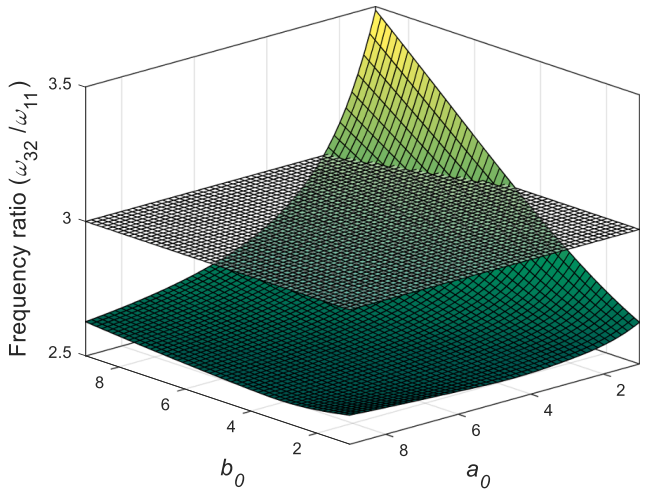

Fig. 29. Natural frequency ratio between ω_{32} and ω_{11} for different lengths and widths.

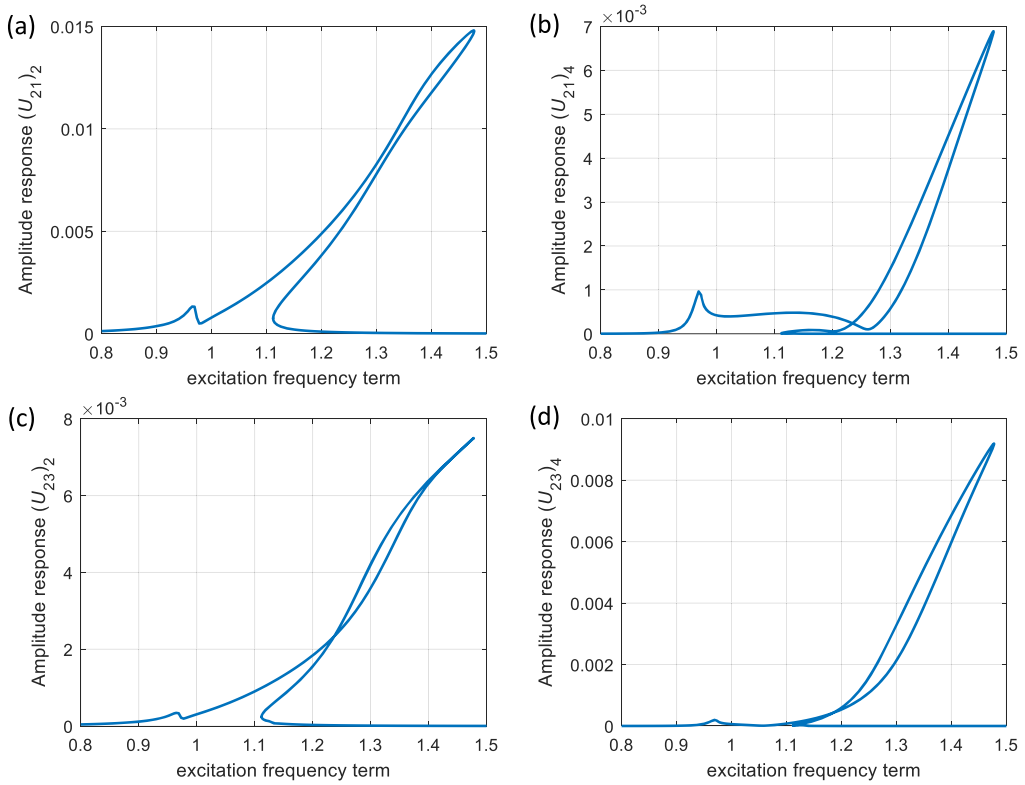

Fig. 30. The maximum in-plane x-direction amplitude-frequency response of the second and fourth dynamic coordinates of the hyperelastic plate close to three-to-one ω_{32}/ω_{11} internal resonance (a) $(U_{21})_2$, (b) $(U_{21})_4$, (c) $(U_{23})_2$, and (d) $(U_{23})_4$.

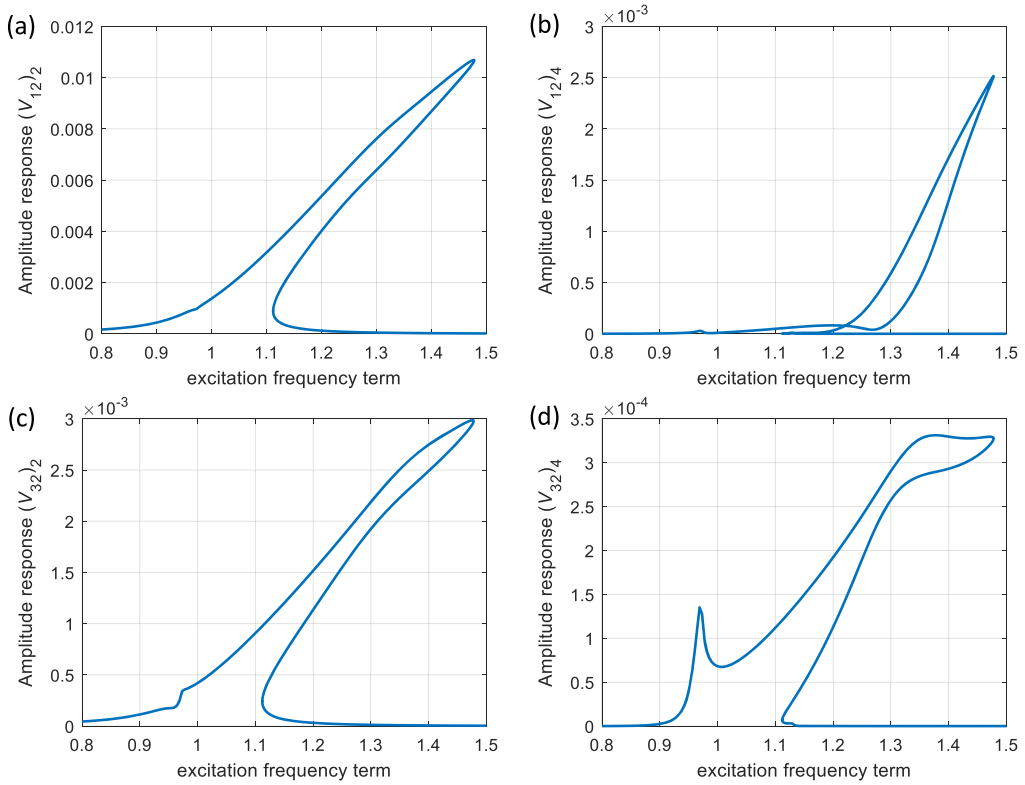

Fig. 31. The maximum in-plane y-direction amplitude-frequency response of the second and fourth dynamic coordinates of the hyperelastic plate close to three-to-one ω_{32}/ω_{11} internal resonance (a) $(V_{12})_2$, (b) $(V_{12})_4$, (c) $(V_{32})_2$, and (d) $(V_{32})_4$.

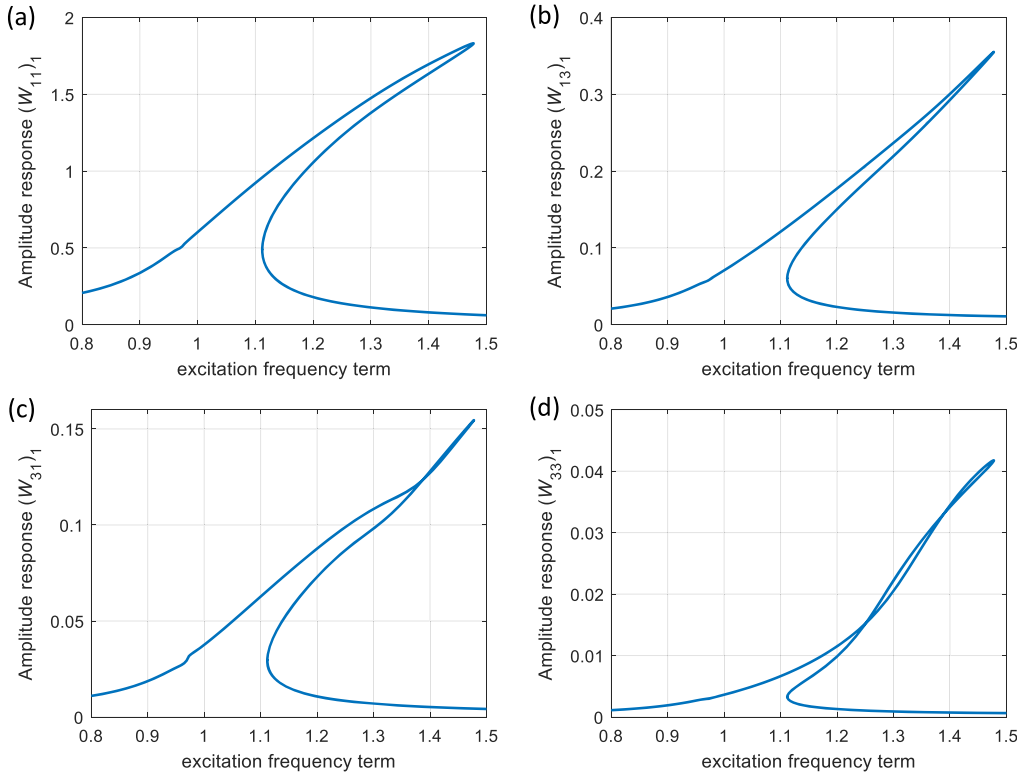

Fig. 32. The maximum transverse amplitude-frequency response of the first dynamic coordinates of the hyperelastic plate close to three-to-one ω_{32}/ω_{11} internal resonance (a) W_{11}, (b) W_{13}, (c) W_{31} and (d) W_{33}.

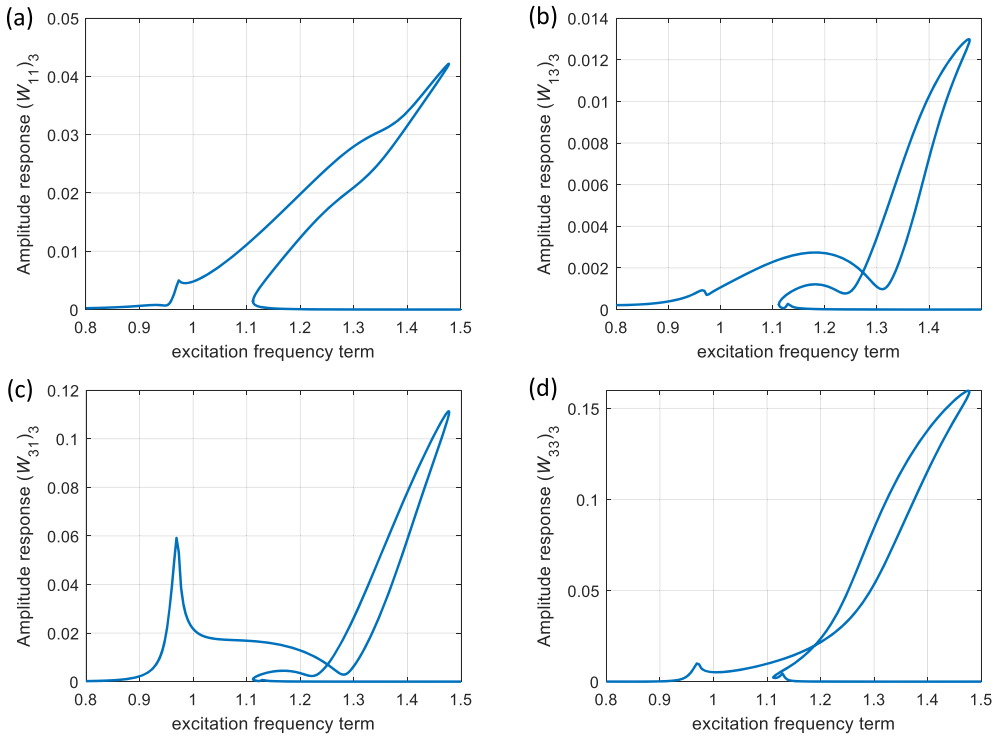

Fig. 33. The maximum transverse amplitude-frequency response of the third dynamic coordinates of the hyperelastic plate close to three-to-one ω_{32}/ω_{11} internal resonance (a) W_{11}, (b) W_{13}, (c) W_{31} and (d) W_{33}.

Data availability

It is a part of a continuing research and cannot be shared.

Acknowledgements

The HDR scholarship support through The University of Adelaide and Faculty of Engineering, Computer & Mathematical Sciences, the University of Adelaide, is acknowledged. This work was supported with supercomputing resources provided by the Phoenix HPC service at the University of Adelaide.

Appendix A

The higher order nonlinear terms are presented for the axial motion as

$$KN_{11} = +12\frac{\eta_a}{\eta_b{}^2}A_1\int_0^1\int_0^1 r_{ij}(x,y)\frac{\partial}{\partial x}\left(r^x_{kl}(x,y)r^x_{mn}(x,y)\right)dxdy$$
$$+\frac{1}{2}\frac{1}{\eta_a}A_3\int_0^1\int_0^1 r_{ij}(x,y)\frac{\partial}{\partial x}\left(r^y_{kl}(x,y)r^y_{mn}(x,y)\right)dxdy+\frac{1}{\eta_a}A_3\int_0^1\int_0^1 r_{ij}(x,y)\frac{\partial}{\partial y}\left(r^x_{kl}(x,y)r^y_{mn}(x,y)\right)dxdy, \tag{A1}$$

$$KN_{12} = -\frac{2}{\eta_b}A_4\int_0^1\int_0^1 r_{ij}(x,y)\frac{\partial}{\partial x}\left(r^x_{kl}(x,y)p^y_{mn}(x,y)\right)dxdy+\frac{1}{\eta_b}A_3\int_0^1\int_0^1 r_{ij}(x,y)\frac{\partial}{\partial x}\left(r^y_{kl}(x,y)p^x_{mn}(x,y)\right)dxdy$$
$$+\frac{\eta_b}{\eta_a{}^2}A_3\int_0^1\int_0^1 r_{ij}(x,y)\frac{\partial}{\partial y}\left(r^y_{kl}(x,y)p^y_{mn}(x,y)\right)dxdy+\frac{1}{\eta_b}A_3\int_0^1\int_0^1 r_{ij}(x,y)\frac{\partial}{\partial y}\left(r^x_{kl}(x,y)p^x_{mn}(x,y)\right)dxdy, \tag{A2}$$

$$KN_{13} = -\frac{1}{\eta_a}A_4\int_0^1\int_0^1 r_{ij}(x,y)\frac{\partial}{\partial x}\left(p^y_{kl}(x,y)p^y_{mn}(x,y)\right)dxdy$$
$$+\frac{1}{2}\frac{\eta_a}{\eta_b{}^2}A_3\int_0^1\int_0^1 r_{ij}(x,y)\frac{\partial}{\partial x}\left(p^x_{kl}(x,y)p^x_{mn}(x,y)\right)dxdy+\frac{1}{\eta_a}A_3\int_0^1\int_0^1 r_{ij}(x,y)\frac{\partial}{\partial y}\left(p^x_{kl}(x,y)p^y_{mn}(x,y)\right)dxdy, \tag{A3}$$

$$KN_{14} = -2\frac{\eta_a}{\eta_b{}^2}A_2\int_0^1\int_0^1 r_{ij}(x,y)\frac{\partial}{\partial x}\left(q^x_{kl}(x,y)q^x_{mn}(x,y)\right)dxdy-\frac{1}{\eta_a}A_2\int_0^1\int_0^1 r_{ij}(x,y)\frac{\partial}{\partial x}\left(q^y_{kl}(x,y)q^y_{mn}(x,y)\right)dxdy$$
$$+\frac{\eta_a{}^3}{\eta_b{}^2}A_1\int_0^1\int_0^1 r_{ij}(x,y)\frac{\partial}{\partial x}\left(q^{xx}_{kl}(x,y)q^{xx}_{mn}(x,y)\right)dxdy-\frac{1}{12}\frac{\eta_b{}^2}{\eta_a}A_4\int_0^1\int_0^1 r_{ij}(x,y)\frac{\partial}{\partial x}\left(q^{yy}_{kl}(x,y)q^{yy}_{mn}(x,y)\right)dxdy$$
$$-\frac{1}{6}\eta_a A_4\int_0^1\int_0^1 r_{ij}(x,y)\frac{\partial}{\partial x}\left(q^{xx}_{kl}(x,y)q^{yy}_{mn}(x,y)\right)dxdy+\frac{1}{6}\eta_a A_3\int_0^1\int_0^1 r_{ij}(x,y)\frac{\partial}{\partial x}\left(q^{xy}_{kl}(x,y)q^{xy}_{mn}(x,y)\right)dxdy$$
$$-\frac{1}{\eta_a}A_2\int_0^1\int_0^1 r_{ij}(x,y)\frac{\partial}{\partial y}\left(q^x_{kl}(x,y)q^y_{mn}(x,y)\right)dxdy+\frac{1}{6}\eta_a A_3\int_0^1\int_0^1 r_{ij}(x,y)\frac{\partial}{\partial y}\left(q^{xx}_{kl}(x,y)q^{xy}_{mn}(x,y)\right)dxdy$$
$$+\frac{1}{6}\frac{\eta_b{}^2}{\eta_a}A_3\int_0^1\int_0^1 r_{ij}(x,y)\frac{\partial}{\partial y}\left(q^{xy}_{kl}(x,y)q^{yy}_{mn}(x,y)\right)dxdy, \tag{A4}$$

$$KN_{15} = +12\frac{{\eta_a}^2}{{\eta_b}^2}A_1\int_0^1\int_0^1 r_{ij}(x,y)\frac{\partial}{\partial x}\left(U^x_{kl}(x,y)q^x_{mn}(x,y)q^x_{op}(x,y)\right)dxdy$$
$$-A_4\int_0^1\int_0^1 r_{ij}(x,y)\frac{\partial}{\partial x}\left(r^x_{kl}(x,y)q^y_{mn}(x,y)q^y_{op}(x,y)\right)dxdy + A_3\int_0^1\int_0^1 r_{ij}(x,y)\frac{\partial}{\partial x}\left(r^y_{kl}(x,y)q^x_{mn}(x,y)q^y_{op}(x,y)\right)dxdy$$
$$+A_3\int_0^1\int_0^1 r_{ij}(x,y)\frac{\partial}{\partial y}\left(r^x_{kl}(x,y)q^x_{mn}(x,y)q^y_{op}(x,y)\right)dxdy + \frac{1}{2}A_3\int_0^1\int_0^1 r_{ij}(x,y)\frac{\partial}{\partial y}\left(r^y_{kl}(x,y)q^x_{mn}(x,y)q^x_{op}(x,y)\right)dxdy$$
$$+\frac{1}{2}\frac{{\eta_b}^2}{{\eta_a}^2}A_3\int_0^1\int_0^1 r_{ij}(x,y)\frac{\partial}{\partial y}\left(r^y_{kl}(x,y)q^y_{mn}(x,y)q^y_{op}(x,y)\right)dxdy, \tag{A5}$$

$$KN_{16} = -\frac{\eta_b}{\eta_a}A_4\int_0^1\int_0^1 r_{ij}(x,y)\frac{\partial}{\partial x}\left(p^y_{kl}(x,y)q^y_{mn}(x,y)q^y_{op}(x,y)\right)dxdy$$
$$+\frac{1}{2}\frac{\eta_a}{\eta_b}A_3\int_0^1\int_0^1 r_{ij}(x,y)\frac{\partial}{\partial y}\left(p^x_{kl}(x,y)q^x_{mn}(x,y)q^x_{op}(x,y)\right)dxdy$$
$$+\frac{1}{2}\frac{\eta_b}{\eta_a}A_3\int_0^1\int_0^1 r_{ij}(x,y)\frac{\partial}{\partial y}\left(p^x_{kl}(x,y)q^y_{mn}(x,y)q^x_{op}(x,y)\right)dxdy + \frac{\eta_b}{\eta_a}A_3\int_0^1\int_0^1 r_{ij}(x,y)\frac{\partial}{\partial y}\left(p^y_{kl}(x,y)q^x_{mn}(x,y)q^y_{op}(x,y)\right)dxdy$$
$$-\frac{\eta_a}{\eta_b}A_4\int_0^1\int_0^1 r_{ij}(x,y)\frac{\partial}{\partial x}\left(p^y_{kl}(x,y)q^x_{mn}(x,y)q^x_{op}(x,y)\right)dxdy + \frac{\eta_a}{\eta_b}A_3\int_0^1\int_0^1 r_{ij}(x,y)\frac{\partial}{\partial x}\left(p^x_{kl}(x,y)q^x_{mn}(x,y)q^y_{op}(x,y)\right)dxdy, \tag{A6}$$

$$KN_{17} = +3\frac{{\eta_a}^3}{{\eta_b}^2}A_1\int_0^1\int_0^1 r_{ij}(x,y)\frac{\partial}{\partial x}\left(q^x_{kl}(x,y)q^x_{mn}(x,y)q^x_{op}(x,y)q^x_{qr}(x,y)\right)dxdy$$
$$-\frac{1}{4}\frac{{\eta_b}^2}{\eta_a}A_4\int_0^1\int_0^1 r_{ij}(x,y)\frac{\partial}{\partial x}\left(q^y_{kl}(x,y)q^y_{mn}(x,y)q^y_{op}(x,y)q^y_{qr}(x,y)\right)dxdy$$
$$-\frac{1}{4}\eta_a A_5\int_0^1\int_0^1 r_{ij}(x,y)\frac{\partial}{\partial x}\left(q^x_{kl}(x,y)q^x_{mn}(x,y)q^y_{op}(x,y)q^y_{qr}(x,y)\right)dxdy$$
$$+\frac{1}{2}\frac{{\eta_b}^2}{\eta_a}A_3\int_0^1\int_0^1 r_{ij}(x,y)\frac{\partial}{\partial y}\left(q^x_{kl}(x,y)q^y_{mn}(x,y)q^y_{op}(x,y)q^y_{qr}(x,y)\right)dxdy$$
$$+\frac{1}{2}\eta_a A_3\int_0^1\int_0^1 r_{ij}(x,y)\frac{\partial}{\partial y}\left(q^x_{kl}(x,y)q^x_{mn}(x,y)q^x_{op}(x,y)q^y_{qr}(x,y)\right)dxdy, \tag{A7}$$

and for the lateral motion as

$$KN_{21} = -\frac{1}{\eta_b}A_4\int_0^1\int_0^1 p_{ij}(x,y)\frac{\partial}{\partial y}\left(r^x_{kl}(x,y)r^x_{mn}(x,y)\right)dxdy + \frac{1}{2}\frac{\eta_b}{{\eta_a}^2}A_3\int_0^1\int_0^1 p_{ij}(x,y)\frac{\partial}{\partial y}\left(r^y_{kl}(x,y)r^y_{mn}(x,y)\right)dxdy$$
$$+\frac{1}{\eta_b}A_3\int_0^1\int_0^1 p_{ij}(x,y)\frac{\partial}{\partial x}\left(r^x_{kl}(x,y)r^y_{mn}(x,y)\right)dxdy, \tag{A8}$$

$$KN_{22} = -\frac{2}{\eta_a}A_4\int_0^1\int_0^1 p_{ij}(x,y)\frac{\partial}{\partial y}\left(r^x_{kl}(x,y)p^y_{mn}(x,y)\right)dxdy + \frac{1}{\eta_a}A_3\int_0^1\int_0^1 p_{ij}(x,y)\frac{\partial}{\partial y}\left(r^y_{kl}(x,y)p^x_{mn}(x,y)\right)dxdy$$
$$+\frac{\eta_a}{{\eta_b}^2}A_3\int_0^1\int_0^1 p_{ij}(x,y)\frac{\partial}{\partial x}\left(r^x_{kl}(x,y)p^x_{mn}(x,y)\right)dxdy + \frac{1}{\eta_a}A_3\int_0^1\int_0^1 p_{ij}(x,y)\frac{\partial}{\partial x}\left(r^y_{kl}(x,y)p^y_{mn}(x,y)\right)dxdy, \tag{A9}$$

$$KN_{23} = +12\frac{\eta_b}{{\eta_a}^2}A_1\int_0^1\int_0^1 p_{ij}(x,y)\frac{\partial}{\partial y}\left(p^y_{kl}(x,y)p^y_{mn}(x,y)\right)dxdy + \frac{1}{2}\frac{1}{\eta_b}A_3\int_0^1\int_0^1 p_{ij}(x,y)\frac{\partial}{\partial y}\left(p^x_{kl}(x,y)p^x_{mn}(x,y)\right)dxdy$$
$$+\frac{1}{\eta_b}A_3\int_0^1\int_0^1 p_{ij}(x,y)\frac{\partial}{\partial x}\left(p^x_{kl}(x,y)p^y_{mn}(x,y)\right)dxdy, \tag{A10}$$

$$KN_{24} = -2\frac{\eta_b}{{\eta_a}^2}A_2\int_0^1\int_0^1 p_{ij}(x,y)\frac{\partial}{\partial y}\left(q^y_{kl}(x,y)q^y_{mn}(x,y)\right)dxdy - \frac{1}{\eta_b}A_2\int_0^1\int_0^1 p_{ij}(x,y)\frac{\partial}{\partial y}\left(q^x_{kl}(x,y)q^x_{mn}(x,y)\right)dxdy$$
$$+\frac{{\eta_b}^3}{{\eta_a}^2}A_1\int_0^1\int_0^1 p_{ij}(x,y)\frac{\partial}{\partial y}\left(q^{yy}_{kl}(x,y)q^{yy}_{mn}(x,y)\right)dxdy - \frac{1}{12}\frac{{\eta_a}^2}{\eta_b}A_4\int_0^1\int_0^1 p_{ij}(x,y)\frac{\partial}{\partial y}\left(q^{xx}_{kl}(x,y)q^{xx}_{mn}(x,y)\right)dxdy$$
$$-\frac{1}{6}\eta_b A_4\int_0^1\int_0^1 p_{ij}(x,y)\frac{\partial}{\partial y}\left(q^{xx}_{kl}(x,y)q^{yy}_{mn}(x,y)\right)dxdy + \frac{1}{6}\eta_b A_3\int_0^1\int_0^1 p_{ij}(x,y)\frac{\partial}{\partial y}\left(q^{xy}_{kl}(x,y)q^{xy}_{mn}(x,y)\right)dxdy \tag{A11}$$
$$-\frac{1}{\eta_b}A_2\int_0^1\int_0^1 p_{ij}(x,y)\frac{\partial}{\partial x}\left(q^x_{kl}(x,y)q^y_{mn}(x,y)\right)dxdy + \frac{1}{6}\frac{{\eta_a}^2}{\eta_b}A_3\int_0^1\int_0^1 p_{ij}(x,y)\frac{\partial}{\partial x}\left(q^{xx}_{kl}(x,y)q^{xy}_{mn}(x,y)\right)dxdy$$
$$+\frac{1}{6}\eta_b A_3\int_0^1\int_0^1 p_{ij}(x,y)\frac{\partial}{\partial x}\left(q^{xy}_{kl}(x,y)q^{yy}_{mn}(x,y)\right)dxdy,$$

$$KN_{25} = +\frac{1}{2}\frac{\eta_b}{\eta_a}A_3\int_0^1\int_0^1 p_{ij}(x,y)\frac{\partial}{\partial x}\left(r^y_{kl}(x,y)q^y_{mn}(x,y)q^y_{op}(x,y)\right)dxdy$$
$$-\frac{\eta_a}{\eta_b}A_4\int_0^1\int_0^1 p_{ij}(x,y)\frac{\partial}{\partial y}\left(r^x_{kl}(x,y)q^x_{mn}(x,y)q^x_{op}(x,y)\right)dxdy + \frac{\eta_a}{\eta_b}A_3\int_0^1\int_0^1 p_{ij}(x,y)\frac{\partial}{\partial x}\left(r^x_{kl}(x,y)q^x_{mn}(x,y)q^y_{op}(x,y)\right)dxdy$$
$$-\frac{\eta_b}{\eta_a}A_4\int_0^1\int_0^1 p_{ij}(x,y)\frac{\partial}{\partial y}\left(r^x_{kl}(x,y)q^y_{mn}(x,y)q^y_{op}(x,y)\right)dxdy + \frac{\eta_b}{\eta_a}A_3\int_0^1\int_0^1 p_{ij}(x,y)\frac{\partial}{\partial y}\left(r^y_{kl}(x,y)q^x_{mn}(x,y)q^y_{op}(x,y)\right)dxdy \tag{A12}$$
$$+\frac{1}{2}\frac{\eta_a}{\eta_b}A_3\int_0^1\int_0^1 p_{ij}(x,y)\frac{\partial}{\partial x}\left(r^y_{kl}(x,y)q^x_{mn}(x,y)q^x_{op}(x,y)\right)dxdy,$$

$$KN_{26} = +12\frac{{\eta_b}^2}{{\eta_a}^2}A_1\int_0^1\int_0^1 p_{ij}(x,y)\frac{\partial}{\partial y}\left(p^y_{kl}(x,y)q^y_{mn}(x,y)q^y_{op}(x,y)\right)dxdy$$
$$-A_4\int_0^1\int_0^1 p_{ij}(x,y)\frac{\partial}{\partial y}\left(p^y_{kl}(x,y)q^x_{mn}(x,y)q^x_{op}(x,y)\right)dxdy + A_3\int_0^1\int_0^1 p_{ij}(x,y)\frac{\partial}{\partial y}\left(p^x_{kl}(x,y)q^x_{mn}(x,y)q^y_{op}(x,y)\right)dxdy$$
$$+A_3\int_0^1\int_0^1 p_{ij}(x,y)\frac{\partial}{\partial x}\left(p^y_{kl}(x,y)q^x_{mn}(x,y)q^y_{op}(x,y)\right)dxdy + \frac{1}{2}A_3\int_0^1\int_0^1 p_{ij}(x,y)\frac{\partial}{\partial x}\left(p^x_{kl}(x,y)q^y_{mn}(x,y)q^y_{op}(x,y)\right)dxdy \tag{A13}$$
$$+\frac{1}{2}\frac{{\eta_a}^2}{{\eta_b}^2}A_3\int_0^1\int_0^1 p_{ij}(x,y)\frac{\partial}{\partial x}\left(p^x_{kl}(x,y)q^x_{mn}(x,y)q^x_{op}(x,y)\right)dxdy,$$

$$
\begin{aligned}
KN_{27} &= +3\frac{{\eta_b}^3}{{\eta_a}^2}A_1\int_0^1\int_0^1 p_{ij}(x,y)\frac{\partial}{\partial y}\left(q^y_{kl}(x,y)q^y_{mn}(x,y)q^y_{op}(x,y)q^y_{qr}(x,y)\right)dxdy\\
&-\frac{1}{4}\frac{{\eta_a}^2}{\eta_b}A_4\int_0^1\int_0^1 p_{ij}(x,y)\frac{\partial}{\partial y}\left(q^x_{kl}(x,y)q^x_{mn}(x,y)q^x_{op}(x,y)q^x_{qr}(x,y)\right)dxdy\\
&-\frac{1}{4}\eta_b A_5\int_0^1\int_0^1 p_{ij}(x,y)\frac{\partial}{\partial y}\left(q^x_{kl}(x,y)q^x_{mn}(x,y)q^y_{op}(x,y)q^y_{qr}(x,y)\right)dxdy\\
&+\frac{1}{2}\frac{{\eta_a}^2}{\eta_b}A_3\int_0^1\int_0^1 p_{ij}(x,y)\frac{\partial}{\partial x}\left(q^x_{kl}(x,y)q^x_{mn}(x,y)q^x_{op}(x,y)q^y_{qr}(x,y)\right)dxdy\\
&+\frac{1}{2}\eta_b A_3\int_0^1\int_0^1 p_{ij}(x,y)\frac{\partial}{\partial x}\left(q^x_{kl}(x,y)q^y_{mn}(x,y)q^y_{op}(x,y)q^y_{qr}(x,y)\right)dxdy,
\end{aligned}
\tag{A14}
$$

and for the transverse motion as

$$
\begin{aligned}
KN_{31} &= -4A_2\frac{\eta_a}{{\eta_b}^2}\int_0^1\int_0^1 q_{ij}(x,y)\frac{\partial}{\partial x}\left(r^x_{kl}(x,y)q^x_{mn}(x,y)\right)dxdy-2A_1\frac{{\eta_a}^3}{{\eta_b}^2}\int_0^1\int_0^1 q_{ij}(x,y)\frac{\partial^2}{\partial x^2}\left(r^x_{kl}(x,y)q^{xx}_{mn}(x,y)\right)dxdy\\
&+\frac{1}{6}A_4\eta_a\int_0^1\int_0^1 q_{ij}(x,y)\frac{\partial^2}{\partial x^2}\left(r^x_{kl}(x,y)q^{yy}_{mn}(x,y)\right)dxdy-\frac{1}{6}A_3\eta_a\int_0^1\int_0^1 q_{ij}(x,y)\frac{\partial^2}{\partial x^2}\left(r^y_{kl}(x,y)q^{xy}_{mn}(x,y)\right)dxdy\\
&+\frac{1}{6}A_4\eta_a\int_0^1\int_0^1 q_{ij}(x,y)\frac{\partial^2}{\partial y^2}\left(r^x_{kl}(x,y)q^{xx}_{mn}(x,y)\right)dxdy+\frac{1}{6}A_4\frac{{\eta_b}^2}{\eta_a}\int_0^1\int_0^1 q_{ij}(x,y)\frac{\partial^2}{\partial y^2}\left(r^x_{kl}(x,y)q^{yy}_{mn}(x,y)\right)dxdy\\
&-\frac{1}{6}A_3\frac{{\eta_b}^2}{\eta_a}\int_0^1\int_0^1 q_{ij}(x,y)\frac{\partial^2}{\partial y^2}\left(r^y_{kl}(x,y)q^{xy}_{mn}(x,y)\right)dxdy-2A_2\frac{1}{\eta_a}\int_0^1\int_0^1 q_{ij}(x,y)\frac{\partial}{\partial y}\left(r^x_{kl}(x,y)q^y_{mn}(x,y)\right)dxdy\\
&-A_2\frac{1}{\eta_a}\int_0^1\int_0^1 q_{ij}(x,y)\frac{\partial}{\partial y}\left(r^y_{kl}(x,y)q^x_{mn}(x,y)\right)dxdy-A_2\frac{1}{\eta_a}\int_0^1\int_0^1 q_{ij}(x,y)\frac{\partial}{\partial x}\left(r^y_{kl}(x,y)q^y_{mn}(x,y)\right)dxdy\\
&-\frac{1}{3}A_3\eta_a\int_0^1\int_0^1 q_{ij}(x,y)\frac{\partial^2}{\partial x\partial y}\left(r^x_{kl}(x,y)q^{xy}_{mn}(x,y)\right)dxdy-\frac{1}{6}A_3\eta_a\int_0^1\int_0^1 q_{ij}(x,y)\frac{\partial^2}{\partial x\partial y}\left(r^y_{kl}(x,y)q^{xx}_{mn}(x,y)\right)dxdy\\
&-\frac{1}{6}A_3\frac{{\eta_b}^2}{\eta_a}\int_0^1\int_0^1 q_{ij}(x,y)\frac{\partial^2}{\partial x\partial y}\left(r^y_{kl}(x,y)q^{yy}_{mn}(x,y)\right)dxdy,
\end{aligned}
\tag{A15}
$$

$$
\begin{aligned}
KN_{32} = &-\frac{1}{6}A_3\frac{{\eta_a}^2}{\eta_b}\int_0^1\int_0^1 q_{ij}(x,y)\,\frac{\partial^2}{\partial x\partial y}\left(p^x_{kl}(x,y)q^{xx}_{mn}(x,y)\right)dxdy\\
&-A_2\frac{1}{\eta_b}\int_0^1\int_0^1 q_{ij}(x,y)\,\frac{\partial}{\partial x}\left(p^x_{kl}(x,y)q^{y}_{mn}(x,y)\right)dxdy-\frac{1}{3}A_3\eta_b\int_0^1\int_0^1 q_{ij}(x,y)\,\frac{\partial^2}{\partial x\partial y}\left(p^y_{kl}(x,y)q^{xy}_{mn}(x,y)\right)dxdy\\
&-\frac{1}{6}A_3\eta_b\int_0^1\int_0^1 q_{ij}(x,y)\,\frac{\partial^2}{\partial x\partial y}\left(p^x_{kl}(x,y)q^{yy}_{mn}(x,y)\right)dxdy-4A_2\frac{\eta_b}{{\eta_a}^2}\int_0^1 q_{ij}(x,y)\,\frac{\partial}{\partial y}\left(p^y_{kl}(x,y)q^{y}_{mn}(x,y)\right)dxdy\\
&-2A_1\frac{{\eta_b}^3}{{\eta_a}^2}\int_0^1\int_0^1 q_{ij}(x,y)\,\frac{\partial^2}{\partial y^2}\left(p^y_{kl}(x,y)q^{yy}_{mn}(x,y)\right)dxdy+\frac{1}{6}A_4\frac{{\eta_a}^2}{\eta_b}\int_0^1\int_0^1 q_{ij}(x,y)\,\frac{\partial^2}{\partial x^2}\left(p^y_{kl}(x,y)q^{xx}_{mn}(x,y)\right)dxdy\\
&-\frac{1}{6}A_3\frac{{\eta_a}^2}{\eta_b}\int_0^1\int_0^1 q_{ij}(x,y)\,\frac{\partial^2}{\partial x^2}\left(p^x_{kl}(x,y)q^{xy}_{mn}(x,y)\right)dxdy+\frac{1}{6}A_4\eta_b\frac{\partial^2}{\partial x^2}\int_0^1\int_0^1 q_{ij}(x,y)\,\frac{\partial^2}{\partial x^2}\left(p^y_{kl}(x,y)q^{yy}_{mn}(x,y)\right)dxdy\\
&+\frac{1}{6}A_4\eta_b\int_0^1\int_0^1 q_{ij}(x,y)\,\frac{\partial^2}{\partial y^2}\left(p^y_{kl}(x,y)q^{xx}_{mn}(x,y)\right)dxdy-\frac{1}{6}A_3\eta_b\int_0^1\int_0^1 q_{ij}(x,y)\,\frac{\partial^2}{\partial y^2}\left(p^x_{kl}(x,y)q^{xy}_{mn}(x,y)\right)dxdy\\
&-2A_2\frac{1}{\eta_b}\int_0^1\int_0^1 q_{ij}(x,y)\,\frac{\partial}{\partial x}\left(p^y_{kl}(x,y)q^{x}_{mn}(x,y)\right)dxdy-A_2\frac{1}{\eta_b}\int_0^1\int_0^1 q_{ij}(x,y)\,\frac{\partial}{\partial y}\left(p^x_{kl}(x,y)q^{x}_{mn}(x,y)\right)dxdy,
\end{aligned}
\tag{A16}
$$

$$
\begin{aligned}
KN_{33} = &+12A_1\frac{{\eta_a}^2}{{\eta_b}^2}\int_0^1\int_0^1 q_{ij}(x,y)\,\frac{\partial}{\partial x}\left(r^x_{kl}(x,y)r^x_{mn}(x,y)q^x_{op}(x,y)\right)dxdy\\
&-A_4\int_0^1\int_0^1 q_{ij}(x,y)\,\frac{\partial}{\partial y}\left(r^x_{kl}(x,y)r^x_{mn}(x,y)q^y_{op}(x,y)\right)dxdy+\frac{1}{2}A_3\int_0^1\int_0^1 q_{ij}(x,y)\,\frac{\partial}{\partial y}\left(r^y_{kl}(x,y)r^y_{mn}(x,y)q^y_{op}(x,y)\right)dxdy\\
&+A_3\int_0^1\int_0^1 q_{ij}(x,y)\,\frac{\partial}{\partial x}\left(r^x_{kl}(x,y)r^y_{mn}(x,y)q^y_{op}(x,y)\right)dxdy+A_3\int_0^1\int_0^1 q_{ij}(x,y)\,\frac{\partial}{\partial y}\left(r^x_{kl}(x,y)r^y_{mn}(x,y)q^x_{op}(x,y)\right)dxdy\\
&+\frac{1}{2}A_3\int_0^1\int_0^1 q_{ij}(x,y)\,\frac{\partial}{\partial x}\left(r^y_{kl}(x,y)r^y_{mn}(x,y)q^x_{op}(x,y)\right)dxdy,
\end{aligned}
\tag{A17}
$$

$$
\begin{aligned}
KN_{34} = &-2A_4\frac{\eta_a}{\eta_b}\int_0^1\int_0^1 q_{ij}(x,y)\,\frac{\partial}{\partial x}\left(r^x_{kl}(x,y)p^y_{mn}(x,y)q^x_{op}(x,y)\right)dxdy\\
&-2A_4\frac{\eta_b}{\eta_a}\int_0^1\int_0^1 q_{ij}(x,y)\,\frac{\partial}{\partial y}\left(r^x_{kl}(x,y)p^y_{mn}(x,y)q^y_{op}(x,y)\right)dxdy+A_3\frac{\eta_a}{\eta_b}\int_0^1\int_0^1 q_{ij}(x,y)\,\frac{\partial}{\partial x}\left(r^y_{kl}(x,y)p^x_{mn}(x,y)q^x_{op}(x,y)\right)dxdy\\
&+A_3\frac{\eta_b}{\eta_a}\int_0^1\int_0^1 q_{ij}(x,y)\,\frac{\partial}{\partial y}\left(r^y_{kl}(x,y)p^x_{mn}(x,y)q^y_{op}(x,y)\right)dxdy+A_3\frac{\eta_a}{\eta_b}\int_0^1\int_0^1 q_{ij}(x,y)\,\frac{\partial}{\partial x}\left(r^x_{kl}(x,y)p^x_{mn}(x,y)q^y_{op}(x,y)\right)dxdy\\
&+A_3\frac{\eta_b}{\eta_a}\int_0^1\int_0^1 q_{ij}(x,y)\,\frac{\partial}{\partial y}\left(r^y_{kl}(x,y)p^y_{mn}(x,y)q^x_{op}(x,y)\right)dxdy+A_3\frac{\eta_b}{\eta_a}\int_0^1\int_0^1 q_{ij}(x,y)\,\frac{\partial}{\partial x}\left(r^y_{kl}(x,y)p^y_{mn}(x,y)q^y_{op}(x,y)\right)dxdy\\
&+A_3\frac{\eta_a}{\eta_b}\int_0^1\int_0^1 q_{ij}(x,y)\,\frac{\partial}{\partial y}\left(r^x_{kl}(x,y)p^x_{mn}(x,y)q^x_{op}(x,y)\right)dxdy,
\end{aligned}
\tag{A18}
$$

$$
\begin{aligned}
KN_{35} &= +12A_1\frac{\eta_b{}^2}{\eta_a{}^2}\int_0^1\int_0^1 q_{ij}(x,y)\frac{\partial}{\partial y}\Big(p^y_{kl}(x,y)p^y_{mn}(x,y)q^y_{op}(x,y)\Big)dxdy \\
&-A_4\int_0^1\int_0^1 q_{ij}(x,y)\frac{\partial}{\partial x}\Big(p^y_{kl}(x,y)p^y_{mn}(x,y)q^x_{op}(x,y)\Big)dxdy+\frac{1}{2}A_3\int_0^1\int_0^1 q_{ij}(x,y)\frac{\partial}{\partial y}\Big(p^x_{kl}(x,y)p^x_{mn}(x,y)q^y_{op}(x,y)\Big)dxdy \\
&+A_3\int_0^1\int_0^1 q_{ij}(x,y)\frac{\partial}{\partial x}\Big(p^x_{kl}(x,y)p^y_{mn}(x,y)q^y_{op}(x,y)\Big)dxdy+A_3\int_0^1\int_0^1 q_{ij}(x,y)\frac{\partial}{\partial y}\Big(p^x_{kl}(x,y)p^y_{mn}(x,y)q^x_{op}(x,y)\Big)dxdy \\
&+\frac{1}{2}A_3\frac{\eta_a{}^2}{\eta_b{}^2}\int_0^1\int_0^1 q_{ij}(x,y)\frac{\partial}{\partial x}\Big(p^x_{kl}(x,y)p^x_{mn}(x,y)q^x_{op}(x,y)\Big)dxdy,
\end{aligned}
\tag{A19}
$$

$$
\begin{aligned}
KN_{36} &= -2A_2\frac{\eta_a{}^2}{\eta_b{}^2}\int_0^1\int_0^1 q_{ij}(x,y)\frac{\partial}{\partial x}\Big(q^x_{kl}(x,y)q^x_{mn}(x,y)q^x_{op}(x,y)\Big)dxdy \\
&-2A_2\frac{\eta_b{}^2}{\eta_a{}^2}\int_0^1\int_0^1 q_{ij}(x,y)\frac{\partial}{\partial y}\Big(q^y_{kl}(x,y)q^y_{mn}(x,y)q^y_{op}(x,y)\Big)dxdy-A_2\int_0^1\int_0^1 q_{ij}(x,y)\frac{\partial}{\partial x}\Big(q^x_{kl}(x,y)q^y_{mn}(x,y)q^y_{op}(x,y)\Big)dxdy \\
&-A_2\int_0^1\int_0^1 q_{ij}(x,y)\frac{\partial}{\partial y}\Big(q^x_{kl}(x,y)q^x_{mn}(x,y)q^y_{op}(x,y)\Big)dxdy+A_1\frac{\eta_a{}^4}{\eta_b{}^2}\int_0^1\int_0^1 q_{ij}(x,y)\frac{\partial}{\partial x}\Big(q^x_{kl}(x,y)q^{xx}_{mn}(x,y)q^{xx}_{op}(x,y)\Big)dxdy \\
&+A_1\frac{\eta_b{}^4}{\eta_a{}^2}\int_0^1\int_0^1 q_{ij}(x,y)\frac{\partial}{\partial y}\Big(q^y_{kl}(x,y)q^{yy}_{mn}(x,y)q^{yy}_{op}(x,y)\Big)dxdy-\frac{1}{12}A_4\eta_b{}^2\int_0^1\int_0^1 q_{ij}(x,y)\frac{\partial}{\partial x}\Big(q^x_{kl}(x,y)q^{yy}_{mn}(x,y)q^{yy}_{op}(x,y)\Big)dxdy \\
&-\frac{1}{12}A_4\eta_a{}^2\int_0^1\int_0^1 q_{ij}(x,y)\frac{\partial}{\partial y}\Big(q^{xx}_{kl}(x,y)q^{xx}_{mn}(x,y)q^y_{op}(x,y)\Big)dxdy-\frac{1}{6}A_4\eta_a{}^2\int_0^1\int_0^1 q_{ij}(x,y)\frac{\partial}{\partial x}\Big(q^x_{kl}(x,y)q^{xx}_{mn}(x,y)q^{yy}_{op}(x,y)\Big)dxdy \\
&-\frac{1}{6}A_4\eta_b{}^2\int_0^1\int_0^1 q_{ij}(x,y)\frac{\partial}{\partial y}\Big(q^{xx}_{kl}(x,y)q^y_{mn}(x,y)q^{yy}_{op}(x,y)\Big)dxdy+\frac{1}{6}A_3\eta_a{}^2\int_0^1\int_0^1 q_{ij}(x,y)\frac{\partial}{\partial x}\Big(q^x_{kl}(x,y)q^{xy}_{mn}(x,y)q^{xy}_{op}(x,y)\Big)dxdy \\
&+\frac{1}{6}A_3\eta_b{}^2\int_0^1\int_0^1 q_{ij}(x,y)\frac{\partial}{\partial y}\Big(q^y_{kl}(x,y)q^{xy}_{mn}(x,y)q^{xy}_{op}(x,y)\Big)dxdy-A_1\frac{\eta_a{}^4}{\eta_b{}^2}\int_0^1\int_0^1 q_{ij}(x,y)\frac{\partial^2}{\partial x^2}\Big(q^x_{kl}(x,y)q^{xx}_{mn}(x,y)q^{xx}_{op}(x,y)\Big)dxdy \\
&-A_1\frac{\eta_b{}^4}{\eta_a{}^2}\int_0^1\int_0^1 q_{ij}(x,y)\frac{\partial^2}{\partial y^2}\Big(q^y_{kl}(x,y)q^{yy}_{mn}(x,y)q^{yy}_{op}(x,y)\Big)dxdy+\frac{1}{12}A_4\eta_b{}^2\int_0^1\int_0^1 q_{ij}(x,y)\frac{\partial^2}{\partial x^2}\Big(q^y_{kl}(x,y)q^{yy}_{mn}(x,y)q^{yy}_{op}(x,y)\Big)dxdy \\
&-\frac{1}{6}A_3\eta_a{}^2\int_0^1\int_0^1 q_{ij}(x,y)\frac{\partial^2}{\partial x\partial y}\Big(q^x_{kl}(x,y)q^y_{mn}(x,y)q^{xx}_{op}(x,y)\Big)dxdy-A_2\int_0^1\int_0^1 q_{ij}(x,y)\frac{\partial}{\partial y}\Big(q^x_{kl}(x,y)q^x_{mn}(x,y)q^y_{op}(x,y)\Big)dxdy \\
&-A_2\int_0^1\int_0^1 q_{ij}(x,y)\frac{\partial}{\partial x}\Big(q^x_{kl}(x,y)q^y_{mn}(x,y)q^y_{op}(x,y)\Big)dxdy+\frac{1}{6}A_3\eta_a{}^2\int_0^1\int_0^1 q_{ij}(x,y)\frac{\partial}{\partial x}\Big(q^{xx}_{kl}(x,y)q^y_{mn}(x,y)q^{xy}_{op}(x,y)\Big)dxdy \\
&-\frac{1}{6}A_3\eta_a{}^2\int_0^1\int_0^1 q_{ij}(x,y)\frac{\partial^2}{\partial x^2}\Big(q^x_{kl}(x,y)q^y_{mn}(x,y)q^{xy}_{op}(x,y)\Big)dxdy+\frac{1}{12}A_4\eta_a{}^2\int_0^1\int_0^1 q_{ij}(x,y)\frac{\partial^2}{\partial x^2}\Big(q^{xx}_{kl}(x,y)q^y_{mn}(x,y)q^y_{op}(x,y)\Big)dxdy \\
&+\frac{1}{12}A_4\eta_b{}^2\int_0^1\int_0^1 q_{ij}(x,y)\frac{\partial^2}{\partial y^2}\Big(q^{xx}_{kl}(x,y)q^y_{mn}(x,y)q^y_{op}(x,y)\Big)dxdy+\frac{1}{12}A_4\eta_a{}^2\int_0^1\int_0^1 q_{ij}(x,y)\frac{\partial^2}{\partial x^2}\Big(q^x_{kl}(x,y)q^x_{mn}(x,y)q^{yy}_{op}(x,y)\Big)dxdy \\
&+\frac{1}{12}A_4\eta_b{}^2\int_0^1\int_0^1 q_{ij}(x,y)\frac{\partial^2}{\partial y^2}\Big(q^x_{kl}(x,y)q^x_{mn}(x,y)q^{yy}_{op}(x,y)\Big)dxdy+\frac{1}{12}A_4\eta_a{}^2\int_0^1\int_0^1 q_{ij}(x,y)\frac{\partial^2}{\partial y^2}\Big(q^x_{kl}(x,y)q^x_{mn}(x,y)q^{xx}_{op}(x,y)\Big)dxdy \\
&-\frac{1}{6}A_3\eta_b{}^2\int_0^1\int_0^1 q_{ij}(x,y)\frac{\partial^2}{\partial y^2}\Big(q^x_{kl}(x,y)q^y_{mn}(x,y)q^{xy}_{op}(x,y)\Big)dxdy-\frac{1}{6}A_3\eta_a{}^2\int_0^1\int_0^1 q_{ij}(x,y)\frac{\partial^2}{\partial x\partial y}\Big(q^x_{kl}(x,y)q^x_{mn}(x,y)q^{xy}_{op}(x,y)\Big)dxdy
\end{aligned}
$$

$$-\frac{1}{6}A_3{\eta_b}^2\int_0^1\int_0^1 q_{ij}(x,y)\frac{\partial^2}{\partial x\partial y}\left(q^y_{kl}(x,y)q^y_{mn}(x,y)q^{xy}_{op}(x,y)\right)dxdy-\frac{1}{6}A_3{\eta_b}^2\int_0^1\int_0^1 q_{ij}(x,y)\frac{\partial^2}{\partial x\partial y}\left(q^x_{kl}(x,y)q^y_{mn}(x,y)q^{yy}_{op}(x,y)\right)dxdy$$
$$+\frac{1}{6}A_3{\eta_a}^2\int_0^1\int_0^1 q_{ij}(x,y)\frac{\partial}{\partial y}\left(q^x_{kl}(x,y)q^{xx}_{mn}(x,y)q^{xy}_{op}(x,y)\right)dxdy+\frac{1}{6}A_3{\eta_b}^2\int_0^1\int_0^1 q_{ij}(x,y)\frac{\partial}{\partial x}\left(q^y_{kl}(x,y)q^{xy}_{mn}(x,y)q^{yy}_{op}(x,y)\right)dxdy$$
$$+\frac{1}{6}A_3{\eta_b}^2\int_0^1\int_0^1 q_{ij}(x,y)\frac{\partial}{\partial y}\left(q^x_{kl}(x,y)q^{xy}_{mn}(x,y)q^{yy}_{op}(x,y)\right)dxdy, \tag{A20}$$

$$KN_{37}=+12A_1\frac{{\eta_a}^3}{{\eta_b}^2}\int_0^1\int_0^1 q_{ij}(x,y)\frac{\partial}{\partial x}\left(r^x_{kl}(x,y)q^x_{mn}(x,y)q^x_{op}(x,y)q^x_{qr}(x,y)\right)dxdy$$
$$-A_4\eta_a\int_0^1\int_0^1 q_{ij}(x,y)\frac{\partial}{\partial x}\left(r^x_{kl}(x,y)q^x_{mn}(x,y)q^y_{op}(x,y)q^y_{qr}(x,y)\right)dxdy$$
$$+A_3\eta_a\int_0^1\int_0^1 q_{ij}(x,y)\frac{\partial}{\partial x}\left(r^y_{kl}(x,y)q^x_{mn}(x,y)q^x_{op}(x,y)q^y_{qr}(x,y)\right)dxdy$$
$$-A_4\eta_a\int_0^1\int_0^1 q_{ij}(x,y)\frac{\partial}{\partial y}\left(r^x_{kl}(x,y)q^x_{mn}(x,y)q^x_{op}(x,y)q^x_{qr}(x,y)\right)dxdy$$
$$-A_4\frac{{\eta_b}^2}{\eta_a}\int_0^1\int_0^1 q_{ij}(x,y)\frac{\partial}{\partial y}\left(r^x_{kl}(x,y)q^y_{mn}(x,y)q^y_{op}(x,y)q^y_{qr}(x,y)\right)dxdy$$
$$+A_3\frac{{\eta_b}^2}{\eta_a}\int_0^1\int_0^1 q_{ij}(x,y)\frac{\partial}{\partial y}\left(r^y_{kl}(x,y)q^x_{mn}(x,y)q^y_{op}(x,y)q^y_{qr}(x,y)\right)dxdy$$
$$+A_3\eta_a\int_0^1\int_0^1 q_{ij}(x,y)\frac{\partial}{\partial x}\left(r^x_{kl}(x,y)q^x_{mn}(x,y)q^y_{op}(x,y)q^y_{qr}(x,y)\right)dxdy \tag{A21}$$
$$+\frac{1}{2}A_3\eta_a\int_0^1\int_0^1 q_{ij}(x,y)\frac{\partial}{\partial x}\left(r^y_{kl}(x,y)q^x_{mn}(x,y)q^x_{op}(x,y)q^y_{qr}(x,y)\right)dxdy$$
$$+\frac{1}{2}A_3\frac{{\eta_b}^2}{\eta_a}\int_0^1\int_0^1 q_{ij}(x,y)\frac{\partial}{\partial x}\left(r^y_{kl}(x,y)q^y_{mn}(x,y)q^y_{op}(x,y)q^y_{qr}(x,y)\right)dxdy$$
$$+A_3\eta_a\int_0^1\int_0^1 q_{ij}(x,y)\frac{\partial}{\partial y}\left(r^x_{kl}(x,y)q^x_{mn}(x,y)q^x_{op}(x,y)q^y_{qr}(x,y)\right)dxdy$$
$$+\frac{1}{2}A_3\eta_a\int_0^1\int_0^1 q_{ij}(x,y)\frac{\partial}{\partial y}\left(r^y_{kl}(x,y)q^x_{mn}(x,y)q^x_{op}(x,y)q^x_{qr}(x,y)\right)dxdy$$
$$+\frac{1}{2}A_3\frac{{\eta_b}^2}{\eta_a}\int_0^1\int_0^1 q_{ij}(x,y)\frac{\partial}{\partial y}\left(r^y_{kl}(x,y)q^x_{mn}(x,y)q^y_{op}(x,y)q^y_{qr}(x,y)\right)dxdy,$$

$$
\begin{aligned}
KN_{38} = {} & +12A_1\frac{{\eta_b}^3}{{\eta_a}^2}\int_0^1\int_0^1 q_{ij}(x,y)\frac{\partial}{\partial y}\left(p^y_{kl}(x,y)q^y_{mn}(x,y)q^y_{op}(x,y)q^y_{qr}(x,y)\right)dxdy \\
& -A_4\eta_b\int_0^1\int_0^1 q_{ij}(x,y)\frac{\partial}{\partial y}\left(p^y_{kl}(x,y)q^x_{mn}(x,y)q^x_{op}(x,y)q^y_{qr}(x,y)\right)dxdy \\
& +A_3\eta_b\int_0^1\int_0^1 q_{ij}(x,y)\frac{\partial}{\partial y}\left(p^x_{kl}(x,y)q^x_{mn}(x,y)q^y_{op}(x,y)q^y_{qr}(x,y)\right)dxdy \\
& -A_4\eta_b\int_0^1\int_0^1 q_{ij}(x,y)\frac{\partial}{\partial x}\left(p^y_{kl}(x,y)q^x_{mn}(x,y)q^y_{op}(x,y)q^y_{qr}(x,y)\right)dxdy \\
& -A_4\frac{{\eta_a}^2}{\eta_b}\int_0^1\int_0^1 q_{ij}(x,y)\frac{\partial}{\partial x}\left(p^y_{kl}(x,y)q^x_{mn}(x,y)q^x_{op}(x,y)q^x_{qr}(x,y)\right)dxdy \\
& +A_3\frac{{\eta_a}^2}{\eta_b}\int_0^1\int_0^1 q_{ij}(x,y)\frac{\partial}{\partial x}\left(p^x_{kl}(x,y)q^x_{mn}(x,y)q^x_{op}(x,y)q^y_{qr}(x,y)\right)dxdy \\
& +A_3\eta_b\int_0^1\int_0^1 q_{ij}(x,y)\frac{\partial}{\partial y}\left(p^y_{kl}(x,y)q^x_{mn}(x,y)q^x_{op}(x,y)q^x_{qr}(x,y)\right)dxdy \\
& +\frac{1}{2}A_3\eta_b\int_0^1\int_0^1 q_{ij}(x,y)\frac{\partial}{\partial y}\left(p^x_{kl}(x,y)q^x_{mn}(x,y)q^x_{op}(x,y)q^y_{qr}(x,y)\right)dxdy \\
& +\frac{1}{2}A_3\frac{{\eta_a}^2}{\eta_b}\int_0^1\int_0^1 q_{ij}(x,y)\frac{\partial}{\partial y}\left(p^x_{kl}(x,y)q^x_{mn}(x,y)q^x_{op}(x,y)q^x_{qr}(x,y)\right)dxdy \\
& +A_3\eta_b\int_0^1\int_0^1 q_{ij}(x,y)\frac{\partial}{\partial x}\left(p^y_{kl}(x,y)q^x_{mn}(x,y)q^y_{op}(x,y)q^y_{qr}(x,y)\right)dxdy \\
& +\frac{1}{2}A_3\eta_b\int_0^1\int_0^1 q_{ij}(x,y)\frac{\partial}{\partial x}\left(p^x_{kl}(x,y)q^y_{mn}(x,y)q^y_{op}(x,y)q^y_{qr}(x,y)\right)dxdy \\
& +\frac{1}{2}A_3\frac{{\eta_a}^2}{\eta_b}\int_0^1\int_0^1 q_{ij}(x,y)\frac{\partial}{\partial x}\left(p^x_{kl}(x,y)q^x_{mn}(x,y)q^x_{op}(x,y)q^y_{qr}(x,y)\right)dxdy,
\end{aligned}
\tag{A22}
$$

$$
\begin{aligned}
KN_{39} = {} & +3A_1\frac{\eta_a{}^4}{\eta_b{}^2}\int_0^1\int_0^1 q_{ij}(x,y)\frac{\partial}{\partial x}\left(q^x_{kl}(x,y)q^x_{mn}(x,y)q^x_{op}(x,y)q^x_{qr}(x,y)q^x_{st}(x,y)\right)dxdy \\
& +3A_1\frac{\eta_b{}^4}{\eta_a{}^2}\int_0^1\int_0^1 q_{ij}(x,y)\frac{\partial}{\partial y}\left(q^y_{kl}(x,y)q^y_{mn}(x,y)q^y_{op}(x,y)q^y_{qr}(x,y)q^y_{st}(x,y)\right)dxdy \\
& -\frac{1}{4}A_4\eta_b{}^2\int_0^1\int_0^1 q_{ij}(x,y)\frac{\partial}{\partial x}\left(q^x_{kl}(x,y)q^y_{mn}(x,y)q^y_{op}(x,y)q^y_{qr}(x,y)q^y_{st}(x,y)\right)dxdy \\
& -\frac{1}{4}A_4\eta_a{}^2\int_0^1\int_0^1 q_{ij}(x,y)\frac{\partial}{\partial y}\left(q^x_{kl}(x,y)q^x_{mn}(x,y)q^x_{op}(x,y)q^x_{qr}(x,y)q^y_{st}(x,y)\right)dxdy \\
& -\frac{1}{4}A_5\eta_a{}^2\int_0^1\int_0^1 q_{ij}(x,y)\frac{\partial}{\partial x}\left(q^x_{kl}(x,y)q^x_{mn}(x,y)q^x_{op}(x,y)q^y_{qr}(x,y)q^y_{st}(x,y)\right)dxdy \\
& -\frac{1}{4}A_5\eta_b{}^2\int_0^1\int_0^1 q_{ij}(x,y)\frac{\partial}{\partial y}\left(q^x_{kl}(x,y)q^x_{mn}(x,y)q^y_{op}(x,y)q^y_{qr}(x,y)q^y_{st}(x,y)\right)dxdy \\
& +\frac{1}{2}A_3\eta_a{}^2\int_0^1\int_0^1 q_{ij}(x,y)\frac{\partial}{\partial x}\left(q^x_{kl}(x,y)q^x_{mn}(x,y)q^x_{op}(x,y)q^y_{qr}(x,y)q^y_{st}(x,y)\right)dxdy \\
& +\frac{1}{2}A_3\eta_b{}^2\int_0^1\int_0^1 q_{ij}(x,y)\frac{\partial}{\partial y}\left(q^x_{kl}(x,y)q^x_{mn}(x,y)q^y_{op}(x,y)q^y_{qr}(x,y)q^y_{st}(x,y)\right)dxdy \\
& +\frac{1}{2}A_3\eta_b{}^2\int_0^1\int_0^1 q_{ij}(x,y)\frac{\partial}{\partial x}\left(q^x_{kl}(x,y)q^y_{mn}(x,y)q^y_{op}(x,y)q^y_{qr}(x,y)q^y_{st}(x,y)\right)dxdy \\
& +\frac{1}{2}A_3\eta_a{}^2\int_0^1\int_0^1 q_{ij}(x,y)\frac{\partial}{\partial y}\left(q^x_{kl}(x,y)q^x_{mn}(x,y)q^x_{op}(x,y)q^x_{qr}(x,y)q^y_{st}(x,y)\right)dxdy.
\end{aligned}
\tag{A23}
$$

References

Ahmetolan, S., & Teymur, M. (2007). Nonlinear modulation of SH waves in an incompressible hyperelastic plate. *Zeitschrift für angewandte Mathematik und Physik, 58*, 457–474.

E.L. Allgower, K. Georg, Introduction to numerical continuation methods, SIAM, 2003.

Allgower, E. L., & Georg, K. (2012). *Numerical continuation methods: An introduction*. Springer Science & Business Media.

Amabili, M., Balasubramanian, P., Breslavsky, I. D., Ferrari, G., Garziera, R., & Riabova, K. (2016). Experimental and numerical study on vibrations and static deflection of a thin hyperelastic plate. *Journal of Sound and Vibration, 385*, 81–92.

Ansari, R., Hassani, R., Faraji Oskouie, M., & Rouhi, H. (2021). Nonlinear bending analysis of hyperelastic Mindlin plates: A numerical approach. *Acta Mechanica, 232*, 741–760.

Argatov, I. I., & Sabina, F. J. (2022). Recovery of information on the depth-dependent profile of elastic FGMs from indentation experiments. *International Journal of Engineering Science, 176*, Article 103659.

Ashok, R., & Manam, S. (2021). Oblique water wave scattering by vertical elastic porous barriers. *International Journal of Engineering Science, 169*, Article 103578.

ASTM, D412: Standard test methods for vulcanized rubber and thermoplastic elastomers–tension, ASTM international, (2006).

Bacciocchi, M., & Tarantino, A. M. (2021). Finite anticlastic bending of hyperelastic laminated beams with a rubberlike core. *Mechanics of Advanced Materials and Structures*, 1–24.

Barber, J., & Klarbring, A. (2003). *Solid mechanics and its applications*. Springer.

Berry, A., Robin, O., & Pierron, F. (2014). Identification of dynamic loading on a bending plate using the virtual fields method. *Journal of Sound and Vibration, 333*, 7151–7164.

Bitter, R., Mohiuddin, T., & Nawrocki, M. (2017). *LabVIEW™ advanced programming techniques*. CRC press.

Bloom, F., & Coffin, D. (2000). *Handbook of thin plate buckling and postbuckling*. CRC Press.

Bonet, J., & Wood, R. D. (1997). *Nonlinear continuum mechanics for finite element analysis*. Cambridge University Press.

Breslavsky, I. D., Amabili, M., & Legrand, M. (2014). Nonlinear vibrations of thin hyperelastic plates. *Journal of Sound and Vibration, 333*, 4668–4681.

C. Brown, T. Nguyen, H. Moody, R. Crawford, A. Oloyede, Assessment of common hyperelastic constitutive equations for describing normal and osteoarthritic articular cartilage, Proceedings of the Institution of Mechanical Engineers, Part H: Journal of Engineering in Medicine, 223 (2009) 643–652.

Chen, W., Wang, L., & Dai, H. (2020). Nonlinear free vibration of hyperelastic beams based on neo-Hookean model. *International Journal of Structural Stability and Dynamics, 20*, Article 2050015.

Chen, W., & Zhao, Y.-P. (2022). Thermo-mechanically coupled constitutive equations for soft elastomers with arbitrary initial states. *International Journal of Engineering Science, 178*, Article 103730.

Darban, H., Luciano, R., & Basista, M. (2022). Free transverse vibrations of nanobeams with multiple cracks. *International Journal of Engineering Science, 177*, Article 103703.
Douhou, A., & Ramtani, S. (2021). Steady diffusion of an ideal fluid through a two-layer thick walled pre-stressed and fiber-reinforced hollow cylinder within the context of mixture theory. *International Journal of Engineering Science, 169*, Article 103575.
Forsat, M. (2020). Investigating nonlinear vibrations of higher-order hyper-elastic beams using the Hamiltonian method. *Acta Mechanica, 231*, 125–138.
Ghayesh, M. H., & Farokhi, H. (2018). Nonlinear behaviour of electrically actuated microplate-based MEMS resonators. In *, 109. Mechanical systems and signal processing* (pp. 220–234).
Hayat, T., & Khan, M. (2005). Homotopy solutions for a generalized second-grade fluid past a porous plate. *Nonlinear Dynamics, 42*, 395–405.
He, L., Lou, J., Kitipornchai, S., Yang, J., & Du, J. (2019). Peeling mechanics of hyperelastic beams: Bending effect. *International Journal of Solids and Structures, 167*, 184–191.
Hu, Y., & Wang, T. (2016). Nonlinear free vibration of a rotating circular plate under the static load in magnetic field. *Nonlinear Dynamics, 85*, 1825–1835.
Islam, S., Bolouri, S. E. S., & Kim, C.-I. (2021). Mechanics of hyperelastic composites reinforced with nonlinear elastic fibrous materials in finite plane elastostatics. *International Journal of Engineering Science, 165*, Article 103491.
Jalaei, M., Thai, H., & Civalek, Ö. (2022). On viscoelastic transient response of magnetically imperfect functionally graded nanobeams. *International Journal of Engineering Science, 172*, Article 103629.
Jeyaraj, P., Padmanabhan, C., & Ganesan, N. (2008). Vibration and acoustic response of an isotropic plate in a thermal environment. *Journal of Vibration and Acoustics*, 130.
Jiang, F., & Yu, W. (2016). Nonlinear variational asymptotic sectional analysis of hyperelastic beams. *AIAA Journal, 54*, 679–690.
Kaplunov, J., Erbaş, B., & Ege, N. (2022). Asymptotic derivation of 2D dynamic equations of motion for transversely inhomogeneous elastic plates. *International Journal of Engineering Science, 178*, Article 103723.
Khadem, S. E., & Rezaee, M. (2000). Introduction of modified comparison functions for vibration analysis of a rectangular cracked plate. *Journal of Sound and Vibration, 236*, 245–258.
Khaniki, H. B., Ghayesh, M. H., Chin, R., & Amabili, M. (2021). Large amplitude vibrations of imperfect porous-hyperelastic beams via a modified strain energy. *Journal of Sound and Vibration, 513*, Article 116416.
Khaniki, H. B., Ghayesh, M. H., Chin, R., & Amabili, M. (2022). A review on the nonlinear dynamics of hyperelastic structures. *Nonlinear Dynamics*, 1–32. https://doi.org/10.1007/s11071-11022-07700-11073
Khaniki, H. B., Ghayesh, M. H., Chin, R., & Chen, L.-Q. (2022). Experimental characteristics and coupled nonlinear forced vibrations of axially travelling hyperelastic beams. *Thin-Walled Structures, 170*, Article 108526.
Khaniki, H. B., Ghayesh, M. H., Chin, R., & Hussain, S. (2022). Nonlinear continuum mechanics of thick hyperelastic sandwich beams using various shear deformable beam theories. *Continuum Mechanics and Thermodynamics, 34*, 781–827.
Kocaturk, T., & Akbas, S. (2010). Geometrically non-linear static analysis of a simply supported beam made of hyperelastic material. *Structural Engineering and Mechanics: An International Journal, 35*, 677–697.
Kubiak, T. (2013). *Static and dynamic buckling of thin-walled plate structures*. Springer.
Kushch, V., & Mogilevskaya, S. (2022). On modeling of elastic interface layers in particle composites. *International Journal of Engineering Science*, Article 103697.
Li, Z., Wang, Q., Du, P., Kadapa, C., Hossain, M., & Wang, J. (2022). Analytical study on growth-induced axisymmetric deformations and shape-control of circular hyperelastic plates. *International Journal of Engineering Science, 170*, Article 103594.
Lu, J., Zhao, X., & Yamada, S. (2016). *Harmonic balance finite element method: Applications in nonlinear electromagnetics and power systems*. John Wiley & Sons.
Makinde, O. (2005). Free convection flow with thermal radiation and mass transfer past a moving vertical porous plate. In *, 32. International communications in heat and mass transfer* (pp. 1411–1419).
Malikan, M., & Eremeyev, V. A. (2022). On a flexomagnetic behavior of composite structures. *International Journal of Engineering Science, 175*, Article 103671.
Malikan, M., Uglov, N. S., & Eremeyev, V. A. (2020). On instabilities and post-buckling of piezomagnetic and flexomagnetic nanostructures. *International Journal of Engineering Science, 157*, Article 103395.
Marckmann, G., & Verron, E. (2006). Comparison of hyperelastic models for rubber-like materials. *Rubber Chemistry and Technology, 79*, 835–858.
Mehta, S., Raju, G., & Saxena, P. (2021). Growth induced instabilities in a circular hyperelastic plate. *International Journal of Solids and Structures, 226*, Article 111026.
Mezzasalma, S. A., Abrami, M., Grassi, G., & Grassi, M. (2022). Rubber elasticity of polymer networks in explicitly non-Gaussian states. Statistical mechanics and LF-NMR inquiry in hydrogel systems. *International Journal of Engineering Science, 176*, Article 103676.
Mittelmann, H. D., & Roose, D. (1990). *Continuation techniques and bifurcation problems*. Springer.
Mooney, M. (1940). A theory of large elastic deformation. *Journal of Applied Physics, 11*, 582–592.
J.M. Ortega, W.C. Rheinboldt, Iterative solution of nonlinear equations in several variables, SIAM, 2000.
Polyanin, A. D., & Zaitsev, V. F. (2003). *Handbook of nonlinear partial differential equations: Exact solutions, methods, and problems*. Chapman and Hall/CRC.
Reddy, J. N. (2003). *Mechanics of laminated composite plates and shells: theory and analysis*. CRC press.
R.J. Schaefer, Mechanical properties of rubber, Harris' shock and vibration handbook, Sixth edition, A. Piersol, T. Paez (Eds), McGraw-Hill Companies Inc, (2010) 33.31–33. 18.
Soni, S., Jain, N., & Joshi, P. (2018). Vibration analysis of partially cracked plate submerged in fluid. *Journal of Sound and Vibration, 412*, 28–57.
Sur, A., & Kanoria, M. (2018). Modeling of memory-dependent derivative in a fibre-reinforced plate. *Thin-Walled Structures, 126*, 85–93.
Wang, J., Wang, Q., & Dai, H.-H. (2018). Stress-free bending of a neo-Hookean plate induced by growth: Exact solution and experiments. *International Journal of Non-Linear Mechanics, 106*, 280–287.
Wang, Y., Zeng, R., & Safarpour, M. (2020). Vibration analysis of FG-GPLRC annular plate in a thermal environment. *Mechanics Based Design of Structures and Machines*, 1–19.
Xia, G., Su, Y., & Chen, W. (2021). Instability of compressible soft electroactive plates. *International Journal of Engineering Science, 162*, Article 103474.
Xiao, X., Xiao, C., & Yin, Y. (2022). A hyperelastic model for corneal stroma accounting for cross-linking and damage. *International Journal of Engineering Science, 176*, Article 103701.
Xu, J., Yuan, X., Zhang, H., Zheng, F., & Chen, L. (2020). Nonlinear vibrations of thermo-hyperelastic moderately thick cylindrical shells with 2: 1 internal resonance. *International Journal of Structural Stability and Dynamics, 20*, Article 2050067.
Xu, W., Zhang, Y., Jiang, J., Liu, Z., & Jiao, Y. (2021). Thermal conductivity and elastic modulus of 3D porous/fractured media considering percolation. *International Journal of Engineering Science, 161*, Article 103456.
Yahia, S. A., Atmane, H. A., Houari, M. S. A., & Tounsi, A. (2015). Wave propagation in functionally graded plates with porosities using various higher-order shear deformation plate theories. *Structural Engineering and Mechanics, 53*, 1143–1165.
Yang, J., Hao, Y., Zhang, W., & Kitipornchai, S. (2010). Nonlinear dynamic response of a functionally graded plate with a through-width surface crack. *Nonlinear Dynamics, 59*, 207–219.
Yang, Y., Fu, C., & Xu, F. (2020). A finite strain model predicts oblique wrinkles in stretched anisotropic films. *International Journal of Engineering Science, 155*, Article 103354.
Zhao, W., Zhang, J., Zhang, W., & Yuan, X. (2021). Internal resonance characteristics of hyperelastic thin-walled cylindrical shells composed of Mooney–Rivlin materials. *Thin-Walled Structures, 163*, Article 107754.
Zheng, Y., Karami, B., & Shahsavari, D. (2022). On the vibration dynamics of heterogeneous panels under arbitrary boundary conditions. *International Journal of Engineering Science, 178*, Article 103727.
Zhou, D., & Cheung, Y. (2000). Vibration of vertical rectangular plate in contact with water on one side. *Earthquake Engineering & Structural Dynamics, 29*, 693–710.

Chapter 8

Doubly-curved hyperelastic shells

Overview

In many applications, shell structures are fabricated using softer materials. For instance, soft shells are used in soft robots, where the shell robots are capable of deforming, and for exploring complicated environments by providing infinite degrees of freedom and large deformations. Moreover, many biological tissues (including bioprosthetic heart valves, inner ears, blood vessels, and bladders) can be analysed using soft shell models. Therefore, this chapter presents comprehensive static, dynamic and internal-resonance analyses on a wide range of curved hyperelastic shell structures, including cylindrical, spherical, doubly-curved, and hyperbolic hyperelastic shallow shells. This study is published and available online as: Khaniki, H. B. & Ghayesh, M. H. (2023). Highly nonlinear hyperelastic shells: Statics and dynamics. International Journal of Engineering Science, 183, 103794. DOI: 10.1016/j.ijengsci.2022.103794

Statement of Authorship

Title of Paper	Highly nonlinear curved hyperelastic shells: statics and dynamics
Publication Status	☐ Published ☐ Accepted for Publication ☑ Submitted for Publication ☐ Unpublished and Unsubmitted w ork w ritten in manuscript style
Publication Details	Khaniki, H. B., & Ghayesh, M. H. (2022). Highly nonlinear hyperelastic shells: statics and dynamics. Submitted for publication to the International Journal of Engineering Science.

Principal Author

Name of Principal Author (Candidate)	Hossein Bakhshi Khaniki		
Contribution to the Paper	I carried out the literature review, conceptualization, formal analysis, investigation, methodology, software, validation, visualization and wrote the manuscript.		
Overall percentage (%)	80%		
Certification:	This paper reports on original research I conducted during the period of my Higher Degree by Research candidature and is not subject to any obligations or contractual agreements with a third party that would constrain its inclusion in this thesis. I am the primary author of this paper.		
Signature		Date	2/11/2022

Co-Author Contributions

By signing the Statement of Authorship, each author certifies that:

i. the candidate's stated contribution to the publication is accurate (as detailed above);

ii. permission is granted for the candidate in include the publication in the thesis; and

iii. the sum of all co-author contributions is equal to 100% less the candidate's stated contribution.

Name of Co-Author	Mergen Ghayesh		
Contribution to the Paper	As the principal supervisor, I helped to construct the manuscript, edit and review the manuscript for submission. I assisted in the conceptualization, investigation, methodology, review and editing. I hereby give consent to Hossein Bakhshi Khaniki to present this paper for examination towards the degree of Doctor of Philosophy.		
Signature		Date	3/11/2022

International Journal of Engineering Science 183 (2023) 103794

Contents lists available at ScienceDirect

International Journal of Engineering Science

journal homepage: www.elsevier.com/locate/ijengsci

Highly nonlinear hyperelastic shells: Statics and dynamics

Hossein B. Khaniki, Mergen H. Ghayesh *

School of Mechanical Engineering, University of Adelaide, South Australia, 5005, Australia

ARTICLE INFO

Keywords:
Hyperelastic shell
Hyperbolic shell
Cylindrical shell
Spherical shell
Nonlinear dynamics
Nonlinear mechanics

ABSTRACT

Investigated in this paper are comprehensive static, dynamic and internal-resonance analyses on a wide range of hyperelastic shell structures, including cylindrical, spherical, doubly-curved, and hyperbolic hyperelastic shallow shells. Donnell's nonlinear shell theory and the Mooney-Rivlin strain energy density model are used to formulate the hyperelastic shell structure. Coupled equations of motion are obtained using Hamilton's principle with highly nonlinear terms due to the curvature in the structure, together with the material nonlinearity and large deformations. The coupled equations of motion are converted to a large set of equations using a two-dimensional Galerkin technique and are solved by employing the Newton-Raphson approach and dynamic equilibrium technique. The strength of the current methodology and model is first verified by comparing the static response of the structure with those obtained by using a finite element software. After verifying the model, a detailed analysis of the bending behaviour of the structure under a time-independent pressure is presented. Moreover, the free and forced vibration responses of the shell structure are presented for different cases, showing that the curvature terms play a significant role in changing the mechanical response of the hyperelastic shell. Furthermore, it is shown that for specific sets of curvatures, internal resonances are present which leads to a complicated, rich nonlinear responses. The nonlinear forced vibration response of the hyperelastic shell is also presented for different shell types and resonances.

1. Introduction

Shell structures are among the most useful structures in many industrial applications due to their high stiffness compared with their individual weight, thereby providing a good load/pressure resistance. Shells have been fabricated with different curvatures through the structure, making cylindrical, spherical, doubly-curved, and hyperbolic shells, each of which has its own unique properties for specific applications. For instance, spherical and cylindrical shell structures have been examined and used for energy-absorption applications (Kan et al., 2021, Tzou and Zhang, 2016), modelling SARS-CoV-2 virus (Dastjerdi et al., 2022), and studying eye conditions (such as Glaucoma (Dastjerdi et al., 2021)). Other well-known applications of a shell structure are liquid/gas storage tanks and pressure vessels (Bakalis and Karamanos, 2021, Sedova and Pronina, 2022), which are fabricated so as to distribute stress and load to avoid buckling and vibration.

For most of the given applications, shells are generally fabricated using stiff materials, such as steel or aluminium alloys. However, in many applications, shell structures should be fabricated using softer materials for different purposes. For instance, in human-machine interactions, shells must be fabricated with soft materials such as airbags (to avoid any injuries). Another application in

* Corresponding author.
E-mail address: mergen.ghayesh@adelaide.edu.au (M.H. Ghayesh).

https://doi.org/10.1016/j.ijengsci.2022.103794
Received 25 October 2022; Received in revised form 15 November 2022; Accepted 20 November 2022
Available online 2 December 2022

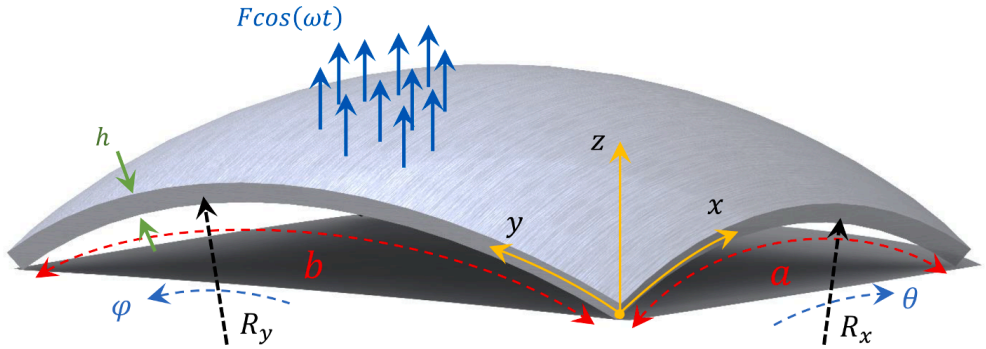

Fig. 1. Schematic of a doubly-curved hyperelastic shell with geometric properties.

which soft shells are used is soft robots, where the shell robots are capable of deforming and exploring complicated environments by providing infinite degrees of freedom and large deformations (Renda et al., 2018, Yang et al., 2021). Soft shell structures have also made their way into many biomechanical applications, of which aortic arch replacement is one of the successful models being used and studied by researchers (Paulis et al., 2017, Detter et al., 2019, Kreibich et al., 2018, Berger et al., 2019). Furthermore, many biological tissues such as bioprosthetic heart valves, inner ears, blood vessels, and bladders can be modelled and analysed accurately using soft shell models (Anani and Rahimi, 2015).

In order to use different types of shell structures properly in any of the mentioned applications, it is important to have a better understanding of the mechanics of shell structures under static and dynamic conditions. Lately, shell theories have been employed in different fields of mechanics such as coating (Nguyen et al., 2020) and drilling (Kaplunov et al., 2020).

For shell structures made of *elastic* materials, researchers have provided a detailed analysis for different static (Kar et al., 2016, Sayyad and Ghugal, 2020, Jiang et al., 2022, Shahmohammadi et al., 2023) and dynamic (Amabili, 2003, Eyvazian et al., 2020, Kar and Panda, 2015, Kiarasi et al., 2021) conditions. Just to discuss a few recent works, for static analysis, Karami et al. (Karami et al., 2022) examined the bending behaviour of anisotropic curved nano-shells using Eringen's nonlocal theory and higher-order shear deformation theory. Malikan et al. (2020) examined the torsional stability of small-scale shells in a magnetic field by using the first-order shear deformation shell theory and the nonlocal strain gradient elasticity approach (Lim et al., 2015, Malikan et al., 2020). A quasi three-dimensional model of functionally graded (FG) shells was presented by Karami and Janghorban (2020) for analysing the buckling and static deformations.

For dynamic analyses of *elastic* shell structures, Zheng et al. (Zheng et al., 2022) examined the linear oscillation behaviour of shell structures with different boundary conditions. Torus-shaped shells made of FG materials have been modelled and studied by Dastjerdi el al. (Dastjerdi et al., 2020) using the first-order shear deformation theory. Using Hamilton's principle, Xu et al. (Xu et al., 2021, Xu et al., 2021) examined the linear forced dynamics of curved nano-shell structures. Detailed analysis and review of the mechanics and dynamics of *elastic* shells can be found in books (Reddy, 2003, Amabili, 2008) and review papers (Amabili and Paidoussis, 2003, Alijani and Amabili, 2014).

Since soft shell structures show nonlinear elastic behaviour and large deformations and strains, these structures show a complicated behaviour under time-dependent and -independent loadings, which requires more accurate modelling. As these structures are used in important applications (biomechanics, soft-robotics, etc.), researchers have developed appropriate methodologies and formulas for modelling soft shell structures.

For circular cylindrical soft shell structures, Amabili et al. (2019) employed the neo-Hookean hyperelastic strain energy density model in the framework of a Lagrangian mechanics to analyse higher-order shear deformable shells with and without perfectly aligned collagen fibres, to study biological tissues and isotropic soft materials. It was concluded that the developed model, which considers material and geometrical nonlinearity, has good accuracy in modelling the static deformation of circular cylindrical shell structures. In another study, Breslavsky et al. (2016) used the same shell theory and analysed the dynamics of circular cylindrical soft shell structures. Zhao et al. (2021) and Xu et al. (2020) analysed the internal resonance phenomena in thin and thick circular cylindrical soft shell structures using the Kirchhoff–Love hypothesis and third-order shear deformation theory, respectively, in the framework of the multiple scale method. Zhang et al. (2019) analysed the nonlinear free vibrations of circular cylindrical soft shell structures by employing the Kirchhoff–Love hypothesis to show that the radius-thickness ratio has a significant effect on changing the vibration modes of circular cylindrical soft shell structures. Anani and Rahimi (2016) analysed the stress in spinning circular cylindrical soft shell structures by using the power-law strain energy function.

Isogeometric methods have been used by Takizawa et al. (2019) and Kiendl et al. (2015) to analyse Kirchhoff–Love shells for the cases of balloon inflation, pinched cylinders, pressurised cylinders and spherical shells. A finite differences scheme was employed by Aranda-Iglesias et al. (2017) to study the oscillations in hyperelastic compressible spherical shells. Zhao et al. (2021) employed Yeoh's strain energy density model for studying spherical incompressible hyperelastic shells under different dynamic conditions. A detailed review study on soft shells and other structures can be found in Refs. (Khaniki et al., 2023, Khaniki et al., 2022).

Previously, the authors have examined the statics and dynamics of different hyperelastic structures including porous-hyperelastic beam structures (Khaniki et al., 2021), axially moving hyperelastic beams (Khaniki et al., 2022), sandwich hyperelastic beams (Khaniki et al., 2022), and hyperelastic plate structures (Khaniki et al., 2023) using both theoretical and experimental approaches.

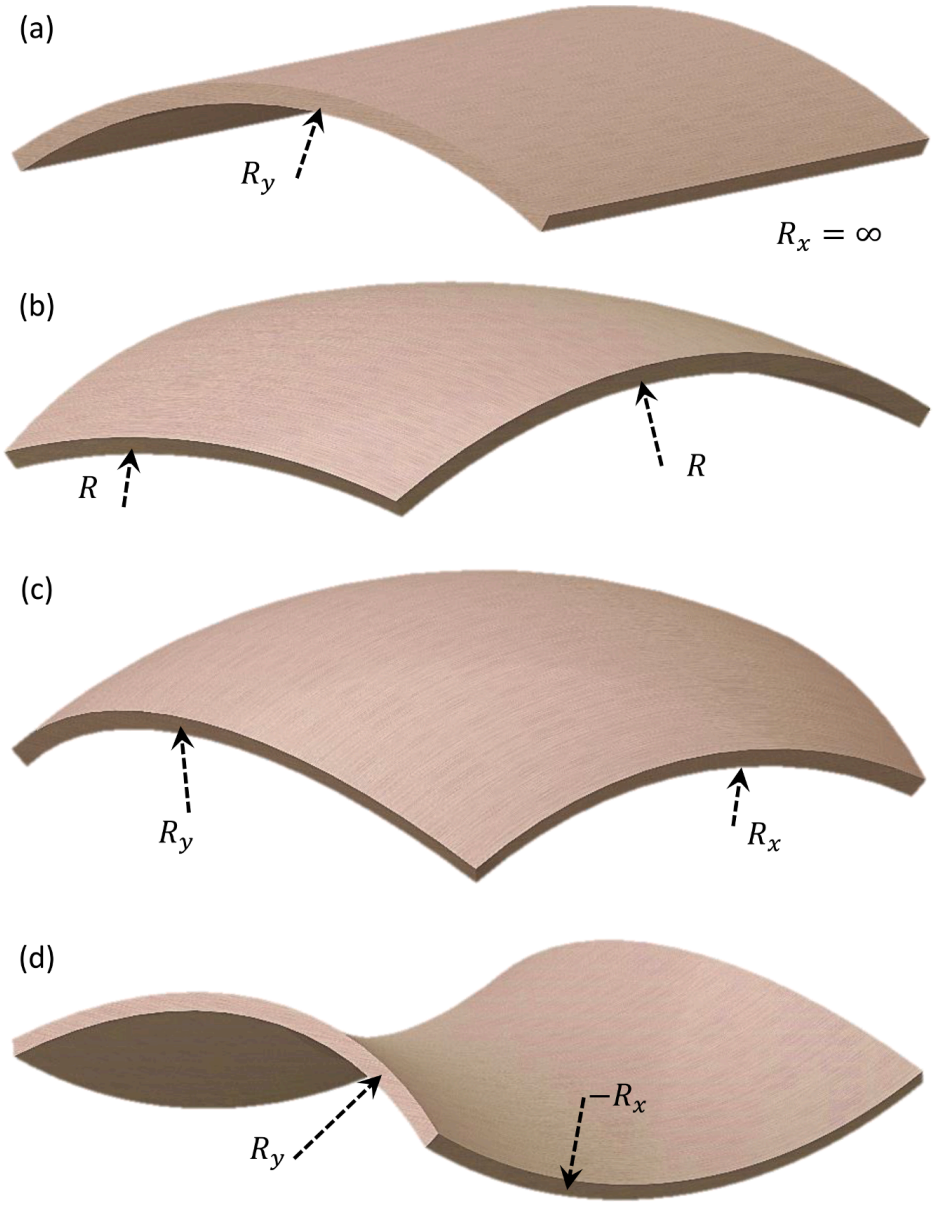

Fig. 2. Different types of hyperelastic shell panels (a) cylindrical, (b) spherical, (c) doubly-curved, and (d) hyperbolic.

However, to the best knowledge of the authors, there has not been a general model for analysing different types of hyperelastic shell structures. Accordingly, in this study, different types of hyperelastic shell structures, namely cylindrical, spherical, double-curved, and hyperbolic hyperelastic shells are analysed under both static and dynamic conditions. The effects of curvature on changing the static deformation, natural frequencies and nonlinear forced vibrations are investigated. Furthermore, internal resonance phenomena, due to curvatures in the hyperelastic shell structure, are investigated in detail. Fig. 1 shows a general model of hyperelastic shell structures, which can be classified in a range of different shell models, including the ones shown in Fig. 2.

2. Hyperelastic doubly-curved shell-structure formulation

Hyperelastic shells with the geometrical properties shown in Fig. 1 can be classified into different types (some shown in Fig. 2), which can be formulated in a general form by employing Donnell's nonlinear shell theory. In this theory, it is assumed that the thickness of the shell is considerably lower than the curvature terms (R_x and R_y), leading to $(1+z/R_x) \cong (1+z/R_y) \cong 1$ (Ghayesh and Farokhi, 2017). For this case, the normal strain terms (ε_x and ε_y) and shear strain term (ε_{xy}) are defined using the in-plane and out-of-plane displacements (u, v, and w) as (Amabili, 2008, Alijani et al., 2011, Reddy, 2006)

$$\varepsilon_x = \frac{1}{R_x}\left(\frac{\partial u}{\partial \theta} + w\right) + \frac{1}{2}\frac{1}{{R_x}^2}\left(\frac{\partial w}{\partial \theta}\right)^2 - z\frac{1}{{R_x}^2}\frac{\partial^2 w}{\partial \theta^2}, \tag{1}$$

$$\varepsilon_y = \frac{1}{R_y}\left(\frac{\partial v}{\partial \varphi} + w\right) + \frac{1}{2}\frac{1}{{R_y}^2}\left(\frac{\partial w}{\partial \varphi}\right)^2 - z\frac{1}{{R_y}^2}\frac{\partial^2 w}{\partial \varphi^2}, \tag{2}$$

$$\varepsilon_{xy} = \frac{1}{2}\left(\frac{1}{R_y}\frac{\partial u}{\partial \varphi} + \frac{1}{R_x}\frac{\partial v}{\partial \theta}\right) - z\frac{1}{R_y}\frac{1}{R_x}\frac{\partial^2 w}{\partial \theta \partial \varphi} + \frac{1}{2}\frac{1}{R_y}\frac{1}{R_x}\frac{\partial w}{\partial \theta}\frac{\partial w}{\partial \varphi}, \tag{3}$$

and by assuming the hyperelastic shell to be an incompressible structure, the normal strain term in the z-direction will not be zero and should be obtained from the incompressibility condition of the shell, as previously obtained in Ref. (Bower, 2009) (and has been used in Ref. (Khaniki et al., 2023)). The left Cauchy-Green deformation tensor (C) is (Bonet et al., 2021)

$$C = \begin{bmatrix} (1+\varepsilon_x)^2 + {\varepsilon_{xy}}^2 & \varepsilon_{xy}(2+\varepsilon_y+\varepsilon_x) & 0 \\ \varepsilon_{xy}(2+\varepsilon_y+\varepsilon_x) & (1+\varepsilon_y)^2 + {\varepsilon_{xy}}^2 & 0 \\ 0 & 0 & (1+\varepsilon_z)^2 \end{bmatrix}. \tag{4}$$

This tensor is used for obtaining the strain invariants of the structure for which, in this study, since the shell is made of soft isotropic materials and undergoes large deformations and strains, the higher-order strain terms should not be ignored. In some studies, since some of the higher-order terms of strains were ignored in defining the strain invariants, the incompressibility equation is different, which can lead to inaccurate modelling of the whole structure. The kinetic energy (KE) of the hyperelastic shell is defined as

$$KE = \frac{1}{2}\rho\int_V \left(W_t^2 + z^2 W_{xt}^2 + z^2 W_{yt}^2 + v_t^2 + u_t^2 - 2zu_t W_{xt} - 2zv_t W_{yt}\right) dV. \tag{5}$$

Since the shell structure is assumed to be made of soft materials, the nonlinear elastic behaviour of the structure is modelled using the Mooney-Rivlin hyperelastic strain energy density model, which has a good accuracy in modelling nonlinear-elastic structures, and is employed as (Rivlin, 1949, Mooney, 1940)

$$HE = C_1[I_1(x,y,z) - 3] + C_2[I_2(x,y,z) - 3], \tag{6}$$

where I_1 and I_2 are the first two strain invariant terms and C_1 and C_2 are the Mooney-Rivlin coefficients. By assuming the hyperelastic shell to be incompressible, the normal strain term in the thickness direction will not be zero ($\varepsilon_z \neq 0$) and should be obtained from the incompressibility condition I_3=0 of the curved shell as

$$\varepsilon_z = 16\varepsilon_x\varepsilon_y(\varepsilon_x+\varepsilon_y) - 16{\varepsilon_{xy}}^2(\varepsilon_x+\varepsilon_y) + 2\varepsilon_x\varepsilon_y + 2{\varepsilon_x}^2 + 2{\varepsilon_{xy}}^2 + 2{\varepsilon_y}^2 - \varepsilon_x - \varepsilon_y. \tag{7}$$

Using Hamilton's principle for a harmonic load of $F\cos(\omega t)$, and for the kinetic energy and potential energy (which for the sake of brevity is neglected here), the equations of motion are obtained for the out-of-plane ξ_3 direction as

$$
\begin{aligned}
&\gamma_{tt}+\Im_{31}\gamma_{\xi_1\xi_1 tt}+\Im_{32}\gamma_{\xi_2\xi_2 tt}+\Im_{33}\alpha_{\xi_1}+\Im_{34}\beta_{\xi_2}+\Im_{35}\gamma_{\xi_1\xi_1\xi_1\xi_1}+\Im_{36}\gamma_{\xi_1\xi_1\xi_2\xi_2}+\Im_{37}\gamma_{\xi_2\xi_2\xi_2\xi_2}+\Im_{38}\gamma\\
&+\Im_{39}{\alpha_{\xi_1}}^2+\Im_{310}{\alpha_{\xi_2}}^2+\Im_{311}{\beta_{\xi_1}}^2+\Im_{312}{\beta_{\xi_2}}^2+\Im_{313}\left(\alpha_{\xi_1}\beta_{\xi_2}\right)+\Im_{314}\left(\alpha_{\xi_2}\beta_{\xi_1}\right)+\Im_{315}\left(\alpha_{\xi_1}\gamma\right)+\Im_{316}\left(\alpha_{\xi_1}\gamma_{\xi_1}\right)\\
&+\Im_{317}\left(\alpha_{\xi_2}\gamma_{\xi_2}\right)+\Im_{318}\left(\alpha_{\xi_1}\gamma_{\xi_2}\right)+\Im_{319}\left(\alpha_{\xi_2}\gamma_{\xi_1}\right)+\Im_{320}\left(\alpha_{\xi_1}\gamma_{\xi_1\xi_1}\right)+\Im_{321}\left(\alpha_{\xi_2}\gamma_{\xi_1\xi_1}\right)+\Im_{322}\left(\alpha_{\xi_1}\gamma_{\xi_2\xi_2}\right)\\
&+\Im_{323}\left(\alpha_{\xi_2}\gamma_{\xi_1\xi_2}\right)+\Im_{324}\left(\alpha_{\xi_1}\gamma_{\xi_1\xi_2}\right)+\Im_{325}\left(\alpha_{\xi_2}\gamma_{\xi_2\xi_2}\right)+\Im_{326}\left(\beta_{\xi_2}\gamma\right)+\Im_{327}\left(\beta_{\xi_1}\gamma_{\xi_1}\right)+\Im_{328}\left(\beta_{\xi_2}\gamma_{\xi_2}\right)\\
&+\Im_{329}\left(\beta_{\xi_1}\gamma_{\xi_2}\right)+\Im_{330}\left(\beta_{\xi_2}\gamma_{\xi_1}\right)+\Im_{331}\left(\beta_{\xi_2}\gamma_{\xi_2\xi_2}\right)+\Im_{332}\left(\beta_{\xi_2}\gamma_{\xi_1\xi_1}\right)+\Im_{333}\left(\beta_{\xi_1}\gamma_{\xi_1\xi_2}\right)+\Im_{334}\left(\beta_{\xi_2}\gamma_{\xi_1\xi_2}\right)\\
&+\Im_{335}\left(\beta_{\xi_1}\gamma_{\xi_2\xi_2}\right)+\Im_{336}\left(\beta_{\xi_1}\gamma_{\xi_1\xi_1}\right)+\Im_{337}\left(\gamma^2\right)+\Im_{338}\left(\gamma\gamma_{\xi_1}\right)+\Im_{339}\left(\gamma\gamma_{\xi_2}\right)+\Im_{340}\left(\gamma\gamma_{\xi_1\xi_1}\right)+\Im_{341}\left(\gamma\gamma_{\xi_2\xi_2}\right)\\
&+\Im_{342}\left(\gamma_{\xi_1}^2\right)+\Im_{343}\left(\gamma_{\xi_2}^2\right)+\Im_{344}\left({\gamma_{\xi_1\xi_1}}^2\right)+\Im_{345}\left({\gamma_{\xi_2\xi_2}}^2\right)+\Im_{346}\left({\gamma_{\xi_1\xi_2}}^2\right)+\Im_{347}\left(\gamma\gamma_{\xi_1\xi_2}\right)+\Im_{348}\left(\gamma_{\xi_1\xi_1}\gamma_{\xi_2\xi_2}\right)\\
&+\Im_{349}\left(\gamma^2\gamma_{\xi_1}\right)+\Im_{350}\left(\gamma^2\gamma_{\xi_2}\right)+\Im_{351}\left(\gamma\gamma_{\xi_1}^2\right)+\Im_{352}\left(\gamma\gamma_{\xi_2}^2\right)+\Im_{353}\left(\gamma_{\xi_1}^3\right)+\Im_{354}\left(\gamma_{\xi_2}^3\right)+\Im_{355}\left(\gamma_{\xi_1}^2\gamma_{\xi_2}\right)\\
&+\Im_{356}\left(\gamma_{\xi_1}\gamma_{\xi_2}^2\right)+\Im_{357}\left(\gamma_{\xi_1}{\gamma_{\xi_1\xi_1}}^2\right)+\Im_{358}\left(\gamma_{\xi_2}{\gamma_{\xi_2\xi_2}}^2\right)+\Im_{359}\left(\gamma_{\xi_1}{\gamma_{\xi_2\xi_2}}^2\right)+\Im_{360}\left({\gamma_{\xi_1\xi_1}}^2\gamma_{\xi_2}\right)+\Im_{361}\left(\gamma_{\xi_1}\gamma_{\xi_1\xi_1}\gamma_{\xi_2\xi_2}\right)\\
&+\Im_{362}\left(\gamma_{\xi_1\xi_1}\gamma_{\xi_2}\gamma_{\xi_2\xi_2}\right)+\Im_{363}\left(\gamma_{\xi_1}{\gamma_{\xi_1\xi_2}}^2\right)+\Im_{364}\left(\gamma_{\xi_2}{\gamma_{\xi_1\xi_2}}^2\right)+\Im_{365}\left(\gamma_{\xi_1}^2\gamma_{\xi_1\xi_1}\right)+\Im_{366}\left(\gamma_{\xi_2}^2\gamma_{\xi_2\xi_2}\right)+\Im_{367}\left(\gamma_{\xi_1\xi_1}\gamma_{\xi_2}^2\right)\\
&+\Im_{368}\left(\gamma_{\xi_1}^2\gamma_{\xi_2\xi_2}\right)+\Im_{369}\left(\gamma_{\xi_1}\gamma_{\xi_2}\gamma_{\xi_1\xi_2}\right)+\Im_{370}\left(\gamma_{\xi_1}^2\gamma_{\xi_1\xi_2}\right)+\Im_{371}\left(\gamma_{\xi_2}^2\gamma_{\xi_1\xi_2}\right)+\Im_{372}\left(\gamma_{\xi_1}\gamma_{\xi_2}\gamma_{\xi_2\xi_2}\right)+\Im_{373}\left(\gamma_{\xi_1}\gamma_{\xi_2}\gamma_{\xi_1\xi_1}\right)\\
&+\Im_{374}\left(\gamma_{\xi_1\xi_1}\gamma_{\xi_2}\gamma_{\xi_1\xi_2}\right)+\Im_{375}\left(\gamma_{\xi_1}\gamma_{\xi_1\xi_1}\gamma_{\xi_1\xi_2}\right)+\Im_{376}\left(\gamma_{\xi_2}\gamma_{\xi_1\xi_2}\gamma_{\xi_2\xi_2}\right)+\Im_{377}\left(\gamma_{\xi_1}\gamma_{\xi_1\xi_2}\gamma_{\xi_2\xi_2}\right)+\Im_{378}\left({\alpha_{\xi_1}}^2\gamma_{\xi_1}\right)\\
&+\Im_{379}\left({\alpha_{\xi_1}}^2\gamma_{\xi_2}\right)+\Im_{380}\left({\alpha_{\xi_2}}^2\gamma_{\xi_2}\right)+\Im_{381}\left(\alpha_{\xi_1}\alpha_{\xi_2}\gamma_{\xi_2}\right)+\Im_{382}\left(\alpha_{\xi_1}\alpha_{\xi_2}\gamma_{\xi_1}\right)+\Im_{383}\left({\alpha_{\xi_2}}^2\gamma_{\xi_1}\right)+\Im_{384}\left({\beta_{\xi_2}}^2\gamma_{\xi_2}\right)\\
&+\Im_{385}\left({\beta_{\xi_2}}^2\gamma_{\xi_1}\right)+\Im_{386}\left({\beta_{\xi_1}}^2\gamma_{\xi_1}\right)+\Im_{387}\left(\beta_{\xi_1}\beta_{\xi_2}\gamma_{\xi_2}\right)+\Im_{388}\left(\beta_{\xi_1}\beta_{\xi_2}\gamma_{\xi_1}\right)+\Im_{389}\left({\beta_{\xi_1}}^2\gamma_{\xi_2}\right)+\Im_{390}\left(\alpha_{\xi_1}\gamma\gamma_{\xi_1}\right)\\
&+\Im_{391}\left(\alpha_{\xi_1}\gamma\gamma_{\xi_1}\right)+\Im_{392}\left(\alpha_{\xi_1}\gamma\gamma_{\xi_2}\right)+\Im_{393}\left(\alpha_{\xi_1}\gamma\gamma_{\xi_2}\right)+\Im_{394}\left(\alpha_{\xi_1}\gamma_{\xi_1}^2\right)+\Im_{395}\left(\alpha_{\xi_1}\gamma_{\xi_2}^2\right)+\Im_{396}\left(\alpha_{\xi_2}\gamma_{\xi_1}\gamma_{\xi_2}\right)\\
&+\Im_{397}\left(\alpha_{\xi_1}\gamma_{\xi_1}^2\right)+\Im_{398}\left(\alpha_{\xi_1}\gamma_{\xi_2}^2\right)+\Im_{399}\left(\alpha_{\xi_2}\gamma_{\xi_1}\gamma_{\xi_2}\right)+\Im_{3100}\left(\alpha_{\xi_2}\gamma\gamma_{\xi_2}\right)+\Im_{3101}\left(\alpha_{\xi_2}\gamma\gamma_{\xi_1}\right)+\Im_{3102}\left(\beta_{\xi_2}\gamma\gamma_{\xi_2}\right)\\
&+\Im_{3103}\left(\beta_{\xi_2}\gamma\gamma_{\xi_2}\right)+\Im_{3104}\left(\beta_{\xi_2}\gamma\gamma_{\xi_1}\right)+\Im_{3105}\left(\beta_{\xi_2}\gamma\gamma_{\xi_1}\right)+\Im_{3106}\left(\beta_{\xi_2}\gamma_{\xi_2}^2\right)+\Im_{3107}\left(\beta_{\xi_2}\gamma_{\xi_1}^2\right)+\Im_{3108}\left(\beta_{\xi_1}\gamma_{\xi_1}\gamma_{\xi_2}\right)\\
&+\Im_{3109}\left(\beta_{\xi_2}\gamma_{\xi_2}^2\right)+\Im_{3110}\left(\beta_{\xi_2}\gamma_{\xi_1}^2\right)+\Im_{3111}\left(\beta_{\xi_1}\gamma_{\xi_1}\gamma_{\xi_2}\right)+\Im_{3112}\left(\beta_{\xi_1}\gamma\gamma_{\xi_1}\right)+\Im_{3113}\left(\beta_{\xi_1}\gamma\gamma_{\xi_2}\right)+\Im_{3114}\left(\alpha_{\xi_1}\beta_{\xi_2}\gamma_{\xi_1}\right)\\
&+\Im_{3115}\left(\alpha_{\xi_1}\beta_{\xi_2}\gamma_{\xi_2}\right)+\Im_{3116}\left(\alpha_{\xi_2}\beta_{\xi_1}\gamma_{\xi_1}\right)+\Im_{3117}\left(\alpha_{\xi_2}\beta_{\xi_1}\gamma_{\xi_2}\right)+\Im_{3118}\left(\alpha_{\xi_1}\beta_{\xi_1}\gamma_{\xi_2}\right)+\Im_{3119}\left(\alpha_{\xi_2}\beta_{\xi_2}\gamma_{\xi_1}\right)\\
&+\Im_{3120}\left(\alpha_{\xi_2}\beta_{\xi_2}\gamma_{\xi_2}\right)+\Im_{3121}\left(\alpha_{\xi_1}\beta_{\xi_1}\gamma_{\xi_1}\right)+\Im_{3122}\left(\alpha_{\xi_1}\gamma_{\xi_1}^3\right)+\Im_{3123}\left(\alpha_{\xi_1}\gamma_{\xi_1}\gamma_{\xi_2}^2\right)+\Im_{3124}\left({\alpha_{\xi_2}}\gamma_{\xi_1}^2\gamma_{\xi_2}\right)\\
&+\Im_{3125}\left(\alpha_{\xi_1}\gamma_{\xi_1}^2\gamma_{\xi_2}\right)+\Im_{3126}\left(\alpha_{\xi_1}\gamma_{\xi_2}^3\right)+\Im_{3127}\left(\alpha_{\xi_2}\gamma_{\xi_1}{\gamma_{\xi_2}}^2\right)+\Im_{3128}\left(\alpha_{\xi_1}\gamma_{\xi_1}{\gamma_{\xi_2}}^2\right)+\Im_{3129}\left(\alpha_{\xi_2}\gamma_{\xi_1}^2\gamma_{\xi_2}\right)\\
&+\Im_{3130}\left(\alpha_{\xi_2}\gamma_{\xi_2}^3\right)+\Im_{3131}\left(\alpha_{\xi_1}{\gamma_{\xi_1}}^2\gamma_{\xi_2}\right)+\Im_{3132}\left(\alpha_{\xi_2}\gamma_{\xi_1}^3\right)+\Im_{3133}\left(\alpha_{\xi_2}\gamma_{\xi_1}\gamma_{\xi_2}^2\right)+\Im_{3134}\left(\beta_{\xi_2}\gamma_{\xi_2}^3\right)+\Im_{3135}\left(\beta_{\xi_2}\gamma_{\xi_1}^2\gamma_{\xi_2}\right)\\
&+\Im_{3136}\left(\beta_{\xi_1}\gamma_{\xi_1}{\gamma_{\xi_2}}^2\right)+\Im_{3137}\left(\beta_{\xi_2}\gamma_{\xi_1}\gamma_{\xi_2}^2\right)+\Im_{3138}\left(\beta_{\xi_2}\gamma_{\xi_1}^3\right)+\Im_{3139}\left(\beta_{\xi_1}{\gamma_{\xi_1}}^2\gamma_{\xi_2}\right)+\Im_{3140}\left(\beta_{\xi_2}{\gamma_{\xi_1}}^2\gamma_{\xi_2}\right)\\
&+\Im_{3141}\left(\beta_{\xi_1}\gamma_{\xi_1}\gamma_{\xi_2}^2\right)+\Im_{3142}\left(\beta_{\xi_1}\gamma_{\xi_1}^3\right)+\Im_{3143}\left(\beta_{\xi_2}\gamma_{\xi_1}{\gamma_{\xi_2}}^2\right)+\Im_{3144}\left(\beta_{\xi_1}\gamma_{\xi_2}^3\right)+\Im_{3145}\left(\beta_{\xi_1}\gamma_{\xi_1}^2\gamma_{\xi_2}\right)+\Im_{3146}\left(\gamma\gamma_{\xi_1}^3\right)\\
&+\Im_{3147}\left(\gamma\gamma_{\xi_2}^3\right)+\Im_{3148}\left(\gamma\gamma_{\xi_1}\gamma_{\xi_2}^2\right)+\Im_{3149}\left(\gamma\gamma_{\xi_1}^2\gamma_{\xi_2}\right)+\Im_{3150}\left(\gamma_{\xi_1}^4\right)+\Im_{3151}\left(\gamma_{\xi_2}^4\right)+\Im_{3152}\left(\gamma_{\xi_1}^2\gamma_{\xi_2}^2\right)+\Im_{3153}\left(\gamma\gamma_{\xi_1}{\gamma_{\xi_2}}^2\right)\\
&+\Im_{3154}\left(\gamma{\gamma_{\xi_1}}^2\gamma_{\xi_2}\right)+\Im_{3155}\left(\gamma_{\xi_1}^5\right)+\Im_{3156}\left(\gamma_{\xi_2}^5\right)+\Im_{3157}\left(\gamma_{\xi_1}\gamma_{\xi_2}^4\right)+\Im_{3158}\left(\gamma_{\xi_1}^4\gamma_{\xi_2}\right)+\Im_{3159}\left(\gamma_{\xi_1}^3{\gamma_{\xi_2}}^2\right)\\
&+\Im_{3160}\left({\gamma_{\xi_1}}^2\gamma_{\xi_2}^3\right)=F^*\cos(\Omega t),
\end{aligned}
\tag{8}
$$

and for the in-plane ξ_1 direction as

$$
\begin{aligned}
&\alpha_{tt}+\mathfrak{F}_{11}\alpha_{\xi_1\xi_1}+\mathfrak{F}_{12}\alpha_{\xi_2\xi_2}+\mathfrak{F}_{13}\beta_{\xi_1\xi_2}+\mathfrak{F}_{14}\gamma_{\xi_1}+\mathfrak{F}_{15}\left(\alpha_{\xi_1}{}^2\right)+\mathfrak{F}_{16}\left(\alpha_{\xi_2}{}^2\right)+\mathfrak{F}_{17}\left(\alpha_{\xi_1}\alpha_{\xi_2}\right)\\
&\quad+\mathfrak{F}_{18}\left(\alpha_{\xi_1}\beta_{\xi_1}\right)+\mathfrak{F}_{19}\left(\alpha_{\xi_2}\beta_{\xi_2}\right)+\mathfrak{F}_{110}\left(\alpha_{\xi_1}\beta_{\xi_2}\right)+\mathfrak{F}_{111}\left(\alpha_{\xi_2}\beta_{\xi_1}\right)+\mathfrak{F}_{112}\left(\alpha_{\xi_1}\gamma\right)+\mathfrak{F}_{113}\left(\alpha_{\xi_2}\gamma\right)\\
&\quad+\mathfrak{F}_{114}\left(\beta_{\xi_2}{}^2\right)+\mathfrak{F}_{115}\left(\beta_{\xi_1}{}^2\right)+\mathfrak{F}_{116}\left(\beta_{\xi_1}\beta_{\xi_2}\right)+\mathfrak{F}_{117}\left(\beta_{\xi_2}\gamma\right)+\mathfrak{F}_{118}\left(\beta_{\xi_1}\gamma\right)+\mathfrak{F}_{119}\left(\gamma^2\right)+\mathfrak{F}_{120}\left(\gamma_{\xi_2}^2\right)\\
&\quad+\mathfrak{F}_{121}\left(\gamma_{\xi_1\xi_1}{}^2\right)+\mathfrak{F}_{122}\left(\gamma_{\xi_1}^2\right)+\mathfrak{F}_{123}\left(\gamma_{\xi_2\xi_2}{}^2\right)+\mathfrak{F}_{124}\left(\gamma_{\xi_1\xi_1}\gamma_{\xi_1\xi_2}\right)+\mathfrak{F}_{125}\left(\gamma_{\xi_1\xi_1}\gamma_{\xi_2\xi_2}\right)+\mathfrak{F}_{126}\left(\gamma_{\xi_1\xi_2}{}^2\right)\\
&\quad+\mathfrak{F}_{127}\left(\gamma_{\xi_1}\gamma_{\xi_2}\right)+\mathfrak{F}_{128}\left(\gamma_{\xi_1\xi_2}\gamma_{\xi_2\xi_2}\right)+\mathfrak{F}_{129}\left(\alpha_{\xi_1}\gamma_{\xi_1}^2\right)+\mathfrak{F}_{130}\left(\alpha_{\xi_1}\gamma_{\xi_2}^2\right)+\mathfrak{F}_{131}\left(\alpha_{\xi_2}\gamma_{\xi_1}\gamma_{\xi_2}\right)\\
&\quad+\mathfrak{F}_{132}\left(\alpha_{\xi_1}\gamma_{\xi_1}\gamma_{\xi_2}\right)+\mathfrak{F}_{133}\left(\alpha_{\xi_2}\gamma_{\xi_1}^2\right)+\mathfrak{F}_{134}\left(\alpha_{\xi_2}\gamma_{\xi_2}^2\right)+\mathfrak{F}_{135}\left(\beta_{\xi_2}\gamma_{\xi_2}^2\right)+\mathfrak{F}_{136}\left(\beta_{\xi_2}\gamma_{\xi_1}^2\right)\\
&\quad+\mathfrak{F}_{137}\left(\beta_{\xi_1}\gamma_{\xi_1}\gamma_{\xi_2}\right)+\mathfrak{F}_{138}\left(\beta_{\xi_1}\gamma_{\xi_1}^2\right)+\mathfrak{F}_{139}\left(\beta_{\xi_1}\gamma_{\xi_2}^2\right)+\mathfrak{F}_{140}\left(\beta_{\xi_2}\gamma_{\xi_1}\gamma_{\xi_2}\right)+\mathfrak{F}_{141}\left(\gamma\gamma_{\xi_1}^2\right)\\
&\quad+\mathfrak{F}_{142}\left(\gamma\gamma_{\xi_2}^2\right)+\mathfrak{F}_{143}\left(\gamma\gamma_{\xi_1}\gamma_{\xi_2}\right)+\mathfrak{F}_{144}\left(\gamma_{\xi_1}^4\right)+\mathfrak{F}_{145}\left(\gamma_{\xi_2}^4\right)+\mathfrak{F}_{146}\left(\gamma_{\xi_1}^2\gamma_{\xi_2}^2\right)\\
&\quad+\mathfrak{F}_{147}\left(\gamma_{\xi_1}^3\gamma_{\xi_2}\right)+\mathfrak{F}_{148}\left(\gamma_{\xi_1}\gamma_{\xi_2}^3\right)=0,
\end{aligned}
\tag{9}
$$

and for the in-plane ξ_2 direction as

$$
\begin{aligned}
&\beta_{tt}+\mathfrak{F}_{21}\alpha_{\xi_1\xi_2}+\mathfrak{F}_{22}\beta_{\xi_2\xi_2}+\mathfrak{F}_{23}\beta_{\xi_1\xi_1}+\mathfrak{F}_{24}\gamma_{\xi_2}+\mathfrak{F}_{25}\left(\alpha_{\xi_1}{}^2\right)+\mathfrak{F}_{26}\left(\alpha_{\xi_2}{}^2\right)+\mathfrak{F}_{27}\left(\alpha_{\xi_1}\alpha_{\xi_2}\right)\\
&\quad+\mathfrak{F}_{28}\left(\alpha_{\xi_1}\beta_{\xi_2}\right)+\mathfrak{F}_{29}\left(\alpha_{\xi_2}\beta_{\xi_1}\right)+\mathfrak{F}_{210}\left(\alpha_{\xi_1}\beta_{\xi_1}\right)+\mathfrak{F}_{211}\left(\alpha_{\xi_2}\beta_{\xi_2}\right)+\mathfrak{F}_{212}\left(\alpha_{\xi_1}\gamma\right)+\mathfrak{F}_{213}\left(\alpha_{\xi_2}\gamma\right)\\
&\quad+\mathfrak{F}_{214}\left(\beta_{\xi_2}{}^2\right)+\mathfrak{F}_{215}\left(\beta_{\xi_1}\beta_{\xi_2}\right)+\mathfrak{F}_{216}\left(\beta_{\xi_1}{}^2\right)+\mathfrak{F}_{217}\left(\beta_{\xi_1}\gamma\right)+\mathfrak{F}_{218}\left(\beta_{\xi_2}\gamma\right)+\mathfrak{F}_{219}\left(\gamma^2\right)+\mathfrak{F}_{220}\left(\gamma_{\xi_2}^2\right)\\
&\quad+\mathfrak{F}_{221}\left(\gamma_{\xi_1}^2\right)+\mathfrak{F}_{222}\left(\gamma_{\xi_2\xi_2}{}^2\right)+\mathfrak{F}_{223}\left(\gamma_{\xi_1\xi_1}{}^2\right)+\mathfrak{F}_{224}\left(\gamma_{\xi_1\xi_1}\gamma_{\xi_2\xi_2}\right)+\mathfrak{F}_{225}\left(\gamma_{\xi_1\xi_2}{}^2\right)+\mathfrak{F}_{226}\left(\gamma_{\xi_1}\gamma_{\xi_2}\right)\\
&\quad+\mathfrak{F}_{227}\left(\gamma_{\xi_1\xi_1}\gamma_{\xi_1\xi_2}\right)+\mathfrak{F}_{228}\left(\gamma_{\xi_1\xi_2}\gamma_{\xi_2\xi_2}\right)+\mathfrak{F}_{229}\left(\alpha_{\xi_1}\gamma_{\xi_1}^2\right)+\mathfrak{F}_{230}\left(\alpha_{\xi_1}\gamma_{\xi_2}^2\right)+\mathfrak{F}_{231}\left(\alpha_{\xi_2}\gamma_{\xi_1}\gamma_{\xi_2}\right)\\
&\quad+\mathfrak{F}_{232}\left(\alpha_{\xi_1}\gamma_{\xi_1}\gamma_{\xi_2}\right)+\mathfrak{F}_{233}\left(\alpha_{\xi_2}\gamma_{\xi_1}^2\right)+\mathfrak{F}_{234}\left(\alpha_{\xi_2}\gamma_{\xi_2}^2\right)+\mathfrak{F}_{235}\left(\beta_{\xi_2}\gamma_{\xi_2}^2\right)+\mathfrak{F}_{236}\left(\beta_{\xi_2}\gamma_{\xi_1}^2\right)\\
&\quad+\mathfrak{F}_{237}\left(\beta_{\xi_1}\gamma_{\xi_1}\gamma_{\xi_2}\right)+\mathfrak{F}_{238}\left(\beta_{\xi_1}\gamma_{\xi_1}^2\right)+\mathfrak{F}_{239}\left(\beta_{\xi_1}\gamma_{\xi_2}^2\right)+\mathfrak{F}_{240}\left(\beta_{\xi_2}\gamma_{\xi_1}\gamma_{\xi_2}\right)+\mathfrak{F}_{241}\left(\gamma\gamma_{\xi_2}^2\right)\\
&\quad+\mathfrak{F}_{242}\left(\gamma\gamma_{\xi_1}^2\right)+\mathfrak{F}_{243}\left(\gamma\gamma_{\xi_1}\gamma_{\xi_2}\right)+\mathfrak{F}_{244}\left(\gamma_{\xi_2}^4\right)+\mathfrak{F}_{245}\left(\gamma_{\xi_1}^4\right)+\mathfrak{F}_{246}\left(\gamma_{\xi_1}^2\gamma_{\xi_2}^2\right)\\
&\quad+\mathfrak{F}_{247}\left(\gamma_{\xi_1}^3\gamma_{\xi_2}\right)+\mathfrak{F}_{248}\left(\gamma_{\xi_1}\gamma_{\xi_2}^3\right)=0,
\end{aligned}
\tag{10}
$$

where

$$
\begin{gathered}
\xi_1=\frac{x}{a},\quad \xi_2=\frac{y}{b},\quad \xi_3=\frac{z}{h},\quad \alpha=\frac{u}{h},\quad \beta=\frac{v}{h},\quad \gamma=\frac{w}{h},\\
\chi_1=\frac{C_1}{C_2},\quad \chi_2=\frac{3C_1+4C_2}{C_2},\quad \chi_3=\frac{18C_1+35C_2}{C_2},\quad \chi_4=\frac{24C_1+70C_2}{C_2},\quad \chi_5=\frac{12C_1+70C_2}{C_2}\\
\Re_x=\frac{a}{R_x},\quad \Re_y=\frac{b}{R_y},\quad \eta_a=\frac{h}{a},\quad \eta_b=\frac{h}{b},\quad \xi=\frac{a}{b},\\
F^*=\frac{Fa^2b^2}{C_2h^4},\quad \Omega=\sqrt{\frac{\rho_0a^2b^2}{C_2h^2}}\omega,\quad t^*=t\sqrt{\frac{C_2h^2}{\rho_0a^2b^2}}=t\frac{h}{ab}\sqrt{\frac{C_2}{\rho_0}}.
\end{gathered}
\tag{11}
$$

Table 1
Comparison of the maximum amplitude of transverse deformation of hyperelastic doubly-curved, hyperbolic and cylindrical shells under different static pressures.

Method	Curvature		Applied static pressure load (Pa)							
	R_x (m)	R_y (m)	-2000	-1500	-1000	-500	500	1000	1500	2000
	Maximum amplitude of transverse deformation – Doubly-curved shell (mm)									
Formula	2/3	2	6.7096	6.0679	5.1047	2.7190	1.0081	1.6658	2.1722	2.5917
ANSYS	2/3	2	6.8894	5.9321	5.0518	2.6112	0.98587	1.5489	2.0902	2.5506
Discrepancy (%)			0.0268	0.0224	0.0104	0.0396	0.0221	0.0702	0.0377	0.0159
	Maximum amplitude of transverse deformation - Hyperbolic shell (mm)									
Formula	2/3	-2	5.7193	5.0937	4.2065	2.5452	1.2142	1.9625	2.5223	2.9782
ANSYS	2/3	-2	5.7257	5.1641	4.1332	2.5949	1.2176	1.9055	2.4738	3.0257
Discrepancy (%)			0.0011	0.0138	0.0174	0.0195	0.0028	0.0290	0.0192	0.0159
	Maximum amplitude of transverse deformation - Cylindrical shell (mm)									
Formula	∞	-2	4.5169	3.9653	3.2410	2.1323	1.7874	2.7423	3.4028	3.9191
ANSYS	∞	-2	4.5524	4.0459	3.2946	2.1403	1.7990	2.7811	3.4793	3.8944
Discrepancy (%)			0.0079	0.0203	0.0165	0.0038	0.0065	0.0141	0.0225	0.0063

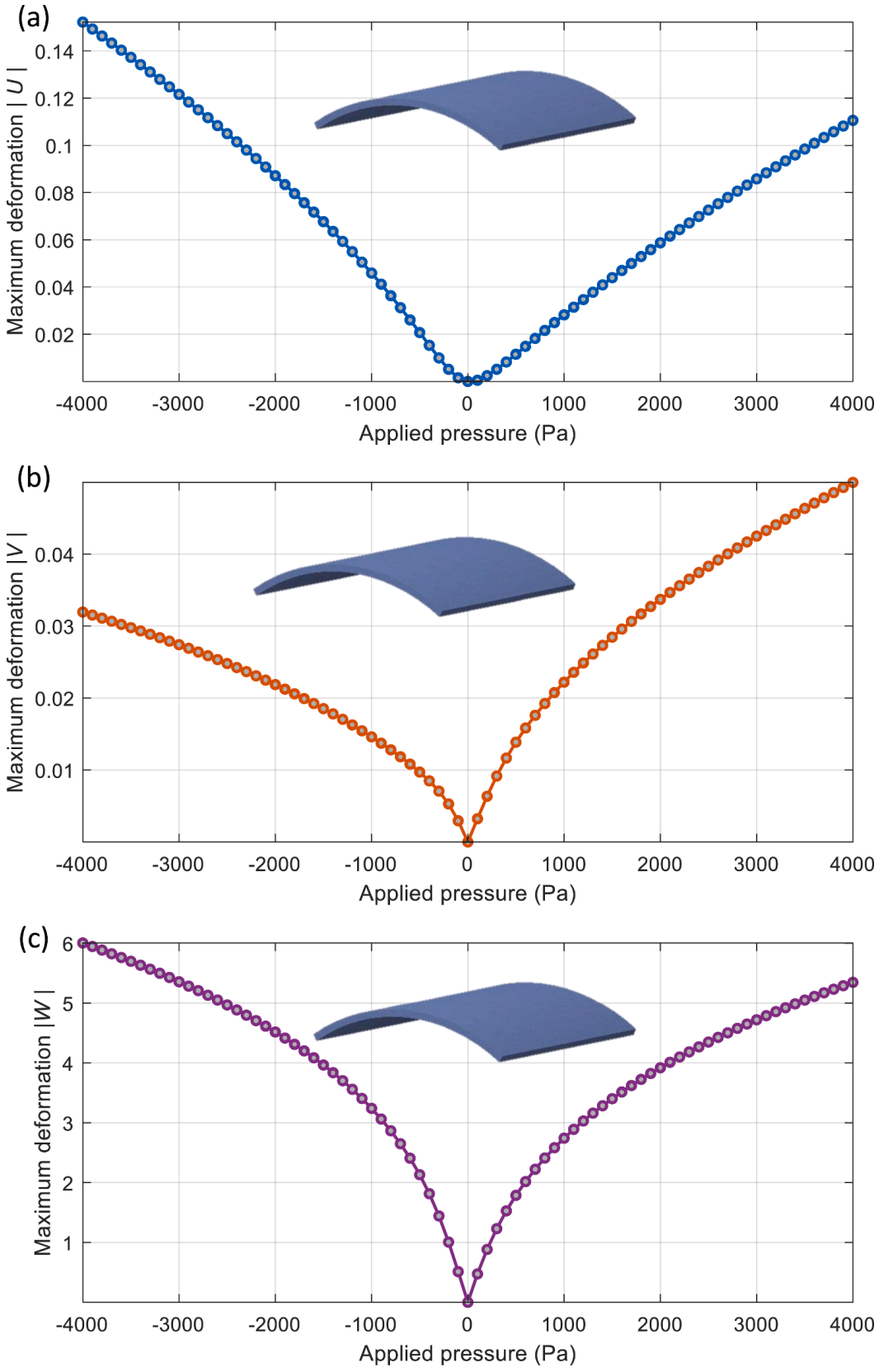

Fig. 3. The maximum magnitude of deformation of a hyperelastic cylindrical shell in millimetres for (a) U, (b) V, and (c) W.

and terms $\mathfrak{F}_{ij}$ are defined in Appendix A. It can be seen that the curvature terms have a significant effect on increasing the coupling and nonlinearity of the equations of motion, which shows the importance of correctly modelling the curvature in the hyperelastic shell structure.

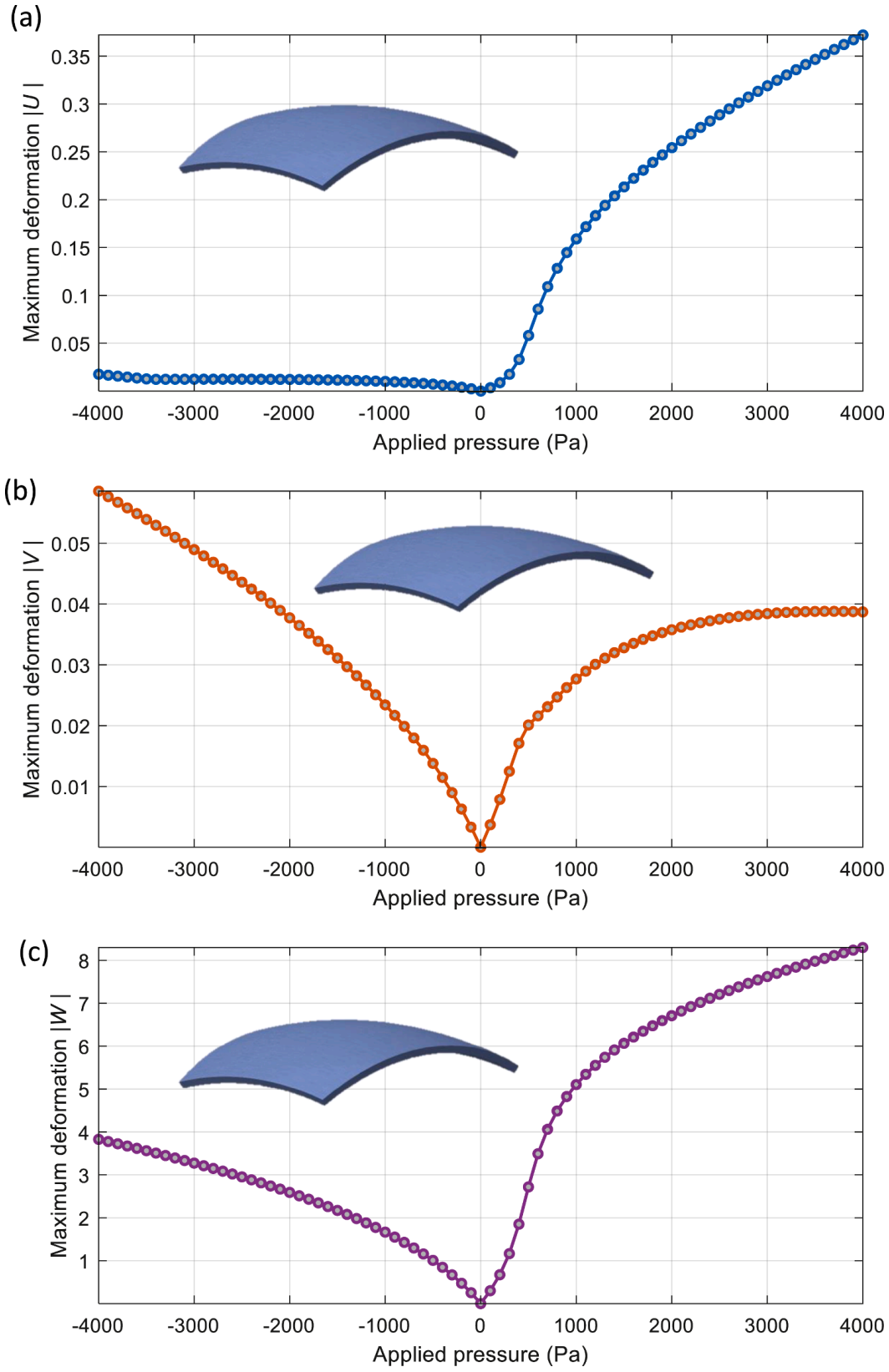

Fig. 4. The maximum magnitude of deformation of a hyperelastic doubly-curved shell in millimetres for (a) U, (b) V, and (c) W.

The presented equations of motion are a general model of curved hyperelastic structures that can be used for any hyperbolic and doubly-curved hyperelastic shells. For specific cases, in order to present a cylindrical hyperelastic shell structure, one of the curvature terms (R_x or R_y) should be infinite equivalent to $\Re_x$ or $\Re_y$ being zero. For a spherical hyperelastic shell structure, the curvature terms have the same magnitude $R_x = R_y = r$ or $\Re_x = \Re_y = \Re$. The elliptical model can also be obtained by having $R_x/2 = R_y = r$ or $2\Re_x = \Re_y =$

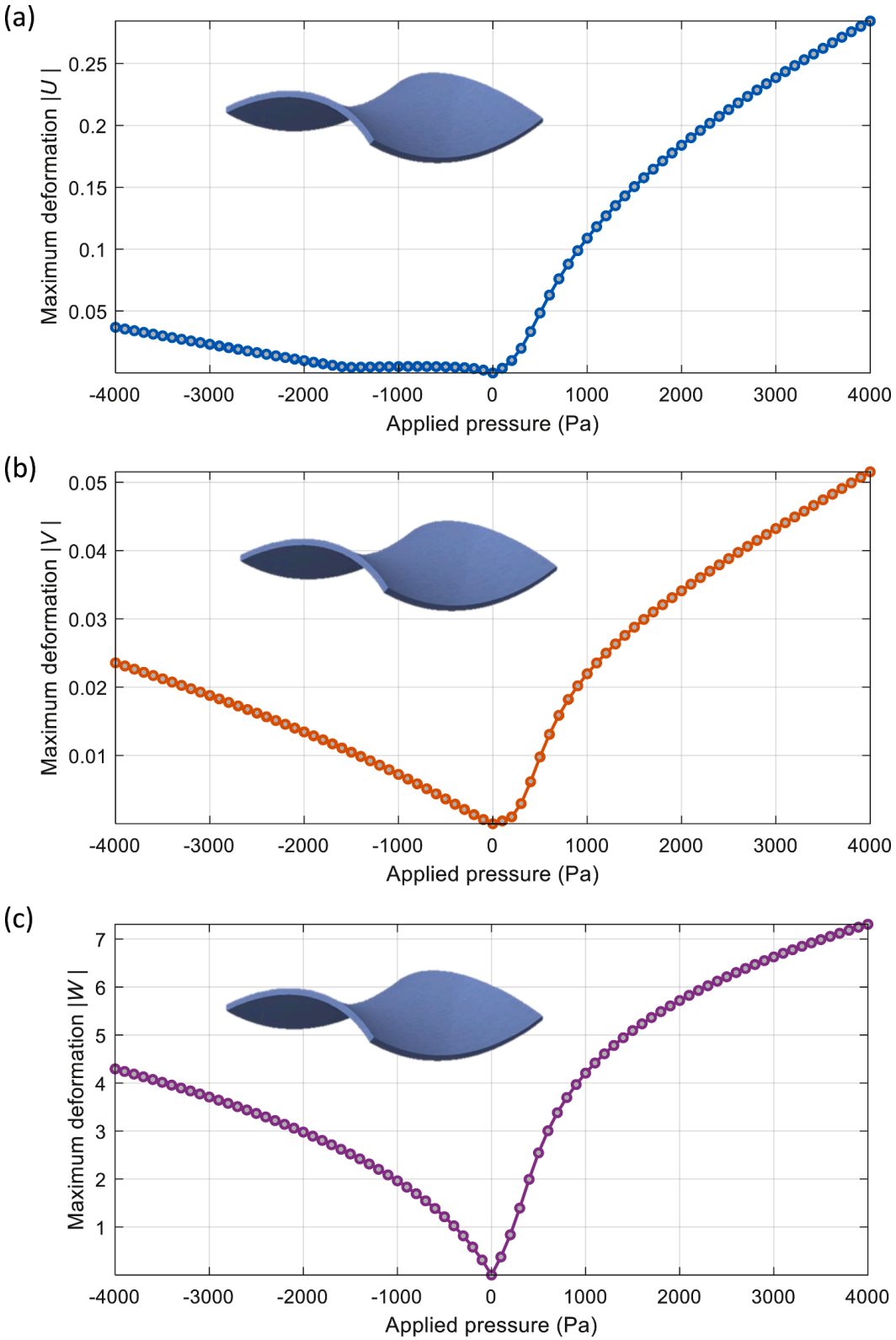

Fig. 5. The maximum magnitude of deformation of a hyperelastic hyperbolic shell in millimetres for (a) U, (b) V, and (c) W.

$\Re$, respectively. In the next section, a solution procedure for the given nondimensional equations of motion of curved hyperelastic structures is presented.

3. Solution procedure

In the previous section, the coupled equations of motion for hyperelastic shell structures were presented, showing highly nonlinear

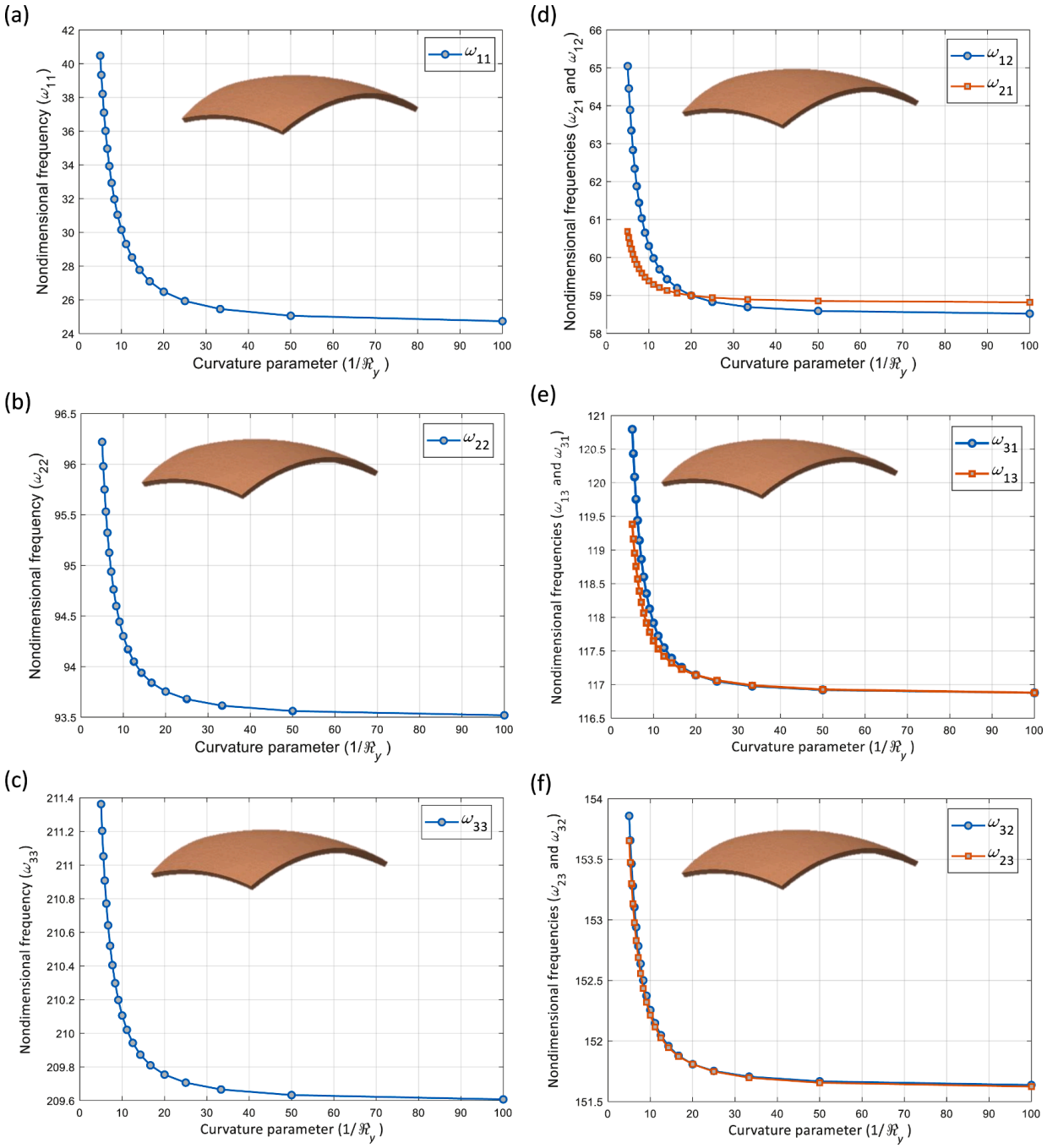

Fig. 6. Nondimensional transverse natural frequencies of a doubly-curved hyperelastic shell with respect to curvature parameter ($1/\Re_y$) for (a) ω_{11}, (b) ω_{22}, (c) ω_{33}, (d) ω_{12} and ω_{21}, (e) ω_{13} and ω_{31}, and (f) ω_{32} and ω_{23}.

terms due to the material nonlinearity, large deformations, and curvature in the shell. The deformation terms α, β, and γ can be presented in a discretised form by using a two-dimensional Galerkin technique, for a simply-supported hyperelastic shell model as (Ghayesh and Farokhi, 2018)

$$\alpha(\xi_1,\xi_2,t)=\sum_{i=1}^{M}\sum_{j=1}^{M}U_{ij}(t)\sin(i\pi\xi_1)\sin(j\pi\xi_2), \tag{12}$$

$$\beta(\xi_1,\xi_2,t)=\sum_{l=1}^{M}\sum_{k=1}^{M}V_{kl}(t)\sin(k\pi\xi_1)\sin(l\pi\xi_2), \tag{13}$$

$$\gamma(\xi_1,\xi_2,t)=\sum_{n=1}^{M}\sum_{m=1}^{M}W_{mn}(t)\sin(m\pi\xi_1)\sin(n\pi\xi_2), \tag{14}$$

The coupled nonlinear equations of motion of hyperelastic shells can be discretised into a large set of ordinary differential equations by using Eqs. (15)-(17)) as

$$
\begin{aligned}
&\sum_{l=1}^{N}\sum_{k=1}^{N} M^{22}_{ijkl}\ddot{W}_{kl} + \sum_{l=1}^{N}\sum_{k=1}^{N}\int_0^1\int_0^1 \sin(i\pi\xi_1)\sin(j\pi\xi_2)\aleph^{31}_{kl}\,d\xi_1 d\xi_2 U_{kl} + \sum_{l=1}^{N}\sum_{k=1}^{N}\int_0^1\int_0^1 \sin(i\pi\xi_1)\sin(j\pi\xi_2)\aleph^{32}_{kl}\,d\xi_1 d\xi_2 V_{kl} \\
&+\sum_{l=1}^{N}\sum_{k=1}^{N} KL^{33}_{ijkl}W_{kl} + \sum_{l=1}^{N}\sum_{k=1}^{N}\int_0^1\int_0^1 \sin(i\pi\xi_1)\sin(j\pi\xi_2)\aleph^{33}_{kl}\,d\xi_1 d\xi_2 W_{kl} \\
&+\sum_{n=1}^{N}\sum_{m=1}^{N}\sum_{l=1}^{N}\sum_{k=1}^{N}\int_0^1\int_0^1 \sin(i\pi\xi_1)\sin(j\pi\xi_2)\aleph^{34}_{klmn}\,d\xi_1 d\xi_2 U_{kl}U_{mn} \\
&+\sum_{n=1}^{N}\sum_{m=1}^{N}\sum_{l=1}^{N}\sum_{k=1}^{N}\int_0^1\int_0^1 \sin(i\pi\xi_1)\sin(j\pi\xi_2)\aleph^{35}_{klmn}\,d\xi_1 d\xi_2 U_{kl}V_{mn} + \sum_{n=1}^{N}\sum_{m=1}^{N}\sum_{l=1}^{N}\sum_{k=1}^{N} KN^{31}_{ijklmn}U_{kl}W_{mn} \\
&+\sum_{n=1}^{N}\sum_{m=1}^{N}\sum_{l=1}^{N}\sum_{k=1}^{N}\int_0^1\int_0^1 \sin(i\pi\xi_1)\sin(j\pi\xi_2)\aleph^{36}_{klmn}\,d\xi_1 d\xi_2 U_{kl}W_{mn} \\
&+\sum_{n=1}^{N}\sum_{m=1}^{N}\sum_{l=1}^{N}\sum_{k=1}^{N}\int_0^1\int_0^1 \sin(i\pi\xi_1)\sin(j\pi\xi_2)\aleph^{37}_{klmn}\,d\xi_1 d\xi_2 V_{kl}V_{mn} + \sum_{n=1}^{N}\sum_{m=1}^{N}\sum_{l=1}^{N}\sum_{k=1}^{N} KN^{32}_{ijklmn}V_{kl}W_{mn} \\
&+\sum_{n=1}^{N}\sum_{m=1}^{N}\sum_{l=1}^{N}\sum_{k=1}^{N}\int_0^1\int_0^1 \sin(i\pi\xi_1)\sin(j\pi\xi_2)\aleph^{38}_{klmn}\,d\xi_1 d\xi_2 V_{kl}W_{mn} \\
&+\sum_{n=1}^{N}\sum_{m=1}^{N}\sum_{l=1}^{N}\sum_{k=1}^{N}\int_0^1\int_0^1 \sin(i\pi\xi_1)\sin(j\pi\xi_2)\aleph^{39}_{klmn}\,d\xi_1 d\xi_2 W_{kl}W_{mn} \\
&+\sum_{p=1}^{N}\sum_{o=1}^{N}\sum_{n=1}^{N}\sum_{m=1}^{N}\sum_{l=1}^{N}\sum_{k=1}^{N} KN^{33}_{ijklmnop}U_{kl}U_{mn}W_{op} + \sum_{p=1}^{N}\sum_{o=1}^{N}\sum_{n=1}^{N}\sum_{m=1}^{N}\sum_{l=1}^{N}\sum_{k=1}^{N} KN^{34}_{ijklmnop}U_{kl}V_{mn}W_{op} \\
&+\sum_{p=1}^{N}\sum_{o=1}^{N}\sum_{n=1}^{N}\sum_{m=1}^{N}\sum_{l=1}^{N}\sum_{k=1}^{N}\int_0^1\int_0^1 \sin(i\pi\xi_1)\sin(j\pi\xi_2)\aleph^{310}_{klmnop}\,d\xi_1 d\xi_2 U_{kl}W_{mn}W_{op} \\
&+\sum_{p=1}^{N}\sum_{o=1}^{N}\sum_{n=1}^{N}\sum_{m=1}^{N}\sum_{l=1}^{N}\sum_{k=1}^{N} KN^{35}_{ijklmnop}V_{kl}V_{mn}W_{op} + \sum_{p=1}^{N}\sum_{o=1}^{N}\sum_{n=1}^{N}\sum_{m=1}^{N}\sum_{l=1}^{N}\sum_{k=1}^{N} KN^{36}_{ijklmnop}W_{kl}W_{mn}W_{op} \\
&+\sum_{p=1}^{N}\sum_{o=1}^{N}\sum_{n=1}^{N}\sum_{m=1}^{N}\sum_{l=1}^{N}\sum_{k=1}^{N}\int_0^1\int_0^1 \sin(i\pi\xi_1)\sin(j\pi\xi_2)\aleph^{311}_{klmnop}\,d\xi_1 d\xi_2 V_{kl}W_{mn}W_{op} \\
&+\sum_{p=1}^{N}\sum_{o=1}^{N}\sum_{n=1}^{N}\sum_{m=1}^{N}\sum_{l=1}^{N}\sum_{k=1}^{N}\int_0^1\int_0^1 \sin(i\pi\xi_1)\sin(j\pi\xi_2)\aleph^{312}_{klmnop}\,d\xi_1 d\xi_2 W_{kl}W_{mn}W_{op} \\
&+\sum_{r=1}^{N}\sum_{q=1}^{N}\sum_{p=1}^{N}\sum_{o=1}^{N}\sum_{n=1}^{N}\sum_{m=1}^{N}\sum_{l=1}^{N}\sum_{k=1}^{N} KN^{37}_{ijklmnopqr}U_{kl}W_{mn}W_{op}W_{qr} \\
&+\sum_{r=1}^{N}\sum_{q=1}^{N}\sum_{p=1}^{N}\sum_{o=1}^{N}\sum_{n=1}^{N}\sum_{m=1}^{N}\sum_{l=1}^{N}\sum_{k=1}^{N} KN^{38}_{ijklmnopqr}V_{kl}W_{mn}W_{op}W_{qr} \\
&+\sum_{r=1}^{N}\sum_{q=1}^{N}\sum_{p=1}^{N}\sum_{o=1}^{N}\sum_{n=1}^{N}\sum_{m=1}^{N}\sum_{l=1}^{N}\sum_{k=1}^{N}\int_0^1\int_0^1 \sin(i\pi\xi_1)\sin(j\pi\xi_2)\aleph^{313}_{klmnopqr}\,d\xi_1 d\xi_2 W_{kl}W_{mn}W_{op}W_{qr} \\
&+\sum_{t=1}^{N}\sum_{s=1}^{N}\sum_{r=1}^{N}\sum_{q=1}^{N}\sum_{p=1}^{N}\sum_{o=1}^{N}\sum_{n=1}^{N}\sum_{m=1}^{N}\sum_{l=1}^{N}\sum_{k=1}^{N} KN^{27}_{ijklmnopqrst}W_{kl}W_{mn}W_{op}W_{qr}W_{st} \\
&-\int_0^1\int_0^1 F^{*}\sin(\pi\xi_1)\sin(\pi\xi_2)\sin(i\pi\xi_1)\sin(j\pi\xi_2)\,d\xi_1 d\xi_2\cos(\Omega t) = 0,
\end{aligned}
\tag{15}
$$

for the out-of-plane equation of motion in ξ_3 direction and

$$
\begin{aligned}
&\sum_{l=1}^{N}\sum_{k=1}^{N} M^{11}_{ijkl}\ddot{U}_{kl} + \sum_{l=1}^{N}\sum_{k=1}^{N} KL^{11}_{ijkl}U_{kl} + \sum_{l=1}^{N}\sum_{k=1}^{N} KL^{12}_{ijkl}V_{kl} + \sum_{l=1}^{N}\sum_{k=1}^{N}\int_0^1\int_0^1 \sin(i\pi\xi_1)\sin(j\pi\xi_2)\aleph^{11}_{kl}d\xi_1 d\xi_2 W_{kl} \\
&+\sum_{n=1}^{N}\sum_{m=1}^{N}\sum_{l=1}^{N}\sum_{k=1}^{N} KN^{11}_{ijklmn}U_{kl}U_{mn} + \sum_{n=1}^{N}\sum_{m=1}^{N}\sum_{l=1}^{N}\sum_{k=1}^{N}\int_0^1\int_0^1 \sin(i\pi\xi_1)\sin(j\pi\xi_2)\aleph^{12}_{klmn}d\xi_1 d\xi_2 U_{kl}W_{mn} \\
&+\sum_{n=1}^{N}\sum_{m=1}^{N}\sum_{l=1}^{N}\sum_{k=1}^{N} KN^{12}_{ijklmn}U_{kl}V_{mn} + \sum_{n=1}^{N}\sum_{m=1}^{N}\sum_{l=1}^{N}\sum_{k=1}^{N}\int_0^1\int_0^1 \sin(i\pi\xi_1)\sin(j\pi\xi_2)\aleph^{13}_{klmn}d\xi_1 d\xi_2 V_{kl}W_{mn} \\
&+\sum_{n=1}^{N}\sum_{m=1}^{N}\sum_{l=1}^{N}\sum_{k=1}^{N} KN^{13}_{ijklmn}KN_{13}V_{kl}V_{mn} + \sum_{n=1}^{N}\sum_{m=1}^{N}\sum_{l=1}^{N}\sum_{k=1}^{N} KN^{14}_{ijklmn}W_{kl}W_{mn} \\
&+\sum_{n=1}^{N}\sum_{m=1}^{N}\sum_{l=1}^{N}\sum_{k=1}^{N}\int_0^1\int_0^1 \sin(i\pi\xi_1)\sin(j\pi\xi_2)\aleph^{14}_{klmn}d\xi_1 d\xi_2 W_{kl}W_{mn} \\
&+\sum_{p=1}^{N}\sum_{o=1}^{N}\sum_{n=1}^{N}\sum_{m=1}^{N}\sum_{l=1}^{N}\sum_{k=1}^{N} KN^{15}_{ijklmnop}U_{kl}W_{mn}W_{op} + \sum_{p=1}^{N}\sum_{o=1}^{N}\sum_{n=1}^{N}\sum_{m=1}^{N}\sum_{l=1}^{N}\sum_{k=1}^{N} KN^{16}_{ijklmnop}V_{kl}W_{mn}W_{op} \\
&+\sum_{p=1}^{N}\sum_{o=1}^{N}\sum_{n=1}^{N}\sum_{m=1}^{N}\sum_{l=1}^{N}\sum_{k=1}^{N}\int_0^1\int_0^1 \sin(i\pi\xi_1)\sin(j\pi\xi_2)\aleph^{15}_{klmnop}d\xi_1 d\xi_2 W_{kl}W_{mn}W_{op} \\
&+\sum_{r=1}^{N}\sum_{q=1}^{N}\sum_{p=1}^{N}\sum_{o=1}^{N}\sum_{n=1}^{N}\sum_{m=1}^{N}\sum_{l=1}^{N}\sum_{k=1}^{N} KN^{17}_{ijklmnopqr}W_{kl}W_{mn}W_{op}W_{qr} = 0,
\end{aligned}
\tag{16}
$$

for the in-plane equation of motion in ξ_1 direction and

$$
\begin{aligned}
&\sum_{l=1}^{N}\sum_{k=1}^{N} M^{22}_{ijkl}\ddot{V}_{kl} + \sum_{l=1}^{N}\sum_{k=1}^{N} KL^{21}_{ijkl}U_{kl} + \sum_{l=1}^{N}\sum_{k=1}^{N} KL^{22}_{ijkl}V_{kl} + \sum_{l=1}^{N}\sum_{k=1}^{N}\int_0^1\int_0^1 \sin(i\pi\xi_1)\sin(j\pi\xi_2)\aleph^{21}_{kl}d\xi_1 d\xi_2 W_{kl} \\
&+\sum_{n=1}^{N}\sum_{m=1}^{N}\sum_{l=1}^{N}\sum_{k=1}^{N} KN^{21}_{ijklmn}U_{kl}U_{mn} + \sum_{n=1}^{N}\sum_{m=1}^{N}\sum_{l=1}^{N}\sum_{k=1}^{N}\int_0^1\int_0^1 \sin(i\pi\xi_1)\sin(j\pi\xi_2)\aleph^{22}_{klmn}d\xi_1 d\xi_2 U_{kl}W_{mn} \\
&+\sum_{n=1}^{N}\sum_{m=1}^{N}\sum_{l=1}^{N}\sum_{k=1}^{N} KN^{22}_{ijklmn}U_{kl}V_{mn} + \sum_{n=1}^{N}\sum_{m=1}^{N}\sum_{l=1}^{N}\sum_{k=1}^{N}\int_0^1\int_0^1 \sin(i\pi\xi_1)\sin(j\pi\xi_2)\aleph^{23}_{klmn}d\xi_1 d\xi_2 V_{kl}W_{mn} \\
&+\sum_{n=1}^{N}\sum_{m=1}^{N}\sum_{l=1}^{N}\sum_{k=1}^{N} KN^{23}_{ijklmn}V_{kl}V_{mn} + \sum_{n=1}^{N}\sum_{m=1}^{N}\sum_{l=1}^{N}\sum_{k=1}^{N} KN^{24}_{ijklmn}W_{kl}W_{mn} \\
&+\sum_{n=1}^{N}\sum_{m=1}^{N}\sum_{l=1}^{N}\sum_{k=1}^{N}\int_0^1\int_0^1 \sin(i\pi\xi_1)\sin(j\pi\xi_2)\aleph^{24}_{klmn}d\xi_1 d\xi_2 W_{kl}W_{mn} \\
&+\sum_{p=1}^{N}\sum_{o=1}^{N}\sum_{n=1}^{N}\sum_{m=1}^{N}\sum_{l=1}^{N}\sum_{k=1}^{N} KN^{25}_{ijklmnop}U_{kl}W_{mn}W_{op} + \sum_{p=1}^{N}\sum_{o=1}^{N}\sum_{n=1}^{N}\sum_{m=1}^{N}\sum_{l=1}^{N}\sum_{k=1}^{N} KN^{26}_{ijklmnop}V_{kl}W_{mn}W_{op} \\
&+\sum_{p=1}^{N}\sum_{o=1}^{N}\sum_{n=1}^{N}\sum_{m=1}^{N}\sum_{l=1}^{N}\sum_{k=1}^{N}\int_0^1\int_0^1 \sin(i\pi\xi_1)\sin(j\pi\xi_2)\aleph^{25}_{klmnop}d\xi_1 d\xi_2 W_{kl}W_{mn}W_{op} \\
&+\sum_{r=1}^{N}\sum_{q=1}^{N}\sum_{p=1}^{N}\sum_{o=1}^{N}\sum_{n=1}^{N}\sum_{m=1}^{N}\sum_{l=1}^{N}\sum_{k=1}^{N} KN^{27}_{ijklmnopqr}W_{kl}W_{mn}W_{op}W_{qr} = 0,
\end{aligned}
\tag{17}
$$

for the in-plane equation of motion in ξ_2 direction. Terms M^{ij}, KL^{ij}, and KN^{ij}, denote the mass, liner stiffness and nonlinear stiffness parameters, respectively, which are similar to those presented in Ref. (Khaniki et al., 2023) and $\aleph^{ij}$ denotes the curvature related terms which are defined in Appendix B. For the static analysis, the time-dependent terms are ignored from Eqs. (15)-17 and the coupled large set of ordinary differential equations (ODEs) are solved using the Newton-Raphson approach (Crisfield, 1979, Pho, 2022). For the dynamic analysis case, a dynamic equilibrium technique (Allgower and Georg, 2003, Mittelmann and Roose, 1990, Allgower and Georg, 2012) is used. The results for different mechanical analyses and different hyperelastic shell structures are discussed in detail in the next section. For this study, the following 27 modes are considered: U_{11}, V_{11}, W_{11}, U_{12}, V_{12}, W_{12}, U_{21}, V_{21}, W_{21}, U_{22}, V_{22}, W_{22}, U_{13}, V_{13}, W_{13}, U_{31}, V_{31}, W_{31}, U_{23}, V_{23}, W_{23}, U_{32}, V_{32}, W_{32}, U_{33}, V_{33}, and W_{33}.

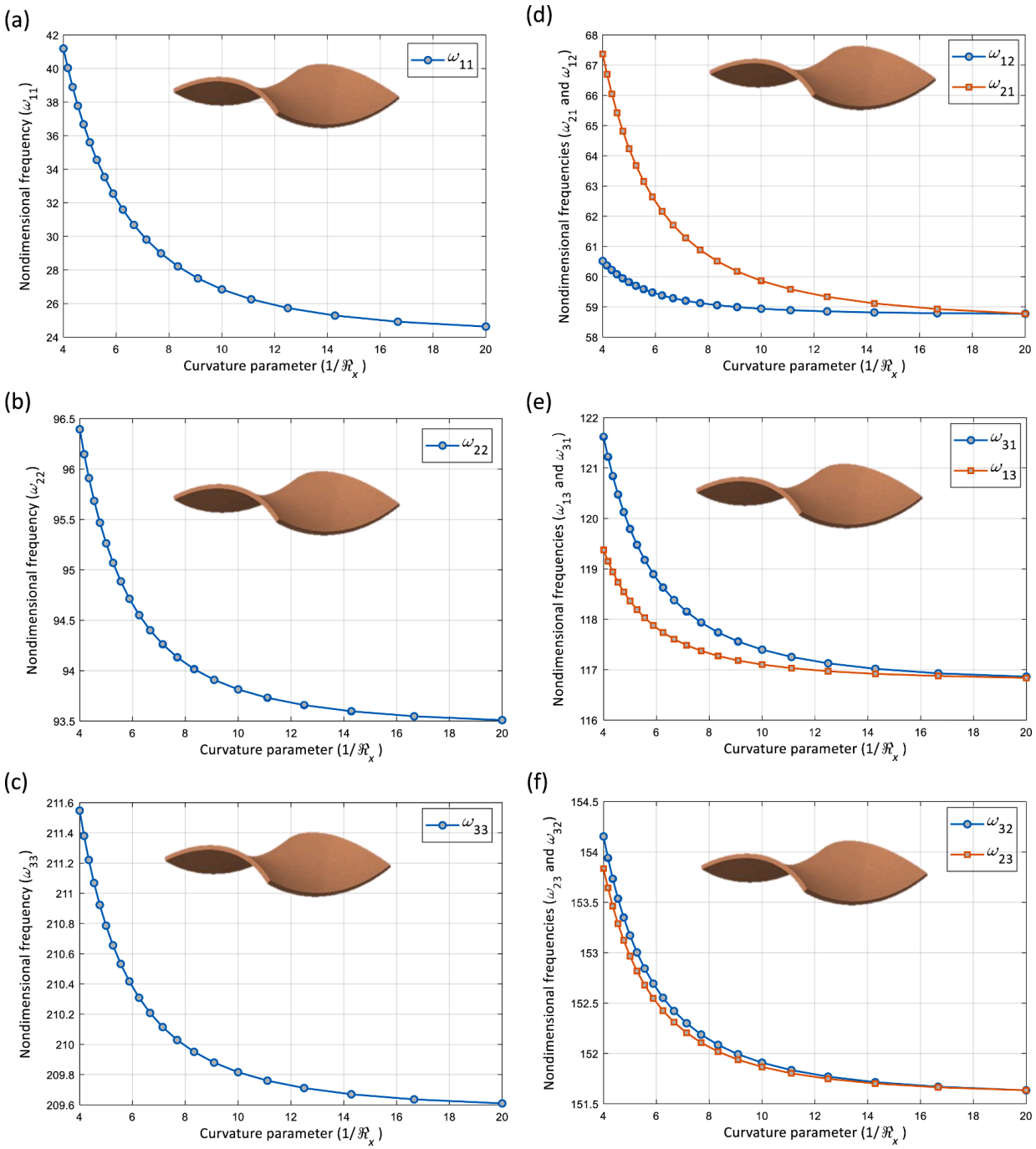

Fig. 7. Nondimensional transverse natural frequencies of a hyperbolic hyperelastic shell with respect to curvature parameter ($1/\Re_x$) for (a) ω_{11}, (b) ω_{22}, (c) ω_{33}, (d) ω_{12} and ω_{21}, (e) ω_{13} and ω_{31}, and (f) ω_{32} and ω_{23}.

4. Results and discussions

A general form of hyperelastic shell structures was formulated and solved in the previous sections, which are applicable to study the statics and dynamics of hyperelastic cylindrical, spherical, doubly-curved and hyperbolic shells. In this section, the results are presented in four subsections by presenting a bending analysis in Section 4.1, linear free vibration analysis in Section 4.2, nonlinear forced vibration in Section 4.3, and resonance analysis in Section 4.4.

4.1. Bending analysis

For the first analysis of this paper, the hyperelastic shell structure is assumed to undergo external time-independent pressures and the static deformations of the structure are investigated. First, in order to perform a static analysis on the hyperelastic shell structure, the accuracy of the current methodology is analysed by applying different pressure loads on the shell and comparing the results with

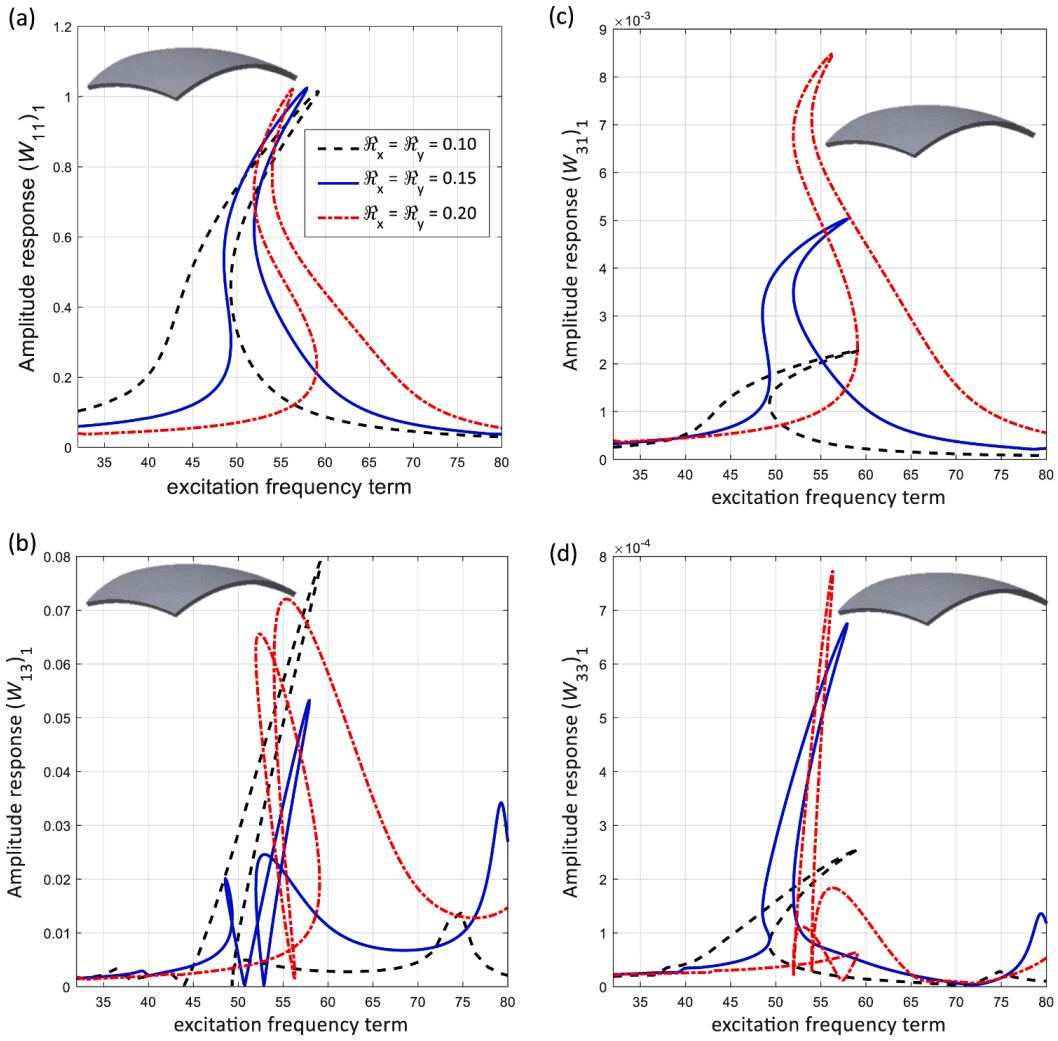

Fig. 8. The maximum nonlinear frequency response of a doubly-curved hyperelastic shell for the first coordinate parameters of (a) W_{11}, (b) W_{13}, (c) W_{31}, and (d) W_{33}.

those obtained by the finite element software ANSYS (ANSYS® MultiphysicsTM 2022). To do this, the geometrical properties of the structures are assumed as $a = 0.10$ m, $b = 0.30$ m, $h = 0.005$ m with curvature terms as $R_x = 2/3$ m and $R_y = 2$ m for the doubly-curved hyperelastic shell model, $R_x = 2/3$ m and $R_y =$ -2 m for the hyperbolic hyperelastic shell model, and $R_x = \infty$ and $R_y = 2$ m for the cylinder hyperelastic shell model. Shells are assumed to be fabricated using silicone rubber, with the material properties as $C_1 =$ 2.463e5 Pa, $C_2 = 3.512$e6 Pa, and $\rho = 1152.5$ kg/m^3. A distributed external time-independent pressure is applied to the structure with the amplitude of $P =$ [-2000 Pa, -1500 Pa, -1000 Pa, -500 Pa, 500 Pa, 1000 Pa, 1500 Pa, 2000 Pa]. The results are obtained and tabulated in Table 1 and compared with those obtained using the finite element software, showing very good agreement.

After verifying the current method for modelling different hyperelastic shell models, the bending behaviour of the structure is analysed. The maximum deformation magnitude of the structures in the in-plane directions ($|U|$ and $|V|$) and out-of-plane direction ($|W|$), under different pressure loads, are presented in Figs. 3–5 for cylindrical, doubly-curved and hyperbolic hyperelastic shells, respectively. The results show that the maximum amplitude of the transverse deformation belongs to the doubly-curved model and the lowest deformation belongs to the hyperelastic cylindrical shell. In addition, the results for the compression and tension pressure loadings are significantly different for hyperbolic and doubly-curved shells, when compared with the cylindrical model for all the *U, V* and *W* direction deformations.

4.2. Linear vibration analysis

For the second analysis of this paper, the influence of the curvature type on the free vibration behaviour of the hyperelastic shell is investigated. For a doubly-curved hyperelastic shell with the geometrical properties $a = 0.20$ m, $b = 0.20$ m, $h = 0.005$m, and $R_x = 4$ m with the other curvature term varying as $R_y = 1$m to 20m, the linear vibration behaviour is analysed. Figs. 6(a)-(f) show the variation of the transverse natural frequencies with respect to varying the curvature term ratio (R_y/b). It can be seen that all the nondimensional natural frequency parameters decrease exponentially by increasing the curvature ratio parameter. The fundamental natural frequency is the most sensitive frequency to variation of the curvature parameter, decreasing around 40% by increasing the curvature parameter

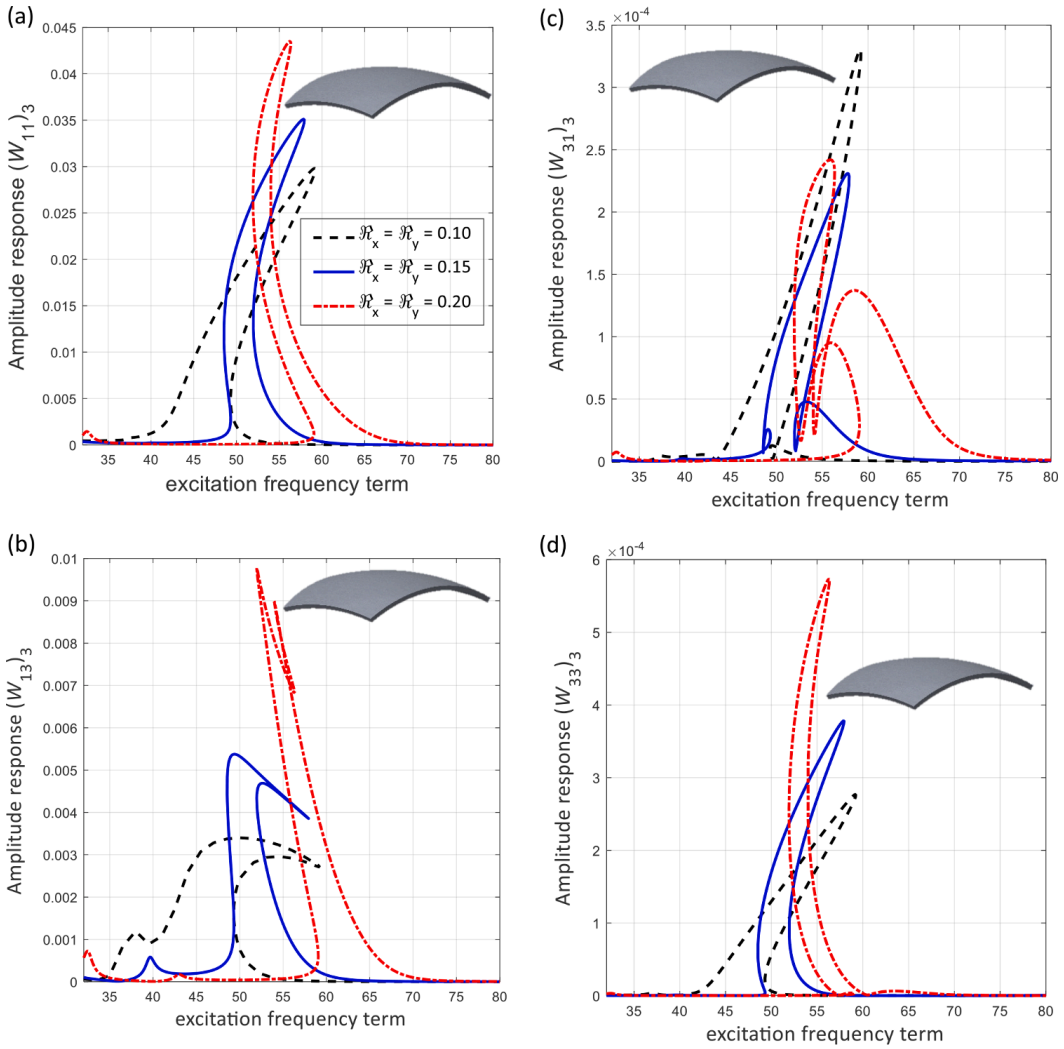

Fig. 9. The maximum nonlinear frequency response of a doubly-curved hyperelastic shell for the third coordinate parameters of (a) W_{11}, (b) W_{13}, (c) W_{31}, and (d) W_{33}.

from 5 to 100 and the least change belongs to the ω_{33} with less than 1% drop in value.

Similarly, for hyperbolic hyperelastic shells, by having $a = 0.20$ m, $b = 0.20$ m, $h = 0.005$m, and $R_y = $ -4 m, the curvature parameter R_x is varied from 0. 667 m to 4 m. The first six transverse natural frequencies of hyperbolic hyperelastic shells are shown in Figs. 7(a)-(f) for different curvature ratio parameters (R_x/a). It can be seen that the linear natural frequencies of the hyperelastic hyperbolic shell model show similar behaviour to the doubly-curved shell in terms of frequency decrements.

4.3. Non-linear vibration analysis

For the case of nonlinear analysis, hyperelastic shell structures are analysed in this section examining different types of curvatures.

Case 1: Doubly-curved hyperelastic shells

For the first analysis of this section, doubly-curved hyperelastic shells are analysed by considering the geometrical properties as $a = 0.10$ m, $b = 0.30$ m, $h = 0.005$ m, and the curvature parameters are varied as $\Re_x = \Re_y = 0.10$, 0.15, and 0.20. Figs. 8(a)-(d) indicate the maximum amplitude response of the hyperelastic doubly-curved shell for the out-of-plane motion with a nondimensional force of 30.75. A simple viscous term of 0.5 has been used in the numerical calculations throughout this section. The results are shown for the dominant coordinates of W_{11}, W_{13}, W_{31}, and W_{33} by varying the curvature terms; it can be seen that when the curvature terms are large $R_x = R_y/3 = 1$ m (or $\Re_x = \Re_y = 0.10$), the first coordinate of the system shows a dominant nonlinear hardening behaviour while, by decreasing the curvature to $R_x = R_y/3 = 0.667$ m (or $\Re_x = \Re_y = 0.15$), the dominant nonlinear hardening behaviour turns into a combination of hardening and softening behaviour. Decreasing the curvature term again to $R_x = R_y/3 = 0.50$ m (or $\Re_x = \Re_y = 0.20$) increases the contribution of the W_{31} coordinate. It is shown that decreasing the curvature parameters R_x and R_y (or increasing $\Re_x$ and $\Re_y$) moves the nonlinear frequency response to higher excitation frequencies. Moreover, the importance of considering higher-order

terms is shown in Figs. 9(a)-(d). It can be seen that as the curvature terms $\Re_x$ and $\Re_y$ increase, the maximum amplitude of the third term of W_{11}, W_{13} and W_{33} also increase.

Case 2: Hyperbolic hyperelastic shells

Similarly, for hyperbolic hyperelastic shells, by considering the geometrical properties to be $a = 0.10$ m, $b = 0.30$ m, $h = 0.005$ m and varying the curvature terms (R_x, R_y), the nonlinear forced vibration behaviour of such structures is analysed. Figs. 10 and 11 show the first and third coordinate terms of the hyperbolic hyperelastic shells under the same external time-dependent load for curvature terms $\Re_x = -\Re_y = 0.10$, 0.15, and 0.20. It can be seen from the results that, unlike the doubly-curved model, increasing the curvature terms $\Re_x$ and $\Re_y$ does not change the dominant nonlinear hardening behaviour of the first dominant transverse coordinate of the hyperbolic hyperelastic shell model. In both the hyperbolic and doubly-curved models, it is seen that increasing the curvature terms $\Re_x$ and $\Re_y$ increases the contribution of W_{31} in the vibration response of the system. It is shown that for both the hyperbolic and doubly-curved hyperelastic shells, the curvature term does not significantly change the maximum amplitude of vibration of the dominant coordinate.

4.4. Internal resonance analysis

In the previous sections it has been shown that the curvatures can significantly affect the linear and nonlinear behaviour of hyperelastic shells. Since the natural frequencies are varied by having different curvature types, in this section, hyperelastic shell structures are analysed for different internal resonances.

Case 1: Hyperbolic hyperelastic shells

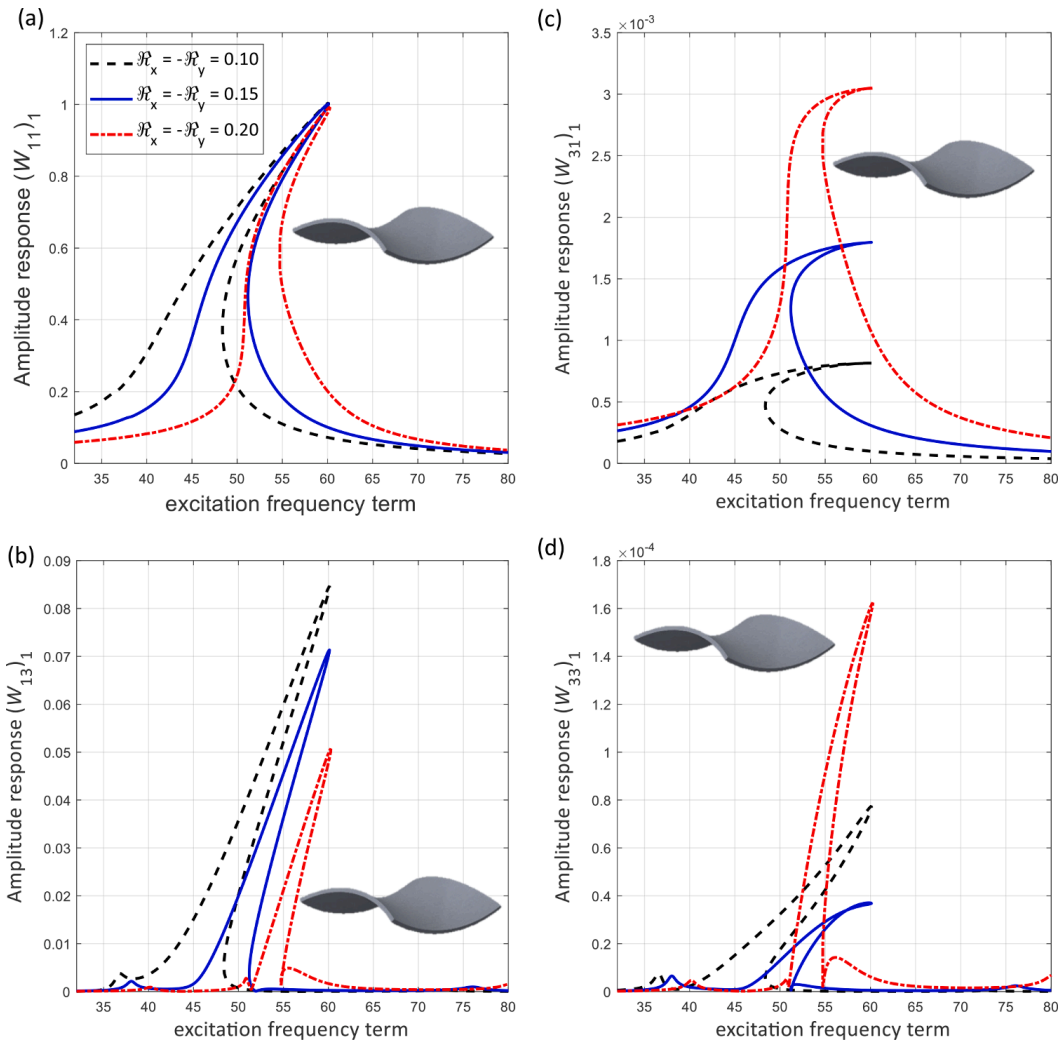

Fig. 10. The maximum nonlinear frequency response of a hyperbolic hyperelastic shell for the first coordinate parameters of (a) W_{11}, (b) W_{13}, (c) W_{31}, and (d) W_{33}.

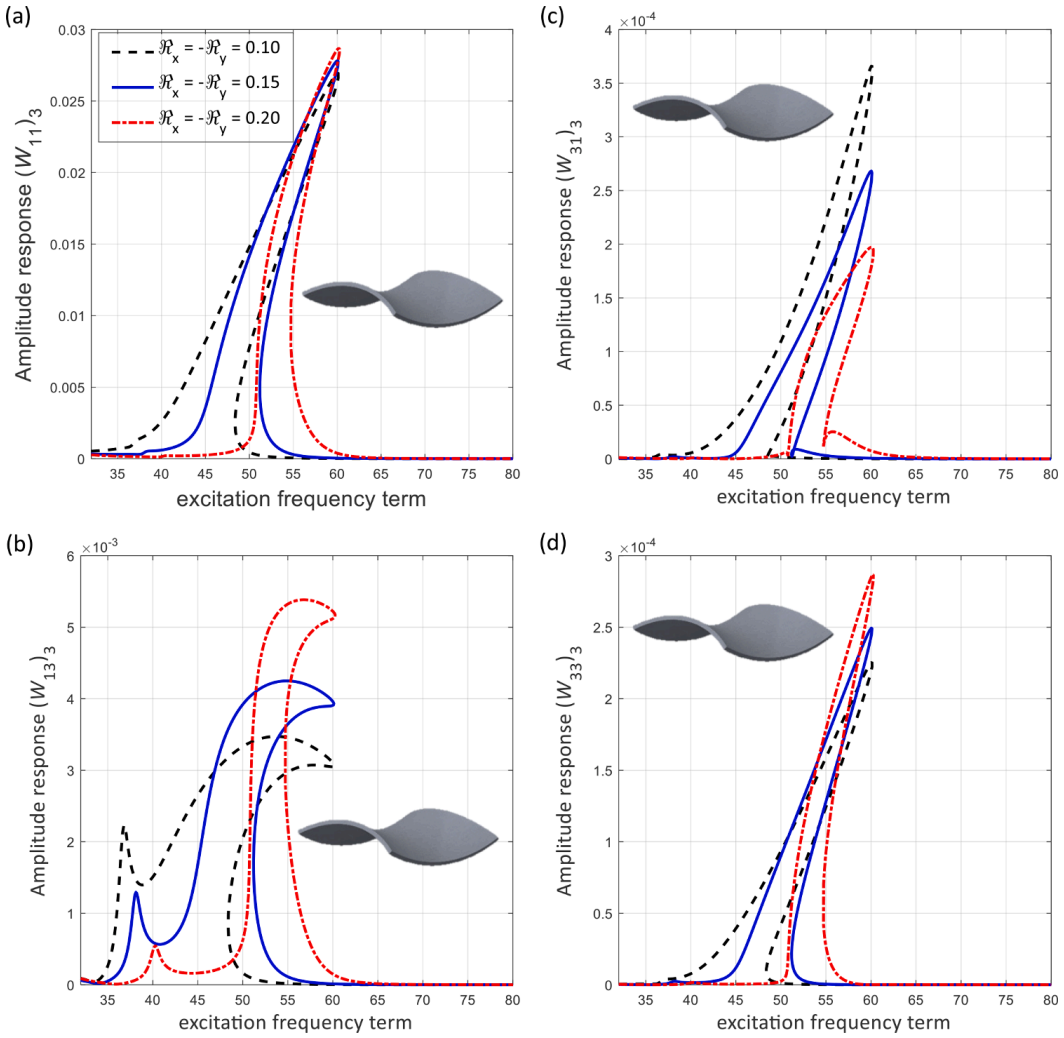

Fig. 11. The maximum nonlinear frequency response of a hyperbolic hyperelastic shell for the third coordinate parameters of (a) W_{11}, (b) W_{13}, (c) W_{31}, and (d) W_{33}.

For a hyperelastic hyperbolic shell with the geometrical properties $a = 0.20$ m, $b = 0.20$ m, $h = 0.005$ m, and R_y = -4 m, the curvature parameter R_x is varied from 0. 667 m to 4 m and the frequency ratio of higher transverse natural frequencies on the fundamental natural frequency is shown in Fig 12. From the natural frequency ratios, it can be seen that when the curvature parameter R_x is around 1.25 m ($\Re_x$ around 0.16) the system in the vicinity of a three-to-one internal resonance between ω_{22} and ω_{11} ($\omega_{22}/\omega_{11} \cong 3$).

Accordingly, by assuming the hyperelastic hyperbolic shell has curvatures $R_x = 1.25$ m and R_y = -4 m, the nonlinear forced vibration of the shell structure is analysed by considering a nondimensional distributed pressure load of 36.45 and a damping term of 0.5. The maximum amplitude-frequency response of the hyperbolic hyperelastic shell in the transverse direction is shown in Fig. 13 for dominant coordinates (W_{11}, W_{31}, W_{13}, and W_{33}). The results show a rich nonlinear behaviour for the dominant coordinates of W_{31} and W_{13}, while the dominant coordinates of W_{11} and W_{33} show a dominant nonlinear hardening behaviour. Similarly, for the in-plane motions, the maximum amplitude of vibration is shown in Figs. 14 and 15 for the U and V directions for the first two dominant coordinates of U_{21}, U_{23}, V_{12}, and V_{32}.

Case 2: Doubly-curved hyperelastic shells

For the case of analysing doubly-curved hyperelastic shells, the geometrical properties are assumed as $a = 0.20$ m, $b = 0.20$ m, $h = 0.005$ m, $R_x = 4$ m, the curvature parameter R_y is varied from 1 m to 20 m and the frequency ratio of higher transverse natural frequencies on the fundamental natural frequency are shown in Fig 16. In order to obtain three-to-one internal resonance phenomena, as shown in Fig. 16, two options are available. For the first model, by having $R_y = 1.74$ m ($\Re_y = 0.115$), the system is prone to a three-to-one internal resonance between ω_{22} and ω_{11} ($\omega_{22}/\omega_{11} \cong 3$). For the given doubly-curved hyperelastic shell model, by actuating the structure with a nondimensional harmonic distributed load $F = 14.57$ and damping term of 0.25, the nonlinear forced vibration behaviour in the internal resonance is analysed. Figs. 17–19 show the maximum amplitude response of the doubly-curved hyperelastic shell at this stage for out-of-plane and in-plane motions. From Fig. 17(a), it can be seen that the structure shows a combination of

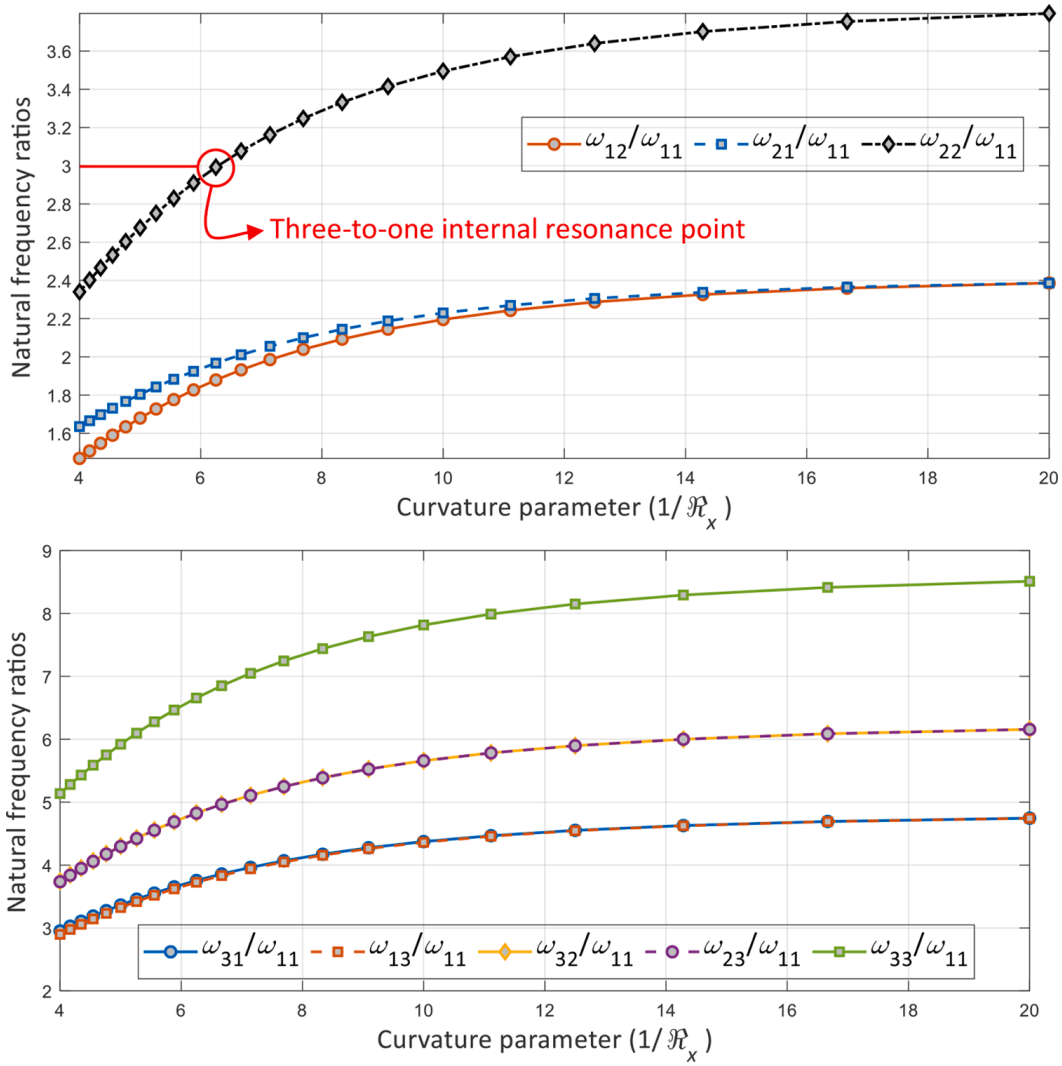

Fig. 12. The natural frequency ratio of a hyperbolic hyperelastic shell for different curvature parameters is shown for (a) $\omega_{12}/\ \omega_{11}$, $\omega_{21}/\ \omega_{11}$ and $\omega_{22}/\ \omega_{11}$, and for (b) $\omega_{13}/\ \omega_{11}$, $\omega_{31}/\ \omega_{11}$, $\omega_{23}/\ \omega_{11}$, $\omega_{32}/\ \omega_{11}$ and $\omega_{33}/\ \omega_{11}$.

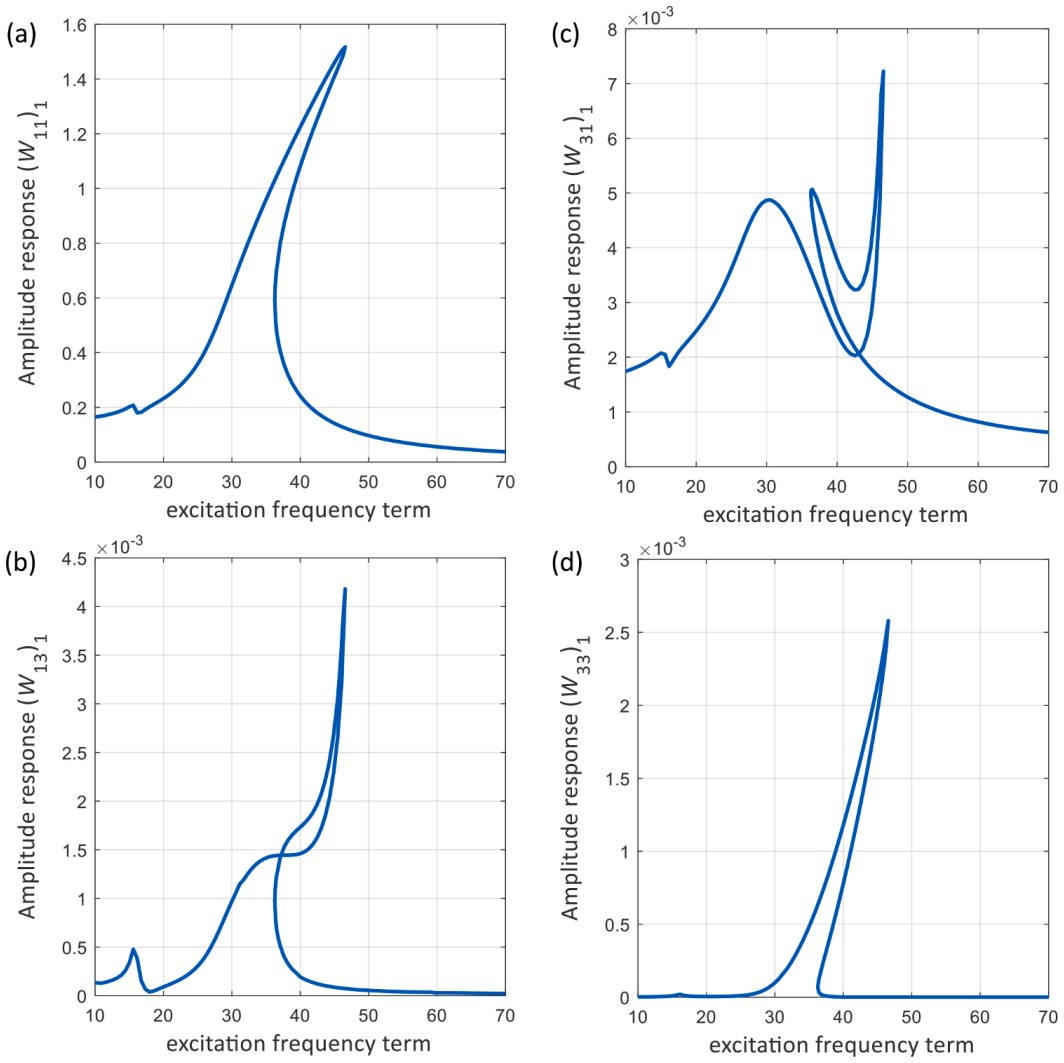

Fig. 13. The maximum out-of-plane nonlinear frequency response of a hyperbolic hyperelastic shell at an internal resonance for (a) W_{11}, (b) W_{13}, (c) W_{31}, and (d) W_{33}.

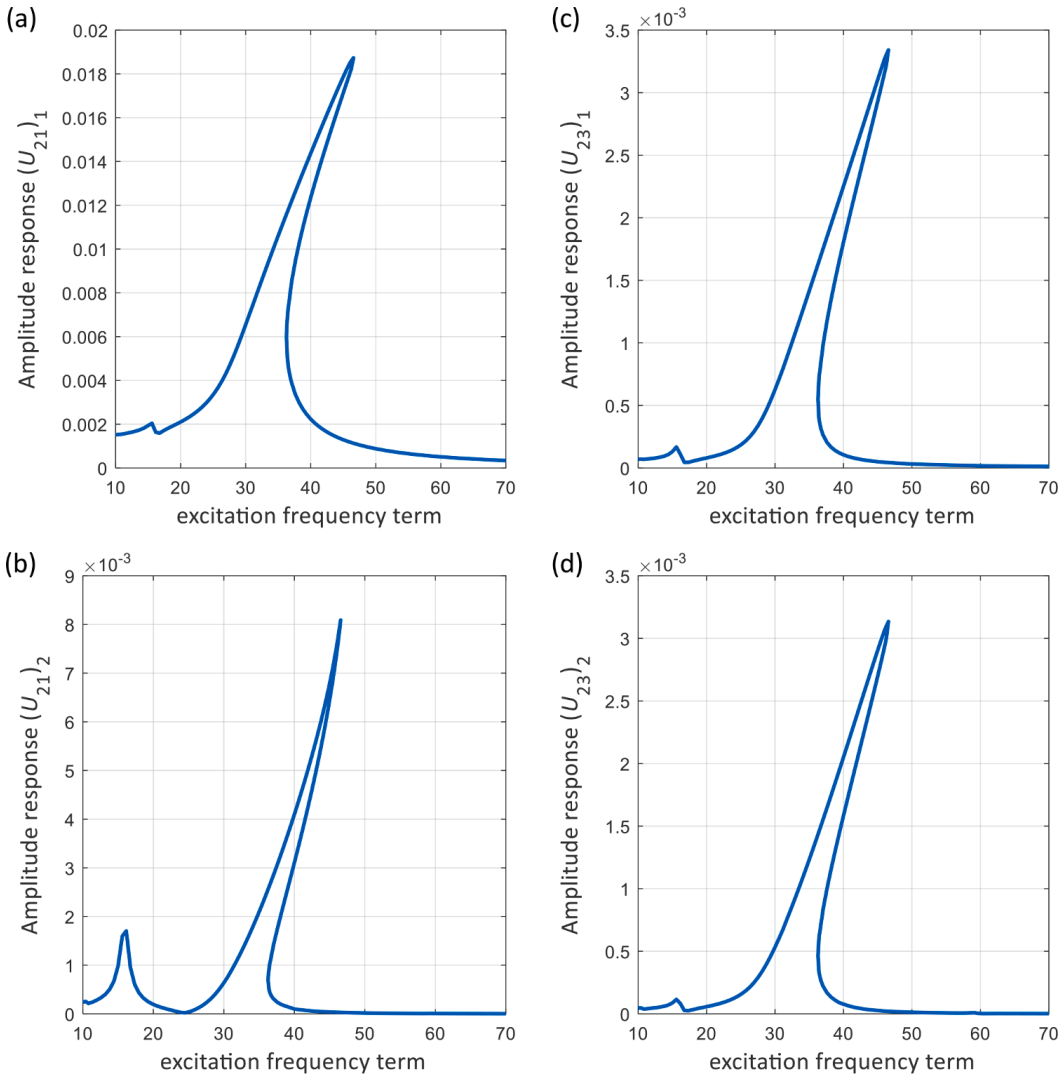

Fig. 14. The maximum in-plane U direction nonlinear frequency response of a hyperbolic hyperelastic shell at an internal resonance for (a) $(U_{21})_1$, (b) $(U_{21})_2$, (c) $(U_{23})_1$, and (d) $(U_{23})_2$.

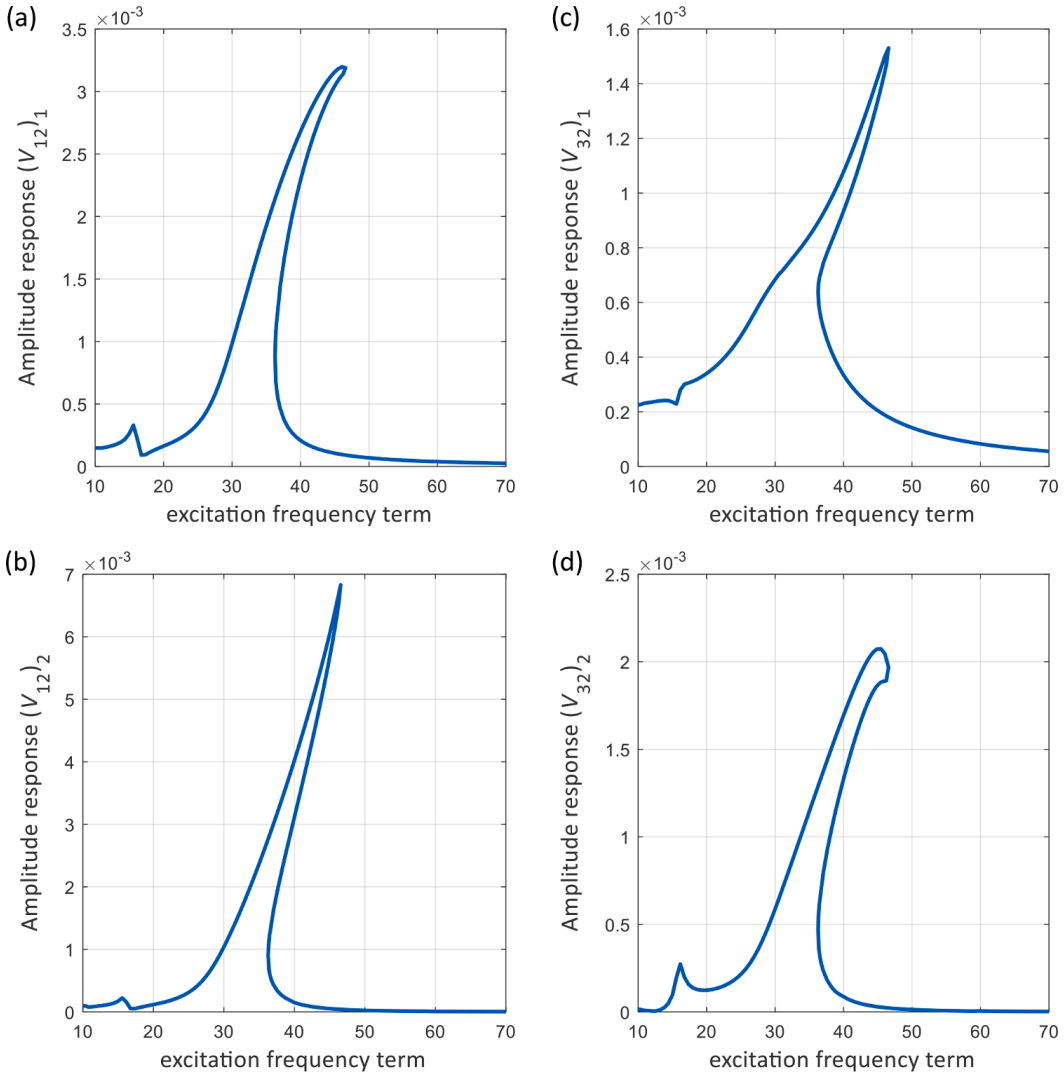

Fig. 15. The maximum in-plane V direction nonlinear frequency response of a hyperbolic hyperelastic shell at an internal resonance for (a) $(V_{12})_1$, (b) $(V_{12})_2$, (c) $(V_{32})_1$, and (d) $(V_{32})_2$.

softening and hardening behaviours for the dominant coordinate W_{11}. For W_{31}, W_{13}, and W_{33}; by increasing the excitation frequency term, the amplitude increases first and this is followed by a sudden drop before reaching the nondimensional excitation frequency of 35 (except for panel (a) in Fig. 17). Figs 18(a) and 19 (a) also show a combination of nonlinear softening and hardening behaviours (with hardening being dominant) for the dominant coordinates of in-plane motions U_{21} and V_{12} and a rich nonlinear behaviour for the rest of the coordinates.

5. Summary and conclusions

In this paper, a general model for hyperelastic shell structures was presented to study the static deformations, linear vibrations, forced nonlinear vibrations and internal resonance phenomena. A combination of Donnell's nonlinear shell theory, together with the Mooney-Rivlin strain energy density model, was used to formulate the hyperelastic shell structure. Using Hamilton's principle, the coupled equations of motion (in-plane and out-of-plane) were derived, which contain a higher order of nonlinear terms due to the material nonlinearity, large deformations and curvatures in the hyperelastic shell. By using a dynamic equilibrium technique, Newton–Raphson method and two-dimensional Galerkin technique, the equations of motion were solved and the accuracy of the model was evaluated (using the FEM for bending) showing good accuracy. Different hyperelastic shells, including cylindrical, spherical, doubly-curved and hyperbolic shells were examined in this study for different mechanical conditions:

- For the bending analysis, it was shown that, for the studied cases, the maximum magnitude of the transverse deformation belongs to the doubly-curved model and the lowest deformation belongs to the hyperelastic cylindrical shell.
- For the free vibration analysis, it was shown that all the nondimensional natural frequency parameters decrease exponentially by increasing the curvature ratio parameter in the studied models. The fundamental natural frequency is the most sensitive frequency to variation of the curvature parameter and the least change belongs to higher modes.

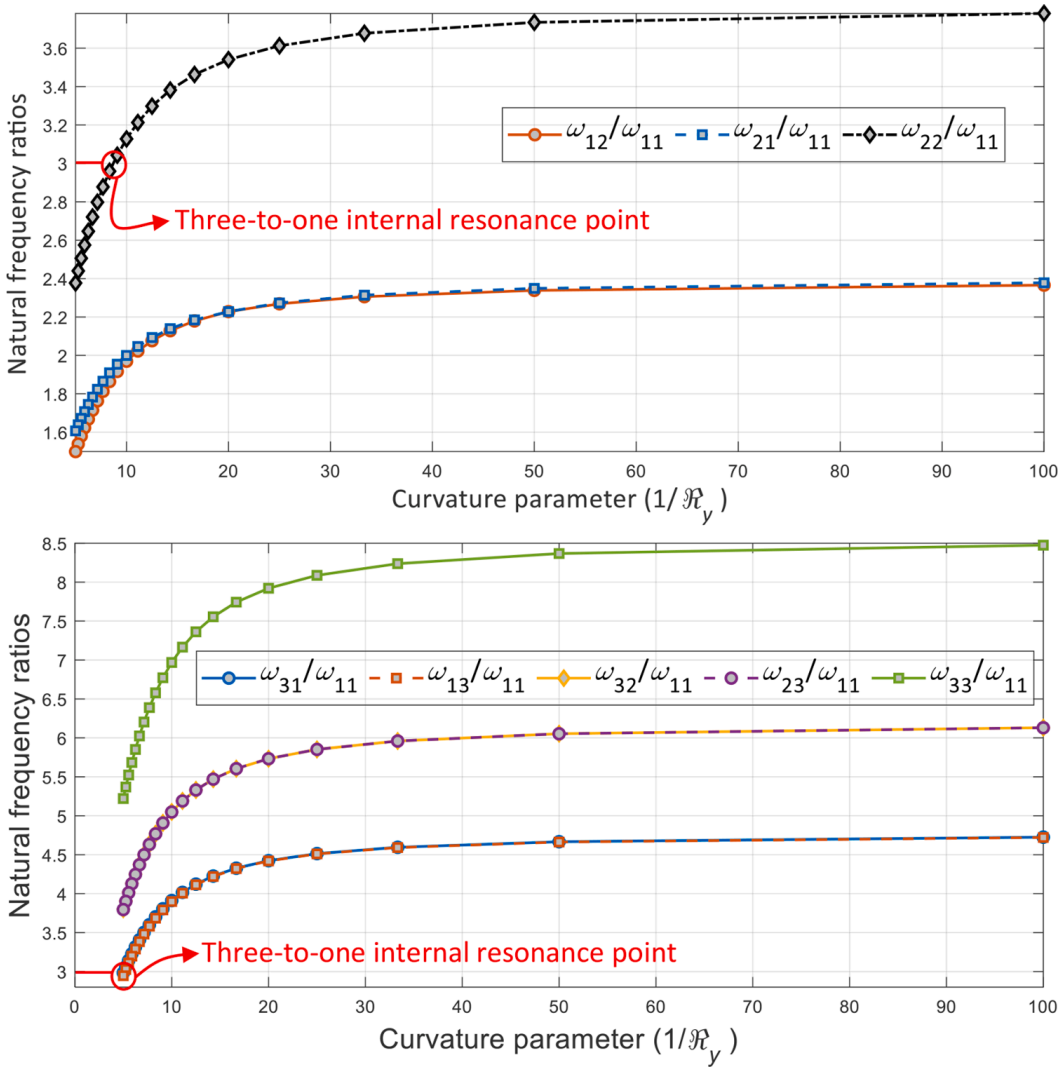

Fig. 16. The natural frequency ratio of a doubly-curved hyperelastic shell for different curvature parameters shown for (a) ω_{12}/ω_{11}, ω_{21}/ω_{11} and ω_{22}/ω_{11}, and for (b) ω_{13}/ω_{11}, ω_{31}/ω_{11}, ω_{23}/ω_{11}, ω_{32}/ω_{11} and ω_{33}/ω_{11}.

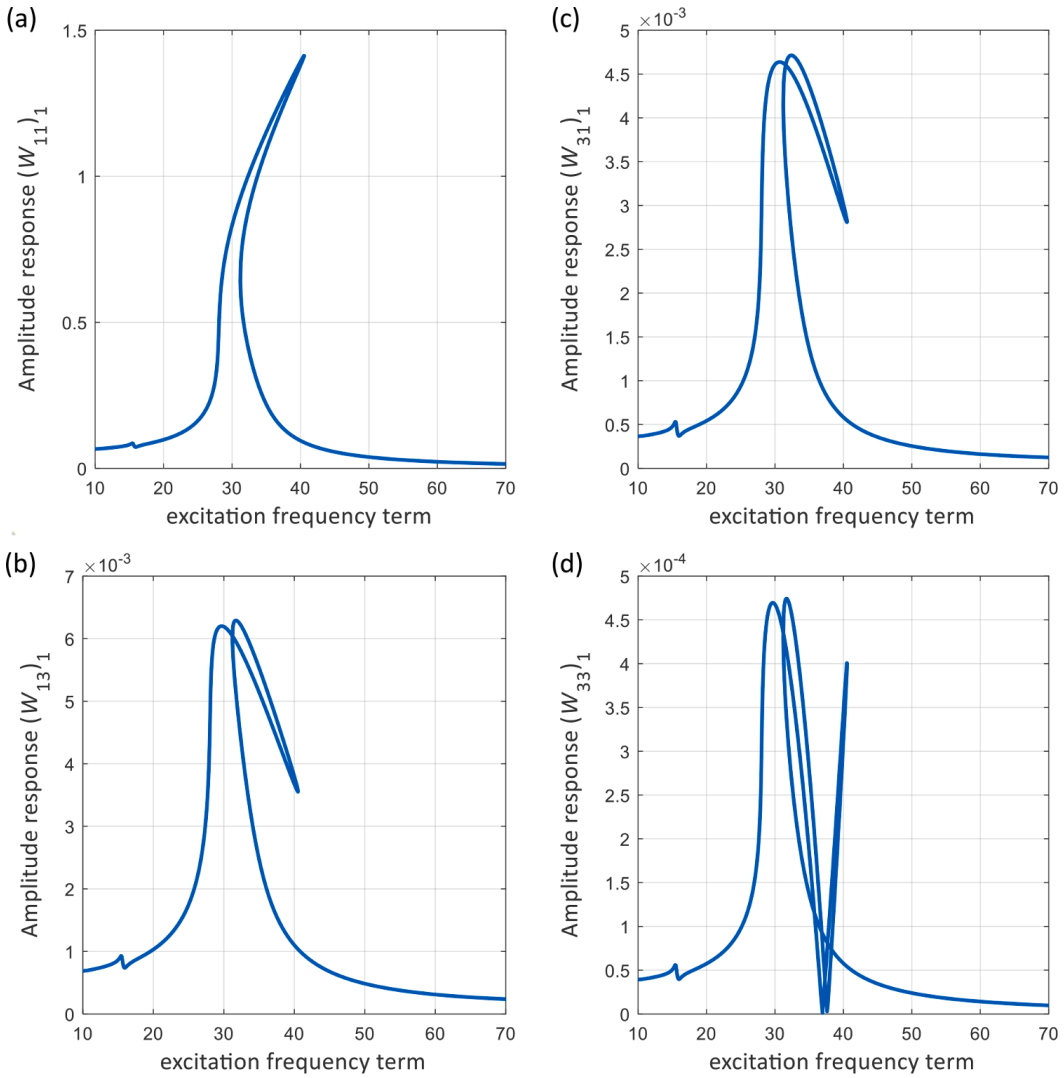

Fig. 17. The maximum out-of-plane nonlinear frequency response of a doubly-curved hyperelastic shell at an internal resonance between ω_{22} and ω_{11} for (a) W_{11}, (b) W_{13}, (c) W_{31}, and (d) W_{33}.

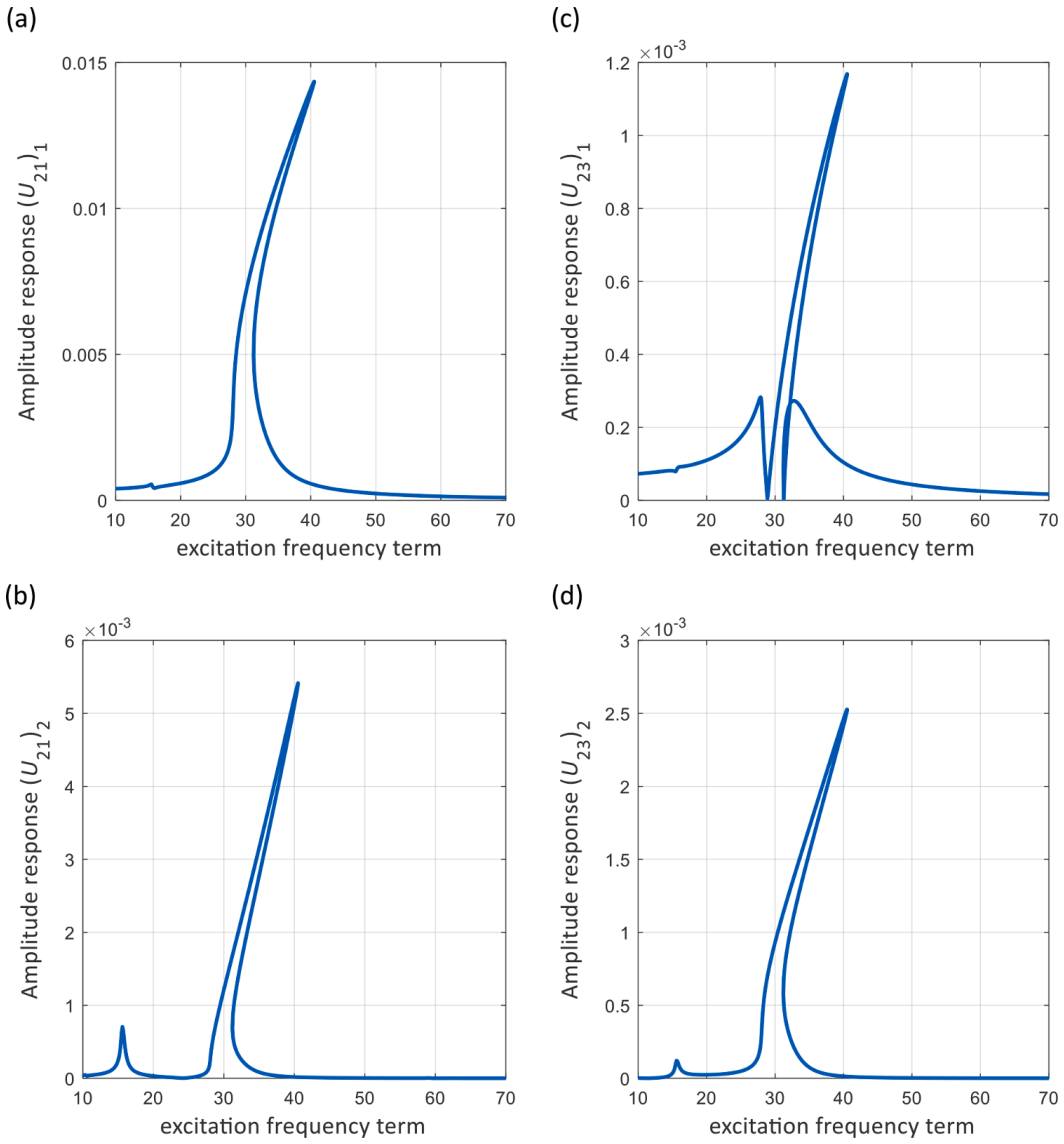

Fig. 18. The maximum in-plane U direction nonlinear frequency response of a doubly-curved hyperelastic shell at an internal resonance between ω_{22} and ω_{11} for (a) $(U_{21})_1$, (b) $(U_{21})_2$, (c) $(U_{23})_1$, and (d) $(U_{23})_2$.

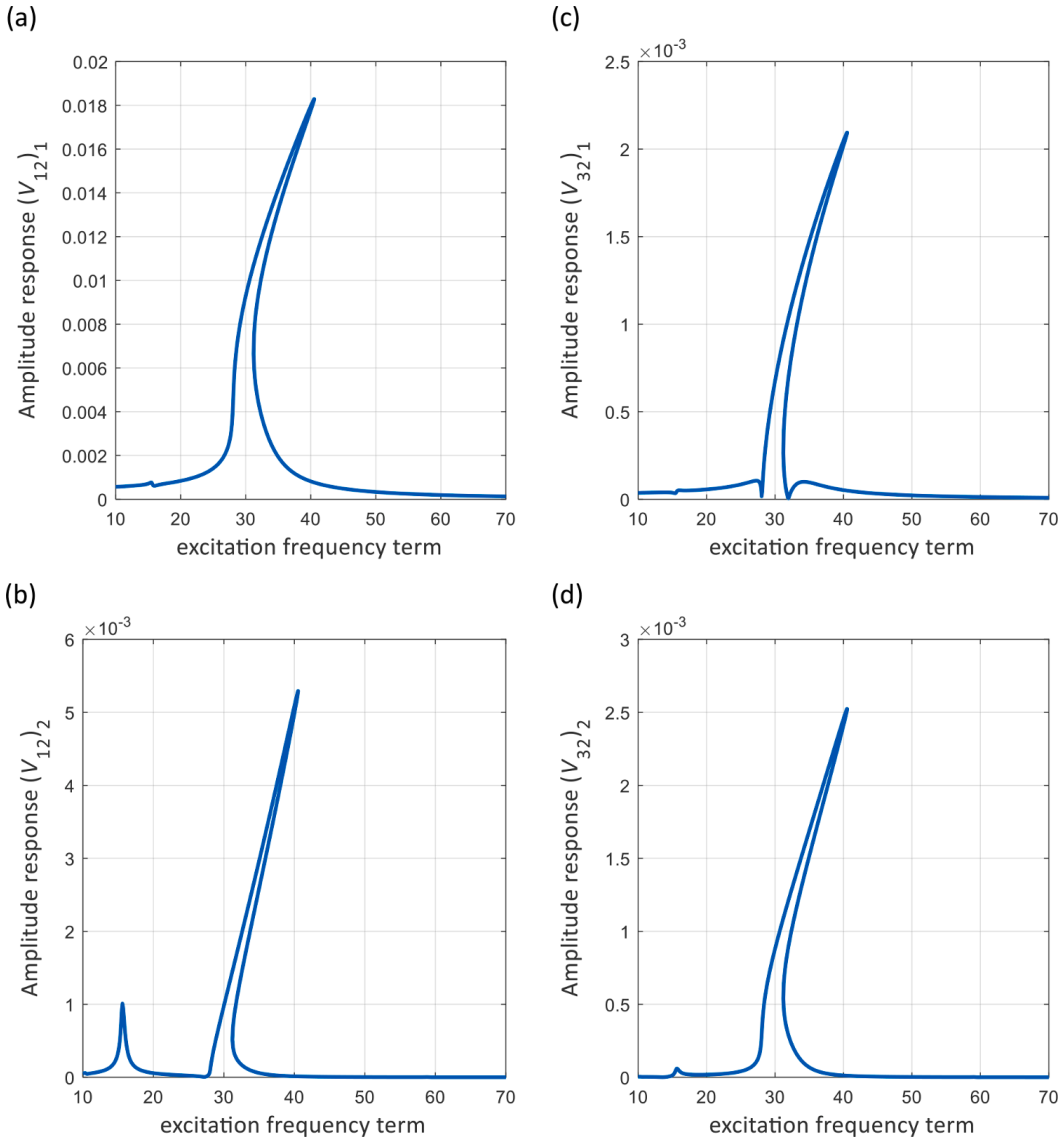

Fig. 19. The maximum in-plane V direction nonlinear frequency response of a doubly-curved hyperelastic shell at an internal resonance between ω_{22} and ω_{11} for (a) $(V_{12})_1$, (b) $(V_{12})_2$, (c) $(V_{32})_1$, and (d) $(V_{32})_2$.

- For the studied doubly-curved hyperelastic shell model, it was shown that when the curvature terms are large ($\Re_x = \Re_y = 0.10$), the first coordinate of the system shows a dominant nonlinear hardening behaviour while, by decreasing the curvature to $R_x = R_y/3 = 0.667$ m (or $\Re_x = \Re_y = 0.15$), the dominant nonlinear hardening behaviour turns into a combination of hardening and softening behaviour.
- Unlike the doubly-curved model, increasing the curvature terms $\Re_x$ and $\Re_y$ does not change the dominant nonlinear hardening behaviour of the first dominant transverse coordinate of the studied hyperbolic hyperelastic shell model.
- Curvature terms can cause different types of internal resonances in hyperelastic shells, which leads to a rich nonlinear frequency response in the shell structure.

Declaration of Competing Interest

The authors declare that they have no known competing financial interests or personal relationships that could have appeared to influence the work reported in this paper.

Data Availability

It is a part of an ongoing research and data cannot be shared.

Acknowledgements

The HDR scholarship support through The University of Adelaide and Faculty of Engineering, Computer & Mathematical Sciences, the University of Adelaide, is acknowledged. This work was supported with supercomputing resources provided by the Phoenix HPC service at the University of Adelaide.

Appendix A

The coefficients of Eqs. (8–10) are defied as

$$
\begin{aligned}
&\mathfrak{I}_{31} = -\frac{1}{12}{\eta_a}^2, \quad \mathfrak{I}_{32} = -\frac{1}{12}{\eta_b}^2, \quad \mathfrak{I}_{33} = 4\chi_2\Re_x\frac{1}{{\eta_b}^2} + 2\chi_2\Re_y\frac{1}{\eta_a\eta_b},\\
&\mathfrak{I}_{34} = 2\chi_2\Re_x\frac{1}{\eta_a\eta_b} + 4\chi_2\Re_y\frac{1}{{\eta_a}^2}, \quad \mathfrak{I}_{35} = \frac{1}{3}\chi_2\frac{1}{\xi^2}, \quad \mathfrak{I}_{36} = \frac{2}{3}\chi_2, \quad \mathfrak{I}_{37} = \frac{1}{3}\chi_2\xi^2,\\
&\mathfrak{I}_{38} = 4\chi_2\left({\Re_x}^2\frac{1}{{\eta_b}^2} + {\Re_y}^2\frac{1}{{\eta_a}^2}\right) + 4\chi_2\Re_x\Re_y\frac{1}{\eta_a\eta_b}, \quad \mathfrak{I}_{39} = -12\chi_1\Re_x\frac{1}{\xi}\frac{1}{\eta_b} + \chi_4\Re_y\frac{1}{\eta_b},\\
&\mathfrak{I}_{310} = -\frac{1}{2}\chi_3\Re_x\frac{1}{\eta_a} + \frac{1}{2}\chi_3\Re_y\frac{1}{\eta_a}\xi, \quad \mathfrak{I}_{311} = -\frac{1}{2}\chi_3\Re_y\frac{1}{\eta_b} - \frac{1}{2}\chi_3\Re_x\frac{1}{\eta_b}\frac{1}{\xi},\\
&\mathfrak{I}_{312} = -12\chi_1\Re_y\frac{1}{\eta_a}\xi + \chi_4\Re_x\frac{1}{\eta_a}, \quad \mathfrak{I}_{313} = 2\chi_4\left(\Re_x\frac{1}{\eta_b} + \Re_y\frac{1}{\eta_a}\right),\\
&\mathfrak{I}_{314} = -\chi_3\left(\Re_x\frac{1}{\eta_b} + \Re_y\frac{1}{\eta_a}\right), \quad \mathfrak{I}_{315} = -24\chi_1\frac{1}{\eta_b}{\Re_x}^2\frac{1}{\xi} + 2\chi_4\Re_y\left(2\Re_x\frac{1}{\eta_b} + \Re_y\frac{1}{\eta_a}\right),\\
&\mathfrak{I}_{316} = -4\chi_2\frac{1}{\xi}\frac{1}{\eta_b}\frac{\partial}{\partial\xi_1}, \quad \mathfrak{I}_{317} = -\chi_2\frac{1}{\eta_a}\frac{\partial}{\partial\xi_1}, \quad \mathfrak{I}_{318} = -2\chi_2\frac{1}{\eta_a}\frac{\partial}{\partial\xi_2}, \quad \mathfrak{I}_{319} = -\chi_2\frac{1}{\eta_a}\frac{\partial}{\partial\xi_2},\\
&\mathfrak{I}_{320} = -2\chi_1\eta_a\frac{1}{\xi^2}\frac{\partial^2}{\partial{\xi_1}^2} + \frac{1}{6}\chi_4\eta_a\frac{\partial^2}{\partial{\xi_2}^2}, \quad \mathfrak{I}_{321} = -\frac{1}{6}\chi_3\eta_a\frac{\partial^2}{\partial\xi_1\partial\xi_2},\\
&\mathfrak{I}_{322} = \frac{1}{6}\chi_4\eta_a\frac{\partial^2}{\partial{\xi_1}^2} + \frac{1}{6}\chi_4\eta_b\xi\frac{\partial^2}{\partial{\xi_2}^2}, \quad \mathfrak{I}_{323} = -\frac{1}{6}\chi_3\eta_a\frac{\partial^2}{\partial{\xi_1}^2} - \frac{1}{6}\chi_3\eta_b\xi\frac{\partial^2}{\partial{\xi_2}^2},\\
&\mathfrak{I}_{324} = -\frac{1}{3}\chi_3\eta_a\frac{\partial^2}{\partial\xi_1\partial\xi_2}, \quad \mathfrak{I}_{325} = -\frac{1}{6}\chi_3\eta_b\xi\frac{\partial^2}{\partial\xi_1\partial\xi_2},\\
&\mathfrak{I}_{326} = -24\chi_1{\Re_y}^2\frac{1}{\eta_a}\xi + 2\chi_4\Re_x\left(\Re_x\frac{1}{\eta_b} + 2\Re_y\frac{1}{\eta_a}\right), \quad \mathfrak{I}_{327} = -\chi_2\frac{1}{\eta_b}\frac{\partial}{\partial\xi_2},\\
&\mathfrak{I}_{328} = -4\chi_2\frac{1}{\eta_a}\xi\frac{\partial}{\partial\xi_2}, \quad \mathfrak{I}_{329} = -\chi_2\frac{1}{\eta_b}\frac{\partial}{\partial\xi_1}, \quad \mathfrak{I}_{330} = -2\chi_2\frac{1}{\eta_b}\frac{\partial}{\partial\xi_1},\\
&\mathfrak{I}_{331} = -2\chi_1\eta_b\xi^2\frac{\partial^2}{\partial{\xi_2}^2} + \frac{1}{6}\chi_4\eta_b\frac{\partial^2}{\partial{\xi_1}^2}, \quad \mathfrak{I}_{332} = \frac{1}{6}\chi_4\eta_a\frac{1}{\xi}\frac{\partial^2}{\partial{\xi_1}^2} + \frac{1}{6}\chi_4\eta_b,\\
&\mathfrak{I}_{333} = -\frac{1}{6}\chi_3\eta_a\frac{1}{\xi}\frac{\partial^2}{\partial{\xi_1}^2} - \frac{1}{6}\chi_3\eta_b\frac{\partial^2}{\partial{\xi_2}^2}, \quad \mathfrak{I}_{334} = -\frac{1}{3}\chi_3\eta_b\frac{\partial^2}{\partial\xi_1\partial\xi_2},\\
&\mathfrak{I}_{335} = -\frac{1}{6}\chi_3\eta_b\frac{\partial^2}{\partial\xi_1\partial\xi_2}, \quad \mathfrak{I}_{336} = -\frac{1}{6}\chi_3\eta_a\frac{1}{\xi}\frac{\partial^2}{\partial\xi_1\partial\xi_2},\\
&\mathfrak{I}_{337} = 3\chi_4\Re_x\Re_y\left(\Re_x\frac{1}{\eta_b} + \Re_y\frac{1}{\eta_a}\right) - 12\chi_1\left({\Re_x}^3\frac{1}{\xi}\frac{1}{\eta_b} + {\Re_y}^3\xi\frac{1}{\eta_a}\right),\\
&\mathfrak{I}_{338} = -4\chi_2\Re_x\frac{1}{\eta_b}\frac{1}{\xi}\frac{\partial}{\partial\xi_1} - 2\chi_2\Re_y\frac{1}{\eta_b}\frac{\partial}{\partial\xi_1},\\
&\mathfrak{I}_{339} = -4\chi_2\Re_y\frac{1}{\eta_a}\xi\frac{\partial}{\partial\xi_2} - 2\chi_2\Re_x\frac{1}{\eta_a}\frac{\partial}{\partial\xi_2},\\
&\mathfrak{I}_{340} = -2\chi_1\Re_x\eta_a\frac{1}{\xi^2}\frac{\partial^2}{\partial{\xi_1}^2} + \frac{1}{6}\chi_4\Re_x\eta_a\frac{\partial^2}{\partial{\xi_2}^2} + \frac{1}{6}\chi_4\Re_y\eta_a\frac{1}{\xi}\frac{\partial^2}{\partial{\xi_1}^2} + \frac{1}{6}\chi_4\Re_y\eta_b\frac{\partial^2}{\partial{\xi_2}^2},
\end{aligned}
\tag{A1}
$$

$$\mathfrak{T}_{341} = -2\chi_1 \Re_y \eta_b \xi^2 \frac{\partial^2}{\partial {\xi_2}^2} + \frac{1}{6}\chi_4 \Re_y \eta_b \frac{\partial^2}{\partial {\xi_1}^2} + \frac{1}{6}\chi_4 \Re_x \eta_b \xi \frac{\partial^2}{\partial {\xi_2}^2} + \frac{1}{6}\chi_4 \Re_x \eta_a \frac{\partial^2}{\partial {\xi_1}^2},$$

$$\mathfrak{T}_{342} = 2\chi_2 \Re_x \frac{1}{\eta_b}\frac{1}{\xi} + \chi_2 \Re_y \frac{1}{\eta_b}, \quad \mathfrak{T}_{343} = 2\chi_2 \Re_y \frac{1}{\eta_a}\xi + \chi_2 \Re_x \frac{1}{\eta_a},$$

$$\mathfrak{T}_{344} = -\chi_1 \Re_x \eta_a \frac{1}{\xi^2} + \frac{1}{12}\chi_4 \Re_y \eta_a \frac{1}{\xi}, \quad \mathfrak{T}_{345} = -\chi_1 \Re_y \eta_b \xi^2 + \frac{1}{12}\chi_4 \Re_x \eta_b \xi,$$

$$\mathfrak{T}_{346} = -\frac{1}{6}\chi_3 \big(\Re_x \eta_a + \Re_y \eta_b\big), \quad \mathfrak{T}_{347} = -\frac{1}{3}\chi_3 \big(\Re_x \eta_a + \Re_y \eta_b\big) \frac{\partial^2}{\partial \xi_1 \partial \xi_2},$$

$$\mathfrak{T}_{348} = \frac{1}{6}\chi_4 \big(\Re_x \eta_a + \Re_y \eta_b\big),$$

$$\mathfrak{T}_{349} = 12\chi_1 {\Re_x}^2 \frac{1}{\xi^2}\frac{\partial}{\partial \xi_1} - 2\chi_4 \Re_x \Re_y \frac{1}{\xi}\frac{\partial}{\partial \xi_1} - \chi_4 {\Re_y}^2 \frac{\partial}{\partial \xi_1},$$

$$\mathfrak{T}_{350} = -\chi_4 {\Re_x}^2 \frac{\partial}{\partial \xi_2} - 2\chi_4 \Re_x \Re_y \xi \frac{\partial}{\partial \xi_2} + 12\chi_1 {\Re_y}^2 \xi^2 \frac{\partial}{\partial \xi_2},$$

$$\mathfrak{T}_{351} = -12\chi_1 {\Re_x}^2 \frac{1}{\xi^2} + \chi_4 \Re_x \Re_y \frac{1}{\xi} + \chi_4 \Re_x \Re_y \frac{1}{\xi} + \chi_4 {\Re_y}^2,$$

$$\mathfrak{T}_{352} = \chi_4 \Re_x \Re_y \xi + \chi_4 {\Re_x}^2 - 12\chi_1 {\Re_y}^2 \xi^2 + \chi_4 \Re_x \Re_y \xi,$$

$$\mathfrak{T}_{353} = -2\chi_2 \frac{1}{\xi^2}\frac{\partial}{\partial \xi_1}, \quad \mathfrak{T}_{354} = -2\chi_2 \xi^2 \frac{\partial}{\partial \xi_2}, \quad \mathfrak{T}_{355} = -2\chi_2 \frac{\partial}{\partial \xi_2}, \quad \mathfrak{T}_{356} = -2\chi_2 \frac{\partial}{\partial \xi_1},$$

$$\mathfrak{T}_{357} = \chi_1 {\eta_a}^2 \frac{1}{\xi^2}\frac{\partial}{\partial \xi_1}, \quad \mathfrak{T}_{358} = \chi_1 {\eta_b}^2 \xi^2 \frac{\partial}{\partial \xi_2}, \quad \mathfrak{T}_{359} = -\frac{1}{12}\chi_4 {\eta_b}^2 \frac{\partial}{\partial \xi_1},$$

$$\mathfrak{T}_{360} = -\frac{1}{12}\chi_4 {\eta_a}^2 \frac{\partial}{\partial \xi_2}, \quad \mathfrak{T}_{361} = -\frac{1}{6}\chi_4 {\eta_a}^2 \frac{\partial}{\partial \xi_1}, \quad \mathfrak{T}_{362} = -\frac{1}{6}\chi_4 {\eta_b}^2 \frac{\partial}{\partial \xi_2},$$

$$\mathfrak{T}_{363} = \frac{1}{6}\chi_3 {\eta_a}^2 \frac{\partial}{\partial \xi_1}, \quad \mathfrak{T}_{364} = \frac{1}{6}\chi_3 {\eta_b}^2 \frac{\partial}{\partial \xi_2}, \quad \mathfrak{T}_{365} = -\chi_1 {\eta_a}^2 \frac{1}{\xi^2}\frac{\partial^2}{\partial {\xi_1}^2} + \frac{1}{12}\chi_4 {\eta_a}^2 \frac{\partial^2}{\partial {\xi_2}^2},$$

$$\mathfrak{T}_{366} = -\chi_1 {\eta_b}^2 \xi^2 \frac{\partial^2}{\partial {\xi_2}^2} + \frac{1}{12}\chi_4 {\eta_b}^2 \frac{\partial^2}{\partial {\xi_1}^2}, \quad \mathfrak{T}_{367} = \frac{1}{12}\chi_4 {\eta_a}^2 \frac{\partial^2}{\partial {\xi_1}^2} + \frac{1}{12}\chi_4 {\eta_b}^2 \frac{\partial^2}{\partial y^2},$$

$$\mathfrak{T}_{368} = \frac{1}{12}\chi_4 {\eta_a}^2 \frac{\partial^2}{\partial {\xi_1}^2} + \frac{1}{12}\chi_4 {\eta_b}^2 \frac{\partial^2}{\partial {\xi_2}^2}, \quad \mathfrak{T}_{369} = -\frac{1}{6}\chi_3 {\eta_a}^2 \frac{\partial^2}{\partial {\xi_1}^2} - \frac{1}{6}\chi_3 {\eta_b}^2 \frac{\partial^2}{\partial {\xi_2}^2},$$

$$\mathfrak{T}_{370} = -\frac{1}{6}\chi_3 {\eta_a}^2 \frac{\partial^2}{\partial \xi_1 \partial \xi_2}, \quad \mathfrak{T}_{371} = -\frac{1}{6}\chi_3 {\eta_b}^2 \frac{\partial^2}{\partial \xi_1 \partial \xi_2}, \quad \mathfrak{T}_{372} = -\frac{1}{6}\chi_3 {\eta_b}^2 \frac{\partial^2}{\partial \xi_1 \partial \xi_2},$$

$$\mathfrak{T}_{373} = -\frac{1}{6}\chi_3 {\eta_a}^2 \frac{\partial^2}{\partial \xi_1 \partial \xi_2}, \quad \mathfrak{T}_{374} = \frac{1}{6}\chi_3 {\eta_a}^2 \frac{\partial}{\partial \xi_1}, \quad \mathfrak{T}_{375} = \frac{1}{6}\chi_3 {\eta_a}^2 \frac{\partial}{\partial \xi_2},$$

$$\mathfrak{T}_{376} = \frac{1}{6}\chi_3 {\eta_b}^2 \frac{\partial}{\partial \xi_1}, \quad \mathfrak{T}_{377} = \frac{1}{6}\chi_3 {\eta_b}^2 \frac{\partial}{\partial \xi_2}, \quad \mathfrak{T}_{378} = 12\chi_1 \frac{1}{\xi^2}\frac{\partial}{\partial \xi_1},$$

$$\mathfrak{T}_{379} = -\chi_4 \frac{\partial}{\partial \xi_2}, \quad \mathfrak{T}_{380} = \frac{1}{2}\chi_3 \xi^2 \frac{\partial}{\partial \xi_2}, \quad \mathfrak{T}_{381} = \chi_3 \frac{\partial}{\partial \xi_1}, \quad \mathfrak{T}_{382} = \chi_3 \frac{\partial}{\partial \xi_2},$$

$$\mathfrak{T}_{383} = \frac{1}{2}\chi_3 \frac{\partial}{\partial \xi_1}, \quad \mathfrak{T}_{384} = 12\chi_1 \xi^2 \frac{\partial}{\partial \xi_2}, \quad \mathfrak{T}_{385} = -\chi_4 \frac{\partial}{\partial \xi_1}, \quad \mathfrak{T}_{386} = \frac{1}{2}\chi_3 \frac{1}{\xi^2}\frac{\partial}{\partial \xi_1},$$

$$\mathfrak{T}_{387} = \chi_3 \frac{\partial}{\partial \xi_1}, \quad \mathfrak{T}_{388} = \chi_3 \frac{\partial}{\partial \xi_2}, \quad \mathfrak{T}_{389} = \frac{1}{2}\chi_3 \frac{\partial}{\partial \xi_2}, \quad \mathfrak{T}_{390} = 24\chi_1 \Re_x \frac{1}{\xi^2}\frac{\partial}{\partial \xi_1},$$

(A2)

$$\mathfrak{F}_{391} = -2\chi_4\Re_y\frac{1}{\xi}\frac{\partial}{\partial\xi_1}, \quad \mathfrak{F}_{392} = -2\chi_4\Re_x\frac{\partial}{\partial\xi_2}, \quad \mathfrak{F}_{393} = -2\chi_4\Re_y\xi\frac{\partial}{\partial\xi_2},$$

$$\mathfrak{F}_{394} = -12\chi_1\Re_x\frac{1}{\xi^2}, \quad \mathfrak{F}_{395} = \chi_4\Re_x, \quad \mathfrak{F}_{396} = -\chi_3\Re_x, \quad \mathfrak{F}_{397} = \chi_4\Re_y\frac{1}{\xi},$$

$$\mathfrak{F}_{398} = \chi_4\Re_y\xi, \quad \mathfrak{F}_{399} = -\chi_3\Re_y\xi, \quad \mathfrak{F}_{3100} = \chi_3\big(\Re_x + \Re_y\xi\big)\frac{\partial}{\partial\xi_1},$$

$$\mathfrak{F}_{3101} = +\chi_3\big(\Re_x + \Re_y\xi\big)\frac{\partial}{\partial\xi_2}, \quad \mathfrak{F}_{3102} = 24\chi_1\Re_y\xi^2\frac{\partial}{\partial\xi_2}, \quad \mathfrak{F}_{3103} = -2\chi_4\Re_x\xi\frac{\partial}{\partial\xi_2},$$

$$\mathfrak{F}_{3104} = -2\chi_4\Re_y\frac{\partial}{\partial\xi_1}, \quad \mathfrak{F}_{3105} = -2\chi_4\Re_x\frac{1}{\xi}\frac{\partial}{\partial\xi_1}, \quad \mathfrak{F}_{3106} = -12\chi_1\Re_y\xi^2, \quad \mathfrak{F}_{3107} = \chi_4\Re_y,$$

$$\mathfrak{F}_{3108} = -\chi_3\Re_x\frac{1}{\xi}, \quad \mathfrak{F}_{3109} = \chi_4\Re_x\xi, \quad \mathfrak{F}_{3110} = \chi_4\Re_x\frac{1}{\xi}, \quad \mathfrak{F}_{3111} = -\chi_3\Re_y,$$

$$\mathfrak{F}_{3112} = \chi_3\left(\Re_x\frac{1}{\xi} + \Re_y\right)\frac{\partial}{\partial\xi_2}, \quad \mathfrak{F}_{3113} = \chi_3\left(\Re_x\frac{1}{\xi} + \Re_y\right)\frac{\partial}{\partial\xi_1}, \quad \mathfrak{F}_{3114} = -2\chi_4\frac{1}{\xi}\frac{\partial}{\partial\xi_1},$$

$$\mathfrak{F}_{3115} = -2\chi_4\xi\frac{\partial}{\partial\xi_2}, \quad \mathfrak{F}_{3116} = \chi_3\frac{1}{\xi}\frac{\partial}{\partial\xi_1}, \quad \mathfrak{F}_{3117} = \chi_3\xi\frac{\partial}{\partial\xi_2}, \quad \mathfrak{F}_{3118} = \chi_3\frac{1}{\xi}\frac{\partial}{\partial\xi_1},$$

$$\mathfrak{F}_{3119} = \chi_3\xi\frac{\partial}{\partial\xi_2}, \quad \mathfrak{F}_{3120} = \chi_3\xi\frac{\partial}{\partial\xi_1}, \quad \mathfrak{F}_{3121} = \chi_3\frac{1}{\xi}\frac{\partial}{\partial\xi_2}, \quad \mathfrak{F}_{3122} = 12\chi_1\eta_a\frac{1}{\xi^2}\frac{\partial}{\partial\xi_1},$$

$$\mathfrak{F}_{3123} = -\chi_4\eta_a\frac{\partial}{\partial\xi_1}, \quad \mathfrak{F}_{3124} = \chi_3\eta_a\frac{\partial}{\partial\xi_1}, \quad \mathfrak{F}_{3125} = -\chi_4\eta_a\frac{\partial}{\partial\xi_2}, \quad \mathfrak{F}_{3126} = -\chi_4\eta_b\xi\frac{\partial}{\partial\xi_2},$$

$$\mathfrak{F}_{3127} = \chi_3\eta_b\xi\frac{\partial}{\partial\xi_2}, \quad \mathfrak{F}_{3128} = \chi_3\eta_a\frac{\partial}{\partial\xi_1}, \quad \mathfrak{F}_{3129} = \frac{1}{2}\chi_3\eta_a\frac{\partial}{\partial\xi_1}, \quad \mathfrak{F}_{3130} = \frac{1}{2}\chi_3\eta_b\xi\frac{\partial}{\partial\xi_1},$$

$$\mathfrak{F}_{3131} = \chi_3\eta_a\frac{\partial}{\partial\xi_2}, \quad \mathfrak{F}_{3132} = \frac{1}{2}\chi_3\eta_a\frac{\partial}{\partial\xi_2}, \quad \mathfrak{F}_{3133} = \frac{1}{2}\chi_3\eta_b\xi\frac{\partial}{\partial\xi_2}, \tag{A3}$$

$$\mathfrak{F}_{3134} = 12\chi_1\eta_b\xi^2\frac{\partial}{\partial\xi_2}, \quad \mathfrak{F}_{3135} = -\chi_4\eta_b\frac{\partial}{\partial\xi_2}, \quad \mathfrak{F}_{3136} = \chi_3\eta_b\frac{\partial}{\partial\xi_2}, \quad \mathfrak{F}_{3137} = -\chi_4\eta_b\frac{\partial}{\partial\xi_1},$$

$$\mathfrak{F}_{3138} = -\chi_4\eta_a\frac{1}{\xi}\frac{\partial}{\partial\xi_1}, \quad \mathfrak{F}_{3139} = \chi_3\eta_a\frac{1}{\xi}\frac{\partial}{\partial\xi_1}\mathfrak{F}_{3140} = \chi_3\eta_b\frac{\partial}{\partial\xi_2}, \quad \mathfrak{F}_{3141} = \frac{1}{2}\chi_3\eta_b\frac{\partial}{\partial\xi_2},$$

$$\mathfrak{F}_{3142} = \frac{1}{2}\chi_3\eta_a\frac{1}{\xi}\frac{\partial}{\partial\xi_2}, \quad \mathfrak{F}_{3143} = \chi_3\eta_b\frac{\partial}{\partial\xi_1}\mathfrak{F}_{3144} = \frac{1}{2}\chi_3\eta_b\frac{\partial}{\partial\xi_1}, \quad \mathfrak{F}_{3145} = \frac{1}{2}\chi_3\eta_a\frac{1}{\xi}\frac{\partial}{\partial\xi_1},$$

$$\mathfrak{F}_{3146} = 12\chi_1\Re_x\eta_a\frac{1}{\xi^2}\frac{\partial}{\partial\xi_1} - \chi_4\Re_y\eta_a\frac{1}{\xi}\frac{\partial}{\partial\xi_1}, \quad \mathfrak{F}_{3147} = 12\chi_1\Re_y\eta_b\xi^2\frac{\partial}{\partial\xi_2} - \chi_4\Re_x\eta_b\xi\frac{\partial}{\partial\xi_2},$$

$$\mathfrak{F}_{3148} = -\chi_4\Re_y\eta_b\frac{\partial}{\partial\xi_1} - \chi_4\Re_x\eta_a\frac{\partial}{\partial\xi_1}, \quad \mathfrak{F}_{3149} = -\chi_4\Re_x\eta_a\frac{\partial}{\partial\xi_2} - \chi_4\Re_y\eta_b\frac{\partial}{\partial\xi_2},$$

$$\mathfrak{F}_{3150} = -3\chi_1\Re_x\eta_a\frac{1}{\xi^2} + \frac{1}{4}\chi_4\Re_y\eta_a\frac{1}{\xi}, \quad \mathfrak{F}_{3151} = -3\chi_1\Re_y\eta_b\xi^2 + \frac{1}{4}\chi_4\Re_x\eta_b\xi,$$

$$\mathfrak{F}_{3152} = \frac{1}{4}\chi_5\big(\Re_x\eta_a + \Re_y\eta_b\big), \quad \mathfrak{F}_{3153} = \chi_3\big(\Re_x\eta_a + \Re_y\eta_b\big)\frac{\partial}{\partial\xi_1},$$

$$\mathfrak{F}_{3154} = \chi_3\big(\Re_x\eta_a + \Re_y\eta_b\big)\frac{\partial}{\partial\xi_2}, \quad \mathfrak{F}_{3155} = 3\chi_1{\eta_a}^2\frac{1}{\xi^2}\frac{\partial}{\partial\xi_1}, \quad \mathfrak{F}_{3156} = 3\chi_1{\eta_b}^2\xi^2\frac{\partial}{\partial\xi_2},$$

$$\mathfrak{F}_{3157} = -\frac{1}{4}\chi_4{\eta_b}^2\frac{\partial}{\partial\xi_1} + \frac{1}{2}\chi_3{\eta_b}^2\frac{\partial}{\partial\xi_1}, \quad \mathfrak{F}_{3158} = -\frac{1}{4}\chi_4{\eta_a}^2\frac{\partial}{\partial\xi_2} + \frac{1}{2}\chi_3{\eta_a}^2\frac{\partial}{\partial\xi_2},$$

$$\mathfrak{F}_{3159} = -\frac{1}{4}\chi_5{\eta_a}^2\frac{\partial}{\partial\xi_1} + \frac{1}{2}\chi_3{\eta_a}^2\frac{\partial}{\partial\xi_1}, \quad \mathfrak{F}_{3160} = -\frac{1}{4}\chi_5{\eta_b}^2\frac{\partial}{\partial\xi_2} + \frac{1}{2}\chi_3{\eta_b}^2\frac{\partial}{\partial\xi_2},$$

$$\mathfrak{I}_{11}=-4\chi_2\frac{1}{\eta_b{}^2},\quad \mathfrak{I}_{12}=-\chi_2\frac{1}{\eta_a{}^2},\quad \mathfrak{I}_{13}=-3\chi_2\frac{1}{\eta_a\eta_b},\quad \mathfrak{I}_{14}=-4\chi_2\Re_x\frac{1}{\eta_b{}^2}-2\chi_2\Re_y\frac{1}{\eta_a\eta_b},$$

$$\mathfrak{I}_{15}=12\chi_1\frac{1}{\eta_b}\frac{1}{\xi}\frac{\partial}{\partial\xi_1},\quad \mathfrak{I}_{16}=\frac{1}{2}\chi_3\frac{1}{\eta_a}\frac{\partial}{\partial\xi_1},\quad \mathfrak{I}_{17}=\chi_3\frac{1}{\eta_a}\frac{\partial}{\partial\xi_2},\quad \mathfrak{I}_{18}=\chi_3\frac{1}{\eta_b}\frac{\partial}{\partial\xi_2},$$

$$\mathfrak{I}_{19}=\chi_3\frac{1}{\eta_a}\xi\frac{\partial}{\partial\xi_2},\quad \mathfrak{I}_{110}=-2\chi_4\frac{1}{\eta_b}\frac{\partial}{\partial\xi_1},\quad \mathfrak{I}_{111}=\chi_3\frac{1}{\eta_b}\frac{\partial}{\partial\xi_1},$$

$$\mathfrak{I}_{112}=24\chi_1\Re_x\frac{1}{\eta_b}\frac{1}{\xi}\frac{\partial}{\partial\xi_1}-2\chi_4\Re_y\frac{1}{\eta_b}\frac{\partial}{\partial\xi_1},\quad \mathfrak{I}_{113}=\chi_3\left(\Re_x+\xi\,\Re_y\right)\frac{1}{\eta_a}\frac{\partial}{\partial\xi_2},$$

$$\mathfrak{I}_{114}=-\chi_4\frac{1}{\eta_a}\frac{\partial}{\partial\xi_1},\quad \mathfrak{I}_{115}=\frac{1}{2}\chi_3\frac{1}{\eta_b}\frac{1}{\xi}\frac{\partial}{\partial\xi_1},\quad \mathfrak{I}_{116}=\chi_3\frac{1}{\eta_a}\frac{\partial}{\partial\xi_2},$$

$$\mathfrak{I}_{117}=-2\chi_4\Re_y\frac{1}{\eta_a}\frac{\partial}{\partial\xi_1}-2\chi_4\Re_x\frac{1}{\eta_b}\frac{\partial}{\partial\xi_1},\quad \mathfrak{I}_{118}=\chi_3\left(\Re_x\frac{1}{\eta_b}+\Re_y\frac{1}{\eta_a}\right)\frac{\partial}{\partial\xi_2},$$

$$\mathfrak{I}_{119}=12\chi_1\Re_x{}^2\frac{1}{\eta_b}\frac{1}{\xi}\frac{\partial}{\partial\xi_1}-\chi_4\Re_y{}^2\frac{1}{\eta_a}\frac{\partial}{\partial\xi_1}-2\chi_4\Re_x\Re_y\frac{1}{\eta_b}\frac{\partial}{\partial\xi_1},$$

$$\mathfrak{I}_{120}=-\chi_2\frac{1}{\eta_a}\frac{\partial}{\partial\xi_1},\quad \mathfrak{I}_{121}=\chi_1\eta_a\frac{1}{\xi^2}\frac{\partial}{\partial\xi_1},\quad \mathfrak{I}_{122}=-2\chi_2\frac{1}{\eta_b}\frac{1}{\xi}\frac{\partial}{\partial\xi_1},$$

$$\mathfrak{I}_{123}=-\frac{1}{12}\chi_4\eta_a\xi^2\frac{\partial}{\partial\xi_1},\quad \mathfrak{I}_{124}=-\frac{1}{6}\chi_4\eta_a\frac{\partial}{\partial\xi_1},\quad \mathfrak{I}_{125}=\frac{1}{6}\chi_3\eta_a\frac{\partial}{\partial\xi_2},$$

$$\mathfrak{I}_{126}=\frac{1}{6}\chi_3\eta_a\frac{\partial}{\partial\xi_1},\quad \mathfrak{I}_{127}=-\chi_2\frac{1}{\eta_a}\frac{\partial}{\partial\xi_2},\quad \mathfrak{I}_{128}=\frac{1}{6}\chi_3\eta_b\xi\frac{\partial}{\partial\xi_2},$$

$$\mathfrak{I}_{129}=12\chi_1\frac{1}{\xi^2}\frac{\partial}{\partial\xi_1},\quad \mathfrak{I}_{130}=-\chi_4\frac{\partial}{\partial\xi_1},\quad \mathfrak{I}_{131}=\chi_3\frac{\partial}{\partial\xi_1},\quad \mathfrak{I}_{132}=\chi_3\frac{\partial}{\partial\xi_2},$$

$$\mathfrak{I}_{133}=\frac{1}{2}\chi_3\frac{\partial}{\partial\xi_2},\quad \mathfrak{I}_{134}=\frac{1}{2}\chi_3\xi^2\frac{\partial}{\partial\xi_2},\quad \mathfrak{I}_{135}=-\chi_4\xi\frac{\partial}{\partial\xi_1},\quad \mathfrak{I}_{136}=-\chi_4\frac{1}{\xi}\frac{\partial}{\partial\xi_1},$$

$$\mathfrak{I}_{137}=\chi_3\frac{1}{\xi}\frac{\partial}{\partial\xi_1},\quad \mathfrak{I}_{138}=\frac{1}{2}\chi_3\frac{1}{\xi}\frac{\partial}{\partial\xi_2},\quad \mathfrak{I}_{139}=\frac{1}{2}\chi_3\xi\frac{\partial}{\partial\xi_2},\quad \mathfrak{I}_{140}=\chi_3\xi\frac{\partial}{\partial\xi_2},$$

$$\mathfrak{I}_{141}=12\chi_1\Re_x\frac{1}{\xi^2}\frac{\partial}{\partial\xi_1}-\chi_4\Re_y\frac{1}{\xi}\frac{\partial}{\partial\xi_1},\quad \mathfrak{I}_{142}=-\chi_4\Re_y\xi\frac{\partial}{\partial\xi_1}-\chi_4\Re_x\frac{\partial}{\partial\xi_1},$$

$$\mathfrak{I}_{143}=\chi_3\left(\Re_x+\Re_y\,\xi\right)\frac{\partial}{\partial\xi_2},\quad \mathfrak{I}_{144}=3\chi_1\eta_a\frac{1}{\xi^2}\frac{\partial}{\partial\xi_1},\quad \mathfrak{I}_{145}=-\frac{1}{4}\chi_4\eta_b\xi\frac{\partial}{\partial\xi_1},$$

$$\mathfrak{I}_{146}=-\frac{1}{4}\chi_5\eta_a\frac{\partial}{\partial\xi_1},\quad \mathfrak{I}_{147}=\frac{1}{2}\chi_3\eta_a\frac{\partial}{\partial\xi_2},\quad \mathfrak{I}_{148}=\frac{1}{2}\chi_3\eta_b\xi\frac{\partial}{\partial\xi_2},$$

(A4)

$$\mathfrak{F}_{21} = -3\chi_2\frac{1}{\eta_a}\frac{1}{\eta_b}, \quad \mathfrak{F}_{22} = -4\chi_2\frac{1}{{\eta_a}^2}, \quad \mathfrak{F}_{23} = -\chi_2\frac{1}{{\eta_b}^2}, \quad \mathfrak{F}_{24} = -4\chi_2\Re_y\frac{1}{{\eta_a}^2} - 2\chi_2\Re_x\frac{1}{\eta_a}\frac{1}{\eta_b},$$

$$\mathfrak{F}_{25} = -\chi_4\frac{1}{\eta_b}\frac{\partial}{\partial\xi_2}, \quad \mathfrak{F}_{26} = \frac{1}{2}\chi_3\frac{1}{\eta_a}\xi\frac{\partial}{\partial\xi_2}, \quad \mathfrak{F}_{27} = \chi_3\frac{1}{\eta_b}\frac{\partial}{\partial\xi_1}, \quad \mathfrak{F}_{28} = -2\chi_4\frac{1}{\eta_a}\frac{\partial}{\partial\xi_2},$$

$$\mathfrak{F}_{29} = \chi_3\frac{1}{\eta_a}\frac{\partial}{\partial\xi_2}, \quad \mathfrak{F}_{210} = \chi_3\frac{1}{\eta_b}\frac{1}{\xi}\frac{\partial}{\partial\xi_1}, \quad \mathfrak{F}_{211} = \chi_3\frac{1}{\eta_a}\frac{\partial}{\partial\xi_1},$$

$$\mathfrak{F}_{212} = -2\chi_4\Re_x\frac{1}{\eta_b}\frac{\partial}{\partial\xi_2} - 2\chi_4\Re_y\frac{1}{\eta_a}\frac{\partial}{\partial\xi_2}, \quad \mathfrak{F}_{213} = \chi_3\left(\Re_x\frac{1}{\eta_b} + \Re_y\frac{1}{\eta_a}\right)\frac{\partial}{\partial\xi_1},$$

$$\mathfrak{F}_{214} = 12\chi_1\frac{1}{\eta_a}\xi\frac{\partial}{\partial\xi_2}, \quad \mathfrak{F}_{215} = \chi_3\frac{1}{\eta_a}\frac{\partial}{\partial\xi_1}, \quad \mathfrak{F}_{216} = \frac{1}{2}\chi_3\frac{1}{\eta_b}\frac{\partial}{\partial\xi_2},$$

$$\mathfrak{F}_{217} = \chi_3\left(\Re_x\frac{1}{\xi}\frac{1}{\eta_b} + \Re_y\frac{1}{\eta_b}\right)\frac{\partial}{\partial\xi_1}, \quad \mathfrak{F}_{218} = 24\chi_1\Re_y\xi\frac{1}{\eta_a}\frac{\partial}{\partial\xi_2} - 2\chi_4\Re_x\frac{1}{\eta_a}\frac{\partial}{\partial\xi_2},$$

$$\mathfrak{F}_{219} = 12\chi_1{\Re_y}^2\frac{1}{\eta_a}\xi\frac{\partial}{\partial\xi_2} - \chi_4{\Re_x}^2\frac{1}{\eta_b}\frac{\partial}{\partial\xi_2} - 2\chi_4\Re_x\Re_y\frac{1}{\eta_a}\frac{\partial}{\partial\xi_2},$$

$$\mathfrak{F}_{220} = -2\chi_2\frac{1}{\eta_a}\xi\frac{\partial}{\partial\xi_2}, \quad \mathfrak{F}_{221} = -\chi_2\frac{1}{\eta_b}\frac{\partial}{\partial\xi_2}, \quad \mathfrak{F}_{222} = \chi_1\eta_b\xi^2\frac{\partial}{\partial\xi_2}, \quad \mathfrak{F}_{223} = -\frac{1}{12}\chi_4\eta_a\frac{1}{\xi}\frac{\partial}{\partial\xi_2}, \tag{A5}$$

$$\mathfrak{F}_{224} = -\frac{1}{6}\chi_4\eta_b\frac{\partial}{\partial\xi_2}, \quad \mathfrak{F}_{225} = \frac{1}{6}\chi_3\eta_b\frac{\partial}{\partial\xi_2}, \quad \mathfrak{F}_{226} = -\chi_2\frac{1}{\eta_b}\frac{\partial}{\partial\xi_1}, \quad \mathfrak{F}_{227} = \frac{1}{6}\chi_3\eta_a\frac{1}{\xi}\frac{\partial}{\partial\xi_1},$$

$$\mathfrak{F}_{228} = \frac{1}{6}\chi_3\eta_b\frac{\partial}{\partial\xi_1}, \quad \mathfrak{F}_{229} = -\chi_4\frac{1}{\xi}\frac{\partial}{\partial\xi_2}, \quad \mathfrak{F}_{230} = -\chi_4\xi\frac{\partial}{\partial\xi_2}, \quad \mathfrak{F}_{231} = \chi_3\xi\frac{\partial}{\partial\xi_2},$$

$$\mathfrak{F}_{232} = \chi_3\frac{1}{\xi}\frac{\partial}{\partial\xi_1}, \quad \mathfrak{F}_{233} = \frac{1}{2}\chi_3\frac{1}{\xi}\frac{\partial}{\partial\xi_1}, \quad \mathfrak{F}_{234} = \frac{1}{2}\chi_3\xi\frac{\partial}{\partial\xi_1}, \quad \mathfrak{F}_{235} = 12\chi_1\xi^2\frac{\partial}{\partial\xi_2},$$

$$\mathfrak{F}_{236} = -\chi_4\frac{\partial}{\partial\xi_2}, \quad \mathfrak{F}_{237} = \chi_3\frac{\partial}{\partial\xi_2}, \quad \mathfrak{F}_{238} = \frac{1}{2}\chi_3\frac{1}{\xi^2}\frac{\partial}{\partial\xi_1}, \quad \mathfrak{F}_{239} = \frac{1}{2}\chi_3\frac{\partial}{\partial\xi_1},$$

$$\mathfrak{F}_{240} = \chi_3\frac{\partial}{\partial\xi_1}, \quad \mathfrak{F}_{241} = 12\chi_1\Re_y\xi^2\frac{\partial}{\partial\xi_2} - \chi_4\Re_x\xi\frac{\partial}{\partial\xi_2}, \quad \mathfrak{F}_{242} = -\chi_4\Re_x\frac{1}{\xi}\frac{\partial}{\partial\xi_2} - \chi_4\Re_y\frac{\partial}{\partial\xi_2},$$

$$\mathfrak{F}_{243} = \chi_3\left(\Re_x\frac{1}{\xi} + \Re_y\right)\frac{\partial}{\partial\xi_1}, \quad \mathfrak{F}_{244} = 3\chi_1\eta_b\xi^2\frac{\partial}{\partial\xi_2}, \quad \mathfrak{F}_{245} = -\frac{1}{4}\chi_4\eta_a\frac{1}{\xi}\frac{\partial}{\partial\xi_2},$$

$$\mathfrak{F}_{246} = -\frac{1}{4}\chi_5\eta_b\frac{\partial}{\partial\xi_2}, \quad \mathfrak{F}_{247} = \frac{1}{2}\chi_3\eta_a\frac{1}{\xi}\frac{\partial}{\partial\xi_1}, \quad \mathfrak{F}_{248} = \frac{1}{2}\chi_3\eta_b\frac{\partial}{\partial\xi_1},$$

Appendix B

The curvature related terms in Eq. (15) are defied as

$$\aleph_{kl}^{31} = 4A_2\Re_x\frac{k\pi}{{\eta_b}^2}\cos(k\pi\xi_1)\sin(l\pi\xi_2) + 2A_2\Re_y\frac{k\pi}{\eta_a\eta_b}\cos(k\pi\xi_1)\sin(l\pi\xi_2), \tag{B1}$$

$$\aleph_{kl}^{32} = 2A_2\Re_x\frac{l\pi}{\eta_a\eta_b}\sin(k\pi\xi_1)\cos(l\pi\xi_2) + 4A_2\Re_y\frac{l\pi}{{\eta_a}^2}\sin(k\pi\xi_1)\cos(l\pi\xi_2), \tag{B2}$$

$$\aleph_{kl}^{33} = 4A_2\left({\Re_x}^2\frac{1}{{\eta_b}^2} + {\Re_y}^2\frac{1}{{\eta_a}^2}\right)\sin(k\pi\xi_1)\sin(l\pi\xi_2) + 4A_2\Re_x\Re_y\frac{1}{\eta_a\eta_b}\sin(k\pi\xi_1)\sin(l\pi\xi_2), \tag{B3}$$

$$\begin{aligned}\aleph_{klmn}^{34} &= -12A_1\Re_x\frac{1}{\xi}\frac{km\pi^2}{\eta_b}(\cos(k\pi\xi_1)\sin(l\pi\xi_2)\cos(m\pi\xi_1)\sin(n\pi\xi_2))\\ &-\frac{1}{2}A_3\Re_x\frac{\ln\pi^2}{\eta_a}(\sin(k\pi\xi_1)\cos(l\pi\xi_2)\sin(m\pi\xi_1)\cos(n\pi\xi_2))\\ &+A_4\Re_y\frac{km\pi^2}{\eta_b}(\cos(k\pi\xi_1)\sin(l\pi\xi_2)\cos(m\pi\xi_1)\sin(n\pi\xi_2))\\ &+\frac{1}{2}A_3\Re_y\xi\frac{\ln\pi^2}{\eta_a}(\sin(k\pi\xi_1)\cos(l\pi\xi_2)\sin(m\pi\xi_1)\cos(n\pi\xi_2)),\end{aligned} \tag{B4}$$

$$\begin{aligned}\aleph_{klmn}^{35} &= 2A_4\left(\Re_x\frac{kn\pi^2}{\eta_b} + \Re_y\frac{kn\pi^2}{\eta_a}\right)(\cos(k\pi\xi_1)\sin(l\pi\xi_2)\sin(m\pi\xi_1)\cos(n\pi\xi_2))\\ &-A_3\left(\Re_x\frac{lm\pi^2}{\eta_b} + \Re_y\frac{lm\pi^2}{\eta_a}\right)(\sin(k\pi\xi_1)\cos(l\pi\xi_2)\cos(m\pi\xi_1)\sin(n\pi\xi_2)),\end{aligned} \tag{B5}$$

$$\begin{aligned}\aleph_{klmn}^{36} &= -24A_1{\Re_x}^2\frac{k\pi}{\eta_b}\frac{1}{\xi}(\cos(k\pi\xi_1)\sin(l\pi\xi_2)\sin(m\pi\xi_1)\sin(n\pi\xi_2))\\ &+2A_4\Re_y\left(2\Re_x\frac{k\pi}{\eta_b} + \Re_y\frac{k\pi}{\eta_a}\right)(\cos(k\pi\xi_1)\sin(l\pi\xi_2)\sin(m\pi\xi_1)\sin(n\pi\xi_2)),\end{aligned} \tag{B6}$$

$$\begin{aligned}\aleph_{klmn}^{37} &= -12A_1\Re_y\frac{\ln\pi^2}{\eta_a}\xi(\sin(k\pi\xi_1)\cos(l\pi\xi_2)\sin(m\pi\xi_1)\cos(n\pi\xi_2))\\ &-\frac{1}{2}A_3\Re_y\frac{km\pi^2}{\eta_b}(\cos(k\pi\xi_1)\sin(l\pi\xi_2)\cos(m\pi\xi_1)\sin(n\pi\xi_2))\\ &+A_4\Re_x\frac{\ln\pi^2}{\eta_a}(\sin(k\pi\xi_1)\cos(l\pi\xi_2)\sin(m\pi\xi_1)\cos(n\pi\xi_2))\\ &-\frac{1}{2}A_3\Re_x\frac{km\pi^2}{\eta_b}\frac{1}{\xi}(\cos(k\pi\xi_1)\sin(l\pi\xi_2)\cos(m\pi\xi_1)\sin(n\pi\xi_2)),\end{aligned} \tag{B7}$$

$$\begin{aligned}\aleph_{klmn}^{38} &= -24A_1{\Re_y}^2\xi\frac{l\pi}{\eta_a}(\sin(k\pi\xi_1)\cos(l\pi\xi_2)\sin(m\pi\xi_1)\sin(n\pi\xi_2))\\ &+2A_4\Re_x\left(\Re_x\frac{l\pi}{\eta_b} + 2\Re_y\frac{l\pi}{\eta_a}\right)(\sin(k\pi\xi_1)\cos(l\pi\xi_2)\sin(m\pi\xi_1)\sin(n\pi\xi_2)),\end{aligned} \tag{B8}$$

$$
\begin{aligned}
\aleph^{39}_{klmn} = & \begin{bmatrix} -12A_1\left(\Re_x{}^3\frac{1}{\xi}\frac{1}{\eta_b}+\Re_y{}^3\xi\frac{1}{\eta_a}\right) \\ +3A_4\Re_x\Re_y\left(\Re_x\frac{1}{\eta_b}+\Re_y\frac{1}{\eta_a}\right) \end{bmatrix}(\sin(k\pi\xi_1)\sin(l\pi\xi_2)\sin(m\pi\xi_1)\sin(n\pi\xi_2)) \\
& +\left(-4A_2\Re_x\frac{m\pi}{\eta_b}\frac{1}{\xi}-2A_2\Re_y\frac{m\pi}{\eta_b}\right)\frac{\partial}{\partial\xi_1}(\sin(k\pi\xi_1)\sin(l\pi\xi_2)\cos(m\pi\xi_1)\sin(n\pi\xi_2)) \\
& +\left(-4A_2\Re_y\frac{n\pi}{\eta_a}\xi-2A_2\Re_x\frac{n\pi}{\eta_a}\right)\frac{\partial}{\partial\xi_2}(\sin(k\pi\xi_1)\sin(l\pi\xi_2)\sin(m\pi\xi_1)\cos(n\pi\xi_2)) \\
& +\left(2A_1\Re_x\eta_a\frac{m^2\pi^2}{\xi^2}-\frac{1}{6}A_4\Re_y\eta_a\frac{m^2\pi^2}{\xi}\right)\frac{\partial^2}{\partial\xi_1{}^2}(\sin(k\pi\xi_1)\sin(l\pi\xi_2)\sin(m\pi\xi_1)\sin(n\pi\xi_2)) \\
& -\frac{1}{6}A_4m^2\pi^2\left(\Re_x\eta_a+\Re_y\eta_b\right)\frac{\partial^2}{\partial\xi_2{}^2}(\sin(k\pi\xi_1)\sin(l\pi\xi_2)\sin(m\pi\xi_1)\sin(n\pi\xi_2)) \\
& +\left(2A_1\Re_y\eta_b\xi^2-\frac{1}{6}A_4\Re_x\eta_b\xi\right)n^2\pi^2\frac{\partial^2}{\partial\xi_2{}^2}(\sin(k\pi\xi_1)\sin(l\pi\xi_2)\sin(m\pi\xi_1)\sin(n\pi\xi_2)) \\
& -\frac{1}{6}A_4n^2\pi^2\left(\Re_y\eta_b+\Re_x\eta_a\right)\frac{\partial^2}{\partial\xi_1{}^2}(\sin(k\pi\xi_1)\sin(l\pi\xi_2)\sin(m\pi\xi_1)\sin(n\pi\xi_2)) \\
& -\frac{1}{3}A_3mn\pi^2\left(\Re_x\eta_a+\Re_y\eta_b\right)\frac{\partial^2}{\partial\xi_1\partial\xi_2}(\sin(k\pi\xi_1)\sin(l\pi\xi_2)\cos(m\pi\xi_1)\cos(n\pi\xi_2)) \\
& +A_2\frac{km\pi^2}{\eta_b}\left(2\Re_x\frac{1}{\xi}+\Re_y\right)(\cos(k\pi\xi_1)\sin(l\pi\xi_2)\cos(m\pi\xi_1)\sin(n\pi\xi_2)) \\
& +A_2\frac{\ln\pi^2}{\eta_a}\left(2\Re_y\xi+\Re_x\right)(\sin(k\pi\xi_1)\cos(l\pi\xi_2)\sin(m\pi\xi_1)\cos(n\pi\xi_2)) \\
& +\left(-A_1\Re_x\eta_a\frac{1}{\xi^2}+\frac{1}{12\xi}A_4\Re_y\eta_a\right)k^2m^2\pi^4(\sin(k\pi\xi_1)\sin(l\pi\xi_2)\sin(m\pi\xi_1)\sin(n\pi\xi_2)) \\
& +\left(-A_1\Re_y\eta_b\xi^2+\frac{\xi}{12}A_4\Re_x\eta_b\right)l^2n^2\pi^4(\sin(k\pi\xi_1)\sin(l\pi\xi_2)\sin(m\pi\xi_1)\sin(n\pi\xi_2)) \\
& +\frac{1}{6}A_4\left(\Re_x\eta_a+\Re_y\eta_b\right)k^2n^2\pi^4(\sin(k\pi\xi_1)\sin(l\pi\xi_2)\sin(m\pi\xi_1)\sin(n\pi\xi_2)) \\
& -\frac{1}{6}A_3\left(\Re_x\eta_a+\Re_y\eta_b\right)klmn\pi^4(\cos(k\pi\xi_1)\cos(l\pi\xi_2)\cos(m\pi\xi_1)\cos(n\pi\xi_2)),
\end{aligned}
\tag{B9}
$$

$$
\begin{aligned}
\aleph^{310}_{klmnop} = & \left(24A_1\Re_x\frac{1}{\xi^2}-2A_4\Re_y\frac{1}{\xi}\right)ko\pi^2\frac{\partial}{\partial\xi_1}\begin{pmatrix}\cos(k\pi\xi_1)\sin(l\pi\xi_2)\sin(m\pi\xi_1)\\ \sin(n\pi\xi_2)\cos(o\pi\xi_1)\sin(p\pi\xi_2)\end{pmatrix} \\
& +\left(-2A_4\Re_x-2A_4\Re_y\xi\right)kp\pi^2\frac{\partial}{\partial\xi_2}\begin{pmatrix}\cos(k\pi\xi_1)\sin(l\pi\xi_2)\sin(m\pi\xi_1)\\ \sin(n\pi\xi_2)\sin(o\pi\xi_1)\cos(p\pi\xi_2)\end{pmatrix} \\
& -12A_1\Re_x\frac{1}{\xi^2}kmo\pi^3\begin{pmatrix}\cos(k\pi\xi_1)\sin(l\pi\xi_2)\cos(m\pi\xi_1)\\ \sin(n\pi\xi_2)\cos(o\pi\xi_1)\sin(p\pi\xi_2)\end{pmatrix} \\
& +\left(A_4\Re_x+A_4\Re_y\xi\right)knp\pi^3\begin{pmatrix}\cos(k\pi\xi_1)\sin(l\pi\xi_2)\sin(m\pi\xi_1)\\ \cos(n\pi\xi_2)\sin(o\pi\xi_1)\cos(p\pi\xi_2)\end{pmatrix} \\
& +\left(-A_3\Re_x-A_3\Re_y\xi\right)lmp\pi^3\begin{pmatrix}\sin(k\pi\xi_1)\cos(l\pi\xi_2)\cos(m\pi\xi_1)\\ \sin(n\pi\xi_2)\sin(o\pi\xi_1)\cos(p\pi\xi_2)\end{pmatrix} \\
& +A_4\Re_y\frac{1}{\xi}kmo\pi^3\begin{pmatrix}\cos(k\pi\xi_1)\sin(l\pi\xi_2)\cos(m\pi\xi_1)\\ \sin(n\pi\xi_2)\cos(o\pi\xi_1)\sin(p\pi\xi_2)\end{pmatrix} \\
& +A_3\left(\Re_x+\Re_y\xi\right)lp\pi^2\frac{\partial}{\partial\xi_1}\begin{pmatrix}\sin(k\pi\xi_1)\cos(l\pi\xi_2)\sin(m\pi\xi_1)\\ \sin(n\pi\xi_2)\sin(o\pi\xi_1)\cos(p\pi\xi_2)\end{pmatrix} \\
& +A_3\left(\Re_x+\Re_y\xi\right)lo\pi^2\frac{\partial}{\partial\xi_2}\begin{pmatrix}\sin(k\pi\xi_1)\cos(l\pi\xi_2)\sin(m\pi\xi_1)\\ \sin(n\pi\xi_2)\cos(o\pi\xi_1)\sin(p\pi\xi_2)\end{pmatrix},
\end{aligned}
\tag{B10}
$$

$$
\begin{aligned}
\aleph^{311}_{klmnop} &= \left(24A_1\Re_y\xi^2 - 2A_4\Re_x\xi\right)lp\pi^2\frac{\partial}{\partial\xi_2}\begin{pmatrix}\sin(k\pi\xi_1)\cos(l\pi\xi_2)\sin(m\pi\xi_1)\\ \sin(n\pi\xi_2)\sin(o\pi\xi_1)\cos(p\pi\xi_2)\end{pmatrix}\\
&+\left(-2A_4\Re_y - 2A_4\Re_x\frac{1}{\xi}\right)lo\pi^2\frac{\partial}{\partial\xi_1}\begin{pmatrix}\sin(k\pi\xi_1)\cos(l\pi\xi_2)\sin(m\pi\xi_1)\\ \sin(n\pi\xi_2)\cos(o\pi\xi_1)\sin(p\pi\xi_2)\end{pmatrix}\\
&-12A_1\Re_y\xi^2 lnp\pi^3\begin{pmatrix}\sin(k\pi\xi_1)\cos(l\pi\xi_2)\sin(m\pi\xi_1)\\ \cos(n\pi\xi_2)\sin(o\pi\xi_1)\cos(p\pi\xi_2)\end{pmatrix}\\
&+\left(A_4\Re_y + A_4\Re_x\frac{1}{\xi}\right)lmo\pi^3\begin{pmatrix}\sin(k\pi\xi_1)\cos(l\pi\xi_2)\cos(m\pi\xi_1)\\ \sin(n\pi\xi_2)\cos(o\pi\xi_1)\sin(p\pi\xi_2)\end{pmatrix}\\
&+\left(-A_3\Re_x\frac{1}{\xi} - A_3\Re_y\right)kmp\pi^3\begin{pmatrix}\cos(k\pi\xi_1)\sin(l\pi\xi_2)\cos(m\pi\xi_1)\\ \sin(n\pi\xi_2)\sin(o\pi\xi_1)\cos(p\pi\xi_2)\end{pmatrix}\\
&+A_4\Re_x\xi lnp\pi^3\begin{pmatrix}\sin(k\pi\xi_1)\cos(l\pi\xi_2)\sin(m\pi\xi_1)\\ \cos(n\pi\xi_2)\sin(o\pi\xi_1)\cos(p\pi\xi_2)\end{pmatrix}\\
&+A_3\left(\Re_x\frac{1}{\xi} + \Re_y\right)ko\pi^2\frac{\partial}{\partial\xi_2}\begin{pmatrix}\cos(k\pi\xi_1)\sin(l\pi\xi_2)\sin(m\pi\xi_1)\\ \sin(n\pi\xi_2)\cos(o\pi\xi_1)\sin(p\pi\xi_2)\end{pmatrix}\\
&+A_3\left(\Re_x\frac{1}{\xi} + \Re_y\right)kp\pi^2\frac{\partial}{\partial\xi_1}\begin{pmatrix}\cos(k\pi\xi_1)\sin(l\pi\xi_2)\sin(m\pi\xi_1)\\ \sin(n\pi\xi_2)\sin(o\pi\xi_1)\cos(p\pi\xi_2)\end{pmatrix},
\end{aligned}
\tag{B11}
$$

$$
\begin{aligned}
\aleph^{312}_{klmnop} &= \left(12A_1{\Re_x}^2\frac{1}{\xi^2} - A_4{\Re_y}^2 - 2A_4\Re_x\Re_y\frac{1}{\xi}\right)o\pi\frac{\partial}{\partial\xi_1}\begin{pmatrix}\sin(k\pi\xi_1)\sin(l\pi\xi_2)\sin(m\pi\xi_1)\\ \sin(n\pi\xi_2)\cos(o\pi\xi_1)\sin(p\pi\xi_2)\end{pmatrix}\\
&-12A_1{\Re_x}^2\frac{1}{\xi^2}o\pi\begin{pmatrix}\sin(k\pi\xi_1)\sin(l\pi\xi_2)\sin(m\pi\xi_1)\\ \sin(n\pi\xi_2)\cos(o\pi\xi_1)\sin(p\pi\xi_2)\end{pmatrix}\\
&+\left(12A_1{\Re_y}^2\xi^2 - A_4{\Re_x}^2 - 2A_4\Re_x\Re_y\xi\right)p\pi\frac{\partial}{\partial\xi_2}\begin{pmatrix}\sin(k\pi\xi_1)\sin(l\pi\xi_2)\sin(m\pi\xi_1)\\ \sin(n\pi\xi_2)\sin(o\pi\xi_1)\cos(p\pi\xi_2)\end{pmatrix}\\
&-12A_1{\Re_y}^2\xi^2 p\pi\begin{pmatrix}\sin(k\pi\xi_1)\sin(l\pi\xi_2)\sin(m\pi\xi_1)\\ \sin(n\pi\xi_2)\sin(o\pi\xi_1)\cos(p\pi\xi_2)\end{pmatrix}\\
&+\left(A_4\Re_x\Re_y\xi + A_4\Re_x\Re_y\xi + A_4{\Re_x}^2\right)np\pi^2\begin{pmatrix}\sin(k\pi\xi_1)\sin(l\pi\xi_2)\sin(m\pi\xi_1)\\ \cos(n\pi\xi_2)\sin(o\pi\xi_1)\cos(p\pi\xi_2)\end{pmatrix}\\
&+\left(A_4\Re_x\Re_y\frac{1}{\xi} + A_4\Re_x\Re_y\frac{1}{\xi} + A_4{\Re_y}^2\right)mo\pi^2\begin{pmatrix}\sin(k\pi\xi_1)\sin(l\pi\xi_2)\cos(m\pi\xi_1)\\ \sin(n\pi\xi_2)\cos(o\pi\xi_1)\sin(p\pi\xi_2)\end{pmatrix},
\end{aligned}
\tag{B12}
$$

$$
\begin{aligned}
\aleph^{313}_{klmnopqr} &= +\frac{1}{4}A_5\left(\Re_x\eta_a + \Re_y\eta_b\right)kmpr\pi^4\begin{pmatrix}\cos(k\pi\xi_1)\sin(l\pi\xi_2)\cos(m\pi\xi_1)\sin(n\pi\xi_2)\\ \sin(o\pi\xi_1)\cos(p\pi\xi_2)\sin(q\pi\xi_1)\cos(r\pi\xi_2)\end{pmatrix}\\
&+\left(-3A_1\Re_x\eta_a\frac{1}{\xi^2} + \frac{1}{4}A_4\Re_y\eta_a\frac{1}{\xi}\right)kmoq\pi^4\begin{pmatrix}\cos(k\pi\xi_1)\sin(l\pi\xi_2)\cos(m\pi\xi_1)\sin(n\pi\xi_2)\\ \cos(o\pi\xi_1)\sin(p\pi\xi_2)\cos(q\pi\xi_1)\sin(r\pi\xi_2)\end{pmatrix}\\
&+\left(12A_1\Re_y\eta_b\xi^2 - A_4\Re_x\eta_b\xi\right)npr\pi^3\frac{\partial}{\partial\xi_2}\begin{pmatrix}\sin(k\pi\xi_1)\sin(l\pi\xi_2)\sin(m\pi\xi_1)\cos(n\pi\xi_2)\\ \sin(o\pi\xi_1)\cos(p\pi\xi_2)\sin(q\pi\xi_1)\cos(r\pi\xi_2)\end{pmatrix}\\
&+\left(-3A_1\Re_y\eta_b\xi^2 + \frac{1}{4}A_4\Re_x\eta_b\xi\right)lnpr\pi^4\begin{pmatrix}\sin(k\pi\xi_1)\cos(l\pi\xi_2)\sin(m\pi\xi_1)\cos(n\pi\xi_2)\\ \sin(o\pi\xi_1)\cos(p\pi\xi_2)\sin(q\pi\xi_1)\cos(r\pi\xi_2)\end{pmatrix}\\
&+\begin{bmatrix}-A_4\Re_y\eta_b - A_4\Re_x\eta_a\\ +A_3\left(\Re_x\eta_a + \Re_y\eta_b\right)\end{bmatrix}mpr\pi^3\frac{\partial}{\partial\xi_1}\begin{pmatrix}\sin(k\pi\xi_1)\sin(l\pi\xi_2)\cos(m\pi\xi_1)\sin(n\pi\xi_2)\\ \sin(o\pi\xi_1)\cos(p\pi\xi_2)\sin(q\pi\xi_1)\cos(r\pi\xi_2)\end{pmatrix}\\
&+\begin{bmatrix}-A_4\Re_x\eta_a - A_4\Re_y\eta_b\\ +A_3\left(\Re_x\eta_a + \Re_y\eta_b\right)\end{bmatrix}mor\pi^3\frac{\partial}{\partial\xi_2}\begin{pmatrix}\sin(k\pi\xi_1)\sin(l\pi\xi_2)\cos(m\pi\xi_1)\sin(n\pi\xi_2)\\ \cos(o\pi\xi_1)\sin(p\pi\xi_2)\sin(q\pi\xi_1)\cos(r\pi\xi_2)\end{pmatrix}\\
&\left(12A_1\Re_x\eta_a\frac{1}{\xi^2} - A_4\Re_y\eta_a\frac{1}{\xi}\right)moq\pi^3\frac{\partial}{\partial\xi_1}\begin{pmatrix}\sin(k\pi\xi_1)\sin(l\pi\xi_2)\cos(m\pi\xi_1)\sin(n\pi\xi_2)\\ \cos(o\pi\xi_1)\sin(p\pi\xi_2)\cos(q\pi\xi_1)\sin(r\pi\xi_2)\end{pmatrix},
\end{aligned}
\tag{B13}
$$

and the curvature related terms in Eq. (16) are defied as

$$\aleph_{kl}^{11} = -4A_2\Re_x\frac{k\pi}{{\eta_b}^2}\cos(k\pi\xi_1)\sin(l\pi\xi_2) - 2A_2\Re_y\frac{k\pi}{\eta_a\eta_b}\cos(k\pi\xi_1)\sin(l\pi\xi_2), \tag{B14}$$

$$\begin{aligned}\aleph_{klmn}^{12} &= +24A_1\Re_x\frac{k\pi}{\eta_b}\frac{1}{\xi}\frac{\partial}{\partial\xi_1}(\cos(k\pi\xi_1)\sin(l\pi\xi_2)\sin(m\pi\xi_1)\sin(n\pi\xi_2))\\ &-2A_4\Re_y\frac{k\pi}{\eta_b}\frac{\partial}{\partial\xi_1}(\cos(k\pi\xi_1)\sin(l\pi\xi_2)\sin(m\pi\xi_1)\sin(n\pi\xi_2))\\ &+A_3\big(\Re_x+\xi\,\Re_y\big)\frac{l\pi}{\eta_a}\frac{\partial}{\partial\xi_2}(\sin(k\pi\xi_1)\cos(l\pi\xi_2)\sin(m\pi\xi_1)\sin(n\pi\xi_2)),\end{aligned} \tag{B15}$$

$$\begin{aligned}\aleph_{klmn}^{13} &= -2A_4\Re_y\frac{l\pi}{\eta_a}\frac{\partial}{\partial\xi_1}(\sin(k\pi\xi_1)\cos(l\pi\xi_2)\sin(m\pi\xi_1)\sin(n\pi\xi_2))\\ &-2A_4\Re_x\frac{l\pi}{\eta_b}\frac{\partial}{\partial\xi_1}(\sin(k\pi\xi_1)\cos(l\pi\xi_2)\sin(m\pi\xi_1)\sin(n\pi\xi_2))\\ &+A_3\left(\Re_x\frac{k\pi}{\eta_b}+\Re_y\frac{k\pi}{\eta_a}\right)\frac{\partial}{\partial\xi_2}(\cos(k\pi\xi_1)\sin(l\pi\xi_2)\sin(m\pi\xi_1)\sin(n\pi\xi_2)),\end{aligned} \tag{B16}$$

$$\begin{aligned}\aleph_{klmn}^{14} &= +12A_1{\Re_x}^2\frac{1}{\eta_b}\frac{1}{\xi}\frac{\partial}{\partial\xi_1}(\sin(k\pi\xi_1)\sin(l\pi\xi_2)\sin(m\pi\xi_1)\sin(n\pi\xi_2))\\ &-A_4{\Re_y}^2\frac{1}{\eta_a}\frac{\partial}{\partial\xi_1}(\sin(k\pi\xi_1)\sin(l\pi\xi_2)\sin(m\pi\xi_1)\sin(n\pi\xi_2))\\ &-2A_4\Re_x\Re_y\frac{1}{\eta_b}\frac{\partial}{\partial\xi_1}(\sin(k\pi\xi_1)\sin(l\pi\xi_2)\sin(m\pi\xi_1)\sin(n\pi\xi_2)),\end{aligned} \tag{B17}$$

$$\begin{aligned}\aleph_{klmnop}^{15} &= +12A_1\Re_x\frac{om\pi^2}{\xi^2}\frac{\partial}{\partial\xi_1}\begin{pmatrix}\sin(k\pi\xi_1)\sin(l\pi\xi_2)\cos(m\pi\xi_1)\\ \sin(n\pi\xi_2)\cos(o\pi\xi_1)\sin(p\pi\xi_2)\end{pmatrix}\\ &-A_4\Re_y np\pi^2\xi\frac{\partial}{\partial\xi_1}\begin{pmatrix}\sin(k\pi\xi_1)\sin(l\pi\xi_2)\sin(m\pi\xi_1)\\ \cos(n\pi\xi_2)\sin(o\pi\xi_1)\cos(p\pi\xi_2)\end{pmatrix}\\ &+A_3\big(\Re_x+\Re_y\,\xi\big)mp\pi^2\frac{\partial}{\partial\xi_2}\begin{pmatrix}\sin(k\pi\xi_1)\sin(l\pi\xi_2)\cos(m\pi\xi_1)\\ \sin(n\pi\xi_2)\sin(o\pi\xi_1)\cos(p\pi\xi_2)\end{pmatrix}\\ &-A_4\Re_y\frac{om\pi^2}{\xi}\frac{\partial}{\partial\xi_1}\begin{pmatrix}\sin(k\pi\xi_1)\sin(l\pi\xi_2)\cos(m\pi\xi_1)\\ \sin(n\pi\xi_2)\cos(o\pi\xi_1)\sin(p\pi\xi_2)\end{pmatrix}\\ &-A_4\Re_x np\pi^2\frac{\partial}{\partial\xi_1}\begin{pmatrix}\sin(k\pi\xi_1)\sin(l\pi\xi_2)\sin(m\pi\xi_1)\\ \cos(n\pi\xi_2)\sin(o\pi\xi_1)\cos(p\pi\xi_2)\end{pmatrix},\end{aligned} \tag{B18}$$

and the curvature related terms in Eq. (17) are defied as

$$\aleph_{kl}^{21} = -4A_2\Re_y\frac{l\pi}{{\eta_a}^2}\sin(k\pi\xi_1)\cos(l\pi\xi_2) - 2A_2\Re_x\frac{l\pi}{\eta_a\eta_b}\sin(k\pi\xi_1)\cos(l\pi\xi_2), \tag{B19}$$

$$\begin{aligned}\aleph_{klmn}^{22} &= -2A_4\Re_x\frac{k\pi}{\eta_b}\frac{\partial}{\partial\xi_2}(\cos(k\pi\xi_1)\sin(l\pi\xi_2)\sin(m\pi\xi_1)\sin(n\pi\xi_2))\\ &-2A_4\Re_y\frac{k\pi}{\eta_a}\frac{\partial}{\partial\xi_2}(\cos(k\pi\xi_1)\sin(l\pi\xi_2)\sin(m\pi\xi_1)\sin(n\pi\xi_2))\\ &+A_3\left(\Re_x\frac{l\pi}{\eta_b}+\Re_y\frac{l\pi}{\eta_a}\right)\frac{\partial}{\partial\xi_1}(\sin(k\pi\xi_1)\cos(l\pi\xi_2)\sin(m\pi\xi_1)\sin(n\pi\xi_2)),\end{aligned} \tag{B20}$$

$$\begin{aligned}\aleph_{klmn}^{23} &= 24A_1\Re_y\xi\frac{l\pi}{\eta_a}\frac{\partial}{\partial\xi_2}(\sin(k\pi\xi_1)\cos(l\pi\xi_2)\sin(m\pi\xi_1)\sin(n\pi\xi_2))\\ &-2A_4\Re_x\frac{l\pi}{\eta_a}\frac{\partial}{\partial\xi_2}(\sin(k\pi\xi_1)\cos(l\pi\xi_2)\sin(m\pi\xi_1)\sin(n\pi\xi_2))\\ &+A_3\left(\Re_x\frac{1}{\xi}\frac{k\pi}{\eta_b}+\Re_y\frac{k\pi}{\eta_b}\right)\frac{\partial}{\partial\xi_1}(\cos(k\pi\xi_1)\sin(l\pi\xi_2)\sin(m\pi\xi_1)\sin(n\pi\xi_2)),\end{aligned} \tag{B21}$$

$$
\begin{aligned}
\aleph^{24}_{klmn} &= 12A_1\Re_y{}^2\frac{1}{\eta_a}\xi\frac{\partial}{\partial\xi_2}(\sin(k\pi\xi_1)\sin(l\pi\xi_2)\sin(m\pi\xi_1)\sin(n\pi\xi_2))\\
&-A_4\Re_x{}^2\frac{1}{\eta_b}\frac{\partial}{\partial\xi_2}(\sin(k\pi\xi_1)\sin(l\pi\xi_2)\sin(m\pi\xi_1)\sin(n\pi\xi_2))\\
&-2A_4\Re_x\Re_y\frac{1}{\eta_a}\frac{\partial}{\partial\xi_2}(\sin(k\pi\xi_1)\sin(l\pi\xi_2)\sin(m\pi\xi_1)\sin(n\pi\xi_2)),
\end{aligned}
\tag{B22}
$$

$$
\begin{aligned}
\aleph^{25}_{klmnop} &= 12A_1\Re_y\xi^2np\pi^2\frac{\partial}{\partial\xi_2}\begin{pmatrix}\sin(k\pi\xi_1)\sin(l\pi\xi_2)\sin(m\pi\xi_1)\\ \cos(n\pi\xi_2)\sin(o\pi\xi_1)\cos(p\pi\xi_2)\end{pmatrix}\\
&-A_4\Re_x\frac{mo\pi^2}{\xi}\frac{\partial}{\partial\xi_2}\begin{pmatrix}\sin(k\pi\xi_1)\sin(l\pi\xi_2)\cos(m\pi\xi_1)\\ \sin(n\pi\xi_2)\cos(o\pi\xi_1)\sin(p\pi\xi_2)\end{pmatrix}\\
&-A_4\Re_y mo\pi^2\frac{\partial}{\partial\xi_2}\begin{pmatrix}\sin(k\pi\xi_1)\sin(l\pi\xi_2)\cos(m\pi\xi_1)\\ \sin(n\pi\xi_2)\cos(o\pi\xi_1)\sin(p\pi\xi_2)\end{pmatrix}\\
&-A_4\Re_x\xi np\pi^2\frac{\partial}{\partial\xi_2}\begin{pmatrix}\sin(k\pi\xi_1)\sin(l\pi\xi_2)\sin(m\pi\xi_1)\\ \cos(n\pi\xi_2)\sin(o\pi\xi_1)\cos(p\pi\xi_2)\end{pmatrix}\\
&+A_3\left(\Re_x\frac{1}{\xi}+\Re_y\right)mp\pi^2\frac{\partial}{\partial\xi_1}\begin{pmatrix}\sin(k\pi\xi_1)\sin(l\pi\xi_2)\cos(m\pi\xi_1)\\ \sin(n\pi\xi_2)\sin(o\pi\xi_1)\cos(p\pi\xi_2)\end{pmatrix},
\end{aligned}
\tag{B23}
$$

References

Alijani, F., & Amabili, M. (2014). Non-linear vibrations of shells: A literature review from 2003 to 2013. *International Journal of Non-Linear Mechanics, 58*, 233–257.

Alijani, F., Amabili, M., Karagiozis, K., & Bakhtiari-Nejad, F. (2011). Nonlinear vibrations of functionally graded doubly curved shallow shells. *Journal of Sound and Vibration, 330*, 1432–1454.

Allgower, E. L., & Georg, K. (2003). *Introduction to numerical continuation methods*. SIAM.

Allgower, E. L., & Georg, K. (2012). *Numerical continuation methods: an introduction*. Springer Science & Business Media.

Amabili, M. (2003). A comparison of shell theories for large-amplitude vibrations of circular cylindrical shells: Lagrangian approach. *Journal of Sound and Vibration, 264*, 1091–1125.

Amabili, M. (2008). *Nonlinear vibrations and stability of shells and plates*. Cambridge University Press.

Amabili, M., Breslavsky, I., & Reddy, J. (2019). Nonlinear higher-order shell theory for incompressible biological hyperelastic materials. *Computer Methods in Applied Mechanics and Engineering, 346*, 841–861.

Amabili, M., & Paidoussis, M. P. (2003). Review of studies on geometrically nonlinear vibrations and dynamics of circular cylindrical shells and panels, with and without fluid-structure interaction. *Applied Mechanics Reviews, 56*, 349–381.

Anani, Y., & Rahimi, G. H. (2015). Stress analysis of thick pressure vessel composed of functionally graded incompressible hyperelastic materials. *International Journal of Mechanical Sciences, 104*, 1–7.

Anani, Y., & Rahimi, G. H. (2016). Stress analysis of rotating cylindrical shell composed of functionally graded incompressible hyperelastic materials. *International Journal of Mechanical Sciences, 108*, 122–128.

ANSYS® Multiphysics™. (2022). Workbench 19.2, Workbench User's Guide, ANSYS Workbench Systems. *Analysis Systems, Modal*.

Aranda-Iglesias, D., Vadillo, G., & Rodríguez-Martínez, J. (2017). Oscillatory behaviour of compressible hyperelastic shells subjected to dynamic inflation: a numerical study. *Acta Mechanica, 228*, 2187–2205.

Bakalis, K., & Karamanos, S. A. (2021). Uplift mechanics of unanchored liquid storage tanks subjected to lateral earthquake loading. *Thin-Walled Structures, 158*, Article 107145.

Berger, T., Weiss, G., Voetsch, A., Arnold, Z., Kreibich, M., Rylski, B., Krombholz-Reindl, P., Winkler, A., Mach, M., & Geisler, D. (2019). Multicentre experience with two frozen elephant trunk prostheses in the treatment of acute aortic dissection. *European Journal of Cardio-Thoracic Surgery, 56*, 572–578.

Bonet, J., Gil, A. J., & Wood, R. D. (2021). *Nonlinear solid mechanics for finite element analysis: dynamics*. Cambridge University Press.

Bower, A. F. (2009). *Applied mechanics of solids*. CRC press.

Breslavsky, I. D., Amabili, M., & Legrand, M. (2016). Static and dynamic behavior of circular cylindrical shell made of hyperelastic arterial material. *Journal of Applied Mechanics, 83*, Article 051002.

Crisfield, M. (1979). A faster modified Newton-Raphson iteration. *Computer Methods in Applied Mechanics and Engineering, 20*, 267–278.

Dastjerdi, S., Akgöz, B., & Civalek, Ö. (2021). On the shell model for human eye in glaucoma disease. *International Journal of Engineering Science, 158*, Article 103414.

Dastjerdi, S., Akgöz, B., Civalek, Ö., Malikan, M., & Eremeyev, V. A. (2020). On the non-linear dynamics of torus-shaped and cylindrical shell structures. *International Journal of Engineering Science, 156*, Article 103371.

Dastjerdi, S., Malikan, M., Akgöz, B., Civalek, Ö., Wiczenbach, T., & Eremeyev, V. A. (2022). On the deformation and frequency analyses of SARS-CoV-2 at nanoscale. *International Journal of Engineering Science, 170*, Article 103604.

Detter, C., Demal, T. J., Bax, L., Tsilimparis, N., Kölbel, T., Von Kodolitsch, Y., Vettorazzi, E., Reichenspurner, H., & Brickwedel, J. (2019). Simplified frozen elephant trunk technique for combined open and endovascular treatment of extensive aortic diseases. *European Journal of Cardio-Thoracic Surgery, 56*, 738–745.

Eyvazian, A., Shahsavari, D., & Karami, B. (2020). On the dynamic of graphene reinforced nanocomposite cylindrical shells subjected to a moving harmonic load. *International Journal of Engineering Science, 154*, Article 103339.

Ghayesh, M. H., & Farokhi, H. (2017). Nonlinear mechanics of doubly curved shallow microshells. *International Journal of Engineering Science, 119*, 288–304.

Ghayesh, M. H., & Farokhi, H. (2018). Nonlinear behaviour of electrically actuated microplate-based MEMS resonators. *Mechanical Systems and Signal Processing, 109*, 220–234.

Jiang, Y., Li, L., & Hu, Y. (2022). A compatible multiscale model for nanocomposites incorporating interface effect. *International Journal of Engineering Science, 174*, Article 103657.

Kan, J., Liao, W., Wang, J., Wang, S., Yan, M., Jiang, Y., & Zhang, Z. (2021). Enhanced piezoelectric wind-induced vibration energy harvester via the interplay between cylindrical shell and diamond-shaped baffle. *Nano Energy, 89*, Article 106466.
Kaplunov, J., Khajiyeva, L., Martyniuk, M., & Sergaliyev, A. (2020). On the dynamics of drilling. *International Journal of Engineering Science, 146*, Article 103184.
Kar, V. R., & Panda, S. K. (2015). Nonlinear flexural vibration of shear deformable functionally graded spherical shell panel. *Steel and Composite Structures, 18*, 693–709.
Kar, V. R., Panda, S. K., & Mahapatra, T. R. (2016). Thermal buckling behaviour of shear deformable functionally graded single/doubly curved shell panel with TD and TID properties. *Advances in Materials Research, 5*, 205.
Karami, B., & Janghorban, M. (2020). On the mechanics of functionally graded nanoshells. *International Journal of Engineering Science, 153*, Article 103309.
Karami, B., Janghorban, M., & Fahham, H. (2022). On the stress analysis of anisotropic curved panels. *International Journal of Engineering Science, 172*, Article 103625.
Khaniki, H. B., Ghayesh, M. H., & Chin, R. (2023). Theory and experiment for dynamics of hyperelastic plates with modal interactions. *International Journal of Engineering Science, 182*, Article 103769.
Khaniki, H. B., Ghayesh, M. H., Chin, R., & Amabili, M. (2021). Large amplitude vibrations of imperfect porous-hyperelastic beams via a modified strain energy. *Journal of Sound and Vibration, 513*, Article 116416.
Khaniki, H. B., Ghayesh, M. H., Chin, R., & Amabili, M. (2022). A review on the nonlinear dynamics of hyperelastic structures. *Nonlinear Dynamics, 110*, 963–994.
Khaniki, H. B., Ghayesh, M. H., Chin, R., & Amabili, M. (2023). Hyperelastic structures: A review on the mechanics and biomechanics. *International Journal of Non-Linear Mechanics, 148*, Article 104275.
Khaniki, H. B., Ghayesh, M. H., Chin, R., & Chen, L.-Q. (2022). Experimental characteristics and coupled nonlinear forced vibrations of axially travelling hyperelastic beams. *Thin-Walled Structures, 170*, Article 108526.
Khaniki, H. B., Ghayesh, M. H., Chin, R., & Hussain, S. (2022). Nonlinear continuum mechanics of thick hyperelastic sandwich beams using various shear deformable beam theories. *Continuum Mechanics and Thermodynamics, 34*, 781–827.
Kiarasi, F., Babaei, M., Mollaei, S., Mohammadi, M., & Asemi, K. (2021). Free vibration analysis of FG porous joined truncated conical-cylindrical shell reinforced by graphene platelets. *Advances in Nano Research, 11*, 361–380.
Kiendl, J., Hsu, M.-C., Wu, M. C., & Reali, A. (2015). Isogeometric Kirchhoff–Love shell formulations for general hyperelastic materials. *Computer Methods in Applied Mechanics and Engineering, 291*, 280–303.
Kreibich, M., Berger, T., Morlock, J., Kondov, S., Scheumann, J., Kari, F. A., Rylski, B., Siepe, M., Beyersdorf, F., & Czerny, M. (2018). The frozen elephant trunk technique for the treatment of acute complicated Type B aortic dissection. *European Journal of Cardio-Thoracic Surgery, 53*, 525–530.
Lim, C., Zhang, G., & Reddy, J. (2015). A higher-order nonlocal elasticity and strain gradient theory and its applications in wave propagation. *Journal of the Mechanics and Physics of Solids, 78*, 298–313.
Malikan, M., Krasheninnikov, M., & Eremeyev, V. A. (2020). Torsional stability capacity of a nano-composite shell based on a nonlocal strain gradient shell model under a three-dimensional magnetic field. *International Journal of Engineering Science, 148*, Article 103210.
Malikan, M., Uglov, N. S., & Eremeyev, V. A. (2020). On instabilities and post-buckling of piezomagnetic and flexomagnetic nanostructures. *International Journal of Engineering Science, 157*, Article 103395.
Mittelmann, H. D., & Roose, D. (1990). *Continuation techniques and bifurcation problems*. Springer.
Mooney, M. (1940). A theory of large elastic deformation. *Journal of Applied Physics, 11*, 582–592.
Nguyen, T.-K., Pham, D.-C., & Nguyen, V.-L. (2020). Conduction in 2-D and 3-D dimensional spherically-symmetric anisotropic-coating inclusion composites. *International Journal of Engineering Science, 154*, Article 103352.
Paulis, G. E. R. D., Czerny, M., Rylski, B., Kari, F. A., Kreibich, M., Morlock, J., Scheumann, J., Kondov, S., Südkamp, M., & Siepe, M. (2017). Technical details making aortic arch replacement a safe procedure using the Thoraflex™ Hybrid prosthesis. *European Journal of Cardio-Thoracic Surgery, 51*, i15–i19.
Pho, K. H. (2022). Improvements of the Newton–Raphson method. *Journal of Computational and Applied Mathematics*, Article 114106.
Reddy, J. N. (2003). *Mechanics of laminated composite plates and shells: theory and analysis*. CRC press.
Reddy, J. N. (2006). *Theory and analysis of elastic plates and shells*. CRC press.
Renda, F., Giorgio-Serchi, F., Boyer, F., Laschi, C., Dias, J., & Seneviratne, L. (2018). A unified multi-soft-body dynamic model for underwater soft robots. *The International Journal of Robotics Research, 37*, 648–666.
Rivlin, R. (1949). Large elastic deformations of isotropic materials VI. Further results in the theory of torsion, shear and flexure. *Philosophical Transactions of the Royal Society of London. Series A, Mathematical and Physical Sciences, 242*, 173–195.
Sayyad, A. S., & Ghugal, Y. M. (2020). Stress analysis of laminated composite and sandwich cylindrical shells using a generalized shell theory. *Composite Materials and Engineering, 2*, 103–124.
Sedova, O., & Pronina, Y. (2022). The thermoelasticity problem for pressure vessels with protective coatings, operating under conditions of mechanochemical corrosion. *International Journal of Engineering Science, 170*, Article 103589.
Shahmohammadi, M. A., Mirfatah, S. M., Salehipour, H., & Civalek, Ö. (2023). On nonlinear forced vibration of micro scaled panels. *International Journal of Engineering Science, 182*, Article 103774.
Takizawa, K., Tezduyar, T. E., & Sasaki, T. (2019). Isogeometric hyperelastic shell analysis with out-of-plane deformation mapping. *Computational Mechanics, 63*, 681–700.
Tzou, H., & Zhang, X. (2016). A flexoelectric double-curvature nonlinear shell energy harvester. *Journal of Vibration and Acoustics*, 138.
Xu, J., Yuan, X., Zhang, H., Zheng, F., & Chen, L. (2020). Nonlinear vibrations of thermo-hyperelastic moderately thick cylindrical shells with 2: 1 internal resonance. *International Journal of Structural Stability and Dynamics, 20*, Article 2050067.
Xu, X., Karami, B., & Janghorban, M. (2021). On the dynamics of nanoshells. *International Journal of Engineering Science, 158*, Article 103431.
Xu, X., Shahsavari, D., & Karami, B. (2021). On the forced mechanics of doubly-curved nanoshell. *International Journal of Engineering Science, 168*, Article 103538.
Yang, Y., Vella, K., & Holmes, D. P. (2021). Grasping with kirigami shells. *Science Robotics, 6*, eabd6426.
Zhang, J., Xu, J., Yuan, X., Ding, H., Niu, D., & Zhang, W. (2019). Nonlinear vibration analyses of cylindrical shells composed of hyperelastic materials. *Acta Mechanica Solida Sinica, 32*, 463–482.
Zhao, W., Zhang, J., Zhang, W., & Yuan, X. (2021). Internal resonance characteristics of hyperelastic thin-walled cylindrical shells composed of Mooney–Rivlin materials. *Thin-Walled Structures, 163*, Article 107754.
Zhao, Z., Yuan, X., Zhang, W., Niu, D., & Zhang, H. (2021). Dynamical modeling and analysis of hyperelastic spherical shells under dynamic loads and structural damping. *Applied Mathematical Modelling, 95*, 468–483.
Zheng, Y., Karami, B., & Shahsavari, D. (2022). On the vibration dynamics of heterogeneous panels under arbitrary boundary conditions. *International Journal of Engineering Science, 178*, Article 103727.

Chapter 9

Conclusions, summary, recommendations and future work

9.1 Conclusions and summary

A detailed computational and experimental investigation of the nonlinear mechanics of hyperelastic structures was presented in this thesis. Due to the wide range of potential applications, multiple structures and mechanical conditions have been discussed to provide a better understanding of the mechanics of hyperelastic structures. The main focus of this thesis was isotropic incompressible hyperelastic laws, which provide good accuracy when studying polymeric structures. Each chapter of this thesis investigated some aspects of the statics and dynamics of soft structures in a combination of analytical, numerical, and experimental analyses. This chapter summarises the achievements and conclusions of this thesis as follows:

In Chapter 2, a state-of-the-art review of the statics and dynamics of different structures was presented in the framework of hyperelastic laws. By gathering together the previous work in this field, up to 2022, it was shown that hyperelastic strain energy models are widely used in different industries and applications, and the number of studies in this field is growing significantly. A major field that employs hyperelastic theories is biomechanics. Modelling the mechanics of biological tissues for surgery simulation, diagnosis and treatment requires an accurate theoretical approach to track the stress-stretch behaviour under different types of loads properly. It is noteworthy that most biological tissues should be modelled as anisotropic/isotropic visco-hyperelastic tissue. This chapter showed the strength of different strain energy density models for modelling different human body organs accurately, concluding that, based on the tissue type, different strain energy laws have superiority. Moreover, the bending, buckling and vibration behaviours of polymeric structures have been reviewed in detail, showing that the field is clearly under-researched as there are many potential and real-world applications that have not yet been investigated properly. Some of these gaps have been addressed in this thesis. The discussions and analyses of Chapter 2 are presented in two separate review papers on the statics and dynamics of hyperelastic structures, and are published in the Journal of *Nonlinear Dynamics* for dynamic analysis [1] and the *International Journal of Non-Linear Mechanics* for statics and biomechanics [2].

In Chapter 3, by considering the applications of axially-moving hyperelastic

structures in different systems including conveyors, technical textile manufacturing processes, belt-operating power transmission systems, roll-to-roll systems and many more, the nonlinear dynamic behaviour of axially-travelling hyperelastic belts was investigated. The structure was assumed to be made of isotropic incompressible thermoplastic and the hyperelastic characteristics were obtained experimentally by fabricating and testing samples using ASTM-D638 guidance. Different strain energy density models (developed using the first strain energy density models) were analysed to find the most accurate hyperelastic law to model the structure. As Yeoh's strain energy density model showed good accuracy in modelling the experimental results, the axially-moving hyperelastic belt was modelled using this constitutive law. The coupled equations of motion were obtained using Hamilton's principle, showing complicated higher-order nonlinear terms. The convergence of the solution method was obtained by considering a higher number of Galerkin modes. This study considered both axial and transverse deformations and the results emphasised that neglecting the axial motion can significantly affect the accuracy of the modelling. A set of case studies have been presented for both linear and nonlinear dynamic analyses. For the linear analysis, the variations of the natural frequencies and mode shapes were examined showing that the axial velocity term and Yeoh's coefficients have a significant effect in changing the natural frequencies and mode shapes. The nonlinear forced vibration behaviour of the axially travelling belt was also investigated, showing that increasing axial velocity leads to a higher coupling between the modes in the nonlinear frequency response. Moreover, the effects of Yeoh's coefficients, tension, and external force on the nonlinear dynamics of the structure were analysed and the sensitivity of the structure to these parameters was presented. The results of this study are useful in designing and using soft belt structures in the mentioned applications. The outcome of this research is published in the journal of *Thin-Walled Structures* [3].

In Chapter 4, the influence of porosity and voids on the dynamic performance of hyperelastic structures were investigated by developing a modified porous-hyperelastic model. In the first part of this study, dumbbell samples with different infill rates were fabricated and the stress-stretch behaviour of each sample was obtained by following the standards. It was shown that porosity in the structure can significantly affect the stress-stretch behaviour of the hyperelastic sample; this effect is nonlinear and it is most effective when the overall porosity rate is low. After obtaining the stress-stretch behaviour for different infill rates, the Mooney-Rivlin strain energy density model was modified with the coefficients as a function of porosity to add the porosity effect into the constitutive model. It was shown that the developed model has good accuracy in tracking the stress-stretch behaviour of hyperelastic samples with different porosities. Using the developed constitutive model, hyperelastic beam structures with porosity were modelled. The porosity was assumed to be either uniform or varied through the length of the hyperelastic beam following power-law and sigmoid functions. The non-linear forced oscillation analysis of the structure shows that the presence of porosity and its variation type through the length can change the nonlinear response of the structure, which can be used by researchers to tune the vibration response based on the application. The results of Chapter 4 are published in the *Journal of Sound and Vibration* [4].

In Chapter 5, the main focus was on layered hyperelastic structures, as it has

been shown that these structures are more useful than single-layered hyperplastic structures in some applications, including laminated tubes and food packaging. The structure was presented as a general multi-layered thick incompressible hyperelastic beam. The effect of shear deformation was added to the model by using five different shear deformation theories. A detailed case study analysis was provided to investigate the effect of layering, layer sorting, material ordering and slenderness ratio of each layer. The results of this chapter show that the designer has the flexibility to change the dynamic behaviour of the sandwich structure by varying the discussed parameters. Furthermore, it has been shown that considering the shear effects in modelling thick hyperelastic asymmetrical structures has a key role in accuracy and the higher order shear deformation theories show a close agreement in results. The results of Chapter 5 are published in the journal of *Continuum Mechanics and Thermodynamics* [5].

Chapter 6 concentrated on considering the viscoelasticity effects in modelling the nonlinear mechanics of hyperelastic structures. An experimentally-proven model of the visco-hyperelastic behaviour was employed from the literature; this model used a combination of Mooney-Rivlin and Kelvin-Voigt models. The bending deformation and nonlinear vibration behaviours of the shallow arch structure were studied by using a third-order shear deformable theory together with von-Karman geometrical nonlinearity. The coupled equations of motion show high-order nonlinear damping and stiffness terms due to the coupling of viscoelasticity and hyperelasticity terms. The static response of the system shows a significant difference in the linear modelling results and higher-order model results, emphasising the importance of modelling the structure accurately. Furthermore, the curvature of the structure was varied so as to reach an internal resonance and the nonlinear forced oscillation behaviour was investigated. It was shown that the rich nonlinear frequency response can be significantly different, depending on the nature and type of the hyperelastic or visco-hyperelastic structure. It is noteworthy that for structures with dominant viscoelastic behaviour, this rich nonlinear behaviour can be fully damped. Since many hyperelastic structures show a combination of hyperelastic and viscoelastic behaviour (including the materials used for fabricating prostheses and implants), the results of this study are useful in comprehending the dynamics of such structures. The results of Chapter 6 are published in the journal of *Continuum Mechanics and Thermodynamics* [6].

In Chapter 7, a joint theoretical and experimental approach for studying the non-linear mechanics of hyperelastic plate structures was presented, focusing on the mass-sensing behaviour of the structure. An experimental setup was developed to study the nonlinear forced vibrations of hyperelastic plates with and without an attached concentrated mass, and the nonlinear frequency responses of the plate under different external excitation loads were obtained. By following the ASTM D-412 standard and using a mould, the dumbbell samples were cut and tested to obtain the hyperelastic coefficients of the isotropic hyperelastic material. After obtaining the hyperelastic characteristics of the plate's material, the coupled in-plane and out-of-plane equations of motion were derived and the nonlinear forced vibration behaviour was modelled. It was shown that the derived model has good accuracy in tracking the nonlinear forced vibration behaviour and mass sensing behaviour of the structure. The internal resonance phenomena due to geometrical ratios and external

masses were analysed and the structure at different resonances was examined. The results show that the soft behaviour of hyperelastic structures gives the advantage of being able to apply them as sensors for sensing attached masses. The results of Chapter 7 are published in the *International Journal of Engineering Science* [7].

In Chapter 8, the bending, vibration and internal resonance behaviours of different types of isotropic incompressible shell structures were presented. Cylindrical, spherical, doubly-curved, and hyperbolic hyperelastic shallow shells were modelled and solved using Donnell's nonlinear shell theory, Hamilton's principle, the two-dimensional Galerkin technique, and the Mooney-Rivlin strain energy density model. It was shown that curvature in the structure can change the nonlinear hardening behaviour to a combination of hardening and softening, which this effect highly depends on the shell type. Internal resonance phenomena were obtained for different shell types based on the curvatures. The proposed modelling and results of this study are useful for different applications, including biomechanics and soft robotics, to understand static and dynamic behaviour under different conditions. The results of Chapter 8 are published in the *International Journal of Engineering Science* [8].

The theoretical models developed through this thesis have been verified using different techniques. Experimental analysis was used to show the accuracy of the developed model for nonlinear forced vibrations of hyperplastic plates. The equations of motion were verified by simplifying the problems and comparing them with those published on linear elastic structures. The solution technique for analysing the nonlinear forced vibration was verified using previous studies on the nonlinear oscillation of axially-travelling elastic beams. The bending and deformation analyses were verified using finite element software for different hyperelastic structures. The linear natural frequencies were also verified using the literature on sandwich elastic structures.

As shown in several chapters of this thesis, hyperelastic structures are very likely to undergo large deformations and strains, which require proper modelling of both material and geometrical nonlinearities in the structure. Depending on the structure type, the geometrical properties, imperfections, boundary conditions and other designing terms, the hyperelastic structure can show a wide range of rich mechanical responses, which, in turn, shows the necessity for developing an effective, accurate model of such structures.

9.2 Future work and recommendations

This thesis investigated the mechanical behaviour of different hyperelastic structures by considering both material and structural nonlinearities. Following the applications, a wide range of mechanical conditions, theoretical models, experimental setups and analyses were presented. Different validation techniques were used to show the strength and accuracy of the developed methodologies. Hyperelastic structures have shown many potential applications and further persuasion and extensions of the current work can be undertaken in different ways. Since this thesis is a fundamental study on the nonlinear mechanics of hyperelastic structures, there are many potential follow-up research topics for this work, for which some of the recommended research directions are listed as follows:

• The volumetric behaviour of the hyperelastic structure is one of the main, important characteristics of the studied systems. The assumption of incompressibility is accurate for materials with nearly-incompressible and incompressible manners such as rubber materials and most polymers [9-11]. However, this assumption cannot be made for some other hyperelastic structures. For instance, foam can undergo large volumetric changes and assuming it to be an incompressible material can cause significant errors. The studies presented in this thesis considered strains in the thickness direction of the structure to fulfil the requirement for having the third strain invariant equal to one ($J = I_3 = 1$). However, for structures fabricated from compressible isotropic materials, the third strain invariant would not be equal to one (as shown in Chapter 2 of this thesis). Based on the application of the compressible hyperelastic structure, its mechanical behaviour can be analysed as a further exploration of this thesis.

• Many materials, such as vulcanised elastomers [12-14], show an ideal hyperelastic behaviour. Soft structures, such as elastomers, usually show a combination of viscoelasticity and hyperelasticity. This thesis mainly challenged the hyperelastic characteristics of soft structures to comprehend the mechanics of hyperelasticity. In Chapter 5, the visco-hyperelastic behaviour of soft structures was investigated, showing a high level of coupling between viscoelasticity and hyperelasticity. The visco-hyperelastic model employed in this study was proposed by Li et al. [15] in their experimental and theoretical analysis. There are a large number of visco-hyperelastic models combining viscosity and hyperelasticity that can be studied further to discuss the strength of each model for different types of soft structures.

• The application of hyperelastic laws in modelling biological tissues has long been a topic of debate between researchers. Since these tissues can be modelled as hyperelastic structures (discussed in Chapter 2), the developed methodologies in this thesis can be extended for such structures. For instance, a common cause of vision loss is Glaucoma, which happens when excessive pressure in the eye leads to optic nerve damage. This can be studied by developing a three-layered hyperelastic spherical model and analysing the pressure effect. This thesis analysed isotropic hyperelastic structures; therefore, the hyperelastic characteristics were obtained by using uniaxial tests alone. However, since biological tissues mostly show an anisotropic behaviour, mechanical characteristic analysis would require both uniaxial and biaxial tests. Therefore, the structural modelling presented in this thesis can be extended for biomechanical applications.

• Prosthetic and implant structures are some of the most important applications of hyperelastic structures. A proper design of such structures can optimise the performance and life cycle in the operating condition. For instance, prosthetic feet [16, 17] undergo periodic loads with different magnitudes and the necessity of having a comfortable design, long lasting structure and optimised geometry can be obtained by expanding the presented works on such structures.

References

[1] H.B. Khaniki, M.H. Ghayesh, R. Chin, M. Amabili, A review on the nonlinear dynamics of hyperelastic structures, Nonlinear Dynamics, 110 (2022) 963–994.

[2] H.B. Khaniki, M.H. Ghayesh, R. Chin, M. Amabili, Hyperelastic structures: A review on the mechanics and biomechanics, International Journal of Non-Linear Mechanics, (2022) 104275.
[3] H.B. Khaniki, M.H. Ghayesh, R. Chin, L.-Q. Chen, Experimental characteristics and coupled nonlinear forced vibrations of axially travelling hyperelastic beams, Thin-Walled Structures, 170 (2022) 108526.
[4] H.B. Khaniki, M.H. Ghayesh, R. Chin, M. Amabili, Large amplitude vibrations of imperfect porous-hyperelastic beams via a modified strain energy, Journal of Sound and Vibration, 513 (2021) 116416.
[5] H.B. Khaniki, M.H. Ghayesh, R. Chin, S. Hussain, Nonlinear continuum mechanics of thick hyperelastic sandwich beams using various shear deformable beam theories, Continuum Mechanics and Thermodynamics, 34 (2022) 781–827.
[6] H.B. Khaniki, M.H. Ghayesh, R. Chin, S. Hussain, Internal resonance and bending analysis of thick visco-hyper-elastic arches, Continuum Mechanics and Thermodynamics, (2022) 1-44.
[7] H.B. Khaniki, M.H. Ghayesh, R. Chin, Theory and experiment for dynamics of hyperelastic plates with modal interactions, International Journal of Engineering Science, 182 (2023) 103769.
[8] H.B. Khaniki, M.H. Ghayesh, Highly nonlinear hyperelastic shells: Statics and dynamics, International Journal of Engineering Science, 183 (2023) 103794.
[9] M. Hossain, D.K. Vu, P. Steinmann, Experimental study and numerical modelling of VHB 4910 polymer, Computational Materials Science, 59 (2012) 65-74.
[10] M. Hossain, P. Steinmann, More hyperelastic models for rubber-like materials: consistent tangent operators and comparative study, Journal of the Mechanical Behavior of Materials, 22 (2013) 27-50.
[11] M. Carroll, A strain energy function for vulcanized rubbers, Journal of Elasticity, 103 (2011) 173-187.
[12] J.S. Bergström, M.C. Boyce, Large strain time-dependent behavior of filled elastomers, Mechanics of Materials, 32 (2000) 627-644.
[13] P. Austrell, Modeling of Elasticity and Damping for Filled Elastomers, Lund University, Lund, Sweden, 1997.
[14] B. Trobentar, S. Glodež, B. Zafošnik, Gear tooth deflection of spur polymer gears, in: 2014 International Gear Conference, Chandos Publishing Lyon, France, 2014, pp. 129-137.
[15] L. Li, A. Maccabi, A. Abiri, Y.-Y. Juo, W. Zhang, Y.-J. Chang, G.N. Saddik, L. Jin, W.S. Grundfest, E.P. Dutson, Characterization of perfused and sectioned liver tissue in a full indentation cycle using a visco-hyperelastic model, Journal of the Mechanical Behavior of Biomedical Materials, 90 (2019) 591-603.
[16] J.E. Edelstein, Prosthetic feet: state of the art, Physical Therapy, 68 (1988) 1874-1881.
[17] G. Klute, J. Berge, Modelling the effect of prosthetic feet and shoes on the heel-ground contact force in amputee gait, Proceedings of the Institution of Mechanical Engineers, Part H: Journal of Engineering in Medicine, 218 (2004) 173-182.